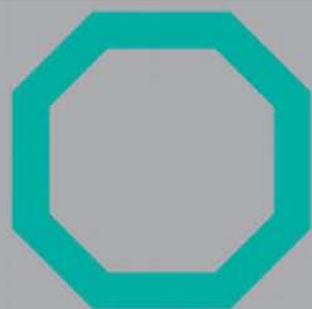
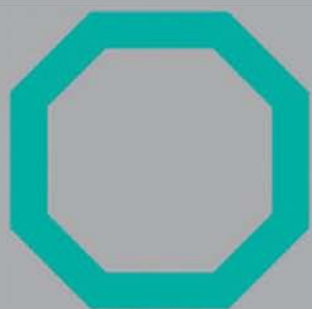


K.A. Gschneidner, Jr.,
J.-C.G. Bünzli and V.K. Pecharsky
Editors

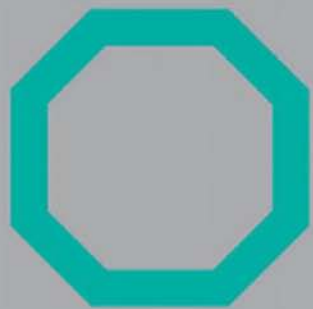
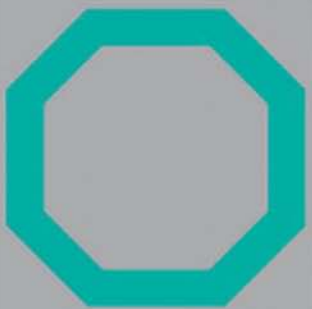
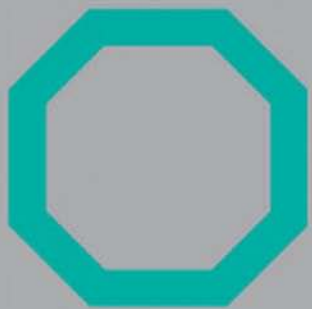


HANDBOOK ON THE
PHYSICS AND CHEMISTRY OF
RARE EARTHS



Volume 41

North-Holland



HANDBOOK ON THE PHYSICS AND CHEMISTRY
OF RARE EARTHS
VOLUME 41

HANDBOOK ON THE PHYSICS AND CHEMISTRY
OF RARE EARTHS

Advisory Editorial Board

G.-y. ADACHI, *Kobe, Japan*

W.J. EVANS, *Irvine, USA*

S.M. KAUZLARICH, *Davis, USA*

G.H. LANDER, *Karlsruhe, Germany*

M.F. REID, *Christchurch, New Zealand*

Editor Emeritus

LeRoy EYRING[‡], *Tempe, USA*

[‡] Deceased.

HANDBOOK ON THE PHYSICS AND CHEMISTRY OF
RARE EARTHS

VOLUME 41

EDITORS

Karl A. GSCHNEIDNER, Jr.

*Member, National Academy of Engineering
The Ames Laboratory, U.S. Department of Energy, and
Department of Materials Science and Engineering
Iowa State University
Ames, Iowa 50011-3020
USA*

Jean-Claude G. BÜNZLI

*Swiss Federal Institute of Technology, Lausanne (EPFL)
Laboratory of Lanthanide Supramolecular Chemistry
BCH 1402
CH-1015 Lausanne
Switzerland*

Vitalij K. PECHARSKY

*The Ames Laboratory, U.S. Department of Energy, and
Department of Materials Science and Engineering
Iowa State University
Ames, Iowa 50011-3020
USA*



Amsterdam • Boston • Heidelberg • London • New York • Oxford
Paris • San Diego • San Francisco • Singapore • Sydney • Tokyo
North-Holland is an imprint of Elsevier



North-Holland is an imprint of Elsevier
Radarweg 29, PO Box 211, 1000 AE Amsterdam, The Netherlands
The Boulevard, Langford Lane, Kidlington, Oxford OX5 1GB, UK

Copyright © 2011 Elsevier B.V. All rights reserved.

No part of this publication may be reproduced, stored in a retrieval system or transmitted in any form or by any means electronic, mechanical, photocopying, recording or otherwise without the prior written permission of the publisher.

Permissions may be sought directly from Elsevier's Science & Technology Rights Department in Oxford, UK: phone (+44) (0) 1865 843830; fax (+44) (0) 1865 853333; email: permissions@elsevier.com. Alternatively you can submit your request online by visiting the Elsevier web site at <http://elsevier.com/locate/permissions>, and selecting, *Obtaining permission to use Elsevier material*.

Notice

No responsibility is assumed by the publisher for any injury and/or damage to persons or property as a matter of products liability, negligence or otherwise, or from any use or operation of any methods, products, instructions or ideas contained in the material herein. Because of rapid advances in the medical sciences, in particular, independent verification of diagnoses and drug dosages should be made.

British Library Cataloguing in Publication Data

A catalogue record for this book is available from the British Library

Library of Congress Cataloging-in-Publication Data

A catalog record for this book is available from the Library of Congress

ISBN: 978-0-444-53590-0

ISSN: 0168-1273

For information on all North-Holland publications
visit our website at books.elsevier.com

Printed and Bound in Great Britain

11 12 10 9 8 7 6 5 4 3 2 1

Working together to grow
libraries in developing countries

www.elsevier.com | www.bookaid.org | www.sabrc.org

ELSEVIER

BOOK AID
International

Sabre Foundation

PREFACE

**Karl A. Gschneidner Jr., Jean-Claude G. Bünzli,
Vitalij K. Pecharsky**

These elements perplex us in our reaches [sic], baffle us in our speculations, and haunt us in our very dreams. They stretch like an unknown sea before us—mocking, mystifying, and murmuring strange revelations and possibilities.

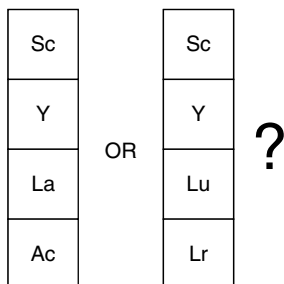
Sir William Crookes (February 16, 1887)

Volume 41 of the *Handbook on the Physics and Chemistry of Rare Earths* adds four chapters to the series: two focus on nanoscale rare-earth materials, while the other two are concerned with divergent topics—the arrangement of the rare-earth elements in the periodic table, and the higher order rare-earth chalcogenide compounds with the elements of the 14th group and also In. The first chapter (248) discusses the various proposals suggested for the location of the rare-earth elements in the periodic table from the time of Mendeleev to the present day. The rare-earth containing buckyballs, that is, carbon fullerenes with encapsulated metal atom(s), which may exhibit a variety of behaviors—metals, semiconductors, and insulators—are described in Chapter 249. The ternary and quaternary rare-earth chalcogenide compounds with the group 14 elements (Si, Ge, Sn and Pb) and In feature a wide range of stoichiometries, and both simple and complex crystal structures, and may have unusual applications (Chapter 250). The final chapter (251) describes the synthesis, chemical behaviors, and physical properties of inorganic compounds at the nanoscale. Each chapter concludes with a perspective of the future of the field.

CHAPTER 248. ACCOMMODATION OF THE RARE EARTHS IN THE PERIODIC TABLE: A HISTORICAL ANALYSIS

By **PIETER THYSSEN AND KOEN BINNEMANS**

Katholieke Universiteit Leuven, Belgium

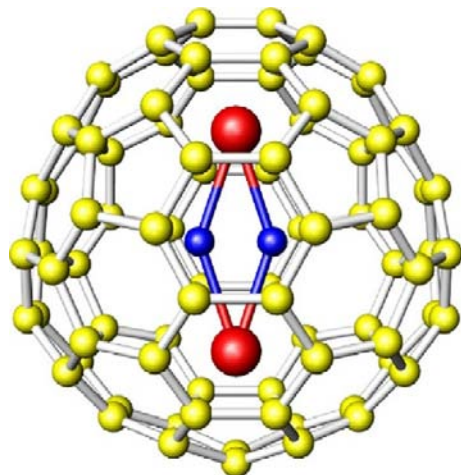


This chapter gives an overview of the evolution of the position of the rare earths in the periodic table, from Mendeleev's time to the present. Three fundamentally different accommodation methodologies have been proposed over the years. Mendeleev considered the rare-earth elements as homologs of the other elements. Other chemists looked upon the rare earths as forming a special intraperiodic group and they clustered the rare-earth elements in one of the groups of the periodic table. Still others adhered to the intergroup accommodation of the rare earths, according to which the rare-earth elements do not show any relationship with the other elements, so that they had to be placed within the periodic table as a separate family of elements. The intergroup accommodation became the preferred one in the twentieth century. The advantages and disadvantages of the different representations of the modern periodic table are discussed.

CHAPTER 249. METALLOFULLERENES

By HISANORI SHINOHARA AND YAHACHI SAITO

Nagoya University, Nagoya, Japan



Endohedral metallofullerenes (fullerenes with metal atom(s) encapsulated) are novel forms of fullerene-based materials that have attracted wide interest during the past decades, not only in physics and chemistry but also in such interdisciplinary areas as material and biological sciences. In this article, advances in the production, separation (isolation), and various spectroscopic characterizations of endohedral metallofullerenes are presented in an attempt to clarify their structural, electronic, and solid-state properties. The endohedral metallofullerenes produced so far are centered on group 2 and 3 metallofullerenes, such as Sr and Ba, and Sc, Y, and La as well as lanthanide metallofullerenes (Ce–Lu). These metal atoms have been encapsulated in higher fullerenes, especially in C_{82} . Synchrotron X-ray diffraction and ^{13}C NMR and ultra-high vacuum scanning tunneling microscopy (UHV-STM) studies have revealed that metal atoms are indeed encapsulated by the carbon cage and that the metal atoms are not in the center of the fullerene cage but sit close to the carbon cage, indicating the presence of a strong metal–cage interaction. Electron spin resonance and theoretical calculations reveal that substantial electron transfer takes place from the engaged metal atom to the carbon cage: intrafullerene electron transfers. One of the most distinct features of such a metallofullerene is superatom character, by which the metallofullerene can be viewed as a positively charged core metal surrounded by a negatively charged carbon cage. Structural and

electronic analyses based on X-ray diffraction and UHV-STM measurements indeed provide evidence of such character. Endohedral metallofullerenes can be metals, small-gap semiconductors, or insulators, depending upon the fullerene size and the kind and the number of metal atoms encapsulated. Finally, some prospective applications of metallofullerenes are presented.

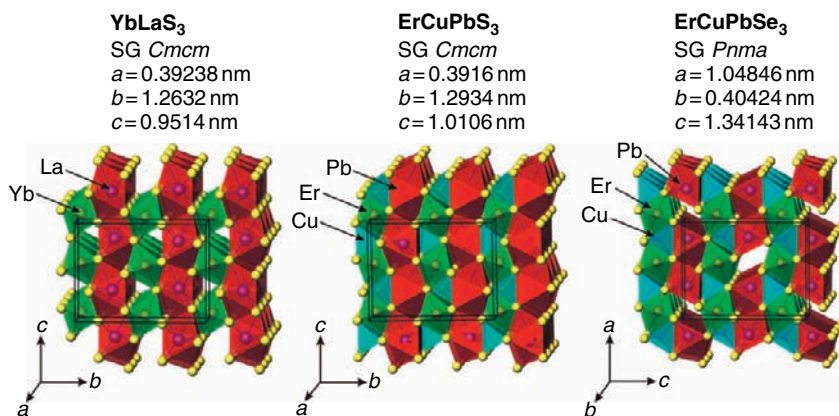
CHAPTER 250. TERNARY AND QUATERNARY CHALCOGENIDES OF Si, Ge, Sn, Pb, and In

By **LUBOMIR D. GULAY**

Volyn National University, Lutsk, Ukraine and

MAREK DASZKIEWICZ

W. Trzebiatowski Institute of Low Temperature and Structure Research, Wrocław, Poland

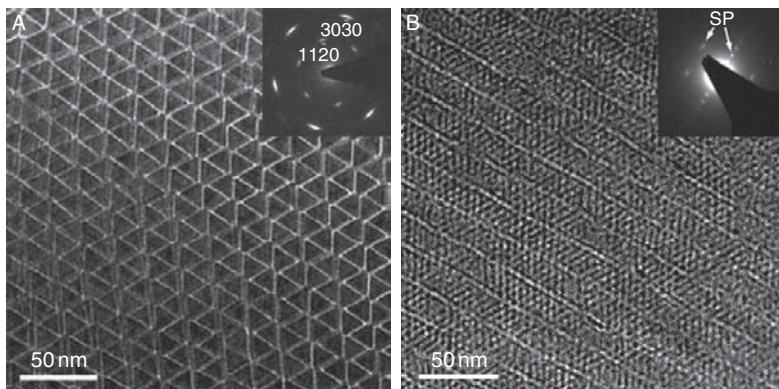


Complex ternary, quaternary, and multicomponent chalcogenides containing rare earths are interesting because of potential applications in the fields of ionic conductivity and nonlinear optics. Gulay and Daszkiewicz review the current knowledge about experimental investigation of phase diagrams, crystallography, crystallographic relationships among known ternary and quaternary rare-earth chalcogenides, and the general principles governing the formation of rare-earth chalcogenides with Si, Ge, Sn, Pb, and In. The information presented in this chapter may serve as a guideline for preparation of small quantities of these novel materials for studies of their basic physical properties, and for those interested in preparing large quantities of materials in order to explore their potential for practical applications.

CHAPTER 251. CONTROLLED SYNTHESIS AND PROPERTIES OF NANOMATERIALS

By **CHUN-HUA YAN, ZHENG-GUANG YAN, YA-PING DU, JIE SHEN, CHAO ZHANG, AND WEI FENG**

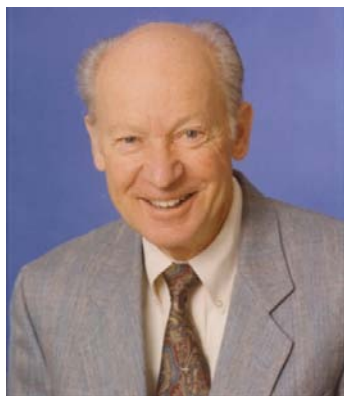
Peking University, Beijing, China



Rare-earth nanomaterials find numerous applications as phosphors, catalysts, permanent magnets, fuel cell electrodes and electrolytes, hard alloys, and superconductors. Yan and coauthors focus on inorganic non-metallic rare-earth nanomaterials prepared using chemical synthesis routes, more specifically, prepared via various solution-based routes. Recent discoveries in synthesis and characterization of properties of rare-earth nanomaterials are systematically reviewed. The authors begin with ceria and other rare-earth oxides, and then move to oxysalts, halides, sulfides, and oxysulfides. In addition to comprehensive description of synthesis routes that lead to a variety of nanoforms of these interesting materials, the authors pay special attention to summarizing most important properties and their relationships to peculiar structural features of nanomaterials synthesized over the last 10–15 years.

Special announcement

With the completion of this volume, the founding and senior editor, Karl A. Gschneidner, Jr., will retire from editing this series of reference books on rare earths. In the Preface of Volume 1, published in 1978 and which was part of a 4-volume successful effort to produce a state-of-the-art overview of the then (and already) fast developing rare earth sciences, Karl A. Gschneidner, Jr. and LeRoy Eyring wrote: *“A goal of these volumes is to attempt to combine and integrate as far as practical the physics and chemistry of these elements.”* Thirty-two years and 41 volumes (featuring 251 chapters) later, this aim seems to have been fully attained. The rare-earth scientific and industrial communities are very grateful to Karl A. Gschneidner, Jr. for his insightful leadership of this endeavor.



Jean-Claude Bünzli will take over the senior editorship of the **HANDBOOK** starting with Volume 42 and Vitalij K. Pecharsky will continue to serve as an editor. A third editor is expected to be added in the near future.

CONTENTS

<i>Preface</i>	v
<i>Contents</i>	xi
<i>Contents of Volumes 1–40</i>	xiii
<i>Index of Contents of Volumes 1–41</i>	xxv
248. Accommodation of the Rare Earths in the Periodic Table: A Historical Analysis	1
Pieter Thyssen and Koen Binnemans	
249. Metallofullerenes	95
Hisanori Shinohara and Yahachi Saito	
250. Ternary and Quaternary Chalcogenides of Si, Ge, Sn, Pb, and In	157
Lubomir D. Gulay and Marek Daszkiewicz	
251. Controlled Synthesis and Properties of Rare Earth Nanomaterials	275
Chun-Hua Yan, Zheng-Guang Yan, Ya-Ping Du, Jie Shen, Chao Zhang, and Wei Feng	
<i>Author Index</i>	473
<i>Subject Index</i>	517

This page intentionally left blank

CONTENTS OF VOLUMES 1–40

VOLUME 1: Metals

1978, 1st repr. 1982, 2nd repr. 1991; ISBN 0-444-85020-1

1. Z.B. Goldschmidt, *Atomic properties (free atom)* 1
 2. B.J. Beaudry and K.A. Gschneidner Jr, *Preparation and basic properties of the rare earth metals* 173
 3. S.H. Liu, *Electronic structure of rare earth metals* 233
 4. D.C. Koskenmaki and K.A. Gschneidner Jr, *Cerium* 337
 5. L.J. Sundström, *Low temperature heat capacity of the rare earth metals* 379
 6. K.A. McEwen, *Magnetic and transport properties of the rare earths* 411
 7. S.K. Sinha, *Magnetic structures and inelastic neutron scattering: metals, alloys and compounds* 489
 8. T.E. Scott, *Elastic and mechanical properties* 591
 9. A. Jayaraman, *High pressure studies: metals, alloys and compounds* 707
 10. C. Probst and J. Wittig, *Superconductivity: metals, alloys and compounds* 749
 11. M.B. Maple, L.E. DeLong and B.C. Sales, *Kondo effect: alloys and compounds* 797
 12. M.P. Dariel, *Diffusion in rare earth metals* 847
- Subject index 877

VOLUME 2: Alloys and intermetallics

1979, 1st repr. 1982, 2nd repr. 1991; ISBN 0-444-85021-X

13. A. Iandelli and A. Palenzona, *Crystal chemistry of intermetallic compounds* 1
 14. H.R. Kirchmayr and C.A. Poldy, *Magnetic properties of intermetallic compounds of rare earth metals* 55
 15. A.E. Clark, *Magnetostrictive RFe₂ intermetallic compounds* 231
 16. J.J. Rhyne, *Amorphous magnetic rare earth alloys* 259
 17. P. Fulde, *Crystal fields* 295
 18. R.G. Barnes, *NMR, EPR and Mössbauer effect: metals, alloys and compounds* 387
 19. P. Wachter, *Europium chalcogenides: EuO, EuS, EuSe and EuTe* 507
 20. A. Jayaraman, *Valence changes in compounds* 575
- Subject index 613

VOLUME 3: Non-metallic compounds – I

1979, 1st repr. 1984; ISBN 0-444-85215-8

21. L.A. Haskin and T.P. Paster, *Geochemistry and mineralogy of the rare earths* 1
22. J.E. Powell, *Separation chemistry* 81
23. C.K. Jørgensen, *Theoretical chemistry of rare earths* 111
24. W.T. Carnall, *The absorption and fluorescence spectra of rare earth ions in solution* 171
25. L.C. Thompson, *Complexes* 209

26. G.G. Libowitz and A.J. Maeland, *Hydrides* 299
27. L. Eyring, *The binary rare earth oxides* 337
28. D.J.M. Bevan and E. Summerville, *Mixed rare earth oxides* 401
29. C.P. Khattak and F.F.Y. Wang, *Perovskites and garnets* 525
30. L.H. Brixner, J.R. Barkley and W. Jeitschko, *Rare earth molybdates (VI)* 609
Subject index 655

VOLUME 4: Non-metallic compounds – II

1979, 1st repr. 1984; ISBN 0-444-85216-6

31. J. Flahaut, *Sulfides, selenides and tellurides* 1
32. J.M. Haschke, *Halides* 89
33. F. Hulliger, *Rare earth pnictides* 153
34. G. Blasse, *Chemistry and physics of R-activated phosphors* 237
35. M.J. Weber, *Rare earth lasers* 275
36. F.K. Fong, *Nonradiative processes of rare-earth ions in crystals* 317
- 37A. J.W. O'Laughlin, *Chemical spectrophotometric and polarographic methods* 341
- 37B. S.R. Taylor, *Trace element analysis of rare earth elements by spark source mass spectroscopy* 359
- 37C. R.J. Conzemius, *Analysis of rare earth matrices by spark source mass spectrometry* 377
- 37D. E.L. DeKalb and V.A. Fassel, *Optical atomic emission and absorption methods* 405
- 37E. A.P. D'Silva and V.A. Fassel, *X-ray excited optical luminescence of the rare earths* 441
- 37F. F.W.V. Boynton, *Neutron activation analysis* 457
- 37G. S. Schuhmann and J.A. Philpotts, *Mass-spectrometric stable-isotope dilution analysis for lanthanides in geochemical materials* 471
38. J. Reuben and G.A. Elgavish, *Shift reagents and NMR of paramagnetic lanthanide complexes* 483
39. J. Reuben, *Bioinorganic chemistry: lanthanides as probes in systems of biological interest* 515
40. T.J. Haley, *Toxicity* 553
Subject index 587

VOLUME 5

1982, 1st repr. 1984; ISBN 0-444-86375-3

41. M. Gasgnier, *Rare earth alloys and compounds as thin films* 1
42. E. Gratz and M.J. Zuckermann, *Transport properties (electrical resistivity, thermoelectric power thermal conductivity) of rare earth intermetallic compounds* 117
43. F.P. Netzer and E. Bertel, *Adsorption and catalysis on rare earth surfaces* 217
44. C. Boulesteix, *Defects and phase transformation near room temperature in rare earth sesquioxides* 321
45. O. Greis and J.M. Haschke, *Rare earth fluorides* 387
46. C.A. Morrison and R.P. Leavitt, *Spectroscopic properties of triply ionized lanthanides in transparent host crystals* 461
Subject index 693

VOLUME 6

1984; ISBN 0-444-86592-6

47. K.H.J. Buschow, *Hydrogen absorption in intermetallic compounds* 1
48. E. Parthé and B. Chabot, *Crystal structures and crystal chemistry of ternary rare earth-transition metal borides, silicides and homologues* 113

49. P. Rogl, *Phase equilibria in ternary and higher order systems with rare earth elements and boron* 335
50. H.B. Kagan and J.L. Namy, *Preparation of divalent ytterbium and samarium derivatives and their use in organic chemistry* 525
Subject index 567

VOLUME 7

1984; ISBN 0-444-86851-8

51. P. Rogl, *Phase equilibria in ternary and higher order systems with rare earth elements and silicon* 1
52. K.H.J. Buschow, *Amorphous alloys* 265
53. H. Schumann and W. Genthe, *Organometallic compounds of the rare earths* 446
Subject index 573

VOLUME 8

1986; ISBN 0-444-86971-9

54. K.A. Gschneidner Jr and F.W. Calderwood, *Intra rare earth binary alloys: phase relationships, lattice parameters and systematics* 1
55. X. Gao, *Polarographic analysis of the rare earths* 163
56. M. Leskelä and L. Niinistö, *Inorganic complex compounds I* 203
57. J.R. Long, *Implications in organic synthesis* 335
Errata 375
Subject index 379

VOLUME 9

1987; ISBN 0-444-87045-8

58. R. Reisfeld and C.K. Jørgensen, *Excited state phenomena in vitreous materials* 1
59. L. Niinistö and M. Leskelä, *Inorganic complex compounds II* 91
60. J.-C.G. Bünzli, *Complexes with synthetic ionophores* 321
61. Zhiquan Shen and Jun Ouyang, *Rare earth coordination catalysis in stereospecific polymerization* 395
Errata 429
Subject index 431

VOLUME 10: High energy spectroscopy

1987; ISBN 0-444-87063-6

62. Y. Baer and W.-D. Schneider, *High-energy spectroscopy of lanthanide materials – An overview* 1
63. M. Campagna and F.U. Hillebrecht, *f-electron hybridization and dynamical screening of core holes in intermetallic compounds* 75
64. O. Gunnarsson and K. Schönhammer, *Many-body formulation of spectra of mixed valence systems* 103
65. A.J. Freeman, B.I. Min and M.R. Norman, *Local density supercell theory of photoemission and inverse photoemission spectra* 165
66. D.W. Lynch and J.H. Weaver, *Photoemission of Ce and its compounds* 231
67. S. Hüfner, *Photoemission in chalcogenides* 301

68. J.F. Herbst and J.W. Wilkins, *Calculation of 4f excitation energies in the metals and relevance to mixed valence systems* 321
69. B. Johansson and N. Mårtensson, *Thermodynamic aspects of 4f levels in metals and compounds* 361
70. F.U. Hillebrecht and M. Campagna, *Bremsstrahlung isochromat spectroscopy of alloys and mixed valent compounds* 425
71. J. Röhler, *X-ray absorption and emission spectra* 453
72. F.P. Netzer and J.A.D. Matthew, *Inelastic electron scattering measurements* 547
Subject index 601

VOLUME 11: Two-hundred-year impact of rare earths on science

1988; ISBN 0-444-87080-6

H.J. Svec, *Prologue* 1

73. F. Szabadváry, *The history of the discovery and separation of the rare earths* 33
74. B.R. Judd, *Atomic theory and optical spectroscopy* 81
75. C.K. Jørgensen, *Influence of rare earths on chemical understanding and classification* 197
76. J.J. Rhyne, *Highlights from the exotic phenomena of lanthanide magnetism* 293
77. B. Bleaney, *Magnetic resonance spectroscopy and hyperfine interactions* 323
78. K.A. Gschneidner Jr and A.H. Daane, *Physical metallurgy* 409
79. S.R. Taylor and S.M. McLennan, *The significance of the rare earths in geochemistry and cosmochemistry* 485
Errata 579
Subject index 581

VOLUME 12

1989; ISBN 0-444-87105-5

80. J.S. Abell, *Preparation and crystal growth of rare earth elements and intermetallic compounds* 1
81. Z. Fisk and J.P. Remeika, *Growth of single crystals from molten metal fluxes* 53
82. E. Burzo and H.R. Kirchmayr, *Physical properties of R₂Fe₁₄B-based alloys* 71
83. A. Szytuła and J. Leciejewicz, *Magnetic properties of ternary intermetallic compounds of the RT₂X₂ type* 133
84. H. Maletta and W. Zinn, *Spin glasses* 213
85. J. van Zytveld, *Liquid metals and alloys* 357
86. M.S. Chandrasekharaiah and K.A. Gingerich, *Thermodynamic properties of gaseous species* 409
87. W.M. Yen, *Laser spectroscopy* 433
Subject index 479

VOLUME 13

1990; ISBN 0-444-88547-1

88. E.I. Gladyshevsky, O.I. Bodak and V.K. Pecharsky, *Phase equilibria and crystal chemistry in ternary rare earth systems with metallic elements* 1
89. A.A. Eliseev and G.M. Kuzmichyeva, *Phase equilibrium and crystal chemistry in ternary rare earth systems with chalcogenide elements* 191
90. N. Kimizuka, E. Takayama-Muromachi and K. Siratori, *The systems R₂O₃–M₂O₃–M'O* 283

91. R.S. Houk, *Elemental analysis by atomic emission and mass spectrometry with inductively coupled plasmas* 385
92. P.H. Brown, A.H. Rathjen, R.D. Graham and D.E. Tribe, *Rare earth elements in biological systems* 423
Errata 453
Subject index 455

VOLUME 14

1991; ISBN 0-444-88743-1

93. R. Osborn, S.W. Lovesey, A.D. Taylor and E. Balcar, *Intermultiplet transitions using neutron spectroscopy* 1
94. E. Dormann, *NMR in intermetallic compounds* 63
95. E. Zirngiebl and G. Güntherodt, *Light scattering in intermetallic compounds* 163
96. P. Thalmeier and B. Lüthi, *The electron–phonon interaction in intermetallic compounds* 225
97. N. Grewe and F. Steglich, *Heavy fermions* 343
Subject index 475

VOLUME 15

1991; ISBN 0-444-88966-3

98. J.G. Sereni, *Low-temperature behaviour of cerium compounds* 1
99. G.-y. Adachi, N. Imanaka and Zhang Fuzhong, *Rare earth carbides* 61
100. A. Simon, Hj. Mattausch, G.J. Miller, W. Bauhofer and R.K. Kremer, *Metal-rich halides* 191
101. R.M. Almeida, *Fluoride glasses* 287
102. K.L. Nash and J.C. Sullivan, *Kinetics of complexation and redox reactions of the lanthanides in aqueous solutions* 347
103. E.N. Rizkalla and G.R. Choppin, *Hydration and hydrolysis of lanthanides* 393
104. L.M. Vallarino, *Macrocyclic complexes of the lanthanide(III), yttrium(III), and dioxouranium (VI) ions from metal-templated syntheses* 443
Errata 513
Subject index 515

CUMULATIVE INDEX, Vols. 1–15

1993; ISBN 0-444-89965-0

VOLUME 16

1993; ISBN 0-444-89782-8

105. M. Loewenhaupt and K.H. Fischer, *Valence-fluctuation and heavy-fermion 4f systems* 1
106. I.A. Smirnov and V.S. Oskotski, *Thermal conductivity of rare earth compounds* 107
107. M.A. Subramanian and A.W. Sleight, *Rare earth pyrochlores* 225
108. R. Miyawaki and I. Nakai, *Crystal structures of rare earth minerals* 249
109. D.R. Chopra, *Appearance potential spectroscopy of lanthanides and their intermetallics* 519
Author index 547
Subject index 579

VOLUME 17: Lanthanides/Actinides: Physics – I

1993; ISBN 0-444-81502-3

110. M.R. Norman and D.D. Koelling, *Electronic structure, Fermi surfaces, and superconductivity in f electron metals* 1
111. S.H. Liu, *Phenomenological approach to heavy-fermion systems* 87
112. B. Johansson and M.S.S. Brooks, *Theory of cohesion in rare earths and actinides* 149
113. U. Benedict and W.B. Holzapfel, *High-pressure studies – Structural aspects* 245
114. O. Vogt and K. Mattenberger, *Magnetic measurements on rare earth and actinide mononictides and monochalcogenides* 301
115. J.M. Fournier and E. Gratz, *Transport properties of rare earth and actinide intermetallics* 409
116. W. Potzel, G.M. Kalvius and J. Gal, *Mössbauer studies on electronic structure of intermetallic compounds* 539
117. G.H. Lander, *Neutron elastic scattering from actinides and anomalous lanthanides* 635
 Author index 711
 Subject index 753

VOLUME 18: Lanthanides/Actinides: Chemistry

1994; ISBN 0-444-81724-7

118. G.T. Seaborg, *Origin of the actinide concept* 1
119. K. Balasubramanian, *Relativistic effects and electronic structure of lanthanide and actinide molecules* 29
120. J.V. Beitz, *Similarities and differences in trivalent lanthanide- and actinide-ion solution absorption spectra and luminescence studies* 159
121. K.L. Nash, *Separation chemistry for lanthanides and trivalent actinides* 197
122. L.R. Morss, *Comparative thermochemical and oxidation – reduction properties of lanthanides and actinides* 239
123. J.W. Ward and J.M. Haschke, *Comparison of 4f and 5f element hydride properties* 293
124. H.A. Eick, *Lanthanide and actinide halides* 365
125. R.G. Haire and L. Eyring, *Comparisons of the binary oxides* 413
126. S.A. Kinkead, K.D. Abney and T.A. O'Donnell, *f-Element speciation in strongly acidic media: lanthanide and mid-actinide metals, oxides, fluorides and oxide fluorides in superacids* 507
127. E.N. Rizkalla and G.R. Choppin, *Lanthanides and actinides hydration and hydrolysis* 529
128. G.R. Choppin and E.N. Rizkalla, *Solution chemistry of actinides and lanthanides* 559
129. J.R. Duffield, D.M. Taylor and D.R. Williams, *The biochemistry of the f-elements* 591
 Author index 623
 Subject index 659

VOLUME 19: Lanthanides/Actinides: Physics – II

1994; ISBN 0-444-82015-9

130. E. Holland-Moritz and G.H. Lander, *Neutron inelastic scattering from actinides and anomalous lanthanides* 1
131. G. Aeppli and C. Broholm, *Magnetic correlations in heavy-fermion systems: neutron scattering from single crystals* 123
132. P. Wachter, *Intermediate valence and heavy fermions* 177

133. J.D. Thompson and J.M. Lawrence, *High pressure studies – Physical properties of anomalous Ce, Yb and U compounds* 383
134. C. Colinet and A. Pasturel, *Thermodynamic properties of metallic systems* 479
Author index 649
Subject index 693

VOLUME 20

1995; ISBN 0-444-82014-0

135. Y. Ōnuki and A. Hasegawa, *Fermi surfaces of intermetallic compounds* 1
136. M. Gasgnier, *The intricate world of rare earth thin films: metals, alloys, intermetallics, chemical compounds, ...* 105
137. P. Vajda, *Hydrogen in rare-earth metals, including RH_{2+x} phases* 207
138. D. Gignoux and D. Schmitt, *Magnetic properties of intermetallic compounds* 293
Author index 425
Subject index 457

VOLUME 21

1995; ISBN 0-444-82178-3

139. R.G. Bautista, *Separation chemistry* 1
140. B.W. Hinton, *Corrosion prevention and control* 29
141. N.E. Ryan, *High-temperature corrosion protection* 93
142. T. Sakai, M. Matsuoka and C. Iwakura, *Rare earth intermetallics for metal–hydrogen batteries* 133
143. G.-y. Adachi and N. Imanaka, *Chemical sensors* 179
144. D. Garcia and M. Faucher, *Crystal field in non-metallic (rare earth) compounds* 263
145. J.-C.G. Bünzli and A. Milicic-Tang, *Solvation and anion interaction in organic solvents* 305
146. V. Bhagavathy, T. Prasada Rao and A.D. Damodaran, *Trace determination of lanthanides in high-purity rare-earth oxides* 367
Author index 385
Subject index 411

VOLUME 22

1996; ISBN 0-444-82288-7

147. C.P. Flynn and M.B. Salamon, *Synthesis and properties of single-crystal nanostructures* 1
148. Z.S. Shan and D.J. Sellmyer, *Nanoscale rare earth–transition metal multilayers: magnetic structure and properties* 81
149. W. Suski, *The ThMn₁₂-type compounds of rare earths and actinides: structure, magnetic and related properties* 143
150. L.K. Aminov, B.Z. Malkin and M.A. Teplov, *Magnetic properties of nonmetallic lanthanide compounds* 295
151. F. Auzel, *Coherent emission in rare-earth materials* 507
152. M. Dolg and H. Stoll, *Electronic structure calculations for molecules containing lanthanide atoms* 607
Author index 731
Subject index 777

VOLUME 23

1996; ISBN 0-444-82507-X

153. J.H. Forsberg, *NMR studies of paramagnetic lanthanide complexes and shift reagents* 1
154. N. Sabbatini, M. Guardigli and I. Manet, *Antenna effect in encapsulation complexes of lanthanide ions* 69
155. C. Görller-Walrand and K. Binnemans, *Rationalization of crystal-field parameterization* 121
156. Yu. Kuz'ma and S. Chykhrij, *Phosphides* 285
157. S. Boghosian and G.N. Papatheodorou, *Halide vapors and vapor complexes* 435
158. R.H. Byrne and E.R. Sholkovitz, *Marine chemistry and geochemistry of the lanthanides* 497
Author index 595
Subject index 631

VOLUME 24

1997; ISBN 0-444-82607-6

159. P.A. Dowben, D.N. McIlroy and Dongqi Li, *Surface magnetism of the lanthanides* 1
160. P.G. McCormick, *Mechanical alloying and mechanically induced chemical reactions* 47
161. A. Inoue, *Amorphous, quasicrystalline and nanocrystalline alloys in Al- and Mg-based systems* 83
162. B. Elschner and A. Loidl, *Electron-spin resonance on localized magnetic moments in metals* 221
163. N.H. Duc, *Intersublattice exchange coupling in the lanthanide-transition metal intermetallics* 339
164. R.V. Skolozdra, *Stannides of rare-earth and transition metals* 399
Author index 519
Subject index 559

VOLUME 25

1998; ISBN 0-444-82871-0

165. H. Nagai, *Rare earths in steels* 1
166. R. Marchand, *Ternary and higher order nitride materials* 51
167. C. Görller-Walrand and K. Binnemans, *Spectral intensities of f-f transitions* 101
168. G. Bombieri and G. Paolucci, *Organometallic π complexes of the f-elements* 265
Author index 415
Subject index 459

VOLUME 26

1999; ISBN 0-444-50815-1

169. D.F. McMorro, D. Gibbs and J. Bohr, *X-ray scattering studies of lanthanide magnetism* 1
170. A.M. Tishin, Yu.I. Spichkin and J. Bohr, *Static and dynamic stresses* 87
171. N.H. Duc and T. Goto, *Itinerant electron metamagnetism of Co sublattice in the lanthanide-cobalt intermetallics* 177

172. A.J. Arko, P.S. Riseborough, A.B. Andrews, J.J. Joyce, A.N. Tahvildar-Zadeh and M. Jarrell, *Photo-electron spectroscopy in heavy fermion systems: Emphasis on single crystals* 265
Author index 383
Subject index 405

VOLUME 27

1999; ISBN 0-444-50342-0

173. P.S. Salamakha, O.L. Sologub and O.I. Bodak, *Ternary rare-earth-germanium systems* 1
174. P.S. Salamakha, *Crystal structures and crystal chemistry of ternary rare-earth germanides* 225
175. B. Ya. Kotur and E. Gratz, *Scandium alloy systems and intermetallics* 339
Author index 535
Subject index 553

VOLUME 28

2000; ISBN 0-444-50346-3

176. J.-P. Connerade and R.C. Karnatak, *Electronic excitation in atomic species* 1
177. G. Meyer and M.S. Wickleder, *Simple and complex halides* 53
178. R.V. Kumar and H. Iwahara, *Solid electrolytes* 131
179. A. Halperin, *Activated thermoluminescence (TL) dosimeters and related radiation detectors* 187
180. K.L. Nash and M.P. Jensen, *Analytical separations of the lanthanides: basic chemistry and methods* 311
Author index 373
Subject index 401

VOLUME 29: The role of rare earths in catalysis

2000; ISBN 0-444-50472-9

P. Maestro, *Foreword* 1

181. V. Paul-Boncour, L. Hilaire and A. Percheron-Guégan, *The metals and alloys in catalysis* 5
182. H. Imamura, *The metals and alloys (prepared utilizing liquid ammonia solutions) in catalysis II* 45
183. M.A. Ulla and E.A. Lombardo, *The mixed oxides* 75
184. J. Kašpar, M. Graziani and P. Fornasiero, *Ceria-containing three-way catalysts* 159
185. A. Corma and J.M. López Nieto, *The use of rare-earth-containing zeolite catalysts* 269
186. S. Kobayashi, *Triflates* 315
Author index 377
Subject index 409

VOLUME 30: High-Temperature Superconductors – I

2000; ISBN 0-444-50528-8

187. M.B. Maple, *High-temperature superconductivity in layered cuprates: overview* 1
188. B. Raveau, C. Michel and M. Hervieu, *Crystal chemistry of superconducting rare-earth cuprates* 31

189. Y. Shiohara and E.A. Goodilin, *Single-crystal growth for science and technology* 67
 190. P. Karen and A. Kjekshus, *Phase diagrams and thermodynamic properties* 229
 191. B. Elschner and A. Loidl, *Electron paramagnetic resonance in cuprate superconductors and in parent compounds* 375
 192. A.A. Manuel, *Positron annihilation in high-temperature superconductors* 417
 193. W.E. Pickett and I.I. Mazin, *RBa₂Cu₃O₇ compounds: electronic theory and physical properties* 453
 194. U. Staub and L. Soderholm, *Electronic 4f-state splittings in cuprates* 491
 Author index 547
 Subject index 621

VOLUME 31: High-Temperature Superconductors – II

2001; ISBN 0-444-50719-1

195. E. Kaldis, *Oxygen nonstoichiometry and lattice effects in YBa₂Cu₃O_x. Phase transitions, structural distortions and phase separation* 1
 196. H.W. Weber, *Flux pinning* 187
 197. C.C. Almasan and M.B. Maple, *Magnetoresistance and Hall effect* 251
 198. T.E. Mason, *Neutron scattering studies of spin fluctuations in high-temperature superconductors* 281
 199. J.W. Lynn and S. Skanthakumar, *Neutron scattering studies of lanthanide magnetic ordering* 315
 200. P.M. Allenspach and M.B. Maple, *Heat capacity* 351
 201. M. Schabel and Z.-X. Shen, *Angle-resolved photoemission studies of untwinned yttrium barium copper oxide* 391
 202. D.N. Basov and T. Timusk, *Infrared properties of high-T_c superconductors: an experimental overview* 437
 203. S.L. Cooper, *Electronic and magnetic Raman scattering studies of the high-T_c cuprates* 509
 204. H. Sugawara, T. Hasegawa and K. Kitazawa, *Characterization of cuprate superconductors using tunneling spectra and scanning tunneling microscopy* 563
 Author index 609
 Subject index 677

VOLUME 32

2001; ISBN 0-444-50762-0

205. N.H. Duc, *Giant magnetostriction in lanthanide-transition metal thin films* 1
 206. G.M. Kalvius, D.R. Noakes and O. Hartmann, *μSR studies of rare-earth and actinide magnetic materials* 55
 207. Rainer Pöttgen, Dirk Johrendt and Dirk Kußmann, *Structure–property relations of ternary equiatomic YbTX intermetallics* 453
 208. Kurima Kobayashi and Satoshi Hirosawa, *Permanent magnets* 515
 209. I.G. Vasilyeva, *Polysulfides* 567
 210. Dennis K.P. Ng, Jianzhuang Jiang, Kuninobu Kasuga and Kenichi Machida, *Half-sandwich tetrapyrrole complexes of rare earths and actinides* 611
 Author index 655
 Subject index 733

VOLUME 33

2003; ISBN 0-444-51323-X

211. Brian C. Sales, *Filled skutterudites* 1
 212. Oksana L. Sologub and Petro S. Salamakha, *Rare earth – antimony systems* 35
 213. R.J.M. Konings and A. Kovács, *Thermodynamic properties of the lanthanide (III) halides* 147
 214. John B. Goodenough, *Rare earth – manganese perovskites* 249
 215. Claude Piguet and Carlos F.G.C. Geraldès, *Paramagnetic NMR lanthanide induced shifts for extracting solution structures* 353
 216. Isabelle Billard, *Lanthanide and actinide solution chemistry as studied by time-resolved emission spectroscopy* 465
 217. Thomas Tröster, *Optical studies of non-metallic compounds under pressure* 515
 Author index 591
 Subject index 637

VOLUME 34

2004; ISBN 0-444-51587-9

218. Yaroslav M. Kalychak, Vasyly I. Zarembo, Rainer Pöttgen, Mar'lyana Lukachuk and Rolf-Dieter Hoffman, *Rare earth–transition metal–indides* 1
 219. P. Thalmeier and G. Zwirner, *Unconventional superconductivity and magnetism in lanthanide and actinide intermetallic compounds* 135
 220. James P. Riehl and Gilles Muller, *Circularly polarized luminescence spectroscopy from lanthanide systems* 289
 221. Oliver Guillou and Carole Daiguebonne, *Lanthanide-containing coordination polymers* 359
 222. Makoto Komiyama, *Cutting DNA and RNA* 405
 Author index 455
 Subject index 493

VOLUME 35

2005; ISBN 0-444-52028-7

223. Natsuko Sakai, Katsuhiko Yamaji, Teruhisa Horita, Yue Ping Xiong and Harumi Yokokawa, *Rare-earth materials for solid oxide fuel cells (SOFC)* 1
 224. Mathias S. Wickleder, *Oxo-selenates of rare-earth elements* 45
 225. Koen Binnemans, *Rare-earth beta-diketonates* 107
 226. Satoshi Shinoda, Hiroyuki Miyake and Hiroshi Tsukube, *Molecular recognition and sensing via rare-earth complexes* 273
 Author index 337
 Subject index 377

VOLUME 36

2006; ISBN 0-444-52142-9

227. Arthur Mar, *Bismuthides* 1
 228. I. Aruna, L.K. Malhotra and B.R. Mehta, *Switchable metal hydride films* 83
 229. Koen Binnemans, *Applications of tetravalent cerium compounds* 281
 230. Robert A. Flowers II and Edamana Prasad, *Samarium (II) based reductants* 393
 Author index 475
 Subject index 511

VOLUME 37: Optical Spectroscopy

2007; ISBN 978-0-444-52144-6

231. Kazuyoshi Ogasawara, Shinta Watanabe, Hiroaki Toyoshima and Mikhail G. Bryk, *First-principles calculations of $4f^n \rightarrow 4f^{n-1} 5d$ transition spectra* 1
232. Gary W. Burdick and Michael F. Reid, *$4f^n - 4f^{n-1} 5d$ transitions* 61
233. Guokui Liu and Xueyuan Chen, *Spectroscopic properties of lanthanides in nanomaterials* 99
234. Takuya Nishioka, Kôichi Fukui and Kazuko Matsumoto, *Lanthanide chelates as luminescent labels in biomedical analyses* 171
235. Steve Comby and Jean-Claude G. Bünzli, *Lanthanide near-infrared luminescence in molecular probes and devices* 217
 Author index 471
 Subject index 503

VOLUME 38

2008; ISBN 978-0-444-52143-9

236. Z.C. Kang, *Lanthanide Higher Oxides: The Contributions of Leroy Eyring* 1
237. Rainer Pöttgen and Ute Ch. Rodewald, *Rare Earth–Transition Metal–Plumbides* 55
238. Takao Mori, *Higher Borides* 105
239. K.-H. Müller, M. Schneider, G. Fuchs and S.-L. Drechsler, *Rare-Earth Nickel Borocarbides* 175
240. Michael T. Pope, *Polyoxometalates* 337
 Author index 383
 Subject index 431

VOLUME 39

2009; ISBN 978-0-444-53221-3

241. W.M. Temmerman, L. Petit, A. Svane, Z. Szotek, M. Lüders, P. Strange, J.B. Staunton, I.D. Hughes, and B.L. Gyorffy, *The Dual, Localized or Band-Like, Character of the $4f$ -States* 1
242. L. Vasylechko, A. Senyshyn, and U. Bismayer, *Perovskite-Type Aluminates and Gallates* 113
243. Toshihiro Yamase, *Luminescence of Polyoxometallolanthanoates and Photochemical Nano-Ring Formation* 297
 Author index 357
 Subject index 381

VOLUME 40

2010; ISBN 978-0-444-53220-6

244. Christiane Görller-Walrand and Linda Fluyt, *Magnetic Circular Dichroism of Lanthanides* 1
245. Z. Zheng, *Cluster Compounds of Rare-Earth Elements* 109
246. François Nief, *Molecular Chemistry of the Rare-Earth Elements in Uncommon Low-Valent States* 241
247. Claude Piguet and Jean-Claude G. Bünzli, *Self-Assembled Lanthanide Helicates: From Basic Thermodynamics to Applications* 301
 Author index 555
 Subject index 583

INDEX OF CONTENTS OF VOLUMES 1–41

- 4f excitation energies, calculations
of **10**, ch. 68, p. 321
- 4f levels, thermodynamic aspects
10, ch. 69, p. 361
- 4f state splittings in cuprates **30**,
ch. 194, p. 491
- 4f states, character of **39**, ch. 241, p. 1
- 4fⁿ-4fⁿ⁻¹5d transitions **37**, ch. 231,
p. 1; **37**, ch. 232, p. 61
- ab-initio calculation of energy
levels **37**, ch. 231, p. 1
- absorption spectra of ions in
solution **3**, ch. 24, p. 171; **18**,
ch. 120, p. 159
- actinide concept, origin of **18**,
ch. 118, p. 1
- activated phosphors **4**, ch. 34, p. 237
- activated thermoluminescence **28**,
ch. 179, p. 187
- aluminates **39**, ch. 242, p. 113
- amorphous alloys **7**, ch. 52, p. 265
- Al- and Mg-based **24**, ch. 161, p. 83
- magnetic **2**, ch. 16, p. 259
- anion interaction in organic solvents **21**,
ch. 145, p. 305
- antimony alloy systems **33**,
ch. 212, p. 35
- atomic properties (free atom) **1**, ch. 1, p. 1
- atomic theory **11**, ch. 74, p. 81
- beta-diketonates **35**, ch. 225, p. 107
- Belousov-Zhabotinsky reactions **36**,
ch. 229, p. 281
- biochemistry **18**, ch. 129, p. 591
- bioinorganic chemistry **4**, ch. 39, p. 515
- biological systems **13**, ch. 92, p. 423
- bioprobes **40**, ch. 247, p. 301
- bismuth alloy systems **36**, ch. 227, p. 1
- borides **6**, ch. 48, p. 113; **6**, ch. 49,
p. 335; **38**, ch. 238, p. 105; **38**,
ch. 239, p. 175
- carbides **15**, ch. 99, p. 61;
38 ch. 239, p. 175
- carbon polyhedral **41**, ch. 249, p. 95
- Carnall, William T. **37**, dedication, p. xiii
- catalysis **29**, foreword, p. 1
- ceria-containing three-way **29**,
ch. 184, p. 159
- metals and alloys **29**, ch. 181, p. 5
- metals and alloys in liquid ammonia
solutions **29**, ch. 182, p. 45
- mixed oxides **29**, ch. 183, p. 75
- zeolites **29**, ch. 185, p. 269
- cerimetry **36**, ch. 229, p. 281
- cerium **1**, ch. 4, p. 337
- cerium compounds
- low-temperature behavior **15**, ch. 98, p. 1
- tetravalent **36**, ch. 229, p. 281
- cerium(IV)
- catalysts **36**, ch. 229, p. 281
- mediated reactions **36**, ch. 229, p. 281
- redox properties **36**, ch. 229, p. 281
- chalcogenides,
- magnetic measurements on mono- **17**,
ch. 114, p. 301
- quaternary **41**, ch. 250, p. 157
- ternary **41**, ch. 250, p. 157
- chemical analysis by
- atomic emission with inductively coupled
plasmas **13**, ch. 91, p. 385
- mass spectrometry, *see* spectroscopy,
mass
- neutron activation **4**, ch. 37F, p. 457
- optical absorption **4**, ch. 37D, p. 405
- optical atomic emission **4**, ch. 37D, p. 405
- polarography **4**, ch. 37A, p. 341; **8**,
ch. 55, p. 163
- spectrophotometry **4**, ch. 37A, p. 341
- trace determination in high-purity
oxides **21**, ch. 146, p. 367
- x-ray excited optical luminescence **4**,
ch. 37E, p. 441
- chemical sensors **21**, ch. 143, p. 179

- chemical understanding and
 classification 11, ch. 75, p. 197
- chirality sensing 35, ch. 226, p. 273
- cluster compounds 40, ch. 245, p. 109
- coherent emission 22, ch. 151, p. 507
- cohesion, theory of 17, ch. 112, p. 149
- complexes 3, ch. 25, p. 209
- antenna effect 23, ch. 154, p. 69
 - beta-diketonates 35, ch. 225, p. 107
 - half-sandwich tetrapyrrole 32, ch. 210, p. 611
 - inorganic 8, ch. 56, p. 203; 9, ch. 59, p. 91
 - low-valent state 40, ch. 246, p. 241
 - macrocycles 15, ch. 104, p. 443
 - molecular recognition in 35, ch. 226, p. 273
 - organometallic π type 25, ch. 168, p. 265
 - polyoxometalates 38, ch. 240, p. 337
 - sensing in 35, ch. 226, p. 273
 - with synthetic ionophores 9, ch. 60, p. 321
- coordination catalysis in stereospecific polymerization 9, ch. 61, p. 395
- coordination in organic solvents 21, ch. 145, p. 305
- coordination polymers 34, ch. 221, p. 359
- corrosion prevention and control 21, ch. 140, p. 29
- corrosion protection 21, ch. 141, p. 93
- cosmochemistry 11, ch. 79, p. 485
- crystal chemistry
- of aluminates 39, ch. 242, p. 113
 - of gallates 39, ch. 242, p. 113
 - of higher borides 38, ch. 238, p. 105
 - of intermetallic compounds 2, ch. 13, p. 1
 - of quaternary systems with chalcogenides 41, ch. 250, p. 157
 - of ternary germanides 27, ch. 174, p. 225
 - of ternary systems with chalcogenides 13, ch. 89, p. 191; 41, ch. 250, p. 157
 - of ternary systems with metallic elements 13, ch. 88, p. 1
 - of ternary transition metal borides 6, ch. 48, p. 113
 - of ternary transition metal plumbides 38, ch. 237, p. 55
 - of ternary transition metal silicides 6, ch. 48, p. 113
 - of ThMn_{12} -type compounds 22, ch. 149, p. 143
- crystal field 2, ch. 17, p. 295
- in non-metallic compounds 21, ch. 144, p. 263
- parametrization, rationalization of 23, ch. 155, p. 121
- crystal structures, *see* crystal chemistry
- cuprates
- 4f state splittings 30, ch. 194, p. 491
 - crystal chemistry 30, ch. 188, p. 31
 - electron paramagnetic resonance (EPR) 30, ch. 191, p. 375
 - electronic theory 30, ch. 193, p. 453
 - flux pinning 31, ch. 196, p. 187
 - Hall effect 31, ch. 197, p. 251
 - heat capacity 31, ch. 200, p. 351
 - infrared properties 31, ch. 202, p. 437
 - magnetoresistance 31, ch. 197, p. 251
 - neutron scattering
 - – magnetic ordering 31, ch. 199, p. 315
 - – spin fluctuations 31, ch. 198, p. 281
 - overview 30, ch. 187, p. 1
 - oxygen nonstoichiometry and lattice effect 31, ch. 195, p. 1
 - phase equilibria 30, ch. 190, p. 229
 - phase transitions, structural distortions and phase separation 31, ch. 195, p. 1
 - photoemission, angle-resolved studies 31, ch. 201, p. 391
 - physical properties 30, ch. 193, p. 453
 - positron annihilation 30, ch. 192, p. 417
 - Raman scattering 31, ch. 203, p. 509
 - scanning tunneling microscopy 31, ch. 204, p. 563
 - single crystals, growth of 30, ch. 189, p. 67
 - superconductivity 30; 31
 - thermochemical properties 30, ch. 190, p. 229
 - tunneling spectra 31, ch. 204, p. 563
- dedications
- F. H. Spedding 11, p. 1
 - Friedrich Hund 14, p. ix
 - LeRoy Eyring 36, p. xi
 - William T. Carnall 37, p. xiii
- diketonates, *see* beta-diketonates
- diffusion in metals 1, ch. 12, p. 847
- divalent samarium in organic chemistry 6, ch. 50, p. 525; 36, ch. 230, p. 393

- divalent ytterbium derivatives in organic chemistry 6, ch. 50, p. 525
- DNA, cutting of 34, ch. 222, p. 405
- dynamical screening of core holes in intermetallic compounds 10, ch. 63, p. 75
- elastic and mechanical properties of metals 1, ch. 8, p. 591
- electron paramagnetic resonance (EPR) 2, ch. 18, p. 387; 24, ch. 162, p. 221
- in cuprate superconductors 30, ch. 191, p. 375
- electronic excitation in atomic species 28, ch. 176, p. 1
- electronic structure
- calculations for molecules 22, ch. 152, p. 607
 - of chalcogenides 39, ch. 241, p. 1
 - of metals 1, ch. 3, p. 233; 17, ch. 110, p. 1; 39, ch. 241, p. 1
 - of oxides 39, ch. 241, p. 1
 - of pnictides 39, ch. 241, p. 1
- electronic theory of cuprates 30, ch. 193, p. 453
- electron-phonon interaction in intermetallic compounds 14, ch. 96, p. 225
- electron-spin resonance, *see* electron paramagnetic resonance
- emission spectra 10, ch. 71, p. 453
- europium chalcogenides 2, ch. 19, p. 507
- exchange coupling in transition metal intermetallics 24, ch. 163, p. 339
- excited state phenomena in vitreous materials 9, ch. 58, p. 1
- Eyring, L.
- dedication 36, p. xi
 - contributions of, higher oxides 38, ch. 236, p. 1
- f-electron hybridization 39, ch. 241, p. 1
- in intermetallic compounds 10, ch. 63, p. 75
- f-element speciation in strongly acidic media (superacids) 18, ch. 126, p. 507
- f-f transitions, spectral intensities 25, ch. 167, p. 101
- f-states: dual, localized, band-like character 39, ch. 241, p. 1
- Fermi surfaces
- of intermetallic compounds 20, ch. 135, p. 1
 - of metals 17, ch. 110, p. 1
- fluorescence spectra of ions in solution 3, ch. 24, p. 171
- fluoride glasses 15, ch. 101, p. 287
- fluorides 5, ch. 45, p. 387
- flux pinning in cuprates 31, ch. 196, p. 187
- fullerenes 41, ch. 249, p. 95
- gallates 39, ch. 242, p. 113
- garnets 3, ch. 29, p. 525
- geochemistry 3, ch. 21, p. 1; 11, ch. 79, p. 485; 23, ch. 158, p. 497
- germanium, ternary systems 27, ch. 173, p. 1
- halides 4, ch. 32, p. 89; 18, ch. 124, p. 365
- metal-rich 15, ch. 100, p. 191
 - simple and complex 28, ch. 177, p. 53
 - thermodynamic properties 18, ch. 122, p. 239 33, ch. 213, p. 147
 - vapors and vapor complexes 23, ch. 157, p. 435
- Hall effect in cuprates 31, ch. 197, p. 251
- heat capacity
- of cuprates 31, ch. 200, p. 351
 - of metals 1, ch. 5, p. 379
- heavy fermions 14, ch. 97, p. 343; 16, ch. 105, p. 1; 19, ch. 132, p. 177
- phenomenological approach 17, ch. 111, p. 87
 - photoelectron spectroscopy 26, ch. 172, p. 265
- helicates 40, ch. 247, p. 301
- high pressure studies 1, ch. 9, p. 707
- anomalous Ce, Yb and U compounds 19, ch. 133, p. 383
 - optical studies of non-metallic compounds 33, ch. 217, p. 515
 - structural aspects 17, ch. 113, p. 245
- high temperature superconductors 30; 31
- history
- of the discovery and separation of rare earths 11, ch. 73, p. 33
 - of the positioning of rare earths in the periodic table 41, ch. 248, p. 1
- Hund, F. 14, dedication, p. ix
- hydration 15, ch. 103, p. 393; 18, ch. 127, p. 529
- hydrides 3, ch. 26, p. 299; 18, ch. 123, p. 293
- switchable films 36, ch. 228, p. 83

- hydrogen absorption in intermetallic compounds 6, ch. 47, p. 1
- hydrogen in metals, including RH_{2+x} phases 20, ch. 137, p. 207
- hydrolysis 15, ch. 103, p. 393; 18, ch. 127, p. 529; 40, ch. 245, p. 109
- hyperfine interactions 11, ch. 77, p. 323
- inelastic electron scattering 10, ch. 72, p. 547
- infrared properties of cuprates 31, ch. 202, p. 437
- inorganic complex compounds 8, ch. 56 p. 203; 9, ch. 59, p. 91
- intermediate valence 19, ch. 132, p. 177
- itinerant electron metamagnetism in cobalt intermetallics 26, ch. 171, p. 177
- kinetics of complexation in aqueous solutions 15, ch. 102, p. 347
- Kondo effect 1, ch. 11, p. 797
- lanthanide-induced shifts 4, ch. 38, p. 483; 23, ch. 153, p. 1; 33, ch. 215, p. 353
- lanthanide chelates
- for sensitizing NIR luminescence 37, ch. 234, p. 171
 - in biomedical analyses 37, ch. 235, p. 217
- laser spectroscopy 12, ch. 87, p. 433
- lasers 4, ch. 35, p. 275
- light scattering in intermetallic compounds 14, ch. 95, p. 163
- liquid metals and alloys 12, ch. 85, p. 357
- LIS, *see* lanthanide-induced shifts
- luminescence
- in biomedical analyses 37, ch. 234, p. 171; 40, ch. 247, p. 301
 - in NIR molecular probes and devices 37, ch. 235, p. 217
 - polyoxometalates 39, ch. 243, p. 297
 - studies of ions 18, ch. 120, p. 159
 - spectra of ions in solution 3, ch. 24, p. 171
- μSR studies of magnetic materials 32, ch. 206, p. 55
- magnetic circular dichroism 40, ch. 244, p. 1
- magnetic and transport properties of metals 1 ch. 6, p. 411
- magnetic correlations in heavy-fermion systems 19, ch. 131, p. 123
- magnetic properties (also see physical properties)
- of borides 38, ch. 238, p. 105
 - of intermetallic compounds 2, ch. 14, p. 55; 20, ch. 138, p. 293
 - of nickel borocarbides 38, ch. 239, p. 175
 - of nonmetallic compounds 22, ch. 150, p. 295
 - of ternary RT_2X_2 type intermetallic compounds 12, ch. 83, p. 133
 - of ThMn_{12} -type compounds 22, ch. 149, p. 143
- magnetic structures 1, ch. 7, p. 489
- magnetism 34, ch. 219, p. 135
- exotic phenomena 11, ch. 76, p. 293
 - surface 24, ch. 159, p. 1
- magnetoresistance in cuprates 31, ch. 197, p. 251
- magnetostriction
- RFe_2 2, ch. 15, p. 231
 - transition metal thin films 32, ch. 205, p. 1
- marine chemistry 23, ch. 158, p. 497
- mechanical alloying 24, ch. 160, p. 47
- mechanically induced chemical reactions 24, ch. 160, p. 47
- metal-hydrogen batteries 21, ch. 142, p. 133
- metallofullerenes, endohedral 41, ch. 249, p. 95
- mineralogy 3, ch. 21, p. 1
- minerals, crystal structures 16, ch. 108, p. 249
- mixed valence systems
- bremsstrahlung isochromat spectroscopy 10, ch. 70, p. 425
 - calculation of $4f$ excitation energies 10, ch. 68, p. 321
 - many-body formulation of spectra 10, ch. 64, p. 103
- molecular recognition 35, ch. 226, p. 273
- molybdates (VI) 3, ch. 30, p. 609
- Mössbauer effect 2, ch. 18, p. 387
- of intermetallic compounds 17, ch. 116, p. 539
- nanostructures and nanomaterials
- Al- and Mg-based systems 24, ch. 161, p. 83
 - ceria 41, ch. 249, p. 95
 - halides 41, ch. 249, p. 95
 - hydroxides 41, ch. 249, p. 95
 - metallofullerenes 41, ch. 249, p. 95
 - oxides 41, ch. 249, p. 95
 - oxysalts 41, ch. 249, p. 95
 - properties 22, ch. 147, p. 1; 41, ch. 251, p. 275

- photochemical ring formation **39**,
ch. 243, 297
- synthesis **22**, ch. 147, p. 1; **41**, ch. 251, p. 275
- spectroscopic properties **37**,
ch. 233, p. 99
- sulfates **41**, ch. 249, p. 95
- transition metal multilayers **22**,
ch. 148, p. 81
- neutron scattering
 - elastic **17**, ch. 117, p. 635
 - inelastic **1**, ch. 7, p. 489
 - intermultiple transitions **14**, ch. 93, p. 1
 - inelastic of anomalous lanthanides **19**,
ch. 130, p. 1
 - in heavy-fermion systems **19**,
ch. 131, p. 123
 - of magnetic ordering in cuprates **31**,
ch. 199, p. 315
 - of spin fluctuations in cuprates **31**,
ch. 198, p. 281
- near-infrared luminescence in molecular
probes and devices **37**, ch. 235, p. 217
- nitride materials, ternary and higher
order **24**, ch. 166, p. 51
- NMR **2**, ch. 18, p. 387
 - in intermetallic compounds **14**,
ch. 94, p. 63
 - lanthanide induced shifts for extracting
solution structures **33**, ch. 215, p. 353
 - of complexes **23**, ch. 153, p. 1
 - of paramagnetic complexes **4**,
ch. 38, p. 483
 - solution structure by paramagnetic NMR
analysis **33**, ch. 215, p. 353
- nonradiative processes in crystals **4**,
ch. 36, p. 317
- nuclear magnetic resonance, *see* NMR

- organic synthesis **8**, ch. 57, p. 335
- organometallic compounds **7**,
ch. 53, p. 446
 - low valent **40**, ch. 246, p. 241
- oxidation – reduction properties **18**, ch.
122, p. 239
- oxides
 - aluminates **39**, ch. 242, p. 113
 - binary **3**, ch. 27, p. 337; **18**, ch. 125,
p. 413
 - gallates **39**, ch. 242, p. 113
 - higher **38**, ch. 236, p. 1
 - mixed **3**, ch. 28, p. 401
 - sesqui, defects in **5**, ch. 44, p. 321
 - sesqui, phase transformation in **5**,
ch. 44, p. 321
 - ternary systems, R_2O_3 - M_2O_3 - $M'O$ **13**,
ch. 90, p. 283
 - oxo-selenates **35**, ch. 224, p. 45
 - oxygen nonstoichiometry and lattice effect
in $YBa_2Cu_3O_x$ **31**, ch. 195, p. 1
- permanent magnets **12**, ch. 82, p. 71; **32**,
ch. 208, p. 515
- periodic table, position of rare earths in **41**,
ch. 248, p. 1
- perovskites **3**, ch. 29, p. 525
 - aluminates **39**, ch. 242, p. 113
 - gallates **39**, ch. 242, p. 113
 - manganese **33**, ch. 214, p. 249
- phase equilibria
 - in cuprates **30**, ch. 190, p. 229
 - in ternary systems with boron **6**,
ch. 49, p. 335; **38**, ch. 238, p. 105
 - in ternary systems with chalcogenides **13**
ch. 89, p. 191
 - in ternary systems with metallic
elements **13** ch. 88, p. 1
 - in ternary systems with lead **38**,
ch. 237, p. 55
 - in ternary systems with silicon **7**,
ch. 51, p. 1
- intra rare earth binary alloys **8**,
ch. 54, p. 1
- phase transitions, structural
distortions and phase separation in
 $YBa_2Cu_3O_x$ **31**, ch. 195, p. 1
- phosphides **23**, ch. 156, p. 285
- photochemical, nano-ring
formations in polyoxometalates **39**,
ch. 243, p. 297
- photoemission
 - angle-resolved studies of untwinned
 $YBa_2Cu_3O_x$ **31**, ch. 201, p. 391
 - in chalcogenides **10**, ch. 67, p. 301
 - inverse spectra, local density supercell
theory **10**, ch. 65, p. 165
 - of Ce and its compounds **10**,
ch. 66, p. 231
 - spectra, local density supercell theory **10**,
ch. 65, p. 165
 - theory of **39**, ch. 241, p. 1
- physical metallurgy **11**, ch. 78, p. 409
- physical properties (also *see* magnetic
properties)
 - of cuprates **30**, ch. 193, p. 453

- of metals 1, ch. 2, p. 173
- of $R_2Fe_{14}B$ -based alloys 12, ch. 82, p. 71
- pnictides 4, ch. 33, p. 153
- magnetic measurements on mono- 17, ch. 114, p. 301
- polyoxometalates 38, ch. 240, p. 337
- luminescence of 39, ch. 243, p. 297
- positron annihilation in high-temperature superconductors 30, ch. 192, p. 417
- preparation and purification of metals 1, ch. 2, p. 173
- pyrochlores 16, ch. 107, p. 225

- quasicrystalline, Al- and Mg-based systems 24, ch. 161, p. 83

- Raman scattering of cuprates 31, ch. 203, p. 509
- redox reactions
 - in aqueous solutions 15, ch. 102, p. 347
 - Ce(IV)/Ce(III) 36, ch. 229, p. 347
- relativistic effects and electronic structure 18, ch. 119, p. 29
- RNA, cutting of 34, ch. 222, p. 405; 36, ch. 229, p. 392
- samarium (II) reductants 36, ch. 230, p. 393
- scandium alloy systems and intermetallics 27, ch. 175, p. 339
- scanning tunneling microscopy of cuprates 31, ch. 204, p. 563
- selenates 35, ch. 224, p. 45
- selenides 4, ch. 31, p. 1
- selenites 35, ch. 224, p. 45
- self-assembly of helicates 40, ch. 247, p. 301
- separation chemistry 3, ch. 22, p. 81; 18, ch. 121, p. 197; 21, ch. 139, p. 1
- analytical, basic chemistry and methods 28, ch. 180, p. 311
- shift reagents 4, ch. 38, p. 483; 23, ch. 153, p. 1; 33, ch. 215, p. 353; 35, ch. 225, p. 107
- single crystals
 - growth from molten metal fluxes 12, ch. 81, p. 53
 - growth of cuprates 30, ch. 189, p. 67
 - growth of metals and intermetallic compounds 12, ch. 80, p. 1
- skutterudites, filled 33, ch. 211, p. 1
- solid electrolytes 28, ch. 178, p. 131; 35, ch. 223, p. 1
- solid oxide fuel cells (SOFC) 35, ch. 223, p. 1
- solution chemistry 15, ch. 103, p. 393; 18, ch. 127, p. 529; 18, ch. 128, p. 559; 21, ch. 145, 305;
- solvation in organic solvents 21, ch. 145, p. 305
- spectroscopic properties in transparent crystals 5, ch. 46, p. 461
- nanomaterials 37, ch. 233, p. 99
- spectroscopy
 - appearance potential 16, ch. 109, p. 519
 - bremsstrahlung isochromat 10, ch. 70, p. 425
 - circularly polarized luminescence 34, ch. 220, p. 289
 - high-energy 10, ch. 62, p. 1
 - magnetic circular dichroism 40, ch. 244, p. 1
 - magnetic resonance 11, ch. 77, p. 323
 - mass
 - – spark source matrices 4, ch. 37C, p. 377
 - – spark source trace element analysis 4, ch. 37B, p. 359
 - – stable-isotope dilution analysis 4, ch. 37G, p. 471
 - – with inductively coupled plasmas analysis 13, ch. 91, p. 385
 - optical 11, ch. 74, p. 81; 37, ch. 233, p. 99; ch. 234, p. 171; 37, ch. 235, p. 217
 - photoelectron in heavy fermion systems 26, ch. 172, p. 265
 - time-resolved emission in solution chemistry 33, ch. 216, p. 465
- Spedding, F. H., 11, prologue, p. 1
- spin glasses 12, ch. 84, p. 213
- stannides, transition metal ternary systems 24, ch. 164, p. 399
- steels 25, ch. 165, p. 1
- stresses, static and dynamic 26, ch. 170, p. 87
- sulfides 4, ch. 31, p. 1
 - poly 32, ch. 209, 567
- superconductivity 1, ch. 10, p. 749; 34, ch. 219, p. 135
- crystal chemistry of cuprates 30, ch. 188, p. 31

- in metals 17, ch. 110, p. 1
- high-temperature layered cuprates:
 - overview 30, ch. 187, p. 1
- nickel borocarbides 38,
 - ch. 239, p. 175
- unconventional and magnetism 34,
 - ch. 219, p. 135
- surfaces
 - adsorption on 5, ch. 43, p. 217
 - catalysis on 5, ch. 43, p. 217
- switchable metal hydride films 36,
 - ch. 228, p. 83
- systematics, intra rare earth binary alloys 8, ch. 54, p. 1
- tellurides 4, ch. 31, p. 1
- ternary equiatomic YbTX intermetallics 32,
 - ch. 207, p. 453
- tetravalent cerium compounds 36, ch. 229,
 - p. 281
- theoretical chemistry 3, ch. 23, p. 111
- thermal conductivity of compounds 16,
 - ch. 106, p. 107
- thermochemical properties 18, ch. 122, p. 239
 - of cuprates 30, ch. 190, p. 229
 - of gaseous species 12, ch. 86, p. 409
 - of metallic systems 19, ch. 134, p. 479
- thin films 5, ch. 41, p. 1; 20,
 - ch. 136, p. 105
- switchable metal hydrides 36,
 - ch. 228, p. 83
- toxicity 4, ch. 40, p. 553
- transition metal-indides 34, ch. 218, p. 1
- transport properties of intermetallics 5,
 - ch. 42, p. 117; 17, ch. 115, p. 409
- triflates 29, ch. 186, p. 315
- tunneling spectra of cuprates 31, ch. 204,
 - p. 563
- valence fluctuations 2, ch. 20, p. 575; 16,
 - ch. 105, p. 1; 39, ch. 241, p. 1
- x-ray absorption spectra 10, ch. 71,
 - p. 453
- x-ray scattering 26, ch. 169, p. 1

This page intentionally left blank

Accommodation of the Rare Earths in the Periodic Table: A Historical Analysis

Pieter Thyssen and **Koen Binnemans**

Contents	List of Symbols and Acronyms	2
	1. Introduction	2
	2. A Short History of the Discovery of the Rare-Earth Elements	4
	3. Dmitrii Ivanovich Mendeleev	8
	3.1 Mendeleev's Attempted System	8
	3.2 Rare Earths as a Primary Group	15
	3.3 Mendeleev's Natural System of Elements	19
	3.4 Homologous Accommodation Methodology	24
	3.5 Mendeleev's Rare-Earth Research	25
	4. Bohuslav Brauner and Sir William Crookes	27
	4.1 Brauner's Rare-Earth Research	27
	4.2 Meta-Elements	38
	4.3 Asteriod Hypothesis	46
	4.4 Intraperiodic Accommodation Methodologies	51
	5. Niels Bohr and Henry Moseley	54
	5.1 Bohr's Atomic Theory	54
	5.2 Moseley's Research on X-Ray Spectra of Elements	56
	5.3 The Controversial Element 72	59
	5.4 The Elusive Element 61	63
	5.5 Intergroup Accommodation Methodologies	67
	6. Seaborg's Actinide Concept	75
	7. Rare-Earth Crisis Anno 2010	77

Department of Chemistry, Katholieke Universiteit Leuven, Celestijnenlaan 200F, P.O. Box 2404, Heverlee, Belgium

8. Conclusions	86
Acknowledgment	88
References	88

List of Symbols and Acronyms

<i>AW</i>	atomic weight
<i>EW</i>	equivalent weight
<i>G</i>	group number
<i>l</i>	angular momentum quantum number
<i>n</i>	principal quantum number
<i>S</i>	series number
<i>X</i>	general element symbol
<i>Z</i>	atomic number

1. INTRODUCTION

The *Periodic System of the Elements*, also known as the *Periodic Table*, represents the cornerstone of modern chemistry because it creates order in the multitude of chemical elements and because it allows the prediction of trends in the chemical properties of the elements (Mazurs, 1974; Puddephatt and Monaghan, 1985; Quam and Battell-Quam, 1934a,b,c; Scerri, 2007; Stewart, 2007; van Spronsen, 1969; Venable, 1896; Wang and Schwarz, 2009). Nearly every textbook of inorganic chemistry contains a graphical representation of the periodic system. Poster versions of the periodic table can be found on the walls of many classrooms and lecture halls. This gives the impression that the shape of the periodic system and the position of the individual elements has been fixed since it was introduced for the first time to the community of chemists by Dmitrii Ivanovich Mendeleev in 1869, and that the only changes are the insertion of newly discovered elements. This impression is wrong. Since Mendeleev's discovery of the periodic law, the periodic system of chemical elements has undergone a strong evolution. Even at present, different standard forms of the periodic table are in use. The most striking differences can be found in group IIIB (group 3) which consists according to some periodic tables of Sc, Y, La, and Ac, whereas this is Sc, Y, Lu, Lr according to other tables, while in still other periodic tables the whole series of the lanthanides and actinides are accommodated in this group. Other topics of discussion are the placement of H, He, Al and the labeling of the element group {Zn, Cd, Hg} as transition metals or not (Bent, 2006; Cronyn, 2003; Habashi, 1997; Jensen, 2003, 2008a; Laing, 2007; Novaro, 2008; Scerri, 2005). Besides the standard forms of the periodic table, hundreds of different varieties have been proposed, including spiral, helical, circular and three-dimensional models (Mazurs, 1974).

The fact that there is still an ongoing debate on the question which elements have to be placed in group IIIB indicates that the accommodation (or placement) of the rare earths in the periodic table has always been a difficult issue. The similarities in their chemical properties and the small differences in atomic weight when going from one element to the next one, have caused many troubles to the earlier investigators of the periodic system (Akeroyd, 2003). Nilson and Pettersson (1880) stated: "The periodic table possesses insurmountable difficulties with the rare earth elements." The problem of the accommodation of the rare earths in the periodic table was complicated even more by assuming wrong values for the valency and atomic weights of these elements. One could also think that the accommodation of the rare earths in the periodic table was difficult because only a few rare earths were known at the time of Mendeleev's seminal work of 1869. From a retrospective point of view however, the classification of the chemical elements would have been next to impossible if all the rare-earth elements had been known at that time (Spronsen, 1969).

While the history of the discovery and the separation of the rare earths is well documented, the story of the accommodation of the rare earths in the periodic table is less well known. Part of the story can be found in the famous book on the periodic system of van Spronsen (1969), but recent investigations in the field of the history and philosophy of chemistry have shed new light on the early episodes of the development of the periodic system after 1869. Moreover, the accommodation of the rare earths in the periodic table is still an active research topic. In 2008 and 2009, there was a debate in the *Journal of Chemical Education* on the position of the lanthanides and actinides in the periodic table (Clark and White, 2008; Lavelle, 2008a,b, 2009; Stewart, 2008; Jensen, 2008b, 2009; Clark, 2008; Scerri, 2009a; Laing, 2009).

The aim of this chapter is to give an overview of the evolution of the position of the rare earths in the periodic table, from Mendeleev's time to the present. It will be shown that three fundamentally different accommodation methodologies have been proposed over the years. Mendeleev considered the rare-earth elements as homologues of the other elements and placed them throughout the system in all different groups from I to VIII. Other chemists looked upon the rare earths as forming a special intraperiodic group and they collectively clustered the rare-earth elements in one of the groups of the periodic table. Still others adhered to the so-called intergroup accommodation of the rare earths, according to which the rare-earth elements do not show any relationship with other elements, so that they had to be placed within the periodic table as a separate family of elements, completely unconnected to the other groups. This was accomplished by accommodating the rare earths in between two groups of the periodic system. The rare-earth elements

thus showed some analogy with the transition metals (according to Mendeleev's definition) in the sense that both types of elements were separated from the rest of the system and that both formed a transition between the two main groups of Mendeleev's system. The intergroup accommodation became the preferred one in the twentieth century, because it was in agreement with Bohr's quantum model of the atom. The contributions of Dmitrii Mendeleev, Bohuslav Brauner, Sir William Crookes, Henry Moseley, Niels Bohr, and Glen Seaborg will be put into a historical context. The advantages and disadvantages of the different representations of the modern periodic table, including the left-step periodic table, will be discussed. Special attention will be paid to the question whether lanthanum (actinium) or rather lutetium (lawrencium) should be located below yttrium in the periodic table. Although it would be scientifically more correct to use the term *relative atomic mass*, the historical term *atomic weight* will be used throughout this chapter. We will use the numbering IIIB (US system) for the group containing scandium and yttrium. This group has been numbered 3 in the more recent IUPAC system and IIIA in the European system.

2. A SHORT HISTORY OF THE DISCOVERY OF THE RARE-EARTH ELEMENTS

In this section of the chapter, a brief account of the fascinating history of the discovery of the rare-earth elements will be given. More detailed information can be found in the works of Weeks (1956), Evans (1996), Niinistö (1997) and in Chapter 73 of this Handbook (Szabadváry, 1988). The story began in 1787, when Carl Axel Arrhenius (1757–1824), a lieutenant of the Swedish army and an amateur mineral collector, went on a trip near the small village of Ytterby on the island of Resarö close to Vaxholm (east of Stockholm) and discovered a heavy black mineral in a feldspar quarry. At first sight, the mineral he later called "black stone" resembled asphalt or coal, but it had a remarkably high mass density. Arrhenius' black mineral was first described in the literature by Bengt Reinhold Geijer (1758–1815), who incorrectly assumed that the heavy mineral contained the newly discovered element tungsten (wolfram). In 1794, Johan Gadolin (1760–1852), a Finnish professor of chemistry and mineralogy in the town of Åbo (now Turku), analyzed a sample of the black mineral given to him by Arrhenius, and he succeeded in isolating a new earth (i.e., a metal oxide) which he subsequently named "Ytterby earth." The unknown white earth had some properties that were reminiscent of alumina, while other properties were more similar to those of calcium oxide. Gadolin's work was published in 1796. His discovery was confirmed a year later by the Swedish chemist Anders Gustav Ekeberg (1767–1813), who analyzed a larger sample. Ekeberg renamed Gadolin's

new earth “yttria” and proposed the name *gadolinite* for the black mineral discovered by Arrhenius, in honor of Gadolin. Back in 1751, the Swedish chemist Axel Frederik Cronstedt (1722–1765), had discovered a heavy stone in the Bastnäs mine in Sweden. Cronstedt’s colleague Tobern Bergman (1735–1784) thought it contained an unknown earth, but it was not until 1803 that Martin Heinrich Klaproth (1743–1817) and Jöns Jacob Berzelius (1779–1848), together with Wilhelm Hisinger (1766–1852), independently isolated a rare-earth element. Klaproth called it “terre ochroite,” because it formed colored salts with acids. Berzelius and Hisinger named it “ceria” after the newly discovered asteroid Ceres, and “ceria” became the name preferred by chemists. Therefore, at the beginning of the nineteenth century two rare-earth elements were known: “yttria” (discovered in 1794) and “ceria” (discovered in 1803). However, both “elements” turned out to be complex mixtures later on. In Figures 1 and 2 the chronology of the splitting of “ceria” and “yttria” in the different rare-earth elements is illustrated.

The pronounced similarity between the chemical and physical properties of the rare-earth elements made their isolation a difficult task. The traditional methods of chemical analysis were to no avail and chemists of

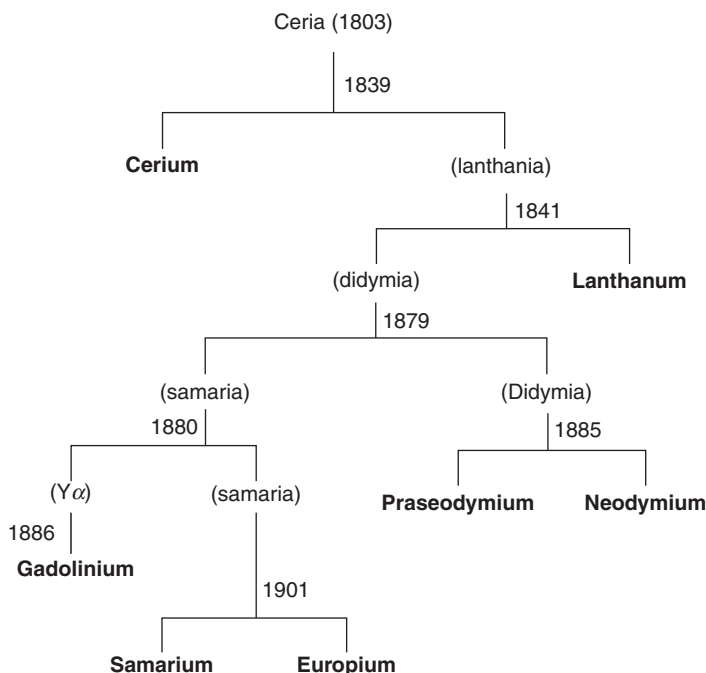


FIGURE 1 Chronology of the splitting of “ceria” in the different composing rare-earth elements.

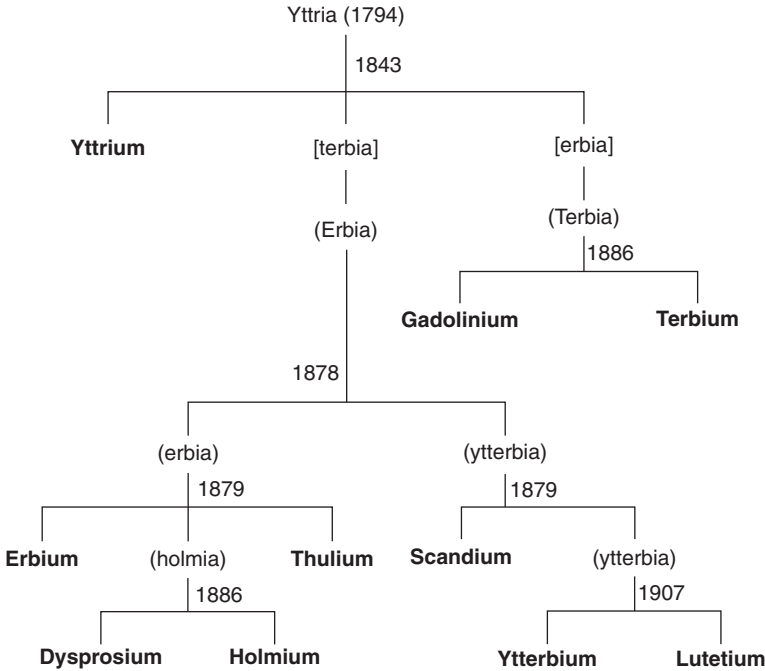


FIGURE 2 Chronology of the splitting of “yttria” in the different composing rare-earth elements.

the early nineteenth century felt obliged to turn to the processes of chemical fractionation (fractional crystallization or fractional precipitation), exploiting the very small differences in the solubility of the rare-earth salts. The number of crystallization steps usually amounted to several thousands, if not tens of thousands. The tedious monotony and dreariness of the exhaustive fractionations is reflected in some of the names of the rare-earth elements. Thus, the Greek origin of lanthanum (La), *λανθάνειν* (*lanthanein*), means “to lie hidden.” Dysprosium (Dy) on the other hand is named after the Greek *dysprositos*, which means that it was “hard to get.” Finally thulium (Tm) refers to its Latin origin, *Thule*, “the farthest northernmost fringe of the civilized world (Evans, 1996).”

It was one of Berzelius’ assistants and the curator of the mineral collections of the Stockholm Academy of Sciences, Carl Gustaf Mosander (1797–1858), who demonstrated the complexity of both “yttria” and “ceria.” When Mosander heated some “cerium” nitrate in 1839, the salt partly decomposed, and on a treatment with dilute nitric acid, he succeeded in extracting a new earth. He called the new element lanthanum (German: Lanthan) and its oxide “lanthana.” Mosander retained the old name *ceria* (Ce) for the insoluble portion of the “ceric” oxide in nitric acid.

In 1841, Mosander discovered another rare earth, “didymium” (Di), in ceria. Unfortunately, “didymium” did not prove to be a genuine element, and it was shown later on that didymium could be separated in two other elements, neodymium and praseodymium (*vide infra*). Having demonstrated the complexity of “ceria” by the identification of at least three elements—cerium, lanthanum, and didymium—Mosander now moved over to his experimental investigations of “yttria” (gadolinite). At the beginning of 1843, Mosander succeeded in splitting his samples of gadolinite in at least three fractions by means of fractional precipitation with ammonium hydroxide. He kept the name *yttria* for the colorless fraction, and named the yellow and rose colored earths “erbia” (Er) and “terbia” (Tb), respectively. The names “erbia” and “terbia” were later interchanged for some obscure reasons and this of course led to confusion among inorganic chemists. The rare-earth story could be briefly recapitulated by noting that “ceria” had been split in cerium, lanthanum and “didymium,” whereas “yttria” had been split in yttrium, “erbium,” and terbium. During the following 35 years (from 1843 to 1878), no new elements were added to the list of rare earths. Thus when Mendeleev introduced his periodic table in 1869, six rare earths were known: yttrium, lanthanum, cerium, “didymium,” “erbium” and terbium.

During the second half of the nineteenth century, a number of rare-earth specialists started applying the various spectroscopic techniques which had been developed by Robert Wilhelm Bunsen (1811–1899) and Gustav Kirchhoff (1824–1887) back in the 1860s in Heidelberg, Germany. Although this new experimental tool proved to be indispensable for the discovery of new elements, it also led to erroneous results. The complexity of absorption and emission spectra, spark spectra and phosphorescent spectra often resulted in wrong interpretations of spectral lines. The combined action of chemical analysis and physical spectroscopy sparked off a multitude of claims and counterclaims for discoveries of new chemical elements, but no one knew how to judge the worth of these assertions. This caused the number of rare-earth elements described in the literature to grow steadily. The chemical community thus witnessed the appearance and disappearance of columbium, damarium, decipium, demonium, euxenium, incognitum, mosandrum, philippium, rogerium, and victorium, to name just a few examples. Fortunately, spectroscopy also aided in discovering a number of genuine rare-earth elements.

The Swiss chemist Jean Charles Galissard de Marignac (1817–1894), was the first in applying these spectroscopic methods. He was 23 years old when he embarked upon his quest for new rare-earth elements. He demonstrated in 1878 that “erbia” was a complex mixture of at least two rare-earth elements, erbium and “ytterbium” (Yb), by heating “erbium” nitrate and extracting the decomposed salt with water. The little Swedish village Ytterby thus holds a distinguished place in the history of the rare-earth elements.

Four rare-earth elements (yttrium, ytterbium, erbium, and terbium) have been named in honor of this village. A year later, the Swedish chemist Lars Fredrik Nilson (1840–1899), discovered another element in “erbia” and he named it *scandium* (Sc) in honor of Scandinavia. At the same time, Nilson’s compatriot, the geologist and chemist Per Theodor Cleve (1840–1905) succeeded in resolving the “erbia” earths yet another step further, when he separated it into three components: erbium, “holmium” (Ho) and thulium (Tm). The name “holmium” refers to Stockholm (Cleve’s native city) and had been independently discovered by the Swiss chemists Marc Delafontaine (1838–1911) and Jacques-Louis Soret (1827–1890), who had coined the metal element X on the basis of its absorption spectrum.

Marignac had been one of the first chemists to question the elemental character of Mosander’s “didymium” back in 1853. It took a quarter of a century before Delafontaine started observing some mysterious variations in the spectra of “didymium.” He thus noted the appearance of two new lines and took it as an indication for the existence of a new element, which he called “decipium” from the Latin “to deceive” or “to stupefy.” However, Paul-Emile Lecoq de Boisbaudran (1838–1912), another specialist in spectroscopic analysis, revealed the real identity of “decipium” in 1879 and he showed it to consist of a mixture of known rare earths. His spectroscopic investigations aided him in the resolution of “didymium” when he isolated “samarium” (Sm) from the mineral samarskite over the course of that same year. Didymium completely ceased to exist in 1885 when Carl Auer von Welsbach (1858–1929) succeeded in splitting it in two fractions, a green fraction which he named *praseodymium* (Pr, from the Greek for “green twin”) and a pink one which he had named *neodymium* (Nd, from the Greek for “new twin”).

Lecoq de Boisbaudran further resolved “samarium” in 1886 in genuine samarium and another rare-earth element which appeared identical with Marignac’s $Y\alpha$, isolated in 1880. Marignac and Lecoq de Boisbaudran decided to name this element *gadolinium* (Gd) after the mineral gadolinite. *Dysprosium* (Dy) was discovered during the same year. *Europium* (Eu) was discovered in 1901 by Eugène-Anatole Demarçay (1852–1904) who was a specialist in spectroscopy. The story about the discovery of lutetium (Lu) and promethium (Pm) will be discussed in Sections 5.3 and 5.4.

3. DMITRII IVANOVICH MENDELEEV

3.1 Mendeleev’s Attempted System

On February 17, 1869 (according to the old Julian calendar), the Russian chemist Dmitrii Ivanovich Mendeleev (1834–1907, Figure 3) wrote a pamphlet entitled “An Attempted System of the Elements Based on



FIGURE 3 Dmitrii Ivanovich Mendeleev (1834–1907). Photo and permission from Edgar Fahs Smith Collection.

Their Atomic Weights and Chemical Analogies” in both the Russian and the French language (Figure 4) (Mendeleev, 1869a). The whole set of chemical elements known at that time had been logically classified in six columns of increasing atomic weight (or relative atomic mass) and 19 rows of natural groups, thus representing the first embodiment of the periodic law and the first version of the periodic table (Gordin, 2004; Kolodkine, 1963; Mendeleev, 1889; Pissarjevski, 1955). By sending the *Attempted System* right away (the actual discovery had been made on the same day), Mendeleev ensured the priority of his discovery. When inspecting Mendeleev’s *Attempted System* in more detail, one can notice an intriguing fact. In general, when reading from top to bottom and from left to right, one should obtain an ever increasing atomic weight sequence. However, this sequence gets interrupted four times. First, when passing from indium (In, 75.6, third column, bottom row) to titanium (Ti, 50, fourth column, top row), and a second time when moving from thorium (Th, 118, fourth column, bottom row) to zirconium (Zr, 90, fifth column, top row). The atomic weight sequence is violated twice more by the inversion of tellurium (Te) and iodine (I), and by the insertion of gold (Au) and bismuth (Bi). The only possible way of restoring the sequence of the In–Ti and the Th–Zr violations would be by eliminating a total of seven elements from the system, namely yttrium (Yt), indium (In), cerium (Ce), lanthanum (La), didymium (Di), erbium (Er) and thorium (Th).

ОПЫТЪ СИСТЕМЫ ЭЛЕМЕНТОВЪ.

ОСНОВАННОЙ НА ИХЪ АТОМНОМЪ ВѢСѢ И ХИМИЧЕСКОМЪ СХОДСТВѢ.

		Ti = 50	Zr = 90	? = 180.
		V = 51	Nb = 94	Ta = 182.
		Cr = 52	Mo = 96	W = 186.
		Mn = 55	Rh = 104,4	Pt = 197,1.
		Fe = 56	Ru = 104,4	Ir = 198.
		Ni = Co = 59	Pd = 106,6	O = 199.
H = 1		Cu = 63,4	Ag = 108	Hg = 200.
	Be = 9,4	Mg = 24	Zn = 65,2	Cd = 112
	B = 11	Al = 27,4	? = 68	U = 116
				Au = 197?
	C = 12	Si = 28	? = 70	Sn = 118
	N = 14	P = 31	As = 75	Sb = 122
				Bi = 210?
	O = 16	S = 32	Se = 79,4	Te = 128?
	F = 19	Cl = 35,5	Br = 80	I = 127
Li = 7	Na = 23	K = 39	Rb = 85,4	Cs = 133
				Tl = 204.
		Ca = 40	Sr = 87,6	Ba = 137
			? = 45	Ce = 92
		?Er = 56	La = 94	
		?Yt = 60	Di = 95	
		?In = 75,5	Th = 118?	

Д. Менделѣевъ

FIGURE 4 An attempted system of the elements based on their atomic weight and chemical analogies. A pamphlet with Mendeleev's first periodic system, distributed on February 17, 1869.

Indeed, if that were the case, the sequence would have passed from the unknown element with an atomic weight of 45 to titanium with an atomic weight of 50, and from strontium with an atomic weight of 87.6 to zirconium with an atomic weight of 90, completely in accordance with the gradual increase in atomic weight. It must be noted that terbium was already known at the time of the first version of the periodic table in 1869, but Mendeleev decided not to include this element in his table, following Bunsen's and Bahr's advice. Nonetheless, all other known rare-earth elements were clearly present in Mendeleev's *Attempted System*, but none of them had been correctly accommodated. Moreover, the atomic weights assigned to the rare-earth elements turned out to be incorrect later on. These wrong values of the atomic weights can be explained by the fact that Mendeleev assumed that the most common valency of the rare-earth elements was 2 and not 3 (*vide infra*).

If Mendeleev was to convince the chemical community of the fundamental character of his system, he had to explain his line of thoughts in more detail. Indeed, his pamphlet did not contain any evidence that might persuade other chemists of the validity of his assertions (Brooks, 2002). Over the course of the next two years (1869–1871), Mendeleev

labored at the clarification, illustration, refinement, and optimization of his periodic classification of the elements. Not surprisingly, the accommodation of the rare-earth elements formed an important part of Mendeleev's research program. During the second half of February 1869, Mendeleev drafted his initial article announcing the discovery of the periodic law and proposing the *Attempted System* as a useful classification of the elements. His paper "On the Correlation between the Properties of the Elements and Their Atomic Weights" was subsequently read by Nikolai Menshutkin on March 6, 1869, at the meeting of the newly founded Russian Chemical Society. Finally, after having received the proofs of the article on April 5, 1869, Mendeleev published his paper in the first volume of the society's new journal, the *Zhurnal Russkogo Khimicheskogo Obshchestva*, in the month of May of that year (Mendeleev, 1869b). This paper was also abstracted in the German language (Mendelejeff, 1869a,b). It should be mentioned that English translations of the most important papers on the periodic law, written by Mendeleev, can be found in the book of Jensen (2002).

As soon as he had finished the writing process, Mendeleev moved over to some experimental research, in the late spring or early summer of 1869. After all, there still remained a number of serious problems connected with his *Attempted System* at the beginning of 1869. Some elements, such as uranium, lead, and thallium, were wrongly accommodated in the system, due to their imprecisely determined atomic weights and doubtful valencies. Thus the atomic weight of uranium was too low, while thallium and lead had been given an incorrect maximum valency of 1 and 2 respectively. Other elements, such as tellurium and iodine, violated the atomic weight sequence as a consequence of their inversed placement which was necessary for the correct grouping of these elements. Mendeleev had also left a number of open places in his system and he boldly proclaimed that these represented some as yet undiscovered elements. Unfortunately, the first version of the periodic table did not prove very useful in determining the characteristic properties of unknown elements. It must be noted that Mendeleev's first representation of the periodic system did not exactly represent all the various chemical and physical relationships between the different elements. The most severe problem however found its origin in the seven elements (Er, Yt, In, Ce, La, Di, and Th) which remained outside the system (*vide supra*). Finally, Mendeleev had not been very clear in his article about the kind of chemical and physical properties of the elements that could be used in order to exemplify the principle of periodicity.

Mendeleev thus began by investigating the atomic volumes of the elements as a possible periodic function of the atomic weight, hoping that his research would confirm the periodic law. His research on the atomic volumes of the elements illustrated that this physical property tended to rise in each short period, reaching a maximum value in the halogens and alkali

metals. But when Mendeleev started examining the longer periods of his system, he first noticed a decrease in the atomic volumes, reaching a minimum at the end of the first half of the period (around the transition metal triads). Once arrived in the second part of the period, the atomic volumes started to increase again. In the case of uranium however, Mendeleev noted a decrease instead of the expected increase. Mendeleev took this as a sign that uranium had been incorrectly accommodated in the *Attempted System*, and he removed the element from its original position in the table between cadmium and tin during the summer of 1869. Mendeleev must have realized that an alteration of the atomic weight and valency of uranium were needed in order to change its position in the system. During the month of August 1869, Mendeleev started writing a paper about his experimental results *Concerning the Atomic Volumes of Simple Bodies* (Gordin, 2004). In August 1869, Mendeleev attended the Second Congress of Russian Physicians and Naturalists in Moscow where he delivered a lecture about his work on the atomic volumes, emphasizing that a comparison of specific weights and specific volumes of the elements belonging to different rows showed to some extent the naturalness of his periodic system.

The naturalness of the system had indeed been proven on the basis of a physical property of the elements, but Mendeleev decided to check whether the chemical properties of the elements would exhibit a periodic relation as well. He immediately turned to an investigation of the higher salt-forming oxides and presented his results on October 2, 1869, during a meeting of the Russian Chemical Society in a paper entitled "On the Quantity of Oxygen in Metal Oxides and on the Valency of the Elements" (Mendeleev, 1870). Mendeleev explained that the periodicity in the valency would only manifest itself in the higher oxides. Mendeleev distinguished seven limiting forms of salt-forming oxides, depending on the highest known oxidation number of a given element: R_2O , $R_2O_2 (= RO)$, R_2O_3 , $R_2O_4 (= RO_2)$, R_2O_5 , $R_2O_6 (= RO_3)$, and R_2O_7 . Every element that is able to react with oxygen forms an oxide, the composition of which can be represented by one of these seven formulae. Mendeleev moreover emphasized the need of considering the salt-forming oxides, since chemists could be drawn to erroneous conclusions about the valency of the elements by mistaking peroxides for oxides (*vide infra*). During the winter of 1869, Mendeleev measured the heat capacity of uranium metal, since this would enable him to correct the atomic weight of uranium (old symbol: Ur). He consequently changed the value from 116 to 240 in early 1870.

Due to the recent discoveries of the rare-earth elements, most of their chemical and physical properties were not yet known in 1869, and Mendeleev had to manage with the limited information that was available at that time. As a consequence, Mendeleev did not succeed in correctly accommodating these elements when he constructed his *Attempted System*. This is not surprising given the fact that Mendeleev still adhered

to the old Berzelian atomic weights of the rare-earth elements. None of these values corresponded with the modern atomic weights. From the well known relationship between the atomic weight (AW) of an element (X), its equivalent weight (EW), and its valency (V):

$$AW(X) = EW(X) \times V(X), \quad (1)$$

one can conclude that these atomic weights were incorrectly determined due to an erroneous estimation of the valence of these elements. Thus, if Mendeleev was using the wrong valency number for some element X , say V_1 , this logically implied a miscalculation of the atomic weight AW_1 :

$$AW_1(X) = EW_1(X) \times V_1(X), \quad (2)$$

where use was made of Eq. (1). In order to obtain the correct atomic weight AW_2 , a correction of the valency number, from V_1 to V_2 , is necessary:

$$AW_2(X) = EW_2(X) \times V_2(X). \quad (3)$$

Due to the constancy of the equivalent weight:

$$EW_1(X) = EW_2(X), \quad (4)$$

eqs. (2) and (3) can be rewritten as follows:

$$\frac{AW_1(X)}{V_1(X)} = \frac{AW_2(X)}{V_2(X)}. \quad (5)$$

Otherwise stated, there exists a relationship between Mendeleev's atomic weight values (AW_1) and the corresponding modern values (AW_2):

$$AW_1(X) = AW_2(X) \times \frac{V_1(X)}{V_2(X)}, \quad (6)$$

which makes it possible to determine the valency as used by Mendeleev in 1869 (V_1):

$$V_1(X) = \frac{AW_1(X)}{AW_2(X)} \times V_2(X). \quad (7)$$

For example, lanthanum was allotted an atomic weight of 94 (AW_1) in Mendeleev's *Attempted System*. The modern value for lanthanum's atomic weight is 138.9 (AW_2) and as all the rare-earth elements typically exhibit the +III oxidation state, its modern valency is 3 (V_2). With the aid of Eq. (7), the valency number V_1 as used by Mendeleev in the beginning of 1869 can be established:

$$V_1(\text{La}) = \frac{AW_1(\text{La})}{AW_2(\text{La})} \times V_2(\text{La}) = \frac{94}{138.8} \times 3 = 2.03 \approx 2. \quad (8)$$

Apparently, Mendeleev believed the valency of lanthanum to be 2 instead of 3. As a consequence, he used the incorrect atomic weight of 94. Application of Eq. (7) to the other six elements with wrong atomic weight values, leads to the following valencies used by Mendeleev:

$$V_1(\text{Er}) = \frac{AW_1(\text{Er})}{AW_2(\text{Er})} \times V_2(\text{Er}) = \frac{56}{167.2} \times 3 = 1.004 \approx 1, \quad (9)$$

$$V_1(\text{Y}) = \frac{AW_1(\text{Y})}{AW_2(\text{Y})} \times V_2(\text{Y}) = \frac{60}{88.9} \times 3 = 2.02 \approx 2, \quad (10)$$

$$V_1(\text{Ce}) = \frac{AW_1(\text{Ce})}{AW_2(\text{Ce})} \times V_2(\text{Ce}) = \frac{92}{140.1} \times 3 = 1.97 \approx 2, \quad (11)$$

$$V_1(\text{Di}) = \frac{AW_1(\text{Di})}{AW_2(\text{Di})} \times V_2(\text{Di}) = \frac{95}{142} \times 3 = 2.007 \approx 2, \quad (12)$$

$$V_1(\text{In}) = \frac{AW_1(\text{In})}{AW_2(\text{In})} \times V_2(\text{In}) = \frac{75.6}{114.8} \times 3 = 1.98 \approx 2, \quad (13)$$

$$V_1(\text{Th}) = \frac{AW_1(\text{Th})}{AW_2(\text{Th})} \times V_2(\text{Th}) = \frac{118}{232} \times 3 = 2.03 \approx 2. \quad (14)$$

It follows from Eqs. (8)–(12) that the known rare-earth elements were considered to be divalent instead of trivalent. Their oxides were generally represented by the formula RO and the higher oxide of cerium was denoted by the formula R₂O₃. Therefore, all atomic weights were incorrectly determined, and this explains why Mendeleev was not able to accommodate these elements into his periodic system. Only with the correct atomic weights at hand, could one try to accommodate them. But this also necessitated a change in valency from 2 to 3. Although Mendeleev would be the first in proposing this modification of valency number, he only did so at the end of the first half of 1870. Before that, during the period 1869–1870, Mendeleev continued to look upon the rare-earth elements as being divalent and he used the wrong atomic weights throughout. On the other hand, it should be noted that Mendeleev started to doubt the positions of the rare-earth elements from the very outset. As he admitted in his 1869 article *On the Correlation between the Properties of the Elements and Their Atomic Weights* (Mendeleev, 1869c; Mendelejeff, 1869c): “With respect to the position of some elements, there exists, quite understandably, complete uncertainty. In particular, this holds for those elements that are little studied and whose correct atomic weight

has hardly been established with any certainty. Among these are, for example, yttrium, thorium, and indium.”

3.2 Rare Earths as a Primary Group

When Lavoisier defined a chemical element in 1789, 26 elements were actually known. Eighty years later, in 1869, a total of 36 new chemical elements had been discovered. As a consequence, more and more chemists felt the need for a systematic organization. Instead of building a periodic table, as Mendeleev did in 1869, they quickly inclined towards putting together elements with similar physical and chemical characteristics, ending up with a network of small, so-called *natural groups*. Examples of natural groups are the highly reactive halogens (F, Cl, Br, I) and the silvery colored and water-reactive alkali metals (Li, Na, K, Rb, Cs). The interesting fact is that Mendeleev clearly recognized the similarity in chemical and physical properties of the rare-earth elements. He therefore considered them as the members of a natural group and he proclaimed this point of view in his 1869 article (Mendeleev, 1869c; Mendelejeff, 1869c): “Only with regard to some groups of elements are there no doubts that they form a whole and represent a natural order of similar manifestations of matter. . . . Such groups are: the halogens, the alkaline earth metals, the nitrogen group, and also—in part—the sulfur group, the companions of platinum, the companions of cerium, and a few others.” Note that Mendeleev considered the other rare earths as the companions of cerium. As a consequence, and in complete analogy with the alkali metals and the halogens, Mendeleev tried to accommodate the rare earths in the periodic table as a group. This fact is clearly exemplified in the *Attempted System* where all the rare-earth elements (Er, Yt, Ce, La, and Di) were grouped together at the bottom of the system. However, Mendeleev understood that the rare earths constituted a very special group of elements and that the whole accommodation issue had its root in the puzzling nature of this elemental group. According to Mendeleev (1869c), “the most interesting problem was the arrangement of elements having such similarities as cerium.”

In order to understand why Mendeleev discriminated this group from the other natural groups (alkali metals, halogens, etc.), it will be necessary to go into a detailed consideration of the construction methodology of the periodic table. In short, a two-step process is needed in order to build a periodic table from scratch. First, all the elements have to be ordered according to increasing atomic weight. Notice that in the modern periodic tables, the ordering is according to increasing atomic number (i.e., the number of protons in the nucleus). This *primary classification* results in a long horizontal sequence of elements, and has been called the *Mendeleev Line* by Henry Bent (Bent, 2006). It will be noted that certain chemical and

physical properties of the elements recur periodically. Therefore, the second step, termed the *secondary classification*, consists of partitioning this Mendeleev Line at certain well defined loci and placing the different sections (i.e., periods) underneath each other so that the elements with similar properties will fall into the same vertical column, thus forming the natural groups and representing the periodic law graphically.

One can conclude at this point that natural, elemental groups (e.g., Li, Na, K, ..., Ag) are formed during the secondary classification. Within such a vertical group, the atomic weights of the congeners will vary in a stepwise way. Thus in the case of the group {Li, Na, K, ..., Ag}, one notices the following sequence of "jumps" between the atomic weights: $7 \rightarrow 23 \rightarrow 39 \rightarrow \dots \rightarrow 108$. One could denominate such a natural group of elements by the term *secondary group*. The members of such a secondary group will be nominated *secondary elements*. Hence, a secondary group can be defined and recognized as follows: (1) Secondary groups are always formed during the secondary classification of the elements; (2) There exists a stepwise relationship between the atomic weights of the congeners. Some examples of secondary groups are the alkali metals, the halogens, the alkaline earth metals, and the noble gases.

In sharp contrast with this type of natural groups, some other groups, e.g., the cerium group {Ce, La, Di}, are formed at an earlier stage of the construction methodology, namely during the primary classification. Worded somewhat differently, due to the fact that the elements constituting such groups succeed one another sequentially in the Mendeleev Line (e.g., Ce = 92, La = 94, Di = 95), the formation of these groups will be noticed during the primary classification. Within such a horizontal group, the atomic weight of the congeners will remain almost constant. Thus in the case of the elemental group {Ce, La, Di}, one observes the following sequence of atomic weights: $92 \rightarrow 94 \rightarrow 95$. Such a natural group of elements can be denominated by the term *primary group* and their congeners by the name *primary elements*. Hence, primary groups can be defined and recognized as follows: (1) Primary groups are always formed during the primary classification of the elements; (2) There exists a steady, almost constant relationship between the atomic weights of the congeners. Other examples of such primary groups are the iron group {Fe = 56, Ni = 59, Co = 59}, the platinum group {Pt = 197.1, Ir = 198, Os = 199}, the palladium group {Rh = 104.4, Rn = 104.4, Pl = 106.6} (in Mendeleev's nomenclature, Rn represented ruthenium and Pl represented palladium), and the erbium group {Er = 56, Yt = 60}. Since the rare-earth elements constituted two primary groups, {Ce, La, Di} and {Er, Yt}, Mendeleev (1869c) considered these groups to be special, because their congeners exhibited atomic weight values which were very close to each other, a fact not to be observed in the "normal" case of secondary groups where the congeners have radically different atomic weights.

At least four important consequences can be drawn from the existence of primary groups. First of all, Mendeleev naturally wondered how one should depict both primary and secondary groups within his *Attempted System*. In contrast to the modern periodic tables, the secondary groups were lying horizontally, whereas the primary groups were depicted vertically. A more significant consequence of the existence of primary groups within the periodic system is their so-called *transitional function*. Mendeleev got this idea when he was examining his *Attempted System*. It appeared to him that the elements of the primary groups at the upper part of his system represented some sort of transition between two (sub)- periods in the periodic table. He remarked that the upper members of the fourth column (Mn, Fe, Co, Ni, Zn) formed a transition to the lower members of the (third) column in which Ca, K, Cl, and similar elements were found, so that the properties and atomic weights of cobalt and nickel, chromium, manganese, and iron represented a transition from copper and zinc to calcium and potassium. At the beginning of 1869, Mendeleev's views on the matter were still rather intuitive and somewhat vague. Indeed, it was not easy to perceive the transitional function of the iron group, the palladium group, and the platinum group in the *Attempted System*. As a consequence of fixing all his attention on the *Attempted System*, Mendeleev immediately recognized how the two primary groups, {Ce, La, Di} and {Er, Yt}, at the bottom part of his system, helped in connecting the periods of the main core. It thus seemed that these primary groups were furnished with a transitional function as well. This brings us to the third important consequence of the existence of primary groups in Mendeleev's classification of the chemical elements. Due to the fact that both the transition metal groups (iron, palladium, and platinum group) and the rare-earth groups (cerium and erbium group) exhibited a transitional function, Mendeleev emphasized the similarity between these two sets of groups. Nevertheless, Mendeleev finally decided not to include the transition metal groups in the lower rows with the two rare-earth groups due to a difference in the basic/acidic properties of the oxides between the congeners of these two sets of groups. The rare earth – transition metal analogy was further exemplified by Mendeleev in his article "Concerning the Atomic Volumes of Simple Bodies" (Mendeleev, 1871; Mendelejeff, 1870). Mendeleev also emphasized the similarity in magnetic properties between the elements of the cerium group and those of the iron group. Repeated references to the rare earth – transition metal analogy were also made in his article "On the Quantity of Oxygen in Metal Oxides and on the Valency of the Elements" (Mendeleev, 1870). A fourth and last consequence of the existence of primary groups is their problematic nature, undermining both the periodic law and the characterization of elements as being defined by their atomic weight. Mendeleev noticed that when the elements are arranged according to their atomic weights, the elements display a distinct periodicity in their

properties. This is clearly seen in the series Li, Be, B, C, N, O, and F, where Li and F are monovalent, Be and O are divalent, B and N trivalent and C tetravalent. The same behavior is found for the series Na, Mg, Al, Si, P, S, and Cl. However, in the case of primary groups, there were of course regular and gradual changes in the size of atomic weights, but these were not accompanied by regular and gradual changes in the distinctive properties of the elements. In the case of the cerium group {Ce, La, Di}, for example, there was a small gradual increase in atomic weight, but the valency remained constant. The same could be said for the iron group, palladium group, platinum group, and the erbium group. The generality of the periodic law got undermined due to the presence of primary groups in the periodic system. This was one of the core problems of the rare-earth elements, laying at the basis of their problematic accommodation.

Mendeleev recognized the dual sense of the nature of chemical elements. He clearly distinguished between the elements as *simple substances* and the elements as *basic substances*. *Simple substances* can be characterized by the plethora of secondary properties (color, taste, smell, etc.), and are therefore observable and isolable (Paneth, 2003). *Basic substances* on the other hand are completely unobservable to our senses. This does not imply however that they are completely devoid of properties. Mendeleev was of the opinion that the more abstract, basic substances were characterized by their atomic weight, and he therefore used this property in accommodating all the chemical elements in his system. According to Mendeleev, the atomic weight of an element determined its place in the periodic table. He concluded for this reason that the magnitude of the atomic weight determined the character of an element to the same extent that the molecular weight determines the properties and many of the reactions of a compound substance. An important consequence of taking the atomic weight as the characteristic property of basic substances was the possibility of distinguishing between the (chemically and physically very similar) congeners of a certain elemental group in the periodic table. The natural group of alkali metals, {Li = 7, Na = 23, K = 39, Rb = 85.4, Cs = 133}, for example, consisted of five metals which shared a lot of similar properties: metallic luster, low melting points and densities, a pronounced reactivity with respect to water, a strongly oxidizing character, etc. It thus seemed that the differences in atomic weights were the only possible way to differentiate between these analogous elements. "Similar elements [in chemical and physical properties] possess different atomic weights," Mendeleev proclaimed (Mendeleev, 1869b). But in the case of the cerium group {Ce = 92, La = 94, Di = 95}, the difference in atomic weights was scarcely noticeable. Indeed, one recalls that in sharp contrast with the secondary groups, which were characterized by a stepwise relationship between the atomic weights of the secondary elements, primary groups represented a steady and almost constant relationship between the atomic weights of the primary elements. Mendeleev

noticed that this observation was not limited to the members of the cerium group. It turned out that similar apperceptions could be made with regard to the transition metal groups, for instance nickel and cobalt, whose atomic weights are very close to each other. Rhodium, ruthenium, and palladium on the one hand, iridium, osmium, and platinum on the other are also elements which closely resemble one another, and which have similar atomic weights. Iron and manganese have similar properties and their atomic weights are also very similar. This implied that, in the case of primary groups, no differentiation between the congeners was possible anymore on the basis of their atomic weights. Otherwise stated, while secondary elements could still be characterized by their atomic weights, primary elements, on the other hand, could not be characterized anymore by the atomic weight. The question naturally presents itself as to how one should differentiate between primary elements. According to Mendeleev, these elements were characterized by “internal differences of matter” (Trifonov, 1970).

Here ended the first period of Mendeleev’s research on the periodic law which lasted from 1869 till the end of the first half of 1870. Mendeleev’s viewpoints could be summarized as follows. According to his opinion, chemists had to draw a sharp distinction between primary (i.e., rare earths, transition metals) and secondary elements (i.e., alkali metals, halogens). Such a differentiation should also be made on the level of primary and secondary groups. The essence of the difficult accommodation of the rare earths in the periodic table rested on the fact that these elements constituted a primary group. Their problematic nature raised a number of serious problems. Both the principle of periodicity and the characterization of primary elements on the basis of their atomic weights became undermined. Mendeleev was also tempted in drawing an analogy between the rare-earth elements and the transition metals on the basis of their transitional functions in the periodic system, and he started questioning the simplicity of these elements on a closer study of the primary groups. He nevertheless continued to use the old atomic weights and erroneous valencies for the rare-earth elements, and his unremitting adherence to the *Attempted System* moreover troubled his views with regard to the different relationships between the chemical and physical properties of these elements.

3.3 Mendeleev’s Natural System of Elements

Mendeleev had been working on the optimization of the periodic law for quite some time now. He had always preferred the long form table (i.e., his *Attempted System*), but in November 1870, Mendeleev created a short form table, his *Natural System of the Elements* (Figure 5) (Mendeleev, 1871; Mendelejeff, 1870). In a long form of the periodic table, the d-block elements are separated from the main group elements, whereas this is

Tabelle II.

Reihen	Gruppe I. R ⁰	Gruppe II. R ⁰	Gruppe III. R ^{0*}	Gruppe IV. R ^{0*}	Gruppe V. R ^{0*}	Gruppe VI. R ^{0*}	Gruppe VII. R ^{0*}	Gruppe VIII. R ^{0*}
1	H=1							
2	Li=7	Be=9,4	B=11	C=12	N=14	O=16	F=19	
3	Na=23	Mg=24	Al=27,3	Si=28	P=31	S=32	Cl=35,5	
4	K=39	Ca=40	—=44	Ti=48	V=51	Cr=52	Mn=55	Fe=56, Co=59, Ni=59, Cu=63.
5	(Cu=63)	Zn=65	—=68	—=72	As=75	Se=78	Br=80	
6	Rb=85	Sr=87	?Yt=88	Zr=90	Nb=94	Mo=96	—=100	Ru=104, Rh=104, Pd=106, Ag=108.
7	(Ag=108)	Cd=112	In=113	Su=118	Sb=122	Te=125	J=127	
8	Cs=133	Ba=137	?Ba=138	?Co=140	—	—	—	—
9	(—)	—	—	—	—	—	—	—
10	—	—	?Er=178	?La=180	Ta=182	W=184	—	Os=195, Ir=197, Pt=198, Au=199.
11	(Au=199)	Hg=200	Tl=204	Pb=207	Bi=208	—	—	—
12	—	—	—	Th=231	—	C=240	—	—

FIGURE 5 Mendeleev's Natural System of the Elements (1871). Reproduced from Mendelejeff (1871).

not the case in a short form of the periodic table. Mendeleev's *Natural System of the Elements* remained the standard format during the next decades, and it succeeded in exhibiting a number of new relationships between the chemical elements (e.g., the close connection between s-, p-, d-, and f-block elements among other aspects).

In following the above mentioned construction methodology (Section 3.2), partitioning the Mendeleev Line after each halogen element, Mendeleev quickly obtained a first sequence of seven elements (Li, Be, B, C, N, O, F) which he denoted as "a short period or series." The lightest element, hydrogen, was solitarily situated above this period, and Mendeleev therefore decided to name it the first series. As a consequence, (Li, Be, B, C, N, O, F) belonged to the second series, (Na, Mg, Al, ...) to the third, etc. However, during the secondary classification, both short and long periods were obtained. Mendeleev noticed that not all of the presently known elements could be placed in short series. Thus, after the third short periods of seven elements, a fourth and longer period (17 elements long) was obtained (Figure 6).

Because of these longer periods, not all of the main block elements were grouped together (e.g., F and Cl were separated from Br and I). Mendeleev therefore had to pursue the secondary classification and the longer periods were cut in half. By partitioning the Mendeleev line before Cu, Ag, and Au, Mendeleev obtained a modified periodic table of chemical elements (Figure 7).

As a result, the fourth period gave rise to two series (the fourth and the fifth) of 10 and 7 elements respectively. The fourth series was termed an *even series*, while the fifth series was called an *odd series*. Mendeleev

H																	
Li	Be	B	C	N	O	F											
Na	Mg	Al	Si	P	S	Cl											
K	Ca	–	Ti	V	Cr	Mn	Fe	Co	Ni	Cu	Zn	–	–	As	Se	Br	
Rb	Sr	–	Zr	Nb	Mo	–	Ru	Rh	Pd	Ag	Cd	In	Sn	Sb	Te	I	
Cs	Ba	–	Ce	–	–	–	–	–	–	–	–	–	–	–	–	–	–
–	–	–	–	Ta	W	–	Os	Ir	Pt	Au	Hg	Tl	Pb	Bi	–	–	
–	–	–	Th	–	U	–	–	–	–	–	–	–	–	–	–	–	

FIGURE 6 Mendeleev's table with eight periods.

1	H																
2	Li	Be	B	C	N	O	F										
3	Na	Mg	Al	Si	P	S	Cl										
4	K	Ca	–	Ti	V	Cr	Mn	Fe	Co	Ni							
5	Cu	Zn	–	–	As	Se	Br										
6	Rb	Sr	–	Zr	Nb	Mo	–	Ru	Rh	Pd							
7	Ag	Cd	In	Sn	Sb	Te	I										
8	Cs	Ba	–	Ce	–	–	–	–	–	–							
9	–	–	–	–	–	–	–										
10	–	–	–	–	Ta	W	–	Os	Ir	Pt							
11	Au	Hg	Tl	Pb	Bi	–	–										
12	–	–	–	Th	–	U	–	–	–	–							

FIGURE 7 Mendeleev's table with 12 periods.

furthermore observed that there exists a very marked difference between the corresponding members of the odd and even series (with the exception of the first two), while, among themselves, the members of the odd series, as well as the members of the even series display much greater analogies. For example, the members of the fourth and sixth series show more similarities among themselves than they do with the members of the fifth or seventh series. Indeed, the alkali metals K and Rb (situated in the fourth and sixth series) are distinctly different from the coinage metals Cu and Ag (situated in the fifth and seventh series). Similarly, chlorine, bromine, and iodine (positioned in the third, fifth, and seventh series, respectively) are all halogens, while Mn (located in the fourth series) certainly is not. In a certain sense, Mendeleev was alluding to the difference in properties between the main block elements (i.e., s-block and p-block elements) and the d-block elements. This was emphasized in his *Natural System* by alternating the elements to the left and the right of each column. At the same time Mendeleev arranged all of the elements which could not be placed in the short periods in order of their properties and atomic weights between the last member of the even series and the first member of the odd series. In this manner Fe, Co, and Ni formed a transition from Cr and Mn, on the one side, to Cu and Zn, on the other.

Mendeleev was thus aided significantly by his construction of the short form table in defining the transition metals more clearly than before as those elements which connected the even and the odd series. Two other triads of transition metals could moreover be discerned in the *Natural System of Elements*. Just as Fe, Co, and Ni follow the 4th series, so Ru, Rh, and Pd follow the 6th, and Os, Ir, and Pt the 10th. Each large period of 17 members thus consisted of two series (one even and one odd), along with the intermediate series of elements given above. Since the intermediate members did not correspond to any of the seven groups of the short periods, they formed an independent group (the eighth, which was indicated by the Roman numeral VIII). Mendeleev also emphasized that the members of this group resembled one another to the same extent as the corresponding members of the even series, with the only difference that they constituted three primary groups, instead of secondary groups as in the case of the elements from the groups I–VII.

Due to the table layout of Mendeleev's *Natural System of the Elements*, consisting of eight groups (I–VIII) and 12 series (1–12), each element (X) could be characterized by two coordinates: its group number (G) and its series number (S). Sodium for example, was located in the first group and the third series, and was therefore given the element coordinates I-3. Magnesium was located in the place II-3, and titanium was characterized by the element coordinates IV-4. The improved format of Mendeleev's table had revealed a number of interesting relationships between the properties of the elements. Encouraged by this new information, Mendeleev began to focus all his attention on predicting the properties of the as yet undiscovered elements (i.e., *eka-boron* in III-4, *eka-aluminium* in III-5, and *eka-silicon* in IV-5).

The *Natural System of Elements* (Figure 5) also contained corrected atomic weights. In his paper "On the Placement of Cerium in the Periodic System of Elements" (Mendelejew, 1870), Mendeleev admitted that the atomic weights of indium, uranium and cerium (and probably its companions, the other rare-earth elements) should be modified because these elements did not fit in the periodic table on the basis of either the formulae of their oxides or their properties according to the periodicity (Trifonov, 1970). He realized that a change in valency would be necessary in order to correct the atomic weight values of the rare earths. The usual representation of their oxides by the formula RO had thus to be modified. Mendeleev was the first in assuming the rare earths to be trivalent, instead of divalent, and he therefore proposed the general formula R_2O_3 for the rare-earth oxides. In the case of cerium, which has two oxidation states, Mendeleev proposed to assign the formula Ce_2O_3 to the oxide of cerium in the lower oxidation state and CeO_2 to the higher oxide (Trifonov, 1966). Similar statements were repeated in his article "Concerning the Natural System of the Elements and Its Application in Determining the Properties

of Undiscovered Elements” (Mendeleev, 1871; Mendelejeff, 1870). These valency shifts also implied that the atomic weights used in his 1869 periodic table would have to be increased by a factor of 1.5:

$$AW_1(X) = AW_2(X) \times \frac{V_1(X)}{V_2(X)} = AW_2(X) \times \frac{3}{2}, \quad (15)$$

where use was made of Eq. (6). AW_1 and V_1 were taken to represent the new atomic weight values and valency numbers, respectively, while AW_2 and V_2 were used for the old values. Application of Eq. (15) to the set of seven elements with incorrect atomic weights leads to the following atomic weight values:

$$AW_1(\text{Er}) = AW_2(\text{Er}) \times \frac{V_1(\text{Er})}{V_2(\text{Er})} = 56 \times \frac{3}{1} = 168 \quad [178], \quad (16)$$

$$AW_1(\text{Y}) = AW_2(\text{Y}) \times \frac{V_1(\text{Y})}{V_2(\text{Y})} = 60 \times \frac{3}{2} = 90 \quad [92], \quad (17)$$

$$AW_1(\text{In}) = AW_2(\text{In}) \times \frac{V_1(\text{In})}{V_2(\text{In})} = 75.6 \times \frac{3}{2} = 113.4 \quad [113], \quad (18)$$

$$AW_1(\text{Ce}) = AW_2(\text{Ce}) \times \frac{V_1(\text{Ce})}{V_2(\text{Ce})} = 92 \times \frac{3}{2} = 138 \quad [138], \quad (19)$$

$$AW_1(\text{La}) = AW_2(\text{La}) \times \frac{V_1(\text{La})}{V_2(\text{La})} = 94 \times \frac{3}{2} = 141 \quad [140], \quad (20)$$

$$AW_1(\text{Di}) = AW_2(\text{Di}) \times \frac{V_1(\text{Di})}{V_2(\text{Di})} = 95 \times \frac{3}{2} = 142.5 \quad [140], \quad (21)$$

$$AW_1(\text{Th}) = AW_2(\text{Th}) \times \frac{V_1(\text{Th})}{V_2(\text{Th})} = 118 \times \frac{4}{2} = 236 \quad [231]. \quad (22)$$

The values in square brackets are those that were effectively used by Mendeleev in 1870. Notice that the atomic weight of erbium was tripled, while the atomic weight of thorium was doubled, just as in the case of uranium:

$$AW_1(\text{U}) = AW_2(\text{U}) \times \frac{V_1(\text{U})}{V_2(\text{U})} = 116 \times \frac{6}{3} = 232 \quad [240]. \quad (23)$$

After having changed the atomic weights of indium, uranium, and cerium, Mendeleev decided to check the correctness of the new values by determining the heat capacity of these elements (Trifonov, 1970).

3.4 Homologous Accommodation Methodology

When the atomic weight of an element X is changed, this logically implies a change in the position of X within the periodic table of elements. Thus, due to the atomic weight corrections of indium, uranium, cerium, lanthanum, didymium, yttrium, erbium, and thorium, all eight elements had to be removed from their usual place, and they had to be accommodated differently. As a consequence, Mendeleev switched from placing the rare-earth elements as a group in the periodic system to the individual placement of each element separately. The change in the atomic weight of indium (from 75.6 to 113) alluded to the fact that it might be accommodated in the position III-5, between cadmium (112) and tin (118). This position had formerly been occupied by uranium. Further support for the relocation of indium was provided by its atomic volume (15.5) which lay midway between the atomic volumes of cadmium (13.0) and tin (16.4). The accommodation of cerium went smoothly as Mendeleev had correctly determined its atomic weight and oxide formulae. Recall that cerium can exhibit two oxidation states (+III and +IV), making its placement in the fourth group very natural. On the basis of its higher degree of oxidation Mendeleev decided to place cerium in the titanium group, in place IV-6 (Figure 5). The placement of lanthanum, didymium and the other rare earths proved much more difficult. Mendeleev finally decided to locate yttrium in position III-4. Lanthanum seemed to fit in position III-6 and didymium was finally given the element coordinates V-6, although Mendeleev was still hesitating and playing with the idea of placing it with lanthanum in the position III-6. All rare-earth elements were thus placed as homologues of the other elements throughout the periods of the periodic system in the groups I-VIII according to a *homologous accommodation methodology*. We will subsequently denote this type of accommodation the *Mendeleev Method*. It must be noted however, that while the individual accommodation of the rare-earth elements had been an interesting step forward, this did not remove all problems. Mendeleev had always used "a web of analogies" in determining the positions of the chemical elements, but this methodology could no longer be applied in the case of the rare earths. The rare-earth elements exposed a serious weakness in Mendeleev's approach to solving the placement of elements in his periodic system. Mendeleev therefore remained very doubtful as to the new positions of the rare-earth elements. Nevertheless, Mendeleev held onto his original conception of the periodic law and he would not permit himself to allow exceptions for the rare-earth elements or any other element (Brooks, 2002).

Mendeleev drew five important conclusions from these rare-earth accommodations. The first one concerned the oxidation states of the rare-earth elements. Lanthanum, a typically trivalent element, was placed

in the third group (III-6). Cerium which could be trivalent as well as tetravalent was accommodated in the fourth group (IV-6). Due to the fact that didymium was located in the fifth group (V-6), Mendeleev presumed that this element could be pentavalent. In other words, the validity of the homologous accommodation methodology could be proven by demonstrating the pentavalent character of didymium. A second consequence of the rare-earth accommodation was the fact that 17 positions remained vacant between the elements cerium ($Ce = 138$) and tantalum ($Ta = 182$). Mendeleev predicted the existence of 17, still undiscovered, rare-earth elements on the basis of their being flanked by two rare earths, cerium, with an atomic weight of 138, and erbium, with an atomic weight of 178. Thirdly, Mendeleev intuitively recognized the existence of the *lanthanide contraction*, because of the close similarities in properties of the element pairs (molybdenum, tungsten), (niobium, tantalum), (antimony, bismuth), and (tin, lead). Fourthly, Mendeleev felt embarrassed by the fact that the seventh period was completely empty, and he put forward the hypothesis that the absence of an entire row of elements is due to their limited stability. Finally, Mendeleev also withdrew his previous claims about the analogy between the rare earths and the iron group. For instance, he observed that the elements of the cerium group are more difficult to reduce than those of the iron group. He also noticed that their normal oxides possess strongly basic properties and do not give characteristic compounds with ammonia and cyanide, in contrast to the iron group elements.

3.5 Mendeleev's Rare-Earth Research

Mendeleev finished writing his paper "Concerning the Natural System of the Elements and Its Application in Determining the Properties of Undiscovered Elements" on November 29, 1870 and he presented his work during a meeting of the Russian Chemical Society in early December 1870 (Mendeleev, 1871). With the predicted properties at hand, Mendeleev soon tried to find the unknown elements. The position of eka-silicon (IV-3) implied that its properties would lie midway between those of titanium and zirconium, and Mendeleev therefore thought it best to initiate his search for this element in the minerals of titanium and zirconium. Two days after the meeting of the Russian Chemical Society, on December 5, 1870, Mendeleev sent a petition to the rector of the University of St. Petersburg, K. F. Kessler, requesting him to contact the Mining Institute to ask them for samples of rare minerals he needed for his scientific work. Mendeleev stressed how especially important it was for him to obtain as large an amount of titanium minerals as possible, and specifically rutile (TiO_2), ilmenite ($FeTiO_3$), and also other minerals: zircon, orthite, or cerite and eschynite. The reason why Mendeleev asked for some specimens of rutile, ilmenite and zirconium is clear. But his

requests of orthite, cerite, and eschynite are less evident. Both cerite and eschynite are rich in cerium (and to a lesser degree also in lanthanum and yttrium). The mineral orthite, on the other hand, is not only abundant in cerium, it also contains substantial amounts of the other rare-earth elements. Obviously, Mendeleev was not only planning to discover the unknown eka-silicon, he also hoped to perform some experimental research on the rare earths in order to resolve their problematic accommodation, and to prove the validity of his homologous accommodation methodology.

Around the same time in July 1871, Mendeleev also started composing his German landmark article on the periodic law. It was translated into German by Felix Wreden and appeared in *Liebig's Annalen* in November 1871, symbolizing Mendeleev's last research paper on the periodic law (Mendelejeff, 1871). According to Brooks (2002), Mendeleev spent considerable time trying to separate the four known rare-earth elements over the course of about one year, but he only met with failure. The difficulty was compounded because two of these rare earths (didymium and erbium) later turned out to be mixtures of several elements. On December 20, 1871, Mendeleev decided to abandon all research on the rare-earth metals, and he set off on a gas project in search of the luminiferous ether (Gordin, 2004). Later he still published papers on the applications of the periodic law to the rare earths (Mendeleev, 1873; Mendelejeff, 1873a,b), on the corrected atomic weight of yttrium (Mendeleev, 1872), and on scandium (Mendeleev, 1881; Mendelejeff, 1881).

This was the end of Mendeleev's experimental research on the periodic law as well as his rare-earth investigations. Without a doubt, Mendeleev had grasped the essence of the difficult accommodation of the rare earths better than anyone else. His train of thought had been meticulously written down in a number of papers on the periodic law during the period 1869–1871. Mendeleev's landmark paper of 1871 in particular proved most valuable for the next generation of chemists who were on the verge of starting their own rare-earth studies (Section 4). But Mendeleev had not only circumscribed the rare-earth problem, he had also significantly aided in partly resolving the problem of their accommodation. Thus Mendeleev had corrected the atomic weight values of the rare-earth elements by increasing their valency from 2 to 3, and he had attempted to accommodate these metals on an individual basis according to a homologous placement. Yet, a definite proof as to the validity of this accommodation methodology was still lacking.

It can be mentioned here that another pioneer of the periodic system, the German Julius Lothar Meyer (1830–1895) did not list the rare earths in his first periodic table, because he was not convinced that the rare earths were genuine elements (van Spronsen, 1969). He also found that their atomic weights had not been determined with sufficient accuracy.

Later, he accepted the elemental nature of the rare earths and he tried to place them in the periodic table according to a homologous accommodation methodology, as Mendeleev did. In 1876, Meyer placed cerium, erbium, and yttrium in the boron group as trivalent elements, but he placed lanthanum in the column of the tetravalent elements.

4. BOHUSLAV BRAUNER AND SIR WILLIAM CROOKES

4.1 Brauner's Rare-Earth Research

The Czech chemist Bohuslav Brauner (1855–1935) (Figure 8) read Mendeleev's 1871 paper about six years later (Brauner, 1930; Druce, 1944). It made such an impression on him that he decided to refocus his experimental research on finding a solution for the question of the position of the rare earths in the periodic system. Brauner became the main defender of the periodic system in late nineteenth century. His rare-earth research has been of great importance in the further resolution of the so-called "rare-earth crisis," i.e., the problematic accommodation of the rare earths in the periodic system. It was especially Mendeleev's change of the atomic weights that had drawn Brauner's attention. It appears that although Brauner doubted the homogeneity (read: elementarity) of

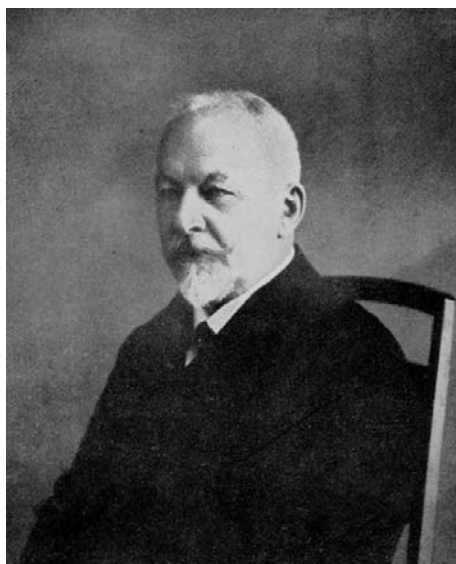


FIGURE 8 Bohuslav Brauner (1855–1935). Photo and permission from Edgar Fahs Smith Collection.

erbium and terbium, he was quite sure that lanthanum, cerium, and didymium were genuine rare-earth elements. Brauner noticed that not only Mendeleev, but also Julius Lothar Meyer (1830–1895) had struggled with the accommodation of these elements in the periodic table. Whereas Mendeleev placed cerium in the fourth group (vertical), he was skeptical about the position of lanthanum and didymium. Meyer, on the other hand, placed cerium in the third group, lanthanum in the fourth group, and didymium provisionally in the sixth group. However, later on he placed all three elements in the third group. In a 1878 paper on the atomic weight of beryllium, Brauner gave his first personal view on the location of the individual members of the rare earths and he proposed to place the cerium metals in the eighth series (horizontal) of the periodic system as follows (Brauner, 1878):

III-8	IV-8	V-8
La = 139	Ce = 141.6	Di = 147

Brauner started his rare-earth research in 1878 when he was working in the laboratory of Robert Bunsen (1811–1899) in Heidelberg (Brauner, 1930). At that time he was working with Bunsen's calorimeter in order to determine the heat capacity of uranium metal. He wanted to prove that the atomic weight of uranium was 240, as predicted by Mendeleev with the aid of his periodic system. After having completed this research topic, he quickly turned to the problem of the accommodation of the rare earths in the periodic table. Brauner was initially trying to apply the above mentioned *Mendeleev Method*. His research program therefore consisted of three steps. First, Brauner would attempt to optimize the currently used fractionation methods in order to isolate the rare-earth elements and to determine the homogeneity of the obtained fractions. These investigations should help in deciding whether the rare-earth elements were really elementary, or rather mixtures of elements. Once this was settled, Brauner planned to establish the atomic weight values of the pure rare earths in order to arrange them according to their increasing atomic weight. With the correct sequence of rare earths at hand, all elements could be placed in the periodic table. Thirdly and most importantly, Brauner realized that he had to investigate the higher oxides of some rare earths, if he was to verify whether the valencies of these elements were in agreement with the number of the group to which they belonged. So, if lanthanum, cerium, and didymium would be genuine elements, and if their sequence as outlined above would prove correct, then Brauner was still to demonstrate the tetravalency of cerium and the pentavalency of didymium.

Therefore, Brauner was highly interested in the higher oxides of didymium. Mosander, de Marignac, Hermann, and Zschiesche had all observed that didymium forms besides the grey oxide Di_2O_3 a higher

oxide of a brown color, but they were unable to determine its true composition. Several other chemists, including Meyer, Cleve, Nilson, and Mendeleev had synthesized this higher oxide, but they had all ascribed it different formulae, ranging from DiO_2 to Di_4O_9 . Brauner on the other hand thought (and obviously hoped) that it would be Di_2O_5 , thus pointing to the pentavalency of didymium. If that brown oxide would really prove to be Di_2O_5 , this would also confirm didymium's accommodation in position V-8 in the periodic table and this would put didymium next to the elements N, P, V, As, Nb, Sb, (Di), Ta, and Bi, which also give two oxides R_2O_3 and R_2O_5 . With didymium (Di) placed at the position V-8, one would have the following horizontal series of oxides: Cs_2O , Ba_2O_2 (= BaO) La_2O_3 , Ce_2O_4 (= CeO_2), Di_2O_5 , ...

Establishing the pentavalency of didymium proved however much more difficult than expected. One of the main problems that Brauner had to cope with can be termed the "oxide problem." From the very outset of his research, Brauner made the crucial distinction between oxides and peroxides, noting that from the peroxides alone, there was not yet sufficient ground to conclude on the valency and placement of the elements in the system. Brauner was thus alluding to the fact that the peroxide anion, O_2^{2-} , contains two oxygen atoms with a valency of -1 , instead of -2 . An example can help to clarify this. If one considers hydrogen peroxide (H_2O_2) to be an oxide instead of a peroxide, then this would also imply that hydrogen has a valency of $+2$ instead of the correct valency number $+1$. Thus, by confusing the two types of oxygen compounds, mistaking peroxides for oxides, chemists could draw erroneous conclusions about the valency of the elements. Consequently, Brauner was led to the question of how to discern peroxides from oxides. Apparently, Mendeleev had already discussed the oxygen problem in his papers on oxygen compounds and peroxides, but Brauner was unaware of these publications. Mendeleev had tried to clarify this issue by showing that the theoretical distinction between peroxides and oxides could also be applied in a practical manner. He explained that all oxygen compounds could be divided into two groups. The first group consisted of the actual peroxides, which did not form salts, while the second group consisted of oxides yielding salts with the aid of mineral acids. In other words, it was the ability to form salts which, according to Mendeleev's opinion, should be taken as the criterion for the existence of higher oxides.

The search for a good method for the synthesis of Di_2O_5 was initiated in Heidelberg, in the laboratory of Bunsen in 1879. Brauner calculated that it had to be theoretically possible to obtain about 109.5 g of Di_2O_5 from 100 g of Di_2O_3 . Brauner only managed to get a maximum of 103.55 g of Di_2O_5 . During the remainder of his stay in Heidelberg (until 1880), Brauner made one fruitless attempt after the other, trying to obtain the pentoxide by another method. He tried to act on Di_2O_3 with oxygen, hydrogen peroxide, barium peroxide, but without success.

Brauner returned to Prague in 1880 and he obtained his degree of Doctor of Philosophy during the course of that same year. In the summer of 1880, Brauner succeeded to prepare a higher oxide of didymium by thermally decomposing didymium oxalate. He thus obtained 106.90 g of a brown oxide out of 100 g of Di_2O_3 , whose color remained unchanged during subsequent calcinations. Brauner had to ascertain whether it was an oxide or a peroxide. He thus immediately proceeded with his investigations and attempted to convert the pentoxide into the corresponding salts.

Meanwhile, Brauner was searching for a foreign inorganic laboratory where he could continue his rare-earth research. He decided in the autumn of 1880 to go to the laboratory of Sir Henry Enfield Roscoe (1833–1915) in Owens College in Manchester. Roscoe was particularly noted for his research on vanadium and for the photochemical investigations he performed in collaboration with Bunsen in Heidelberg in 1852, where he studied the formation of hydrogen chloride from hydrogen and chlorine. Five years later, Roscoe was called to the chair of chemistry at Owens College in Manchester. In view of the fact that Roscoe and Bunsen became lifelong friends, it seems very probable that Bunsen advised Brauner to head for Manchester. It was during his sojourn in Owens College that Brauner succeeded in demonstrating the tetravalent character of cerium for the very first time. He dissolved the higher oxide of cerium in strong HF, and dried the product at 100°C , thus preparing the hydrated tetrafluoride $\text{CeF}_4 \cdot \text{H}_2\text{O}$. He also converted CeF_3 in CeO_2 and he used the hydrated dioxide for synthesizing the double salt $3\text{KF} \cdot 2\text{CeF}_4 \cdot 2\text{H}_2\text{O}$. Based on the existence of CeF_4 , Brauner was able to show that this element should be placed in group IV-8. It must be noted that Mendeleev came to the same conclusion on the basis of the composition CeO_2 of the higher oxide of cerium, but without conclusive experimental evidence. Brauner also continued his study of the oxide of didymium. He realized that he needed to convert it into salts if he was to prove the pentavalency of didymium. Brauner tried almost everything that came to his mind in order to form the pentafluoride, DiF_5 , as well as its double salts, but it was to no avail. His research was moreover clouded by the fact that didymium did not appear to be a genuine element, but rather a mixture of elements. Brauner discovered that even the most pure, crystalline products of didymium represented a mixture of two elements. He endeavored to purify his didymium samples by the repeated process of fractionated precipitations with oxalic acid, but he did not manage to obtain it in a pure, elementary state. Amidst all his confusing work on didymium, Brauner also attempted to redetermine the atomic weight of lanthanum, as well as to determine its place in the periodic system. After having verified the purity of his lanthanum specimens with the aid of spark spectroscopy, he ultimately concluded that there is no tetravalent lanthanum, but only trivalent lanthanum with an atomic weight of 138.27. Even though

Brauner had not yet succeeded in preparing the pentafluoride of didymium or its double salts with KF, the existence of Di_2O_5 had already been firmly established. He was very confident that it would soon turn out to be a real oxide, and he therefore thought the pentavalency of didymium a proven fact. Even though the results of his fractionated precipitations had made him question the complexity of didymium, he still believed it to be a genuine element with an atomic weight of 146.18. All these facts spoke in favor of the correctness of the Mendeleev method. Adhering to the individual placement of the rare-earth elements in successive groups, he came to the following accommodation which was in full compliance with the periodic law:

III-8	IV-8	V-8
La = 138.27	Ce = 141.60	Di = 146.18

Brauner published his first papers on the rare earths in 1881. On September 21, 1881, Brauner attended in Salzburg (Austria) the meeting of Naturalists and Doctors where he presented two papers on his rare-earth explorations and their accommodation in the periodic table. Both these papers were subsequently published in the proceedings of the Salzburg meeting (Brauner, 1881a,b) and they were also included in the *Berichte* in a summarized format (Brauner, 1882a). In December 1881, Brauner visited the Academy of Vienna where he delivered a lecture on his rare-earth research. His paper was published soon after in the journal *Monatshefte* (Brauner, 1882b) and translated into French, in *Le Moniteur Scientifique* (Brauner, 1882c). The results of his first investigations were also presented during a meeting of the Chemical Society in London on December 15, 1881, by Sir Henry Roscoe (Brauner, 1882d). Whilst Brauner's experiments were in progress, Nilson and Pettersson published a series of objections to the periodic system, one of which consisted in the statement that insurmountable difficulties presented themselves to the classification in the system of the numerous rare-earth elements (Akeroyd, 2003; Nilson and Pettersson, 1880). But Brauner objected that the results described in his paper proved that with the metals cerium, lanthanum, and didymium, this was not the case, but that, on the contrary, each of these metals was found to occupy its own characteristic position in the system. Brauner published a periodic table in which all rare-earth elements had been individually laid down; Sc in III-4, Y in III-6, La in III-8, Ce in IV-8, Di in V-8, Tb in VI-8, Er in V-9, and Yb in III-10 (Figure 9) (Brauner, 1882a). Brauner's belief in the pentavalency of didymium convinced him that all other rare-earth elements would be successfully accommodated in due time. He thus placed terbium in group VI and erbium in group V, even though their hexa- and pentavalency had not yet been demonstrated. Brauner was moreover under the impression that the

Das periodische System der Elemente.

Gruppen	I.	II.	III.	IV.	V.	VI.	VII.	VIII.
Reihen	(R ₂ X ₇) R ₂ O	(R ₂ X ₆) R ₂ O ₂	(R ₂ X ₅) R ₂ O ₂	RH ₄ R ₂ O ₄	RH ₃ R ₂ O ₄	RH ₂ R ₂ O ₅	RH R ₂ O ₇	(R ₂ H) (R ₂ O ₂) } Verbindungs- formen
1.	1 Li							
2.	Li 7	Be 9	B 11	C 12	N 14	O 16	F 19	
3.	23 Na	24 Mg	27 Al	28 Si	31 P	32 S	35.5 Cl	
4.	K 39	Ca 40	Sc 44	Ti 48	V 51	Cr 52	Mn 55	Fe 56, Co 59, Ni 59, Cu 63
5.	(63 Cu)	65 Zn	69 Ga	72 ?	75 As	78 Se	80 Br	
6.	Rb 85	Sr 87	Y 89	Zr 90	Nb 94	Mo 96	? 100	Ru 104, Rh 104, Pd 106, Ag 108
7.	(108 Ag)	112 Cd	114 In	118 Sn	120 Sb	126 Te	127 J	
8.	Cs 133	Ba 137	La 139	Ce 141.6	Di 146.7	Tb 148.8 ?	Sm 150 ?	? 152, ? 153, ? 154, ? 156
9.	150 ?	158 ?	? 159 Y _a ?	162 ?	166 Er?	167 ?	? 169 Tm?	
10.	? 170	? 172	Yb 173	? 177	Ta 183	W 184	? 190	Os 193 ¹⁾ , Jr 193, Pt 195, Au 197
11.	(197 Au)	200 Hg	204 Tl	207 Pb	210 Bi	? 214 Ng?	219 ?	
12.	? 221	? 225	? 230	Th 234	? 237	U 240	? 244	

¹⁾ Aus der Dampfdichte des Os O₄ (Deville und Debray, Ann. chim. phys. (3) 56, 476) ergibt sich die Zahl 193 als Atomgewicht des Osmiums.

FIGURE 9 Brauner's periodic table of 1882 with a homologous accommodation of the rare-earth elements (reproduced from Brauner, 1882a).

rare earths consisted of 19 elements, beginning with lanthanum in III-8 and ending with ytterbium in III-10. Thirteen of these elements were still unknown, according to Brauner's opinion. It therefore appears that Brauner did not accept the discoveries of samarium (by Delafontaine in 1878 and by Lecoq de Boisbaudran in 1879), holmium (by Delafontaine and Soret in 1878 and by Cleve in 1879), thulium (by Cleve in 1879), and gadolinium (by Marignac and Soret in 1880).

Brauner left Manchester during the summer of 1882 and returned to Prague where he was appointed lecturer in chemistry at Charles University. Despite Brauner's laborious efforts in the field of the rare earths, in particular his quest for the salts of pentavalent didymium, most of his results remained disappointing. The reason for this was twofold. First, Di_2O_5 appeared to be a peroxide after all, given that it could not be converted into salts and double salts. Secondly, the evidence for the complex character of didymium was mounting up. It turned out that didymium was not a genuine rare-earth element but rather a mixture of two or more rare earths.

Brauner came very close to the discovery of praseodymium and neodymium. He found that didymium could be separated in two fractions, which he called $\text{Di}\alpha$ and $\text{Di}\beta$. The fraction containing $\text{Di}\beta$ gave a black higher oxide and salts of green color. In the fraction $\text{Di}\alpha$, which gave pink-violet salts and a higher oxide of light brown shade, several absorption lines were absent, which were intensified in the $\text{Di}\beta$ fraction. Brauner had discussed this in the spring of 1882 with Roscoe and intended to call this new element "bunsenium," in honor of Robert Bunsen. At that time appeared a communication of Cleve from Upsala (Sweden), in which this great authority in rare earths denied that didymium would be a mixture rather than a single element. Brauner was convinced that Cleve was wrong, but he decided to wait in order to be able to contradict him after having thoroughly worked out the problem. Unfortunately he postponed the publication of his work too long and finally, in 1885, Carl Auer von Welsbach in Vienna (Austria) succeeded in isolating two new elements from didymium compounds, which he called praseodymium and neodymium and which were in fact identical to the $\text{Di}\beta$ and $\text{Di}\alpha$ fractions of Brauner (1930). Brauner later on blamed von Welsbach of not having mentioned his earlier work on didymium.

In 1884, Brauner presumed that terbium and erbium would not fit into the positions VI-8 and V-9, because didymium did not fit in V-8. All his attempts to obtain the rare earths in a higher stage of oxidation had come to nothing. It thus seemed as if all rare-earth elements were trivalent (with the exception of tetravalent cerium). Brauner therefore wrote that one had to be ready to accept a number of anomalies within the eighth and ninth series of the periodic system, which could not be found in other rows. In view of the fact that the rare-earth elements were not analogous to the alkaline metals and alkaline earths in groups I and II, and due to the fact that they did not exhibit any similarity with the members of groups V, VI,

VII, and VIII (as a consequence of their failing to display valencies higher than three), Brauner had to conclude that the individual placement of the rare-earth elements (i.e., Mendeleev methodology) had failed. Trifonov (1963) explained this anomaly by stating that a change in the properties of the rare-earth elements along the horizontal did not agree with the change in properties along the vertical. This “horizontal anomaly” got of course more and more pronounced as the years passed and more rare-earth elements were brought to light. Unfortunately, Brauner was blinded by the *Mendeleev Method*, and he kept searching for new experimental evidence that would speak in favor of the individual accommodation of the rare earths. Only in 1902, after 25 years of fruitless endeavors, did Brauner change his view and did he propose an alternative placement for the rare-earth elements (see Section 4.3).

Brauner turned to the experimental determination of the atomic weights of the rare-earth elements. He published at least ten papers on lanthanum, cerium, praseodymium and neodymium (or didymium) during the period 1882–1903, with emphasis on the atomic weights of these elements (Brauner, 1882e, 1883, 1885a,b, 1891, 1898a,b, 1901a,b, 1903a,b; Brauner and Batek, 1903; Brauner and Pavlicek, 1901, 1902). These determinations fitted in with Brauner’s life’s aim to fix the position of the so-called *rare elements* and especially those of the rare earths in Mendeleev’s system. Indeed, by having the exact atomic weights in one’s possession, all rare earths could be ordered sequentially according to their increasing atomic weight. We cannot prevent ourselves however from raising some questions as to the usefulness of Brauner’s new research program. The difficulty of accommodating the rare earths was not caused by an erroneous, out of order sequence of rare earths, but rather by the fact that these elements did not exhibit higher valencies. It was their pronounced similarity and unique nature that was undermining the Mendeleev method. Brauner also investigated the atomic weight of tellurium, which was another anomaly in Mendeleev’s system, since its atomic weight of 128 was higher than that of iodine (127), although everyone agreed that tellurium was to *precede* iodine in the periodic table on the basis of its chemical properties. In 1888, Brauner also advocated the adoption of oxygen instead of hydrogen as the standard for calculating atomic weights (Brauner, 1888a,b). When, during that same period, a whole new group of elements was discovered (the noble or inert gases), Brauner was at first unwilling to recognize these as genuine elements (Brauner, 1896). He thus started some investigations of his own and went so far as to propose that helium might be an allotrope of hydrogen. He also put forward the claim that argon was triatomic nitrogen. As mentioned before, Brauner never lost faith in the success of the *Mendeleev Method* for accommodating the rare earths during the period 1884–1902. Thus in 1895, for example, Brauner wrote a short paper about cerium for *Chemical*

News in which he stated the following question (Brauner, 1895): “Where is there a place in the periodic system for the numberless rare-earth metals (true chemical asteroids) the atomic weight of which varies between 140 and 170?,” and he wrote:

Beryllium, Be = 9, is undoubtedly a divalent rare-earth element, with the oxide RO, as was shown by the author in 1878, 1881, and 1882. Then come the trivalent elements: scandium, Sc = 44; yttrium, Y = 89; lanthanum, La = 138; and ytterbium, Yb = 173, with the oxides, R₂O₃. Cerium, Ce = 140, forms a transition to the tetravalent earth elements, being both trivalent and tetravalent, with the oxides R₂O₃ and R₂O₄. Thorium, Th = 232, is only tetravalent with the oxide R₂O₄, though a lower oxide, Th₂O₃, may exist, corresponding to the lower oxides of niobium and tantalum. At the present limit of the periodic system and outside it rare-earth elements may be expected, possessing the oxides R₂O₅, R₂O₆, and perhaps even R₂O₇ and R₂O₈, with distinct basic properties. Very probably the atomic weight of either neodymium (R''' = 140.5) or praseodymium (R''' = 143.5) will be 235 and the oxide R₂O₅, or 282 and the oxide R₂O₆ (a true Neptune of the periodic system), for only one of both constituents of the old didymium, more probably praseodymium, yielding salts of the higher oxide, which seems to be as unstable as is CeCl₄ [. . .], will find its place in the eighth series next to cerium.

Brauner clearly held on to his conviction that all rare-earth elements could be accommodated on an individual basis in the different groups of the periodic table. Brauner therefore concluded that the valency of the rare-earth elements increased with increasing atomic weight, so that the periodicity was not undermined by the presence of the rare earths. In 1898, he repeated his claim that the pure oxides of praseodymium and neodymium would probably be found to have the formulae Pr₂O₅ and Nd₂O₆, so that the eighth series of the periodic system would assume the following form (Brauner, 1898b):

I-8	II-8	III-8	IV-8	V-8	VI-8
Cs = 133	Ba = 137.4	La = 138.2	Ce = 139.7	Pr = 141	Nd = 143.6

Despite Brauner's belief in the validity of the Mendeleev methodology, he also had to admit that he had not yet succeeded in resolving the rare-earth crisis. Thus Brauner wrote in 1901 with reference to praseodymium that its maximum valency was tetravalent, like that of cerium but that no place had been found in the periodic table for an element possessing the physical and chemical properties of praseodymium and its compounds (Brauner, 1901b). He also admitted that the difficulties of finding a place for neodymium in the periodic table were even greater than in the case of praseodymium.

At the beginning of the twentieth century, only scandium, yttrium, lanthanum, and cerium had been accommodated in the periodic system with some certainty, but all other rare earths remained homeless. As a result, more and more chemists were starting to question the strength of the periodic table. They were losing faith in the universality and the naturalness of the periodic law, and became skeptical about the dictum that all the properties of the chemical elements are periodic functions of their atomic weights. Some of them, like Nilson and Pettersson, put forward their doubts and uncertainties. The French chemist Grégoire Wyruboff (1843–1913) recognized that the periodic system was a very interesting and highly ingenious table of analogies and dissimilarities between the simple bodies, but he also noticed some problems, as for example the accommodation of the rare earths. Since the laws of nature admitted no exceptions, Wyruboff felt somewhat surprised that the periodic law was accepted (Wyruboff, 1896). He concluded that there was nothing which merits the name of law or system and claimed that the periodic law had to be rejected as a whole. He downgraded Mendeleev's system to nothing more than a *catalogue raisonné* of the elements. Wyruboff gave the following critique about the accommodation of the rare earths in the periodic table (Wyruboff, 1896):

Prof. Mendeleeff admits for the three cerite metals La = 138, Ce = 140, and Di = 192. He required this succession, since cerium yielding a higher oxide should not be placed upon the ascending branch of the curve before lanthanum. But Marignac, Bunsen, Jørgensen, Rammelsberg, and Wolf have found Ce = 138, with deviations not exceeding one or two units of the first decimal. Prof. Brauner alone has obtained 140 by the calcinations of the sulfate, a process absolutely defective, as Schützenberger has recently pointed out. As for lanthanum, the majority of recent determinations lead to a figure very near 138.5. Mendeleeff, to give more symmetry to his curve, selected that which presents the lowest figure. As for didymium, it is especially embarrassing for the periodic classification. In 1886 it was split up by Auer von Welsbach into neodymium (Nd = 141) and praseodymium (Pr = 143.6). Now, this latter gives on calcination an oxide higher than R_2O_3 , whence neodymium ought to be placed on the same horizontal line as lanthanum. This part of the curve would then become quite irregular, whence Mendeleeff retains in his table of 1889 the old didymium, contenting himself with asserting that the two new metals ought not to be simple bodies, and that there is no occasion to occupy ourselves with them. The arbitrary selection of oxides and of atomic weights is the gravest critique which we are justified in addressing to Prof. Mendeleeff.

In spite of the somewhat exaggerated character of Wyruboff's sharp critique, there was some truth in his statement that Mendeleev's disbelief

in the elementarity of praseodymium and neodymium was too easy an answer. As a matter of fact, it appears as if Mendeleev was starting to doubt the validity of his system as well. This was due to a number of reasons. First, there had been the discovery of the noble gases which had severely threatened the periodic law, until Errera and Ramsay, independently of each other, put forward the hypothesis to accommodate them into a whole new group of elements (group VIII or 0). Secondly, the inversed placements of tellurium and iodine; argon and potassium; and cobalt and nickel remained a mystery and thirdly, the rare-earth crisis was only growing worse. It thus seems as if Mendeleev preferred to look away from these threats, and he clearly withdrew himself more and more from the ongoing discussions. Trifonov (1970) very well described this change in Mendeleev's attitude towards the rare earths:

If in the first stage Mendeleev presumed the existence of a whole series of undiscovered rare-earth elements on the basis of the periodic system, in the second stage of development a majority of these elements were actually discovered and they were generally trivalent. The problem about their position in the table was, therefore, unprecedentedly serious. If in the first stage Mendeleev was actively engaged in the problem of the position of rare-earth elements in the system, discussing different versions for the position of different elements, then in the second stage his views were characterized by maximum caution.

The crux of the rare-earth problem was obvious. Despite all experimental attempts of Brauner and other chemists, the rare-earth elements refused to exhibit valencies higher than three. This implied that their properties were not regularly changing with ascending atomic weight, as was the case with all other members. The Mendeleev methodology for accommodating the rare earths had failed and nobody knew what alternative to propose. Their pronounced similarity baffled the whole chemical community, and everyone wondered how these resemblances could be explained, and whether this explanation could help in solving the problematic accommodation of the rare earths in the periodic table.

It should be mentioned here that there had been a close contact between Mendeleev and Brauner via correspondence (Brauner, 1930; Kedrov and Chentsova, 1955). The correspondence between Brauner and Mendeleev is of great historical interest. Its content clearly demonstrates how these two chemists mutually influenced each other during the period 1881–1907, and it provides us with new insights into Brauner's rare-earth research. Luckily, Mendeleev was a very orderly man, who carefully maintained even the most minor notes and letters which he received from others, especially when the content of these letters was related to his scientific activities. Mendeleev brought all these letters

together in chronological order and he carefully pasted them in large albums, which are currently stored in the Mendeleev Museum and Archive in his university apartment in St. Petersburg. Most of Brauner's letters were as such pasted down in Mendeleev's albums. The first part of their correspondence, covering the period 1881–1888, consisted of more than 20 letters. One can conclude on the basis of Mendeleev's response that Brauner had written Mendeleev in his first letter about his wish to further investigate the rare-earth elements, pointing out the importance of the higher oxide of didymium. Mendeleev's cordial reply was dated February 8, 1881 (according to the Gregorian calendar). Mendeleev also wrote of the rare earths and their problematic accommodation in the periodic table. He was happy to offer Brauner the following advice (Brauner, 1930):

If you have begun to work on rare elements, allow me to direct your attention to the fact, that the solution of all is to be looked for in didymium, which is little known and even this little not exact. It is didymium which is the most interesting. Seven years ago I worked at it, but I have not published anything; yet I think, judging from the number of the bodies, that in its higher form of oxidation didymium gives salts, and that the ordinary compounds of didymium are mixtures, that they are not pure. If you like I shall send you the oxide of didymium I possess (may be I have about 80 g) for your work. I have also much of zircon, the mineral from Ural, which I can offer you if it will help your research. I have little of gadolinites; yet my determination of the atomic weight of yttrium was proved by later works.

Mendeleev ended his letter by repeating once more that he was delighted to know that the periodic system had got a defender like Brauner. Brauner was particularly pleased by Mendeleev's letter because it confirmed his own views about the rare-earth elements. Brauner gladly accepted Mendeleev's offer to send him samples of didymium oxide and some other rare-earth specimens. He reported to him that he had been experimenting with the higher oxide of didymium since 1878 and meticulously described his experimental endeavors of the last four years. In his letter of February 23, 1881, Mendeleev agreed that the higher oxide of didymium was especially important and confessed that he had himself thought of it and directed his research to this problem.

4.2 Meta-Elements

Bohuslav Brauner had approached the rare-earth crisis from a traditional chemical point of view. Both the search for higher valencies and complicated atomic weight determinations had been central to his research during the last quarter of the nineteenth century, but neither of these methodologies allowed to prove the validity of the homologous accommodation. Brauner's adherence to the *Mendeleev method* had led him to a

dead end and a change was called for. Not the classical techniques of chemical analysis, but the novel methods of spectroscopic investigation came to the rescue of the rare-earth specialists. Bunsen and Kirchhoff had built their first spectroscope in 1859. The usefulness of this instrument was established a few months later, when the two German scientists discovered a novel element, cesium. Another alkaline metal, rubidium, was discovered by Bunsen in 1861, and Sir William Crookes (1832–1919, Figure 10) spoke about the existence of a new element, which he named thallium during that same year. Reich and Richter discovered indium in 1863 and Lecoq de Boisbaudran tracked down Mendeleev's eka-aluminium (i.e., gallium) in 1886. Throughout these 30 years, spectroscopic research had yielded rich rewards, and many new elements had been characterized by their unique spectrum.

During his research on electrical discharges in cathode ray tubes in the late 1870s, Sir William Crookes noticed that a large number of substances emitted phosphorescent light when they were exposed to a discharge by means of an induction coil in a highly exhausted vacuum tube (Brock, 2008). Some substances emitted light of the greatest intensity, while others showed only a faint phosphorescence. Still others showed no sign of phosphorescence at all. He found that diamond had the most brilliant

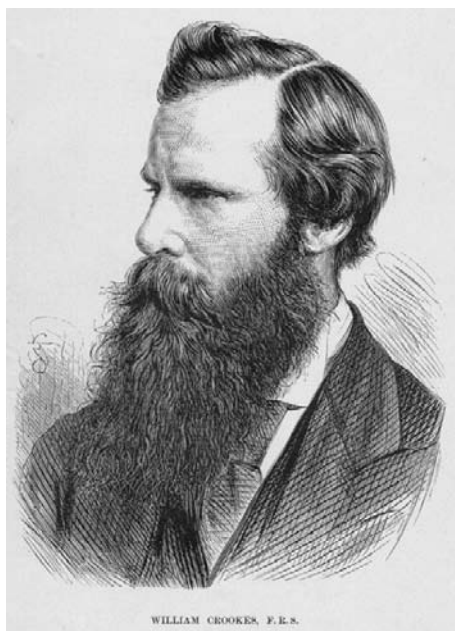


FIGURE 10 Sir William Crookes (1832–1919). Photo and permission from Edgar Fahs Smith Collection.

phosphorescence intensity, followed by ruby. When this phosphorescent light was examined with the aid of a spectroscope, it turned out that most bodies gave out continuous spectra, but sometimes the spectrum of the phosphorescent light was discontinuous, and a number of beautifully colored spectrum lines or bands appeared on the dark background. Crookes' attention in the early 1880s was directed towards these latter bodies, and he called the study of their spectra *radiant matter spectroscopy* (Crookes, 1879, 1884a,b; DeKosky, 1973). Crookes was convinced of the possibility of correlating the observed bands with known and unknown elements, just as he had been able to discover a new element, thallium, during his spectroscopic researches in 1861. He started to investigate the spectra of the rare earths (Crookes, 1884a,b, 1886f,g,h,i,j, 1889b). After Crookes had characterized the spectra of yttrium and samarium, his attention was drawn by a mysterious orange spectral line. The anomalous line did not come from yttrium or samarium, and Crookes therefore postulated the existence of a new element. This was a bold hypothesis. Chemical elements were usually characterized by a unique spectrum of bands and lines, but this time Crookes claimed that he had demonstrated the existence of a new element, based on a single spectral line.

The repeated chemical fractionations of yttrium resulted in mysterious changes in its spectrum. Finally, Crookes was able to obtain a number of fractions and each fraction gave a spectrum which corresponded with one line of the spectrum of yttrium. In analogy with the orange line, Crookes considered this as an indication of the existence of new elements. Yttrium did no longer meet the criteria of homogeneity and elementarity and it appeared to consist of seven constituents (Crookes, 1886k). Crookes speculated that all chemical elements could be split into a number of constituents by advanced fractionations. Because this hypothesis was steadily increasing the number of elements, Crookes developed his famous concept of *meta-elements* (Crookes, 1888a,b,c,d,e). According to Crookes, the term *element* had to be replaced by the term *elemental group*. Each element was made up of a collection of *meta-elements* (or *elementoids*). These meta-elements differed slightly from each other in their atomic weight, chemical and physical properties. Crookes had thus succeeded in splitting the element yttrium in seven meta-elements. He stated that the atomic weight which was ascribed to yttrium merely represented a mean value around which the actual weights of the individual atoms of the "element" range within certain limits. According to Crookes chemical fractionation was the method par excellence to split an elemental group in its meta-elements (Crookes, 1886a,b,c,d,e).

Crookes' radiant matter spectroscopic research on the rare earths seemed to point towards the complexity of the elements. It thus provided an excellent empirical basis for his influential lecture "On the nature and the probable, or at least possible, origin of the so called elements" which

he presented during his presidential address before the Chemical Section of the British Association on September 2, 1886 (Crookes, 1886b). The epistemological nature of the elements was considered one of the greatest riddles for the chemical sciences throughout the nineteenth century. Many chemists had attempted to unravel the secret composition of the so-called elements, but all had been in vain. Since the chemical revolution in 1789 and the pioneering research of Antoine Laurent Lavoisier (1743–1794), chemical elements had been defined as the endpoint of chemical analysis. But according to Crookes' opinion, all these traditional operational definitions were worthless. There was a complete uncertainty about the elementary character of the chemical elements, and nothing prevented chemists from putting forward the hypothesis that the chemical elements might turn out to be composite bodies after all. As a matter of fact, many renowned chemists and physicists, e.g., Faraday, Stokes and Graham had played with the idea of complex elements. Crookes started his lecture by mentioning the most famous hypothesis concerning the ultimate constituents of the elements which had been suggested by Prout in 1816. According to Prout's hypothesis, all chemical elements were complex aggregates of hydrogen since their atomic weights were all approximate multiples of the atomic weight of hydrogen. A more complete agreement between the hypothetical (theoretical) and practical atomic weights could be obtained by assuming that the *protyle* (i.e., a hypothetical primitive substance from which the chemical elements were supposed to have been formed) was not hydrogen, but a half or fourth part of the hydrogen atom or another simple substance of low atomic weight. Although Crookes had repeatedly spoken about the possible complexity of the elements, he nevertheless had to admit that not even the highest temperatures or the most powerful electric currents had been able to dissociate the chemical elements.

Crookes was also convinced that the chemical elements had evolved out of some primordial and rudimentary form of matter via a *process of genesis* (Crookes, 1887, 1889a). Laplace's cosmological theories about the evolution of the heavenly bodies as well as Darwin's recently published work "On the Origin of Species" inspired Crookes to compare the periodic kingdom of elements with the organic world of fauna and flora, a comparison first made by the astrophysicist Norman Lockyer (1836–1920) (Leone and Robotti, 2000, 2003). Both kingdoms were seen as the outcome of a process of evolutionary development which had been subjected to the laws of nature. The concerted action of a struggle for existence and the survival of the fittest had determined which elements survived and which became extinct. Crookes noticed that both elements and animals display species that are common and species that are rare. The analogy could not be pushed too far however, since there was no fossil record of extinct elements. The mineral kingdom, on the other hand, pointed towards the genesis of the elements as well. The heterogenous distribution of the

elements in the earth's crust had puzzled both geologists and chemists. An explanation for the simultaneous occurrence of sodium and chlorine, or lead and sulfur (as sodium chloride and lead sulfide) could be given on the basis of their opposite chemical affinities. But Crookes also mentioned the grouped occurrence of strongly related elements that showed absolutely no affinity for each other, such as nickel and cobalt, the two platinum groups, and the rare-earth elements. It appeared more logical to claim that these elements had been formed under nearly identical circumstances during the genesis of the elements.

This elemental evolution, according to Crookes' opinion, began at extremely high temperatures and ultra gaseous conditions. Atoms had not yet formed in the beginning of time, and only the *protyle* permeated throughout the universe. But as time progressed, the *protyle* cooled down and all rudimentary matter started to granulate until the first atoms were formed. This condensation process could result in atoms of all possible weights, but since hydrogen (or perhaps helium) was the simplest element from a structural point of view, this element was created first during the agglomeration of the *protyle*. Soon after, as the temperature had lowered a little more, a second element of greater atomic weight was formed. As a result, each element evolved from the *protyle* at a well defined temperature. The longer this temperature of formation was sustained (i.e., the slower the cooling rate at that region of temperatures), the sharper defined the resulting element. For instance, hydrogen, oxygen, and other clear cut elements had all been formed during these long periods of slow cooling. At irregular rates of cooling, on the other hand, less defined elements were produced. A stage of rapid cooling thus caused the formation of groups of closely related elements, such as the transition metal triads with very similar atomic weights. At certain times during the evolutionary history of the elements, the temperature dropped even faster and the set of rare-earth elements was formed. This evolutionary process did not only determine the birth of each element, it also established their atomic weights, affinities and chemical positions in the periodic table. Crookes thought the cooling process had never been slow enough to create elements with atoms of identical weight, and postulated that the atomic weights merely represented a mean value around which the actual atomic weights of the atoms varied within certain narrow limits.

All these statements seemed of course very bold and hypothetical at first sight, but Crookes knew he could provide his daring and provocative thesis about the complexity and genesis of the elements with a scientific underpinning, thanks to his rare-earth research. In 1886 Crookes drew up an alternative representation of the periodic table, his *Mighty Pendulum* (Figure 11), in which he modeled a possible scenario of elementary evolution (Crookes, 1886). This format was inspired by Reynolds' "Note on a Method of Illustrating the Periodic Law" (Reynolds, 1886). In order to fully grasp the meaning of this new table layout, it is constructive to

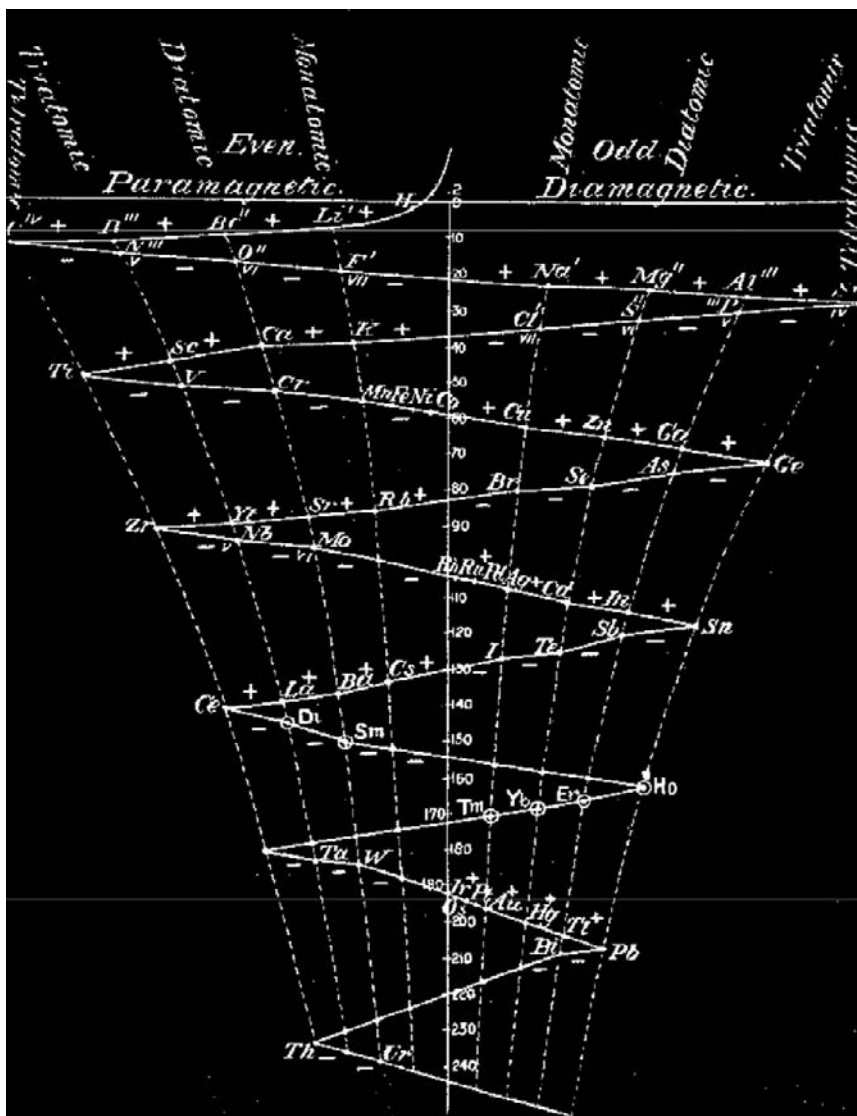


FIGURE 11 Crookes' mighty pendulum of 1886. Reproduced from Crookes (1886l).

consider the first period of the periodic table, {Li, Be, B, C, N, O, F}. The properties of the elements change step by step according to a gradual transition from lithium to fluorine. The first element of a given period therefore stands in sharp contrast with the last one. The next step from fluorine to sodium moreover happens *per saltum* according to an abrupt transition since sodium is again an alkaline metal. A point of mean

variation can consequently be found in the middle of each period with carbon and silicon as representatives of the class of the so-called *meso-elements*. The triad of elements to the right of a given *meso-element* consists of electropositive members, while the elements to the left are all electronegative. The elements at opposite sides of a *meso-element* form pairs of elements with analogous valencies:

Li = 7	Be = 9.4	B = 11	C = 12	N = 14	O = 16	F = 19	
<i>Valency</i>	1	2	3	4	3	2	1

All this could be represented by some sort of zigzag curve, but Crookes slightly altered Reynolds' diagram and he presented the periodic law as a *mighty pendulum* with the *meso-elements*—carbon, silicon, titanium, germanium, etc.—situated at the apex of each pendulous swing. In between these tetratomic elements lay the monatomic, diatomic and triatomic elements with valencies 1, 2, and 3 respectively. All elements could be uniquely determined by the Cartesian coordinate system in which the abscissa denoted the combining capacity of the element in question, whilst the ordinate represented its atomic weight. Gaps alluded to the possible existence of undiscovered elements. Thus the elemental evolution started at the top of Crookes' mighty pendulum and ended with the formation of thorium and uranium, at the bottom of the diagram. The zigzag curve moreover suggested the presence of two forces, acting simultaneously on the original *protyle* in both the vertical and the horizontal direction. The first creative force represented time and was tied up with a sinking of the temperature from the dissociation point of hydrogen down to the dissociation point of the heaviest elements. The horizontal force periodically oscillated from left to right and was connected with electricity, the vertical axis representing neutrality. The further removed from this neutral center line, the greater the atomicity of the elements concerned. Paramagnetic elements were formed at the left hand side of the center line; diamagnetic elements on the right hand side. On approaching the center line, electronegative elements were formed. Electropositive elements, conversely, came into being on the retreating halves of the pendulous swing. In 1888, Crookes decided to alter the *mighty pendulum* to his *vis generatrix* by attempting to project the plane pendulum into three dimensions and considered a figure of eight or lemniscate the best representation of his zigzag diagram since it allowed the curve to pass twice through the neutral point in each cycle (Figure 12) (Crookes, 1888a, 1898). Crookes' viewpoints threw considerable light upon the outlandish nature of the transition metals, and the concept of meta-elements greatly facilitated the development of alternative accommodation methodologies for the rare-earth elements (*vide infra*).

Neither Crookes' *mighty pendulum* (Crookes, 1886l) nor his *vis generatrix* (Crookes, 1888a, 1898) had offered an alternative accommodation for

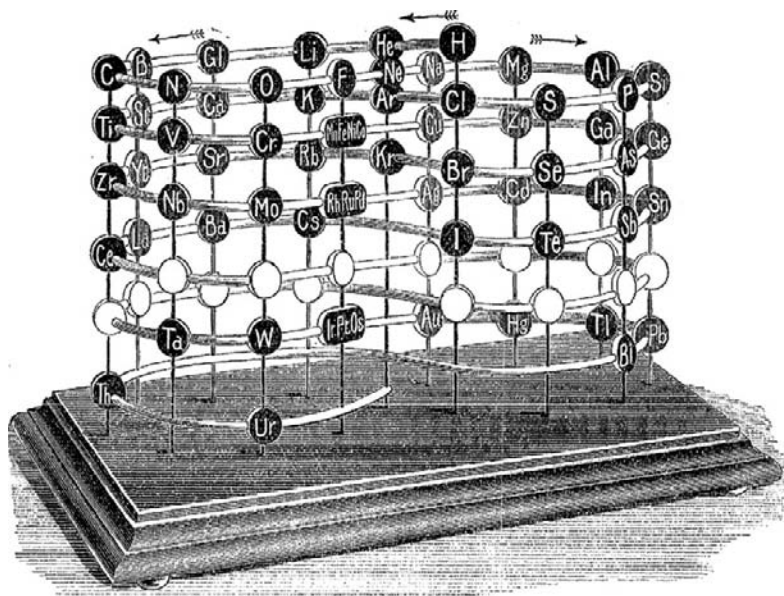


FIGURE 12 Model of Crookes' vis generatrix of 1898—built by his assistant, Gardiner. The vertical scale represents the atomic weight of the elements from H = 1 to Ur = 239. Missing elements are represented by a white circle. Similar elements appear underneath each other (reproduced from Crookes, 1898).

the set of chemical elements. Both systems differed from Mendeleev's 1871 table in their peculiar two- and three-dimensional layout, but the placement of the elements in primary and secondary groups, short and long periods, odd and even series, had remained the same. Crookes' most valuable contribution to the development of the periodic system consisted in providing a reasonable explanation of the periodic law by means of its relation with the unity of matter and inorganic evolution. The peculiar accommodation of the transition metals, however, needs some further consideration. Crookes had located the triplets (iron, nickel, cobalt), (rhodium, ruthenium, palladium), and (osmium, iridium, platinum) as three independent groups near the center line of his mighty pendulum (Figure 11). When the pretzel-shaped model of the periodic law was drawn up two years later, Crookes did not hesitate to cluster the transition metals once again as three triads near the neutral axis (Figure 12). He called these elements *interperiodic*, both because their atomic weights excluded them from the small periods into which the other elements fell, and because their chemical relations with certain members of the adjacent periods showed that they were probably interperiodic in the sense of being transitional. Crookes' interperiodic accommodation methodology was therefore identical with the one advocated by Mendeleev in his paper

of 1871. It must moreover be observed that Mendeleev had chosen to overcrowd the boxes of his eighth group with sets of four elements each, instead of accommodating the transition elements in four different boxes. Thus one finds in his 1871 table, at the end of the fourth series, a tetrad of elements (iron, cobalt, nickel, and copper), occupying just one position, in complete analogy with Crookes' collective grouping of these metals between manganese and copper in his zigzag curve.

Both Mendeleev and Crookes were thus accused of violating the concept of single occupancy, by placing more than one element in the same position of the periodic table. One recalls however that Crookes had offered a way out in his papers on the complexity of the elements, given the fact that he proclaimed that the members of each triplet had to be regarded as modifications of one single form of matter. He did not consider the closely related elements platinum, osmium, and iridium to be genuine elements, but rather looked upon them as constituents of one single transition element. According to Crookes' terminology, platinum, osmium, and iridium had to be regarded as meta-elements of one elemental group. Consequently, there was no more a violation of the concept of single occupancy as with all other elements (i.e., elemental groups), since Crookes was accommodating just one elemental group in the case VIII-10. Would it not be justified according to this line of reasoning to consider the even more closely allied rare-earth elements as meta-elements of one elemental group? Would it not be tempting to collectively cluster these trivalent elements in one case of the periodic system, according to a so-called *intraproductic accommodation methodology*? Quite surprisingly, Crookes did not adhere to this method and he preferred to place the rare earths as ordinary elements throughout the higher periods of his mighty pendulum. In spite of this, Crookes had encircled most of the rare-earth elements, meaning that they were out of place, owing to their atomic weights not having been correctly determined. He also thought that several rare-earth elements still had to be discovered. Crookes did not put his ideas into action and decided not to include the rare-earth elements in his *vis generatrix* (with the exception of lanthanum and cerium), but his proposal would soon be taken up by the Bohuslav Brauner, who was still struggling with the problematic accommodation of the rare earths.

4.3 Asteriod Hypothesis

In a lecture at the 11th Congress of Russian Natural Scientists in St. Petersburg in 1902, Brauner proposed a completely different accommodation methodology for the rare earths according to which all rare earths had to be put in the fourth group. Brauner termed this idea the *asteroid hypothesis*, because just as the entire group of asteroids occupies an

orbit in the solar system on which normally one single planet would be expected to move, exactly in the same way does the entire group of elements known as the rare earths occupy one single place in the system which would have been ordinarily occupied by a single element (Brauner, 1902). According to Brauner's opinion, chemists tended more and more to the idea that chemical elements were composed of some primordial matter. He thus imagined that the condensation of the *Ursubstanz* (i.e., primary matter) had not proceeded as far during the formation of the rare earths as in the other elements and concluded that it would be best to accommodate them in one and the same place in the fourth group and eighth row of the periodic system, where only cerium had hitherto been located. He provided his hypothesis with a more solid ground on the basis of the pronounced similarities among the rare earths and the fact that they all exhibited approximately equal atomic volumes in the free state. The eighth row would therefore proceed as shown in Figure 13.

Brauner naturally wondered whether one still had to presuppose the existence of analogues of niobium, molybdenum, manganese, and the three platinum metals in V-8, VI-8, VII-8, and VIII-8 respectively, and he also doubted whether the ninth row would ever be filled by seven more heavy elements. He preferred to consider the rare earths as forming a direct transition from tetravalent cerium to pentavalent tantalum. Brauner was also tempted to draw an analogy between the rare-earth elements and the transition metals since both types of elements had been collectively placed in one "pigeonhole" of the system (*interperiodically* in the case of the transition metals, and *intrapperiodically* in the case of the rare earths). Brauner pushed the analogy even further on the basis of their oxide forms. Theoretically, the limiting degree of oxidation for the transition metals was RX_8 , but only osmium and ruthenium exhibited these forms of oxidation (i.e., OsO_4 en RuO_4). Similarly, the highest form of oxidation for the rare-earth elements had to be RX_4 , but this was only manifested in the oxides of cerium and praseodymium. It thus appears that Brauner had reached the same conclusions in 1902 as Mendeleev had in 1869 with regard to the transitional function of the primary groups and the rare earth – transition metal analogy.

Cs = 133	Ba = 137.4	La = 139.0	Ce = 140.2	–?	–?
			Pr = 141		
			Nd = 144		
			Sm = 148		
			Eu = 151		
			Gd = 156		
			etc.		

FIGURE 13 Position of the rare earths in the periodic table according to Brauner's asteroid hypothesis.

Instead of writing all rare earths underneath each other in IV-8, Brauner thought it more convenient to write them next to each other in groups of four, as with the transition elements (Figure 14). An even more compact method of representation consisted of writing "Ce etc. 140–178" in the case IV-8 of the periodic table (Figure 15). There were a number of interesting advantages connected with this type of accommodation. First of all, the periodicity was no longer undermined by the presence of the rare earths. Secondly, the astonishing similarities in the chemical and physical properties of the rare earths were accentuated by the placement of these metals in one case only. Finally, Brauner made it clear that the gap between La and Ta would be filled by rare earths and rare earths only. He thus delineated the boundaries of the rare-earth family.

One could be inclined to conclude that Brauner had been heavily influenced by the concept of Crookes' meta-elements when he proposed his asteroid hypothesis in 1902 (Stewart, 1909). After all, a violation of the concept of single occupancy could only be avoided by assuming the rare-earth elements to be constituent meta-elements of one and the same rare-earth elemental group. The link between Brauner and Crookes could be further substantiated by the following clues and indications. First of all, Brauner was tempted to compare the rare-earth elements with the asteroids of the solar system, in complete analogy with Crookes, who had referred to this class of metals as "the asteroids among the elements" (Crookes, 1886). Secondly, Brauner tried to provide his asteroid hypothesis with a scientific underpinning by imagining the condensation of the *Ursubstanz* during the formation of the rare-earth elements, just as Crookes had done in his lectures of 1886–1888. More than that, Brauner actually referred to Crookes in a footnote when he was writing about the primordial *Ursubstanz*. Finally, the two rare-earth specialists knew each other personally from the time when Brauner was working in Manchester, and they corresponded a lot during their lifetime. However, the influence of Crookes' concept of meta-elements should not be pushed too far. First of all, Brauner had spoken for the first time about the "confusion in this area of the chemistry of asteroids" in a letter to Mendeleev, dated February 17, 1881 (i.e., five years before Crookes' presidential address of 1886). Secondly, when he spoke about *die Kondensation der Ursubstanz*, Brauner at first referred to one of his own lectures, claiming that he had proposed this evolutionary hypothesis for the first time before the *Chemical Society of London* in March 17, 1898. How could Brauner maintain his priority if Crookes had developed his viewpoints on the epistemological nature of the concept of elements 10 years earlier, during the period 1886–1888? As a matter of fact, Brauner did not make any reference to this trilogy of papers, but he relegated his reading public to Crookes' paper of June 9, 1898 "On the Position of Helium, Argon, and Krypton in the Scheme of Elements" (Crookes, 1898). Apparently,

A. Periodisches System der Elemente (volle Gestalt).

Reihe	Gruppe 0	Gruppe I	Gruppe II	Gruppe III	Gruppe IV	Gruppe V	Gruppe VI	Gruppe VII	Gruppe VIII			
	—	—	—	—	RH ₄	RH ₃	RH ₂	RH	—			
	R	R ₂ O	RO	R ₂ O ₃	RO ₂	R ₂ O ₃	RO ₃	R ₂ O ₇	RO ₄			
1		1 H										
2	He 4	Li 7	Be 9	B 11	C 12	N 14	O 16	F 19				
8	20 Ne	23 Na	24 Mg	27 Al	28 Si	31 P	32 S	35.5 Cl				
4	A 40	K 39	Ca 40	Sc 44	Ti 48	V 51	Cr 52	Mn 55	Fe 56	Co 59	Ni 59	Cu 68
5		63 Cu	65 Zn	70 Ga	72 Ge	75 As	79 Se	80 Br				
6	Kr 82	Rb 85	Sr 87	Y 89	Zr 90	Nb 94	Mo 96	— 100	Ru 102	Rh 108	Pd 106	Ag 108
7		108 Ag	112 Cd	114 In	119 Sn	120 Sb	128 Te	127 J				
8	Xe 128	Ce 138	Ba 137	La 139	Ce 140	Pr 141	Nd 144	— 145				
					— 147	Sm 148	Eu 151	— 152				
					— 155	Gd 156	— 159	— 160				
					Tb 168	Ho 165	Er 166	— 167				
					Tm 171	Yb 178	— 176					
					— 178	Ta 182	W 184	— 190	Os 191	Ir 198	Pt 195	Au 197
9		197 Au	200 Hg	204 Tl	207 Pb	209 Bi	212—	214—				
10	— 218	— 220	Rd 226?	— 230	Th 238	— 235	U 239					

FIGURE 14 Brauner's periodic table of 1902 with an intraperiodic accommodation of the rare-earth elements (long form). Reproduced from Brauner (1902).

B. Periodisches System der Elemente (abgekürzte Form).

Reihe	Gruppe 0	Gruppe I	Gruppe II	Gruppe III	Gruppe IV	Gruppe V	Gruppe VI	Gruppe VII	Gruppe VIII
	—	—	—	—	RH ₄	RH ₃	RH ₂	RH	— Höchste Wasserstoffverbindungen
	R	R ₂ O	RO	R ₂ O ₃	RO ₂	R ₂ O ₅	RO ₃	R ₂ O ₇	RO ₄ Höchste Oxyde
1		1 H							
2	He 4	Li 7	Be 9	B 11	C 12	N 14	O 16	F 19	Erste kleine Periode
3	20 Ne	23 Na	24 Mg	27 Al	28 Si	31 P	32 S	35.5 Cl	Zweite kleine Periode
4	A 40	K 39	Ca 40	Sc 44	Ti 48	V 51	Cr 52	Mn 55	Fe 56 Co 59 Ni 59 Cu 68
5		63 Cu	65 Zn	70 Ga	72 Ge	75 As	79 Se	80 Br	Erste große Periode
6	Kr 82	Rb 85	Sr 87	Y 89	Zr 90	Nb 94	Mo 96	—100	Ru 102 Rh 108 Pd 108 Ag 108
7		108 Ag	112 Cd	114 In	119 Sn	120 Sb	128 Te	127 J	Zweite große Periode
8	Xe 128	Cs 133	Ba 137	La 138	Ce etc. 140—178	Ta 182	W 184	—190	Os 191 Ir 198 Pt 195 Au 197
9		197 Au	200 Hg	204 Tl	207 Pb	209 Bi	212—	214—	Dritte große Periode
10	—218	—220	Rd 225?	—280	Th 233	—235	U 239		
									Vierte große Periode

FIGURE 15 Brauner's compact periodic table of 1902 with an intraperiodic accommodation of the rare-earth elements. Reproduced from Brauner (1902).

Brauner was completely unaware of the existence of Crookes' 1886–1888 lectures. This also explains why Brauner never mentioned the terms meta-elements and elemental groups in his 1902 paper. Indeed, the asteroid hypothesis of Brauner could be approved on the basis of Crookes' concept of meta-elements, but Brauner himself did never take this step.

4.4 Intraperiodic Accommodation Methodologies

Brauner's asteroid hypothesis is an *intraperiodic accommodation methodology* (Brauner, 1902). The rare earths are considered as forming a special intraperiodic group and they are collectively clustered in one of the groups of the periodic system. Although the asteroid hypothesis is credited to Brauner, the original idea to compare the accommodation of the rare earths with the placement of the asteroids in the solar system did not come from Crookes' papers, and neither did it come from Brauner's creative mind. About seven years before Brauner's lecture of 1902, an article from Retgers (1895) had appeared in the *Zeitschrift für physikalische Chemie*, entitled "Über einige Änderungen im periodischen System der Elemente" (On some Modifications in the Periodic System of Elements). On the second page of his paper, Retgers mentioned the group of planetoids, which occurred between Mars and Jupiter in the planetary system, and which occupied the orbit of one planet. Not surprisingly, Retgers adhered to an intraperiodic accommodation methodology and he clustered La, Ce, Di, Sm, Er and Yb in one and the same spot of the periodic system (Figure 16). It therefore seems more correct to speak about the *asteroid hypothesis of Retgers*. As a matter of fact, the whole idea of clustering the rare earths in one pigeonhole appears to have been in the air of science, since a whole spectrum of articles about the periodic table emerged at the dawn of the twentieth century, every one of them putting forward the same asteroid like hypothesis and claiming that it provided the long sought after solution for the rare-earth crisis.

Thus, Biltz devised a periodic table in 1902 where Mn, Fe, Co, and Ni were grouped together, as well as Ru, Rh, Pd; Os, Ir, Pt; and the rare earths La, Ce, Pr, Nd (Figure 17) (Biltz, 1902). He named each group after the best known member and symbolized the clusters by the summation symbol Σ . The iron group ΣFe , the palladium group ΣPd , and the platinum group ΣPt , were all located in group VII. The cerium group ΣCe , on the other hand, was placed among the trivalent elements in group III. Some authors preferred to treat the rare earths as an *intermediate group* and located them in both the third and fourth group of the periodic system. Rudorf (1903) and Benedicks (1904) (Figure 18) adhered to this type of accommodation when they published their periodic tables in 1903 and 1904 respectively. The German chemist, Stefan Meyer proposed a similar placement of the rare-earth elements in 1918 (Figure 19). Several textbook authors too were

I	II	III	IV	V	VI	VII
einwertig	einwertig	zweiwertig	dreiwertig	vierwertig	dreiwertig	zweiwertig
<i>H</i>	<i>Li</i>	<i>Be</i>	<i>Bo</i>	<i>C</i>	<i>N</i>	<i>O</i>
<i>Fl</i>	<i>Na</i>	<i>Mg</i>	<i>Al</i>	<i>Si</i>	<i>P</i>	<i>S</i>
<i>Cl</i>	<i>K</i>	<i>Ca</i>	<i>Sc</i>	<i>Ti</i>	<i>V</i>	<i>Cr, Mn, Fe, Co, Ni</i>
	<i>Cu</i>	<i>Zn</i>	<i>Ga</i>	<i>Ge</i>	<i>As</i>	<i>Se</i>
<i>Br</i>	<i>Rb</i>	<i>Sr</i>	<i>Y</i>	<i>Zr</i>	<i>Nb</i>	<i>Mo, Ru, Rh, Pd</i>
	<i>Ag</i>	<i>Cd</i>	<i>Jn</i>	<i>Sn</i>	<i>Sb</i>	<i>Te</i>
<i>J</i>	<i>Cs</i>	<i>Ba</i>	<i>La, Ce, Di, Sm, Er, Yb</i>		<i>Ta</i>	<i>W, Os Ir, Pt</i>
	<i>Au, Hg, Tl</i>	<i>Pb</i>			<i>Bi</i>	<i>Th, U.</i>

FIGURE 16 Periodic Table of Retgers (1895) with an intraperiodic accommodation of the rare earths. Reproduced from Retgers (1895).

Periodensystem der Elemente.

He	Li	Be	B	C	N	O	F
Ne	Na	Mg	Al	Si	P	S	Cl
Ar	K	Ca	Sc	Ti	V	Cr	Σ Fe
Kr	Cu	Zn	Ga	Ge	As	Se	Br
X	Rb	Sr	Y	Zr	Nb	Mo	Σ Pd
	Ag	Cd	Jn	Sn	Sb	Te	J
	Cs	Ba	Σ Ce		Ex		
	Au	Hg	Yb	Pb	Ta	W	Σ Pt
			Tl	Th	Bi	U	

Untergruppen.

Σ Ce = La	Ce	Pr	Nd	Σ Fe = Mn	Fe	Co	Ni
				Σ Pd = Ru	Rh	Pd	
				Σ Pt = Os	Ir	Pt	

FIGURE 17 Periodic Table of Biltz (1902) with an intraperiodic accommodation of the rare earths. Reproduced from Biltz (1902).

	O	I	II	III	IV	V	VI	VII	VIII
		H							
1	He	Li	Be	B	C	N	O	F	
2	Ne	Na	Mg	Al	Si	P	S	Cl	
3	A	K	Ca	Sc	Ti	V	Cr	Mn	Fe, Co, Ni
4		Cu	Zn	Ga	Ge	As	Se	Br	
5	Kr	Rb	Sr	Y	Zr	Nb	Mo	—	Ru, Rh, Pd
6		Ag	Cd	In	Sn	Sb	Te	J	
7	Xe	Cs	Ba	[La, Ce... Yb]		Ta	W	—	Os, Ir, Pt
8		Au	Hg	Tl	Pb	Bi	—	—	
9	—	—	Ra	—	Th	—	U	—	

FIGURE 18 Periodic Table of Benedicks (1904) with an intraperiodic accommodation of the rare earths. Reproduced from Benedicks (1904).

Tabelle I. Periodisches System der Elemente.

		I								0								
		H								He								
		1.008								4.00								
		1								2								
Wertigkeit bez. Gruppennummer Symbol Atom-Gewicht Ordnungszahl (Kernladung)	1	I	II	III	IV	V	VI	VII	0	I	II	III	IV	V	VI	VII	0	
	2	Li	Be	B	C	N	O	F	Ne	Die Atomvolumina nehmen von der Mitte nach beiden Seiten zu.	Li	Be	B	C	N	O	F	Ne
	3	Na	Mg	Al	Si	P	S	Cl	Ar	Na	Mg	Al	Si	P	S	Cl	Ar	
		23.0	24.3	27.1	28.3	31.0	32.1	35.5	39.9	11	12	13	14	15	16	17	18	

	I	II	III	IV	V	VI	VII	VIII	I	II	III	IV	V	VI	VII	0		
4	K	Ca	Sc	Ti	V	Cr	Mn	Fe	Co	Ni	Cu	Zn	Ga	Ge	As	Se	Br	Kr
	39.1	40.1	45.1	48.1	51.0	52.0	54.9	55.8	58.9	58.7	63.6	65.4	69.9	72.5	75.0	79.2	79.9	82.9
	19	20	21	22	23	24	25	26	27	28	29	30	31	32	33	34	35	36
5	Rb	Sr	Y	Zr	Nb	Mo		Ru	Rh	Pd	Ag	Cd	Jn	Sn	Sb	Te	J	X
	85.5	87.6	88.7	90.6	93.5	96.0	?	101.1	102.9	106.4	107.9	112.4	114.8	118.7	120.2	127.5	126.9	130.2
	37	38	39	40	41	42	43	44	45	46	47	48	49	50	51	52	53	54
6	Cs	Ba	seltene Erden		Ta	W		Os	Jr	Pt	Au	Hg	Tl	Pb	Bi	Po	?	Em
	132.8	137.4	139.0 bis 178		181.5	184.0	?	198.9	193.1	195.2	197.2	200.6	204.0	207.2	208.0	210	?	222
	55	56	57 bis 72		73	74	75	76	77	78	79	80	81	82	83	84	85	86
7		Ra	Ac	Th	Bv	U												
		226.0		232.1	234	238.2												
		88		90	91	92												

	La	Ce	Pr	Nd	?	Sm	Eu	Gd	Tb	Dy	Ho	Er	TuI	Ad	Cp	TuII
	138.0	140.3	140.9	144.3	?	150.4	152.0	157.3	158.9	162.5	163.5	167.3	168.5	173.5	175.0	-
	57	58	59	60	61	62	63	64	65	66	67	68	69	70	71	72

FIGURE 19 Periodic Table of Meyer (1918) with an intraperiodic accommodation of the rare earths. Reproduced from Meyer (1918).

quick at adopting Brauner's asteroid hypothesis. The first editions of the books of Jones (1903) and Smith (1906) both accommodated the rare earths in group IV of the periodic system. Ostwald (1904), on the other hand, preferred to cluster the rare earths in group III. Six more textbook authors converted to the intraperiodic accommodation methodology during the

period 1914–1921. Arnold in 1914, Newell in 1916, Walker in 1919, and Holmyard in 1922 located the rare earths in group IV. Friend et al. (1917), on the other hand, chose group III, and Norris in 1921 opted for a grouped accommodation in the groups II, III, and IV.

5. NIELS BOHR AND HENRY MOSELEY

5.1 Bohr's Atomic Theory

Thomson's model of the atom could not provide an explanation for the large angle deflections of α particles as first observed in the laboratory of Rutherford (1871–1937) in Manchester. Rutherford consequently improved Thomson's model by postulating the existence of a central nucleus in 1911. He thus provided an explanation for the anomalous scattering phenomena, but he realized that his nuclear model was unstable according to the doctrines of classical physics. The permanent radiation remained a problem until the summer of 1912, when Niels Bohr (1885–1962, Figure 20) provided a solution on the basis of his quantum theory and postulated the existence of electron orbits within the atom. When electrons occupied these stationary states, no energy was radiated. Bohr moreover ascribed each orbit a certain energy value and this



FIGURE 20 Niels Henrik David Bohr (1885–1962). Photo and permission from Edgar Fahs Smith Collection.

permitted him to derive the formula of Balmer with regard to the spectral lines of the hydrogen spectrum. Bohr published his atomic theory in three voluminous papers, "On the Constitution of Atoms and Molecules," which appeared in the *Philosophical Magazine* between July and November 1913 (Bohr, 1913a,b,c). Although Bohr's theory was primarily of a physical nature, a number of chemical aspects were included as well. He was heavily influenced by the concepts from inorganic chemistry, and he was especially interested in the theoretical explanation of the periodic table (Kragh, 1977). Bohr attempted to explain the various chemical and physical characteristics of the elements by deriving their electronic configurations. This type of approach was not entirely new. As a matter of fact, J. J. Thomson (1856–1940), the discoverer of the electron, had developed the first electronic arrangements in 1904 on the basis of his *plum pudding model* of the atom. Inspired by Victorian vortex chemistry, Thomson had tried to give an explanation of the periodic law, but his attempt had not been very successful (Kragh, 2001). Bohr on the other hand adhered to a *stability condition*, and he selected the least energetic configurations as the most probable ones. Nevertheless, Bohr did not succeed in deriving these configurations deductively from his quantum theories. He was forced to use some inductive reasoning and he had to rely upon his chemical knowledge.

Bohr did not further develop the chemical aspects of his 1913 theory in the subsequent years. He only returned to the subject matter in 1921 when he offered an explanation of the periodic system in terms of electron configurations (Bohr, 1921, 1922a). Bohr referred to the natural system of Mendeleev and Lothar Meyer at the beginning of his Nobel Lecture in Copenhagen in 1922, and he offered his audience a diagrammatic representation of the periodic law in a somewhat modified form of a table first given by Julius Thomsen (Figure 21) (Bohr, 1922b). He noted that the characteristic features of the natural system had found a surprisingly simple interpretation in that the ordinal number of an element in the periodic table, the so-called *atomic number*, is just equal to the number of electrons which move about the nucleus in the neutral atom. He also referred to Moseley's investigations of the X-ray spectra of the elements as convincing support for this law (see Section 5.2).

According to Bohr's opinion, the rare-earth group consisted of elements where the four-quantum level was gradually filled up from 18 to 32 electrons. The number of electrons in the five- and six-quantum levels on the other hand remained unchanged. Bohr's quantum theory thus served as a useful explanation for the pronounced similarity between the chemical and physical properties of the rare-earth elements. He mentioned that their mutual similarity must be ascribed to the fact that we have here to do with the development of an electron group that lies deeper in the atom. He moreover emphasized that lutetium ($Z = 71$) had to be considered the last rare-earth element. Element 72 on the other hand did not belong to

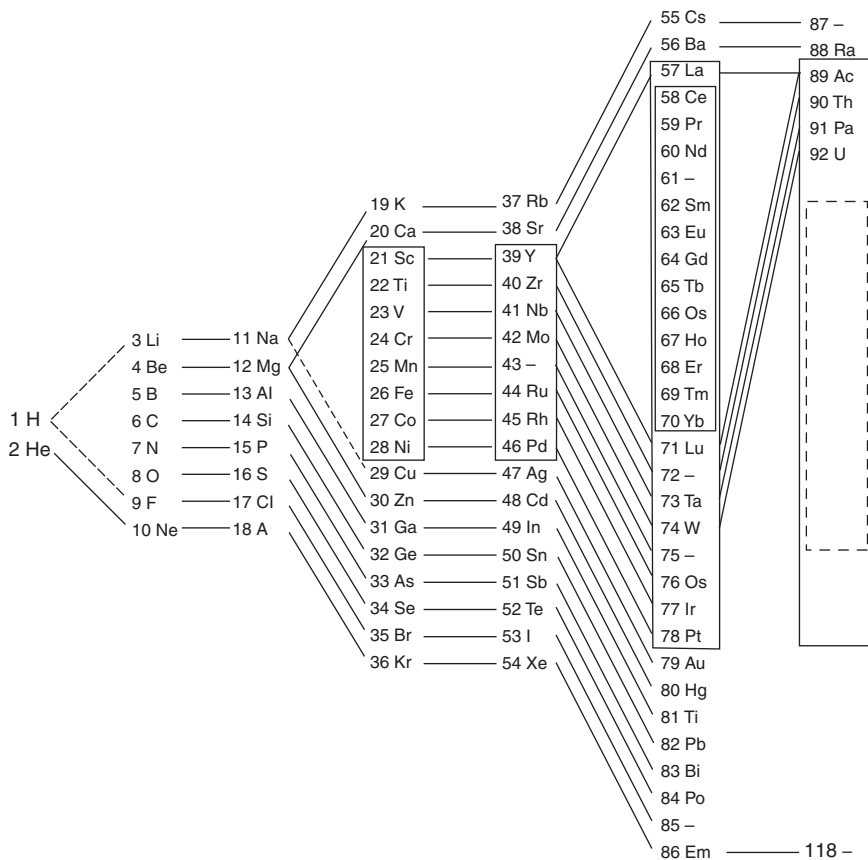


FIGURE 21 Bohr's periodic table (1922). Reproduced with permission (Copyright Nobel Foundation, 1922).

the group of trivalent rare earths, but had to be seen as a tetravalent zirconium homologue. Bohr observed that in many representations of the table a place is left open for this element in the rare-earth family, but he noted that in Julius Thomsen's representation of the natural system, this hypothetical element was given a position homologous to titanium and zirconium (Figure 21).

5.2 Moseley's Research on X-Ray Spectra of Elements

After his graduation as M.A. in Natural Sciences at Trinity College, Oxford, in 1910, Henry Moseley (1887–1915, Figure 22) headed for Manchester where he was welcomed in the laboratory of Rutherford (Hogg, 1975). His measurements of the X-ray emission spectra of the



FIGURE 22 Henry Gwyn Jeffreys Moseley (1887–1915). Photo and permission from Edgar Fahs Smith Collection.

chemical elements rendered the correlation possible between the X-ray frequencies and the atomic numbers of the elements. The main objectives of Moseley's research were to clarify the anomalies in the periodic table and to solve the puzzle of the total number of rare earths (Heimann, 1967). As Moseley observed, "there are some [chemists] who would split almost every one of these rare-earth elements into three or four" (Heimann, 1968). The success of Bohr's theory in the explanation of the hydrogen spectrum undoubtedly led Moseley to speculate on the connection between the frequency, ν , of X-rays and the nuclear charge of the emitting element (Gorin, 1996; Haigh, 1995; Heimann, 1967, 1968; Heimann and Heilbron, 1967; Lesk, 1980). Moseley could thus explain the order of the elements in the periodic table. The reversals of tellurium and iodine, potassium and argon, nickel and cobalt in the periodic system were explained on the basis of their atomic numbers.

Moseley was still working in Rutherford's group in Manchester when he published his first paper on the high frequency spectra of the elements in the issue of the *Philosophical Magazine* for December 1913 (Moseley and Darwin, 1913). Moseley had been investigating the K radiation of at least

10 transition elements from calcium to zinc (with the exception of scandium). At the end of the year, in December 1913, Moseley left the research group of Rutherford and headed for Oxford with the aim of investigating the K spectra of all the other elements, as well as the L spectra of the elements with high atomic weights. The reason for this move to Oxford could be the fact that Moseley was anxious to get full credit for all his research and felt that as long as he stayed in Manchester he was in danger of being overshadowed not only by Rutherford but also by other members of the team which at that time included Geiger, Bohr, Marsden and others (Hogg, 1975). Unfortunately, Moseley's research in Oxford advanced with many difficulties. His X-ray tube had not survived the trip from Manchester to Oxford, and the Clarendon Laboratory in Oxford was in a poor state. Fortunately, Moseley could restart his work soon and he began investigating the K spectra of yttrium, zirconium, niobium, molybdenum, ruthenium, palladium and silver. Elements with an atomic weight greater than $\text{Ag} = 107.8$ could not be studied since the laboratories in Oxford were not built to handle such high voltages.

On January 18, 1914, Moseley enthusiastically wrote to de Hevesy (1885–1966) in Manchester: “[It will] be possible to put every rare-earth element into its right pigeonhole, to settle if any of them are really complex, and where to look for new ones” (Heimann, 1967). His enthusiasm must have faded away however as soon as he moved over to a study of the softer L radiation. The penetrating character of these X-rays was not high enough and the radiation did not pass through the aluminium windows of the spectrometer. Neither did it penetrate through the protective wrapping of the photographic plates. Apparently, two centimeters of air already halted the propagation of the L radiation. His targets moreover volatilized at the high temperatures inside the X-ray tubes. Moseley had to solve these practical problems one at a time. He decided to perform his experiments in the dark and attempted to work with a highly exhausted spectrometer. Since none of the pumps available in Oxford could reach the required high vacuum, Moseley felt obliged to borrow one from the laboratory in Balliol (Hogg, 1975). The L spectra of all the elements from zirconium to gold were subsequently investigated and Moseley observed that the advantage of his method lay in the simplicity of the spectra and the impossibility of one substance making the radiation from another (Heimann, 1968). He thus concluded that his method could even lead to the discovery of missing elements, because of the possibility to predict the position of their characteristic lines.

Soon afterwards, Moseley wrote a second paper on the X-ray spectra of the elements, in which he stated that every element from aluminium to gold (which marked the boundaries of his studies) was characterized by an integer N which determined its X-ray spectrum. This integer N was the atomic number of the element and it was identified with the number of

positive units of electricity contained in the atomic nucleus. Thus, the frequency of any line in the X-ray spectrum is approximately proportional to $A(N - b)^2$, where A and b are constants (Moseley, 1914). The latter statement has been termed *Moseley's law* in his honor (Heimann, 1967). However, the concept of the atomic number was not introduced by Moseley, but by the Dutch amateur scientist Antonius Van den Broek (1870–1926) (Scerri, 2007; Van den Broek, 1913; van Spronsen, 1969). The term “atomic number” was first used by Rutherford (Rutherford, 1913). When the chemical elements were classified on the basis of their atomic number, Moseley immediately observed that elements 43, 61, and 75 were still missing. Moseley's investigations were not only important in establishing the correct order of the elements in the periodic table. They also provided an experimental vindication of the atomic number hypothesis, and therefore increased the explanatory power of the Rutherford–Bohr model (Heimann, 1968). Moseley was killed in the First World War during the battle of the Dardanelles in August, 1915 at the age of 27.

5.3 The Controversial Element 72

At the end of his Noble Lecture to the Swedish Academy of Sciences on December 11, 1922 Niels Bohr announced the discovery of element 72 by George de Hevesy and Dirk Coster (1889–1950) in Copenhagen (Bohr, 1922b). This was a very surprising statement since the French chemist Georges Urbain (1872–1938) had already claimed the discovery of this element in 1911 (Heimann, 1967; Kragh, 1979, 1980, 1996; Scerri, 1994; Urbain, 1911; Weeks, 1956). Urbain had named the element *celtium* and he had recently published some further proof for its existence in collaboration with Alexandre Dauvillier (1892–1979). Urbain was a French chemist and professor of mineral chemistry at the Faculté des Sciences de l'Université de Paris. He was a rare-earth specialist, as well as an amateur composer, painter and sculptor. Urbain became the president of the International Committee on Atomic Weights in 1907 after Henri Moissan (1852–1907) had died, and he must have realized how tactical a position it was during his priority dispute with Auer von Welsbach (1858–1929) (*vide infra*). Urbain improved the current methods of fractionation by selecting a number of more efficient reagents and he was a pioneer in the application of double salts of bismuth during the chemical fractionation of rare earths. This allowed him to disprove Crookes results on radiant matter spectroscopy. Pure rare-earth samples did not show any phosphorescent spectrum, according to Urbain. Urbain was moreover a philosophically inclined scientist and he wrote a number of books on the changing concept of element. In analogy with Crookes' viewpoints, Urbain did not attach great importance to the operational definitions of Lavoisier with regard to the concept of elements, and he also questioned

the trustworthiness of atomic weight determinations in determining the homogeneity of the chemical elements. He therefore proposed to adhere to the magnetic susceptibility of the rare-earth elements as a criterion for their elementarity. Despite the fact that Urbain clearly belonged to the traditional chemists of the nineteenth century and that he approached the rare-earth crisis from a chemical point of view, it appears that he was swift in adopting Moseley's X-ray spectroscopic techniques of analysis. Urbain had initiated his researches in 1907, after having discovered neo-ytterbium (Yb) and lutetium (Lu), and he worked for four years, until he finally obtained a number of new lines in the optical spectrum of one of his fractions and concluded that they had to be attributed to a new element, *celtium* (Ct).

It appears that Moseley had heard about Urbain's discovery and moreover believed in the existence of celtium when he continued his research in Oxford in 1914. Due to a small calculation error, Moseley had ascribed each element from yttrium an atomic number which was one unit too high. For example, yttrium was not allotted the correct atomic number 39, but instead 40. As a consequence, the atomic number 39 remained unused and Moseley wrote to Rutherford on March 4, 1914 that it seemed very probable that N₃₉ would be celtium. Moseley's prediction was in contradiction with Urbain's claim that celtium belonged to the family of rare-earth elements. Moseley soon discovered the flaw in his argument and he redeemed his own mistake the next day on March 5, 1914. He wrote a postcard to Rutherford, claiming that the element between strontium and yttrium was a myth (Heimann, 1967). In his second article of April 1914, Moseley summarized the results of his rare-earth research (Moseley, 1914). He had obtained most rare-earth samples from Crookes and from Schuchard which he subsequently rubbed on the surface of nickel plates (Hogg, 1975). He had begun investigating the spectra of the whole rare-earth family in the middle of February 1914 and ascribed these elements the following atomic numbers:

57	58	59	60	61	62	63	64	65	66	67	68	69	70	71	72
La	Ce	Pr	Nd	–	Sm	Eu	Gd	Tb	Ho	Dy	Er	TmI	TmII	Yb	Lu

Notice that Moseley had made a minor mistake in the atomic number determinations of both holmium and dysprosium. The atomic number of holmium is namely 67, and dysprosium has an atomic number of 66. It also appears that Moseley attached some credence to the investigation of Auer von Welsbach who had demonstrated the complexity of thulium in 1911 by splitting it into three components. Moseley had incorporated two of these components (TmI and TmII) in his atomic number sequence. Moseley therefore ascribed Urbain's neo-ytterbium and lutetium too high an atomic number (in reality the atomic numbers of ytterbium and

lutetium are 70 and 71 respectively). As a consequence, only one case remained vacant (number 61) and Moseley therefore explained to de Hevesy that he was tempted to accommodate celtium in this spot. A few weeks later, Moseley had obtained a number of new samples of ytterbium, lutetium, terbium and dysprosium from Urbain, and he subsequently wrote a second letter to de Hevesy on April 23, 1914, concluding that TmII does not exist, and that he had got the order dysprosium, holmium wrong (Heimann, 1967). Moseley had thus adjusted the sequence of elements and he included the following list in his letter for de Hevesy, with element 61 still missing and celtium having ascribed an atomic number of 72:

57	58	59	60	61	62	63	64	65	66	67	68	69	70	71	72
La	Ce	Pr	Nd	–	Sm	Eu	Gd	Tb	Dy	Ho	Er	Tm	Yb	Lu	Ct

At the end of May 1914, Urbain visited Moseley in Oxford to examine together the X-ray spectrum of celtium. Moseley could not find other lines in the spectra than those of lutetium and ytterbium. Urbain accepted the negative results of Moseley's research, but he did not lose faith in the elementarity of celtium. Urbain started his own X-ray investigations in collaboration with Alexandre Dauvillier in Paris. They announced in May 1922, seven months before Bohr's Nobel Lecture, their discovery of two new X-ray lines which they attributed to celtium on the basis of Moseley's theory, even though the spectrum was very faint and the lines corresponded only roughly with Moseley's predictions.

When Bohr returned from a series of lectures which he had delivered in Göttingen in June 1922, he read a note by Rutherford in *Nature* communicating Urbain and Dauvillier's results. Celtium was considered to be a trivalent rare-earth element. This was in contradiction with Bohr's theory of atomic structure, according to which element 71 was the last rare earth, and element 72 had to be a tetravalent zirconium homologue. But Bohr at first believed he had been wrong, and he accepted Urbain's discovery. Nevertheless, Bohr soon decided to consult with Dirk Coster in Lund (Sweden). Coster was a specialist in X-ray spectroscopy given the fact that he had been the assistant of Manne Siegbahn (1886–1978), the Swedish pioneer in X-ray investigations after Moseley's death. Coster questioned Urbain and Dauvillier's findings, and Siegbahn, who had visited the two Frenchmen in Paris, had not even been able to see the two faint lines on the photographic plates. Bohr asked Coster, when he came to Copenhagen in September 1922, to search for element 72, but Coster was at first reluctant. de Hevesy, however, soon convinced him and the two started their hunt for element 72 in a number of Norwegian zirconium containing minerals which they had obtained from the Mineralogy Museum of Copenhagen. de Hevesy had to perform intensive chemical investigations for almost two weeks, but they finally

succeeded on Saturday, December 9, 1922, to obtain six very pronounced X-ray spectral lines which pointed to the existence of a new element, element 72, according to Moseley's theory. Coster and Kramers decided to name the element *hafnium*, but Bohr, de Hevesy, Bjerrum and Christiansen preferred *danium*. Due to an error of the editor of *Nature*, the element was named *hafnium* after all, in reference to the Latinized name of Copenhagen (*Hafnia*). Their results were published on January 20, 1923.

A first response came from the British chemist and mineralogist at the British Museum, Alexander Scott, who claimed he had discovered element 72 in the period 1913–1918 when analyzing black sand from New Zealand. He had called the element *oceanium*. This finally turned out to be a mixture of iron, aluminium, and titanium. More importantly, a priority dispute between the French school (i.e., Urbain and Dauvillier) and the Copenhagen school (i.e., Bohr, de Hevesy, and Coster) began. It must be noted that while both teams consisted of chemists and physicists, they definitely adhered to different research paradigms: the classic, chemical approach versus the physical, quantum mechanical approach. The French school rested on an enormous chemical knowledge with regard to the rare-earth elements and its members were very skeptical about the theoretical viewpoints of Bohr. Bohr had not soiled his own hands, and he had never personally experienced the troubles of chemical fractionation. How could such a theoretical physicist possibly say anything meaningful about the rare earths? The Copenhagen school on the other hand accepted Bohr's theory of the atom with open arms. They relied upon quantum mechanical viewpoints and were therefore convinced that element 72 would prove to be a zirconium homologue. The Copenhagen school was supported by scientists from Scandinavia, Holland and Germany. The German chemist, Fritz Paneth backed up Coster and de Hevesy in their claims. Auer von Welsbach had lost the priority dispute with Urbain about the elements 70 and 71 and therefore supported the Copenhagen team as well. The French school was mainly supported by French and British scientists. Bohuslav Brauner who had lost the priority dispute with Auer von Welsbach with regard to the splitting of didymium and subsequent discovery of praseodymium and neodymium also supported the team of Urbain. Besides the internal reasons for a priority dispute, there also were a number of external ones. Both nationalistic feelings and personal relations contributed to the whole conflict. The sudden interest from British scientists when Scott had claimed priority over the discovery of element 72 clearly emphasizes the important role of patriotism in priority disputes. The political situation after the First World War also contributed to the conflict between the French and Copenhagen school. French and English scientists were of the opinion that German science formed a threat and they heavily tried to isolate it from the rest of the world.

In February 1923, Urbain and Dauvillier stated in a piercing critique that Coster and de Hevesy had only succeeded in rediscovering the rare-earth element, celtium, in zirconium minerals (Scerri, 1994). Coster and de Hevesy replied by underlining the differences in chemical and physical properties between hafnium and celtium. While the claim of the French scientists rested on two very faint lines in the X-ray spectrum, their claim to the discovery of element 72 rested on six pronounced X-ray lines. Bohr too said he had reason to believe that the observation of Dauvillier was a self illusion. de Hevesy's chemical investigations had moreover proven that hafnium was a tetravalent zirconium analogue, and that it did not behave as a typical, trivalent rare-earth element. They had studied the optical spectrum of hafnium and noticed the enormous differences with Urbain's, 1911 spectra. In the spring of 1923, Urbain and Dauvillier felt obliged to admit that element 72 was a zirconium homologue, but this did not end the dispute. The French team maintained that they had been the first in discovering element 72. Meanwhile, de Hevesy continued his chemical investigations, determining the atomic weight of element 72, as well as the solubility of its salts, mineralogical and magnetic properties. The dispute came to an end when Bohr received some rare-earth samples from Auer von Welsbach, which demonstrated that the optical lines obtained by Urbain were not due to celtium, but were characteristic of lutetium. Urbain's celtium samples of 1911 were just very pure lutetium specimens. They did not contain any new elements. This also meant that his lutetium samples of 1907 had been impure, and did contain only a trace of lutetium. Auer von Welsbach's cassiopeium samples on the other hand had been pure in 1907, and he was to be seen as the real discoverer of element 71 (Paneth, 1923).

5.4 The Elusive Element 61

In 1902, Bohuslav Brauner suspected the existence of an element between neodymium and samarium on the basis of the rather large difference in atomic weights of these two elements, but he could not give experimental evidence for his claim (Brauner, 1902, 1926). In 1913, Moseley had just discovered the atomic numbers of neodymium and samarium to be 60 and 62 respectively (Moseley, 1914; Moseley and Darwin, 1913). Apparently, element 61 was still missing. The quest for this rare-earth element had thus begun (Marinsky, 1996; Trifonov, 1963, 1984; Trifonov and Trifonov, 1982; Weeks, 1956). The physicists had pointed towards the existence of the unknown element and this inspired a number of chemists to start looking for it. Making predictions as to the existence of unknown elements would have been impossible before Moseley's pioneering work. Admittedly, Mendeleev had successfully predicted the existence and

properties of gallium, scandium, and germanium on the basis of his periodic table, but this was due to the fact that these vacant spaces were completely surrounded by known elements. Mendeleev had never been that clear when it came to predicting the properties of eka-caesium (francium), eka-iodine (astatine), dvi-tellurium (polonium), eka-manganese (technetium), dvi-manganese (rhenium), and especially the rare-earth elements.

"I have been searching unsuccessfully for the unknown element," Moseley wrote on April 23, 1914. "Either it is very rare, or as is quite likely, only occurs in a few minerals. I hardly think that it does not exist" (Heimann, 1967). Most chemists however were quite surprised by Moseley's prediction. It was known since the 1920s that the rare-earth elements were not rare at all. Their abundance in the earth's crust was greater than those of tin, lead, silver, antimony, mercury, and gold. The family of rare earths was moreover subdivided into two groups. The cerium group contained all rare-earth elements with low atomic weights. The yttrium group on the other hand was constituted of rare earths with high atomic weights. Both chemists and geologists knew that the members from the cerium group were more abundant than those of the yttrium group. Moseley's investigations, on the other hand, demonstrated that all members of the yttrium group were known. Strangely enough, the unknown element appeared to belong to the cerium group. Clearly, the mysterious element 61 was completely different from the other cerium group elements. Its abundance had in all probability been too low in order to render its discovery possible with the aid of the current methods of analysis (Yntema, 1924). However, in April 1926 an article appeared in *Nature* from the hand of the American chemists James Allen Harris, Leonard Yntema, and B. Smith Hopkins from the University of Illinois at Urbana-Campaign, who claimed to have discovered element 61 in natural minerals (Harris et al., 1926a,b). They named the element *illinium* (II). Apparently, Yntema had performed thousands of fractional crystallization, after which all the neodymium and samarium containing fractions had been investigated by Harris and Hopkins with the aid of optical spectroscopy and X-ray spectroscopy. But despite the fact that their spectroscopic results pointed towards the presence of element 61, the team of American scientists had not yet succeeded in isolating illinium. It must also be noted that at that time all chemical elements had been discovered by European scientists. The past "element" discoveries of American chemists had all proved to be erroneous. This made the discovery of element 61 all the more important.

However, shortly after this announcement two Italian chemists, Luigi Rolla (1882–1960) and Lorenzo Fernandes (1902–1977), who were working at the University of Florence, claimed to have discovered element 61 in monazite from Brazil two years before the Americans, back in 1924 (Rolla and Fernandes, 1926, 1927a,b,c, 1928). All their results had been meticulously written down in two long papers, but they had decided not to

publish it for some obscure reasons. The articles were instead filed away in a sealed envelope and subsequently placed in safekeeping in the *Accademia dei Lincei* in Rome. Not surprisingly, a priority dispute commenced between the Americans and the Italians. Everyone wondered who had been the true discover of element 61 and whether one should call it illinium or rather *florentium*, as the Italians preferred? Two German chemists, the rare-earth specialist Wilhelm Prandtl (1878–1956) and his assistant Hans Grimm had investigated more than 50 different rare-earth minerals with the aid of X-ray spectroscopy, but they could not retrace the element 61 (Prandtl, 1926; Prandtl and Grimm, 1924, 1926). They concluded that the element 61 differed from the rare-earth metals in its chemical behavior or that it does not exist at all. They had constructed a periodic table and noticed that the elements 43, 61, 75, and 93 in the periodic table were all located underneath each other in the manganese group VIIb. They stated that the empty slots 43, 61, 75, and 93 could be a manifestation of some periodic regularity and that it was possible that they would never be filled.

Auer von Welsbach was another chemist who doubted the validity of the American results. Finally, the married couple, Ida Noddack (née Tacke, 1896–1978) and Walter Noddack (1893–1960), embarked upon a quest for the element 61. Husband and wife were greatly stimulated by their recent discoveries of masurium and rhenium. The Noddacks, in collaboration with Berg, began their investigations with an enormous amount of rare-earth minerals (Noddack et al., 1925). They first of all produced a number of very pure samples of neodymium and samarium. They made use of the most sensitive and accurate methods of analysis of that time, allowing to detect element 61 if it were 10 million times more rare than neodymium and samarium. However, their work remained without success.

Ida Noddack suspected that element 61 was radioactive and presumed its half-life to be less than the age of the earth. The geochemists on the other hand could not believe such a statement. In view of the fact that all the members of the cerium group were both abundant and stable, they were quite certain about the possibility of finding element 61 in nature. They had also observed that the rare-earth elements did not always exhibit a valency of three, and that some rare earths possessed a valency value of two or four. Europium, for example, formed stable compounds when its oxidation state was +II. Perhaps, something similar could be observed with element 61. Maybe all chemists had just been looking for this element in the wrong place. Instead of analyzing rare-earth minerals, why not looking in minerals containing bivalent alkaline earths? The Noddacks did not attach much credence to this viewpoint, but they nevertheless pursued their research in the latter type of minerals. Unfortunately, all appeared to be in vain.

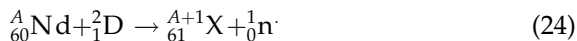
It was the German theoretical physicist, Josef Mattauch (1895–1976), who proved Ida Noddack to be correct, when he proposed the *Mattauch rule* (also

known as the *Mattauch isobar rule*) (Mattauch, 1934). According to this rule, if the nuclear charges of two isobars (i.e., nuclides with the same mass number) differ by unity, one of the isobars must be radioactive. Another formulation of this rule is that if two adjacent elements have nuclides of the same mass, then at least one of them must be radioactive. Isobars can only be stable when they are separated by more than one atomic mass unit. The mass numbers of the stable isotopes of neodymium and samarium are:

Nd	142	143	144	145	146	–	148	–	150
Sm	–	–	144	–	–	147	148	149	150

All the possible mass numbers between 142 and 150 are already taken by neodymium ($Z = 60$) and samarium ($Z = 62$), so that no stable isotope is expected for element 61. They would all be radioactive, just as in the case of technetium ($Z = 43$). The Mattauch rule however was not capable of ascribing these radioactive isotopes a certain half-life. A number of uranium and thorium isotopes are also radioactive, but their half-lives are great enough so that one can still find them in nature. During that same year, in 1934, the American physicist and future Noble Prize winner, Willard Libby (1908–1980), discovered that neodymium is a β emitter (Libby, 1934). According to Soddy's displacement laws, this should imply that when neodymium decays, isotopes of element 61 should be formed.

Due to these recent discoveries, chemists did not lose their faith and they still hoped to discover the element 61 in nature. But most of them realized that it would probably be more successful to synthesize the element artificially. Technetium, the first artificially prepared element, had been formed in 1937 in the Berkeley cyclotron (Perrier and Sègre, 1937, 1947). One year later, in July 1938, the American physicists Pool and Quill of the University of Ohio started bombarding a neodymium target with fast deuterons (Pool and Quill, 1938). They were hoping that the proton would be taken up by the neodymium nuclei, with the formation of element 61 as a consequence:



Unfortunately, the produced amount of element 61 was too small to study its properties. Pool and Quill were nevertheless convinced that they had synthesized an isotope of element 61 with mass number 144 and half-life of 12.5 h. More isotopes of element 61, with mass number 144, 147, and 149, were produced two years later in collaboration with Kurbatov, Law and MacDonald (Kurbatov et al., 1942; Law et al., 1941). Pool and his team decided to name the element *cyclonium* (symbol: Cy) in honor of the cyclotron in which all artificial elements had been formed. Most chemists however questioned the validity of their assertions, and doubted that the neodymium targets had been entirely pure. Every presence of impurities

would have been bombarded too and these could have formed some rare-earth isotopes.

In the year 1932, the *neutron* was discovered by Sir James Chadwick (1891–1974) as a new, neutral elementary particle which constituted the atomic nucleus (Chadwick, 1932). Since it was not electrically charged, it proved very useful to penetrate the nuclei of other atoms in order to form new nuclides. Physicists soon discovered the processes of fission when they started bombarding certain uranium isotopes with neutrons. They produced daughter nuclides ranging from zinc to gadolinium. It thus appeared that isotopes of the element 61 could be produced during the fission process of uranium-235 as well. A number of chemists, physicists, and engineers studied the formation of these isotopes during the Manhattan Project in 1942. A whole range of new techniques had to be developed in order to separate the different nuclides. The ion exchange chromatographic methods proved very valuable. Polymers were used as ion exchangers. The American chemists Jacob Akiba Marinsky (1918–2005), Lawrence Elgin Glendenin (1918–2008) and Charles Dubois Coryell (1912–1971) working at Oak Ridge National Laboratory (ORNL) in Tennessee soon succeeded in separating the different lanthanide nuclides. They also obtained some fractions which contained element number 61. In 1945, a millionth of a gram was obtained of the isotopes with mass number 147 and 149. These isotopes had been generated by two different methods: nuclear fission of uranium and bombardment of neodymium with neutrons. Finding a name for element 61 proved however as difficult as the production of its isotopes. It was Coryell's wife Grace Mary who proposed to name the element *promethium* (symbol: Pm). The mythical Prometheus, one of the titans in Greek mythology, had stolen the fire from the gods for the benefit of mankind. Zeus decided to punish Prometheus for his acts and he chained him to a big rock. An eagle came to visit him each day and always ate a small piece of his liver, just small enough so that it could grow again in one day. The choice of their name was twofold. For one thing, it referred to the harnessing of nuclear energy by humans in order to synthesize new elements. On the other hand, the name warned everybody for the "eagle of war." The discovery of promethium was first announced at an American Chemical Society Meeting in New York in September 1947 (Marinsky et al., 1947). On July 28, 1948, a total of 3 mg of yellow promethium chloride and pink promethium nitrate were exhibited before the American Chemical Society.

5.5 Intergroup Accommodation Methodologies

According to the *intergroup accommodation methodology*, the rare-earth elements did not show any relationship with the other elements. They had to be placed within the periodic table as a separate family of elements,

completely unconnected to the other groups. This was accomplished by accommodating the rare earths in between two groups of the periodic table. The rare-earth elements thus showed some analogy with the transition metals in view of the fact that both types of elements were separated from the rest of the system and that both formed in a sense the transition between two main groups of Mendeleev's system. This type of placement was in complete agreement with Bohr's quantum theory of the atom, and consequently became the preferred methodology in the twentieth century.

A particularly interesting classification was the one with horizontal groups and vertical periods proposed by the Danish thermochemist Hans Peter Jørgen Julius Thomsen (1826–1909) in 1895 (Figure 23) (Thomsen, 1895). Such a pyramidal/ladder form representation had already been proposed by the English scientist Thomas Bayley in 1882 (Figure 24), but

Elektropositive Elemente.

				Cs 133
				Ba 137
				La 138
				Ce 140
				Ne 141
				Pr 144
				— —
				Sm 150
				— —
				Gd 156
				Trb 160
				— —
				Er 166
				— —
				Thu 171
				Yb 173
				— —
				— —
				Ta 183
				W 184
				— —
				Os 191
				Ir 193
				Pt 195
				Au 197
				Hg 200
				Tl 204
				Pb 207
				Bi 209
				— —
				— —

Elektronegative Elemente.

FIGURE 23 Julius Thomsen's pyramidal periodic table (1895). Reproduced from Thomsen (1895).

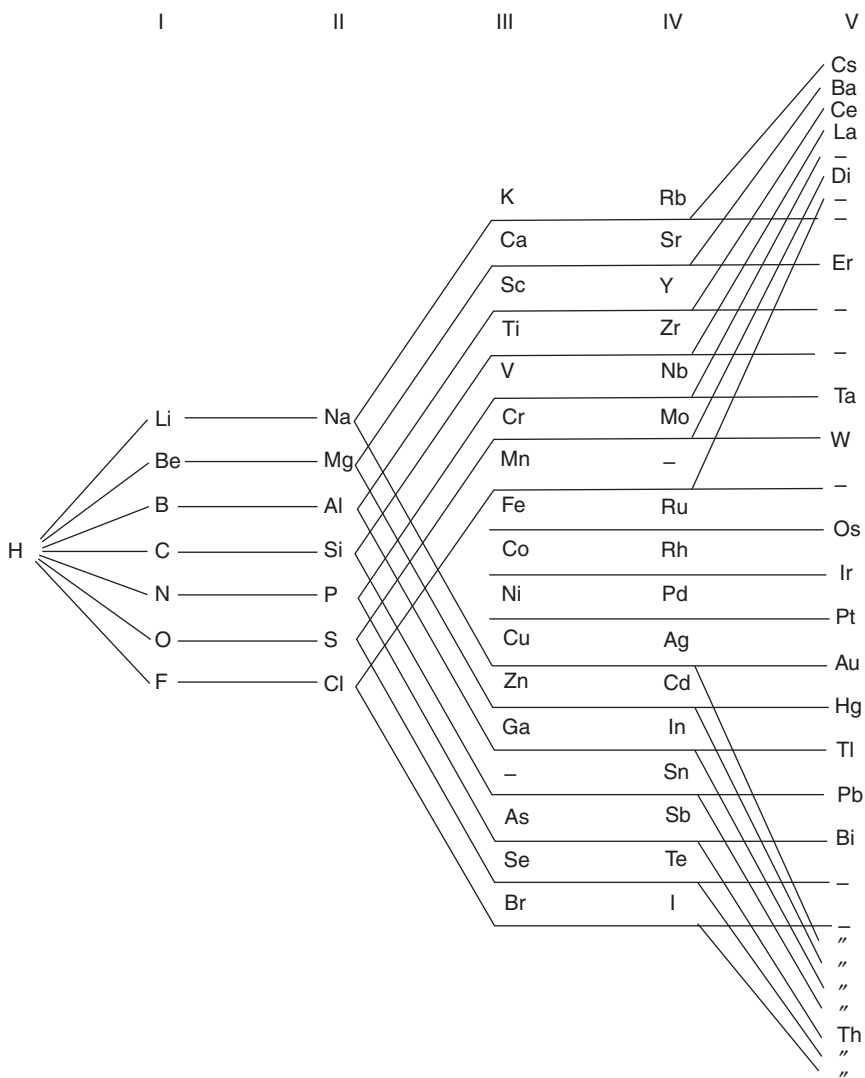


FIGURE 24 Bayley's pyramidal periodic table (1882). Reproduced from Bayley (1882).

Thomsen's system differed from Bayley's pyramid in an important way. Both tables consisted of three main parts. The first part contained the elements of the short periods (Li–F and Na–Cl); the second part included the long periods of 17 elements (K–Br and Rb–I); and the third section covered the remaining 31 elements from cesium to uranium. Analogous elements were connected by lines and due to the existence of odd and even series, most elements were related to a pair of elements. Thus Na was related

with K and Cu (and therefore also with Rb and Ag). Some elements remained completely unconnected. These were the transition metal triads {Fe, Co, Ni}, {Ru, Rh, Pd}, and {Os, Ir, Pt} which represented a transition from the odd to the even series. The important difference between the two tables is that Thomsen connected the elements Rb–Ag with only one element, instead of two as Bayley did. The consequences were explained by Thomsen in his paper:

Just as silicon in the first group shows similarities with titanium on the one hand and with germanium on the other, there exists in exactly the same way a relationship between the elements of the 2nd and 3rd groups, for example from zirconium to cerium with an atomic weight of 140 on the one hand and from zirconium to an unknown element with an atomic weight around 181 on the other. There are a large number of rare-earth elements in between these two elements which are related to one another like the central elements of the 3rd series placed between manganese and zinc. (Thomsen, 1895; Trifonov, 1966).

Thomsen even tried to explain the analogy between the rare-earth elements on the one hand and the elements from group VIII on the other, just as Mendeleev had tried 26 year earlier (see Section 3). But the most important aspect of Thomsen's table was not the apparent analogy with the transition metals, but the fact that the rare-earth elements did not bear any relationship with the elements of the preceding period from Rb to I (except for La, Ce and Yb). The rare earths did not belong to any of the eight groups and they were fitted in between group IV and V as an intergroup. Thomsen moreover correctly predicted the existence of a total of 15 rare earths from lanthanum to the unknown element after ytterbium. The element with atomic weight 181 did not belong to the rare-earth elements, but was a zirconium homologue. One thus starts to understand why Bohr preferred this table and why he used it during his Noble Lecture in 1922 (Figure 21) (Bohr, 1922b). The element after ytterbium was lutetium, a genuine trivalent rare earth, while element 72 clearly was a tetravalent zirconium homologue. Bohr remembered this table from his student time. A large version of Thomsen's table hung in one of the auditoria of the Polytechnical Institute where Bohr was following the lectures on inorganic chemistry from Niels Bjerrum (1879–1958).

The sequence of rare earths in Thomsen's table was almost correct. He left a number of vacant spaces between Pr and Sm for element 61 (Pm), between Sm and Gd for Eu, between Tb and Er and between Er and Tm for Dy/Ho, and after Yb for Lu and Hf. Bohr was not the first to grasp the advantages of Thomsen's intergroup layout. Both Richards (1898) and the Australian chemist Steele (1901) adhered to the intergroup methodology. It must also be noted that Thomsen's system was not the first so-called

inverted system, with horizontal groups and vertical periods. The chemist Henry Bassett (1892) had proposed a similar system and he also adhered to the intergroup methodology (Figure 25). The rare-earth elements thus formed a separate group and consisted of 18 elements. If these systems would be reverted again, vertical groups and horizontal periods would be obtained.

Alfred Werner (1866–1919) was the first to publish a long form table according to the intergroup methodology (Figure 26) (Werner, 1905a,b). The rare-earth elements (La–Yb) were isolated from the other elements and formed an intergroup between group II and group III. Lanthanum did not belong to the same group as scandium and yttrium. Lutetium on

				Cs	133		226?		
				Ba	137		?		
				La	138·2		?		
				Ce	140·2	Th	232·6		
				Ndy	140·8		?		
				Pdy	143·6	U	239·6		
					148?		241?		
				Sm	150		?		
					?		?		
					?		?		
					154?		248?		
					?		?		
				Tb	159·5		?		
				Ho	162		?		
					?		?		
				Er	166·3		?		
					169?		263?		
				Tm	170·4				
					?				
				Yb	173				
			K	39·1	Rb	85·5	174?		
			Ca	40	Sr	87·6	?		
			Sc	44	Y	89·1	?		
			Ti	48	Zr	90·6	?		
			V	51·4	Nb	94	Ta 182·6		
			Cr	52·1	Mo	96	W 184		
			Mn	55		100?	189?		
			Fe	56	Ru	101·6	Os 191·7		
			Ni	58·7	Rh	103·5	Ir 193·1		
			Co	59	Pd	106·6	Pt 195		
Li	7	Na	23	Cu	63·4	Ag	107·9	Au	197·3
Be	9	Mg	24·3	Zn	65·3	Cd	112	Hg	200
B	11	Al	27	Ga	69	In	113·7	Tl	204·2
C	12	Si	28·4	Ge	72·3	Sn	119	Pb	207
N	14	P	31	As	75	Sb	120	Bi	208·9
O	16	S	32·1	Se	79	Te	125		?
F	19	Cl	35·5	Br	80	I	126·9		216?

FIGURE 25 Bassett's periodic table (1892). Reproduced from Bassett (1892).

																He													
																4													
																Be	B	C	N	O	VI	Ne							
																9,1	12	14,04	16,00	19	20								
F																													
1,008																													
																Mg	Al	Si	P	S	Cl	A							
																24,36	27,1	28,4	31,0	32,06	35,45	39,9							
Li																													
7,09																													
Na																													
23,05																													
K	Ca													Sc	Ti	V	Cr	Mn	Fe	Cu	Ni	Zn	Ga	Ge	As	Se	Br	Kr	
39,10	40,1													44,1	48,1	51,2	52,1	55,0	55,9	59,0	58,7	63,6	65,4	70	72	75,0	79,1	79,96	81,12
Eb	Br													Y	Zr	Nb	Mo	Ru	Rh	Pd	Ag	Cd	In	Sn	Sb	Te	J	X	
85,4	87,6													89,0	90,7	94	95,0	101,7	103,0	106	107,83	112,9	114	118,5	120	127,6	126,36	128	
Ce	Ba	La	Ce	Pr	Sm	Eu	Gd	Tb	Ho	Er	Tm	Yb			Os	Ir	Pt	Au	Hg	Tl	Pb	Bi							
133	137,4	138	140	140,9	140,9	151,79	158	160	162	166	171	173,0			191	193,0	194,8	197,2	200,5	204,1	208,0	209,0							
Ra	La	Tb											U											Po	Bi	Te			
225	173	232,0											238,0																

FIGURE 26 Werner's periodic table with an intergroup accommodation of the rare-earth elements (1905). Reproduced from Werner (1905b).

the other hand, according to Werner's table, was not a rare-earth element, but a transition metal (see also Section 7). Werner was moreover the first to suggest the existence of another intergroup of heavier elements, below and analogous to the rare-earth elements. This idea was taken up by Glenn Seaborg and is now known as the *actinide hypothesis* (see also Section 6). In Werner's system, the pair praseodymium–neodymium has been arranged according to decreasing atomic weight: Werner placed neodymium (143.6) before praseodymium (140.5). The reason given by Werner for this proposal was the similarity in color of the hydrated cobalt (II) and neodymium(III) salts which are violet on the one hand, and the similarity in color of the hydrated nickel(II) and praseodymium(III) salts which are green on the other hand. The order cobalt–nickel in the periodic table suggested Werner to choose the order neodymium–praseodymium as well. Notice that the pair cobalt–nickel is an example of the deviation from increasing atomic weight in the periodic table. Baur (1911) published a similar table, but he included the rare earths between group IV and V (except La and Ce, see Figure 27). The best representation, according to the authors' opinion, was the *left-step periodic table* which had been devised in the period 1927–1929 by the French engineer, inventor and biologist Charles Janet (1849–1932) (see Section 7). A remarkable periodic system is the circular system of Janet (Janet, 1929), which was based on his left-step table (Figure 28). The advantage of this representation is its compactness. Janet's table gives equal value to all the elements, including

Nullte Gruppe	Erste Gruppe		Zweite Gruppe		Dritte Gruppe		Vierte Gruppe		Gruppe der seltenen Erden	Fünfte Gruppe		Sechste Gruppe		Siebente Gruppe	Eisen-Platin-Gruppe
	Haupt- gruppe	Neben- gruppe	Haupt- gruppe	Neben- gruppe	Haupt- gruppe	Neben- gruppe	Haupt- gruppe	Neben- gruppe		Haupt- gruppe	Neben- gruppe	Haupt- gruppe	Neben- gruppe		
He	Li	Be	B	[C					N	O	F				
Ne	Na	Mg	Al] [Si					P	S	Cl				
Ar	K	Cu	Sc	Ti						V	Cr			{ Mn Ni Fe Co	
		Cu	Zn	Ga	Ge				[As	Se	Br				
Kr	Rb	Sr	Y	Zr					Nb	Mo				Ru Rh Pd	
		Ag	Cd	In	Sn				[Sb	Te	J				
X	Cs	Ba	La	Ce] { Pr Sm Gd Dy Er Yb Nd Eu Tb Ho Tm Lu				Ta	W				Os Ir Pt	
		Au	Hg	Tl	Pb				[Bi	Pol.	Supra- jod				
Em	Supra- cäs.	Ra	Akt.	Th					Supra- tantal	U					

FIGURE 27 Baur's periodic table (1911). Reproduced from Baur (1911).

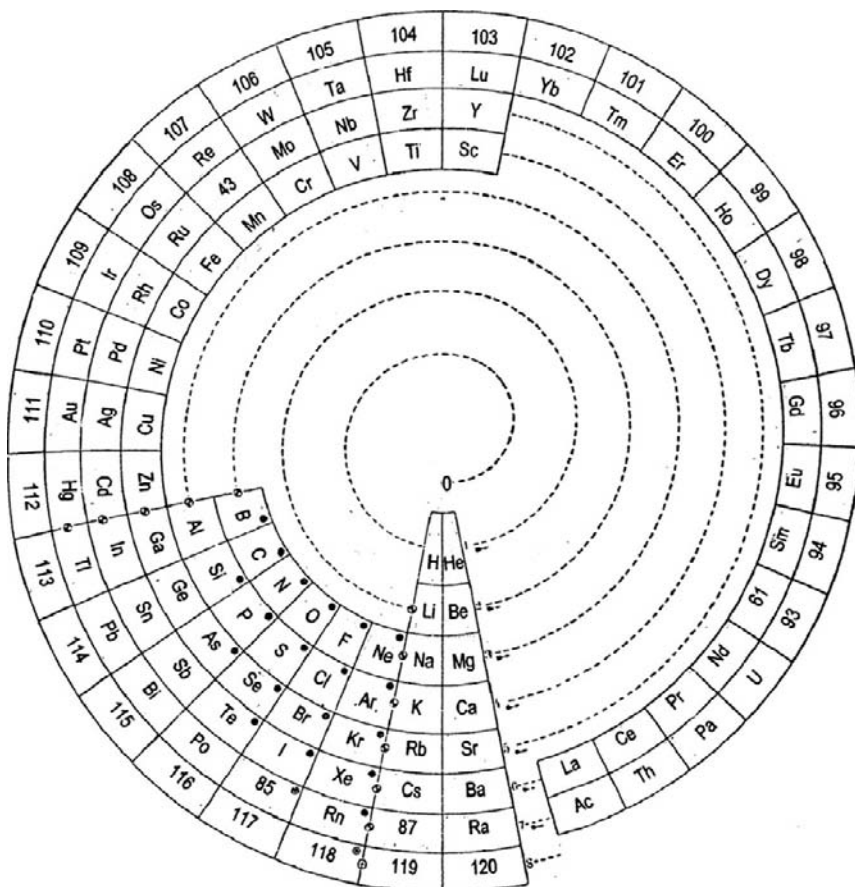


FIGURE 28 Modified circular system of Janet (1929). Reproduced from Stewart (2007), with permission of Springer.

the rare earths. Notice that Janet places lutetium and not lanthanum below yttrium (see Section 7).

A survey of about 100 educational and professional textbooks in the field of descriptive inorganic chemistry was entailed by one of the authors (P.T.) in order to investigate the popularity of the three types of accommodation. A total of 92 chemistry textbooks for both undergraduate and graduate students from the period 1846–1963 was selected at random and thoroughly investigated. Only 54 manuals out of the 92 did contain a periodic table. One handbook exhibited a spiral form of the periodic table (Shepard, 1886), but all other textbooks represented short and long forms of the periodic table. An important observation rested on the fact that almost all textbooks adhered to one of two possible accommodation

methodologies. Thus 40 textbooks placed the rare-earth elements according to a homologous accommodation, and the other 14 adhered to the intraperiodic accommodation methodology. The first intergroup accommodation only appeared in 1946 (Yost and Russell, 1946). Indeed, the well known placement of both lanthanides and actinides underneath the main body of the “modern” periodic table became only popular after the Second World War.

6. SEABORG'S ACTINIDE CONCEPT

Although Bohr considered thorium, protactinium, and uranium as members of a second series of rare earths, the majority of chemists remained convinced that these elements were homologues of hafnium, tantalum and tungsten, for a time after Bohr had formulated his atomic theory. The reason for the delay of acceptance of a second rare-earth series was mainly due the fact that the highest valence states of thorium (+IV), protactinium (+V) and uranium (+VI) suggested that these elements were transition metals. Moreover, with the exception of thorium and cerium, there are, besides the similarities in electronic configuration, only few similarities in chemical properties between the early actinide elements and the lanthanides. The chemical properties of uranium seem to differ very much from those of neodymium, whereas on the other hand there are striking similarities between uranium and the elements of group 5 (Cr, Mo, W). For instance, uranium and tungsten both form hexachlorides (UCl_6 and WCl_6). Uranium forms the ion $\text{U}_2\text{O}_7^{2-}$ and the compound UO_2Cl_2 , while chromium forms $\text{Cr}_2\text{O}_7^{2-}$ and CrO_2Cl_2 . However, one should note that the dissimilarities between uranium and neodymium are only evident when hexavalent uranium (the most common oxidation state for uranium) and trivalent neodymium (the most common oxidation state for neodymium) are compared. Uranium(III) on one hand, shows many similarities with neodymium(III), whereas on the other hand, uranium(IV) resembles thorium(IV) and cerium(IV). Another point of confusion was the very small energy differences between the 5f- and 6d-shell, even in the range of the chemical binding energy, so that it was difficult to predict when the 5f-shell started to be filled. It was assumed that in thorium, protactinium, and uranium the 6d-shell was being filled. Goldschmidt (1924) predicted that the transuranium elements up to element 96 would be platinum group elements. Nevertheless, several researchers believed in the existence of a second series of rare earths, even before the introduction of Bohr's atomic theory in 1922. As early as 1892, Bassett considered thorium and uranium to be analogous to cerium and praseodymium, respectively (Bassett, 1892). It should be noted that he preferred the order {Ce, Nd, Pr} rather than {Ce, Pr, Nd} for the

lanthanides. Werner considered thorium as an analogue of cerium and uranium as an analogue of europium. Both authors reserved open spaces in their periodic tables for other members of the second rare earths series that were still undiscovered at that time.

In 1926, Goldschmidt demonstrated the analogies between the elements {Th, Pa, U} and the lanthanides on the basis of the observation that the volumes of Th^{4+} and U^{4+} showed the same contractions as the ions of the lanthanide series. Striking early examples of periodic tables in which actinium, thorium, protactinium, and uranium are considered as homologues of the rare earths lanthanum, cerium, praseodymium, and neodymium are the circular system and left-step table of Charles Janet (Janet, 1929).

Seaborg (1944, 1945) noticed that whereas thorium, protactinium, and uranium showed similarities in chemical behavior with zirconium, tantalum, and tungsten, respectively, neptunium and plutonium did not show such similarities with rhenium and osmium, or with technetium and ruthenium. For instance, in contrast to the volatiles osmium tetroxide and ruthenium tetroxide, there exists no volatile plutonium tetroxide. On the other hand, the chemical properties of neptunium and plutonium are very similar to those of thorium and uranium. These four elements have a stable +IV oxidation state. ThO_2 , UO_2 , NpO_2 , and PuO_2 are isomorphous and there is a steady decrease of the metallic ion radius when going from Th^{4+} to Pu^{4+} . Other evidence was based on magnetic susceptibility data, on the absorption spectra of the ions in aqueous solution and in crystals, on the spectra of the gaseous atoms, and on additional crystallographic and chemical data. These observations made Seaborg propose the existence of a second rare-earth series that begins with actinium, in the same sense as that the lanthanide series begins with lanthanum. He termed this second rare-earth series the "*actinide series*." The actinide elements do not tend to occupy the 6d orbital, but there is a gradual filling of the 5f shell over the actinide series. Although Seaborg assumed that thorium would be the first element at which the 5f orbital becomes occupied, he also considered the possibility that thorium and protactinium do not have 5f electrons, and that uranium has three 5f electrons. The actinide concept has as a consequence that +III is a characteristic oxidation state for the actinides. However, a striking difference between the lanthanide and actinide series is the existence of oxidation states higher than +IV in the actinide series (+V and +VI). This is an indication that the 5f electrons are less tightly bonded than the 4f electrons. Seaborg (1949) introduced the form of the periodic table with which so many chemists are familiar with: one that considers the lanthanides and actinides as footnotes of the main body of the periodic table. A detailed account of the development of the actinide concept can be found in Chapter 118 in this Handbook (Seaborg, 1994).

7. RARE-EARTH CRISIS ANNO 2010

In a note in the *Journal of Chemical Education*, Clark and White (2008) recently described the three most common ways of representing the f-block elements in the medium-long form periodic table (Figures 29–31). As should be clear from all these different representations, especially the positions of lanthanum (La), actinium (Ac), lutetium (Lu) and lawrencium (Lr) remain problematic. In response to the short paper of Clark and White, several scientists and teachers gave their opinion in subsequent issues of the *Journal of Chemical Education* (Lavelle, 2008a,b, 2009; Stewart, 2008; Jensen, 2008b, 2009; Clark 2008; Scerri, 2009a; Laing, 2009). Everyone seems to wonder how the boundaries of the lanthanides and the actinides should be marked. Some chemists consider the f-block to consist of two blocks of 15 elements each, with La, Ac, Lu, and Lr as the boundary elements. This type of accommodation is represented in the 15LaAc tables (Figure 29), the type which is preferred by IUPAC. Others limit the number

	1																		18
	1A	2																	0
1	H	2																	He
2	Li	Be																	Ne
3	Na	Mg	3	4	5	6	7	8	9	10	11	12							Ar
			IIIB	IVB	VB	VIB	VII	VIII	IX	X	XI	XII							
4	K	Ca	Sc	Ti	V	Cr	Mn	Fe	Co	Ni	Cu	Zn	Ga	Ge	As	Se	Br	Kr	
5	Rb	Sr	Y	Zr	Nb	Mo	Tc	Ru	Rh	Pd	Ag	Cd	In	Sn	Sb	Te	I	Xe	
6	Cs	Ba		Hf	Ta	W	Re	Os	Ir	Pt	Au	Hg	Tl	Pb	Bi	Po	At	Rn	
7	Fr	Ra		Rf	Db	Sg	Bh	Hs	Mt	Ds	Rg	Cn							
6	La	Ce	Pr	Nd	Pm	Sm	Eu	Gd	Tb	Dy	Ho	Er	Tm	Yb	Lu				
7	Ac	Th	Pa	U	Np	Pu	Am	Cm	Bk	Cf	Es	Fm	Md	No	Lr				

15LaAc medium-long form periodic table

	1																		18																				
	1A	2																	0																				
1	H	2																	He																				
2	Li	Be																	Ne																				
3	Na	Mg	3										4	5	6	7	8	9	10	11	12																		
			IIIB										IVB	VB	VIB	VII	VIII	IX	X	XI	XII																		
4	K	Ca	Sc										Ti	V	Cr	Mn	Fe	Co	Ni	Cu	Zn	Ga	Ge	As	Se	Br	Kr												
5	Rb	Sr	Y										Zr	Nb	Mo	Tc	Ru	Rh	Pd	Ag	Cd	In	Sn	Sb	Te	I	Xe												
6	Cs	Ba	La	Ce	Pr	Nd	Pm	Sm	Eu	Gd	Tb	Dy	Ho	Er	Tm	Yb	Lu	Hf	Ta	W	Re	Os	Ir	Pt	Au	Hg	Tl	Pb	Bi	Po	At	Rn							
7	Fr	Ra	Ac	Th	Pa	U	Np	Pu	Am	Cm	Bk	Cf	Es	Fm	Md	No	Lr	Rf	Db	Sg	Bh	Hs	Mt	Ds	Rg	Cn													

15LaAc long form periodic table

s-block f-block and d-block p-block

FIGURE 29 A medium-long form and long form depiction of the 15LaAc periodic table. In this representation, the whole f-block belongs to group 3 (IIIB) of the periodic table and consists of 15 groups of f-block elements with lanthanum (La) and actinium (Ac) as the first representatives of each row and lutetium (Lu) and lawrencium (Lr) as the last ones. As should be clear from the long form periodic table, an intermingling occurs between the f-block and d-block.

	1																		18
	IA																		0
1	H	2																	He
	IIA																		
2	Li	Be																	Ne
3	Na	Mg	3	4	5	6	7	8	9	10	11	12							
			IIIB	IVB	VB	VIB	VII B	VIII B	IX	X	IB	IIB							
4	K	Ca	Sc	Ti	V	Cr	Mn	Fe	Co	Ni	Cu	Zn							
5	Rb	Sr	Y	Zr	Nb	Mo	Tc	Ru	Rh	Pd	Ag	Cd							
6	Cs	Ba	La	Hf	Ta	W	Re	Os	Ir	Pt	Au	Hg							
7	Fr	Ra	Ac	Rf	Db	Sg	Bh	Hs	Mt	Ds	Rg	Cn							
6	Ce	Pr	Nd	Pm	Sm	Eu	Gd	Tb	Dy	Ho	Er	Tm	Yb	Lu					
7	Th	Pa	U	Np	Pu	Am	Cm	Bk	Cf	Es	Fm	Md	No	Lr					

14CeTh medium-long form periodic table

	1																		18
	IA																		0
1	H	2																	He
	IIA																		
2	Li	Be																	Ne
3	Na	Mg	3																
			IIIB																
4	K	Ca	Sc																
5	Rb	Sr	Y																
6	Cs	Ba	La	Ce	Pr	Nd	Pm	Sm	Eu	Gd	Tb	Dy	Ho	Er	Tm	Yb	Lu		
7	Fr	Ra	Ac	Th	Pa	U	Np	Pu	Am	Cm	Bk	Cf	Es	Fm	Md	No	Lr		

s-block d f-block d-block p-block

14CeTh long form periodic table

FIGURE 30 A medium-long form and long form depiction of the 14CeTh periodic table. In this representation, the f-block consists of 14 groups of f-elements with cerium (Ce) and thorium (Th) as the first representatives of each row and lutetium (Lu) and lawrencium (Lr) as the last ones. Lanthanum (La) and actinium (Ac) are accommodated as d-block elements in group 3 (IIIB) of the periodic table, below scandium (Sc) and yttrium (Y). The d-block has been torn apart in the long form, due to the insertion of the f-block.

of f-block elements to 28 (i.e., 2×14), but there exist two different opinions. The first group of chemists adheres to the 14CeTh tables (Figure 30) and they consider Ce and Th to be the first representatives of the lanthanides and actinides respectively, while Lu and Lr form the other boundary. The second group of chemists, on the other hand, shifts the boundary one box to the left and they look upon La and Ac as the first representatives of the f-block elements, and Yb and No as the last ones. This type of accommodation is represented in the 14LaAc tables (Figure 31). In the 15LaAc table, it seems that the two boxes below scandium (Sc) and yttrium (Y) in group IIIB (group 3) remain vacant, but as Jensen (2008b) correctly pointed out, they rather contain the symbols La–Lu and Ac–Lr, respectively, thus indicating that all these 30 elements in the footnote belong in just those two boxes. This becomes clear when expanding the medium-long form into the long form. However, this interpretation does not go back to the electronic interpretations of the 1920s, as Jensen stated, but to Bohuslav Brauner's asteroid hypothesis of 1902, in which the entire group

		1 IA																	18 0
1	H	2 IIA											13 IIIA	14 IVA	15 VA	16 VIA	17 VIIA	He	
2	Li	Be											B	C	N	O	F	Ne	
3	Na	Mg	3 IIIB	4 IVB	5 VB	6 VIB	7 VIIB	8 VIIIB	9 VIIIB	10 VIIIB	11 IB	12 IIB	Al	Si	P	S	Cl	Ar	
4	K	Ca	Sc	Ti	V	Cr	Mn	Fe	Co	Ni	Cu	Zn	Ga	Ge	As	Se	Br	Kr	
5	Rb	Sr	Y	Zr	Nb	Mo	Tc	Ru	Rh	Pd	Ag	Cd	In	Sn	Sb	Te	I	Xe	
6	Cs	Ba	La	Hf	Ta	W	Re	Os	Ir	Pt	Au	Hg	Tl	Pb	Bi	Po	At	Rn	
7	Fr	Ra	Lr	Rf	Db	Sg	Bh	Hs	Mt	Ds	Rg	Cn							

6	La	Ce	Pr	Nd	Pm	Sm	Eu	Gd	Tb	Dy	Ho	Er	Tm	Yb
7	Ac	Th	Pa	U	Np	Pu	Am	Cm	Bk	Cf	Es	Fm	Md	No

14LaAc medium-long form periodic table

		1 IA																	18 0
1	H	2 IIA																	He
2	Li	Be																	Ne
3	Na	Mg																	Ar
4	K	Ca																	Kr
5	Rb	Sr																	Xe
6	Cs	Ba	La	Ce	Pr	Nd	Pm	Sm	Eu	Gd	Tb	Dy	Ho	Er	Tm	Yb			Rn
7	Fr	Ra	Ac	Th	Pa	U	Np	Pu	Am	Cm	Bk	Cf	Es	Fm	Md	No			

s-block f-block d-block p-block

14LaAc long form periodic table

FIGURE 31 A medium-long form and long form depiction of the 14LaAc periodic table. In this representation, the f-block consists of 14 groups of f-elements with lanthanum (La) and actinium (Ac) as the first representatives of each row and ytterbium (Yb) and nobelium (No) as the last ones. Lutetium (Lu) and lawrencium (Lr) are accommodated as d-block elements in group 3 (IIIB) of the periodic table, below scandium (Sc) and yttrium (Y). The 14LaAc periodic table is in perfect agreement with the Madelung rule.

of rare earths should occupy a single place in the system which ordinarily would belong to a single element (Section 4.3). Admittedly, this is the only representation where the similarity of the lanthanide elements is rendered clear. Nevertheless, one cannot agree with this type of accommodation because the whole f-block gets included into the d-block, and no intermingling of the s-, p-, d-, and f-blocks is allowed in the modern periodic table. As a consequence, the discussion gets shifted from where the lanthanides and actinides should be placed as a whole to which two elements should come underneath scandium (Sc) and yttrium (Y) in the third group (IIIB). This could be either lanthanum (La) and actinium (Ac) as depicted in the 14CeTh table, or lutetium (Lu) and lawrencium (Lr) as in the 14LaAc table. When taking the 14CeTh table into consideration, one notices that the d-block has been torn apart due to the insertion of the f-block. Of course, the d-block could be restored by merging the two parts together, but this would result in a non-logical table where the natural sequence of atomic numbers gets interrupted twice, as depicted in Scerri's letter (Scerri,

2009a). In the 14LaAc table, on the other hand, the d-block has remained intact. Thus, from just having a quick look at both tables, one has to admit that the 14LaAc table looks more “natural.” This intuitive thesis can be moreover scientifically substantiated.

There is quite a lot of chemical evidence that lutetium, instead of lanthanum, should be placed in the same column of the periodic table as scandium and yttrium. This issue has been addressed by several authors (Dash, 1967; Hamilton, 1965; Hamilton and Jensen, 1963; Jensen, 2009; Laing, 2005; Lavelle, 2008a; Merz and Ulmer, 1967; Nuroh and Wendin, 1981; Sanderson, 1964; Scerri, 2009a; Villar, 1966) and in a very convincing way by Jensen (1982). Even simple physical and structural properties of the elements are in favor of placing lutetium and not lanthanum below yttrium in the periodic table. The melting point of La is 918 °C, while those of Sc, Y, and Lu are 1,541 °C, 1,522 °C, and 1,663 °C, respectively (Beaudry and Gschneidner, 1978). The room-temperature crystal structure of Sc, Y, and Lu is the hexagonal closed packed (hcp) structure, whereas La has a different hexagonal structure, which is also found for the lanthanides and for the transuranium elements. Sc_2O_3 , Y_2O_3 , and Lu_2O_3 have the same crystal structure, but the crystal structure of La_2O_3 is different. Also ScCl_3 , YCl_3 and LuCl_3 belong to the same structural type, but LaCl_3 does not. X-ray spectroscopy has shown that lutetium, but not lanthanum, has a structure of its conduction band that is similar to that of transition metals (Nuroh and Wendin, 1981). Scandium, yttrium and lutetium are not superconductive at atmospheric pressure, but lanthanum metal becomes conducting at 4.9 K (Probst and Wittig, 1978). Also trends in the atomic radii, the sum of the first two ionization potentials, and the electronegativity favor the grouping (Sc, Y, Lu) instead of (Sc, Y, La). Lanthanum occurs together with the cerium group elements in minerals, whereas lutetium and yttrium occur together with the other yttrium group elements.

With so much chemical and physical evidence supporting the accommodation of lutetium below yttrium in the periodic system, one can wonder why in so many periodic tables lanthanum is placed below yttrium. The answer lies according to Jensen (1982) in incorrect older electronic configurations. The accommodation of the elements in the periodic table is based on electronic configurations and the concept of the differentiating electron. Earlier spectroscopic work seemed to indicate that, with a few exceptions, the ground state electronic configuration of the rare earth atoms was of the form $[\text{Noble Gas}](n-2)f^{x-1}(n-1)d^1ns^2$. Ytterbium was assigned the ground state $[\text{Xe}]4f^{13}5d^16s^2$ and lutetium the ground state $[\text{Xe}]4f^{14}5d^16s^2$. These two ground state configurations differ only in the number of electrons in the 4f orbitals. Lutetium has a 4f differentiating electron, so that it was assumed to be the last member of the f-block for period 6. The ground state configurations of barium and lanthanum are $[\text{Xe}]6s^2$ and $[\text{Xe}]5d^16s^2$, respectively, so that lanthanum has a 5d differentiating electron and should be accommodated in group IIIB (group 3) as the

first member of the d-block of period 6. Moreover, the ground state of lanthanum seemed to be similar with those of the other elements of group IIIB: $[\text{Ar}]3d^14s^2$ for scandium and $[\text{Kr}]4d^15s^2$ for yttrium.

More recent spectroscopic work showed that only lanthanum, gadolinium, and lutetium have a ground state of the type $[\text{Xe}]4f^{x-1}5d^16s^2$, whereas the ground state of all the other lanthanides is $[\text{Xe}]4f^x6s^2$. Thus, the electronic configuration of Yb is $[\text{Xe}]4f^{14}6s^2$. With $[\text{Xe}]4f^{14}5d^16s^2$ representing the ground state of Lu, the differentiating electron for Lu clearly is a 5d electron. For the actinides only seven members (Ac, Pa, U, Np, Pu, Cm, Lr) have the old electronic configuration $[\text{Rn}]5f^{x-1}6d^17s^2$. The ground state configuration of thorium is $[\text{Rn}]6d^27s^2$, while that of the remaining actinide atoms is $[\text{Rn}]5f^x7s^2$. The ground state configuration of nobelium is $[\text{Rn}]5f^{14}7s^2$ while that of lawrencium is $[\text{Rn}]5f^{14}6d^17s^2$. This results in a 6d differentiating electron for lawrencium, just as was the case for lutetium. All this evidence shows that lanthanum and actinium should be considered as the first members of the f-block (not cerium and thorium), while ytterbium and nobelium should be considered as the last members of the f-block (not lutetium and lawrencium). Lutetium and lawrencium are the first members of the d-block for period 6 and 7, and should be accommodated along with scandium and yttrium in group IIIB (group 3). This also implies that the preferred representation of the medium-long form periodic table is 14LaAc (Figure 31).

It should be noted that although for decennia lanthanum and actinium could be found below yttrium in most periodic tables, some authors have placed lutetium below yttrium in the past. For instance, in the periodic table of Werner (1905a,b), there is an open place below yttrium at the position where lutetium is expected, but it should be realized that at that time lutetium had not yet been discovered (this was in 1907). However, Werner did not consider lanthanum as a homologue of yttrium, because of the differences in chemical properties between these two elements. Also in the circular system of Janet (Figure 28), the left-step table of Janet (Figure 32) and in the periodic table of Bohr (Figure 21), lutetium was placed below yttrium.

A major disadvantage of the medium-long forms of the periodic table is that the lanthanides and actinides are dissected from the main body of the periodic table and degraded to footnotes. The medium-long forms give the impression that the lanthanides and actinides are unimportant elements. This notion of unimportance is even enforced by the IUPAC notation of the groups in the medium-long form of the periodic table from 1 to 18, so that the lanthanides and actinides are not numbered at all. The long forms of the periodic table are preferred over the medium-long forms, because they give equal importance to the s-, p-, d-, and f-blocks. In this respect, the long-form of the 14LaAc table is a better conventional representation of the periodic system than the medium-long form of the 14LaAc table.

																	H	He	1													
																	Li	Be	2													
															B	C	N	O	F	Ne	Na	Mg	3									
															Al	Si	P	S	Cl	Ar	K	Ca	4									
													Sc	Ti	V	Cr	Mn	Fe	Co	Ni	Cu	Zn	Ga	Ge	As	Se	Br	Kr	Rb	Sr	5	
													Y	Zr	Nb	Mo	Tc	Ru	Rh	Pd	Ag	Cd	In	Sn	Sb	Te	I	Xe	Cs	Ba	6	
La	Ce	Pr	Nd	Pm	Sm	Eu	Gd	Tb	Dy	Ho	Er	Tm	Yb	Lu	Hf	Ta	W	Re	Os	Ir	Pt	Au	Hg	Tl	Pb	Bi	Po	At	Rn	Fr	Ra	7
Ac	Th	Pa	U	Np	Pu	Am	Cm	Bk	Cf	Es	Fm	Md	No	Lr	Rf	Db	Sg	Bh	Hs	Mt	Ds	Rg	Cn								8	

f-block

 d-block

 p-block

 s-block

FIGURE 32 The left-step periodic table. In this representation, the f-block consists of 14 groups of f-elements with lanthanum (La) and actinium (Ac) as the first representatives of each row and ytterbium (Yb) and nobelium (No) as the last ones. Lutetium (Lu) and lawrencium (Lr) are accommodated as d-block elements in the periodic table, below scandium (Sc) and yttrium (Y). The left-step periodic table is in perfect agreement with the Madelung rule.

Another reason why the 14LaAc table is the preferred representation of the periodic table is because it can be derived from the so-called *Madelung Rule*, which is named after Erwin Madelung (1881–1972). The Madelung rule is also called *Klechkowski's rule* in some countries. Niels Bohr was one of the first scientists who attempted to understand the periodic table by relying on electronic configurations (Section 5.1). His calculations on the hydrogen atom had indicated that the energy of this one-electron system increases with increasing value of n . Therefore, it seemed logical that the electronic shells of the other 85 known elements would be filled in exactly the same way, according to the following sequence:

$$1s < 2s < 2p < 3s < 3p < 3d < 4s < 4p < 4d < 4f < 5s < 5d < 5f < \dots$$

If this had been the case, the old quantum theory would have been complete. Unfortunately, the investigation of atomic spectra made it clear that the shells are not filled in that strictly sequential manner, but rather in a more complex way, as described by the following order:

$$1s < 2s < 2p < 3s < 3p < 4s < 3d < 4p < 5s < 4d < 5p < 6s < 4f < 5d < \dots$$

Thus it appeared that the fourth shell started to be filled, even before the third shell had been completely filled. Therefore, the electronic configuration of potassium (K, $Z = 19$) was not $1s^2 2s^2 3s^2 3p^6 3d^1$ as expected, but $1s^2 2s^2 2p^6 3s^2 3p^6 4s^1$. In other words, the simple (n, l) rule, according to which the orbitals are filled in order of increasing n (and l for the same value of n), failed to construct the exact filling sequence. Consequently, the correct order had to be deduced in a semi-empirical way (i.e., with the aid of spectroscopic experiments). Only then could one derive the exact electronic configurations of the elements. But in 1936, Madelung

published his empirical $(n + l, n)$ rule, which correctly predicted the filling sequence in neutral atoms (Madelung, 1936):

- (1) With increasing nuclear charge Z , the orbitals are filled in order of increasing $N = n + l$.
- (2) For a fixed value of N , the orbitals are filled in the order of increasing n .

Thus, with the help of the Madelung rule, it could be explained why the 4s-orbital ($n = 4, l = 0 \rightarrow n + l = 4$) gets filled before the 3d-orbital ($n = 3, l = 2 \rightarrow n + l = 5$). Application of the Madelung rule gives rise to the data shown in Table 1. From this table, it is evident that the 4f-block starts with lanthanum (La, $Z = 57$) and ends with ytterbium (Yb, $Z = 70$). Consequently, lutetium (Lu, $Z = 71$) is the first member of the 5d-block. In analogy, one can state that the 5f-block starts with actinium (Ac, $Z = 89$), while the last member of this group is nobelium (No) with an atomic number of $Z = 102$. Finally, the next element in line, lawrencium (Lr, $Z = 103$), will start the 6d-block. Thus, according to the Madelung rule, lutetium (Lu) and lawrencium (Lr) should be placed in the third group (IIIB) underneath scandium (Sc) and yttrium (Y), whereas lanthanum (La) and actinium (Ac) should be regarded as the first representatives of the f-block elements. Therefore, only the 14LaAc table is in perfect agreement with the Madelung rule. Alternatively, one could also use Table 1 as a framework or quantum map for a new representation of the periodic system, as depicted in Figure 32. This form, known as the *Left-Step Table* or *Janet Periodic Table*, was first devised by Charles Janet in 1929 (Janet, 1929) and it offers certain advantages in comparison with the more conventional medium-long form (Bent, 2006; Katz, 2001). For example, the number of elements in the eight periods of the Janet table are given by the following sequence $\{2, 2, 8, 8, 18, 18, 32, 32\}$. Thus, due to the pairing of all the periods, one obtains the distinctive stepped profile of

TABLE 1 Application of the empirical $(n + l, n)$ rule (Madelung rule) according to which the orbitals in neutral atoms are filled in order of increasing $n + l$, and n for fixed $n + l$. The exact filling sequence is obtained by reading the quantum map from left to right, and top to bottom

$n + l$	$l = 3$	$l = 2$	$l = 1$	$l = 0$	N_{n+l}^{\max}	$Z_i \rightarrow Z_f$	$X_i \rightarrow X_f$
1	–	–	–	$1s^2$	2	$1 \rightarrow 2$	H \rightarrow He
2	–	–	–	$2s^2$	2	$3 \rightarrow 4$	Li \rightarrow Be
3	–	–	$2p^6$	$3s^2$	8	$5 \rightarrow 22$	B \rightarrow Mg
4	–	–	$3p^6$	$4s^2$	8	$23 \rightarrow 30$	Al \rightarrow Ca
5	–	$3d^{10}$	$4p^6$	$5s^2$	18	$31 \rightarrow 48$	Sc \rightarrow Sr
6	–	$4d^{10}$	$5p^6$	$6s^2$	18	$49 \rightarrow 56$	Y \rightarrow Ba
7	$4f^{14}$	$5d^{10}$	$6p^6$	$7s^2$	32	$57 \rightarrow 88$	La \rightarrow Ra
8	$5f^{14}$	$6d^{10}$	$7p^6$	$8s^2$	32	$89 \rightarrow 120$	Ac \rightarrow 120

the left-step table. This is in sharp contrast with the conventional periodic table, where the seven periods give rise to a more artificial sequence of cardinalities {2, 8, 8, 18, 18, 32, 32}. Secondly, the periods in the Janet table are characterized by a constant value of $n + l$, and this without any exception. In the medium-long form, on the other hand, it seems that the periods are characterized by a constant value of n , but this rule gets violated several times. For example, when the 3d-block unexpectedly appears in the fourth period or when all of the sudden a 4f-block emerges into the sixth period. Finally, the ordering of the blocks is more natural in the left-step table (i.e., f-d-p-s) than in the conventional long form table (i.e., s-f-d-p) since it reads s-p-d-f from right to left (in contrast to the meaningless p-d-f-s in the long-form table). An odd feature of the left-step table is the position of the noble gas helium above the alkaline-earth metal beryllium, rather than above the noble gas neon as in the conventional periodic tables. However, several arguments can be made in favor of placing helium above beryllium. For instance, the valence shell of helium ($1s^2$) is more similar to that of beryllium ($[\text{He}]2s^2$) than that of neon ($[\text{He}]2s^22p^6$).

In Table 2 both the predicted and experimentally determined electronic configurations are listed for lanthanum (La), actinium (Ac), lutetium (Lu) and lawrencium (Lr). Apparently, the Madelung rule predicts the wrong ground state configurations for lanthanum (La) and actinium (Ac). Instead of having one outer electron in an f-orbital, both lanthanum (La) and actinium (Ac) are characterized by an electron in a d-orbital outside their inert gas core. It is this fact which lies at the origin of the whole La–Ac–Lu–Lr discussion. Moreover, this is not an isolated case. In fact, it appears that for more than 30% of the transition elements, the Madelung rule predicts electronic configurations that are deviant from the empirical ones. Of course, one cannot neglect the discrepancies between the theoretically and empirically determined ground state configurations. Nevertheless, we wonder if this fact provides sufficient

TABLE 2 The theoretically predicted and experimentally observed ground state configurations of lanthanum (La), lutetium (Lu), actinium (Ac), and lawrencium (Lr)^a

Element	Z	Predicted Madelung ground state	Empirically determined ground state
La	57	$[\text{Xe}]4f^16s^2$	$[\text{Xe}]5d^16s^2$
Lu	71	$[\text{Xe}]4f^{14}5d^16s^2$	$[\text{Xe}]4f^{14}5d^16s^2$
Ac	89	$[\text{Rn}]5f^17s^2$	$[\text{Rn}]6d^17s^2$
Lr	103	$[\text{Rn}]5f^{14}6d^17s^2$	$[\text{Rn}]5f^{14}6d^17s^2$

^a The ground state configuration of lawrencium (Lr) is not empirically known, but predicted and it may not have a 6d-electron but a 6p-electron according to more recent calculations. In that case, lawrencium would form another exception to the Madelung rule.

ground to start a discussion about the correct grouping of the elements into columns. As more than 80% of all the elements are characterized by a ground state configuration that is in perfect agreement with the Madelung rule, one has every right to consider the other 19 elements (with “non-Madelung” ground states) as mere exceptions to a seemingly more general and fundamentally correct quantum rule. Actually, this is exactly the way most chemists normally behave. Hardly any chemist claims for example that the d-block should end with copper (Cu), $[\text{Ar}] 3d^{10}4s^1$, palladium (Pd), $[\text{Kr}]4d^{10}$, and gold (Au), $[\text{Xe}]4f^{14}5d^{10}6s^1$, because these elements are characterized by 10 electrons in a d-orbital. Consciously or subconsciously, most chemists seem to agree that these electronic configurations are exceptional, and that the d-block should end with zinc (Zn), $[\text{Ar}]3d^{10}4s^2$, cadmium (Cd), $[\text{Kr}]4d^{10}5s^2$, and mercury (Hg), $[\text{Xe}]4f^{14}5d^{10}6s^2$, as predicted by the Madelung rule.

A very unconventional way to accommodate the lanthanides can be found in a new periodic table introduced by the South-African chemist Michael Laing (2004, 2005) (Figure 33). He divides the lanthanides into three subgroups according to their important +II, +III, and +IV oxidation states: La to Sm, Eu to Tm, and Yb and Lu. In Laing’s Table, Eu and

																		1																			1	2						
																		H																			H	He						
																		1.0																			1.0	4.00						
2	3	4	5	6	7	8	9	10	11	12	13	14	15	16	17	18	19	20	21	22	23	24	25	26	27	28	29	30	31	32	33	34	35	36										
He	Li	Be	B	C	N	O	F	Ne	Na	Mg	Al	Si	P	S	Cl	Ar	K	Ca	Sc	Ti	V	Cr	Mn	Fe	Co	Ni	Cu	Zn	Ga	Ge	As	Se	Br	Kr										
4.0	6.9	9.0	10.8	12.0	14.0	16.0	19.0	20.18	23.0	24.3	26.98	28.09	30.97	35.45	39.95	39.95	39.95	40.08	44.96	47.88	50.9	52.0	54.9	55.85	58.9	58.93	63.55	68.9	69.7	72.64	74.9	78.9	79.9	83.8										
10	11	12	13	14	15	16	17	18	19	20	21	22	23	24	25	26	27	28	29	30	31	32	33	34	35	36	37	38	39	40	41	42	43	44	45	46	47	48	49	50	51	52	53	54
Ne	Na	Mg	Al	Si	P	S	Cl	Ar	K	Ca	Sc	Ti	V	Cr	Mn	Fe	Co	Ni	Cu	Zn	Ga	Ge	As	Se	Br	Kr	Rb	Sr	Y	Zr	Nb	Mo	Tc	Ru	Rh	Pd	Ag	Cd	In	Sn	Sb	Te	I	Xe
20.18	23.0	24.3	26.98	28.09	30.97	35.45	39.95	39.95	39.95	40.08	44.96	47.88	50.9	52.0	54.9	55.85	58.9	58.93	63.55	68.9	69.7	72.64	74.9	78.9	79.9	83.8	85.47	87.6	88.9	91.2	92.9	95.9	101.1	102.9	106.4	107.8	112.4	114.8	118.7	121.8	127.6	126.9	131.3	
54	55	56	57	58	59	60	61	62																																				
Xe	Cs	Ba	La	Ce	Pr	Nd	Pm	Sm																																				
131.3	132.9	137.3	138.9	140.9	144.2	(145)	150.4																																					
			63	64	65	66	67	68	69																																			
			Eu	Gd	Tb	Dy	Ho	Er	Tm																																			
			162.0	157.2	158.9	162.5	164.9	167.3	168.9																																			
			70	71	72	73	74	75	76	77	78	79	80	81	82	83	84	85	86																									
			Yb	Lu	Hf	Ta	W	Re	Os	Ir	Pt	Au	Hg	Tl	Pb	Bi	Po	At	Rn																									
			173.0	175.0	178.5	180.9	183.8	186.2	190.2	192.2	195.1	197.0	200.6	204.4	207.2	209.0	(209)	(210)	(222)																									
86	87	88	89	90	91	92	93	94																																				
Rn	Fr	Ra	Ac	Th	Pa	U	Np	Pu																																				
(222)	(223)	226.0	227.0	232.0	231.0	238.0	237.0	(244)																																				
		95	96	97	98	99	100	101																																				
		Am	Cm	Bk	Cf	Es	Fm	Md																																				
		(243)	(247)	(247)	(251)	(252)	(257)	(258)																																				
102	103	104	105	106	107	108	109	110	111	112	113	114	115	116	117	118	119	120																										
No	Lr	Rf	Db	Sg	Bh	Hs	Mt					114																																
(259)	(260)	(261)	(262)	(263)	(262)	(265)	(266)																																					

FIGURE 33 Laing’s periodic table (Laing, 2005). Reproduced with permission from Springer.

Yb fall directly below Ba in group 2. For these elements +II is a common oxidation state. La, Gd and Lu form a column directly below Y in group IIIB. These elements have all +III as the dominant oxidation state. Ce and Tb fall in a vertical line between Zr and Hf in group 4. Ce, Tb, Zr, and Hf all have +IV as a stable oxidation state. Laing remarks that Pm falls below Tc, which is remarkable, because both are radioactive and have no long-living isotopes. From this table, it can also be derived that Am and No can easily be obtained in the +II oxidation state, and Bk in the +IV oxidation state. A weakness of Laing's table is that several elements are duplicated, so that his table is more an instrumental tool which is used to explain as many chemical properties as possible rather than being a representation of the periodic law. Moreover, Laing still adheres to Mendeleev's homologous accommodation of the rare earths. Laing (2009) also emphasized the role of gadolinium as central metal in the lanthanide series.

8. CONCLUSIONS

One notices in the alternative accommodation methodologies of the rare-earth elements, a gradual evolution going hand in hand with a growing detachment of the rare earths from the other chemical elements. Such a progression of events is easily accounted for on the basis of their unique character and perplexing properties. Mendeleev in his time was swift at discerning the primary rare-earth elements from the secondary elements, and he clearly emphasized the many consequences of the existence of primary groups within his periodic table. He thus referred to their transitional function, the apparent analogy with the transition metals, and their problematic representation within the periodic table. Mendeleev moreover explained how the presence of these primary elements resulted in both elementary characterization issues and problems of undermined periodicity. Nevertheless, throughout his lifetime, Mendeleev continuously adhered to a *homologous accommodation methodology*, thus placing the rare earths as homologues of the other elements throughout the periods of the system in the many groups I to VIII. As a consequence, all rare earths remained connected with the other elements and many chemists (Brauner in particular) eagerly tried to obtain the higher valencies of the rare-earth elements, e.g., his search for the pentavalency of didymium.

Bohuslav Brauner in 1902 pursued the detachment process by clustering the rare-earth elements within the eighth period in only one pigeon-hole of Mendeleev's system according to an *intra-periodic accommodation methodology*. In many ways, Brauner's asteroid hypothesis was analogous to the collective grouping of the transition metals in between two periods according to an *inter-periodic accommodation methodology*. Without a

doubt, both types of placement violated the concept of single occupancy, but this problem could be removed by adhering to the meta-element concept of Crookes who considered the rare-earth elements to be meta-elements of one elemental group. Brauner had revived Mendeleev's rare earth – transition metal analogy and he moreover explicated how the rare earths formed a transition from lanthanum to tantalum, thus pointing to the transitional function of primary elements. By placing the rare-earth elements in one particular group of the system (typically in groups III and IV), Brauner moreover emphasized the similarity of the rare earths metals and he resolved the problem of undermined periodicity. He also rendered their limited relationship with the other elements clear by connecting them with the congeners of one group only.

Niels Bohr concluded the detachment process by locating the rare earths as a whole in between two groups of the periodic system according to an *intergroup accommodation methodology*. He thus broke off all relations with the other elements and consequently placed the individuality of the rare-earth elements in the spotlights. Bohr furthermore removed the characterization issues by explaining the peculiar nature of primary elements on the basis of the arrangement of their innermost electrons. Moseley's investigations on X-ray spectroscopy aided as well in the resolution of the characterization problem by pointing to the existence of atomic numbers. His methods proved extremely valuable in deciding upon the homogeneity and elementarity of the rare-earth elements, and they permitted the chemical community to draw up a correct sequence of rare earths on the basis of their increasing atomic number.

The detachment process has been further emphasized nowadays by removing the rare earths from the main body and by locating them as a footnote at the periphery of Mendeleev's system. Contemporary discussions on the "rare-earth crisis" have shifted from the accommodation of the rare earths as a whole to the placement of lanthanum and lutetium in particular. Since the actinides are placed underneath the lanthanides, similar problems are posed for this group of elements and most discussions therefore center on the location of actinium and lawrencium. Chemists are thus arguing about the methods to draw the boundaries of the rare-earth island. According to the authors, the representations to be preferred are the long form of the 14LaAc periodic table and the left-step periodic table, because these do not degrade the lanthanides and actinides to footnotes of the main body of the table, and agree with the Madelung rule. The authors also discourage the use of the IUPAC numbering of the groups in the periodic table from 1 to 18, because this numbering totally neglects the existence of the lanthanides and actinides.

ACKNOWLEDGMENT

Pieter Thyssen is a research assistant of the Flemish Research Council (FWO-Vlaanderen). The authors thank Prof. Geert Vanpaemel (K.U.Leuven) for stimulating discussions.

REFERENCES

- Akeroyd, F.M., 2003. *J. Gen. Phil. Sci.* 34, 337.
- Arnold, C., 1914. *A Compendium of Chemistry, Including General, Inorganic, and Organic Chemistry*. American Science Series—Advanced Course, 1st ed. John Wiley & Sons, New York.
- Bassett, H., 1892. *Chem. News*. 65 (3), 19.
- Baur, E., 1911. *Z. Phys. Chem.* 76, 659.
- Bayley, T., 1882. *London, Edinburgh, Dublin Philos. Mag. J. Sci.* 13, 26.
- Beaudry, B.J., Gschneidner Jr., K.A., 1978. Preparation and basic properties of the rare earth metals. In: Gschneidner Jr., K.A., Eyring, L. (Eds.), *Handbook on the Physics and Chemistry of Rare Earths*, vol. 1. Elsevier, Amsterdam, pp. 173–232. Chapter 2.
- Benedicks, C., 1904. *Z. Anorg. Chem.* 39, 41.
- Bent, H.A., 2006. *New Ideas in Chemistry from Fresh Energy for the Periodic Law*. AuthorHouse, Bloomington.
- Biltz, H., 1902. *Ber.* 35 (562), 4242.
- Bohr, N., 1913a. *Phil. Mag.* 26, 1.
- Bohr, N., 1913b. *Phil. Mag.* 26, 476.
- Bohr, N., 1913c. *Phil. Mag.* 26, 857.
- Bohr, N., 1921. *Nature* 107, 104.
- Bohr, N., 1922a. *The Theory of Spectra and Atomic Constitution*. Three Essays. Cambridge University Press, Cambridge.
- Bohr, N., 1922b. *The Structure of the Atom*. Nobel Lecture. http://nobelprize.org/nobel_prizes/physics/laureates/1922/bohr-lecture.pdf.
- Brauner, B., 1878. *Ber.* 11, 872.
- Brauner, B., 1881a. *Tageblatt der Versammlung deutscher Naturforscher und Aerzte in Salzburg* 48.
- Brauner, B., 1881b. *Tageblatt der Versammlung deutscher Naturforscher und Aerzte in Salzburg* 49.
- Brauner, B., 1882a. *Ber.* 15, 115.
- Brauner, B., 1882b. *Monatshefte* 3, 1.
- Brauner, B., 1882c. *Moniteur Sci.* 24, 595.
- Brauner, B., 1882d. *J. Chem. Soc.* 41, 68.
- Brauner, B., 1882e. *Compt. Rend.* 94, 1718.
- Brauner, B., 1883. *Trans. Chem. Soc.* 43, 278.
- Brauner, B., 1885a. *Monatshefte* 6, 785.
- Brauner, B., 1885b. *J. Chem. Soc.* 47, 879.
- Brauner, B., 1888a. *Chem. News* 58, 307.
- Brauner, B., 1888b. *Ber.* 22, 1186.
- Brauner, B., 1891. *Ber.* 24, 1328.
- Brauner, B., 1895. *Chem. News* 71, 283.
- Brauner, B., 1896. *Chem. News* 74, 223.
- Brauner, B., 1898a. *Proc. Chem. Soc.* 14, 69.
- Brauner, B., 1898b. *Proc. Chem. Soc.* 14, 70.
- Brauner, B., 1901a. *Proc. Chem. Soc.* 17, 65.
- Brauner, B., 1901b. *Proc. Chem. Soc.* 17, 66.

- Brauner, B., 1902. *Z. Anorg. Chem.* 32, 1.
- Brauner, B., 1903a. *Z. Anorg. Chem.* 33, 317.
- Brauner, B., 1903b. *Z. Anorg. Chem.* 34, 207.
- Brauner, B., 1926. *Nature* 118, 84.
- Brauner, B., 1930. *Coll. Czech. Chem. Commun.* 2, 219.
- Brauner, B., Batek, A., 1903. *Z. Anorg. Chem.* 34, 103.
- Brauner, B., Pavlicek, F., 1901. *Proc. Chem. Soc.* 17, 63.
- Brauner, B., Pavlicek, F., 1902. *J. Chem. Soc.* 81, 1243.
- Brock, W.H., 2008. *William Crookes (1832–1919) and the commercialization of science.* In: Knight, D., Levere, T. (Eds.), *Science, Technology and Culture, 1700–1945.* Ashgate, Hampshire.
- Brooks, N.M., 2002. *Found. Chem.* 4, 128.
- Chadwick, J., 1932. *Nature* 129, 312.
- Clark, R.W., 2008. *J. Chem. Educ.* 85, 1493.
- Clark, R.W., White, G.D., 2008. *J. Chem. Educ.* 85, 497.
- Cronyn, M.W., 2003. *J. Chem. Educ.* 80, 947.
- Crookes, W., 1879. *Nature* 20, 419, 436.
- Crookes, W., 1884a. *Philos. Trans. R. Soc. Lond.* 174, 891.
- Crookes, W., 1884b. *Proc. R. Soc. Lond.* 38, 414.
- Crookes, W., 1886a. *Chem. News* 54, 131.
- Crookes, W., 1886b. *Br. Assoc. Rep.* 558.
- Crookes, W., 1886c. *Br. Assoc. Rep.* 583.
- Crookes, W., 1886d. *Br. Assoc. Rep.* 586.
- Crookes, W., 1886e. *Chem. News* 54, 239.
- Crookes, W., 1886f. *Philos. Trans. R. Soc. Lond.* 176, 691.
- Crookes, W., 1886g. *Proc. R. Soc. Lond.* 40, 77.
- Crookes, W., 1886h. *Proc. R. Soc. Lond.* 40, 236.
- Crookes, W., 1886i. *Proc. R. Soc. Lond.* 40, 502.
- Crookes, W., 1886j. *Chem. News* 54, 27.
- Crookes, W., 1886k. *Chem. News* 54, 39.
- Crookes, W., 1886l. *Chem. News* 54, 115.
- Crookes, W., 1887. *Chem. News* 55, 83, 95.
- Crookes, W., 1888a. *J. Chem. Soc.* 53, 487.
- Crookes, W., 1888b. *Chem. News* 57, 198.
- Crookes, W., 1888c. *Chem. News* 57, 206.
- Crookes, W., 1888d. *Chem. News* 57, 216.
- Crookes, W., 1888e. *Chem. News* 57, 226.
- Crookes, W., 1889a. *Proc. R. Inst.* 12, 37.
- Crookes, W., 1889b. *J. Chem. Soc.* 55, 255.
- Crookes, W., 1898. *Proc. R. Soc. Lond.* 63, 408.
- Dash, H.H., 1967. *J. Inorg. Nucl. Chem* 29, 1811.
- DeKosky, R.K., 1973. *Br. J. Hist. Sci.* 6, 400.
- Druce, G., 1944. *Two Czech Chemists. Bohuslav Brauner (1855–1935) & Frantisek Wald (1861–1930).* The New Europe Publishing Company Limited, London.
- Evans, C.H., 1996. *Episodes from the History of the Rare Earth Elements.* Kluwer Academic Publishers, Dordrecht.
- Friend, N.J., Little, H.F.V., Turner, W.E.S., Briscoe, H.V.A., 1917. Part I—An Introduction to Modern Inorganic Chemistry, Part II—The Inert Gases. In: Friend, N.J. (Ed.), *A Text-Book of Inorganic Chemistry*, vol. I, 2nd ed. Charles Griffin and Company Limited, London.
- Goldschmidt, V.M., 1924. *Geochemische Verteilungsgesetze der Elemente*, vol. II. *Nor. Vidensk.-Akad. Skrifter*, Kristiania.

- Gordin, M.D., 2004. *A Well-Ordered Thing: Dmitrii Mendeleev and the Shadow of the Periodic Table*. Basic Books, New York.
- Gorin, G., 1996. *J. Chem. Educ.* 73, 490.
- Habashi, F., 1997. *Interdiscip. Sci. Rev.* 22, 53.
- Haigh, C.W., 1995. *J. Chem. Educ.* 1012, 72.
- Hamilton, D.C., 1965. *Am. J. Phys.* 33, 637.
- Hamilton, D.C., Jensen, M.A., 1963. *Phys. Rev. Lett.* 11, 205.
- Harris, J.A., Yntema, L.F., Hopkins, B.S., 1926a. *Nature* 117, 792.
- Harris, J.A., Yntema, L.F., Hopkins, B.S., 1926b. *J. Am. Chem. Soc.* 48, 1585.
- Heimann, P.M., 1967. *Ann. Sci.* 4, 249.
- Heimann, P.M., 1968. *Centaurus* 12, 261.
- Heimann, P.M., Heilbron, J.L., 1967. *Isis* 58, 232.
- Hogg, J.T., 1975. *J. Chem. Educ.* 52, 325.
- Holmyard, E.J., 1922. *Inorganic Chemistry. A Textbook for Schools*, 1st ed. Edward Arnold & Co., London.
- Janet, C., 1929. *Chem. News* 138, 372, 388.
- Jensen, W.B., 1982. *J. Chem. Educ.* 59, 634.
- Jensen, W.B., 2002. *Mendeleev on the Periodic Law: Selected Writings, 1869–1905*. Dover Publications, Mineola, NY.
- Jensen, W.B., 2003. *J. Chem. Educ.* 80, 952.
- Jensen, W.B., 2008a. *J. Chem. Educ.* 85, 1182.
- Jensen, W.B., 2008b. *J. Chem. Educ.* 85, 1491.
- Jensen, W.B., 2009. *J. Chem. Educ.* 86, 1186.
- Jones, H.C., 1903. *Elements of Inorganic Chemistry*, 1st ed. The MacMillan Company, New York.
- Katz, G., 2001. *Chem. Educator* 6, 324.
- Kedrov, B.M., Chentsova, T.N., 1955. Brauner – Spodvizhnik Mendeleeva. K Stoletiiu So Dnia Rozhdeniia Boguslava Braunera. Akademiia Nauk SSSR, Moscow.
- Kolodkine, P., 1963. *Dmitri Mendel'ëv et la Loi Périodique*. Éditions Seghers, Paris.
- Kragh, H., 1977. *J. Chem. Educ.* 54, 208.
- Kragh, H., 1979. *J. Chem. Educ.* 56, 456.
- Kragh, H., 1980. *Centaurus* 23, 275.
- Kragh, H., 1996. Elements No. 70, 71 and 72: discoveries and controversies. In: Evans, C.H. (Ed.), *Episodes from the History of the Rare Earth Elements*. Kluwer Academic Publishers, London, pp. 67–90.
- Kragh, H., 2001. *Found. Chem.* 333, 129.
- Kurbatov, J.D., MacDonald, D.C., Pool, M.L., Quill, L.L., 1942. *Phys. Rev.* 61, 106.
- Laing, M., 2004. *S. Afr. J. Sci.* 100, 198.
- Laing, M., 2005. *Found. Chem.* 7, 203.
- Laing, M., 2007. *Found. Chem.* 9, 127.
- Laing, M., 2009. *J. Chem. Educ.* 86, 188.
- Laing, M., 2009. *J. Chem. Educ.* 86, 1189.
- Lavelle, L., 2008a. *J. Chem. Educ.* 85, 1482.
- Lavelle, L., 2008b. *J. Chem. Educ.* 85, 1491.
- Lavelle, L., 2009. *J. Chem. Educ.* 86, 1187.
- Law, H.B., Pool, M.L., Kurbatov, J.D., Quill, L.L., 1941. *Phys. Rev.* 59, 936.
- Leone, M., Robotti, N., 2000. *Ann. Sci.* 57, 241.
- Leone, M., Robotti, N., 2003. *Phys. Perspect.* 5, 360.
- Lesk, A.M., 1980. *Am. J. Phys.* 48, 492.
- Libby, W.F., 1934. *Phys. Rev.* 46, 196.
- Madelung, E., 1936. *Mathematische Hilfsmittel des Physikers*. Springer Verlag, Berlin.

- Marinsky, J.A., 1996. The search for element 61. In: Evans, C.H. (Ed.), *Episodes from the History of the Rare Earth Elements*. Kluwer Academic Publishers, London, pp. 91–108.
- Marinsky, J.A., Glendenin, L.E., Coryell, C.D., 1947. *J. Am. Chem. Soc.* 69, 2781.
- Mattauch, J., 1934. *Z. Phys.* 91, 361.
- Mazurs, E., 1974. *The Graphic Representation of the Periodic System During 100 Years*. University of Alabama Press, Tuscaloosa.
- Mendeleev, D.I., 1869a. *An Attempted System of the Elements Based on Their Atomic Weights and Chemical Analogies (flyer)*.
- Mendeleev, D.I., 1869b. *Zhur. Russ. Khim. Obshch.* 1, 60.
- Mendeleev, D.I., 1869c. *Zhur. Russ. Khim. Obshch.* 1, 229.
- Mendeleev, D.I., 1870. *Zhur. Russ. Khim. Obshch.* 2, 14.
- Mendeleev, D.I., 1871. *Zhur. Russ. Khim. Obshch.* 3, 25.
- Mendeleev, D.I., 1872. *Zhur. Russ. Khim. Obshch.* 4, 7.
- Mendeleev, D.I., 1873. *Zhur. Russ. Khim. Obshch.* 5, 119.
- Mendeleev, D.I., 1881. *Zhur. Russ. Khim. Obshch.* 13, 516.
- Mendeleev, D.I., 1889. *J. Chem. Soc.* 55, 634.
- Mendelejeff, D., 1869a. *J. Prakt. Chem.* 106, 251.
- Mendelejeff, D., 1869b. *Z. Chem.* 5, 405.
- Mendelejeff, D., 1869c. *Ber.* 2, 553.
- Mendelejeff, D., 1870. *Ber.* 3, 990.
- Mendelejeff, D., 1871. *Ann. Suppl.* VIII, 139.
- Mendelejeff, D., 1873a. *Ber.* 6, 558.
- Mendelejeff, D., 1873b. *Ann.* 168, 45.
- Mendelejeff, D., 1881. *Ber.* 14, 2821.
- Mendelejew, D., 1870. *Bull. Acad. Imp. Sci. (St. Petersburg)* 16, 45.
- Merz, H., Ulmer, K., 1967. *Phys. Lett. A* 26, 6.
- Meyer, S., 1918. *Phys. Z.* 19, 178.
- Moseley, H.G.J., 1914. *London, Edinburgh, Dublin Philos. Mag. J. Sci.* 27, 703.
- Moseley, H.G.J., Darwin, C.G., 1913. *London, Edinburgh, Dublin Philos. Mag. J. Sci.* 26, 210.
- Newell, L.C., 1916. *A Course in Inorganic Chemistry for Colleges*, 1st ed. D.C. Heath & Co., Boston.
- Niinistö, L., 1997. Discovery and separation of rare earths. In: Sáez Puche, R., Caro, P.A. (Eds.), *Rare Earths*. Editorial Complutense, Madrid, pp. 25–42.
- Nilson, L.F., Pettersson, O., 1880. *Ber.* 13, 1451.
- Noddack, W., Tacke, I., Berg, O., 1925. *Naturwissenschaften* 13, 567.
- Norris, J.F., 1921. *A Textbook of Inorganic Chemistry for Colleges*, 1st ed. McGraw-Hill, New York.
- Novaro, O., 2008. *Found. Chem.* 10, 3.
- Nuroh, K., Wendin, G., 1981. *Phys. Rev. B* 24, 5533.
- Ostwald, W., 1904. *The Principles of Inorganic Chemistry*, 2nd ed. MacMillan and Co., London.
- Paneth, F.A., 1923. *Ergeb. Exakten. Naturwiss.* 2, 168.
- Paneth, F.A., 2003. *Found. Chem.* 5, 113. (reprint of a lecture given in 1931).
- Perrier, C., Sègre, E., 1937. *Rend. Lincei* 25, 723.
- Perrier, C., Sègre, E., 1947. *Nature* 159, 24.
- Pissarjevski, O., 1955. *Dmitri Ivanovitch Mendeleev: Sa Vie et son Oeuvre La Science Russe Et Ses Hommes*. Editions en Langues Etrangères, Moscou.
- Pool, M.L., Quill, L.L., 1938. *Phys. Rev.* 53, 437.
- Prandtl, W., 1926. *Angew. Chem.* 39, 897.
- Prandtl, W., Grimm, A., 1924. *Z. Anorg. Allg. Chem.* 136, 283.
- Prandtl, W., Grimm, A., 1926. *Angew. Chem.* 39, 1333.

- Probst, C., Wittig, J., 1978. Superconductivity: metals, alloys and compounds. In: Gschneidner Jr., K.A., Eyring, L. (Eds.), *Handbook on the Physics and Chemistry of Rare Earths*, vol. 1. Elsevier, Amsterdam, pp. 749–796. Chapter 10.
- Puddephatt, R.J., Monaghan, P.K., 1985. *The Periodic Table of the Elements*. Oxford University Press, Oxford.
- Quam, G.N., Battell-Quam, M., 1934a. *J. Chem. Educ.* 11, 27.
- Quam, G.N., Battell-Quam, M., 1934b. *J. Chem. Educ.* 11, 217.
- Quam, G.N., Battell-Quam, M., 1934c. *J. Chem. Educ.* 11, 288.
- Retgers, J.W., 1895. *Z. Phys. Chem.* 16, 644.
- Reynolds, J.E., 1886. *Chem. News* 54, 1.
- Richards, T.W., 1898. *Am. Chem. J.* 20, 543.
- Rolla, L., Fernandes, L., 1926. *Z. Anorg. Allg. Chem.* 157, 371.
- Rolla, L., Fernandes, L., 1927a. *Nature* 119, 637.
- Rolla, L., Fernandes, L., 1927b. *Z. Anorg. Allg. Chem.* 160, 190.
- Rolla, L., Fernandes, L., 1927c. *Z. Anorg. Allg. Chem.* 163, 40.
- Rolla, L., Fernandes, L., 1928. *Z. Anorg. Allg. Chem.* 169, 319.
- Rudorf, G., 1903. *Z. Anorg. Chem.* 37, 176.
- Rutherford, E., 1913. *Nature* 92, 423.
- Sanderson, R.T., 1964. *J. Chem. Educ.* 41, 187.
- Scerri, E.R., 1994. *Ann. Sci.* 51, 137.
- Scerri, E.R., 2005. *Hyle* 11, 127.
- Scerri, E.R., 2007. *The Periodic Table, Its Story and Its Significance*. Oxford University Press, Oxford.
- Scerri, E.R., 2009a. *J. Chem. Educ.* 86, 1188.
- Scerri, E.R., 2009b. *Int. J. Quantum Chem.* 109, 959.
- Seaborg, G.T., 1944. Metallurgical Project Report CK-1968 (A-2845) (July 17). Metallurgical Laboratory Memorandum, MUC-GTS-858.
- Seaborg, G.T., 1945. *Chem. Eng. News* 23, 2190.
- Seaborg, G.T., 1949. Electronic structure of the heaviest elements, paper 21.1. In: Seaborg, G.T., Katz, J.J., Manning, W.M. (Eds.), *The Transuranium Elements—Research Papers*, National Nuclear Energy Series IV, vol. 14B, Part II. McGraw Hill, New York, p. 1492.
- Seaborg, G.T., 1994. Origin of the actinide concept. In: Gschneidner Jr., K.A., Eyring, L. (Eds.), *Handbook on the Physics and Chemistry of Rare Earths*, vol. 18. Elsevier, Amsterdam, pp. 1–28. Chapter 118.
- Shepard, J.H., 1886. *Elements of Inorganic Chemistry*, 1st ed. D.C. Heath & Co., Boston.
- Smith, A., 1906. *Introduction to General Inorganic Chemistry*, 1st ed. The Century Co., New York.
- Steele, B.D., 1901. *Chem. News* 84, 245.
- Stewart, A.W., 1909. The place of the rare earth elements in the periodic system. *Recent Advances in Physical and Inorganic Chemistry*. Longmans, London pp. 168–175.
- Stewart, P.J., 2007. *Found. Chem.* 9, 235.
- Stewart, P.J., 2008. *J. Chem. Educ.* 85, 1490.
- Szabadváry, F., 1988. The history of the discovery and separation of the rare earths. In: Gschneidner Jr., K.A., Eyring, L. (Eds.), *Handbook on the Physics and Chemistry of Rare Earths*, vol. 11. Elsevier, Amsterdam, pp. 33–80. Chapter 73.
- Thomsen, J., 1895. *Z. Anorg. Chem.* 9, 190.
- Trifonov, D.N., 1963. *The Rare-Earth Elements*. The MacMillan Company, New York.
- Trifonov, D.N., 1966. *Problems in the Study of Rare Earths*. Translated by J. Schmorak. Israel Program for Scientific Translations, Jerusalem.
- Trifonov, D.N., 1970. Views of D. I. Mendeleev on Rare Earths. *Rare-Earth Elements and Their Position in the Periodic System*. Indian National Scientific Documentation Centre, New Delhi, pp. 31–52.

- Trifonov, D.N., 1984. *The Price of Truth: The Story of Rare-Earth Elements*. Mir Publishers, Moscow.
- Trifonov, D.N., Trifonov, V.D., 1982. *Chemical Elements. How They Were Discovered*. Mir Publishers, Moscow.
- Urbain, G., 1911. *Compt. Rend. Hebd. Acad. Sci.* 151, 141.
- Van den Broek, A.J., 1913. *Nature* 92, 372.
- van Spronsen, J., 1969. *The Periodic System of the Chemical Elements, the First One Hundred Years*. Elsevier, Amsterdam.
- Venable, F.P., 1896. *The Development of the Periodic Law*. Chemical Publishing Co., Easton.
- Villar, G.E.J., 1966. *Inorg. Nucl. Chem* 28, 25.
- Walker, J., 1919. *Inorganic Chemistry*, 11th ed. G. Bell & Sons, Ltd., London.
- Wang, S.G., Schwarz, W.H.E., 2009. *Angew. Chem. Int. Ed.* 48, 3404.
- Weeks, M.E., 1956. *Discovery of the Elements*, 6th ed. Mack Printing Co., Easton, PA.
- Werner, A., 1905a. *Ber. Dtsch. Chem. Ges.* 38, 914.
- Werner, A., 1905b. *Neuere anschauungen auf dem gebiete der anorganischen chemie*. Verlag Friedrich Vieweg.
- Wyrouboff, G., 1896. *Chem. News* 74, 31.
- Yntema, L.F., 1924. *J. Am. Chem. Soc.* 46, 37.
- Yost, D.M., Russell Jr., H., 1946. *Systematic Inorganic Chemistry of the Fifth and Sixth Group Nonmetallic Elements*, 1st ed. Prentice-Hall, New York.

This page intentionally left blank

Metallofullerenes

Hisanori Shinohara* and Yahachi Saito†

Contents	List of Abbreviations	96
	1. Historical Introduction	96
	1.1 The first detection and synthesis of endohedral metallofullerenes	99
	2. Synthesis, Extraction from Soot, and Separation/Purification	101
	2.1 Synthesis of endohedral metallofullerenes	101
	2.2 Solvent extraction from primary soot containing metallofullerenes	105
	3. Purification and Isolation of Metallofullerenes	106
	3.1 Purification by liquid chromatography	106
	3.2 HPLC purification on metallofullerenes	106
	4. Molecular and Crystal Structures of Metallofullerenes	109
	4.1 Endohedral or exohedral?	109
	4.2 Structural isomers obeying the so-called IPR	110
	4.3 Confirmation on endohedral structures as determined by synchrotron X-ray diffraction	111
	4.4 Crystal structures	119
	5. Carbide Metallofullerenes	120
	6. Electronic States and Structures	121
	6.1 Intrafullerene electron transfer within the carbon cage	121
	6.2 ESR detection of structural isomers of metallofullerenes	122
	6.3 Electrochemistry on metallofullerenes	126
	6.4 Similarity of UV–Vis–NIR absorption spectra	128
	6.5 The Fermi level and the electronic structure	132

* Department of Chemistry and Institute for Advanced Research, Nagoya University, Nagoya 464-8602, Japan

† Department of Quantum Engineering, Nagoya University, Nagoya 464-8603, Japan

7. Meta-cage Vibration within Metallofullerenes	133
8. STM Studies on Metallofullerenes	135
8.1 STM studies of metallofullerenes on clean surfaces	135
8.2 Metallofullerenes as superatoms	137
9. Magnetism of Metallofullerenes	139
10. M@C ₆₀ : A Big Mystery and a Big Challenge	141
11. Applications to Radiochemistry and MRI Contrast Agents	144
12. Conclusions and Future Prospects	145
Acknowledgments	146
References	146

List of Abbreviations

CV	cyclic voltammetry
DC	direct current
DOS	density of state
DTPA	diethylenetriamine- <i>N,N,N',N'',N''</i> -pentaacetic acid
ESEEM	electron spin-echo envelope modulation
ESR	electron spin resonance
EXAFS	extended X-ray absorption fine structure
FT-ICR	Fourier transform ion cyclotron resonance
hfc	hyperfine constant
hfs	hyperfine structure
HOMO	highest occupied molecular orbital
HPLC	high-performance liquid chromatography
HRTEM	high-resolution transmission electron microscopy
IPR	isolated pentagon rule
LC	liquid chromatography
LUMO	lowest unoccupied molecular orbital
MEM	maximum entropy method
MRI	magnetic resonance imaging
SAM	self-assembled monolayer
SCF	self-consistent field
SOMO	singly occupied molecular orbital
SQUID	superconducting quantum interference device
STM	scanning tunneling microscopy
UHV	ultra-high vacuum
UPS	ultraviolet photoelectron spectroscopy
UV-Vis-NIR	ultraviolet-visible-near IR
XPS	X-ray photoelectron spectroscopy
XRD	X-ray diffraction

1. HISTORICAL INTRODUCTION

Rare earth endohedral metallofullerenes are an interesting class of fullerenes because electron transfer from the encaged metal atom to the carbon cage has been known to occur and this dramatically alters electronic and magnetic properties of the fullerenes.

A week after the first observation of the “magic number” soccerball-shaped C_{60} in a laser-vaporized cluster beam mass spectrum by Kroto et al. (1985), the same research group also found a magic number feature due to LaC_{60} in a mass spectrum prepared by laser vaporization of a $LaCl_3$ impregnated graphite rod (Heath et al., 1985). They observed a series of C_n^+ and LaC_n^+ ion species with LaC_{60}^+ as a magic number ion in the mass spectrum (Figure 1) and concluded that a La atom was encaged within the (then hypothetical) soccerball-shaped C_{60} . This was obviously the first proposal of the so-called “endohedral metallofullerene” concept based on experiments. They first tried Fe with no success and found that La is a correct atom for encapsulation within fullerenes. It is interesting to note that even today Fe has not been encapsulated by fullerenes.

Further circumstantial (not direct) evidence that metal atoms may be encaged in C_{60} was also reported by the Rice group, showing that LaC_{60}^+ ions did not react with H_2 , O_2 , NO , and NH_3 (Weiss et al., 1988), suggesting that reactive metal atoms are protected from the surrounding gases and are indeed trapped inside the C_{60} cage.

The first direct evidence of the soccerball (truncated icosahedron) C_{60} was amply demonstrated in 1990 by a historical experiment done by Kraetschmer, Huffman and co-workers. They succeeded in producing macroscopic quantities of soccerball-shaped C_{60} by using resistive heating of graphite rods under a He atmosphere (Kraetschmer et al., 1990a,b). The resistive heating method was then superseded by the so-called contact arc discharge method (Haufler et al., 1991) since the arc discharge method can produce fullerenes order of magnitudes larger than by resistive heating. Since then, the arc discharge method has become a standard method for fullerene synthesis.

The first production of macroscopic quantities of endohedral metallofullerenes were also reported by the Rice group (Chai et al., 1991). They used high-temperature laser vaporization of La_2O_3 /graphite composite rods and the corresponding contact arc technique to produce various sizes of La-metallofullerenes. Contrary to expectation, only the $La@C_{82}$ fullerene survived in a solvent and was extractable by toluene even though $La@C_{60}$ and $La@C_{70}$ were also seen in the mass spectra of the sublimed film from soot. In other words, the major La-metallofullerene with air stability is $La@C_{82}$, and $La@C_{60}$ and $La@C_{70}$ are somehow unstable in air and in solvents.

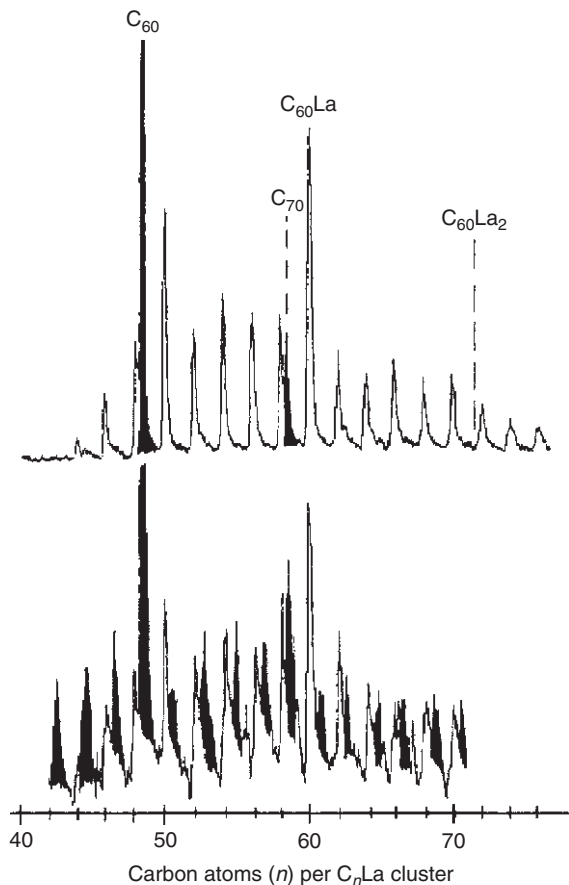


FIGURE 1 Laser-vaporization supersonic cluster-beam time-of-flight mass spectrum of various lanthanum–carbon clusters. LaC₆₀ is seen as an enhanced (magic number) peak.

The symbol @ is conventionally used to indicate that atoms listed to the left of the @ symbol are encaged in the fullerenes. For example, a C₆₀-encaged metal species (M) is then written as M@C₆₀ (Chai et al., 1991). The corresponding IUPAC nomenclature is different from this conventional M@C₆₀ representation. It is recommended by IUPAC that La@C₈₂ should be called [82] fullerene-*incar*-lanthanum and be written *i*LaC₈₂ (Godly and Taylor, 1997). However, throughout this review the conventional M@C_{2n} description is used for endohedral metallofullerenes for brevity, unless otherwise noted.

1.1 The first detection and synthesis of endohedral metallofullerenes

Figure 2 shows a FT-ICR mass spectrum of hot toluene extract of fullerene materials produced by laser vaporization of a 10% La_2O_3 /graphite composite rod (Chai et al., 1991). In addition to empty fullerenes, only the La@C_{82} metallofullerene is seen and La@C_{60} and La@C_{70} are completely absent in the mass spectrum of the solvent extracts. The speciality of the La@C_{82} fullerene was soon confirmed by Whetten and co-workers (Alvarez et al., 1991). However, they also observed that at relatively high loading ratios of La_2O_3 in composite rods a di-lanthanofullerene, $\text{La}_2\text{@C}_{80}$, was also produced by the resistive-heating method and found to be another solvent-extractable major lanthanofullerene (Alvarez et al., 1991; Yerezian et al., 1992).

The first important information on the electronic structure of La@C_{82} was provided by the IBM Almaden research group. The charge state of the engaged La atom was studied by Johnson et al. (1992) using electron spin resonance (ESR). The ESR hyperfine splitting (hfs) analysis of La@C_{82} revealed that the La atom is in the 3+ charge state and that the formal charge state of La@C_{82} is written as $\text{La}^{3+}\text{@C}_{82}^{3-}$: three outer electrons of La transferring to the C_{82} cage (Bethune et al., 1993).

Several other research groups extended their work to endohedral yttrium compounds. The Rice–Minnesota University (Weaver et al., 1992) and Nagoya University (Shinohara et al., 1992a) research groups also reported solvent-extractable Y@C_{82} and $\text{Y}_2\text{@C}_{82}$ fullerenes and observed the ESR hfs of Y@C_{82} . From the hfs analyses both groups concluded that the charge state of the Y atom is 3+ and that a similar

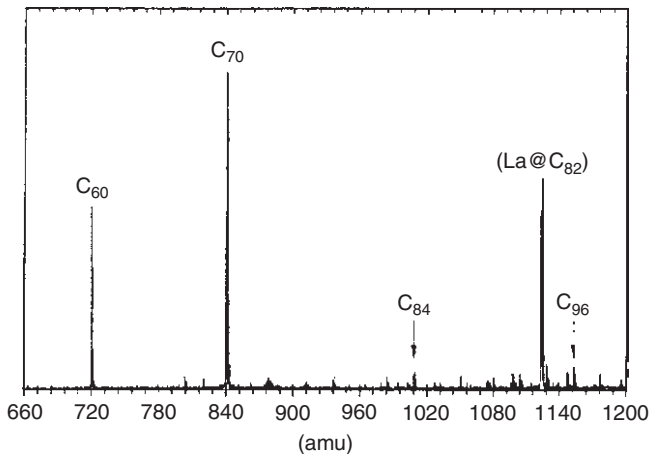


FIGURE 2 An FT-ICR mass spectrum of hot toluene extract of fullerene soot produced by high-temperature laser vaporization of a 10% La_2O_3 /graphite composite rod.

intra-fullerene electron transfer was taking place in $Y@C_{82}$ as in $La@C_{82}$. These results were also confirmed by the NRL group (Ross et al., 1992). In addition, they also reported the production of mixed di-metallofullerenes like $(LaY)@C_{80}$. McElvany (1992) reported the production of a series of yttrium fullerenes, $Y_m@C_n$ including $Y@C_{82}$, by direct laser vaporization of samples containing graphite, yttrium oxide and fullerenes in the gas phase.

Scandium metallofullerenes were also produced in macroscopic quantity and solvent-extracted by Shinohara et al. (1992b) and Yannoni et al. (1992). The Sc fullerenes exist in extracts as a variety of species (mono-, di-, tri- and even tetra-scandium fullerenes), typically as $Sc@C_{82}$, $Sc_2@C_{74}$, $Sc_2@C_{82}$, $Sc_2@C_{84}$, $Sc_3@C_{82}$, and $Sc_4@C_{82}$. It was found that $Sc_3@C_{82}$ was also an ESR-active species whereas di- and tetra-scandium fullerenes like $Sc_2@C_{84}$ and $Sc_4@C_{82}$ were ESR-silent. (See Section 5 for the present correct assignment for some of the di- and tri-scandium metallofullerenes.) A detailed discussion on the electronic structures of the scandium fullerenes accrued from these ESR experiments is given in Section 6.1.

The formation of lanthanide metallofullerenes $R@C_{82}$ ($R = Ce, Pr, Nd, Sm, Eu, Gd, Tb, Dy, Ho, Er, Yb, \text{ and } Lu$) was also reported by the UCLA (Gillan et al., 1992) and SRI international (Moro et al., 1993) groups. These metallofullerenes were also based on the C_{82} fullerene.

In addition to group 3 (Sc, Y, La) and the lanthanide metallofullerenes, group 2 metal atoms (Ca, Sr, Ba) were also found to form endohedral metallofullerenes, and have been produced and isolated in milligram quantity (Dennis and Shinohara, 1997a,b, 1998; Dennis et al., 1998; Wan et al., 1997, 1998; Xu et al., 1996). These metal atoms have been engaged not only by C_{82} and C_{84} but also by such smaller fullerenes as C_{72} , C_{74} , and C_{80} . Furthermore, group 4 metallofullerenes (Ti, Zr, Hf) were synthesized and isolated (Cao et al., 2001, 2002).

Other important C_{60} -based endohedral fullerenes which have been produced are $Ca@C_{60}$ (Guo et al., 1992; Kubozono et al., 1995; L Wang et al., 1993a,b; Y Wang et al., 1993f) and $U@C_{60}$ (Guo et al., 1992). The $Ca@C_{60}$ and $U@C_{60}$ fullerenes are unique metallofullerenes in which Ca and U atoms are engaged by C_{60} , and are quite different from group 3 and lanthanide, $R@C_{82}$ type, metallofullerenes. An *ab initio* SCF Hartree-Fock calculation indicates that the Ca ion in $Ca@C_{60}$ is displaced by 0.7 Å from the center and that the electronic charge of Ca is 2+ (Scuseria, 1992; L Wang et al., 1993a). A similar theoretical prediction has been made on $Sc@C_{60}$ by Scuseria and co-workers (Guo et al., 1994). Metallofullerenes based on C_{60} are known to be unstable in air and in normal fullerene solvents such as toluene and carbon disulfide. We will discuss the stability and properties of C_{60} -based metallofullerenes together with an inability to extract and purify these in Section 10. The metal atoms which have been reported to form endohedral metallofullerenes are shown in Table 1.

TABLE 1 A “bucky periodic table” showing the elements which have been reported to form endohedral metallofullerenes and isolated as purified forms (as of June 2009). The black elements form endohedral metallofullerenes which have been purified, whereas the gray elements form endohedral non-metallofullerenes

Bucky periodic table																			
1													13	14	15	16	17	18	
H													B	C	N	O	F	Ne	
Li	Be													Al	Si	P	S	Cl	Ar
Na	Mg	3	4	5	6	7	8	9	10	11	12	Ga	Ge	As	Se	Br	Kr		
K	Ca	Sc	Ti	V	Cr	Mn	Fe	Co	Ni	Cu	Zn	In	Sn	Sb	Te	I	Xe		
Rb	Sr	Y	Zr	Nb	Mo	Tc	Ru	Rh	Pd	Ag	Cd	Hg	Tl	Pb	Bi	Po	At		
Cs	Ba	La	Ce	Pr	Nd	Pm	Sm	Eu	Gd	Tb	Dy	Ho	Er	Tm	Yb	Lu	Rn		
Fr	Ra	Ac	Th	Pa	U	Np	Pu	Am	Cm	Bk	Cf	Es	Fm	Md	No	Lr			

In the following sections, the major advances in production, separation, structures, electronic/magnetic and solid state properties of endohedral metallofullerenes will be discussed in an effort to shed light on this fascinating new class of fullerene-related materials.

2. SYNTHESIS, EXTRACTION FROM SOOT, AND SEPARATION/PURIFICATION

2.1 Synthesis of endohedral metallofullerenes

Metallofullerenes can be synthesized typically in two ways similar to the synthesis of empty fullerenes, which involves the generation of a carbon-rich vapor or plasma in He or Ar gas atmosphere. The two methods have been routinely used to date for preparing macroscopic amounts of metallofullerenes: the high-temperature laser vaporization or “laser-furnace” method (Chai et al., 1991; Haufler et al., 1991; Ying et al., 1994) and the standard direct current (DC) arc discharge method (Haufler et al., 1990). Both methods simultaneously generate a mixture of hollow fullerenes (C_{60} , C_{70} , C_{76} , C_{78} , C_{84} , ...) together with metallofullerenes. The production of metallofullerenes can be followed by procedures to extract from soot and to separate/purify the metallofullerenes from the hollow fullerenes (see Sections 2.2, 3.1, and 3.2).

There is a less common but important method called the metal ion implantation technique for metallofullerene synthesis. This technique

has been used to produce alkaline metallofullerenes (Campbell et al., 1997; Tellgmann et al., 1996a,b) and nitrogen atom endofullerenes (Knapp et al., 1997; Mauser et al., 1997; Murphy et al., 1996) such as Li@C_{60} and N@C_{60} , respectively. Also, Hirata et al. (1996) reported the production of K@C_{60} by introducing negatively charged C_{60} into a low-temperature (ca 0.2 eV) potassium plasma column by a strong axial magnetic field. However, isolation and structural characterization of metallofullerenes prepared by the above methods have not been performed yet due to the insufficiency of the materials produced by the implantation and the plasma techniques, although partial high-performance liquid chromatography (HPLC) separation on Li@C_{60} has been reported (Krawez et al., 1998). In the following, we review the current status of the laser furnace and arc discharge methods for the synthesis of endohedral metallofullerenes.

In the laser-furnace method (Figure 3), a target composite rod or disc for laser vaporization, which is composed of metal-oxide/graphite with a high-strength pitch binder, is placed in a furnace at 1,200 °C (Haufler et al., 1991). A frequency-doubled Nd:YAG laser at 532 nm is focused onto the target rod, which is normally rotating/translating to ensure a fresh surface, in an Ar gas flow (100–200 Torr) condition. Metallofullerenes and empty fullerenes are produced by the laser vaporization and then flow down the tube with the Ar gas carrier, and are finally trapped on the quartz tube wall near the end of the furnace.

To produce fullerenes and metallofullerenes, a temperature above 800 °C was found to be necessary, and below this critical temperature no fullerenes were produced (Haufler et al., 1991; Suzuki et al., 1997a; Wakabayashi et al., 1997), suggesting that relatively slow thermal annealing processes are required to form fullerenes and metallofullerenes. The laser-furnace method is suited to the study of growth mechanism of fullerenes and metallofullerenes (Curl and Smalley, 1991; Haufler et al., 1991;

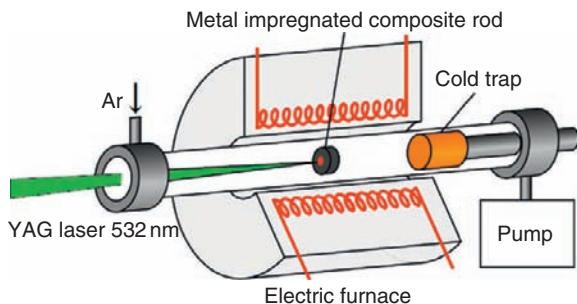


FIGURE 3 Schematic diagram of the high-temperature laser-furnace apparatus to produce fullerenes and metallofullerenes by laser vaporization of a rotating metal-impregnated graphite target in an electric furnace with flowing argon carrier gas.

Smalley, 1992; Wakabayashi and Achiba, 1992; Wakabayashi et al., 1993; Ying et al., 1994). The laser-furnace method is also known to be an efficient production method for single-wall carbon nanotubes when Ni/Co or Ni/Fe binary metal is stuffed with graphite powder for target composite rods (Thess et al., 1996).

Figure 4 represents a third-generation large-scale DC arc discharge apparatus for the production of metallofullerenes developed and installed at Nagoya (Dennis and Shinohara, 1998; Nakane et al., 1997; Shinohara, 1998, 2000; Shinohara et al., 1996a). The arc generator consists

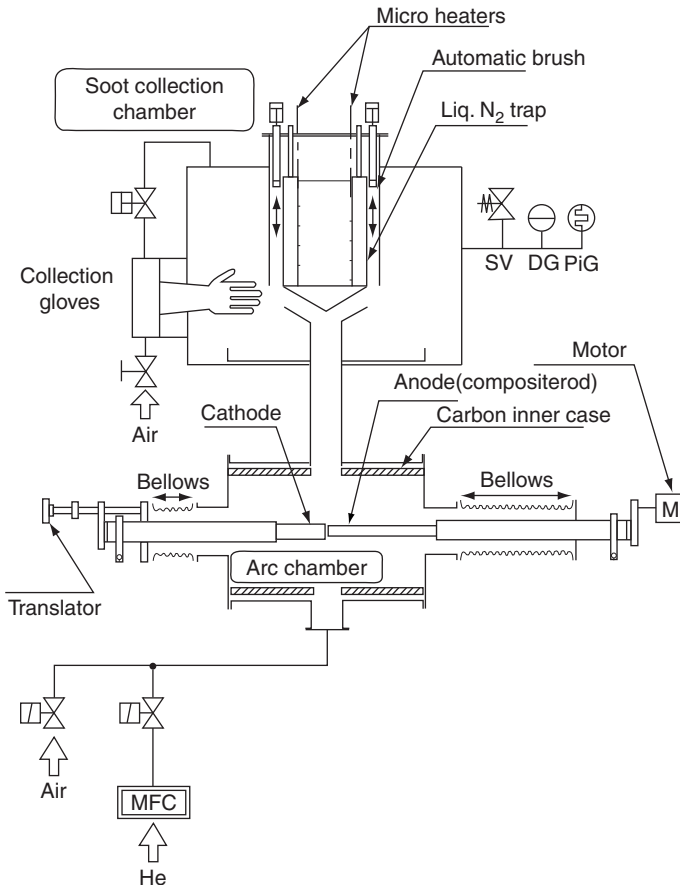


FIGURE 4 A cross-sectional view of the third-generation DC arc discharge apparatus (in Nagoya University) with an anaerobic collection and sampling mechanism. The produced metallofullerene-containing soot is effectively trapped by the liquid N_2 trap installed in the center of the collection chamber. Typical arc discharge conditions: 40–100 Torr He flow, 300–500 A, and 25–30 V.

of a production chamber and a collection chamber, equipped with an anaerobic sampling and collection mechanism of raw soot containing metallofullerenes (Bandow et al., 1993; Shinohara et al., 1994a). Anaerobic sampling of the soot is preferred to conventional collection under ambient conditions because many of the metallofullerenes in primary soot are air (moisture)-sensitive and may be subjected to degradation during the soot handling.

Metal-oxide/graphite composite rods, e.g., La_2O_3 to prepare La@C_{82} , are normally used as positive electrodes (anodes) after a high-temperature (above ca 1,600 °C) heat treatment where the composite rods are cured and carbonized. At such high temperatures, various metal carbides in the phase of MC_2 are formed in the composite rods (Adachi et al., 1991), which actually is crucial to an efficient production of endohedral metallofullerenes: uniformly dispersed metal atoms as metal-carbides in a composite rod provide metallofullerenes in higher yields.

For example, the yield of La@C_{82} is increased by a factor of ten or more when LaC_2 -enriched composite rods are used for the arc generation of soot instead of using La_2O_3 as a starting material for the composite rods (Bandow et al., 1993). The rods (20 mm diameter \times 500 mm long), are arced in the DC (300–500 A) spark mode under 50–100 Torr He flow conditions (Figure 4). The soot so produced is collected under totally anaerobic conditions to avoid unnecessary degradation of the metallofullerenes produced during the soot collection and handling. It was found that the soot collected in the upper chamber contains a substantial amount of metallofullerenes compared to that collected in the arc discharge (lower) chamber. The fullerene smoke (soot) which rises along a convection flow around the evaporation source has the maximum content of metallofullerenes (Saito et al., 1996). Furthermore, the extraction efficiency of the anaerobic soot is much higher than that of the ambient soot in the lower chamber.

In general, the yield of a metallofullerene varies sensitively on He buffer gas pressure during the arc synthesis. An optimum He pressure depends on arc conditions such as the size of a composite rod, DC current, and the arc gap of the two electrodes, which is normally close to that of empty higher fullerenes such as C_{82} and C_{84} . It has been reported that the formation of La@C_{82} , for example, is closely related to the evaporation rate of a composite rod; the maximum yield of La@C_{82} is attained at the highest evaporation rate of the rod (Saito et al., 1996). Mieno (1998) reported that the production of endohedral metallofullerenes can be much enhanced under gravitation-free arc discharge conditions as compared with the normal gravitational condition. This is due to the fact that the gravitation-free conditions suppress thermal convection of hot gas in the arc region and thus enable long-duration hot reaction of carbon clusters suited to metallofullerene production.

The production of scandium fullerenes, Sc_nC_{82} and/or $\text{Sc}_n\text{C}_2\text{C}_{80}$ ($n = 1-4$), is especially interesting, because scandium fullerenes exist in a solvent extract as mono-, di-, and tri-scandium fullerenes (Shinohara et al., 1992b; Yannoni et al., 1992), which is quite unique compared to the other rare earth metallofullerenes. Even a tetra-scandium fullerene, $\text{Sc}_4\text{C}_2\text{C}_{80}$, has also been produced and isolated (Kuroki et al., 1999; Wang et al., 2009). The synthesis of the mono-, di-, tri- and tetra-scandium fullerene was found to be sensitive to the mixing ratio of scandium and carbon atoms in the composite rods; the relative abundance of di-, tri- and tetra-scandium fullerenes increases as the carbon/scandium ratio decreases. For example, with a carbon/scandium (atomic) ratio of 86.2, the formation of mono- and di-scandium fullerenes such as ScC_{82} and $\text{Sc}_2\text{C}_2\text{C}_{82}$ was dominant, and the production of $\text{Sc}_3\text{C}_2\text{C}_{80}$ and $\text{Sc}_4\text{C}_2\text{C}_{80}$ was almost negligible. It was observed that the major scandium fullerene produced was $\text{Sc}_2\text{C}_2\text{C}_{82}$ over a wide range of the carbon/scandium mixing ratios (10–100) (Shinohara et al., 1992a,b).

2.2 Solvent extraction from primary soot containing metallofullerenes

The so-called solvent extraction method by toluene, *o*-xylene or carbon disulfide is the most common and frequently used extraction method, in which metallofullerenes and hollow fullerenes are preferentially dissolved in solvents. The so-called Soxhlet extraction (a continuous and hot solvent extraction) or ultrasonic extraction is normally employed to increase the solvent extraction efficiency (Khemani et al., 1992). Insolubles in soot are easily separated from this solution by filtration. However, in many cases, the toluene or CS_2 extraction is not sufficient, since nearly half of the metallofullerene still remains in the residual soot even after the extensive CS_2 extraction. It has been found that metallofullerenes are further extracted from the residual soot by such solvents as pyridine (Inakuma et al., 1995) and 1,2,4-trichlorobenzene (Yamamoto et al., 1994a,b). The metallofullerenes were found to be concentrated in this pyridine or trichlorobenzene extracted fraction. When necessary, the metallofullerene extracts can be stored in carbon disulfide solution for an extended period of time, up to a year.

In a sublimation method (Chai et al., 1991; Diener et al., 1997; Yeretizian et al., 1993), as in the case of empty fullerenes (Abrefah et al., 1992; Averitt et al., 1994; Cox et al., 1991; Kraetschmer et al., 1990b; Pan et al., 1991; Taylor et al., 1990), the raw soot containing metallofullerenes is heated in He gas or in vacuum up to 400 °C, where metallofullerenes such as LaC_{82} and Y@C_{82} start to sublime. The metallofullerenes then condense in a cold trap, leaving the soot and other nonvolatiles behind in the sample holder. However, a complete separation of metallofullerenes

has not been achieved to date by sublimation. Extraction by sublimation has the advantage over solvent extraction for obtaining "solvent-free" extracts, whereas the latter method is suited to large-scale extraction of metallofullerenes.

3. PURIFICATION AND ISOLATION OF METALLOFULLERENES

3.1 Purification by liquid chromatography

As in the case of hollow fullerenes (Ajie et al., 1990; Scrivens et al., 1992; Taylor et al., 1990), liquid chromatography (LC) is the main purification technique for metallofullerenes. LC has been frequently and traditionally used in separation chemistry. One of the most powerful LC techniques is HPLC which allows separation of fullerenes according to their molecular weight, size, shape or other parameters (Jinno and Saito, 1996; Kikuchi et al., 1991, 1992; Klute et al., 1992; Meier and Selegue, 1992). The HPLC technique can even allow us to separate structural isomers of various metallofullerenes (Shinohara, 2000).

The purification of endohedral metallofullerenes via HPLC had been difficult, mainly because the content of metallofullerenes in raw soot is normally very limited and, furthermore, the solubility in normal HPLC solvents is generally lower than that of various empty higher fullerenes. It took almost two years for metallofullerenes to be completely isolated by the HPLC method (Kikuchi et al., 1993; Shinohara et al., 1993a) after the first extraction of La@C₈₂ by the Rice group (Chai et al., 1991). Following these first isolations of metallofullerenes, isolation with different HPLC columns was also reported (Savina et al., 1994; Yamamoto et al., 1994a). The success of the purification/isolation was a real breakthrough for further characterization of the endohedral metallofullerenes.

3.2 HPLC purification on metallofullerenes

Scandium metallofullerenes are, in particular, interesting in terms of separation and purification because, as described in Section 2.1, scandium fullerenes appear as mono-, di-, tri- and even tetra-scandium fullerenes with several structural isomers which can be separated completely by HPLC. As an example, the HPLC separation of scandium fullerenes is briefly described in the following.

The scandium fullerenes, such as Sc@C₈₂, Sc₂C₂@C₈₂, and Sc₃C₂@C₈₀, were separated and isolated from various hollow (C₆₀–C₁₁₀) fullerenes by the so-called two-stage HPLC method (Kikuchi et al., 1993; Shinohara, 2000; Shinohara et al., 1993a, 1994a). The two-stage HPLC method uses two complementary HPLC columns, which have different types of

fullerene adsorption mechanisms and are suited for a complete separation of the metallofullerenes. The two-stage HPLC method was first successfully applied to the isolation of several di-scandium fullerenes including $\text{Sc}_2\text{@C}_{74}$, $\text{Sc}_2\text{@C}_{82}$ and $\text{Sc}_2\text{C}_2\text{@C}_{82}$ (Shinohara et al., 1993a) as shown in Figure 5. To simplify the separation, an automated HPLC separation on some endohedral metallofullerenes has been also reported by Stevenson et al. (1994a,b).

In the first HPLC stage, the toluene solution of the extracts was separated by a preparative recycling HPLC system (Japan Analytical Industry LC-908- C_{60}) with a Trident-Tri-DNP column (Buckyclutcher I, 21 mm \times 500 mm: Regis Chemical) or a 5-PBB (pentabromobenzyl) column (20 mm \times 250 mm, Nacalai Tesque) with CS_2 eluent. In this HPLC process, the scandium fullerene-containing fractions were separated from other fractions including C_{60} , C_{70} , and higher fullerenes (C_{76} – C_{110}). The complete purification and isolation of various scandium fullerenes were performed in the second HPLC stage by using a Cosmosil Buckyprep column (20 mm \times 250 mm, Nacalai Tesque) with a 100% toluene eluent. Figure 6 shows the first and the second HPLC stages of the purification of Sc@C_{82} as an example.

It has been found (Inakuma et al., 1995; Yamamoto et al., 1994a,b) that most of the monometallofullerenes, M@C_{82} , have at least two types of structural isomers (conventionally called I and II), which can be separated by the two-stage HPLC technique.

The retention times of isomers I are normally shorter than those of isomers II and, in general, isomers I are much more stable than isomers II

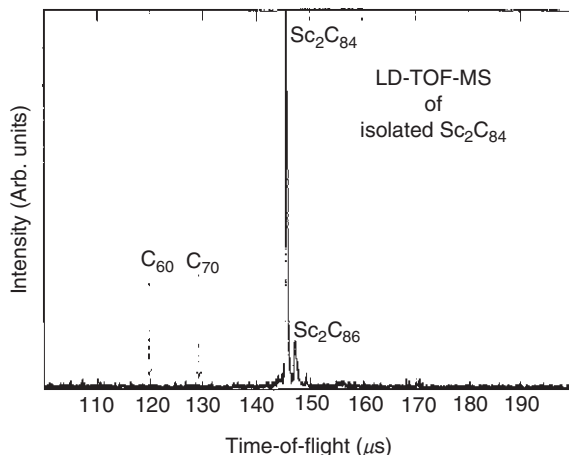


FIGURE 5 The first mass spectra of isolated metallofullerenes: Sc_2C_{84} (which is currently identified as $\text{Sc}_2\text{C}_2\text{@C}_{82}$).

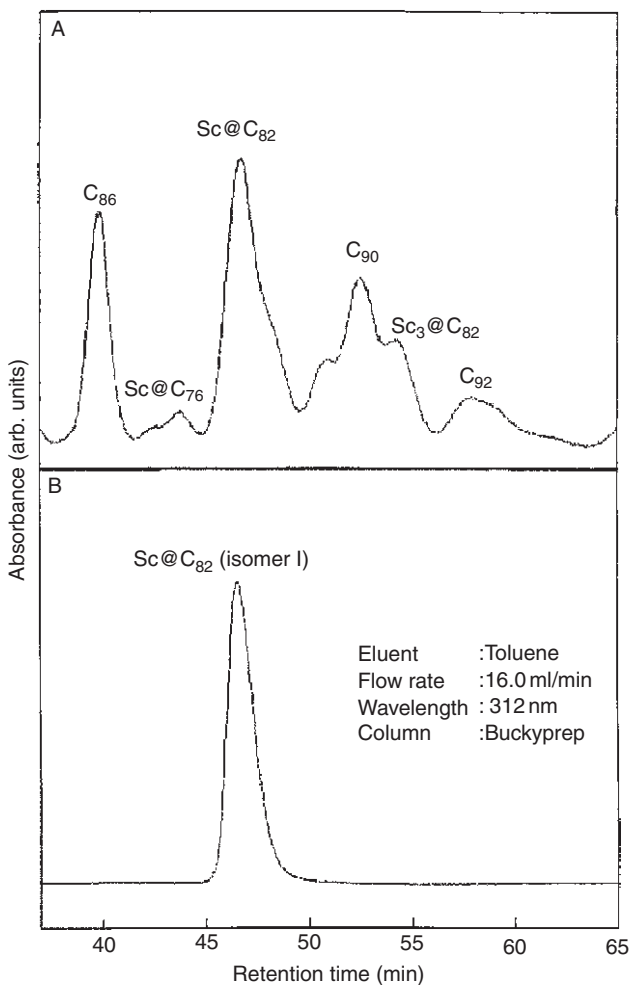


FIGURE 6 (A) An overall HPLC spectrum for the fraction which contains various scandium metallofullerenes in the first HPLC stage. (B) An isolated HPLC chromatogram for the Sc@C₈₂ (I) after the second HPLC stage. The experimental conditions are presented in the lower right of the figure.

in air and in various solvents. In some cases, several isomers have been found for a metallofullerene. For example, a mono-calcium fullerene, Ca@C₈₂, has four isomers (I–IV) which have been produced, isolated, and characterized (Xu et al., 1996). Unless otherwise noted, we discuss the structural and electronic properties of “major isomers” (mostly isomer I) in this article.

Normally, the isolation of various metallofullerenes is confirmed by laser-desorption time-of-flight mass spectrometry. For ESR-active metallofullerenes, the observation of the corresponding hyperfine structures can further confirm the identification and isolation.

4. MOLECULAR AND CRYSTAL STRUCTURES OF METALLOFULLERENES

4.1 Endohedral or exohedral?

Since the first studies on production and solvent extraction of metallofullerenes, such as La/Y/Sc@C₈₂, there had been great controversy as to whether or not the metal atom is really trapped inside the fullerene cage (Bethune et al., 1993; Chai et al., 1991). In the gas phase, the stability of endohedral metallofullerenes has been studied by laser photofragmentation for La@C₈₂ and Sc₂C₂@C₈₂ (Suzuki et al., 1997b; Wakabayashi et al., 1996), collisional fragmentation with atomic and molecular targets for La@C₈₂ and Gd@C₈₂ (Lorents et al., 1995) and fragmentation induced by surface impact for La₂@C₈₀ (Yeretzian et al., 1992), La@C₈₂, La₂@C₁₀₀ (Beck et al., 1996b), La@C₆₀ (Kimura et al., 1999a), Ce@C₈₂ and Ce₂@C₁₀₀ (Beck et al., 1996a), Y@C₈₂ and Ca@C₈₄ (Kimura et al., 1999b).

Although the most extensive fragmentation was observed in the laser photofragmentation, the general tendency of the fragmentation induced by the three excitations was found to be similar: the main fragments from La@C₈₂ were C₂-loss species such as La@C₈₀, La@C₇₈, La@C₇₆, etc., and the empty C₈₂ fragment was not observed. This result was interpreted as being due to the endohedral nature of La@C₈₂ since exohedral La(C₆₀) (Huang and Freiser, 1991) and Fe(C₆₀) (Roth et al., 1991) prepared by gas phase reactions gave C₆₀ as the main product upon collisional fragmentation against rare-gas targets.

However, in the solid state, the evidence for the endohedral nature of the contradictory results were reported for extended X-ray absorption fine structure (EXAFS) experiments on an unpurified extract of Y@C₈₂ (i.e., a mixture of Y@C₈₂ and empty fullerenes). Soderholm et al. (1992) reported that the yttrium atom is exohedrally attached from the outside to the C₈₂ cage, whereas Park et al. (1993) reported an endohedral nature of Y@C₈₂: the nearest-neighbor C–Y distances obtained were 2.53 ± 0.02 and 2.4 Å, respectively. Kikuchi et al. (1994a) performed an EXAFS experiment on a purified La@C₈₂ powder material and reported that the nearest and next-to-nearest-neighbor C–La distances are 2.47 ± 0.02 and 2.94 ± 0.07 Å, respectively.

Most of the major experimental evidence suggested, however, the endohedral nature of the metallofullerenes: the IBM Almaden group

reported a high-resolution transmission electron microscopy (HRTEM) experiment on a purified $\text{Sc}_2\text{C}_2@\text{C}_{82}$ (III) material which suggests that the two scandium atoms are encapsulated in the C_{82} cage (Beyers et al., 1994).

Similar evidence on the endohedral nature based on HRTEM images was reported on $\text{Gd}@\text{C}_{82}$ by Tanaka et al. (1996). The UCLA group reported a high-energy collision experiment on $\text{La}_2@\text{C}_{80}$ against silicon surfaces and found that no collision fragments such as La atoms and C_{80} were observed, also suggesting an endohedral structure of $\text{La}_2@\text{C}_{80}$ (Alvarez et al., 1991). Similar surface-induced dissociation experiments were done on $\text{La}@\text{C}_{82}$ and $\text{La}@\text{C}_{60}$ (Kimura et al., 1999a) against a self-assembled monolayer (SAM) film and on $\text{Y}@\text{C}_{82}$, $\text{Ca}@\text{C}_{82}$, and $\text{Ca}@\text{C}_{84}$ against solid (silicon and gold) surfaces and SAM films (Kimura et al., 1999b), all of which indicated the endohedral nature of these metallofullerenes.

The Tohoku–Nagoya group reported a series of ultra-high vacuum scanning tunneling microscopy (UHV-STM) studies on $\text{Sc}_2\text{C}_2@\text{C}_{82}$ and $\text{Y}@\text{C}_{82}$ adsorbed on silicon and copper clean surfaces, respectively (Sakurai et al., 1996; Shinohara et al., 1993b; X Wang et al., 1993c). All of the obtained STM images showed spherical shape which strongly suggests that the metal atoms are encapsulated in the fullerene cages. Gimzewski also studied $\text{Sc}_2\text{C}_2@\text{C}_{82}$ molecules deposited from a CS_2 solution onto Au(110) by STM and obtained some internal structure on the top part of the images (Gimzewski, 1996).

Although the above experimental results strongly suggest an endohedral nature of the metallofullerenes, the final confirmation of the endohedral nature and detailed endohedral structures of the metallofullerenes was obtained by synchrotron X-ray diffraction measurements on purified powder samples (Takata et al., 1995).

4.2 Structural isomers obeying the so-called IPR

A fullerene molecule has structural isomers with different five- and six-membered ring patterns. The most important structural isomers are called isolated-pentagon rule (IPR) isomers (Kroto, 1987; Schmalz et al., 1988). IPR is considered as the most important and essential rule governing the geometry of fullerenes, stating that the most stable fullerenes are those in which all pentagons are surrounded by five hexagons. In fact, all the empty fullerenes produced, isolated, and structurally characterized to date have been known to satisfy IPR. IPR can be best understood as a logical consequence of minimizing the number of dangling bonds and steric strain of fullerenes (Fowler and Manolopoulos, 1995).

As a result, the smallest IPR-satisfying fullerene is C_{60} , and C_{70} is the second smallest; there are no IPR fullerenes between C_{60} and C_{70} . Although IPR has been equally applied for metallofullerenes, IPR isomers of a metallofullerene can be different from those of the corresponding

empty fullerene (Dennis et al., 1998; Takata et al., 1998). Electron transfers from a caged metal atom to the carbon cage may alter the stability of the fullerene.

4.3 Confirmation on endohedral structures as determined by synchrotron X-ray diffraction

4.3.1 Y@C₈₂ mono-metallofullerene

Previous experimental evidence including EXAFS (Kikuchi et al., 1994a; Park et al., 1993) and HRTEM (Beyers et al., 1994) suggested that the metal atoms are inside the fullerenes. Theoretical calculations also indicated that such endohedral metallofullerenes are stable (Andreoni and Curioni, 1996a,b; Chang et al., 1991; Cioslowski and Fleishmann, 1991; Guo et al., 1994; Laasonen et al., 1992; Manolopoulos and Fowler, 1991, 1992; Nagase and Kobayashi, 1993; Rosen and Waestberg, 1988, 1989; Saito and Sawada, 1992; L Wang et al., 1993a). However, the first conclusive experimental evidence on the endohedral nature of a metallofullerene, Y@C₈₂, was obtained by a synchrotron X-ray diffraction study. The result indicated that the yttrium atom is encapsulated within the C₈₂ fullerene and is strongly bound to the carbon cage (Takata et al., 1995).

The space group was assigned to P2₁, which is monoclinic for Y@C₈₂. The experimental data were analyzed in an iterative way of a combination of Rietveld analysis (Rietveld, 1969) and the maximum entropy method (MEM) (Bricogne, 1988; Collins, 1982). The MEM can produce an electron density distribution map from a set of X-ray structure factors without using any structural model. By the MEM analysis (Kumazawa et al., 1993; Sakata and Sato, 1990), the R_1 becomes as low as 1.5% for Y@C₈₂.

By using the revised structural model based on the previous MEM map and MEM analysis, a series of iterative steps involving Rietveld analysis were carried out until no significant improvement was obtained. Eventually, the R_1 factor improved from 14.4% to 5.9% ($R_{WP} = 3.0\%$). In Figure 7, the best fit of the Rietveld analysis of the Y@C₈₂ is shown. To display the endohedral nature of the Y@C₈₂, the MEM electron density distribution of Y@C₈₂ is shown in Figure 8. There exists a high-density area just inside the C₈₂ cage. The density maximum at the interior of the C₈₂ cage corresponds to the yttrium atom, indicating the endohedral structure of the metallofullerene.

It was also found that the cage structure of Y@C₈₂ differs from that of the hollow C₈₂ fullerene. There are many local maxima along the cage in Y@C₈₂, whereas electron densities of the C₈₂ cage are relatively uniform. This suggests that in Y@C₈₂ the rotation of the C₈₂ cage is very limited around a certain axis even at room temperature, whereas that in C₈₂ is almost free.

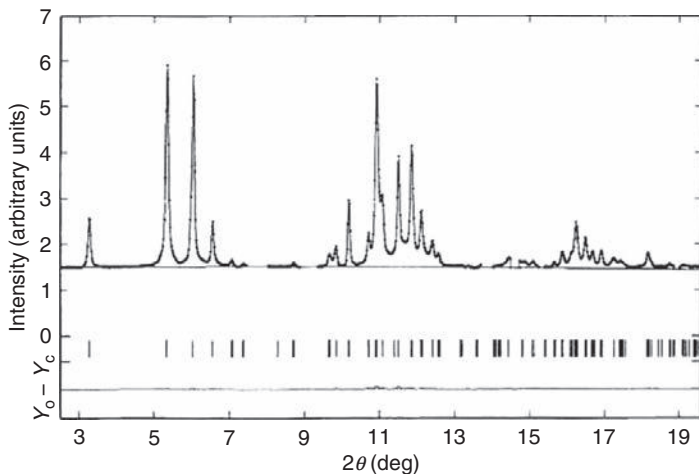


FIGURE 7 Powder X-ray (synchrotron) diffraction patterns and the corresponding fitting results of $Y@C_{82}$ based on the calculated intensities from the MEM electron density.

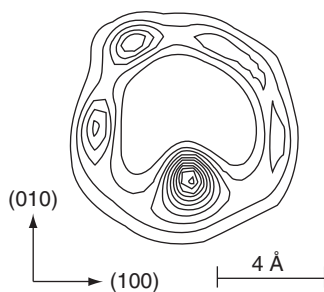


FIGURE 8 The MEM electron density distribution of $Y@C_{82}$ for the (001) section. The density maximum corresponds to Y atom.

The MEM electron density map further reveals that the yttrium atom does not reside at the center of the C_{82} cage but is very close to the carbon cage, as suggested theoretically (Andreoni and Curioni, 1996a,b; Guo et al., 1994; Laasonen et al., 1992; Nagase and Kobayashi, 1993; Nagase and Kobayashi, 1994a). The ESR (Shinohara et al., 1992a; Weaver et al., 1992) and theoretical (Nagase and Kobayashi, 1993; Schulte et al., 1996) studies suggest the presence of a strong charge transfer interaction between the Y^{3+} ion and the C^{3-} cage which may cause the aspherical electron density distribution of atoms. The Y-C distance calculated from the MEM map is $2.9(3)$ Å which is slightly longer than a theoretical prediction of 2.55 – 2.65 Å (Nagase and Kobayashi, 1993). The X-ray

study also reveals that the $Y@C_{82}$ molecules are aligned along the [001] direction in a head-to-tail ($\dots Y@C_{82} \dots Y@C_{82} \dots Y@C_{82} \dots$) order in the crystal, indicating the presence of a strong dipole-dipole and charge transfer interactions among the $Y@C_{82}$ fullerenes.

4.3.2 $Sc@C_{82}$ metallofullerene

The endohedral structure of $Sc@C_{82}$ was also studied by synchrotron X-ray diffraction with MEM analysis (Takata et al., 1998). The $Sc@C_{82}$ crystal includes solvent toluene molecules and has $P2_1$ space group as in the $Y@C_{82}$ case. The MEM electron charge density distribution of $Sc@C_{82}$ is shown in Figure 9. The Sc atom is not at the center of the fullerene but close to one of the six membered rings of the cage. The nearest-neighbor Sc-C distance estimated from the MEM map is 2.53(8) Å, which is very close to a theoretical value, 2.52–2.61 Å (Nagase and Kobayashi, 1993). There are in total nine IPR (isolated-pentagon rule) satisfying structural isomers for C_{82} . These are $C_2(a)$, $C_2(b)$, $C_2(c)$, C_{2v} , $C_s(a)$, $C_s(b)$, $C_s(c)$, $C_{3v}(a)$, and $C_{3v}(b)$. The X-ray result indicates that the carbon cage of $Sc@C_{82}$ has C_{2v} symmetry (Figure 9).

There has been controversy as to whether the engaged Sc atom has a divalent state or a trivalent state (Nagase and Kobayashi, 1993; Ruebsam et al., 1996b; Schulte et al., 1998; Shinohara et al., 1992b). The synchrotron X-ray result shows that the number of electrons around the Sc atom is $18.8e$, indicating that the Sc atom in the cage is in a divalent state,

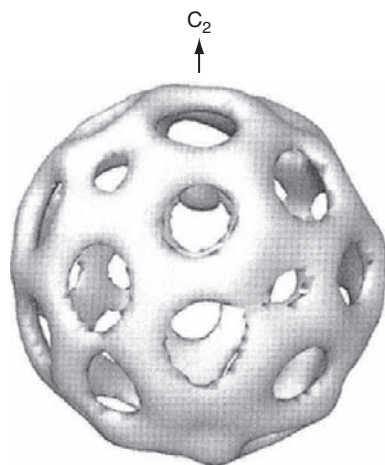


FIGURE 9 Equi-contour density map of the MEM charge density for the side view of $Sc@C_{82}$ molecule. The Sc atom is drawn inside the upper hemisphere of the fullerene. The C_2 axis is indicated.

$\text{Sc}^{2+}@\text{C}_{82}^{2-}$. The charge state is consistent with an ultraviolet photoelectron spectroscopy (UPS) experiment (Hino et al., 1998).

4.3.3 $\text{La}@\text{C}_{82}$ metallofullerene

The $\text{La}@\text{C}_{82}$ metallofullerene is one of the first endohedral metallofullerenes that was macroscopically produced and solvent extracted (Chai et al., 1991). Suematsu et al. (1994) first reported the crystal structure of $\text{La}@\text{C}_{82}$ precipitated from CS_2 solution via synchrotron X-ray powder diffraction. The composition of the microcrystal is expressed by $\text{La}@\text{C}_{82}(\text{CS}_2)_{1.5}$. The crystal has the cubic structure. The results suggest a molecular alignment in the unit cell, in which the molecules align in the [111] direction with the molecular axis orienting in the same [111] direction. Watanuki et al. (1995, 1996) performed synchrotron X-ray diffraction measurements on solvent-free powder samples of $\text{La}@\text{C}_{82}$, and concluded that the major part of the crystal has fcc lattice. Their results strongly suggest the endohedral nature of $\text{La}@\text{C}_{82}$ where the La atom is displaced from the center of the C_{82} cage by 1.9 Å.

The detailed endohedral structure of $\text{La}@\text{C}_{82}$ was revealed experimentally (Nishibori et al., 2000). The electron density distribution of $\text{La}@\text{C}_{82}$ based on the MEM analysis of the powder X-ray diffraction data is presented in Figure 10. The result shows that the La atom is encapsulated by the C_{2v} isomer of C_{82} as in $\text{Sc}@\text{C}_{82}$ described above. As is seen from the figure, the La atom is not at rest in the cage but rather is in a floating motion along the nearest six-membered ring at room temperature. The result is different from the $\text{Sc}@\text{C}_{82}$ and $\text{Y}@\text{C}_{82}$ cases in which Sc and Y atoms are almost at a standstill in the cage even at room temperature.



FIGURE 10 The section of the equi-charge density surface of $\text{La}@\text{C}_{82}$ molecule.

A light metal atom such as Sc seems to be more strongly bound to the fullerene cage than a heavy La atom.

4.3.4 Movement of metal atoms within the cage

Intrafullerene metal motions have been theoretically predicted by Andreoni and Curioni (1996a,b, 1997, 1998) on La@C₆₀ and La@C₈₂ on the basis of molecular dynamics simulations. Experimentally, dynamical motion of metal atoms has been reported on La@C₈₂ (Nishibori et al., 2000), Sc₂C₂@C₈₂ (Miyake et al., 1996) and La₂@C₈₀ (Akasaka et al., 1995b, 1997). It is noted that La atom is moving in the C₈₂ cage at room temperature (Figure 10).

A particularly interesting case has been found in La₂@C₈₀. La₂@C₈₀ metallofullerene was first produced by Whetten and co-workers (Alvarez et al., 1991) and was first isolated by Kikuchi et al. (1994a). The empty C₈₀ has seven IPR structures (D_2 , D_{5d} , C_{2v} , C_{2v} , D_3 , D_{5h} , and I_h). A ¹³C NMR study indicated that the most abundant C₈₀ has D_2 symmetry (Hennrich et al., 1996). However, theoretical calculations (Kobayashi et al., 1995a,b) have shown that encapsulation of two La atoms inside the I_h -C₈₀ cage is most favorable. This is due to the fact that the I_h -C₈₀ cage has only two electrons in the fourfold degenerate highest occupied molecular orbital (HOMO) level and can accommodate six more electrons to form the stable closed-shell electronic state of (La³⁺)₂@C₈₀⁶⁻ with a large HOMO–LUMO (lowest unoccupied molecular orbital) gap.

On the basis of ¹³C NMR and ¹³⁹La NMR results, Akasaka et al. (1995b, 1997) reported a circular motion of engaged La atoms in the C₈₀ cage. Two La atoms may circuit the inside of the spherical I_h -C₈₀ cage. The energy barrier for the circuit of the metal cations is very small (about 5 kcal mol⁻¹). The dynamic behavior of metal atoms should also be reflected in the ¹³⁹La NMR linewidth, since circulation of two La³⁺ cations produces a new magnetic field inside the cage. Such a linewidth broadening was actually observed with increasing temperature from 305 to 363 K (Akasaka et al., 1997).

A similar but greatly restricted intrafullerene dynamics of engaged metal ions has been reported by Miyake et al. (1996) on Sc₂C₂@C₈₂. They observed a single ⁴⁵Sc NMR line, indicating that two Sc atoms in the cage are equivalent. However, in contrast to the La₂@C₈₀ case, the internal rotation is hindered by a large barrier of about 50 kcal mol⁻¹ (Nagase and Kobayashi, 1994b).

Nishibori et al. revealed a detailed La dynamic motion in C₈₀ cage by synchrotron X-ray powder diffraction (Figure 11, Nishibori et al., 2001), where a perfect pentagonal-dodecahedral charge density of La₂ was seen in an icosahedral I_h -C₈₀ cage. The characteristic charge density results from a highly selective trajectory of the two La atoms, which hop along the hexagonal rings of the I_h -C₈₀ polyhedral network. This highly

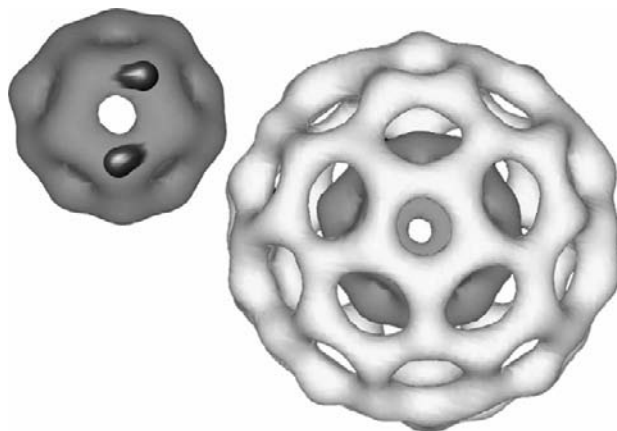


FIGURE 11 MEM charge density of $\text{La}_2@C_{80}$ as the equal-density contour surface along the S_{10} axis. The La_2 dodecahedral charge density is colored in dark and is also additionally shown beside the fullerene molecule.

symmetrical hopping of the two La atoms in C_{80} cage was supported and analyzed in detail by a quantum chemical study (Shimotani et al., 2004).

An intrafullerene dynamics of Ce atom in the C_{82} cage was also studied by time-differential perturbed angular correlation measurements (Sato et al., 1998). The observed angular correlation shows the presence of two different chemical species of $\text{Ce}@C_{82}$. The data at low temperatures reveal that Ce stays at a certain site for one of the species, whereas for the other the atom has an intramolecular dynamic motion.

4.3.5 A di-metallofullerene: $\text{Sc}_2\text{C}_2@C_{82}$

Various metallofullerenes supposed to encapsulate two or three metal atoms within fullerene cages, such as $\text{La}_2@C_{80}$ (Akasaka et al., 1995b, 1997; Alvarez et al., 1991; Kikuchi et al., 1994a; Suzuki et al., 1995a,b), $\text{La}_2@C_{72}$ (Bethune et al., 1994, 1996; Stevenson et al., 1998; van Loosdrecht et al., 1994a,b), $\text{Y}_2@C_{82}$ (Shinohara et al., 1992a; Weaver et al., 1992), $\text{Sc}_2@C_{74}$ (Shinohara et al., 1993a, X Wang et al., 1993c), $\text{Sc}_2@C_{82}$ (Shinohara et al., 1992a; Yannoni et al., 1992), $\text{Sc}_2\text{C}_2@C_{82}$ (Beyers et al., 1994; Shinohara et al., 1992a,b; Takahashi et al., 1995; Takata et al., 1997; Yamamoto et al., 1996; Yannoni et al., 1992), $\text{Sc}_3\text{C}_2@C_{80}$ (Anderson et al., 1997b; Kato et al., 1995a; Shinohara et al., 1992b, 1994a; Stevenson et al., 1994a,b; van Loosdrecht et al., 1994a,b; Yannoni et al., 1992) and $\text{Er}_2@C_{82}$ (Ding et al., 1997; Dorn et al., 1995; Macfarlane et al., 1997) have been successfully synthesized and purified. Among them the scandium di-metallofullerenes, $\text{Sc}_2\text{C}_2@C_{82}$, are especially interesting, because three structural isomers have been found and isolated so far (Yamamoto et al., 1996).

Ab initio theoretical studies (Nagase and Kobayashi, 1997; Nagase et al., 1996) and the experimental results on $\text{Sc}_2\text{C}_2@\text{C}_{82}$ including STM (Shinohara et al., 1993b, X Wang et al., 1993c), TEM (Beyers et al., 1994) and ^{13}C NMR (E Yamamoto et al., 1996) have suggested an endohedral nature. Similar to the mono-metallofullerenes, a synchrotron powder X-ray study is reported on $\text{Sc}_2\text{C}_2@\text{C}_{82}$ (isomer III) based on the Rietveld/MEM analysis (Takata et al., 1997). Figure 12 shows a structural model based on a three-dimensional MEM electron density distribution of $\text{Sc}_2@\text{C}_{84}$ (III), which is now identified as $\text{Sc}_2\text{C}_2@\text{C}_{82}$ (III) carbide metallofullerene as described in Section 5 (Iiduka et al., 2006; Nishibori et al., 2006a,b).

The number of electrons around each maximum inside the cage is 18.8, which is close to that of a divalent scandium ion Sc^{2+} (19.0). A theoretical study predicted that the formal electronic structure of $\text{Sc}_2\text{C}_2@\text{C}_{82}$ is well represented by $(\text{Sc}_2\text{C}_2)_2^{2+}@\text{C}_{82}^{4-}$, where two 4s electrons of each Sc atom transfer to the C_{82} cage (Nagase and Kobayashi, 1997). The positive charge of the Sc atom from the MEM charge density is +2.2 which is in good agreement with the theoretical value. Furthermore, Pichler et al. (2000) reported that comparison of the Sc 2p–3d X-ray absorption spectrum with calculated ionic multiplet spectra shows a formal charge transfer to the fullerene cage of 2.6.

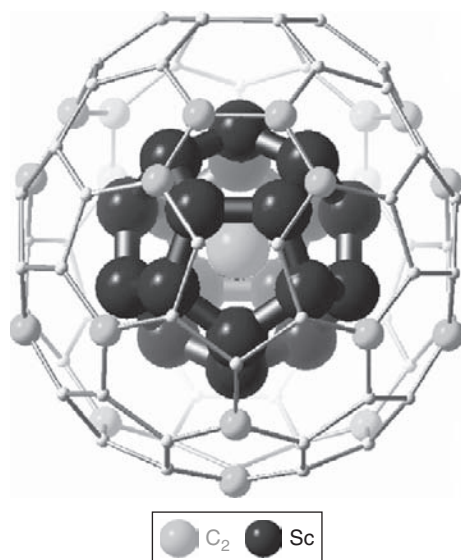


FIGURE 12 The molecular structure of $(\text{Sc}_2\text{C}_2)@\text{C}_{82}$ (III) carbide metallofullerene [formerly considered to be $\text{Sc}_2@\text{C}_{84}$ (III)].

4.3.6 A tri-metallofullerene $\text{Sc}_3\text{C}_2@C_{80}$

A tri-scandium fullerene, $\text{Sc}_3@C_{82}$ (currently identified as $\text{Sc}_3\text{C}_2@C_{80}$, cf. Section 5), has been produced (Shinohara et al., 1992b; Yannoni et al., 1992) and characterized by ESR (see Section 5). A synchrotron X-ray structural study on $\text{Sc}_3@C_{82}$ has been reported recently based on Rietveld/MEM analysis (Takata et al., 1999). The result revealed an intriguing feature of this metallofullerene: three Sc atoms are encapsulated in the form of a triangle Sc_3 cluster inside the $C_{3v}\text{-}C_{82}$ fullerene cage. Furthermore, the charge state of the encaged Sc_3 cluster is 3+ leading to a formal molecular charge state of $(\text{Sc}_3)^{3+}@C_{82}^{3-}$ as a result of an intrafullerene electron transfer. This was the first example in which a metal cluster is encaged by a fullerene. The presence of a Sc_3 trimer in the cage is consistent with an extended Hückel calculation (Ungerer and Hughbanks, 1993).

As is described in Section 5, the detailed X-ray diffraction studies currently indicate that $\text{Sc}_3@C_{82}$ should be $\text{Sc}_3\text{C}_2@C_{80}$ carbide metallofullerene (Iiduka et al., 2005; Nishibori et al., 2006a,b), where a C_2 molecule is encapsulated in $C_{80}\text{-}I_h$ cage. The encapsulated three Sc atoms form a triangle. A spherical charge distribution originating from the C_2 molecule is located at the center of the triangle. Intraatomic distances between Sc and Sc are 3.61(3) Å in the triangle. The distance between Sc and the center of the C_2 molecule is 2.07(1) Å. The molecular structure is shown in Figure 13.

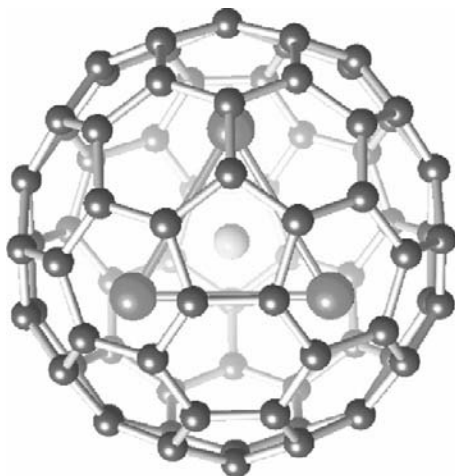


FIGURE 13 The molecular structure model of $\text{Sc}_3\text{C}_2@C_{80}$ along the S_{10} axis determined by the MEM/Rietveld method from the synchrotron X-ray power diffraction data. The large atoms forming a triangle are Sc, and the central sphere represents C_2 molecule averaged by rotation.

4.4 Crystal structures

Microcrystals of a metallofullerene grown from solution and those from solvent-free conditions generally have different crystal structures because of the presence of solvent molecules in the former case. For example, solvent-free La@C₈₂ crystals prepared by sublimation have fcc structure (Watanuki et al., 1995, 1996), whereas La@C₈₂ crystals grown from toluene and carbon disulfide exhibit monoclinic (Nishibori et al., 2000) and cubic (Suematsu et al., 1994) structures, respectively. Crystals of Y@C₈₂ (Takata et al., 1995), Sc@C₈₂ (Takata et al., 1997), Sc₂C₂@C₈₂ (Takata et al., 1998) and Sc₃C₂@C₈₀ (Takata et al., 1999) grown from toluene solutions also have monoclinic structures. Crystals of empty higher fullerenes such as C₇₆ and C₈₂ grown from toluene solutions also show monoclinic structures (Kawata et al., 1995). The observed crystal data and structural parameters of La@C₈₂, Y@C₈₂, and Sc@C₈₂ are listed in Table 2.

One of the important findings in the crystal structures of the mono-metallofullerenes is the alignment of molecules in a certain direction in the crystal. For example, the Y@C₈₂ molecules are aligned along the [001] direction in a head-to-tail (...Y@C₈₂...Y@C₈₂...Y@C₈₂...) configuration

TABLE 2 X-ray structural data for Sc@C₈₂, Y@C₈₂, and La@C₈₂ determined by synchrotron powder X-ray diffraction

	Lattice type ^a	Space group	Parameters	Metal-carbon distance (Å)
Sc@C ₈₂	monoclinic	P2 ₁	a = 18.362(1) Å b = 11.2490(6) Å c = 11.2441(7) Å β = 107.996(9)°	2.53(8)
Y@C ₈₂	monoclinic	P2 ₁	a = 18.401(2) Å b = 11.281(1) Å c = 11.265(1) Å β = 108.07(1)°	2.40(15) ^d
La@C ₈₂	monoclinic	P2 ₁	a = 18.3345(8) Å b = 11.2446(3) Å c = 11.2320(3) Å β = 107.970(6)°	2.55(7)
La@C ₈₂	cubic ^b	I-43d	a ₀ = 25.72 ± 0.007 Å	2.55(7)
La@C ₈₂	fcc ^b	Fm 3 m ^c	a ₀ = 15.78 Å	2.55(7)

^a All crystals as grown from toluene solution have monoclinic lattice.

^b Crystals containing as grown from CS₂ solution have cubic lattice, whereas solvent-free crystals have fcc lattice.

^c Patterson symmetry.

^d The structure with five positional disorder of Y atom.

in the crystal, indicating the presence of a strong dipole–dipole and charge transfer interactions among the $Y@C_{82}$ fullerenes (Takata et al., 1995). The crystal data in Table 2 also support this idea since the c parameter of $Y@C_{82}$ (11.265 Å) is shorter than that of C_{82} (11.383 Å), whereas the parameter of $Y@C_{82}$ is much longer than that of C_{82} , indicating a shrinkage in crystal packing in the [001] direction.

5. CARBIDE METALLOFULLERENES

The production and isolation of the first carbide metallofullerene was reported on $Sc_2@C_{86}$ ($=Sc_2C_2@C_{84}$) in 2001 (Wang et al., 2001). In fact, this study has revealed that the major part of the di-scandium metallofullerenes may have $Sc_2C_2@C_{2n-2}$ carbide structure rather than $Sc_2@C_{2n}$ including $Sc_2@C_{84}$ (isomers III) (Iiduka et al., 2006; Nishibori et al., 2006a,b).

The schematic molecular structure is shown in Figure 14. It was found that the C_2 molecule in the C_{84} cage rotates like a rigid-rotor at low temperatures below 60 K (Krause et al., 2004). Furthermore, it has been found that $Sc_3@C_{82}$ was actually a scandium carbide fullerene, $Sc_3C_2@C_{80}$, as revealed by X-ray diffraction (Iiduka et al., 2005; Nishibori et al., 2006a,b). The possibility of such carbide structure of $Sc_3C_2@C_{80}$ instead of $Sc_3@C_{82}$ was reported by Sugai et al. by gas-phase ion mobility measurements (Sugai et al., 2001). Even in non-IPR metallofullerenes (Stevenson et al., 2000; Wang et al., 2000), the presence of a carbide fullerene, $Sc_2C_2@C_{68}$, was reported and structurally characterized (Shi et al., 2006).

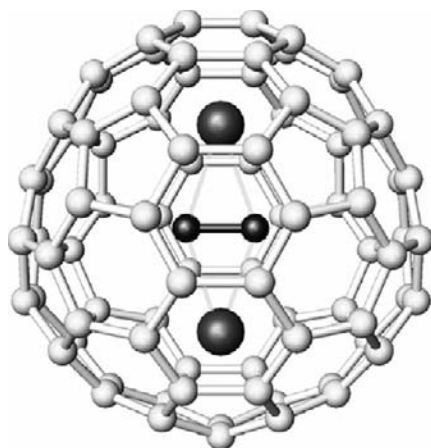


FIGURE 14 Schematic molecular structure of the $(Sc_2C_2@C_{84})$ carbide metallofullerene based on the synchrotron X-ray powder diffraction and ^{13}C NMR experiments. The two (top and bottom) spheres in the fullerene correspond to Sc atoms, whereas the C_2 molecules are depicted between the Sc atoms.

The carbide metallofullerenes are now widely observed for the various kind of di-metallofullerenes such as $Y_2C_2@C_{82}$ (Inoue et al., 2003, 2004) and $Er_2C_2@C_{82}$ (isomers I, II, III) (Ito et al., 2007a,b). One of the main causes for the prevalence of carbide di- or tri-metallofullerenes is that two or three positively charged metal atoms in fullerene cages can be bound tightly together around a negatively charged C_2 molecule (Inoue et al., 2004).

6. ELECTRONIC STATES AND STRUCTURES

6.1 Intrafullerene electron transfer within the carbon cage

Group 3 (Sc, Y, La) metallofullerenes exhibit ESR hfs, which provides us with important information on the electronic structures of the metallofullerenes. Typical ESR-active monometallofullerenes are $La@C_{82}$, $Y@C_{82}$, and $Sc@C_{82}$. The ESR hfs of a metallofullerene was first observed in $La@C_{82}$ by the IBM Almaden group (Johnson et al., 1992) (Figure 15) and was discussed within the framework of an intrafullerene electron transfer. The observation of eight equally spaced lines provides evidence of isotropic electron–nuclear hyperfine coupling (hfc) to ^{139}La with a nuclear spin quantum number $I = 7/2$. The observed electron g -value of 2.0010, close to that measured for the C_{60} radical anion (Allemand et al., 1991; Krusic et al., 1991), indicates that a single unpaired electron resides in the LUMO of the carbon cage. They also observed ^{13}C hyperfine

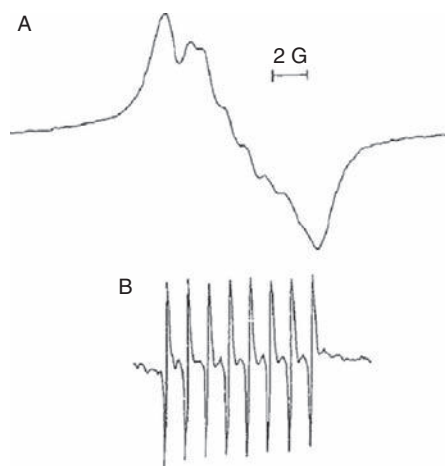


FIGURE 15 The first ESR hyperfine spectra (9.112 GHz) of $La@C_{82}$ at room temperature of (A) solid degassed toluene extract and (B) a degassed solution of the dried extract in 1,1,2,2-tetrachloroethane.

satellites, provided the unpaired electron couples to both the ^{139}La and the carbon atoms. The observed hfc (1.2 G) is very small compared with that (50 G) measured for La^{2+} substituted in CaF_2 (Pilla and Bill, 1984). Therefore, it was concluded that the La atom in the C_{82} cage must be in the 3+ state, which gives a formal charge state of $\text{La}^{3+}@\text{C}_{82}^{3-}$. UPS (Hino et al., 1993; Poirier et al., 1994) and recent X-ray diffraction results (Nishibori et al., 2000) strongly support this conclusion.

ESR hfs obtained for $\text{Y}@\text{C}_{82}$ indicated that the yttrium in C_{82} is also in the 3+ oxidation state (Shinohara et al., 1992a; Weaver et al., 1992). However, there has been controversy as to whether $\text{Sc}@\text{C}_{82}$ has 3+ or 2+ charge state, as described in Section 4.3.2 (Nagase and Kobayashi, 1993; Ruebsam et al., 1996a; Shinohara et al., 1992b). Recent X-ray diffraction (Takata et al., 1998) and UPS (Hino et al., 1998) results indicate a 2+ state leading to $\text{Sc}^{2+}@\text{C}_{82}^{2-}$. Theoretical calculations suggest that the electronic structure of $\text{Sc}@\text{C}_{82}$ is well represented by $\text{Sc}^{2+}@\text{C}_{82}^{2-}$ (Nagase and Kobayashi, 1993, 1994a,c, 1996). Unlike $\text{La}@\text{C}_{82}$ and $\text{Y}@\text{C}_{82}$, $\text{Sc}@\text{C}_{82}$ forms a divalent state and an electron residing in the $\text{Sc}(3d)$ orbital, owing to a large energy separation between the 3d and 4s orbitals, might be responsible for the observed ESR hfs.

The temperature-dependent linewidths of the ESR hfs of $\text{La}@\text{C}_{82}$, $\text{Sc}@\text{C}_{82}$ and $\text{Gd}@\text{C}_{82}$ have been discussed by Kato et al. (1993, 1995a,b, 1996) in terms of the spin-rotation coupling interaction. Dinse and co-workers (Ruebsam et al., 1995, 1996a,b) investigated temperature dependence of ESR line widths of $\text{La}@\text{C}_{82}$, $\text{La}@\text{C}_{90}$, and $\text{Sc}@\text{C}_{82}$ in different solvents and obtained information on the nuclear quadrupole interactions in these metallofullerenes. Dunsch and co-workers (Bartl et al., 1994, 1997; Seifert et al., 1998) studied ^{13}C satellite structures of $\text{M}@\text{C}_{82}$ ($\text{M} = \text{Sc}, \text{Y}, \text{La}$) in detail and reported that the manifold of ^{13}C hfc (hyperfine constants) could be interpreted by the calculated spin density distributions.

ESR spectra of $\text{La}@\text{C}_{82}$, $\text{Y}@\text{C}_{82}$, $\text{Ho}@\text{C}_{82}$, and $\text{Tm}@\text{C}_{82}$ taken from the solid soot extract were reported by Bartl et al. (1994, 1995a,b, 1996) and showed low resolved but split hyperfine structure, indicating that the metal atoms exist in ionic form in the fullerene cage also in the solid state. The research group also reported (Knorr et al., 1998) the principal values of the hyperfine tensor A and the relative orientation of g and A tensors of $\text{M}@\text{C}_{82}$ ($\text{M} = \text{Sc}, \text{Y}, \text{La}$) applying three- and four-pulse electron spin-echo envelope modulation techniques (ESEEM).

6.2 ESR detection of structural isomers of metallofullerenes

Suzuki et al. (1992) reported the presence of structural isomers of $\text{M}@\text{C}_{82}$ ($\text{M} = \text{Sc}, \text{Y},$ and La) via ESR hfs measurements and also hfs to ^{13}C in natural abundance on the fullerene cage. Figure 16 shows ESR spectra of $\text{Sc}@\text{C}_{82}$, $\text{Y}@\text{C}_{82}$, and $\text{La}@\text{C}_{82}$ which exhibit ^{13}C hfs. Hoinkis et al. (1992)

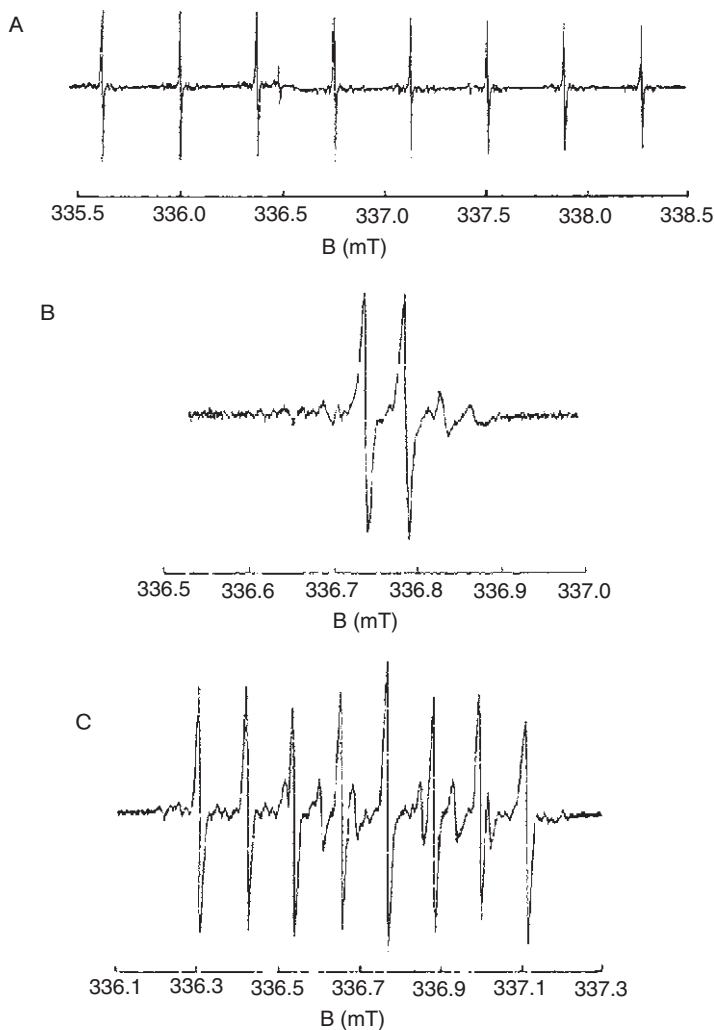


FIGURE 16 ESR spectra of (A) Sc@C_{82} in CS_2 (9.4325 GHz, 0.1 mW); (B) Y@C_{82} in toluene (9.4296 GHz, 0.1 mW); (C) La@C_{82} in toluene (9.4307 GHz, 0.1 mW).

similarly reported the presence of isomers of La@C_{82} and Y@C_{82} . Bandow et al. (1992) also found the structural isomers of La@C_{82} as well as the presence of other La-fullerenes such as La@C_{76} and La@C_{84} by ESR hfs measurements only when anaerobic sampling of soot containing La-fullerenes was employed.

These structural isomers of M@C_{82} have been separated and isolated by HPLC (Section 3). The minor isomer of La@C_{82} , i.e., La@C_{82} (II), was isolated by Yamamoto et al. (1994b). Similar to the major isomer,

La@C₈₂ (I), La@C₈₂ (II) exhibits an equally spaced octet line but with a smaller hfs constant. Sc@C₈₂ also has two structural isomers (I and II) which have been separated and isolated (Inakuma et al., 1995). The two Sc@C₈₂ isomers show equally spaced, eight narrow ESR hfs owing to the hfc to the scandium nucleus (Inakuma et al., 1995; Shinohara et al., 1992b; Yannoni et al., 1992). The hfs of Sc@C₈₂ is much bigger than that of La@C₈₂.

Two isomers of Y@C₈₂ (I, II) have been separated and isolated by the two-stage HPLC method (Inakuma et al., 1995; Kikuchi et al., 1994b; Shinohara et al., 1995a,b). Both isomers of Y@C₈₂ show distinct ESR hyperfine doublets due to $I = 1/2$ yttrium nucleus. The overall ESR spectral patterns of Y@C₈₂ (I, II) in CS₂ solution at room temperature are similar, but the hfs values differ. Moreover, the appearance of the small satellite peaks due to ¹³C, adjacent to the main doublets, is much less clear in Y@C₈₂ (II). Obviously, the electronic structures of the two isomers are different. It has been found that isomer (II) is less stable in air and much more reactive toward various solvents than isomer (I). Yamamoto et al. (1997) produced and isolated three isomers of La@C₉₀ (I–III) and observed the hfs. The observed hfc values are much smaller than those of La@C₈₂ (I, II).

Other mono-metallofullerenes are either simply ESR-silent or show fine structures (instead of hfs) only at low temperature. For example, the Gd@C₈₂ metallofullerene exhibits a fine structure at low temperature (Kato et al., 1995b, 1996). Di-metallofullerenes, such as La₂@C₈₀, Y₂@C₈₂, and Sc₂C₂@C₈₂, are known to be ESR-silent, indicating that these species are diamagnetic. Knapp et al. (1998) observed ESR signals of Lu@C₈₂ arising from unresolved hyperfine interaction with $I = 7/2$ nuclear spin of ¹⁷⁵Lu, whereas no ESR signals were detected for Ho@C₈₂. The unobservability of solution and frozen matrix ESR on Ho@C₈₂ can be attributed to a high spin state (a ⁵I₈ ground state for Ho³⁺) leading to strong spin lattice relaxation and rigid limit spectral broadening (Knapp et al., 1998). The general inability to observe well-resolved ESR hfs for the lanthanide metallofullerenes Ln@C₈₂ (Ln = Ce, . . . , Lu) as in group 3 metallofullerenes might also be due to this strong nuclear spin relaxation.

The tri-scandium fullerene, Sc₃C₂@C₈₀ (formerly assigned as Sc₃@C₈₂), has so far been the only ESR-active metallofullerene identified other than the mono-metallofullerenes of the type M@C₈₂ (R = Sc, Y, La). Figure 17 shows perfectly symmetric, equally spaced, 22 narrow ESR hfs, which is a manifestation of the isotropic hfc of three scandium nuclei with $I = 7/2$ in the C₈₀ cage (Shinohara et al., 1992b; Yannoni et al., 1992). The presence of the perfectly symmetric 22 hfs lines suggests the geometrical equivalence of the three scandium atoms in the C₈₀ cage (Anderson et al., 1997b; Kato et al., 1994, 1995a; Shinohara et al., 1992b, 1993c; Stevenson et al., 1994b; van Loosdrecht et al., 1994b; Yannoni et al., 1992). Based on the appearance of the perfectly symmetric 22 hfs and the results of theoretical

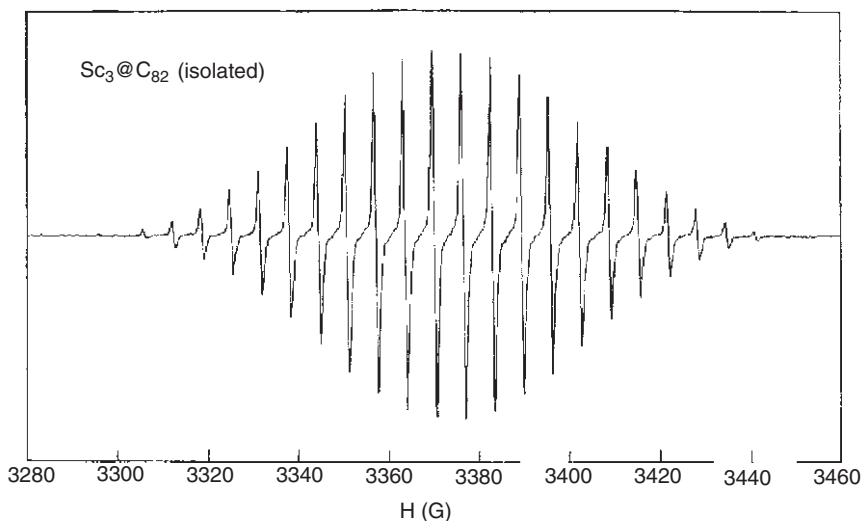


FIGURE 17 ESR spectrum (X-band, 9.4360 GHz) for $\text{Sc}_3\text{C}_2@C_{80}$ in CS_2 solution at 220 K, showing well resolved, equally spaced and perfectly symmetric 22 hfs ($g = 1.9985$, $\text{hfs} = 6.51$, $\Delta H_{\text{pp}} = 0.770$ G).

calculations (Ungerer and Hughbanks, 1993), three scandium atoms form an equilateral Sc_3 trimer within the C_{80} cage so as to retain a threefold axis as an entire $\text{Sc}_3\text{C}_2@C_{80}$ molecule. The result is consistent with a recent X-ray structural study on $\text{Sc}_3\text{C}_2@C_{80}$ as described in Section 4.3.6. The molecular structure of $\text{Sc}_3\text{C}_2@C_{80}$ is shown in Figure 13.

The temperature dependence of the 22 hfs lines can provide us with further structural information on $\text{Sc}_3\text{C}_2@C_{80}$ (Kato et al., 1995b; van Loosdrecht et al., 1994b). The H (magnetic field) value has a minimum at 220 K above which the hfs linewidth increases as temperature increases. A similar temperature dependence has been reported for $\text{La}@C_{82}$ (Bandow et al., 1992; Kato et al., 1993). Even at this temperature, the hfs linewidth of $\text{Sc}_3\text{C}_2@C_{80}$ ($H_{\text{pp}} = 0.4$ G at 220 K) is about ten times as broad as that of $\text{Sc}@C_{82}$ (0.036 G at 300 K). Such a large linewidth could be due to incomplete motional averaging of local field variations due to strong magnetic anisotropy of the entire molecule (van Loosdrecht et al., 1994b). The intramolecular dynamics is the inherent nature of the Sc_3 trimer encapsulated in the C_{80} cage. In addition to $\text{Sc}_3\text{C}_2@C_{80}$ described above, Suzuki et al. (1994) observed a series of ESR hfs due to non-equivalent Sc trimers encaged in fullerene cages other than C_{80} .

The observed ESR hyperfine parameters for $M@C_{82}$ ($R = \text{Sc}, \text{Y}, \text{La}$), $\text{La}@C_{90}$ and $\text{Sc}_3\text{C}_2@C_{80}$ are summarized in Table 3.

TABLE 3 ESR parameters for some isolated metallofullerenes

Species	hfc (G)	g-value	H_{pp} (G)
Sc@C ₈₂ (I)	3.82	1.9999	0.036 (300 K)
Sc@C ₈₂ (II)	1.16	2.0002	0.019 (300 K)
Sc@C ₈₄	3.78	1.9993	0.017 (300 K)
Sc ₃ C ₂ @C ₈₂	6.45	1.999	0.4 (220 K)
Y@C ₈₂ (I)	0.48	2.0004	0.087 (300 K)
Y@C ₈₂ (II)	0.34	2.0002	0.12 (300 K)
La@C ₈₂ (I)	1.20	2.0008	0.049 (300 K)
La@C ₈₂ (II)	0.83	2.0002	0.052 (220 K)
La@C ₉₀ (I)	0.60	2.0010	
La@C ₉₀ (II)	0.53	2.0011	
La@C ₉₀ (III)	0.12	2.0022	

6.3 Electrochemistry on metallofullerenes

Electronic properties of endohedral metallofullerenes based on reduction/oxidation (redox) properties have also been investigated electrochemically by using cyclic voltammetry (CV). Suzuki et al. (1993) measured cyclic voltammograms on La@C₈₂ and found unusual redox properties of the metallofullerene which differ significantly from those of empty fullerenes. Figure 18 shows the CV of La@C₈₂. The first reversible oxidation potential is approximately equal to that of ferrocene, indicating that La@C₈₂ is a moderate electron donor. The first reduction and oxidation potentials indicate that it should form both cationic and anionic charge transfer complexes. In addition, La@C₈₂ is a stronger electron acceptor than empty fullerenes such as C₆₀, C₇₀ and C₈₄. A schematic energy level diagram of La@C₈₂ is presented in Figure 19. The CV results on La@C₈₂ revealed that La@C₈₂ is a good electron donor as well as a good electron acceptor and that at least five electrons can be transferable to the C₈₂ cage while maintaining the 3+ charge state of the encaged La atom, i.e., (La³⁺@C₈₂³⁻)⁵⁻.

The CV measurements indicate that the oxidation state of the yttrium atom in Y@C₈₂ (Suzuki et al., 1996) was close to that of La@C₈₂, probably 3+. The electrochemistry of Y@C₈₂ is almost identical to that of La@C₈₂ (Anderson et al., 1997a; Suzuki et al., 1996). Other mono-metallofullerenes such as Y@C₈₂, Ce@C₈₂ and Gd@C₈₂ have a similar tendency in their redox properties (Suzuki et al., 1996). Anderson et al. (1997b) reported CV data on Sc₃C₂@C₈₀. CV measurements were also taken on other lanthanide fullerenes such as Pr@C₈₂, Nd@C₈₂, Tb@C₈₂, Dy@C₈₂, Ho@C₈₂, Er@C₈₂ and Lu@C₈₂ by Wang et al. (1997). The first reduction potentials of all seven M@C₈₂ were found to locate within a close vicinity

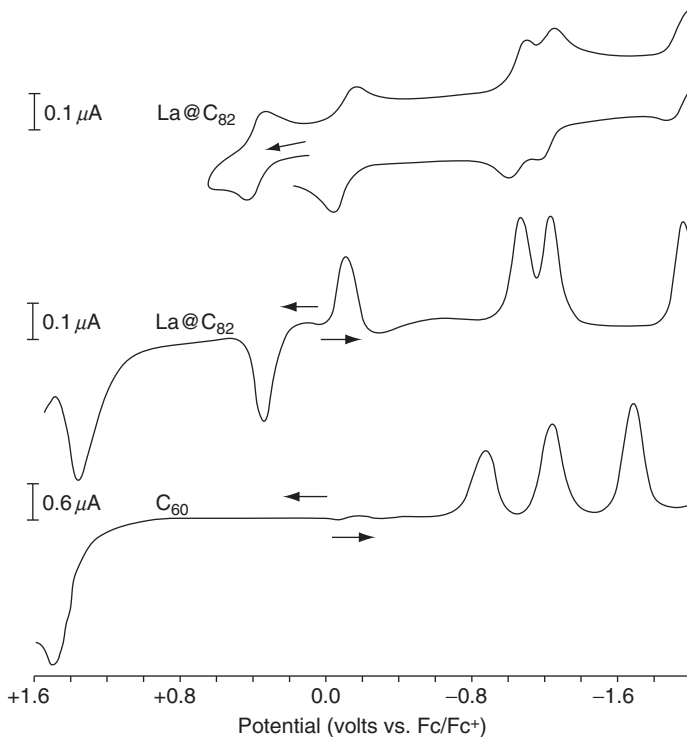


FIGURE 18 Cyclic voltammogram of La@C_{82} and differential pulse voltammograms of La@C_{82} and C_{60} in *o*-dichlorobenzene.

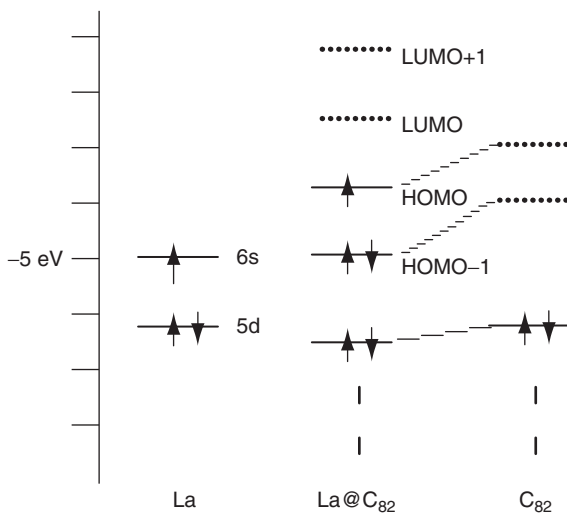


FIGURE 19 Schematic energy level diagram of La@C_{82} . The vertical energy spacing is 1.0 eV.

to each other, suggesting that all the entrapped metal atoms adopt a similar valence state, presumably a trivalent cation state.

Dunsch and co-workers (Bartl et al., 1996; Dunsch et al., 1995, 1997; Petra et al., 1996) studied electron transfers in metallofullerenes by CV coupled with *in situ* ESR experiments. The electron transfer to the endohedral La@C₈₂ molecule studied by this method gives evidence of a charge in the electronic state of the fullerene; the electrochemical reaction in the anodic scan causes the formation of La³⁺@C₈₂⁴⁻, and during the cathodic scan the spin concentration decreases as the La³⁺@C₈₂²⁻ structure formed by reduction is not paramagnetic.

6.4 Similarity of UV–Vis–NIR absorption spectra

Absorption spectra of endohedral metallofullerenes in the ultraviolet–visible–near IR (UV–Vis–NIR) region are unique as compared with those of empty fullerenes. Normally, the absorption spectra of metallofullerenes have long tails to the red down to 1,500 nm or more. The absorption spectra of the major isomers of mono-metallofullerenes M@C₈₂ (M = Y, La, Ce, Pr, Nd, Gd, Tb, Dy, Ho, Er, Lu) are similar to each other and well represented by a sharp peak around 1,000 nm and a broad peak around 1,400 nm. These absorption peaks may be related to the intrafullerene electron transfers from the engaged metal atom to the carbon cage.

Figure 20 shows UV–Vis–NIR absorption spectra for the isolated group 3 metallofullerenes: La@C₈₂ (Kikuchi et al., 1993; Yamamoto et al., 1994a), Y@C₈₂ (Kikuchi et al., 1994b) and Sc@C₈₂ (Inakuma et al., 1995) in carbon disulfide solution. The spectrum of Sc@C₈₂ is very different from those of Y@C₈₂ and La@C₈₂, indicating that the electronic structure of Sc@C₈₂ is different from those of Y@C₈₂ and La@C₈₂. As described in Section 4.3.2, the charge state of Sc²⁺@C₈₂²⁻ (divalency) is different from those of La³⁺@C₈₂³⁻ and Y³⁺@C₈₂³⁻ (trivalency) (Hino et al., 1993; Nagase and Kobayashi, 1993; Takata et al., 1995). The UV–Vis–NIR absorption spectra of many mono-metallofullerenes encapsulating lanthanide elements, Ln@C₈₂ (Ln = Ce–Nd, Gd–Er, Lu) (Ding et al., 1996b; Suzuki et al., 1996), Pr (Ding and Yang, 1996; Shinohara et al., 1994b), Nd (Ding et al., 1996a), Gd (Kikuchi et al., 1994c; Shinohara et al., 1994b), Tb (Shi et al., 2003), Dy (Kikuchi et al., 1998; Tagmatarchis and Shinohara, 2000), Ho (Knapp et al., 1998; W Wang et al., 1997), Er (Ito et al., 2007a,b; Kikuchi et al., 1998), Lu (Knapp et al., 1998)), are similar to those of La@C₈₂ and Y@C₈₂. However, the absorption spectra of the C₈₂ based metallofullerenes containing the divalent lanthanide elements (i.e., Sm, Eu, Tm, and Yb) (Kikuchi et al., 1997; Kirbach and Dunsch, 1996; Okazaki et al., 2000) are different from those of La@C₈₂, Y@C₈₂ and Ln@C₈₂ but are similar to

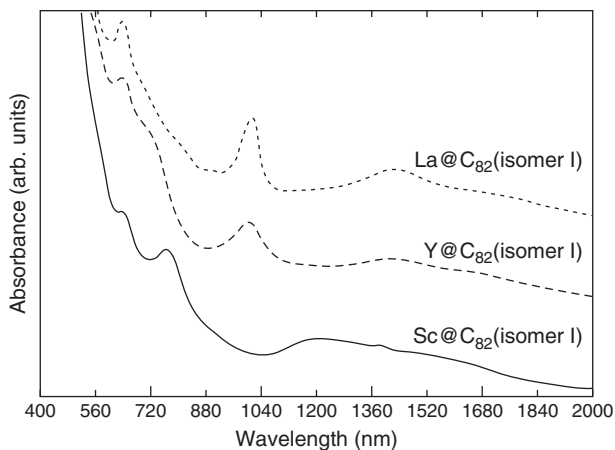


FIGURE 20 UV-Vis-NIR absorption spectra of $\text{La@C}_{82}(\text{I})$, $\text{Y@C}_{82}(\text{I})$, and $\text{Sc@C}_{82}(\text{I})$. The spectral feature of Sc@C_{82} is different from those of Y@C_{82} and La@C_{82} . The absorption spectra of M@C_{82} ($\text{M} = \text{Ce}, \text{Pr}, \text{Gd}, \text{Tb}, \text{Dy}, \text{Ho}, \text{Er}, \text{and Lu}$) are essentially the same as that of La@C_{82} .

that of Sc@C_{82} in that the sharp absorption peak at 1,000 nm are missing in these divalent metallofullerenes.

UV-Vis-NIR absorption spectra of structural isomers for a metallofullerene generally differ from each other. Such differences stem from the fullerene cage (isomer) structure as well as from the difference in charge state of the fullerene. For example, isomers I and II of La@C_{82} (Yamamoto et al., 1994b), Y@C_{82} (Inakuma et al., 1995) and Sc@C_{82} (Inakuma and Shinohara, 2000) have different spectral features in their respective absorption spectra (cf. Figure 21).

The absorption spectra of group 2 metallofullerenes are quite different from those of group 3 metallofullerenes. Figure 22 shows the UV-Vis-NIR absorption spectra of major isomers of Ca@C_{82} (Dennis and Shinohara, 1997a,b, 1998; Dennis et al., 1998; Nakane et al., 1998; Xu et al., 1996). This is due to the fact that the charge state of the engaged metal atoms for these group 2 metallofullerenes is $2+$ rather than $3+$. Similar to the group 3 case, the absorption spectra of structural isomers of group 2 metallofullerenes also differ from each other. Such an example has been found for the four structural isomers of Ca@C_{82} (I-IV) (Xu et al., 1996) (Figure 22). A similar observation has been reported for the three structural isomers of Tm@C_{82} (A, B, C) (Dunsch et al., 1997; Kirbach and Dunsch, 1996). The absorption spectra of the three isomers (A, B, C) of Tm@C_{82} are almost exactly the same as three structural isomers (III, I, IV) of Ca@C_{82} , respectively, suggesting that each isomer shares the same isomer structure. Furthermore, the absorption spectrum of Ca@C_{82} (IV)

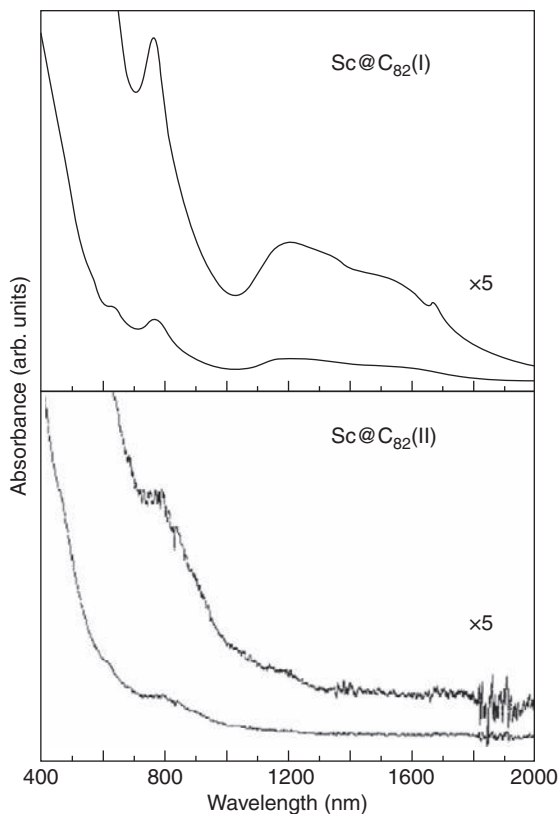


FIGURE 21 UV-Vis-NIR absorption spectra of isolated Sc@C₈₂ (I, II) in CS₂ solution. The energy of the onset Sc@C₈₂ (II) (<0.95 eV) is much larger than that of Sc@C₈₂ (I) (0.62 eV). The overall spectral features are quite different with each other.

was found to be similar to that of Sc@C₈₂ (I), indicating that the Ca and Sc atoms are trapped within the same structural isomer having the same oxidation state of 2+.

Judging from the similarity on the absorption spectra, Ln@C₈₂ (Ln = Ce, Pr, Nd, Gd, Tb, Dy, Ho, Er, Lu) metallofullerenes have 3+ charge state similar to La@C₈₂ and Y@C₈₂, whereas the charge state of Ln@C₈₂ (Ln = Sm, Eu, Tm, Yb) is 2+ as that of Sc@C₈₂. It is interesting to note that the HPLC retention times of Ln@C₈₂ (Ln = Ce, Pr, Nd, Gd, Tb, Dy, Ho, Er, Lu) are similar to each other but are different from those of Ln@C₈₂ (Ln = Sm, Eu, Tm, Yb) which are also almost the same as each other (Kikuchi et al., 1997; Sueki et al., 1997). Yang and co-workers also made a systematic study on lanthanide metallofullerenes from the standpoint of Vis-NIR absorption spectra (Ding and Yang, 1997) together with their HPLC elution behavior (Huang and Yang, 1988). They found that there is

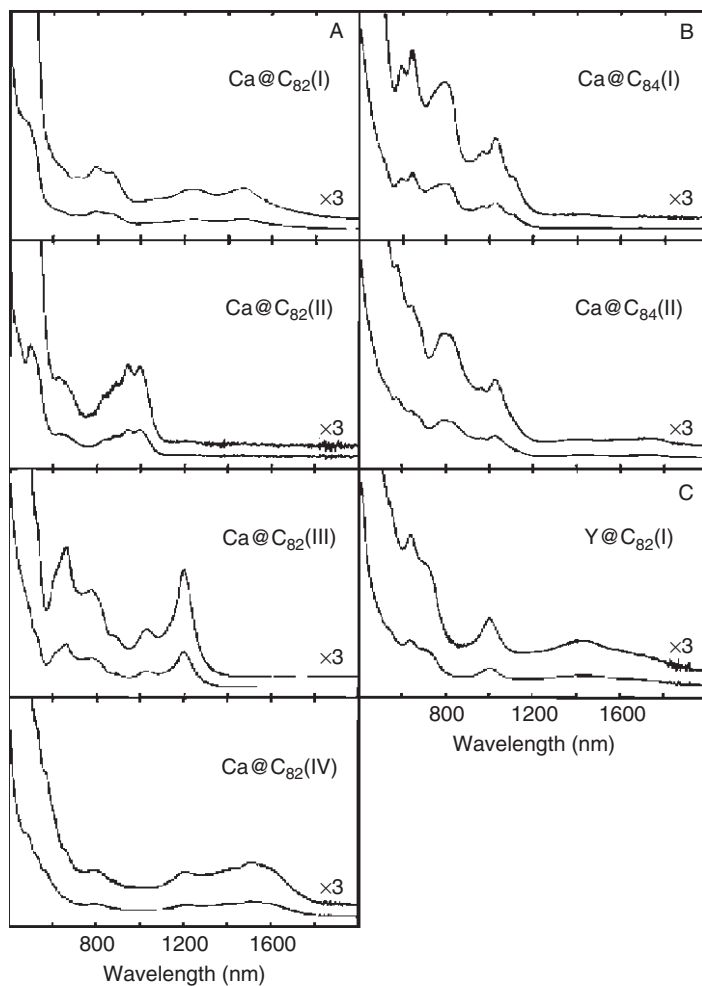


FIGURE 22 UV-Vis-NIR absorption spectra of (A) Ca@C_{82} (I-IV), (B) Ca@C_{84} (I, II), and (C) Y@C_{82} (I) for comparison.

a fairly good correlation between the relative HPLC retention time and the charge state (i.e., divalent or trivalent) of encapsulated metal atoms. According to their results, the four lanthanide atoms Sm, Eu, Tm, and Yb have divalent state whereas the other lanthanide elements (La, Ce, Pr, Nd, Gd, Tb, Dy, Ho, Er, Lu) form a trivalent state in the C_{82} cage which is consistent with the former results.

Here we are able to derive an empirical rule regarding the relationship between absorption features and the isomer structure of a metallofullerene: “a UV-Vis-NIR absorption spectrum of a metallofullerene

($M@C_{82}$: M = metal atom) is very similar to that of another metallofullerene irrespective of the kind of encaged metal atom when the cage (isomer) structure and the charge state of the atoms are the same." This empirical rule can be best understood by molecular excitations of the isomer cage which should not be changed as long as the cage and the filling of the molecular levels are the same.

Fluorescence experiments of endohedral metallofullerenes, on the other hand, have been limited because of their weak emission feature. IR emissions from Er^{3+} for $Er_2@C_{82}$ around $1.5 \mu m$ have been observed (Ding et al., 1997; Hoffman et al., 1997; Ito et al., 2007a,b; Macfarlane et al., 1997; Plant et al., 2009). The emission was ascribed by the characteristic intraconfigurational $4f^{11}$ fluorescence of the trivalent Er ${}^4I_{13/2} \rightarrow {}^4I_{15/2}$ transition.

6.5 The Fermi level and the electronic structure

The electronic properties of several metallofullerenes in the solid state have been studied by UPS (Hino et al., 1993; Kessler et al., 1997; Pichler et al., 1997, 1998; Poirier et al., 1994). Figure 23 is a UPS spectrum of $La@C_{82}$ (Poirier et al., 1994). The first (small peak is 0.64 eV (number 1, and a in the difference plot) below the Fermi level corresponding to the singly occupied molecular orbital (SOMO) level of $La@C_{82}$ where the spectral onset is 0.35 eV from the Fermi level. Hino et al. (1993) also observed peaks at 0.9 and 1.6 eV below the Fermi level in their UPS measurement on $La@C_{82}$ which are absent in the corresponding empty C_{82} spectrum. The peaks at 1.6 and 0.9 eV correspond to electron transfers from the La atom to the LUMO and (LUMO+1) levels of $La@C_{82}$ which are now occupied, respectively (see Figure 19). Since the observed intensity ratio of the two peaks is about 2:1, they concluded that three electrons of the La atom are transferred to the fullerene cage, i.e., $La^{3+}@C_{82}^{3-}$, which is consistent with the results obtained by ESR hfs (see Section 6.1). Eberhardt and co-workers also studied the valency of $La@C_{82}$ by UPS measurements on the sublimed layers. They observed a resonant enhancement of the La-derived valence states via the La 3d to 4f transition (Kessler et al., 1997). They concluded that, in contrast to the interpretations of the La core-level photoemission studies described above, the La valence electrons are not completely delocalized on the fullerene cage. They estimated that about one-third of an electron charge is left in the La-valence orbitals for $La@C_{82}$. It seems that a complex picture involving several La-fullerene hybridized states can better describe the electronic structure of $La@C_{82}$ than a simple charge transfer.

Pichler et al. (1997) studied the valency of the Tm ion in the endohedral $Tm@C_{82}$ fullerene by UPS and XPS. The resemblance of the Tm 4d core level photoemission spectrum to that calculated for Yb^{3+} suggests a $4f^{13}$

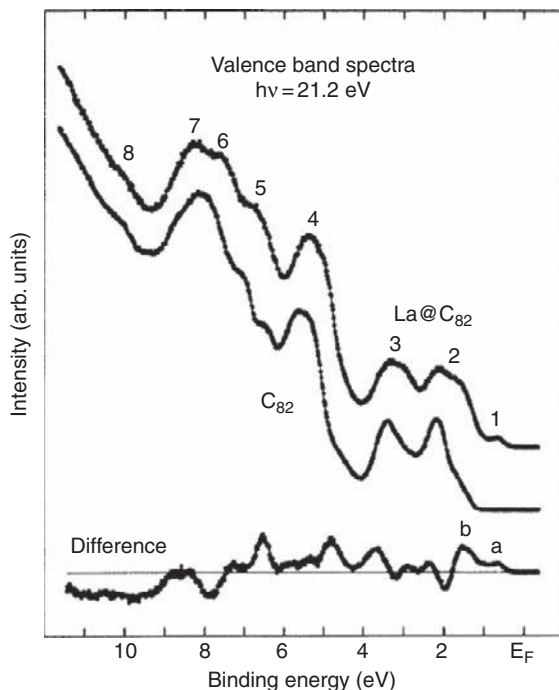


FIGURE 23 Comparison of valence band spectra for C_{82} and $La@C_{82}$ measured at 21.2 eV. The observed onset at 0.35 eV indicates insulating character for solid $La@C_{82}$. Peaks 1–3 and 4–8 are assigned as due to the π and σ electrons, respectively. The difference curve at the bottom is obtained after shifting the C_{82} spectrum by -0.18 eV for the best overall alignment.

ground state configuration of the Tm ion. The UPS measurements on $Sc_2C_2@C_{82}$ (III) (Takahashi et al., 1995), $Gd@C_{82}$ (Hino et al., 1997), $Sc@C_{82}$ (I) (Hino et al., 1998) and $Ca@C_{82}$ (I, III) (Hino et al., 2001) were also reported in which band gaps of these metallofullerenes were obtained.

7. META-CAGE VIBRATION WITHIN METALLOFULLERENES

Vibrational structures of several metallofullerenes have been studied by IR and Raman spectroscopy (Dunsch et al., 1998a; Hulman et al., 1997; Kikuchi et al., 1993; Lebedkin et al., 1998a,b; Pichler et al., 1996). Some of the vibrational absorption lines of $Sc_2C_2@C_{82}$ (III) are strongly enhanced if compared with the spectrum of the empty cage (Hulman et al., 1997; Krause et al., 1999; Pichler et al., 1996). With decreasing temperature, a dramatic narrowing of the lines was observed. The linewidth shows an

Arrhenius-like behavior between 200 and 300 K provided that the main contribution to it comes from rotational diffusion.

Lebedkin et al. (1998a,b) reported vibrations due to the encapsulated metal ions in the cage for $M@C_{82}$ ($M = La, Y, Ce, Gd$) based on IR and Raman measurements. Figure 24 shows Raman spectra of $M@C_{82}$ ($M = La, Y, Ce, Gd$) (Lebedkin et al., 1998b). The peaks around 150 cm^{-1} can be attributed to internal vibrational modes, most probably metal-to-cage vibrations. Almost all peaks are observed at similar positions. These peaks were strongly broadened when the samples were exposed to air. This result is in agreement with a near-edge X-ray absorption fine-structure study (Buerk et al., 1996) where the pronounced effect of air on the

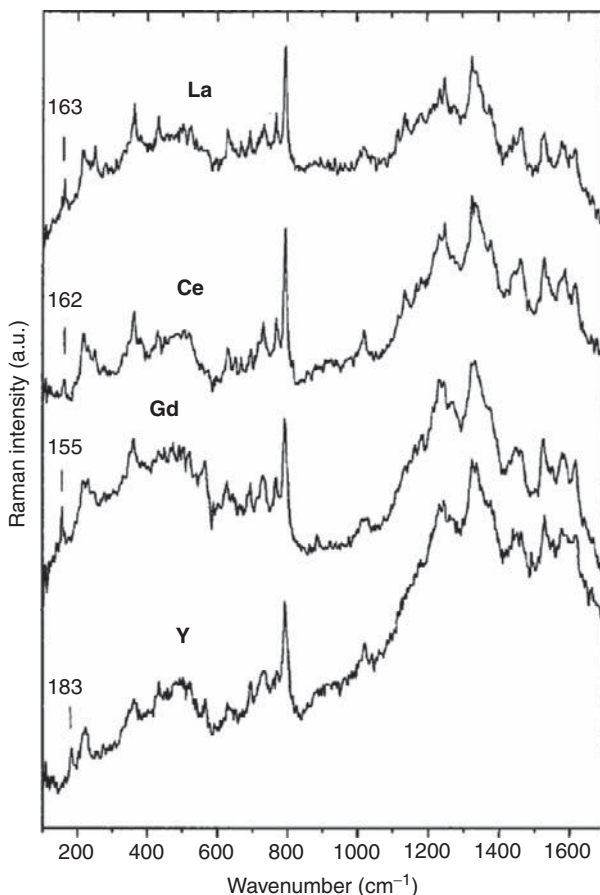


FIGURE 24 Raman spectra of $M@C_{82}$ ($M = La, Ce, Gd, Y$) metallofullerenes. The spectra are shifted for clarity.

spectra of La@C₈₂ films could be reduced only by heating them to 600 °C. The far-IR spectra of M@C₈₂ (M = La, Y, Ce) (Lebedkin et al., 1998b) support the picture derived from the Raman measurements. The metal-dependent far-IR peaks between 150 and 200 cm⁻¹ correspond well to their Raman counterparts.

More detailed IR and Raman measurements were reported by Dunsch and co-workers (Dunsch et al., 1998b) on the three isomers of Tm@C₈₂ (Dunsch et al., 1997; Kirbach et al. 1996). The frequency of the metal-to-cage vibration is only slightly affected by the fullerene cage isomerization, but it strongly depends on the kind of metal ion inside the fullerene. Generally, the metal-to-cage peaks around 100 cm⁻¹ are almost invariant among the isomers but are much smaller than those of M@C₈₂ (M = La, Y, Ce, Gd) described above. It was proposed that the metal-to-cage vibration is sensitive toward the charge state of the encaged metal atom; the frequencies of this vibration for the trivalent metallofullerenes, M@C₈₂ (M = La, Y, Ce, Gd), are much higher than those of the divalent metallofullerenes such as Tm@C₈₂ and Eu@C₇₄ (Dunsch et al., 1998a). This is expected if the metal–cage bonding is basically electrostatic (Kobayashi and Nagase, 1998; Takata et al., 1995) and the metals bear the same charge.

A systematic Raman and IR study on di-metallofullerenes, Sc₂@C₈₄ (I, II, III), was reported by Krause et al. (1999, 2000). As in the mono-metallofullerenes they observed metal (Sc)–cage vibrations below 300 cm⁻¹. They concluded that the amount of metal-to-fullerene charge transfer and the distance between the oppositely charged centers determines the carbon cage–metal bond strength.

Inelastic neutron scattering results for La@C₈₂ and Y@C₈₂ (Lebedkin et al., 1998a,b) also presented evidence of metal-to-cage vibrations at 180, 150, and 85 cm⁻¹. The interval from 100 to 200 cm⁻¹ in the Raman and FIR spectra of M@C₈₂ (M = divalent and trivalent metal atoms) can be regarded as a “metal-fingerprint” range.

8. STM STUDIES ON METALLOFULLERENES

8.1 STM studies of metallofullerenes on clean surfaces

STM has been a powerful technique for studying structural and electronic properties of endohedral metallofullerenes. In fullerenes, the STM technique was first applied to study the morphology of C₆₀ on Au(111) (Wilson et al., 1990), highly oriented pyrolytic graphite (Wragg et al., 1990), GaAs(110) (Li et al., 1991), Si(100) (Hashizume et al., 1992), Si(111) (Wang et al., 1992), Cu(111) (Cuberes et al., 1996; Hashizume et al., 1993a) and Au(110) (Joachim et al., 1995) surfaces. In particular, UHV-STM has been proven to be a crucial technique for the study of endohedral metallofullerenes, and was reviewed extensively by Sakurai et al. (1996).

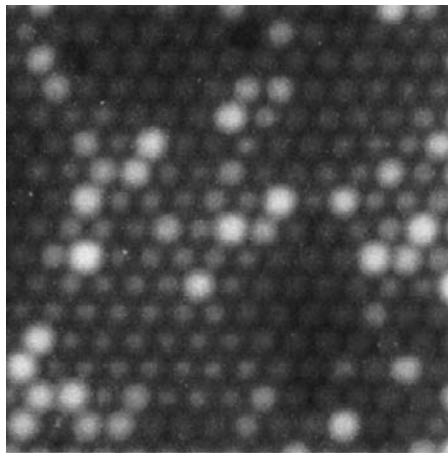


FIGURE 25 STM image of the third layer of $\text{Sc}_2\text{C}_2@C_{82}$ fullerenes on the $\text{Si}(100) 2 \times 1$ clean surface at a bias voltage of -3.0 V (tunneling current = 20 pA). The white contrasts correspond to the $\text{Sc}_2\text{C}_2@C_{82}$ fullerenes which are slightly get ahead of the other close-packed fullerenes.

Figure 25 shows a UHV-STM image of a small ($141 \text{ \AA} \times 141 \text{ \AA}$) area of the $\text{Si}(100) 2 \times 1$ surface covered with $\text{Sc}_2\text{C}_2@C_{82}$ molecules with a coverage of approximately three mono-layers at room temperature (Shinohara et al., 1993b, X Wang et al., 1993d). Pure scandium fullerenes were evaporated from a tantalum boat heated to approximately 700 °C onto the clean $\text{Si}(100) 2 \times 1$ surface in an UHV condition (5×10^{-11} Torr). The $\text{Sc}_2\text{C}_2@C_{82}$ molecules reside in the trough separated by the Si dimer rows and they are distributed randomly on the surface with a minimum separation of 11.7 \AA . The STM image of the $\text{Sc}_2\text{C}_2@C_{82}$ molecules shows small deviation (within ca 10%) from the perfectly circular shape. The first layer of $\text{Sc}_2\text{C}_2@C_{82}$ has provided only a short-range local ordering. When the first layer was completed, the second $\text{Sc}_2\text{C}_2@C_{82}$ layer began to form and island formation was observed. The second layer was still somewhat irregular. However, the $\text{Sc}_2\text{C}_2@C_{82}$ molecule overlayers (the third layer and up) grown on the second layer were well ordered and perfectly close-packed, indicating that the overlayer film was basically formed by van der Waals interaction without interference from the Si substrate, similar to the case of the C_{60} (Hashizume et al., 1992) and C_{84} (Wang et al., 1992) depositions on the $\text{Si}(100) 2 \times 1$ surface.

The STM images present strong evidence that the two scandium atoms are indeed encapsulated by the C_{84} fullerene cage: the STM images of the $\text{Sc}_2\text{C}_2@C_{82}$ molecules show no characteristic bright (or dark) spots (which may correspond to the position of scandium atoms) on and around the carbon cage, and all images are essentially the same as those of hollow C_{84}

molecules (Hashizume et al., 1993b, X Wang et al., 1993e). The two scandium atoms are trapped securely inside the C_{82} cage, which is consistent with HRTEM (Beyers et al., 1994), high-resolution ^{13}C NMR (Yamamoto et al., 1996) and synchrotron X-ray diffraction (Iiduka et al., 2006; Nishibori et al., 2006a,b; Takata et al., 1997) results.

In contrast to the STM observation on the Si(100) 2×1 surface, Gimzewski (1996) found that STM images of $Sc_2C_2@C_{82}$ on a Au(110) (Joachim et al., 1995) surface show a characteristic internal structure. The appearance of the internal structure indicates that the interaction between $Sc_2C_2@C_{82}$ and the Si and Au surfaces differ from each other and that the electronic structures near the Fermi levels might be also different.

8.2 Metallofullerenes as superatoms

A typical large-scale ($400 \text{ \AA} \times 400 \text{ \AA}$) STM image of a small amount [23 molecules ($1,000 \text{ \AA}^{-2}$)] of $Y@C_{82}$ on Cu(111) 1×1 surface at room temperature shows a preferential adsorption at the terrace edges (Figure 26) (Hasegawa et al., 1997; Shinohara et al., 1995a,b). The $Y@C_{82}$ molecules are sublimated from the tantalum boat onto the copper surface and impinge on the terrace of the surface with a kinetic energy corresponding to about $400 \text{ }^\circ\text{C}$. The $Y@C_{82}$ molecules are mobile on the surface and segregate to the terrace edges. The impinging $Y@C_{82}$ molecules migrate to the edges following adsorption since the bonding to the substrate surface is relatively weak. The C_{60} adsorption on the

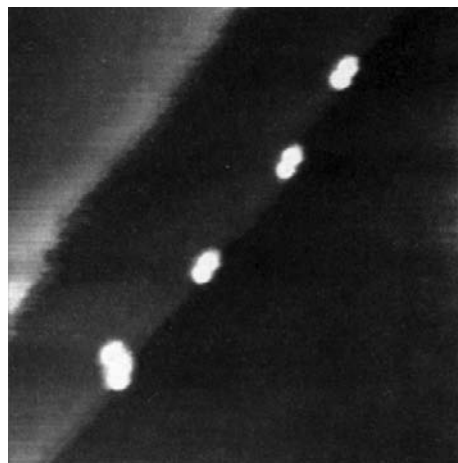


FIGURE 26 Typical large-scale ($400 \text{ \AA} \times 400 \text{ \AA}$) STM image of $(Y@C_{82})_2$ dimers adsorbed on a terrace edge of Cu(111) 1×1 clean surface.

Cu(111) 1×1 surface showed a similar mobile tendency (Hashizume et al., 1993a). This is in sharp contrast to the adsorption of fullerenes on Si(100) and Si(111) surfaces in which the fullerenes such as C_{60} (Hashizume et al., 1992), C_{70} (Wang et al., 1994) and C_{84} (X Wang et al., 1993e) do not freely migrate.

One of the most intriguing observation here is that the $Y@C_{82}$ fullerenes predominantly form clusters, $(Y@C_{82})_n$ ($n = 2-6$), and in particular dimers, $(Y@C_{82})_2$, on the Cu(111) surface even at the very initial stage of adsorption (Shinohara et al., 1995a,b). The distribution of the $(Y@C_{82})_n$ clusters has the maximum at dimers and shows that more than 60% of the $Y@C_{82}$ molecules on the Cu(111) surface exist as dimers or larger clusters (Hasegawa et al., 1997). Previous STM results on higher fullerenes indicate that, like C_{60} , the higher fullerenes, such as C_{70} and C_{84} , also exist mostly as monomers in the initial stage of deposition on the copper and silicon surfaces (X Wang et al., 1993e; Wang et al., 1994). These results indicate that the $Y@C_{82}$ metallofullerenes have a very special tendency to form dimers and larger clusters on the copper surface. The dimerization energy of $Y@C_{82}$ on the Cu(111) surface was estimated to be about 180 meV (Hasegawa et al., 1997). In addition, large dipole moments of metallofullerenes may also play a crucial role in the dimerization, since the calculated and experimental dipole moments of $La@C_{82}$ are 3–4 D (debye) (Laasonen et al., 1992; Poirier et al., 1994) and 4.4 ± 0.4 D (Fuchs and Rietschel, 1996), respectively.

As discussed in Section 6.1 hfs analysis of the ESR measurements of $Y@C_{82}$ indicates that the encaged Y atom donates three valence electrons to the C_{82} cage to form an endohedral metallofullerene of the type $Y^{3+}@C_{82}^{3-}$ (Shinohara et al., 1992a; Weaver et al., 1992). An *ab initio* theoretical calculation (Nagase and Kobayashi, 1994a,c) reveals that the charge on the encaged yttrium, i.e., $3+$, is little changed even when $Y@C_{82}$ ejects or accepts an additional electron. Namely, the $Y@C_{82}$ metallofullerene can be regarded as a positively charged core metal and a negatively charged carbon cage. Such a molecule has a great similarity to the superatom concept proposed first by Watanabe and Inoshita (1986) and Inoshita et al. (1986) in a semiconductor heterostructure composed of spherically symmetric positively charged core. Superatoms have also been discussed theoretically in relation to endohedral metallofullerenes by Rosen and Waestberg (1988, 1989), Saito (1990) and Nagase and Kobayashi (1994a,c).

The STM observation of the $Y@C_{82}$ dimers and clusters is direct experimental evidence that $Y@C_{82}$ molecules exhibit the superatom feature. The observed interfullerene distance is 11.2 Å, which is shorter than that of the simple $Y@C_{82}-Y@C_{82}$ van der Waals distance (11.4 Å), suggesting that the interfullerene interaction is not a simple dispersion type of weak interaction but a relatively strong interaction. A large dipole moment of $Y@C_{82}$ also plays an important role in the tight binding between $Y@C_{82}$

molecules, particularly in the solid state. In fact, a synchrotron X-ray diffraction study on a powder $Y@C_{82}$ sample (Takata et al., 1995) reveals the presence of such a charge-transfer-type interaction from the analysis of the total electron density distribution map of the $Y@C_{82}$ microcrystal. In an $Y@C_{82}-Y@C_{82}$ fullerene interaction, the positively charged ($Z = +3$) yttrium core on one side of $Y@C_{82}$ attracts the negatively charged ($Z = -3$) C_{82} cage of the other $Y@C_{82}$ molecule. The $Y@C_{82}-Y@C_{82}$ molecule can be viewed just like a Li-Li molecule but with much weaker interaction. The superatom character of such a metallofullerene might in future lead to novel solid state properties.

9. MAGNETISM OF METALLOFULLERENES

Magnetic properties of powder samples of $La@C_{82}$ and $Gd@C_{82}$, grown from toluene solution, have been studied by Funasaka et al. (1994, 1995). Magnetization data for a powder sample of $Gd@C_{82}$ have been obtained employing a SQUID magnetometer. The results indicate that the data fall on a curve fitted to a Brillouin function consistent with $J = 3.38$ and $g = 2$: a signature of paramagnetic behavior. They also observed that the powder sample of $La@C_{82}$ showed Curie-Weiss behavior at low temperature (<40 K), see Figure 27. The observed effective magnetic moment per

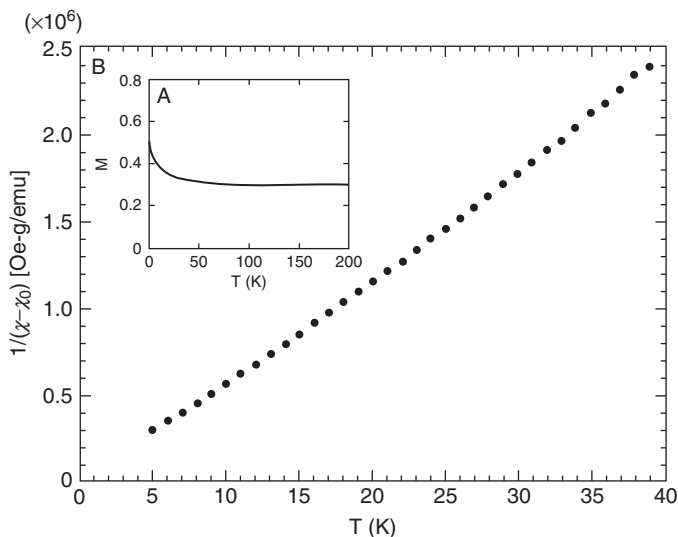


FIGURE 27 (A) Magnetization (emu/g) versus temperature for a $La@C_{82}$ powder sample containing solvent molecules, measured at an applied field of 5 T; (B) Inverse susceptibility data as a function of temperature using the data (A).

La@C₈₂ was 0.38 μ B, equivalent to 0.22 of an electron spin per fullerene molecule. This is quite different from the value of 1.0 which would be expected for $S = 1/2$ La@C₈₂. A similar magnetic property for Gd@C₈₂ has been obtained by Dunsch et al. (1988b): the susceptibility follows a Curie law and the magnetization can be described by a Brillouin function. They also reported that the two Eu fullerenes, Eu@C₇₄ and Eu@C₈₂, show the same $M(H/T)$ magnetic behavior as that of Gd@C₈₂ if all magnetization values are normalized to the saturation magnetization at high fields.

Powder samples of Y@C₈₂ exhibited localized-electron behavior both at temperatures above 200 K and temperatures below 90 K, but with different Curie–Weiss curves (Allen, 1998). The Curie–Weiss curve at low temperature corresponded to 0.29(4) electrons per fullerene similar to that of La@C₈₂, with a small Curie constant of $-2.7(8)$ K, and to 1.0(1) electrons at high temperature, with an extremely large Curie constant of 280(30) K. This single electron spin clearly agrees with the single unpaired electron which is expected, and as observed in solution ESR experiments (see Section 6.1). The high-temperature susceptibility is weakly temperature dependent, and if it arises from a metal then the density of state (DOS) is 10(1) states per molecule per electronvolt at 294 K.

The above magnetic measurements were, however, done on samples which contained solvent molecules, so magnetic behaviors of the powder samples of sublimed (thus solvent-free) pure metallofullerenes might be different. The magnetic properties on a solvent-free powder sample of La@C₈₂, which was prepared by sublimation, was reported by Watanuki et al. (1997). They performed ESR experiments on the sample between 7 and 300 K. The results indicate that the paramagnetic component is almost temperature independent above 80 K, indicating Pauli paramagnetism of the conducting electrons. Based on the observed temperature dependence of the spin susceptibility, ESR linewidth and the g -value, they concluded that solvent-free La@C₈₂ is metallic between 80 and 300 K. Magnetic measurements on solvent-free powder samples of metallofullerenes will be needed to further clarify the bulk magnetic properties of endohedral metallofullerenes.

The apparent discrepancy in the results between this ESR magnetic measurement (metallic) and the UPS studies on La@C₈₂ (insulator) (Hino et al., 1993; Poirier et al., 1994) as described in Section 6.5 might be due to sample preparation, i.e., sample purity together with the thickness of the sublimed samples. This is suggested because a more recent UPS measurement by Eberhardt and co-workers (Kessler et al., 1997) has shown DOSs at the Fermi level, suggesting a metallic behavior for La@C₈₂ consistent with the ESR result.

Cerium endohedral metallofullerene (Ce@C₈₂) can be regarded as a π - f composite nanomagnet, where anisotropic f -electron spin is expected to couple with the rotational motion of the fullerene cage that has

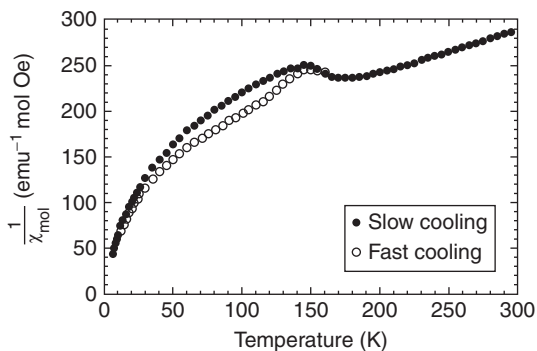


FIGURE 28 Temperature dependence of the inverse magnetic susceptibility of solvent-free Sc@C₈₂ crystal for slow and fast cooling.

π -electron spin. Inakuma et al. (2003) found that in Ce@C₈₂ crystals the crystal field effects in the metallofullerene cage is considerably reduced in contrast to that of ordinary rare-earth compounds. This is consistent with their study of a small electronic coupling between the f and π electrons, and the shallow potentials of the C₈₂ fullerene cage surrounding the Ce ion. As a consequence the crystal field effect is emphasized in the low-temperature range (below 100 K).

Ito et al., 2007a,b studied magnetic properties of solvent-free crystals of the Sc@C₈₂. They found that the crystal is a paramagnet and the magnetic susceptibility decreases below 150 K with evidence of antiferromagnetic-like interactions by slow cooling. X-ray crystal analysis shows the presence of a phase transition at 150 K, which can be attributed to an orientational ordering transition of the fullerene molecules (Figure 28).

10. M@C₆₀: A BIG MYSTERY AND A BIG CHALLENGE

It had been expected, before the first macroscopic production and extraction of La@C₈₂ (Chai et al., 1991), that metallofullerenes based on the C₆₀ cage would be the most abundant metallofullerenes that were prepared in macroscopic amounts, as was the case in empty fullerenes. This is simply because that C₆₀ is the most abundant fullerene which can be easily produced by either the arc-discharge or the laser furnace method (cf. Section 2.1). In fact, an earlier gas phase experiment on the production of carbon clusters containing La via the laser-vaporization cluster-beam technique (Heath et al., 1985) indicated that La@C₆₀ is a prominent “magic number” species among various La@C_{*n*} (44 < *n* < 80) clusters (Figure 1).

A series of gas phase ion chromatographic studies on metallofullerenes in the gas phase done by Jarrold and co-workers (Clemmer and Jarrold, 1994; Clemmer et al., 1994a,b,c; Hunter et al., 1993; Shelimov et al., 1994) have presented important clues on the stability and growth mechanism of endohedral metallofullerenes. They showed that laser vaporization of a La_2O_3 /graphite rod produces a number of LaC_{60}^+ and a variety of different isomers including the endohedral La@C^+ in which the lanthanum atom seems to be bound to polycyclic polyynes rings (Clemmer et al., 1994c) and also to be networked into the fullerene cage (Shelimov et al., 1994). Interestingly, when heated, nearly all of the different ring isomers convert spontaneously into endohedral metallofullerenes, trapping the metal atom inside the cage with high efficiency (>98%) (Clemmer et al., 1994b). Figure 29 shows a drift-time distribution recorded for LaC_{60}^+ with injection energy of 400 eV. The main peak corresponds to the endohedral La@C_{60}^+ . Based on these results it was proposed that in the first step of the thermal annealing process the La atom acts as a nucleation center and the carbon rings arrange themselves around the La atom before converting into a fullerene cage.

The extraction of the M@C_{60} -type (M = metal) metallofullerene has been difficult because all of the M@C_{60} metallofullerenes so far produced in soot have not been soluble in normal fullerene solvents such as toluene and carbon disulfide. Several M@C_{60} -type metallofullerenes have, however, been extracted by such solvents as pyridine and aniline. Ca@C_{60} has been extracted by pyridine (L Wang et al., 1993a,b) and aniline (Kubozono et al., 1995). Other M@C_{60} (M = La, Y, Ba, Ce, Pr, Nd, Gd) metallofullerenes have been similarly extracted from soot by aniline (Kubozono et al., 1996a,b). Since pyridine and aniline are not suited for HPLC solvent (eluent) for purification, purification and isolation of the M@C_{60} -type metallofullerenes has been extremely difficult. The inability to purify such metallofullerenes has prevented us from any detailed structural and electronic studies on these fullerenes. A similar unconventional stability and solubility property has been observed for Li@C_{60} which was prepared by Li^+ ion implantation onto C_{60} thin films (Campbell et al., 1997; Gromov et al., 2003; Tellmann et al., 1996a,b).

Despite these difficulties, Ogawa et al. (2000) performed the first isolation of an M@C_{60} -type metallofullerene, Er@C_{60} . The isolation was done by using a combined technique of vacuum sublimation of soot containing Er@C_{60} together with higher erbium metallofullerenes Er@C_{2n} ($70 < 2n < 120$), which was followed by a Buckyclutcher HPLC purification (see Section 3.2) with a 100% aniline eluent. Er@C_{60} may be greatly stabilized in aniline solution by forming charge transfer complexes of the type $(\text{Er@C}_{60})-(\text{aniline})_n$. A similar result was reported for Eu@C_{60} by Inoue et al. (2000).

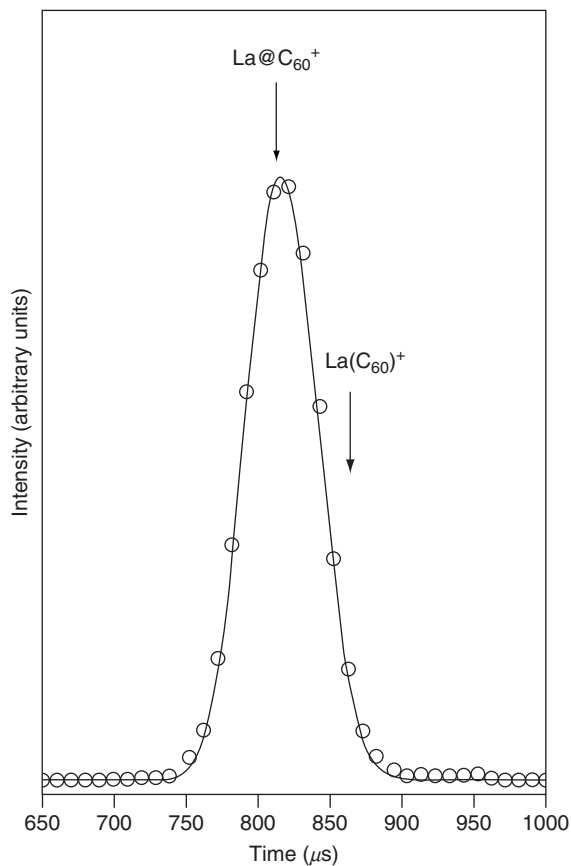


FIGURE 29 Drift-time distribution recorded for LaC_{60}^+ with injection energy of 400 eV. The curve shows the drift-time distribution calculated from the transport equation for ions in the drift tube. The arrows show the expected drift times for endohedral La@C_{60}^+ and exohedral $\text{La}(\text{C}_{60})^+$ complexes. The mobility was calculated using a simple hard-sphere collision model.

At present, it is still not known why the M@C_{60} -type metallofullerenes behave quite differently from the conventional M@C_{82} type fullerenes in terms, for example, of the solubility property. This may correlate to high reactivity of M@C_{60} toward moisture and/or air: M@C_{60} can possibly form weak complexes to stabilize themselves only with pyridine or aniline through their nonbonding electrons. Another possible rationale is that the carbon cage structures of the M@C_{60} so far produced somehow do not satisfy the IPR, which again leads to high chemical reactivity of the species. To fully understand “the M@C_{60} mystery” future studies on structural and electronic properties of these elusive metallofullerenes are definitely needed.

11. APPLICATIONS TO RADIOCHEMISTRY AND MRI CONTRAST AGENTS

Studies of endohedral metallofullerenes directed to application have been reported since the metallofullerenes are structurally and electronically much more unique than the normal empty fullerenes.

The advantages and uniqueness of radiochemical techniques in metallofullerene studies have been pointed out by the Tokyo Metropolitan group (Kikuchi et al., 1994c; Kobayashi et al., 1995a,b; Ohtsuki et al., 1996a; Sueki et al., 1997) and Cagle et al. (1996). The HPLC behavior of metallofullerenes of 14 lanthanide elements was studied with the use of radiotracers (Sueki et al., 1997). From the radiochromatographic HPLC elution behavior, the 14 lanthanide elements forming metallofullerenes were found to be grouped into two, i.e., Sm, Eu, Tm, and Yb as one group and the rest of the elements as another. The former elements have 2+ charge state in the C₈₂ cage, whereas the latter elements have 3+ charge state (see Section 6.4). Radioactive endohedral ⁷Be@C₆₀ can also be detected using radiochemical and radiochromatographic techniques in solvents (Ohtsuki et al., 1996b).

The distribution of metallofullerenes among organs when they are administered to an animal can be best studied by radioisotopically labeled fullerenes. The HPLC fractions of ¹⁴⁰La-labeled La@C₈₂ and La₂@C₈₀ were made into emulsion and injected into the hearts of rats. The rats were dissected after 24 h and the radioactivity remaining in each organ was determined by γ -ray spectrometry. Large portions of La-fullerenes were found in the liver and blood (Kobayashi et al., 1995a,b). Although the physiological meaning of the results is not clear at present, it certainly suggests possible biological applications of metallofullerene chemistry.

Kikuchi et al. (1994c) showed that the endohedral form of metallofullerenes was not affected by the recoil energy of the metal atom resulting from the emission of electrons in the β -decay in which nuclear reaction and decay processes are related to ¹⁵⁹Ga@C₈₂, ¹⁶¹Tb@C₈₂, and ¹⁵³Gd@C₈₂. Successful encapsulation of radioactive atoms inside the fullerene cage will widen the potential use of metallofullerenes not only in materials science and technology but in biological and even medical science.

Akiyama et al. (2001) synthesized and isolated some light actinide metallofullerenes such as U@C₈₂, Np@C₈₂, and Am@C₈₂ and found the valency of U atom in C₈₂ cage is 3+, showing almost exactly the same UV-Vis-NIR absorption spectrum as that of the trivalent lanthanide C₈₂ metallofullerenes such as La@C₈₂ and Gd@C₈₂.

Shinohara et al. (1996b), Cagle et al. (1997), Mikawa et al. (2001) and Kato et al. (2003) have evaluated the use of an endohedral metallofullerene as a magnetic resonance imaging (MRI) contrast agent. MRI is one of

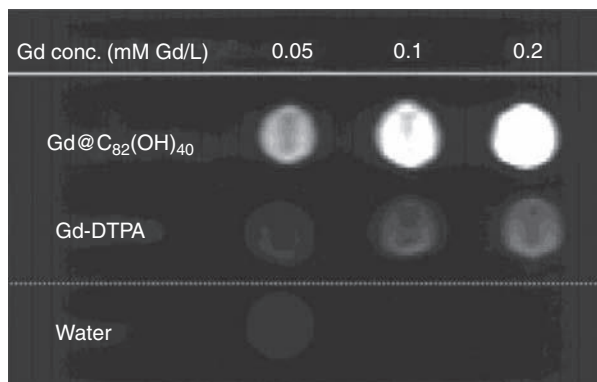


FIGURE 30 T_1 -weighted MRI of Gd@C₈₂(OH)₄₀ and Gd-DTPA phantom at the concentration of 0.05, 0.1, and 0.2 mmol Gd/L, respectively. Extremely strong signals of Gd@C₈₂(OH)₄₀ are seen at the Gd concentration of 0.05 mM, whereas Gd-DTPA of the same concentration shows only a slight enhancement of MRI signals as compared with pure water.

the most common medical techniques for the diagnostic examination of human patients (Lauffer, 1987). The commercially available MRI contrast agents usually employ Gd³⁺ ($S = 7/2$) to enhance the relaxation rate of water protons. Purified Gd@C₈₂ fullerene was organic functionalized to obtain a water-soluble property and was then evaluated for use as an MRI contrast agent in terms of relaxivity measurements. Cagle et al. (1997) reported relatively low relaxivity at 20 MHz as compared with other conventional Gd-containing MRI contrast agents. However, recent measurements on a purified (99.9% up) Gd@C₈₂(OH)_{*n*} by Mikawa et al. (2001) gave high R_1 relaxivity (81 L mmol⁻¹ s⁻¹ at pH = 7.5) which is more than 20 times greater than commercial Gd-MRI contrast agents such as Gd-DTPA (4.3 L mmol⁻¹ s⁻¹) (Figure 30). This is encouraging for the prospects of future use of this water-soluble Gd-metallofullerene.

12. CONCLUSIONS AND FUTURE PROSPECTS

Lanthanide metallofullerenes are novel forms of fullerene-related materials which were first obtained in their purified form in January 1993 (Shinohara et al., 1993a). Since then, as detailed in this paper, numerous investigations into various aspects of metallofullerenes have been intensively carried out by various research groups. These studies have revealed unique structural and novel electronic properties of the metallofullerenes.

Even so, there still remain many potentially important and intriguing problems which should be clarified in the not too distant future.

For instance, the solid state properties such as electric conductivity and magnetic behavior are not well known apart from for a few metallofullerenes. Only a limited number of such studies have been reported. Organic functionalizations of the metallofullerenes (Akasaka et al., 1995a,b,c; Kato et al., 1996; Suzuki et al., 1995c) will be an important direction for the synthesis of further novel materials based on endohedral metallofullerenes because, as Akasaka et al. (1995a,b,c) have found, metallofullerenes are generally more reactive, either thermally or photochemically, than the corresponding empty fullerenes, due to the small HOMO–LUMO gaps.

Metallofullerenes will also become an important nanostructured material for future nanoscale electronic devices, because the band gaps of endohedral metallofullerenes, for example, can be varied between 1.0 and 0.2 eV depending on the fullerene size, the kind of metal atom(s) as well as the number of metal atoms encapsulated.

Since the amount of metallofullerenes so far produced and isolated has been small, studies on the solid state properties of metallofullerenes have been limited. However, scaling-up of production and isolation of metallofullerenes is possible by using a large-scale arc discharge system as well as by using a preparative HPLC system with a large column (30 mm diameter \times 250 mm length). With this system, up to 100 mg of purified metallofullerenes might be obtained in a week or so.

As described in the preceding section, physiological and medical applications of the endohedral metallofullerenes will become extremely important in relation to tracer chemistry in biological systems, and await further studies. In any case, the endohedral metallofullerenes will continue to tantalize physicists, chemists and materials scientists for years to come.

ACKNOWLEDGMENTS

The authors are indebted to my collaborators C-R Wang (Chinese Academy of Science, Beijing), T.J.S. Dennis (London University), N. Tagmatarchis (National Hellenic Institute, Athens), B-Y Sun (Chinese Academy of Science, Beijing), T. Sugai (Toho University), T. Okazaki (AIST) and R. Kitaura (Nagoya University). The present study was partially supported by a JST CREST (Japan Science and Technology Agency, Core Research for Evolutional Science and Technology) program on “Novel Carbon Nano-materials.”

REFERENCES

- Abrefah, J., Olander, D.R., Balooch, M., Siekhaus, W.J., 1992. *Appl. Phys. Lett.* 60, 1313.
Adachi, G., Imanaka, N., Fuzhong, Z., 1991. In: Gschneidner Jr., K.A., Eyring, L. (Eds.), *Handbook on the Physics and Chemistry of Rare Earths*, vol 15. Elsevier, Amsterdam, pp. 61–189.
Ajie, H., et al., 1990. *J. Phys. Chem.* 94, 8630.

- Akasaka, T., Kato, T., Kobayashi, K., Nagase, S., Yamamoto, K., Funasaka, H., Takahashi, T., 1995a. *Nature* 374, 600.
- Akasaka, T., Nagase, S., Kobayashi, K., Suzuki, T., Kato, T., Kikuchi, K., Achiba, Y., Yamamoto, K., Funasaka, H., Takahashi, T., 1995b. *Angew. Chem. Int. Ed. Engl.* 34, 2139.
- Akasaka, T., Nagase, S., Kobayashi, K., Suzuki, T., Kato, T., Yamamoto, K., Funasaka, H., Takahashi, T., 1995c. *J. Chem. Soc. Chem. Commun.* 1343.
- Akasaka, T., Nagase, S., Kobayashi, K., Waelchli, M., Yamamoto, K., Funasaka, H., Kako, M., Hoshino, T., Erata, T., 1997. *Angew. Chem. Int. Ed. Engl.* 36, 1643.
- Akiyama, K., et al., 2001. *J. Am. Chem. Soc.* 123, 181.
- Allemand, P.M., Srdanov, G., Koch, A., Khemani, K., Wudl, F., Rubin, Y., Diederich, F., Alvarez, M.M., Anz, S.J., Whetten, R.L., 1991. *J. Am. Chem. Soc.* 113, 2780.
- Allen, K., 1998. PhD Thesis. Oxford University.
- Alvarez, M.M., Gillan, E.G., Holczer, K., Kaner, R.B., Min, K.S., Whetten, R.L., 1991. *J. Phys. Chem.* 95 (10), 561.
- Anderson, M.R., Dorn, H.C., Burbank, P.M., Gibson, J.R., 1997a. In: Kadish, K., Ruoff, R. (Eds.), *Fullerenes: Recent Advances in the Chemistry and Physics of Fullerenes and Related Materials*, vol 4. Electrochemical Society, Pennington, pp. 448–456.
- Anderson, M.R., Dorn, H.C., Stevenson, S., Burbank, P.M., Gibson, J.R., 1997b. *J. Am. Chem. Soc.* 119, 437.
- Andreoni, W., Curioni, A., 1996a. *Phys. Rev. Lett.* 77, 834.
- Andreoni, W., Curioni, A., 1996b. In: Andreoni, W. (Ed.), *The Chemical Physics of Fullerenes 10 (and 5) Years Later*. Kluwer, Dordrecht, pp. 183–196.
- Andreoni, W., Curioni, A., 1997. In: Kadish, K., Ruoff, R. (Eds.), *Fullerenes: Recent Advances in the Chemistry and Physics of Fullerenes and Related Materials*, vol 4. Electrochemical Society, Pennington, pp. 516–522.
- Andreoni, W., Curioni, A., 1998. *Appl. Phys. A* 66, 299.
- Averitt, R.D., Alford, J.M., Halas, N.J., 1994. *Appl. Phys. Lett.* 65, 374.
- Bandow, S., Kitagawa, H., Mitani, T., Inokuchi, H., Saito, Y., Yamaguchi, H., Hayashi, N., Sato, H., Shinohara, H., 1992. *J. Phys. Chem.* 96, 9609.
- Bandow, S., Shinohara, H., Saito, Y., Ohkohchi, M., Ando, Y., 1993. *J. Phys. Chem.* 97, 6101.
- Bartl, A., Dunsch, L., Froehner, J., Kirbach, U., 1994. *Chem. Phys. Lett.* 229, 115.
- Bartl, A., Dunsch, L., Kirbach, U., 1995a. *Solid State Commun.* 94, 827.
- Bartl, A., Dunsch, L., Kirbach, U., Schandert, B., 1995b. *Synth. Met.* 70, 1365.
- Bartl, A., Dunsch, L., Kirbach, U., 1996. *Appl. Magn. Reson.* 11, 301.
- Bartl, A., Dunsch, L., Kirbach, U., Seifert, G., 1997. *Synth. Met.* 86, 2395.
- Beck, R.D., Weis, P., Rockenberger, J., Kappes, M.M., 1996a. *Surf. Sci. Lett.* 3, 771.
- Beck, R.D., Weis, P., Rockenberger, J., Michel, R., Fuchs, D., Benz, M., Kappes, M.M., 1996b. *Surf. Sci. Lett.* 3, 881.
- Bethune, D.S., Johnson, R.D., Salem, J.R., de Vries, M.S., Yannoni, C.S., 1993. *Nature* 366, 123.
- Bethune, D.S., et al., 1994. *Materials Research Society Fall Meeting Abstract* 255.
- Bethune, D.S., et al., 1996. In: Andreoni, W. (Ed.), *The Chemical Physics of Fullerenes 10 (and 5) Years Later*. Kluwer, Dordrecht, pp. 165–181.
- Beyers, R., et al., 1994. *Nature* 370, 196.
- Bricogne, G., 1988. *Acta Crystallogr. A* 44, 517.
- Buerk, M., Schmidt, M., Cummins, T.R., Nuecker, N., Ambruster, J.F., Schuppler, S., Fuchs, D., Adelman, P., Michel, R.H., Kappes, M.M., 1996. In: Kuzmany, H., Fink, J., Mehring, M., Roth, S. (Eds.), *Fullerenes and Fullerene Nanostructures*. World Scientific, London, pp. 196–199.
- Cagle, D.W., Thrash, T.P., Wilson, L.J., Ehrhardt, G.J., Alford, J., Chibante, L.P.F., 1996. In: Kadish, K., Ruoff, R. (Eds.), *Fullerenes: Recent Advances in the Chemistry and Physics of Fullerenes and Related Materials*, vol 3. Electrochemical Society, Pennington, pp. 854–868.

- Cagle, D.W., Alford, J.M., Tien, J., Wilson, L.J., 1997. In: Kadish, K., Ruoff, R. (Eds.), *Fullerenes: Recent Advances in the Chemistry and Physics of Fullerenes and Related Materials*, vol 4. Electrochemical Society, Pennington, pp. 361–368.
- Campbell, E.E.B., Tellgmann, R., Krawez, N., Hertel, I.V., 1997. *J. Phys. Chem. Solids* 58, 1763.
- Cao, B.P., et al., 2001. *J. Am. Chem. Soc.* 123, 9679.
- Cao, B.P., Suenaga, K., Okazaki, T., Shinohara, H., 2002. *J. Phys. Chem. B* 106, 9295.
- Chai, Y., Guo, T., Jin, C., Haufler, R.E., Chibante, L.P.F., Fure, J., Wang, L., Alford, J.M., Smalley, R.E., 1991. *J. Phys. Chem.* 95, 7564.
- Chang, A.H.H., Ermler, W.C., Pitzer, R.M., 1991. *J. Chem. Phys.* 94, 5004.
- Cioslowski, J., Fleishmann, E.D., 1991. *J. Chem. Phys.* 94, 3730.
- Clemmer, D.E., Jarrold, M.F., 1994. *J. Am. Chem. Soc.* 117, 8841.
- Clemmer, D.E., Hunter, J.M., Shelimov, K.B., Jarrold, M.F., 1994a. *Nature* 372, 248.
- Clemmer, D.E., Shelimov, K.B., Jarrold, M.F., 1994b. *Nature* 367, 718.
- Clemmer, D.E., Shelimov, K.B., Jarrold, M.F., 1994c. *J. Am. Chem. Soc.* 116, 5971.
- Collins, D.M., 1982. *Nature* 298, 49.
- Cox, D.M., et al., 1991. *J. Am. Chem. Soc.* 113, 2940.
- Cuberes, M.T., Schlittler, R.R., Gimzewski, J.K., 1996. *Appl. Phys. Lett.* 69, 3016.
- Curl, R.F., Smalley, R.E., 1991. *Sci. Am.* 265, 54.
- Dennis, T.J.S., Shinohara, H., 1997a. *Chem. Phys. Lett.* 278, 107.
- Dennis, T.J.S., Shinohara, H., 1997b. In: Kadish, K., Ruoff, R. (Eds.), *Fullerenes: Recent Advances in the Chemistry and Physics of Fullerenes and Related Materials*, vol 4. Electrochemical Society, Pennington, pp. 182–190.
- Dennis, T.J.S., Shinohara, H., 1998. *Appl. Phys. A* 66, 243.
- Dennis, T.J.S., Kai, T., Tomiyama, T., Shinohara, H., 1998. *J. Chem. Soc. Chem. Commun.* 619.
- Diener, M.D., Smith, C.A., Veirs, D.K., 1997. *Chem. Mater.* 9, 1773.
- Ding, J., Yang, S., 1996. *J. Am. Chem. Soc.* 118 (11), 254.
- Ding, J., Yang, S., 1997. *J. Phys. Chem. Solids* 11, 1661.
- Ding, J., Lin, N., Weng, L., Cue, N., Yang, S., 1996a. *Chem. Phys. Lett.* 261, 92.
- Ding, J., Weng, L., Yang, S., 1996b. *J. Phys. Chem.* 100 (11), 120.
- Ding, X., Alford, J.M., Wright, J.C., 1997. *Chem. Phys. Lett.* 269, 72.
- Dorn, H.C., et al., 1995. In: Bernier, P. et al., (Ed.), *Science and Technology of Fullerenes*. Materials Research Society, Pittsburgh, pp. 123–135.
- Dunsch, L., Bartl, A., Kirbach, U., Froehner, J., 1995. In: Kadish, K., Ruoff, R. (Eds.), *Fullerenes: Recent Advances in the Chemistry and Physics of Fullerenes and Related Materials*, vol 2. Electrochemical Society, Pennington, pp. 182–190.
- Dunsch, L., Kuran, P., Kirbach, U., Scheller, D., 1997. In: Kadish, K., Ruoff, R. (Eds.), *Fullerenes: Recent Advances in the Chemistry and Physics of Fullerenes and Related Materials*, vol 4. Electrochemical Society, Pennington, pp. 523–536.
- Dunsch, L., Kuran, P., Krause, M., 1998a. In: Kadish, K., Ruoff, R. (Eds.), *Fullerenes: Recent Advances in the Chemistry and Physics of Fullerenes and Related Materials*, vol 6. Electrochemical Society, Pennington, pp. 1031–1038.
- Dunsch, L., Eckert, D., Froehner, J., Bartl, A., Kuran, P., Wolf, M., Mueller, K.H., 1998b. In: Kadish, K., Ruoff, R. (Eds.), *Fullerenes: Recent Advances in the Chemistry and Physics of Fullerenes and Related Materials*, vol 6. Electrochemical Society, Pennington, pp. 955–966.
- Fowler, P.W., Manolopoulos, D.E., 1995. *An Atlas of Fullerenes*. Clarendon, Oxford.
- Fuchs, D., Rietschel, H., 1996. In: Kuzmany, H., Fink, J., Mehring, M., Roth, S. (Eds.), *Fullerenes and Fullerene Nanostructures*. World Scientific, London, pp. 186–190.
- Funasaka, H., Sakurai, K., Oda, Y., Yamamoto, K., Takahashi, T., 1994. *Chem. Phys. Lett.* 232, 273.
- Funasaka, H., Sugiyama, K., Yamamoto, K., Takahashi, T., 1995. *J. Phys. Chem.* 99, 1826.

- Gillan, E., Yeretian, C., Min, K.S., Alvarez, M.M., Whetten, R.L., Kaner, R.B., 1992. *J. Phys. Chem.* 96, 6869.
- Gimzewski, J.K., 1996. In: Andreoni, W. (Ed.), *The Chemical Physics of Fullerenes 10 (and 5) Years Later*, vol 316. Kluwer, Dordrecht, pp. 117–136.
- Godly, E.W., Taylor, R., 1997. *Pure Appl. Chem.* 69, 1411.
- Gromov, A., Ostrovskii, D., Lassesson, A., Jonsson, M., Campbell, E.E.B., 2003. *J. Phys. Chem. B* 107, 11290.
- Guo, T., Diener, M.D., Chai, Y., Alford, M.J., Haufler, R.E., McClure, S.M., Ohno, T., Weaver, J.H., Scuseria, G.E., Smalley, R.E., 1992. *Science* 257, 1661.
- Guo, T., Odom, G.K., Scuseria, G.E., 1994. *J. Phys. Chem.* 98, 7745.
- Hasegawa, Y., Ling, Y., Yamazaki, S., Hashizume, T., Shinohara, H., Sakai, A., Pickering, H. W., Sakurai, T., 1997. *Phys. Rev. B* 56, 6470.
- Hashizume, T., Wang, X.D., Nishina, Y., Shinohara, H., Saito, Y., Kuk, Y., Sakurai, T., 1992. *Japan J. Appl. Phys.* 31, L880.
- Hashizume, T., et al., 1993a. *Phys. Rev. Lett.* 71, 2959.
- Hashizume, T., Wang, X.D., Nishina, Y., Shinohara, H., Saito, Y., Sakurai, T., 1993b. *Japan J. Appl. Phys.* 32, L132.
- Haufler, R.E., Conceicao, J., Chibante, L.P.F., Chai, Y., Byrne, N.E., Flanagan, S., Haley, M.M., O'Brien, S.C., Pan, C., Xiao, Z., Billups, W.E., Ciufolini, M.A., Hauge, R.H., Margrave, J.L., Wilson, L.J., Curl, R.F., Smalley, R.E., 1990. *J. Phys. Chem.* 94, 8634.
- Haufler, R.E., Chai, Y., Chibante, L.P.F., Conceicao, J., Jin, C., Wang, L.S., Maruyama, S., Smalley, R.E., 1991. In: *Averback, R.S., Bernhoc, J., Nelson, D.L. (Eds.), Cluster-Assembled Materials*, vol 206. Materials Research Society, Pittsburgh, pp. 627–637.
- Heath, J., O'Brien, S.C., Zhang, Q., Liu, Y., Curl, R.F., Kroto, H.W., Tittel, F.K., Smalley, R.E., 1985. *J. Am. Chem. Soc.* 107, 7779.
- Henrich, F.H., Michel, R.H., Fisher, A., Richard-Schneider, S., Gilb, S., Kappes, M.M., Fuchs, D., Buerk, M., Kobayashi, K., Nagase, S., 1996. *Angew. Chem. Int. Ed. Engl.* 35, 1732.
- Hino, S., Takahashi, H., Iwasaki, K., Matsumoto, K., Miyazaki, T., Hasegawa, S., Kikuchi, K., Achiba, Y., 1993. *Phys. Rev. Lett.* 71, 4261.
- Hino, S., Umishita, K., Iwasaki, K., Miyazaki, T., Miyamae, T., Kikuchi, K., Achiba, Y., 1997. *Chem. Phys. Lett.* 281, 115.
- Hino, S., Umishita, K., Iwasaki, K., Miyamae, T., Inakuma, M., Shinohara, H., 1998. *Chem. Phys. Lett.* 300, 145.
- Hino, S., Umishita, K., Iwasaki, K., Miyamae, T., Inakuma, M., Shinohara, H., 1999. *Chem. Phys. Lett.* 300, 145–151.
- Hino, S., Umishita, K., Iwasaki, K., Aoki, M., Kobayashi, K., Nagase, S., Dennis, T.J.S., Nakane, T., Shinohara, H., 2001. *Chem. Phys. Lett.* 337, 65.
- Hirata, T., Hatakeyama, R., Mieno, T., Sato, N., 1996. *J. Vac. Sci. Technol. A* 14, 615.
- Hoffman, K.R., Norris, B.J., Merle, R.B., 1997. In: *Kadish, K., Ruoff, R. (Eds.), Fullerenes: Recent Advances in the Chemistry and Physics of Fullerenes and Related Materials*, vol 4. Electrochemical Society, Pennington, pp. 475–484.
- Hoinkis, M., Yannoni, C.S., Bethune, D.S., Salem, J.R., Johnson, R.D., Crowder, M.S., de Vries, M.S., 1992. *Chem. Phys. Lett.* 198, 461.
- Huang, Y., Freiser, B.S., 1991. *J. Am. Chem. Soc.* 113, 9418.
- Huang, H., Yang, S., 1988. *J. Phys. Chem.* 102 (10), 196.
- Hulman, M., Pichler, T., Kuzmany, H., Zerbetto, F., Yamamoto, E., Shinohara, H., 1997. *J. Mol. Struct.* 408–409, 359.
- Hunter, J., Fye, J., Jarrold, M.F., 1993. *Science* 260, 784.
- Iiduka, Y., Wakahara, T., Nakahodo, T., Tsuchiya, T., Sakuraba, A., Maeda, Y., Akasaka, T., Yoza, K., Horn, E., Kato, T., Liu, M.T., Mizorogi, N., Kobayashi, K., Nagase, S., 2005. *J. Am. Chem. Soc.* 127, 12500.
- Iiduka, Y., Wakahara, T., Nakajima, K., Tsuchiya, T., Nakahodo, T., Maeda, Y., Akasaka, T., Mizorogi, N., Nagase, S., 2006. *Chem. Commun.* 2057.

- Inakuma, M., Shinohara, H., 2000. *J. Phys. Chem.* 104, 7595.
- Inakuma, M., Ohno, M., Shinohara, H., 1995. In: Kadish, K., Ruoff, R. (Eds.), *Fullerenes: Recent Advances in the Chemistry and Physics of Fullerenes and Related Materials*, vol 2. Electrochemical Society, Pennington, pp. 330–342.
- Inakuma, M., Kato, H., Taninaka, A., Shinohara, H., Enoki, T., 2003. *J. Phys. Chem. B* 107, 6965.
- Inoshita, T., Ohnishi, S., Oshiyama, A., 1986. *Phys. Rev. Lett.* 57, 2560.
- Inoue, T., et al., 2000. *Chem. Phys. Lett.* 316, 381.
- Inoue, T., Tomiyama, T., Sugai, T., Shinohara, H., 2003. *Chem. Phys. Lett.* 382, 226.
- Inoue, T., Tomiyama, T., Sugai, T., Okazaki, T., Suematsu, T., Fujii, N., Utsumi, H., Nojima, K., Shinohara, H., 2004. *J. Phys. Chem. B* 108, 7573.
- Ito, Y., Fujita, W., Okazaki, T., Sugai, T., Awaga, K., Nishibori, E., Takata, M., Sakata, M., Shiohara, H., 2007a. *Chem. Phys. Chem.* 8, 1019.
- Ito, Y., Okazaki, T., Okuba, S., Akachi, M., Ohno, Y., Mizutani, T., Nakamura, T., Kitaura, R., Sugai, T., Shinohara, H., 2007b. *ACS Nano* 1, 456.
- Jinno, K., Saito, Y., 1996. *Adv. Chromatogr.* 36, 65.
- Joachim, C., Gimzewski, J.K., Schlittler, R.R., Chavy, C., 1995. *Phys. Rev. Lett.* 74, 2102.
- Johnson, R.D., de Vries, M.S., Salem, J., Bethune, D.S., Yannoni, C.S., 1992. *Nature* 355, 239.
- Kato, T., Suzuki, S., Kichuchi, K., Achiba, Y., 1993. *J. Phys. Chem.* 97 (13), 425.
- Kato, T., Bandow, S., Inakuma, M., Shinohara, H., Hayashi, N., Saito, Y., 1994. In: Kadish, K., Ruoff, R. (Eds.), *Fullerenes: Recent Advances in the Chemistry and Physics of Fullerenes and Related Materials*, vol 1. Electrochemical Society, Pennington, pp. 1361–1381.
- Kato, T., Bandow, S., Inakuma, M., Shinohara, H., 1995a. *J. Phys. Chem.* 99, 856.
- Kato, T., Suzuki, T., Yamamoto, K., Funasaka, H., Takahashi, T., 1995b. In: Kadish, K., Ruoff, R. (Eds.), *Fullerenes: Recent Advances in the Chemistry and Physics of Fullerenes and Related Materials*, vol 2. Electrochemical Society, Pennington, pp. 733–739.
- Kato, T., Akasaka, T., Kobayashi, K., Nagase, S., Yamamoto, K., Funasaka, H., Takahashi, T., 1996. *Appl. Magn. Reson.* 11, 293.
- Kato, H., Kanazawa, Y., Okumura, M., Taninaka, A., Yokawa, T., Shinohara, H., 2003. *J. Am. Chem. Soc.* 125, 4391.
- Kawata, H., Fujii, Y., Nakao, H., Murakami, Y., Watanuki, T., Suematsu, H., Kikuchi, K., Achiba, Y., Ikemoto, I., 1995. *Phys. Rev. B* 51, 8723.
- Kessler, B., Bringer, A., Cramm, S., Schlebusch, E., Wberhardt, W., Suzuki, S., Achiba, Y., Esch, F., Barnaba, M., Cocco, D., 1997. *Phys. Rev. Lett.* 79, 2289.
- Khemani, K.C., Prato, M., Wudl, F., 1992. *J. Organ. Chem.* 57, 3254.
- Kikuchi, K., et al., 1991. *Chem. Lett.* 1607.
- Kikuchi, K., et al., 1992. *Chem. Phys. Lett.* 188, 177.
- Kikuchi, K., Suzuki, S., Nakao, Y., Nakahara, N., Wakabayashi, T., Shiromaru, H., Saito, I., Ikemoto, I., Achiba, Y., 1993. *Chem. Phys. Lett.* 216, 67.
- Kikuchi, K., Nakao, Y., Achiba, Y., Nomura, M., 1994a. In: Kadish, K., Ruoff, R. (Eds.), *Fullerenes: Recent Advances in the Chemistry and Physics of Fullerenes and Related Materials*, vol 1. Electrochemical Society, Pennington, pp. 1300–1308.
- Kikuchi, K., Nakao, Y., Suzuki, S., Achiba, Y., Suzuki, T., Maruyama, Y., 1994b. *J. Am. Chem. Soc.* 116, 9367.
- Kikuchi, K., Kobayashi, K., Sueki, K., Suzuki, S., Nakahara, H., Achiba, Y., 1994c. *J. Am. Chem. Soc.* 116, 9775.
- Kikuchi, K., Sueki, K., Akiyama, K., Komada, T., Nakahara, H., Ikemoto, I., Akasaka, T., 1997. In: Kadish, K., Ruoff, R. (Eds.), *Fullerenes: Recent Advances in the Chemistry and Physics of Fullerenes and Related Materials*, vol 4. Electrochemical Society, Pennington, pp. 408–416.
- Kimura, T., Sugai, T., Shinohara, H., 1999a. *Chem. Phys. Lett.* 304, 211.
- Kimura, T., Sugai, T., Shinohara, H., 1999b. *J. Chem. Phys.* 110, 9681.

- Kirbach, U., Dunsch, L., 1996. *Angew. Chem. Int. Ed. Engl.* 35, 2380.
- Klute, R.C., Dorn, H.C., Mc Nair, H.M., 1992. *J. Chromatogr. Sci.* 30, 438.
- Knapp, C., Dinse, K.-P., Pietzak, B., Waiblinger, M., Weidinger, A., 1997. *Chem. Phys. Lett.* 272, 433.
- Knapp, C., Weiden, N., Dinse, K.P., 1998. *Appl. Phys. A* 66, 249.
- Knorr, S., Grupp, A., Mehring, M., Kirbach, U., Bartl, A., Dunsch, L., 1998. *Appl. Phys. A* 66, 257.
- Kobayashi, K., Nagase, S., 1998. *Chem. Phys. Lett.* 282, 325.
- Kobayashi, K., Nagase, S., Akasaka, T., 1995a. *Chem. Phys. Lett.* 245, 230.
- Kobayashi, K., Kuwano, Sueki, K., Kikuchi, K., Achiba, Y., Nakahara, H., Ni, Kananish, Watanabe, M., Tomura, K., 1995b. *J. Radio Anal. Nucl. Chem.* 192, 81.
- Kraetschmer, W., Fostiropoulos, K., Huffman, D.R., 1990a. *Chem. Phys. Lett.* 170, 167.
- Kraetschmer, W., Fostiropoulos, K., Lamb, L.D., Huffman, D.R., 1990b. *Nature* 347, 354.
- Krause, M., Hulman, M., Kuzmany, H., Dennis, T.J.S., Inakuma, M., Shinohara, H., 1999. *J. Chem. Phys.* 111, 7976.
- Krause, M., Hulman, M., Kuzmany, H., Kuran, P., Dunsch, L., Dennis, T.J.S., Inakuma, M., Shinohara, H., 2000. *J. Mol. Struct.* 521, 325.
- Krause, M., Hulman, M., Kuzmany, H., Dubay, O., Kresse, G., Vietze, K., Seifert, G., Wang, C., Shinohara, H., 2004. *Phys. Rev. Lett.* 93, 137403-1.
- Krawez, N., Tellgmann, R., Gromov, A., Kraetschmer, W., Campbell, E.E.B., 1998. In: Kuzmany, H., Fink, J., Mehring, M., Roth, S. (Eds.), *Molecular Nanostructures*. World Scientific, London, pp. 184–188.
- Kroto, H., 1987. *Nature* 329, 529.
- Kroto, H., Heath, J.R., O'Brien, S.C., Curl, R.F., Smalley, R.F., 1985. *Nature* 318, 162.
- Krusic, P.J., Wasserman, E., Parkinson, B.A., Malone, B., Holler, E.R., 1991. *J. Am. Chem. Soc.* 113, 6274.
- Kubozono, Y., Ohta, T., Hayashibara, T., Maeda, H., Ishida, H., Kashino, S., Oshima, K., Yamazaki, H., Ukita, S., Sogabe, T., 1995. *Chem. Lett.* 457.
- Kubozono, Y., et al., 1996a. *Chem. Lett.* 1061.
- Kubozono, Y., Maeda, H., Takabayashi, Y., Hiraoka, K., Nakai, T., Kashino, S., Emura, S., Ukita, S., Sogabe, T., 1996b. *J. Am. Chem. Soc.* 118, 6998.
- Kumazawa, S., Kubota, Y., Tanaka, M., Sakata, M., Ishibashi, Y., 1993. *J. Appl. Crystallogr.* 26, 453.
- Kuroki, K., Kuriyama, T., Inakuma, M., Shinohara, H., 1999. (unpublished results).
- Laasonen, K., Andreoni, W., Parrinello, M., 1992. *Science* 258, 1916.
- Lauffer, R.B., 1987. *Chem. Rev.* 87, 901.
- Lebedkin, S., Renker, B., Heid, R., Rietschel, H., Schober, H., 1998a. In: Kuzmany, H., Fink, J., Mehring, M., Roth, S. (Eds.), *Molecular Nanostructures*. World Scientific, London, pp. 203–206.
- Lebedkin, S., Renker, B., Heid, R., Schober, H., Rietschel, H., 1998b. *Appl. Phys. A* 66, 273.
- Li, Y.Z., Patrin, J.P., Chander, M., Weaver, J.W., Chibante, L.P.F., Smalley, R.E., 1991. *Science* 252, 547.
- Lorents, D.C., Yu, D.H., Brink, C., Jensen, N., Hvelplund, P., 1995. *Chem. Phys. Lett.* 236, 141.
- Macfarlane, R.M., Wittmann, G., van Loosdrecht, P.H.M., de Vries, M.S., Bethune, D.S., Stevenson, S., Dorn, H.C., 1997. *Phys. Rev. Lett.* 79, 1397.
- Manolopoulos, D.E., Fowler, P.W., 1991. *Chem. Phys. Lett.* 187, 1.
- Manolopoulos, D.E., Fowler, P.W., 1992. *J. Chem. Soc. Faraday Trans.* 88, 1225.
- Mausser, H., van Hommes, E., Clark, T., Hirsch, A., Pietzak, B., Weidinger, A., Dunsch, L., 1997. *Angew. Chem. Int. Ed. Engl.* 36, 2835.
- McElvany, S.W., 1992. *J. Phys. Chem.* 96, 4935.
- Meier, M.S., Selegue, J.P., 1992. *J. Organ. Chem.* 57, 1924.
- Mieno, T., 1998. *Japan J. Appl. Phys.* 37, L761.

- Mikawa, M., Kato, H., Okumura, M., Narazaki, M., Kanazawa, Y., Miwa, N., Shinohara, H., 2001. *Bioconj. Chem.* 12, 510.
- Miyake, Y., Suzuki, S., Kojima, Y., Kikuchi, K., Kobayashi, K., Nagase, S., Kainosho, M., Achiba, Y., Maniwa, Y., Fisher, K., 1996. *J. Phys. Chem.* 100, 9579.
- Moro, L., Ruoff, R.S., Becker, C.H., Lorents, D.C., Malhotra, R., 1993. *J. Phys. Chem.* 97, 6801.
- Murphy, T.A., Pawlik, T., Weidinger, A., Hoehne, M., Alcalá, R., Spaeth, J.M., 1996. *Phys. Rev. Lett.* 77, 1075.
- Nagase, S., Kobayashi, K., 1993. *Chem. Phys. Lett.* 214, 57.
- Nagase, S., Kobayashi, K., 1994a. *Chem. Phys. Lett.* 228, 106.
- Nagase, S., Kobayashi, K., 1994b. *Chem. Phys. Lett.* 231, 319.
- Nagase, S., Kobayashi, K., 1994c. *J. Chem. Soc. Chem. Commun.* 1837.
- Nagase, S., Kobayashi, K., 1997. *Chem. Phys. Lett.* 276, 55.
- Nagase, S., Kobayashi, K., Akasaka, T., 1996. *Bull. Chem. Soc. Japan* 69, 2131.
- Nakane, T., Xu, Z., Yamamoto, E., Sugai, T., Tomiyama, T., Shinohara, H., 1997. *Fullerene Sci. Technol.* 5, 829.
- Nakane, T., Xu, Z., Yamamoto, E., Kai, T., Tomiyama, T., Shinohara, H., Kobayashi, Y., 1998. In: Kuzmany, H., Fink, J., Mehring, M., Roth, S. (Eds.), *Fullerenes and Fullerene Nanostructures*. World Scientific, London, pp. 193–281.
- Nishibori, E., Sakata, M., Takata, M., Hasegawa, M., Shinohara, H., 2000. *Chem. Phys. Lett.* 330, 497.
- Nishibori, E., Takata, M., Sakata, M., Taninaka, A., Shinohara, H., 2001. *Angew. Chem. Int. Ed. Engl.* 40, 2998.
- Nishibori, E., Terauchi, I., Sakata, M., Takata, M., Ito, Y., Sugai, T., Shinohara, H., 2006a. *J. Phys. Chem. B* 110, 19215.
- Nishibori, E., Ishihara, M., Takata, M., Sakata, M., Ito, Y., Inoue, T., Shinohara, H., 2006b. *Chem. Phys. Lett.* 433, 120.
- Ogawa, T., Sugai, T., Shinohara, H., 2000. *J. Am. Chem. Soc.* 122, 3538.
- Ohtsuki, T., Masumoto, K., Kikuchi, K., Sueki, K., 1996a. *Mater. Sci. Eng. A* 217–218, 38.
- Ohtsuki, T., Masumoto, K., Ohno, K., Maruyama, Y., Kawazoe, Y., Sueki, K., Kikuchi, K., 1996b. *Phys. Rev. Lett.* 77, 3522.
- Okazaki, T., Lian, Y., Gu, Z.N., Suenaga, K., Shinohara, H., 2000. *Chem. Phys. Lett.* 320, 435.
- Pan, C., Sampson, M.P., Chai, Y., Hauge, R.H., Margrave, J.L., 1991. *J. Phys. Chem.* 95, 2944.
- Park, C.H., et al., 1993. *Chem. Phys. Lett.* 213, 196.
- Petra, A., Dunsch, L., Neudeck, A., 1996. *J. Electroanalytic. Chem.* 412, 153.
- Pichler, T., Kuzmany, H., Yamamoto, E., Shinohara, H., 1996. In: Kuzmany, H. et al., (Ed.), *Fullerenes and Fullerene Nanostructures*. World Scientific, London, pp. 178–181.
- Pichler, T., Golden, M.S., Knupfer, M., Fink, J., Kirbach, U., Kuran, P., Dunsch, L., 1997. *Phys. Rev. Lett.* 79, 3026.
- Pichler, T., Hu, Z., Grazioli, C., Legner, S., Knupfer, M., Golden, M.S., Fink, J., de Groot, F.M.F., Hunt, M.R.C., Rudolf, P., Follath, R., Jung, Ch., Kjeldgaard, L., Bruehwiler, P., Inakuma, M., Shinohara, H., 2000. *Phys. Rev. B* 62, 13196.
- Pilla, O., Bill, H., 1984. *J. Phys. C: Solid State Phys.* 17, 3263.
- Plant, S.R., et al., 2009. *Chem. Phys. Lett.* 476, 41.
- Poirier, M.D., Knupfer, M., Weaver, J.H., Andreoni, W., Laasonen, K., Parrinello, M., Bethune, D.S., Kikuchi, K., Achiba, Y., 1994. *Phys. Rev. B* 49 (17), 403.
- Rietveld, H.M., 1969. *J. Appl. Crystallogr.* 2, 65.
- Rosen, A., Waestberg, B., 1988. *J. Am. Chem. Soc.* 110, 8701.
- Rosen, A., Waestberg, B., 1989. *Z. Phys. D* 12, 387.
- Ross, M.M., Nelson, H.H., Callahan, J.H., McElvany, S.W., 1992. *J. Phys. Chem.* 96, 5231.
- Roth, L.M., Huang, Y., Schwedler, J.T., Cassady, C.J., Ben-Amotz, D., Kahr, B., Freiser, B.S., 1991. *J. Am. Chem. Soc.* 113, 6298.

- Ruebsam, M., Plueschau, M., Schweitzer, P., Dinse, K.P., Fuchs, D., Rietschel, H., Michel, R.H., Benz, M., Kappes, M.M., 1995. In: Kuzmany, H. et al., (Ed.), *Physics and Chemistry of Fullerenes and Derivatives*. World Scientific, London, pp. 117–121.
- Ruebsam, M., Schweitzer, P., Dinse, K.P., 1996a. In: Kuzmany, H. et al., (Ed.), *Fullerenes and Fullerene Nanostructures*. World Scientific, London, pp. 173–177.
- Ruebsam, M., Knapp, C.P., Schweitzer, P., Dinse, K.P., 1996b. In: Kadish, K., Ruoff, R. (Eds.), *Fullerenes: Recent Advances in the Chemistry and Physics of Fullerenes and Related Materials*, vol 3. Electrochemical Society, Pennington, pp. 602–608.
- Saito, S., 1990. In: Averback, R.S. et al., (Ed.), *Clusters and Cluster-Assembled Materials*, vol 206. Materials Research Society, Pittsburgh, pp. 115–120.
- Saito, S., Sawada, S., 1992. *Chem. Phys. Lett.* 198, 466.
- Saito, Y., Yokoyama, S., Inakuma, M., Shinohara, H., 1996. *Chem. Phys. Lett.* 250, 80.
- Sakata, M., Sato, M., 1990. *Acta Crystallogr. A* 46, 263.
- Sakurai, T., Wang, X.D., Xue, Q.K., Hasegawa, Y., Hashizume, T., Shinohara, H., 1996. *Prog. Surf. Sci.* 51, 263.
- Sato, W., Sueki, K., Kikuchi, K., Kobayashi, K., Suzuki, S., Achiba, Y., Nakahara, H., Ohkubo, Y., Ambe, F., Asai, K., 1998. *Phys. Rev. Lett.* 80, 133.
- Savina, M., Martin, G., Xiao, J., Milanovich, N., Meyerhoff, M.E., Francis, A.H., 1994. In: Kadish, K., Ruoff, R. (Eds.), *Fullerenes: Recent Advances in the Chemistry and Physics of Fullerenes and Related Materials*, vol 1. Electrochemical Society, Pennington, pp. 1309–1319.
- Schmalz, T.G., Seits, W.A., Klein, D.J., Hite, G.E., 1988. *J. Am. Chem. Soc.* 110, 1113.
- Schulte, J., Boehm, M.C., Dinse, K.P., 1996. *Chem. Phys. Lett.* 259, 48.
- Schulte, J., Boehm, M.C., Dinse, K.P., 1998. In: Kuzmany, H. et al., (Ed.), *Molecular Nanostructures*. World Scientific, London, pp. 189–192.
- Scrivens, W.A., Bedworth, P.V., Tour, M.J., 1992. *J. Am. Chem. Soc.* 114, 7917.
- Scuseria, G.E., 1992. *J. Chem. Phys.* 97, 7528.
- Seifert, G., Bartl, A., Dunsch, L., Ayuela, A., Rockenbauer, A., 1998. *Appl. Phys. A* 66, 265.
- Shelimov, K.B., Clemmer, D.E., Jarrold, M.F., 1994. *J. Phys. Chem.* 98 (12), 819.
- Shi, Z.J., Okazaki, T., Shimada, T., Sugai, T., Suenaga, K., Shinohara, H., 2003. *J. Phys. Chem. B* 107, 2485.
- Shi, Z.Q., Wu, X., Wang, C.R., Lu, X., Shinohara, H., 2006. *Angew. Chem. Int. Ed.* 45, 2107.
- Shimotani, H., Ito, T., Iwasa, Y., Taninaka, A., Shinohara, H., Nishibori, E., Takata, M., Sakata, M., 2004. *J. Am. Chem. Soc.* 126, 364.
- Shinohara, H., 1998. In: Duncan, M. (Ed.), *Advances in Metal and Semiconductor Clusters*, vol 4. JAI Press, New York, pp. 205–226.
- Shinohara, H., 2000. *Rep. Prog. Phys.* 63, 843.
- Shinohara, H., Sato, H., Saito, Y., Ohkohchi, M., Ando, Y., 1992a. *J. Phys. Chem.* 96, 3571.
- Shinohara, H., Sato, H., Ohkohchi, M., Ando, Y., Kodama, T., Shida, T., Kato, T., Saito, Y., 1992b. *Nature* 357, 52.
- Shinohara, H., Yamaguchi, H., Hayashi, N., Sato, H., Ohkohchi, M., Ando, Y., Saito, Y., 1993a. *J. Phys. Chem.* 97, 4259.
- Shinohara, H., Hayashi, N., Sato, H., Saito, Y., Wang, X.D., Hashizume, T., Sakurai, T., 1993b. *J. Phys. Chem.* 97 (13), 438.
- Shinohara, H., Yamaguchi, H., Hayashi, N., Sato, H., Inagaki, M., Saito, Y., Bandow, S., Kitagawa, H., Mitani, T., Inokuchi, H., 1993c. *Mater. Sci. Eng. B* 19, 25.
- Shinohara, H., Inakuma, M., Hayashi, N., Sato, H., Saito, Y., Kato, T., Bandow, S., 1994a. *J. Phys. Chem.* 98, 8597.
- Shinohara, H., Kishida, M., Nakane, T., Kato, T., Bandow, S., Saito, Y., Wang, X.D., Hashizume, T., Sakurai, T., 1994b. In: Kadish, K., Ruoff, R. (Eds.), *Fullerenes: Recent Advances in the Chemistry and Physics of Fullerenes and Related Materials*, vol 1. Electrochemical Society, Pennington, pp. 1361–1381.

- Shinohara, H., Ohno, M., Kishida, M., Yamazaki, S., Hashizume, T., Sakurai, T., 1995a. In: Kadish, K., Ruoff, R. (Eds.), *Fullerenes: Recent Advances in the Chemistry and Physics of Fullerenes and Related Materials*, vol 2. Electrochemical Society, Pennington, pp. 763–773.
- Shinohara, H., Inakuma, M., Kishida, M., Yamazaki, S., Hashizume, T., Sakurai, T., 1995b. *J. Phys. Chem.* 99 (13), 769.
- Shinohara, H., Takata, M., Sakata, M., Hashizume, T., Sakurai, T., 1996a. *Mater. Sci. Forum* 232, 207.
- Shinohara, H., Yagi, K., Nakamura, J., 1996b. Japanese Patent No 143478.
- Smalley, R.E., 1992. *Acc. Chem. Res.* 25, 98.
- Soderholm, L., Wurcz, P., Lykke, K.R., Parker, D.H., Lytle, F.W., 1992. *J. Phys. Chem.* 96, 7153.
- Stevenson, S., et al., 1994a. *Anal. Chem.* 66, 2675.
- Stevenson, S., et al., 1994b. *Anal. Chem.* 66, 2680.
- Stevenson, S., et al., 1998. *J. Phys. Chem.* 102, 2833.
- Stevenson, S., et al., 2000. *Nature* 408, 427.
- Sueki, K., et al., 1997. *Fullerene Sci. Technol.* 5, 1435.
- Suematsu, H., Murakami, Y., Kawata, H., Fujii, Y., Hamaya, N., Kikuchi, K., Achiba, Y., Ikemoto, I., 1994. *Proc. Mat. Res. Soc. Symp.* 349, 213.
- Sugai, T., Inakuma, M., Hudgins, R., Dugourd, P., Fye, J.L., Jarrold, M.F., Shinohara, H., 2001. *J. Am. Chem. Soc.* 123, 6427.
- Suzuki, S., Kawata, S., Shiromaru, H., Yamauchi, K., Kikuchi, K., Kato, T., Achiba, Y., 1992. *J. Phys. Chem.* 96, 7159.
- Suzuki, T., Maruyama, Y., Kato, T., Kikuchi, K., Achiba, K., 1993. *J. Am. Chem. Soc.* 115 (11), 006.
- Suzuki, S., Kojima, Y., Nakao, Y., Wakabayashi, T., Kawata, S., Kikuchi, K., Achiba, Y., Kato, T., 1994. *Chem. Phys. Lett.* 229, 512.
- Suzuki, T., Maruyama, Y., Kato, T., Kikuchi, K., Nakao, Y., Achiba, Y., Kobayashi, K., Nagase, S., 1995a. *Angew. Chem. Int. Ed. Engl.* 107, 1228.
- Suzuki, T., Maruyama, Y., Kato, T., Kikuchi, K., Nakao, Y., Achiba, Y., Kobayashi, K., Nagase, S., 1995b. *Angew. Chem. Int. Ed. Engl.* 34, 1094.
- Suzuki, T., Maruyama, Y., Kato, T., Akasaka, T., Kobayashi, K., Nagase, S., Yamamoto, K., Funasaka, H., Takahashi, T., 1995c. *J. Am. Chem. Soc.* 117, 9606.
- Suzuki, T., Kikuchi, K., Oguri, F., Nakao, Y., Suzuki, S., Achiba, Y., Yamamoto, K., Funasaka, H., Takahashi, T., 1996. *Tetrahedron* 52, 4973.
- Suzuki, S., Kasuya, D., Suganuma, T., Shiromaru, H., Achiba, Y., Kataura, H., 1997a. In: Kadish, K., Ruoff, R. (Eds.), *Fullerenes: Recent Advances in the Chemistry and Physics of Fullerenes and Related Materials*, vol 4. Electrochemical Society, Pennington, pp. 485–489.
- Suzuki, S., Kojima, Y., Shiromaru, H., Achiba, Y., Walabayashi, T., Tellgmann, R., Campbell, E.E.B., Hertel, I.V., z. 1997b. *Phys. D* 40, 410.
- Tagmatarchis, N., Shinohara, H., 2000. *Chem. Mater.* 12, 3222.
- Takahashi, T., Ito, A., Inakuma, M., Shinohara, H., 1995. *Phys. Rev. B* 52 (13), 812.
- Takata, M., Umeda, B., Nishibori, E., Sakata, M., Saito, Y., Ohno, M., Shinohara, H., 1995. *Nature* 377, 46.
- Takata, M., Nishibori, E., Umeda, B., Sakata, M., Yamamoto, E., Shinohara, H., 1997. *Phys. Rev. Lett.* 78, 3330.
- Takata, M., Nishibori, E., Umeda, B., Sakata, M., Inakuma, M., Shinohara, H., 1998. *Chem. Phys. Lett.* 298, 79.
- Takata, M., Nishibori, E., Sakata, M., Inakuma, M., Yamamoto, Y., Shinohara, H., 1999. *Phys. Rev. Lett.* 83, 2214.
- Tanaka, N., Honda, Y., Kawahara, M., Kishida, M., Shinohara, H., 1996. *Thin Solid Films* 281–282, 613.

- Taylor, R., Hare, J.P., Abdul-Sada, A.K., Kroto, H.W., 1990. *J. Chem. Soc. Chem. Commun.* 1423.
- Tellgmann, R., Krawez, N., Lin, S.-H., Hertel, I.V., Campbell, E.E.B., 1996a. *Nature* 382, 407.
- Tellgmann, R., Krawez, N., Hertel, I.V., Campbell, E.E.B., 1996b. In: Kuzmany, H., Fink, J., Mehring, M., Roth, S. (Eds.), *Fullerenes and Fullerene Nanostructures*. World Scientific, London, pp. 168–172.
- Thess, A., et al., 1996. *Science* 273, 483.
- Ungerer, J.R., Hughbanks, T., 1993. *J. Am. Chem. Soc.* 115, 2054.
- van Loosdrecht, P.H.M., et al., 1994a. In: Kadish, K., Ruoff, R. (Eds.), *Fullerenes: Recent Advances in the Chemistry and Physics of Fullerenes and Related Materials*, vol 1. Electrochemical Society, Pennington, pp. 1320–1330.
- van Loosdrecht, P.H.M., Johnson, R.D., Bethune, D.S., Dorn, H.C., Burbank, P., Stevenson, S., 1994b. *Phys. Rev. Lett.* 73, 3415.
- Wakabayashi, T., Achiba, Y., 1992. *Chem. Phys. Lett.* 190, 465.
- Wakabayashi, T., Kikuchi, K., Shiromaru, H., Suzuki, S., Achiba, Y., 1993. *Z. Phys. D* 26, S258.
- Wakabayashi, T., Shiromaru, H., Suzuki, S., Kikuchi, K., Achiba, Y., 1996. *Surf. Rev. Lett.* 3, 793.
- Wakabayashi, T., Kasuya, D., Shiromaru, H., Suzuki, S., Kikuchi, K., Achiba, Y., 1997. *Z. Phys. D* 40, 414.
- Wan, S.M., Zhang, H.-W., Tso, T.S.C., Kwong, K.P., Wong, T., Ruoff, R.S., Inakuma, M., Shinohara, H., 1997. In: Kadish, K., Ruoff, R. (Eds.), *Fullerenes: Recent Advances in the Chemistry and Physics of Fullerenes and Related Materials*, vol 4. Electrochemical Society, Pennington, pp. 490–506.
- Wan, S.M., Zhang, H.-W., Nakane, T., Xu, Z., Inakuma, M., Shinohara, H., Kobayashi, K., Nagase, S., 1998. *J. Am. Chem. Soc.* 120, 6806.
- Wang, X.D., Hashizume, T., Shinohara, H., Saito, Y., Nishina, Y., Sakurai, T., 1992. *Japan J. Appl. Phys.* 31, L983.
- Wang, L.S., Alford, J.M., Chai, Y., Diener, M., Zang, J., McClure, S.M., Guo, T., Scuseria, G.E., Smalley, R.E., 1993a. *Chem. Phys. Lett.* 207, 354.
- Wang, L.S., Alford, J.M., Chai, Y., Diener, M., Smalley, R.E., 1993b. *Z. Phys. D* 26, S297.
- Wang, X.D., Hashizume, T., Xue, Q., Shinohara, H., Saito, Y., Nishina, Y., Sakurai, T., 1993c. *Chem. Phys. Lett.* 216, 409.
- Wang, X.D., Xue, Q., Hashizume, T., Shinohara, H., Nishina, Y., Sakurai, T., 1993d. *Phys. Rev. B* 48 (15), 492.
- Wang, X.D., Hashizume, T., Shinohara, H., Saito, Y., Nishina, Y., Sakurai, T., 1993e. *Phys. Rev. B* 47 (15), 923.
- Wang, Y., Tomanek, D., Ruoff, R., 1993f. *Chem. Phys. Lett.* 208, 79.
- Wang, X.D., Yurov, V.Y., Hashizume, T., Shinohara, H., Sakurai, T., 1994. *Phys. Rev. B* 49 (14), 746.
- Wang, W., Ding, J., Yang, S., Li, X.Y., 1997. In: Kadish, K., Ruoff, R. (Eds.), *Fullerenes: Recent Advances in the Chemistry and Physics of Fullerenes and Related Materials*, vol 4. Electrochemical Society, Pennington, pp. 417–428.
- Wang, C.R., Kai, T., Tomiyama, T., Yoshida, T., Kobayashi, Y., Nishibori, E., Takata, M., Sakata, M., Shinohara, H., 2000. *Nature* 408, 426.
- Wang, C.R., Kai, T., Yomiya, T., Yoshida, T., Kobayashi, Y., Nishibori, E., Takata, M., Sakata, M., Shinohara, H., 2001. *Angew. Chem. Int. Ed. Engl.* 113, 411.
- Wang, T.S., et al., 2009. *J. Am. Chem. Soc.* 131, 16646.
- Watanabe, H., Inoshita, T., 1986. *Optoelectron. Devices Technol.* 1, 33.
- Watanuki, T., et al., 1995. *Photon Factory Rep.* 13, 333.
- Watanuki, T., et al., 1996. *Photon Factory Rep.* 14, 403.
- Watanuki, T., Suematsu, H., Nakao, Y., Kikuchi, K., Schiba, Y., Maniwa, Y., 1997. *The 13th Fullerene Symp Abstract (Nagano)* 83.

- Weaver, J.H., et al., 1992. *Chem. Phys. Lett.* 190, 460.
- Weiss, F.D., Elkind, J.L., O'Brien, S.C., Curl, R.F., Smalley, R.E., 1988. *J. Am. Chem. Soc.* 110, 4464.
- Wilson, R.J., Meijer, G., Bethune, D.S., Johnson, R.D., Chambliss, D.D., de Vries, M.S., Hunziker, H.E., Wendt, H.R., 1990. *Nature* 348, 621.
- Wragg, J.L., Chamberlain, J.E., White, H.W., Kraetschmer, W., Huffman, D.R., 1990. *Nature* 348, 623.
- Xu, Z., Nakane, T., Shinohara, H., 1996. *J. Am. Chem. Soc.* 118 (11), 309.
- Yamamoto, K., Funasaka, H., Takahashi, T., Akasaka, T., 1994a. *J. Phys. Chem.* 98, 2008.
- Yamamoto, K., Funasaka, H., Takahashi, T., Akasaka, T., Suzuki, T., Maruyama, Y., 1994b. *J. Phys. Chem.* 98 (12), 831.
- Yamamoto, E., Tansho, M., Tomiyama, T., Shinohara, H., Kawahara, H., Kobayashi, Y., 1996. *J. Am. Chem. Soc.* 118, 2293.
- Yamamoto, Y., Ishiguro, T., Sakurai, K., Funasaka, H., 1997. In: Kadish, K., Ruoff, R. (Eds.), *Fullerenes: Recent Advances in the Chemistry and Physics of Fullerenes and Related Materials*, vol 4. Electrochemical Society, Pennington, pp. 375–389.
- Yannoni, C.S., Hoinkis, M., de Vries, M.S., Bethune, D.S., Salem, J.R., Crowder, M.S., Johnson, R.D., 1992. *Science* 256, 1191.
- Yeretzian, C., Hansen, K., Alvarez, M.M., Min, K.S., Gillan, E.G., Holczer, Kaner, R.B., Whetten, R.L., 1992. *Chem. Phys. Lett.* 196, 337.
- Yeretzian, C., Wiley, J.B., Holczer, K., Su, T., Nguyen, S., Kaner, R.B., Whetten, R.L., 1993. *J. Phys. Chem.* 97 (10), 097.
- Ying, Z.C., Jin, C., Hettich, R.L., Puretzky, A.A., Haufler, R.E., Compton, R.N., 1994. In: Kadish, K., Ruoff, R. (Eds.), *Fullerenes: Recent Advances in the Chemistry and Physics of Fullerenes and Related Materials*, vol 1. Electrochemical Society, Pennington, pp. 1402–1412.

CHAPTER 250

Ternary and Quaternary Chalcogenides of Si, Ge, Sn, Pb, and In

Lubomir D. Gulay* and Marek Daszkiewicz†

Contents	Symbols and Abbreviations	158
	1. Introduction	158
	2. Synthesis Conditions	159
	3. Ternary Systems	159
	3.1 Ternary R–Si–X (X = S, Se, Te) systems	160
	3.2 Ternary R–Ge–X (X = S, Se, Te) systems	160
	3.3 Ternary R–Sn–X (X = S, Se, Te) systems	160
	3.4 Ternary R–Pb–X (X = S, Se, Te) systems	160
	3.5 Ternary R–In–X (X = S, Se, Te) systems	168
	3.6 Structure types of ternary systems	168
	4. Quaternary Systems	206
	4.1 Quaternary R_2X_3 – M_2X – ZX_2 (M = Cu, Ag; Z = Si, Ge, Sn, X = S, Se) systems	206
	4.2 Quaternary R_2X_3 – M_2X – PbX (M = Cu, Ag; X = S, Se, Te) systems	214
	4.3 Quaternary R_2X_3 – M_2X – In_2X_3 (M = Cu, Ag; X = S, Se) systems	219
	4.4 Structure types of quaternary systems	222
	5. Crystallographic Relationships of Ternary and Quaternary Rare Earth Chalcogenides of Si, Ge, Sn, Pb and In	252

* Department of Ecology and Protection of Environment, Volyn National University, Lutsk, Ukraine

† W. Trzebiatowski Institute of Low Temperature and Structure Research, Polish Academy of Sciences, Wrocław, Poland

5.1	Crystallographic peculiarities of R_3MZX_7 ($M = \text{Cu(I), Ag(I), } 1/2\text{Ag(II), } 1/3\text{Ag(III), } Z = \text{Si, Ge, Sn; } X = \text{S, Se), } R_3Z_{1,25}X_7$ ($Z = \text{Si, Ge, Sn; } X = \text{S, Se), and } \text{La}_3\text{In}_{1,67}X_7$ ($X = \text{S, Se) compounds}$	252
5.2	Crystallographic peculiarities of rare earth—lead chalcogenides	258
5.3	Formation of superstructures	266
5.4	The role of voids in the crystal structures of chalcogenides	269
	References	270

Symbols and Abbreviations

a, b, c	unit cell dimensions (in nm)
α, β, γ	unit cell angles (in °)
x, y, z	Fractional atomic coordinates (same as $x/a, y/b, z/c$)
SG	Space group
Z	Number of formula units per unit cell
CP	Coordination polyhedron
CN	Coordination number
M	d-element
Z	Group 13 and 14 element (Si, Ge, Sn, Pb, In)
X	Group 16 element (S, Se, Te)

1. INTRODUCTION

The present chapter consists of two main parts. The first part (paragraph 3) deals with crystal structures of ternary rare earth chalcogenides of Si, Ge, Sn, Pb, and In. The compounds for which at least a structure type has been assigned are included in the chapter. Since phase diagrams of ternary systems have been described by Eliseev and Kuzmichyeva (1990) only the crystal structures of ternary chalcogenides are described here. The second part (paragraph 4) deals with phase diagrams of quaternary rare earth chalcogenides of Si, Ge, Sn, Pb, and In systems and crystal structures of quaternary compounds.

Crystallographic peculiarities of rare earth chalcogenides of Si, Ge, Sn, Pb, and In are shortly discussed at the end of this chapter.

2. SYNTHESIS CONDITIONS

Direct synthesis of the elemental constituents in evacuated quartz ampoules was used in most reported cases. The ampoules with the mixtures of elements were heated to different preset maximum temperature, for example 1420 K, and were kept at this temperature for a few hours. Afterward, the ampoules were cooled slowly to a respective annealing temperature, for example 870 K, and annealed at this temperature for many hours. In some cases, the flux method was used. Detailed experimental conditions can be found in the original cited papers.

3. TERNARY SYSTEMS

This section describes ternary chalcogenides of silicon, germanium, tin, lead, and indium systems. All of these elements, except indium, belong to Group 14 in the periodic table of elements and therefore, theoretically, all of them have stable +4 oxidation states. Thus, a substitution one element of Group 14 by another could result in a similar structure. However, structural relationships among the ternary compounds seem to not be as straightforward as this may appear.

The effective ionic radius of a cation depends on (a) the charge and (b) the coordination number (Shannon, 1976). It appears that the charge is a very important parameter in tin and lead compounds, where the +2 oxidation state is possible. This follows from the fact that as many as ~37% of structures of all tin chalcogenides deposited in the Inorganic Crystal Structure Database (ICSD) contain Sn^{2+} ions and none of the chalcogenides structures deposited in the ICSD contains tetravalent lead. Besides, the ionic radius increases significantly for the four-valent ions of Group 14 elements, that is $r(\text{Si}^{4+}) = 0.40 \text{ \AA}$, $r(\text{Ge}^{4+}) = 0.53 \text{ \AA}$, $r(\text{Sn}^{4+}) = 0.69 \text{ \AA}$ and $r(\text{Pb}^{4+}) = 0.79 \text{ \AA}$. On the other hand, a smaller difference of the ionic radii is observed for the lanthanide series that is 1.30 Å for eight-coordinate La^{3+} and 1.12 Å for eight-coordinate Lu^{3+} . Moreover, when the ionic radius of the divalent lead ion (1.43 Å) is compared with those of the lanthanide series elements, it appears that Pb^{2+} can substitute for R^{3+} ions. So, it is not a simple substitution among the elements of Group 14, and therefore, synthesis of the rare earth chalcogenides with silicon, germanium, tin, or lead should result in non-isostructural compounds. Finally, occupational disorder in the crystal structures of these materials is also possible, because the ionic radii of Pb^{2+} and R^{3+} ions are similar.

Indium ions are even more different than, for example, silicon ions, because the former occurs in the +3 oxidation state. This fact suggests that In^{3+} ions could substitute for lanthanide ions. However, the In^{3+} ion

has a smaller ionic radius than R^{3+} ions and it prefers tetrahedral or octahedral locations in crystal structures.

3.1 Ternary R–Si–X (X = S, Se, Te) systems

The R–Si–X (X = S, Se, Te) systems have been investigated mainly across the R_2X_3 – SiX_2 sections. Ternary compounds known in these systems are listed in Table 1. Among all of these compounds, stoichiometric $R_4Si_3X_{12}$ and nonstoichiometric $R_3Si_{1.25}X_7$ chalcogenides exhibiting hexagonal symmetry can be found. Many monoclinic compounds of general formulae R_2SiX_5 , R_2SiX_4 , and $R_4Si_3X_{12}$ have been obtained. Triclinic $R_6Si_4X_{17}$ crystals are also known in the R–Si–X (X = S, Se) systems. No ternary compounds have been reported for Te systems.

3.2 Ternary R–Ge–X (X = S, Se, Te) systems

The R–Ge–X (X = S, Se, Te) systems have been investigated mainly across the R_2X_3 – GeX_2 sections. Ternary compounds reported in these systems are listed in Table 2. Like silicon chalcogenides, they crystallize in hexagonal and monoclinic crystal systems. However, no triclinic $R_6Ge_4X_{17}$ compounds have been reported. No ternary compounds are known for the systems with Te.

3.3 Ternary R–Sn–X (X = S, Se, Te) systems

The R–Sn–X (X = S, Se, Te) systems have been investigated mainly across the R_2X_3 – SnX_2 sections. Known ternary compounds are listed in Table 3. No ternary compounds are known for the systems with Te. An extended series of orthorhombic (SG *Pbam*) R_2SnS_5 compounds has been synthesized, and also hexagonal nonstoichiometric $La_3Sn_{1.25}S_7$ compound has been found. An investigation of the Eu–Sn–X (X = S, Se) systems resulted in five different chalcogenides that adopt orthorhombic symmetry.

3.4 Ternary R–Pb–X (X = S, Se, Te) systems

The R–Pb–X (X = S, Se, Te) systems have been investigated mainly across the R_2X_3 – PbX sections. Ternary compounds that form in these systems are listed in Table 4. Many compounds with general formula $R_{2+2x/3}Pb_{1-x}X_4$ ($x = 0-1$) have been prepared. They crystallize in the cubic body-centered and orthorhombic primitive, and face-centered unit cells. No hexagonal nonstoichiometric $R_3Pb_{0.5}X_7$ compounds were found. Two chalcogen-poor La_5Pb_3S and La_5Pb_3Se compounds (SG *P6₃/mcm*) have been synthesized in the R–Pb–X (X = S, Se) systems. No ternary compounds are known for the Te systems.

TABLE 1 Crystallographic data for ternary rare earth silicon chalcogenides

Compound	Structure type	Space group	Lattice parameters (nm)			Reference(s)
			<i>a</i>	<i>b</i>	<i>c</i>	
Y ₃ Si _{1.25} S ₇	Dy ₃ Ge _{1.25} S ₇	<i>P6</i> ₃	0.97449	–	0.56985	Lychmanyuk et al. (2006a)
La ₂ Si ₅	La ₂ GeS ₅	<i>P2</i> ₁ / <i>c</i>	0.7620	1.2640 <i>β</i> = 101.55°	0.7899	Daszkiewicz et al. (2007a)
Ce ₂ Si ₅	La ₂ GeS ₅	<i>P2</i> ₁ / <i>c</i>	0.75475	1.2558 <i>β</i> = 101.55°	0.78286	Gauthier et al. (2003)
Ce ₄ Si ₃ S ₁₂	La ₄ Ge ₃ S ₁₂	<i>R3c</i>	1.91745	–	0.79943	Gauthier et al. (2003)
Ce ₆ Si ₄ S ₁₇	Ce ₆ Si ₄ S ₁₇	<i>P</i> $\bar{1}$	0.89576 <i>α</i> = 82.188°	1.00022 <i>β</i> = 86.889°	1.4265 <i>γ</i> = 89.515°	Gauthier et al. (2003)
Pr ₂ Si ₅	La ₂ GeS ₅	<i>P2</i> ₁ / <i>c</i>	0.7514	1.2489 <i>β</i> = 101.62°	0.7775	Michelet et al. (1970)
Pr ₄ Si ₃ S ₁₂	La ₄ Ge ₃ S ₁₂	<i>R3c</i>	1.911	–	0.793	Perez and Duale (1969)
Pr ₆ Si ₄ S ₁₇	Ce ₆ Si ₄ S ₁₇	<i>P</i> $\bar{1}$	0.8902 <i>α</i> = 82.19°	0.9934 <i>β</i> = 86.94°	1.4206 <i>γ</i> = 89.40°	Gulay et al. (2008a)
Nd ₂ Si ₅	La ₂ GeS ₅	<i>P2</i> ₁ / <i>c</i>	0.7480	1.2434 <i>β</i> = 101.66°	0.7740	Michelet et al. (1970)
Nd ₄ Si ₃ S ₁₂	La ₄ Ge ₃ S ₁₂	<i>R3c</i>	1.906	–	0.790	Perez and Duale (1969)
Nd ₆ Si ₄ S ₁₇	Ce ₆ Si ₄ S ₁₇	<i>P</i> $\bar{1}$	0.8880 <i>α</i> = 82.11°	0.9903 <i>β</i> = 87.04°	1.4168 <i>γ</i> = 89.31°	Gulay et al. (2008a)
Sm ₄ Si ₃ S ₁₂	La ₄ Ge ₃ S ₁₂	<i>R3c</i>	1.897	–	0.783	Perez and Duale (1969)
Sm ₆ Si ₄ S ₁₇	Ce ₆ Si ₄ S ₁₇	<i>P</i> $\bar{1}$	0.88300 <i>α</i> = 82.126°	0.9779 <i>β</i> = 87.338°	1.4047 <i>γ</i> = 89.018°	Gulay et al. (2008a)

(continued)

Table 1 (continued)

Compound	Structure type	Space group	Lattice parameters (nm)			Reference(s)
			<i>a</i>	<i>b</i>	<i>c</i>	
Eu ₂ SiS ₄	Sr ₂ GeS ₄	<i>P</i> 2 ₁ / <i>m</i>	0.6524	0.6591 $\beta = 108.29^\circ$	0.8205	Johrendt and Pocha (2001)
Gd ₃ Si _{1.25} S ₇	Dy ₃ Ge _{1.25} S ₇	<i>P</i> 6 ₃	0.987	–	0.571	Michelet and Flahaut (1969)
Gd ₄ Si ₃ S ₁₂	La ₄ Ge ₃ S ₁₂	<i>R</i> 3 <i>c</i>	1.889	–	0.779	Perez and Duale (1969)
Gd ₄ Si ₃ S ₁₂	Tb ₄ Si ₃ S ₁₂	<i>P</i> 2 ₁ / <i>n</i>	0.9867	1.09969 $\beta = 102.67^\circ$	1.6462	Hatscher and Urland (2003)
Tb ₃ Si _{1.25} S ₇	Dy ₃ Ge _{1.25} S ₇	<i>P</i> 6 ₃	0.982	–	0.570	Michelet and Flahaut (1969)
Tb ₄ Si ₃ S ₁₂	Tb ₄ Si ₃ S ₁₂	<i>P</i> 2 ₁ / <i>n</i>	0.9836	1.0964 $\beta = 102.76^\circ$	1.6391	Hatscher and Urland (2002a)
Dy ₃ Si _{1.25} S ₇	Dy ₃ Ge _{1.25} S ₇	<i>P</i> 6 ₃	0.975	–	0.570	Michelet and Flahaut (1969)
Dy ₄ Si ₃ S ₁₂	Tb ₄ Si ₃ S ₁₂	<i>P</i> 2 ₁ / <i>n</i>	0.9813	1.0938 $\beta = 102.86^\circ$	1.6360	Hatscher and Urland (2002b)
Ho ₃ Si _{1.25} S ₇	Dy ₃ Ge _{1.25} S ₇	<i>P</i> 6 ₃	0.97306	–	0.57001	Lychmanyuk et al. (2007a)
Pr ₃ Si _{1.25} Se ₇	Dy ₃ Ge _{1.25} S ₇	<i>P</i> 6 ₃	1.05268	–	0.60396	Gulay and Lychmanyuk (2008)
Nd ₃ Si _{1.25} Se ₇	Dy ₃ Ge _{1.25} S ₇	<i>P</i> 6 ₃	1.04760	–	0.60268	Gulay and Lychmanyuk (2008)
Sm ₃ Si _{1.25} Se ₇	Dy ₃ Ge _{1.25} S ₇	<i>P</i> 6 ₃	1.04166	–	0.59828	Gulay and Lychmanyuk (2008)

TABLE 2 Crystallographic data for ternary rare earth germanium chalcogenides

Compound	Structure type	Space group	Lattice parameters (nm)			Reference(s)
			<i>a</i>	<i>b</i>	<i>c</i>	
Y ₃ Ge _{1.25} S ₇	Dy ₃ Ge _{1.25} S ₇	<i>P6</i> ₃	0.9730	–	0.5826	Gulay et al. (2006a)
La ₃ Ge _{1.67} S ₇	Dy ₃ Ge _{1.25} S ₇	<i>P6</i> ₃	1.038	–	0.581	Michelet and Flahaut (1969)
La ₃ Ge _{1.25} S ₇	Dy ₃ Ge _{1.25} S ₇	<i>P6</i> ₃	1.0297	–	0.5812	Zeng et al. (2008)
La ₂ GeS ₅	La ₂ GeS ₅	<i>P2</i> ₁ / <i>c</i>	0.7641	1.2702 $\beta = 101.39^\circ$	0.7893	Mazurier and Etienne (1973)
La ₄ Ge ₃ S ₁₂	La ₄ Ge ₃ S ₁₂	<i>R3c</i>	1.940	–	0.810	Mazurier and Etienne (1974)
La ₅ Ge ₃ S	Hf ₅ CuSn ₃	<i>P6</i> ₃ / <i>mcm</i>	0.8992	–	0.7031	Guloy and Corbett (1993)
Ce ₃ Ge _{1.67} S ₇	Dy ₃ Ge _{1.25} S ₇	<i>P6</i> ₃	1.030	–	0.580	Michelet and Flahaut (1969)
Ce ₃ Ge _{1.25} S ₇	Dy ₃ Ge _{1.25} S ₇	<i>P6</i> ₃	1.022	–	0.583	Michelet and Flahaut (1969)
Ce ₄ Ge ₃ S ₁₂	La ₄ Ge ₃ S ₁₂	<i>R3c</i>	1.9375	–	0.8029	Choudhury and Dorhout (2008)
Pr ₃ Ge _{1.67} S ₇	Dy ₃ Ge _{1.25} S ₇	<i>P6</i> ₃	1.019	–	0.576	Michelet and Flahaut (1969)
Pr ₃ Ge _{1.25} S ₇	Dy ₃ Ge _{1.25} S ₇	<i>P6</i> ₃	1.010	–	0.581	Bakakin et al. (1974)
Pr ₄ Ge ₃ S ₁₂	La ₄ Ge ₃ S ₁₂	<i>R3c</i>	1.92856	–	0.798049	Helmholdt et al. (2003)
Nd ₃ Ge _{1.67} S ₇	Dy ₃ Ge _{1.25} S ₇	<i>P6</i> ₃	1.010	–	0.576	Michelet and Flahaut (1969)
Nd ₃ Ge _{1.25} S ₇	Dy ₃ Ge _{1.25} S ₇	<i>P6</i> ₃	1.005	–	0.582	Michelet and Flahaut (1969)
Nd ₄ Ge ₃ S ₁₂	La ₄ Ge ₃ S ₁₂	<i>R3c</i>	1.9250	–	0.7949	Choudhury and Dorhout (2008)
Sm ₃ Ge _{1.67} S ₇	Dy ₃ Ge _{1.25} S ₇	<i>P6</i> ₃	1.003	–	0.574	Michelet and Flahaut (1969)
Sm ₃ Ge _{1.25} S ₇	Dy ₃ Ge _{1.25} S ₇	<i>P6</i> ₃	0.994	–	0.582	Michelet and Flahaut (1969)
Sm ₄ Ge ₃ S ₁₂	La ₄ Ge ₃ S ₁₂	<i>R3c</i>	1.919	–	0.796	Michelet et al. (1966)
EuGeS ₃	β -CaSiO ₃	<i>P</i> $\bar{1}$	0.8468	1.176	0.8389	Bugli et al. (1978)
Eu ₂ GeS ₄	Eu ₂ GeS ₄	<i>P2</i> ₁	0.6638	$\alpha = 90.49^\circ$ $\beta = 104.56^\circ$ $\beta = 108.20^\circ$	$\gamma = 69.52^\circ$ 0.8146	Bugli et al. (1979)

(continued)

Table 2 (continued)

Compound	Structure type	Space group	Lattice parameters (nm)			Reference(s)
			<i>a</i>	<i>b</i>	<i>c</i>	
Eu ₂ GeS ₄	Sr ₂ GeS ₄	<i>P2₁/m</i>	0.6643	0.6674 $\beta = 108,19^\circ$	0.8162	Tampier and Johrendt (2001)
Gd ₃ Ge _{1.25} S ₇	Dy ₃ Ge _{1.25} S ₇	<i>P6₃</i>	0.984	–	0.582	Michelet and Flahaut (1969)
Gd ₄ Ge ₃ S ₁₂	La ₄ Ge ₃ S ₁₂	<i>R3c</i>	1.909	–	0.790	Michelet et al. (1966)
Tb ₃ Ge _{1.25} S ₇	Dy ₃ Ge _{1.25} S ₇	<i>P6₃</i>	0.979	–	0.582	Michelet and Flahaut (1969)
Dy ₃ Ge _{1.25} S ₇	Dy ₃ Ge _{1.25} S ₇	<i>P6₃</i>	0.973	–	0.582	Michelet et al. (1975)
Ho ₃ Ge _{1.25} S ₇	Dy ₃ Ge _{1.25} S ₇	<i>P6₃</i>	0.9686	–	0.5819	Lychmanyuk et al. (2007a)
Er ₃ Ge _{1.33} S ₇	Dy ₃ Ge _{1.25} S ₇	<i>P6₃</i>	0.9593	–	0.5849	Zeng et al. (2008)
La ₃ Ge _{1.5} Se ₇	Dy ₃ Ge _{1.25} S ₇	<i>P6₃</i>	1.075	–	0.609	Guittard and Julien-Pouzol (1970)
La ₃ Ge _{1.25} Se ₇	Dy ₃ Ge _{1.25} S ₇	<i>P6₃</i>	1.067	–	0.610	Loireau-Lozac'h and Guittard (1977)
La ₅ Ge ₃ Se	Hf ₅ CuSn ₃	<i>P6₃/mcm</i>	0.9112	–	0.7161	Guloy and Corbett (1993)
Ce ₃ Ge _{1.5} Se ₇	Dy ₃ Ge _{1.25} S ₇	<i>P6₃</i>	1.064	–	0.607	Guittard and Julien-Pouzol (1970)
Pr ₃ Ge _{1.5} Se ₇	Dy ₃ Ge _{1.25} S ₇	<i>P6₃</i>	1.059	–	0.606	Guittard and Julien-Pouzol (1970)
Nd ₃ Ge _{1.5} Se ₇	Dy ₃ Ge _{1.25} S ₇	<i>P6₃</i>	1.053	–	0.600	Guittard and Julien-Pouzol (1970)
Sm ₃ Ge _{1.5} Se ₇	Dy ₃ Ge _{1.25} S ₇	<i>P6₃</i>	1.045	–	0.603	Guittard and Julien-Pouzol (1970)
Eu ₂ GeSe ₄	Eu ₂ GeS ₄	<i>P2₁</i>	0.6964	0.7055 $\beta = 108.12^\circ$	0.8400	Tampier et al. (2002)
Eu ₂ GeSe ₄	Sr ₂ GeS ₄	<i>P2₁/m</i>	0.6969	0.7059 $\beta = 107.99^\circ$	0.8516	Tampier et al. (2002)
Eu ₂ Ge ₂ Se ₅	Sr ₂ Ge ₂ Se ₅	<i>P2₁/n</i>	0.8421	1.2235 $\beta = 93.67^\circ$	0.9127	Tampier et al. (2002)
Gd ₃ Ge _{1.5} Se ₇	Dy ₃ Ge _{1.25} S ₇	<i>P6₃</i>	1.031	–	0.605	Guittard and Julien-Pouzol (1970)
Tb ₃ Ge _{1.5} Se ₇	Dy ₃ Ge _{1.25} S ₇	<i>P6₃</i>	1.026	–	0.609	Guittard and Julien-Pouzol (1970)
Dy ₃ Ge _{1.5} Se ₇	Dy ₃ Ge _{1.25} S ₇	<i>P6₃</i>	1.018	–	0.609	Guittard and Julien-Pouzol (1970)

TABLE 3 Crystallographic data for ternary rare earth tin chalcogenides

Compound	Structure type	Space group	Lattice parameters (nm)			Reference(s)
			<i>a</i>	<i>b</i>	<i>c</i>	
La ₃ Sn _{1.25} S ₇	Dy ₃ Ge _{1.25} S ₇	<i>P6₃</i>	1.0277	–	0.6003	Zeng et al. (2008)
La ₂ SnS ₅	La ₂ SnS ₅	<i>Pbam</i>	0.7915	1.122	0.396	Jaulmes (1974)
Ce ₂ SnS ₅	La ₂ SnS ₅	<i>Pbam</i>	0.786	1.124	0.395	Guittard et al. (1976)
Pr ₂ SnS ₅	La ₂ SnS ₅	<i>Pbam</i>	0.78195	1.1214	0.39462	Daszkiewicz et al. (2008a)
Nd ₂ SnS ₅	La ₂ SnS ₅	<i>Pbam</i>	0.7772	1.1218	0.39272	Daszkiewicz et al. (2008a)
Sm ₂ SnS ₅	La ₂ SnS ₅	<i>Pbam</i>	0.7773	1.1276	0.3895	Julien-Pouzol and Jaulmes (1979)
Gd ₂ SnS ₅	La ₂ SnS ₅	<i>Pbam</i>	0.7733	1.1290	0.38217	Daszkiewicz et al. (2008a)
Tb ₂ SnS ₅	La ₂ SnS ₅	<i>Pbam</i>	0.7717	1.1246	0.38056	Daszkiewicz et al. (2008a)
Dy ₂ SnS ₅	La ₂ SnS ₅	<i>Pbam</i>	0.775	1.114	0.386	Guittard et al. (1976)
Eu ₂ SnS ₅	Eu ₂ SnS ₅	<i>Pbam</i>	1.1507	1.5612	0.4100	Jaulmes et al. (1982)
Eu ₃ Sn ₂ S ₇	Eu ₃ Sn ₂ S ₇	<i>Pbam</i>	1.1542	1.2690	0.3974	Jaulmes and Julien-Pouzol (1977a)
Eu ₅ Sn ₃ S ₁₂	Eu ₅ Sn ₃ S ₁₂	<i>Pmc2₁</i>	0.3924	2.0212	1.1509	Jaulmes and Julien-Pouzol (1977b)
Eu ₂ SnS ₄	Eu ₂ SnS ₄	<i>Pnma</i>	1.1187	0.8768	0.7538	Pocha et al. (2003)
Eu ₂ SnSe ₅	Eu ₂ SnSe ₅	<i>P2₁2₁2</i>	1.1990	1.6425	0.8543	Evenson and Dorhout (2001)

TABLE 4 Crystallographic data for ternary rare earth lead chalcogenides

Compound	Structure type	Space group	Lattice parameters (nm)			Reference(s)
			<i>a</i>	<i>b</i>	<i>c</i>	
Sc ₂ PbS ₄	CaFe ₂ O ₄	<i>Pnma</i>	1.1642	0.3757	1.3711	Shemet et al. (2006a)
Y ₂ PbS ₄	Er ₂ PbS ₄	<i>Cmc</i> ₂₁	0.79301	2.86966	1.20511	Gulay et al. (2008b)
La _{2+2/3x} Pb _{1-x} S ₄ (<i>x</i> = 0–1)	Th ₃ P ₄	<i>I</i> 43 <i>d</i>	0.8767 (<i>x</i> = 0)	–	–	Patrie et al. (1969)
La ₅ Pb ₃ S	Hf ₅ CuSn ₃	<i>P</i> 6 ₃ / <i>mcm</i>	0.9547	–	0.7022	Guloy and Corbett (1994)
Ce _{2+2/3x} Pb _{1-x} S ₄ (<i>x</i> = 0–1)	Th ₃ P ₄	<i>I</i> 43 <i>d</i>	0.8705 (<i>x</i> = 0)	–	–	Patrie et al. (1969)
Pr _{2+2/3x} Pb _{1-x} S ₄ (<i>x</i> = 0–1)	Th ₃ P ₄	<i>I</i> 43 <i>d</i>	0.8675 (<i>x</i> = 0)	–	–	Patrie et al. (1969)
Pr _{2+2/3x} Pb _{1-x} S ₄ (<i>x</i> = 0–0.54)	Th ₃ P ₄	<i>I</i> 43 <i>d</i>	0.86513 (<i>x</i> = 0)	–	–	Marchuk et al. (2006a)
Nd _{2+2/3x} Pb _{1-x} S ₄ (<i>x</i> = 0–1)	Th ₃ P ₄	<i>I</i> 43 <i>d</i>	0.8632 (<i>x</i> = 0)	–	–	Patrie et al. (1969)
Sm _{2+2/3x} Pb _{1-x} S ₄ (<i>x</i> = 0–1)	Th ₃ P ₄	<i>I</i> 43 <i>d</i>	0.8572 (<i>x</i> = 0)	–	–	Patrie et al. (1969)
Gd _{2+2/3x} Pb _{1-x} S ₄ (<i>x</i> = 0–1)	Th ₃ P ₄	<i>I</i> 43 <i>d</i>	0.8522 (<i>x</i> = 0)	–	–	Patrie et al. (1969)
Tb _{2+2/3x} Pb _{1-x} S ₄ (<i>x</i> = 0.13–1)	Th ₃ P ₄	<i>I</i> 43 <i>d</i>	0.8485 (<i>x</i> = 0.13)	–	–	Patrie et al. (1969)
Tb _{2+2/3x} Pb _{1-x} S ₄ (<i>x</i> = 0–0.6)	Th ₃ P ₄	<i>I</i> 43 <i>d</i>	0.85021–0.83954	–	–	Hvaleba et al. (2006)
Dy _{2+2/3x} Pb _{1-x} S ₄ (<i>x</i> = 0.16–1)	Th ₃ P ₄	<i>I</i> 43 <i>d</i>	0.8449 (<i>x</i> = 0.16)	–	–	Patrie et al. (1969)
Dy _{2+2/3x} Pb _{1-x} S ₄ (<i>x</i> = 0.44–0.50)	Th ₃ P ₄	<i>I</i> 43 <i>d</i>	0.84250–0.84062	–	–	Gulay et al. (2007a)
Dy ₂ PbS ₄	Er ₂ PbS ₄	<i>Cmc</i> ₂₁	0.79484	2.8721	1.2039	Gulay et al. (2008b)
Ho _{2+2/3x} Pb _{1-x} S ₄ (<i>x</i> = 0.43–1)	Th ₃ P ₄	<i>I</i> 43 <i>d</i>	0.8366 (<i>x</i> = 0.43)	–	–	Patrie et al. (1969)
Ho ₂ PbS ₄	Er ₂ PbS ₄	<i>Cmc</i> ₂₁	0.79081	2.86222	1.20220	Gulay et al. (2008b)
Er ₂ PbS ₄	Er ₂ PbS ₄	<i>Cmc</i> ₂₁	0.7863	2.8525	1.1995	Gulay et al. (2008b)
Tm ₂ PbS ₄	Er ₂ PbS ₄	<i>Cmc</i> ₂₁	0.78419	2.84184	1.19655	Gulay et al. (2008b)
Yb ₂ PbS ₄	Tm ₂ PbSe ₄	<i>Pnma</i>	1.1899	0.39015	1.4127	Gulay et al. (2008c)
Lu ₂ PbS ₄	Tm ₂ PbSe ₄	<i>Pnma</i>	1.1919	0.38890	1.4103	Gulay et al. (2008c)
Sc ₂ PbSe ₄	CaFe ₂ O ₄	<i>Pnma</i>	1.22029	0.39061	1.42801	Shemet et al. (2006a)
Y _{4,2} Pb _{0,7} Se ₇	Y _{4,2} Pb _{0,7} Se ₇	<i>Cm</i>	1.3357	0.40469	1.22356	Shemet et al. (2005)

$$\beta = 104.529^\circ$$

$Y_6Pb_2Se_{11}$	$Y_6Pb_2Se_{11}$	<i>Cmcm</i>	0.40610	1.3467	3.7624	Gulay et al. (2005a)
$La_{2+2/3x}Pb_{1-x}Se_4$ ($x = 0-1$)	Th_3P_4	$\bar{I}43d$	0.9106 ($x = 0$)	–	–	Patrie et al. (1969)
La_5Pb_3Se	Hf_5CuSn_3	<i>P6₃/mcm</i>	0.9553	–	0.7035	Guloy and Corbett (1994)
$Ce_{2+2/3x}Pb_{1-x}Se_4$ ($x = 0-1$)	Th_3P_4	$\bar{I}43d$	0.9045 ($x = 0$)	–	–	Patrie et al. (1969)
$Pr_{2+2/3x}Pb_{1-x}Se_4$ ($x = 0-1$)	Th_3P_4	$\bar{I}43d$	0.8996 ($x = 0$)	–	–	Patrie et al. (1969)
$Pr_{2+2/3x}Pb_{1-x}Se_4$ ($x = 0-1$)	Th_3P_4	$\bar{I}43d$	0.89916 ($x = 0$)	–	–	Marchuk et al. (2006b)
$Nd_{2+2/3x}Pb_{1-x}Se_4$ ($x = 0-1$)	Th_3P_4	$\bar{I}43d$	0.8968 ($x = 0$)	–	–	Patrie et al. (1969)
$Sm_{2+2/3x}Pb_{1-x}Se_4$ ($x = 0-1$)	Th_3P_4	$\bar{I}43d$	0.8909 ($x = 0$)	–	–	Patrie et al. (1969)
$Gd_{2+2/3x}Pb_{1-x}Se_4$ ($x = 0.31-1$)	Th_3P_4	$\bar{I}43d$	0.8857 ($x = 0.31$)	–	–	Patrie et al. (1969)
$Tb_{2+2/3x}Pb_{1-x}Se_4$ ($x = 0.69-1$)	Th_3P_4	$\bar{I}43d$	0.8737 ($x = 0.69$)	–	–	Patrie et al. (1969)
$Tb_{2+2/3x}Pb_{1-x}Se_4$ ($x = 0.21-0.57$)	Th_3P_4	$\bar{I}43d$	0.87672 ($x = 0.50$)	–	–	Gulay et al. (2006b)
$Dy_6Pb_2Se_{11}$	$Y_6Pb_2Se_{11}$	<i>Cmcm</i>	0.40772	1.3458	3.7589	Gulay et al. (2005a)
$Ho_6Pb_2Se_{11}$	$Y_6Pb_2Se_{11}$	<i>Cmcm</i>	0.40603	1.3397	3.7542	Gulay et al. (2006c)
Er_2PbSe_4	Tm_2PbSe_4	<i>Pnma</i>	1.2541	0.40810	1.4865	Gulay et al. (2007b)
Tm_2PbSe_4	Tm_2PbSe_4	<i>Pnma</i>	1.2505	0.40630	1.4820	Gulay et al. (2006d)
Yb_2PbSe_4	Tm_2PbSe_4	<i>Pnma</i>	1.2501	0.40380	1.4707	Gulay et al. (2007b)
Lu_2PbSe_4	Tm_2PbSe_4	<i>Pnma</i>	1.24718	0.40345	1.47338	Gulay et al. (2006d)

3.5 Ternary R–In–X (X = S, Se, Te) systems

The R–In–X (X = S, Se, Te) systems have been investigated mainly across the R_2X_3 – In_2X_3 sections. No ternary compounds are known for Te systems. Ternary compounds found in these systems are listed in Table 5. Almost all compounds from this group crystallize in the orthorhombic symmetry. The crystal structure of the La_3InS_6 published by Carré et al. (1978) should be solved in $Pnmm$ space group and not in $P2_12_12$. The PLATON program (Spek, 2003) finds additional symmetry elements for this structure deposited in the ICSD. Hexagonal nonstoichiometric $La_3In_{1.67}X_7$ (X = S, Se) compounds were also found in the R–In–X (X = S, Se) systems.

3.6 Structure types of ternary systems

3.6.1 Structure type $Dy_3Ge_{1.25}S_7$

Structure type $Dy_3Ge_{1.25}S_7$ (Michelet et al., 1975) (Figure 1, Table 6). SG $P6_3$, $Z = 2$, $a = 0.973$, $c = 0.582$ nm. The dysprosium atoms are located in monocapped trigonal prismatic arrangement of the S atoms. The shortest Dy–S distance is 0.267 nm. The Ge1 and Ge2 atoms lie on the threefold rotation axis and sixfold screw axis, respectively. The sulfur atoms create tetrahedral coordination sphere around the Ge1 and create octahedral sphere around the Ge2. The shortest Ge–S distances are 0.207 and 0.251 nm. The S1 atom is located outside a trigonal bipyramid (i.e., to say, the pyramid is centered outside) formed by 3Dy and 2Ge atoms. S2 and S3 atoms have CN = 4 and a tetrahedral arrangement, coordinated by 3Dy and 1Ge atoms. The increase of the Ge content observed for some compounds with the $Dy_3Ge_{1.25}S_7$ structure type can be explained by the reduction of the Ge charge (Zeng et al., 2008).

3.6.2 Structure type La_2GeS_5

Structure type La_2GeS_5 (Mazurier and Etienne, 1973) (Figure 2, Table 7). SG $P2_1/c$, $Z = 4$, $a = 0.7641$, $b = 1.2702$, $c = 0.7893$ nm, $\beta = 101.39^\circ$. The La1 and La2 atoms are located in bi- and tricapped trigonal prisms, respectively. The shortest La–S distance is 0.2833 nm. The germanium atoms are located in tetrahedra formed by the S atoms. The shortest Ge–S distance is 0.2181 nm. S1, S3, and S5 atoms are located in the tetrahedral arrangement of 3La and 1Ge atoms. The S2 atom is also located in a tetrahedron; however, this CP is formed exclusively by the La atoms. The S4 atom is located in a trigonal bipyramid composed by 3La and 2Ge atoms.

TABLE 5 Crystallographic data for ternary rare earth indium chalcogenides

Compound	Structure type	Space group	Lattice parameters (nm)			Reference(s)
			<i>a</i>	<i>b</i>	<i>c</i>	
Sc ₃ InS ₆	La ₃ InS ₆	<i>Pnmm</i>	1.374	1.676	0.390	Aliev (1980)
Y ₃ InS ₆	La ₃ InS ₆	<i>Pnmm</i>	1.378	1.682	0.398	Aliev (1980)
Y ₄ In ₅ S ₁₃	Nd ₄ In ₅ S ₁₃	<i>Pbam</i>	1.165	2.116	0.394	Aliev (1980)
La ₃ InS ₆	La ₃ InS ₆	<i>P2₁2₁2</i>	1.3946	1.6912	0.4079	Carré et al. (1978)
La ₃ In _{1.67} S ₇	Ce ₃ Al _{1.67} S ₇	<i>P6₃</i>	1.0196	–	0.62792	Gulay et al. (2008d)
La ₄ In ₅ S ₁₃	Nd ₄ In ₅ S ₁₃	<i>Pbam</i>	1.1843	2.1393	0.4061	Guseinov et al. (1979a)
La _{3.92} In _{4.76} S ₁₃	La _{3.92} In _{4.76} S ₁₃	<i>Pbam</i>	1.1814	2.1280	0.40384	Gulay et al. (2008d)
Ce ₃ InS ₆	La ₃ InS ₆	<i>Pnmm</i>	1.3944	1.691	0.4081	Aliev (1980)
Ce ₄ In ₅ S ₁₃	Nd ₄ In ₅ S ₁₃	<i>Pbam</i>	1.181	2.130	0.399	Aliev (1980)
Ce _{3.88} In _{4.79} S ₁₃	La _{3.92} In _{4.76} S ₁₃	<i>Pbam</i>	1.1794	2.1247	0.39933	Gulay et al. (2008d)
Pr ₃ InS ₆	La ₃ InS ₆	<i>Pnmm</i>	1.392	1.689	0.407	Aliev (1980)
Pr ₄ In ₅ S ₁₃	Nd ₄ In ₅ S ₁₃	<i>Pbam</i>	1.199	2.126	0.399	Aliev (1980)
Pr _{3.92} In _{4.76} S ₁₃	La _{3.92} In _{4.76} S ₁₃	<i>Pbam</i>	1.1758	2.1197	0.39695	Gulay et al. (2008d)
Nd ₃ InS ₆	La ₃ InS ₆	<i>Pnmm</i>	1.390	1.687	0.404	Aliev (1980)
Nd ₄ In ₅ S ₁₃	Nd ₄ In ₅ S ₁₃	<i>Pbam</i>	1.1774	2.1254	0.3968	Guseinov et al. (1979b)
Nd _{3.90} In _{4.76} S ₁₃	La _{3.92} In _{4.76} S ₁₃	<i>Pbam</i>	1.1754	2.1211	0.39514	Gulay et al. (2008d)
Sm ₃ InS ₆	U ₃ ScS ₆	<i>Pnmm</i>	1.3632	1.6513	0.3901	Messain et al. (1977)
Sm ₄ In ₅ S ₁₃	Nd ₄ In ₅ S ₁₃	<i>Pbam</i>	1.173	2.120	0.395	Aliev (1980)
EuIn ₂ S ₄	SrAl ₂ Se ₄	<i>Cccm</i>	0.650	1.049	1.036	Aliev et al. (1976)
Gd ₃ InS ₆	U ₃ ScS ₆	<i>Pnmm</i>	1.3544	1.6502	0.38686	Gulay et al. (2008d)
Gd ₄ In ₅ S ₁₃	Nd ₄ In ₅ S ₁₃	<i>Pbam</i>	1.171	2.117	0.393	Aliev (1980)
Tb ₃ InS ₆	La ₃ InS ₆	<i>Pnmm</i>	1.384	1.684	0.4014	Aliev (1980)
Tb ₄ In ₅ S ₁₃	Nd ₄ In ₅ S ₁₃	<i>Pbam</i>	1.170	2.115	0.393	Aliev (1980)

(continued)

Table 5 (continued)

Compound	Structure type	Space group	Lattice parameters (nm)			Reference(s)
			<i>a</i>	<i>b</i>	<i>c</i>	
Tb ₃ In ₅ S ₁₂	Tb ₃ In ₅ S ₁₂	<i>P2₁/m</i>	1.0998	2.1259 $\beta = 96.36^\circ$	0.3897	Carré (1977)
Dy ₃ InS ₆	La ₃ InS ₆	<i>Pnmm</i>	1.382	1.682	0.400	Aliev (1980)
Dy ₄ In ₅ S ₁₃	Nd ₄ In ₅ S ₁₃	<i>Pbam</i>	1.169	2.114	0.392	Aliev (1980)
Ho ₃ InS ₆	La ₃ InS ₆	<i>Pnmm</i>	1.376	1.680	0.396	Aliev (1980)
Ho ₄ In ₅ S ₁₃	Nd ₄ In ₅ S ₁₃	<i>Pbam</i>	1.168	2.111	0.392	Aliev (1980)
Er ₃ InS ₆	La ₃ InS ₆	<i>Pnmm</i>	1.374	1.679	0.394	Aliev (1980)
Er ₄ In ₅ S ₁₃	Nd ₄ In ₅ S ₁₃	<i>Pbam</i>	1.167	2.103	0.390	Aliev (1980)
Tm ₃ InS ₆	La ₃ InS ₆	<i>Pnmm</i>	1.372	1.677	0.390	Aliev (1980)
Yb ₃ InS ₆	La ₃ InS ₆	<i>Pnmm</i>	1.370	1.675	0.387	Aliev (1980)
Yb _{4/3} In _{4/3} S ₄	Yb ₂ FeS ₄	<i>Fd$\bar{3}m$</i>	1.0873	–	–	Likforman and Guittard (1993)
Yb ₁₈ In _{7.33} S ₃₆	Yb ₁₈ In _{7.33} S ₃₆	<i>P6₃/m</i>	2.0688	–	0.3861	Lemoine et al. (1989)
YbIn ₂ S ₄	YbIn ₂ S ₄	<i>P3</i>	2.0859	–	0.38743	Amirov et al. (1984)
YbIn ₂ S ₄	SrAl ₂ Se ₄	<i>Cccm</i>	1.040	0.618	1.052	Aliev et al. (1976)
Lu ₃ InS ₆	La ₃ InS ₆	<i>Pnmm</i>	1.367	1.672	0.386	Aliev (1980)
La ₃ In _{1.67} Se ₇	Ce ₃ Al _{1.67} S ₇	<i>P6₃</i>	1.050	–	0.650	Patrie and Guittard (1969)
La ₄ In _{4.67} Se ₁₃	La ₄ In _{4.67} Se ₁₃	<i>Pbam</i>	1.2442	2.2146	0.41969	Gulay et al. (2007c)
Ce ₄ In _{4.67} Se ₁₃	La ₄ In _{4.67} Se ₁₃	<i>Pbam</i>	1.23725	2.2144	0.41463	Gulay et al. (2007c)
Ce ₃ InSe ₆	U ₃ ScS ₆	<i>Pnmm</i>	1.75642	1.43792	0.41681	Huch et al. (2006a)
Pr ₃ InSe ₆	U ₃ ScS ₆	<i>Pnmm</i>	1.7413	1.4275	0.4109	Aleandri and Ibers (1989)
Nd ₃ InSe ₆	U ₃ ScS ₆	<i>Pnmm</i>	1.74343	1.42766	0.40995	Huch et al. (2006a)
Sm ₃ InSe ₆	U ₃ ScS ₆	<i>Pnmm</i>	1.4177	1.7352	0.40625	Tougait and Ibers (2000)
EuIn ₂ Se ₄	SrAl ₂ Se ₄	<i>Cccm</i>	0.670	1.110	1.088	Aliev et al. (1976)
Gd ₃ InSe ₆	U ₃ ScS ₆	<i>Pnmm</i>	1.4071	1.7286	0.40202	Tougait and Ibers (2000)
YbIn ₂ Se ₄	SrAl ₂ Se ₄	<i>Cccm</i>	0.636	1.080	1.094	Aliev et al. (1976)

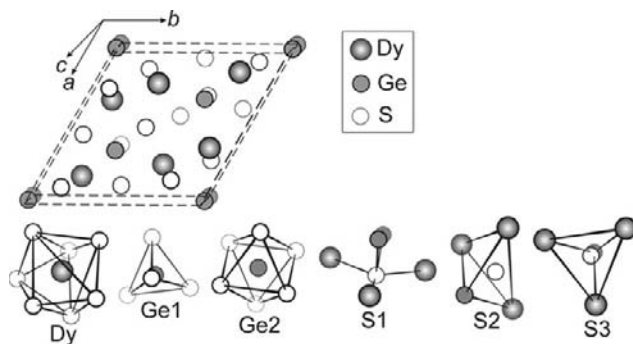


FIGURE 1 Crystal structure of $\text{Dy}_3\text{Ge}_{1.25}\text{S}_7$ and CPs of atoms.

TABLE 6 Atomic parameters for $\text{Dy}_3\text{Ge}_{1.25}\text{S}_7$

Atom	Position	Fractional coordinates			Atomic arrangement
		<i>x</i>	<i>y</i>	<i>z</i>	
Dy	6c	0.359	0.140	0.250	7S
Ge1	2b	1/3	2/3	0.175	4S
Ge2 ^a	2a	0	0	0.047	6S
S1	6c	0.251	0.100	0.818	3Dy 2Ge
S2	6c	0.523	0.427	0.504	3Dy 1Ge
S3	2b	1/3	2/3	0.531	3Dy 1Ge

^a Occupancy 25%.

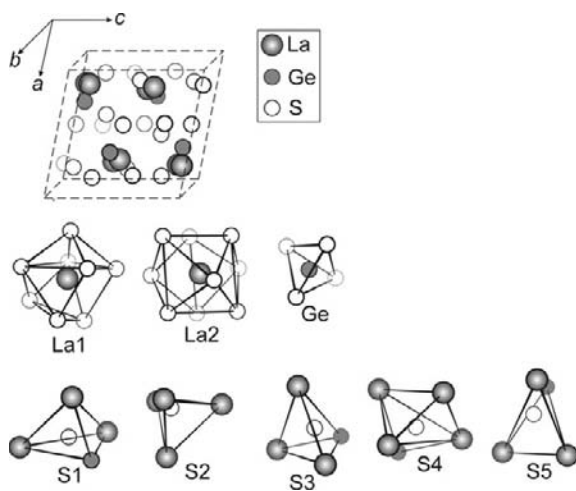
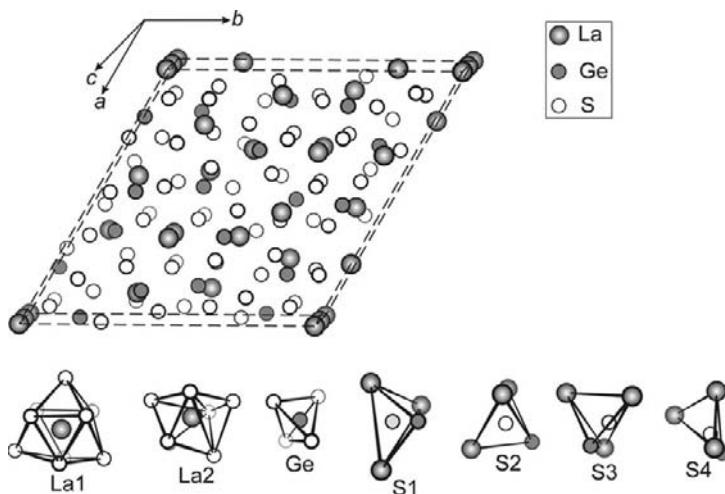


FIGURE 2 Crystal structure of La_2GeS_5 and CPs of atoms.

TABLE 7 Atomic parameters for La_2GeS_5

Atom	Position	Fractional coordinates			Atomic arrangement	
		x	y	z		
La1	4e	0.2395	0.0935	0.0419	8S	
La2	4e	0.8401	0.1667	0.3649	9S	
Ge	4e	0.3380	0.1165	0.5912	4S	
S1	4e	0.1706	0.0259	0.3815	3La	1Ge
S2	4e	0.8613	0.3790	0.5004	4La	
S3	4e	0.5784	0.0061	0.2163	3La	1Ge
S4	4e	0.1287	0.2051	0.6977	4La	1Ge
S5	4e	0.5349	0.2326	0.5474	3La	1Ge

**FIGURE 3** Crystal structure of $\text{La}_4\text{Ge}_3\text{S}_{12}$ and CPs of atoms.

3.6.3 Structure type $\text{La}_4\text{Ge}_3\text{S}_{12}$

Structure type $\text{La}_4\text{Ge}_3\text{S}_{12}$ (Mazurier and Etienne, 1974) (Figure 3, Table 8). SG $R3c$, $Z = 6$, $a = 1.940$, $c = 0.810$ nm. The sulfur atoms create tri- and monocapped trigonal prismatic arrangement around the La1 and La2 atoms, respectively. The shortest La–S distance is 0.2864 nm. The Ge atoms are situated in tetrahedral arrangement of the S atoms. The shortest Ge–S distance is 0.2193 nm. Tetrahedrally shaped coordination sphere of each of the four independent sulfur atoms is formed by 3La and 1Ge atoms.

TABLE 8 Atomic parameters for $\text{La}_4\text{Ge}_3\text{S}_{12}$

Atom	Position	Fractional coordinates			Atomic arrangement	
		x	y	z		
La1	6a	0	0	0	9S	
La2	18b	0.0030	0.2307	0.2028	7S	
Ge	18b	0.2000	0.1875	0.1523	4S	
S1	18b	0.1549	0.3789	0.1618	3La	1Ge
S2	18b	0.1246	0.0643	0.2511	3La	1Ge
S3	18b	0.1145	0.2005	0.9974	3La	1Ge
S4	18b	0.3960	0.0593	0.1817	3La	1Ge

3.6.4 Structure type $\text{Ce}_6\text{Si}_4\text{S}_{17}$

Structure type $\text{Ce}_6\text{Si}_4\text{S}_{17}$ (Gauthier et al., 2003) (Figure 4, Table 9). SG $P\bar{1}$, $Z = 4$, $a = 0.89576$, $b = 1.00022$, $c = 1.4265$ nm, $\alpha = 82.188^\circ$, $\beta = 86.889^\circ$, $\gamma = 89.515^\circ$. The Ce4 atom is located in monocapped trigonal prismatic arrangement of the sulfur atoms. The Ce1, Ce3, Ce5, and Ce6 atoms are situated in bicapped trigonal prisms, while the Ce2 atom has tricapped trigonal prismatic surrounding. The shortest Ce–S distance is 0.2771 nm. Each silicon atom has tetrahedral coordination sphere made of the S atoms and the shortest Si–S distance equals to 0.2076 nm. Each of the S6, S7, S13, S15, and S17 atoms has triangular surroundings of 1Si and 2Ce atoms. The S2 atom is located in a tetragonal pyramid formed by 4Ce and 1Si atoms. The remaining sulfur atoms have tetrahedral coordination spheres. However, the S9 and S16 atoms are located outside of the tetrahedra.

3.6.5 Structure type Sr_2GeS_4

Structure type Sr_2GeS_4 (Ribes et al., 1970) (Figure 5, Table 10). SG $P2_1/m$, $Z = 2$, $a = 0.6524$, $b = 0.6591$, $c = 0.8205$ nm, $\beta = 108.29^\circ$ for Eu_2SiS_4 (Johrendt and Pocha, 2001). Two independent europium atoms have trigonal prismatic surroundings made of the sulfur atoms. The shortest Eu–S distance is 0.2940 nm. One independent silicon atom is located in a tetrahedron formed by the S atoms. The shortest Si–S distance is 0.2121 nm. Three crystallographically independent sulfur atoms are located in trigonal bipyramids formed by 4Eu and 1Si atoms.

3.6.6 Structure type $\text{Tb}_4\text{Si}_3\text{S}_{12}$

Structure type $\text{Tb}_4\text{Si}_3\text{S}_{12}$ (Hatscher and Umland, 2002a) (Figure 6, Table 11). SG $P2_1/n$, $Z = 4$, $a = 0.9836$, $b = 1.0964$, $c = 1.6361$ nm, $\beta = 102.76^\circ$.

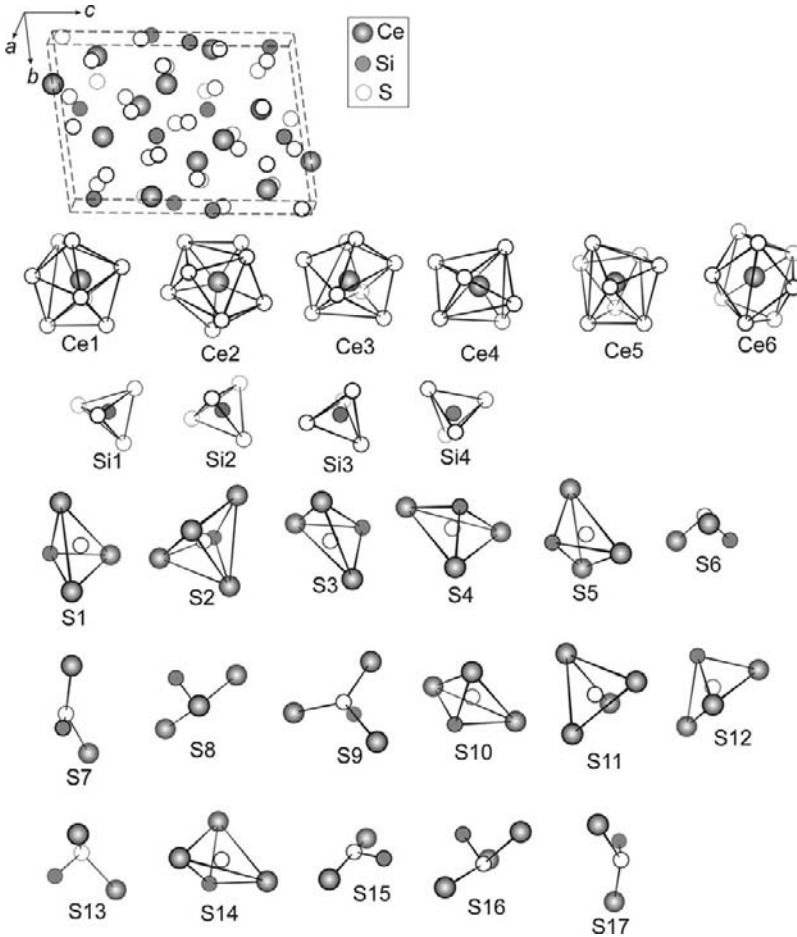


FIGURE 4 Crystal structure of $Ce_6Si_4S_{17}$ and CPs of atoms.

The sulfur atoms create bicapped trigonal prismatic arrangement around the Tb1, Tb2, and Tb3 atoms. Monocapped trigonal prism occurs only around the Tb4 atoms. The shortest Tb–S distance is 0.2692 nm. The silicon atom is located in a tetrahedron formed by the S atoms. The shortest Si–S distance is 0.2059 nm. The S1, S3, S6, S10, and S11 atoms have triangular surroundings formed by 2Tb and 1Si atoms. All other independent sulfur atoms have tetrahedral coordination spheres. Several of them, that is the S2, S4, S5, S7, and S8 atoms are located outside their respective tetrahedra. Each CP of the sulfur atom is formed by 3Tb and 1Si atoms.

TABLE 9 Atomic parameters for $\text{Ce}_6\text{Si}_4\text{S}_{17}$

Atom	Position	Fractional coordinates			Atomic arrangement
		x	y	z	
Ce1	2i	0.47753	0.73133	0.54087	8S
Ce2	2i	0.58162	0.57886	0.16660	9S
Ce3	2i	0.83025	0.91349	0.34206	8S
Ce4	2i	0.12796	0.43096	0.32673	7S
Ce5	2i	0.39393	0.11542	0.18165	8S
Ce6	2i	0.94665	0.23952	0.00062	8S
Si1	2i	0.2500	0.0000	0.4154	4S
Si2	2i	0.2487	0.4410	0.0773	4S
Si3	2i	0.7311	0.9382	0.0987	4S
Si4	2i	0.7735	0.5567	0.3949	4S
S1	2i	0.8407	0.5015	0.0567	3Ce 1Si
S2	2i	0.4863	0.0036	0.3771	4Ce 1Si
S3	2i	0.3159	0.5179	0.4673	3Ce 1Si
S4	2i	0.6059	0.7000	0.3460	3Ce 1Si
S5	2i	0.1785	0.0192	0.0428	3Ce 1Si
S6	2i	0.7972	0.4107	0.3047	2Ce 1Si
S7	2i	0.5097	0.8719	0.1133	2Ce 1Si
S8	2i	0.2415	0.6149	0.1498	3Ce 1Si
S9	2i	0.4578	0.3527	0.0476	3Ce 1Si
S10	2i	0.1145	0.2886	0.1605	3Ce 1Si
S11	2i	0.4282	0.3547	0.2790	4Ce
S12	2i	0.2054	0.1905	0.4598	3Ce 1Si
S13	2i	0.1883	0.8649	0.5373	2Ce 1Si
S14	2i	0.8674	0.7844	0.1666	3Ce 1Si
S15	2i	0.1445	-0.0297	0.2926	2Ce 1Si
S16	2i	0.7477	0.1134	0.1681	3Ce 1Si
S17	2i	0.9818	0.6520	0.3981	2Ce 1Si

3.6.7 Structure type Hf_5CuSn_3

Structure type Hf_5CuSn_3 (Rieger et al., 1965) (Figure 7, Table 12). SG $P6_3/mcm$, $Z = 2$, $a = 0.8992$, $c = 0.7031$ nm for $\text{La}_5\text{Ge}_3\text{S}$ (Guloy and Corbett, 1993). Four chalcogenides of rare earths with structure type Hf_5CuSn_3 are known. The atomic parameters of these compounds are not refined. The La1 atom is situated in 13-vertex polyhedron formed by 6La, 5Ge, and 2S atoms. The La2 atom is surrounded by a bicapped hexagonal prism formed by 8La and 6Ge atoms. The Ge atom is located in a nine-vertex polyhedron formed by 9La atoms. The S atom has octahedral coordination sphere formed by 6La atoms.

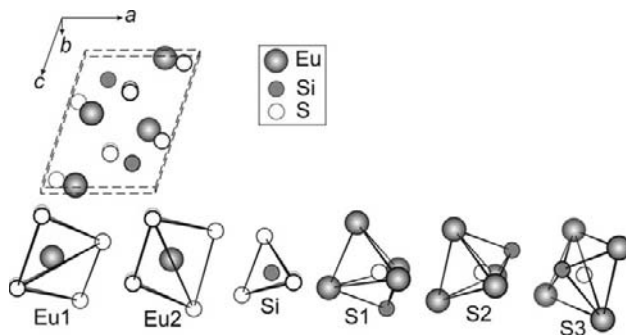


FIGURE 5 Crystal structure of Eu_2SiS_4 (structure type Sr_2GeS_4) and CPs of atoms.

TABLE 10 Atomic parameters for Eu_2SiS_4

Atom	Position	Fractional coordinates			Atomic arrangement
		x	y	z	
Eu1	2e	0.71526	1/4	0.04825	6S
Eu2	2e	0.77759	1/4	0.57195	6S
Si1	2e	0.2807	1/4	0.2040	4S
S1	2e	0.1140	1/4	-0.0638	4Eu 1Si
S2	2e	0.0833	1/4	0.3663	4Eu 1Si
S3	4f	0.4948	-0.0010	0.26449	4Eu 1Si

3.6.8 Structure type $\beta\text{-CaSiO}_3$

Structure type $\beta\text{-CaSiO}_3$ (Trojer, 1968) (Figure 8, Table 13). SG $P\bar{1}$, $Z = 6$, $a = 0.8468$, $b = 1.176$, $c = 0.8389$ nm, $\alpha = 90.49^\circ$, $\beta = 104.56^\circ$, $\gamma = 69.52^\circ$ for EuGeS_3 (Bugli et al., 1978). The coordination sphere of the Eu1 atom is octahedrally shaped, but the Eu2 and Eu3 atoms are located inside mono- and bicapped trigonal prisms. The shortest Eu–S distance is 0.2911 nm. Each of the three germanium atoms is situated in a tetrahedron formed by 4S atoms. The shortest Ge–S distance is 0.2150 nm. Three of the sulfur atoms, that is S1, S5, and S8 atoms, have triangular surroundings formed by 1Eu and 2Ge atoms. The other six crystallographically independent sulfur atoms are located in various tetrahedra formed by 3Eu and 1Ge atoms.

3.6.9 Structure type Eu_2GeS_4

Structure type Eu_2GeS_4 (Bugli et al., 1979) (Figure 9, Table 14). SG $P2_1$, $Z = 2$, $a = 0.6638$, $b = 0.6672$, $c = 0.8146$ nm, $\beta = 108.20^\circ$. The sulfur atoms create monocapped trigonal prismatic arrangement around both

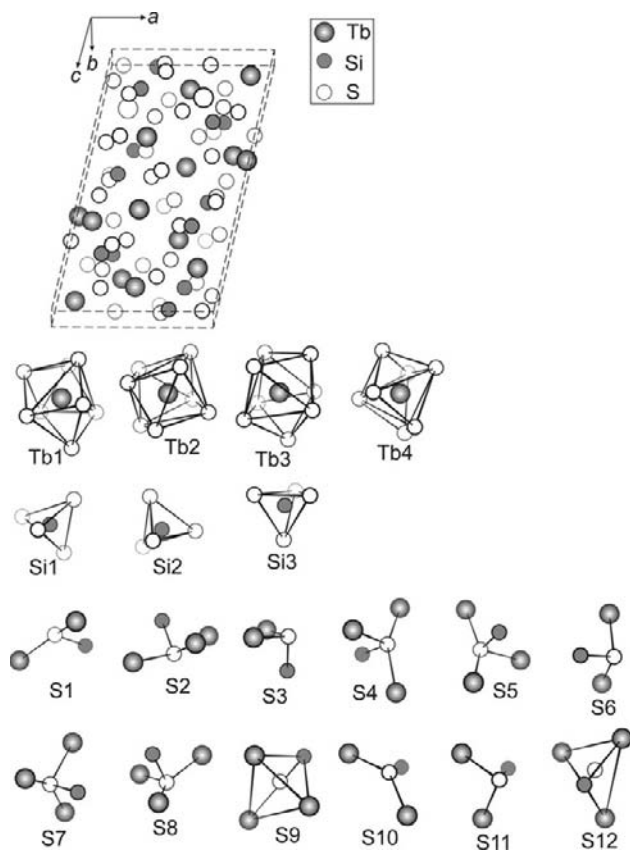


FIGURE 6 Crystal structure of $Tb_4Si_3S_{12}$ and CPs of atoms.

of the symmetry independent Eu atoms. The shortest Eu–S distance is 0.2950 nm. Ge atom is situated in a tetrahedron formed by the S atoms, and the shortest Ge–S distance is 0.2191 nm. All of the S atoms are located in trigonal bipyramids formed by 4Eu and 1Ge atoms.

3.6.10 Structure type $Sr_2Ge_2Se_5$

Structure type $Sr_2Ge_2Se_5$ (Johrendt and Tampier, 2000) (Figure 10, Table 15). SG $P2_1/n$, $Z = 4$, $a = 0.8421$, $b = 1.2235$, $c = 0.9127$ nm, $\beta = 93.67^\circ$ for $Eu_2Ge_2Se_5$ (Tampier et al., 2002). The Eu1 and Eu2 atoms are situated in tri- and bicapped trigonal prisms, respectively. The shortest Eu–Se distance is 0.3054 nm. Each of the two independent Ge atoms is situated in a tetrahedron formed by 3Se and 1Ge atoms, and the shortest Ge–S distance is 0.2319 nm. In this structure, close Ge1–Ge2 contacts (0.2431 nm) exist. The Se1 atom is located outside its coordinating

TABLE 11 Atomic parameters for $\text{Tb}_4\text{Si}_3\text{S}_{12}$

Atom	Position	Fractional coordinates			Atomic arrangement	
		x	y	z		
Tb1	4e	0.6108	0.9836	0.1250	8S	
Tb2	4e	0.8768	0.6523	0.0599	8S	
Tb3	4e	0.5316	0.3768	0.1306	8S	
Tb4	4e	0.3225	0.7601	0.2891	7S	
Si1	4e	0.2220	0.5540	0.1173	4S	
Si2	4e	0.7003	0.8839	-0.0607	4S	
Si3	4e	0.7090	0.7163	0.2332	4S	
S1	4e	0.5047	0.7781	0.1889	2Tb	1Si
S2	4e	0.4191	0.1531	0.1838	3Tb	1Si
S3	4e	0.7482	0.2131	0.1359	2Tb	1Si
S4	4e	0.8474	0.8363	0.1879	3Tb	1Si
S5	4e	0.6124	0.7606	0.0133	3Tb	1Si
S6	4e	0.9097	0.8473	-0.0535	2Tb	1Si
S7	4e	0.0429	0.4369	0.0943	3Tb	1Si
S8	4e	0.3497	0.4807	0.2285	3Tb	1Si
S9	4e	0.6661	0.4733	-0.0228	3Tb	1Si
S10	4e	0.1516	0.7318	0.1264	2Tb	1Si
S11	4e	0.6580	0.0587	-0.0276	2Tb	1Si
S12	4e	0.7567	0.5432	0.1878	3Tb	1Si

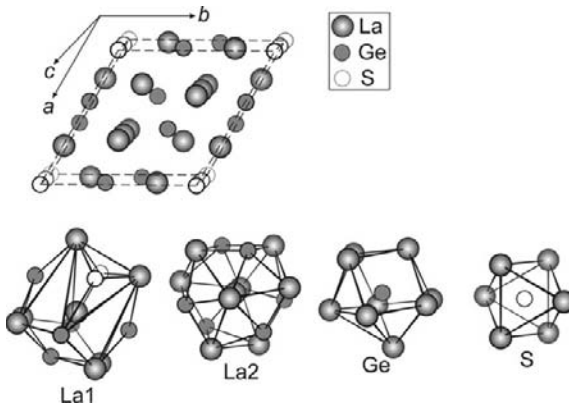
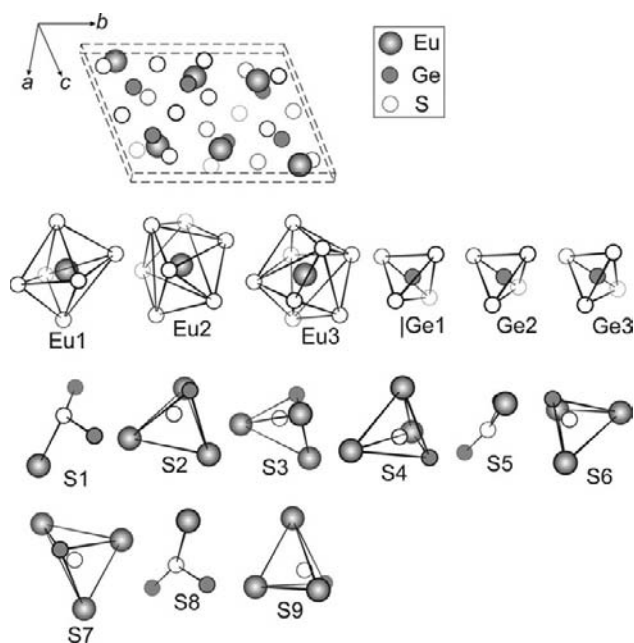
**FIGURE 7** Crystal structure of $\text{La}_5\text{Ge}_3\text{S}$ (structure type Hf_5CuSn_3) and CPs of atoms.

TABLE 12 Atomic parameters for $\text{La}_5\text{Ge}_3\text{S}^a$

Atom	Position	Fractional coordinates			Atomic arrangement		
		x	y	z			
La1	6g	0.27	0	1/4	6La	5Ge	2S
La2	4d	1/3	2/3	0	8La	6Ge	
Ge	6g	0.62	0	1/4	9La		
S	2b	0	0	0	6La		

^a Atomic coordinates are as for the structure Hf_5CuSn_3 (Rieger et al. 1965).

**FIGURE 8** Crystal structure of EuGe_3 (structure type $\beta\text{-CaSiO}_3$) and CPs of atoms.

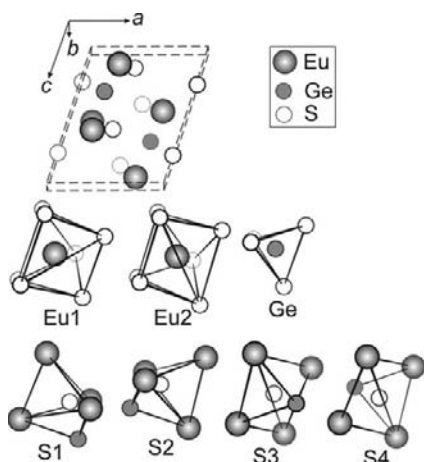
tetrahedron formed by 3Eu and 1Ge atoms. The Se2, Se3, and Se5 atoms are situated in tetragonal pyramids formed by 4Eu and 1Ge atoms. The Se4 atom has triangular surroundings of the 1Eu and 2Ge atoms.

3.6.11 Structure type La_2SnS_5

Structure type La_2SnS_5 (Jaulmes, 1974) (Figure 11, Table 16). SG $Pbam$, $Z = 2$, $a = 0.7915$, $b = 1.122$, $c = 0.396$ nm. The lanthanum atom is situated in a tricapped trigonal prism formed by the S atoms. The shortest

TABLE 13 Atomic parameters for EuGeS_3

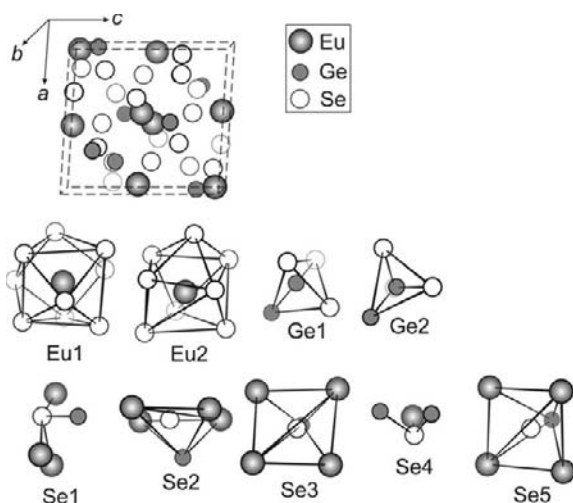
Atom	Position	Fractional coordinates			Atomic arrangement	
		<i>x</i>	<i>y</i>	<i>z</i>		
Eu1	<i>2i</i>	0.76017	0.18730	0.42324	6S	
Eu2	<i>2i</i>	0.12501	0.13791	0.10454	7S	
Eu3	<i>2i</i>	0.76033	0.49961	0.75341	8S	
Ge1	<i>2i</i>	0.64430	0.19535	0.90516	4S	
Ge2	<i>2i</i>	0.29381	0.18706	0.55366	4S	
Ge3	<i>2i</i>	0.25534	0.46771	0.76970	4S	
S1	<i>2i</i>	0.4950	0.0809	0.7815	1Eu	2Ge
S2	<i>2i</i>	0.8131	0.2349	0.7739	3Eu	1Ge
S3	<i>2i</i>	0.9346	0.4052	0.1216	3Eu	1Ge
S4	<i>2i</i>	0.3873	0.2338	0.3530	3Eu	1Ge
S5	<i>2i</i>	0.8148	0.0695	0.1184	1Eu	2Ge
S6	<i>2i</i>	0.1108	0.3510	0.6398	3Eu	1Ge
S7	<i>2i</i>	0.1392	0.0769	0.4563	3Eu	1Ge
S8	<i>2i</i>	0.6325	0.4613	0.3906	1Eu	2Ge
S9	<i>2i</i>	0.4629	0.3564	0.9930	3Eu	1Ge

**FIGURE 9** Crystal structure of Eu_2GeS_4 and CPs of atoms.

La–S distance is 0.2803 nm. The tin atom is located in an octahedral arrangement of the sulfur atoms. The shortest Sn–S distance is 0.2529 nm. The S1 atoms adopt a square coordination sphere of the four lanthanum atoms. The S2 and S3 atoms have five-coordination spheres.

TABLE 14 Atomic parameters for Eu_2GeS_4

Atom	Position	Fractional coordinates			Atomic arrangement	
		x	y	z		
Eu1	2a	0.21839	0.0000	0.55209	7S	
Eu2	2a	0.26732	-0.0022	0.06775	7S	
Ge	2a	0.2269	0.5157	0.2999	4S	
S1	2a	0.5968	0.0389	0.4233	4Eu	1Ge
S2	2a	0.4217	0.5302	0.1262	4Eu	1Ge
S3	2a	0.0154	0.2552	0.2424	4Eu	1Ge
S4	2a	0.0054	0.2628	0.7641	4Eu	1Ge

**FIGURE 10** Crystal structure of $\text{Eu}_2\text{Ge}_2\text{Se}_5$ (structure type $\text{Sr}_2\text{Ge}_2\text{Se}_5$) and CPs of atoms.

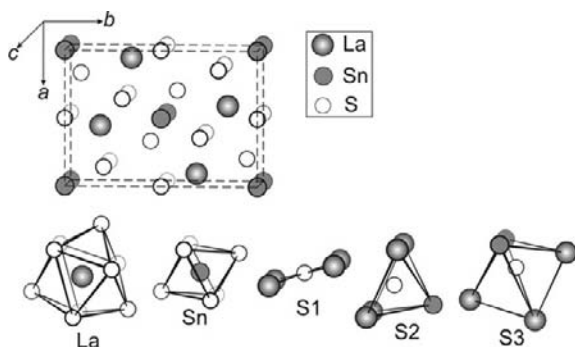
The CP of the former is a tetragonal pyramid ($4\text{La} + 1\text{Sn}$) and the CP of the latter is a trigonal bipyramid ($3\text{La} + 2\text{Sn}$).

3.6.12 Structure type Eu_2SnS_5

Structure type Eu_2SnS_5 (Jaulmes et al., 1982) (Figure 12, Table 17). SG $Pbam$, $Z = 4$, $a = 1.1507$, $b = 1.5612$, $c = 0.4100$ nm. The two independent europium atoms are situated in trigonal prisms with four additional atoms, formed exclusively by the sulfur atoms. The shortest Eu-S distance is 0.2997 nm. The tin atom occupies two positions, Sn1 and Sn2. The sulfur atoms form a tetrahedron and an octahedron around the Sn1 and Sn2 atoms, respectively. The shortest Sn-S distance is 0.2322 nm. The S1 and

TABLE 15 Atomic parameters for $\text{Eu}_2\text{Ge}_2\text{Se}_5$

Atom	Position	Fractional coordinates			Atomic arrangement	
		x	y	z		
Eu1	4e	0.0434	0.1625	0.0302	9Se	
Eu2	4e	0.5588	0.3040	0.0208	8Se	
Ge1	4e	0.4934	0.0505	0.3351	3Se	1Ge
Ge2	4e	0.7999	0.4796	0.3131	3Se	1Ge
Se1	4e	0.2032	0.4423	0.4556	3Eu	1Ge
Se2	4e	0.5360	0.5076	0.2157	4Eu	1Ge
Se3	4e	0.3136	0.2133	0.7913	4Eu	1Ge
Se4	4e	0.1590	0.4104	0.0591	1Eu	2Ge
Se5	4e	0.3423	0.2057	0.2780	4Eu	1Ge

**FIGURE 11** Crystal structure of La_2SnS_5 and CPs of atoms.**TABLE 16** Atomic parameters for La_2SnS_5

Atom	Position	Fractional coordinates			Atomic arrangement	
		x	y	z		
La	4h	0.07434	0.33106	1/2	9S	
Sn	2a	0	0	0	6S	
S1	2c	0	1/2	0	4La	
S2	4g	0.3571	0.2984	0	4La	1S
S3	4h	0.1869	0.0694	1/2	3La	2S

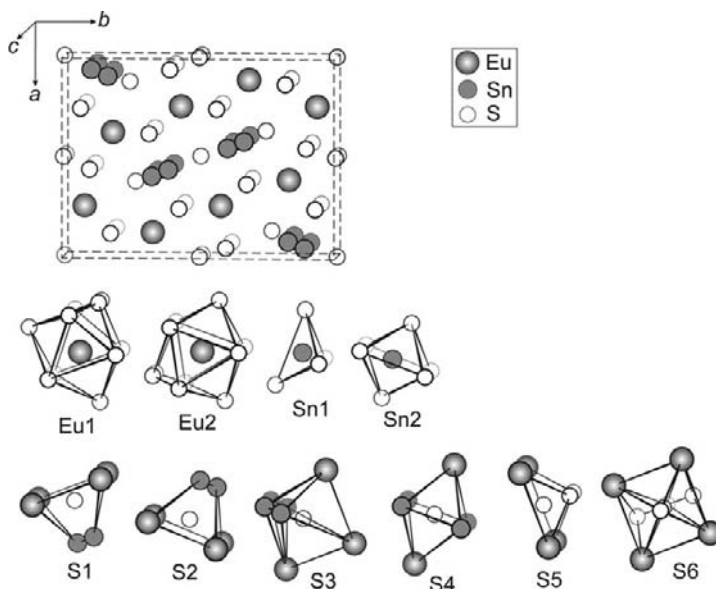


FIGURE 12 Crystal structure of Eu_2SnS_5 and CPs of atoms.

TABLE 17 Atomic parameters for Eu_2SnS_5

Atom	Position	Fractional coordinates			Atomic arrangement	
		<i>x</i>	<i>y</i>	<i>z</i>		
Eu1	4 <i>h</i>	0.2511	0.42716	1/2	10S	
Eu2	4 <i>h</i>	0.38273	0.1769	1/2	10S	
Sn1 ^a	4 <i>g</i>	0.0882	0.1692	0	4S	
Sn2 ^a	4 <i>g</i>	0.0553	0.1088	0	6S	
S1	4 <i>g</i>	0.3747	0.3209	0	4Eu	1Sn
S2	4 <i>g</i>	0.2498	0.0693	0	4Eu	1Sn
S3	4 <i>h</i>	0.1283	0.2394	1/2	3Eu	2Sn
S4	2 <i>b</i>	0	0	1/2	2Eu	4Sn
S5	4 <i>g</i>	0.0545	0.3975	0	4Eu	1S
S6 ^a	4 <i>f</i>	0	1/2	0.277	4Eu	4S

^a Occupancy 50%.

S2 atoms are located in tetragonal pyramids formed by 4Eu and 1Sn atoms. The S3 atom is located in a trigonal bipyramid formed by 3Eu and 2Sn atoms. The S4 atom has octahedral surroundings formed by 2Eu and 4Sn atoms. A close S5–S6 contact (0.2061 nm) exists in this structure

type. Since S6 atoms occupy a disordered position, each S5 atom is located in a tetragonal pyramid formed by 4Eu and 1S atoms. The S6 atom has bicapped trigonal prismatic surroundings (4Eu + 4S).

3.6.13 Structure type $\text{Eu}_3\text{Sn}_2\text{S}_7$

Structure type $\text{Eu}_3\text{Sn}_2\text{S}_7$ (Jaulmes and Julien-Pouzol, 1977a) (Figure 13, Table 18). SG $Pbam$, $Z = 2$, $a = 1.1542$, $b = 1.2690$, $c = 0.3974$ nm. The sulfur atoms create, respectively, distorted cubic and monocapped

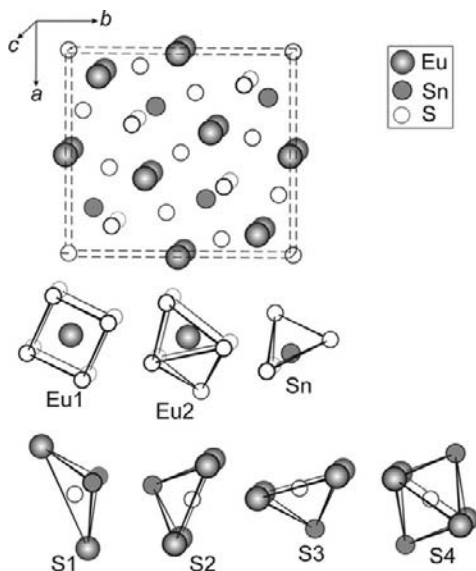


FIGURE 13 Crystal structure of $\text{Eu}_3\text{Sn}_2\text{S}_7$ and CPs of atoms.

TABLE 18 Atomic parameters for $\text{Eu}_3\text{Sn}_2\text{S}_7$

Atom	Position	Fractional coordinates			Atomic arrangement	
		x	y	z		
Eu1	2c	0	1/2	0	8S	
Eu2	4g	0.38672	0.64649	0	7S	
Sn	4h	0.2737	0.38827	1/2	4S	
S1	4g	0.3482	0.2951	0	2Eu	2Sn
S2	4h	0.2951	0.0647	1/2	4Eu	1Sn
S3	4h	0.0757	0.3191	1/2	4Eu	1Sn
S4	2b	0	0	1/2	4Eu	2Sn

trigonal prismatic arrangements around the Eu1 and Eu2 atoms. The shortest Eu–S distance is 0.2989 nm. The tin atom is situated in a tetrahedron, and the shortest Sn–S distance is 0.2376 nm. The S1 atom has tetrahedral surroundings of 2Eu and 2Sn atoms. The S2 and S3 atoms are located in tetragonal pyramids (4Eu + 1Sn), and the S4 atom occupies octahedrally shape surroundings (4Eu + 2Sn).

3.6.14 Structure type $\text{Eu}_5\text{Sn}_3\text{S}_{12}$

Structure type $\text{Eu}_5\text{Sn}_3\text{S}_{12}$ (Jaulmes and Julien-Pouzol, 1977b) (Figure 14, Table 19). SG $Pmc2_1$, $Z = 2$, $a = 0.3924$, $b = 2.0212$, $c = 1.1509$ nm. The Eu5 atom is located inside a monocapped trigonal prism, and the other europium atoms have bicapped trigonal prismatic surroundings made of the sulfur atoms. The shortest Eu–S distance is 0.2810 nm. Two of the three independent tin atoms, that is Sn1 and Sn2, have octahedrally shaped surroundings, and the third—Sn3—atom has trigonal bipyramidal one. The shortest Sn–S distance is 0.2407 nm. The S1 atom is located in a

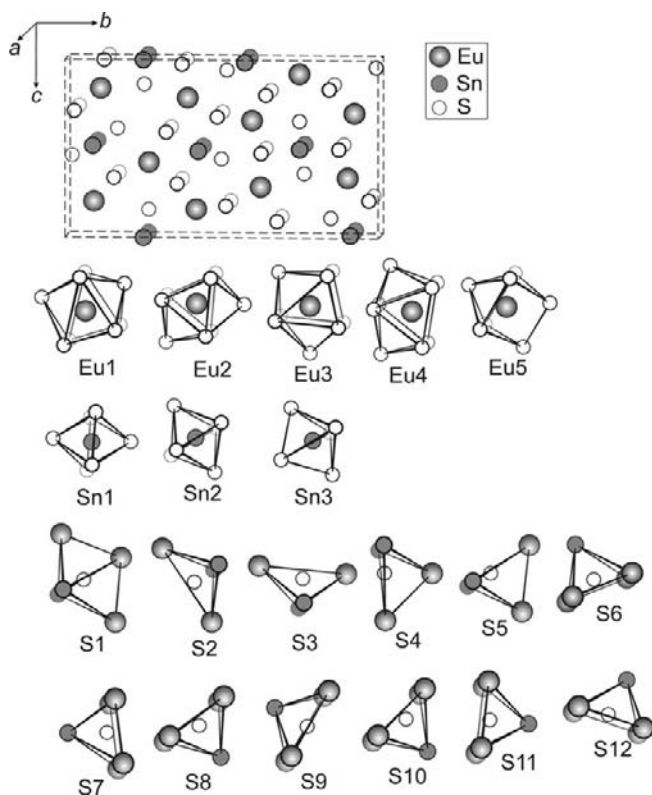


FIGURE 14 Crystal structure of $\text{Eu}_5\text{Sn}_3\text{S}_{12}$ and CPs of atoms.

TABLE 19 Atomic parameters for $\text{Eu}_5\text{Sn}_3\text{S}_{12}$

Atom	Position	Fractional coordinates			Atomic arrangement	
		x	y	z		
Eu1	2b	1/2	0.38383	0.2271	8S	
Eu2	2b	1/2	0.58892	0.3529	8S	
Eu3	2b	1/2	0.25954	0.5905	8S	
Eu4	2b	1/2	0.08403	0.8111	8S	
Eu5	2b	1/2	0.10598	0.1749	7S	
Sn1	2a	0	0.2505	0.0	6S	
Sn2	2a	0	0.0887	0.4834	6S	
Sn3	2a	0	0.5744	0.0128	5S	
S1	2b	1/2	0.0147	0.552	3Eu	2Sn
S2	2b	1/2	0.1596	0.4002	2Eu	2Sn
S3	2b	1/2	0.2447	0.1512	2Eu	2Sn
S4	2b	1/2	0.7407	0.356	2Eu	2Sn
S5	2b	1/2	0.5089	0.0703	2Eu	2Sn
S6	2a	0	0.0299	0.2875	4Eu	1Sn
S7	2a	0	0.1255	0.0001	4Eu	1Sn
S8	2a	0	0.1562	0.6624	4Eu	1Sn
S9	2a	0	0.3232	0.4062	4Eu	1Sn
S10	2a	0	0.6417	0.1967	4Eu	1Sn
S11	2a	0	0.374	0.0238	4Eu	1Sn
S12	2a	0	0.4865	0.3199	4Eu	1Sn

trigonal bipyramid formed by 3Eu and 2Sn atoms. The S2, S3, S4, and S5 atoms have tetrahedral surroundings of the (2Eu + 2Sn) atoms. The remaining sulfur atoms are located in tetragonal pyramids created by 4Eu and 1Sn atoms.

3.6.15 Structure type Eu_2SnS_4

Structure type Eu_2SnS_4 (Pocha et al., 2003) (Figure 15, Table 20). SG $Pnma$, $Z = 4$, $a = 1.1187$, $b = 0.8768$, $c = 0.7538$ nm. The single independent europium atom is located in a monocapped trigonal prism, and the shortest Eu–S distance is 0.2954 nm. The tin atom occupies inner position in a tetrahedron, and the shortest Sn–S distance is 0.2388 nm. The S1 and S2 atoms are located in tetragonal pyramids formed by 4Eu and 1Sn atoms. The nearest surrounding of the S3 atom is tetrahedral (3Eu + 1Sn).

3.6.16 Structure type Eu_2SnSe_5

Structure type Eu_2SnSe_5 (Evenson and Dorhout, 2001) (Figure 16, Table 21). SG $P2_12_12$, $Z = 8$, $a = 1.1990$, $b = 1.6425$, $c = 0.8543$ nm. All of the four independent europium atoms have similar tricapped trigonal

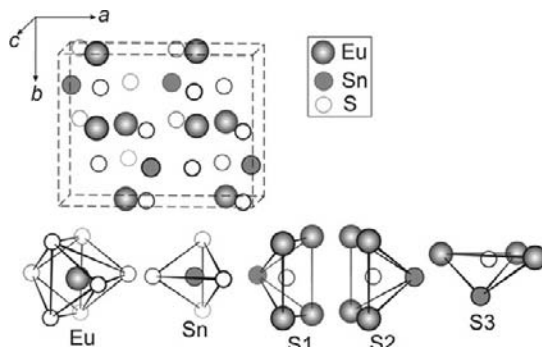


FIGURE 15 Crystal structure of Eu_2SnS_4 and CPs of atoms.

TABLE 20 Atomic parameters for Eu_2SnS_4

Atom	Position	Fractional coordinates			Atomic arrangement	
		x	y	z		
Eu	8d	0.3107	0.5049	0.3804	7S	
Sn	4c	0.0307	1/4	0.3888	4S	
S1	4c	0.1926	1/4	0.5995	4Eu	1Sn
S2	4c	0.3170	1/4	0.0955	4Eu	1Sn
S3	8d	0.0635	0.0184	0.2294	3Eu	1Sn

prismatic coordination spheres. The shortest Eu–Se distance is 0.3083 nm. The Sn1 and Sn2 atoms are located in octahedral and tetrahedral sites, respectively. The shortest Sn–Se distance is 0.2521 nm. The Se1, Se2, Se5, and Se6 atoms are inside of the respective tetragonal pyramids. Each CP is formed by 4Eu and 1Sn atoms. The Se3 and Se4 atoms are located in tetrahedrally shaped surroundings of 2Eu and 2Sn atoms. The Se7 and Se8 atoms are situated in tetragonal bipyramids formed by 4Eu and 2Se atoms. The Se9 and Se11 atoms are situated inside distorted octahedra formed by 3Eu, 2Sn, and 1Se atoms. The Se10 and Se12 atoms are situated in trigonal prisms formed by 4Eu and 2Se atoms.

3.6.17 Structure type CaFe_2O_4

Structure type CaFe_2O_4 (Hill et al., 1956) (Figure 17, Table 22). SG $Pnma$, $Z = 4$, $a = 1.1642$, $b = 0.3757$, $c = 1.3711$ nm for Sc_2PbS_4 (Shemet et al., 2006a). Both of the independent scandium atoms are located in octahedra formed by the S atoms. The shortest Sc–S distance is 0.2542 nm. The lead atom is located in a bicapped trigonal prismatic surrounding of the sulfur

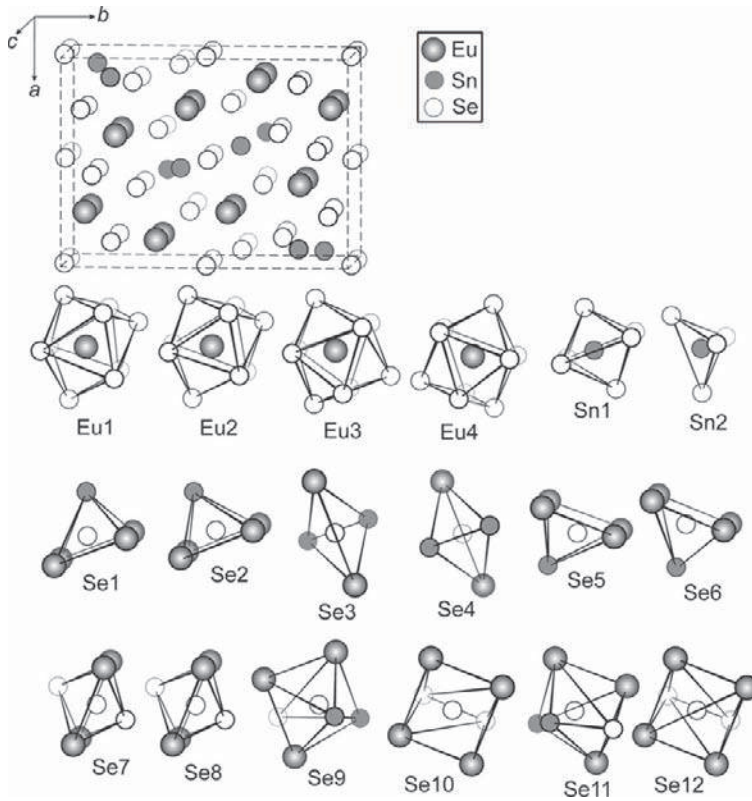


FIGURE 16 Crystal structure of Eu_2SnSe_5 and CPs of atoms.

atoms. The shortest Pb–S distance is 0.3026 nm. The S3 atom is located in a trigonal bipyramid formed by 3Sc and 2Pb atoms. The remaining three independent sulfur atoms occupy inner positions in tetragonal pyramids formed by 3Sc and 2Pb atoms.

3.6.18 Structure type Er_2PbS_4

Structure type Er_2PbS_4 (Gulay et al., 2008b) (Figure 18, Table 23). SG $Cmc2_1$, $Z = 16$, $a = 0.7863$, $b = 2.8525$, $c = 1.1995$ nm. All of the six independent erbium atoms are located in octahedral coordination spheres of the sulfur atoms, and the shortest Er–S distance is 0.263 nm. Each of the four independent lead atoms is located in monocapped trigonal prisms, and the shortest Pb–S distance is 0.276 nm. The Pb3 and Pb4 atoms occupy split position. The S1 and S12 atoms have tetrahedral surroundings, and the S2 atom is located in a trigonal bipyramid. The remaining crystallographically independent sulfur atoms have tetragonal pyramidal

TABLE 21 Atomic parameters for Eu_2SnSe_5

Atom	Position	Fractional coordinates			Atomic arrangement		
		x	y	z			
Eu1	4c	0.6153	0.8220	0.7447	9Se		
Eu2	4c	0.6171	0.8213	0.2414	9Se		
Eu3	4c	0.7473	0.5712	0.7581	9Se		
Eu4	4c	0.2483	0.9286	0.7394	9Se		
Sn1	4c	0.4464	0.6049	0.4996	6Se		
Sn2	4c	0.4088	0.6720	0.0148	4Se		
Se1	4c	0.6209	0.6752	0.0054	4Eu	1Sn	
Se2	4c	0.6303	0.6822	0.5048	4Eu	1Sn	
Se3	2a	1/2	1/2	0.7289	2Eu	2Sn	
Se4	2a	1/2	1/2	0.2766	2Eu	2Sn	
Se5	4c	0.7527	0.9314	0.9868	4Eu	1Sn	
Se6	4c	0.7410	0.9281	0.4857	4Eu	1Sn	
Se7	4c	0.4389	0.8918	0.9887	4Eu	2Se	
Se8	4c	0.4422	0.8905	0.4884	4Eu	2Se	
Se9	4c	0.8697	0.7616	0.7199	3Eu	2Sn	1Se
Se10	2b	1/2	0	0.1600	4Eu	2Se	
Se11	4c	0.3674	0.7468	0.7638	3Eu	2Sn	1Se
Se12	2b	1/2	0	0.6555	4Eu	2Se	

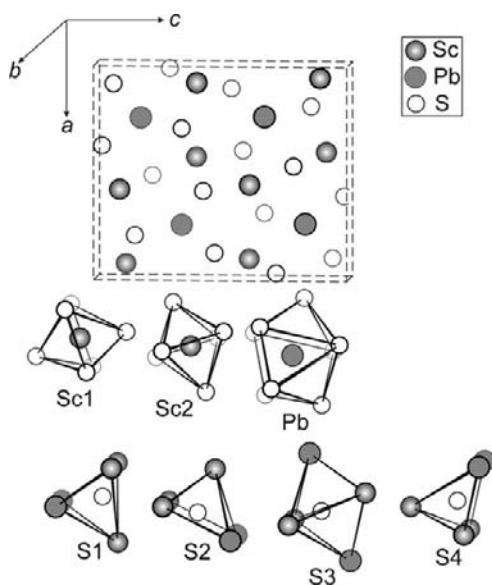
**FIGURE 17** Crystal structure of Sc_2PbS_4 (structure type CaFe_2O_4) and CPs of atoms.

TABLE 22 Atomic parameters for Sc_2PbS_4

Atom	Position	Fractional coordinates			Atomic arrangement	
		x	y	z		
Sc1	4c	0.4420	1/4	0.3893	6S	
Sc2	4c	0.4178	1/4	0.9025	6S	
Pb	4c	0.76042	1/4	0.33074	8S	
S1	4c	0.2037	1/4	0.8424	3Sc	2Pb
S2	4c	0.1221	1/4	0.5279	3Sc	2Pb
S3	4c	0.5293	1/4	0.2156	3Sc	2Pb
S4	4c	0.4119	1/4	0.5729	3Sc	2Pb

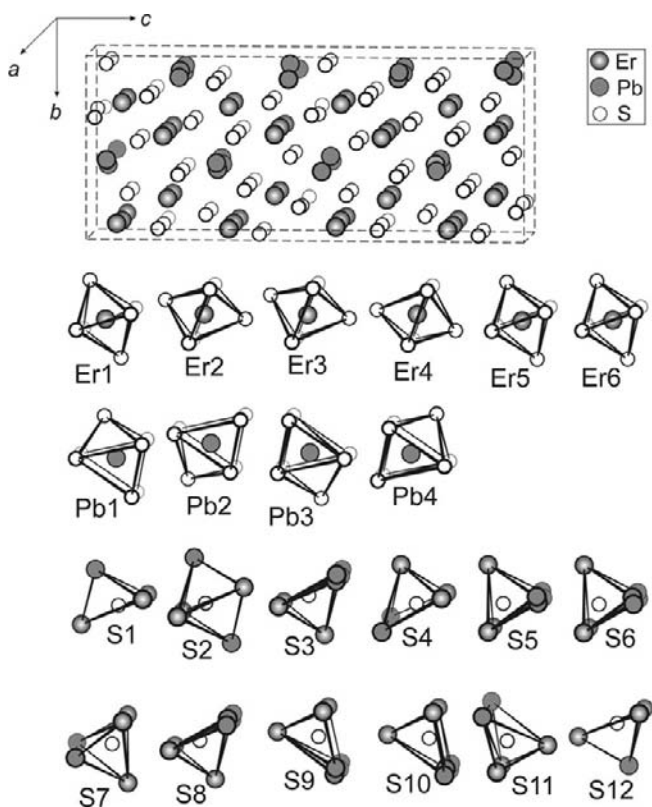
**FIGURE 18** Crystal structure of Er_2PbS_4 and CPs of atoms.

TABLE 23 Atomic parameters for Er₂PbS₄

Atom	Position	Fractional coordinates			Atomic arrangement	
		x	y	z		
Er1	8 <i>b</i>	0.2494	0.0757	0.2693	6S	
Er2	4 <i>a</i>	0	0.0694	0.9122	6S	
Er3	4 <i>a</i>	0	0.5700	0.9217	6S	
Er4	8 <i>b</i>	0.2503	0.1800	0.7869	6S	
Er5	4 <i>a</i>	0	0.6740	0.4369	6S	
Er6	4 <i>a</i>	0	0.1751	0.4343	6S	
Pb1	4 <i>a</i>	0	0.04629	0.5653	7S	
Pb2	4 <i>a</i>	0	0.53800	0.6213	7S	
Pb3 ^a	8 <i>b</i>	0.250	0.2068	0.126	7S	
Pb4 ^a	8 <i>b</i>	0.251	0.2079	0.094	7S	
S1	8 <i>b</i>	0.247	0.0392	0.059	3Er	1Pb
S2	4 <i>a</i>	0	0.6396	0.227	3Er	2Pb
S3	4 <i>a</i>	0	0.1640	0.938	3Er	2Pb
S4	4 <i>a</i>	0	0.6650	0.940	3Er	2Pb
S5	8 <i>b</i>	0.252	0.0881	0.765	3Er	2Pb
S6	4 <i>a</i>	0	0.0191	0.338	3Er	2Pb
S7	4 <i>a</i>	0	0.5151	0.313	3Er	2Pb
S8	8 <i>b</i>	0.252	0.2332	0.377	3Er	2Pb
S9	4 <i>a</i>	0	0.1391	0.222	3Er	2Pb
S10	8 <i>b</i>	0.248	0.1118	0.479	3Er	2Pb
S11	4 <i>a</i>	0	0.7077	0.647	3Er	2Pb
S12	4 <i>a</i>	0	0.2080	0.648	3Er	1Pb

^a Occupancy 50%.

surroundings of 3Er and 2Pb atoms. These tetragonal pyramids contain disordered lead atoms in some of their vertices.

3.6.19 Structure type Th₃P₄

Structure type Th₃P₄ (Meisel, 1939) (Figure 19, Table 24). SG $I\bar{4}3d$, $Z = 4$, $a = 0.89916$ nm for Pr₂PbSe₄ (Marchuk et al., 2006b). Randomly distributed Pr and Pb atoms (M) are located in eight-vertex polyhedra formed by the Se atoms and the shortest M–Se distance is 0.3012 nm. The selenium atom has octahedral surrounding of the M atoms.

3.6.20 Structure type Tm₂PbSe₄

Structure type Tm₂PbSe₄ (Gulay et al., 2006d) (Figure 20, Table 25). SG $Pnma$, $Z = 4$, $a = 1.2505$, $b = 0.40630$, $c = 1.4820$ nm. Both of the two independent thulium atoms have octahedral coordination spheres made

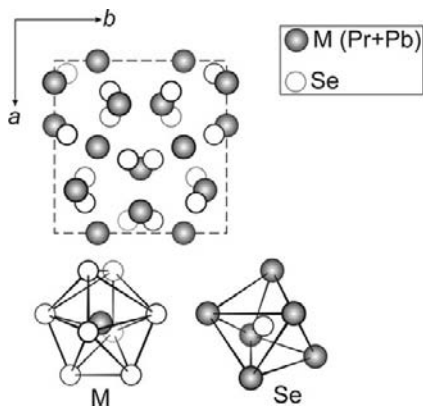


FIGURE 19 Crystal structure of Pr_2PbSe_4 (structure type Th_3P_4) and CPs of atoms.

TABLE 24 Atomic parameters for Pr_2PbSe_4

Atom	Position	Fractional coordinates			Atomic arrangement
		x	y	z	
M^a	$12a$	$3/8$	0	$1/4$	8
Se	$16c$	0.0728	x	x	6 M

^a Occupancy 66.7% Pr + 33.3% Pb.

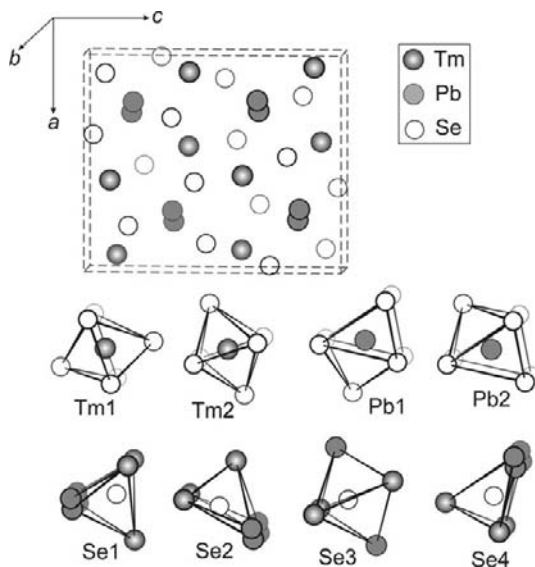


FIGURE 20 Crystal structure of Tm_2PbSe_4 and CPs of atoms.

TABLE 25 Atomic parameters for Tm_2PbSe_4

Atom	Position	Fractional coordinates			Atomic arrangement	
		x	y	z		
Tm1	4c	0.43884	1/4	0.39019	6Se	
Tm2	4c	0.41590	1/4	0.90440	6Se	
Pb1 ^a	4c	0.7888	1/4	0.3365	7Se	
Pb2 ^a	4c	0.7325	1/4	0.3216	7Se	
Se1	4c	0.2056	1/4	0.8326	3Tm	2Pb
Se2	4c	0.1280	1/4	0.5308	3Tm	2Pb
Se3	4c	0.5268	1/4	0.2152	3Tm	2Pb
Se4	4c	0.4093	1/4	0.5762	3Tm	2Pb

^a Occupancy 50%.

of the selenium atoms. The shortest Tm–Se distance is 0.2782 nm. The selenium atoms create monocapped trigonal prismatic arrangements around the lead atom occupying split positions, and the shortest Pb–Se distance is 0.3011 nm. The Se3 atom is located in a trigonal bipyramid formed by 3Tm and 2Pb atoms. The other three independent selenium atoms are surrounded by 3Tm and 2Pb atoms creating tetragonal pyramids.

3.6.21 Structure type $\text{Y}_{4.2}\text{Pb}_{0.7}\text{Se}_7$

Structure type $\text{Y}_{4.2}\text{Pb}_{0.7}\text{Se}_7$ (Shemet et al., 2005) (Figure 21, Table 26). SG Cm , $Z = 2$, $a = 1.3357$, $b = 0.40469$, $c = 1.22356$ nm, $\beta = 104.529^\circ$. The selenium atoms create octahedral arrangements around all the three independent ordered yttrium atoms. The shortest Y–Se distance is 0.261 nm. The two positions of the Y and Pb atoms (M) are disordered, and these atoms are located inside monocapped trigonal prisms. The shortest M–Se distance is 0.269 nm. The Se1 and Se3 atoms have tetrahedral surrounding made of the 2Y and 2M atoms. The Se6 atom is located practically in the center of a square formed by 4Y atoms. The remaining independent selenium atoms have tetragonal pyramidal surroundings made of the yttrium and M atoms.

3.6.22 Structure type $\text{Y}_6\text{Pb}_2\text{Se}_{11}$

Structure type $\text{Y}_6\text{Pb}_2\text{Se}_{11}$ (Gulay et al., 2005a) (Figure 22, Table 27). SG $Cmcm$, $Z = 4$, $a = 0.40610$, $b = 1.3467$, $c = 3.7624$ nm. The selenium atoms create octahedral arrangements around all the ordered yttrium atoms, and the shortest Y–Se distance is 0.2808 nm. One site is disordered and is occupied by the Y and Pb atoms (M), and these atoms are located in

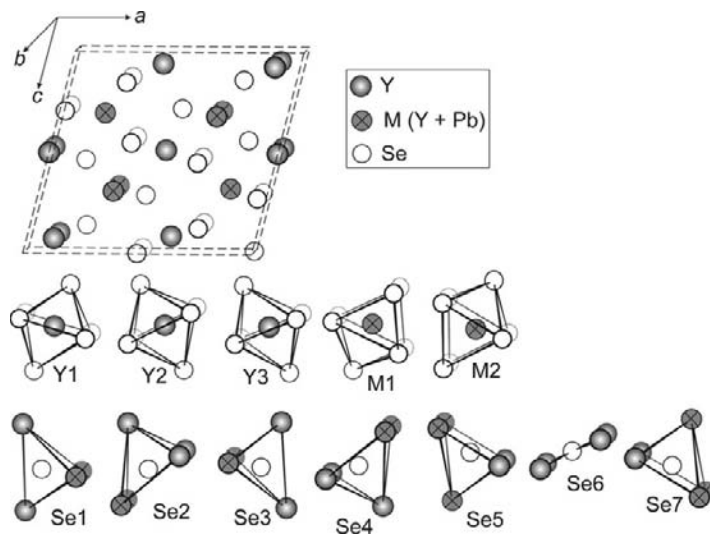


FIGURE 21 Crystal structure of $Y_{4.2}Pb_{0.7}Se_7$ and CPs of atoms.

TABLE 26 Atomic parameters for $Y_{4.2}Pb_{0.7}Se_7$

Atom	Position	Fractional coordinates			Atomic arrangement	
		x	y	z		
Y1	$2a$	0.000	0	0.500	6Se	
Y2	$2a$	0.890	0	0.072	6Se	
Y3	$2a$	0.119	0	0.925	6Se	
M1 ^a	$2a$	0.692	0	0.318	7Se	
M2 ^b	$2a$	0.325	0	0.690	7Se	
Se1	$2a$	0.024	0	0.294	2Y	2M
Se2	$2a$	0.260	0	0.152	3Y	2M
Se3	$2a$	0.962	0	0.723	2Y	2M
Se4	$2a$	0.738	0	0.872	3Y	2M
Se5	$2a$	0.349	0	0.450	2Y	3M
Se6	$2a$	0.499	0	0.997	4Y	
Se7	$2a$	0.660	0	0.548	2Y	3M

^a Occupancy 70% Y + 20% Pb.

^b Occupancy 50% Y + 50% Pb.

monocapped trigonal prisms. The ordered position occupied by the lead atoms has a bicapped trigonal prism as the coordination polyhedron, and the shortest Pb–Se distance equals to 0.2847 nm. The Se1 and Se6 atoms

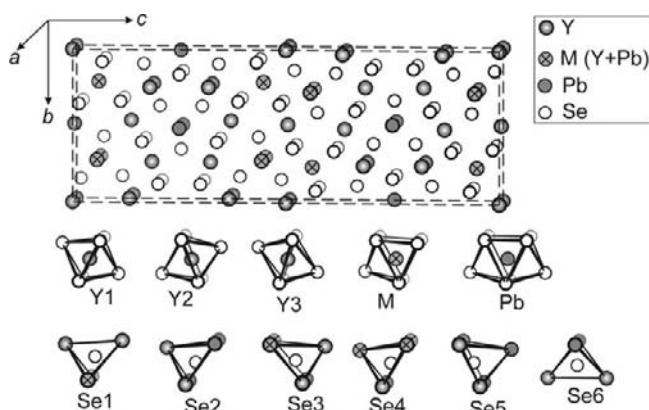


FIGURE 22 Crystal structure of $Y_6Pb_2Se_{11}$ and CPs of atoms.

TABLE 27 Atomic parameters for $Y_6Pb_2Se_{11}$

Atom	Position	Fractional coordinates			Atomic arrangement	
		x	y	z		
Y1	8f	0	0.0257	0.63328	6Se	
Y2	8f	0	0.2462	0.18144	6Se	
Y3	4a	0	0	0	6Se	
M ^a	8f	0	0.2761	0.55707	7Se	
Pb	4c	0	0.5148	1/4	8Se	
Se1	8f	0	0.0810	0.06902	2Y	2M
Se2	8f	0	0.1203	0.70071	3Y	2Pb
Se3	8f	0	0.3394	0.11226	3Y	2M
Se4	8f	0	0.3575	0.01521	2Y	3M
Se5	8f	0	0.6047	0.16219	4Y	1Pb
Se6	4c	0	0.1629	1/4	2Y	2Pb

^a Occupancy 50% Y + 50% Pb.

have tetrahedrally shaped surroundings formed by 2Y and 2M (Pb) atoms. The remaining selenium atoms are located in tetragonal pyramids.

3.6.23 Structure type La_3InS_6

Structure type La_3InS_6 (Carré et al., 1978) (Figure 23, Table 28). SG $P2_12_12$, $Z = 4$, $a = 1.3946$, $b = 1.6912$, $c = 0.4079$ nm. The sulfur atoms form bicapped trigonal prismatic arrangements around the La1 and La2 atoms; the La3 atom is located in a monocapped trigonal prism.

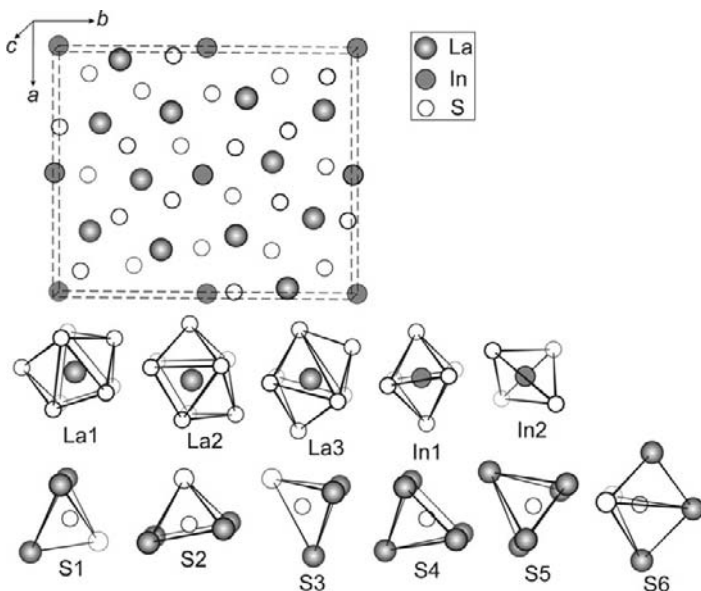


FIGURE 23 Crystal structure of La_3InS_6 and CPs of atoms.

TABLE 28 Atomic parameters for La_3InS_6

Atom	Position	Fractional coordinates			Atomic arrangement	
		x	y	z		
La1	4c	0.53715	0.28022	0.2452	8S	
La2	4c	0.74931	0.10858	0.2413	8S	
La3	4c	0.30957	0.14302	0.2457	7S	
In1	2b	0	1/2	0.2537	6S	
In2	2a	0	0	0.0873	4S	
S1	4c	0.3988	0.413	0.266	3La	1In
S2	4c	0.1863	0.5173	0.253	4La	1In
S3	4c	0.1079	0.1058	0.255	3La	1In
S4	4c	0.1774	0.2827	0.259	5La	
S5	4c	0.113	0.7446	0.252	5La	
S6	4c	0.5205	0.1018	0.247	3La	2In

The shortest La–S distance is 0.2871 nm. The In1 and In2 atoms are coordinated by sulfur octahedra and tetrahedra, respectively. The shortest In–S distance is 0.2436 nm. The S1 and S3 atoms have tetrahedral

surroundings of the 3La and 1In. The remaining sulfur atoms are five-coordinated, of which S2, S4, and S5 are located in tetragonal pyramids and the S6 atom is located in a trigonal bipyramid.

3.6.24 Structure type $\text{Nd}_4\text{In}_5\text{S}_{13}$

Structure type $\text{Nd}_4\text{In}_5\text{S}_{13}$ (Guseinov et al., 1979b) (Figure 24, Table 29). SG $P6_{3m}$, $Z = 2$, $a = 1.1774$, $b = 2.1254$, $c = 0.3968$ nm. The sulfur atoms create bi- and monocapped trigonal prismatic arrangements around the Nd1 and Nd2 atoms, respectively. The shortest Nd–S distance is 0.2871 nm. The In1 and In2 atoms are situated in deformed octahedra; the coordination sphere of the In3 atom is trigonal bipyramidal. The shortest In–S distance is 0.2365 nm. The S1, S2, and S3 atoms are located in tetragonal pyramids. The S4, S5, and S6 atoms are situated in tetrahedra. A square surrounding of the indium atoms is found around the S7 atom.

3.6.25 Structure type $\text{Ce}_3\text{Al}_{1.67}\text{S}_7$

Structure type $\text{Ce}_3\text{Al}_{1.67}\text{S}_7$ (de Saint-Giniez et al., 1968) (Figure 25, Table 30). SG $P6_3$, $Z = 2$, $a = 1.0196$, $c = 0.62792$ nm for $\text{La}_3\text{In}_{1.67}\text{S}_7$ (Gulay et al., 2008d). The lanthanum atom is located in a monocapped trigonal prism, and the shortest La–S distance equals to 0.28747 nm. The sulfur atoms form tetrahedral and trigonal antiprismatic (i.e., octahedral) arrangements around the In1 and In2, respectively. The shortest In–S

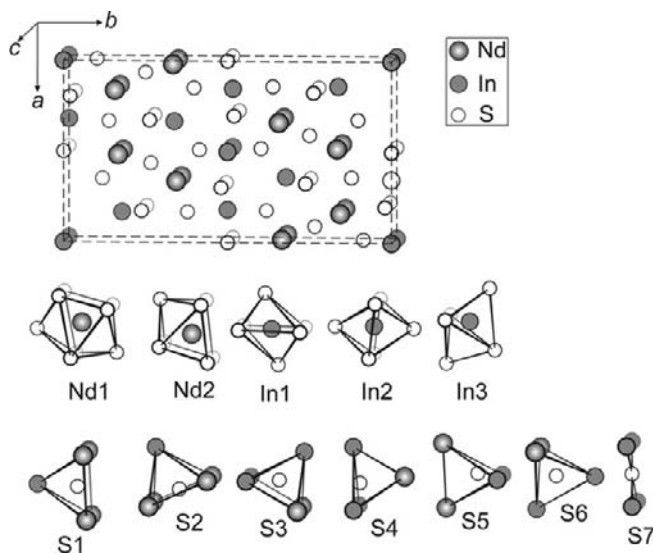
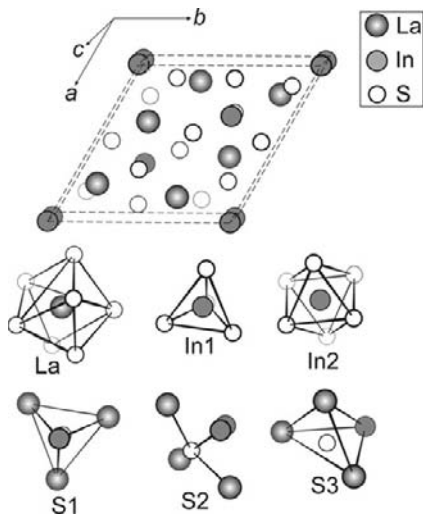


FIGURE 24 Crystal structure of $\text{Nd}_4\text{In}_5\text{S}_{13}$ and CPs of atoms.

TABLE 29 Atomic parameters for $\text{Nd}_4\text{In}_5\text{S}_{13}$

Atom	Position	Fractional coordinates			Atomic arrangement	
		x	y	z		
Nd1	4g	0.1622	0.1562	0	8S	
Nd2	4g	0.0183	0.3341	0	7S	
In1 ^a	2a	0	0	0	6S	
In2	4h	0.3342	0.0084	1/2	6S	
In3	4h	0.3475	0.3296	1/2	5S	
S1	4h	0.3463	0.1301	1/2	4Nd	1In
S2	4h	0.0781	0.2421	1/2	4Nd	1In
S3	4h	0.0044	0.0941	1/2	2Nd	3In
S4	4g	0.1977	0.0197	0	1Nd	3In
S5	4g	0.327	0.2623	0	2Nd	2In
S6	4h	0.163	0.3898	1/2	2Nd	2In
S7	2c	0	1/2	0		4In

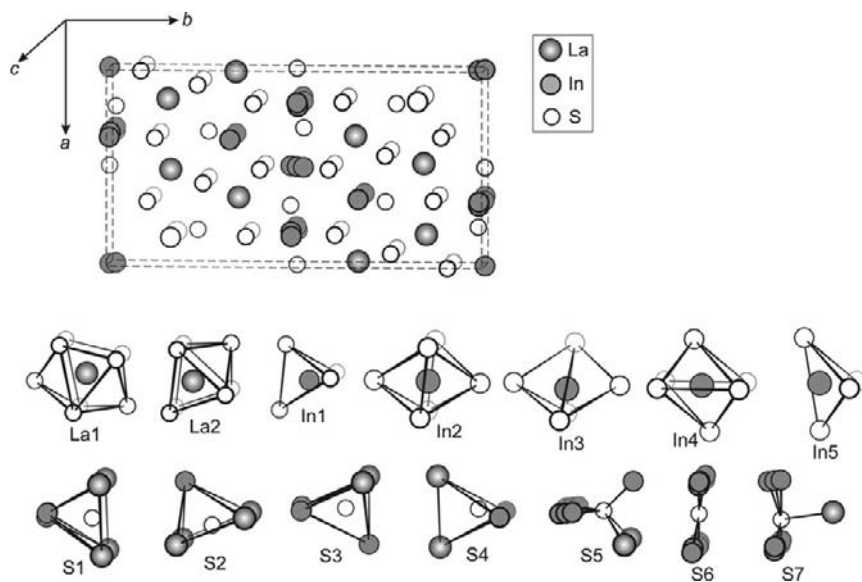
^a Occupancy 91%.

**FIGURE 25** Crystal structure of $\text{La}_3\text{In}_{1.67}\text{S}_7$ (structure type $\text{Ce}_3\text{Al}_{1.67}\text{S}_7$) and CPs of atoms.

distances are 0.2392 and 0.2658 nm, respectively. The S1 and S3 atoms have CN of 4 and tetrahedral arrangements formed by 3La and 1In atoms. The S2 atom is located outside a trigonal bipyramid.

TABLE 30 Atomic parameters for $\text{La}_3\text{In}_{1.67}\text{S}_7$

Atom	Position	Fractional coordinates			Atomic arrangement	
		x	y	z		
La	6c	0.22805	0.85279	0.25786	7S	
In1	2b	1/3	2/3	0.83212	4S	
In2 ^a	2a	0	0	0.4669	6S	
S1	2b	1/3	2/3	0.4511	3La	1In
S2	6c	0.1459	0.9000	0.7081	3La	2In
S3	6c	0.4298	0.5141	0.9984	3La	1In

^a Occupancy 67%.**FIGURE 26** Crystal structure of $\text{La}_{3.92}\text{In}_{4.76}\text{S}_{13}$ and CPs of atoms.

3.6.26 Structure type $\text{La}_{3.92}\text{In}_{4.76}\text{S}_{13}$

Structure type $\text{La}_{3.92}\text{In}_{4.76}\text{S}_{13}$ (Gulay et al., 2008d) (Figure 26, Table 31). SG $Pbam$, $Z = 2$, $a = 1.1814$, $b = 2.1280$, $c = 0.40384$ nm. The La1 and La2 atoms are located in bi- and monocapped trigonal prisms, respectively. The shortest La–S distance is 0.29071 nm. The sulfur atoms form various coordination spheres around the five independent indium atoms. The In1 and In5 atoms are located in tetrahedra, the In2 and In4 atoms occupy octahedral sites, and the In3 atom has trigonal bipyramidal surrounding. The shortest In–S distance is 0.2294 nm. The In2, In3, In4, and In5 atoms

TABLE 31 Atomic parameters for $\text{La}_{3.92}\text{In}_{4.76}\text{S}_{13}$

Atom	Position	Fractional coordinates			Atomic arrangement	
		x	y	z		
La1 ^a	4h	0.15820	0.15577	1/2	8S	
La2	4h	0.51922	0.16279	1/2	7S	
In1	4g	0.84981	0.17089	0	4S	
In2 ^b	4g	0.6593	0.9924	0	6S	
In3 ^c	8i	0.6810	0.9907	0.941	5S	
In4 ^b	2b	0	0	1/2	6S	
In5 ^d	4h	0.996	0.0169	1/2	4S	
S1	4g	0.3438	0.12878	0	4La	1In
S2	4g	0.0724	0.24262	0	4La	1In
S3	4g	0.6670	0.10872	0	2La	2In
S4	4h	0.3233	0.26470	1/2	2La	2In
S5	4g	0.0015	0.09167	0	2La	3In
S6	2d	1/2	0	1/2	4In	
S7	4h	0.1978	0.01764	1/2	1La	3In

^a Occupancy 96%.^b Occupancy 50%.^c Occupancy 25%.^d Occupancy 13%.

occupy disordered positions, and because of this numerous polyhedra can be found around the sulfur atoms. The S1, S2, and S5 atoms are located in tetragonal pyramids. Each of the S3, S4, and S7 atoms has tetrahedral surroundings, and the S6 atom is situated in a square made of In atoms.

3.6.27 Structure type U_3ScS_6

Structure type U_3ScS_6 (Noël and Vovan, 1976) (Figure 27, Table 32). SG $Pn\bar{m}$, $Z = 4$, $a = 1.3632$, $b = 1.6513$, $c = 0.3901$ nm for Sm_3InS_6 (Messain et al., 1977). The sulfur atoms create bicapped trigonal prismatic arrangements around the Sm1 and Sm2 atoms, and the Sm3 atom is located in a monocapped trigonal prism. The shortest Sm–S distance is 0.2763 nm. The two independent indium atoms are located in octahedra formed by the sulfur atoms. The shortest In–S distance is 0.2428 nm. The S4 atom has a tetrahedral surrounding of 3Sm and 1In. Five other independent sulfur atoms have five-coordinate nearest neighbor spheres. Among these, the S6 atom is located in a trigonal bipyramid and the other sulfur atoms are located in tetragonal pyramids.

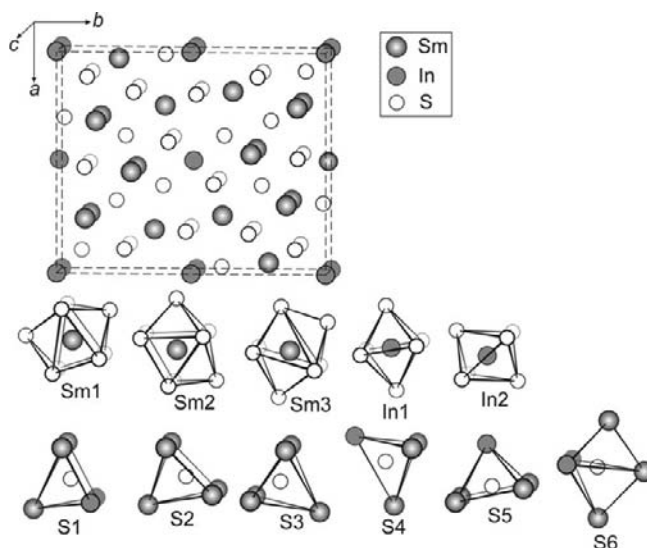


FIGURE 27 Crystal structure of Sm_3InS_6 (structure type U_3ScS_6) and CPs of atoms.

TABLE 32 Atomic parameters for Sm_3InS_6

Atom	Position	Fractional coordinates			Atomic arrangement	
		x	y	z		
Sm1	4g	0.54075	0.27764	0	8S	
Sm2	4g	0.75205	0.10614	0	8S	
Sm3	4g	0.31191	0.14605	0	7S	
In1	2c	0	1/2	0	6S	
In2	2a	0	0	0	6S	
S1	4g	0.4049	0.416	0	3Sm	2In
S2	4g	0.1816	0.2868	0	5Sm	
S3	4g	0.1107	0.7475	0	5Sm	
S4	4g	0.1131	0.1136	0	3Sm	1In
S5	4g	0.1904	0.5196	0	4Sm	1In
S6	4g	0.5215	0.104	0	3Sm	2In

3.6.28 Structure type SrAl_2Se_4

Structure type SrAl_2Se_4 (Klee and Schäfer, 1978) (Figure 28, Table 33). SG $Cccm$, $Z = 2$, $a = 0.650$, $b = 1.049$, $c = 1.036$ nm for EuIn_2S_4 (Aliev et al., 1976). Only four chalcogenide compounds with the structure type SrAl_2Se_4 are known. The atomic parameters of these compounds are not

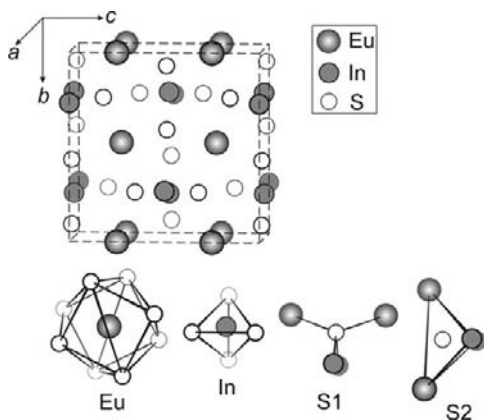


FIGURE 28 Crystal structure of EuIn_2S_4 (structure type SrAl_2Se_4) and CPs of atoms.

TABLE 33 Atomic parameters for $\text{EuIn}_2\text{S}_4^a$

Atom	Position	Fractional coordinates			Atomic arrangement	
		<i>x</i>	<i>y</i>	<i>z</i>		
Eu	$4a$	0	0	$1/4$	8S	
In	$8l$	0.505	0.232	0	4S	
S1	$8l$	0.237	0.08	0	2Eu	2In
S2	$8k$	$1/4$	$1/4$	0.333	2Eu	2In

^a Atomic coordinates are as for the structure EuIn_2S_4 (Klee and Schäfer, 1978).

refined. The sulfur atoms create tetragonal antiprismatic arrangement around the europium atoms. The single independent indium atom is located in a tetrahedron. The S1 and S2 atoms are located in tetrahedra, but for the S1 atom the tetrahedron is centered outside.

3.6.29 Structure type $\text{Tb}_3\text{In}_5\text{S}_{12}$

Structure type $\text{Tb}_3\text{In}_5\text{S}_{12}$ (Carré, 1977) (Figure 29, Table 34). SG $P2_1/m$, $Z = 2$, $a = 1.0998$, $b = 2.1259$, $c = 0.3897$ nm, $\beta = 96.36^\circ$. The Tb1 and Tb2 atoms are located in bicapped trigonal prisms, and the Tb3 atom has monocapped trigonal prismatic surroundings. The shortest Tb–S distance is 0.2725 nm. The sulfur atoms form tetrahedron around the In2 atom, and the other indium atoms have octahedral surroundings. The shortest In–S distance is 0.2449 nm. Each of the S7 and S9 atoms has triangular surroundings formed by 3In atoms. Each of the S1, S5, S6, S10, and S11 atoms is located in a tetragonal pyramid. The remaining sulfur atoms are located in tetrahedra.

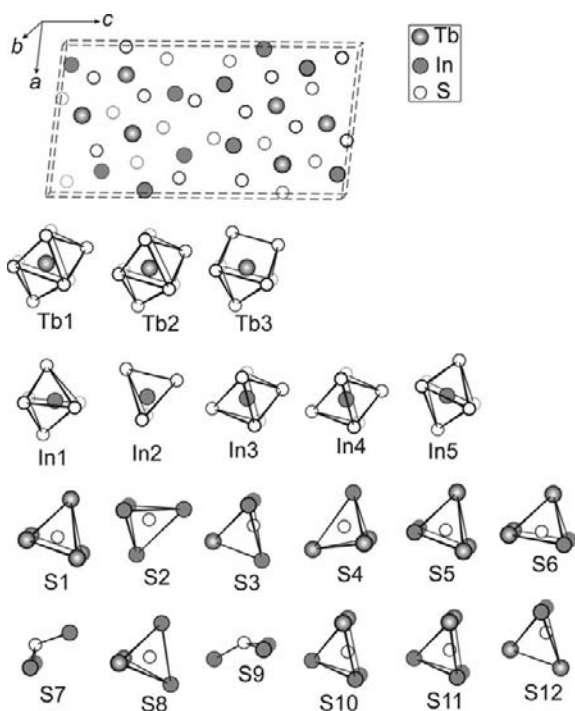


FIGURE 29 Crystal structure of $Tb_3In_5S_{12}$ and CPs of atoms.

3.6.30 Structure type Yb_2FeS_4

Structure type Yb_2FeS_4 (Tomas and Guittard, 1977) (Figure 30, Table 35). SG $Fd\bar{3}m$, $Z = 8$, $a = 1.0873$ nm for $Yb_{4/3}In_{4/3}S_4$ (Likforman and Guittard, 1993). The sulfur atoms create octahedral arrangement around the single ordered site occupied by Yb atoms. The disordered site occupied by both Yb and In atoms (M) also has octahedral coordination. The shortest Yb–S and M–S distances are 0.2784 and 0.2655 nm, respectively. The In atom has tetrahedral coordination sphere with the shortest In–S distance of 0.2465 nm. The sulfur atom is located in an octahedron formed by 3Yb and 3M with an additional In atom centering one of the triangular faces of the octahedron.

3.6.31 Structure type $Yb_{18}In_{7.33}S_{36}$

Structure type $Yb_{18}In_{7.33}S_{36}$ (Lemoine et al., 1989) (Figure 31, Table 36). SG $P6_3/m$, $Z = 2$, $a = 2.0688$, $c = 0.3861$ nm. The coordination spheres of Yb and In atoms are ideally described as trigonal prisms with the shortest Yb–S and In–S distances of 0.2802 and of 0.3484 nm, respectively. The disordered position of the randomly distributed Yb and In atoms (M) is

TABLE 34 Atomic parameters for $Tb_3In_5S_{12}$

Atom	Position	Fractional coordinates			Atomic arrangement	
		x	y	z		
Tb1	2e	0.2163	1/4	0.21583	8S	
Tb2	2e	0.41197	1/4	0.73356	8S	
Tb3	2e	0.52933	1/4	0.91099	7S	
In1	2e	0.33844	1/4	0.38816	6S	
In2	2e	0.7424	1/4	0.44173	4S	
In3	2e	0.85237	1/4	0.16872	6S	
In4	2e	0.03984	1/4	0.67118	6S	
In5	2e	0.1533	1/4	0.0262	6S	
S1	2e	0.4657	1/4	0.1854	5Tb	
S2	2e	0.9227	1/4	0.055	4In	
S3	2e	0.1092	1/4	0.3466	1Tb	3In
S4	2e	0.3768	1/4	0.0081	3Tb	1In
S5	2e	0.6618	1/4	0.709	3Tb	2In
S6	2e	0.7779	1/4	0.8861	3Tb	2In
S7	2e	0.1213	1/4	0.5597	3In	
S8	2e	0.5621	1/4	0.3605	2Tb	2In
S9	2e	0.6324	1/4	0.5358	3In	
S10	2e	0.7928	1/4	0.2851	2Tb	3In
S11	2e	0.9835	1/4	0.7882	2Tb	3In
S12	2e	0.2977	1/4	0.8485	2Tb	2In

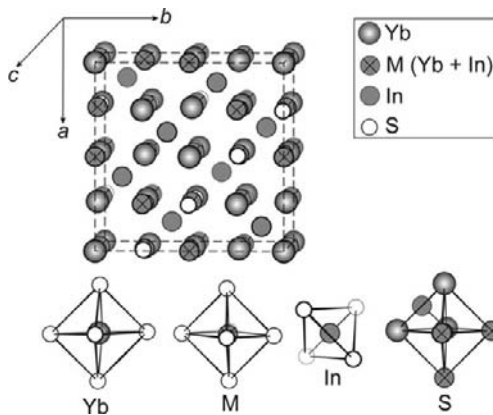
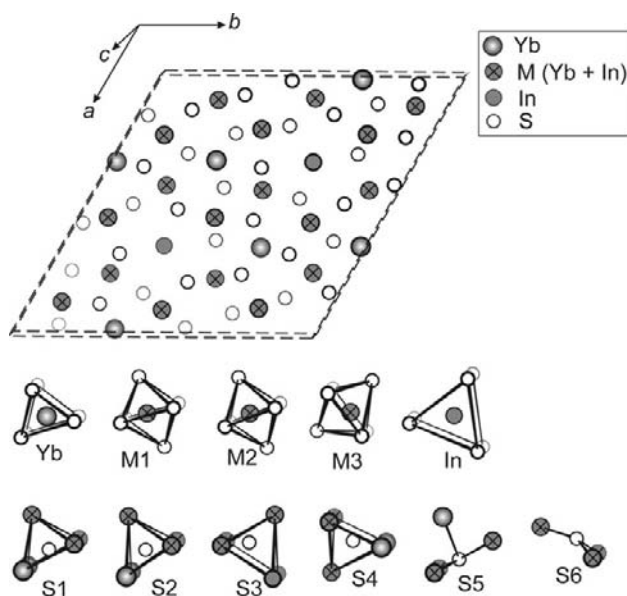
**FIGURE 30** Crystal structure of $Yb_{4/3}In_{4/3}S_4$ (structure type Yb_2FeS_4) and CPs of atoms.

TABLE 35 Atomic parameters for $\text{Yb}_{4/3}\text{In}_{4/3}\text{S}_4$

Atom	Position	Fractional coordinates			Atomic arrangement		
		<i>x</i>	<i>y</i>	<i>z</i>			
Yb^a	16 <i>c</i>	0	0	0	6S		
M^b	16 <i>d</i>	1/2	1/2	1/2	6S		
In^c	8 <i>a</i>	1/8	1/8	1/8	4S		
S	32 <i>e</i>	0.2559	0.2559	0.2559	3Yb	3M	1In

^a Occupancy 16.7%.^b Occupancy 50% Yb + 41.7% In.^c Occupancy 50%.**FIGURE 31** Crystal structure of $\text{Yb}_{18}\text{In}_{7.33}\text{S}_{36}$ and CPs of atoms.

located in an octahedron. The shortest M–S distance is 0.2569 nm. The S6 atom has triangular surroundings formed by 3M atoms, whilst the four-coordination sphere of the S5 atom can be described as a trigonal pyramid or a distorted tetrahedron, which is centered outside. The remaining independent sulfur atoms have tetragonal pyramidal surroundings.

3.6.32 Structure type YbIn_2S_4

Structure type YbIn_2S_4 (Amirov et al., 1984) (Figure 32, Table 37). SG P3, $Z = 9$, $a = 2.0859$, $c = 0.38743$ nm. The sulfur atoms create trigonal prismatic arrangement around the Yb1, Yb2, Yb3, and Yb5 atoms, and

TABLE 36 Atomic parameters for $\text{Yb}_{18}\text{In}_{7.33}\text{S}_{36}$

Atom	Position	Fractional coordinates			Atomic arrangement
		x	y	z	
Yb	6h	0.3453	0.0165	1/4	6S
M1 ^a	6h	0.1078	0.2336	1/4	6S
M2 ^b	6h	0.4495	0.9010	1/4	6S
M3 ^b	6h	0.4351	0.2259	1/4	6S
In	2d	2/3	1/3	1/4	6S
S1	6h	0.5812	0.0234	1/4	2Yb 3M
S2	6h	0.2356	0.3546	1/4	2Yb 3M
S3	6h	0.2052	0.5169	1/4	2In 3M
S4	6h	0.3137	0.2361	1/4	2Yb 3M
S5	6h	0.5071	0.1514	1/4	1Yb 3M
S6	6h	0.169	0.0322	1/4	3M

^a Occupancy 66.7% Yb+22.2% In.

^b Occupancy 66.7% Yb+33.3% In.

monocapped trigonal prismatic polyhedra around the Yb4 and Yb6 atoms. The Yb4 and Yb6 atoms occupy split positions. The shortest Yb–S distance is 0.2794 nm. Each of the In1, In3, and In6 atoms is located in an octahedron, whilst the In2 and In4 atoms occupy inner position of tetrahedra. A trigonal bipyramid is the coordination polyhedron of the In5 atom. The shortest In–S distance is 0.2111 nm. The S7 atom has triangular surroundings formed by 3In atoms. Each of the S2, S3, S5, S10, and S12 atoms is located in a tetrahedron. The remaining sulfur atoms have tetragonal pyramidal surroundings.

4. QUATERNARY SYSTEMS

This section describes known quaternary chalcogenide systems containing silicon, germanium, tin, lead, and indium.

4.1 Quaternary $\text{R}_2\text{X}_3\text{--M}_2\text{X--ZX}_2$ (M = Cu, Ag; Z = Si, Ge, Sn, X = S, Se) systems

The R–M–Z–X (M = Cu, Ag; Z = Si, Ge, Sn, X = S, Se) systems have been investigated mainly across the $\text{R}_2\text{X}_3\text{--M}_2\text{X--ZX}_2$ sections. No quaternary compounds are known for Te systems. Quaternary compounds that form in these systems are listed in Table 38. Among all of these 105 quaternary chalcogenides only four compounds crystallize in SG other than P6_3 . In several series of the silver compounds, occupational disorder for the silver atom has been found.

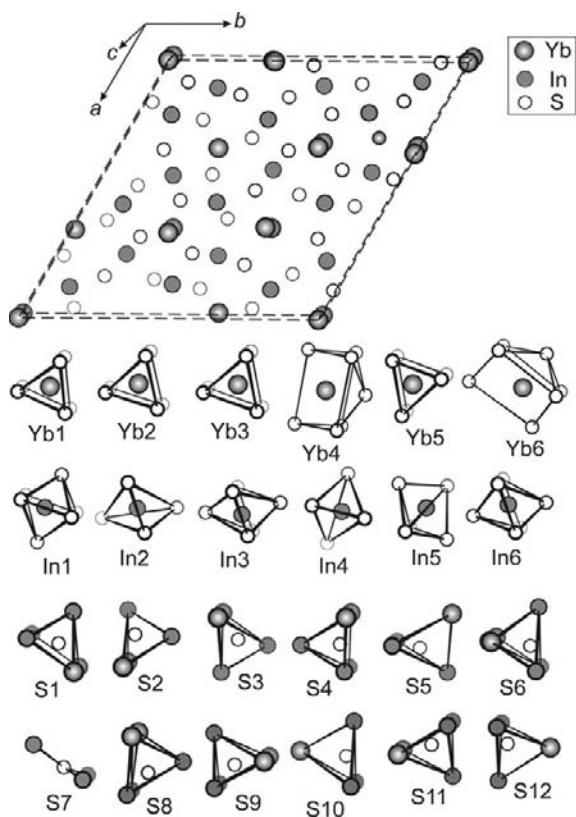


FIGURE 32 Crystal structure of YbIn_2S_4 and CPs of atoms.

The isothermal sections of the systems $\text{Y}_2\text{S}_3\text{-Cu}_2\text{S-SiS}_2$ (Lychnanyuk et al., 2006a), $\text{Pr}_2\text{S}_3\text{-Cu}_2\text{S-SiS}_2$ (Lychnanyuk et al., 2007b), $\text{Ho}_2\text{S}_3\text{-Cu}_2\text{S-SiS}_2$ (Lychnanyuk et al., 2007a), $\text{Y}_2\text{Se}_3\text{-Cu}_2\text{Se-SiSe}_2$ (Lychnanyuk et al., 2006a), $\text{Pr}_2\text{Se}_3\text{-Cu}_2\text{Se-SiSe}_2$ (Lychnanyuk et al., 2007b), and $\text{Ho}_2\text{Se}_3\text{-Cu}_2\text{Se-SiSe}_2$ (Lychnanyuk et al., 2007a) are shown in Figures 33–38, respectively.

The isothermal sections of the systems $\text{Y}_2\text{S}_3\text{-Cu}_2\text{S-GeS}_2$ (Gulay et al., 2006a), $\text{Pr}_2\text{S}_3\text{-Cu}_2\text{S-GeS}_2$ (Lychnanyuk et al., 2007b), $\text{Ho}_2\text{S}_3\text{-Cu}_2\text{S-GeS}_2$ (Lychnanyuk et al., 2007a), $\text{Y}_2\text{Se}_3\text{-Cu}_2\text{Se-GeSe}_2$ (Lychnanyuk et al., 2006b), $\text{Pr}_2\text{Se}_3\text{-Cu}_2\text{Se-GeSe}_2$ (Lychnanyuk et al., 2007b), and $\text{Ho}_2\text{Se}_3\text{-Cu}_2\text{Se-GeSe}_2$ (Lychnanyuk et al., 2007a) are shown in Figures 39–44, respectively.

The isothermal sections of the systems $\text{Y}_2\text{S}_3\text{-Cu}_2\text{S-SnS}_2$ (Shemet et al., 2006b), $\text{Y}_2\text{S}_3\text{-Cu}_2\text{S-SnS}$ (Shemet et al., 2006c), $\text{La}_2\text{S}_3\text{-Cu}_2\text{S-SnS}_2$ (Shemet and Gulay, 2007), $\text{Sm}_2\text{S}_3\text{-Cu}_2\text{S-SnS}_2$ (Shemet and Gulay, 2007), $\text{Tb}_2\text{S}_3\text{-Cu}_2\text{S-SnS}_2$ (Shemet and Gulay, 2007), $\text{Er}_2\text{S}_3\text{-Cu}_2\text{S-SnS}_2$ (Shemet and Gulay, 2007), $\text{Sc}_2\text{Se}_3\text{-Cu}_2\text{Se-SnSe}_2$ (Gulay et al., 2008e), $\text{Y}_2\text{Se}_3\text{-Cu}_2\text{Se-SnSe}_2$ (Shemet et al., 2006b), $\text{Y}_2\text{Se}_3\text{-Cu}_2\text{Se-SnSe}$ (Shemet et al., 2005),

TABLE 37 Atomic parameters for YbIn_2S_4

Atom	Position	Fractional coordinates			Atomic arrangement	
		x	y	z		
Yb1	1a	0	0	0	6S	
Yb2	1c	2/3	1/3	0	6S	
Yb3	1b	1/3	2/3	0	6S	
Yb4	3d	0.0083	0.345	0.51	7S	
Yb5	3d	0.348	0.333	0.498	6S	
Yb6	3d	0.002	0.356	0.995	7S	
In1	3d	0.220	0.113	0.527	6S	
In2	3d	0.4623	0.2329	0.12	4S	
In3	3d	0.5573	0.4324	0.506	6S	
In4	3d	0.1212	0.2126	0.19	4S	
In5	3d	0.2351	0.4424	0.515	5S	
In6	3d	0.1141	0.561	0.016	6S	
S1	3d	0.248	0.224	0.017	2Yb	3In
S2	3d	0.551	0.307	0.47	2Yb	2In
S3	3d	0.094	0.105	0.48	2Yb	2In
S4	3d	0.460	0.361	0.004	2Yb	3In
S5	3d	0.142	0.304	0.502	1Yb	3In
S6	3d	0.026	0.49	0.491	2Yb	3In
S7	3d	0.181	0.022	0.03	3In	
S8	3d	0.156	0.467	0.137	2Yb	3In
S9	3d	0.357	0.571	0.474	2Yb	3In
S10	3d	0.356	0.154	0.46	1Yb	3In
S11	3d	0.317	0.422	0.039	2Yb	3In
S12	3d	0.630	0.496	0.002	1Yb	3In

$\text{La}_2\text{Se}_3\text{-Cu}_2\text{Se-SnSe}_2$ (Shemet and Gulay, 2007), $\text{Sm}_2\text{Se}_3\text{-Cu}_2\text{Se-SnSe}_2$ (Shemet and Gulay, 2007), $\text{Er}_2\text{Se}_3\text{-Cu}_2\text{Se-SnSe}_2$ (Shemet and Gulay, 2007), $\text{Lu}_2\text{Se}_3\text{-Cu}_2\text{Se-SnSe}_2$ (Shemet and Gulay, 2007), and $\text{Y}_2\text{Te}_3\text{-Cu}_2\text{Te-SnTe}$ (Shemet et al., 2006c) are shown in Figures 45–58, respectively.

Formation of one quaternary compound R_3CuZX_7 of hexagonal symmetry (structure type $\text{La}_3\text{CuSiS}_7$, SG $P6_3$) has been observed in each of the $\text{R}_2\text{X}_3\text{-Cu}_2\text{X-ZX}_2$ ($Z = \text{Si, Ge, Sn, X} = \text{S, Se}$) systems with large R (La–Er). Only in the $\text{Y}_2\text{S}_3\text{-Cu}_2\text{S-SnS}_2$ system two compounds have been found. No quaternary compounds has been found in the $\text{R}_2\text{X}_3\text{-Cu}_2\text{X-ZX}_2$ ($Z = \text{Si, Ge, Sn, X} = \text{S, Se}$) systems with small R (Tm–Lu). Only one quaternary compound with cubic symmetry exists in the $\text{Sc}_2\text{Se}_3\text{-Cu}_2\text{Se-SnSe}_2$ system. No quaternary compounds exist in the systems with Sn(II): $\text{Y}_2\text{X}_3\text{-Cu}_2\text{X-SnX}$ ($X = \text{S, Se, Te}$).

TABLE 38 Crystallographic data for quaternary chalcogenides of the $R_2X_3-M_2X-ZX_2$ ($M = Cu, Ag; Z = Si, Ge, Sn, X = S, Se$) systems

Compound	Structure type	Space group	Lattice parameters (nm)			Reference(s)
			<i>a</i>	<i>b</i>	<i>c</i>	
Y ₃ CuSiS ₇	La ₃ CuSiS ₇	<i>P</i> 6 ₃	0.9854	–	0.5656	Gulay et al. (2005b)
La ₃ CuSiS ₇	La ₃ CuSiS ₇	<i>P</i> 6 ₃	1.0310	–	0.5794	Collin and Laruelle (1971)
Ce ₃ CuSiS ₇	La ₃ CuSiS ₇	<i>P</i> 6 ₃	1.0236	–	0.5767	Gulay et al. (2007d)
Ce ₃ CuSiS ₇	La ₃ CuSiS ₇	<i>P</i> 6 ₃	1.02219	–	0.57628	Hartenbach et al. (2007)
Pr ₃ CuSiS ₇	La ₃ CuSiS ₇	<i>P</i> 6 ₃	1.01615	–	0.57474	Gulay et al. (2007d)
Nd ₃ CuSiS ₇	La ₃ CuSiS ₇	<i>P</i> 6 ₃	1.0116	–	0.5725	Gulay et al. (2007d)
Sm ₃ CuSiS ₇	La ₃ CuSiS ₇	<i>P</i> 6 ₃	1.00193	–	0.56968	Gulay et al. (2007d)
Gd ₃ CuSiS ₇	La ₃ CuSiS ₇	<i>P</i> 6 ₃	0.99459	–	0.56703	Hartenbach et al. (2006)
Tb ₃ CuSiS ₇	La ₃ CuSiS ₇	<i>P</i> 6 ₃	0.98897	–	0.56582	Gulay et al. (2007d)
Dy ₃ CuSiS ₇	La ₃ CuSiS ₇	<i>P</i> 6 ₃	0.98689	–	0.56582	Gulay et al. (2007d)
Ho ₃ CuSiS ₇	La ₃ CuSiS ₇	<i>P</i> 6 ₃	0.98144	–	0.56422	Lychmanyuk et al. (2007a)
Er ₃ CuSiS ₇	La ₃ CuSiS ₇	<i>P</i> 6 ₃	0.97929	–	0.56518	Gulay et al. (2007d)
Y ₃ CuSiSe ₇	La ₃ CuSiS ₇	<i>P</i> 6 ₃	1.0269	–	0.5954	Gulay et al. (2005b)
La ₃ CuSiSe ₇	La ₃ CuSiS ₇	<i>P</i> 6 ₃	1.07116	–	0.60754	Gulay et al. (2007d)
Ce ₃ CuSiSe ₇	La ₃ CuSiS ₇	<i>P</i> 6 ₃	1.06215	–	0.60386	Gulay et al. (2007d)
Pr ₃ CuSiSe ₇	La ₃ CuSiS ₇	<i>P</i> 6 ₃	1.05854	–	0.60367	Gulay et al. (2007d)
Nd ₃ CuSiSe ₇	La ₃ CuSiS ₇	<i>P</i> 6 ₃	1.05600	–	0.60313	Gulay et al. (2007d)
Sm ₃ CuSiSe ₇	La ₃ CuSiS ₇	<i>P</i> 6 ₃	1.05042	–	0.60244	Gulay et al. (2007d)
Gd ₃ CuSiSe ₇	La ₃ CuSiS ₇	<i>P</i> 6 ₃	1.04643	–	0.60240	Gulay et al. (2007d)
Tb ₃ CuSiSe ₇	La ₃ CuSiS ₇	<i>P</i> 6 ₃	1.04115	–	0.60132	Gulay et al. (2007d)
Dy ₃ CuSiSe ₇	La ₃ CuSiS ₇	<i>P</i> 6 ₃	1.03823	–	0.60192	Gulay et al. (2007d)
Ho ₃ CuSiSe ₇	La ₃ CuSiS ₇	<i>P</i> 6 ₃	1.02294	–	0.59554	Lychmanyuk et al. (2007a)
La ₃ AgSiS ₇	La ₃ CuSiS ₇	<i>P</i> 6 ₃	1.0421	–	0.5785	Wu and Huang (2005)
La ₃ Ag _{0.90} SiS ₇	La ₃ Ag _{0.82} SnS ₇	<i>P</i> 6 ₃	1.04168	–	0.57825	Daszkiewicz et al. (2008b)

(continued)

Table 38 (continued)

Compound	Structure type	Space group	Lattice parameters (nm)			Reference(s)
			<i>a</i>	<i>b</i>	<i>c</i>	
Ce ₃ Ag _{0.82} SiS ₇	La ₃ Ag _{0.82} SnS ₇	<i>P</i> 6 ₃	1.0312	–	0.57395	Daszkiewicz et al. (2008b)
Pr ₃ Ag _{0.85} SiS ₇	La ₃ Ag _{0.82} SnS ₇	<i>P</i> 6 ₃	1.0248	–	0.57223	Daszkiewicz et al. (2008b)
Nd ₃ Ag _{0.81} SiS ₇	La ₃ Ag _{0.82} SnS ₇	<i>P</i> 6 ₃	1.0192	–	0.57020	Daszkiewicz et al. (2008b)
Sm ₃ Ag _{0.77} SiS ₇	La ₃ Ag _{0.82} SnS ₇	<i>P</i> 6 ₃	1.0100	–	0.56643	Daszkiewicz et al. (2008b)
La ₃ AgSiS ₇	La ₃ CuSiS ₇	<i>P</i> 6 ₃	1.0578	–	0.5987	Lin et al. (1997)
La ₃ AgSiSe ₇	La ₃ CuSiS ₇	<i>P</i> 6 ₃	1.0817	–	0.60640	Daszkiewicz et al. (2009a)
Ce ₃ AgSiSe ₇	La ₃ CuSiS ₇	<i>P</i> 6 ₃	1.0731	–	0.6031	Daszkiewicz et al. (2009a)
Pr ₃ AgSiSe ₇	La ₃ CuSiS ₇	<i>P</i> 6 ₃	1.0655	–	0.6005	Daszkiewicz et al. (2009a)
Nd ₃ AgSiSe ₇	La ₃ CuSiS ₇	<i>P</i> 6 ₃	1.0602	–	0.5988	Daszkiewicz et al. (2009a)
Sm ₃ Ag _{0.85} SiSe ₇	La ₃ Ag _{0.82} SnS ₇	<i>P</i> 6 ₃	1.0497	–	0.59466	Daszkiewicz et al. (2009a)
Gd ₃ Ag _{0.81} SiSe ₇	La ₃ Ag _{0.82} SnS ₇	<i>P</i> 6 ₃	1.0433	–	0.59367	Daszkiewicz et al. (2009a)
Tb ₃ Ag _{0.70} SiSe ₇	La ₃ Ag _{0.82} SnS ₇	<i>P</i> 6 ₃	1.0362	–	0.59296	Daszkiewicz et al. (2009a)
Dy ₃ Ag _{0.72} SiSe ₇	La ₃ Ag _{0.82} SnS ₇	<i>P</i> 6 ₃	1.0332	–	0.59494	Daszkiewicz et al. (2009a)
Y ₃ CuGeS ₇	La ₃ CuSiS ₇	<i>P</i> 6 ₃	0.9835	–	0.5765	Gulay et al. (2006a)
La ₃ CuGeS ₇	La ₃ CuSiS ₇	<i>P</i> 6 ₃	1.0294	–	0.5862	Poduska et al. (2002)
Ce ₃ CuGeS ₇	La ₃ CuSiS ₇	<i>P</i> 6 ₃	1.0225	–	0.58350	Gulay et al. (2006e)
Pr ₃ CuGeS ₇	La ₃ CuSiS ₇	<i>P</i> 6 ₃	1.0168	–	0.58223	Gulay et al. (2006e)
Nd ₃ CuGeS ₇	La ₃ CuSiS ₇	<i>P</i> 6 ₃	1.0123	–	0.57942	Gulay et al. (2006e)
Sm ₃ CuGeS ₇	La ₃ CuSiS ₇	<i>P</i> 6 ₃	1.00144	–	0.57714	Gulay et al. (2006e)
Gd ₃ CuGeS ₇	La ₃ CuSiS ₇	<i>P</i> 6 ₃	0.99428	–	0.57592	Gulay et al. (2006e)
Tb ₃ CuGeS ₇	La ₃ CuSiS ₇	<i>P</i> 6 ₃	0.98863	–	0.57535	Gulay et al. (2006e)
Dy ₃ CuGeS ₇	La ₃ CuSiS ₇	<i>P</i> 6 ₃	0.98371	–	0.57552	Gulay et al. (2006e)
Ho ₃ CuGeS ₇	La ₃ CuSiS ₇	<i>P</i> 6 ₃	0.97865	–	0.57606	Lychmanyuk et al. (2007a)

Er ₃ CuGeSe ₇	La ₃ CuSiS ₇	P6 ₃	0.97415	–	0.57835	Gulay et al. (2006e)
Y ₃ CuGeSe ₇	La ₃ CuSiS ₇	P6 ₃	1.02368	–	0.60569	Lychmanyuk et al. (2006b)
La ₃ CuGeSe ₇	La ₃ CuSiS ₇	P6 ₃	1.0725	–	0.6133	Poduska et al. (2002)
Ce ₃ CuGeSe ₇	La ₃ CuSiS ₇	P6 ₃	1.0643	–	0.60973	Gulay et al. (2006f)
Pr ₃ CuGeSe ₇	La ₃ CuSiS ₇	P6 ₃	1.0559	–	0.6084	Gulay et al. (2006f)
Nd ₃ CuGeSe ₇	La ₃ CuSiS ₇	P6 ₃	1.0519	–	0.60707	Gulay et al. (2006f)
Sm ₃ CuGeSe ₇	La ₃ CuSiS ₇	P6 ₃	1.04216	–	0.60447	Gulay et al. (2006f)
Gd ₃ CuGeSe ₇	La ₃ CuSiS ₇	P6 ₃	1.03491	–	0.60395	Gulay et al. (2006f)
Tb ₃ CuGeSe ₇	La ₃ CuSiS ₇	P6 ₃	1.02940	–	0.60387	Gulay et al. (2006f)
Dy ₃ CuGeSe ₇	La ₃ CuSiS ₇	P6 ₃	1.02499	–	0.60322	Huang and Ibers (1999)
Ho ₃ CuGeSe ₇	La ₃ CuSiS ₇	P6 ₃	1.01978	–	0.60612	Gulay et al. (2006f)
Y ₃ Ag _{0.50} GeS ₇	Tb ₃ Ag _{0.59} GeS ₇	P6 ₃	0.9809	–	0.5805	Daszkiewicz et al. (2009b)
La ₃ Ag _{0.82} GeS ₇	La ₃ Ag _{0.82} SnS ₇	P6 ₃	1.0405	–	0.5828	Daszkiewicz et al. (2009b)
Ce ₃ Ag _{0.88} GeS ₇	La ₃ Ag _{0.82} SnS ₇	P6 ₃	1.0390	–	0.5842	Daszkiewicz et al. (2009b)
Pr ₃ Ag _{0.90} GeS ₇	La ₃ Ag _{0.82} SnS ₇	P6 ₃	1.0229	–	0.5776	Daszkiewicz et al. (2009b)
Nd ₃ Ag _{0.84} GeS ₇	La ₃ Ag _{0.82} SnS ₇	P6 ₃	1.0193	–	0.5769	Daszkiewicz et al. (2009b)
Sm ₃ Ag _{0.74} GeS ₇	La ₃ Ag _{0.82} SnS ₇	P6 ₃	1.0080	–	0.5760	Daszkiewicz et al. (2009b)
Eu _{1.75} Ag _{0.5} GeS ₄	Pb _{1.75} Ag _{0.5} GeS ₄	I43d	1.3949	–	–	Iyer et al. (2004)
Gd ₃ Ag _{0.63} GeS ₇	La ₃ Ag _{0.82} SnS ₇	P6 ₃	0.9963	–	0.5766	Daszkiewicz et al. (2009b)
Tb ₃ Ag _{0.59} GeS ₇	Tb ₃ Ag _{0.59} GeS ₇	P6 ₃	0.9900	–	0.5765	Daszkiewicz et al. (2009b)
Dy ₃ Ag _{0.51} GeS ₇	Tb ₃ Ag _{0.59} GeS ₇	P6 ₃	0.9800	–	0.5787	Daszkiewicz et al. (2009b)
Ho ₃ Ag _{0.50} GeS ₇	Tb ₃ Ag _{0.59} GeS ₇	P6 ₃	0.9740	–	0.5799	Daszkiewicz et al. (2009b)
Er ₃ Ag _{0.50} GeS ₇	Tb ₃ Ag _{0.59} GeS ₇	P6 ₃	0.9692	–	0.5830	Daszkiewicz et al. (2009b)
La ₃ Ag _{0.94} GeSe ₇	La ₃ Ag _{0.82} SnS ₇	P6 ₃	1.0806	–	0,6111	Daszkiewicz et al. (2009a)
Ce ₃ Ag _{0.89} GeSe ₇	La ₃ Ag _{0.82} SnS ₇	P6 ₃	1.0711	–	0.60719	Daszkiewicz et al. (2009a)
Pr ₃ Ag _{0.89} GeSe ₇	La ₃ Ag _{0.82} SnS ₇	P6 ₃	1.0619	–	0.6070	Daszkiewicz et al. (2009a)
Nd ₃ Ag _{0.87} GeSe ₇	La ₃ Ag _{0.82} SnS ₇	P6 ₃	1.0621	–	0.60531	Daszkiewicz et al. (2009a)

(continued)

Table 38 (continued)

Compound	Structure type	Space group	Lattice parameters (nm)			Reference(s)
			<i>a</i>	<i>b</i>	<i>c</i>	
Sm ₃ Ag _{0.81} GeSe ₇	La ₃ Ag _{0.82} SnS ₇	<i>P6₃</i>	1.0479	–	0.60258	Daszkiewicz et al. (2009a)
Gd ₃ Ag _{0.85} GeSe ₇	La ₃ Ag _{0.82} SnS ₇	<i>P6₃</i>	1.0428	–	0.60321	Daszkiewicz et al. (2009a)
Tb ₃ Ag _{0.82} GeSe ₇	La ₃ Ag _{0.82} SnS ₇	<i>P6₃</i>	1.0364	–	0.60399	Daszkiewicz et al. (2009a)
Dy ₃ Ag _{0.72} GeSe ₇	La ₃ Ag _{0.82} SnS ₇	<i>P6₃</i>	1.0271	–	0.6057	Daszkiewicz et al. (2009a)
Sc _{1.02} Cu _{0.54} Sn _{1.10} S ₄	Yb _{1.84} Fe _{1.23} S ₄	<i>Fd$\bar{3}m$</i>	1.04176	–	–	Shemet et al. (2006d)
Y ₃ Cu _{1–4x} Sn _{1+x} S ₇ (<i>x</i> = 0)	La ₃ CuSiS ₇	<i>P6₃</i>	0.96766–	–	0.61717–	Gulay et al. (2005c),
0 < <i>x</i> ≤ 0.09	Y ₃ Cu _{0.64} Sn _{1.09} S ₇		0.9694		0.6168	Shemet et al. (2006b)
Y ₂ Cu _{0.20} Sn _{0.95} S ₅	Y ₂ Cu _{0.20} Sn _{0.95} S ₅	<i>Pbam</i>	1.12491	0.76994	0.37850	Shemet et al. (2006b)
La ₃ CuSnS ₇	La ₃ CuSiS ₇	<i>P6₃</i>	1.0317	–	0.60274	Gulay et al. (2005d)
Ce ₃ CuSnS ₇	La ₃ CuSiS ₇	<i>P6₃</i>	1.0209	–	0.60150	Gulay et al. (2005d)
Pr ₃ CuSnS ₇	La ₃ CuSiS ₇	<i>P6₃</i>	1.01417	–	0.60210	Gulay et al. (2005d)
Nd ₃ CuSnS ₇	La ₃ CuSiS ₇	<i>P6₃</i>	1.0075	–	0.60212	Gulay et al. (2005d)
Sm ₃ CuSnS ₇	La ₃ CuSiS ₇	<i>P6₃</i>	0.99288	–	0.60800	Gulay et al. (2005d)
Gd ₃ CuSnS ₇	La ₃ CuSiS ₇	<i>P6₃</i>	0.98087	–	0.61511	Gulay et al. (2005d)
Tb ₃ CuSnS ₇	La ₃ CuSiS ₇	<i>P6₃</i>	0.97512	–	0.61573	Gulay et al. (2005d)
Dy ₃ CuSnS ₇	La ₃ CuSiS ₇	<i>P6₃</i>	0.97024	–	0.61694	Gulay et al. (2005d)
Ho ₃ CuSnS ₇	La ₃ CuSiS ₇	<i>P6₃</i>	0.96527	–	0.61731	Gulay et al. (2005d)
Sc _{0.96–1.18} Cu _{0.37} Sn _{1.19–1.02} Se ₄	Yb _{1.84} Fe _{1.23} S ₄	<i>Fd$\bar{3}m$</i>	1.0822–	–	–	Gulay et al. (2005e)
			1.0935			Gulay et al. (2008e)
Y ₃ CuSnSe ₇	La ₃ CuSiS ₇	<i>P6₃</i>	1.01270	–	0.63951	Gulay et al. (2004)
La ₃ CuSnSe ₇	La ₃ CuSiS ₇	<i>P6₃</i>	1.07211	–	0.62770	Gulay and Olekseyuk (2005a)
Ce ₃ CuSnSe ₇	La ₃ CuSiS ₇	<i>P6₃</i>	1.0637	–	0.6254	Gulay et al. (2005f)
Pr ₃ CuSnSe ₇	La ₃ CuSiS ₇	<i>P6₃</i>	1.05613	–	0.62532	Gulay and Olekseyuk (2005a)

Nd ₃ CuSnSe ₇	La ₃ CuSiS ₇	P6 ₃	1.05002	–	0.62523	Gulay and Olekseyuk (2005a)
Sm ₃ CuSnSe ₇	La ₃ CuSiS ₇	P6 ₃	1.03809	–	0.62848	Gulay and Olekseyuk (2005a)
Gd ₃ CuSnSe ₇	La ₃ CuSiS ₇	P6 ₃	1.02435	–	0.63409	Gulay and Olekseyuk (2005a)
Tb ₃ CuSnSe ₇	La ₃ CuSiS ₇	P6 ₃	1.01894	–	0.63642	Gulay and Olekseyuk (2005a)
Dy ₃ CuSnSe ₇	La ₃ CuSiS ₇	P6 ₃	1.01359	–	0.63809	Gulay and Olekseyuk (2005a)
La ₃ AgSnS ₇	La ₃ CuSiS ₇	P6 ₃	1.0378	–	0.5990	Zeng et al. (2008)
La ₃ Ag _{0.82} SnS ₇	La ₃ Ag _{0.82} SnS ₇	P6 ₃				
at 298 K			1.0399	–	0.6016	Daszkiewicz et al. (2007b)
at 450 K			1.0404	–	0.6039	Daszkiewicz et al. (2007b)
at 530 K			1.0408	–	0.6050	Daszkiewicz et al. (2007b)
Ce ₃ Ag _{0.81} SnS ₇	La ₃ Ag _{0.82} SnS ₇	P6 ₃				
at 12 K			1.0302	–	0.5969	Daszkiewicz et al. (2007b)
at 298 K			1.0300	–	0.6002	Daszkiewicz et al. (2007b)
at 450 K			1.0292	–	0.6033	Daszkiewicz et al. (2007b)
at 530 K			1.0299	–	0.6041	Daszkiewicz et al. (2007b)
La ₃ AgSnSe ₇	La ₃ CuSiS ₇	P6 ₃	1.0805	–	0.6246	Daszkiewicz et al. (2007b)

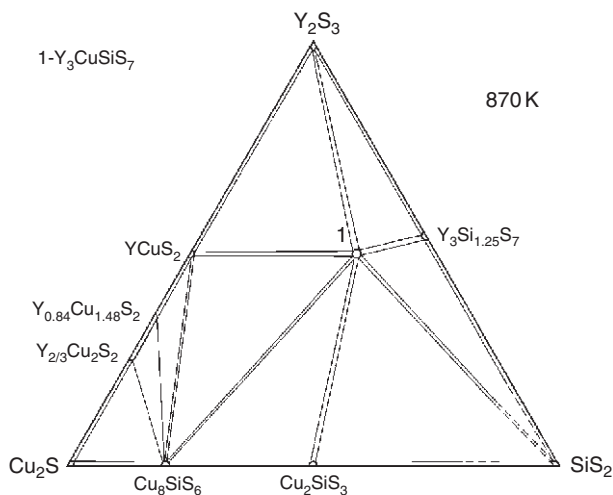


FIGURE 33 Isothermal section of the Y_2S_3 - Cu_2S - SiS_2 system at 870 K.

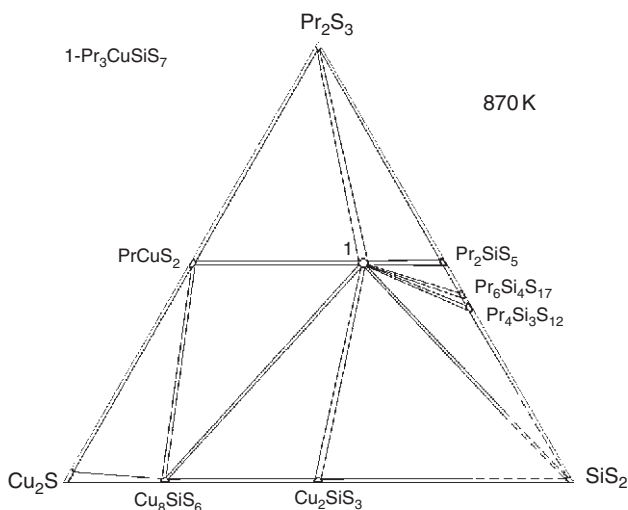


FIGURE 34 Isothermal section of the Pr_2S_3 - Cu_2S - SiS_2 system at 870 K.

4.2 Quaternary R_2X_3 - M_2X - PbX ($M = Cu, Ag$; $X = S, Se, Te$) systems

The R - M - Pb - X ($M = Cu, Ag$; $X = S, Se, Te$) systems have been investigated mainly across the R_2X_3 - M_2X - PbX sections. No quaternary compounds are known for Te systems and all systems of Ag . Quaternary

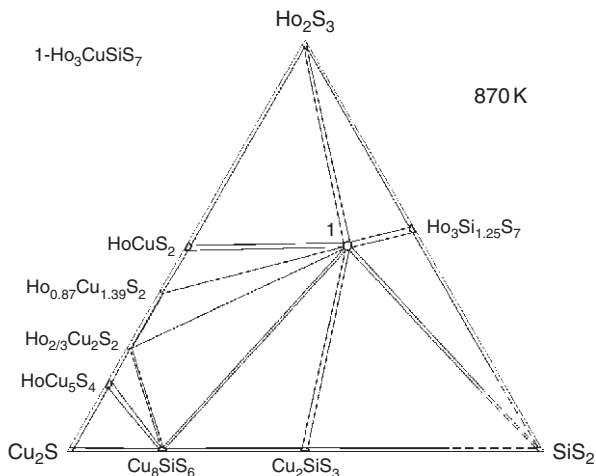


FIGURE 35 Isothermal section of the $\text{Ho}_2\text{S}_3\text{-Cu}_2\text{S-SiS}_2$ system at 870 K.

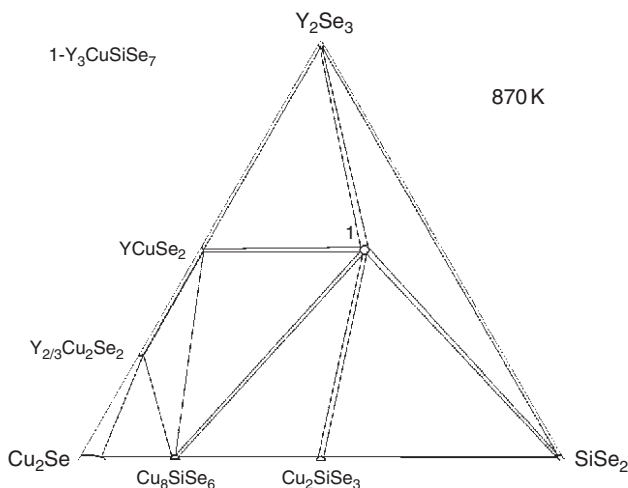


FIGURE 36 Isothermal section of the $\text{Y}_2\text{Se}_3\text{-Cu}_2\text{Se-SiSe}_2$ system at 870 K.

compounds prepared in $\text{R}_2\text{X}_3\text{-Cu}_2\text{X-PbX}$ ($\text{X} = \text{S, Se}$) system crystallize in (a) monoclinic Cm space group with $\text{Y}_{3.33}\text{CuPb}_{1.5}\text{S}_7$ structure type, (b) orthorhombic $Cmcm$ space group with $\text{Er}_5\text{CuPb}_3\text{Se}_{11}$ and ErCuPbS_3 structure types, and (c) orthorhombic $Pnma$ space group with $\beta\text{-BaLaCuSe}_3$ and LaCuPbS_3 structure types (Table 39).

The isothermal sections of the systems $\text{Y}_2\text{S}_3\text{-Cu}_2\text{S-PbS}$ (Gulay et al., 2007a), $\text{Pr}_2\text{S}_3\text{-Cu}_2\text{S-PbS}$ (Marchuk et al., 2006a), $\text{Tb}_2\text{S}_3\text{-Cu}_2\text{S-PbS}$

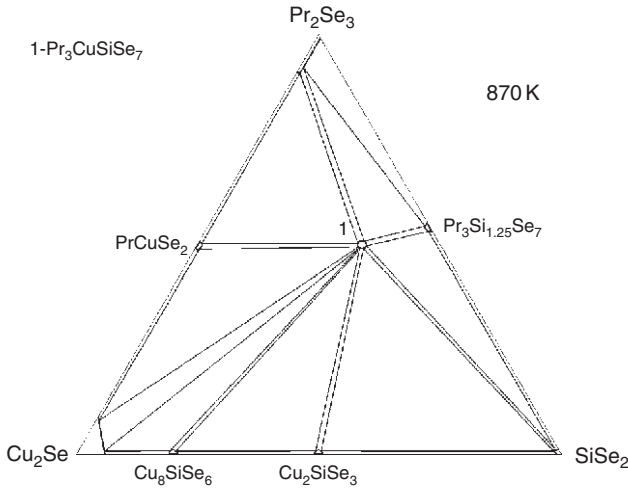


FIGURE 37 Isothermal section of the Pr_2Se_3 - Cu_2Se - SiSe_2 system at 870 K.

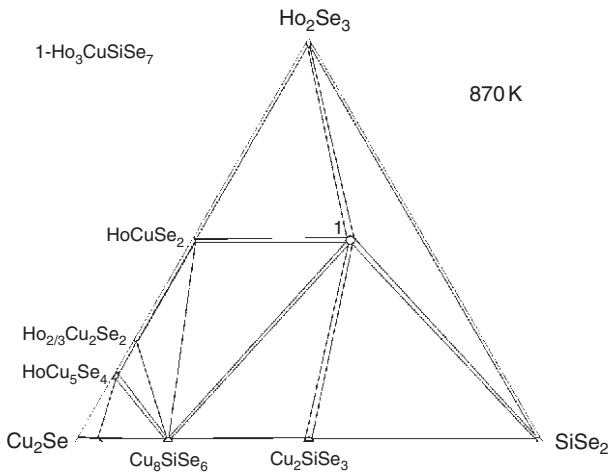


FIGURE 38 Isothermal section of the Ho_2Se_3 - Cu_2Se - SiSe_2 system at 870 K.

(Hvaleba et al., 2006), Dy_2S_3 - Cu_2S - PbS (Gulay et al., 2007a), Ho_2S_3 - Cu_2S - PbS (Gulay et al., 2007a), Er_2S_3 - Cu_2S - PbS (Gulay et al., 2007a), Sc_2Se_3 - Cu_2Se - PbSe (Gulay et al., 2008e), Y_2Se_3 - Cu_2Se - PbSe (Shemet et al., 2005), Pr_2Se_3 - Cu_2Se - PbSe (Marchuk et al., 2006b), Tb_2Se_3 - Cu_2Se - PbSe (Gulay et al., 2006b), Dy_2Se_3 - Cu_2Se - PbSe (Gulay et al., 2006b), Ho_2Se_3 - Cu_2Se - PbSe (Gulay et al., 2006g), Er_2Se_3 - Cu_2Se - PbSe (Gulay et al., 2006g), Tm_2Se_3 - Cu_2Se - PbSe (Gulay et al., 2006d), Lu_2Se_3 - Cu_2Se - PbSe (Gulay

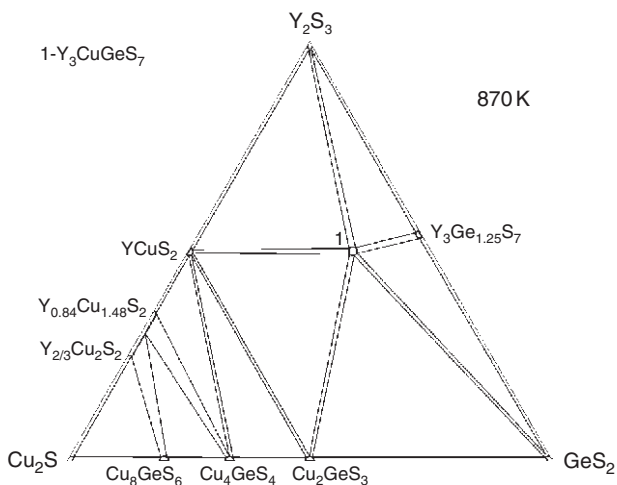


FIGURE 39 Isothermal section of the Y_2S_3 - Cu_2S - GeS_2 system at 870 K.

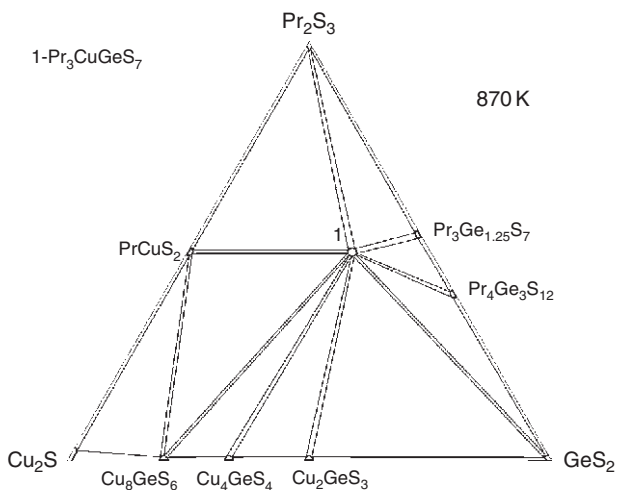


FIGURE 40 Isothermal section of the Pr_2S_3 - Cu_2S - GeS_2 system at 870 K.

et al., 2006d), Y_2Te_3 - Cu_2Te - $PbTe$ (Shemet et al., 2006e), Tb_2Te_3 - Cu_2Te - $PbTe$ (Marchuk et al., 2008), Dy_2Te_3 - Cu_2Te - $PbTe$ (Marchuk et al., 2008), Ho_2Te_3 - Cu_2Te - $PbTe$ (Gulay and Olekseyuk, 2006a), Er_2Te_3 - Cu_2Te - $PbTe$ (Gulay and Olekseyuk, 2006a), Tm_2Te_3 - Cu_2Te - $PbTe$ (Gulay and Olekseyuk, 2006a), Pr_2Se_3 - Ag_2Se - $PbSe$ (Marchuk et al., 2006b), Tb_2Te_3 - Ag_2Te - $PbTe$ (Marchuk et al., 2008), and Dy_2Te_3 - Ag_2Te - $PbTe$ (Marchuk et al., 2008) are shown in Figures 59–82, respectively.

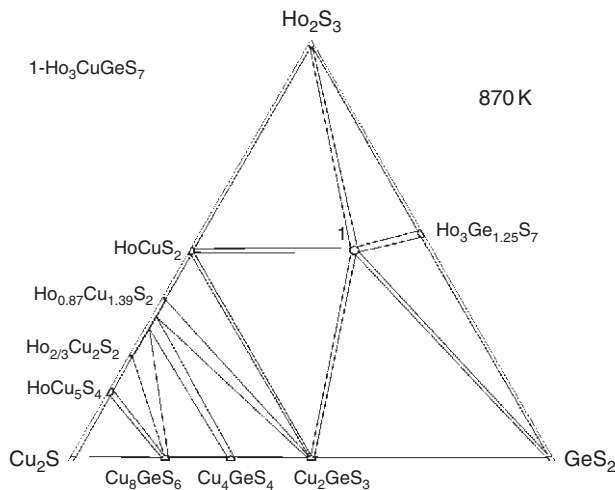


FIGURE 41 Isothermal section of the Ho_2S_3 - Cu_2S - GeS_2 system at 870 K.

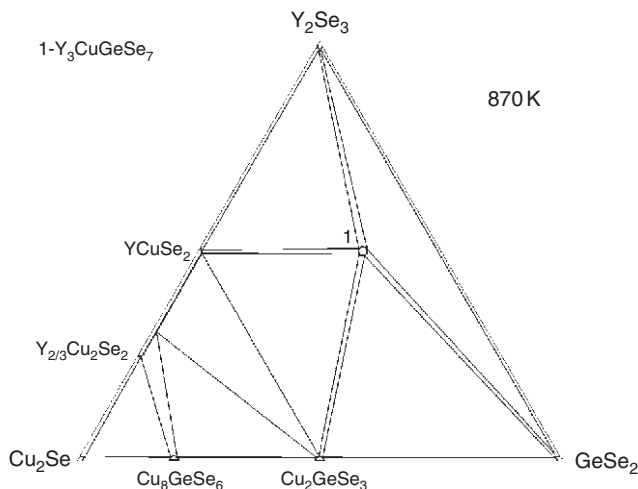


FIGURE 42 Isothermal section of the Y_2Se_3 - Cu_2Se - GeSe_2 system at 870 K.

Formation of two or three quaternary compounds has been observed in the R_2X_3 - Cu_2X - PbX ($\text{X} = \text{S}, \text{Se}$) systems with small R (Gd-Lu). No quaternary compound (except LaCuPbS_3) has been observed in the R_2X_3 - Cu_2X - PbX ($\text{X} = \text{S}, \text{Se}$) systems with large R (La-Sm). No quaternary compounds has been observed in the R_2X_3 - Ag_2X - PbX ($\text{X} = \text{S}, \text{Se}, \text{Te}$) and R_2Te_3 - Cu_2Te - PbTe systems. Compounds with RMX_2 stoichiometry can be prepared in all of the R-Cu-X and (Tb, Dy)-Ag-Te systems.

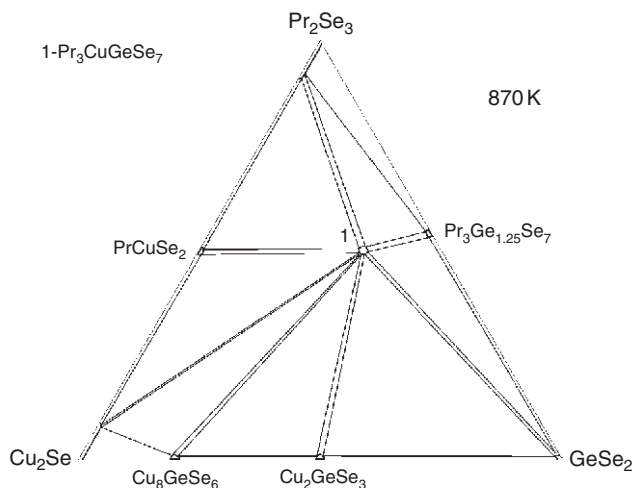


FIGURE 43 Isothermal section of the Pr_2Se_3 - Cu_2Se - GeSe_2 system at 870 K.

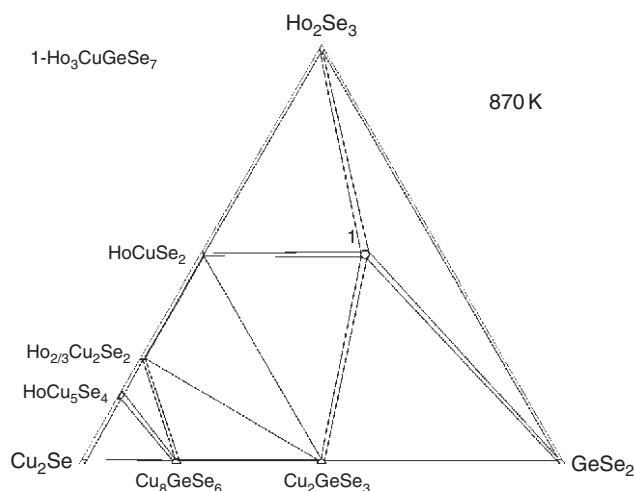


FIGURE 44 Isothermal section of the Ho_2Se_3 - Cu_2Se - GeSe_2 system at 870 K.

4.3 Quaternary R_2X_3 - M_2X - In_2X_3 ($\text{M} = \text{Cu}, \text{Ag}$; $\text{X} = \text{S}, \text{Se}$) systems

The R-M-In-X ($\text{M} = \text{Cu}, \text{Ag}$; $\text{X} = \text{S}, \text{Se}, \text{Te}$) systems have been investigated mainly across the R_2X_3 - M_2X - In_2X_3 sections, and no quaternary compounds have been reported for Te. A small series of the copper quaternary compounds have been prepared in these systems (Table 40).

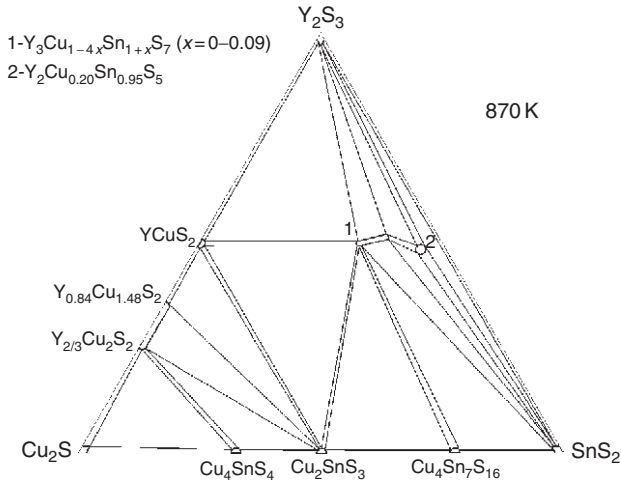


FIGURE 45 Isothermal section of the Y_2S_3 - Cu_2S - SnS_2 system at 870 K.

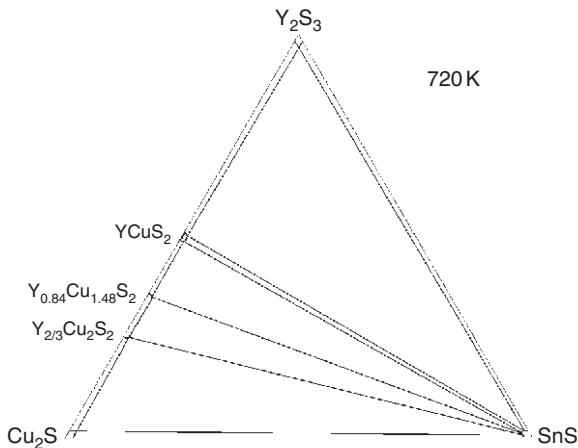


FIGURE 46 Isothermal section of the Y_2S_3 - Cu_2S - SnS system at 720 K.

The copper-containing chalcogenides crystallize in orthorhombic symmetry, SG $Pnma$. Only one silver quaternary compound, $La_4Ag_2In_4S_{13}$, has been reported. It crystallizes with relatively large a and b lattice parameters.

The isothermal sections of the systems Y_2S_3 - Cu_2S - In_2S_3 (Huch et al., 2007a), La_2S_3 - Cu_2S - In_2S_3 (Huch et al., 2007a), Pr_2S_3 - Cu_2S - In_2S_3 (Huch et al., 2007a), Er_2S_3 - Cu_2S - In_2S_3 (Huch et al., 2007a), Y_2Se_3 - Cu_2Se - In_2Se_3 (Huch et al., 2007b), La_2Se_3 - Cu_2Se - In_2Se_3 (Huch et al., 2007b), Pr_2Se_3 - Cu_2Se - In_2Se_3 (Huch et al., 2007b), and Er_2Se_3 - Cu_2Se - In_2Se_3 (Huch et al., 2007b) are shown in Figures 83–90, respectively.

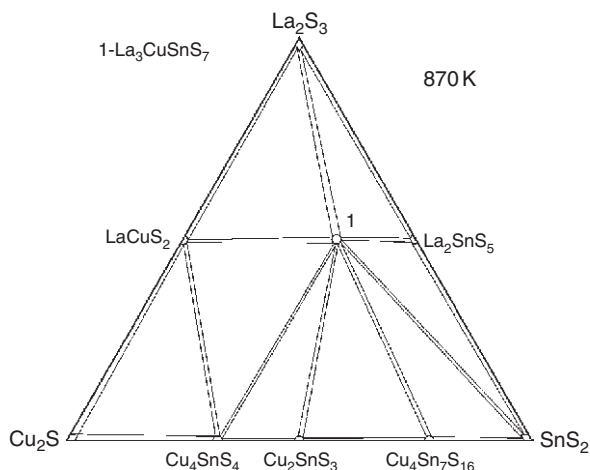


FIGURE 47 Isothermal section of the La_2S_3 - Cu_2S - SnS_2 system at 870 K.

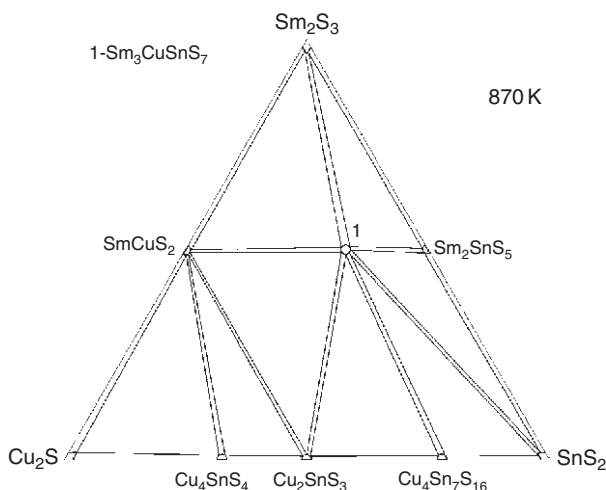


FIGURE 48 Isothermal section of the Sm_2S_3 - Cu_2S - SnS_2 system at 870 K.

Formation of one quaternary compound having R_2CuInX_5 stoichiometry with orthorhombic symmetry (SG $Pnma$) has been observed in R_2X_3 - M_2X - In_2X_3 ($\text{X} = \text{S}, \text{Se}$) systems with large R (La-Sm). No quaternary compounds has been observed in the R_2X_3 - M_2X - In_2X_3 ($\text{X} = \text{S}, \text{Se}$) systems with small R (Gd-Lu), except for the Er_2S_3 - Cu_2S - In_2S_3 system, where $\text{Er}_4\text{Cu}_2\text{In}_4\text{S}_{13}$ phase was isolated. Many of the ternary indium-rich compounds were prepared in the selenium-containing R_2Se_3 - M_2Se - In_2Se_3 systems.

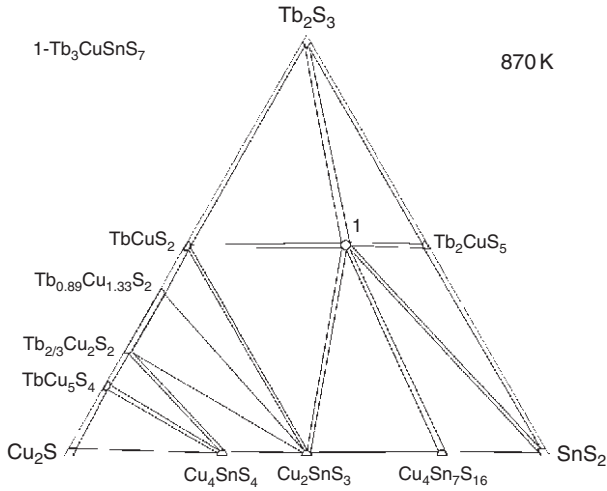


FIGURE 49 Isothermal section of the Tb_2S_3 - Cu_2S - SnS_2 system at 870 K.

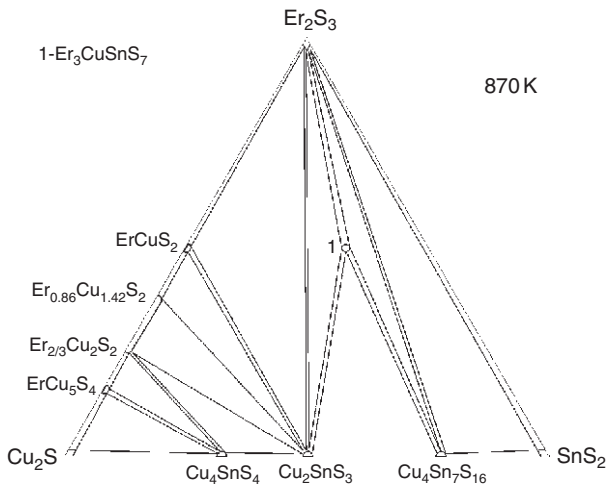


FIGURE 50 Isothermal section of the Er_2S_3 - Cu_2S - SnS_2 system at 870 K.

4.4 Structure types of quaternary systems

4.4.1 Structure type $\text{La}_3\text{CuSiS}_7$

Structure type $\text{La}_3\text{CuSiS}_7$ (Collin and Laruelle, 1971) (Figure 91, Table 41). SG $P6_3$, $Z = 2$, $a = 1.0310$, $c = 0.5794$ nm. The sulfur atoms form bicapped trigonal prismatic arrangement around the lanthanum atom, and the shortest La-S distance is 0.2869 nm. The copper atom is located on the

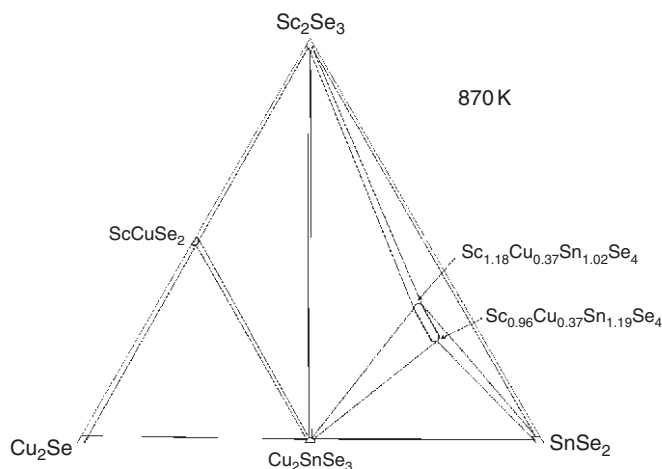


FIGURE 51 Isothermal section of the Sc_2Se_3 - Cu_2Se - SnSe_2 system at 870 K.

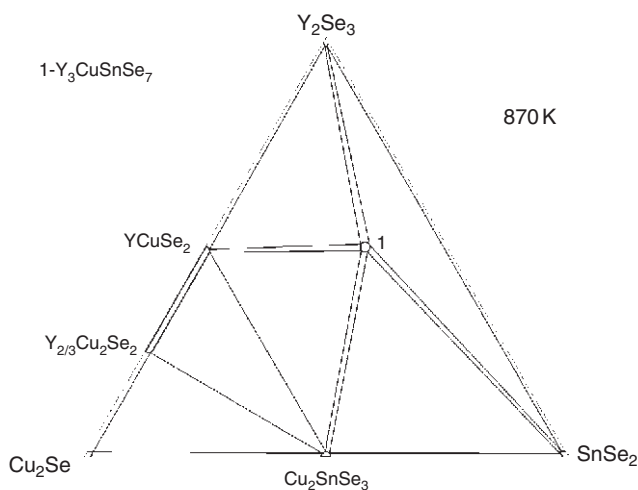


FIGURE 52 Isothermal section of the Y_2Se_3 - Cu_2Se - SnSe_2 system at 870 K.

sixfold screw axis and has triangular surrounding formed by the sulfur atoms. The shortest Cu-S distance is 0.2272 nm. The Si atoms have a tetrahedrally shaped coordination sphere and the shortest Si-S distance is 0.2086 nm. The S1 atoms are located in trigonal bipyramids, and the S2 and S3 atoms have CN of 4 and a tetrahedral arrangement formed by 3La and 1Si atoms.

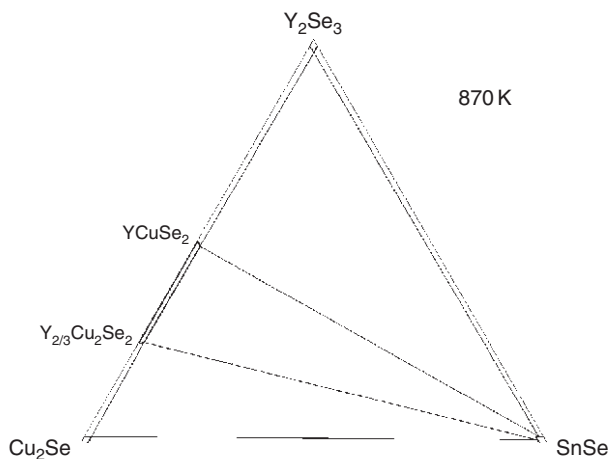


FIGURE 53 Isothermal section of the Y_2Se_3 - Cu_2Se - $SnSe$ system at 870 K.

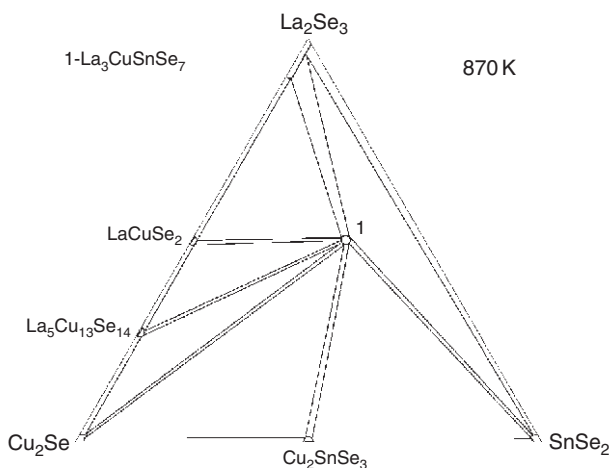


FIGURE 54 Isothermal section of the La_2Se_3 - Cu_2Se - $SnSe_2$ system at 870 K.

4.4.2 Structure type $La_3Ag_{0.82}SnS_7$

Structure type $La_3Ag_{0.82}SnS_7$ (Daszkiewicz et al., 2007b) (Figure 92, Table 42). SG $P6_3$, $Z = 2$, $a = 1.04168$, $c = 0.57825$ nm. The structure is *quasi*-isostructural to La_3CuSiS_7 , two sites for the silver atoms have been established. The Ag1 and Ag2 atoms have triangular and trigonal antiprismatic surroundings, respectively, formed by the S atoms, with the shortest Ag1-S and Ag2-S distances equal to 0.24331 and 0.2813 nm. The shortest La-S distance is 0.29125 nm. The Sn atoms are situated in a

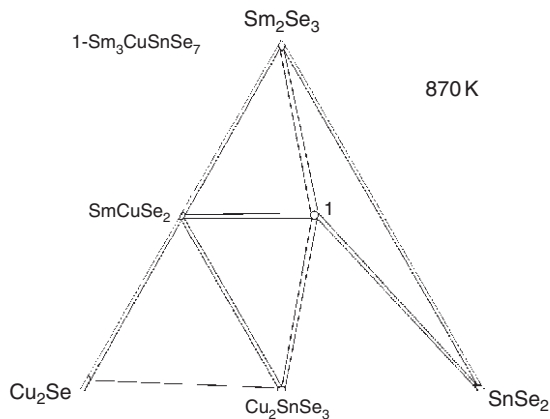


FIGURE 55 Isothermal section of the Sm_2Se_3 – Cu_2Se – SnSe_2 system at 870 K.

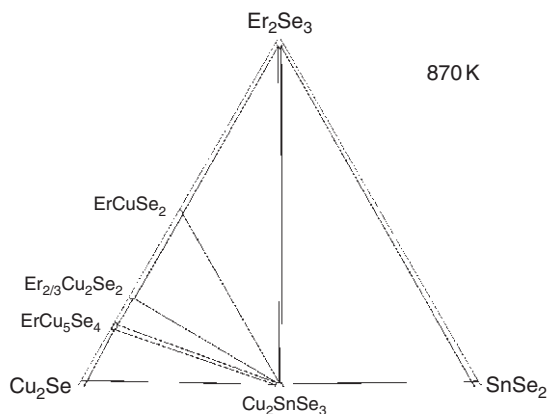


FIGURE 56 Isothermal section of the Er_2Se_3 – Cu_2Se – SnSe_2 system at 870 K.

tetrahedral coordination sphere, and the shortest Sn–S distance is 0.2344 nm. S1 and S3 atoms have CN of 4 and tetrahedral arrangements formed by 3La and 1Sn atoms. Since Ag atoms occupy defect positions, each S2 atom is located in tetragonal bipyramid formed by 4La and 2Ag atoms.

4.4.3 Structure type $\text{Tb}_3\text{Ag}_{0.59}\text{GeS}_7$

Structure type $\text{Tb}_3\text{Ag}_{0.59}\text{GeS}_7$ (Daszkiewicz et al., 2009b) (Figure 93, Table 43). SG $P6_3$, $Z = 2$, $a = 0.9809$, $c = 0.5805$ nm. The structure is *quasi*-isostructural to $\text{La}_3\text{Ag}_{0.82}\text{SnS}_7$; however, only the octahedral position of the silver atom has been confirmed with the shortest Ag–S distance

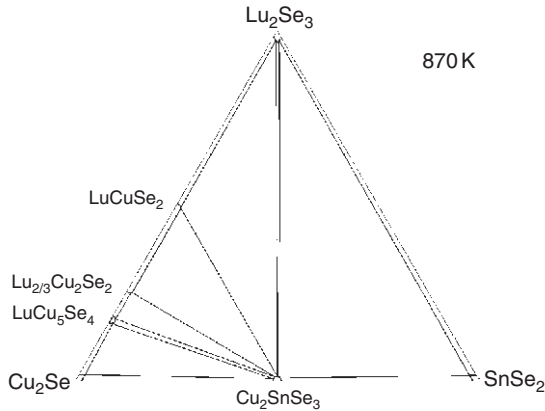


FIGURE 57 Isothermal section of the Lu_2Se_3 – Cu_2Se – SnSe_2 system at 870 K.

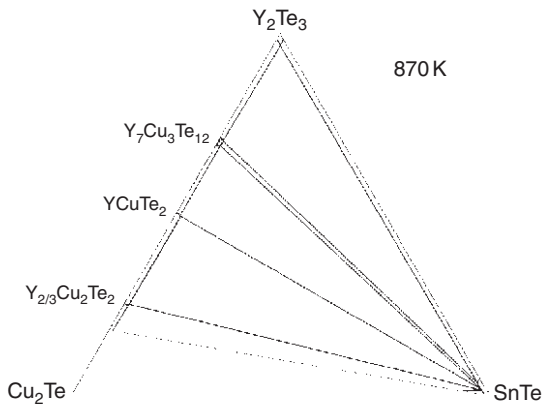


FIGURE 58 Isothermal section of the Y_2Te_3 – Cu_2Te – SnTe system at 870 K.

of 0.2504 nm. The sulfur atoms create monocapped trigonal prismatic arrangement around the terbium atom and the shortest Tb–S distance is 0.2805 nm. The germanium atom is situated in tetrahedral surrounding of the sulfur atoms. The shortest Ge–S distance is 0.2175 nm. Each of the S1 and S3 atoms has tetrahedral surroundings of the 3Tb and 1Ge atoms. The S2 atom is located in trigonal bipyramid centered outside.

4.4.4 Structure type $\text{Pb}_{1.75}\text{Ag}_{0.5}\text{GeS}_4$

Structure type $\text{Pb}_{1.75}\text{Ag}_{0.5}\text{GeS}_4$ (Iyer et al., 2004) (Figure 94, Table 44). SG $\bar{I}43d$, $Z = 16$, $a = 1.3949$ nm for $\text{Eu}_{1.75}\text{Ag}_{0.5}\text{GeS}_4$ (Iyer et al., 2004). The sulfur atoms create octahedral arrangement around the europium atoms

TABLE 39 Crystallographic data for quaternary chalcogenides of the R_2X_3 - Cu_2X - PbX ($X = S, Se$) systems

Compound	Structure type	Space group	Lattice parameters (nm)			Reference(s)
			<i>a</i>	<i>b</i>	<i>c</i>	
$Y_{5+x}Cu_{1-x}Pb_{3-x}S_{11}$ ($x = 0.28$)	$Er_5CuPb_3Se_{11}$	<i>Cmcm</i>	0.39423	1.3007	3.6386	Gulay et al. (2007a)
$Y_{3.33}CuPb_{1.5}S_7$	$Y_{3.33}CuPb_{1.5}S_7$	<i>Cm</i>	1.30246	0.39421	1.20671	Gulay et al. (2005g)
$YCuPbS_3$	β -BaLaCuSe ₃	<i>Pnma</i>	1.01957	0.39370	1.29625	Gulay et al. (2005c)
$LaCuPbS_3$	$LaCuPbS_3$	<i>Pnma</i>	0.8091	0.4093	1.5996	Brennan and Ibers (1992)
$Tb_{3.33}CuPb_{1.5}S_7$	$Y_{3.33}CuPb_{1.5}S_7$	<i>Cm</i>	1.3129	0.39791	1.2176	Gulay and Olekseyuk (2006b)
$TbCuPbS_3$	$ErCuPbS_3$	<i>Cmcm</i>	0.39413	1.2885	1.0262	Gulay et al. (2005h)
$Dy_5CuPb_3S_{11}$	$Er_5CuPb_3Se_{11}$	<i>Cmcm</i>	0.39604	1.3068	3.6653	Gulay et al. (2007a)
$Dy_{3.33}CuPb_{1.5}S_7$	$Y_{3.33}CuPb_{1.5}S_7$	<i>Cm</i>	1.3079	0.39591	1.2119	Gulay and Olekseyuk (2006b)
$DyCuPbS_3$	$ErCuPbS_3$	<i>Cmcm</i>	0.39297	1.2891	1.0205	Gulay et al. (2005h)
$Ho_5Cu_{1+x}Pb_{3-x/2}S_{11}$ ($x = 0.25$)	$Er_5CuPb_3Se_{11}$	<i>Cmcm</i>	0.39400	1.3022	3.6707	Gulay et al. (2007a)
$Ho_{3.33}CuPb_{1.5}S_7$	$Y_{3.33}CuPb_{1.5}S_7$	<i>Cm</i>	1.3047	0.39462	1.2090	Gulay and Olekseyuk (2006b)
$HoCuPbS_3$	$ErCuPbS_3$	<i>Cmcm</i>	0.3925	1.2916	1.0161	Gulay et al. (2005h)
$Er_5CuPb_3S_{11}$	$Er_5CuPb_3Se_{11}$	<i>Cmcm</i>	0.39329	1.3004	3.6664	Gulay et al. (2007a)
$Er_{3.33}CuPb_{1.5}S_7$	$Y_{3.33}CuPb_{1.5}S_7$	<i>Cm</i>	1.3011	0.39313	1.20606	Gulay and Olekseyuk (2006b)
$ErCuPbS_3$	$ErCuPbS_3$	<i>Cmcm</i>	0.3916	1.2934	1.0106	Gulay et al. (2005h)
$TmCuPbS_3$	$ErCuPbS_3$	<i>Cmcm</i>	0.39096	1.29539	1.0078	Gulay et al. (2005h)
$YbCuPbS_3$	$ErCuPbS_3$	<i>Cmcm</i>	0.3911	1.2956	1.0064	Gulay et al. (2005h)

(continued)

Table 39 (continued)

Compound	Structure type	Space group	Lattice parameters (nm)			Reference(s)
			<i>a</i>	<i>b</i>	<i>c</i>	
Lu _{3.33} CuPb _{1.5} S ₇	Y _{3.33} CuPb _{1.5} S ₇	<i>Cm</i>	1.29262	0.38948 $\beta = 104.794^\circ$	1.19916	Gulay and Olekseyuk (2006b)
LuCuPbSe ₃	ErCuPbS ₃	<i>Cmcm</i>	0.3889	1.2920	1.0030	Gulay et al. (2005h)
Y _{3.33} CuPb _{1.5} Se ₇	Y _{3.33} CuPb _{1.5} S ₇	<i>Cm</i>	1.35675	0.40959 $\beta = 104.661^\circ$	1.26026	Gulay et al. (2005g)
YCuPbSe ₃	β -BaLaCuSe ₃	<i>Pnma</i>	1.05438	0.40524	1.33840	Gulay et al. (2004)
GdCuPbSe ₃	β -BaLaCuSe ₃	<i>Pnma</i>	1.0687	0.40858	1.3443	Gulay and Olekseyuk (2005b)
Tb _{3.33} CuPb _{1.5} Se ₇	Lu _{3.33} CuPb _{1.5} Se ₇	<i>Cm</i>	1.3624	0.41144 $\beta = 104.68^\circ$	1.2645	Gulay and Olekseyuk (2005c)
TbCuPbSe ₃	β -BaLaCuSe ₃	<i>Pnma</i>	1.0603	0.40680	1.3414	Gulay and Olekseyuk (2005b)
Dy _{3.33} CuPb _{1.5} Se ₇	Lu _{3.33} CuPb _{1.5} Se ₇	<i>Cm</i>	1.3557	0.4091 $\beta = 104.59^\circ$	1.2574	Gulay and Olekseyuk (2005c)
DyCuPbSe ₃	β -BaLaCuSe ₃	<i>Pnma</i>	1.05606	0.40594	1.34236	Gulay and Olekseyuk (2005b)
Ho _{3.33} CuPb _{1.5} Se ₇	Lu _{3.33} CuPb _{1.5} Se ₇	<i>Cm</i>	1.35314	0.40819 $\beta = 104.577^\circ$	1.25609	Gulay and Olekseyuk (2005c)
HoCuPbSe ₃	β -BaLaCuSe ₃	<i>Pnma</i>	1.0516	0.40470	1.3410	Gulay et al. (2006g)
Er ₅ CuPb ₃ Se ₁₁	Er ₅ CuPb ₃ Se ₁₁	<i>Cmcm</i>	0.40710	1.3480	3.8092	Gulay et al. (2006i)
Er _{3.33} CuPb _{1.5} Se ₇	Lu _{3.33} CuPb _{1.5} Se ₇	<i>Cm</i>	1.35018	0.40693 $\beta = 104.492^\circ$	1.25433	Gulay and Olekseyuk (2005c)
ErCuPbSe ₃	β -BaLaCuSe ₃	<i>Pnma</i>	1.04846	0.40424	1.34143	Gulay and Olekseyuk (2005b)
Tm ₅ CuPb ₃ Se ₁₁	Er ₅ CuPb ₃ Se ₁₁	<i>Cmcm</i>	0.40582	1.3429	3.7979	Gulay et al. (2006i)

$\text{Tm}_{3.33}\text{CuPb}_{1.5}\text{Se}_7$	$\text{Lu}_{3.33}\text{CuPb}_{1.5}\text{Se}_7$	<i>Cm</i>	1.34584	0.40560 $\beta = 104.342^\circ$	1.25083	Gulay and Olekseyuk (2005c)
TmCuPbSe_3	$\beta\text{-BaLaCuSe}_3$	<i>Pnma</i>	1.0447	0.40400	1.3423	Gulay and Olekseyuk (2005b)
$\text{Yb}_5\text{CuPb}_3\text{Se}_{11}$	$\text{Er}_5\text{CuPb}_3\text{Se}_{11}$	<i>Cmcm</i>	0.40487	1.33993	3.7876	Gulay et al. (2006i)
$\text{Yb}_{3.33}\text{CuPb}_{1.5}\text{Se}_7$	$\text{Lu}_{3.33}\text{CuPb}_{1.5}\text{Se}_7$	<i>Cm</i>	1.3425	0.40437 $\beta = 104.381^\circ$	1.2484	Gulay and Olekseyuk (2005c)
YbCuPbSe_3	$\beta\text{-BaLaCuSe}_3$	<i>Pnma</i>	1.0407	0.40350	1.3401	Gulay et al. (2006h)
$\text{Lu}_{3.33}\text{CuPb}_{1.5}\text{Se}_7$	$\text{Lu}_{3.33}\text{CuPb}_{1.5}\text{Se}_7$	<i>Cm</i>	1.3404	0.40307 $\beta = 104.36^\circ$	1.2475	Gulay and Olekseyuk (2005c)
LuCuPbSe_3	$\beta\text{-BaLaCuSe}_3$	<i>Pnma</i>	1.03857	0.40248	1.34056	Gulay and Olekseyuk (2005b)

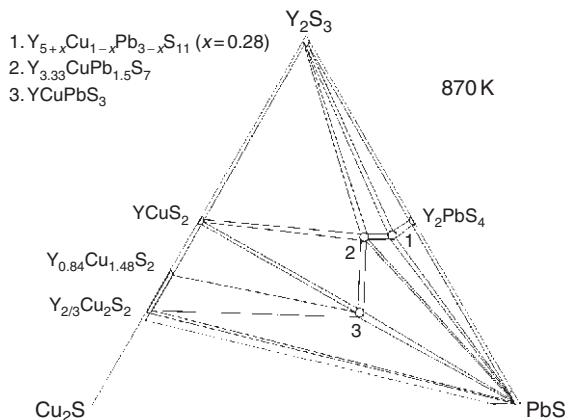


FIGURE 59 Isothermal section of the Y_2S_3 - Cu_2S - PbS system at 870 K.

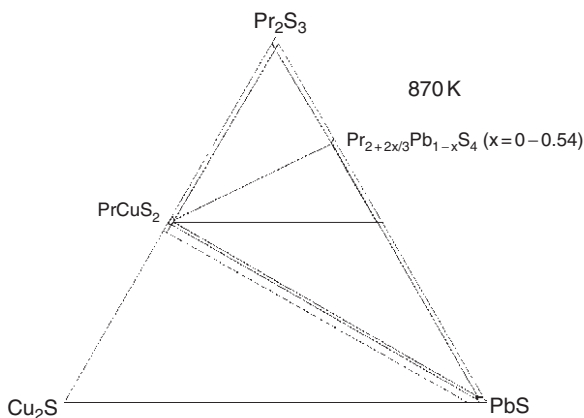


FIGURE 60 Isothermal section of the Pr_2S_3 - Cu_2S - PbS system at 870 K.

and the shortest Eu-S distance is 0.2475 nm. The silver and germanium atoms have tetrahedral surroundings formed by the S atoms, and the shortest Ag-S and Ge-S distances are 0.2574 and 0.2179 nm, respectively. The S1 atom is located in a tetrahedron formed by 3Eu and 1Ge atoms. Due to the occupational disorder of the silver and europium atoms, the nearest coordination sphere of the S2 atom is complex and contains 4Eu, 1Ag, and 1Ge atoms.

4.4.5 Structure type $Y_3Cu_{0.64}Sn_{1.09}S_7$

Structure type $Y_3Cu_{0.64}Sn_{1.09}S_7$ (Shemet et al., 2006b) (Figure 95, Table 45). SG $P6_3$, $Z = 2$, $a = 0.9694$, $c = 0.6168$ nm. The structure is *quasi*-isostructural to $La_3Ag_{0.82}SnS_7$. The sulfur atoms create a monocapped trigonal

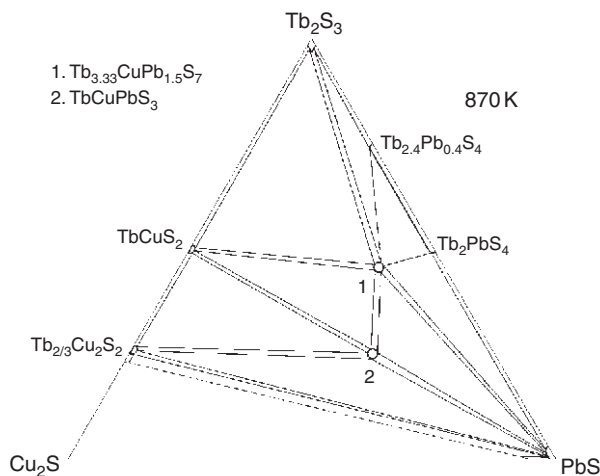


FIGURE 61 Isothermal section of the Tb_2S_3 - Cu_2S - PbS system at 870 K.

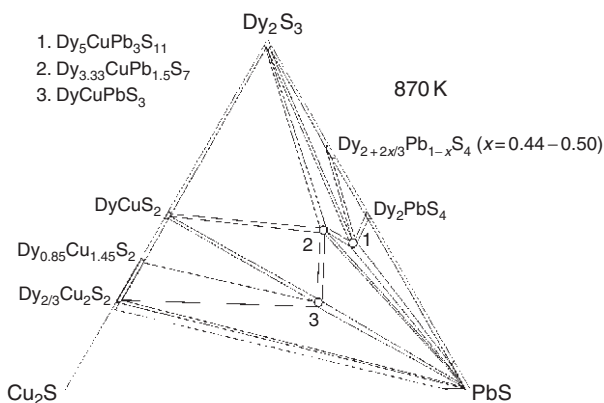


FIGURE 62 Isothermal section of the Dy_2S_3 - Cu_2S - PbS system at 870 K.

prismatic arrangement around the yttrium atom, and the shortest Y-S distance is 0.2713 nm. The positions of the Cu and the Sn2 atoms correspond to the Ag1 and Ag2 in $La_3Ag_{0.82}SnS_7$, respectively. The shortest Cu-S distance is 0.2216 nm. The other tin atom, Sn1, has a tetrahedral coordination sphere. The shortest Sn2-S distance (trigonal antiprismatic site), 0.2618 nm, is longer than the shortest Sn1-S distance (tetrahedral site), 0.2360 nm. Since Cu and Sn2 atoms occupy defect positions, the S1 atom is located in a trigonal bipyramid formed by 3Y, 1Cu, and 1Sn atoms. Further, the S2 and S3 atoms have CN of 4 and tetrahedral surroundings made of the 3Y and 1Sn atoms.

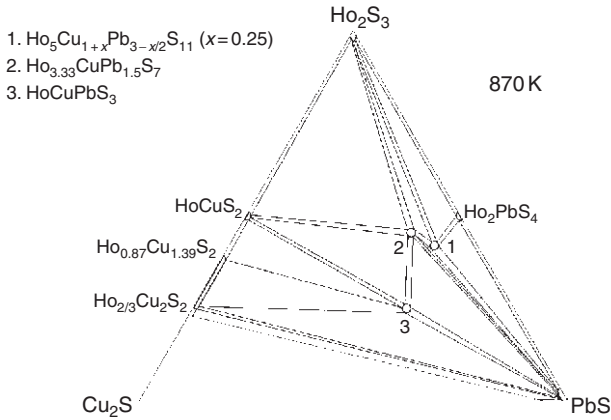


FIGURE 63 Isothermal section of the Ho_2S_3 - Cu_2S - PbS system at 870 K.

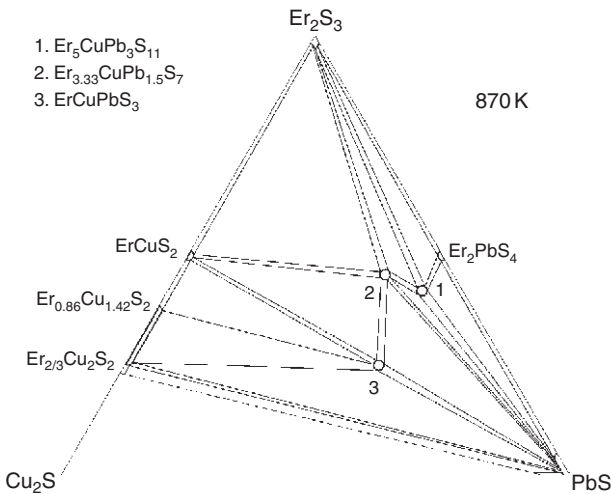


FIGURE 64 Isothermal section of the Er_2S_3 - Cu_2S - PbS system at 870 K.

4.4.6 Structure type $\text{Y}_2\text{Cu}_{0.20}\text{Sn}_{0.95}\text{S}_5$

Structure type $\text{Y}_2\text{Cu}_{0.20}\text{Sn}_{0.95}\text{S}_5$ (Shemet et al., 2006b) (Figure 96, Table 46). SG *Pbam*, $Z = 2$, $a = 1.12491$, $b = 0.76994$, $c = 0.37850$ nm. The sulfur atoms create bicapped trigonal prismatic, tetrahedral and octahedral arrangement around the yttrium, copper and tin atoms, respectively. The shortest interatomic distances among these coordination spheres are $d(\text{Y-S}) = 0.2718$ nm, $d(\text{Cu-S}) = 0.208$ nm, and $d(\text{Sn-S}) = 0.2507$ nm. Two of the three independent sulfur atoms—S1 and S2—have CN of 6 and pseudo-octahedral surroundings. The S3 atom is located in a

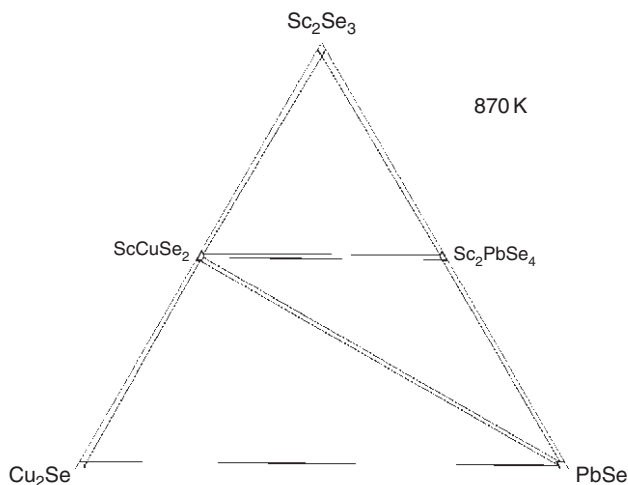


FIGURE 65 Isothermal section of the Sc_2Se_3 – Cu_2Se – PbSe system at 870 K.

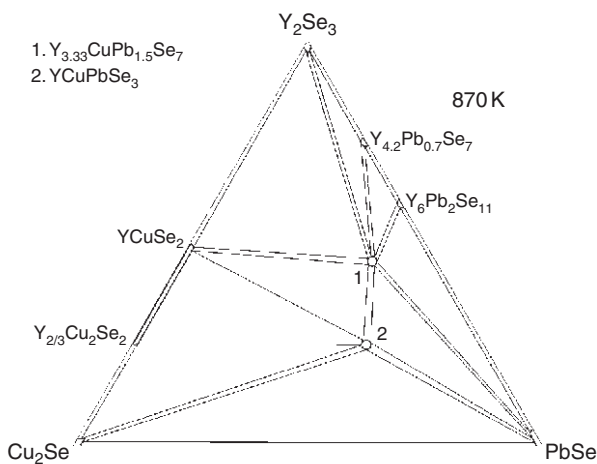


FIGURE 66 Isothermal section of the Y_2Se_3 – Cu_2Se – PbSe system at 870 K.

six-vertex polyhedron formed by 2Y , 2Cu , and 2Sn atoms which resembles a distorted pentagonal pyramid.

4.4.7 Structure type $\text{Yb}_{1.84}\text{Fe}_{1.23}\text{S}_4$

Structure type $\text{Yb}_{1.84}\text{Fe}_{1.23}\text{S}_4$ (Tomas et al., 1992) (Figure 97, Table 47). SG $Fd\bar{3}m$, $Z = 4$, $a = 1.08827$ nm for $\text{Sc}_{1.09}\text{Cu}_{0.37}\text{Sn}_{1.09}\text{Se}_4$ (Gulay et al., 2005e). The Sc atoms are located in octahedra formed by the Se atoms and the

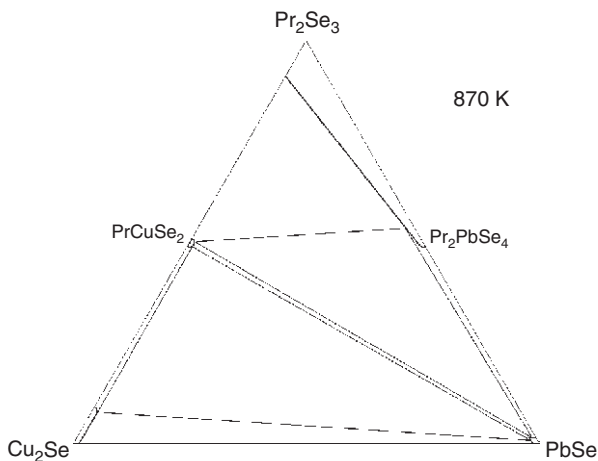


FIGURE 67 Isothermal section of the Pr_2Se_3 - Cu_2Se - PbSe system at 870 K.

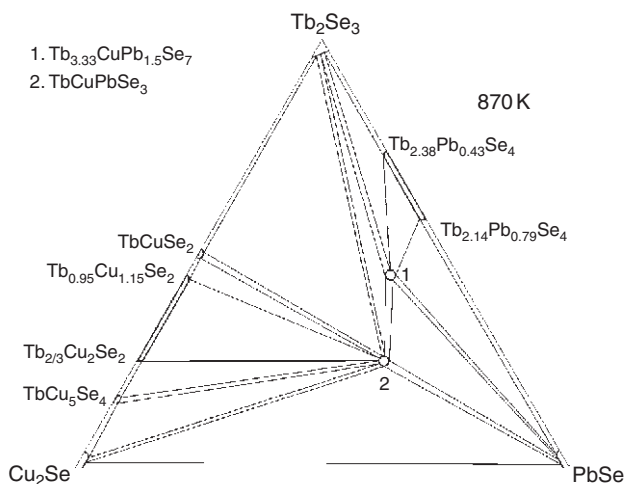


FIGURE 68 Isothermal section of the Tb_2Se_3 - Cu_2Se - PbSe system at 870 K.

shortest Sc-Se distance is 0.2747 nm. The randomly distributed Sc and Sn atoms (M) are also located in an octahedral site with the shortest M-Se distance 0.2695 nm. Each copper atom has a tetrahedral surrounding of the selenium atoms. The shortest Cu-Se distance is 0.2401 nm. The Se atoms are located in an octahedron formed by 3Sc and 3M with one additional atom Cu atom centering one of the faces.

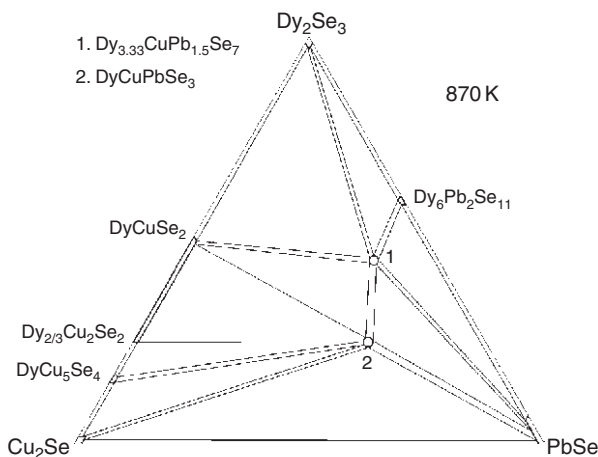


FIGURE 69 Isothermal section of the Dy_2Se_3 - Cu_2Se - PbSe system at 870 K.

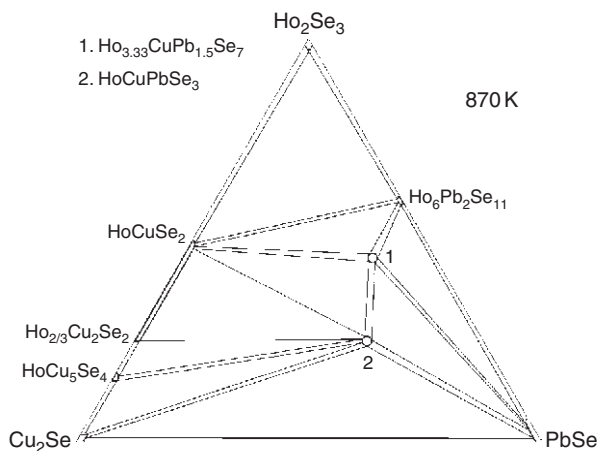


FIGURE 70 Isothermal section of the Ho_2Se_3 - Cu_2Se - PbSe system at 870 K.

4.4.8 Structure type $\text{Er}_5\text{CuPb}_3\text{Se}_{11}$

Structure type $\text{Er}_5\text{CuPb}_3\text{Se}_{11}$ (Gulay et al., 2006i) (Figure 98, Table 48). SG $Cmcm$, $Z = 4$, $a = 0.40710$, $b = 1.3480$, $c = 3.8092$ nm. The erbium and copper atoms are located in distorted octahedra and tetrahedra, respectively. The shortest interatomic distances among these coordination spheres are $d(\text{Er}-\text{Se}) = 0.2795$ nm and $d(\text{Cu}-\text{Se}) = 0.240$ nm. The selenium atoms create mono- and bicapped trigonal prismatic arrangements around the Pb1 and Pb2 atoms, respectively, and the shortest Pb-Se distance is 0.2877 nm. The Se1 and Se6 atoms are located in octahedra

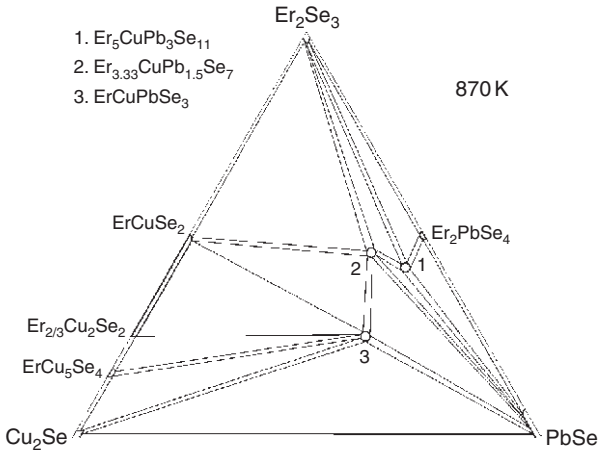


FIGURE 71 Isothermal section of the Er_2Se_3 – Cu_2Se – PbSe system at 870 K.

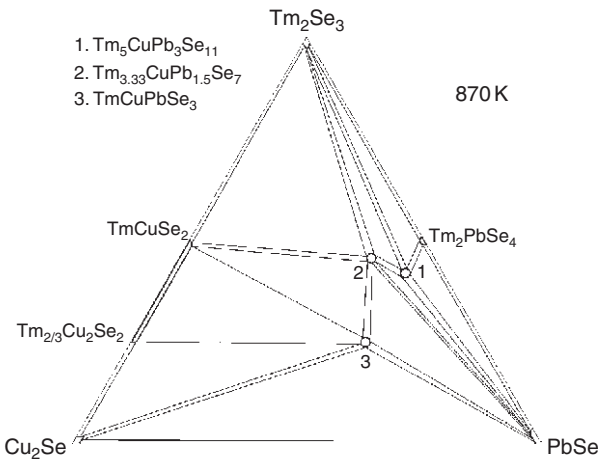


FIGURE 72 Isothermal section of the Tm_2Se_3 – Cu_2Se – PbSe system at 870 K.

formed by 2Er, 2Cu, and 2Pb atoms. The Se2 and Se3 atoms are situated in octahedra formed by 3Er, 1Cu, and 2Pb atoms. The Se4 atoms are located in octahedra formed by 2Er, 1Cu, and 3Pb atoms. The Se5 atoms are located in a tetragonal pyramid formed by 4Er and 1Pb atoms.

4.4.9 Structure type $\text{Y}_{3.33}\text{CuPb}_{1.5}\text{S}_7$

Structure type $\text{Y}_{3.33}\text{CuPb}_{1.5}\text{S}_7$ (Gulay et al., 2005g) (Figure 99, Table 49). SG Cm , $Z = 2$, $a = 1.30246$, $b = 0.39421$, $c = 1.20671$ nm, $\beta = 104.953^\circ$. All three independent Y atoms are located in octahedra formed by the S

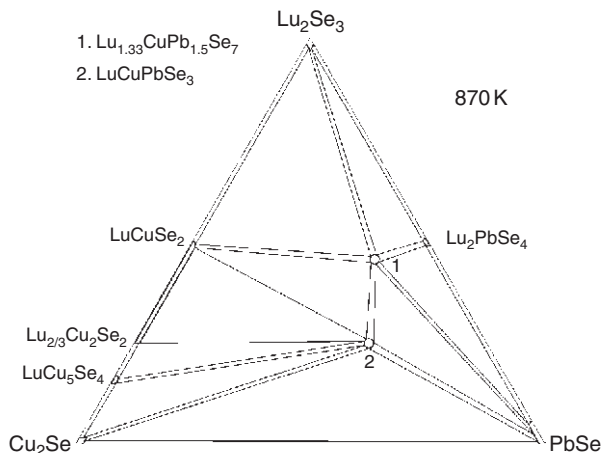


FIGURE 73 Isothermal section of the Lu_2Se_3 – Cu_2Se – PbSe system at 870 K.

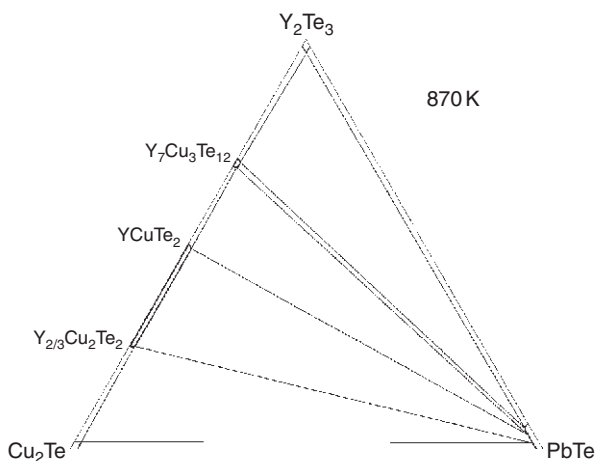


FIGURE 74 Isothermal section of the Y_2Te_3 – Cu_2Te – PbTe system at 870 K.

atoms, and the shortest Y–S distance is 0.243 nm. The randomly distributed Y and Pb atoms (M) are located in a monocapped trigonal prism, and the shortest M–S distance is 0.284 nm. The Cu and Pb atoms are located in tetrahedra and monocapped trigonal prisms formed by the S atoms. The shortest Cu–S and Pb–S distances among these polyhedra are 0.215 and 0.275 nm, respectively. S1 atom is located in a tetrahedron formed by 2Y and 2M atoms. The S2 and S5 atoms are located in tetragonal pyramids. The S3, S4, and S7 atoms have octahedral surroundings, and the S6 atom is located practically in the center of a square formed by 4Y atoms.

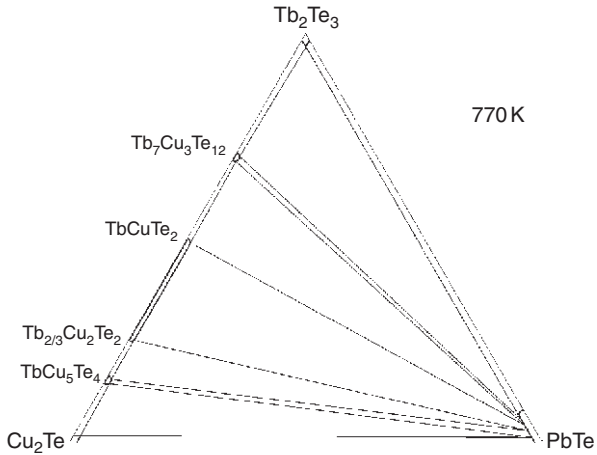


FIGURE 75 Isothermal section of the Tb_2Te_3 - Cu_2Te - PbTe system at 770 K.

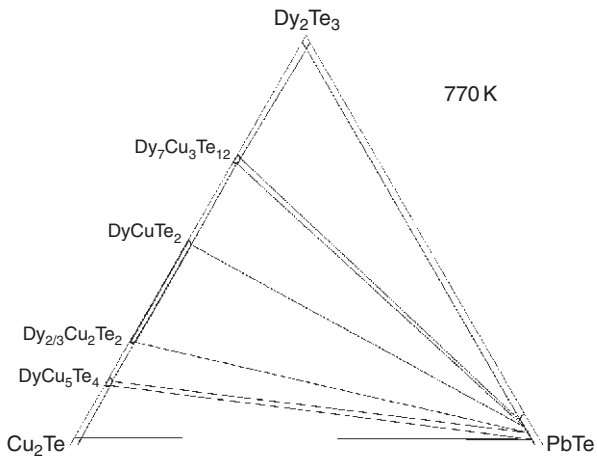


FIGURE 76 Isothermal section of the Dy_2Te_3 - Cu_2Te - PbTe system at 770 K.

4.4.10 Structure type $\text{Lu}_{3.33}\text{CuPb}_{1.5}\text{Se}_7$

Structure type $\text{Lu}_{3.33}\text{CuPb}_{1.5}\text{Se}_7$ (Gulay and Olekseyuk, 2005c) (Figure 100, Table 50). SG Cm , $Z = 2$, $a = 1.3404$, $b = 0.40307$, $c = 1.2475$ nm, $\beta = 104.36^\circ$. The structure is *quasi*-isostructural to $\text{Y}_{3.33}\text{CuPb}_{1.5}\text{S}_7$. The positions of the Lu atoms correspond to the octahedral positions of the Y atoms in $\text{Y}_{3.33}\text{CuPb}_{1.5}\text{S}_7$. The shortest Lu-Se distance is 0.2721 nm. The difference between the $\text{Y}_{3.33}\text{CuPb}_{1.5}\text{S}_7$ and $\text{Lu}_{3.33}\text{CuPb}_{1.5}\text{Se}_7$ crystal structures is in split positions of the Pb and M (Lu + Pb) atoms. The shortest Pb-Se and M-Se distances equal to 0.2703 and 0.2842 nm,

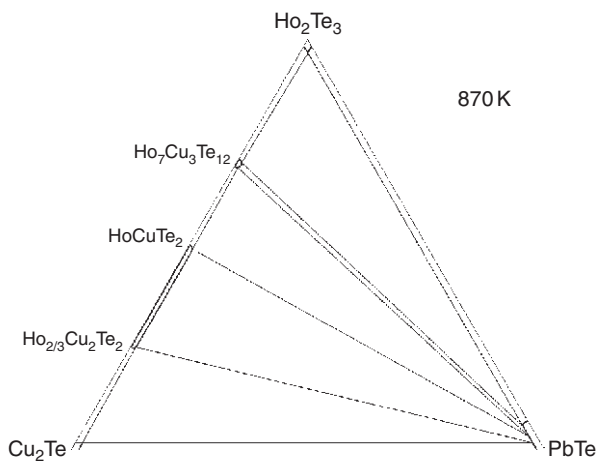


FIGURE 77 Isothermal section of the Ho_2Te_3 - Cu_2Te - PbTe system at 870 K.

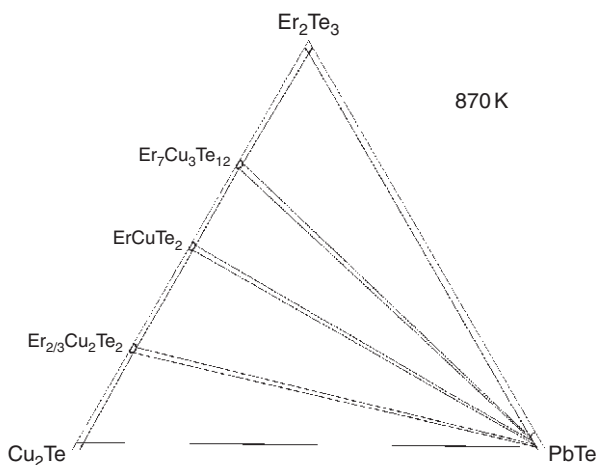


FIGURE 78 Isothermal section of the Er_2Te_3 - Cu_2Te - PbTe system at 870 K.

respectively. The Cu atoms are located in tetrahedra formed by the Se atoms, and the shortest Cu-Se distance is 0.241 nm. The surroundings of each of the seven independent selenium atoms are similar to the coordination spheres of the sulfur atoms in $\text{Y}_{3.33}\text{CuPb}_{1.5}\text{S}_7$.

4.4.11 Structure type β -BaLaCuSe₃

Structure type β -BaLaCuSe₃ (Christuk et al., 1994) (Figure 101, Table 51). SG *Pnma*, $Z = 4$, $a = 1.0407$, $b = 0.40350$, $c = 1.3401$ nm for YbCuPbSe_3 (Gulay et al., 2006h). The selenium atoms form octahedral and monocapped

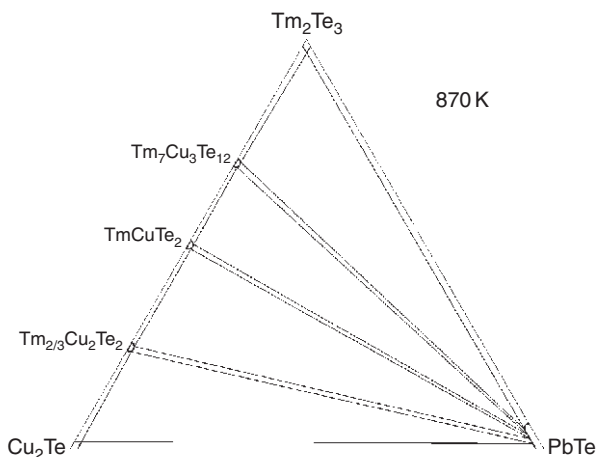


FIGURE 79 Isothermal section of the Tm_2Te_3 – Cu_2Te – PbTe system at 870 K.

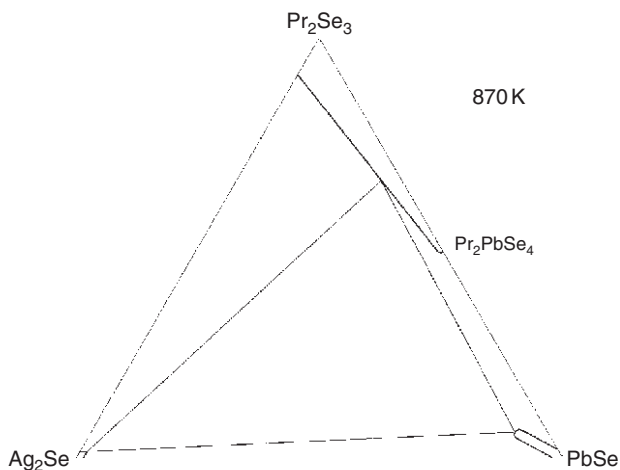


FIGURE 80 Isothermal section of the Pr_2Se_3 – Ag_2Se – PbSe system at 870 K.

trigonal prismatic arrangements around the Yb and Pb atoms, respectively. The shortest Yb–Se and Pb–Se distances equal to 0.2804 and 0.3095 nm, respectively. The Se1 and S3 atoms are located in octahedra, while the Se2 atom is situated in a tetragonal pyramid centered outside.

4.4.12 Structure type ErCuPbS_3

Structure type ErCuPbS_3 (Gulay et al., 2005h) (Figure 102, Table 52). SG $Cmcm$, $Z = 4$, $a = 0.3916$, $b = 1.2934$, $c = 1.0106$ nm. The sulfur atoms create octahedral and monocapped trigonal prismatic arrangements

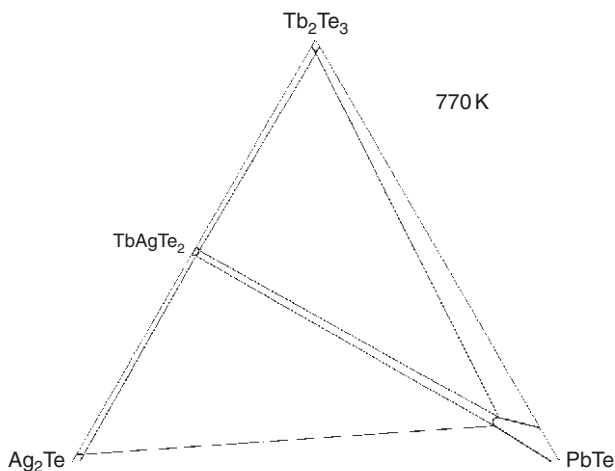


FIGURE 81 Isothermal section of the Tb_2Te_3 - Ag_2Te - PbTe system at 770 K.

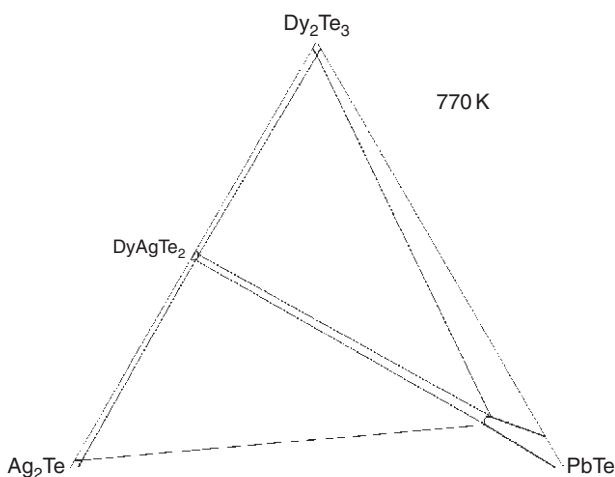


FIGURE 82 Isothermal section of the Dy_2Te_3 - Ag_2Te - PbTe system at 770 K.

around the erbium and lead atoms, respectively, and the shortest Er-S and Pb-S distances equal to 0.2701 and 0.2957 nm. The Pb atoms occupy split position. The Cu atoms are located in tetrahedra and the shortest Cu-S distance is 0.2327 nm. The S1 atom is located in an octahedron formed by 2Er, 2Cu, and 2Pb atoms. The S2 atom is located inside in an octahedron formed by 2Er, 1Cu, and 3Pb atoms.

TABLE 40 Crystallographic data for quaternary chalcogenides of the $R_2X_3-M_2X-In_2X_3$ ($M = Cu, Ag; X = S, Se$) systems

Compound	Structure type	Space group	Lattice parameters (nm)			Reference(s)
			<i>a</i>	<i>b</i>	<i>c</i>	
La ₂ CuInS ₅	La ₂ CuInS ₅	<i>Pnma</i>	1.1487	0.39760	1.6911	Huch et al. (2006b)
Ce ₂ CuInS ₅	La ₂ CuInS ₅	<i>Pnma</i>	1.14396	0.39361	1.6804	Huch et al. (2006b)
Pr ₂ CuInS ₅	La ₂ CuInS ₅	<i>Pnma</i>	1.14123	0.39119	1.6737	Huch et al. (2006b)
Nd ₂ CuInS ₅	La ₂ CuInS ₅	<i>Pnma</i>	1.13948	0.38933	1.66886	Huch et al. (2006b)
Sm ₂ CuInS ₅	La ₂ CuInS ₅	<i>Pnma</i>	1.13671	0.38594	1.6603	Huch et al. (2006b)
La ₂ CuInSe ₅	La ₂ CuInSe ₅	<i>Pnma</i>	1.20382	0.41185	1.7556	Gulay et al. (2007e)
Ce ₂ CuInSe ₅	La ₂ CuInSe ₅	<i>Pnma</i>	1.19997	0.40855	1.7464	Huch et al. (2007b)
Pr ₂ CuInSe ₅	La ₂ CuInSe ₅	<i>Pnma</i>	1.1973	0.40649	1.7408	Huch et al. (2007b)
La ₄ Ag ₂ In ₄ S ₁₃	La ₄ Ag ₂ In ₄ S ₁₃	<i>Pbam</i>	2.0523	2.5118	0.40241	Gulay et al. (2008d)

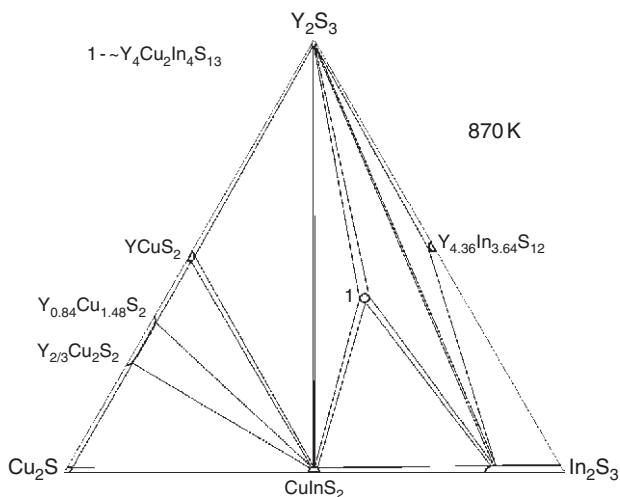


FIGURE 83 Isothermal section of the Y_2S_3 - Cu_2S - In_2S_3 system at 870 K.

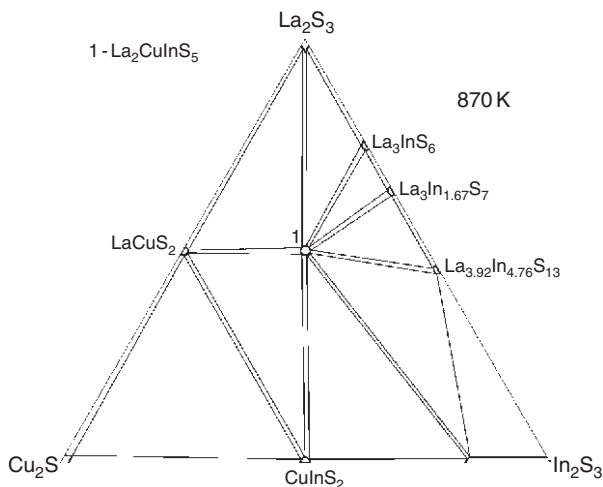


FIGURE 84 Isothermal section of the La_2S_3 - Cu_2S - In_2S_3 system at 870 K.

4.4.13 Structure type $LaCuPbS_3$

Structure type $LaCuPbS_3$ (Brennan and Ibers, 1992) (Figure 103, Table 53). SG $Pnma$, $Z = 4$, $a = 0.8091$, $b = 0.4093$, $c = 1.5996$ nm. The randomly distributed La and Pb atoms (M) are located in monocapped trigonal prisms formed by the S atoms. The shortest M-S distance is 0.2864 nm. The sulfur atoms create a tetrahedral arrangement around the single independent copper atom, and the shortest Cu-S distance is 0.2334 nm.

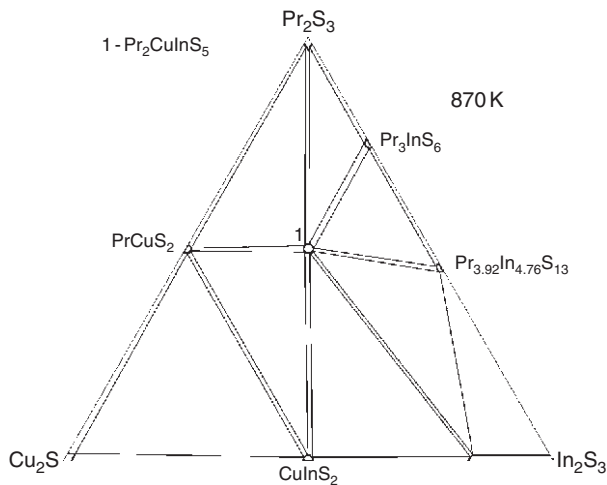


FIGURE 85 Isothermal section of the Pr_2S_3 – Cu_2S – In_2S_3 system at 870 K.

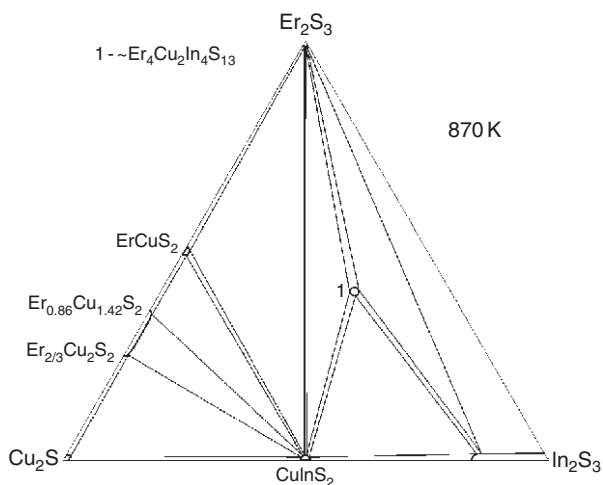


FIGURE 86 Isothermal section of the Er_2S_3 – Cu_2S – In_2S_3 system at 870 K.

The S1 atom has octahedral surroundings of 4M and 2Cu atoms. The S2 and S3 atoms are located in octahedra formed by 5M and 1Cu atoms.

4.4.14 Structure type $\text{La}_2\text{CuInS}_5$

Structure type $\text{La}_2\text{CuInS}_5$ (Huch et al., 2006b) (Figure 104, Table 54). SG $Pnma$, $Z = 4$, $a = 1.1487$, $b = 0.39760$, $c = 1.6911$ nm. The La atoms are located in bicapped trigonal prisms formed by the S atoms, and the

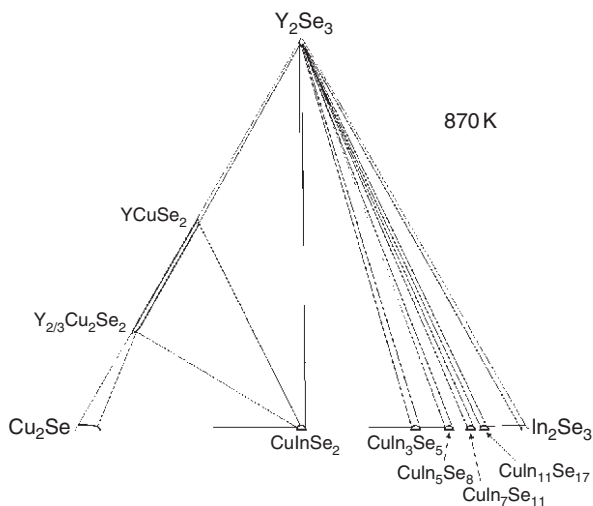


FIGURE 87 Isothermal section of the Y_2Se_3 - Cu_2Se - In_2Se_3 system at 870 K.

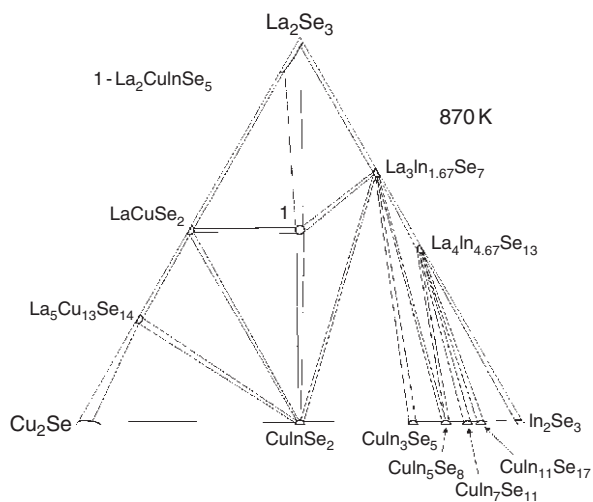


FIGURE 88 Isothermal section of the La_2Se_3 - Cu_2Se - In_2Se_3 system at 870 K.

shortest La-S distance is 0.2914 nm. The copper atoms occupy disordered positions. The sulfur atoms create tetrahedral arrangements around the copper atoms, and form an octahedral arrangement around the indium atom. The shortest Cu-S and In-S distances equal to 0.222 and 0.2553 nm, respectively. The S1 atom is located in a trigonal bipyramid formed by 3La and 2In atoms. The S2 and S3 atoms are situated in octahedra. The S4 and S5 atoms are located in tetragonal pyramids.

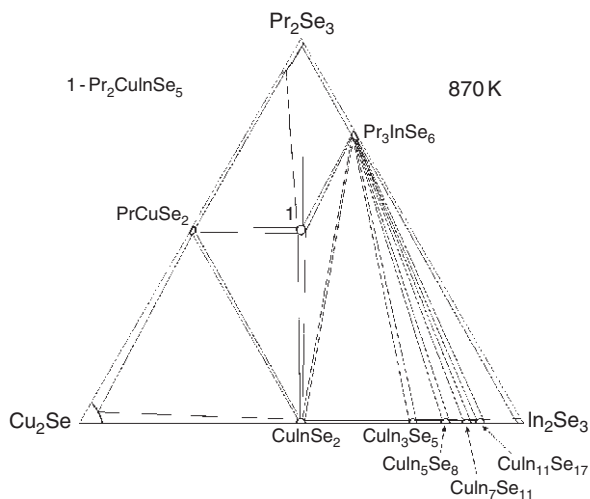


FIGURE 89 Isothermal section of the Pr_2Se_3 – Cu_2Se – In_2Se_3 system at 870 K.

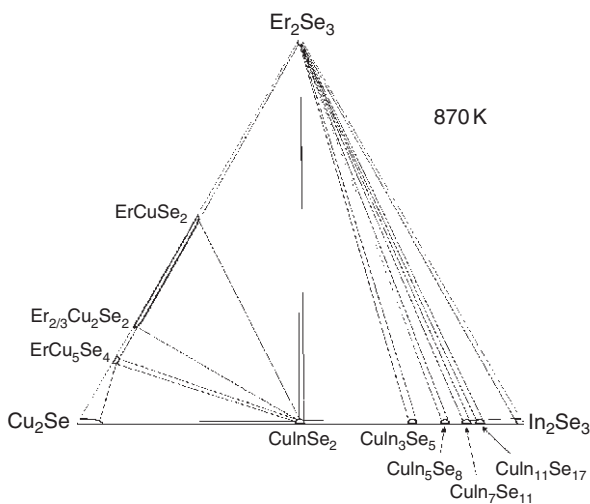


FIGURE 90 Isothermal section of the Er_2Se_3 – Cu_2Se – In_2Se_3 system at 870 K.

4.4.15 Structure type $\text{La}_2\text{CuInSe}_5$

Structure type $\text{La}_2\text{CuInSe}_5$ (Gulay et al., 2007e) (Figure 105, Table 55). SG $Pnma$, $Z = 4$, $a = 1.20382$, $b = 0.41185$, $c = 1.7556$ nm. The structure of $\text{La}_2\text{CuInSe}_5$ is *quasi*-isostructural to $\text{La}_2\text{CuInS}_5$. The main difference is in the ordered position of the copper atom in $\text{La}_2\text{CuInSe}_5$. Despite this, the copper atom has tetrahedral surroundings like in the $\text{La}_2\text{CuInS}_5$ type

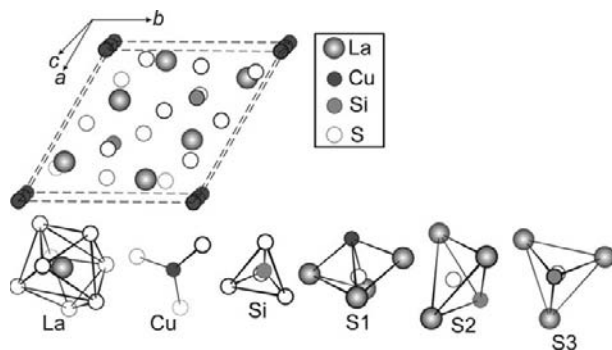


FIGURE 91 Crystal structure of $\text{La}_3\text{CuSiS}_7$ and CPs of atoms.

TABLE 41 Atomic parameters for $\text{La}_3\text{CuSiS}_7$

Atom	Position	Fractional coordinates			Atomic arrangement	
		<i>x</i>	<i>y</i>	<i>z</i>		
La	6 <i>c</i>	0.123	0.357	0.028	8S	
Cu	2 <i>a</i>	0	0	0.000	3S	
Si	2 <i>b</i>	1/3	2/3	0.614	4S	
S1	6 <i>c</i>	0.250	0.165	0.017	4La	1Cu
S2	6 <i>c</i>	0.526	0.116	0.255	3La	1Si
S3	2 <i>b</i>	1/3	2/3	0.254	3La	1Si

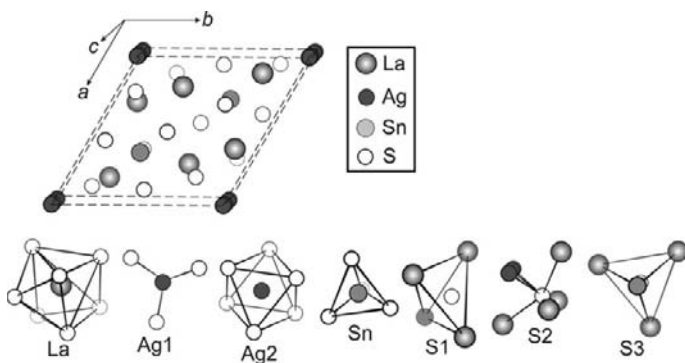
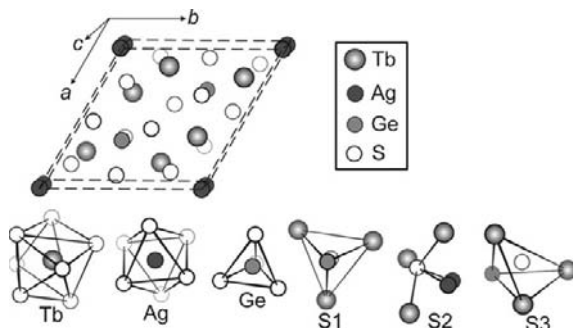


FIGURE 92 Crystal structure of $\text{La}_3\text{Ag}_{0.82}\text{SnS}_7$ and CPs of atoms.

TABLE 42 Atomic parameters for $\text{La}_3\text{Ag}_{0.82}\text{SnS}_7$

Atom	Position	Fractional coordinates			Atomic arrangement	
		x	y	z		
La	6c	0.35851	0.13233	0.04973	7S	
Ag ¹ ^a	2a	0	0	0.4660	3S	
Ag ² ^b	2a	0	0	0.284	6S	
Sn	2b	1/3	2/3	0.12629	4S	
S1	6c	0.51639	0.42295	0.79230	3La	1Sn
S2	6c	0.16456	0.26446	0.0267	4La	2Ag
S3	2b	1/3	2/3	0.7365	3La	1Sn

^a Occupancy 65.9%.^b Occupancy 16.1%.**FIGURE 93** Crystal structure of $\text{Tb}_3\text{Ag}_{0.59}\text{GeS}_7$ and CPs of atoms.**TABLE 43** Atomic parameters for $\text{Tb}_3\text{Ag}_{0.59}\text{GeS}_7$

Atom	Position	Fractional coordinates			Atomic arrangement	
		x	y	z		
Tb	6c	0.86677	0.64133	0.2500	7S	
Ag ^a	2a	0	0	0.0324	6S	
Ge	2b	1/3	2/3	0.3305	4S	
S1	2b	1/3	2/3	0.9534	3Tb	1Ge
S2	6c	0.9002	0.7379	0.7165	3Tb	2Ag
S3	6c	0.5790	0.4798	0.9894	3Tb	1Ge

^a Occupancy 58.6%.

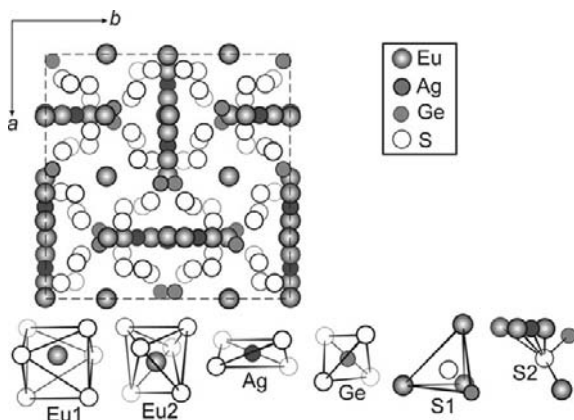


FIGURE 94 Crystal structure of $\text{Eu}_{1.75}\text{Ag}_{0.5}\text{GeS}_4$ (structure type $\text{Pb}_{1.75}\text{Ag}_{0.5}\text{GeS}_4$) and CPs of atoms.

TABLE 44 Atomic parameters for $\text{Eu}_{1.75}\text{Ag}_{0.5}\text{GeS}_4$

Atom	Position	Fractional coordinates			Atomic arrangement		
		x	y	z			
Eu1 ^a	24d	0.6561	0	3/4	6S		
Eu2	24d	0.9760	0	3/4	6S		
Ag ^b	12b	5/8	0	3/4	4S		
Ge	16c	0.7654	0.7654	0.7654	4S		
S1	16c	0.8556	0.8556	0.8556	3Eu	1Ge	
S2	48e	0.9092	0.9003	0.5681	4Eu	1Ag	1Ge

^a Occupancy 16.6%.

^b Occupancy 66.7%.

structure. The shortest Cu–Se distance is 0.2392 nm. The sulfur atoms form bicapped trigonal prismatic and octahedral arrangements around the lanthanum and indium atoms, respectively. The shortest La–Se and In–Se distances are 0.30323 and 0.26754 nm, respectively. Surroundings of five independent selenium atoms are similar to those found for the sulfur atoms in $\text{La}_2\text{CuInS}_5$.

4.4.16 Structure type $\text{La}_4\text{Ag}_2\text{In}_4\text{S}_{13}$

Structure type $\text{La}_4\text{Ag}_2\text{In}_4\text{S}_{13}$ (Gulay et al., 2008d) (Figure 106, Table 56). SG $Pbam$, $Z = 4$, $a = 2.0523$, $b = 2.5118$, $c = 0.40241$ nm. All four independent lanthanum atoms are located in bicapped trigonal prisms made of sulfur, and the shortest La–S distance is 0.2933 nm. The silver atoms

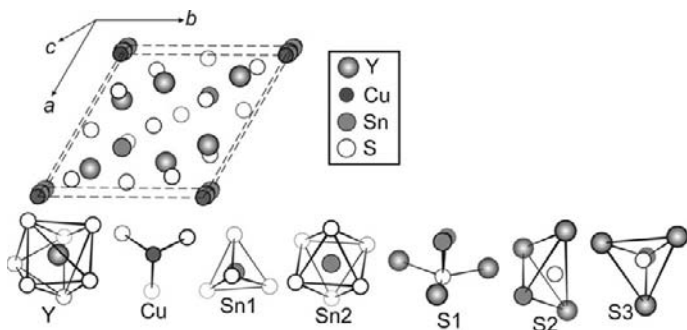


FIGURE 95 Crystal structure of $Y_3Cu_{0.64}Sn_{1.09}S_7$ and CPs of atoms.

TABLE 45 Atomic parameters for $Y_3Cu_{0.64}Sn_{1.09}S_7$

Atom	Position	Fractional coordinates			Atomic arrangement		
		x	y	z			
Y	6c	0.36090	0.15623	0.3795	7S		
Cu ^a	2a	0	0	0.0000	3S		
Sn1	2b	1/3	2/3	0.3160	4S		
Sn2 ^b	2a	0	0	0.225	6S		
S1	6c	0.2616	0.1182	0.9555	3Y	1Cu	1Sn
S2	6c	0.5239	0.4425	0.6368	3Y	1Sn	
S3	2b	1/3	2/3	0.6986	3Y	1Sn	

^a Occupancy 64%.

^b Occupancy 9%.

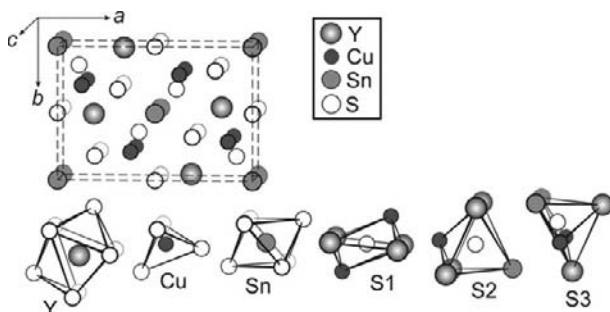
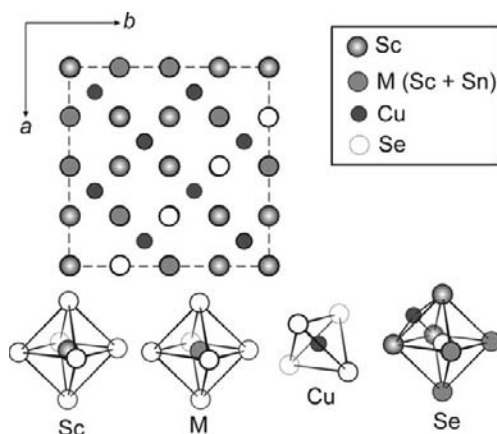


FIGURE 96 Crystal structure of $Y_2Cu_{0.20}Sn_{0.95}S_5$ and CPs of atoms.

TABLE 46 Atomic parameters for $Y_2Cu_{0.20}Sn_{0.95}S_5$

Atom	Position	Fractional coordinates			Atomic arrangement
		x	y	z	
Y	4h	0.3276	0.0274	1/2	8S
Cu ^a	4g	0.125	0.291	0	4S
Sn ^b	2a	0	0	0	6S
S1	2c	0	1/2	0	4Y 2Cu
S2	4g	0.309	0.322	0	4Y 1Cu 1Sn
S3	4h	0.096	0.161	1/2	2Y 2Cu 2Sn

^a Occupancy 10%.^b Occupancy 95%.**FIGURE 97** Crystal structure of $Sc_{1.09}Cu_{0.37}Sn_{1.09}Se_4$ (structure type $Yb_{1.84}Fe_{1.23}S_4$) and CPs of atoms.

have octahedral coordination spheres formed by the S atoms, and the shortest Ag–S distance is 0.2647 nm. The In1, In3, In4, and In6 atoms are located in octahedra, the In2, In5, and In7 atoms are located in tetrahedra. The In4–In7 atoms occupy defect positions. The shortest In–S distance is 0.2401 nm. The S1 and S4 atoms are located in tetragonal pyramids formed by 2La, 2Ag, and 1In atoms. Each of the S2, S3, S5, and S7 atoms is located in tetragonal pyramids formed by 4La and 1In atoms. The S6 and S12 atoms are located in trigonal bipyramidal arrangements of the 3La and 2In atoms. The S8 atom is located in a tetrahedron formed by 2Ag and 2In atoms. The S9 and S10 atoms are located in tetragonal pyramids centered outside. These polyhedra are formed by 2La, 2Ag, and 1In atoms. The S11 and S13 atoms have tetragonal bipyramidal arrangements of 1La, 1Ag, and 4In atoms.

TABLE 47 Atomic parameters for $\text{Sc}_{1.09}\text{Cu}_{0.37}\text{Sn}_{1.09}\text{Se}_4$

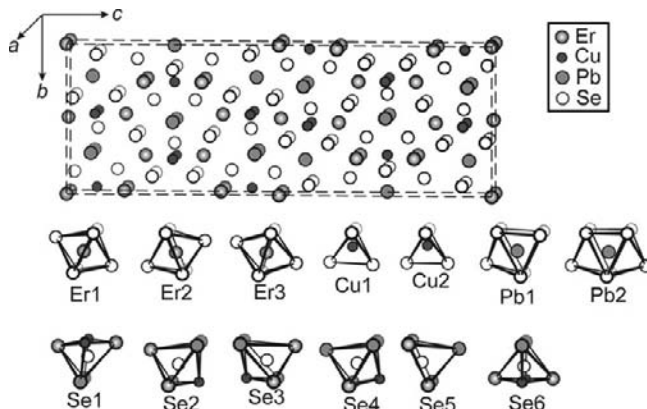
Atom	Position	Fractional coordinates			Atomic arrangement		
		x	y	z			
Sc ^a	16c	0	0	0	6Se		
Sc ^b	16d	1/2	1/2	1/2	6Se		
Sn ^c	16d	1/2	1/2	1/2	6Se		
Cu ^d	8a	1/8	1/8	1/8	4Se		
Se	32e	0.2524	x	x	3Sc	3M	1Cu

^a Occupancy 10%.

^b Occupancy 45% Sc.

^c Occupancy 55% Sn.

^d Occupancy 36% Cu.

**FIGURE 98** Crystal structure of $\text{Er}_5\text{CuPb}_3\text{Se}_{11}$ and CPs of atoms.

5. CRYSTALLOGRAPHIC RELATIONSHIPS OF TERNARY AND QUATERNARY RARE EARTH CHALCOGENIDES OF SI, GE, SN, PB AND IN

5.1 Crystallographic peculiarities of R_3MZX_7 ($\text{M} = \text{Cu(I)}, \text{Ag(I)}, 1/2\text{Ag(II)}, 1/3\text{Ag(III)}$), $\text{Z} = \text{Si, Ge, Sn}$; $\text{X} = \text{S, Se}$), $\text{R}_3\text{Z}_{1.25}\text{X}_7$ ($\text{Z} = \text{Si, Ge, Sn}$; $\text{X} = \text{S, Se}$), and $\text{La}_3\text{In}_{1.67}\text{X}_7$ ($\text{X} = \text{S, Se}$) compounds

The members of the following structure types: $\text{Dy}_3\text{Ge}_{1.25}\text{S}_7$, $\text{Ce}_3\text{Al}_{1.67}\text{S}_7$, $\text{La}_3\text{CuSiS}_7$, $\text{La}_3\text{Ag}_{0.82}\text{SnS}_7$, $\text{Tb}_3\text{Ag}_{0.59}\text{GeS}_7$, and $\text{Y}_3\text{Cu}_{0.64}\text{Sn}_{1.09}\text{S}_7$ represent a large group of compounds with similar structural motifs. The packing of the $[\text{RX}_8]$ trigonal prisms and of the $[\text{ZX}_4]$ tetrahedra (Figure 107) is similar for

TABLE 48 Atomic parameters for $\text{Er}_5\text{CuPb}_3\text{Se}_{11}$

Atom	Position	Fractional coordinates			Atomic arrangement		
		x	y	z			
Er1	8f	0	0.02404	0.63604	6Se		
Er2	8f	0	0.24919	0.18200	6Se		
Er3	4a	0	0	0	6Se		
Cu1 ^a	8f	0	0.5357	0.5674	4Se		
Cu2 ^b	4c	0	0.762	1/4	4Se		
Pb1	8f	0	0.2735	0.55737	7Se		
Pb2	4c	0	0.5175	1/4	8Se		
Se1	8f	0	0.0688	0.07002	2Er	2Cu	2Pb
Se2	8f	0	0.1197	0.70150	3Er	1Cu	2Pb
Se3	8f	0	0.3442	0.11543	3Er	1Cu	2Pb
Se4	8f	0	0.3602	0.01446	2Er	1Cu	3Pb
Se5	8f	0	0.6082	0.16276	4Er	1Pb	
Se6	4c	0	0.1683	1/4	2Er	2Cu	2Pb

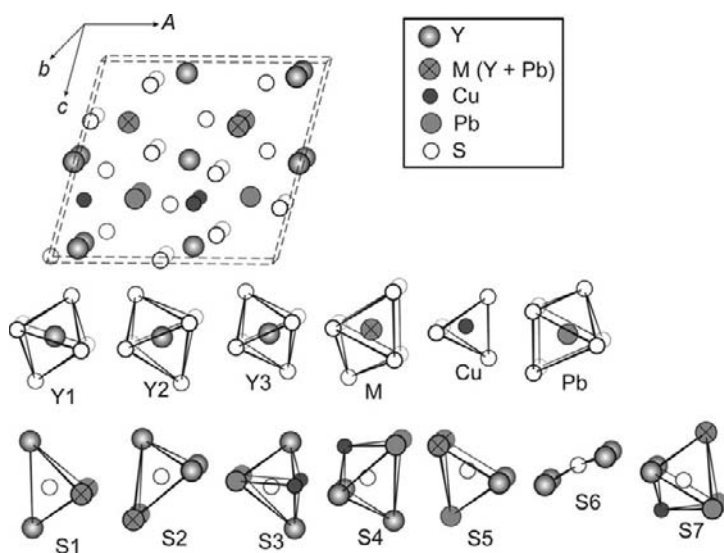
^a Occupancy 44%.^b Occupancy 12%.**FIGURE 99** Crystal structure of $\text{Y}_{3.33}\text{CuPb}_{1.5}\text{S}_7$ and CPs of atoms.

TABLE 49 Atomic parameters for $Y_{3.33}CuPb_{1.5}S_7$

Atom	Position	Fractional coordinates			Atomic arrangement		
		x	y	z			
Y1	2a	0.000	0	0.500	6S		
Y2	2a	0.886	0	0.071	6S		
Y3	2a	0.120	0	0.929	6S		
M ^a	2a	0.686	0	0.317	7S		
Cu	2a	0.580	0	0.702	4S		
Pb	2a	0.315	0	0.681	7S		
S1	2a	0.026	0	0.298	2Y	2M	
S2	2a	0.249	0	0.116	3Y	2M	
S3	2a	0.968	0	0.722	2Y	2Cu	2Pb
S4	2a	0.719	0	0.859	3Y	1Cu	2Pb
S5	2a	0.335	0	0.453	2Y	2M	1Pb
S6	2a	0.501	0	0.985	4Y		
S7	2a	0.644	0	0.555	2Y	1M	1Cu 2Pb

^a Occupancy 33% Y + 50% Pb.

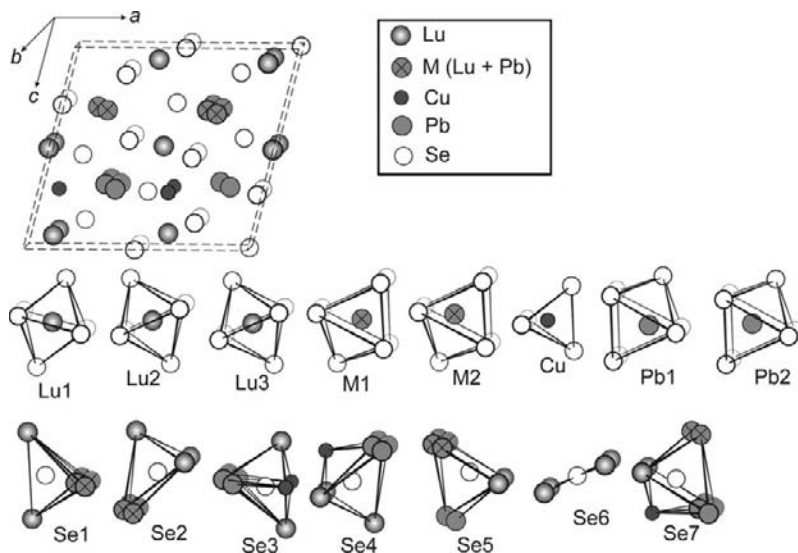
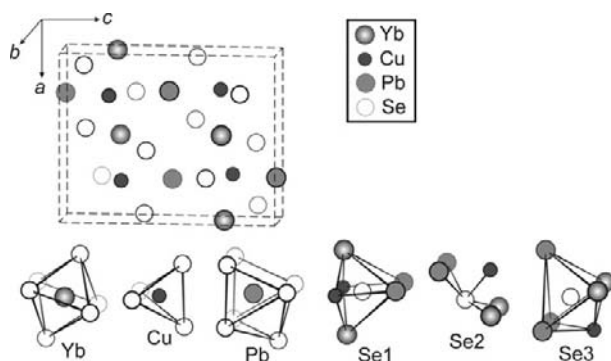
**FIGURE 100** Crystal structure of $Lu_{3.33}CuPb_{1.5}Se_7$ and CPs of atoms.

TABLE 50 Atomic parameters for $\text{Lu}_{3.33}\text{CuPb}_{1.5}\text{Se}_7$

Atom	Position	Fractional coordinates			Atomic arrangement			
		x	y	z				
Lu1	2a	0.0000	0	0.5000	6Se			
Lu2	2a	0.8806	0	0.0713	6Se			
Lu3	2a	0.1196	0	0.9313	6Se			
M1 ^a	2a	0.7092	0	0.3249	7Se			
M2 ^a	2a	0.6635	0	0.3076	7Se			
Cu	2a	0.5821	0	0.7141	4Se			
Pb1 ^b	2a	0.3426	0	0.7002	7Se			
Pb2 ^b	2a	0.2944	0	0.6765	7Se			
Se1	2a	0.0102	0	0.2849	2Lu	2M		
Se2	2a	0.2620	0	0.1341	3Lu	2M		
Se3	2a	0.9807	0	0.7239	2Lu	2Cu	2Pb	
Se4	2a	0.7344	0	0.8654	3Lu	1Cu	2Pb	
Se5	2a	0.3493	0	0.4581	2Lu	2M	1Pb	
Se6	2a	0.498	0	0.000	4Lu			
Se7	2a	0.6494	0	0.5444	2Lu	1M	1Cu	2Pb

^a Occupancy 17% Lu + 25% Pb.

^b Occupancy 50%.

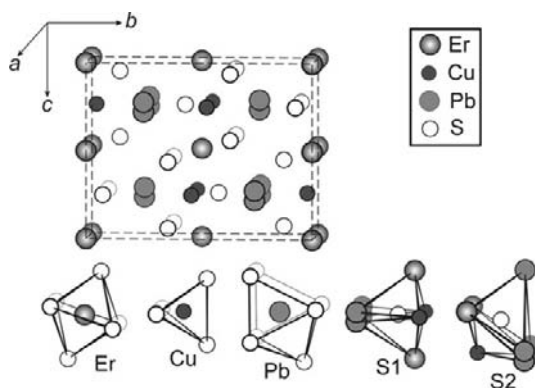
**FIGURE 101** Crystal structure of YbCuPbSe_3 (structure type $\beta\text{-BaLaCuSe}_3$) and CPs of atoms.

all structures. The differences are only for the occupations of trigonal antiprisms located along the c axes. All of these compounds can be divided into three groups:

Group 1: Only one atomic position exists within the same antiprism. This position is located close to the triangular face of the antiprism, and actually, a triangular coordination occurs for the central atom. Stoichiometric $\text{R}_3\text{M}_{1-\delta}\text{TX}_7$ ($\delta = 0$) ($\text{M} = \text{Cu}, \text{Ag}$) compounds belong to the first group.

TABLE 51 Atomic parameters for YbCuPbSe_3

Atom	Position	Fractional coordinates			Atomic arrangement		
		<i>x</i>	<i>y</i>	<i>z</i>			
Yb	4 <i>c</i>	0.50736	1/4	0.25312	6Se		
Cu	4 <i>c</i>	0.7452	1/4	0.7826	4Se		
Pb	4 <i>c</i>	0.7615	1/4	0.49687	7Se		
Se1	4 <i>c</i>	0.2560	1/4	0.3284	2Yb	2Cu	2Pb
Se2	4 <i>c</i>	0.4323	1/4	0.6083	2Yb	1Cu	2Pb
Se3	4 <i>c</i>	0.0528	1/4	0.6114	2Yb	1Cu	3Pb

**FIGURE 102** Crystal structure of ErCuPbS_3 and CPs of atoms.**TABLE 52** Atomic parameters for ErCuPbS_3

Atom	Position	Fractional coordinates			Atomic arrangement		
		<i>x</i>	<i>y</i>	<i>z</i>			
Er	4 <i>a</i>	0	0	0	6S		
Cu	4 <i>c</i>	0	0.5337	1/4	4S		
Pb ^a	8 <i>f</i>	0	0.25436	0.2774	7S		
S1	4 <i>c</i>	0	0.9262	1/4	2Er	2Cu	2Pb
S2	8 <i>f</i>	0	0.6377	0.0621	2Er	1Cu	3Pb

^a Occupancy 50%.

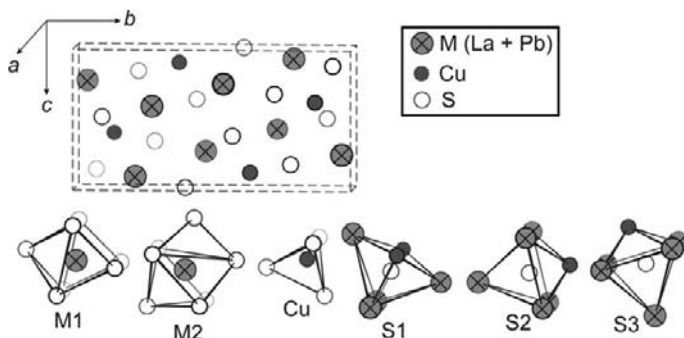


FIGURE 103 Crystal structure of LaCuPbS_3 and CPs of atoms.

TABLE 53 Atomic parameters for LaCuPbS_3

Atom	Position	Fractional coordinates			Atomic arrangement	
		<i>x</i>	<i>y</i>	<i>z</i>		
M1 ^a	4c	0.0891	1/4	0.78001	7S	
M2 ^b	4c	0.2501	1/4	0.03674	7S	
Cu	4c	0.1212	1/4	0.3669	4S	
S1	4c	0.0124	1/4	0.6000	4M	2Cu
S2	4c	0.18064	1/4	0.2209	5M	1Cu
S3	4c	0.3809	1/4	0.4304	5M	1Cu

^a Occupancy 33% La + 67% Pb.

^b Occupancy 67% La + 33% Pb.

Group 2: Two atomic positions are found within the same antiprism. The first position is located close to the triangular face of the antiprism, and it is occupied by Ag (M1) atoms. The second position is located close to the center of the antiprism, and it is occupied by either the Ag (M2) or Sn (Z2) atoms. Slightly defective $\text{R}_3\text{Ag}_{1-\delta}\text{TX}_7$ ($0 < \delta \leq 0.38$) and $\text{Y}_3\text{Cu}_{0.64}\text{Sn}_{1.09}\text{S}_7$ compounds belong to this group.

Group 3: Only the central atomic position exists within the same antiprism, and it is occupied by Ag (M2) or Z (Z2) atoms. All strongly defect ternary and quaternary $\text{R}_3\text{Ag}_{1-\delta}\text{TX}_7$ ($0.38 < \delta \leq 0.50$) compounds belong to the third group.

All of the $\text{R}_3\text{M}_{1-\delta}\text{ZX}_7$ ($\text{M} = \text{Cu}, \text{Ag}, \text{Z} = \text{Si}, \text{Ge}, \text{Sn}$, and $\text{X} = \text{S}, \text{Se}$) compounds are listed in Table 57.

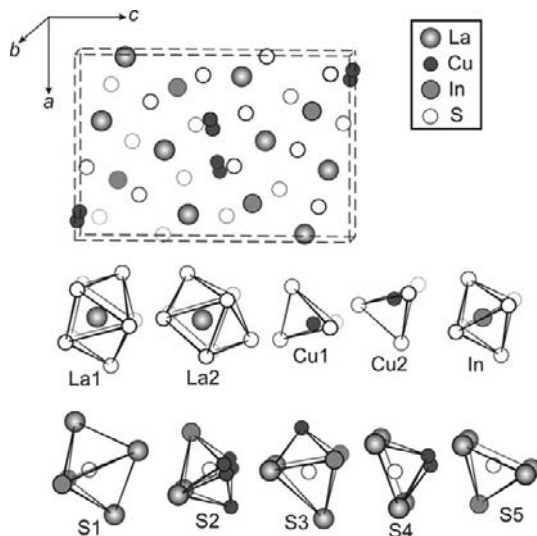


FIGURE 104 Crystal structure of $\text{La}_2\text{CuInS}_5$ and CPs of atoms.

TABLE 54 Atomic parameters for $\text{La}_2\text{CuInS}_5$

Atom	Position	Fractional coordinates			Atomic arrangement		
		x	y	z			
La1	4c	0.48086	1/4	0.67851	8S		
La2	4c	0.13548	1/4	0.59233	8S		
Cu1 ^a	4c	0.5960	1/4	0.5032	4S		
Cu2 ^b	4c	0.6478	1/4	0.5123	4S		
In	4c	0.19638	1/4	0.35820	6S		
S1	4c	0.7404	1/4	0.7293	3La	2In	
S2	4c	0.3971	1/4	0.4253	2La	3Cu	1In
S3	4c	0.8851	1/4	0.5380	3La	1Cu	2In
S4	4c	0.6826	1/4	0.3826	4La	1Cu	
S5	4c	0.4878	1/4	0.1939	4La	1In	

^a Occupancy 82%.

^b Occupancy 18%.

5.2 Crystallographic peculiarities of rare earth—lead chalcogenides

Ternary and quaternary rare earth—lead compounds in the $\text{R}_2\text{X}_3\text{—PbX}$ and $\text{R}_2\text{X}_3\text{—Cu}_2\text{X—PbX}$ ($\text{X} = \text{S}, \text{Se}$) systems are listed in Table 58. The ternary and quaternary chalcogenides have very similar structures for

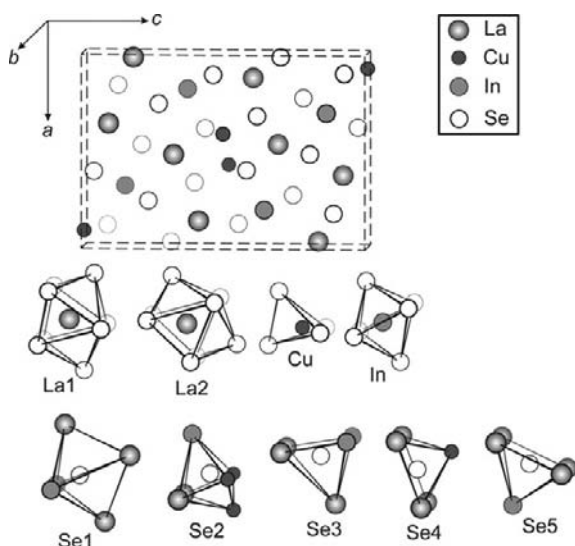


FIGURE 105 Crystal structure of $\text{La}_2\text{CuInSe}_5$ and CPs of atoms.

TABLE 55 Atomic parameters for $\text{La}_2\text{CuInSe}_5$

Atom	Position	Fractional coordinates			Atomic arrangement
		<i>x</i>	<i>y</i>	<i>z</i>	
La1	4c	0.47993	1/4	0.67902	8Se
La2	4c	0.13680	1/4	0.59252	8Se
Cu	4c	0.58400	1/4	0.50300	4Se
In	4c	0.19371	1/4	0.35994	6Se
Se1	4c	0.74095	1/4	0.72918	3La 2In
Se2	4c	0.39751	1/4	0.42335	2La 3Cu 1In
Se3	4c	0.88864	1/4	0.53794	3La 2In
Se4	4c	0.68170	1/4	0.38456	4La 1Cu
Se5	4c	0.48589	1/4	0.19359	4La 1In

the less complex compounds and therefore all of them can be divided into five groups:

1. Quaternary RCuPbX_3 compounds (structure types ErCuPbS_3 and $\beta\text{-BaLaCuSe}_3$) are related to YbLaS_3 (Mitchell et al., 2004). The ErCuPbX_3 compounds can be derived from YbLaS_3 according to the relationship $\text{La}^{3+} \rightarrow \text{Pb}^{2+} + \text{Cu}^+$ (Figure 108). Additionally, split position of the Pb atoms is observed in ErCuPbS_3 compared with the same position in ErCuPbSe_3 , which is ordered.

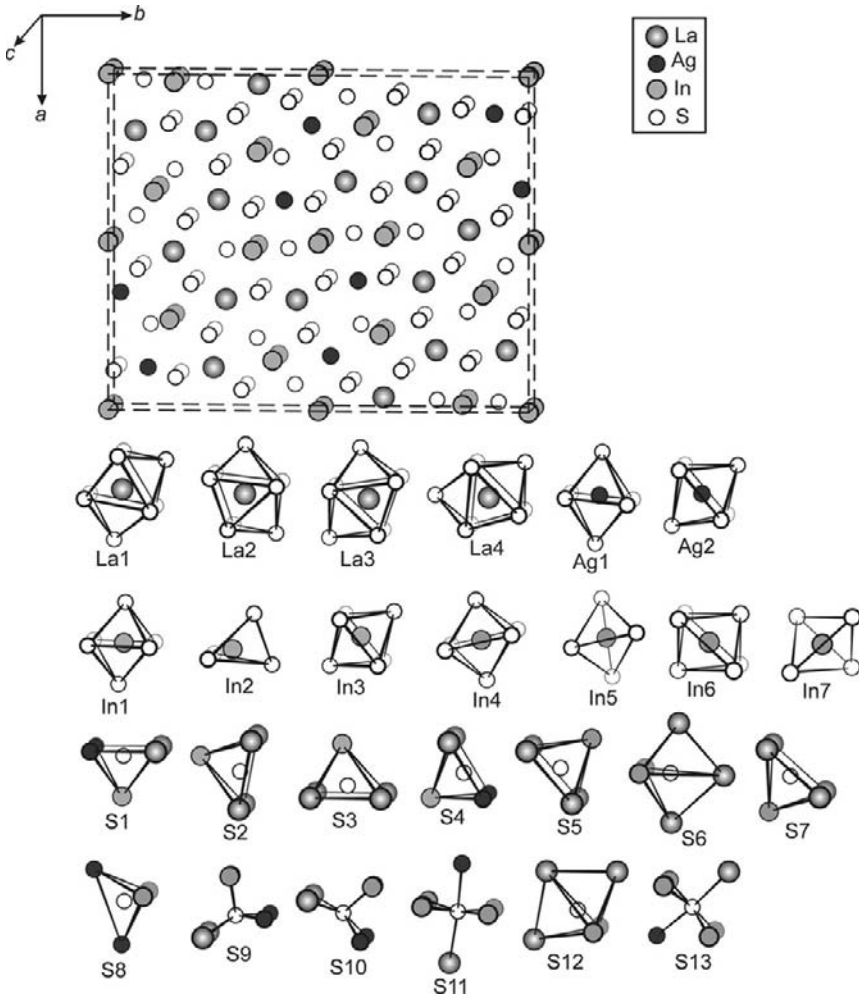


FIGURE 106 Crystal structure of $\text{La}_4\text{Ag}_2\text{In}_4\text{S}_{13}$ and CPs of atoms.

- The $\text{La}^{3+} \rightarrow \text{Pb}^{2+} + \text{Cu}^+$ substitution results in the LaCuPbS_3 type structure derived from the binary La_2S_3 parent (Bazançon et al., 1969) (Figure 109).
- The $\text{Y}_{4.2}\text{Pb}_{0.7}\text{Se}_7$ and $\text{R}_{3.33}\text{CuPb}_{1.5}\text{X}_7$ compounds are related to the binary Y_5Se_7 compound (Kim and Franzen, 1988) (Figure 110). The ternary $\text{Y}_{4.2}\text{Pb}_{0.7}\text{Se}_7$ compound can be derived from the binary Y_5Se_7 according to the following relationship $\text{Y}^{2+} \rightarrow \text{Pb}^{2+}$. A subsequent substitution $\text{Y}^{3+} \rightarrow \text{Pb}^{2+} + \text{Cu}^+$ results in the quaternary $\text{R}_3\text{CuPb}_2\text{X}_7$ compounds from the ternary $\text{Y}_{4.2}\text{Pb}_{0.7}\text{Se}_7$ compound. As a result of this particular substitution, it is also possible to derive the $\text{Y}_{3.33}\text{CuPb}_{1.5}\text{S}_7$

TABLE 56 Atomic parameters for $\text{La}_4\text{Ag}_2\text{In}_4\text{S}_{13}$

Atom	Position	Fractional coordinates			Atomic arrangement		
		x	y	z			
La1	4h	0.88013	0.24395	1/2	8S		
La2	4h	0.67626	0.27385	1/2	8S		
La3	4h	0.67644	0.44179	1/2	8S		
La4	4h	0.03505	0.35155	1/2	8S		
Ag1	4h	0.88092	0.08797	1/2	6S		
Ag2	4h	0.15697	0.47730	1/2	6S		
In1	4g	0.02257	0.15688	0	6S		
In2	4g	0.72937	0.14592	0	4S		
In3	4g	0.84973	0.39152	0	6S		
In4 ^a	2a	1/2	1/2	0	6S		
In5 ^b	4e	1/2	1/2	0.092	4S		
In6 ^c	2c	0	1/2	0	6S		
In7 ^d	4f	0	1/2	0.877	4S		
S1	4g	0.90132	0.16056	0	2La	2Ag	1In
S2	4g	0.77430	0.24004	0	4La	1In	
S3	4g	0.64624	0.35616	0	4La	1In	
S4	4g	0.77443	0.47033	0	2La	2Ag	1In
S5	4g	0.93783	0.31722	0	4La	1In	
S6	4h	1.02864	0.22437	1/2	3La	2In	
S7	4h	0.62271	0.19710	1/2	4La	1In	
S8	4h	0.75159	0.09433	1/2	2Ag	2In	
S9	4g	0.61736	0.51303	0	2La	2Ag	1In
S10	4g	0.07939	0.42976	0	2La	2Ag	1In
S11	4h	0.02335	0.07796	1/2	1La	1Ag	4In
S12	4h	0.79108	0.34789	1/2	3La	2In	
S13	4h	0.07115	0.56190	1/2	1La	1Ag	4In

^a Occupancy 40%.^b Occupancy 30%.^c Occupancy 56%.^d Occupancy 22%.

type structure. The latter is also related to $\text{Lu}_{3.33}\text{CuPb}_{1.5}\text{Se}_7$, where splitting of the Pb positions is observed contrary to an ordered position of the lead atom in $\text{Y}_{3.33}\text{CuPb}_{1.5}\text{S}_7$.

4. The $\text{R}_6\text{Pb}_2\text{Se}_{11}$ and $\text{R}_5\text{CuPb}_3\text{X}_{11}$ compounds are related to Tm_8S_{11} (Zhang et al., 1990) (Figure 111). The ternary $\text{Y}_6\text{Pb}_2\text{Se}_{11}$ compound can be derived from the binary Tm_8S_{11} according to the relationship $\text{Tm}^{2+} \rightarrow \text{Pb}^{2+}$. Quaternary $\text{Er}_5\text{CuPb}_3\text{Se}_{11}$ compound can be derived from the ternary $\text{Y}_6\text{Pb}_2\text{Se}_{11}$ according to the relationship $\text{Y}^{3+} \rightarrow \text{Pb}^{2+} + \text{Cu}^+$.

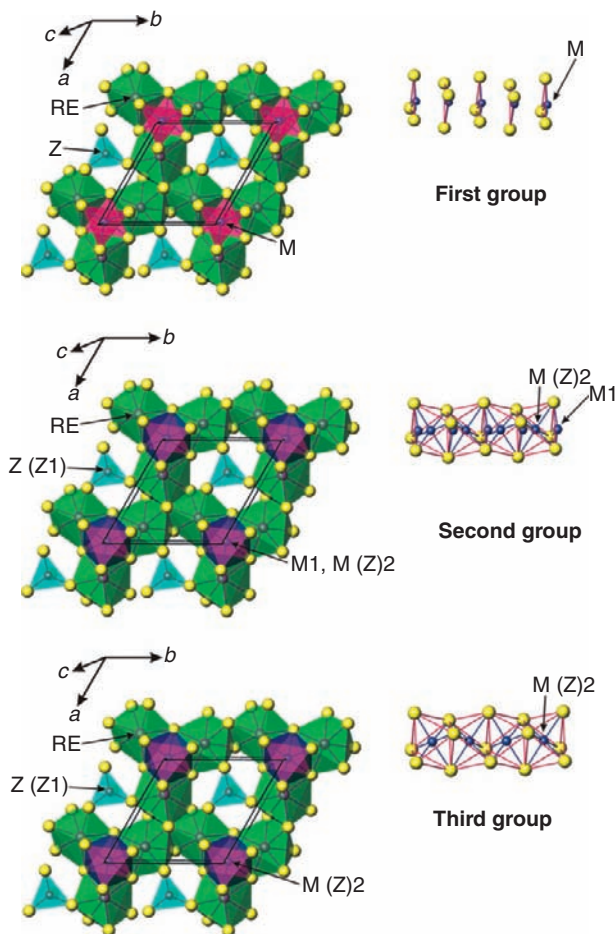


FIGURE 107 Crystal structures of R_3MX_7 ($M = \text{Cu(I)}, \text{Ag(I)}, 1/2\text{Ag(II)}, 1/3\text{Ag(III)}$, $Z = \text{Si}, \text{Ge}, \text{Sn}$; $X = \text{S}, \text{Se}$), $R_3Z_{1.25}X_7$ ($Z = \text{Si}, \text{Ge}, \text{Sn}$; $X = \text{S}, \text{Se}$), and $\text{La}_3\text{In}_{1.67}X_7$ ($X = \text{S}, \text{Se}$) compounds.

5. The $R_2\text{PbX}_4$ compounds (structure types Fe_2CaO_4 , Tm_2PbSe_4 , and Er_2PbS_4) can be derived from Er_2EuS_4 [Lemoine et al., 1985] according to the relationship $\text{Eu}^{2+} \rightarrow \text{Pb}^{2+}$ (Figure 112).

The relationships between the crystal structures of ternary compounds found in the $R_2X_3\text{-PbX}$ ($X = \text{S}, \text{Se}$) systems are shown in Figure 113. Specifically, in the crystal structure of Er_2PbS_4 half of the positions of the lead atoms are ordered and the remaining half are disordered. On the other hand, all of the Pb positions are disordered in Tm_2PbSe_4 , while they are ordered in Sc_2PbS_4 . Thus, the crystal structure of Er_2PbS_4 contains fragments of both Tm_2PbSe_4 and Sc_2PbS_4 types of crystal structure. At the

TABLE 57 The $R_3M_{1-\delta}ZX_7$ ($M = \text{Cu, Ag, Z} = \text{Si, Ge, Sn, and X} = \text{S, Se}$) compounds

Compounds	La	Ce	Pr	Nd	Sm	Gd	Tb	Dy	Ho	Y	Er	Tm	Yb	Lu
$R_3Cu_{1-\delta}SiS_7$ ($\delta = 0$)	1	1	1	1	1	1	1	1	1	1	1	–	–	–
$R_3Cu_{1-\delta}GeS_7$ ($\delta = 0$)	1	1	1	1	1	1	1	1	1	1	1	–	–	–
$R_3Cu_{1-\delta}SnS_7$ ($\delta = 0$)	1	1	1	1	1	1	1	1	1	1	–	–	–	–
$R_3Cu_{1-\delta}SiSe_7$ ($\delta = 0$)	1	1	1	1	1	1	1	1	1	1	1	–	–	–
$R_3Cu_{1-\delta}GeSe_7$ ($\delta = 0$)	1	1	1	1	1	1	1	1	–	1	–	–	–	–
$R_3Cu_{1-\delta}SnSe_7$ ($\delta = 0$)	1	1	1	1	1	1	1	1	–	1	–	–	–	–
$R_3Ag_{1-\delta}SiS_7$ ($\delta = 0.10\text{--}0.23$)	2	2	2	2	2	–	–	–	–	–	–	–	–	–
$R_3Ag_{1-\delta}GeS_7$ ($\delta = 0.11\text{--}0.50$)	2	2	2	2	2	2	3	3	3	3	3	–	–	–
$R_3Ag_{1-\delta}SnS_7$ ($\delta = 0.18\text{--}0.19$)	2	2	–	–	–	–	–	–	–	–	–	–	–	–
$R_3Ag_{1-\delta}SiSe_7$ ($\delta = 0\text{--}0.30$)	1	1	1	1	2	2	2	2	–	–	–	–	–	–
$R_3Ag_{1-\delta}GeSe_7$ ($\delta = 0.06\text{--}0.28$)	2	2	2	2	2	2	2	2	–	–	–	–	–	–
$R_3Ag_{1-\delta}SnSe_7$ ($\delta = 0$)	1	–	–	–	–	–	–	–	–	–	–	–	–	–

1, first group; 2, second group; 3, third group.

TABLE 58 Ternary and quaternary rare earth lead compounds of the R_2X_3 -PbX and R_2X_3 -Cu₂X-PbX (X = S, Se) systems

Series	Composition	Structure type	X	R														
				La	Ce	Pr	Nd	Sm	Gd	Tb	Dy	Ho	Y	Er	Tm	Yb	Lu	Sc
1	RCuPbX ₃	ErCuPbS ₃ , β-BaLaCuSe ₃	S	-	-	-	-	-	+	+	+	+	+	+	+	+	-	
			Se	-	-	-	-	-	-	+	+	+	+	+	+	+	+	-
2	RCuPbX ₃	LaCuPbS ₃	S	+	-	-	-	-	-	-	-	-	-	-	-	-	-	
			Se	-	-	-	-	-	-	-	-	-	-	-	-	-	-	-
3	R _{4,2} Pb _{0,7} X ₇	Y _{4,2} Pb _{0,7} Se ₇	S	-	-	-	-	-	-	-	-	-	-	-	-	-	-	
			Se	-	-	-	-	-	-	-	-	-	+	-	-	-	-	-
4	R _{3,33} CuPb _{1,5} X ₇	Y _{3,33} CuPb _{1,5} S ₇ , Lu _{3,33} CuPb _{1,5} Se ₇	S	-	-	-	-	-	-	-	+	+	+	+	-	-	+	
			Se	-	-	-	-	-	-	+	+	+	+	+	+	+	+	-
	R ₆ Pb ₂ X ₁₁	Y ₆ Pb ₂ Se ₁₁	S	-	-	-	-	-	-	-	-	-	-	-	-	-	-	
			Se	-	-	-	-	-	-	-	+	+	+	-	-	-	-	-
R ₅ CuPb ₃ X ₁₁	Er ₅ CuPb ₃ Se ₁₁	S	-	-	-	-	-	-	-	-	+	+	+	+	-	-	-	
		Se	-	-	-	-	-	-	-	-	-	-	+	+	+	+	-	
5	R ₂ PbX ₄	Fe ₂ CaO ₄ ,	S	-	-	-	-	-	-	-	-	+	+	+	+	+	+	
		Tm ₂ PbSe ₄ ,	Se	-	-	-	-	-	-	-	-	-	-	-	+	+	+	+
		Er ₂ PbS ₄	Se	-	-	-	-	-	-	-	-	-	-	-	+	+	+	+

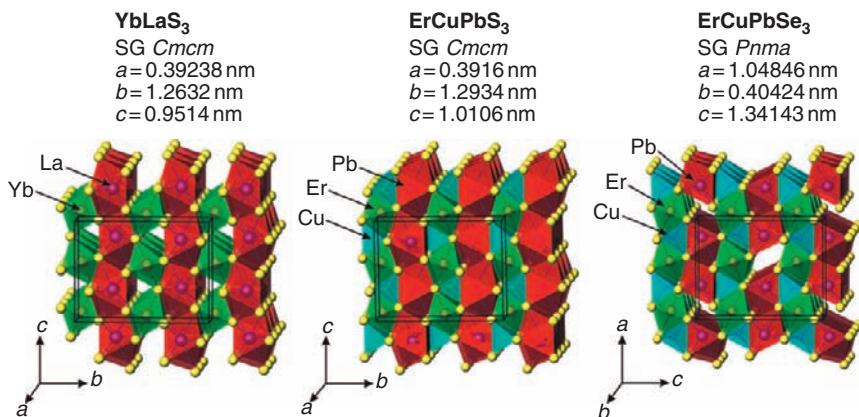


FIGURE 108 Crystallographic relationships among YbLaS₃, ErCuPbS₃, and ErCuPbSe₃ compounds.

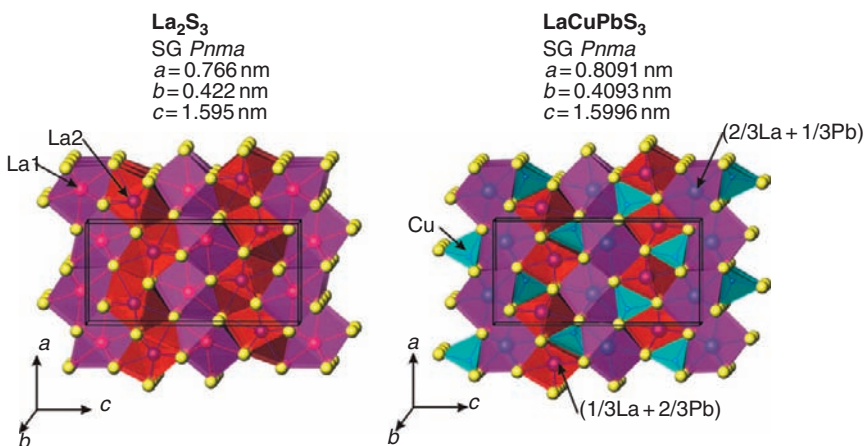


FIGURE 109 Crystallographic relationships between La₂S₃ and LaCuPbS₃ compounds.

same time, the crystal structure of the Y₆Pb₂Se₁₁ consists of structural fragments found in R₂PbX₄ and Y_{4.2}Pb_{0.7}S₇.

Similar relationships are also observed for quaternary compounds found in the R₂X₃–Cu₂X–PbX (X = S, Se) systems (Figure 114). Structural fragments from the RCuPbSe₃ and R₂Se₃ (Flahaut et al., 1965) types can be found in the crystal structures of the R_{3.33}CuPb_{1.5}Se₇ compounds. Furthermore, structural fragments of the R_{3.33}CuPb_{1.5}Se₇ type can be found in the crystal structure of R₅CuPb₃Se₁₁ compounds. The unit cell of the R₅CuPb₃Se₁₁ compounds can be completely constructed from the fragments of the R_{3.33}CuPb_{1.5}Se₇ and R₂PbSe₄ compounds.

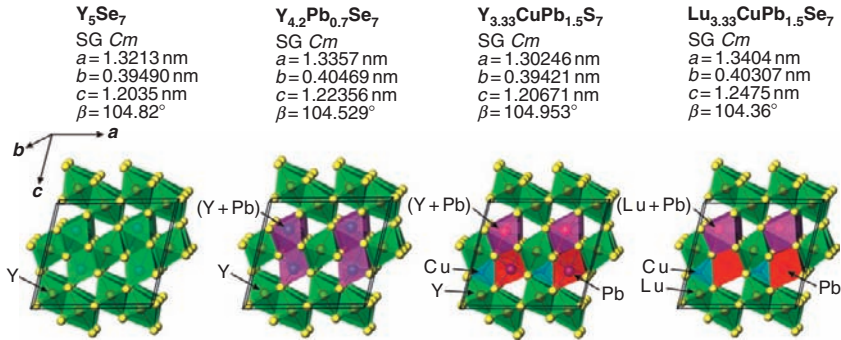


FIGURE 110 Crystallographic structure relationships among Y₅Se₇, Y_{4.2}Pb_{0.7}Se₇, Y_{3.33}CuPb_{1.5}S₇, and Lu_{3.33}CuPb_{1.5}Se₇ compounds.

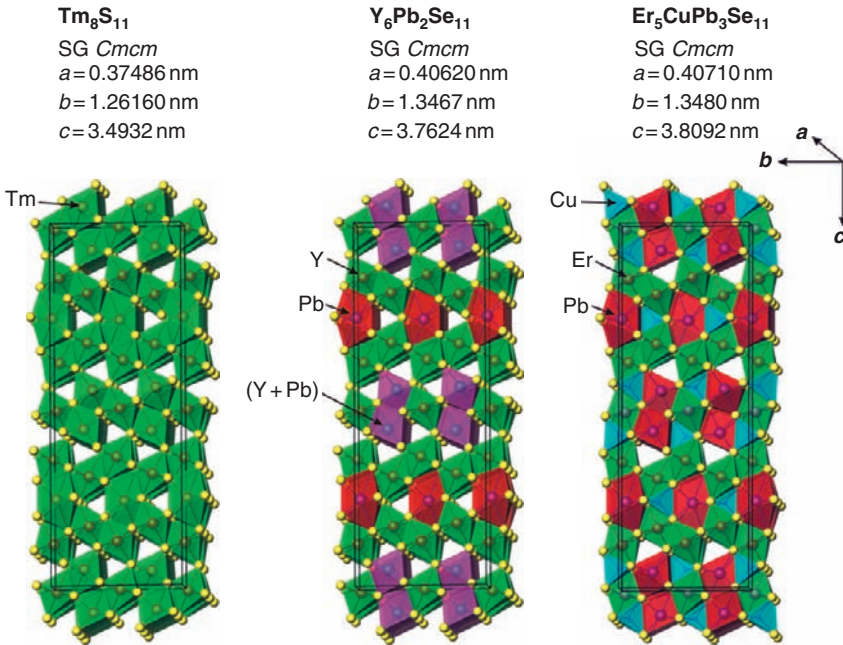


FIGURE 111 Crystallographic relationships among Tm₈S₁₁, Y₆Pb₂Se₁₁, and Er₅CuPb₃Se₁₁ compounds.

5.3 Formation of superstructures

The crystal structures of ternary and quaternary rare earth chalcogenides of Si, Ge, Sn, Pb, and In can be formed according to the following principles:

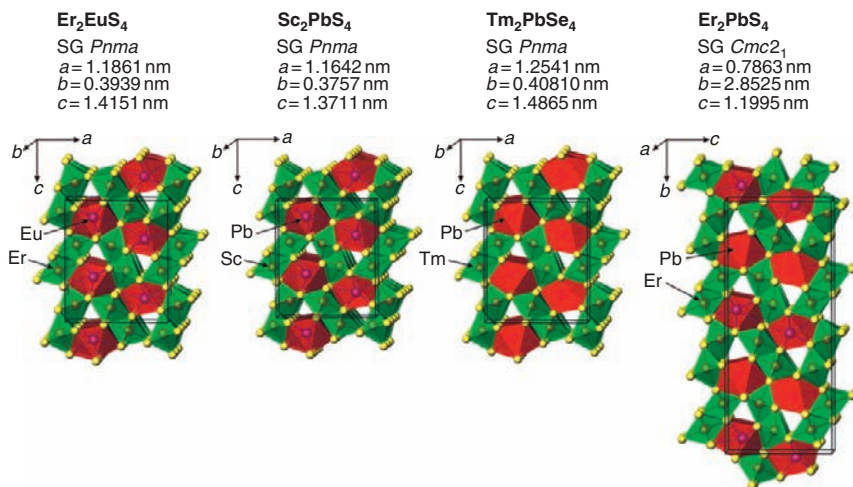


FIGURE 112 Crystallographic relationships among Er₂EuS₄, Sc₂PbS₄, Tm₂PbSe₄, and Er₂PbS₄ compounds.

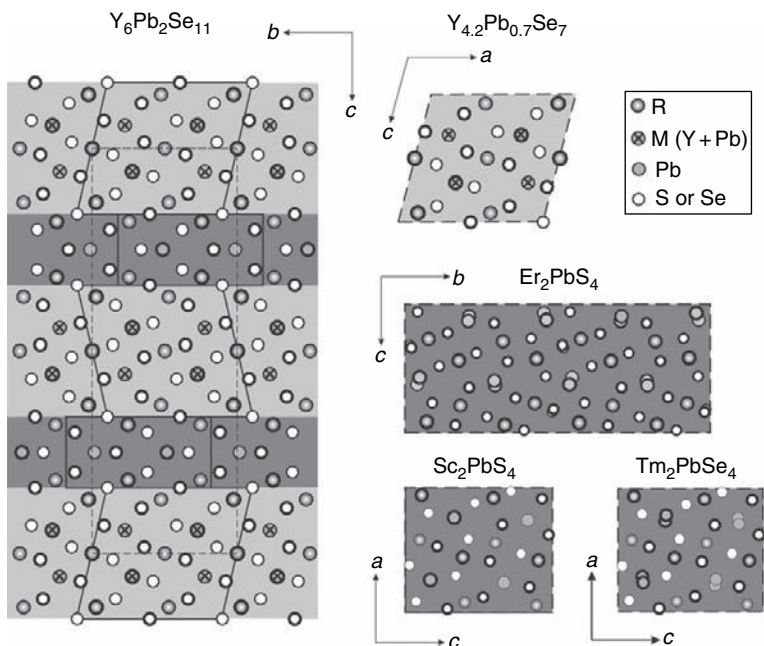


FIGURE 113 Relationships between crystal structures of ternary compounds in the R₂X₃-PbX (X = S, Se) systems.

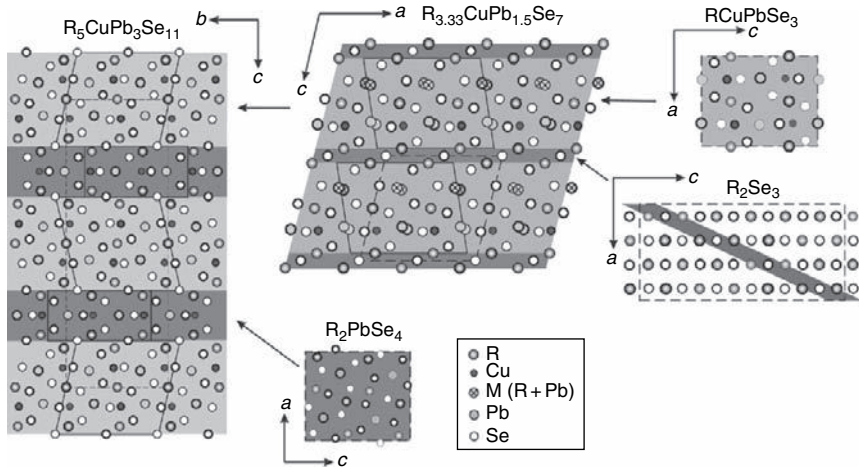


FIGURE 114 Relationships between crystal structures of quaternary compounds in the R_2Se_3 – Cu_2Se – $PbSe$ systems.

- (I) Ordered substitutions of atoms carrying identical charges. This kind of substitution is observed in the formation of ternary structures from the corresponding binary parents. For example, the crystal structure of the ternary $Y_6Pb_2Se_{11}$ can be derived from the binary Tm_8S_{11} parent by the substitution of Tm^{2+} by Pb^{2+} (Figure 111).
- (II) Ordered substitutions of atoms carrying different charges. The number of crystallographic positions is then different for the underlying parent structure and for the superstructure. This kind of substitution is observed for the formation of quaternary structures from the corresponding binary or ternary parent structures. For example, the crystal structure of the quaternary $Er_5CuPb_3Se_{11}$ can be derived from the ternary $Y_6Pb_2Se_{11}$ by the simple substitution of Y^{3+} by Pb^{2+} (Figure 111). Additional site for the Cu atoms is created in $Er_5CuPb_3Se_{11}$.
- (III) Ordering (disordering) of positions of some atoms. The number of positions either decreases or increases for a superstructure in comparison with the original parent structure. For example, the crystal structure of Tm_2PbSe_4 can be derived from Sc_2PbS_4 by splitting of the Pb positions (Figure 113).
- (IV) The crystal structure of a complex compound contains fragments of simpler structures. For example, the unit cell of $Y_6Pb_2Se_{11}$ can be completely constructed from the fragments of the unit cells of R_2PbX_4 and $Y_{4.2}Pb_{0.7}S_7$ (Figure 113).

According to these rules, a general scheme describing the formation of the crystal structures of ternary and quaternary rare earth lead chalcogenides can be constructed, and it is shown in Figure 115.

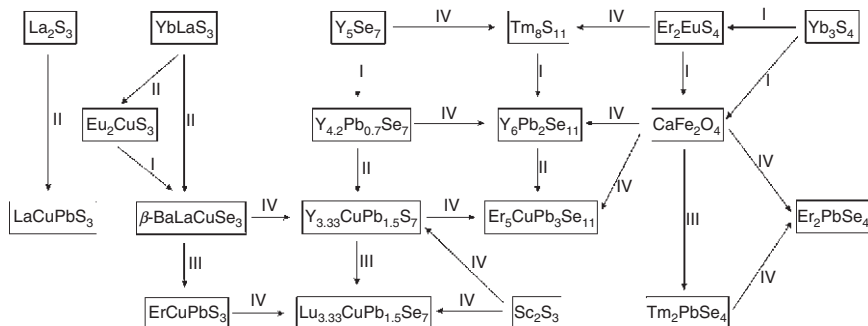


FIGURE 115 Formation of structures of ternary and quaternary rare earth lead chalcogenides.

5.4 The role of voids in the crystal structures of chalcogenides

In the case of quaternary compounds, it is observed that the copper atoms occupy new positions in comparison with their parent structures (see rule II, above). The copper atoms have tetrahedral coordination spheres and their positions, for example, in $Y_{4.2}Pb_{0.7}S_7$, are related to the existence of voids (large spacing) that are found between Y and Pb atoms in $Y_{4.2}Pb_{0.7}S_7$. By placing Cu atoms in such voids it was possible to derive the quaternary $Y_{3.33}CuPb_{1.5}S_7$ compound (Figure 110). It appears that the crystal structure of the $Er_5CuPb_3Se_{11}$ compound is formed in a similar fashion, that is via filling of the voids present in the less complex parent structure (Figure 111). However, what is origin of these large voids in the parent structures?

In many crystal structures, the chalcogenide atoms, that is sulfur or selenium, create a trigonal prismatic arrangement around the R atoms. These trigonal prisms can be mono-, bi-, or tricapped, and therefore, the coordination numbers of the R atoms are 7 (6 + 1), 8 (6 + 2), or 9 (6 + 3). The additional coordination sites are intentionally distinguished here, because the six $R-X_{in}$ distances in the trigonal prism itself are usually shorter than the capping $R-X_{out}$ distances in the same trigonal prism. These long distances become longer for heavy lanthanides, because the heavy lanthanides have smaller ionic radius. Moreover, the same is also reflected in the bond valence sums for the $R-X_{out}$ (Brown, 1996), where this contribution is smaller than for $R-X_{in}$. When the contribution to the bond valence sum of R^{3+} ion is small, the $R-X_{out}$ becomes too long to be recognized as the bonding interaction and the void is created. Thus, small ions, for example Cu^+ ion, can occupy this position, and a new quaternary chalcogenide is formed. Additionally, this newly formed compound has a very similar crystal structure architecture as its parent structure.

Summing up, synthesis of new compounds with predictable crystal structures resembles laying building blocks. However, the more crystal structures we know, the more predictable synthetic results will become. This fact is as important as crystal engineering, which is still looking for new compounds with predictable structure and with new (or predictable) properties.

REFERENCES

- Aleandri, L.E., Ibers, J.A., 1989. *J. Solid State Chem.* 81, 317.
- Aliev, O.M., 1980. *Neorg. Mater.* 16, 1514 (in Russian).
- Aliev, O.M., Kurbanov, T.K., Rustamov, P.G., Alidzhanov, M.A., Salmanov, S.M., 1976. *Neorg. Mater.* 12, 1944 (in Russian).
- Amirov, A.S., Shnulin, A.N., Guseinov, G.G., Mamedov, Kh.S., 1984. *Kristallografiya* 29, 787 (in Russian).
- Bakakin, V.V., Ipatova, E.N., Solov'eva, L.P., 1974. *Zhurn. Strukt. Khim.* 15, 460.
- Basançon, P., Adolphe, C., Flahaut, J., Laruelle, P., 1969. *Mater. Res. Bull.* 4, 227.
- Brennan, T.D., Ibers, J.A., 1992. *J. Solid State Chem.* 97, 377.
- Brown, I.D., 1996. *J. Appl. Cryst.* 29, 479. http://www.ccp14.ac.uk/ccp/web-mirrors/i_d_brown.
- Bugli, G., Carré, D., Barnier, S., 1978. *Acta Cryst.* B34, 3186.
- Bugli, G., Dugué, J., Barnier, S., 1979. *Acta Cryst.* B35, 2690.
- Carré, D., 1977. *Acta Cryst.* B33, 1163.
- Carré, D., Guittard, M., Adolphe, C., 1978. *Acta Cryst.* B34, 3499.
- Choudhury, A., Dorhout, P.K., 2008. *Z. Anorg. Allg. Chem.* 634, 649.
- Christuk, A.E., Wu, P., Ibers, J.A., 1994. *J. Solid State Chem.* 110, 330.
- Collin, G., Laruelle, P., 1971. *Bull. Soc. Fr. Mineral. Cristallogr.* 94, 175.
- Daszkiewicz, M., Gulay, L.D., Ruda, I.R., Marchuk, O.V., Pietraszko, A., 2007a. *Acta Cryst.* E63, i197.
- Daszkiewicz, M., Gulay, L.D., Pietraszko, A., Shemet, V.Ya., 2007b. *J. Solid State Chem.* 180, 2053.
- Daszkiewicz, M., Gulay, L.D., Shemet, V.Ya., 2008a. *Acta Cryst.* B64, 172.
- Daszkiewicz, M., Gulay, L.D., Lychmanyuk, O.S., Pietraszko, A., 2008b. *J. Alloys Compd.* 460, 201.
- Daszkiewicz, M., Gulay, L.D., Lychmanyuk, O.S., Pietraszko, A., 2009a. *J. Alloys Compd.* 467, 168.
- Daszkiewicz, M., Gulay, L.D., Lychmanyuk, O.S., 2009b. *Acta Cryst.* B65, 126.
- de Saint-Giniez, D., Laruelle, P., Flahaut, J., 1968. *R.C. Seances Acad. Sci. Ser. C* 267, 1029.
- Eliseev, A.A., Kuzmichyeva, G.M., 1990. *Handbook on the Physics and Chemistry of Rare Earths*. Elsevier Science Publishers B.V. 13, Chapter 89, pp. 191–281.
- Evenson, C.R., Dorhout, P.K., 2001. *Z. Anorg. Allg. Chem.* 627, 2178.
- Flahaut, J., Laruelle, P., Pardo, M.P., Guittard, M., 1965. *Bull. Soc. Chim. Fr.* 1399.
- Gauthier, G., Jobic, S., Evain, M., Koo, H.-J., Whangbo, M.-H., Fouassier, C., Brec, R., 2003. *Chem. Mater.* 15, 828.
- Guittard, M., Julien-Pouzol, M., 1970. *Bull. Soc. Chim. Fr.* 2467.
- Guittard, M., Julien-Pouzol, M., Jaulmes, S., 1976. *Mater. Res. Bull.* 11, 1073.
- Gulay, L.D., Lychmanyuk, O.S., 2008. *J. Alloys Compd.* 458, 174.
- Gulay, L.D., Olekseyuk, I.D., 2005a. *J. Alloys Compd.* 388, 274.
- Gulay, L.D., Olekseyuk, I.D., 2005b. *J. Alloys Compd.* 387, 160.
- Gulay, L.D., Olekseyuk, I.D., 2005c. *J. Alloys Compd.* 396, 233.

- Gulay, L.D., Olekseyuk, I.D., 2006a. *Visnyk Volyn University Khim. Nauky* 4, 101 (in Ukrainian).
- Gulay, L.D., Olekseyuk, I.D., 2006b. *J. Alloys Compd.* 413, 122.
- Gulay, L.D., Shemet, V.Ya., Olekseyuk, I.D., 2004. *J. Alloys Compd.* 385, 160.
- Gulay, L.D., Shemet, V.Ya., Stępień-Damm, J., Pietraszko, A., Olekseyuk, I.D., 2005a. *J. Alloys Compd.* 403, 206.
- Gulay, L.D., Lychmanyuk, O.S., Stępień-Damm, J., Pietraszko, A., Olekseyuk, I.D., 2005b. *J. Alloys Compd.* 402, 201.
- Gulay, L.D., Shemet, V.Ya., Olekseyuk, I.D., 2005c. *J. Alloys Compd.* 388, 59.
- Gulay, L.D., Olekseyuk, I.D., Wołczyr, M., Stępień-Damm, J., 2005d. *Z. Anorg. Allg. Chem.* 631, 1919.
- Gulay, L.D., Shemet, V.Ya., Olekseyuk, I.D., 2005e. *J. Alloys Compd.* 393, 174.
- Gulay, L.D., Kaczorowski, D., Pietraszko, A., 2005f. *J. Alloys Compd.* 403, 49.
- Gulay, L.D., Shemet, V.Ya., Olekseyuk, I.D., 2005g. *J. Alloys Compd.* 394, 250.
- Gulay, L.D., Olekseyuk, I.D., Wołczyr, M., Stępień-Damm, J., 2005h. *J. Alloys Compd.* 399, 189.
- Gulay, L.D., Lychmanyuk, O.S., Stępień-Damm, J., Pietraszko, A., Olekseyuk, I.D., 2006a. *J. Alloys Compd.* 414, 113.
- Gulay, L.D., Wołczyr, M., Olekseyuk, I.D., 2006b. *Pol. J. Chem.* 80, 805.
- Gulay, L.D., Kaczorowski, D., Shemet, V.Ya., Pietraszko, A., 2006c. *J. Alloys Compd.* 421, 87.
- Gulay, L.D., Wołczyr, M., Pietraszko, A., Olekseyuk, I.D., 2006d. *Pol. J. Chem.* 80, 1703.
- Gulay, L.D., Lychmanyuk, O.S., Wołczyr, M., Pietraszko, A., Olekseyuk, I.D., 2006e. *J. Alloys Compd.* 425, 159.
- Gulay, L.D., Lychmanyuk, O.S., Olekseyuk, I.D., Pietraszko, A., 2006f. *J. Alloys Compd.* 422, 203.
- Gulay, L.D., Olekseyuk, I.D., Wołczyr, M., Stępień-Damm, J., Pietraszko, A., 2006g. *J. Alloys Compd.* 416, 173.
- Gulay, L.D., Kaczorowski, D., Pietraszko, A., 2006h. *J. Alloys Compd.* 413, 26.
- Gulay, L.D., Stępień-Damm, J., Pietraszko, A., Olekseyuk, I.D., 2006i. *J. Alloys Compd.* 413, 90.
- Gulay, L.D., Shemet, V.Ya., Olekseyuk, I.D., Stępień-Damm, J., Pietraszko, A., Koldun, L.V., Filimonyuk, J.O., 2007a. *J. Alloys Compd.* 431, 77.
- Gulay, L.D., Daszkiewicz, M., Stępień-Damm, J., Pietraszko, A., 2007b. *J. Alloys Compd.* 429, 111.
- Gulay, L.D., Huch, M.R., Olekseyuk, I.D., Pietraszko, A., 2007c. *J. Alloys Compd.* 429, 216.
- Gulay, L.D., Lychmanyuk, O.S., Olekseyuk, I.D., Daszkiewicz, M., Stępień-Damm, J., Pietraszko, A., 2007d. *J. Alloys Compd.* 431, 185.
- Gulay, L.D., Daszkiewicz, M., Huch, M.R., Pietraszko, A., 2007e. *Acta Cryst.* E63, i182.
- Gulay, L.D., Daszkiewicz, M., Lychmanyuk, O.S., Pietraszko, A., 2008a. *J. Alloys Compd.* 453, 197.
- Gulay, L.D., Daszkiewicz, M., Shemet, V.Ya., 2008b. *Z. Anorg. Allg. Chem.* 634, 1887.
- Gulay, L.D., Daszkiewicz, M., Shemet, V.Ya., Pietraszko, A., 2008c. *J. Alloys Compd.* 453, 143.
- Gulay, L.D., Daszkiewicz, M., Huch, M.R., 2008d. *J. Solid State Chem.* 181, 2626.
- Gulay, L.D., Daszkiewicz, M., Shemet, V.Ya., Pietraszko, A., 2008e. *Polish J. Chem.* 82, 1001.
- Guloy, A.M., Corbett, J.D., 1993. *Inorg. Chem.* 32, 3532.
- Guloy, A.M., Corbett, J.D., 1994. *J. Solid State Chem.* 109, 352.
- Guseinov, G.G., Mamedov, F.H., Mamedov, H.S., 1979a. *Dokl. Akad. Nauk Azerb. SSSR* 35, 50 (in Russian).
- Guseinov, G.G., Mamedov, F.H., Shnulin, A.N., Mamedov, H.S., 1979b. *Dokl. Akad. Nauk Azerb. SSSR* 246, 1360 (in Russian).
- Hartenbach, I., Müller, A.C., Schleid, T., 2006. *Z. Anorg. Allg. Chem.* 632, 2147.
- Hartenbach, I., Nilges, T., Schleid, T., 2007. *Z. Anorg. Allg. Chem.* 633, 2445.

- Hatscher, S.T., Urland, W., 2002a. *Z. Anorg. Allg. Chem.* 628, 1673.
- Hatscher, S.T., Urland, W., 2002b. *Acta Cryst.* E58, i74.
- Hatscher, S.T., Urland, W., 2003. *J. Solid State Chem.* 172, 417.
- Helmholdt, R.B., Goubitz, K., Sonneveld, E.J., Schenk, H., 2003. *Acta Cryst.* E59, i119.
- Hill, P.M., Peiser, H.S., Rait, J.R., 1956. *Acta Cryst.* 9, 981.
- Huang, F.Q., Ibers, J.A., 1999. *Acta Cryst.* C55, 1210.
- Huch, M.R., Gulay, L.D., Olekseyuk, I.D., 2006a. *Visnyk Volyn University Khim. Nauky* 4, 54 (in Ukrainian).
- Huch, M.R., Gulay, L.D., Olekseyuk, I.D., Pietraszko, A., 2006b. *J. Alloys Compd.* 425, 230.
- Huch, M.R., Gulay, L.D., Olekseyuk, I.D., 2007a. *Visnyk Volyn University Khim. Nauky* 13, 15 (in Ukrainian).
- Huch, M.R., Gulay, L.D., Olekseyuk, I.D., 2007b. *J. Alloys Compd.* 439, 156.
- Hvaleba, N.V., Gulay, L.D., Zmiy, O.F., Olekseyuk, I.D., 2006. *Visnyk Volyn University Khim. Nauky* 4, 112 (in Ukrainian).
- Iyer, R.G., Aitken, J.A., Kanatzidis, M.G., 2004. *Solid State Sci.* 6, 451.
- Jaulmes, S., 1974. *Acta Cryst.* B30, 2283.
- Jaulmes, S., Julien-Pouzol, M., 1977a. *Acta Cryst.* B33, 3898.
- Jaulmes, S., Julien-Pouzol, M., 1977b. *Acta Cryst.* B33, 1191.
- Jaulmes, S., Julien-Pouzol, M., Laruelle, P., Guittard, M., 1982. *Acta Cryst.* B38, 79.
- Johrendt, D., Pocha, R., 2001. *Acta Cryst.* E57, i57.
- Johrendt, D., Tampier, M., 2000. *Chem. Eur. J.* 6, 994.
- Julien-Pouzol, M., Jaulmes, S., 1979. *Acta Cryst.* B35, 2672.
- Kim, S.-J., Franzen, H.F., 1988. *J. Less-Comm. Met.* 138, L29.
- Klee, W., Schäfer, H., 1978. *Z. Naturforsch.* B33, 829.
- Lemoine, P., Carré, D., Guittard, M., 1985. *Acta Cryst.* C41, 667.
- Lemoine, P., Tomas, A., Carré, D., Guittard, M., Likforman, A., 1989. *Acta Cryst.* C45, 1858.
- Likforman, A., Guittard, M., 1993. *Acta Cryst.* C49, 1270.
- Lin, S.-H., Mao, J.-G., Guo, G.-C., Huang, J.-S., 1997. *J. Alloys Compd.* 252, L8.
- Loireau-Lozac'h, A., Guittard, M., 1977. *Mater. Res. Bull.* 12, 887.
- Lychmanyuk, O.S., Gulay, L.D., Olekseyuk, I.D., 2006a. *Visnyk Volyn University Khim. Nauky* 4, 118 (in Ukrainian).
- Lychmanyuk, O.S., Gulay, L.D., Olekseyuk, I.D., 2006b. *Polish J. Chem.* 80, 463.
- Lychmanyuk, O.S., Gulay, L.D., Olekseyuk, I.D., Stepień-Damm, J., Daszkiewicz, M., Pietraszko, A., 2007a. *Polish J. Chem.* 81, 353.
- Lychmanyuk, O.S., Gulay, L.D., Olekseyuk, I.D., 2007b. *Visnyk Volyn University Khim. Nauky* 15, 10 (in Ukrainian).
- Marchuk, O.V., Gulay, L.D., Olekseyuk, I.D., 2006a. *Visnyk Volyn University Khim. Nauky* 4, 96 (in Ukrainian).
- Marchuk, O.V., Gulay, L.D., Shemet, V.Ya., Olekseyuk, I.D., 2006b. *J. Alloys Compd.* 416, 106.
- Marchuk, O.V., Daszkiewicz, M., Gulay, L.D., Olekseyuk, I.D., Pietraszko, A., 2008. *J. Alloys Compd.* 455, 186.
- Mazurier, A., Etienne, J., 1973. *Acta Cryst.* B29, 817.
- Mazurier, A., Etienne, J., 1974. *Acta Cryst.* B30, 759.
- Meisel, K., 1939. *Z. Anorg. Allg. Chem.* 240, 300.
- Messain, D., Carré, D., Laruelle, P., 1977. *Acta Cryst.* B33, 2540.
- Michelet, A., Flahaut, J., 1969. *R.C. Seances Acad. Sci. Ser. C* 268, 326.
- Michelet, A., Laruelle, P., Flahaut, J., 1966. *R.C. Seances Acad. Sci. Ser. C* 262, 753.
- Michelet, A., Perez, G., Etienne, J., Darriet Duale, M., 1970. *R.C. Seances Acad. Sci. Ser. C* 271, 513.
- Michelet, A., Mazurier, A., Collin, G., Laruelle, P., Flahaut, J., 1975. *J. Solid State Chem.* 13, 65.
- Mitchell, K., Somers, R.C., Huang, F.Q., Ibers, J.A., 2004. *J. Solid State Chem.* 177, 709.
- Noël, R., Vovan, T., 1976. *Acta Cryst.* B32, 2705.

- Patrie, M., Guittard, M., 1969. R.C. Seances Acad. Sci. Ser. C 268, 1136.
- Patrie, M., Guittard, M., Pardo, M.-P., 1969. Bull. Soc. Chim. Fr. 3832.
- Perez, G., Duale, M., 1969. R.C. Seances Acad. Sci. Ser. C 269, 984.
- Pocha, R., Tampier, M., Hoffmann, R.-D., Mosel, B.D., Pöttgen, R., Johrendt, D., 2003. Z. Anorg. Allg. Chem. 629, 1379.
- Poduska, K.M., DiSalvo, F.J., Min, K., Halasyamani, P.S., 2002. J. Alloys Compd. 335, L5.
- Ribes, M., Philippot, E., Maurin, M., 1970. R.C. Seances Acad. Sci. Ser. C 270, 716.
- Rieger, W., Nowotny, H., Benesovsky, F., 1965. Monatsh. Chem. 96, 232.
- Shannon, R.D., 1976. Acta Cryst. A32, 751.
- Shemet, V.Ya., Gulay, L.D., 2007. Mizvyzivskiy Zbirnyk Inzhenerna Mekhanika 20, 558 (in Ukrainian).
- Shemet, V.Ya., Gulay, L.D., Olekseyuk, I.D., 2005. Polish J. Chem. 79, 1315.
- Shemet, V.Ya., Gulay, L.D., Stępień-Damm, J., Pietraszko, A., Olekseyuk, I.D., 2006a. J. Alloys Compd. 407, 94.
- Shemet, V.Ya., Gulay, L.D., Stępień-Damm, J., Pietraszko, A., Olekseyuk, I.D., 2006b. Polish J. Chem. 80, 943.
- Shemet, V.Ya., Gulay, L.D., Olekseyuk, I.D., 2006c. Visnyk Volyn University Khim. Nauky 4, 124 (in Ukrainian).
- Shemet, V.Ya., Gulay, L.D., Olekseyuk, I.D., 2006d. J. Alloys Compd. 426, 186.
- Shemet, V.Ya., Gulay, L.D., Stępień-Damm, J., Pietraszko, A., Olekseyuk, I.D., 2006e. J. Alloys Compd. 420, 58.
- Spek, A.L., 2003. J. Appl. Cryst. 36, 7.
- Tampier, M., Johrendt, D., 2001. J. Solid. State Chem. 158, 343.
- Tampier, M., Johrendt, D., Pöttgen, R., Kotzyba, G., Rosenhahn, C., Mosel, B.D., 2002. Z. Naturforsch. B57, 133.
- Tomas, A., Guittard, M., 1977. Mater. Res. Bull. 12, 1043.
- Tomas, A., Palazzi, M., Chaqour, S.M., Guittard, M., Guymont, M., 1992. Mater. Res. Bull. 27, 1083.
- Tougait, O., Ibers, J.A., 2000. Inorg. Chem. 39, 1790.
- Trojer, F., 1968. Naturwissenschaften 55, 442.
- Wu, L.-B., Huang, F.-Q., 2005. Z. Kristallogr. NST 220, 307.
- Zeng, H.-Y., Zheng, F.-K., Guo, G.-C., Huang, J.-S., 2008. J. Alloys Compd. 458, 123.
- Zhang, Y., Franzen, H.F., Harbrecht, B.J., 1990. Less-Comm. Met. 166, 135.

This page intentionally left blank

Controlled Synthesis and Properties of Rare Earth Nanomaterials

**Chun-Hua Yan,* Zheng-Guang Yan,*[†] Ya-Ping Du,*
Jie Shen,* Chao Zhang,* and Wei Feng***

Contents	List of Symbols and Abbreviations	276
	1. Introduction	278
	2. Nanomaterials of Rare Earth Oxides and Hydroxides	281
	2.1 Ceria	281
	2.2 R ₂ O ₃	311
	2.3 Other rare earth oxides	325
	2.4 Rare earth hydroxides	326
	3. Nanomaterials of Rare Earth Oxysalts	329
	3.1 Rare earth phosphates	329
	3.2 Rare earth vanadates	350
	3.3 Rare earth borates	379
	3.4 Rare earth silicates	385
	3.5 Other rare earth oxysalts	387
	4. Nanomaterials of Rare Earth Halides	404
	4.1 Rare earth fluorides	405
	4.2 Rare earth oxyhalides	418
	4.3 ARF ₄ compounds	420
	5. Nanomaterials of Rare Earth Sulfides and Oxysulfides	433
	5.1 Rare earth sulfides	433
	5.2 Rare earth oxysulfides	440
	6. Conclusions and Perspectives	448
	Acknowledgments	451
	References	451

* Beijing National Laboratory for Molecular Sciences, State Key Laboratory of Rare Earth Materials Chemistry and Applications, PKU-HKU Joint Laboratory in Rare Earth Materials and Bioinorganic Chemistry, Peking University, Beijing, China

[†] Institute of Microscopy and Properties of Advanced Materials, Beijing University of Technology, Beijing, China

List of Symbols and Abbreviations

1D	one dimensional
2D	two dimensional
3D	three dimensional
ac	acetate
acac	acetylacetonate
AHA	6-aminohexanoic acid
AOT	bis(2-ethylhexyl) sulfosuccinate
BA	benzoylacetate
BA	borate absorption
Bipy	2,2'-bipyridine
CBD	chemical bath deposition
CIE	international commission on illumination
CL	cathodo-luminescent
CP	coprecipitation
CT	charge transfer
CTA	hexadecyltrimethylammonium
CTAB	hexadecyltrimethylammonium bromide
CTL	catalytic luminescence
CVD	chemical vapor deposition
CW	continuous wave
DC	down-conversion
DDAB	di- <i>n</i> -didodecyldimethylammoniumbromide
Ddtc	diethyldithiocarbamate
DEG	diethylene glycol
DMDCS	dimethyldichlorosilane
DMF	dimethylformamide
DMSO	dimethyl sulfoxide
DNA	deoxyribonucleic acid
DP	deposition-precipitation
DTE	diarylethene
ED	electron diffraction
EDS	energy dispersive spectra
EDTA	ethylenediaminetetraacetic acid
E_g	energy of band gap
EHPNA	2-ethylhexyl phosphonic acid mono-2-ethylhexyl ester
EISA	evaporation induced self assembly
ET	excitonic transfer
Et-	ethano-
FFT	fast Fourier transform
FITC	fluorescein isothiocyanate

FRET	fluorescence resonance energy-transfer or Förster resonance energy transfer
GOx	glucose oxidase
H_C	coercivity
HEDP	1-hydroxyethane-1,1-diphosphonic acid
HEEDA	<i>N</i> -(2-hydroxyethyl)-ethylenediamine
HRTEM	high-resolution transmission electron microscopy
IL	ionic liquids
IR	infrared
KB cells	a cell line derived from a human carcinoma of the nasopharynx
Ln	lanthanide
LRET	luminescence resonance energy transfer
MCM-41	one of the most common mesoporous silicates
MOCVD	metalorganic chemical vapor deposition
mPEG	polyethylene glycol monomethyl ether
MRI	magnetic resonance imaging
NC	nanocrystal
NEXAFS	near edge X-ray absorption fine structure
NIR	near-infrared
NMR	nuclear magnetic resonance
NP	nanoparticle
NR	nanorod
NT	nanotube
NW	nanowire
OA	oleic acid
ODE	1-octadecene
OM	oleylamine
OSC	oxygen storage capacity
PAAc	poly(acrylic acid)
PAh	poly(alkylamine hydrochloride)
PEG	poly(ethylene glycol)
PEI	polyethylenimine
Phen	1,10-phenanthroline
PL	photo luminescence
PLD	pulsed laser deposition
PMMA	poly(methyl methacrylate)
PPA	phosphino polyacrylic acid
PSS	poly(sodium 4-styrenesulfonate)
PVA	poly(vinyl alcohol)
PVP	polyvinylpyrrolidone
QD	quantum dot
QY	quantum yield

R	rare earth
R_w	water/oil ratio in microemulsion systems
SAED	selected area electron diffraction
SBA-15	one of the most common mesoporous silicates
SDS	sodium dodecyl sulfate
SEM	scanning electron microscopy
SOD	superoxide dismutase
SOFC	solid oxide fuel cell
SP	superlattice
Span 83	sorbitan sesquioleate
SWNT	single wall carbon nanotube
T_c	curie temperature
TEM	transmission electron microscopy
TEOS	tetraethylorthosilicate
TOA	trioctylamine
TOPO	trioctylphosphine oxide
TPP	tripolyphosphate ($\text{Na}_5\text{P}_3\text{O}_{10}$)
TPR	temperature-programmed reduction
TWC	three way catalyst
UC	up-conversion
UV	ultraviolet
VUV	vacuum ultraviolet
WGS	water gas shift reaction
XPS	X-ray photoelectron spectroscopy
XRD	X-ray diffraction
YBCO	yttrium barium copper oxide
YSZ	yttria stabilized zirconia
ZBLAN	a type of glass made of a mixture of zirconium, barium, lanthanum, aluminum, and sodium fluorides
ZDDP	zinc di-iso-amyl-octyl-dithiophosphate

1. INTRODUCTION

Since the discovery of carbon nanotubes (Iijima, 1991), nanoscience and nanotechnology has been one of the most attractive issues in materials science. Nanomaterials are notable for their featured small size, which means that at least one dimension is in the range of 1–100 nm. This characteristic also endows nanomaterials with size- and shape-dependent physical and chemical properties because of the high surface/volume ratio and quantum effects.

Up to now, different nanomaterials have been developed into several large families. The carbon nanomaterials, including the carbon nanotubes, fibers, graphene, fullerenes, and many other forms (Delgado et al., 2008) show potential for applications in electronics, optics and even mechanics (Deheer et al., 1995; Fan et al., 1999; Tans et al., 1998; Thess et al., 1996; Treacy et al., 1996). Recently, the graphene, that is, one or a few single atomic layer(s) of carbon, has attracted increasing attention (Geim and Novoselov, 2007; Novoselov et al., 2005) for both practical and theoretical research interests.

The semiconductor nanocrystals, known as quantum dots/rods, are significant for their optical and electronic properties (Alivisatos, 1996; Bruchez et al., 1998; Murray et al., 1993). They make an important contribution to the interdisciplinary research between nanotechnology and biology, since quantum dots have been widely utilized as fluorescent bioprobes. On the other hand, ZnO nanomaterials have found substantial interest among researchers for lasing action and piezoelectric nanogenerators (Ozgur et al., 2005; Wang and Song, 2006).

The metallic nanocrystals are remarkable due to their localized surface plasmon resonance (SPR) phenomenon, that is, the excitation of surface plasma by light. It ensures these nanocrystals to be color based sensors (Homola et al., 1999; Kelly et al., 2003). The metallic nanocrystals could also sensitize the Raman signals from their adsorbed organic molecules. This surface enhanced Raman scattering (SERS) effect potentially raises the detection sensitivity to single molecule level (Kneipp et al., 1997; Nie and Emery, 1997).

Rare earth (Sc, Y, and La–Lu) nanomaterials are also being paid great attention during this “nanomania”. With the previous success in conventional applications, including phosphors, catalysts, magnets, fuel cell electrodes/electrolyte, hard alloys, and superconductors (Xu, 2005), rare earth compounds keep on showing new properties and applications in the nanoscaled field. Some important achievements have already emerged in the luminescence (Liu and Chen, 2007b), catalysis (Bernal et al., 1999), and ceramics related fields (Kleinlogel and Gauckler, 2001). Different from quantum dots, the typical rare earth nanomaterials show certain size-insensitive luminescence behaviors. Their quasi-line emissions mostly rely on the intra-4f electron transitions and have much longer decay lifetimes. Another important characteristic, the apparent quenching concentration of luminescent dopants in rare earth nanomaterials is higher relative to that for corresponding bulk phosphors. This is usually attributed to the large surface effect of nanocrystalline materials. However, the increased surface status interrupts the energy transfer pathway of luminescence, and the luminescence efficiency could not be improved by merely raising the doping concentration. One proper solution is to employ further surface modification/coating to fabricate

core/shell structured nanocrystals. Moreover, we can make use of the lattice aberrance in nanomaterials to modulate the emission of rare earth ions. Especially for Eu^{3+} , its local symmetry definitely affects the intensity ratio of red/orange luminescence signals. On the other hand, the luminescence behavior of Eu^{3+} also probes the symmetry of local environment. Besides the optical-related applications, the catalysis research on rare earth nanomaterials extends our traditional knowledge too. Ceria (CeO_2) has a considerable oxygen storage capability by the interconversion between Ce(III) and Ce(IV) and nano-sized ceria crystallites will increase the surface areas, exposing more surface-active sites. It benefits noble metal catalysts dispersed into the ceria to reach orders of a magnitude of higher catalytic activity. The importance of such catalysts in fuel, energy, and waste gas processing has attracted lots of attention. The traditional CO oxidation mechanism and some new reactions are under active research.

In the past decade, a great amount of effort has been devoted to the research field of rare earth nanomaterials. First of all, some classical chemical synthesis methodologies have been validated in these works, including aqueous reactions, hydrothermal/solvothermal reactions, microemulsion route, high-boiling solvent route, sonication or microwave reactions, as well as molten salt route, solid state reactions, and combustion method. Now we could precisely control the phase purity, crystallinity, morphology, and surface status of the products in preparation. Second, some complex mesostructures, composite materials, and superlattices are fabricated for new potential applications, as well as in response to demands of the developing nanotechnology. In addition, simulations and theoretical modeling of rare earth based nanomaterials have also been attempted with classical atomistic models as well as first principle techniques.

One of the chapters of this handbook has already made an in-depth discussion on luminescence of rare earth doped nanomaterials, presented by Liu and Chen (2007b). So in this chapter, we will focus on the chemical synthesis technology of inorganic rare earth nanomaterials, especially on the versatile solution-based routes, and recent discoveries and milestones in the synthesis and properties studies are systemically reviewed. The general physical synthesis routes, such as MOCVD, PLD, magnetron sputtering, would not be specifically mentioned in our chapter.

The subsequent sections are assigned by following the compound sequence of rare earth nanomaterials. Rare earth oxides are often regarded as the most important compound class while rare earth hydroxides are frequently used as their synthesis precursors. Therefore, we discuss the nanomaterials of ceria, R_2O_3 and other rare earth oxides along with the rare earth oxyhydroxides and hydroxides in Section 2. Rare earth oxysalts, such as phosphates, vanadates, and borates are

widely used in the lighting industry, while complex oxides of rare earth and other metal ions also promise applications in optics, magnetism, superconductivity, and many other areas. We review these nanomaterials in Section 3. Rare earth fluorides are another class of insoluble rare earth salts, and NaYF_4 is one of the best hosts for upconversion photoluminescence. Other rare earth halides and rare earth oxyhalides provide applications like scintillators. So, all discussion on rare earth halide-related nanomaterials is included in Section 4. Rare earth sulfides and oxysulfides provide another class of photo-luminescent materials, and corresponding nanomaterials will be discussed in Section 5. Finally, we would attempt to summarize the chapter and provide a brief prospective in Section 6. These materials, mainly based on other elements and doped with rare earths, such as yttria-stabilized zirconia (YSZ), yttrium barium copper oxide (YBCO), rare earth-doped phosphors, would not be covered in our work.

2. NANOMATERIALS OF RARE EARTH OXIDES AND HYDROXIDES

2.1 Ceria

As one of the most frequently investigated rare earth compounds in recent years, ceria (CeO_2) is an example of the cation with a valence of 4. Ceria adopts a cubic fluorite structure with space group $Fm\bar{3}m$ from room temperature up to the melting point (m.p.). Ce^{4+} occupies the 4a sites (0, 0, 0) and O^{2-} occupies the 8c sites (1/4, 1/4, 1/4). The fluorite structure could be maintained under intensive reduction due to reducing atmosphere or elevated temperature to a large extent. With reduction processes, the alteration of cation valence states from Ce^{4+} to Ce^{3+} is accompanied by the formation of oxygen vacancies, which provide highly active reaction sites and oxygen storage capabilities for catalytic activities.

Ceria affords a number of important applications, such as catalysts in redox reactions (Kašpar et al., 1999, 2000; Trovarelli, 2002), electrode and electrolyte materials in fuel cells, optical films, polishing materials, and gas sensors. In order to improve the performance and/or stability of ceria materials, the doped materials, solid solutions and composites based on ceria are fabricated. For example, the ceria-zirconia solid solution is used in the three way catalyst, rare earth (such as Sm, Gd, or Y) doped ceria is used in solid state fuel cells, and ceria-noble metal or ceria-metal oxide composite catalysts are used for water-gas-shift (WGS) reaction and selective CO oxidation.

The nanosciences and nanotechniques bestow new perspectives on ceria-based materials in various ways. Compared with the correspondent bulk materials, nanoceria exhibits impressive novel or enhanced

properties, such as lattice expansion and distortion, phase transformation, mixed and tunable Ce valence states, blue shift in UV–Vis spectra, and especially enhanced catalytic properties, such as redox or oxygen storage promoters in the three-way catalysts, catalysts for H₂ production from fuels, and solid state conductors for fuel cells. Pure ceria and ceria-metal oxide solid solution nanomaterials have been reviewed many times, for example, by Fernández-García *et al.* (2004). Yan *et al.* have also presented a recent feature article on the controlled synthesis and assembly of ceria-based nanomaterials (Yuan *et al.*, 2009). Although ceria nanomaterials themselves should deserve a single monograph, we attempt to cover the typical results in our short review concentrating on the synthesis routes, their properties and applications.

2.1.1 Synthesis of ceria nanostructures

In the past decade, controlled synthesis of ceria based nanomaterials, such as obtaining the pure phase, doping for desirable composition, controlling uniform size, shape, and nanostructure, tuning surfaces, fabricating composites, assemblies and mesostructures, have been the targets of active research since ceria-based materials exhibits unique properties when their sizes are reduced to nanometer scale.

In the past decade, controlled synthesis of ceria based nanomaterials has been active with lots of new developed routes. The general targets of nanomaterials synthesis, that is, to obtain the pure phase, desired composition, uniform size, shape, and nanostructure, to modify the surfaces, to fabricate the composites, assemblies, and mesostructures, are also the key points for ceria.

Pure fluorite type CeO₂ is obtained straightforwardly via solid state thermal decomposition or aqueous precipitation. In the recent years, novel synthetic routes and techniques have been applied for the synthesis of nanoceria. In this section, the synthesis through aqueous and nonaqueous solution-based methods as well as the dry and post annealing routes toward ceria nanomaterials are illustrated with examples. And the related systems as well as the simulation works providing instructive results are also discussed.

2.1.1.1 Aqueous methods and conversion methods In aqueous solutions, the Ce⁴⁺ ions would precipitate even in quite acidic solutions while the Ce³⁺ ions would precipitate as Ce(OH)₃ at much higher pH values (7–9); Ce(OH)₃ precipitate could be oxidized into ceria in air. In nonaqueous solutions, ceria forms with decomposition of appropriate precursor, with or without the oxidation by air or other oxidative species. If doping is a target, the doping ions would be introduced during the synthesis, and the coprecipitation, sol-gel, combustion/spray pyrolysis, or hydrothermal techniques are usually employed for such a task.

In one way, ceria nanocrystals could be produced directly through aqueous hydrolysis routes without post sintering processes, with either Ce(III) or Ce(IV) soluble salts as Ce sources. For conventional solution reaction, the particle sizes and shapes could be controlled by fine-tuning the experimental conditions, such as temperature, pH value, concentration, reaction time, as well as utilizing chelating agents, mineralizers, or surface-selective modifying agents. In another way, the ceria NCs could be obtained by conversion from an appropriate intermediate, such as a hydroxide, a carbonate, or an organic precursor, usually through post-heating in air.

The size and shape of ceria NCs are proven to appreciably change the chemical and physical properties; hence, their control in synthesis is one chief objective for study, and various nanoparticles, nanocubes, nanooctahedra, nanowires, and nanotubes have been obtained for this purpose. Owing to the cubic fluorite structure, ceria tends to form isometric particles, which present sphere-like morphology and are usually intermediates between the shape of cubes and octahedra. The major exposed crystal surfaces for ceria NCs are low index ones, that is, {100}, {110}, and {111}, with considerable surface relaxation and reconstructions. Figure 1 shows some typical morphologies of ceria NCs.

A great number of works on the aqueous synthesis of ceria NPs have been reported from very early years, since the ultrafine ceria powders are re-examined from the view point of nanotechnology; for example, the simple precipitation methods (Zhang et al., 2002a), the microemulsion methods (Masui et al., 1997; Zarur and Ying, 2000), urea assisted hydrothermal methods (Hirano and Inagaki, 2000; Hirano and Kato, 1999), hydrothermal methods with supercritical conditions (Adschiri et al., 2001).

It should be noted that the real ceria NPs vary from cubic and octahedral shapes. A statistical 3D model for ceria NPs was demonstrated by Kaneko et al. (2007) (Figure 2). The illustrated ceria NPs were obtained through a typical hydrothermal method with precipitation by NaOH, aging, washing, and the hydrothermal treatments with small amount of decanoic acid at 400 °C for 10 min. The obtained ceria NPs are highly crystalline and exhibit truncated cube morphology with an edge length of 4–8 nm. The 3D volume-rendered images revealed that the CeO₂ nanocrystals exposed predominantly {200} cubic facets with truncations of the corners exposing {111} facets and at the edges showing {220} facets. The ideal shape of ceria NPs are definitely an intermediate of cubes and octahedra, without spherical symmetry. The results could be compared with the molecular dynamics simulation carried out by Sayle et al. (2004) (Figure 2), where a truncated octahedra morphology is proposed.

The microwave irradiation heating methods are facile, quick, and productive for synthesis of ceria NPs. Ultrafine crystalline ceria powder

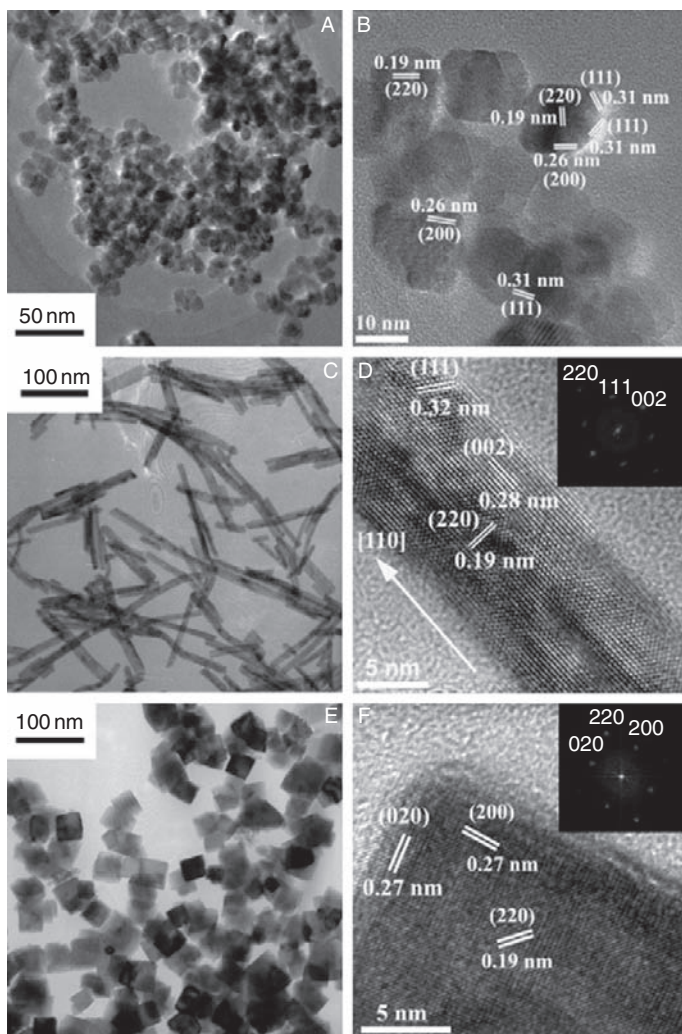


FIGURE 1 TEM (A) and HRTEM (B) images of CeO_2 nanopolyhedra. TEM (C) and HRTEM (D) images of CeO_2 nanorods, inset is a fast Fourier transform (FFT) analysis. TEM (E) and HRTEM (F) images of CeO_2 nanocubes, inset is a fast Fourier transform (FFT) analysis. Reprinted with permission from Mai *et al.* (2005). Copyright 2005 American Chemical Society.

of ca. 2 nm could be prepared under microwave irradiation by hydrolysis of $(\text{NH}_4)_2\text{Ce}(\text{NO}_3)_6$ in aqueous solution containing PEG-2000 and NaAc (Liao *et al.*, 2001). Pr doped ceria powder was synthesized through coprecipitation method, while microwave irradiation is applied to dry and

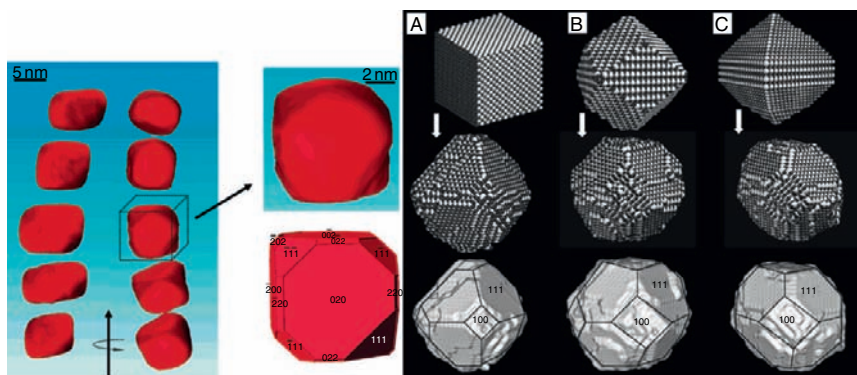


FIGURE 2 *Left part:* 3D volume rendered images indicating the presence of {111} at each corner and {220} at each edge. Reprinted with permission from Kaneko et al. (2007). Copyright 2007 American Chemical Society. *Right part:* Graphical representation of the atom positions comprising each nanoparticle in molecular dynamics. *Top, starting configurations, left to right:* (a): {100}; (b): {110}; (c): {111} and {110}; *middle, final configurations;* *bottom, final configurations with surface filling representation to aid interpretation.* Cerium is white and oxygen, black. Reprinted with permission from Sayle et al. (2004). Copyright 2004 Royal Chemical Society.

calcine the powder to efficiently improve the quality of the powder (Bondioli et al., 2001).

The small ceria NPs exhibit high trend of assembly and agglomeration, for example, in ice mold or with egg white. Karakoti et al. (2008) reported the formation of ceria nanorods during the freezing, after the aging of frozen ceria nanoparticles suspensions. Ceria nanoparticles suspensions are formed with cerium nitrate solution mixed with PEG-600 and oxidized with H_2O_2 . After having frozen in ice, the ceria nanoparticles form zigzag alignment, agglomerate, and form NRs in days and weeks. Maensiri et al. obtained the plate-like clusters of CeO_2 NPs of 6–30 nm. Cerium(III) acetate hydrate and freshly extracted egg white are mixed, dried, and calcined at 400, 500, and 600 °C before the crystallized products are obtained (Maensiri et al., 2007).

Since ceria exhibits a cubic fluorite crystal structure, the noncubic nanostructures, such as NRs, NWs, and nanoplates, are fabricated under experimental conditions that are suitable to break down the symmetry. One general way is to exploit an appropriate intermediate, such as $\text{Ce}(\text{OH})_3$ or $\text{Ce}(\text{OH})\text{CO}_3$. The rare earth hydroxide crystalline NRs/NWs/NTs are obtained in basic solutions under hydrothermal treatment, which is discussed in Section 2.3. If certain oxidant is present in the hydrothermal treatment, the ceria NCs could be obtained in a one pot manner. In this way, rod-like, wire-like, or tube-like nanoceria could be synthesized. If the hydrothermal treatment is carried out under oxygen free

conditions, the ceria hydroxide nanocrystal intermediates could be separated and converted into ceria nanocrystals with a carefully conducted post annealing. We reported the formation of ceria NRs through a facile hydrothermal route. Single crystalline ceria NRs of $10 \text{ nm} \times (50\text{--}200) \text{ nm}$ with a growth direction of [110] are obtained at 100°C with over 6 mol L^{-1} NaOH, by virtue of the temporary formation of hexagonal $\text{Ce}(\text{OH})_3$. The obtained NRs exhibited high oxygen storage capacity (OSC) compared with differently shaped NCs, which might be related to the certain shapes and exposed facets (Mai *et al.*, 2005). The growth of ceria NRs is quite a subtle procedure affected by multiple factors, such as temperature in the whole process. Du *et al.* reported that ceria nanoparticles, pearl-chain-like nanostructures, and NRs along the [211] or [110] direction form with different mixing temperatures of $\text{Ce}(\text{NO}_3)_3$ and NaOH with a short refluxing time at 100°C , respectively (Du *et al.*, 2007). With a mixing temperature of 100°C , which could be taken as the nucleation temperature, the formation of NRs is favored; with nucleation temperature of $70\text{--}90^\circ\text{C}$, the pearl-chain-like nanostructures are formed; even lower nucleation temperature lead to nanoparticles. The formation of such NRs and pearl-chain-like nanostructures is ascribed to an oriented attachment mechanism by self-organization of truncated octahedral ceria nanocrystals, sharing the {111} or {200} planes with each other. Leite *et al.* reported the microwave assisted hydrothermal treatment at 130°C to form the Gd doped ceria NRs (Godinho *et al.*, 2008). The microwave oven heat treatment drastically decreased the treatment time required to obtain the ceria NRs and obviously the oriented attachment mechanism is responsible for anisotropic growth. Han *et al.* (2005) reported the formation of ceria NWs, NTs, and NPs, by the balance of Ce(III) and Ce(IV) (see Figure 3). Ammonia is used to precipitate the ceria powders at 100°C with 3 min postheating and the precipitates were aged for a long time of 45 days. Tang *et al.* obtained $\text{Ce}(\text{OH})_3$ NTs through a standard alkali thermal process under oxygen-free conditions. Then, CeO_2 NTs are prepared by annealing the $\text{Ce}(\text{OH})_3$ NTs at 450°C under a mild controlled condition, that is, using reducing atmosphere instead of air. The temperature is raised slowly to allow the smooth structure modification during the conversion (Tang *et al.*, 2005b). Zhou and Yang *et al.* reported the synthesis of $\text{Ce}(\text{OH})_3$ NTs with large cavity and thin walls using $\text{Ce}_2(\text{SO}_4)_3$ and 10 M NaOH with hydrothermal treatment at 130°C , then the hydroxide NTs are exposed to air and finally oxidized by H_2O_2 under ultrasonication (Zhou *et al.*, 2007a). The ceria NWs could also be obtained with one pot hydrothermal treatments assisted by H_2O_2 as oxidizer (Tang *et al.*, 2005a).

The cerium hydroxyl carbonate could be obtained through hydrothermal treatments, for example the hydrothermal treatment of cerium oxalate (Li *et al.*, 1996). The most feasible way is to utilize the sealed reaction of Ce^{3+} with urea $\text{CO}(\text{NH}_2)_2$ in aqueous solution. The hydrolysis of urea in water leads to $(\text{NH}_4)_2\text{CO}_3$ and provides the base to change the

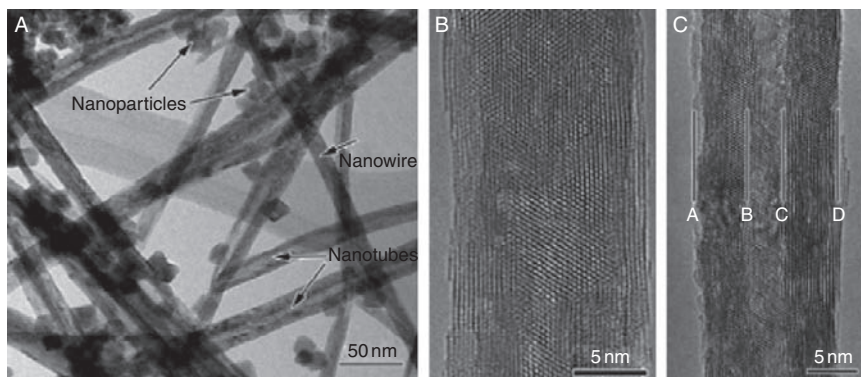


FIGURE 3 Typical morphology of the ceria samples produced by a hydrothermal route. There are three kinds of nanostructures: (A) nanoparticles, NWs, and NTs as marked in the figure. (B) High-resolution image of a NW. (C) High-resolution image of a NT. Reprinted with permission from Han et al. (2005). Copyright 2005 American Chemical Society.

pH value and give the precipitates (Wang and Lu, 2002). Then, ceria could be obtained by calcination. The spindle like orthorhombic $\text{Ce}(\text{OH})\text{CO}_3$ nanocrystals could be obtained through a hydrothermal synthesis with urea at 100°C (Lu and Wang, 2002). With higher temperature, the hexagonal $\text{Ce}(\text{OH})\text{CO}_3$ nanocrystals could be obtained, for example, flower-like NR bundles of hexagonal $\text{Ce}(\text{OH})\text{CO}_3$ are obtained at 200°C (Han et al., 2000). Micron-scale rods and plates of orthorhombic $\text{Ce}(\text{OH})\text{CO}_3$ are obtained at 160°C (Wang and Li, 2002) Yu et al. (Chen et al., 2004) reported the solvothermal synthesis of $\text{Ce}(\text{OH})\text{CO}_3$ and CeO_2 in mixed solvents of water and ethanol. Cerium nitrate hydrate and urea are used as starting materials and the heat treatment is carried out at 80°C for 1 day. The obtained products strongly depend on the composition of reaction media, and with increasing concentration of ethanol, the products change from orthorhombic $\text{Ce}(\text{OH})\text{CO}_3$ to metastable hexagonal $\text{Ce}(\text{OH})\text{CO}_3$ particles, and finally to CeO_2 particles. Du et al. reported that the uniform triangular plate-like and shuttle-like ceria nanocrystals are obtained via $\text{Ce}(\text{OH})\text{CO}_3$ intermediates assisted by CTAB or PVA hydrothermally and the intermediates are converted into ceria by calcination in air (Guo et al., 2006, 2008). Zhang et al. reported the synthesis of rhombic ceria microplates by $\text{Ce}(\text{NO}_3)_3$, urea, and CTAB in aqueous solution at room temperature (Zhang et al., 2008b). Li et al. (Sun et al., 2006a) reported the synthesis of nearly monodisperse $\text{Ce}(\text{OH})\text{CO}_3$ flower-like sphere nanosheet assemblies by a simultaneous polymerization precipitate process. The glucose, acrylamide, and ammonia are used in the reaction and a gel is obtained at pH 10 and exposed in air for hours. The

subsequent hydrothermal treatment at 180 °C yields the $\text{Ce}(\text{OH})\text{CO}_3$ products, and CeO_2 products could be obtained with postheat treatment.

Li *et al.* reported the general synthesis of a series of metal oxide hollow spheres including SnO_2 , Al_2O_3 , La_2O_3 , Y_2O_3 , Lu_2O_3 , CeO_2 , TiO_2 , ZrO_2 , and other metal oxides. Carbonaceous polysaccharide microspheres are used as templates and the metal ions are absorbed into the functional surface layer of carbonaceous saccharide microspheres and then densification and cross-linking take place in the post calcination and oxidation (Sun *et al.*, 2006b).

The surface functionalization of ceria, which is crucial for the bioapplications, could be readily done by mixing the ceria sol with surface capping agents. For example, colloidal ceria nanoparticles are obtained by hydrolysis of Ce(IV) in aqueous solution at 70 °C and mixing the sol with phosphonate-PEG solution. The well-anchored PPEG layer is sufficient to disperse the particles and expand the stability of original sol (pH 3) up to pH 9. The functionalized nanoparticles exhibit strong UV absorption capability and high redistributability (Qi *et al.*, 2008). Colloidal ceria nanoparticles stabilized by phosphonate-PEG oligomers are obtained by simply mixing the ceria NP sol and oligomer solution. The products show excellent redispersible and UV absorption properties. The complexation of laurate ligands grafted onto the surface of cerium(IV) oxide nanoparticles can be probed and quantified *in situ*, by pulsed field gradient ^1H NMR through the dependence of the diffusion coefficient on the size of the species (Ribot *et al.*, 2005). Zhang *et al.* reported the synthesis of ceria polycrystalline NRs of 5–10 nm in diameter and 50–150 nm in length via ultrasonication using polyethylene glycol (PEG) as a structure-directing agent (Zhang *et al.*, 2007a).

The addition of appropriate chelating agents has strong effects, both on the phase and on the morphology of NCs by drastically affecting the thermodynamics and kinetics of the crystal nucleation and growth process. Sub-microrods of cubic CeO_2 were selectively prepared via an EDTA-assisted route via an incomplete reaction while uniform nanoparticles were formed through a complete reaction between NaClO_3 and Ce-EDTA complexes (Chen *et al.*, 2007c).

Using $\text{Na}_3\text{PO}_4 \cdot 6\text{H}_2\text{O}$ as mineralizer in hydrothermal process at 170 °C to synthesize ceria nanocrystals leads to single-crystalline CeO_2 nanooctahedrons and NRs by temporal evolution. The added Na_3PO_4 does not leave impurity on the products. During the synthesis, the octahedral morphology of ceria forms at first. Then, the octahedra gradually disappear while the NRs form (Yan *et al.*, 2008a).

Sun *et al.* reported the polycrystalline ceria NWs synthesized using sodium bis(2-ethylhexyl) sulfosuccinate as a structure-directing agent (Sun *et al.*, 2004). The obtained CeO_2 NWs were 30–120 nm in diameters and 0.2–5 μm in lengths, consisting of 7 nm sized nanocrystallites.

The microemulsion method utilizes a water/oil/surfactant system to construct a micro reactor, in which NCs could be synthesized. The microemulsions have a wide range of applications from oil recovery to the synthesis of nanoparticles. Microemulsion is a system of water, oil, and surfactant, and it is an optically isotropic and thermodynamically stable solution. At molecular scale, the microemulsion is heterogeneous with an internal structure either of nanospherical monosized droplets (micelles or reverse micelles) or a bicontinuous phase, depending on the given temperature as well as the ratio of its constituents (Eriksson et al., 2004). The small droplets could be utilized as microreactors in order to synthesize the fine NCs in a controllable way.

Adachi et al. (Masui et al., 1997) reported a typical synthesis of ultra-fine ceria particle by a microemulsion method. The microemulsion system used in this work was composed of surfactant OP-10, cosurfactant *n*-hexyl alcohol, cyclohexane, and water. Two microemulsions containing cerium nitrate and ammonium hydroxide were directly mixed and stirred until a colloidal suspension form. The BET specific surface area of the products was between 153 and 185 m² g⁻¹, which corresponds to the particle sizes between 4.4 and 5.4 nm, assuming the particles are all spherical in shape. The water/oil ratio (R_w) has strong effect on the particle sizes, and small R_w values lead to small sizes and narrow size distribution, and vice versa. With higher cerium ion concentration, the particle size would become slightly larger. The microemulsion method of preparation can yield slightly agglomerated nanosized cubic CeO₂ with higher specific surface areas than ceria obtained via the traditional thermal decomposition method. AOT (sodium bis(2-ethylhexyl) sulfosuccinate), DDAB (di-*n*-didodecyldimethylammoniumbromide), or DDAB + Brij 35 surfactant mixtures were applied by Bumajdad et al. to form the microemulsions. The obtained NPs exhibit surface areas up to 250 m² g⁻¹ while the surface area could be retained to be several tens of m² g⁻¹ after heat treatment at 800 °C (Bumajdad et al., 2004). Well-defined polyhedral-shaped ceria nanoparticles around 3.7 nm are prepared using reverse micellar synthesis, using cerium nitrate as starting material, sodium hydroxide as precipitating agent, *n*-octane as oil phase, CTAB as surfactant, and 1-butanol as cosurfactant (Sathyamurthy et al., 2005).

2.1.1.2 Nonaqueous solution methods In addition to the aqueous methods, ceria nanocrystals could also be obtained through a number of nonaqueous solution methods, such as the solvothermal methods, ionic liquids routes, polyol routes, as well as reactions in coordinating high-boiling oil solvents.

The ceria nanocrystals could be synthesized through solvothermal routes, where a nonaqueous reaction media, such as ethanol, CCl₄, or mixed solvents, are used (Li et al., 2001; Verdon et al., 1995;

Wang *et al.*, 1996, 2002). Zhang *et al.* reported the solvothermal synthesis of ceria nanoparticles in ethanol (Zhang *et al.*, 2003a). $\text{Ce}(\text{NO}_3)_3 \cdot 6\text{H}_2\text{O}$ and $(\text{NH}_4)_2\text{Ce}(\text{NO}_3)_6$ are used as cerium source respectively with KOH or NaOH powders. The alcoholothermal treatment was performed at 180 °C to produce ceria nanocrystals. To attain full crystallization via a dissolution and recrystallization mechanism, small amount of water is required in the reactions.

The solvothermal synthesis assisted by long carbon chain acid could produce high quality nanocrystals, where the mixed solvents would be usually used. Chen *et al.* (Sun *et al.*, 2005) reported the synthesis of ceria NRs of 40–50 nm in diameter and 0.3–2 μm in length through a solvothermal method, where octadecylamine and ethylenediamine were used. Yang and coworkers reported a solvothermal route toward high quality ceria nanocubes (Yang and Gao 2006; Figure 4). Ceria nitrate aqueous solution is mixed with toluene and oleic acid, and *tert*-butylamine is used as base to give out OH^- . The solvothermal treatment is carried out at 180 °C for 24 h. Li *et al.* reported the solvothermal one-pot synthesis of monodisperse CeO_2 nanocrystals and their superlattices in ethanol–water mixed solvent mediated by oleic acid, using $(\text{NH}_4)_2\text{Ce}(\text{NO}_3)_6$ as precursor

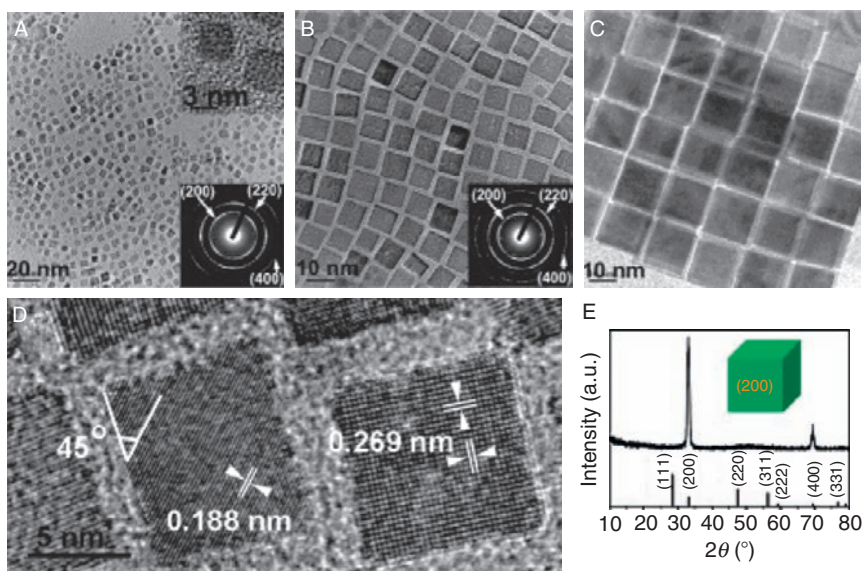


FIGURE 4 (A–C) TEM images of ceria nanocubes with the average sizes of (A) 4.43 nm, (B) 7.76 nm, and (C) 15.65 nm; the insets are SAED patterns and individual NPs. (D) HRTEM image of the ceria nanocubes. (E) A typical XRD pattern of the ceria nanocubes assembled on a Si wafer; the inset is the schematic illustration of the facets of an individual cube. Reprinted with permission from Yang and Gao (2006). Copyright 2006 American Chemical Society.

(Huo et al., 2008). The synthesis could be carried out in a gram scale and the selection of precursor is crucial for the results.

The ionic liquids could also be used in the preparation of ceria-based materials. Ionic liquids provide a good candidate as supporting surfactants for the general methodology to obtain crystalline metal oxides with mesoporous morphologies. Brezesinski et al. reported mesoporous $\text{Ce}_{0.5}\text{Zr}_{0.5}\text{O}_2$ with a distorted cubic structure which was obtained with KLE polymer $((\text{CH}_2\text{CH}_2\text{CH}_2(\text{CH})\text{CH}_2\text{CH}_3)_{79}(\text{OCH}_2\text{-CH}_2)_{89}\text{OH})$ and ionic liquid as the template (Brezesinski et al., 2005). Li et al. reported the preparation of nearly monodisperse spherical aggregates of CeO_2 nanocrystals using ionic liquid 1-hexadecyl-3-methylimidazolium bromide (C16MimBr) both as the template and solvent. The spherical aggregates exhibit average diameter of 100–150 nm and are composed of ca. 3.5 nm CeO_2 nanocrystals as building units and 3D open mesoporous structures (Li et al., 2008i; Figure 5).

The polyol method is applied to obtain a series of inorganic nanoparticles including ceria (Feldmann, 2003). Yu et al. reported the synthesis of ceria nanocrystals through a polyol method. Thermal decomposition of $(\text{NH}_4)_2\text{Ce}(\text{NO}_3)_6$ in refluxing ethylene glycol with PVP (ca. 190 °C) is carried out to produce sphere-like, rod-like, and spindle-like nanocrystals (Ho et al., 2005).

Zhou et al. reported the synthesis of flower-like ceria NPs by thermal decomposition of $(\text{NH}_4)_2\text{Ce}(\text{NO}_3)_6$ in OA/OM solvents at 230–300 °C. The small ceria nanoparticles form, assemble, and fuse mainly via (111) faces by oriented attachment. Monitoring by *in situ* electrical resistance measurements shows that the conductive species are diminished when the flower-like nanostructures form (Zhou et al., 2008a; Figure 6). Ceria nanoflowers and nanocubes are also obtained in octadecylamine, with higher temperature for nanoflower and lower temperature for nanocubes. The obtained colloidal nanoparticles can be self-assembled into nanospheres assisted by SDS surfactants (Wang et al., 2008a).

Nearly monodisperse ceria NRs can be synthesized along [100] direction by thermal decomposition of ceria–oleate complex in the presence of oleic acid at 200 °C for 2–14 days. A striking feature is that the ceria NRs are slowly and selectively shortened with time, while the diameter does not change. Adding octadecylamine to the reaction mixture leads to the growth of ceria nanodumbbells and nanospheres (Ahniyaz et al., 2008).

Gu and Soucek reported the synthesis of ceria nanoparticle in hydrocarbon solvents. Cerium–oleate complex was refluxed in high boiling point organic solvents such as octyl ether, 1-tetradecene, decalin, dipropylene glycol monomethyl ether, dipropylene glycol *n*-butyl ether, and 2,2,4-trimethyl-1,3-pentanediol monoisobutyrate, to decompose and form ceria nanocrystals. The sizes of the nanocrystals are uniform and could be

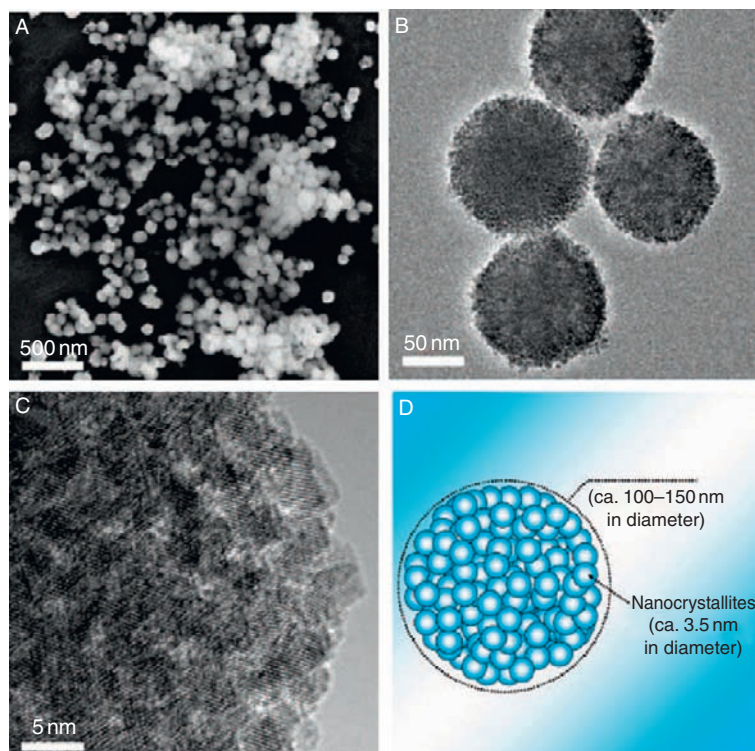


FIGURE 5 Morphology and structure of CeO_2 NCs spherical aggregates prepared with ILs. (A) SEM image. (B) TEM image. (C) HRTEM image. (D) A schematic diagram. Reprinted with the permission from Li *et al.* (2008i). Copyright 2008, American Chemical Society.

controlled from 5 to 20 nm by choice of solvent, reaction time, and reactant concentration without size sorting (Gu and Soucek, 2007).

Ceria NWs (1.2 nm in width) and tadpole-shaped nanocrystals (3.7 nm in width) are obtained by a nonhydrolytic sol-gel process in presence of diphenyl ether in a mixed high boiling solvent of oleic acid and oleylamine at 320 °C (Yu *et al.*, 2005c; Figure 7). The NWs reported by Yu *et al.* are among the thinnest ones known with a reasonable yield, showing a growth direction of [100] of the fluorite structure. Spherical ceria nanocrystals of 3.5 nm could also be obtained if oleic acid is absent from the system.

2.1.1.3 Other methods The traditional methods, such as gas condensation, sol-gel methods, precipitation with postheating methods, and mechanical milling methods are widely used for the synthesis of nanocrystalline ceria materials and ceria based catalysts (Fu *et al.*, 2001;

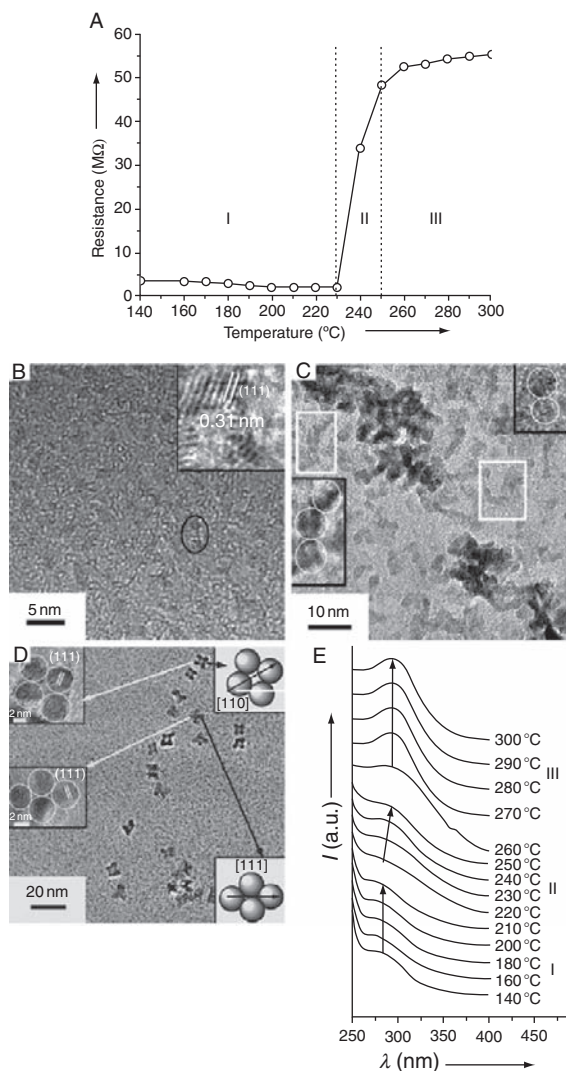


FIGURE 6 (A) Electrical resistance as a function of temperature in the synthesis of CeO₂ nanoflowers. TEM, HRTEM images (inset), and models (inset) of CeO₂ nanocrystals obtained at (B) 140, (C) 230, and (D) 240 $^{\circ}$ C. (E) Dependence of UV/Vis absorption on temperature for the synthesis of CeO₂ nanoflowers. Reprinted with permission from Zhou et al. (2008a). Copyright 2008 Wiley-VCH.

Guillou et al., 1997; Kleinlogel and Gauckler, 2000; Purohit et al., 2001; Trovarelli et al., 1997). The method by annealing of cerium hydroxides or cerium hydroxyl carbonates with special nanostructures is used to obtain ceria nanostructure, which has been discussed above.

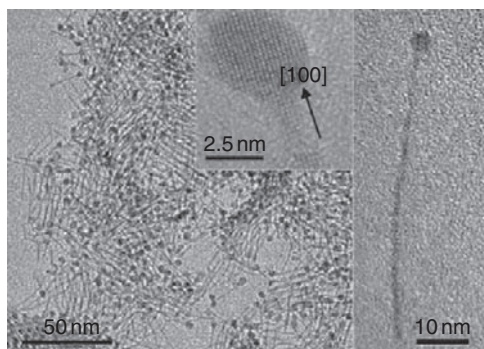


FIGURE 7 TEM images of the tadpole-shaped ceria nanocrystals. The inset is the HRTEM image of a tadpole shaped nanocrystal. Reprinted with permission from Yu *et al.* (2005c). Copyright 2005 Wiley-VCH.

There are also other newly developed dry routes toward ceria NCs. The molten salt-based methods have been used to synthesize various ceria NCs. Okuyama *et al.* reported a salt-assisted aerosol decomposition method mediated by eutectic mixture of potassium and sodium nitrates to yield ceria NPs. Spherical ceria NPs with size between 20 and 120 nm could be produced, while the conventional aerosol decomposition would produce submicron to micron sized powders (Xia *et al.*, 2001). The composite hydroxide method uses molten alkaline hydroxide composite as solvents. Ba-doped CeO₂ NWs are obtained from CeO₂ particles through a facile composite-hydroxide-mediated route utilizing the eutectic mixture of NaOH and KOH. Humidity sensors based on the Ba-doped ceria NWs were constructed (Hu *et al.*, 2006a; Zhang *et al.*, 2007e). Huang *et al.* reported highly crystallized ceria nanoparticles with mean size less than 10 nm through the composite hydroxide method and the particle size was controlled by reaction time and temperature (Huang *et al.*, 2006a).

The combustion and flame-based methods are facile to produce ceria fine powders with high specific areas. Purohit *et al.* reported a combustion synthesis using glycine and nitrate to obtain voluminous ceria ultrafine powders with a size of 2.5–12 nm and a specific surface area of 75 m² g⁻¹ (Purohit *et al.*, 2001). Pratsinis *et al.* (Madler *et al.*, 2002) reported a flame spray pyrolysis method to produce ceria NPs with high specific surface areas up to 101–240 m² g⁻¹. Cerium acetate was mixed with fuels of iso-octane/2-butanol mixture and the process was controlled by the composition of mixture as well as oxygen dispersion and liquid precursor flow rates through the flame. In a more recent attempt, a so-called nanoexplosion method was reported by Vasylykiv and Sakka, and ceria nanopowders were obtained. The nanoexplosion of C₃H₆N₆O₆ NPs breaks apart the agglomerates and allows

the formation of multicomponent ceramic nanopowders with controlled morphologies (Vasylykiv and Sakka, 2005).

2.1.1.4 Related systems It should be noted that specific properties for applications could be enhanced by using solid solutions, doped materials, and composites, instead of pure ceria. For example, ceria–zirconia solid solution is a well known ceria based material for enhanced OSC and high ionic conductivity for solid state fuel cell components. It is also used in the three way catalysts for automobile waste gas cleaning, because of the improved thermal stability, surface area, and reducibility. The synthesis, structure, and properties of ceria–zirconia have been actively studied for a long time. Di Monte and Kašpar et al. presented feature articles on the nanostructured ceria–zirconia-mixed oxides. The studies on phase, structures, as well as the microstructures are discussed and reviewed (Di Monte et al., 2004).

The aqueous methods such as precipitation and hydrothermal routes (Cabanas et al., 2000; Wright et al., 2007) have been applied to obtain gram scale microcrystalline ceria–zirconia powders. For example, Deshpande et al. (2004) synthesized $\text{Ce}_{1-x}\text{Zr}_x\text{O}_2$ nanoparticle sols ($x = 0-1$) by hydroxide coprecipitation from a mixed precursor solution of cerium ammonium nitrate and zirconyl chloride, followed with redispersion in an aqueous medium by sonication using nitric acid as the peptizing agent. Cabanas et al. (2000) reported the synthesis carried out continuously in a near-critical water flow reactor at ca. 300 °C and 25 MPa. This rapid hydrothermal coprecipitation process produces ceria–zirconia NPs with the composition determined by the initial concentrations of Ce^{4+} and Zr^{4+} ions in the starting solution. Wang and Li et al. (Liang et al., 2008) reported the synthesis of ceria–zirconia nanocages assisted by a route utilizing the Kirkendall effect. The monodisperse ceria NPs are prepared via a hydrolysis process in glycol, and a further reaction with Zr^{4+} produces the nanocages.

Ceria–zirconia is also obtained through dry methods. Stark et al. (2003) reported the pyrolysis method. Cerium and zirconium precursors dissolved in carboxylic acids were sprayed into a methane–oxygen flame and produced well-structured nanocrystals of ceria–zirconia, with high temperature stability and high surface area up to $170 \text{ m}^2 \text{ g}^{-1}$, which would decrease to $68-82 \text{ m}^2 \text{ g}^{-1}$ after sintering at 900 °C. Trovarelli et al. (1997) reported the preparation of ceria–zirconia catalysts by a room temperature high-energy mechanical milling method. The nano-phase ceria–zirconia solid solution is synthesized in a wide composition range, which is confirmed by the XRD and TPR. A strong enhancement of the redox properties of CeO_2 was observed by introduction of ZrO_2 .

Ceria–zirconia could also be synthesized through aqueous process followed by heating, such as urea assisted sol-gel method (Thammachart

et al., 2001), impregnation on Al_2O_3 (Di Monte *et al.*, 2000) or spray-freezing route. Wang *et al.* reported a spray freezing to produce homogeneous ceria–zirconia fine particles (Wang *et al.*, 2008e). A mixed aqueous solution of $\text{Ce}(\text{NO}_3)_3$ and $\text{ZrO}(\text{NO}_3)_2$ is sprayed onto a surface at liquid nitrogen temperature and a high-surface-area material with nanoscale heterogeneity consisting of Ce-rich cores surrounded by Zr rich shells will form.

Mesoporous ceria–zirconia nanostructures could be obtained through evaporation induced self assembly process (Yuan *et al.* 2007; Figure 8). Such ordered nanostructures may show promising applications in catalysis and sensors with special selectivities.

2.1.1.5 Atomistic simulation assisted synthesis and investigations The classical atomistic simulation techniques based on the pair potentials are suitable for the simulations of ceria nanoparticles even with a real sized model. Molecular dynamics studies with several thousands of ions and up to hundreds of nanoseconds in a time scale have been carried out to interpret the diffusion, and crystal growth behaviors for pure and doped-ceria nanoparticles. Traditionally, the technique has been used to explore the oxygen ionic conductivity in ionic conductors such as ceria and zirconia (Maicaneanu *et al.*, 2001; Sayle *et al.*, 2006).

Sayle *et al.* (2004) reported (Figure 2) a molecular dynamics study on the shape of ceria nanoparticles. A simulated amorphization and recrystallization of ceria NPs are carried out in order to avoid the artificial effect for selecting the initial models. Ten nanometres NP comprising 16,000 atoms become amorphous after being scaled in size and high temperature MD. The continued MD simulation leads to the recrystallization. Finally,

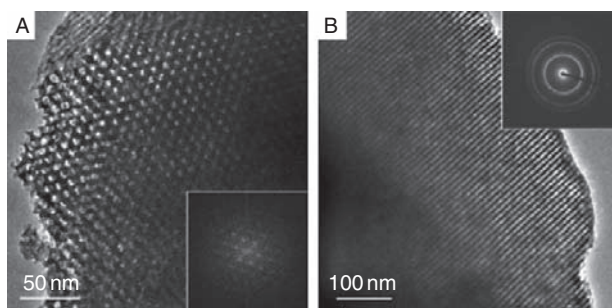


FIGURE 8 TEM images of the mesoporous $\text{Ce}_{1-x}\text{Zr}_x\text{O}_2$ ($x = 0.5$) recorded along the (A) [001] and (B) [110] orientations. The inset in (A) is the corresponding FFT (fast Fourier transform) diffraction image, and the one in (B) is the corresponding SAED pattern. Reprinted with permission from Yuan *et al.* (2007). Copyright 2007 American Chemical Society.

a ceria NP with truncated octahedral shape was obtained. The exposed surfaces are {100} and {111}, which is irrelevant to the initial configurations. The applicability of classical potentials of ceria in molecular dynamics simulation of NPs was demonstrated. Other successful application of the simulated amorphization and recrystallization method includes the simulation of partially reduced ceria NP, where a small portion of the Ce^{4+} was replaced with Ce^{3+} (Sayle et al., 2005), and Rh-doped ceria NPs (Sayle et al., 2007b).

Parker et al. reported (Martin et al., 2007) another atomistic simulation for the ceria NTs. A multilayer structure was proposed for the model and it is believed that the polycrystalline structure would stabilize the oxygen vacancies at surfaces, grain boundaries, and triple junctions, therefore, the ceria NTs would have enhanced catalytic activities.

Sayle et al. (2008) also developed (Figure 9) a route exploiting the classical atomistic simulation to make combined studies of theoretical and experimental works. A typical selected system is ceria. Since the pair potential model based on electrostatic interaction and Buckingham short range presentations are often adequate to describe the fluorite structure of ceria, Sayle et al. explored the application of such models in nano-sized particles. A series of works have been reported on the assembly behaviors of nano-building blocks into complex nanostructures, including the ceria nanoparticles self assembly in ice mold (Karakoti

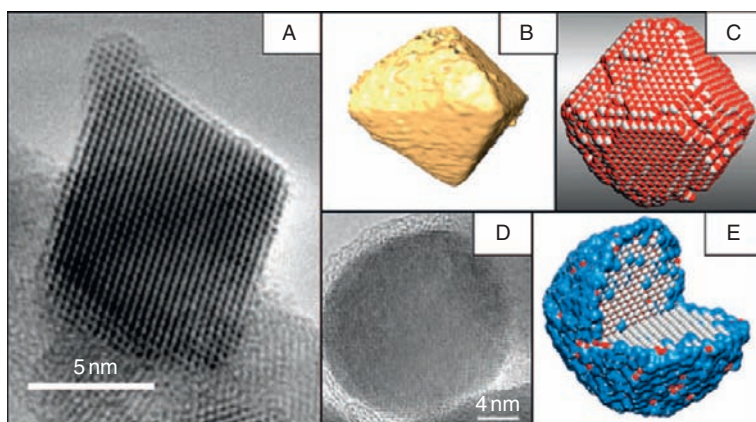


FIGURE 9 Nano building blocks: (A) HRTEM of a CeO_2 nanocrystal; (B) three-dimensional tomogramme of a CeO_2 nanocrystal generated from computer-aided tomography of sequentially oriented TEM images; (C) atomistic model of a CeO_2 nanocrystal; (D) Ti-doped CeO_2 nanocrystal showing the (amorphous) TiO_2 shell encapsulating the inner (crystalline) CeO_2 core rendering it spherical; (E) atomistic model of a Ti-doped CeO_2 nanocrystal. Reprinted with permission from Sayle et al. (2008). Copyright 2008 American Chemical Society.

et al., 2008) and the small octahedral building blocks assembly into larger ceria nanoparticles (Kuchibhatla *et al.*, 2007, 2009).

Wang and Feng (2003) reported a systematical study on the shapes of ceria nanoparticles. They suggest that ceria NPs with sizes between 3 and 10 nm favor a truncated octahedral shape defined by {100} and {111} facets, while in larger sized ceria NPs, the fast growth along <100> directions diminishes the {100} facets and leads to octahedral shapes. The ceria NPs also have tendency of forming lattice matched agglomerates as well as textured depositions through the formation of lattice matched coherent interfaces. Feng and Wang *et al.* further reported (Feng *et al.*, 2006) the large-scale synthesis of spherical shaped ceria nanocrystals based on these studies on the shape of ceria NPs. The ceria nanospheres are particularly useful in the abrasive materials to reduce the polishing defects and increase the silica removal rate for chemical-mechanical planarization of advanced integrated circuits. The doping of ceria with titanium is done using flame spray synthesis and the molecular dynamics simulation helps to understand the phenomena better. With the synthesis conditions, a molten shell of titania in liquid state would minimize the surface energy, therefore, the inner ceria core evolves in a single crystal spherical shape without faceting. Sayle *et al.* simulated CeO₂ and Ti-doped CeO₂ NRs through a “simulated synthesis” methodology. In particular, they predict that Ti doping will “smooth” the surfaces: hexagonal prism shaped CeO₂ NRs with (111) and (100) surfaces will become cylindrical (Sayle *et al.*, 2007a; see Figure 9).

2.1.2 Properties and applications

Nano sized ceria particles exhibit significant size-induced property changes compared with bulk materials, such as lattice expansion, blue shift in ultraviolet absorption spectra, Raman-allowed modes shifting and broadening, and pressure-induced phase transformation. Size induced lattice relaxation is observed by TEM and XRD in ceria nanoparticles with average sizes of 4–60 nm. The finest particles do not show strain induced line broadening while the particles with larger grain sizes by high temperature annealing might show significant strains (Zhou and Huebner, 2001). Wang *et al.* reported the pressure induced effects in nanoceria, such as phase transition and size change (Wang *et al.*, 2001b, 2004d). The phase transition was observed by *in situ* synchrotron X-ray diffraction to study size-induced compressional effect in nanocrystalline CeO₂ up to a pressure of 38 GPa. The results indicate that at a critical pressure of 20 GPa, a significant weakening of the size-induced effect occurs. Tsunekawa *et al.* (2000a) reported the electron diffraction studies on anomalous lattice expansions in monodisperse CeO_{2-x} nanoparticles. XPS results suggest that the valence reduction of Ce ions, would lead to a decrease of electrostatic force and therefore is the origin of expansion. In addition, Tsunekawa *et al.* (2000b) studied the UV absorption spectra of

monodisperse CeO_{2-x} ($0 < x < 0.5$) nanoparticles. The NPs shows blue shifts of absorption edge about 310–400 nm, which could be related to the particle sizes. They also explained the blue shift with a valence change of Ce ions. Herman et al. (Spanier et al., 2001) reported Raman spectra studies on CeO_2 NPs. The size dependent properties of ceria nanoparticles, including the Raman peak red shifting and broadening and asymmetric line shape with the smaller particle size are explained with the combined effect of strain and phonon confinement effects. The lattice constants increased with decreased particle sizes, and therefore, the Raman peaks shift to low energy direction. The line width change was explained by the inhomogeneous strain broadening with the small dispersion in particle size and by phonon confinement.

2.1.2.1 Catalysis of ceria nanomaterials In recent years, ceria and ceria-containing materials like ceria–zirconia solid solution have been under intense studies as catalysts and as structural and electronic promoters of heterogeneous catalytic reactions. Ceria exhibit very high oxygen storage/release capacity (OSC) through the conversion between Ce(IV) and Ce(III) and formation of oxygen related defects. A number of reactions could be catalyzed by ceria and ceria based catalysts (ceria/noble metal, ceria/transition metal oxides), such as the water gas shift reaction, CO selective oxidation by oxygen, catalytic combustion of volatile organic compounds, selective dehydrogenation processes, as well as the CO oxidation in automobile waste gas. Therefore, the investigation on catalysis of ceria nanomaterials is primarily about the catalytic oxidation of CO in various gas mixtures and conditions.

Fuel cells represent an attractive new power-generation technology that converts chemical energy directly into electricity with high efficiency and low pollution. The solid-oxide fuel cell (SOFC) is operated with three processes, including reduction of molecular O_2 at the cathode, diffusion of O^{2-} through an oxygen ionic electrolyte, and oxidation of fuel at the anode. Ceria has proved to be an applicable component of anode materials for the self-cleaning usage of hydrocarbon fuels with appropriate operation conditions (Murray et al., 1999; Park et al., 2000). Cerium oxide and lanthanide oxide are used to adsorb and remove H_2S in the fuel gas stream to protect the anodes from sulfurization (Flytzani-Stephanopoulos et al., 2006). Ceria or doped ceria nanomaterials could be used as the buffer layer between electrodes and electrolytes to improve ionic conductivity (Azad et al., 2005), which is related to the nanoscaled crystallite sizes (Anselmi-Tamburini et al., 2006). The nanostructured electrodes in fuel cells will provide advantageous catalytic properties related to the enhanced surface vacancy concentration and increased ionic and electronic conductivities. Though the stability of the nanostructured components under elevated operation temperature raises issues of

concern, extended stability have been shown with hundreds of cycles in fuel cell systems (Sholklipper *et al.*, 2007). In contrast to the application in the SOFCs, ceria nanomaterials show more important applications for the fuel pretreatment by the catalysis in WGS and selective CO oxidations.

Ceria/noble metal (such as Ru, Rh, and Pd) catalysts are composed of noble metal species such as nanoparticles and clusters dispersed on the ceria supports. The catalysts show typical strong metal-support interactions (SMSI) (Bernal *et al.*, 1999), that is, the catalysts exhibit a number of features for SMSI effects including: (1) reducible supports; (2) "high temperature" reduction treatments; (3) heavily disturbed chemical properties and significant changes in catalytic behavior of the dispersed metal phase; (4) reversible for recovering the conventional behavior of the supported metal phase. In these cases, the reducibility of ceria NPs is greatly enhanced by the noble metal species and the catalytic activities of the noble metals are enhanced by ceria NPs.

The water gas shift reaction (WGS , $\text{CO} + \text{H}_2\text{O} \leftrightarrow \text{H}_2 + \text{CO}_2$) is one of the critical processes to provide hydrogen for industrial applications. Ceria-noble metal composite catalysts have proved to be a competitive alternative for the traditional catalysts in low temperature water gas shift (LTS).

Flytzani-Stephanopoulos *et al.* reported a series of studies on nanostructured ceria-gold composite catalysts for LTS (Fu *et al.*, 2001, 2003a,b). The composite is made of ceria or La doped ceria NPs and gold NPs and/or ionic species. Three different preparation routes: the deposition-precipitation (Liu and Flytzani-Stephanopoulos, 1995a,b), coprecipitation, and urea-assisted gelation method (Fu *et al.*, 2001), were used. They found that with gold loading of 5–8 wt%, the composite is a very good catalyst for LTS. The TPR results showed that the addition of gold significantly increases the reducibility of the ceria surface oxygen, independent to the different preparation routes. The CO conversion profile with temperature shows that the conversion rates are affected by the loading amount of Au and the crystal size of ceria. With increased gold loading and smaller ceria size, the WGS activity was increased while the gold particle size does not have significant effect on the catalysis activity (Fu *et al.*, 2001). However, without the gold species, the activity of ceria NPs is much lower. The WGS light-off temperature of gold or copper-modified ceria samples is below 120 °C, while ceria itself is inactive below 300 °C (Fu *et al.* 2003a). As the XPS tests suggest that in the nanostructured ceria-gold catalysts, most of the gold species are metallic while there are also the ionic species. Fu *et al.* tested the significance of ionic species in the catalysis by leaching the gold metal NPs away from the ceria/gold NP composite catalyst. The results are striking in that the catalytic activity in WGS with or without gold NPs is the same, given that the ionic gold species exist. Therefore, it is suggested that the nonmetallic Au species instead of the NPs play the major role in the WGS process catalyzed by

Au–ceria catalysts (Fu et al. 2003b). Since only the nonmetallic gold species would have strong effect on the reaction, much lower content of the gold could be used in this catalyst for economical reasons. The low gold content catalyst is free of metallic gold NPs while exhibiting high catalytic activity (Fu et al., 2005; Figure 10).

The known WGS catalysts based on ceria or copper oxide both suffer greatly from the deactivation with time-on-stream and/or in shut-down/restart operation. The mechanism of such deactivation was ascribed to the

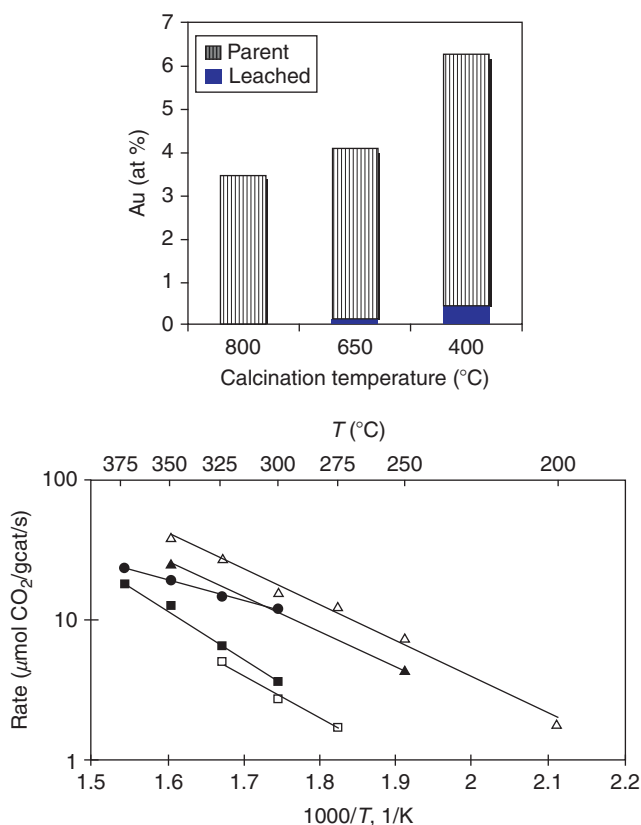


FIGURE 10 The composition and activity in WGS of low content gold–ceria catalysts. *Upper part*: the gold amount before and after leaching with different calcination temperature. *Lower part*: steady-state WGS reaction rates. *Solid triangles*: 4.7Au–10%La doped ceria (deposition–precipitation); *open triangles*: leached 0.44Au–10%La doped ceria (deposition–precipitation, NaCN); Other reference catalysts are also shown: *solid circles*: 0.62Au–TiO₂ (deposition–precipitation), *solid squares*: 2.02Au–Fe₂O₃ (coprecipitation), *open squares*: leached 0.73Au–Fe₂O₃ (coprecipitation, NaCN). Reprinted with permission from Fu et al. (2005). Copyright 2004 Elsevier.

blockage of the active sites by carbonates and/or formates formed during the WGS reaction or overreduction of ceria. Flytzani-Stephanopoulos *et al.* studied the deactivation of ceria–gold or ceria–platinum composite catalysts in a practical fuel cell (Deng and Flytzani-Stephanopoulos, 2006). The formation of cerium (III) hydroxycarbonate in the ceria–gold catalysts is identified during the shutdown process. Therefore, the addition of a small amount of gaseous oxygen to the reaction gas mixture is proposed as a solution. In this way, both Au–ceria and Pt–ceria catalysts showed remarkable stability in the WGS reaction in the full fuel–gas mixture at various temperatures and in a cyclic shut-down/start-up operation.

The selective oxidation or preferential oxidation of CO in hydrogen-rich stream is another important object for ceria based catalysts. The gas mixture from steam reforming/partial oxidation of alcohols or hydrocarbons, followed by the WGS reaction contains mainly H₂, CO₂ and a small portion of CO, H₂O, and N₂. When such gaseous stream would be taken as input for hydrogen fuel cells, the CO has to be removed to avoid poisoning of the anode electrocatalysts. Ceria based nanomaterials, such as ceria/gold, ceria/copper oxide catalysts exhibit suitable catalytic activities and selectivities for CO PROX process.

Corma *et al.* reported that the activity of gold on nanocrystalline CeO₂ for CO oxidation is increased by 2 orders of magnitude with respect to a conventionally precipitated CeO₂ support. The characteristics of the cerium oxide surface are extremely important in determining whether a CeO₂-supported gold catalyst is active or not for CO oxidation (Carrettin *et al.*, 2004). Corma *et al.* carried out time resolved spectroscopy studies on the working catalysts of gold nanocluster/ nanocrystalline ceria (Guzman *et al.*, 2005). The CO-TPR, XPS and *in situ* Raman and IR spectra proved that nanocrystalline CeO₂ supplies reactive oxygen in the form of surface superoxide species and peroxide species at the one-electron defect site to the supported active species of gold for the oxidation of CO. The reactive oxygen species are not formed on conventionally prepared CeO₂ and the presence of the gold enhances the formation the reactive oxygen species on nanocrystalline ceria. In addition, Corma *et al.* reported that the nanocrystalline CeO₂ and Y₂O₃ could stabilize the Au(III) species on the surface and that the catalytic activity of CO oxidation is proportional to the concentration of these Au(III) surface species (Carrettin *et al.*, 2005).

Nanocrystalline CuO–CeO₂ catalysts show nearly ideal selectivity and promising activity for the removal of CO from reformed fuels by selective oxidation (Avgouropoulos and Ioannides, 2003). The ultrafine nanocrystalline CuO–CeO₂ catalysts were made by a urea–nitrate combustion method. CuO–CeO₂ catalysts are inactive for H₂ oxidation at temperatures up to ca. 120 °C and CO does not influence the rate of hydrogen oxidation. The addition of small amount of H₂O shows adverse influence

of CO oxidation. The catalysts also showed stable activity in long-term experiments with the realistic feeds. Hočevár et al. reported the study on the kinetics of CO selective oxidation in excess hydrogen over a nanostructured $\text{Cu}_{0.1}\text{Ce}_{0.9}\text{O}_{2-y}$ catalyst prepared by a sol-gel method (Sedmak et al., 2003). A steady state Mars and van Krevelen kinetic model is proposed for the reaction, and kinetic parameters of the reaction were found to be as follows: apparent activation energy for CO oxidation step, 57.2 kJ mol^{-1} , and for the catalyst reoxidation step, 60.2 kJ mol^{-1} . Ratnasamy et al. (2004) reported the $\text{CuO-CeO}_2\text{-ZrO}_2$ nanocrystalline catalysts made by a coprecipitation method for the CO selective oxidation. The composition of the support markedly influenced the PROX activity. Meanwhile, both CuO-CeO_2 and $\text{CuO-CeO}_2\text{-ZrO}_2$ catalysts exhibited higher activity and selectivity in CO oxidation than CuO-ZrO_2 .

Nanoparticulated gold supported by nanocrystalline or mesostructured nanocrystalline ceria catalysts represents an alternative to catalysts for selective aerobic oxidation of aliphatic and aromatic aldehydes which is much better than the gold supported by the precipitated ceria (Corma and Domine, 2005). The ceria or yttria supported Au are also active and extremely selective for the homocoupling of arylboronic acids, and the activity is directly correlated with Au(III) (Carrettin et al., 2005).

Mononuclear Au(III) species supported on ceria powder (averaged 46 nm) is catalytically active for CO oxidation, and would aggregate into gold clusters with even increased catalytic properties, proved by X-ray adsorption study (Aguilar-Guerrero and Gates, 2007).

Other oxidation/reduction related reactions are also explored with ceria based catalysts. For example, Murugan and Ramaswamy (2007) reported the oxidative dehydrogenation of ethylbenzene on nanocrystalline ceria using N_2O as the oxidant; Concepcion et al. (2004) reported the chemoselective hydrogenation of crotonaldehyde catalyzed by Pt on mesostructured CeO_2 NPs embedded within layers of SiO_2 binder.

In addition to the selective oxidation, the complete oxidation and catalytic combustion processes are also important topics in catalytic fields.

The air pollutants of volatile organic compounds emitted from many industrial processes and transportation activities could be abated by catalytic combustion processes. Scirè et al. reported the catalytic combustion of 2-propanol, methanol, and toluene on ceria-gold catalysts. The catalysts were prepared with coprecipitation and deposition-precipitation methods. The gold significantly enhanced the catalytic activity of ceria for the oxidation of these volatile organic compounds. The supposed reason is that the gold NPs weakened the mobility/reactivity of surface lattice oxygen (Scirè et al., 2003).

Since the advent of three way catalysts (TWCs) for vehicle waste gas treatment in the 1980s, the demand for pollutant removing has been on the rise. The TWCs remove the pollutants by converting the nitrogen oxides,

carbon monoxide, as well as unburnt hydrocarbons into harmless H_2O , CO_2 , and N_2 simultaneously. When, the air to fuel ratios equal to the stoichiometric conditions, the TWCs would perform most efficiently, and the deviations from the ideal ratios severely decrease the efficiency of TWCs. The addition of CeO_2 could limit this disadvantage by acting as an oxygen buffer by storing/releasing O_2 with $\text{Ce}^{4+}/\text{Ce}^{3+}$ redox couple (Kašpar *et al.*, 1999).

The defective structure in nanocrystalline ceria based catalysts proved to have strong effect on the OSC. Mamontov *et al.* (2000) reported the neutron diffraction studies of the atomic structures of nanocrystalline powder of ceria and ceria–zirconia solid solution. They found that the concentration of vacancy-interstitial oxygen defects has a direct correlation with the OSC. This effect is stronger than the correlation of surface area with OSC. Zirconia reduces ceria and preserves oxygen defects to retard the degradation of ceria–zirconia in OSC. Yan *et al.* observed the strong correlation between OSC and the lattice strain in nanosized ceria–zirconia, which could be measured via XRD (Si *et al.*, 2004; Figure 11).

In addition to the size effect of ceria nanomaterials on the catalytic activities, the exposed specific crystal facets of various ceria nanocrystals also play a role (Mai *et al.*, 2005; Si and Flytzani-Stephanopoulos, 2008; Zhou *et al.*, 2005; Figure 12). The OSC of CeO_2 nanopolyhedra, NRs, and nanocubes are compared with bulk materials, and the {100}/{110}-dominated structures are more reactive for CO oxidation than the {111}-dominated one (Mai *et al.*, 2005). Gold supported by ceria catalyst active for water–gas shift reaction shows dependence on the various exposed facets of nanoceria related to the shape of ceria nanocrystals (Si and Flytzani-Stephanopoulos, 2008). Rodriguez *et al.* investigated the WGS reaction of Cu and Au NPs supported on CeO_2 (111) and ZnO (000-1) surfaces experimentally and theoretically. Au/ CeO_2 (111) was an excellent catalyst with activity similar to that of Cu/ CeO_2 (111). The most difficult step in this WGS reaction is the dissociation of H_2O which could be realized when the O vacancy exists on ceria (111) surface. The metal NPs facilitate the partial reduction of ceria by CO and help to form the O vacancies, illustrating a cooperative effect (Liu and Rodriguez, 2007).

Corma *et al.* (Abad *et al.*, 2006) reported chemoselectivity exhibited by the gold NPs supported by nanocrystalline ceria for the aerobic oxidation of allylic alcohols. Pd NPs and Au/Pd core shell NPs are also examined and the Au NPs are more active and chemoselective for both solvent free and in organic media situations. The results show that the gold/ceria system is a general and reusable catalyst for the oxidation of allylic alcohols without solvent or in organic media. The catalytic activity in toluene correlates linearly with the total number of external gold atoms, and with the surface coverage of the supporting ceria nanostructures (Abad *et al.*, 2008).

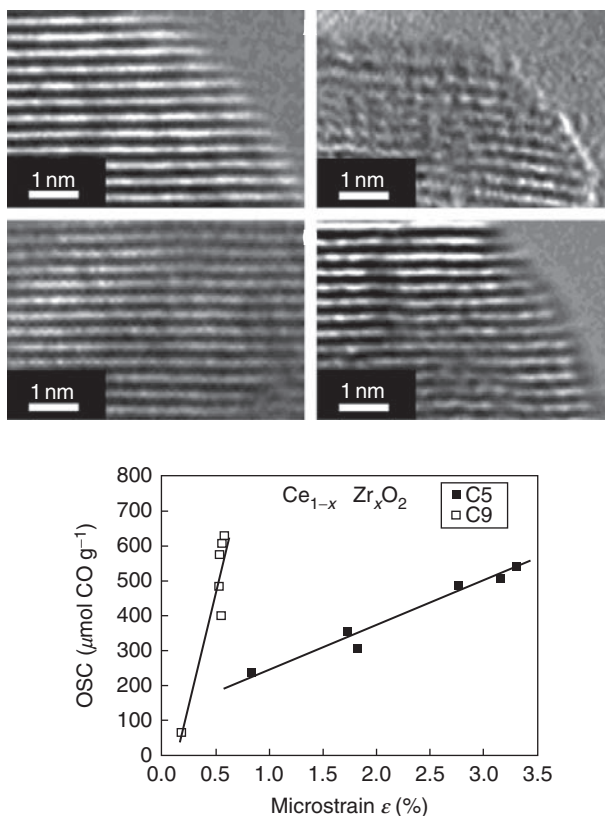


FIGURE 11 HRTEM images of the $\text{Ce}_{1-x}\text{Zr}_x\text{O}_2$ samples: (A) $x = 0$, calcined at 773 K; (B) $x = 0.5$, calcined at 773 K; (C) $x = 0$, calcined at 1173 K; (D) $x = 0.5$, calcined at 1173 K. Right: CO-OSC values of the $\text{Ce}_{1-x}\text{Zr}_x\text{O}_2$ ($x = 0-0.8$) catalysts as a function of the microstrain in the crystal lattice. Reprinted with permission from Si et al. (2004). Copyright 2004 American Chemical Society.

2.1.2.2 Sensors The ceria NPs could also be used in biosensors as well as the gas sensors. The redox catalytic activity and the semiconductivity of ceria allow it to be used as gas sensors for the reductive and oxidative gases such as CO, NO_2 , O_2 , and alcohols by the resistivity or cataluminescence measurements. The noble metals or metal oxides which could activate the catalytic process of ceria could also help to increase the sensitivity of ceria for gas sensing.

Barreca et al. reported the preparation of columnar CeO_2 nanostructures on Si(100) and Al_2O_3 substrates by a catalyst-free CVD process at 623–723 K (Barreca et al., 2006, 2007). $\text{Ce}(\text{hfa})_3 \cdot \text{diglyme}$ (hfa = 1,1,1,5,5,5-hexafluoro-2,4-pentanedione; diglyme = bis(2-methoxyethyl)ether) is used as the cerium molecular source. The obtained CeO_2 columnar

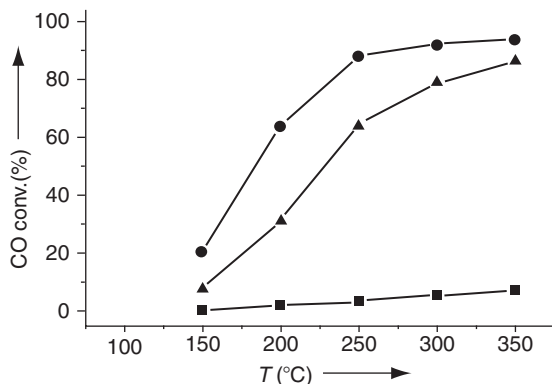


FIGURE 12 WGS reaction “light-off” profiles for 1% Au on CeO₂ nanorods (●), cubes (■), and polyhedra (▲). Reprinted with permission from Si and Flytzani-Stephanopoulos (2008). Copyright 2008 Wiley-VCH.

nanostructures exhibited higher sensitivity in the detection of gaseous ethanol and NO₂ compared with the continuous CeO₂ thin films. Liao *et al.* demonstrated a single NW gas sensor based on the ceria NW (Mai *et al.*, 2005) deposited with Pt NPs. The nanodevice exhibited high selectivity in detecting CO over other reductive gases, such as H₂, H₂S, ethanol, and gasoline (Liao *et al.*, 2008; Figure 13).

Xu *et al.* reported the cataluminescence and catalysis studies of ethanol on nanosized Ce_{1-x}Zr_xO₂ materials. The ceria-rich solid solutions ($x = 0.05\text{--}0.25$) showed high cataluminescence activity at 220 °C and were supposed to be efficient low temperature CTL sensors for ethanol (Ye *et al.*, 2006). Lv *et al.* (Xuan *et al.*, 2009) reported the cataluminescence studies of CS₂ on ceria NRs, nanocubes, and nanospheres. The chemiluminescence is used as a sensitive gas sensor for the determination of CS₂ and a high selectivity over a number of organic gases was demonstrated.

Ansari *et al.* (2008) reported a nanostructured ceria film immobilizing glucose oxidase (GOx) deposited on Au electrode for glucose sensor fabricated by a sol-gel method. Glucose biosensor with its importance for monitoring blood glucose for treatment of both diabetics and nondiabetics could be fabricated through immobilization of glucose oxidase. CeO₂ is known to have a wide band gap of 3.4 eV, high isoelectric point of 9.0, which is an advantage for immobilization of low isoelectric point enzyme such as glucose oxidase (GOx, isoelectric point 4.2) via electrostatic interactions, and good retention of biological activity for protein binding. This nanostructured GOx/CeO₂/Au bioelectrode exhibits sensitivity of 0.00287 μA mg dL⁻¹ cm². Gupta *et al.* (Saha *et al.*, 2009) also reported a glucose sensor of PLD deposited ceria nanoporous thin films on Pt coated glass plate immobilized with glucose oxidase.

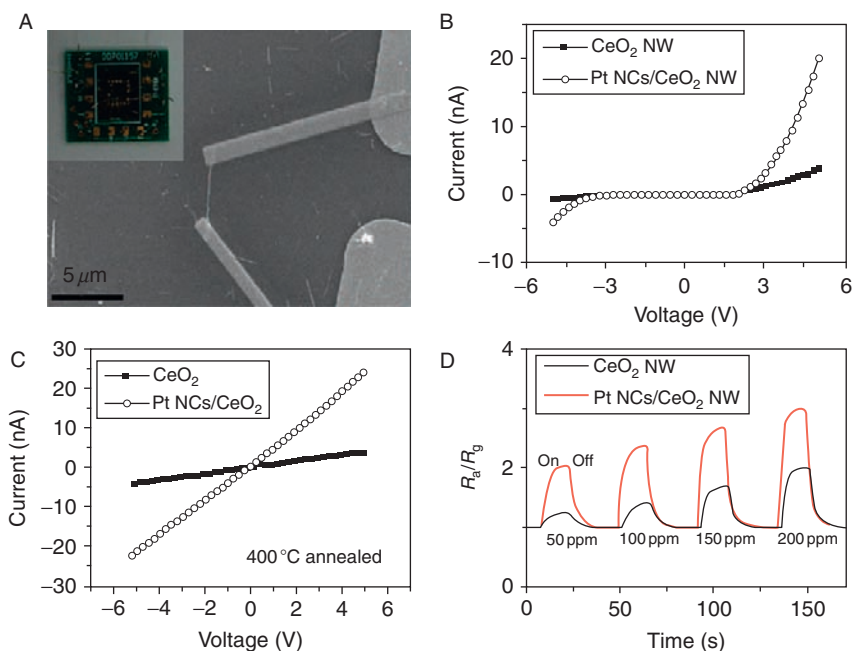
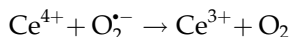
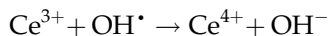
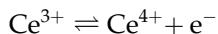


FIGURE 13 (A) SEM image of a single CeO_2 NW gas sensor, inset showing an optical image of the NW sensor chip; I - V curves of a single CeO_2 NW and a single Pt NC/ CeO_2 NW before (B) and after annealing at 400°C for 1 h (C). (D) The gas sensibility response curves of a single CeO_2 NW and a single Pt NCs/ CeO_2 NW, after being annealed, for different CO concentrations. Reprinted with permission from Liao et al. (2008). Copyright 2008 American Chemical Society.

Zhang et al. reported a nanocomposite membrane of shuttle shaped ceria nanocrystals (Guo et al., 2008), SWNTs, and ILs1-butyl-3-methylimidazolium hexafluorophosphate (BMIMPF_6), which was incorporated on the glassy carbon electrode for electrochemical sensing of the immobilization and hybridization of DNA (Zhang et al., 2009). The electron transfer resistance (R_{et}) of the electrode surface increased after the immobilization of probe ssDNA on the CeO_2 -SWNTs- BMIMPF_6 membrane and rose further after the hybridization of the probe ssDNA with its complementary sequence.

2.1.2.2 Toward bioapplications Since cerium occurs in both trivalent (+3) state and tetravalent (+4) state, it may switch between these two states in a redox reaction in ceria to make excellent oxygen buffers. Therefore, ceria NPs with increased surface area and oxygen vacancies exhibit excellent catalytic activities. In biological systems, reports indicated that ceria NPs

show potent free-radical scavenger behaviors with neuroprotective, radio protective, and anti-inflammatory properties (Chen *et al.*, 2006a).



Tarnuzzer *et al.* (2005) reported the vacancy engineered ceria nanostructures for protection from radiation-induced cellular damage. The applied ceria NPs provided almost 99% protection from radiation-induced cell death for normal cell, whereas the same concentration showed almost no protection of tumor cells MCF-7. The photoreceptor cells are exposed to lights and show high rate of oxygen metabolism. These cells are exposed to continuous elevated levels of toxic reactive oxygen intermediates. Although the causes of retinal diseases resulting in loss of vision are complex, oxygen radicals that damage the sensitive cells in the retina are thought to play a central role. Chen *et al.* reported the *in vivo* studies of vacancy-engineered mixed-valence-state cerium oxide NPs scavenging these reactive oxygen intermediates to prevent degenerative retinal disorders in rats (Chen *et al.*, 2006a; Figure 14). Therefore, ceria NPs may be used to treat problems that cause blindness. Niu *et al.* (2007) show the ceria NPs could protect cells *in vivo* in mice from lethal endoplasmic reticulum stress. The effect of ceria NPs on cardiac function is also assessed.

Korsvik *et al.* reported ceria NPs used as catalysts mimicking superoxide dismutase (SOD) (Korsvik *et al.*, 2007). The polycrystalline 3–5 nm sized ceria NPs show excellent catalytic rate constant even exceeding that of enzyme SOD. The mechanism should be further elucidated.

Perez *et al.* reported the bio-active monodisperse, water-soluble, and highly crystalline dextran-coated ceria NPs with pH dependent antioxidant activity, which are made through room temperature hydrolysis in ammonia aqueous solution in the presence of dextran T-10 (Perez *et al.*, 2008). The obtained water soluble NPs contained a ratio of $\text{Ce}^{4+}/\text{Ce}^{3+}$ approximately 3/2, which became 2/3 after adding some H_2O_2 . Later, the NPs could regenerate the original ratio 10 days under pH 7.4 while there is no regeneration under pH 4.

2.1.2.3 Optical applications Ceria also exhibits optical properties suitable for potential applications. Ceria is a transparent oxide in the visible and near-IR spectral region. Thin films of ceria exhibit high refractive index, and dc dielectric constant, being suitable for applications in optical,

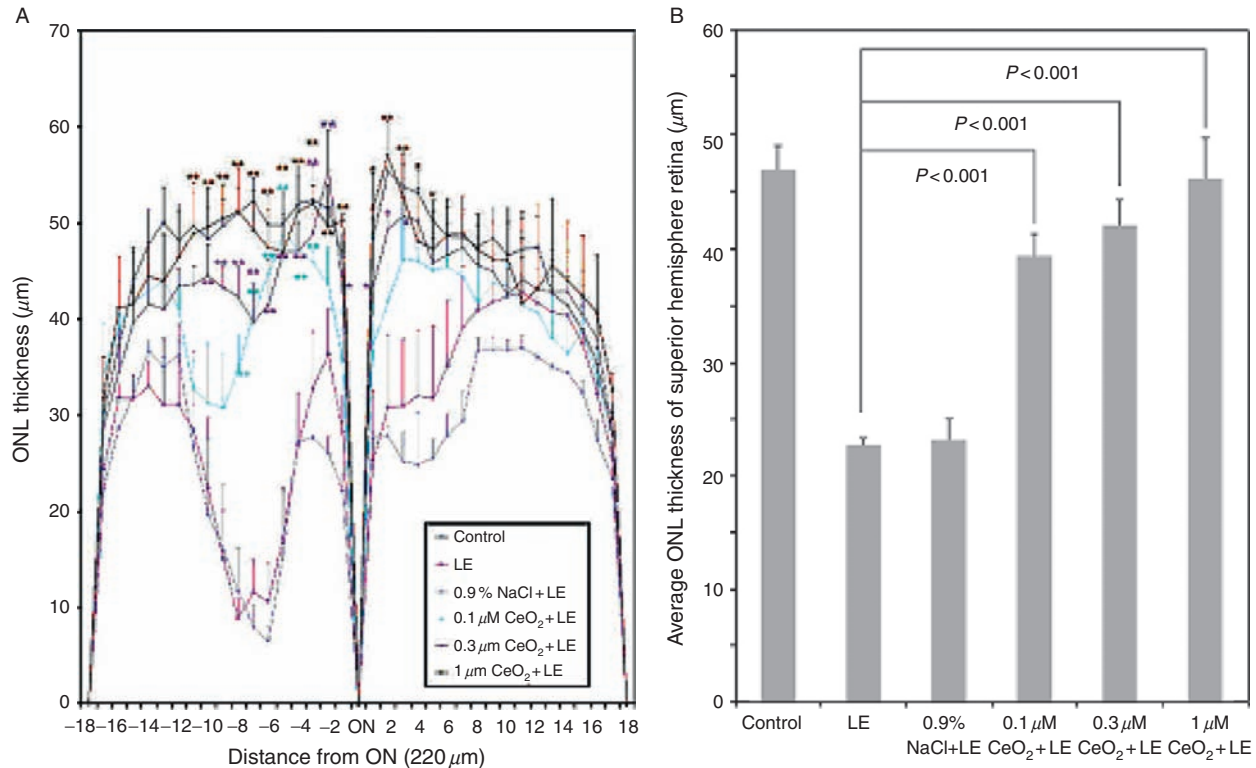


FIGURE 14 Nanoceria particles provide pan-retinal protection against light damage. The thickness of the ONL of the retina was measured along the vertical meridian every 220 mm, starting at the optic nerve. Reprinted with permission from Chen et al. (2006a). Copyright 2006 Nature Publishing Group.

electro-optical, microelectronic, and optoelectronic devices. Patsalas *et al.* reported the electron beam evaporation (EBE) growth of nanocrystalline ceria films, and measured the optical properties and the energy gap and the refractive index that can be tailored by varying the substrate temperature or using Ar^+ ion beams (Patsalas *et al.*, 2002).

Ceria only exhibits weak luminescence; therefore, doping with rare earths such as Eu^{3+} can enhance the visible emission required for imaging. Babu *et al.* reported the Eu^{3+} doped 10 nm ceria NPs synthesized by room temperature chemical precipitation and post annealing at 500 and 900 °C (Babu *et al.*, 2008). A fraction of Ce^{3+} exists in the ceria NPs, and it decreases after annealing. Emission intensity varies with the wavelength of excitation and observed transitions indicate the presence of Eu^{3+} in different symmetry environments.

Waterhouse *et al.* reported the inverse opal ceria photonic crystal films prepared through a colloidal template sol-gel procedure with PMMA spheres (Waterhouse *et al.*, 2008; Waterhouse and Waterland, 2007; Figure 15). The obtained films exhibited 3D ordered macroporous structures and a photonic band gap in the visible region. Filling the macropores of the CeO_2 inverse opal with solvent caused a red-shift in the position of the photonic band gap, with the magnitude of the shift being directly proportional to the refractive index of the solvent. Refractive index sensing with a sensitivity of $n = 0.001$ or better is achievable using inverse opal CeO_2 thin films.

Ceria is used as UV-shielding materials for cosmetics. CeO_2 has a charge transfer band gap of 3.2 eV, which is at the border between UV and visible range similar to the bandgap of ZnO (3.4 eV) or TiO_2 (3.1–3.25 eV). Because of the high refractive index of ceria in the visible range (2.05 eV), ceria is quite transparent to visible light, but has excellent

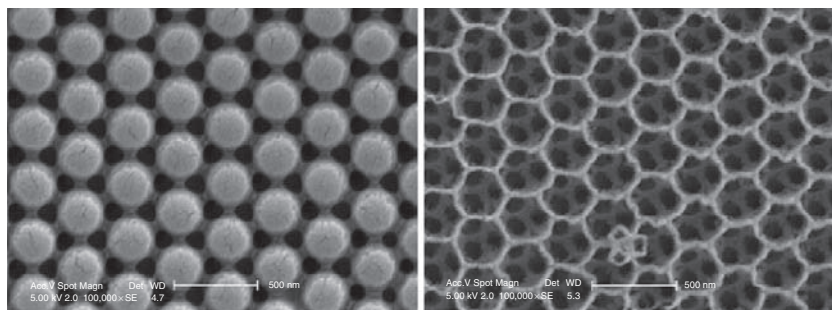


FIGURE 15 (A) SEM image of PMMA opal photonic crystal; (B) SEM image of ceria inverted opal photonic crystal made from the PMMA template. Reprinted with permission from Waterhouse and Waterland (2007). Copyright 2008 American Chemical Society.

ultraviolet absorption ability, and appears natural on the skin without imparting an excessively pale white look. However, the photocatalytic activity of ceria, which facilitates the generation of reactive oxygen species and raises safety concerns, must be suppressed for such applications. The activity can be reduced in various ways, such as doping ceria with calcium, making the ceria into NPs, as well as coating the ceria NPs with silica shells (El-Toni et al., 2005, 2006; Yabe and Sato, 2003).

2.1.3 Remarks

Ceria-based nanomaterials have been developed successfully during the last decade. A large variety of synthesis methods have been developed for the synthesis of ceria nanocrystals. The synthesis of high quality nanocrystals with controlled particle sizes, shapes, advanced nanostructures, as well as the doping, composition, and surface status have been well investigated. The simulation techniques utilizing both the classical atomistic methods and the first principle calculations based on the density functional theory methods have also shown efficiency in understanding a range of phenomena in ceria based nanomaterials.

2.2 R_2O_3

Rare earth oxides provided the materials for luminescent phosphors. R_2O_3 have three phases at ambient conditions: the hexagonal phase (A phase), monoclinic phase (B phase), and cubic phase (C phase). The most stable phase for each rare earth elements changes along with the cationic radii, where the hexagonal phase is most stable for larger ions, the cubic phase is most stable for smaller ions, and the monoclinic phase is most stable for some medium ones.

2.2.1 Synthesis

The synthesis of R_2O_3 nanocrystals has been extensively studied. The dry methods and gel based routes, like the gas phase condensation, combustion method, sol-gel method, and coprecipitation method mainly lead to NPs with relatively wide size distribution. The newly developed hydrothermal methods usually produce an intermediate such as hydroxide, which could be converted into R_2O_3 through postheating. The precipitation from high-boiling solvents, including OA, TOPO and poly alcohols would directly produce rare earth oxide nanocrystals from solution and might produce monodisperse high quality nanocrystals. The obtained rare earth oxide nanocrystals might exhibit varied phase, size, shape, surface status, and therefore lead to varied luminescence properties.

2.2.1.1 Dry methods and postcalcination methods The industrial micron sized R_2O_3 powder is commonly made by thermal pyrolysis of rare earth carbonates or oxalates at a temperature of 600–1000 °C. The dry methods usually result in fine powders with a relatively wide size distribution. After the sintering, the surface OH^- and other solvent related species are generally removed, therefore, the powder may exhibit better luminescence efficiency and longer decay time. Nano-sized rare earth oxide products could be obtained from finely selected precursors like hydroxides gels, premade nanostructures, through heat treatment, spray pyrolysis, combustion, and sol-gel processes.

The laser ablation or laser-heated gas phase condensation process could produce NPs less than 50 nm with broad-size distributions. For example, Eilers and Tissue reported that the Eu_2O_3 NPs could be made by a laser-heated gas phase condensation process. The particles are polydisperse in a range of 2–30 nm (Eilers and Tissue, 1995).

The combustion technique, such as the solution combustion, spray pyrolysis, flame pyrolysis, utilizes the high temperature of burning process to quickly decompose the precursor and crystallize the fine powders. Usually, large quantities of highly porous or fine particles are produced, varied composition and doping are achieved, and the volatile quenching impurities are removed. However, the particles also exhibit a wide size distribution which might be partially alleviated by size selection process. The spray pyrolysis could be used to fabricate luminescent Y_2O_3 films (Hao *et al.*, 2001), and the flame spray pyrolysis could be used to obtain $Y_2O_3:Eu$, Gd_2O_3 and $Gd_2O_3:Eu$ NPs with a designed burner (Dosev *et al.*, 2006; Goldys *et al.*, 2006).

In contrast to the dry methods, there are other conventional methods related to post heat treatment from precipitates from the aqueous solutions. The ambient aqueous routes and the hydrothermal methods at elevated temperature usually lead to rare earth precipitates like hydroxides, carbonates, instead of oxides. In fact, the hydrothermal treatment of rare earth oxide powders results in a hydration process to form hydroxides. Subsequently, the precursor could be used to produce rare earth oxide nanocrystals with post annealing at varied temperatures and in appropriate atmosphere.

The sol-gel methods are also widely applied to obtain the rare earth oxide NPs, for example, $Y_2O_3:Tb$ (Goldburt *et al.*, 1997), $Y_2O_3:Eu$ (Dhanaraj *et al.*, 2001). Additional techniques like freeze drying or so called sol-lyophilization are also used to obtain good quality and uniform NPs, like $Gd_2O_3:Eu$ (Louis *et al.*, 2003). The sol-gel method could be well combined with hard templates to obtain complex nanostructures, such as Eu_2O_3 nanotubes from AAO templates. (Wu *et al.*, 2004). The urea assisted coprecipitation methods could also produce nanocrystalline luminescent Y_2O_3 nanocrystals (Cress *et al.*, 2008; Wakefield *et al.*, 2001).

The conversion from rare earth hydroxide nanocrystals would be discussed in Section 2.4 for rare earth hydroxide nanomaterials. In this way, the rare earth oxide nanowires, nanorods, nanotubes could be obtained (Fang et al., 2003b; Hu et al., 2007; Wang and Li, 2003a; Yada et al., 2002). The recent examples include the preparation of $Y_2O_3:Tb$ hollow spheres in supercritical solvothermal processes using water and ethanol mixed solvents (Devaraju et al., 2009), and $3\ \mu m$ $Y_2O_3:Eu$ spheres obtained by a route assisted by sodium acetate (Yang et al., 2007a).

In addition to the hydroxides, the hydroxyl carbonates could be used as intermediates before calcination is carried out. The urea mediated hydrothermal methods could well lead to the production of these nanostructures of rare earth hydroxyl carbonates. Recent examples include the $Y_2O_3:Eu$ hollow spheres (Jia et al., 2009).

The formation of rare earth organic-inorganic hybrid nanostructure could be realized via nonaqueous or aqueous solution based methods. Later, the products could be converted into rare earth oxides by calcination in air. The nanostructures could be partially or mostly preserved.

Yada et al. reported the synthesis of rare earth oxide nanotubes templated by SDS, where the precursors obtained in solution are probably hydroxides or hydroxycarbonates, which could be converted into rare earth oxides after calcination (see Figure 16; Yada et al., 2002, 2004).

Pinna et al. (Karmaoui et al., 2006, 2007; Pinna, 2007; Pinna et al., 2005) reported a series of works on the nonaqueous synthesis of yttria mesostructures (Figure 17). The synthesis procedures were performed water-free and oxygen-free in a glovebox. Yttrium isopropoxide ($Y_5O(OC_3H_7)_{13}$) or mixture of yttrium isopropoxide and anhydrous $Eu(III)$ chloride was added to anhydrous benzyl alcohol, 4-*tert*-butyl benzyl alcohol, or 4-biphenylmethanol. The heat treatment was performed at 250–300 °C for 2 days. The products were centrifuged, washed, and dried. Yttria was obtained through calcinations in air at 550 °C. A highly ordered lamellar nanocomposite consisting of yttria layers with thickness of about 0.6 nm, separated by organic layers of intercalated benzoate or biphenolate molecules depending on the solvents used, respectively. For the benzoates, two organic reactions were observed; a C–C bond formation occurred between benzyl alcohol and the isopropanolate ligand and yttrium oxide catalyzed hydride-transfer reactions to form benzoic acid and toluene from benzyl alcohol via benzaldehyde. Chen et al. reported a method based on the lanthanide coordination polymer foams (Shen et al., 2008b). By a facile hydrothermal route, lanthanide salt was added to *L*-asparagine aqueous solution and heated at 160 °C. The obtained monolith could be converted into rare earth oxide by calcination in air. Another work from the same group reports the synthesis of rare earth oxide microspheres and hollow spheres by thermolysis of rare earth coordination compounds also by a hydrothermal reaction with lanthanide ions and asparagines (Shen et al., 2009; Figure 18).

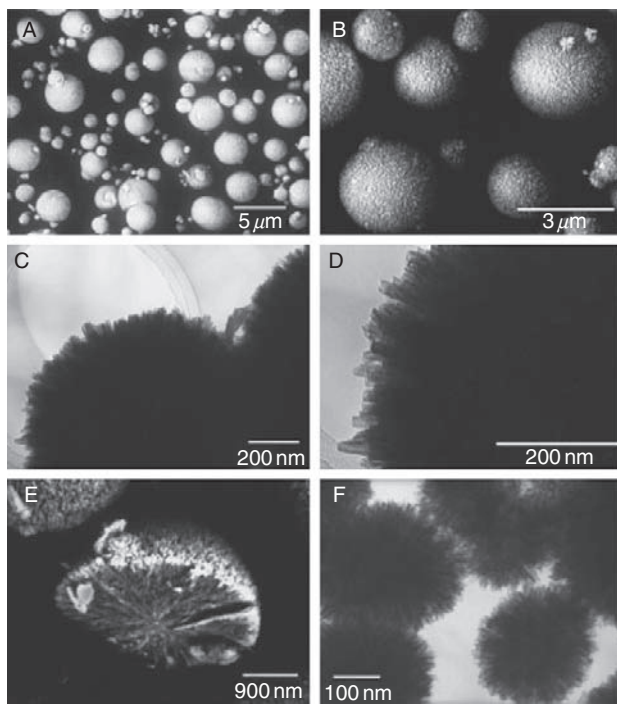


FIGURE 16 SEM and TEM image of spherical particles composed of ytterbium compound nanotubes. Reprinted with permission from Yada *et al.* (2004). Copyright 2004 Wiley-VCH.

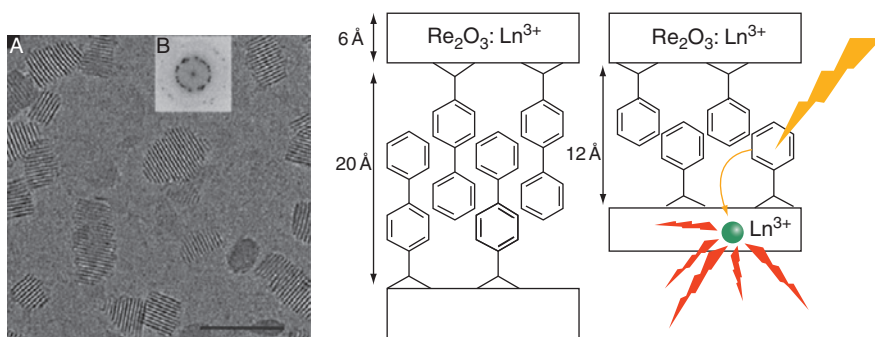


FIGURE 17 Left: TEM images of the yttria nanocomposite synthesized in 4-*tert*-butyl benzyl alcohol (A) and its Fourier transform (B). Scale bar = 50 nm. Reprinted with permission from Pinna *et al.* (2005). Copyright 2005 Wiley-VCH. Right: Structures of a unit cell of the biphenolate and benzoate based hybrid materials. Reprinted with permission from Pinna (2007). Copyright 2007 the Royal Chemical Society.

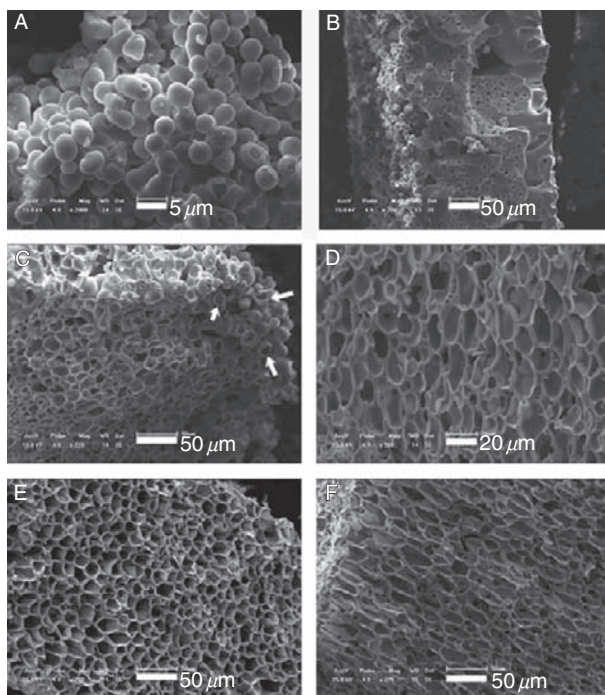


FIGURE 18 SEM images of La-organic coordination polymers synthesized with varied reaction times. Reprinted with the permission from Shen et al. (2008b). Copyright 2008 Wiley-VCH.

2.2.1.2 Colloidal synthesis The aqueous synthesis routes could not yield rare earth oxides directly without postheat treatment, while the dry routes usually lead to products with relatively wide size distribution and the nanocrystals could not be dispersed as colloidal solutions. Therefore, it is highly desirable to synthesize R_2O_3 nanocrystals in suitable nonaqueous solutions. However, the decomposition of rare earth precursor and crystallization of rare earth oxide nanocrystals would require an elevated temperature. Therefore, the solvents are usually with a high boiling point, which are called “high-boiling solvents.”

The synthesis method in high-boiling solvents has been developed to obtain high quality nanocrystals of a number of metals, metal oxides, semiconductors, and inorganic salts. For rare earth compounds, the synthesis of rare earth oxides, phosphates and halides would be discussed in this and latter sections of this chapter. The synthesis route is considered as colloidal synthesis since the products are usually well dispersed NCs in the reaction solution or certain solvents, and the products could only be separated with particular techniques.

The colloidal synthesis in high-boiling solvent systems is a versatile and reliable process, usually with the thermolysis of organometallic precursors or precipitation finely controlled by experimental parameters such as ligands, precursors, and reaction temperature. Therefore, the kinetics and thermodynamics of the nucleation and growth of nanocrystals are tuned, and the size and shape are controlled to obtain redispersible, high quality monodisperse and uniformly sized colloidal nanocrystals with varied shapes, including nanoparticles, nanorods, nanowires, nanotubes, and nanoplates. For rare earth oxide nanocrystals, the research interest has sought out new synthesis approaches to take advantages of their robust optical properties effectively, for which, the size and shape control, crystallinity, as well as the colloidal stability and suitability for luminescence applications are key issues.

The earlier works were performed in trioctylphosphine oxide (TOPO). Wakefield *et al.* (1999a,b) reported the synthesis of Tb_2O_3 and Eu_2O_3 nanocrystals through a colloidal precipitation method. The RCl_3 methanol solution was added to TOPO and a controlled amount of NaOH methanol solution was added later to initiate the precipitation. The dehydrating properties of the alcohol result in the formation of oxide, not hydroxides. The obtained NPs are covered with TOPO and the size could be controlled by tuning the ratio of solvents. However, the particle size distribution is still broad.

Bazzi *et al.* (2003, 2004) reported (Figure 19) the colloidal precipitation from polyalcohol solution to obtain stable colloidal suspensions of luminescent doped rare earth oxide nanocrystals with an average grain

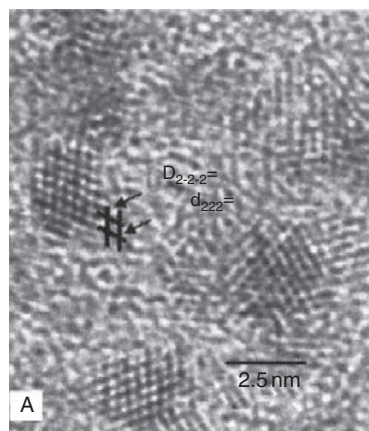


FIGURE 19 High-resolution electron micrographs of some typical sub-5 nm lanthanide nanoparticles: Eu_2O_3 . Reprinted with permission from Bazzi *et al.* (2003). Copyright 2003 Elsevier.

diameter in the range of 2–5 nm. The mixed rare earth chloride salts were dispersed in DEG. Later aqueous NaOH solution was added, and the mixture was heated at 140 °C to completely dissolve the compounds. The reaction was carried out at 180 °C and transparent suspension of particles dispersed in organic solvent was obtained.

The current works on colloidal synthesis of rare earth oxide nanocrystals in high boiling are usually carried out in OA/OM/ODE mixed solvents. The composition of the solvents, the precursor, as well as the heating parameters would have effects on the obtained nanocrystals. A typical synthesis process in high-boiling solvents, for example, OA/OM/ODE could be divided in several steps. First, the precursor solution mixture for pyrolysis is prepared with one or more selected precursors dissolved in the solvents. Second, since usually appropriate precursor hydrate is added to the solvents at room temperature, the low-boiling point fractions, including water, should be removed under vacuum at about 100 °C. Then, the reaction is performed with rapid heating to the target temperature, for example, 250–330 °C, and maintaining this temperature for a certain time, usually under protective atmosphere. After the solution cools down, another solvent, such as ethanol is poured in to precipitate the nanocrystals. The as-precipitated nanocrystals are dispersible in nonpolar solvents such as hexane, toluene, and cyclohexane to form colloidal solutions. With evaporation of the solvents, the nanocrystals would self assemble into superlattices under appropriate conditions (Cao 2004, Si et al., 2005, 2007; see Figure 20).

The rare earth oxide nanocrystals are obtained through thermolysis of single or multiple metal complex precursors and their derivatives in exchangeable surfactant solutions. Cao reported colloidal synthesis of highly uniform square Gd_2O_3 nanoplates. The nanoplates simultaneously form superlattice structures via a self-organization process (Cao, 2004). Yan et al. reported systematic synthesis of R_2O_3 and CeO_2 nanocrystals by thermolysis of rare earth benzoylacetate (BA), acetylacetate (acac), and acetate (ac) complex precursors in OA/OM/ODE-mixed solvents. Rare earth oxide nanoplates and nanopolyhedra with high dispersibility and crystallinity were obtained (Si et al., 2005, 2007). Furthermore, Yu et al. reported the synthesis of 1.1 nm-wide nanowires of Sm_2O_3 in practical scale, and the rectangular-shape nanowires were actually with a single unit cell thickness (Yu et al., 2006b).

In addition to the conventional heating scheme, the microwave irradiation methodology featuring rapid heating, which is suitable for the pyrolysis in high-boiling solvents, is also studied (Panda et al., 2007). The uniform, single crystalline rare earth oxide nanorods and nanoplates on the order of several nanometers were obtained. Microwave heating allows rapid direct transfer of energy to the reactants avoiding thermal gradient effects, and therefore, the rapid decomposition of precursors is facilitated.

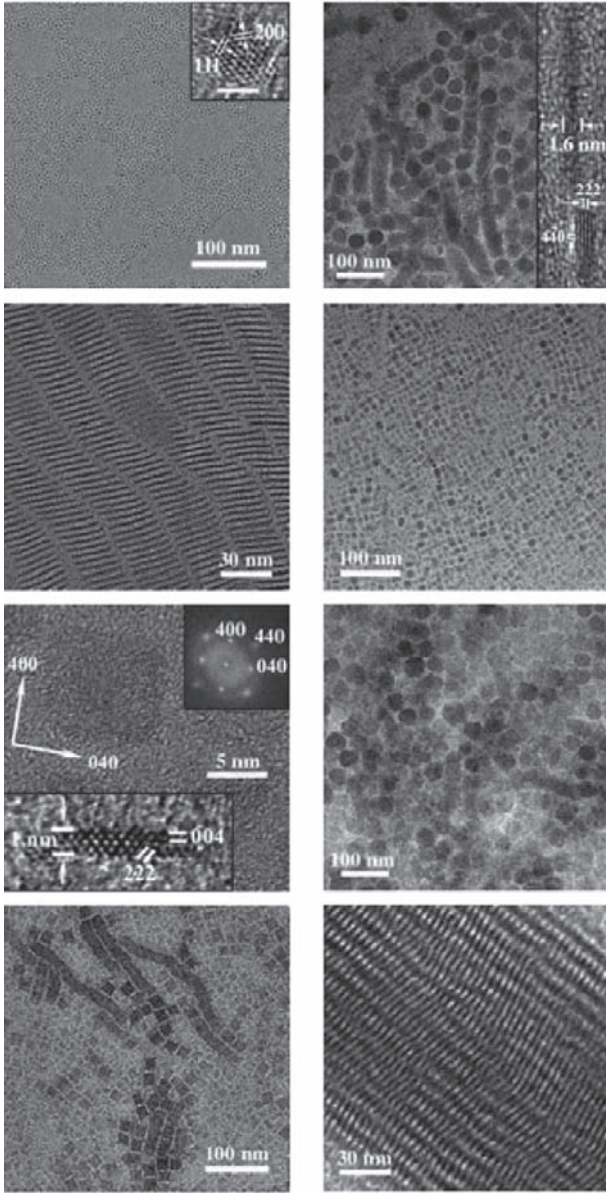


FIGURE 20 TEM image of CeO_2 nanopolyhedra, Eu_2O_3 nanodisks and nanoplates Reprinted with permission from Si *et al.* (2005). Copyright 2005 Wiley-VCH.

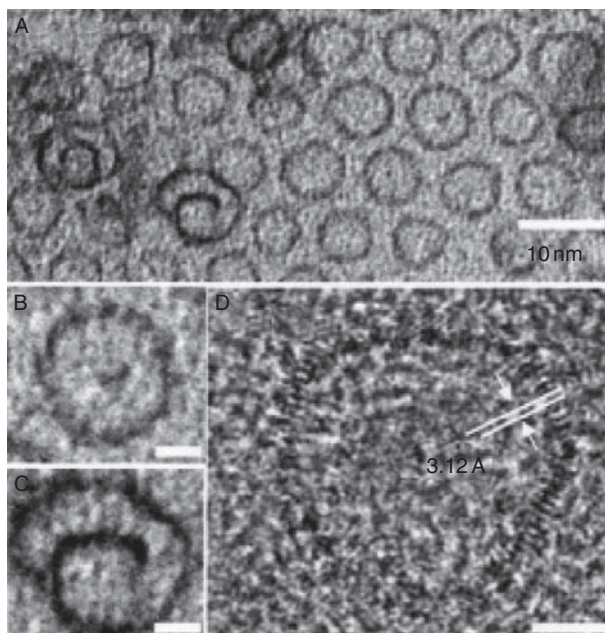


FIGURE 21 TEM image of Gd_2O_3 nanorings. Unlabeled scale bars correspond to 2.5 nm. Reprinted with permission from Paek et al. (2007). Copyright 2007 American Chemical Society.

Paek et al. (2007) reported the synthesis of colloidal nanorings and nanoplates of several rare earth metal oxides from thermal dehydration of hydrolyzed metal precursor-surfactant aggregates (Figure 21). The $\text{Gd}(\text{acac})_3$ precursor was hydrolyzed at a low temperature of 90°C and latter, the hydrolyzed precursor-surfactant aggregates were heated to 320°C for thermal decomposition. Colloidal cubic R_2O_3 nanorings and nanoplates were obtained.

Han et al. (2008) reported the synthesis of heavy lanthanide sesquioxide (R_2O_3 , $\text{R} = \text{Y}, \text{Dy}, \text{Ho}, \text{Er}$) nanobelts by thermolysis of solid rare earth nitrate hydrates in a dodecylamine/1-octadecene mixed solvent system. The nitrate hydrates showed poor solubility in the mixed solvent, and the heat-transport differences between the liquid and the solid assisted in separation of the nucleation and growth processes.

Nakamura and Maeda et al. reported the synthesis of several doped rare earth oxide nanocrystal such as $\text{Y}_2\text{O}_3:\text{Eu}$ nanocrystal in OA/OM/TOPO high-boiling solvent system (Wang et al., 2005b). Xu et al. reported the self assembly of $\text{Y}_2\text{O}_3:\text{Tb}$ nanocrystals into nanorods at similar conditions (Zhang et al., 2007d).

Yang et al. reported the study on $\text{Gd}_2\text{O}_3:\text{Eu}$ and $\text{Gd}_2\text{O}_3:\text{Er}$ nanocrystals prepared using hot solution chemistry. The synthesis started with rare

earth (III) acetate precursors, which was dissolved in oleic acid, and the pyrolysis was performed in a mixture of two coordinating solvents, trioctylamine (TOA) and TOPO, at 200–280 °C for 4–6 h (Yang *et al.*, 2005a). The products are believed to be capped with both TOA and TOPO ligands and therefore redispersible in organic solvents such as hexane, chloroform, and toluene. Square-shaped nanoplates with 11–16 nm edge length and 1.05 nm edge thickness were obtained. Notably, Yang *et al.* indexed the Gd_2O_3 nanoplates as a metastable monoclinic phase. If only TOA is used without TOPO, the yield drops with even longer reaction time and the products are not redispersible. Mahajan and Dickerson reported the synthesis of monodisperse stable sub-3 nm cubic rare earth oxide colloidal nanocrystals using a similar method (Mahajan and Dickerson, 2007).

In summary, the capping agents of OA and OM have strong effect on phase, crystal growth, and assembly of the obtained rare earth oxide nanocrystals. For all rare earths, R_2O_3 nanoplates are formed in the cubic phase, except CeO_2 , as determined from the XRD patterns. The nanoplates exhibit a thickness comparable to the unit cell dimension. On this scale, the interactions on the exposed faces obviously could affect the whole nanocrystal. Since the cubic phase is not a common product at ambient conditions for light and medium lanthanide oxides, the cubic phase is mainly controlled and stabilized by these capping agents. In addition, the plate-like morphology also shows the template effects of the capping agents through the assembly behaviors of long carbon chains. The capped nanocrystals show interesting self-assembly behavior enabled by the long carbon chains. Fine-tuning of the polarity of a mixed solvent and the concentration of the nanocrystals allows the fabrication of micron-scaled superlattices on TEM grids.

When the interaction between the metal oxide nanoparticle surface and the employed surfactant is strong and the size of the nanoparticle is small, the surface energy could usually dominate both the polymorphism and the crystal growth behavior of metal oxide nanoparticle. Herein, the OA chelated R_2O_3 nanocrystals are fixed to be cubic phase and a 2D morphology is shown. If the interaction between the metal oxide nanoparticle surface and the employed surfactant is not strong enough to guide the anisotropic crystal growth at high temperatures, the resulting nanocrystals would usually be in the spherical form, and sometimes in anisotropic form as the result of the intrinsic crystal growth behavior. The CeO_2 nanopolyhedron is a typical example. The surface ligands with long carbon chains both allow the dispersibility of these nanocrystals in non-polar organic solvents and enable the interesting self organization of the nanocrystals into superlattices. Due to the variety of shapes of these nanocrystals, the superlattices present more diversity in the structure.

2.2.2 Properties of R_2O_3

2.2.2.1 Luminescence Photoluminescence of rare earth oxide nanocrystals is one of their most significant properties of interest for applications. The photoluminescence features of rare earth doped nanomaterials have been reviewed by Liu and Chen in an earlier chapter (Liu and Chen, 2007b). Therefore, we only review some related aspects, such as the major variations in the luminescence features of nanophased rare earth oxides, the application of rare earth doped nanocrystals as multicolor phosphors and as bioimaging probes.

A large portion of early efforts was devoted to the so-called size effects in rare earth doped nanocrystals, for example, Eu and Tb doped rare earth oxides. The luminescent rare earth oxide nanocrystals mainly are doped Y_2O_3 , Gd_2O_3 , La_2O_3 , and Lu_2O_3 , and the hosts do not emit lights themselves in the visible light range. Buissette et al. (2006a) presented a feature article for lanthanide doped phosphate and vandate nanophosphors, and the feature article also briefly covered some common characteristics for other rare earth nanocrystals including rare earth oxides. The spectroscopic effects, change in luminescence yield, in quenching concentration, and decay curves have been widely studied. There is a review of doped Y_2O_3 and Gd_2O_3 nanophosphors presented by Lebbou et al. (2005).

A significant part of the spectroscopic studies was for Eu^{3+} doped NPs, especially in $Y_2O_3:Eu$. The stable phase of Y_2O_3 is cubic C phase while the monoclinic B phase is also frequently studied (Bihari et al., 1997). Tissue et al. (Williams et al., 1999; Figure 22) reported the size dependent luminescence spectra and decay lifetimes in nanocrystalline monoclinic $Y_2O_3:Eu$ with sizes decreased from 15 to 7 nm. With decreased particle sizes, the spectra show increased line broadening. The 5D_0 lifetimes increase and the decay transients become non-single exponential with decreased particle size below 13 nm. As is well known, Eu^{3+} is a good probe for their local environment. There would be changes in the relative intensities, the position of excitation and emission bands as well as a systematic increase in the bandwidths for fine 4f–4f transitions with decreased crystalline size below 50 nm. The broadening is mainly attributed to the structural disorder in NPs and the high surface/volume ratio. The charge transfer excitation band exhibits red shift due to the increase of Eu–O bond length in NPs caused by the expansion of the cell. The decrease of luminescence efficiency is mostly related to the surface of NPs and the optimal doping concentration depends on the alteration of energy transfer in NPs.

$Y_2O_3:Tb$ nanocrystalline material shows only a 40% luminescence efficiency compared with $LaOBr:Tb$ phosphors (Goldburt et al., 1997). However, the luminescent efficiency in doped nanocrystalline $Y_2O_3:Tb$

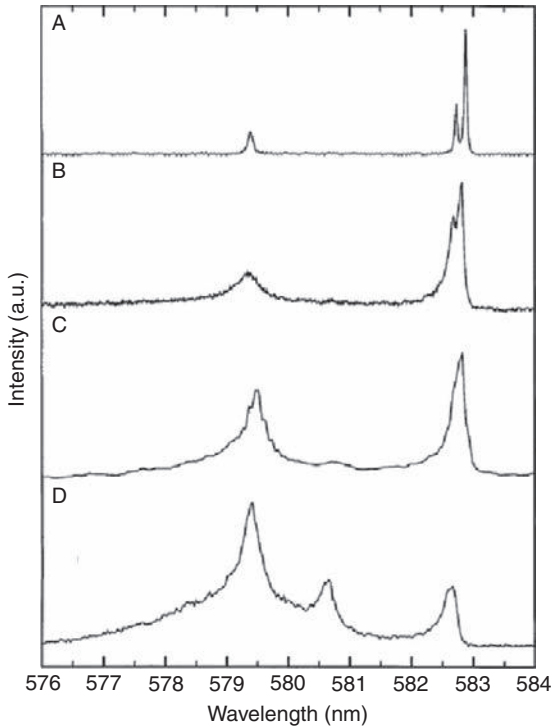


FIGURE 22 $F_0 \rightarrow D_0$ excitation spectra of differently sized 0.1% $Y_2O_3:Eu$ at approximately 13 K excited at 614 nm. (A) Bulk; (B) 15 nm; (C) 13 nm; (D) 7 nm. Reprinted with permission from Williams *et al.* (1999). Copyright 1999 Elsevier.

phosphors was found to increase with the decrease in the particle size from 10 to 4 nm. The light output per Tb^{3+} ion in nanocrystalline phosphors exceeded that in the standard $LaOBr:Tb^{3+}$ phosphor.

Sm^{3+} presents a complex spectroscopic feature due to its multiplet structure (Goldys *et al.*, 2006; Zhou *et al.*, 2003). The energy transfer from rare earth oxide hosts to Sm^{3+} is not efficient. When codoped with Bi^{3+} , the sensitization effect of Bi^{3+} ions on the emission of Sm^{3+} ions is significant and varies with Bi^{3+} concentration (Liu *et al.*, 2008a). Vetrone *et al.* (2004) reported that the nanosized $Y_2O_3:Sm$ sample made by a combustion method might exhibit a longer decay time feature in ${}^4G_{5/2}$ level compared with the bulk correspondent, which is strongly dependent on the index of refraction of the media.

Luminescent UC materials are those excited by a long wavelength light source and give a short wavelength emission. Such materials have been known for over 50 years. The rare earth based UC materials, such as those codoped with Yb^{3+} and Er^{3+} , exhibit high photo stability and

low cytotoxicity, which are promising candidates for medical applications, for example, as FRET donors in biological assays (Morgan and Mitchell, 2007).

The upconversion luminescent rare earth phosphors could emit a range of tunable colors. Glaspell et al. reported the synthesis of UC Y_2O_3 NPs using laser vaporization/controlled condensation route. Y_2O_3 nanocrystals doped with Yb^{3+} , Er^{3+} , Ho^{3+} , and Tm^{3+} are obtained and the samples could generate red, green, blue, and white light under 980 nm, laser excitation (Glaspell et al., 2008). Yang et al. reported the synthesis of $Yb^{3+}/Er^{3+}/Tm^{3+}$ -doped Lu_2O_3 UC nanoparticles via a glycol mediated dehydration route. By controlling the concentration of dopants, the white color emission could be achieved (Yang et al., 2009).

2.2.2.2 Bioimaging and bio-compatibility The surface modification of luminescent rare earth NPs not only allows the NPs to be dispersible in appropriate solvents as colloidal solutions, but also tune the surface chemistry and helps to increase the luminescence efficiency significantly. Peng et al. reported (Yu et al., 2007) the surface modification of Nd_2O_3 NPs with a silane coupling agent of the dimethyldichlorosilane (DMDCS). The modified NPs exhibit good fluorescent properties and could be dispersed as a liquid medium. Traina and Schwartz reported (Traina and Schwartz, 2007) the surface modification of Y_2O_3 NPs with various phosphonic acids, which are synthesized to be hydrophilic, hydrophobic, or intermediates, therefore, the phosphonates readily bond to yttrium oxide nanoparticle surfaces and the hydrophilic characteristics of these particles can be controlled by choice of the phosphonic acid. Das and Tan reported the synthesis of doped luminescent Y_2O_3 NCs, which could be potentially used as bioimaging probes (Das and Tan, 2008). A solvothermal process assisted with oleic acid was carried out, therefore NPs and NRs of doped Y_2O_3 are obtained. Then, the NCs are coated with silica, functionalized, and tested with their *in vitro* cytotoxicity.

Fluorescent labeling of molecules is important for biological studies. In addition to the organic dyes, quantum dots, as well as rare earth chelates, rare earth oxide based NPs also provide an attractive way for bioimaging probes. Kennedy et al. provided an example in an immunoassay for atrazine (Feng et al., 2003; Figure 23). Eu_2O_3 NPs are functionalized and atrazine-derivatized; therefore, they could be used to interact with atrazine antibodies and magnetic beads linked to mouse antibodies. Finally, the magnetic beads could be removed from the solution by magnets, which leave the solution with luminescent NPs only if free atrazine is present in the assay. Kennedy et al. reported an example to visualize proteins using $Gd_2O_3:Eu$ NPs (Dosev et al., 2005); the NPs are coated with avidin through physical adsorption and the protein linked to biotin could thus be visualized by the affinity of biotin and avidin.

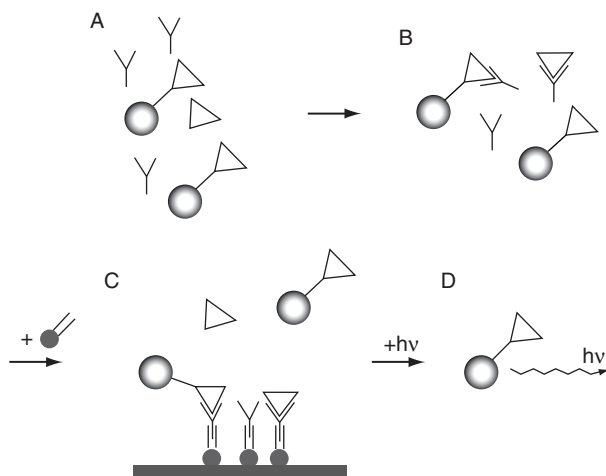


FIGURE 23 Schematic presentation of the competitive assay using magnetic separation. Reprinted with permission from Feng *et al.* (2003). Copyright 2003 American Chemical Society.

Recent advancements in nanotechnology reveal the opportunities for nanoscaled upconversion (UC) materials in bioimaging because there are hardly few biomaterials that would exhibit UC properties and the injected UC materials would be distinguished easily. Nagasaki *et al.* reported the UC $\text{Y}_2\text{O}_3:\text{Yb},\text{Er}$ NPs co-immobilized with poly(ethylene glycol)-*b*-poly(acrylic acid) (PEG-*b*-PAAc) and streptavidin, and therefore the NPs could specifically recognize biotinylated antibodies and emit strong upconversion luminescence upon near-infrared excitation (Kamimura *et al.*, 2008). Hilderbrand *et al.* reported the UC $\text{Y}_2\text{O}_3:\text{Yb},\text{Er}$ NPs suitable for *in vivo* imaging. The obtained NPs are aqueously dispersible and modified with PEG polymers and NIR emitting carbocyanine fluorophores. The attached carbocyanine fluorophores, which could be excited with 750 nm, enable a dual channel imaging in addition to the UC Y_2O_3 NPs. The NPs also show low cytotoxicity in preliminary *in vivo* tests (Hilderbrand *et al.*, 2009).

Bifunctional biolabels with magnetic and luminescent properties are highly desirable for *in vitro* and *in vivo* bioimaging. There are several strategies to use NPs to comprise such biolabels, such as core/shell NPs, for example, the magnetic cores of iron oxide doped with cobalt and neodymium and luminescent shells of $\text{Gd}_2\text{O}_3:\text{Eu}$ (Dosev *et al.*, 2005, 2007).

2.2.2.3 Catalysis Rare earth oxides exhibit a basic oxide surface and therefore rare earth oxides are used as substrates or additives in catalysts.

Gate et al. reported (Fierro-Gonzalez et al., 2005) the catalysts of mononuclear La_2O_3 -supported Au-III complexes. The catalyst was synthesized from $\text{Au-III}(\text{CH}_3)_2\text{C}_5\text{H}_7\text{O}_2$ and was highly active and stable for CO oxidation at room temperature. Guzman and Corma reported the catalyst of mesostructured Y_2O_3 -gold (Guzman and Corma, 2005). The support shows ability in stabilizing catalytically active gold species, while Au NPs are not required (Fu et al., 2003b). Qiu et al. reported (Sun et al., 2004) the catalytic activity for steam reforming of ethanol at low temperature in nano-sized nickel catalysts using Y_2O_3 , La_2O_3 , or Al_2O_3 as substrate. The rare earth oxide based catalysts shows high activity and long term stability for ethanol steam reforming.

Weckhuysen et al. found the destruction of carbon tetrachloride (CCl_4) on CeO_2 or La_2O_3 in the presence of oxidants. In the process, the rare earth oxides are chlorinated (Weckhuysen et al., 1999). Later they reported the catalytic destruction of CCl_4 over a series of lanthanide and alkaline-earth metal oxides based catalysts in the presence of water steam (Van der Avert et al., 2004). The catalysts combined the destruction on basic oxide surface and concurrent dechlorination of the partially chlorinated solid by steam. The two noncatalytic reactions combined into a catalytic cycle in this way.

2.3 Other rare earth oxides

Most of the rare earth elements form oxides in the form of R_2O_3 with R(III), but CeO_2 , EuO , YbO , Tb_4O_7 , and Pr_6O_{11} are also common. The nanomaterials of the latter four compounds will be discussed in this section.

The low-valence rare earth compounds containing Eu(II) and Yb(II) are usually obtained using techniques providing protection against the oxidation from environment, such as reductive atmosphere, surface modification or coating, and protective polymeric matrix. EuO exhibits a cubic rock salt structure, and it is a ferromagnetic semiconductor with a band gap of 1.1 eV and a bulk Curie temperature (T_c) of 69 K. Hasegawa et al. reported the synthesis of spindle-shaped EuO nanocrystals with average size of 280 nm in length and 95 nm in width from Eu metal in liquid ammonia (Thongchant et al., 2001). Later, they reported the synthesis of smaller EuO nanocrystals with average diameter of 3.4 nm by photochemical reduction of $\text{Eu}(\text{NO}_3)_3$ in methanol (Hasegawa et al., 2002). EuO nanorods could be obtained through a multi-step conversion route. Bierman et al. (2007) reported the synthesis of polycrystalline EuO NRs. $\text{Eu}(\text{OH})_3$ nanorods were first precipitated from $\text{Eu}(\text{NO}_3)_3$ by hexamethylenetetramine at 95 °C, avoiding impurities like Na^+ or K^+ which might affect the magnetic properties. Then the precipitates are calcined at 800 °C to obtain Eu_2O_3 powder samples, followed by the reduction in Eu metal atmosphere to form EuO . Reports on YbO nanomaterials are scarce.

The mixed-valenced rare earth oxides of Tb_4O_7 and Pr_6O_{11} are usually obtained through calcinations in air. In solution, normal oxides like Tb_2O_3 and Pr_2O_3 may form, however, after appropriate oxidation processes, the mixed-valenced products will form. Pr_6O_{11} nanocrystals are usually obtained by heating $Pr(OH)_3$ nanocrystals in air (Ma *et al.*, 2007b; Yan *et al.*, 2008b). The heating temperature is crucial for the morphology and phase. With a low temperature (450 °C), there may be residue of hydroxides, while with a high temperature (800 °C), the original morphology can collapse into nanoparticles. Only with a moderate temperature (600 °C), the morphology would be preserved (Huang *et al.*, 2006b; Yan *et al.*, 2008b). Tb_4O_7 nanotubes are also obtained through heating of $Tb(OH)_3$ nanotubes (Fang *et al.*, 2003b). The sol-gel method utilizing propylene oxide, citrate acid, or Pechini method could also be used to obtain nanostructured Pr_6O_{11} materials (Borchert *et al.*, 2008). The size of the nanocrystalline domains was in the range of about 10 nm. Wang *et al.* reported the synthesis of single crystalline Pr_6O_{11} nanotubes through a molten-salt route (Wang *et al.*, 2004c). NaCl and Pr_6O_{11} powders are mixed, ground, and calcined at 840 °C (NaCl, m.p. 801 °C). After cooling to room temperature, NaCl is washed away by water. About 30% of the raw Pr_6O_{11} microparticles have been converted into nanotubes, grown along [1–10] axis. The impurity of Na^+ or Cl^- was not observed. Since Pr is similar to Ce, its neighbor in the periodic table, Pr_6O_{11} with cubic fluorite-like structure are often considered and compared to CeO_2 . The Pr_6O_{11} nanopowders (Borchert *et al.*, 2008) and nanorods loaded with gold (Huang *et al.*, 2006b) exhibit catalytic activity for CO oxidation.

2.4 Rare earth hydroxides

2.4.1 Synthesis of rare earth hydroxide nanostructures

Rare earth hydroxide nanocrystals are commonly synthesized via the precipitation of R^{3+} to form gel-like $R(OH)_3$ in basic aqueous solutions, which is quite straightforward with appropriate pH values of 6–8 for Y and La–Lu. Sc^{3+} would precipitate even in an acidic solution. The crystallized rare earth hydroxide is then obtained after annealing or aging the gel-like precipitation with mother liquor. With elevated temperature, the dried rare earth hydroxides could be dehydrated into oxyhydroxide and oxide in steps.

Rare earth hydroxides themselves find scarce applications, because of their instability in the presence of CO_2 . In addition, the presence of OH^- introduces deterioration effects for photoluminescence emissions. However, rare earth hydroxides can be easily converted into a number of other rare earth compounds through dry and solution chemical routes, therefore, they are often taken as intermediates for the synthesis of rare earth oxides, sulfides, and fluorides.

The hydrothermal treatment of gel-like $R(\text{OH})_3$ in mother liquor yields crystallized $R(\text{OH})_3$ nanocrystals with particle-like, sheet-like, rod-like, and tube-like morphologies. The results are mostly affected by the basicity and treatment temperatures. Wang and Li reported the synthesis of rare earth nanowires/nanorods through hydrothermal methods with strong basicity in mother liquor. A serial synthesis of rare earth hydroxide nanowires with growth directions along [001] is done with pH 14 or concentrated NaOH of 5–10 M (Wang and Li, 2002; Figure 24). They suggest that an optimal concentration of the alkaline base exists for the biggest aspect ratio. Higher concentrations of NaOH hinder the anisotropic growth by lowering the mobility of rare earth ions, whereas pH 7–8 typically leads to sheet-like morphology (Wang and Li, 2002). Liu et al. reported the nanosheet of $\text{Lu}(\text{OH})_3$ and Lu_2O_3 obtained through a hydrothermal route with medium pH values (Wang et al., 2007a). Wang and Li reported the fullerene-like nanoparticles of rare earth hydroxide obtained through a hydrothermal route (Wang and Li, 2003a,b; Figure 25C). The hollow NPs are formed with curved layers of the hexagonal rare earth hydroxides. The rare earth hydroxide nanotubes could also be obtained in the hydrothermal routes, with a temperature of 120–140 °C (Wang and Li, 2003a).

For heavy lanthanides like Yb and Sc, the hydrothermal treatment may lead to the formation of oxyhydroxides ROOH . The use of alkali hydroxide or ammonia has strong effect on the phase and morphology of ScOOH (Zhang et al., 2005c). With NaOH as precipitator, pH values in 10–14, or with 2.5 mol L^{-1} NaOH, α - ScOOH nanorods are obtained, similar to that of YbOOH obtained by Wang and Li (2002). However, when higher

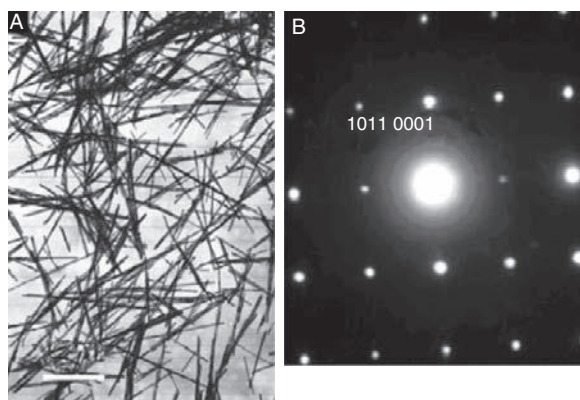


FIGURE 24 (A) TEM image of $\text{La}(\text{OH})_3$ nanowires (KOH, 5 mol L, bar 1 μm); (B) Electron diffraction pattern of a single $\text{La}(\text{OH})_3$ nanowire; reprinted with permission from Wang and Li (2002). Copyright 2002 Wiley-VCH.

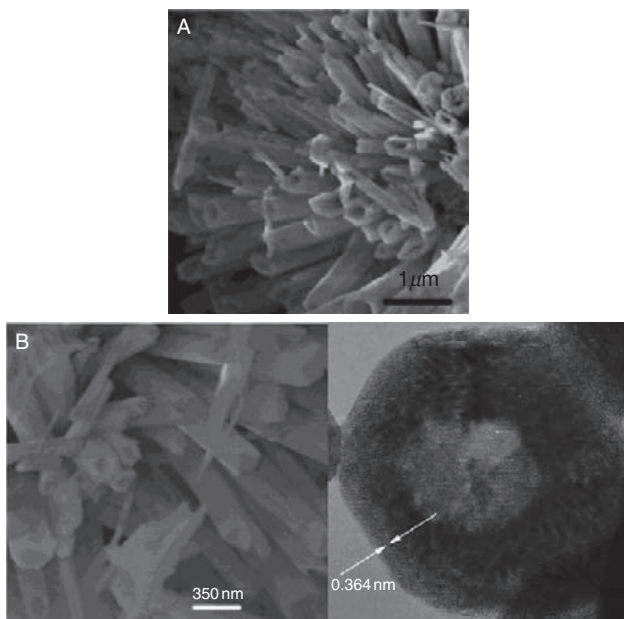


FIGURE 25 SEM images of $\text{Dy}(\text{OH})_3$ (A) and Dy_2O_3 (B) nanotubes. Reprinted with permission from Xu *et al.* (2003). Copyright 2002, American Chemical Society. (C) HRTEM image of an individual $\text{Eu}(\text{OH})_3$ fullerene like nanoparticle with diameter about 45 nm. Reprinted with permission from Wang and Li (2003a). Copyright 2003 Wiley-VCH.

concentrations of NaOH (5 mol L^{-1}) are used, the products become $\text{Sc}(\text{OH})_3$ submicron crystals. $\text{NH}_3 \cdot \text{H}_2\text{O}$ leads to meta-stable $\gamma\text{-ScOOH}$ nanoparticles, probably due to the weaker mineralization effect.

The heat treatment temperature for synthesizing hydroxide nanocrystals mostly affects the morphology, as well as the crystallinity. If the temperature is low, for example 100°C , long time is often used for reaction or aging (Yan *et al.*, 2008b; Zhu *et al.*, 2008c).

The utilization of soft templates is helpful for the construction of rare earth hydroxide nanotubes. The synthesis of $\text{Y}(\text{OH})_3$ nanotubes could be assisted by PEG (Tang *et al.*, 2003) or grafted with PMMA (Li *et al.*, 2004; Mo *et al.*, 2005). Hard templates like AAO are also studied for the fabrication of rare earth hydroxide nanowires (Bocchetta *et al.*, 2007).

Hu and coworkers developed a composite hydroxide method (CHM) to synthesize highly crystallized rare earth hydroxide and oxide nanocrystals (Hu *et al.*, 2007). The eutectic mixture of alkaline hydroxides ($\text{NaOH}:\text{KOH} = 51.5:48.5$, m.p. 165°C) is used as solvent and the real synthetic process is done at approximately 200°C in a sealed vessel. The highly crystallized $\text{La}(\text{OH})_3$ nanobelts are obtained through this method

with a growth direction of [110], which is different from the hydrothermally obtained nanowires.

There are also other ways to obtain rare earth hydroxide nanocrystals. The formation of rare earth hydroxide needles or nanotubes was observed as a corrosion product with LaNi_5 in KOH (Maurel et al., 2000). Fang and Xu et al. reported that with medium pH values, that is, near the precipitation pH value of rare earth hydroxides, the hydration of medium rare earth (Tb, Dy, Y) oxides with a hydrothermal treatment will lead to rare earth hydroxide nanotubes (Fang et al., 2003a; Xu et al., 2003; Figure 25). Lee and Byeon reported the hydration of LaOCl for the synthesis of $\text{La}(\text{OH})_3$ nanostructures (Lee and Byeon, 2006).

Rare earth hydroxides are rarely obtained in nonaqueous systems. However, Djerdj et al. reported the synthesis of $\text{La}(\text{OH})_3$ nanorods/nanofibers and manganese oxide nanoparticles through a nonaqueous sol-gel process involving the reaction of $\text{La}(\text{OiPr})_3$ (lanthanum *i*-propoxide) and KMnO_4 with organic solvents such as benzyl alcohol, 2-butanone, and their mixture (Djerdj et al., 2007).

2.4.2 Properties and applications of rare earth hydroxide nanostructures

$\text{R}(\text{OH})_3$ do not provide many applications themselves, though there are some reports on tribology (Zhang et al., 1998, 2001a), sensing (Liu and Song, 2006), and photonic crystal fabricated with monodisperse silica shell (Lin et al., 2007b).

However, hydroxides proved to be applicable intermediate for preparing various nanocrystals of rare earth oxide, oxysulphide, oxyfluoride, and other rare earth compounds. In this route, the crystallized $\text{R}(\text{OH})_3$ nanocrystals instead of gels were obtained and collected, later a next step is performed to convert the $\text{R}(\text{OH})_3$ nanocrystals into other compounds, without destroying the morphology. The obtained new nanocrystals may or may not have a certain crystal growth direction related to the precursor. A selection of typical works on the conversion of rare earth hydroxide nanostructures are listed in Table 1.

3. NANOMATERIALS OF RARE EARTH OXYSALTS

3.1 Rare earth phosphates

There are four different phases of rare earth orthophosphate (RPO_4), mostly depending on the cationic radius of rare earth element: Monazite (monoclinic, dehydrate, for light lanthanides), xenotime (also typed as zircon, tetragonal, dehydrate or hydrate, for heavy lanthanides and Y^{3+}), rhabdophane (hexagonal, mostly hydrate, across the series), and

TABLE 1 The conversion from rare earth hydroxide nanocrystals

Morphology	Target compound	Conversion method	Conversion condition	Crystal relations	Reference
Hydroxide, nanowires, nanotubes	R_2O_3	Heating dehydration	500 °C	Not reported	Wang and Li (2003a)
Hydroxide, nanowires, nanotubes	R_2O_2S	Sulfur	700 °C, 2 h	Not reported	Wang and Li (2003a)
Hydroxide, nanowires, nanotubes	$R(OH)_x F_{3-x}$	F, hydrothermal	120 °C	Not reported	Wang and Li (2003a)
Tb(OH) ₃ , Y(OH) ₃ , Dy(OH) ₃ , nanotubes	Oxide, Tb ₄ O ₇ , Y ₂ O ₃ , Dy ₂ O ₃	Heating in air	450 °C	[001] to [011] for Dy	Xu et al. (2003), Fang et al. (2003b)
Ce(OH) ₃ nanotubes	Oxide, CeO ₂	Heating in air	450 °C	[100] to [110]	Tang et al. (2005b)
La(OH) ₃ , Nd(OH) ₃ , nanowires	Sulfide, LnS ₂	Boron–sulfur method	400–450 °C, 24 h, more S	Not observed	Huang et al. (2008b)
La(OH) ₃ , Nd(OH) ₃ , nanowires	Oxysulfide, Ln ₂ O ₂ S, Ln ₂ O ₂ S ₂	Boron–sulfur method	500 °C, 10 min, with Ln(OH) ₃ /S = 1 or 0.5	Not observed	Huang et al. (2008b)
Gd(OH) ₃ nanorods	Vanadate, GdVO ₄	Hydrothermal reaction with Na ₃ VO ₄	180 °C 18 h, pH 13	[001] to [001]	Gu et al. (2008c)
Eu(OH) ₃ nanorods	EuO	Heating in air to Eu ₂ O ₃ and reduction in Eu vapor to EuO		Polycrystalline	Bierman et al. (2007)

churchite (also named weinschenkite, monoclinic, hydrate, for heavy lanthanides and Y^{3+}) (Wickleder, 2002). It should be noted that the so-called orthorhombic phase is probably a mixture of xenotime and rhabdophane (Assaouadi et al., 2000).

RPO_4 have a number of advantageous properties, including very low solubility in water (Firsching and Brune, 1991), high thermal stability with melting points around 2300°C (Rouanet et al., 1981), low thermal conductivity, high refractive indexes (Jellison et al., 2000), high luminescence quantum efficiency, chemical capability of containing lanthanides and actinides, and unusual magnetic behaviors. Therefore rare earth orthophosphates find applications in various fields, such as phosphors, sensors, proton conductors (Norby and Christiansen, 1995; Yu and De Jonghe, 2007), catalysts (Onoda et al., 2002), hosts for radioactive nuclear waste (Ordenez-Regil et al., 2002), and heat-resistant ceramic materials. The most significant applications for rare earth orthophosphates are the optical ones, such as the scintillators for X-ray and γ -ray detection for medical imaging (Lempicki et al., 1993), thermo luminescence phosphors (Iaconi et al., 2001), laser hosts (Laporta et al., 1999), compact fluorescent lamps, and plasma display panels. Especially, $\text{LaPO}_4:\text{Ce}^{3+},\text{Tb}^{3+}$ is a highly efficient commercial green phosphor ($^5D_4 \rightarrow ^7F_5$ transition of Tb^{3+} at 543 nm) used in fluorescent lamps.

In addition to the orthophosphates, there are also a small number of reports on nanomaterials of other rare earth phosphate salts (Tang et al., 2005c). In this section, we will discuss the chemical synthesis of rare earth orthophosphates in aqueous solutions, nonaqueous solutions, and dry methods, together with the brief discussion of the luminescent properties, as well as the applications in biosensing.

3.1.1 Synthesis of rare earth orthophosphate nanostructures

The synthesis of rare earth orthophosphate nanomaterials involves obtaining pure phase, uniform morphology, as well as the surface structures, in order to fulfill the requirement for applications such as phosphors. The rare earth orthophosphate NCs could be obtained through precipitation in aqueous or nonaqueous solutions and dry methods.

3.1.1.1 Ambient aqueous routes and hydrothermal routes The synthesis of rare earth orthophosphate NCs could be carried out in aqueous solutions by the precipitation of rare earth cations by phosphate anions, due to the low aqueous solubility of RPO_4 . A typical synthesis begins with soluble rare earth salts in aqueous solution, such as nitrates or chlorides, and a phosphate source like phosphate $M_n\text{H}_{3-n}\text{PO}_4$, triphosphate $M_5\text{P}_3\text{O}_{10}$ ($M = \text{Na}, \text{K}, \text{or } \text{NH}_4$), or H_3PO_4 . The two solutions are mixed at room temperature or elevated temperature to form gel-like precipitation as precursor. Then the mixture of precipitation and mother liquor is

subjected to appropriate controlled heat treatment, for example, a hydrothermal process or in oil/water bath at a certain temperature to complete the crystallization process. After a certain reaction time, the system is cooled to room temperature, and the precipitated rare earth phosphate NCs are collected and washed. The obtained rare earth orthophosphate products exhibit varied phases and morphologies, depending strongly on the cationic radii, acidity, and reaction temperatures. For light lanthanides (La–Gd), hexagonal rhabdophane and monazite phase rod-like or wire-like products could be obtained (Yan *et al.*, 2004; Zhang *et al.*, 2003b). With a temperature of 180–240 °C, the products become the monazite phase with the morphology strongly affected by the acidity (Figure 26). With smaller cationic radius, the required temperature to obtain this pure monoclinic phase is higher. Rod-like or wire-like monoclinic light lanthanides orthophosphate products also need higher temperature

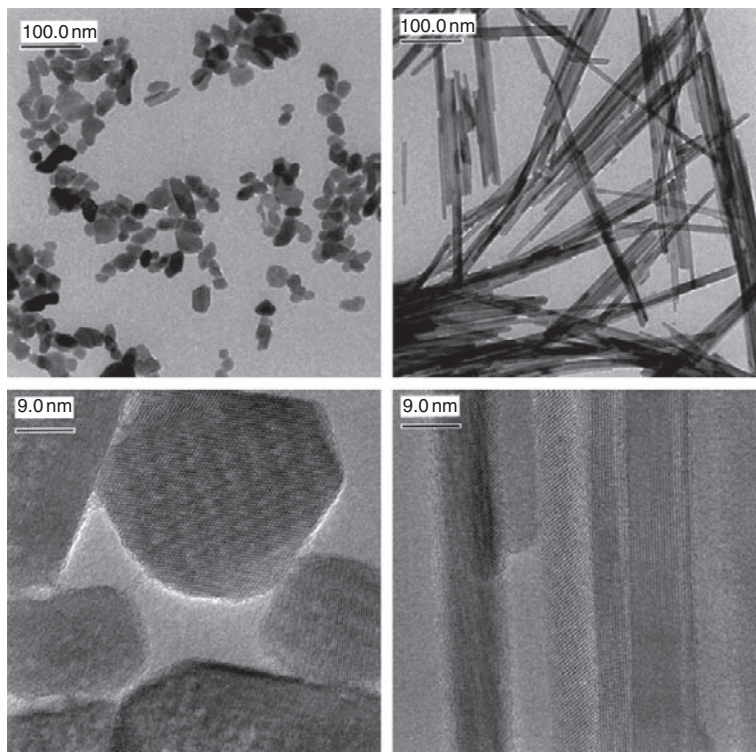


FIGURE 26 TEM (upper part) and HRTEM (lower part) micrographs of $\text{LaPO}_4:\text{Eu}$ NCs synthesized by a hydrothermal route, which is prepared at $\text{pH}_{\text{start}} = 1.7$ (right) and at $\text{pH}_{\text{start}} = 12.5$ (left), respectively. Reprinted with permission from Meyssamy *et al.* (1999). Copyright 1999 Wiley-VCH.

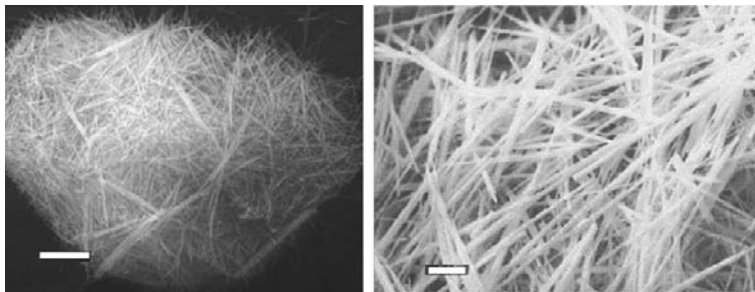


FIGURE 27 SEM image of LaPO_4 NWs (left) and EuPO_4 NWs (right), the scale bar is 1 μm .

(for example, 200–240 °C) and similar mother liquor acidity of pH 1–2 (Figure 27). Monoclinic NCs with smaller aspect ratios can be obtained, with lower acidity of pH 2–6 or higher acidity by adding concentrated phosphoric acid and with a higher temperature (Guan and Zhang 2004; Zhang and Guan, 2003; Zhang et al., 2003b). With basic solution of pH 10–12 and a temperature of 200 °C, monazite type NPs, for example, LaPO_4 :Eu will form (Meyssamy et al., 1999; Figure 26). With neutral pH values, hexagonal NPs with round or slightly elongated shape will form at moderate temperature, for example, $\text{EuPO}_4 \cdot n\text{H}_2\text{O}$ (Zollfrank et al., 2008). This hexagonal phase NCs can also form at 100–140 °C in an acidic solution with pH value of 1–2 (Figure 28). Pure and doped hexagonal LaPO_4 NRs with typical dimensions of 8 nm in diameter and 80 nm in length are prepared from NaH_2PO_4 and LaCl_3 aqueous solutions at 100 °C. Compositional analysis by X-ray photoelectron spectroscopy demonstrated that LaPO_4 NRs had an anion-rich surface, which may be the main reason for their colloidal stabilities (Wang and Gao, 2006).

For heavy lanthanides (Ho–Lu) and Y, a synthesis temperature as low as 70 °C is required to obtain hydrated monoclinic churchite phase, for example, YPO_4 NWs (Di et al., 2007b). Higher temperature leads to tetragonal zircon phase. Usually, a particle-like morphology is obtained with acidic conditions. When a chelating agent like EDTA is introduced, the hydrated hexagonal NRs of YPO_4 could be obtained (Yan et al., 2005).

For intermediate lanthanides (Gd, Tb, Dy), hexagonal, tetragonal, and monoclinic phases may coexist. Therefore, results are more complex. Typically, rhabdophane type TbPO_4 NRs form at low temperature and zircon type TbPO_4 nanocubes form at high temperature, both with acidic mother liquors (Zhang et al., 2003b). Hexagonal DyPO_4 NR bundles (Fang et al., 2003a) form at low temperature. Heating of the thus obtained hydrate rare earth phosphate NCs leads to dehydrates. Usually, the rhabdophane products of light rare earths convert to monazite products, while the churchite phase converts to zircon products with heat treatment

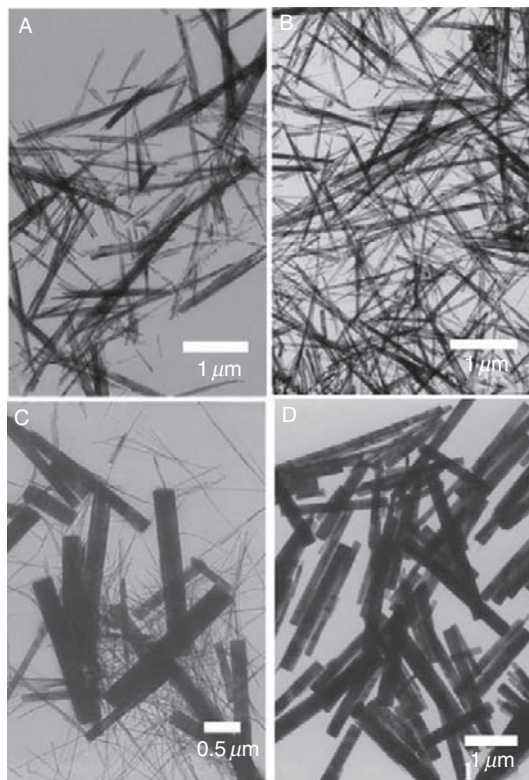


FIGURE 28 TEM images of hexagonal $\text{LnPO}_4 \cdot n\text{H}_2\text{O}$ products synthesized by a hydrothermal route: (A) La, (B) Ce, (C) Eu, (D) Gd. Reprinted with permission from Yan *et al.* (2004). Copyright 2004 Elsevier.

(Fang *et al.*, 2005b). Like the DyPO_4 NR bundles, the rare earth phosphate NRs obtained via hydrothermal process tend to attach to each other via the side faces to form bundles at low pH value of 1 and moderate temperature (Di *et al.*, 2007a; Fang *et al.*, 2003a; Yan *et al.*, 2004). Bu *et al.* reported the uniform spindle-shaped NR bundles obtained in the presence of block copolymer Pluronic P123 (Bu *et al.*, 2007). Similar results could also be obtained, when the hydrothermal synthesis is conducted using a standard household microwave oven (Patra *et al.*, 2005).

In addition to the orthophosphates, other rare earth phosphates could also be obtained through hydrothermal routes. Tang *et al.* reported the synthesis of so-called CeP (with a composition of $\text{Ce}(\text{HPO}_4)_2 \cdot \text{H}_2\text{O}$) nanotubes (Tang *et al.*, 2005c). Concentrated phosphoric acid solution of 6 M was heated to a temperature ranging from 50 to 110 °C to form a condensed linear polyphosphate $(\text{P}_n\text{O}_{3n+1})_{n+2}^-$. Then, the $(\text{NH}_4)_2\text{Ce}(\text{NO}_3)_6$ solution is

added slowly. After 2 h, cellulose paper-like material with a fiber like morphology is obtained. Although the crystal structure of the product is unknown, a hexagonal and an orthorhombic phase could be identified with the composition of $\text{Ce}(\text{HPO}_4)_2 \cdot \text{H}_2\text{O}$. The cerium phosphate nanotubes at 105 °C with hexagonal structure could be obtained. Li et al. also reported the hydrothermal synthesis of microporous nanofibers of rare earth organophosphates (Li et al., 2008h).

Sonochemistry is one of the early techniques for the synthesis of nanosized compounds (Gedanken, 2004). The sonochemical synthesis is fast, simple, and usually carried out at ambient conditions. The sonochemical synthesis of rare earth phosphate nanomaterials has been investigated in aqueous solutions without additional surfactant or chelating agents. The current results are to some extent very similar to those of the hydrothermal routes. Brown et al. reported the sonochemical synthesis of hexagonal $\text{LaPO}_4\text{:Ce}$ NRs and NPs, at pH 1 and 12, respectively (Brown et al., 2005). Zhu et al. reported a sonochemical synthesis of $\text{CePO}_4\text{:Tb}$ NRs $\text{CePO}_4\text{:Tb@LaPO}_4$ core/shell NRs under ambient conditions for 2 h (Zhu et al., 2006). The crystallinity and uniformity of the NRs are relatively high, though a substantial reduction in reaction time and temperature is used compared with the hydrothermal process. Yu et al. reported a sonochemical synthesis of LnPO_4 ($\text{Ln} = \text{La, Ce, Pr, Nd, Sm, Eu, Gd, Tb, Dy, Ho}$) NCs under ambient conditions without any surfactant or template. The hexagonal phase products ($\text{Ln} = \text{La, Ce, Pr, Nd, Sm, Eu, Gd}$) exhibit NR bundles morphology, and the tetragonal phase products ($\text{Ln} = \text{Tb, Dy, Ho}$) exhibit NP morphology (Yu et al., 2008a).

The surfactants, chelating agents, as well as block copolymers are used to control and tune the size and shape of rare earth phosphate NCs. Bu et al. reported a P123-assisted hydrothermal synthesis of $\text{CePO}_4\text{:Tb}$ single-crystalline thin NRs of 10–12 nm in width. The surfactant Pluronic P123 was found to play a crucial role both to improve luminescence properties and NC homogeneity (Bu et al., 2004). When the pH value of reaction system is adjusted to below 1.0, uniform spindle like NW bundles of LaPO_4 could be obtained (Bu et al., 2007). Zhang et al. (Guan et al., 2007) reported the synthesis of hollow and core-shell microspheres composed of single-crystal NRs fabricated by a P123 and $\text{H}_6\text{P}_4\text{O}_{13}$ assisted route.

Nishihama et al. reported the synthesis of submicron hexagonal rare earth orthophosphate fine particles using an emulsion liquid membrane system consisting of Span 83 (sorbitan sesquioleate) as surfactant and EHPNA (2-ethylhexyl phosphonic acid mono-2-ethylhexyl ester) as extractant (cation carrier). The fine particles obtained were changed to monoclinic structure by calcination at 1373 K (Nishihama et al., 2002). Cao et al. reported the synthesis of LaPO_4 and CePO_4 NR/NWs in a microemulsion system (Cao et al., 2005). Xing et al. reported the synthesis of uniform CePO_4 NRs by reaction of aqueous $[(\text{CTA})_3\text{PO}_4]$ micelles with

[Ce(AOT)₃] reverse micelles prepared in isooctane (Xing *et al.*, 2006). Ghosh *et al.* reported the synthesis of LaPO₄:Er,Yb and LaPO₄:Er@YbPO₄ NP and NRs using a reverse micelles system (Ghosh *et al.*, 2008).

Buissette *et al.* reported the aqueous colloidal synthesis of LaPO₄:Ce, Tb and LaPO₄:Eu NPs assisted with tripolyphosphate (Na₅P₃O₁₀, TPP). The rare earth nitrate solutions are mixed with TPP and aged at 90 °C to form colloidal suspensions. The excess ions are removed by dialyzing (Buissette *et al.*, 2004). TPP acts as both complexing agent and orthophosphate precursor. The complexing agents like TPP or citrate acid (Boakye *et al.*, 2005) greatly increase the stability of colloidal solutions and enable the applications for various luminescent devices. Li *et al.* reported an OA-assisted solvothermal routes in mixed solution of water and ethanol for the synthesis of uniform hexagonal RPO₄·*n*H₂O NCs at 140 °C (Huo *et al.*, 2007; Figure 29).

In order to obtain bulk materials, nanocrystalline materials, and films, the sol-gel processes were exploited for the synthesis of rare earth phosphates. The rare earth phosphates deposited from aqueous solution usually contain hydrated phases, while the preferred dehydrates are obtained after postheat treatment. For example, Yu *et al.* reported doped LaPO₄ films on the silicon or quartz substrate fabricated via a Pechini sol-gel and dip-coating method. The films are further patterned with soft lithography. After annealing, pure monazite phase products with high luminescent efficiency are obtained (Yu *et al.*, 2003). Nanocrystalline CePO₄ with an average particle size of 50 nm is synthesized from cerium

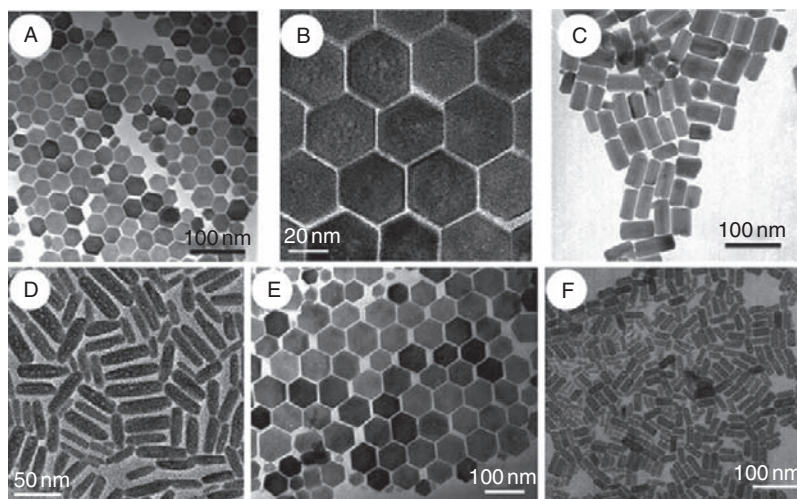


FIGURE 29 TEM image of RPO₄·*n*H₂O NCs: (A) Dy, (B) Er, (C) Ho, (D) Tm, (E) Yb, and (F) Lu. Reprinted with permission from Huo *et al.* (2007). Copyright 2007 Wiley-VCH.

nitrate and orthophosphoric acid by a sol-gel process involving controlled precipitation followed by peptization using nitric acid and deagglomeration of sol particles using ultrasonication (Rajesh et al., 2004). $\text{LaPO}_4\text{:Eu}^{3+}$ NPs sols are synthesized through an EDTA mediated method with pH values of 8.5–9. The sols are deposited onto substrate with porous alumina membrane templates of varied average pore diameters. After a short-time of permeation and aging, the gel forms in the template. After removing the template, nanotubes with sizes of 20–200 nm are synthesized (Fisher et al., 2008).

The assembly behavior during the synthesis of rare earth orthophosphates has been observed. Li et al. (2008g) reported a one pot synthesis of CePO_4 NWs attached to CeO_2 octahedral micrometer crystals. $\text{Ce}(\text{NO}_3)_3 \cdot 6\text{H}_2\text{O}$ and $(\text{NH}_4)_2\text{HPO}_4$ are used in a molar ratio of 2:1, pH value is tuned to be about 1, and the treatment temperature is 180 °C. The authors reported that the photoluminescence properties of CePO_4 NWs attached to CeO_2 octahedral micrometer crystals are enhanced strongly in comparison with pure CePO_4 NWs. Tang et al. (Li et al., 2007b) reported the formation of 1D nanostructures via the oriented linear aggregation of $\text{LaPO}_4\text{:Ce,Tb}$ luminescent NPs. Rare earth nitrates and $(\text{NH}_4)_2\text{HPO}_4$ are mixed with a pH value less than 1 and adjusted to 9.0 to form lanthanum phosphate colloidal suspension, followed by aging at room temperature for more than 1 day to obtain NPs. A 1% aqueous suspension of the NPs was prepared and the linear aggregation of these particles was initiated by lowering the pH value of the suspension to 2.0 with different aggregation periods of 1–7 days. The authors reported that the oriented aggregation of nanophosphors can significantly enhance the luminescent efficiency. Yeh et al. (Huang et al., 2008a) reported a low temperature solution reflux synthesis of GdPO_4 NRs. KH_2PO_4 was dissolved in aqueous solution with small amount of ethanol and refluxed at 88 °C with addition of GdCl_3 aqueous solution. Highly viscous $\text{GdPO}_4 \cdot \text{H}_2\text{O}$ hydrogels were prepared by suspending $\text{GdPO}_4 \cdot \text{H}_2\text{O}$ NRs in distilled water, where the as-prepared $\text{GdPO}_4 \cdot \text{H}_2\text{O}$ NRs with a length of 200–300 nm would aggregate and self-assemble into NWs extending over micrometers.

3.1.1.2 Nonaqueous solution methods The syntheses of rare earth phosphate NCs in nonaqueous solutions mainly include the solvothermal method, polyol method, the synthesis in ionic liquids, and the synthesis in high-boiling coordinating solvents like TOPO or OA.

The polyol method could be applied to synthesis $\text{LaPO}_4\text{:Ce,Tb}$ and other rare earth orthophosphate NCs. The so-called polyol method is the precipitation of a solid while heating sufficient precursors in multivalent and high-boiling alcohol like diethylene glycol (DEG) with a boiling point of 246 °C. Therefore, spherical NPs of 20–300 nm in size, usually metal

oxides, are typically obtained. For $\text{LaPO}_4\cdot\text{Ce,Tb}$, a typical size of 30–40 nm was obtained after the reaction at 190 °C (Feldmann, 2003).

Feldmann *et al.* developed the synthesis route based on ionic liquids (ILs) as reaction media to obtain luminescent rare earth phosphate NCs. In recent years, ILs have attracted considerable research interest because of their exceptional features including wide liquid range, high thermal stability, non-coordinating effect, high electrochemical stability, as well as adjustable polarity. ILs have been applied in the synthesis of organic molecules and inorganic NC. The synthesis usually starts with a solution of rare earth chlorides in IL tributylmethylammonium triflylimide and a cosolvent (for example, ethanol, dimethylformamide (DMF), dimethyl sulfoxide (DMSO), or pyridine). This rare earth solution is added to the phosphate precursor solution in IL and cosolvent at a temperature of 70 °C and the rare earth phosphate precipitate forms immediately. Then, the mixture is heated to 300 °C within 10 s by microwave to allow the NCs to crystallize. The obtained NCs were redispersible in ethanol. $\text{LaPO}_4\cdot\text{Ce,Tb}$ NC phosphors of 9–12 nm in size are obtained this way and the products exhibit Tb related quantum yields of 70% (Bühler and Feldmann, 2006; Figure 30). The obtained colloidal luminescent NCs show capability of constructing devices through inkjet printing and applications in dielectric barrier discharge lamp as “luminescent windows” (Bühler and Feldmann, 2007; Zharkouskaya *et al.*, 2008).

The synthesis in high-boiling coordinating solvents gives out a number of advantageous features for the synthesis of doped REPO_4 NCs. The binding of the solvent molecules to particle surface allows the particles to be well-separated and dispersible in a range of solvents to be colloidal solutions. In such a synthesis processes, with optimized process parameters like concentration and temperature, in addition to a suitable solvent or mixed solvent chosen for the reaction, the obtained NPs exhibit pure phase, high crystallinity, uniform shape, narrow particle size distribution, and properties suitable for applications. Doped RPO_4 with their interesting luminescence properties could be made as colloidal NCs via the synthesis process in high boiling solvents.

Haase and coworkers presented a series of works on the synthesis of rare earth phosphate and related materials in high-boiling coordinating solvents (Riwotzki *et al.*, 2001). For a typical process, the hydrated rare earth salts are dissolved and mixed in a methanol solution with appropriated high-boiling solvents. Later, methanol and water are distilled out at a moderate temperature. Dry phosphoric acid in high-boiling solvent is then added, and the reaction is carried out at high temperature. When the reaction is finished, that is, the controlled reaction time runs out, the solution is cooled down and usually, a transparent colloidal solution is obtained. Afterwards, the NCs would be separated with precipitation method by adding suitable solvents such as methanol. Since the obtained

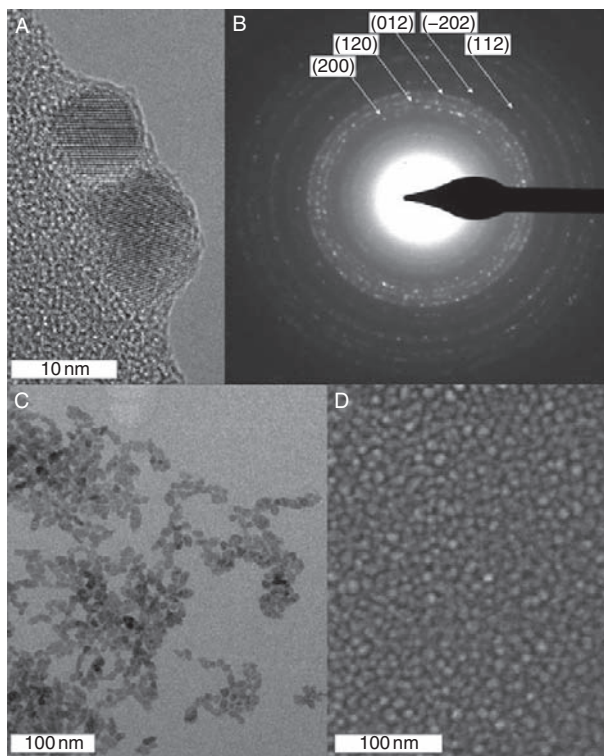


FIGURE 30 TEM and SEM images of the $\text{LaPO}_4:\text{Ce,Tb}$ NCs prepared in ionic liquids: (A) high-resolution TEM image; (B) electron diffraction pattern; (C) TEM, and (D) SEM images. Reprinted with permission from Bühler and Feldmann (2006). Copyright 2006 Wiley-VCH.

NCs are covered with solvent molecules, they could be re-dispersed in suitable solvents. $\text{LaPO}_4:\text{Eu}$ and $\text{CePO}_4:\text{Tb}$ colloidal NPs are synthesized in tris(ethylhexyl)phosphate, RCl_3 , H_3PO_4 , and trioctylamine are dissolved in tris(ethylhexyl)phosphate to form a colorless transparent liquid, and then the liquid is degassed and heated to refluxing. The initial temperature is $200\text{ }^\circ\text{C}$, while during the reaction some of the tris(ethylhexyl)phosphate are cleaved and the temperature drops to $170\text{--}180\text{ }^\circ\text{C}$. The NPs could be collected by adding methanol to the transparent colloid. The precipitated NPs could be redispersed in propanol with small quantity of tetrabutylammonium hydroxide methanol solution (Riwotzki et al., 2000). $\text{LaPO}_4:\text{Ce,Tb}$ colloidal NPs are also synthesized by the same method (Riwotzki et al., 2001). $\text{RCl}_3 \cdot n\text{H}_2\text{O}$ methanol solution is mixed with tributyl phosphate and diphenyl ether followed by the distillation of methanol and water. Then, trihexylamine and dry phosphoric acid in dihexyl ether are added, and the mixture is heated to $200\text{ }^\circ\text{C}$ and kept

under dry nitrogen for 2 h. After that, the doped RPO_4 NPs with dispersibility to be colloid in nonpolar solvents are obtained via repeated filtration pressed under N_2 and rotary evaporation (Lehmann *et al.*, 2003). This method was successfully applied by Heer *et al.* to synthesize colloidal NPs of $\text{LuPO}_4:\text{Er}$, $\text{YbPO}_4:\text{Er}$, $\text{LuPO}_4:\text{Yb,Er}$ and these doped NPs show upconversion photo luminescence properties (Heer *et al.*, 2003). The as prepared $\text{CePO}_4:\text{Tb}$ colloidal NPs could be used in the synthesis of core/shell NPs of $\text{CePO}_4:\text{Tb}@\text{LaPO}_4$ in a secondary synthesis process, where the phosphoric acid and La^{3+} are added to the core NPs colloidal solution step by step at 200°C (Kompe *et al.*, 2003; Figure 31).

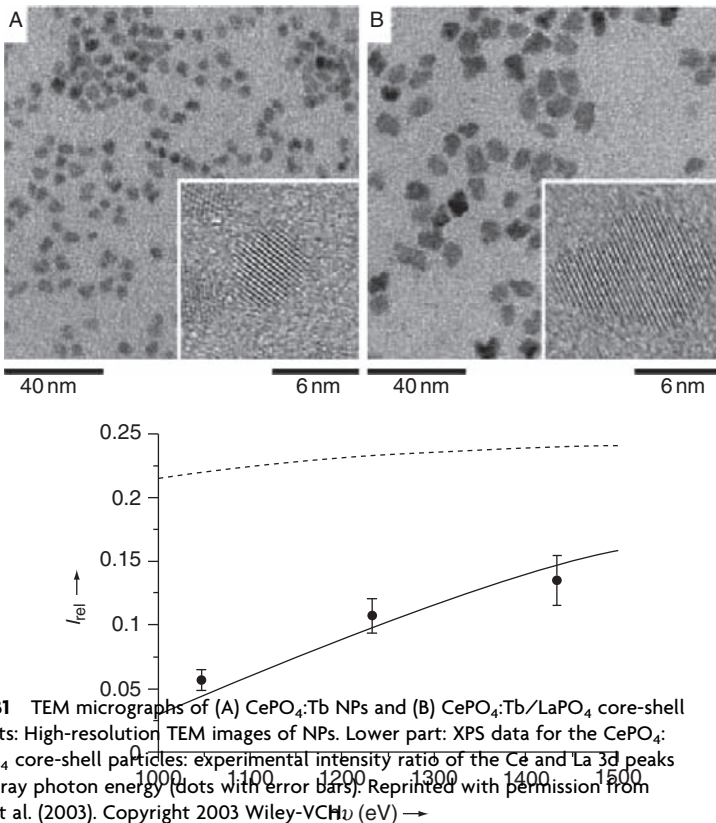


FIGURE 31 TEM micrographs of (A) $\text{CePO}_4:\text{Tb}$ NPs and (B) $\text{CePO}_4:\text{Tb}@\text{LaPO}_4$ core-shell NPs. Insets: High-resolution TEM images of NPs. Lower part: XPS data for the $\text{CePO}_4:\text{Tb}@\text{LaPO}_4$ core-shell particles: experimental intensity ratio of the Ce and La 3d peaks versus X-ray photon energy (dots with error bars). Reprinted with permission from Kompe *et al.* (2003). Copyright 2003 Wiley-VCH. $h\nu$ (eV) \rightarrow

Using the colloidal luminescent $\text{LaPO}_4\cdot\text{R}$ ($\text{R} = \text{Ce}, \text{Tb}, \text{Eu}, \text{and Dy}$) NPs (Riwotzki et al., 2000), nanostructured thin films on planar quartz supports as well as on polystyrene (PS) microspheres are fabricated by electrostatically assembling aided by oppositely charged polyelectrolyte interlayers (Schuetz and Caruso, 2002).

The thin films of those obtained RPO_4 NPs of 2–5 nm in size could be fabricated via spin coating. Therefore, the NEXAFS studies could be carried out (Suljoti et al., 2008). The results show that the light lanthanides tend to form monoclinic monazite phase of 3–5 nm in size and the heavy lanthanides tend to form the tetragonal zircon phase of 3–5 nm in size, while the medium lanthanides tend to form a mixture of the two phases with 2 nm in sizes.

A series of high-quality dispersible RPO_4 NCs with shapes of nanopolyhedra, quasinanorods, NRs, and NWs are synthesized at 180–260 °C in oleic acid and oleylamine solvents via a limited anion-exchange mechanism (Mai et al., 2007; Figure 32).

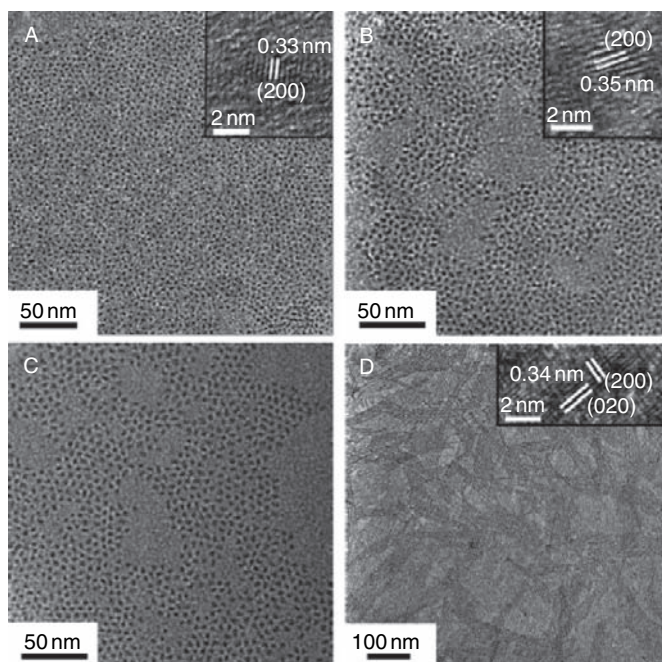


FIGURE 32 TEM and HRTEM images (insets) of (A) LaPO_4 polyhedra and (B) EuPO_4 polyhedra. (C) TEM image of TbPO_4 polyhedra. (D) TEM and HRTEM images (inset) of YPO_4 NWs. Reprinted with permission from Mai et al. (2007). Copyright 2007 American Chemical Society.

3.1.1.3 Dry routes The combustion technique is used to produce very fine, high-purity, crystalline oxide powders in recent years and the products may be homogeneous, unagglomerated, and multicomponent. Typically, the combustion synthesis starts with an aqueous solution containing a suitable organic fuel and corresponding metal salts like nitrates. The mixture solution is heated to boil until the mixture ignites, therefore, a self-sustaining rapid combustion reaction (exothermic but nonexplosive) takes place, and a dry, usually crystalline fine powder is produced.

Gallini *et al.* reported the combustion synthesis of monazite type $\text{LaPO}_4:\text{Sr}^{2+}$ NPs using $\text{La}(\text{NO}_3)_3$, $\text{Sr}(\text{NO}_3)_2$, and $(\text{NH}_4)_2\text{HPO}_4$ precursors with urea as fuel (Gallini *et al.*, 2005). $\text{LaPO}_4:\text{Sr}$ NPs have potential applications as protonic conductor in fuel cells and humidity sensors, for which the purity of materials is especially important. The solution based syntheses usually introduce impurities like phosphate acid, hydrated phase, NH_4NO_3 , or HNO_3 , which could only be removed after calcination at high temperature. Therefore, by the facile combustion method, the contamination is avoided and high quality products are obtained.

Liu *et al.* reported the combustion synthesis of 30–50 nm sized luminescent tetragonal $\text{YPO}_4:\text{Nd}^{3+}$ NPs (Liu *et al.*, 2008b). The obtained NCs exhibited spherical morphology with some agglomeration. The luminescence intensities strongly depended on the concentration of Nd^{3+} and the ratio of urea to Y^{3+} .

Ball milling is another widely used dry method to get NCs. Rhabdophane-type $\text{LaPO}_4 \cdot n\text{H}_2\text{O}$ NCs are obtained by ball milling a mixture of $\text{La}(\text{NO}_3)_3 \cdot 6\text{H}_2\text{O}$ and Na_2HPO_4 for 3 h. Mostly, the needle-like morphology is obtained. These rhabdophane NCs could be converted into monazite type particles after calcination at 600 °C (Diaz-Guillen *et al.*, 2007).

As noted above, rare earth orthophosphate hydrates could be converted into dehydrated phased through appropriate heat treatment. Rhabdophane type of rare earth orthophosphates could also be converted into monazite or xenotime phase via calcination. For La–Tb, rhabdophane NRs or NWs are converted into monazite type NRs or NWs after calcination at 900 °C in air for 3 h (Fang *et al.*, 2003b). The calcination may result in a significant increase in particle size (Zollfrank *et al.*, 2008).

Electrospinning is a simple and versatile method for generating ultra-thin fibers for a large variety of materials including polymers, composites, and ceramics (Li and Xia, 2004). Hou *et al.* (2009) reported the preparation of doped LaPO_4 nanofibers and microbelts through a combined sol-gel and electrospinning process. The obtained nanofibers and microbelts are made up of small NPs.

3.1.2 Properties and applications of rare earth phosphate nanomaterials

3.1.2.1 Luminescence Buissette et al. (2006a) presented a feature article on the aqueous colloidal synthesis and luminescence of rare earth phosphates and vanadates, which could be a good reference for the works in this field.

Among rare earth phosphates, $\text{LaPO}_4:\text{Ce,Tb}$ is the most well-known and commercially used green phosphors in fluorescent lamps. The strong green emission of $\text{LaPO}_4:\text{Ce,Tb}$ comes from the $^5\text{D}_4 \rightarrow ^7\text{F}_j$ ($J = 6, 5, 4, 3$) transitions of Tb^{3+} with the strongest peak located around 543 nm with $J = 5$. The LaPO_4 host absorbs UV excitation efficiently while the coactivator Ce^{3+} helps to pass this energy to Tb^{3+} through a wide $4f \rightarrow 5d$ transition band located around 330 nm. Various forms of $\text{LaPO}_4:\text{Ce,Tb}$ nanophosphors have been studied in recent important works, such as colloidal NCs (Riwotzki et al., 2000, 2001), further electrostatically assembled and patterned ultrathin films (Schuetz and Caruso, 2002; Yu et al., 2003), and coating on ceramic fibers (Chawla et al., 2000).

The $\text{LaPO}_4:\text{Ce,Tb}$ NCs display the same spectral features compared with bulk materials and the same energy transfer from Ce^{3+} to Tb^{3+} was observed (Meysamy et al., 1999). As discussed above, the NCs synthesized through well controlled aqueous or nonaqueous routes could be dispersible in appropriate solvent to form colloidal solutions, gaining this capability by surface modification or chelating with selected molecules. However, the NCs exhibit lower luminescent intensity and quantum efficiencies due to the energy transfer and loss to the defects, considering the large surface area in nano systems. The quantum yields are strongly affected by the solvent and particle surface termination (Stouwdam et al., 2003).

In order to improve the luminescence efficiency, core/shell structures are fabricated. Kompe et al. (2003, 2006) reported the $\text{CePO}_4:\text{Tb}/\text{LaPO}_4$ core-shell NPs, where the core $\text{CePO}_4:\text{Tb}$ NPs are coated with a layer of LaPO_4 . The photoluminescence quantum yield had a drastic increase from 43% for the core particle to 70% for the core-shell NPs, which is comparable to the bulk materials. Other ways of manipulating the surface status such as fabrication of silica coated NPs (Yu et al., 2006a) and surface modifications (Stouwdam and van Veggel, 2004), are also studied for the enhancement of luminescent properties. Notably, the core/shell NPs still exhibit the same emission spectra compared with $\text{LaPO}_4:\text{Ce,Tb}$. Compared with the NPs, the $\text{LaPO}_4:\text{Ce,Tb}$ NWs, submicron rods mainly exhibit similar spectra (Yu et al., 2005a). The so-called nano cable or core-shell structured NWs are fabricated through multiple steps of synthesis and the luminescence was also enhanced (Bu et al., 2005; Fang et al., 2005a; Zhu et al., 2006).

Surface modifications of NCs can enhance their solubility in a range of solvents, enable the biofunctionalization, protect the surface ions from oxidation, or improve the photoluminescence properties. The coordinated organic ligands can be modified by a quantitative exchange reaction in solution or by introducing functionalized ligands during the synthesis. Aqueous colloidal solution of rhabdophane core/shell structured $\text{LaPO}_4 \cdot x\text{H}_2\text{O}$ around Ce^{3+} and Tb^{3+} doped NPs is prepared with TPP salts both as phosphate source and stabilizing agents (Buissette *et al.*, 2006b). Stouwdam and van Veggel reported the surface modification of luminescent LaPO_4 and LaF_3 NPs (Stouwdam and van Veggel, 2004). The surface of as-prepared LaPO_4 NPs consists of phosphate groups and some bound ethylhexyl chains left before surface modification and the NPs was soluble in polar aprotic solvents, like dimethylformamide (DMF) and dimethyl sulfoxide (DMSO). The surface modification of LaPO_4 NPs was made with activation of OPCl_3 and subsequent reaction with dodecanol. After the modification, the NPs were dispersible in nonpolar solvents like toluene, dichloromethane, and chloroform. The NPs can be solubilized in methanol and 2-propanol, by the addition of tetraalkylammonium hydroxides while the addition of tetraalkylammonium bromides have no effect, showing that the base is necessary to deprotonate the surface OH groups to obtain negatively charged surface capable of attracting the tetraalkylammonium cations for the solubility.

The Ce exhibits a +3 valence in CePO_4 which is driven by the thermodynamics. However, Ce could be partially oxidized to +4 valence, which would greatly affect the photoluminescence in the phosphate nanophosphors. Li and Yam reported the utilization of +4 valenced Ce to develop a redox luminescence switch (Li and Yam, 2007; Figure 33). A room temperature aqueous precipitation protocol was performed to obtain urchin like NW assemblies of $\text{CePO}_4:\text{Tb}$. The samples showed strong green PL emission under UV excitation (256 nm), when KMnO_4 is added to oxidize the surface Ce to +4 valence, the emission vanished while when ascorbic acid is added to reduce the Ce ions, the PL emission recovered.

The luminescent spectroscopic studies are frequently reported on Eu^{3+} doped NCs, for example, $\text{LaPO}_4:\text{Eu}$ while other doped systems are also studied. Van Veggel *et al.* (Stouwdam *et al.*, 2003) studied the luminescent properties of RPO_4 NCs doped with a series of R^{3+} cations, which were obtained by a colloidal synthesis in high boiling solvents (Riwotzki *et al.*, 2000, 2001). In the doped NCs, the lanthanide ions are incorporated in the inorganic host of the particles to substitute the site occupied by host R^{3+} . The luminescent lifetimes of the activator ions are increased by orders of magnitude compared to those in organic complexes, showing the effective shielding of the lanthanide ions from nonradiative decay of the excited state through the vibrations of the solvents.

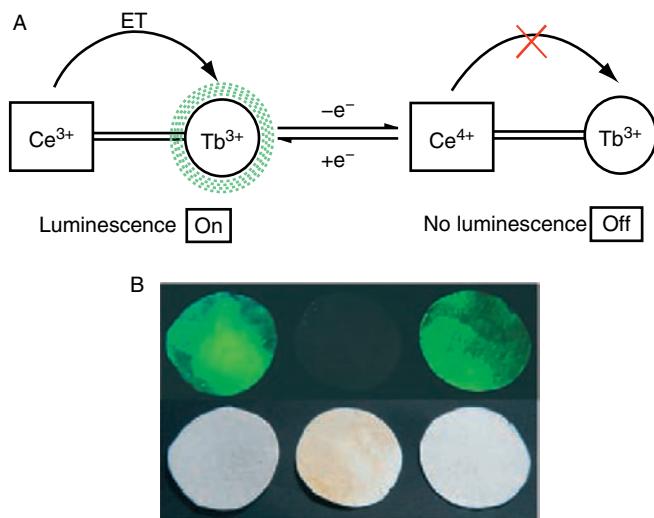


FIGURE 33 The redox luminescence switch based on the $\text{CePO}_4\text{:Tb}$ NWs. (A) the illustration. (B) Photographs: samples of $\text{CePO}_4\text{:Tb}$ (left), $\text{CePO}_4\text{:Tb} + \text{KMnO}_4$ (middle), and $\text{CePO}_4\text{:Tb} + \text{KMnO}_4 + \text{ascorbic acid}$ (right); impregnated on filter paper with (top) and without (bottom) UV irradiation. Reprinted with permission from Li and Yam (2007). Copyright 2007 Wiley-VCH.

Eu^{3+} ion was often used as a probe to detect the crystal environment in which the ion is located. In LaPO_4 , Eu^{3+} can be excited at 260 nm because of a charge transfer band caused by the electron transfer in the $\text{Eu}^{3+}\text{-O}^{2-}$ bond. In the emission spectrum of Eu^{3+} , the ratio of the different peaks of the ${}^5\text{D}_0 \rightarrow {}^7\text{F}_j$ ($J = 1, 2$) transitions gives information about the symmetry of the crystal site in which Eu^{3+} is located, which is C_1 in the monazite type LaPO_4 , the same as in the bulk materials (Stouwdam et al., 2003).

The luminescence decay rate also gives information on the influence of quenching from the organic solvent and ligand outside the particle and impurities from inside the particle. The decay curve of $\text{LaPO}_4\text{:Eu}$ could be acceptably fitted with two exponentials, however, the effect of quenching from the solvent and the ligand on the surface should not be considered as “only two” exponentials. Van Veggel et al. proposed a model to interpret the luminescence decay results successfully (Stouwdam et al., 2003). The effect of surface is considered with dividing a particle into a number of shells, and relating the lifetimes of different shells with an effective radiative lifetime and a quenching factor depending on the distance to the surface. In addition, van Veggel et al. discussed the effect of the difference in refractive index between the NC and the surroundings. Such difference would have effect on the long component of the two lifetimes, not on the short one which is mostly determined by surface quenching.

The structure of doped LaPO_4 core/shell NPs are studied by constructing the $\text{LaPO}_4:\text{Eu}$ core/shell NPs. Haase *et al.* reported the $\text{LaPO}_4:\text{Eu}$ core/shell NPs obtained from high-boiling coordinating solvents mixture (Lehmann *et al.*, 2004). Up to three different lattice sites could be identified in the interior of LaPO_4 NPs by site-selective spectroscopy, which is not known from bulk LaPO_4 . There are also surface sites, which could be converted into bulk sites by the shell fabrication, and obtained by the reaction of Eu^{3+} with pure LaPO_4 NPs. The differently shaped $\text{RPO}_4:\text{Eu}^{3+}$ NCs would exhibit different sites and therefore varied spectroscopic features. For example, $\text{LaPO}_4:\text{Eu}$ NWs show a strong emission about 625 nm which is different from $\text{LaPO}_4:\text{Eu}$ NPs (Song *et al.*, 2004; Yu *et al.*, 2004a,b).

In addition, the NIR emission spectra of Nd^{3+} , Er^{3+} , Pr^{3+} , Ho^{3+} are also discussed by van Veggel *et al.* The differences in the luminescence spectra are smaller than that for Eu^{3+} compared with bulk materials or coordinating complexes. The variation in local crystal symmetry leads to the change in emission peak shapes and relative intensities. There are also studies on Dy doped YPO_4 NCs, for example, which are synthesized via coprecipitation (Lai *et al.*, 2008) or combustion routes (Xiu *et al.*, 2006).

The upconversion RPO_4 NCs have been fabricated in the form of colloidal NPs (Heer *et al.*, 2003; Figure 34), organic/inorganic nanocomposite sol-gel films (Ahn *et al.*, 2006), or polymer matrix embedded NPs (Jung *et al.*, 2005). The hexagonal NaYF_4 presents low phonon energy and is a good host for rare earth upconversion materials, which will be discussed in Section 4.

3.1.2.2 Biosensing Nanoparticles conjugated with biomolecules have shown great potential in biomedical applications. Inorganic fluorescent NPs have attracted attention from biologists. Quantum dots (QDs) have shown their advantages like tunable size and composition dependent luminescence, narrow emission bandwidth, high quantum yield, considerable chemical and photo-stability, single source excitation with multiplex detection, as well as size comparable with biomolecules (<10 nm). Therefore, the QD bioconjugates are used in the fluorescent imaging of cells, immunoassay, single molecule detection, and so on. The shortcomings of QDs such as the hydrophobicity, toxicity, and high cost of synthesis still calls for new bio-labeling materials. Rare earth nanomaterials can display sharp fluorescent emission and high stability for chemical environment or photo-bleaching and are therefore proposed as a class of attractive candidates.

Haase *et al.* obtained the monodisperse fluorescent NPs of doped LaPO_4 through hydrothermal reactions, solvothermal methods, or precipitation in high-boiling solvents (Meyssamy *et al.*, 1999; Riwozki *et al.*, 2000, 2001). Caruso *et al.* demonstrated biofunctionalization of nano-sized

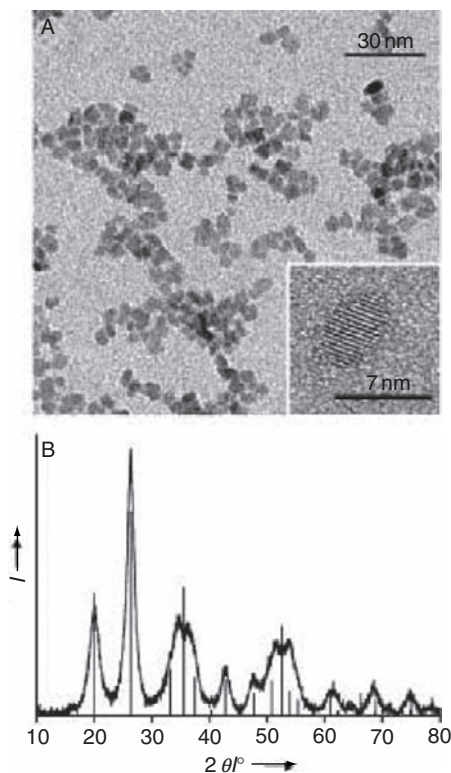


FIGURE 34 (A) TEM micrograph of $\text{LuPO}_4:49\%\text{Yb},1\%\text{Tm}$ NCs. Inset: High-resolution image of a nanocrystal. (B) Powder XRD pattern of $\text{LuPO}_4:49\%\text{Yb},1\%\text{Tm}$ NCs. The line spectrum corresponds to the literature data of bulk LuPO_4 (PDF No. 84–337 reference pattern, body-centered tetragonal, space group $I41/amd$). Reprinted with permission from Heer et al. (2003). Copyright 2003 Wiley-VCH.

fluorescent colloidal LaPO_4 NPs. $\text{LaPO}_4:\text{Ce},\text{Tb}$ NPs with green fluorescent emissions are dispersed in aqueous solution containing 6-aminohexanoic acid (AHA) to obtain AHA modified NPs. Then the NPs are conjugated to avidin, a model protein, to utilize the binding of avidin to biotin molecules (Meiser et al., 2004; Figure 35). The NP functionalization could be examined by analytical ultracentrifugation, microelectrophoresis, absorption and fluorescence spectroscopy, dynamic light scattering, as well as TEM observations.

The luminescence resonance energy transfer (LRET) system from lanthanide-doped NP donors and gold NP acceptors are constructed through electrostatic interactions between the oppositely charged NPs. The negatively charged water soluble $\text{YVO}_4:\text{Eu}$ and $\text{LaPO}_4:\text{Ce},\text{Tb}$ luminescent NPs are obtained through a polymer-assisted hydrothermal

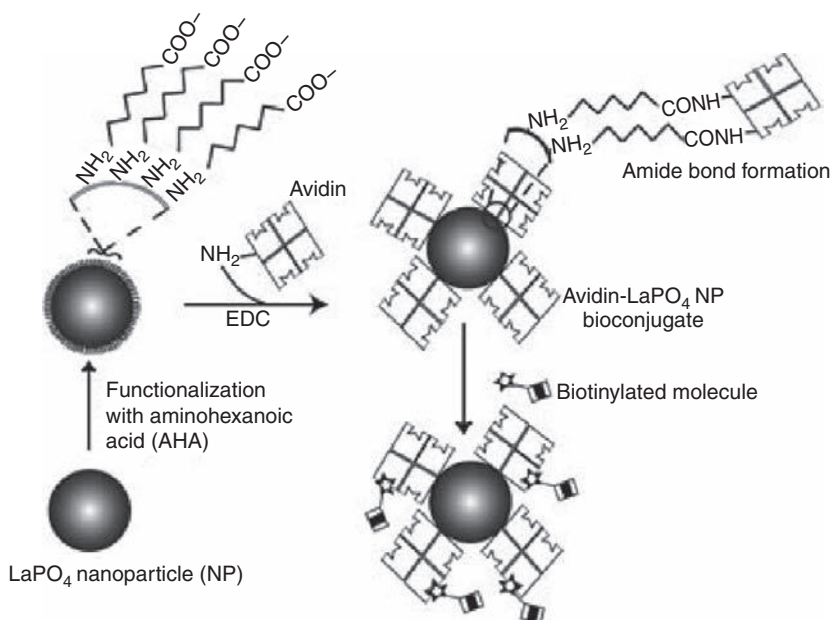
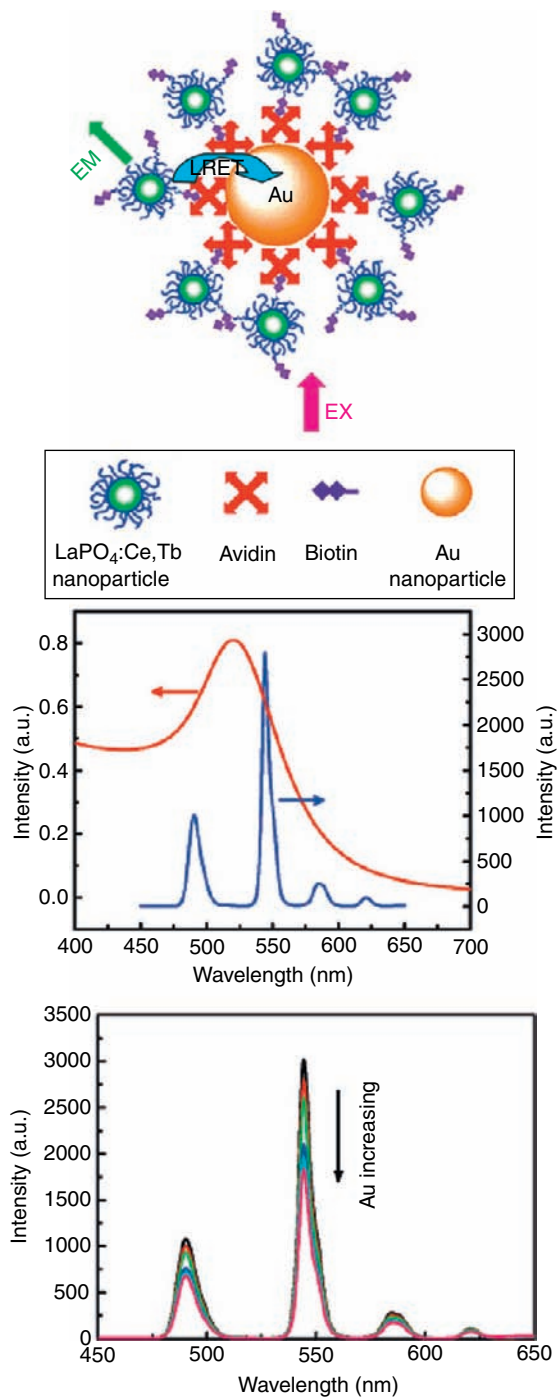


FIGURE 35 Schematic illustration showing the biofunctionalization of fluorescent Ce/Tb-doped LaPO₄ NPs with avidin. Reprinted with permission from Meiser *et al.* (2004). Copyright 2004 Wiley-VCH.

method. The positively charged polyhedral and spherical gold NPs, synthesized through a seed-mediated cetyltrimethylammonium bromide (CTAB)-assisted method, exhibit SPR bands centered at 623 and 535 nm, respectively. Assemblies of the oppositely charged donors and acceptors are developed into LRET-based sensors exhibiting donor quenching efficiency close to 100% (Gu *et al.*, 2008b). The LaPO₄:Ce,Tb NPs are paired with differently sized gold NPs through the well-established binding affinity of biotin and avidin. The spectral overlap between the emission of lanthanide NPs and the absorption of gold NPs meets the prerequisite for energy transfer, and the resonance energy transfer process is characterized by both steady-state and time decay luminescent measurements. (Gu *et al.*, 2008a; Figure 36) Wang *et al.* reported a fluorescence resonance energy-transfer (FRET) system with CePO₄:Tb³⁺ NCs as energy donor and Rhodamine B dye as energy acceptor (Wang *et al.*, 2008d).

The traditional radioimmunoassay technique could be utilized with rare earth phosphate NPs. Lin *et al.* reported the LuPO₄-apoferritin core-shell NPs synthesized in apoferritin templates. The NPs were further modified with biotin and exhibited affinity for streptavidin-modified magnetic beads or streptavidin-modified fluorescein isothiocyanate. Radioactive ¹⁷⁷Lu was used to label the NPs (Wu *et al.*, 2008a).

**FIGURE 36** (Continued)

In addition to NPs, other shaped NCs could also be used in biosensing. Patra *et al.* reported the attempt of using hexagonal $\text{EuPO}_4 \cdot n\text{H}_2\text{O}$ and $\text{TbPO}_4 \cdot n\text{H}_2\text{O}$ NRs for cell imaging. The red or green emitting NRs are internalized by the cells and localize mainly in the cytoplasm. Confocal fluorescence microscopy is used to give an image (Patra *et al.*, 2007). Meng *et al.* (2009) reported the synthesis of monoclinic CePO_4 nanotubes by a hydrothermal route and their application in biosensing. The heme proteins/enzymes with myoglobin were immobilized on the nanotubes and their electrochemistry properties were examined with voltammetry, showing applicability as biosensors.

3.1.2.3 Catalytic properties Phosphorus is known to have deactivation effects for some automotive catalysts and the formation of CePO_4 has been identified in phosphorus contaminated catalysts (Uy *et al.*, 2003). Nanocrystalline LaPO_4 would act as Lewis acid in a catalytic process, which could be determined by a temperature-programmed ammonia adsorption/desorption process (Onoda *et al.*, 2002; Rajesh *et al.*, 2004, 2007). In addition, the rare earth phosphate NCs could act as supports; for example, Pd, Pt, or Rh supported on RPO_4 show excellent catalytic reduction of NO into N_2 and O_2 (Tamai *et al.*, 2000), and gold supported on RPO_4 shows catalytic activity and stability for CO oxidation.

Dai *et al.* reported an ultra stable gold nanocatalyst supported on nanosized LaPO_4 particles (Yan *et al.*, 2006). The rhabdophane LaPO_4 NPs of 6–8 nm in size were synthesized by a sonication method (Brown *et al.*, 2005) and commercially purchased monazite LaPO_4 NPs of about 10 nm were used for comparison. The rhabdophane LaPO_4 -supported gold nanocatalysts exhibit high activity for low temperature CO oxidation, even after calcination at 500 °C which would deactivate a majority of these kinds of catalysts. Further study (Ma *et al.*, 2008b) on gold/phosphate catalysts, including a number of RPO_4 also shows high CO conversions below 50 °C as well as stability under 500 °C calcination.

3.2 Rare earth vanadates

Rare earth orthovanadates (RVO_4) typically include two isomorphous phase structures with rare earth orthophosphates, monoclinic (*m*-) monazite type, and tetragonal (*t*-) zircon type. The selectivity also relies on the

FIGURE 36 (A) Schematic illustration of the LRET process from the biotinylated LaPO_4 :Ce,Tb NPs to avidin-coated gold NPs based on the high affinity of biotin and avidin. (B) Extinction spectrum of colloidal gold NPs with a diameter of ca. 13 nm and emission spectrum of LaPO_4 :Ce,Tb NPs. (C) Evolution of emission intensity of biotinylated LaPO_4 :Ce,Tb NPs with the addition of avidin coated gold NPs. Reprinted with permission from Gu *et al.* (2008a). Copyright 2008 American Chemical Society.

radius of R^{3+} , only that the zircon type is the stable phase for all rare earth orthovanadates while the monoclinic type exists for $LaVO_4$ and $CeVO_4$. Based on different lanthanide ion components, RVO_4 compounds exhibit unique optical, magnetic, catalytic, and electrical properties for various applications. Nevertheless, the optical characteristics are their most prominent feature. For example, single-crystalline yttrium orthovanadate is utilized as polarizer and laser host material, while its crystalline powder with europium dopant ($YVO_4:Eu^{3+}$) is the previous generation of red phosphor in cathode ray tubes and fluorescent lamps. Due to narrow excitation lines and low absorbency cross-section of Ln^{3+} , it is difficult to directly excite Ln^{3+} emitters. The host energy migration process of vanadate matrix overcomes this problem easily, which produces a strong charge-transfer absorption band located at 200–350 nm. The excited host could transfer its energy to adjacent emitters (i.e., Ln ions) via thermally activated migration, so most kinds of Ln emitters could be sensitized with a high efficiency.

Usually, industry adopts solid-state synthesis to produce rare earth orthovanadate, using rare earth oxide and vanadium pentoxide as raw materials. This method consumes too much energy, and the calcined products with extensive aggregation are inconvenient for refined machining. Over the past decade, there has been an upsurge to develop solution-phase preparation of crystalline ceramics. Some studies focus on the corresponding nanomaterials based on these wet chemical methods. In this section, we will discuss the RVO_4 nanomaterials grouped by different synthesis methodologies, including atmospheric aqueous method, hydrothermal method, microemulsion/modified hydrothermal method, microwave/ultrasonic irradiation method, and sol-gel method. Meanwhile, the properties and related applications of RVO_4 nanomaterials will be briefly discussed at the end of this section.

3.2.1 Synthesis

3.2.1.1 Ambient aqueous routes Due to the low water-solubility, rare earth vanadates could be obtained by aqueous precipitation reactions under ambient temperature and pressure. This facile route saves energy. The reaction pH value is the most important parameter for preparing rare earth vanadates in aqueous system. Below pH 8, the VO_4^{3-} anions easily polymerize into oligomers, such as $V_3O_9^{3-}$ and $V_{10}O_{28}^{6-}$, whereas a strong basic media generates a competition between rare earth vanadates and rare earth hydroxides byproducts. Hence the optimized pH value is commonly around 11 for the preparation of $REVO_4$ NCs.

Among numerous rare earth vanadate compounds, $YVO_4:Eu^{3+}$ has been investigated most for its value in practical use. Its bulk polycrystals could reach a quantum yield (QY) of ca. 70% as commercial red phosphor. Huignard et al. obtained *t*- $YVO_4:Eu^{3+}$ NPs with sizes around 15–30 nm

from room temperature coprecipitation of Y^{3+} , Eu^{3+} and VO_4^{3-} ions (Huignard *et al.*, 2000). By the aid of sodium hexametaphosphate, the as-prepared $YVO_4:Eu^{3+}$ NPs were further stabilized into a colloidal solution. Eu^{3+} quenching concentration increased and luminescence efficiency for nanosized $YVO_4:Eu^{3+}$ reduced. This was attributed to the nonradiative recombination from the surface defects. Succeeding hydrothermal aging could remedy this drawback to a certain extent.

To better confine the growth of $YVO_4:Eu^{3+}$ NPs, Huignard and co-workers added sodium citrate to R^{3+} solution before introduction of Na_3VO_4 (Huignard *et al.*, 2002). The competition for R^{3+} between chelation and precipitation led to the formation of ca. 10 nm NPs. The citrate groups also formed a capping layer to stabilize $YVO_4:Eu^{3+}$ NPs in water. Although the NPs were encapsulated by citrate ligands, surface energy quenching has obstructed the luminescent efficiency. An increased QY from D_2O dispersed $YVO_4:Eu^{3+}$ colloidal NPs suggested the quenching effect of water molecule (OH groups).

Further coating with a silicate shell could reduce the optimal doping ratio of europium, but also failed to prevent energy quenching. It seems that annealing was indispensable for the improvement of QY (Huignard *et al.*, 2003). By the aid of citrate, Isobe's group prepared *t*- $YVO_4:Bi^{3+}, Eu^{3+}$ NPs. The codoped Bi^{3+} acted as cosensitizer for Eu^{3+} through the energy transfer from Bi^{3+} 6s orbit to V^{5+} 3d orbit. This charge transfer process extended the excitation band to the region between 300 and 400 nm. Such excitation red shift potentially broadened the application of vanadate phosphor. However, the hydrolyzation of Bi^{3+} was a difficult problem while strong acid media did not suit the crystallization of rare earth vanadates. So Isobe *et al.* used bismuth (III) citrate compound instead, which was partially soluble in water. The reaction of Y–Eu–Bi citrates and Na_3VO_4 was carried out at 60 °C, with a pH value of 12.5. Considering bismuth (III) is markedly different from R^{3+} ions with respect to the physical and chemical properties, the authors carefully studied the variations of NPs structure, composition, and photoluminescence throughout the whole aging process. According to XRD and X-ray fluorescent data, the NPs crystallization was nearly accomplished post ca. 200 min of reaction. Polycrystalline *t*- $YVO_4:Bi^{3+}, Eu^{3+}$ NPs around 40 nm were observed under TEM. During the prolonged aging period, the ionic exchange induced an increase of Bi^{3+} and a decrease of Y^{3+} on NPs surface. The luminescence intensity also gradually decreased by increasing the aging time and the authors concluded that enriched Bi^{3+} ions near the NP surface could quench the transfer of energy (Takeshita *et al.*, 2008).

In ethanol/water media at 75 °C, van Veggel *et al.* prepared *t*- $LaVO_4$ NPs with series of Ln^{3+} dopants ($Ln = Eu, Tm, Nd, Er, Ho, Dy, Sm, Pr$). The coprecipitation reaction was administrated by adding $Ln(NO_3)_3$ aqueous solution into the ethanol/water mixture that contained Na_3VO_4

and $\text{NH}_4(n\text{-C}_{18}\text{H}_{37}\text{O})_2\text{PS}_2$. The ionized dithiophosphate acted as electro-negative ligand to limit the growth of LaVO_4 NPs. As a representative, $t\text{-LaVO}_4\cdot\text{Eu}^{3+}$ NPs had irregular shapes with a size around 6–10 nm. These NPs were soluble in nonpolar solvents due to the hydrophobic surface ligands (Stouwdam et al., 2005).

3.2.1.2 Hydrothermal routes Under ambient conditions, the low reaction temperature and fast precipitation rate have deleterious effect on the crystallization and optical performance of rare earth vanadate nanomaterials. Referring to traditional solid-state reactions, bulk $\text{YVO}_4\cdot\text{Eu}^{3+}$ phosphors require a calcinations temperature above 1300 K, but it is too high for the preparation of nanomaterials. Alternatively, hydrothermal routes could provide the adequate energy for solution phase reactions, which have been widely described in preparation of ceramic powders. The high pressure and temperature largely promote the dissolution–reprecipitation process, so as to decrease the lattice defects of NCs. With fine modulation, this method is also efficient to produce nano-sized crystals.

Riwotzki and Haase introduced hydrothermal method into preparation of rare earth vanadate NPs for the first time (Riwotzki and Haase, 1998). In the case of tetragonal phase $\text{YVO}_4\cdot\text{Eu}^{3+}$ NPs, Na_3VO_4 and a slight excess of $\text{Y}(\text{NO}_3)_3/\text{Eu}(\text{NO}_3)_3$ were mixed at ambient temperature, then the mixture was transferred to a Teflon vessel for a 200 °C hydrothermal aging at different pH value, that is, 4.8 and 12.5, respectively. Both the acid and basic conditions resulted in highly crystalline NPs in the size range of 10–30 nm, but the alkaline medium seemed to yield a product with better defined crystal facets and edges than that of the acidic medium. The spectral analysis verified that the Y^{3+} ions were randomly replaced by Eu^{3+} dopants without phase separation, the same as for the bulk materials.

YVO_4 matrix was also suitable for doping other Ln emitters. The YVO_4 NPs doped with Sm^{3+} or Dy^{3+} could be synthesized via a similar method (Haase et al., 2000; Riwotzki and Haase, 1998). Wu et al. systemically researched synthesis parameters for $t\text{-YVO}_4$ nano-/microcrystals, including reactant ratio, pH value, hydrothermal temperature, and aging duration. They used V_2O_5 powder as the vanadium source directly, which only started dissociating to produce VO_4^{3-} at hydrothermal conditions. The pH value had a major influence on the experimental results. In acidic medium, vanadate anions incorporated into a small quantity of oligomers as nuclei. The shortage of nuclei together with the fast migration of Y^{3+} ions then resulted in YVO_4 NCs. Contrarily, Y^{3+} cations formed a mass of $\text{Y}(\text{OH})_3$ nuclei in basic condition. It took time for VO_4^{3-} anions to corrode $\text{Y}(\text{OH})_3$ and so as to form YVO_4 NPs. As the minor factor, reactant stoichiometric ratio could influence the product purity. It was divided into two situations. In acidic system, only equal ratio of yttrium and vanadium resulted in pure YVO_4 . When the Y/V ratio was changed

from 1, $Y_8V_2O_{17}$ or V_2O_5 were detected. In basic solution, the excess V_2O_5 promoted the formation of $Y(OH)_3$ into YVO_4 . The remnant vanadium could be neutralized in the form of VO_4^{3-} . Thus $Y(OH)_3$ was the sole impurity due to the strong hydrolysis effect of rare earth ions. Furthermore, higher aging temperature and longer duration was preferred for the reaction completeness (Wu et al., 2003a).

Li and coworkers operated the hydrothermal route under extremely acidic conditions and observed single crystalline t - YVO_4 with nanobelt morphology. Compared with other growth directions, the crystal growth along the [010] direction seemed to be less perturbed by hydrated proton at pH value of 1. Below this acidity, polyhedron microcrystals were the primary product, which agree with previous reports (Li et al., 2008f).

Among the rare earth elements, cerium is an exception. The impurity of $CeVO_4$ NPs prepared under high alkaline conditions was CeO_2 , rather than cerium hydroxides, because $Ce(OH)_3$ was prone for dehydration and oxidation. Chen synthesized $CeVO_4$ NPs from NH_4VO_3 and $Ce(NO_3)_3$ in hydrothermal reactions with different pH (ranging from 9 to 14). The pH value of 12 was shown to be the upper threshold for pure vanadate NPs (Chen 2006).

In the absence of surfactants and chelating agents, materials generally exhibit their intrinsic nucleation and growth. However, for certain application, one needs to manipulate their crystallization behavior. Introducing chelating agent may be a powerful tool to restrict crystal growth and regulate the crystallization. Sun et al. adopted rare earth citrate as precursors in hydrothermal synthesis of t - $YVO_4:Er^{3+}$ NPs. Their experimental procedure was similar to that reported by Boilot et al., (Mialon et al., 2008) except that the crude precipitate NPs have gone through a 200 °C hydrothermal treatment. Via violent recrystallization, the 7 nm crude NPs with irregular shapes grew into 40 nm tetragonal NPs. It was believed that citrate anions accelerated the recrystallization process (Sun et al., 2006c).

Qian et al. compared the effect of several chelating agents in the hydrothermal synthesis system. The trisodium citrate (Na_3cit), sodium tartrate (Na_2tar) and sodium malate (Na_2mal) revealed different capability in morphology, mediation of YVO_4 nanomaterials. As coprecipitation precursors, Y^{3+}/mal^{2-} complex had the smallest hindrance for combining VO_4^{3-} , whereas Y^{3+}/cit^{3-} and Y^{3+}/tar^{2-} provided enough spatial hindrance to restrict the crystalline growth along the [100] and [010] directions. Therefore, Na_2mal induced small t - YVO_4 NPs with irregular shape. Similar morphology was observed in low concentration Na_3cit/Na_2tar conditions or without any additives. If the quantity of Na_3cit or Na_2tar was beyond twofold molar ratio of Y^{3+} , a preferential growth will arise to form t - YVO_4 nanoplates. Meanwhile, Na_3cit and Na_2tar assembled these nanoplates into hierarchical complex morphologies by electrostatic and coordinating effects (Figure 37). The heavy rare earth ions, like

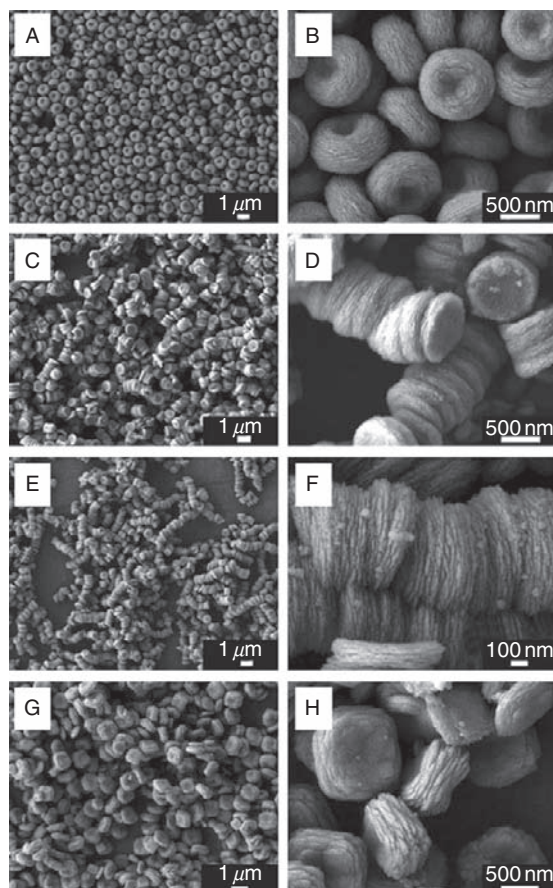


FIGURE 37 SEM images of monodisperse YVO_4 assemblies obtained from 24 h hydrothermal reaction at 140°C . Different chelating agents were used. (A, b) 2:1 molar ratio of $\text{cit}^{3-}/\text{Y}^{3+}$; (C, D), 3:1 molar ratio of $\text{cit}^{3-}/\text{Y}^{3+}$; (E, F), 4:1 molar ratio of $\text{cit}^{3-}/\text{Y}^{3+}$; (G, H), 2:1 molar ratio of $\text{tar}^{2-}/\text{Y}^{3+}$. (Herein cit is for citrate and tar is for tartrate). Reprinted with permission from Qian et al. (2009). Copyright 2009 Wiley-VCH.

Dy^{3+} and Er^{3+} , have close ionic diameters to that of Y^{3+} , thus DyVO_4 and ErVO_4 exhibit similar morphology variation under the previous reaction conditions. The Ce^{3+} and Gd^{3+} are light lanthanide elements, and the preparation generated irregular CeVO_4 and GdVO_4 NPs (Qian et al., 2009).

Some coordinating polymers also have been used as chelating reagents. Chen et al. selected PVP to assist the hydrothermal preparation. With gradual increase of the alkalinity from pH 8 to 12, the aspect ratio of $\text{YVO}_4:\text{Eu}^{3+}$ NPs was decreased and their crystallinity was increased (Chen et al., 2006b). Yan et al. utilized phosphino polyacrylic acid (P-PAA) as both chelating agent and surface stabilizer. Its functional

mechanism was similar to that of citrate assisted hydrothermal system, but PPA also provided bigger steric and electrostatic repulsions to NPs than other small chelating molecules did. The colloidal NPs solution was directly obtained after the 180 °C hydrothermal treatment. Due to the surface protection from P-PAA, the *t*-YVO₄:Eu³⁺ NPs reached a total QY of ca. 54%, and could be well dispersed in buffer solution or pure water. The surface carboxyl groups of PPA also provided modifiable sites for succeeding functionalization (Gu et al., 2008a; Shen et al., 2008a).

To avoid the concentration quenching of Ln emitters, dilution cations (such as Y³⁺) are always necessary in rare earth luminescent materials. Gd³⁺ could also take this role due to its stable ground state with half-filled *f* shell. Actually, GdVO₄:Eu³⁺ and YVO₄:Eu³⁺ were both important commercial red-emitting phosphors. Wu and Yan codoped Gd³⁺ and Eu³⁺ into YVO₄ NPs by hydrothermal reaction without surfactant and chelating ligands. The NPs product had a mean particle size of ca. 180 nm. The Gd³⁺ was considered as potential sensitizer for Eu³⁺ dopants. The experimental data showed that the Y_xGd_{1-x}VO₄:Eu³⁺ NPs had an optimal luminescence intensity at *x* = 0.2 (Wu and Yan, 2008). Lanthanum has an empty 4*f* electron shell as the first element of Ln series. Its cation (La³⁺) is optically inert with the fully occupied electron configuration. Different from YVO₄, thermodynamically stable LaVO₄ exhibited monoclinic phase structure. However, Eu³⁺ needs higher coordination symmetry to reach the best performance. Since phase modulation is the first task for LaVO₄-based phosphors, wet chemistry routes and nano-sized materials become a possible way to archive this purpose. It is known that mild synthesis conditions could result in metastable polymorphs. Nanomaterials may not follow the rules followed by bulk materials.

Yan et al. used ethylenediamine tetra-acetic acid (EDTA) assisted hydrothermal method and obtained *t*-LaVO₄:Eu³⁺ NRs. The rod-like products had diameters distributed from 20 to 60 nm and lengths from 100 to 300 nm. The transformation from monazite phase to the metastable zircon structure dramatically enhanced the luminescence intensity of LaVO₄:Eu³⁺, validating the correlation between structure and properties of materials (Jia et al., 2004). They subsequently demonstrated the importance of chelating ligands in this phase transformation process. Weak coordinating ligands like sodium acetate or sodium citrate, only promote the crystallization of LaVO₄, but have little effect on the polymorph selection for the tetragonal phase. Chelating ligand EDTA (simplified as H₄A) evidently facilitates the formation of *t*-LaVO₄ NCs, because La³⁺ was forced to crystallize with smaller coordination number to depress the steric repulsion between A⁴⁻ ligands and lattice coordinating oxygen atoms at the lattice/solution interface. This inducement could be varied at different pH values based on the different coordination ability of H₃A⁻, H₂A²⁻, HA³⁻, and A⁴⁻. The thermal stability of nanosized *t*-LaVO₄ was

also enhanced. High-temperature XRD studies showed the critical point for *t*- to *m*- phase transition was 250 °C, which is higher than that of bulk compound. This characteristic also benefits the application as catalysts in oxidative dehydrogenation reactions (Jia et al., 2005).

Ma et al. omitted acid treatments and used V₂O₅ and La₂O₃ bulk powders in direct hydrothermal synthesis. Only EDTA mediated experiment could produce pure *t*-LaVO₄ NRs, or else, monoclinic phase product was obtained (Ma et al., 2008a). With EDTA-hydrothermal route, Wang et al. obtained high aspect ratio *t*-LaVO₄ NRs. It was presumed that the adsorption ability of EDTA on the (020) and the (200) planes of *t*-LaVO₄ was stronger than on the (002) planes, so that the anisotropic growth preferred the [001] direction. This inducing effect of EDTA required appropriate alkalinity for ligand deprotonation. Even at pH 9.0, there was a little *m*-LaVO₄ impurity mixed in the product due to the inefficient coordinating action. Too high pH value (the author used ammonia here) also perturbed the coordination, and the optimal pH value was locked in the range of 9.0–9.5. Additionally, this paper reported the interaction between crystallographic anisotropy of *t*-LaVO₄ NR and its magnetocrystalline anisotropy (Wang et al., 2007d).

EDTA was also used to control the size and morphology of *t*-CeVO₄ in hydrothermal reaction. Different morphologies like hollow woolen spheres, solid spheres, and NRs were observed via adjusting the hydrothermal temperature, solution pH and EDTA/Ce³⁺ ratio (Figure 38). Moreover, EDTA prevented the oxidation of Ce³⁺ ions during the hydrothermal treatment. The X-ray photoelectron spectral data showed that the surface Ce³⁺/(Ce³⁺ + Ce⁴⁺) ratio in the *t*-CeVO₄ NPs without EDTA was 0.95, that is, a little lower than in other samples with EDTA. The different distribution of cerium valence state was also detected in magnetic susceptibility measurement, based on the contribution from paramagnetic Ce³⁺ and diamagnetic Ce⁴⁺ (Luo et al., 2005). The CeVO₄ 1D NRs could be further converted into CeVO₃ NCs by deoxidization in flowing hydrogen (Luo et al., 2004).

LaVO₄ nanomaterials have also been prepared without chelating ligands or surfactants in hydrothermal systems. Sun and coworkers contributed several reports on this subject. NaVO₃ and La(NO₃)₃ were mixed to form a yellow suspension of *m*-LaVO₄ first. Then, the crude precipitates were transformed into *t*-LaVO₄ NRs during a 48 h hydrothermal treatment at 180 °C. The obtained NRs had average diameters of 20 nm and lengths close to 100 nm along [001] direction. Other *t*-LnVO₄ NRs (Ln = Nd, Sm, Eu, Dy) were prepared by the same way, but tetragonal phase precipitates were formed directly without phase transition (Fan et al., 2004). The phase structure and morphology of LaVO₄ are dominated by aqueous pH value. Below pH 3.5, LaVO₄ crystallizes into irregular shaped *m*-phase NPs. The *t*-phase NRs only form in the pH range of 4.5–6.0.

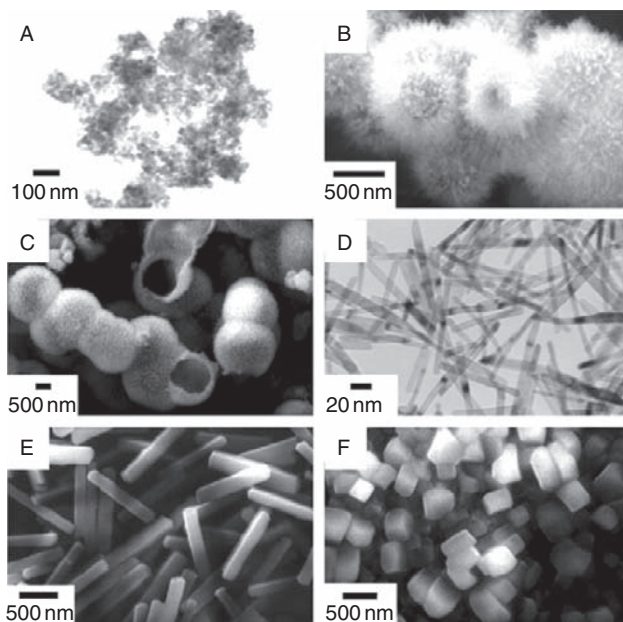


FIGURE 38 SEM and TEM images of CeVO_4 samples with typical shapes obtained at (A) pH = 10, 180 °C, 24 h, EDTA/Ce = 0; (B) pH = 1, 180 °C, 24 h, EDTA/Ce = 1.5; (C) pH = 3, 180 °C, 24 h, EDTA/Ce = 1.5; (D) pH = 10, 180 °C, 24 h, EDTA/Ce = 1.0; (E) pH = 10, 180 °C, 24 h, EDTA/Ce = 3.0; and (F) pH = 10, 220 °C, 24 h, EDTA/Ce = 3.0. Reprinted with permission from Luo *et al.* (2005). Copyright 2005 American Chemical Society.

Further increasing the pH value decreases the aspect ratio of NRs, and finally leads to particle-like $t\text{-LaVO}_4$ (Fan *et al.*, 2007a). Interestingly, the initial La^{3+} sources were responsible for the product morphology. $\text{La}(\text{NO}_3)_3$, LaCl_3 , and $\text{La}_2(\text{SO}_4)_3$ were utilized with the same hydrothermal procedures for comparison. Both lanthanum chloride and lanthanum nitrate led to similar $t\text{-LaVO}_4$ NRs, whereas lanthanum sulfate yielded the product with nanowisker morphology (Figure 39). This was attributed to the different coordinating ability of the three kinds of anions (Fan *et al.*, 2006).

Hard template materials are reliable tools for preparation of special nanostructures. Wu *et al.* prepared $\text{YVO}_4:\text{Eu}^{3+}$ short NRs based on porous silicon templates. At first, rare earth vanadates were deposited onto surface-activated silicon during hydrothermal aging. Then porous silicon was corroded by alkali and NRs were left. They also tried to use V_2O_5 NWs as templates, but the NWs morphology was not maintained (Wu *et al.*, 2006b). $(\text{NH}_4)_{0.5}\text{V}_2\text{O}_5$ NWs have served as reactive templates for the deposition of Nd^{3+} in hydrothermal condition. And NdVO_4 NRs

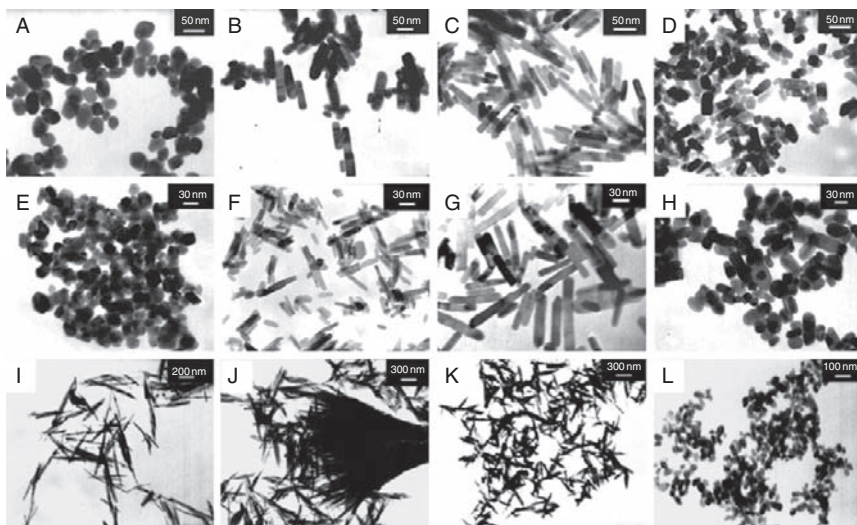


FIGURE 39 The TEM images of LaVO_4 NCs prepared from different La source at 180°C for 48 h. Using $\text{La}(\text{NO}_3)_3$ at (A) pH = 2.5; (B) pH = 3.5; (C) pH = 4.5; (D) pH = 6.0; Using LaCl_3 at (E) pH = 2.5; (F) pH = 3.5; (G) pH = 4.5; (H) pH = 6.0; Using $\text{La}_2(\text{SO}_4)_3$ at (I) pH = 2.0; (J) pH = 3.0; (K) pH = 4.5; (L) pH = 6.5. Reprinted with permission from Fan et al. (2006). Copyright 2006 American Chemical Society.

originated from the $(\text{NH}_4)_{0.5}\text{V}_2\text{O}_5$ matrix surface. When the matrix was used up, $t\text{-NdVO}_4$ dendrites were left. These NRs were single crystalline with cross-section of ca. $60 \times 60 \text{ nm}^2$ and lengths about $400 \sim 700 \text{ nm}$, which typically grew along $[312]$ or $[101]$ directions (Wu et al., 2005). In preparation of YVO_4 via the same method, the phenomenon was slightly different. The morphology of $(\text{NH}_4)_{0.5}\text{V}_2\text{O}_5$ NWs partially remained in product YVO_4 , which showed diameters of $140\text{--}250 \text{ nm}$ and lengths up to $50 \mu\text{m}$. Some $(\text{NH}_4)_{0.5}\text{V}_2\text{O}_5$ nanowires with bigger diameters form hollow YVO_4 microtubes, with outer diameters in the range of $1.2\text{--}1.6 \mu\text{m}$ and wall thickness of $0.5 \mu\text{m}$. Both NRs and microtubes were composed of assembled YVO_4 NPs (Wu et al., 2006a).

Rare earth hydroxides could serve as reactive templates, $\text{Y}(\text{OH})_3\text{:Eu}^{3+}$ wire-like microcrystals were synthesized by hydrothermal method first. Then Na_3VO_4 eroded the hydroxide templates to form $\text{YVO}_4\text{:Eu}^{3+}$ during the second hydrothermal procedure. Due to the slow diffusion of ions in solid lattices, the core section of hydroxide templates remained in the final product NRs, whereas the outer coating layer was made up of polycrystalline $\text{YVO}_4\text{:Eu}^{3+}$ NPs (Pan et al., 2007a). Using smaller $\text{Gd}(\text{OH})_3$ NRs as templates, they could be thoroughly corroded by VO_4^{3-} and formed single-crystalline $t\text{-GdVO}_4$ NRs. The intermediate product was captured from an unfinished hydrothermal treatment (Figure 40). In a typical TEM

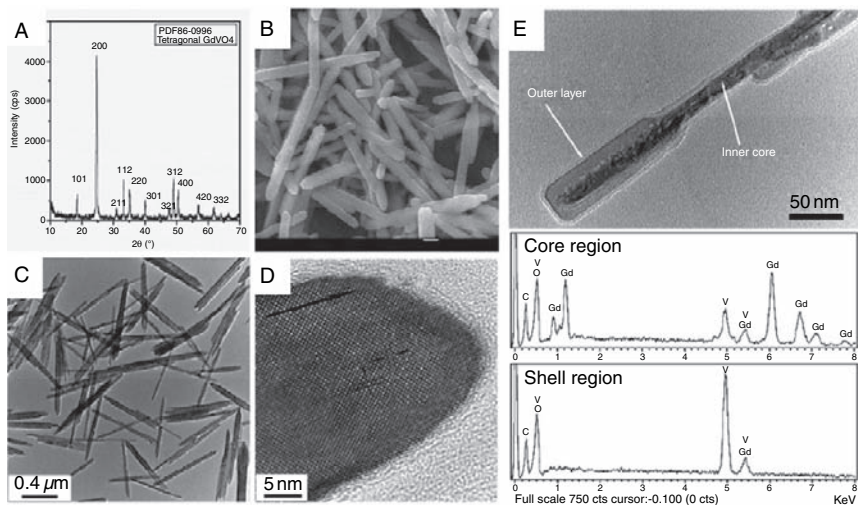


FIGURE 40 Characterization of GdVO_4 NRs in (A) XRD pattern, (B) SEM (C) TEM, and (D) HRTEM images. (E) The intermediate product after 4 h hydrothermal reaction. TEM image and EDS clearly distinguish the inner core and outer shell. Reprinted with permission from Gu *et al.* (2008c). Copyright 2008 American Chemical Society.

image, the core/shell structure was observed based on the contrast difference. The EDS analysis indicated a heterogeneous distribution of metal elements, that is, the gadolinium enriched core section and the vanadium enriched outer layer. Dissolution–precipitation process was validated as the growth mechanism for GdVO_4 NRs. The final products were about 70–80 nm in diameters, and several micrometers in lengths. The growth direction was confirmed as [001] (Gu *et al.*, 2008c).

Some anion dopants have been introduced into rare earth vanadate materials for functional modulation. Tetragonal rare earth vanadates and phosphates had the same crystal structure. They could form a homogeneous solid solution, and the component ratio of P/V was continuously adjustable. When VO_4^{3-} was partly replaced by the isomorphous PO_4^{3-} , the luminescent performance of RVO_4 phosphors was improved. The preparation of nano-sized $\text{YP}_x\text{V}_{1-x}\text{O}_4$ could follow these hydrothermal routes mentioned above, with or without the aid of chelating agents. The only modification was adding adequate phosphate source into the coprecipitation system (Riwotzki and Haase, 2001; Wang *et al.*, 2008b; Zhu *et al.*, 2008b).

3.2.1.3 Microemulsion methods and modified hydrothermal methods In hydrothermal synthesis, hydrophobic surfactants and precursors are unpractical raw materials. The mixed-solvent-thermal routes reaction could overcome this limitation by adjusting the polarity of the solution phase. One of

the advantages is that hydrophobic surfactant makes the product soluble in nonpolar solvents and polymers. It will benefit further processing of nanomaterials such as spin-coating, Langmuir-Blodgett film assembly, and copolymerization. Another advantage is saving the cost on high boiling-point organic solvent, but achieving products with similar quality.

Usually, water-soluble alkyl alcohol is utilized to decrease the solution polarity. Chen et al. prepared $\text{YVO}_4:\text{Dy}^{3+}$ NRs in *n*-propyl alcohol/water mixture. The complete crystallization required a 24 h solvent-thermal treatment at 150 °C (Chen et al., 2008b). Masih et al. prepared $\text{YV}_{0.7}\text{P}_{0.3}\text{O}_4:\text{Eu}^{3+}$, Bi^{3+} NPs in ethylene glycol/water mixture after 2 h aging at 200 °C. No hydrophobic ligands appeared in these two studies. Li and coworkers modified hydrothermal process with phase-transfer and separation to synthesize hydrophobic NPs (Wang et al., 2005d). This strategy has recently been extended to rare earth vanadates NPs (Liu and Li, 2007a). In brief, NaOH and NH_4VO_3 were mixed in water to produce Na_3VO_4 first, and ethanol-diluted oleic acid was added under strong agitation. Solution of $\text{Ln}(\text{NO}_3)_3$ was introduced at last, followed by 140 °C autoclave treatment. The ethanol promoted the dispersion and neutralization of hydrophobic oleic acid, which coordinated with Ln^{3+} ions. Then $\text{Ln}(\text{OA})_x$ complex reacted with VO_4^{3-} for nucleation at the interface of oleic acid and ethanol/water. Due to the phase separation of two precursors, the seed growth was confined at this interface. When the NPs were too big to be suspended in the solution, they fell to the reactor bottom and the growth was terminated. For *t*- $\text{LaVO}_4:\text{Eu}^{3+}$, the as-prepared NPs were 40 nm × 40 nm × 10 nm in shapes, with a square plate morphology. The oleic acid, adsorbed on certain crystal surfaces, often played a crucial role in shape-controlled synthesis of NPs. In this research, the (001) facet of LaVO_4 was greatly restricted by oleic acid, even though the (100) and (010) facets were also covered by oleic acid. Moreover, the uniform NCs could self-assemble into ordered 2D arrays along with the evaporation of organic solvents, motivated by the hydrophobic interaction of surface alkyl chains (Figure 41). As a complementary work, Li's group subsequently synthesized a series of *t*- RVO_4 colloidal NCs by using this heterogeneous hydrothermal method. They found the preferential growth direction of NCs was decided by the steric repulsions of active points on crystal facets. LaVO_4 , CeVO_4 , and PrVO_4 NCs revealed a square sheet-like morphology since their [100] and [010] directions had smaller rejection. With reducing ionic radius, YVO_4 , NdVO_4 , SmVO_4 , and EuVO_4 showed similar square morphology, but the corners and edges of the nanoplates were broken or damaged. From EuVO_4 to LuVO_4 , the breakage on NCs edges became more pronounced and the proportion of irregular NCs gradually increased. For TmVO_4 and LuVO_4 , the selectivity of crystalline growth direction almost disappeared (Liu and Li, 2007b).

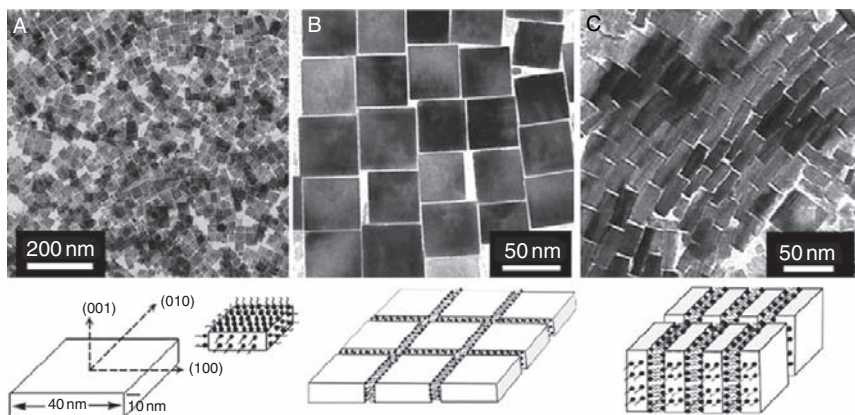


FIGURE 41 TEM images of the $t\text{-LaVO}_4\text{:Eu}$ NPs. Schematic diagram showing their self-assembled structure. Reprinted with permission from Liu and Li (2007a). Copyright 2007 Wiley-VCH.

Microemulsion methodology provides large numbers of small containers for individual reaction. Theoretically, each microemulsion droplet affords a confined environment for the crystallization of one single NC, so the size and morphology of product could be well controlled. Althues *et al.* designed a special reverse microemulsion system to synthesize $\text{YVO}_4\text{:Eu}^{3+}$ NPs in methyl methacrylate (MMA) liquid (Althues *et al.*, 2007). The $\text{R}(\text{NO}_3)_3$ and Na_3VO_4 aqueous solution was stabilized by CTAB (cetyltrimethyl ammonium bromide) and BDMA (butanediol monoacrylate) into two microemulsion reactants whereas MMA monomers acted as the organic dispersed phase. Then the two kinds of microemulsions were mixed together to generate $\text{YVO}_4\text{:Eu}^{3+}$ NPs at 50°C . The hydrodynamic size of NPs could be controlled in the range of 6–90 nm based on the proportion of water/surfactant/MMA. This liquid mixture was subsequently converted into a solid polymer matrix by the polymerization of MMA. Due to the low light scattering of $\text{YVO}_4\text{:Eu}^{3+}$ NPs, the polymer plates had high transparency in the visible light range (400–800 nm), meanwhile the $\text{YVO}_4\text{:Eu}^{3+}$ inclusions preserved red photoluminescence under UV excitation.

On the other hand, microemulsion system could combine hydrothermal methodology to enhance the crystallization of NPs. Yan *et al.* synthesized $t\text{-YVO}_4$ NPs by CTAB microemulsion assisted hydrothermal reaction (Sun *et al.*, 2002). As a typical four-component reverse micelle system, the solution contained surfactant CTAB, cosurfactant n -hexanol, oil phase n -heptane and water phase with inorganic salt. When the W value (the molar ratio of water/CTAB) was below 16, the sizes of NPs could be mediated in the range of 9–50 nm by adjusting the

microemulsion pH value. In a sodium dodecyl sulfate (SDS)/cyclohexane/*n*-hexanol/water quaternary microemulsion mediated hydrothermal reaction, Fan et al. obtained *t*-LaVO₄ NWs and nanotubes after 170 °C treatment (Fan et al., 2007b). Actually, this inverse microemulsion system was only stable at room temperature, and the product size was far beyond the droplet diameter. Thus it was presumed that the surfactants directed the NC growth through other complex interactions. By altering the SDS concentration, the morphology of LaVO₄ was variable between NWs and NRs, and the aspect ratio along the [001] direction could reach 100 (see Figure 42). Moreover, an interesting tube-like morphology of LaVO₄ was observed, but the growth mechanism was uncertain yet.

Deng et al. dispersed a small volume of Ln(NO₃)₃ and Na₃VO₄ aqueous solution stepwise into *L*-octadecene/oleic acid/oleylamine mixture without any other surfactant (Deng et al., 2008). The authors considered that the aqueous component formed reverse microemulsions after vigorous stirring. The Ln (RCOO)_x coordinates may stabilize the water nanodroplets in the hydrophobic organic solvent. Under ambient conditions, the phase separation restrained the nucleation and growth of NCs, and a solvo/hydrothermal strategy evidently accelerated the reaction. By regulating reaction time and pH value, both CeVO₄ and NdVO₄ NPs realized morphology modulation between H-shape and square-plate shape. The formation mechanism was related to chemical etching.

3.2.1.4 Microwave and ultrasonic irradiation methods Heat source is an important factor in chemical synthesis for enhancing the reactivity of reactants. Ordinary heating process could be classified into three mechanisms: radiation, heat conduction, and convection. These heating modes are relatively low efficient, and unavoidably introduce temperature gradients into the reaction media. Thus it takes time to reach an equilibrium state.

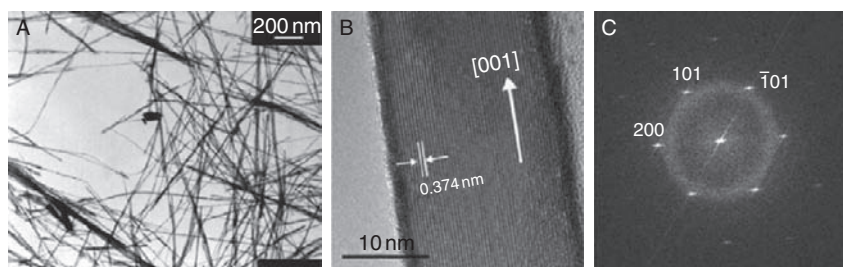


FIGURE 42 (A) TEM and (B) HRTEM images of The *t*-LaVO₄ NWs prepared under conditions of [SDS] = 0.25 M, water/SDS = 13.3, and *n*-hexanol/SDS = 5.78, at 170 °C for 48 h. (C) Fast Fourier transform pattern of the image (B). Reprinted with permission from Fan et al. (2007b). Copyright 2007 Elsevier.

Microwave and ultrasound assisted heating methods have the potential to overcome these problems via totally different calefaction processes.

Microwave technique is a fast and energy efficient way for heating, as well as for driving chemical synthesis. High-penetrating microwaves could be directly absorbed by polar molecules via relaxation or resonance, so the reaction system is heated homogeneously. Meanwhile, microwave radiation has good selectivity for certain molecular targets. The *in situ* heating and high-speed ascending temperature easily lead to an explosive nucleation of crystal seeds and rapid crystallization, which benefit the formation of small NP products. Wang's group reported a simple method to obtain *t*-YVO₄ NPs using a household microwave oven (Xu *et al.*, 2004). The mixture of adequate Y(NO₃)₃ and NaVO₃ solution was kept in a refluxing system and then it went through a 10-min microwave irradiation in ambient air. The particle size ranged from 5 to 18 nm according to different reaction pH. The smallest NPs appeared at pH 7. This group also investigated the photocatalytic property of YVO₄ NPs (Xu *et al.*, 2007). The microwave-synthesized 5 nm YVO₄ NPs showed better efficiency than the further annealed product (with bigger particle size) in photo-decolorization of methyl orange solution under UV irradiation. Another kind of potential oxidative catalysts, CeVO₄ NPs were fabricated in the same way (Wang *et al.*, 2004b). Row and coworkers added polyethylene glycol (6000) to mediate the precipitation of tetragonal phase Ln vanadate NPs in microwave synthesis (Mahapatra *et al.*, 2008). The obtained CeVO₄, PrVO₄, and NdVO₄ NPs had particle size of 25–30 nm. CeVO₄ NPs showed even higher photocatalytic activity than the commercial TiO₂ (Degussa P-25) did, while two materials had similar particle size and surface area. This can be attributed to the smaller band gap of the orthovanadates.

Like electromagnetic microwaves, intensive ultrasound waves could rapidly heat up the liquid media (aqueous system was used most). Its heating mechanism originates from the formation and cracking of small bubbles. The implosive collapse of bubbles may occur with an instantaneous high temperature of 5000 K and an extremely rapid cooling rate. These bubbles act as hot spots and continually deliver heat energy to the aqueous reaction medium. Free of surfactant or template, Cao *et al.* used the sonochemical method to prepare CeVO₄ and YVO₄:Eu³⁺ nanomaterials. A high-intensity ultrasonic probe promoted the reaction in ambient air, and the average solution temperature was maintained around 70 °C. When using Ce(NO₃)₃, NH₄VO₃, and ammonia in the experiment, the formed CeVO₄ NRs had a diameter of ca. 5 nm and a length of 100–150 nm, probably due to the collision of NPs under the action of ultrasound. In the case of YVO₄:Eu³⁺, spindle-like NPs which composed of tiny grains inside were obtained. If NH₄VO₃ and ammonia was replaced by NaVO₃ and NaOH, the CeVO₄ NPs grew up to 20 nm with pore sizes of 5–7 nm (Zhu *et al.*, 2007a,c).

3.2.1.5 Sol-gel methods Sol-gel methodology is highly versatile for producing inorganic powders and film materials. It does not belong to solution phase synthesis, because its crystallization process depends on the solid-state annealing. Traditional sol-gel protocols are incapable of avoiding agglomeration, unless proper modifications are introduced. For instance, Hou et al. combined electrospinning technique and sol-gel process for preparing $t\text{-YPO}_{0.8}\text{VO}_{0.2}\text{O}_4\text{:Ln}^{3+}$ nanofibers and $t\text{-YVO}_4\text{:Ln}^{3+}$ microbelts (Ln = Eu, Sm, Dy) (Hou et al., 2008). The sol precursors were molded into 1D shape by physical force, and then crystallized via calcination. On the other hand, sol-gel methods have an advantage for efficient loading or coating certain materials onto the ready-made templates. For example, the $\text{YVO}_4\text{:Ln}^{3+}$ sol precursor could be coated onto a planar substrate via dip-coating or soft lithography. Then high temperature annealing will turn it to a compact, and a flat film consisted of NPs (Yu et al., 2002). If the templates have small sizes and good dispersibility, the final composite products would be also in nano- or micrometer scale.

Silica spheres are one kind of facile template materials with any required diameter, thus depositing luminescent materials on SiO_2 spheres was a good choice to yield core-shell structured nano-phosphors. This core-shell strategy also cuts down the cost of luminescent material by introducing cheap silica inclusions. Lin's group did a series of studies on $\text{SiO}_2/\text{RVO}_4$ phosphors. In a typical experimental procedure, SiO_2 spheres were added into the sol mixture of $\text{R}(\text{NO}_3)_3$, NH_4VO_3 , PEG, and citric acid. Then the soaked SiO_2 spheres were collected for drying and annealing steps. The final products preserved the morphology of original templates through the sol-gel process. XRD and TEM characterization confirmed that RVO_4 NCs were well crystallized on the surfaces of amorphous silica. Repeating the deposition/annealing cycle could increase the shell thickness. Following this sol-gel protocol, sub-micrometer sized SiO_2 spheres were successfully coated by uniform shells of $\text{YVO}_4\text{:Eu}^{3+}$, $\text{YVO}_4\text{:Dy}^{3+}$, $\text{YVO}_4\text{:Sm}^{3+}$, or $\text{GdVO}_4\text{:Eu}^{3+}$ (Figure 43). These composite particles possessed fine optical performance similar to that of corresponding bulk phosphors (Li et al., 2006a; Liu et al., 2006; Wang et al., 2006d; Yu et al., 2005b). Mesoporous silica materials are also candidates as sol-gel reaction templates. Because of the good biocompatibility and high surface area, mesoporous silica has been proposed as carriers for drug delivery. If the carrier was modified with luminescent compounds, tracking their migration and studying the metabolism *in vivo* becomes easier. Following the previous sol-gel process, Lin's group modified the ordered mesoporous SBA-15 and MCM-41 silica particles with $\text{YVO}_4\text{:Eu}^{3+}$ shell. Then the composite particles were filled by ibuprofen as a simulation of drug delivery carrier (Yang et al., 2007b,c). Chang et al. reported triplex core/shell structured $\text{Y}_2\text{O}_3\text{:Eu}^{3+}@\text{SiO}_2@\text{YVO}_4\text{:Eu}^{3+}$ phosphors. At first, $\text{Y}_2\text{O}_3\text{:Eu}^{3+}$ around 23 nm were generated from urea homogeneous precipitation

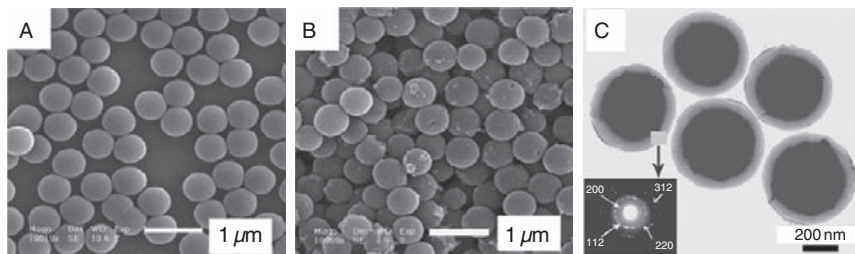


FIGURE 43 SEM images of (A) SiO_2 sheres and (B) the $\text{SiO}_2@\text{Gd}_{0.95}\text{Eu}_{0.05}\text{VO}_4$ by four deposition/annealing cycles; (C) TEM image of $\text{Gd}_{0.95}\text{Eu}_{0.05}\text{VO}_4$ spheres; Inset of (C): electron diffraction pattern of the selected shell region. Reprinted with permission from Li *et al.* (2006a). Copyright 2006 Elsevier.

of $\text{Y}(\text{NO}_3)_3$ and $\text{Eu}(\text{NO}_3)_3$. Then these $\text{Y}_2\text{O}_3:\text{Eu}^{3+}$ NPs served as cores for TEOS hydrolysis in a modified stöber process. The as-synthesized $\text{Y}_2\text{O}_3:\text{Eu}^{3+}@\text{SiO}_2$ spheres encapsulated tens of $\text{Y}_2\text{O}_3:\text{Eu}^{3+}$ NPs, with a total diameter of 200 nm. The final step was a typical sol-gel method for depositing rare earth vanadate, and the smooth surface of former spheres was covered by a rough thin layer of $\text{YVO}_4:\text{Eu}^{3+}$ NPs (Chang and Tie, 2008).

Some research groups changed the sol composition in order to produce nanocrystals. Zhang *et al.* adopted polyacrylamide gel as dispersant and obtained 20 nm $t\text{-YVO}_4:\text{Eu}^{3+}$ NPs with only small aggregates (Zhang *et al.*, 2004a). Acrylamide monomers, cross-linkers and polymerization initiators were added into the reacting solution to form the polymeric gel together with inorganic precursors (Y_2O_3 , Eu_2O_3 , NH_4VO_3 , critic acid, and dilute HNO_3). For polymerization, the side reaction between cations and acrylamide was eliminated by critic acid. The obtained gel well dispersed rare earth and vanadium species based on its porous framework. This static separation reduced the aggregating of products when the organic residues were burned out. Using polymeric glucose gel instead, this group also synthesized $t\text{-YVO}_4:\text{Tm}^{3+}$ NPs (Zhang *et al.*, 2004b). In Zhang's recent report, soluble starch powder was utilized as both chelating agent and gel substance in preparation of $\text{YVO}_4:\text{Sm}^{3+}$ and $\text{YVO}_4:\text{Dy}^{3+}$ NPs. The starch backbone consisted of long-chain glucose units. Some hydroxyl groups of the glucose units were oxidized to COO^- by the excess HNO_3 , so as to bind the NPs and limit their size (Zhang *et al.*, 2008d).

Recently, Boilot *et al.* utilized sol-gel method as the subsequent annealing treatment for the preparation of $\text{YVO}_4:\text{Eu}^{3+}$ NPs (Mialon *et al.*, 2008). At room temperature, water-phase precipitation always produced inorganic NPs with low crystallinity, so the author re-dispersed the crude $\text{YVO}_4:\text{Eu}^{3+}$ NPs into a polymeric silica sol for sol-gel thermal annealing. The silica matrix could prevent the aggregation and growth of NPs even

at 1000 °C. After annealing process, silica was dissolved by hydrofluoric acid, and highly crystallized $\text{YVO}_4:\text{Eu}^{3+}$ NPs were obtained. These NPs were dispersible in PAA/water solution, and their QY were an evidently increased. This annealing protocol was also efficient for other metal oxide nanomaterials.

3.2.2 Properties of rare earth vanadate nanomaterials

Multicolored luminescence is the most attractive property of rare earth-based compounds. Lanthanide ions possess many sharp emission lines that cover the visible and near infrared (NIR) region due to the abundant transitions of *f*-orbital configurations. However, the forbidden *f*-*f* transitions induce narrow excitation lines for most rare earth ions. This low absorbency cross-section is the bottleneck in practical application, so host-sensitized emission mode is commonly employed by rare earth phosphors. The vanadate matrix is one of the candidates, which excites lanthanide ions via charge-transfer energy migration.

Attributed to different cation size, rare earth orthovanadates have two kinds of phase structure, *m*-type (monoclinic phase) and *t*-type (tetragonal phase). One of the commercial red phosphors, bulk $\text{YVO}_4:\text{Eu}^{3+}$ belongs to zircon type crystal (*t*-type), when the $^5\text{D}_0$ to $^7\text{F}_2$ emission of Eu^{3+} shows strong promotion in D_{2d} symmetry sites. And *t*- $\text{YVO}_4:\text{Eu}^{3+}$ nanomaterial preserves this optical property. Riwotzki et al. carefully scanned the emission spectra of 5 mol% Eu^{3+} doped *t*- YVO_4 colloidal NPs. Each emission line was well assigned according to the theoretical Eu^{3+} energy level diagram, including the conventional $^5\text{D}_0$ to $^7\text{F}_j$ transitions and several weak signals originating from $^5\text{D}_1$ and $^5\text{D}_2$ level. In their report, the maximum quantum yield at room temperature was only 15%, just one fifth of the value of bulk $\text{YVO}_4:\text{Eu}^{3+}$. Although the hydrothermal method (200 °C) ensured the high crystallinity of NPs, the luminescence efficiency still seemed to be depressed by surface energy trapping without surface passivating (Riwotzki and Haase, 1998). Referring to Boilot's reports, a coprecipitation method at low temperature produced *t*- $\text{YVO}_4:\text{Eu}^{3+}$ NPs also with a maximum quantum yield of 15% (Huignard et al., 2000, 2002). Boilot et al. considered that the emission process was weakened by nonradiative recombination at NPs' surface. For aqueous colloid NPs, the surface-adsorbed H_2O molecule and chemically bonded OH groups dissipated a majority of the energy that was transferred among the vanadate lattices. Only in deuterated water the NPs quantum yield could increase to 28%, since deuterated water quenched rare earth compounds with a much lower probability (Huignard et al., 2000). Haase et al. ascribed this quenching to the radiationless recombination of surface vanadate groups, supported by spectroscopy techniques. They found that the Eu^{3+} luminescence lifetime for the $^5\text{D}_0$ level was barely affected by temperature and surrounding medium, but the luminescence

properties of VO_4^{3-} were correlated to the two above mentioned factors. It was not in conflict with the fact that all Eu^{3+} ions were excited via VO_4^{3-} sensitization, because energy transfer from one VO_4^{3-} to the neighboring Eu^{3+} was much faster than radiationless processes at this VO_4^{3-} group. After eliminating the quenching possibility of surface Eu^{3+} , they further compared the temperature dependent luminescence spectra of $\text{YVO}_4:\text{Eu}^{3+}$ NPs and $\text{YP}_{0.95}\text{V}_{0.05}\text{O}_4:\text{Eu}^{3+}$ NPs. The phosphate dopant served as diluting anions to suppress the energy transfer between adjacent vanadate groups. With rising temperature, the luminescence intensity and lifetime of VO_4^{3-} decreases much faster in the case of $\text{YVO}_4:\text{Eu}^{3+}$ than $\text{YP}_{0.95}\text{V}_{0.05}\text{O}_4:\text{Eu}^{3+}$ NPs, whereas the emission of its Eu^{3+} was not increased along with the enhancing thermally activated energy transfer from vanadate groups (Figure 44).

Thus, it seemed impossible for europium to receive the energy transferred from distant vanadate groups in NC environment. Considering that the energy migration did happen in $\text{YVO}_4:\text{Eu}^{3+}$ NPs, this portion of energy must follow another route for radiationless recombination, for example assuming deactivation of the excited vanadate on surface sites (Riwotzki and Haase, 2001). Boilot's group validated this conclusion on

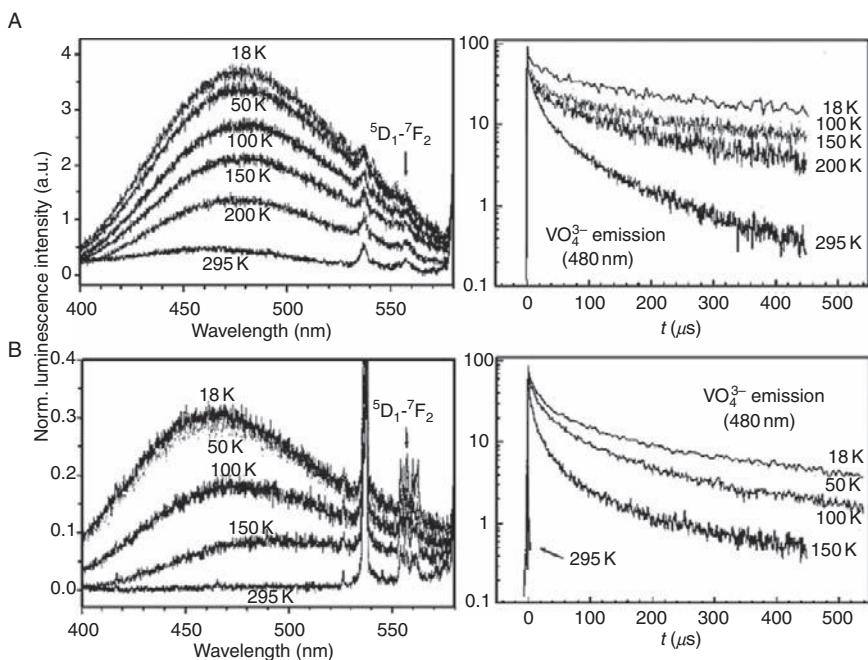


FIGURE 44 Temperature-dependent luminescence and the corresponding luminescence decay of vanadate in (A) $\text{YP}_{0.95}\text{V}_{0.05}\text{O}_4:\text{Eu}$ NPs and (B) $\text{YVO}_4:\text{Eu}$ NPs. Reprinted with permission from Riwotzki and Haase (2001). Copyright 2001 American Chemical Society.

the side of optimal europium-doping ratio. The dopants concentration influences the QY via two competitive effects. To increase the probability of host-to-emitter energy transfer, high doping ratio is desired. But excess dopant leads to self-quenching of excited emitters. The $Y_{1-x}Eu_xVO_4$ NPs from low temperature precipitation had a maximal quantum yield at $x = 0.20$, which was far beyond the optimal concentration of 5% for bulk material (Huignard et al., 2000, 2002). The lifetime of $Eu^{3+} {}^5D_0$ emission steadily decreased from 1.2 ms to 0.6 ms along with varying x from 0.05 to 0.3, indicating the remarkable concentration quenching, but these lifetime values were still higher than those of standard bulk phosphors. Obviously, the surface quenching of excited Eu^{3+} was not the primary reason for the low QY. And a high Eu^{3+} concentration was necessary for the competition with radiationless recombination of excited vanadate groups.

It is worth noting that the optimal doping ratio was not a constant in different rare earth nanomaterials and researchers have to check this parameter taking the corresponding bulk material as a reference. Inspired by core/shell structured QDs, Boilot's group passivated the crude $YVO_4:Eu^{3+}$ NPs by silicate shell. The product showed a clear decrease in the optimal Eu^{3+} doping ratio, but the QY and the 5D_0 lifetime of Eu^{3+} was only elevated slightly. Maybe amorphous SiO_2 shell did not completely eliminate the OH quenchers. This passivation efficiency became evident only after an annealing treatment at 600 °C. The QY then reached 52% while the 5D_0 lifetime increased up to 1.7 ms (Huignard et al., 2003).

With this understanding, the spectra of Eu^{3+} could probe the microstructure of nanomaterials, because the 5D_0 to 7F_1 transition was very sensitive to the site symmetry. Yan et al. used laser selective excitation technique to research the high-resolution spectra of $t-YVO_4:Eu^{3+}$ NPs (Yan et al., 2003a). When the Eu^{3+} dopants approach the NPs surface, the D_{2d} symmetry is broken. In emission spectra this is reflected by several points: the increased number of emission lines; the shortened luminescent lifetime, the enhanced splitting of energy levels, and the broadened emission peaks.

Simulating the existent bulk phosphors, Isobe's group doped Bi^{3+} into $t-YVO_4:Eu^{3+}$ NPs in order to extend the host excitation band (Takeshita et al., 2008). The Bi^{3+} primarily altered the electronic structure of vanadate matrix when its 6s orbital was incorporated into the host valence band. Energy could be transferred from the 6s orbital of Bi^{3+} to the 3d orbital of V^{5+} , and finally, to sensitize the Eu^{3+} dopants. In the excitation spectrum, a new band was observed between 300 and 400 nm, corresponding to the charge transfer from Bi^{3+} to V^{5+} . However, due to the different crystallization characteristics, $BiVO_4$ and YVO_4 were difficult to combine together via homogeneous precipitation. Prolonging the hydrothermal aging only led to a phase separation of Bi^{3+} and Y^{3+} , but did not help to form

$\text{BiVO}_4/\text{YVO}_4$ solid solution. The luminescence intensity also drops from the maximum value when surface-enriched Bi^{3+} quenches the host migrating energy (Figure 45). Lü *et al.* codoped Li^+ into $t\text{-YVO}_4:\text{Eu}^{3+}$ NPs via sol-gel combustion method (Zhang *et al.*, 2006a). With 5 mol% Li^+ additive, the emission of Eu^{3+} could be increased by a fraction of 11. There were two possible reasons. When Li^+ ions replaced Y^{3+} or partly enter into the interstices in the crystal lattice, the site symmetry of Eu^{3+} is

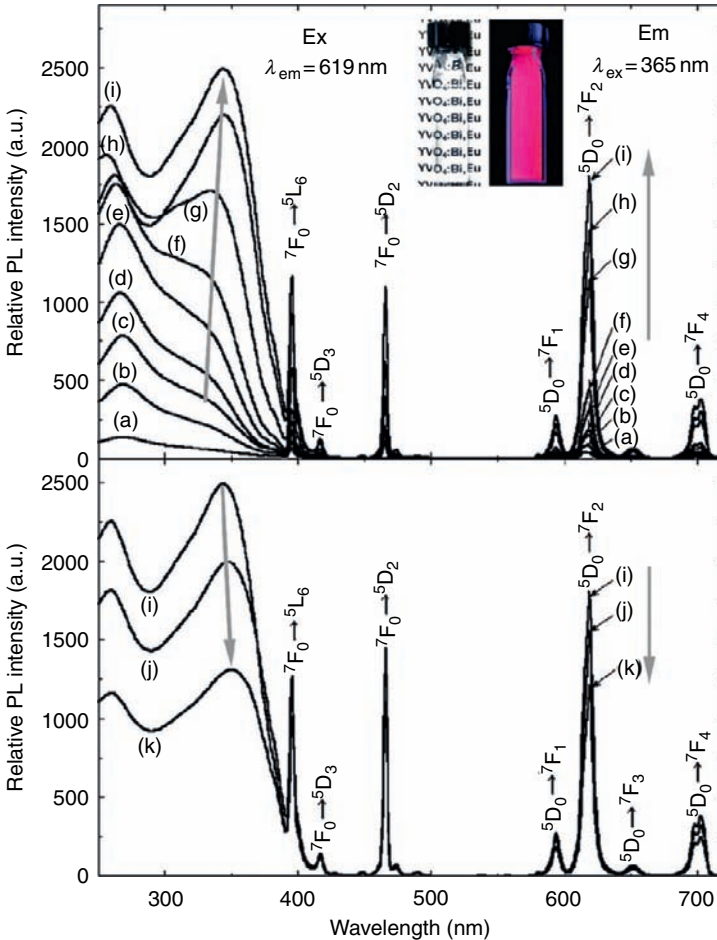


FIGURE 45 Emission and excitation spectra of $t\text{-YVO}_4:\text{Bi}, \text{Eu}$ NPs powder samples aged at 60°C for different time (min): (a) 0, (b) 1, (c) 15, (d) 30, (e) 45, (f) 60, (g) 120, (h) 180, (i) 240, (j) 300, and (k) 420. And the Bi–V charge transfer band between 300 and 400 nm showed a red shift with increasing reaction time. Reprinted with permission from Takeshita *et al.* (2008). Copyright 2008 Elsevier.

reduced. Then the loss of selection rules leads to an enhancement of luminescence. Another possibility is that Li^+ dopants bring oxygen vacancies into the lattice for charge neutrality, which promotes the energy transfer to the Eu^{3+} emitters.

Lanthanum ion has an empty 4f electron shell. In its trivalent ion form it is totally transparent to light irradiation, but the thermodynamics of the *m*-phase structure of LaVO_4 makes it capable as a host material. The relatively low symmetry of the monoclinic structure suppresses the host energy transition process. The Ln^{3+} -doped bulk *m*- LaVO_4 materials often form with phase separation of *t*- LnVO_4 due to the size mismatch of cations. Different from bulk material, nanocrystalline LaVO_4 could be stable in the tetragonal phase, which is the optimal structure for Eu^{3+} emitters. It has been proved that europium doped *t*- LaVO_4 NPs remarkably improve the luminescent intensity and spectral homochromy (see Figure 46) (Fan et al., 2006, 2007a; Jia et al., 2004, 2005). The *t*- $\text{LaVO}_4:\text{Eu}^{3+}$ NPs displayed luminescent properties similar to those of *t*- $\text{YVO}_4:\text{Eu}^{3+}$ NPs. The excitation peak around 280 nm is the typical absorbance of VO_4^{3-} matrix. The emission spectrum consists of several portions ranging from 580 to 720 nm, corresponding to the transitions of $^5\text{D}_0$ to $^7\text{F}_J$ ($J = 0, 1, 2, 3, 4$) levels, respectively. The $^5\text{D}_0 \rightarrow ^7\text{F}_2$ transition provides the strongest peak at 610–620 nm, so this kind of a phosphor shows a red luminescence (Liu and Li, 2007a). In principle, the intensity ratios of different $^5\text{D}_0$ to $^7\text{F}_J$ transitions rely on the symmetry of Eu^{3+} local environment. For Eu^{3+} ions, the $^5\text{D}_0 \rightarrow ^7\text{F}_1$ is the permitted magnetic dipole transition while the $^5\text{D}_0 \rightarrow ^7\text{F}_2$ is the forbidden electric dipole transition. But if the Eu^{3+} sites are not on the inversion centers, such as the D_{2d} sites in the tetragonal vanadate matrix phase, this situation can be partially overcome. That was the reason for the high purity and intensity of red emission of *t*- $\text{LaVO}_4:\text{Eu}^{3+}$ NPs. Moreover, the $^5\text{D}_0 \rightarrow ^7\text{F}_2$ transition is sensitive to the tiny change of Eu^{3+} local environment. Fan et al. compared the emission spectra of *t*- $\text{LaVO}_4:\text{Eu}^{3+}$ NPs and NRs. The intensity ratio of the $^5\text{D}_0 \rightarrow ^7\text{F}_2$ to $^5\text{D}_0 \rightarrow ^7\text{F}_1$ transitions and the split shape of the $^5\text{D}_0 \rightarrow ^7\text{F}_2$ peak were obviously different, but the position of each peak was fixed on the wavelength axis. It could be explained by lattice distortion in nano-sized crystals, which influenced the crystal field symmetry (Fan et al., 2007a).

The optical properties of other Ln ions in nano-sized vanadate matrix were enumerated as follows. The *t*- $\text{LaVO}_4:\text{Pr}^{3+}$ NPs revealed three emission peaks via vanadate host sensitizing. According to the energy level of praseodymium ion, they were identified as the $^3\text{P}_0 \rightarrow ^3\text{H}_4$ (480 nm) transition, the $^1\text{D}_2 \rightarrow ^3\text{H}_4$ (603 nm) transition, and the $^3\text{P}_0 \rightarrow ^3\text{H}_6$ (655 nm) transition, respectively (Stouwdam et al., 2005). Besides the ordinary absorption band of the vanadate host, $\text{LaVO}_4:\text{Nd}^{3+}$ and NdVO_4 NPs revealed absorption peaks of Nd^{3+} with medium intensity (Liu and Li, 2007b; Stouwdam et al., 2005). Wu et al. observed four peaks located at

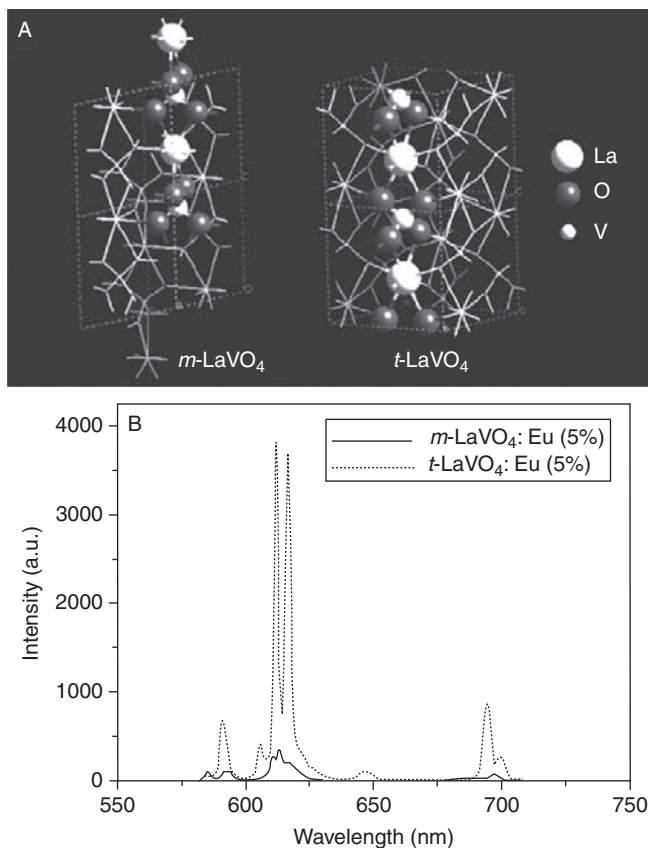


FIGURE 46 (A) Simulated crystal structures of $m\text{-LaVO}_4$ (left) and $t\text{-LaVO}_4$ (right). (B) Luminescence spectra of m - and $t\text{-LaVO}_4\text{:Eu}$ NPs (5 mol% Eu) excited at 310 nm. Reprinted with permission from Jia *et al.* (2005). Copyright 2005 American Chemical Society.

593, 753, 807, and 878 nm from the $t\text{-NdVO}_4$ NRs sample, which were attributed to the Nd^{3+} intrinsic transitions from the $^4\text{I}_{9/2}$ level to the $^4\text{G}_{5/2}$, $^4\text{F}_{7/2}$, $^4\text{F}_{5/2}$, and $^4\text{F}_{3/2}$ levels, respectively (Liu and Li, 2007b). The emission of Nd^{3+} mainly composed of UV and blue light under excitation of 310 nm. Two emission peaks at 362 and 467 nm could be distinguished easily, corresponding to the $^4\text{D}_{3/2} \rightarrow ^4\text{I}_{9/2}$ and the $^4\text{G}_{11/2} \rightarrow ^4\text{I}_{9/2}$ transitions. The rest of emissions at 396, 420, 450, 482, and 492 nm were shoulder peaks that almost incorporated into broad bands. van Veggel *et al.* measured NIR emission of $\text{LaVO}_4\text{:Nd}^{3+}$ NPs with excitation at 280 nm. The typical emissions at 880, 1060, and 1330 nm were assigned to transitions from the $^4\text{F}_{3/2}$ level to the $^4\text{I}_{13/2}$, $^4\text{I}_{11/2}$, and $^4\text{I}_{9/2}$ levels, respectively (Stouwdam *et al.*, 2005).

Deng et al. discovered a unique upconverted avalanche luminescence phenomenon in their synthesized *t*-CeVO₄ and *t*-NdVO₄ NPs under the near-infrared excitation (720–920 nm, tunable Ti:Sapphire CW laser). NdVO₄ NPs displayed three emission bands centered at 530, 593, and 670 nm with $\lambda_{\text{ex}} = 800$ nm. The corresponding avalanche threshold excitation intensity (P_c) was ca. 8 mW, and above this P_c value the avalanche slope was 15. Furthermore, the P_c value and avalanche slope of *t*-NdVO₄ NPs showed a functional dependence on excitation wavelength. When the λ_{ex} matched the resonance wavelength of the Nd³⁺ metastable levels, that is, the $^4I_{9/2} \rightarrow ^4F_{5/2}$ state (810 nm) and the $^4I_{9/2} \rightarrow ^4F_{3/2}$ state (885 nm), P_c value decreased 80% to a minimum. The avalanche slope had similar variation trend, showing a decrease about 18% with the resonance excitation. The *t*-CeVO₄ NPs were more difficult for upconverted avalanche emission, which displayed a broad band centered at 584 nm with the P_c value ca. 22 mW at $\lambda_{\text{ex}} = 800$ nm. No resonance excitation was observed due to the energy level difference (Deng et al., 2008).

Riwotzki and Haase prepared *t*-YVO₄:Sm³⁺ (2% doping ratio) and *t*-YVO₄:Dy³⁺ (1% doping ratio) colloidal NPs via hydrothermal routes (Riwotzki and Haase, 1998). The spectra were identical with those of the corresponding bulk materials, and each emission line could be assigned to the known transitions of Sm³⁺ or Dy³⁺ (Figure 47). Zhang et al. examined the fine excitation spectra of YVO₄:Sm³⁺ and YVO₄:Dy³⁺ NPs in the region of 340–500 nm. The weak excitation lines belonged to the f–f

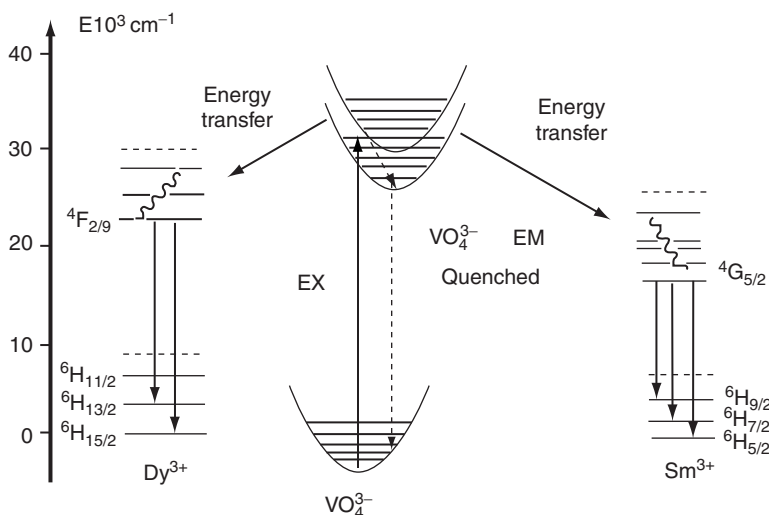


FIGURE 47 Scheme of energy transfer from VO_4^{3-} to Dy^{3+} and Sm^{3+} . Reprinted with permission from Wang et al. (2006d). Copyright 2006 Elsevier.

transitions of Ln ions (Zhang et al., 2008d). Using LaVO_4 host instead, the excitation and emission properties of Dy^{3+} and Sm^{3+} were all the same. Nano-sized $t\text{-LaVO}_4\text{:Sm}^{3+}$ (5% doping ratio) displayed three typical emission peaks at 565, 602, and 646 nm, which were generated by the ${}^4\text{G}_{5/2}$ to the ${}^6\text{H}_{5/2}$, ${}^6\text{H}_{7/2}$, and ${}^6\text{H}_{11/2}$ transitions, respectively. This material emitted red light as commonly reported. Only the intensity ratio of three peaks varies in different literature. For example, the square sheet-like NPs coated by oleic acid showed the dominant emission middle peak at 602 nm (Liu and Li, 2007a), while the NRs with bare surface had similar integral area for the 602 and 646 nm emission peaks (Fan et al., 2007a). With UV excitation, nanosized $t\text{-LaVO}_4\text{:Dy}^{3+}$ (5% doping ratio) displayed yellow luminescence, which was dominated by the ${}^4\text{F}_{9/2} \rightarrow {}^6\text{H}_{13/2}$ transition. The blue-emission of the ${}^4\text{F}_{9/2} \rightarrow {}^6\text{H}_{15/2}$ line was a bit lower. It was probably screened in bright yellow light as observed by naked eyes. And the ${}^4\text{F}_{9/2} \rightarrow {}^6\text{H}_{11/2}$ transition was faint, almost merged in baseline (Fan et al., 2007a; Liu and Li, 2007a).

Erbium ion is an important emitter for upconverting infrared photons to visible photons, due to its electronic level scheme with equally spaced and long-lived excited states. The Er^{3+} could be sensitized by vanadate matrix, too. In the report of Sun et al., $t\text{-YVO}_4\text{:Er}^{3+}$ (2% doping) NPs were prepared by a hydrothermal method with an average diameter of 35 nm. With exciting the vanadate host at 280 nm, the NPs emitted green light at 523 and 557 nm, associated with the ${}^2\text{H}_{11/2} \rightarrow {}^4\text{I}_{15/2}$ and the ${}^4\text{S}_{3/2} \rightarrow {}^4\text{I}_{15/2}$ transitions of Er^{3+} , respectively. Under the 980 nm radiation, the Er^{3+} ions were directly excited and also gave out green luminescence. The ${}^2\text{H}_{11/2}$, ${}^4\text{S}_{3/2} \rightarrow {}^4\text{I}_{15/2}$ transitions occupy the principal part in the emission spectra, and the ${}^4\text{F}_{9/2} \rightarrow {}^4\text{I}_{15/2}$ transition (red, between 650 and 670 nm) was quite weak. Both portions were attributed to a two-photon process, confirmed by the relation between excitation power and upconverted luminescence intensity (Sun et al., 2006c). The NIR emission of $t\text{-LaVO}_4\text{:Ho}^{3+}$ and $t\text{-LaVO}_4\text{:Er}^{3+}$ NPs was reported in van Veggel's paper (Stouwdam et al., 2005). With 280 nm excitation, $\text{LaVO}_4\text{:Ho}^{3+}$ exhibited the ${}^5\text{F}_5 \rightarrow {}^5\text{I}_7$ transition (960 nm) and the ${}^5\text{F}_5 \rightarrow {}^5\text{I}_6$ transition (1460 nm) in NIR region. Another peak of the ${}^5\text{F}_5 \rightarrow {}^5\text{I}_8$ transition (650 nm) belongs to visible light region. The NIR emission of $\text{LaVO}_4\text{:Er}^{3+}$ NPs located at 980 and 1530 nm, corresponding to the ${}^4\text{I}_{11/2} \rightarrow {}^4\text{I}_{15/2}$ transition and the ${}^4\text{I}_{13/2} \rightarrow {}^4\text{I}_{15/2}$ transition of Er^{3+} , respectively. The $t\text{-LaVO}_4\text{:Tm}^{3+}$ NPs emitted intense blue light under 280 nm excitation, which originated from the ${}^1\text{G}_4 \rightarrow {}^3\text{H}_6$ transition of Tm^{3+} (around 475 nm). The ${}^1\text{G}_4 \rightarrow {}^3\text{H}_4$ and ${}^3\text{F}_4 \rightarrow {}^3\text{H}_6$ transitions brought relatively weak emission, locating at 650 and 790 nm, respectively (Stouwdam et al., 2005). $t\text{-Y}_{0.75}\text{Yb}_{0.25}\text{VO}_4$ NPs had a NIR absorption peak at 978 nm, consistent with the ${}^2\text{F}_{7/2} \rightarrow {}^2\text{F}_{5/2}$ transition of Yb^{3+} . Under excitation at 970 nm, the luminescence spectrum showed a broad band from 980 to 1050 nm. It originated from the ${}^2\text{F}_{5/2} \rightarrow {}^2\text{F}_{7/2}$ transition, just as a reverse process of

absorption (Buissette et al., 2003). In fact, Yb^{3+} was widely used as codopant together with Er^{3+} or Tm^{3+} to increase the NIR absorption efficiency. There was an efficient resonant energy transfer from excited Yb^{3+} ions to $\text{Er}^{3+}/\text{Tm}^{3+}$ emitters for much easier pumping.

Zircon type GdVO_4 was another ideal host for Eu^{3+} emitters. The $t\text{-GdVO}_4:\text{Eu}^{3+}$ NRs (5% doping ratio) synthesized by Gu et al. showed the maximum absorption band around 307 nm. The emission spectrum was consistent with data of other Eu^{3+} -incorporated rare earth vanadate nanomaterials (Gu et al., 2008c). Liu et al. reported four types of oleic acid capped $t\text{-LnVO}_4:\text{Eu}^{3+}$ ($\text{Ln} = \text{Y}, \text{La}, \text{Gd}, \text{Lu}$) NPs. They exhibited almost the same emission spectra with $\lambda_{\text{ex}} = 280$ nm (Liu and Li, 2007b). Li et al. studied both the photoluminescence and low voltage cathodoluminescence properties of $\text{SiO}_2@\text{GdVO}_4:\text{Eu}^{3+}$ nanospheres. Under the excitation of electron beam (1–5 kV), the ${}^5\text{D}_1 \rightarrow {}^7\text{F}_1, {}^7\text{F}_2$ and ${}^5\text{D}_0 \rightarrow {}^7\text{F}_j$ ($j = 1, 2, 3, 4$) transitions of Eu^{3+} were observed. The intensity ratio of different peaks was basically in agreement with that of the photoluminescence emission spectrum (Li et al., 2006a). Wu et al. prepared $t\text{-Y}_{0.8}\text{Gd}_{0.2}\text{VO}_4:\text{Eu}^{3+}$ NPs and considered the codoped Gd^{3+} served as sensitizer for Eu^{3+} . The $4f^n$ high energy level of Gd^{3+} is located at the host absorption band of vanadate groups (around 200 nm). Hence, there was a potential energy transfer from the host matrix to Gd^{3+} . Meanwhile, the ${}^6\text{G}_j \rightarrow {}^6\text{P}_j$ transition of Gd^{3+} had a similar energy gap as that for the ${}^7\text{F}_1 \rightarrow {}^5\text{D}_0$ transition of Eu^{3+} , thus Gd^{3+} in ${}^6\text{G}_j$ state could excite Eu^{3+} up to the ${}^5\text{D}_0$ state by resonance energy transfer. With a fixed Eu^{3+} concentration (5 mol%), the $\text{Y}_{0.8}\text{Gd}_{0.2}\text{VO}_4:\text{Eu}^{3+}$ NPs revealed stronger luminescence than $\text{YVO}_4:\text{Eu}^{3+}$ NPs (Wu and Yan, 2008).

Partial replacement of vanadate anions was another route to adjust the luminescence properties. Riwozki and Haase introduced phosphate into vanadate matrix and prepared $t\text{-YP}_{0.95}\text{V}_{0.05}\text{O}_4:\text{Eu}^{3+}$ NPs via a hydrothermal reaction. By phosphate dilution, the energy transfer between vanadate groups was restrained, so radiationless recombination of excited VO_4^{3-} was weakened, especially on particle surface. As a result, more excited VO_4^{3-} groups transferred its energy to their neighboring Eu^{3+} ions. Compared with $\text{YVO}_4:\text{Eu}^{3+}$ NPs, $\text{YP}_{0.95}\text{V}_{0.05}\text{O}_4:\text{Eu}^{3+}$ NPs had an improved emission intensity, while the ${}^5\text{D}_0 \rightarrow {}^7\text{F}_j$ ($j = 1, 2, 3, 4$) transition showed larger area in spectra, but the intensity ratio was altered (Riwozki and Haase, 2001). Due to the dilution effect of phosphate, the luminescence of VO_4^{3-} was also enhanced. Liu et al. modulated the emission color of $t\text{-YP}_{0.75}\text{V}_{0.25}\text{O}_4:\text{Ln}^{3+}$ NPs by altering the intensity ratios of $\text{YP}_{0.75}\text{V}_{0.25}\text{O}_4$ host emission and host-sensitized Ln^{3+} emission. The vanadate emission was a broad peak centered at ca. 435 nm (deep blue). With increasing the concentrations of Eu^{3+} , Dy^{3+} , or Sm^{3+} dopants (0.2–5 mol%), vanadate emission is gradually depressed due to the resonant energy transfer (Figure 48). Therefore, the emission color was

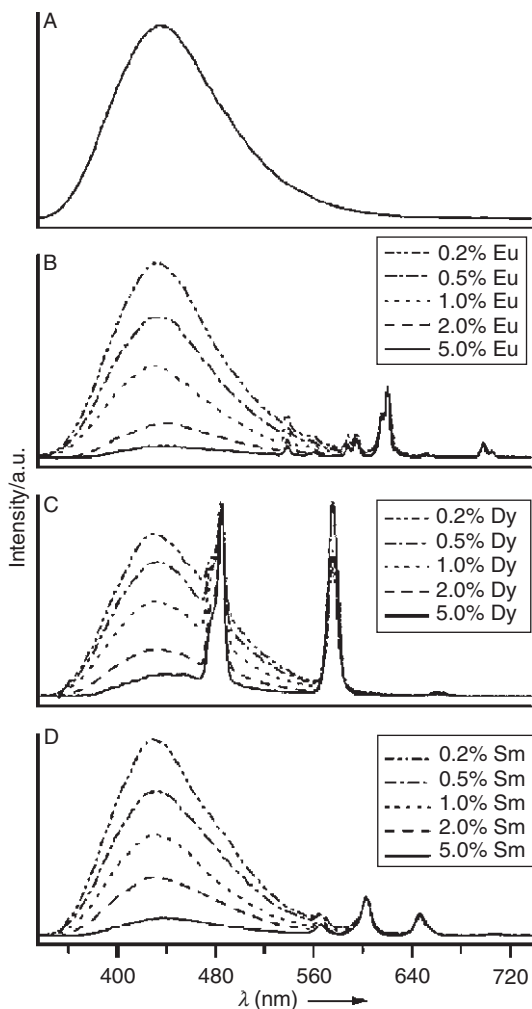


FIGURE 48 Room-temperature emission spectra of (A) $\text{YP}_{0.75}\text{V}_{0.05}\text{O}_4$ NPs, (B) $\text{YP}_{0.75}\text{V}_{0.25}\text{O}_4:\text{Eu}$ NPs (normalized to Eu 618 nm emission), (C) $\text{YP}_{0.75}\text{V}_{0.25}\text{O}_4:\text{Dy}$ NPs (normalized to Dy 485 nm emission), and (D) $\text{YP}_{0.75}\text{V}_{0.25}\text{O}_4:\text{Sm}$ NPs (normalized to Sm 604 nm emission) with various dopants concentrations under 280 nm excitation. Reprinted with permission from Wang *et al.* (2008b). Copyright 2008 Wiley-VCH.

continuously tuned from deep blue to green (for Dy^{3+}), red (for Eu^{3+}), or yellow (for Sm^{3+}), respectively (Wang *et al.*, 2008b). Similar luminescence modulation was realized in $\text{YP}_{0.8}\text{V}_{0.2}\text{O}_4:\text{Ln}^{3+}$ nanofibers in Lin's report (Hou *et al.*, 2008).

$\text{YBO}_3:\text{Eu}^{3+}$ had a high quantum yield under vacuum ultraviolet (VUV) excitation, but its $^5\text{D}_0$ to $^7\text{F}_1$ (orange) and $^5\text{D}_0$ to $^7\text{F}_2$ (red) transitions contributed in nearly equal proportions to the emission spectra. This poor chromaticity largely limited its application. Pan et al. modified $\text{YBO}_3:\text{Eu}^{3+}$ NPs with $\text{YVO}_4:\text{Eu}^{3+}$ in order to combine the optical advantages of two phosphors. The as-synthesized $\text{YBO}_3:\text{Eu}^{3+}$ NPs were corroded by Na_3VO_4 during the second hydrothermal step, and a small quantity of $\text{YVO}_4:\text{Eu}^{3+}$ was confirmed to form on the surface of YBO_3 phase. With excitation at 240 nm (i.e., the charge-transfer band of YBO_3), the composite phosphor singularly revealed $^5\text{D}_0 \rightarrow ^7\text{F}_2$ (red) dominated transition, which was close to the performance of $\text{YVO}_4:\text{Eu}^{3+}$. Using the intrinsic excitation lines of Eu^{3+} did not generate this phenomenon. It suggested most of Eu^{3+} ions were still in the YBO_3 matrix. Thus, a new energy-transfer process of $\text{YBO}_3 \rightarrow \text{YVO}_4 \rightarrow \text{Eu}^{3+}$ (in YVO_4 lattice) was proposed. This research extended the excitation band of europium phosphors to VUV region with preserved red emission purity (Pan et al., 2006).

The applications of RVO_4 nanomaterials were mainly focused on $\text{YVO}_4:\text{Eu}^{3+}$ NPs because of their high QY. Theoretically, nano-sized $\text{YVO}_4:\text{Eu}^{3+}$ could imitate standard polycrystalline material in most cases. The good dispersibility and low scattering of light by nanomaterials may bring even better performance. On the other hand, $\text{YVO}_4:\text{Eu}^{3+}$ NPs were proposed as a new kind of biological probes. $\text{YVO}_4:\text{Eu}^{3+}$ NPs possess common advantages of rare earth phosphors, like large Stokes shift, narrow emission width, long luminescent lifetime, and high photostability. These points address the shortages of QDs and organic dyes. Therefore, $\text{YVO}_4:\text{Eu}^{3+}$ NPs have the potential to strengthen the current bio-probe system.

Tetrodotoxin and saxitoxin belong to the natural guanidinium toxins that target Na^+ channels of cell membranes. Since guanidine (Gua) functionalized NPs could specifically anchor to the entrance of Na^+ channel, Alexandrou et al. prepared $\text{YVO}_4:\text{Eu}^{3+}@\text{SiO}_2\text{-Gua}$ NPs and used them to label cell membranes of frog live cardiac myocytes. As the luminescent lifetime of Eu^{3+} (0.7 ms) was far beyond that of cell auto-fluorescence, a simple chopper was adequate for the time-gated imaging to screen out background noise, and the location of Na^+ channels was clearly visualized (Figure 49). Additionally, no blinking behavior was observed, probably due to the large numbers of emitters incorporated in each NP (Beaurepaire et al., 2004; Giaume et al., 2005).

Fluorescence resonance energy transfer (FRET) luminescence occurs when donor phosphor decreases its emission intensity and luminescent lifetime, while acceptor phosphor lights up. As the precondition of FRET, the donor emission and the acceptor absorption require adequate spectra overlaps. The spatial distance of donor-acceptor pair is the second factor. Only within a small range, the energy could be transferred from donors to

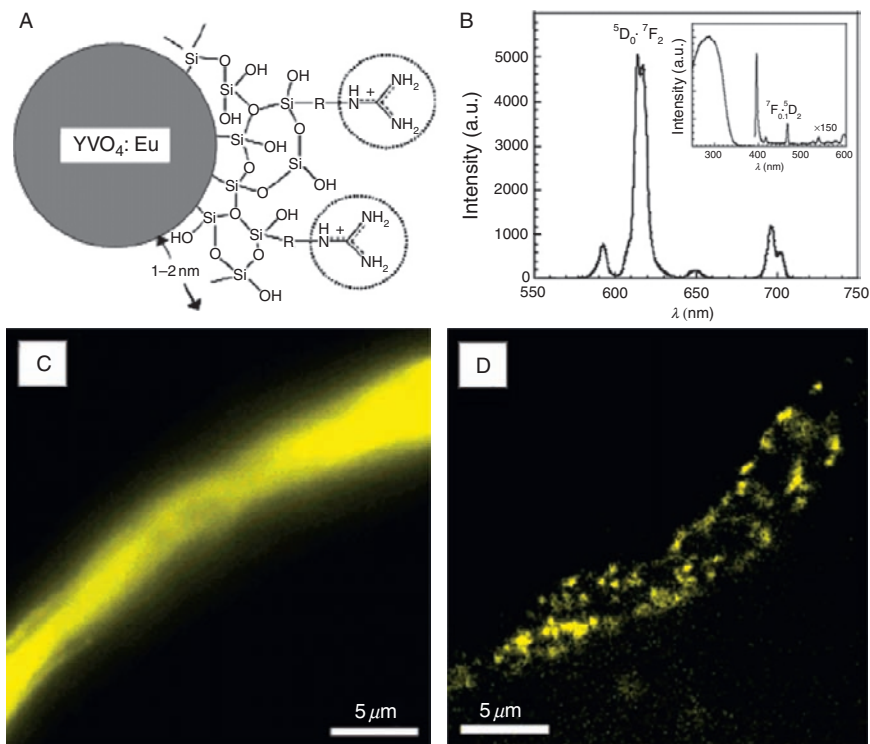


FIGURE 49 (A) Scheme of guanidine-labeled YVO₄:Eu NPs. (B) the emission spectrum with insertion of excitation lines. (C) wide-field image, and (D) time-gated image of Na channels on cell membrane probed by YVO₄:Eu NPs. Reprinted with permission from Beaupaire *et al.* (2004). Copyright 2004 American Chemical Society.

acceptors via nonradiative dipole-dipole interactions. Thus FRET was widely utilized as a molecule-sized ruler in biological studies. Dye-based FRET experiments often suffer from spectral cross-talk problems due to the small Stokes shift of organic phosphors. Using rare earth compound donors is an effective method to improve the detection sensitivity, because its atomic-like emission and large Stokes shift suppress the direct acceptor excitation and donor emission leaking in FRET luminescence channel. Alexandrou's group studied the FRET behavior between Y_{0.6}Eu_{0.4}VO₄ NPs and cyanine 5 (Cy5) at both ensemble and single-particle level. The Cy5 could attach to the NPs by coordinating interaction, and its absorption band overlays the ⁵D₀ to ⁷F_J (*J* = 1, 2, 3, 4) transitions of Eu³⁺. Having aimed at a single Cy5-coated NP on spin-coated silica coverslip, an increase of donor emission was observed after the photobleaching of acceptors (Casanova *et al.*, 2006b). Based on the difference in

photostability, Alexandrou et al. used $Y_{0.6}Eu_{0.4}VO_4$ NPs and Alexa488 in a double-tag imaging experiment for protein/NP ratio counting. The NPs were functionalized by SiO_2-NH_2 shell and then conjugated to Alexa488-labeled- α -bungarotoxin protein. To check the protein number in each protein-NP conjugate, the number of Alexa488 in each bright spot with Eu^{3+} emission was counted via a stepwise-photobleaching manner (Casanova et al., 2007; Giaume et al., 2008). Moreover, single-molecule imaging technique has been used to determine the size of rare earth phosphor NPs. According to the luminescent mechanism, the luminosity of individual rare earth NP was proportional to the number of inner doped emitters, indicating that the NP volume could be calculated from the detectable photon number. In Alexandrou's report, the size distribution of $Y_{0.6}Eu_{0.4}VO_4$ NPs measured by optical microscopy was in agreement with the TEM data. The minimum detectable size for $Y_{0.6}Eu_{0.4}VO_4$ NPs was 13 nm. Further improvements require UV laser for excitation (Casanova et al., 2006a).

3.3 Rare earth borates

$YBO_3:Eu^{3+}$ exhibits a vaterite-type crystal structure with a $P6_3/m$ space group (Chadeyron et al., 1997). The crystal structures of the low- and high-temperature polymorphs of vaterite rare earth orthoborate were established from neutron powder diffraction. In the low-temperature structure, boron atoms are all tetrahedrally coordinated to form B_3O_9 units, while in the high-temperature polymorph, the boron atoms are all in triangular coordination (Ren et al., 1999). Both the low- and high-temperature phases are not the typical vaterite structure. However, they do retain some structural features typical for vaterite (Lin et al., 2004). First principle calculations using extended Hückel formalism suggest that the VUV absorption of borates is significantly affected by the structure of borate ions, and vaterite type orthoborates represent the best properties for optical applications (Yang et al., 2000). The polyborates like (La,Gd) MgB_5O_{10} (Lin et al., 2006) and the ternary compounds like $Sr_3Y_2(BO_3)_4$ and $Ca_3La_3(BO_3)_5$ (Zhang and Li, 2004; Zhang et al., 2005b) were also studied as potential photoluminescence host candidates.

Rare earth orthoborates (RBO_3) show high transparency over visible region, exceptional optical damage threshold, and good UV absorption properties (Moine et al., 2001). Therefore, these materials are candidates for optical applications ranging from VUV phosphors to high-damage threshold ultraviolet optical components in lamps or plasma display flat-panels (Ronda, 1997). Rare earth orthoborates NPs are also investigated for applications in tribology (Hu et al., 2000).

3.3.1 Synthesis

The conventional synthesis of rare earth borates, such as solid-state reaction between rare earth oxides and boric acid, flux-aided solid-state reaction at temperatures above 1000 °C, and milling, leads to a poor crystalline integrity and damaged luminescent properties. Other methods like coprecipitation methods through wet process (Boyer *et al.*, 1999) are also studied.

The combustion method is used to obtain rare earth orthoborates such as vaterite type YBO_3 and GdBO_3 and aragonite type LaBO_3 (Tukia *et al.*, 2005). Soft chemistry methods such as coprecipitation–combustion method, salt assisted combustion method, and emulsion method are employed to prepare the red phosphor $(\text{Y,Gd})\text{BO}_3:\text{Eu}$ (Cui *et al.*, 2008).

Sol-gel method is a facile route to obtain rare earth orthoborates, for example, the sol-gel processes through rare earth alkoxides (Boyer *et al.*, 1999). The thermal decomposition of H_3BO_3 –EDTA complex precursor has been applied in the fabrication of hexagonal $(\text{Y,Gd})\text{BO}_3:\text{Eu}$ NCs (Wei *et al.*, 2002a). $\text{Y}_{0.9}\text{Eu}_{0.1}\text{BO}_3$ phosphor layers deposited on monodisperse SiO_2 particles of different sizes were fabricated via a sol-gel process to form core/shell-structured $\text{SiO}_2@(\text{Y}_{0.9}\text{Eu}_{0.1})\text{BO}_3$ particles (Lin *et al.*, 2007a).

The controlled hydrothermal synthesis of rare earth borates results in various nanostructures. The hydrothermal method at 300 °C yields sub-micron sized $\text{GdBO}_3:\text{Eu}^{3+}$ powders (Wang *et al.*, 2001a). Well-crystallized $\text{YBO}_3:\text{Eu}^{3+}$ NCs were prepared by a mild hydrothermal method in the presence of urea, and a pure hexagonal phase could be obtained at a lower temperature of 200 °C (Jiang *et al.*, 2003).

Hydrothermal treatment with intermediate pH mother liquors leads to doughnut-like $\text{YBO}_3:\text{Eu}$ NP assemblies. The assemblies are sub-micron in size, composed of small NPs or plates (Jiang *et al.*, 2004b; Figure 50). Similar $\text{LuBO}_3:\text{Eu}$ nanoflake assemblies were obtained with varied pH values and temperatures. With a basic pH value, the vaterite type borate forms with flake-like morphology, while particle like assemblies of calcite phase form with pH value of 4. Higher temperature and shorter time result in individual nanoflakes, while moderate temperature and longer time result in nanoflake assemblies (Yang *et al.*, 2008a). Similar products are also obtained for TbBO_3 (Yang *et al.*, 2008b). In fact, the pH values of 8–10 might allow possible hydroxide intermediates to form and the intermediate significantly affects the crystal growth process and the morphology. The so-called O-HT process with Nd_2O_3 and B_2O_3 as reactants in hydrothermal synthesis also results in a similar nanoflake assembly morphology, which might be understood considering the hydration of rare earth oxide under mild hydrothermal conditions into hydroxide (Ma *et al.*, 2007a). Introducing a moderate concentration of NaOH leads

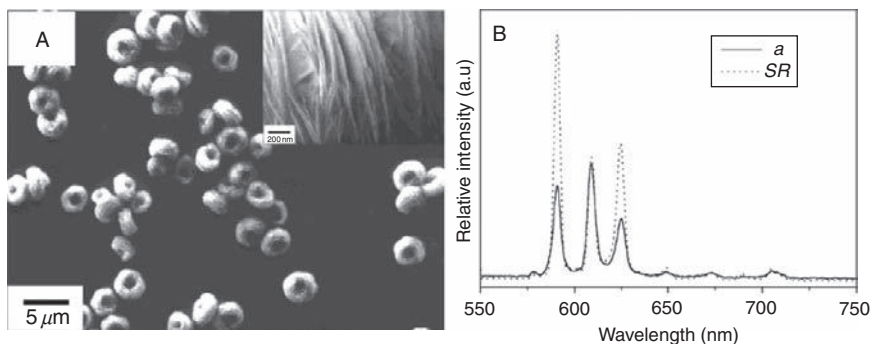


FIGURE 50 (A) SEM images of $\text{YBO}_3\text{:Eu}$ doughnut-like NP assembly, prepared by a hydrothermal method at 180°C . The inset is a magnification of the edge of a single “doughnut.” (B) Emission spectra of $\text{YBO}_3\text{:Eu}$ doughnut-like NP assembly and the bulk $\text{YBO}_3\text{:Eu}$ sample from solid state reaction under 240 nm UV excitation. Reprinted with permission from Jiang et al. (2004b). Copyright 2004 American Chemical Society.

to nanobelt assemblies which might also be a conversion product from the hydroxide NWs (Pan et al., 2007b).

Chelating agents and surfactants usually have strong effects on the morphology of NCs. For rare earth orthoborates, the surfactants like CTAB (Zhang and Lin, 2004) and DEG (Yang et al., 2008a) do not change the morphology greatly while the chelating agent EDTA changes the morphology to irregular NP assemblies (Zhang and Lin, 2004). Uniform drum-like microcrystals of $\text{YBO}_3\text{:Eu}^{3+}$ are obtained in the presence of high-concentration ammonium acetate, which acts both as a buffer reagent and ligand. The acetate ions were found to be responsible for the especially good uniformity and high crystallinity of the products (Jiang et al. 2004c; Figure 52). Well-dispersed, lense-like $\text{YBO}_3\text{:Eu}$ NCs have been fabricated by a solvothermal method in ethanol mediated by oleic ligands (Li et al., 2007c; Figure 51). Song et al. obtained narrow and size-controllable (40–500 nm) $\text{YBO}_3\text{:Eu}$ NTs and NWs by an electrospinning method (Song et al., 2008).

3.3.2 Properties and applications

3.3.2.1 Luminescence of $\text{YBO}_3\text{:Eu}^{3+}$ The excitation and emission spectra of $\text{YBO}_3\text{:Eu}^{3+}$ vary with the synthetic route. The $\text{YBO}_3\text{:Eu}^{3+}$ powder synthesized through a sol-gel method exhibit three Eu^{3+} sites identified by site selective excitation. The Eu^{3+} concentration dependence of emission intensity and Eu^{3+} luminescence decay from 300 to 15 K prove that the energy migration is phononassisted. (Boyer et al., 2003).

YBO_3 is an excellent VUV luminescent host. $\text{YBO}_3\text{:Eu}^{3+}$ exhibits good emission intensities as a phosphor, however, the Eu^{3+} emission of

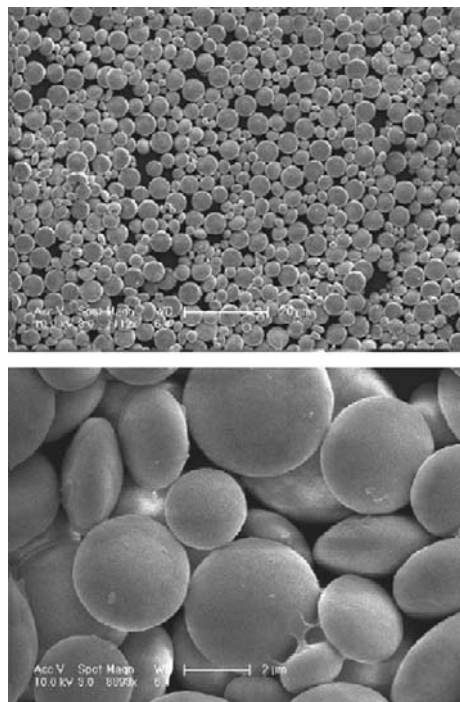


FIGURE 51 SEM images of $\text{YBO}_3:\text{Eu}$ NCs prepared by the liquid–solid-solution method using 8 mL oleic acid at 210°C for 24 h. Reprinted with permission from Li *et al.* (2007c). Copyright 2007 Wiley-VCH.

$\text{YBO}_3:\text{Eu}^{3+}$ is in the orange-red color with poor color purity. In this case, the strong orange emission peak near 590 nm of $\text{Eu}^{3+} {}^5\text{D}_0 \rightarrow {}^7\text{F}_1$ and red emission peak near 610 and 625 nm of $\text{Eu}^{3+} {}^5\text{D}_0 \rightarrow {}^7\text{F}_2$ transitions give almost equal contributions. In order to improve the color purity, that is, increase the ratio of the intensity of red emission over the intensity of orange emission (R/O value), the local symmetry of Eu^{3+} must be lowered so as to decrease the contribution of ${}^5\text{D}_0 \rightarrow {}^7\text{F}_1$ transition.

Pure hexagonal vaterite-typed $\text{YBO}_3:\text{Eu}^{3+}$ NCs are fabricated by a facile sol-gel pyrolysis of R-EDTA precursors. Taking $\text{Y}(\text{NO}_3)_3$, $\text{Eu}(\text{NO}_3)_3$, H_3BO_3 , and $(\text{NH}_4)_2\text{EDTA}$ as starting reagents, the mixed homogeneous aqueous solution with a pH value of 6–7 is slowly evaporated to form complex precursors. After drying, the precursor is calcined at 650–1100 $^\circ\text{C}$ to obtain the nanophosphor (Wei *et al.*, 2002a). The NCs provide both improved intensity and red-orange-ratio compared with the bulk samples obtained from solid state reactions. The quenching concentration also increases with the smaller particle size (Wei *et al.*, 2002b). The XRD patterns and IR spectra confirm that the lattices of $\text{YBO}_3:\text{Eu}^{3+}$ NCs are

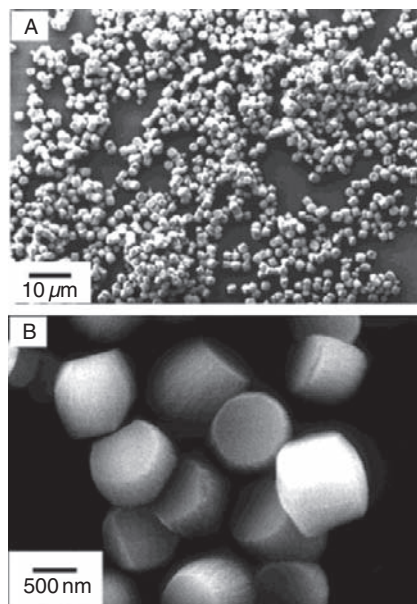


FIGURE 52 SEM images of $\text{YBO}_3:\text{Eu}$ prepared under 200°C with $1.5\text{ mol/L NH}_4\text{Ac}$. (A) A panorama; (B) a magnified image. Reprinted with permission from Jiang et al. (2004c). Copyright 2004 American Chemical Society.

distorted due to small particle size. The site-selective excitation spectra indicate that Eu^{3+} ions exhibit three different sites, two of which are only identified in the NCs. Eu^{3+} ions exhibit enhanced R/O values in these two specific sites, which might be ascribed to the distorted lattices (Wei et al., 2002c). The analysis of EXAFS results shows that the size-dependent chromaticity could be attributed to the disorder in NCs. No direct correlation between size and chromaticity exists, while the size-dependent chromaticity is caused by the poor crystallization and the resulting high levels of disorder as the particle size decreased (Wei et al., 2003a).

Studying the VUV excitation and corresponding emission properties of the $\text{YBO}_3:\text{Eu}^{3+}$ NCs, Wei and coworkers also revealed that as the particle size decreased, the excitonic transfer (ET) and CT bands showed a blue-shift and red-shift, respectively. At the same time, the spectral lines of the CT and borate absorption (BA) bands are narrowed. And BA/CT is decreased, while ET/CT exhibited an increase followed by a decrease. What is more interesting is that a peak located at 130 nm was present (Wei et al., 2003b).

Sheet-like, flower-like, and bundle-like $\text{YBO}_3:\text{Eu}^{3+}$ NCs are synthesized via a hydrothermal route. The time-resolved emission spectra

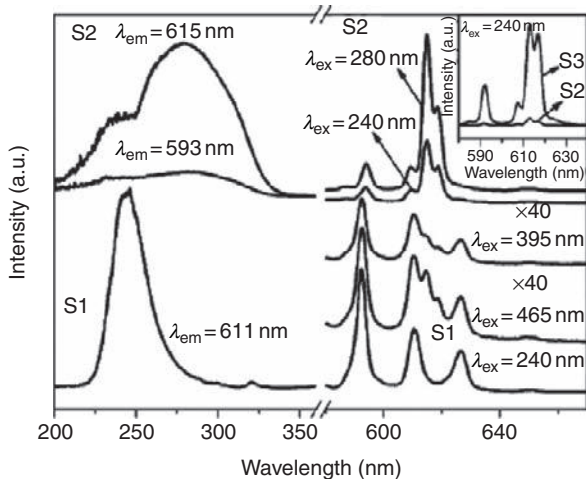


FIGURE 53 Excitation (left) and emission spectra (right) of sample $\text{YBO}_3/\text{YVO}_4$ nanocomposite in contrast to those of YBO_3 nanosheet assembly. Inset is a comparison of emission spectra of $\text{YBO}_3/\text{YVO}_4$ nanocomposite with those of $\text{YBO}_3/\text{YVO}_4$ bulk composite. Reprinted with permission from Pan *et al.* (2006). Copyright 2006 American Chemical Society.

excited by 266 nm laser also suggest that there are interior and surface sites for the Eu^{3+} activators. The surface Eu^{3+} exhibit faster decay characteristics compared with the interior Eu^{3+} (Pan *et al.*, 2007b; Figure 53).

Another way of improving the color purity of rare earth borate phosphor is via fabricating composites. $\text{YVO}_4:\text{Eu}^{3+}/\text{YBO}_3:\text{Eu}^{3+}$ composite was fabricated by chemical corrosion through a two-step hydrothermal process, that is, first by preparation of $\text{YBO}_3:\text{Eu}^{3+}$ NCs and by subsequent chemical corrosion by Na_3VO_4 solution. The energy-transfer and luminescent route via UV and VUV excitation was identified as YBO_3 phase \rightarrow YVO_4 phase \rightarrow Eu^{3+} ions in the YVO_4 phase. High quantum yield was maintained, and considerably improved color purity was reported (Pan *et al.*, 2006).

3.3.2.2 Luminescence of other doped rare earth borate nanophosphors

Hexagonal flake shaped submicron Sb^{3+} and Eu^{3+} codoped YBO_3 crystals have been synthesized using Y_2O_3 , B_2O_3 , SbCl_3 and Eu_2O_3 as raw materials through a hydrothermal method at 473 K for 3 days. The spectrum of Sb^{3+} doped YBO_3 shows an emission band ranging from 350 to 600 with the emission peak at about 450 nm attributed to the $^3\text{P}_1 \rightarrow ^1\text{S}_0$ transition of Sb^{3+} . The color of the emission can be changed through changing the ratio of $\text{Sb}^{3+}/\text{Eu}^{3+}$ (Wen *et al.*, 2005). NIR quantum-cutting in $\text{GdBO}_3:\text{Tb}^{3+}$, Yb^{3+} nanophosphors was investigated. Upon excitation of Tb^{3+} with a

visible photon at 486 nm, two NIR photons could be emitted by Yb^{3+} through cooperative energy transfer from Tb^{3+} to two Yb^{3+} ions (Zhang et al., 2007c). Hydrothermal synthesis of $\text{TbBO}_3:\text{Eu}$ microsphere phosphor is realized at pH 8 and 200 °C. An efficient energy transfer can occur from Tb^{3+} to Eu^{3+} in TbBO_3 host (Yang et al., 2008b). Other rare earth ions doped YBO_3 NCs are also fabricated through sol-gel method. For example, the VUV excited spectroscopy of $\text{YBO}_3:\text{Pr}^{3+}$ could be studied (You et al., 2007). The lanthanide(III)-doped NPs with NIR luminescence emission would be of particular interest in telecommunication components, lasers, and polymer displays, and fluorescent label in bioassays. An urea assisted hydrothermal method (Jiang et al., 2003) is used to obtain vaterite $\text{Y}_{1-x}\text{BO}_3:\text{Nd}_x$ NPs. The narrow emission peaks (excited at 800 nm) that were observed around 1050 and 1320 nm are attributed to the $4\text{F}_{3/2} \rightarrow 4\text{I}_{11/2}$ and $4\text{F}_{3/2} \rightarrow 4\text{I}_{13/2}$ transitions of Nd^{3+} ions, respectively. The concentration quenching occurs at higher dopant concentration of Nd^{3+} ions in smaller NPs compared with the bulk sample (Wang et al., 2004a).

3.4 Rare earth silicates

Rare earth silicates exhibit potential applications as stable luminescent materials for phosphors, scintillators, and detectors. Silica and silicon substrates are frequently used for thin films fabrication, and their nanostructures including monodisperse sphere, NWs are also reliable templates and substrates. However, the composition, structure, and phase of rare earth silicates are rather complex, for example, there are many phases like silicate R_2SiO_5 , disilicate $\text{R}_2\text{Si}_2\text{O}_7$ (A-type, tetragonal), hexagonal $\text{R}_x(\text{SiO}_4)_6\text{O}_2$ oxyapatite, etc. The controlled synthesis of single-phase rare earth silicate nanomaterials can only be reached with precisely controlled experimental conditions. A number of heat treatment based routes, such as solid state reaction of rare earth oxides with silica/silicon substrate, sol-gel methods, and combustion method, as well as physical routes like pulsed laser ablation, have been applied to prepare various rare earth silicate powders and films. The optical properties of rare earth silicate nanocrystalline films and powders have been studied.

Eu doped Y_2SiO_5 and $\text{Y}_2\text{Si}_2\text{O}_7$ films could be prepared through metal-organic decomposition sol-gel process. The red/orange ratio (${}^3\text{D}_0 \rightarrow {}^7\text{F}_2$ emission over ${}^3\text{D}_0 \rightarrow {}^7\text{F}_1$ emission) exhibit strong correlation with the annealing temperature and crystal structure (Zhang et al., 2002b). Taghavinia et al. reported Eu doped $\alpha\text{-Y}_2\text{Si}_2\text{O}_7$ NPs grown inside a porous silicon oxide matrix by chemical impregnation of porous silicon layers and postheating at about 1100 °C (Taghavinia et al., 2004). Single phase silicates were obtained, however, the size distribution was broad. Gonzalez-Ortega et al. reported white-emitting nanocrystalline rare earth activated Y_2SiO_5 synthesized by combustion synthesis or pulsed

laser ablation (Gonzalez-Ortega *et al.*, 2005). The $\text{Y}_2\text{SiO}_5\text{:Ce,Tb}$ was excited at 358 nm while both the $\text{Ce}^{3+} 5d \rightarrow {}^2\text{F}_j$ emission around 390–440 nm and the emission of $\text{Tb}^{3+} {}^5\text{D}_4 \rightarrow {}^7\text{F}_j$ were observed and could be tuned with the composition.

Cerium silicate nanomaterials exhibit violet/blue emissions with correlation to their microstructures. Kepinski *et al.* carried out a series of studies of cerium silicates (Kepinski *et al.*, 2002a,b). Heating nanocrystallites of CeO_2 supported on SiO_2 substrate in hydrogen up to 1100 °C leads to the formation of spreaded ceria, cerium silicate $\text{Ce}_6(\text{Si}_4\text{O}_{13})(\text{SiO}_4)_2$ and tetragonal disilicate $\text{Ce}_2\text{Si}_2\text{O}_7$ (elongated NPs/NRs) in turn. The nanocrystalline $\text{Ce}_2\text{Si}_2\text{O}_7$ exhibits a typical emission band around 410 nm.

The modern silicon-based microelectronics led to the miniaturization of electronic devices. However, delays caused by metallic interconnections became a bottleneck for the improvement of their performances. One possible solution of this problem is to use optical interconnections for the transfer of information, and, therefore, silicon compatible materials and devices that are able to generate, guide, amplify, switch, modulate, and detect light are needed. Rare earth silicates with luminescent rare earths and compatibility with silicon may be a good choice for these applications (Miritello *et al.*, 2007). Miritello *et al.* presented the study on nanocrystalline erbium silicate thin films fabricated on silicon/silica substrates. The obtained films exhibit strong photoluminescence emission around 1540 nm with room temperature excitation by 488 nm Ar^+ laser.

Ananias *et al.* reported NPs of layered $\text{Ln}_2(\text{SiO}_4\text{H})(\text{OH})_2(\text{H}_2\text{O})\text{Cl}$ (where Ln = Eu, Gd, and Tb) and their microcrystalline correspondence with mixed Eu/Gd or Tb/Gd rare earths (Ananias *et al.*, 2008). These materials display energy transfer between different pairs $\text{Eu}^{3+}/\text{Gd}^{3+}$ and $\text{Tb}^{3+}/\text{Gd}^{3+}$. The PL properties of the mixed $\text{Eu}^{3+}/\text{Gd}^{3+}$ sample change upon F^- for Cl^- ion exchange, with potential application for sensing.

Suh *et al.* reported the study on Er^{3+} luminescence and cooperative upconversion in $\text{Er}_x\text{Y}_{2-x}\text{SiO}_5$ NC aggregates fabricated using Si NWs (Suh *et al.*, 2008). The composition of the final NCs can be varied continuously from pure Y_2SiO_5 to pure Er_2SiO_5 while keeping the crystal structure. The cooperative upconversion coefficient of Er^{3+} in these NCs is much lower than that reported for Er-doped silica showing viability of using such silicates for compact, high-gain Si-based optical material for Si photonics.

Choi and Shin *et al.* reported the fabrication of Si/Silica/ $\text{Er}_2\text{Si}_2\text{O}_7$ core-shell NWs of about 120 nm in diameter, grown vertically on Si substrates by the vapor–liquid–solid mechanism in an Si–Er–Cl– H_2 system using Au catalyst, which is shown in Figure 54 (Choi *et al.*, 2005). The NWs showed promising 1.54 μm Er^{3+} optical activity viable for light source applications.

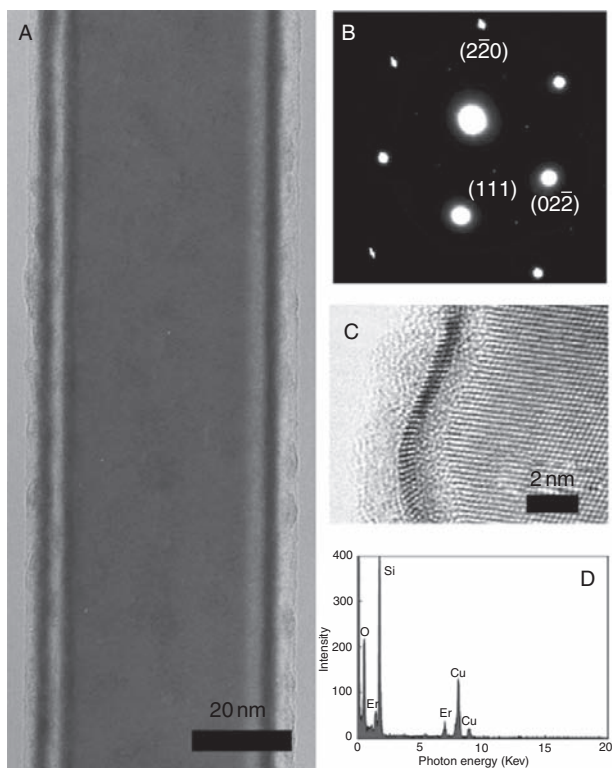


FIGURE 54 A single Si/Er₂Si₂O₇/SiO₂ core-shell NW: (A) TEM image. (B) SAED pattern taken along the [111] zone axis of Si NW in (A). (C) HRTEM image. (D) EDS spectrum measured the edge part of the NW, showing the presence of Er, Si, and O. Reprinted with permission from Choi et al. (2005). Copyright 2005 American Chemical Society.

3.5 Other rare earth oxysalts

This section covers some other heterometallic rare earth oxides, including Al, Ti, Zr, Sn, Mo, W, Mn, Fe, Co, Ni, and Cu complex oxides, while certain well-known oxysalts, Y–Ba–Cu–O, for example, will not be specifically discussed. For these heterometallic compounds, due to their relatively complex compositions, it is usually difficult to obtain phase-pure products, especially when some dopant ions are added. At elevated temperatures, some of these oxides undergo phase transitions, which may significantly change their physical and chemical properties such as thermal expansion coefficient and ionic conductivity. And for those oxides with variable metal valencies, different nonstoichiometric compositions may also result in distinct functionalities in magnetism and catalysis.

3.5.1 Rare earth aluminates

Perovskite-structured RAIO_3 and garnet-structure $\text{R}_3\text{Al}_5\text{O}_{12}$ are the two most important categories of rare earth aluminates, which could be obtained through conventional solid state reactions; however, the high sintering temperature imposes technological constraints for the synthesis and processing, while nanoscience can yield homogeneous fine powders to lower the sintering temperature. The rare earth aluminate NPs can be prepared through aerosol synthesis, coprecipitation, sol-gel, and combustion methods.

RAIO_3 exhibit high dielectric constants, zero temperature coefficients of resonant frequency, and provide excellent lattice and thermal expansion matches for Y–Ba–Cu–O and Bi–Sr–Ca–Cu–O superconductors, and hence find applications in catalysis and as substrates for depositing superconducting thin films. Behera *et al.* reported ultrasonic assisted combined gel synthesis of LaAlO_3 nanospheres with sizes in the range 25–40 nm (Behera *et al.*, 2004). Phase-pure powders were obtained by calcination at 600 °C for 4 h. Sahu *et al.* prepared LaAlO_3 with gelation-precipitation technique, and the influence of chloride ions on phase evolution and morphology was studied (Sahu *et al.*, 2004). The results showed that chloride-free samples crystallized to pure LaAlO_3 perovskite phase at 600 °C. Hreniak *et al.* reported Eu^{3+} -doped LaAlO_3 via sol-gel derived Pechini method, and an enhancement of luminescence lifetimes with decreasing of the NCs sizes was found (Hreniak *et al.*, 2006). Same method was employed by Daren *et al.* to prepare luminescent Tb^{3+} -doped LaAlO_3 (Deren *et al.*, 2007). Cizauskaite *et al.* synthesized GdAlO_3 nanocrystalline ceramics via ethanediol assisted sol-gel route (Cizauskaite *et al.*, 2007). Single-phase GdAlO_3 perovskite was obtained after calcination at 1000 °C for 10 h.

$\text{R}_3\text{Al}_5\text{O}_{12}$ perform as good laser hosts for luminescent centers. Xia *et al.* prepared Eu^{3+} -doped $\text{Y}_3\text{Al}_5\text{O}_{12}$ garnet (YAG) phosphors by a facile sol-gel combustion method (Xia *et al.*, 2005). YAG phase is obtained through sintering at 900 °C for 2 h without intermediate phases observed. The charge transfer band of the nanophosphors shows a blue-shift compared to that of amorphous ones due to lower covalency of Eu–O bond in nanocrystalline phosphors. Capponetti *et al.* reported Nd^{3+} -doped YAG by coprecipitation method, in which a substitution rate as high as 24 at.% was found (Capponetti *et al.*, 2007a,b). The formation of a single phase cubic garnet structure was attained at temperatures as low as 900 °C with neodymium loading less than 5–6 at.%. For neodymium loading higher than 5–6 at.% the garnet structure may be substantially affected by the presence of monoclinic $\text{Y}_4\text{Al}_2\text{O}_9$ and orthorhombic distorted perovskite-like YAlO_3 phases. Purwanto *et al.* prepared Ce^{3+} -doped YAG from urea-added nitrate aqueous precursor by flame-assisted spray pyrolysis

(Purwanto, et al., 2008). An optimal quantum efficiency of 45.0% was observed for the sample with 4.0 at% substitution. Zhang et al. reported $(Y_{1-x}Ln_x)_3Al_5O_{12}:Ce$ ($Ln = Gd, La$) by *in situ* esterification (Zhang et al., 2008e). The effects of Gd^{3+} and La^{3+} ions on structure and luminescence were investigated. For Gd^{3+} -doped YAG, a maximum substitution ratio of 50 mol% was found and 20 mol% for La^{3+} -doped samples. As the doping concentration of Gd^{3+} and La^{3+} increased, the maximum emission band showed red shift. The doped samples exhibited lower emission intensity and shorter luminescent lifetime due to distorted structure. Chaudhury et al. synthesized a series of gadolinium aluminates including $GdAlO_3$, $Gd_3Al_5O_{12}$, and $Gd_4Al_2O_9$ via solution combustion method in glycerol (Chaudhury et al., 2007). Thermophysical properties including thermal expansion and specific heat were studied.

3.5.2 Rare earth titanates, zirconates, and stannates

Titanates, zirconates and stannates of rare earths have a general formula $A_2B_2O_7$, where A represents Ln^{3+} ion, and B represents Ti^{4+} , Zr^{4+} or Sn^{4+} ions. In general, these compounds exhibit high melting-points, high thermal stability, high thermal expansion coefficients, good chemical resistance, low thermal conductivity, and high ionic conductivity, which promise their potential applicability in thermal barrier coatings, hosts for luminescence centers, hosts for nuclear wastes, oxygen monitoring sensors, high-temperature catalysts, and solid electrolytes in high-temperature fuel cells. When these materials are fabricated as NPs, the reduced particle size and enlarged specific surface area may result in varied phase transition temperatures, enhanced catalytic activity, and improved processability. Generally, these rare earth complex oxide nanomaterials can be prepared by conventional solid-state reactions, coprecipitation, sol-gel, hydrothermal, and self-propagation methods.

The conventional solid-state reactions involve a series of laborious cycles of heating at high temperature and repeated grinding, and the resulting powders show low phase purity, inhomogeneous composition and extensive agglomeration. Notably, Henkes et al. developed a NP-directed approach for the rapid low-temperature synthesis of bulk-scale $Y_2Ti_2O_7$ and $Eu_2Ti_2O_7$ oxides, which employs readily available binary oxide NPs as precursors to form nanocomposites, which may then be thermally transformed rapidly at low temperatures into a predesigned product phase (Henkes et al., 2006). Following this strategy, NPs were prepared from nanomodulated precursors comprising Y_2O_3/Eu_2O_3 and TiO_2 NPs. This alternative approach effectively reduces diffusion distances to the nanometer scale and allows reaction to occur within reduced reaction time and under relatively low temperatures, typically 400–700 °C lower than is necessary for conventional routes.

In contrast to solid-state reactions, solution-based soft chemical methods are expected to yield chemically homogeneous and phase-pure products with narrow particle size distribution and low crystallization temperatures.

Coprecipitation method gives pure phase with relatively simple experimental procedures and availability of mass production. Shlyakhtina *et al.* reported $Y_2Ti_2O_7$ nanoceramics prepared from coprecipitated and freeze-dried precursors (Shlyakhtina *et al.*, 2005). A fluorite–pyrochlore–fluorite transformation with transition temperatures respectively around 800 and 1670 °C was established. For the $Y_2Ti_2O_7$ with grain size of about 30 nm sintered at 1670 °C, a linear correlation between electrical conductivity and temperature was observed over the entire temperature range. Wang *et al.* reported the ammonia coprecipitation preparation of $La_2Sn_2O_7$ NPs from stannic chloride pentahydrate and lanthanum nitrate (Wang *et al.*, 2006g). The size of particles synthesized by the reverse-drop method (adding the salt solution to aqueous ammonia) was smaller than those synthesized by the nature-drop method (adding aqueous ammonia to the salt solution), and the NPs became large rapidly with the dilution of the original reagent solution.

Zhang *et al.* reported citric acid assisted sol-gel synthesis of well crystallized square-like $Dy_2Ti_2O_7$ NPs with heat treatment at 700 °C for 2 h (Zhang *et al.*, 2008f). The photoactivity was investigated via decomposition of methyl orange. A decomposition ratio of 98.6% within 60 min was observed. Lu *et al.* developed a CTAB-assisted sol-gel method to prepare Eu^{3+} -doped 40-nm $Y_2Sn_2O_7$ NPs with good crystallinity. The as-synthesized materials display intense and prevailing emission at 589 nm belonging to the $^5D_0 \rightarrow ^7F_1$ magnetic dipole transition (Lu *et al.*, 2004b). Fujihara *et al.* prepared Eu^{3+} -doped $Y_2Sn_2O_7$ thin films with citric acid as chelating agent and poly(ethylene glycol) as cross-linking agent (Fujihara and Tokumo, 2005). The sol was dip-coated on quartz glass substrate and immediately heated at 800–1000 °C for 1 h. A film with the thickness of approximately 150 nm was obtained, displaying five predominant orange-red band emissions at a single-wavelength ultraviolet excitation due to doubly split magnetic-dipole $^5D_0 \rightarrow ^7F_1$ and electric-dipole $^5D_0 \rightarrow ^7F_2$ transitions. Ion *et al.* reported a nitrate-modified alkoxide-based sol-gel route for preparing single phase $La_2Zr_2O_7$ NPs (Ion *et al.*, 2007). The nitrates acted as an oxidizing agent for the organic groups of the precursor and enabled their removal. The decomposition of the precursor started with a strongly exothermic reaction, yielding a porous powder that crystallized into a pyrochlore phase at 800 °C. The powder that was heated at 900 °C for 1 h was composed of friable agglomerates of approximately 60-nm-sized NPs. Li *et al.* reported a polymeric complex method to prepare nanocrystalline $La_{1.5}Ln_{0.5}Ti_2O_7$ ($Ln = Pr, Gd, Er$) (Li *et al.*, 2006e). $La_{1.5}Gd_{0.5}Ti_2O_7$ was found to show

the highest photocatalytic activity in the decomposition of methyl orange. The authors attributed the activity to the half-filled electronic configuration of Gd^{3+} .

Hydrothermal method is expected to result in homogeneous chemical composition, narrow particle size distribution and fine crystallinity at relatively low temperature. Chen et al. reported first hydrothermal synthesis of fluorite and pyrochlore $La_2Zr_2O_7$ NPs (Chen and Xu, 1998). The NPs were prepared under moderate conditions from lanthanum chloride and titanium chloride/zirconium oxychloride, respectively, and with KOH as the mineralizer. Li et al. reported the one-step hydrothermal synthesis of $La_2Ti_2O_7$ nanosheets (Li et al., 2006d). With NaOH as the mineralizer, 2D $La_2Ti_2O_7$ nanosheets were obtained at 200 °C for 24 h. Experiments of decoloration of methyl orange and evolution of hydrogen indicated an enhanced photocatalytic activity. Moon et al. reported $La_2Sn_2O_7$ nanospheres synthesized via the hydrothermal method (Moon, 2001). The reaction was performed under 200 °C for 36 h, resulting in phase-pure and well-crystallized NPs. SEM and TEM observation for morphologic evolution and kinetic analysis during crystallization indicated that $La_2Sn_2O_7$ formation probably proceeds via a two-step reaction. $Ln_2Sn_2O_7$ ($Ln = La, Sm, \text{ and } Gd$) NPs prepared by hydrothermal reactions were reported by Park et al. (2003). Addition of manganese to the rare earth pyrochlore improves the catalytic activity in methane combustion. Li et al. reported hydrothermally synthesized $Y_2Sn_2O_7$ NPs using different organic agents (PMMA, CTAB, EDTA) (Li et al., 2006c). BET analysis revealed that PMMA does not significantly influence the surface area compared with samples prepared without organic agent, while with the addition of CTAB or EDTA, the surface area is reduced by approximately 40% and 70%, respectively. Zeng et al. reported nanocubic $La_2Sn_2O_7$ (Figure 55), and the influence of several experimental parameters (alkaline concentration, reaction time, and reaction temperature) was also investigated (Zeng et al., 2007). A three-stage morphology evolution mechanism was proposed. Photocatalytic activity was examined via degradation of methyl orange and generation of hydrogen.

Self-propagating high temperature synthesis utilizes reaction heat to drive the expected phase transition, resulting in good quality nonagglomerated submicron or nanometer sized powders, which can be sintered to high density at relatively low temperatures. Joseph et al. (2008) reported self-propagating synthesis of $Ln_2Ti_2O_7$ ($Ln = La, Nd, \text{ and } Gd$) NPs with urea. The powders were slowly heated, and a spontaneous incandescent reaction took place vigorously at approximately 350 °C. The mixture self-ignited at about 400 °C along with evolution of large amount of gases, and the resulting powders formed a foam-like highly porous network. The photoluminescence of $La_2Ti_2O_7$ around 610 nm was attributed to the presence of Ti^{3+} ions. Wang et al. reported Dy^{3+} -doped $La_2Sn_2O_7$

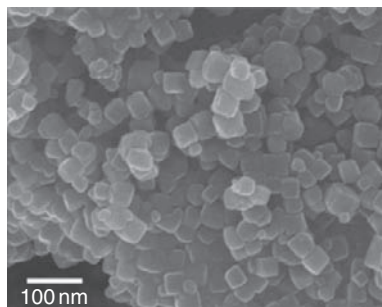


FIGURE 55 SEM photographs of $\text{La}_2\text{Sn}_2\text{O}_7$ nanocubes synthesized at 200 °C for 12 h. Reprinted with permission from Zeng *et al.* (2007). Copyright 2007 American Chemical Society.

NPs with sizes less than 50 nm (Wang *et al.*, 2007e). Energy transfer from host to Dy^{3+} was observed which leads to the strong emission around 485 and 578 nm.

Several alternative synthetic methods have also been developed. Arney *et al.* reported a rapid and simple one-step molten-salt flux synthesis of $\text{La}_2\text{Ti}_2\text{O}_7$ platelet particles (Arney *et al.*, 2008). Stoichiometric mixture of La_2O_3 and TiO_2 (preheated and dried) was ground and then combined with the $\text{Na}_2\text{SO}_4/\text{K}_2\text{SO}_4$ salt flux to give $\text{La}_2\text{Ti}_2\text{O}_7$. Platelet-like particle morphologies were obtained in high purity and with homogeneous microstructures that range in size from approximately 500–6000 nm, with thicknesses of less than 100 nm. The particle size decreases with increasing amount of flux used in the synthesis. High photocatalytic activity was observed, which was assigned to the exposed crystallite edges and the (010) and (001) crystal faces.

Tong *et al.* reported $\text{Ln}_2\text{Zr}_2\text{O}_7$ NPs synthesized via stearic acid method, which uses stearic acid as both the reactant and dispersant (Tong *et al.*, 2008). The photocatalytic activity was found strongly dependent of Ln, decreasing in the sequence of $\text{Dy} > \text{Nd} > \text{Er} > \text{Sm} > \text{La}$.

Li *et al.* reported pyrochlore-structured $\text{La}_2\text{Zr}_2\text{O}_7$ prepared by electrospinning technique from PVP/lanthanum nitrate/zirconium oxychloride as precursors, which was then calcinated at 1000 °C for 12 h, with a diameter of 100–500 nm (Figure 56) (Li *et al.*, 2006b). The fiber structure shows a low sintering ability, which could be attributed to the random stacking of fiber, resulting in a structure with low contact area between fibers.

3.5.3 Rare earth molybdates and tungstates

Rare earth molybdates and tungstates share a general formula of $\text{A}_2\text{B}_2\text{O}_9$, where A represents rare earth, and B represents molybdenum or tungsten. Usually, they show reversible phase transition from a monoclinic

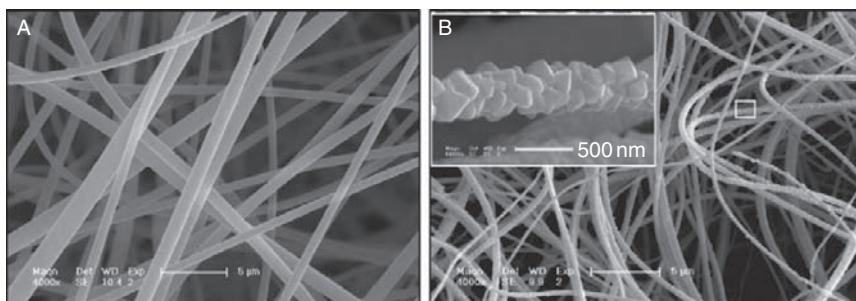


FIGURE 56 SEM micrographs for PVP-precursor fibers (A) and $\text{La}_2\text{Zr}_2\text{O}_7$ fibers calcined at 1000°C (B). Reprinted with permission from Li et al. (2006b). Copyright 2006 Elsevier.

α -polymorph to a cubic β -polymorph at high temperature in association with long-range oxygen vacancy ordering. Molybdates with cubic structure are good conductors with ionic conductivity comparable to that of YSZ and gadolinium doped ceria, which may find applications in electrolyte material for SOFCs, membrane materials for oxygen separation, and oxygen sensors. However, the drastic drop in conductivity below 560°C and possible mechanical failure due to the high thermal expansion of the unit cell volume during phase transition hinders their application. Consequently, a wide range of substitutions have been investigated in order to stabilize the β -polymorph. Particularly, the redox stability of $\text{La}_2\text{Mo}_2\text{O}_9$ -based materials can be improved by partial substitution of Mo by W. The similar ionic radius of Mo and W, 0.59 and 0.60 Å, respectively, permits high levels of substitution up to 80%, maintaining the cubic beta- $\text{La}_2\text{Mo}_2\text{O}_9$ structure and the high ionic conductivity.

Marrero-Lopez et al. reported the synthesis of $\text{La}_2\text{Mo}_2\text{O}_9$ from freeze-dried powder precursors (Marrero-Lopez, et al., 2004). Eu^{3+} -doped samples exhibited improved stability and enhanced ionic conductivity, and optical characterization indicated that an NC-size dependent energy transfer process from matrix to the europium ions occurs. These $\text{La}_2\text{Mo}_2\text{O}_9$ NPs were sintered and investigated by impedance measurement. A significant grain boundary resistance was found for sintered samples prepared at temperatures below 1173 K, which was minimized upon sintering at temperatures above 1173 K (Marrero-Lopez, et al., 2005). Some other cations (Ca^{2+} , Sr^{2+} , Ba^{2+} and K^+) were also doped in the $\text{La}_2\text{Mo}_2\text{O}_9$ matrix for stabilization. The dependence of overall conductivity on both the ionic radius and dopant content was studied (Marrero-Lopez, et al., 2007). They also prepared $\text{La}_2\text{W}_2\text{O}_9$ with similar method, and different substitution (Sr^{2+} , Ba^{2+} , K^+ , Nb^{5+} , and V^{5+}) were performed. Nanocrystalline materials obtained by a freeze-drying precursor method at 600°C exhibit mainly the β - $\text{La}_2\text{W}_2\text{O}_9$ structure, however,

the triclinic α -form is stabilized as the firing temperature increases and the crystallite size grows. Only high levels of Ba^{2+} and V^{5+} substitutions retained the cubic form at room temperature after firing above $1100\text{ }^\circ\text{C}$ (Marrero-Lopez *et al.*, 2008).

Subramania *et al.* reported Pr^{3+} -doped $\text{La}_2\text{Mo}_2\text{O}_9$ by pyrolysis of polyacrylate salt precursors via *in situ* polymerization of the metal salts and acrylic acid (Subramania, *et al.*, 2007). Electrical characterization shows that the oxide-ion conductivity increases with increasing Pr content and the maximum conductivity is attained at $x = 0.5$ in $\text{La}_{2-x}\text{Pr}_x\text{Mo}_2\text{O}_9$. They also reported microwave-assisted combustion synthesis of $\text{La}_2\text{Mo}_2\text{O}_9$, which affords a highly pure nanocrystalline powder at shorter times (Saradha *et al.*, 2008). Aspartic acid is selected both as the fuel and dispersing agent in combustion process. The synthesized nanocrystalline powder showed good sinterability and reached more than 97% of theoretical density even after treatment at low temperature of $800\text{ }^\circ\text{C}$ for 5 h. The sintered $\text{La}_2\text{Mo}_2\text{O}_9$ sample exhibited a conductivity of 0.159 S/cm in air at $750\text{ }^\circ\text{C}$.

Zhuang *et al.* prepared $\text{La}_2\text{Mo}_2\text{O}_9$ films with sol-gel method and spin-coating technique (Zhuang *et al.*, 2008). The thickness of the films was more than 200 nm for single-layered films. The electrical conductivity of the films reaches 0.06 S/cm at $600\text{ }^\circ\text{C}$ that was almost more than one order of magnitude higher than that of the corresponding bulk material.

3.5.4 Rare earth manganites, ferrites, cobaltites, nickelates

Rare earth manganites, ferrites, cobaltites and nickelates share a general formula RMO_3 , and usually possess a perovskite-type structure. These heterometallic oxides, featured by their nonstoichiometric structures, attract extensive fundamental and practical interests by virtue of their rich functionality, particularly in catalysis, magnetism and conductivity (including semiconductivity and superconductivity). For example, LaCoO_3 shows a semiconducting behavior up to 400 K, and metallic conductivity at temperature above 1200 K, and variable Co^{3+} spin states at different temperatures; LaNiO_3 is an intrinsic n-type metallic oxide characterized by a low electron density at the Fermi level similar to that of high- T_C superconducting oxides, and exhibits a very sharp metal to insulator (MI) transition. These interesting properties draw attention in the fields of catalysts, sensors, solid oxide fuel cells, and magnetic media. Generally, these compounds can be obtained via solid-state reactions, combustion, coprecipitation, sol-gel, hydrothermal/solvothermal method, and there are also some other methods reported, including decomposition of heterometallic complexes, epitaxial growth, electrospinning and so on. Recently, techniques to fabricate mesoporous structures and nanocomposites of RMO_3 have also been developed.

Conventional solid-state reaction is a facile method to prepare RMO_3 nanopowders, with relatively poor size control and wide size distribution, though. Royer et al. reported LaCoO_3 , LaMnO_3 , $\text{La}_{0.6}\text{Sr}_{0.4}\text{MnO}_3$, $\text{La}_{0.9}\text{Ce}_{0.1}\text{MnO}_3$ NPs synthesized by reactive grinding (Royer, et al., 2008). The catalytic activity on wet air oxidation of stearic acid was studied. LaCoO_3 samples presented the highest initial activity for this reaction, while pure and substituted LaMnO_3 samples show weaker activity.

Zhang et al. reported nanoscale $\text{LaCo}_{1-x}\text{Cu}_x\text{O}_3$, $\text{LaMn}_{1-x}\text{Cu}_x\text{O}_3$ perovskites prepared by reactive grinding, and the reduction of NO by CO over these compounds (Zhang et al., 2006b). Compared to LaMnO_3 , LaCoO_3 exhibits better catalytic performance. After 20% Cu substitution, the catalytic activity for LaCoO_3 can be improved, which is attributed to the ease of generation of anion vacancies after Cu incorporation and enhanced lattice oxygen mobility.

Li et al. developed a solid-state reaction process to synthesize perovskite-type LaCoO_3 NCs with grain diameters of 15–40 nm (Li et al., 2002). In the first step of the preparation, ~5 nm composite hydroxide NPs were synthesized by grinding metal nitrates liquid paste and mixing with KOH. Then the composite powders were calcined at ~800 °C, yielding a single-phase oxide. Tien-Thao et al. prepared $\text{LaCo}_x\text{Cu}_{1-x}\text{O}_{3-\delta}$ ($x < 0.3$) by mechano-synthesis (Tien-Thao et al., 2008). The sample has various distinct Co^{3+} ions in the perovskite lattice, which are more reducible. The reduced catalyst surface comprising cobalt and copper atoms is very selective for the hydrogenation of CO.

Combustion method featured by its short reaction time and low cost is also widely employed. Qi et al. prepared nanosized LaFeO_3 NPs using an auto-combustion route, and the obtained perovskite sample exhibited a high coercivity around 99 G and a low saturation magnetization of 2.75 emu g^{-1} (Qi et al., 2002). Berger et al. reported combustion synthesis of pure and Sr^{2+} -doped LaMnO_3 nanopowders using metal nitrate as oxidants and different organic compounds as fuels (Berger et al., 2007). Chen et al. prepared perovskite LaMnO_3 and NdCoO_3 powders with an average crystallite size, respectively, of 12.5 and 9 nm via combustion reactions (Chen et al., 2006c, 2007d). Wang et al. reported LaMO_3 ($M = \text{Fe, Co, Ni}$) NPs prepared by a glycine combustion method, and examined their catalytic activity during thermal decomposition of NH_4ClO_4 (Wang et al., 2006i).

Dey and Nath employed a pyrophoric reaction process to obtain $\text{La}_{0.7}\text{Ca}_{0.3}\text{MnO}_3$ NPs, and they investigated the effect of grain size modulation on the magnetic and electronic transport properties of the NPs (Dey and Nath, 2006). With decreased grain sizes, the metal-insulator transition temperature drops gradually, while ferromagnetic-paramagnetic transition temperature remains almost constant. A phenomenological model based on a spin-polarized tunneling mechanism was proposed to explain the observed electronic transport behavior over the

whole temperature range (20–300 K). With a similar method, they also prepared nanosized $\text{La}_{0.7}\text{Sr}_{0.3}\text{MnO}_3$ and investigated the effect of nanometric grain size modulation on the magnetoimpedance (MI) behavior (Dutta *et al.*, 2007). The experimental results show that MI increases with the increase in nanometric grain size for the series of samples, which can be related to the dependency of skin depth on external magnetic field and applied AC signal frequency.

Nagabhushana prepared a series of alkaline-earth-metal-doped (Ca^{2+} , Sr^{2+} , Ba^{2+}) LaMnO_3 NPs via combustion method (Nagabhushana, *et al.*, 2005, 2006, 2007, 2008). For all doped samples, a cubic to rhombohedral phase transition is observed. With increased dopant content, the particle size was reduced and the surface area was accordingly increased. All the samples exhibit metal-insulator transitions. Particularly, the $\text{La}_{0.9}\text{Ba}_{0.1}\text{MnO}_3$ sample exhibits field-induced ferromagnetic ordering and negative magnetoresistance.

Coprecipitation route was employed by Kharrazi *et al.* to prepare TbMnO_3 NPs, and they also investigated their structural, magnetic and dielectric properties (Kharrazi *et al.*, 2006). Liang *et al.* synthesized $\text{La}_{0.5}\text{Sr}_{0.5}\text{MnO}_3$ cubes and NPs by coprecipitation and hydrothermal method, respectively (Liang *et al.*, 2007a). The effect of Jahn-Teller distortion on the catalytic performance during CO and CH_4 oxidation were elucidated.

As reports on the sol-gel synthesis of these compounds are quite abundant, only a few representative works will be reviewed here. Tiwari and Rajeev prepared nanocrystalline $\text{LaMnO}_{3+\delta}$ with nitrate salts and citric acid, and studied their magnetic properties with respect to oxygen stoichiometry (Tiwari and Rajeev, 1997). It was found that as the excess oxygen concentration decreases, the magnitude of the AC susceptibility and ferromagnetic-paramagnetic transition temperature decreases, and ultimately ferromagnetism vanishes completely.

Dezanneau *et al.* reported $\text{La}_{1-x}\text{MnO}_{3+\delta}$ nanocrystalline powders prepared by an acylamide polymerization sol-gel method (Dezanneau *et al.*, 2002a,b, 2003). The composition analysis revealed that for $\text{La}/\text{Mn} < 0.9$ the Mn_3O_4 phase was present, while for $\text{La}/\text{Mn} > 0.9$, the high oxygen excess led to considerable vacancies on cationic sites. The Curie temperature remained constant at 295 K for the former case, while decreased Curie temperatures were observed for the latter case, due to the increasing amount of Mn vacancies.

Zhang *et al.* prepared nanosized YMnO_3 powders via a modified citric acid method, and investigated the size effect on the microstructure and stoichiometry (Zhang *et al.*, 2004c). A remarkable broadening of reflection peaks in Raman and IR spectra was found with decreased grain size, identifying the significant surface structure relaxation effect for small-size powders.

Popa prepared pure single-phase LaMeO_3 (Me = Mn, Fe, Co) nanopowders with homogeneous microstructure (Popa et al. 2002a,b, 2003a,b). Raman spectral properties of these samples were investigated, which were found to be related to the particle size, oxygen content, symmetry, temperature, and oxygen partial pressure during preparation. Particularly, the magnetization curves of LaMnO_3 powders indicated the ferromagnetic behavior.

Markovich et al. employed citrate method to prepare LaMnO_3 sample with different particle sizes (20, 25, 30 nm), and investigated the size effects on magnetic properties (Markovich et al., 2007, 2008a,b). All NPs exhibited a paramagnetic to ferromagnetic transition at a Curie temperature above 200 K. It was found that the relative volume of the ferromagnetic phase increases for larger particle size.

Niu et al. prepared a series of RFeO_3 (R = Nd, Sm, Eu, Gd, Dy, Ho,) perovskites using sol-gel method, and examined their performances in gas-sensing (including H_2 , H_2S , CO, etc.) and photocatalytic degradation of several water-soluble dyes (Niu et al., 2003, 2004a,b, 2005a,b,c).

Malavasi et al. (2003) prepared nanocrystalline $\text{La}_{1-x}\text{Na}_x\text{MnO}_3$ samples with polyacrylamide-based sol-gel method and propellant synthesis. Both samples showed superparamagnetic behaviors, while the former was more evidenced due to the smaller grain size. An enhanced low-field (<1 T) magnetoresistance was also observed.

Wang et al. reported sol-gel preparation of $\text{La}_{1-x}\text{K}_x\text{MnO}_3$ NPs, and examined their catalytic activity for the combustion of diesel soot particles (Wang et al., 2005a). It was found that as the K content increases, the combustion temperature decreases, and the samples with $x = 0.20$ and 0.25 are good candidate catalysts for the soot particle removal reaction under loose contact conditions.

Gnanasekar et al. prepared nanocrystalline $\text{La}_{1-x}\text{Sr}_x\text{MnO}_3$ ($x < 0.3$) by a glycine-based sol-gel technique, and the crystallization temperature was as low as 575°C (Gnanasekar et al., 2002). Nanocrystalline thin films were deposited by pulsed laser ablation technique, and atomic force microscope (AFM) characterization revealed the highly granular feature of the film with an average grain size of 100–150 nm.

Cherivin et al. developed a non-alkoxide sol-gel method for the preparation of homogeneous nanocrystalline powders of $\text{L}_{0.85}\text{Sr}_{0.15}\text{MnO}_3$ (Cherivin et al., 2006). Calcination of the dried gels resulted in the crystallization of single-phase products at 700°C with discrete particles free of hard agglomeration (Figure 57).

Morales et al. prepared Sn^{4+} -doped LaMnO_3 NPs via the sol-gel method and studied the solubility of Sn in the LaMnO_3 perovskite structure (Morales et al., 2000, 2002), which was found to be strongly dependent on the synthesis temperature.

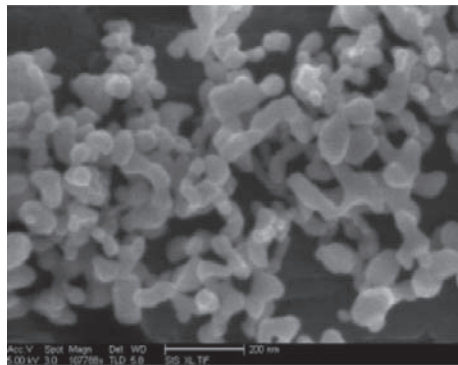


FIGURE 57 SEM micrographs of $\text{La}_{0.85}\text{Sr}_{0.15}\text{MnO}_3$ NPs calcined at $1000\text{ }^\circ\text{C}$ for 1 h. Reprinted with permission from Cherivin *et al.* (2006). Copyright 2006 American Chemical Society.

Song *et al.* reported nanocrystalline $\text{La}_{0.8}\text{Pb}_{0.2}\text{FeO}_3$ prepared by sol-gel method (Song *et al.*, 2005). The obtained product had a mean crystallite size about 19 nm. They examined its sensing behaviors to hydrogen, and observed an elevated conductance compared to that of the undoped sample. Zhang *et al.* also reported the sol-gel synthesis of $\text{La}_{0.68}\text{Pb}_{0.32}\text{FeO}_3$ nanomaterials. Compared to LaFeO_3 sample, the doped sample showed higher conductance, higher sensitivity to CO, and lower operation temperature (Zhang *et al.*, 2005a).

Krishnamoorthy *et al.* developed a citrate-complex method to prepare single-phase $\text{La}_{1-x}\text{Ce}_x\text{MnO}_3$ ($x = 0.15, 0.2, 0.3$) nanopowders (Krishnamoorthy *et al.*, 2007a,b). All samples show ferro- to paramagnetic transition, and ZFC/FC curves suggest cluster glass behavior. For the samples with $x = 0.2$ and 0.3 , a metal to insulator transition was observed. In the ferromagnetic regime, the magnetoresistance decreases with increasing temperature.

Soderlind *et al.* (2008) reported ultrasmall perovskite GdFeO_3 NCs (around 4 nm) via a polyol route. The small size and hydrophilic surface suggests potential application as contrast agents in bioimaging.

Buassi-Monroy *et al.* (2004) employed the sol-gel method to prepare highly crystalline YCoO_3 . The synthetic process was carried out at a relatively low temperature ($900\text{ }^\circ\text{C}$), without the need for high oxygen pressure.

Zhou *et al.* (2007b) investigated the structural and magnetic properties of LaCoO_3 NPs prepared by a sol-gel method. A ferromagnetic order with $T_C \sim 85\text{ K}$ has been observed. The infrared spectra give evidence for stabilizing of higher spin state and a reduced Jahn-Teller distortion in the NPs with respect to the bulk LaCoO_3 , and proposed to be the possible origin of the observed ferromagnetic order in LaCoO_3 .

Kundu et al. (2007) employed the citric acid sol-gel method to prepare a nanoscale ordered perovskite cobaltite, which consists of 90° ordered domains of the layered "112" $\text{LaBaCo}_2\text{O}_6$. This perovskite exhibits a high magnetic anisotropy in contrast to the disordered and ordered phases. The authors explained that the locking of the cobalt spins due to the existence of 90° oriented nanostructure domains is responsible for the observed anisotropy.

Fita et al. (2008) also reported LaCoO_3 NPs synthesized via the citrate method, and their magnetic properties were investigated. All NPs exhibit weak ferromagnetism below $T_C \sim 85$ K. With decreasing particle size, the unit-cell volume increases monotonically, and the ferromagnetic moment increases as well. On the other hand, an applied hydrostatic pressure suppresses strongly the ferromagnetic phase. However, T_C does not change visibly with size and external pressure.

Krishnan et al. (2005) prepared undoped and Ca^{2+} -doped LaCoO_3 powder via sol-gel method. Undoped LaCoO_3 perovskite powders were obtained at temperatures between 700 and 1000 $^\circ\text{C}$.

Robert et al. (2005) synthesized $\text{La}_{1-x}\text{CaCoO}_3$ ($0 < x < 0.4$), $\text{La}_{1-x}\text{Ca}_x\text{Co}_{0.99}\text{Ti}_{0.01}\text{O}_3$ ($0 < x < 0.2$), and $\text{Ca}_3\text{Co}_4\text{O}_9$ phases by thermal decomposition of the corresponding amorphous citrate precursors with the substitution ratio varying from 1% to 50%. The thermoelectric properties of different systems were investigated, which revealed that electrical conductivity of the nanostructured compounds is high in spite of the increased grain boundary influence.

Armelaio et al. (2005) fabricated LaCoO_3 thin films by the combination of chemical vapor deposition (CVD) and sol-gel methods. Two sequences were adopted to prepare the target film: (i) sol-gel of Co–O on CVD La–O; (ii) CVD of Co–O on sol-gel La–O. Losurdo et al. (2005) further investigated the spectroscopic properties of these films by ellipsometry in the near-IR and UV range. The former film has a larger crystallite size, a lower refractive index, and a higher extinction coefficient. It also presents a semiconductor-to-metal transition at a temperature of 530 K. Contrarily, the latter film has a smaller crystallite size, a higher refractive index, a lower extinction coefficient and a semiconductor behavior.

Cheng et al. (2008) reported LaCoO_3 nanopowders for intermediate temperature solid oxide fuel cells prepared by an aqueous gel-casting technique at 600 $^\circ\text{C}$. The performance of La–Sr–Mn–O (LSM) electrode impregnated with as-synthesized LaCoO_3 nanopowders showed a significant improvement.

Le et al. (2006) employed "amorphous citrate" gel method to prepare single phase ceramic powders of LaNiO_3 with controlled grain size by thermal annealing. The target product was obtained at 650 $^\circ\text{C}$ with particle sizes from 30 to 65 nm at annealing temperatures from 650 to 750 $^\circ\text{C}$, while the crystalline sized varied from 10 to 15 nm. Accordingly, a wide

Raman peak at 392 cm^{-1} with decreasing half-width at increasing temperatures was observed.

Hydrothermal/solvothermal synthesis of RMO_3 is also extensively adopted, by virtue of the low reaction temperature and well-crystallized products. Vazquez-Vazquez and Lopez-Quintela (2006) reported the solvothermal synthesis of $\text{La}_{1-x}\text{A}_x\text{MnO}_3$ ($\text{A} = \text{Ca}, \text{Sr}, \text{Ba}$) NPs in benzyl alcohol and acetophenone. The obtained precipitate was annealed to form crystalline products and acetophenone was found to be more suited to obtain clean perovskite phase. Zhu *et al.* (2008a) prepared single-crystalline YbMnO_3 and LuMnO_3 nanoplates via hydrothermal method. The products were found to be hexagonal phases. A possible formation mechanism was proposed, which involves the formation of ROOH phase as intermediate.

There are some reports on the synthesis of RMO_3 via other methods, including thermal decomposition of heteronuclear complex precursors (Aono *et al.*, 2001; Sadaoka *et al.*, 1998; Traversa *et al.*, 1996, 1998, 1999, 2000), decomposition of mixed-metal organic framework precursors (Mahata *et al.*, 2007), pulsed laser deposition (Yanagida *et al.*, 2004), sonochemical synthesis (Sivakumar, *et al.*, 2004a,b), chemical solution deposition (Ghosh, *et al.*, 2005), microemulsion method (Giannakas *et al.*, 2003, 2004, 2006; Yuasa *et al.*, 2007), epitaxial growth using pulsed laser ablation (Jiang *et al.*, 2004a), radio frequency magnetron sputtering (Malavasi *et al.*, 2006), CVD process (Conchon, *et al.*, 2007), high-temperature flux method (Galstyan, *et al.*, 2008), and electrospinning to obtain nanofibers (Zhou *et al.*, 2008b). Notably, Mathur *et al.* developed a synthetic route for RFeO_3 ($\text{R} = \text{Gd}, \text{Y}$) NPs from a heterobimetallic precursor $[\text{RFe}(\text{OPr}^i)_6(\text{HOPr}^i)_2]$ (Mathur *et al.*, 2002, 2004), and then Xu *et al.* (2008) further developed a general synthetic method to prepare RFeO_3 ($\text{R} = \text{La}, \text{Pr}, \text{Nd}, \text{Sm}, \text{Eu}, \text{Gd}$) NPs using metal oleates as precursors, which was calcined at a relatively low temperature ($500\text{ }^\circ\text{C}$) to yield the target products.

Some research efforts have been devoted to fabricate RMO_3 perovskites with unique morphologies and structures. Wang *et al.* developed a two-step method to prepare single-crystalline LaFeO_3 nanotubes. The as-prepared nanotubes with rough walls were further fabricated into gas sensors, which showed good selectivity and stability to Cl_2 at room temperature (Wang *et al.*, 2006a).

Wang *et al.* reported ordered mesoporous LaCoO_3 perovskites synthesized via nanocasting strategy by hard template from citrate complex precursors (Wang *et al.*, 2008f). The ordered mesoporous structure can be seen in TEM images (Figure 58). This material showed high activity in complete methane oxidation.

Teng *et al.* synthesized LaCoO_3 NWs using carbon nanotubes via citric acid method (Teng *et al.*, 2007). After calcination at $750\text{ }^\circ\text{C}$ for 48 h, the

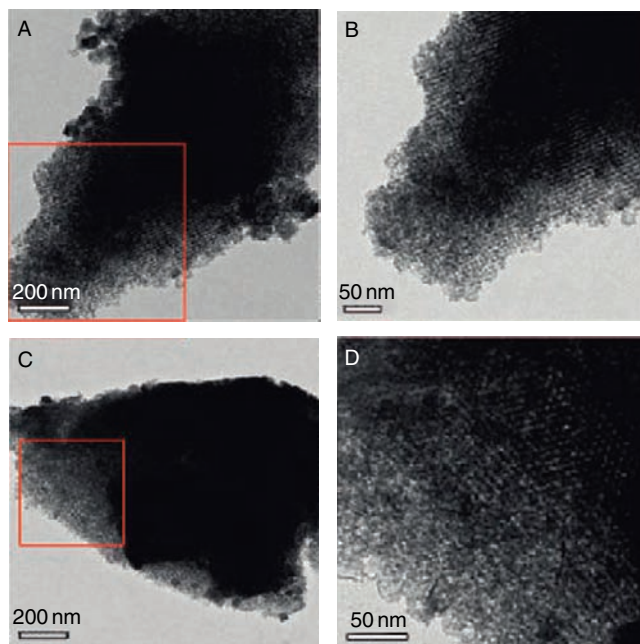


FIGURE 58 TEM images of the mesoporous LaCo_3 which were taken from different regions. Reprinted with permission from Wang et al. (2008f). Copyright 2007 American Chemical Society.

LaCoO_3 NWs showed higher thermal stability and activity of CO oxidation, compared with the nanoparticulate counterpart. Yang et al. reported the synthesis of highly ordered LaNiO_3 perovskite NWs within a porous anodic aluminium oxide (AAO) templated via a sol-gel method (Yang et al., 2005b). The NWs had a uniform length and diameter (Figure 59), which were determined by the thickness and pore diameter of the used AAO template. SAED results revealed that the NWs were polycrystalline, and XPS/EDX analysis confirmed the stoichiometric composition. Later they also reported the LaFeO_3 NWs using a similar method (Yang et al., 2006). LaMnO_3 NW arrays were fabricated by Hu et al. (2006b).

Also, some research devoted to prepare nanocomposites involving RMO_3 have been published. Kida et al. obtained $\text{LaMnO}_3/\text{CdS}$ nanocomposites by a reverse micelle method (Kida, et al., 2003a,b), and examined their photocatalytic activity for hydrogen production from water containing electron donors (Na_2S and Na_2SO_3) under visible light ($\lambda > 420$ nm). The prepared nanocomposites showed higher activity than CdS. It was proposed that the photogenerated holes in the valence band of CdS can move to that of LaMnO_3 and react with Na_2S while the photogenerated electrons remain in the conduction band of CdS and react with water to produce H_2 .

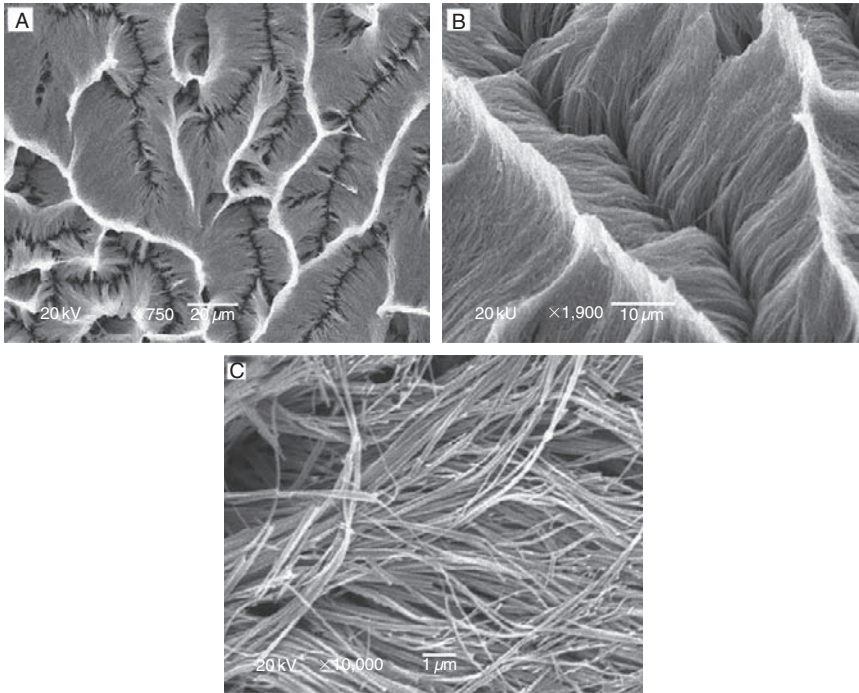


FIGURE 59 SEM images of LaNiO_3 NWs with the AAO template partly dissolved. Reprinted with permission from Yang *et al.* (2005b) Copyright 2005 Elsevier.

Frolova-Borchert *et al.* fabricated nanocomposites comprised of fluorite-like Gd- or Pr-doped ceria and perovskite LaMnO_3 using Pechini route (Frolova-Borchert, *et al.*, 2006). Interaction between components is reflected in the increase of doped ceria lattice parameters and disordering of Mn coordination sphere. Despite this interaction, nanocomposites possess a high conductivity and a high lattice oxygen mobility and reactivity.

Svensson *et al.* prepared catalysts with 20% LaMnO_3 supported on MgO via CTAB-1-butanol-iso-nitrate salt microemulsion (Svensson *et al.* 2006). By varying the synthetic procedure, an attempt to vary the interaction between LaMnO_3 and MgO was made. Compared with bulk LaMnO_3 , the LaMnO_3 supported on MgO showed a greatly improved activity.

Yi *et al.* reported LaCoO_3 perovskite NPs confined in SBA-15 silica by a microwave-assisted process with a La-Co citrate complex precursor (Yi *et al.*, 2005). This method allows the incorporation of up to 60 wt% LaCoO_3 perovskites into the mesopores. The obtained material exhibited high catalytic activity in the complete methane oxidation.

Kira *et al.* synthesized LaMnO_3 NPs in a mesoporous silica MCM-41 via the impregnation method (Kira, *et al.* 2007). Ferromagnetic and

antiferromagnetic regions were found to coexist in the sample, and the ferromagnetic behavior with a magnetization hysteresis was observed below 280 K.

Shi et al. combined a novel NH_3 converter based on nanosized LaCoO_3 (prepared from heteronuclear complex) with chemiluminescence detector for the determination of NH_3 gas (Shi et al., 2003). NH_3 gas is oxidized on the catalyst to produce NO_x , which can react with luminol to generate chemiluminescent emission. This method offers advantages of long lifetime of the converter, fast response and high selectivity to NH_3 over foreign substances such as hydrogen, oxygen, nitrogen, formaldehyde, acetone, and gasoline.

3.5.5 Rare earth cuprates

RE_2CuO_4 perovskites exhibit important and varying magnetic and electrical characteristics, and they are broadly studied as potential high- T_c superconductive materials. At room temperature, they show p-type semiconducting behaviors, and are used as electrode materials in fuel batteries. The catalytic properties of the perovskite oxides also make them effective in various oxidation and reduction reaction, hence they are considered as promising substitutes to the classical Pt/Rh-based catalysts applied to automotive pollution control.

Zhu et al. prepared nanosized La_2CuO_4 perovskite oxide using an amorphous heteronuclear complex $\text{La}_2\text{Cu}(\text{DTPA})_{1.6} \cdot 6\text{H}_2\text{O}$ as a precursor at a low temperature of 650 °C (Zhu et al., 2000). The grain size was in nano-scale even though the precursor was calcined at 900 °C. The crystal size barely changes with calcination temperature above 650 °C and the calcination time.

Yusupov et al. prepared a series of La_2CuO_4 samples with different grain sizes (0.2, 0.7, 1.5, 4 μm), and examined their magnetization behaviors (Yusupov et al., 2007a,b). Ferromagnetic single-domain spin clusters are shown to spontaneously form at the surface of fine grains as well as paramagnetic defects. Hysteresis loops and thermomagnetic irreversibility are observed in a wide temperature range 5–350 K with the remnant moment and coercivity gradually decreasing with increasing temperature. Possible origins of the spontaneous surface ferromagnetic clusters and the relation of the data to the appearance of unusual magnetic phenomena and phase separation of doped cuprates are discussed.

Gao et al. reported hydrothermal synthesis of La_2CuO_4 nanofibers obtained under mild conditions at a temperature around 60 °C templated with single-wall carbon nanotubes (Gao et al., 2006). The crystals grew from needle-like (5 h) through stick-like (20 h) and finally plate-like fibers. Twenty hours is an optimal reaction time to obtain regular crystal fibers. The catalytic activity of the nanofibers was investigated by methanol steam reforming and NO decomposition (Gao et al., 2008a,b). At the low

temperature of 150 °C and the steam/methanol ratio of 1.3, methanol was completely converted to H₂ and CO₂ without the generation of CO. Above 300 °C NO was completely converted to N₂ and O₂. The high catalytic activity was attributed to the special structure, high specific area, appropriate Cu⁺/Cu²⁺ ratio and uncompetitive O₂ and NO adsorptions.

White *et al.* synthesized nanometric La₂CuO₄ through three techniques: auto-ignition, Pechini method, and coprecipitation (White *et al.*, 2008). The NPs were used to fabricate sensing electrodes for NO_x, and the effect of electrode microstructure on the sensitivity and response time was studied. The response times of the sensors were exponentially dependent on electrode grain size. Sensors with fine-grained electrodes were able to produce a steady-state and consistent voltage at lower temperatures, which improved their response sensitivity.

Zhou *et al.* prepared lightly doped La_{2-x}Sr_xCuO₄ ($x = 0.04$) NPs using sol-gel method (Zhou *et al.*, 2007c). All samples were single phase and had an orthorhombic unit cell. As the particle size was reduced, it was found that the IR band around 685 cm⁻¹ corresponding to the in-plane Cu–O asymmetrical stretching mode shifts to higher frequency and the magnetization exhibits a large enhancement at low temperature. The magnetic susceptibility of all samples follows a modified Curie law between ~20 and ~100 K, and the Curie constant displays a strong dependence on the particle size. The sample with the smallest particle sizes exhibits no visible spin-glass transition under a relatively weak external field, in contrast to the sample with the largest particle sizes.

4. NANOMATERIALS OF RARE EARTH HALIDES

Rare earth halides and their derivatives are important functional materials with great potentials in many areas, especially the lanthanide doped ones that are broadly used in solid state lasers, vacuum ultraviolet (VUV) excited downconversion (DC), and near-infrared (NIR) excited upconversion (UC) phosphors in lightings and displays (Akdeniz *et al.*, 2001; Blasse and Grabmaier, 1994; Meyer and Wickleder, 2000; Shionoya and Yen, 1999). On one hand, the high coordination numbers for the hosted rare earth ions in halide lattices result in diverse crystal structures and properties; on the other hand, the high ionicity of the rare earth to halide bond leads to a wide band-gap and very low vibration energies. These two structural features particularly benefit their applications in optical, electrical, magnetic, and catalytic fields etc (Akdeniz *et al.*, 2001; Blasse and Grabmaier, 1994; Meyer and Wickleder, 2000; Reisfeld and Jorgensen, 1977; Shionoya and Yen, 1999).

According to the coordination states of rare earth, previous studies have classified the rare earth halides complex A_{*m*}RX_{*n*} (A = alkali and/or

alkaline earth metal; R = rare earth; X = halogen) compounds as follows: (1) ARX_4 , a fourfold coordination of the rare earth atom is accompanied by twofold or threefold coordination of the alkali and/or alkaline earth atom. (2) A_2RX_5 , a fivefold coordination of the rare earth atom is energetically more stable than a fourfold one. (3) A_3RX_6 , the fivefold and sixfold coordination of the rare earth atom are energetically competitive, and (4) in both A_2RX_5 and A_3RX_6 each coordination state can be realized in various forms that differ in detail but are close in energy (Akdeniz et al., 2001; Meyer and Wickleder, 2000).

During the past two decades, nanomaterials have captivated the materials research field with the great promise of exciting applications in science and technology. Manipulation of lanthanide-doped rare earth halide NCs has led to important modulations of their optical properties in terms of excited states, emission profiles, and efficiencies. Meanwhile, the successful preparation of rare earth halide nanomaterials have opened the pathways for finding new properties, and concurrently, the performance of their macroscopic counterparts can be conserved in the nanometer regime. In this chapter, we will focus primarily on the developments in the synthesis, properties, and potential applications of rare earth halides and their derivative NCs.

4.1 Rare earth fluorides

Among the rare earth halide NCs, rare earth fluorides are second to none of the excellent hosts for optical applications, such as industrial lighting, display, and biological imaging by both DC and UC processes (Nakajima et al., 2000; Sommerdijk and Bril, 1974). On the other hand, to satisfy the low phonon energy environment and good chemical/mechanical stability, the transparent oxyfluoride glasses (ceramics doped with rare earth fluorides NCs) have been found with applications in optical waveguide amplifiers, light wave circuits, and UC lasers (Auzel, 2004). For example, the so-called ZBLAN is a type of a glass made of a mixture of zirconium, barium, lanthanum, aluminum, and sodium fluorides. With higher refractive index, rare earth doped ZBLAN can transmit the intense infrared light (Auzel, 2004). The RF_3 NCs are generally prepared by wet chemical routes involving the modified precipitation, hydrothermal treatment, microemulsion, and polyol methods, which are all mainly based on the liquid reaction between the rare earth salts (such as nitrates/chlorides) and metal fluorides (such as NaF/ NH_4F). Recently, the non-hydrolytic approach using single source precursor in the solution phase offers a convenient and reproducible route for the fabrication of high quality (monodisperse, single-crystalline, well shaped, and phase-pure) RF_3 NCs (Sun et al., 2007).

4.1.1 Synthesis of RF_3 nanocrystals

4.1.1.1 Coprecipitation method Coprecipitation is a convenient technique for synthesizing rare earth fluoride NCs. Compared with other techniques, it shows high output and is fast and low cost for both equipment and raw materials. Early, van Veggel *et al.* prepared of $\text{LaF}_3\text{:R}^{3+}$ ($\text{R} = \text{Eu}, \text{Er}, \text{Nd}, \text{and Ho}$) NPs by a precipitation process between rare earth nitrates and NaF in ethanol/water solvent. Ammonium di-*n*-octadecyldithiophosphate was used as capping ligand to stabilize the particles against aggregation, and the as-obtained NPs were readily dispersible in organic solvents (Stouwdam and van Veggel, 2002). Later, Chow *et al.* expanded this coprecipitation method to prepare multicolor UC fluorescent LaF_3 NCs with $\text{Yb}^{3+}\text{-Er}^{3+}$, $\text{Yb}^{3+}\text{-Ho}^{3+}$, and $\text{Yb}^{3+}\text{-Tm}^{3+}$ codopants (Yi and Chow, 2005). Also employing the precipitation strategy, Zhang *et al.* grew lanthanide doped LaF_3 on the surface of silica sub-microspheres and obtained raspberry-like nanostructures (Zhang and Lu, 2007). Cao *et al.* prepared hexagonal CeF_3 NCs with different morphologies in disk, rod, and dot shapes. The aqueous coprecipitation of $\text{Ce}(\text{NO}_3)_3$ assisted by ultrasound, and different fluorine sources (KBF_4 , NaF, NH_4F) were compared (Zhu *et al.*, 2007b). They also obtained EuF_3 nanoflowers using a similar process (Zhu *et al.*, 2007d). Liu *et al.* obtained doughnut- and shuttle-shaped EuF_3 superstructures by using sodium tetrafluoroborate (NaBF_4) to react with $\text{Eu}(\text{NO}_3)_3$ in aqueous solutions without organic additives or surfactants. The EuF_3 superstructures were controllably fabricated by changing the concentrations and molar ratio of NaBF_4 and $\text{Eu}(\text{NO}_3)_3$, which were formed through oriented attachment procedure (Miao *et al.*, 2007). Chen *et al.* synthesized a variety of nanostructures (nanoplates, nanospheres, nanobundles, nanorods, and nanowires) of EuF_3 NCs with orthorhombic and hexagonal phases via precipitation route. Many different fluoride sources (XF , $\text{X} = \text{K}^+, \text{H}^+, \text{NH}_4^+, \text{Na}^+, \text{Rb}^+, \text{and Cs}^+$) have been tried in their work (Figure 60) (Wang *et al.*, 2006e,f). Recently, Ansari *et al.* prepared the pyridine functionalized TbF_3 NPs through the reaction of $\text{Tb}(\text{NO}_3)_3$, NaF and pyridine in water/ethanol system (Ansari and Singh, 2008).

4.1.1.2 Hydrothermal method Hydrothermal route is an easy and effective synthetic way yielding NCs. The high reaction pressure and temperature benefit the crystallization of products. Li *et al.* prepared the hexagonal $\text{Yb}^{3+}\text{-Er}^{3+}$, $\text{Yb}^{3+}\text{-Ho}^{3+}$ codoped LaF_3 uniform nanoplates from oleic acid assisted hydrothermal reaction of sodium oleate, rare earth nitrate, NaF, and oleic acid in water/ethanol mixture (Hu *et al.*, 2008a). Using linoleate acid as capping reagent in solvothermal synthesis, Li *et al.* successfully prepared the LaF_3 as well as other classes of rare earth fluoride NCs with diverse shapes (Wang *et al.*, 2006h), such as

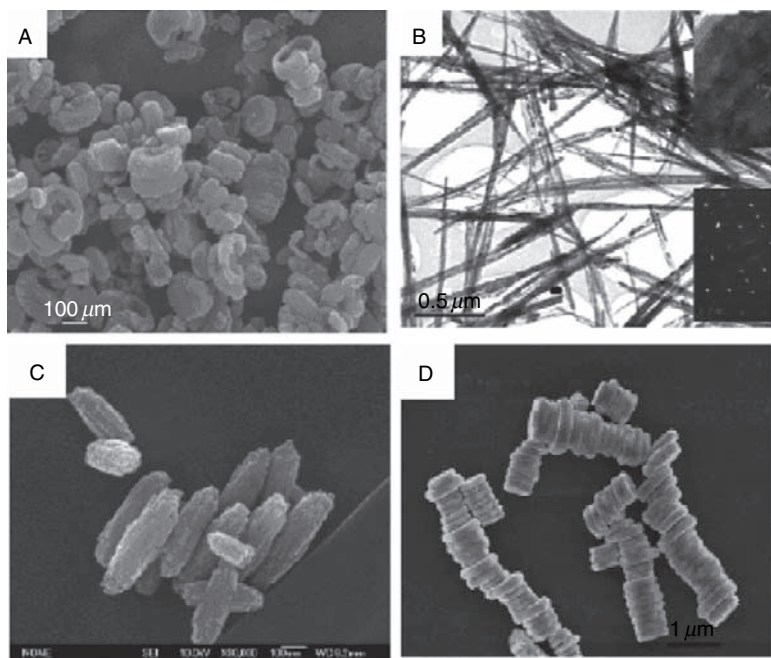


FIGURE 60 (A) SEM image of hexagonal EuF_3 lunate nanoplates, and (B) TEM image, HRTEM image, and ED patterns of orthorhombic EuF_3 nanowires. Reprinted with permission from Wang et al. (2006e). Copyright 2006 American Chemical Society. SEM images of (C) orthorhombic EuF_3 nanospindles and (D) hexagonal EuF_3 nanodisks. Reprinted with permission from Wang et al. (2006f). Copyright 2006 American Chemical Society.

monodisperse rare earth doped LaF_3 nanorods (Wang et al., 2007c; Figure 61). Recently, Lin et al. demonstrated a general synthesis of RF_3 NCs with diverse morphologies (elongated particles, aggregates, and octahedra) by hydrothermal method, where, the rare earth nitrates or chlorides, NaBF_4 , and trisodium citrate were the precursors, and the pH of the solution was adjusted with diluted HCl (Li et al., 2008e).

With PVP (polyvinyl pyrrolidone) stabilization, Qin et al. obtained water-soluble hexagonal phase colloidal $\text{La}_{0.78}\text{Yb}_{0.20}\text{Er}_{0.02}\text{F}_3/\text{SiO}_2$ core/shell structured NCs by hydrothermal method (Wang et al., 2007). Chen et al. obtained the multicolor UC fluorescent $\text{Yb}^{3+}\text{-Er}^{3+}$, $\text{Yb}^{3+}\text{-Tm}^{3+}$, and $\text{Yb}^{3+}\text{-Ho}^{3+}$ codoped LaF_3 NCs by decomposition of the corresponding rare earth trifluoroacetates combined with a solvothermal technique (Liu and Chen 2007a). Using the same synthetic approach based on the solvothermal synthesis, Kumar et al. synthesized the $\text{LaF}_3:\text{Nd}^{3+}$ NCs with highly efficient infrared emissions (Kumar et al., 2007). Lin et al. prepared CeF_3 , $\text{CeF}_3:\text{Tb}^{3+}$, and core/shell structured $\text{CeF}_3:\text{Tb}^{3+}@\text{LaF}_3$ nanoplates by organic additive and trisodium citrate (Cit^{3-}) assisted hydrothermal

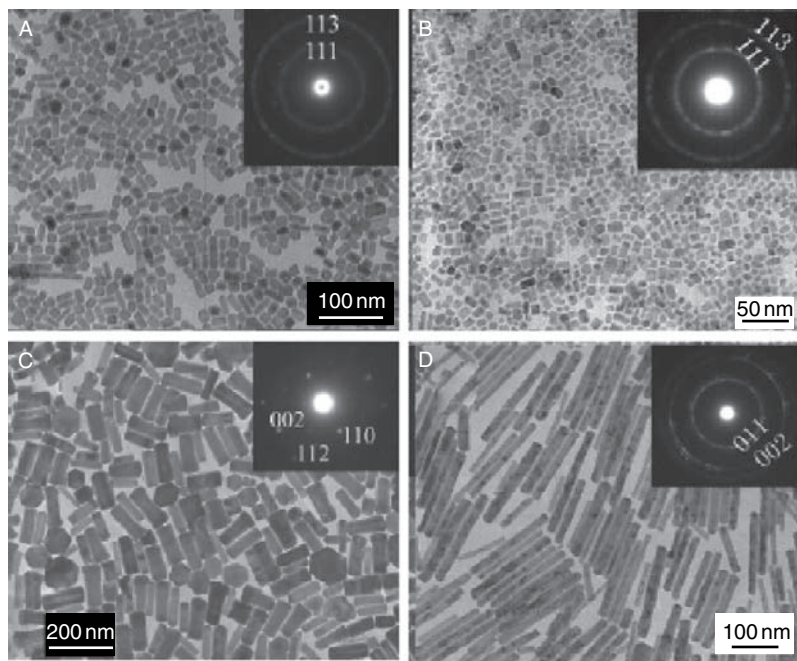


FIGURE 61 TEM images of (A) LaF_3 :5%Ce,5%Tb, (B) LaF_3 :18%Yb,2%Er nanorods, (C) NaLaF_4 :18%Yb,2%Er, and (D) NaLaF_4 :5%Ce,5%Tb nanorods. Insets are their corresponding SAED patterns. Reprinted with permission from Wang *et al.* (2007c). Copyright 2007 Wiley-VCH.

method (Li *et al.*, 2008a). Hu *et al.* reported the hydrothermal preparation of hollow CeF_3 nanostructures with nanocages, nanorings, nanococoons, and circular hollow disks morphologies. A classical Belousov-Zhabotinsky oscillating reaction in the bromate–citric acid– Ce(IV) – H_2SO_4 system was responsible for the formation of hollow nanostructures. The cerium ions catalyzed oxidation of citric acid by bromate ion in sulfuric acid solution, and the valences of cerium ions were periodically changed between Ce(III) and Ce(IV) (Wu *et al.*, 2008b). Li *et al.* prepared the LaF_3 and PrF_3 fullerene-like NPs using a routine hydrothermal method at a relatively low temperature (80–180 °C) (Wang and Li 2003a,b). The formation of fullerene-like nanostructure required designated hydrothermal temperature and pH conditions. Chen *et al.* obtained the hollow structured PrF_3 NPs by microwave assisted hydrothermal method, and dissolution–recrystallization process was the likely growth mechanism (Ma *et al.*, 2007c).

Qian *et al.* prepared spindle-like lanthanide doped YF_3 luminescent NCs by hydrothermal treatment of YCl_3 , NaF, and EDTA at relatively low

temperature of 140 °C (Zhang et al., 2007f). Li et al. synthesized the nanocrystalline $\text{YF}_3:\text{Ln}^{3+}$ phosphors via sonochemistry-assisted hydrothermal route (Yan and Li, 2005). Recently, Yao et al. prepared the highly uniform and monodisperse YF_3 nanosized and sub-microsized truncated octahedra in large quantities. Their hydrothermal treatment was assisted with ethylenediamine tetraacetic acid disodium salt ($\text{Na}_2\text{H}_2\text{EDTA}$). At low temperature (around 100 °C), significant activity of Eu^{2+} was observed in aqueous solution, so the Eu^{2+} emission was observed in the Eu-doped YF_3 products (Tao et al., 2007a,b).

4.1.1.3 Microemulsion method The microemulsion method is a convenient route for preparing monodisperse NPs with controllable size. By mixing different microemulsion containing reactants, chemical reactions could be performed inside each individual reverse micelle water pool, just like in a nanoreactor. Moreover, the growth of NPs is limited by the micelle size. Ritcey et al. prepared YF_3 quadrilateral shaped NPs with water in cyclohexane reverse microemulsion by polyoxyethylene isooctylphenyl ether (igepal CO520) stabilization. The microemulsion was formed by mixing aqueous YCl_3 and igepal CO520 in cyclohexane, then the aqueous NH_4HF_2 was added to produce the YF_3 NPs (Figure 62) (Lemyre and Ritcey, 2005).

Shi et al. prepared $\text{CeF}_3:\text{Lu}^{3+}$ NPs from the quaternary reverse micelle system, which contained CTAB, *n*-butanol, *n*-octane, and water. The characteristic emission of Lu^{3+} was observed (Lian et al., 2004). Similarly, Qin et al. obtained $\text{Yb}^{3+}\text{-Tm}^{3+}$ codoped YF_3 nanobundles through a microemulsion method in another quaternary reverse microemulsion system with water/CTAB/cyclohexane/1-pentanol (Wang et al., 2008c).

4.1.1.4 Methods using hard templates Mesoporous materials could serve as efficient hard templates for the fabrication of ordered mesostructured arrays. As mentioned above, most of the established synthetic methods for metal fluorides are based on liquid precipitation reaction between soluble metal salts and alkali fluorides. Zhao et al. fabricated ordered mesoporous LaF_3 nanowire arrays via nanocasting route by the aid of mesoporous silica SBA-15 template and $\text{La}(\text{CF}_3\text{COO})_3$ precursor (Zhang et al., 2008c). Qiu et al. fabricated CeF_3 nanowires using carbon nanotubes as template (Wang et al., 2007f).

4.1.1.5 Polyol hydrolyzed method The polyol hydrolysis method is arisen growing strategy for the preparation of NCs, in which the reducing properties of high-boiling alcohol (e.g., glycerol, glycol) are adequately utilized. Lin et al. reported water soluble colloidal CeF_3 , $\text{CeF}_3:\text{Tb}^{3+}$, and $\text{CeF}_3:\text{Tb}^{3+}/\text{LaF}_3$ core/shell structured NPs by this route, where, the NH_4F and rare earth nitrates was dissolved in diethylene glycol to produce final

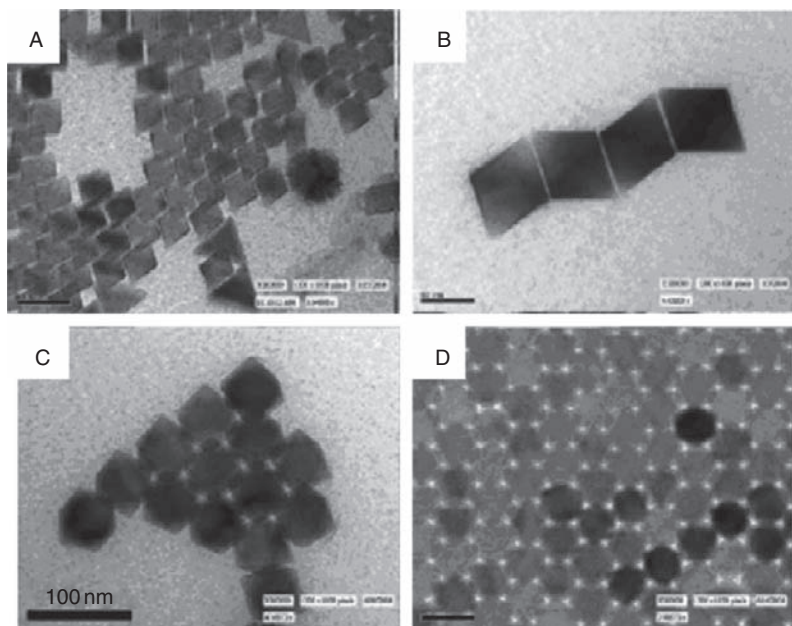


FIGURE 62 TEM images of different morphologies of YF_3 NCs: (A) typical mixtures of predominant YF_3 particles morphologies. (B) YF_3 quadrilateral shaped NCs. (C) YF_3 hexagonal NCs. (D) self-assembly of YF_3 hexagonal NCs. Reprinted with permission from Lemyre and Ritcey (2005). Copyright 2005 American Chemical Society.

nanocrystalline products (Wang *et al.*, 2006j). Song *et al.* obtained hexagonal LaF_3 nanoplates via a polyol-mediated route in ethylene glycol solvent; increased the chemical potential caused by the addition of NaNO_3 mineralizer in this reaction system made LaF_3 nanoplates formed initially unstable and transformed into stable regular hexagonal LaF_3 nanoplates during a slow dissolution–recrystallization process (Qin *et al.*, 2009).

4.1.1.6 Thermal decomposition in high boiling coordinating solvents During the past 5 years, thermal decomposition method is perhaps one of the most efficacious techniques to synthesize rare earth fluoride NCs with narrow size distribution and controllable shapes. Yan *et al.* first explored a thermolysis method based on the decomposition of single source precursor, that is, $\text{La}(\text{CF}_3\text{COO})_3$ in oleic acid and 1-octadecene solutions. High quality triangular LaF_3 nanoplates were obtained and they could further assemble into superstructures (Figure 63) (Zhang *et al.*, 2005d). This method has merits of one-step, mass production, and easy extension to other high quality (monodisperse, single-crystalline, well shaped, and

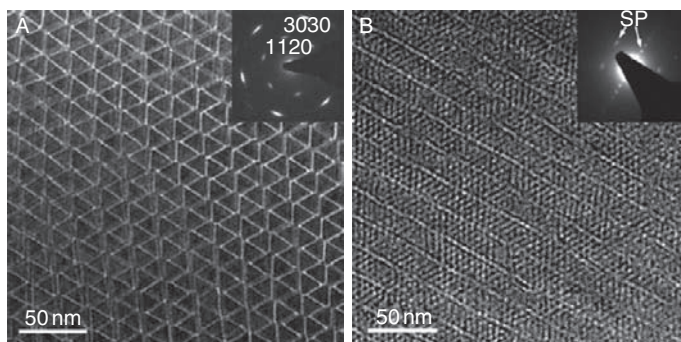


FIGURE 63 TEM (transmission electron microscopy) images of the (A) edge-to-edge and (B) face-to-face superlattices of LaF_3 nanoplates. Insets are the SAED patterns. Reprinted with permission from Zhang et al. (2005d). Copyright 2005 American Chemical Society.

phase-pure) RF_3 NCs (Sun et al., 2007), including ScF_3 . Analogously, Zhuravleva et al. synthesized TOPO (trioctylphosphine oxide)-capped EuF_3 NPs by decomposition of europium trifluoroacetate complex in TOPO solvent (Zhuravleva et al., 2005).

4.1.1.7 Other methods Chen et al. demonstrated a simple room temperature solid-state reaction route for preparing EuF_3 and SmF_3 NPs (Huang et al., 2007). Wang et al. demonstrated that highly crystallized $\text{LaF}_3:\text{Ce}^{3+}$, Tb^{3+} NPs could be prepared in a capillary microreactor, using diethylene glycol as solvent by well-controlled temperature steps (Zhu et al., 2008d). Recently, Xiao et al. demonstrated a combustion-fluorination method to prepare Eu^{3+} doped and Yb^{3+} - Ho^{3+} codoped LuF_3 and YF_3 NPs. The precursor solution containing rare earth nitrate and glycine was concentrated by evaporation until the spontaneous ignition occurred. Then the resultant ash was mixed with NH_4HF_2 for high temperature fluorination in a closed corundum crucible (Yang et al., 2008c; Xiao et al., 2007). Chen et al. synthesized uniform RF_3 ($\text{R} = \text{La, Ce, Pr, Nd, Sm, Eu, and Er}$), $\text{CeF}_3:\text{Tb}^{3+}$, as well as $\text{LaF}_3:\text{Eu}^{3+}$ NC in different ionic liquids (ILs) (1-octyl-3-methylimidazolium hexafluorophosphate, 1-octyl-3-methylimidazolium tetrafluoroborate, and 1-butyl-3-methylimidazolium hexafluorophosphate). The ILs acted as both solvents and templates, and partial hydrolysis of PF_6^- and BF_4^- could provide fluorine source (Zhang et al., 2008a).

4.1.2 Properties and applications of RF_3 nanocrystals

Surface defects and ligands coordinating small particles strongly suppress the luminescence and reduce the quantum efficiency. To increase the optical efficiency, the so-called core/shell structures are proposed, in

which a shell of pure (undoped) host material could protect the light emitting ions from solvent molecules and capping ligands. Following this protocol, the core/shell structured LaF₃ NCs have been demonstrated to possess more efficient luminescence, since the nonradiative processes at or near the NC surface are generally suppressed (Lezhnina *et al.*, 2006; Stouwdam and van Veggel, 2004).

Currently, the applications of optically robust and water-soluble rare earth fluoride NCs in biological imaging are becoming an active interdisciplinary research area. These optical bioprobes largely profit from their long luminescent lifetimes, wide range of non-overlapping emissions, and photo-bleaching immunity (Shen *et al.*, 2008a).

For bio-applications, the NCs must have a suitable surface chemistry, which could be realized either by using functionalized ligands during the synthesis or by ligand exchange after the synthesis. Van Veggel *et al.* reported the one-step synthesis and optical properties of water soluble, luminescent lanthanide doped LaF₃ NPs coordinated with a hydrophilic (RO)PO₃²⁻ ligand (Diamente and van Veggel, 2005). Then they showed the synthesis of silica-coated lanthanide doped LaF₃ NPs using sol-gel method, and demonstrated the bio-conjugation to FITC-avidin (FITC = fluorescein isothiocyanate) for down- and up-converting luminescent biolabels (Diamente *et al.*, 2006; Sivakumar *et al.*, 2006). Recently, Li *et al.* described a simple method for converting hydrophobic up-converting LaF₃:20%Yb³⁺, 1%Ho³⁺ nanophosphors into amphiphilic ones by epoxidation of the surface oleic acid ligands. After further coupling with polyethylene glycol monomethyl ether (mPEG-OH), the NCs possessed low cytotoxicity and good cell membrane permeability for bioimaging purposes (Figure 64) (Hu *et al.*, 2008b).

Zhang *et al.* synthesized highly water-soluble LaF₃ NCs in aqueous solution without any capping ligands, various rare earth ions (Eu³⁺, Ce³⁺, Tb³⁺, and Nd³⁺) with characteristic emissions in the visible and near-infrared spectra regions were discerned (Wang *et al.*, 2006b). They also prepared biocompatible LaF₃ and chitosan/LaF₃:Eu³⁺ NCs via facile coprecipitation with natural biopolymer additives (Wang *et al.*, 2006c). Chen *et al.* reported the well-crystallized and water soluble LaF₃:Yb³⁺, Er³⁺ NPs synthesized by the polyol (glycol, diethylene glycol, and glycerol) hydrolyzed method (Wei *et al.*, 2007). More recently, Charbonnière demonstrated one-step synthetic method toward water-soluble LaF₃:Eu³⁺ NPs with bipyCOO⁻ (6-carboxy-50-methyl-2,20-bipyridine) coating. By the surface antenna effect, the absorbed energy of bipyCOO⁻ moieties could be converted into intense emission of europium ions (Charbonnière *et al.*, 2008). Wang *et al.* used poly(St-co-MAA) polymer-coated luminescent LaF₃:Ce³⁺/Tb³⁺ NCs for DNA detection. Under optimum conditions, the fluorescence intensity was proportional to the concentration of the introduced DNA for calf thymus DNA (ctDNA) and fish sperm DNA

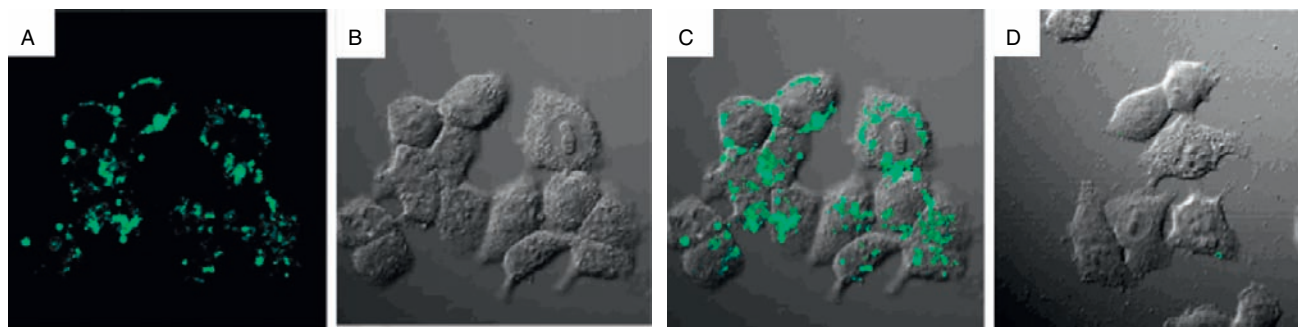


FIGURE 64 (A) Confocal luminescence images of cells stained with mPEG modified $\text{LaF}_3:20\%\text{Yb},1\%\text{Ho}$ NCs ($\lambda_{\text{ex}} = 980$ nm). (B) Bright-field image of cells. (C) Overlay image of (A) and (B). (D) Overlay image of confocal luminescence and bright field images of cells stained with mPEG modified $\text{LaF}_3:20\%\text{Yb},1\%\text{Ho}$ NCs. Reprinted with permission from Hu et al. (2008b). Copyright 2008 American Chemical Society.

(fsDNA), respectively (Wang *et al.*, 2009a). Recently, Wang *et al.* prepared uniform surfactant-free $\text{NdF}_3/\text{SiO}_2$ core/shell structured NCs by precipitation route. The as-obtained NCs showed high fluorescent efficiency *in vivo* (Yu *et al.*, 2008b).

On the other hand, unique physical properties and potential applications of nanoscaled lanthanide-doped LaF_3 have been discussed in many reports. For instance, van Veggel *et al.* reported the bright white light through up-conversion of a single near-infrared source by thin film of $\text{LaF}_3:\text{Yb}^{3+}$, $\text{Eu}^{3+}/\text{Er}^{3+}/\text{Tm}^{3+}$ NPs (Figure 65) (Sivakumar *et al.*, 2005). And the silica films with R^{3+} (Er^{3+} , Nd^{3+} , and Ho^{3+}) doped LaF_3 NPs possessed the visible white luminescence (Sudarsan *et al.*, 2005).

By employing sol-gel procedure, van Veggel made the bright green and red luminescent thin films composed of $\text{La}_{0.45}\text{Yb}_{0.50}\text{Er}_{0.05}\text{F}_3$ NPs (Sivakumar *et al.*, 2007a), as well as thin films of In_2O_3 , HfO_2 , ZrO_2 contained $\text{LaF}_3:\text{R}^{3+}$ ($\text{R} = \text{Er}$, Nd , and Eu) NPs. The as-obtained films showed sensitized emission of the rare earth ions, which great potentials for lighting applications (Sivakumar *et al.*, 2007b). Rodríguez *et al.* synthesized nanostructured Eu^{3+} doped $\text{LaF}_3\text{-SiO}_2$ transparent glass-ceramics

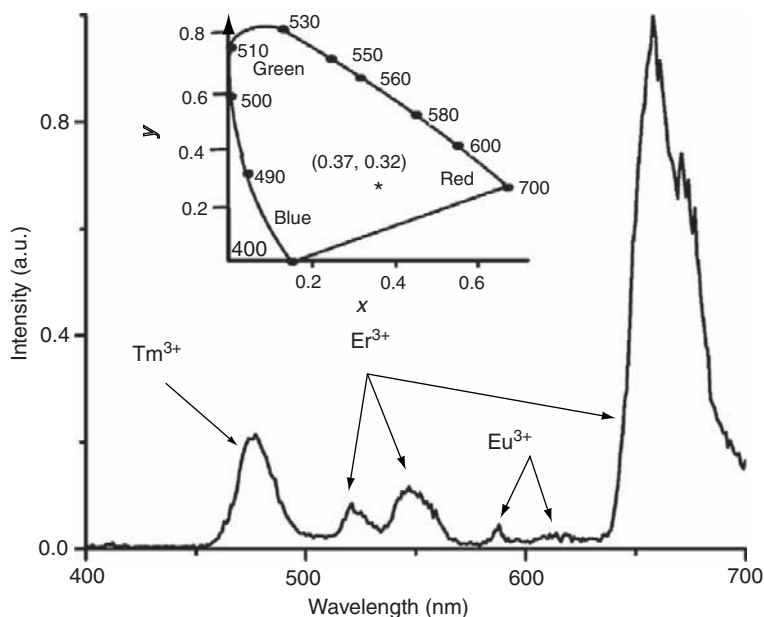


FIGURE 65 Up-conversion emission spectrum of silica thin film made with $\text{La}_{0.45}\text{Yb}_{0.5}\text{Er}_{0.05}\text{F}_3$, $\text{La}_{0.75}\text{Yb}_{0.2}\text{Tm}_{0.05}\text{F}_3$, and $\text{Yb}_{0.75}\text{La}_{0.2}\text{Eu}_{0.05}\text{F}_3$ NPs under 980 nm laser excitation (the insets show the CIE color coordinates of the resulting white light). Reprinted with permission from Sivakumar *et al.* (2005). Copyright 2005 American Chemical Society.

by a simple sol-gel method, and observed the strong Eu^{3+} emission (Yanes et al., 2007). Using complex core/shell structures, DiMaio et al. detected the white light emissions from single species of NPs doped with multiple trivalent rare earths (Eu^{3+} , Tb^{3+} , and Tm^{3+}) (DiMaio et al., 2006).

Zhen et al. recently synthesized oleic acid ligands modified $\text{LaF}_3:\text{Er}^{3+}$, Yb^{3+} NPs and dispersed them into polymethylmethacrylate (PMMA) matrix to form NC-polymer hybrid materials. The product exhibited strong emission around the 1550 nm telecommunication window with excitation at 980 nm, proposed to be promising materials for polymer-based optical waveguide amplifiers (Wang et al., 2007b). Dekker et al. reported stimulated emission at 863 nm in hybrid Si_3N_4 waveguides with $\text{LaF}_3:\text{Nd}^{3+}$ NP in PMMA top cladding material (Dekker et al., 2004). Meltzera et al. detected interesting photon echo signals for the $^3\text{H}_4 \rightarrow ^3\text{P}_0$ transition of Pr^{3+} in LaF_3 NCs embedded in oxyfluoride glass ceramics (Meltzera et al., 2004). Zhang et al. first studied the antiwear and extreme pressure additive of surface sulfur/phosphate coated LaF_3 NPs in liquid paraffin (Zhou et al., 2001). As an oil additive, LaF_3 NPs improved the load-carrying capacity and antiwear properties of the base oil. They had better friction-reduction compared to ZDDP (zinc di-iso-amyl-octyl-dithiophosphate) (Zhang et al., 2001a,b). Qiu et al. synthesized CeF_3 NPs from polyisobutene-butanediimede (T154)/cyclohexane/water microemulsions. The tribological properties as lubricating oil additives were studied (Qiu et al., 1999, 2000), since previous studies indicated that CeF_3 was a good solid lubricant due to its layered structure (Aldorf, 1985).

Li et al. described $\text{LaF}_3:\text{Yb}^{3+},\text{Ho}^{3+}$ nanophosphors synthesized from a modified hydrothermal process. Then they employed a DTE (diarylethene) derivative in $\text{LaF}_3:\text{Yb}^{3+},\text{Ho}^{3+}$ loaded PMMA film, and demonstrated a unique up-conversion luminescent "switch" by an intermolecular energy transfer process (Figure 66) (Zhou et al., 2008c). For exploring potential applications of LaF_3 NCs in transparent glass, Qiu et al. recently fabricated the $\text{Tm}^{3+}-\text{Yb}^{3+}$ codoped transparent oxyfluoride glass ceramics by thermal treatment LaF_3 NCs on the as-made glasses. The infrared quantum cutting involving Yb^{3+} 950–1100 nm ($^2\text{F}_{5/2} \rightarrow ^2\text{F}_{7/2}$) emission was obtained upon the excitation of the $^1\text{G}_4$ energy level of Tm^{3+} at 468 nm (Ye et al., 2008). Wang et al. fabricated $\text{Fe}_3\text{O}_4@(\text{PAH}/\text{PSS})_2$ bifunctional composite NPs with a facile layer-by-layer assembly technique. The nanocomposites were generated by absorbing the negatively charged $\text{LaF}_3:\text{Ce}^{3+}$, $\text{Tb}^{3+}@(\text{PAH}/\text{PSS})_2$ (PAH, poly(alkylamine hydrochloride) and PSS, poly(sodium 4-styrenesulfonate)) luminescent NPs onto the positively charged $\text{Fe}_3\text{O}_4@(\text{PAH}/\text{PSS})_2/\text{PAH}$ magnetic particles through electrostatic interaction (Wang et al., 2009b).

By melt quenching and subsequent heating procedure, Wang et al. fabricated transparent $\text{SiO}_2-\text{Al}_2\text{O}_3-\text{LiF}-\text{YF}_3$ glass ceramic with NdF_3 NPs

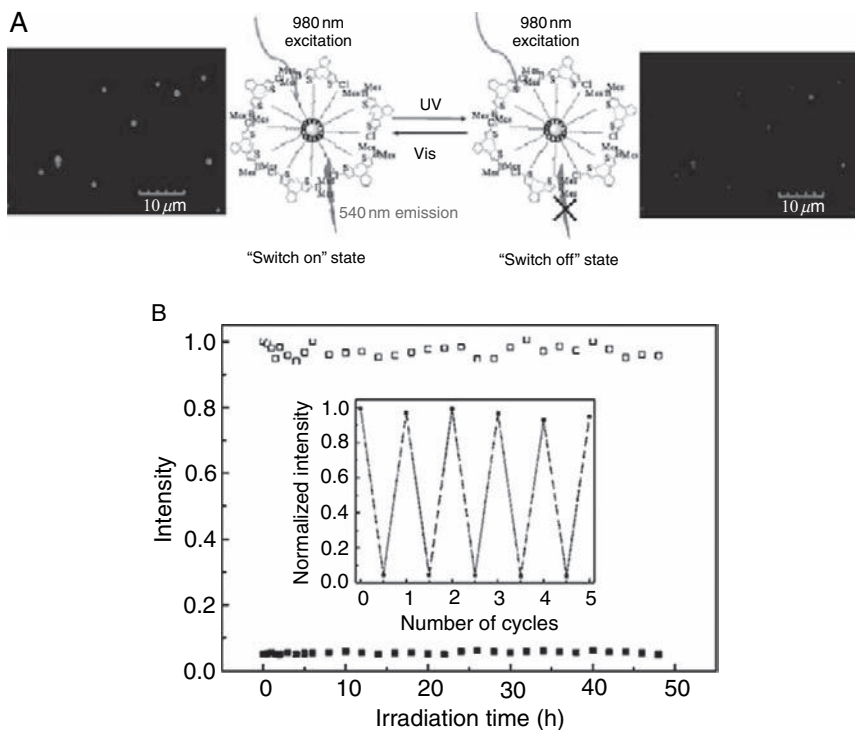


FIGURE 66 (A) Principle and confocal luminescence images of the up-conversion luminescent switch consisting of $\text{LaF}_3:\text{Yb}^{3+},\text{Ho}^{3+}$ loaded PMMA film. (B) Nondestructive readout capability of $\text{LaF}_3:\text{Yb}^{3+},\text{Ho}^{3+}$ loaded PMMA film in the open state and in the PSS (photostationary state) state. Reprinted with permission from Zhou *et al.* (2008c). Copyright 2008 American Chemical Society.

doping. This material exhibited excellent infrared emission performance (Chen *et al.*, 2007a). This group also prepared NdF_3 NPs by the hydrothermal reaction of NH_4F and $\text{Nd}(\text{NO}_3)_3$. The as-obtained NPs could self-assemble into plate-built chains through typical oriented aggregations (Bao *et al.*, 2006). Wang *et al.* fabricated oxyfluoride glass ceramics with LaF_3 and ErF_3 NCs doping (Hu *et al.*, 2006c). Seddona *et al.* synthesized ErF_3 NCs doped ultra-transparent oxyfluoride glass ceramics (Tikhomirov *et al.*, 2002). Prentice *et al.* investigated the incorporation of YbF_3 NPs into glass ionomer cement, which could significantly reduce compressive strength and surface hardness, as well as accelerate the glass ionomer curing reaction (Prentice *et al.*, 2006). Wang *et al.* synthesized $\text{Tm}^{3+}-\text{Yb}^{3+}$ doped YF_3 NCs and embedded them into oxyfluoride glass

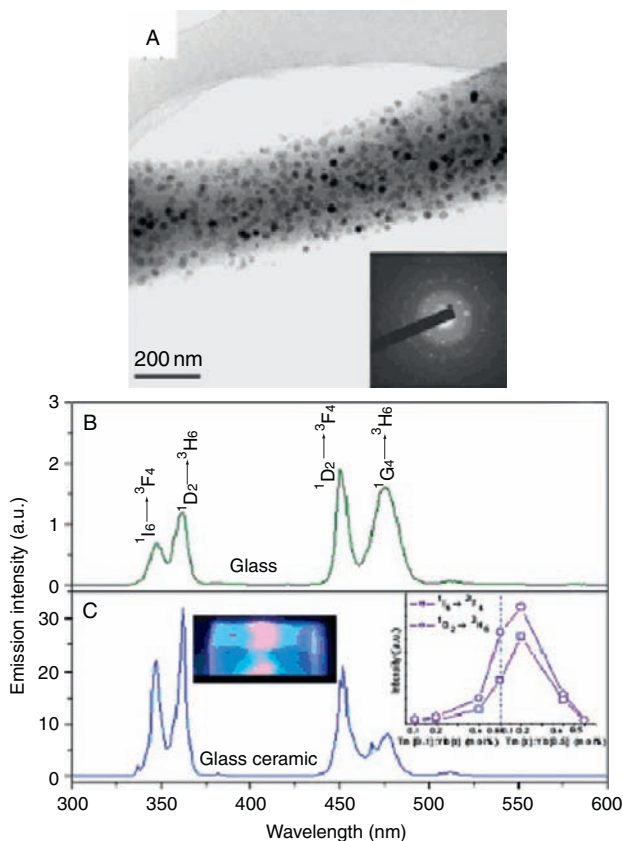


FIGURE 67 (A) TEM image and the SAED pattern of the glass ceramic. Up-conversion emission spectra of (B) the precursor glass and (C) the glass ceramic, the inset of (C) shows the photograph of the glass ceramic with blue luminescence (left) and the variation of the ultraviolet upconversion luminescence on the Yb^{3+} and Tm^{3+} concentration (right). Reprinted with permission from Chen et al. (2007b). Copyright 2007 American Institute of Physics.

ceramic by solid state reaction. The as-obtained glass yielded intense UC luminescence (Figure 67) (Chen et al., 2007b).

The mercury-free fluorescent lamps and plasma display panels require alternative luminescent materials for efficient conversion of ultraviolet radiation to visible light. The quantum cutting (two photon luminescence or photon-cascade emission) was demonstrated in famous “ Eu^{3+} - Gd^{3+} pair” containing system employing the concept of down-conversion, which means that two visible photons are emitted after

absorption of each VUV photon (Wegh *et al.*, 1999). With the excitation of 6G_J or higher state of Gd^{3+} in Eu^{3+}/Gd^{3+} system, the energy from the ${}^6G_J \rightarrow {}^6P_J$ transition of Gd^{3+} can be transferred to Eu^{3+} , and 6P_J energy level of Gd^{3+} also can sensitize 5D_J level of Eu^{3+} , resulting in the emission of two visible photons by Eu^{3+} for every high-energy photon absorbed (quantum efficiency approaches 200%). The extraordinary matching of Gd^{3+}/Eu^{3+} energy levels makes GdF_3 an important material for quantum cutting. In addition, GdF_3 is expected to be good MRI contrast agents due to the large magnetic moment of Gd^{3+} . The $4f^7$ configuration of Gd^{3+} greatly shortens the 1H NMR relaxation times of its coordinated H_2O molecules (Westbrook, 1999). Hua *et al.* obtained $GdF_3:Eu^{3+}$ NCs by microemulsion-mediated hydrothermal process, and the visible quantum efficiency of $GdF_3:Eu^{3+}$ NC was calculated to ca. 170% (Hua *et al.*, 2006). Van Veggel *et al.* synthesized water-soluble NPs consisting of either a solid core of GdF_3 or a mixture of GdF_3 and LaF_3 by using a coprecipitation approach. After the stabilization by 2-aminoethyl phosphate, the GdF_3/LaF_3 NCs were used as NMR and MRI (magnetic resonance imaging) relaxation agents (Evanics *et al.*, 2006). Wang *et al.* fabricated transparent glass ceramics containing hexagonal GdF_3 NCs by melt-quenching and subsequent heating of glass with composition of $44SiO_2-28Al_2O_3-17NaF-11GdF_3$ (Chen *et al.*, 2008a). Fujihara *et al.* prepared transparent porous thin films of a $SiO_2/(Gd,Eu)F_3$ nanocomposite structure, in which $(Gd, Eu)F_3$ NCs were dispersed in a silica matrix, and the films showed interesting luminescence of Gd^{3+} and Eu^{3+} (Fujihara *et al.*, 2004).

4.2 Rare earth oxyhalides

Rare earth oxyhalides (ROX, X = F, Cl, Br) have been investigated for their applications as phosphors, ionic conductors, magnets, and catalysts (Au *et al.*, 1997; Chao *et al.*, 1995; Gruehn and Glaum, 2000; Hölsä *et al.*, 1998; Mello *et al.*, 1995; Wells, 1962). For example, rare earth ions activated oxyfluoride glass-ceramics are important photonic materials, which combine the low-phonon-energy environment of fluoride crystals and the high chemical/mechanical stability of oxide glasses. The general synthesis of rare earth oxyhalides is based on the solid-state reaction of rare earth oxides and ammonium halide (Meyer and Staffel, 1986). This method gives good control over the crystallinity and stoichiometry of the products, but is difficult to adopt to produce nanosized particles. Up to now, the majority of research on ROX has been done using their bulk crystals or thin films materials, while only a few of reports deal with the fabrication of nanosized materials by solution method. Barreca *et al.* fabricated thin film of $LaOF$ NPs (crystallite size < 30 nm) on SiO_2 and Si (100) by CVD (chemical

vapor deposition) method. Herein, $\text{La}(\text{hfa})_3 \cdot \text{diglyme}$ ($\text{hfa} = 1,1,1,5,5,5$ -hexafluoro-2,4-pentanedione; diglyme = bis(2-methoxyethyl) ether) was used as a precursor (Barreca et al., 2005). Malandrino et al. deposited nanostructured oxyfluoride (LaOF) films on Si (100) glass by MOCVD method using $\text{La}(\text{hfa})_3$ (Htmhd = 2,2,6,6-tetramethyl-3, 5-heptanedione) single source precursor (Malandrino et al., 2006). Fujihara et al. fabricated porous nanoparticulate LaOF films on glass substrates from ion modified lanthanum diacetate hydroxide by CBD (chemical bath deposition) (Hosono et al., 2004). Zhang et al. synthesized nanosized LaOF powders by mechanochemical processing in air using rare earth oxide and polytetrafluoroethylene as the solid reactants (Lee et al., 2003). Recently, Zeng et al. synthesized YOF NPs by decomposition of an air-stable single-source precursor, sodium yttrium fluorocarbonate under mild hydrothermal conditions, followed by thermal treatments (Zeng et al., 2009). Yan et al. reported a series of monodisperse ROF and rare earth doped NCs by controlled fluorination in oleic acid and oleylamine mixture solvents. Using $\text{R}(\text{CF}_3\text{COO})_3$ complexes as precursors, the rare earth doped ROF NCs presented excellent luminescence properties (Figure 68) (Du et al., 2008).

For ROCl, Byeon et al. synthesized PbFCl-type (tetragonal) Eu^{3+} doped LaOCl and GdOCl sub-microcrystals with controlled morphology by three different synthetic methods, viz. the coprecipitation reaction of different R_2O_3 in HCl solution followed by calcination process, the solvothermal reaction of rare earth chlorides in absolute ethanol, and the oleic acid surfactant-assisted solvothermal reaction (Lee et al., 2007). Zhang et al. synthesized LaOCl and LaOBr NPs by grinding the mixture of rare earth oxides, chlorides, and bromides in air followed by mechanochemical method (Lee et al., 2001). Konishi et al. prepared LaOCl: $\text{Yb}^{3+}, \text{Er}^{3+}$ NPs through a self-hydrolysis process of lanthanum and erbium hydrated chlorides. The as-obtained NPs emitted green and red UC emissions under laser irradiation at 980 nm (Konishi et al., 2007). More recently, Yan et al. developed the synthesis of monodisperse ultrathin LaOCl nanoplates (ca. 4.0 nm in thickness) and their superlattice assemblies via the decomposition of $(\text{La}(\text{CCl}_3\text{COO})_3)$ in long chain amines and 1-octadecene. By tuning the category of long chain amines (oleylamine, hexadecylamine, and octadecylamine), the LaOCl nanoplates could be aligned into "face to face" and "side to side" mixed superstructures, nanowire-like, and nanorod-like superstructures. This variety of self-assembled configurations could be attributed to the different interaction strengths of amine capping ligands. (Figure 69) (Du et al., 2009a).

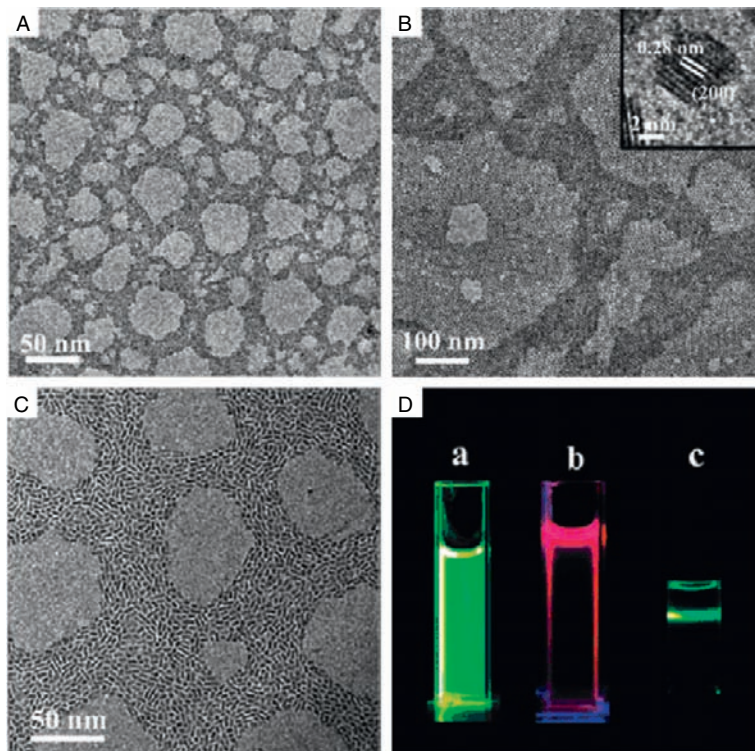


FIGURE 68 TEM images of (A) 2.9 nm LaOF:45%Ce,15%Tb nanopolyhedra, (B) 6.3 nm GdOF:5%Eu nanopolyhedra, and (C) 2.3 nm \times 6.2 nm GdOF:20%Yb,2%Er elongated NCs. (D) Fluorescence photographs of (a) LaOF:45%Ce,15%Tb nanopolyhedra and (b) GdOF:5% Eu nanopolyhedra dispersed in cyclohexane under irradiation of a 254 nm UV lamp. (c) Upconversion fluorescence photograph of GdOF:20%Yb,2%Er elongated NCs dispersed in cyclohexane under a 980 nm laser excitation. Reprinted with permission from Du *et al.* (2008). Copyright 2008 American Chemical Society.

4.3 ARF₄ compounds

The chemical formula of complex rare earth fluorides could be generally presented as ARF₄ (A, alkali metal; R, rare earth). Common structure types include tetragonal anti-scheelite (LiYF₄), hexagonal (NaN₂F₄), trigonal (KErF₄), and orthorhombic (KCeF₄) type (Brunton, 1969; Burns, 1965; le Fur *et al.*, 1992; Thoma *et al.*, 1961). Additionally, an unusual high-temperature modality also exists, which has A⁺ and R³⁺ cations at the Ca²⁺ sites of cubic CaF₂ structure with statistical distribution. For example, the cation sites in the hexagonal β -NaRF₄ contain three types:

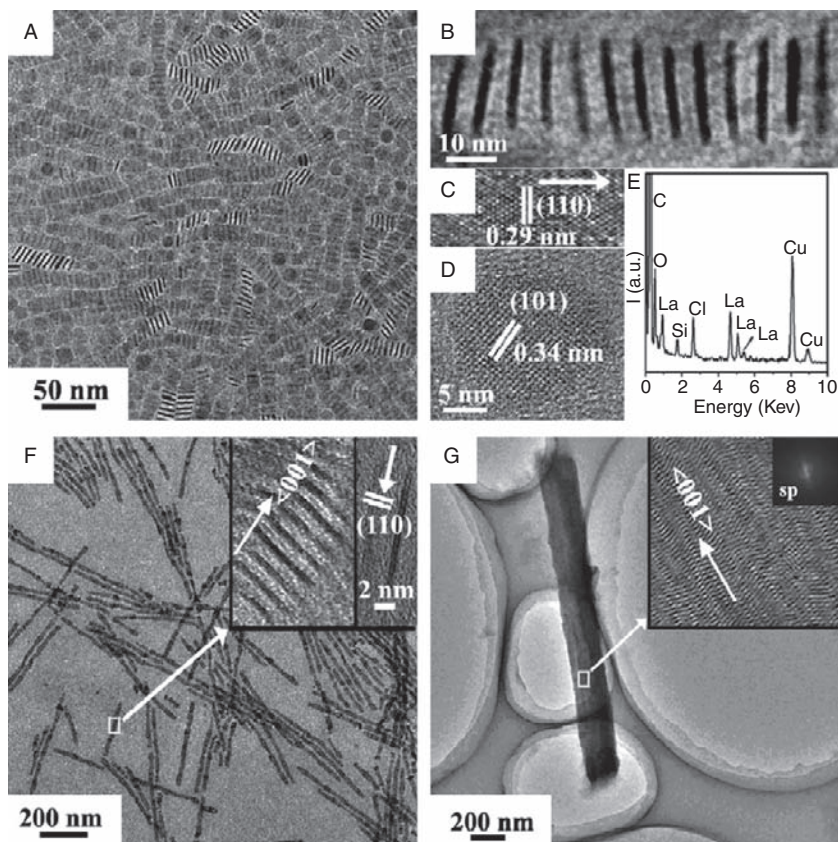


FIGURE 69 (A) TEM image of oleylamine (OM)-capped LaOCl nanoplate arrays. (B) TEM image of an aligned OM-capped LaOCl nanoplate (standing on the edge) array. (C) HRTEM image of a single OM-capped LaOCl nanoplate standing on the edge. (D) HRTEM image of a single OM-capped LaOCl nanoplate lying flat on the face. (E) EDAX spectrum of the LaOCl nanoplates. (F) TEM and HRTEM (inset) images of nanowire-like LaOCl nanoplate arrays composed of single-linear standing nanoplates capped with hexadecylamine via the face-to-face formation. (G) TEM image of a single nanorod-like LaOCl nanoplate array composed of multi-linear standing nanoplates capped with octadecylamine via the face-to-face formation; insets are the HRTEM image of the nanoplate superlattice (SP) and the corresponding FFT pattern. Reprinted with permission from Du et al. (2009a). Copyright 2009 American Chemical Society.

a onefold site occupied by R^{3+} , a onefold site occupied randomly by $1/2Na^+$ and $1/2R^{3+}$, and a twofold site occupied randomly by Na^+ and vacancies. But in the cubic $\alpha-NaRF_4$, Na^+ and R^{3+} cations are randomly distributed in the cationic sublattice (Thoma et al., 1966).

ARF₄ compounds with unique luminescent, insulating/magnetic, and piezoelectric properties attract great attention for their applications in solid-state lasers, 2D flat-panel displays, and low-intensity IR imaging. Up to present, wet synthetic approaches for ARF₄ NCs have been well developed. Especially, the well-known upconverting luminescent ARF₄ NCs are promising bioprobe candidates since the NIR excitation could eliminate auto-fluorescence background of the biomaterials (Choi et al., 2000; Cooke et al., 1975; Ghosh et al., 2003; Karbowski et al., 2005a).

4.3.1 Synthesis of ARF₄ nanocrystals

4.3.1.1 Coprecipitation methods The room temperature coprecipitation is the simplest route for complex rare earth fluoride NPs as well as their derivatives. For example, Chen et al. prepared ternary metal fluorides, such as hexagonal NaEuF₄ and cubic Na₅Eu₉F₃₂ NCs by reacting Eu(NO₃)₃ and NaF in water. Experimentally, the bundle-like EuF₃ nanostructure was formed first, and they reacted with NaF to form NaEuF₄ with 1D morphology. The NaEuF₄ nanorods could be transformed into Na₅Eu₉F₃₂ nanospheres by prolonging the reaction time in excess NaF (Wang et al., 2005c). Chen et al. prepared nearly monodisperse NaYF₄:Yb, Er NPs by coprecipitation of Y³⁺, Yb³⁺, Er³⁺ with NaF in the presence of EDTA. The particle size could be controlled effectively by the EDTA/R³⁺ ratio. Their preliminary results demonstrated the NPs to be promising up-converting fluorescent labels in biological detection (Yi et al., 2004). Karbowski et al. synthesized cubic KGdF₄ and KGdF₄:Eu³⁺ NCs using Gd₂O₃, Eu₂O₃, hydrochloric acid, and NH₄HF₂ as starting materials based on coprecipitation process (Karbowski et al., 2004, 2005b).

4.3.1.2 Solvothermal method The solvothermal (including hydrothermal and its derivatives) method is widely used to prepare ARF₄ NCs. Lin et al. reported uniform hexagonal NaYF₄:R³⁺ (R = Eu, Tb, Yb/Er, and Yb/Tm) submicroprism crystals through hydrothermal reaction of RCl₃, sodium citrate, and NaF. The ratio of sodium citrate and R³⁺ was found to strongly influence the shape and size of the products (Figure 70) (Li et al., 2007a).

Li et al. developed a water/alcohol/surfactant solvothermal system to prepare NaYF₄ NCs with predictable size, shape, and phase structure. The starting materials include R(NO₃)₃, NaF, NaOH, C₂H₅OH, and oleic acid. The NaF concentration, reactant concentration, synthesis temperature and time govern the size, shape and phase of NaYF₄ NCs (Figure 71) (Liang et al., 2007b,c; Wang and Li, 2007; Zeng et al., 2005). By the aid of other surfactants such as CTAB and EDTA, more novel NaYF₄ nanostructures could be prepared (Zeng et al., 2005; Zhuang et al., 2007). By modifying the additive in the hydrothermal route, Lin et al. synthesized NaYbF₄ sub-microcrystals with different phase structures and diverse morphologies, such as β-NaYbF₄ microdisks, microprisms, microtubes,

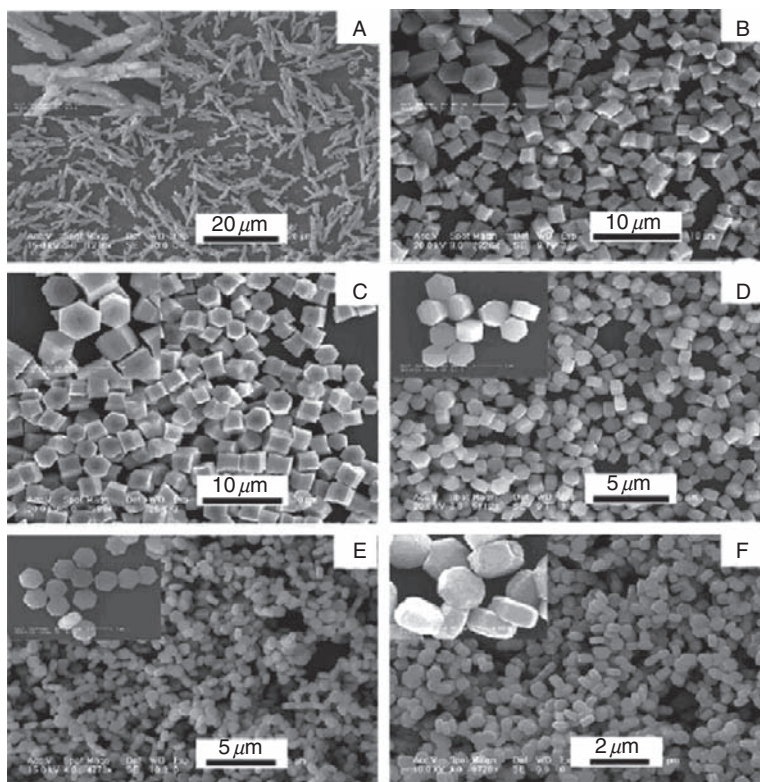


FIGURE 70 SEM images for β - NaYF_4 :5%Tb samples prepared with different molar ratios of sodium citrate and RE, (A) without sodium citrate, (B) 1:2, (C) 1:1, (D) 2:1, (E) 4:1, (F) 8:1. Insets are higher-magnification images for the corresponding samples. Reprinted with permission from Li et al. (2007a). Copyright 2007 American Chemical Society.

and α - NaYbF_4 submicrospheres (Li et al., 2008c). They also prepared hexagonal NaLuF_4 microprisms, microdisks, microtubes, cubic NaLuF_4 submicrospheres via Cit^{3-} and EDTA aided hydrothermal route (Li et al., 2008b). Similarly, Wu et al. prepared prismatic NaHoF_4 microtubes and NaSmF_4 nanotubes by EDTA modified hydrothermal method (Liang et al., 2004). Recently, Lin et al. demonstrated a simple trisodium citrate assisted hydrothermal method to synthesize monodisperse β - NaLuF_4 sub-microplates (Li et al., 2008d).

Li et al. prepared NaYF_4 : Eu^{2+} microcrystals with an intense blue luminescence via solvothermal route. OA and CTAB were served as the surfactants to tune the morphology, while citric acid stabilized the β - NaYF_4 and reduced Eu^{3+} to Eu^{2+} (Su et al., 2008).

Zhao et al. obtained NaYF_4 nanostructured arrays by solvothermal reaction of NaF , $\text{R}(\text{NO}_3)_3$ and oleic acid. A reverse micelle dissolution-

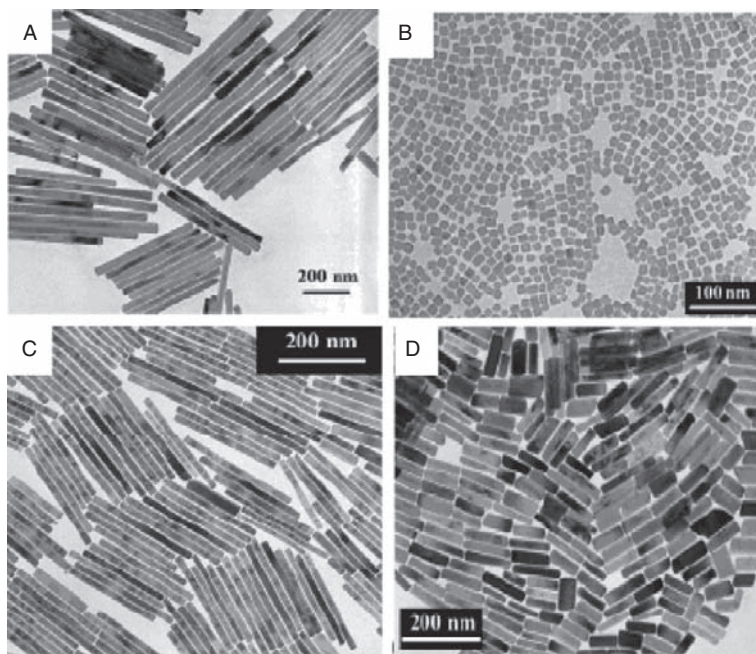


FIGURE 71 TEM image of (A) NaYF₄:Eu nanorods, (B) NaYF₄:Tb NCs, (C) NaYF₄:Tb nanorods, and (D) NaYF₄:Yb,Er nanorods. Reprinted with permission from Wang and Li (2007). Copyright 2007 American Chemical Society.

reconstruction process was supposed to be the chemical mechanism (Figure 72) (Zhang *et al.*, 2007b). They also fabricated uniform β -NaRF₄ nanotubes through a hydrothermal *in situ* ion-exchange reaction by rare earth hydroxide precursors [R(OH)₃] (Zhang and Zhao, 2009).

4.3.1.3 Thermo-decomposition method Yan *et al.* first reported the synthesis of high quality of NaRF₄ NCs by cothermolysis of Na(CF₃COO) and R(CF₃COO)₃ in high boiling organic surfactants, that is, oleic acid, oleylamine and 1-octadecene. Both metal (Na and R) and fluorine elements were integrated in the same precursor, providing a much better controlled synthesis of fluoride NCs than the liquid precipitation methods. By tuning the ratio of Na/R, solvent composition, reaction temperature and time, the phase structure and morphology the NaRF₄ NCs could be manipulated. Their research also showed that LaF₃ and CeF₃ preferred to segregate along with NaF, instead of forming NaLaF₄ or NaCeF₄. Pure α -NaRF₄ could be obtained at a low temperature with a low ratio of Na/R in OA/OM/ODE in a relatively short reaction time, while the formation of β -NaRF₄ preferred the reverse conditions (Figure 73) (Mai *et al.*, 2006). As

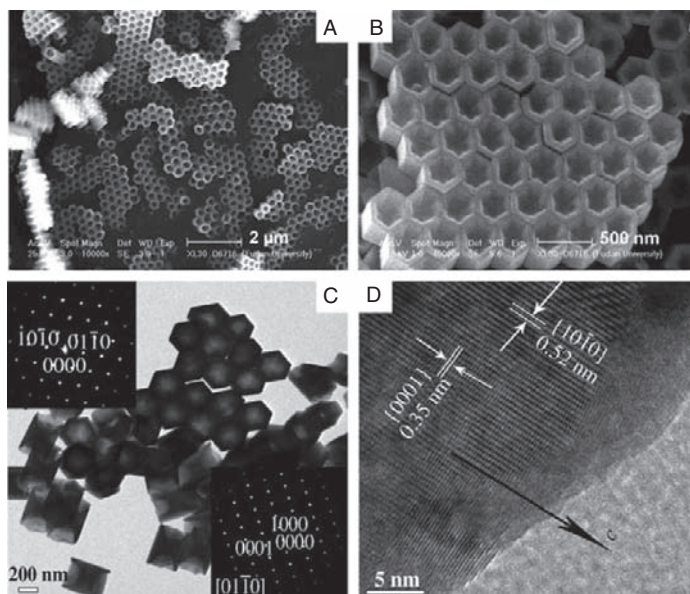


FIGURE 72 (A, B) SEM images of arrays of hexagonal nanotubes of β - NaYF_4 . (C) TEM image of the nanotubes and corresponding ED patterns (insets). (D) HRTEM image of a nanotube. Reprinted with permission from Zhang et al. (2007b). Copyright 2007 Wiley-VCH.

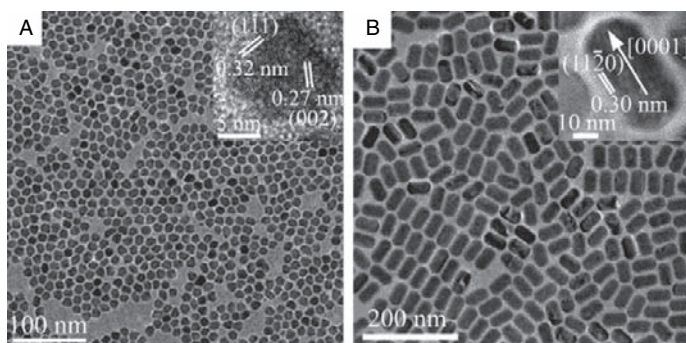


FIGURE 73 TEM and HRTEM (inset) images of high quality (A) cubic and (B) hexagonal phases of NaYF_4 nanopolyhedra and nanorods. Reprinted with permission from Mai et al. (2006). Copyright 2006 American Chemical Society.

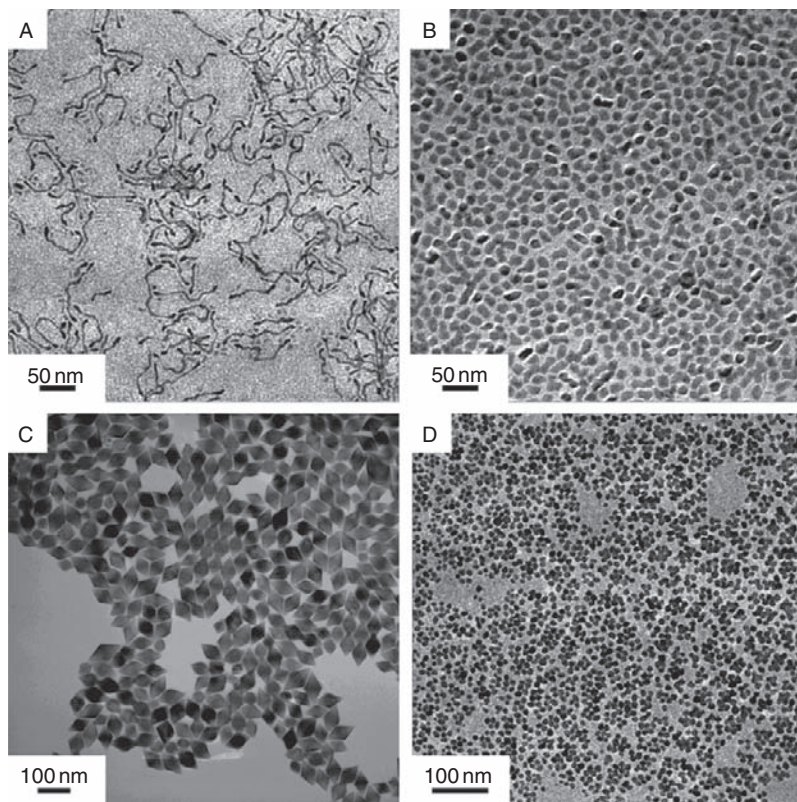


FIGURE 74 TEM images of (A) KLaF_4 nanowires, (B) KEuF_4 nanopolyhedra, (C) LiTmF_4 nanoplates, and (D) LiLuF_4 nanopolyhedra (Du *et al.*, 2009b). Reprinted with permission from Du *et al.* (2009). Copyright 2009, The Royal Society of Chemistry.

a subsequent work, this group developed a general synthesis for near-monodisperse KRF_4 and LiRF_4 NCs by cothermolysis of corresponding metal trifluoroacetate precursors in hot surfactants of OA, OM, and ODE (Figure 74) (Du *et al.*, 2009b).

4.3.1.4 Other methods A few other synthetic methods for ARF_4 NCs are listed below. Song *et al.* fabricated Yb^{3+} , Tm^{3+} codoped and Yb^{3+} , Er^{3+} , Tm^{3+} doped NaYF_4/PVP ($M_w = 1,300,000$) composite fibers with an average diameter of 300–800 nm by electrospinning method where, the doped NaYF_4 NCs were prepared by the polyol method using NaF, rare earth nitrates, and diethylene glycol as starting materials, the doped NaYF_4/PVP nanocomposite were subjected to the electrospinning setup operated at 13 kV (Dong *et al.*, 2008). Qiu *et al.* also fabricated uniform and

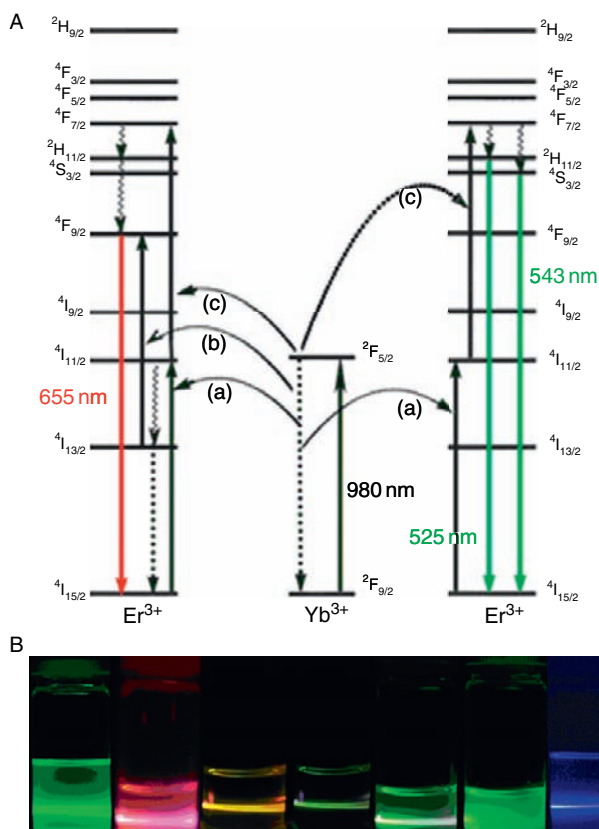


FIGURE 75 (A) Schematic illustration of the two-photon mechanism UC process of Er with Yb as the promoter for $\text{NaYF}_4:\text{Yb,Er}$ NCs (red emission at 655 nm; right, green emissions at 525 and 543 nm). (B) Multicolor up-conversion emission of rare earth doped NaYF_4 NCs.

smooth Ag NP embedded $\text{NaYF}_4:\text{Ce}^{3+}, \text{Tb}^{3+}/\text{PVP}$ composite nanofibers by adopting the similar electrospinning procedure (Dong et al., 2009).

4.3.2 Properties and applications of ARF_4 nanocrystals

Upconversion emission of rare earth doped ARF_4 NCs presents some attractive advantages in biological research (Suyver et al., 2005; Wang and Liu, 2009). With near infrared (NIR) excitation in the region of 700–900 nm, which is known as the biological spectral window, the UC luminescence minimizes the background autofluorescence and photo-damage of biological specimens.

Moreover, the excitation intensity required for UC process is much lower than for the general two-photon process. As shown in the scheme in Figure 75 need reference?, Yb^{3+} ion in ground-state $^2\text{F}_{7/2}$ absorbs a NIR photon to reach its excited-state of $^2\text{F}_{5/2}$, and then drops back to the ground state while transfer the energy to excite an adjacent Er^{3+} ion to its $^4\text{I}_{11/2}$ level. A second 980 nm photon also follows this transferring process but has the opportunity to further pump the Er^{3+} ion to its $^4\text{F}_{7/2}$ level. Then the Er^{3+} ion relaxes nonradiatively to the $^2\text{H}_{11/2}$ or $^4\text{S}_{3/2}$ levels, followed by green $^2\text{H}_{11/2} \rightarrow ^4\text{I}_{15/2}$ or $^4\text{S}_{3/2} \rightarrow ^4\text{I}_{15/2}$ emissions. Alternatively, the Er^{3+} ion can further relax and populate the $^4\text{F}_{9/2}$ level, leading to the red $^4\text{F}_{9/2} \rightarrow ^4\text{I}_{15/2}$ emission. Also, the Er^{3+} ion in the $^4\text{I}_{11/2}$ state may nonradiatively decay to the $^4\text{I}_{13/2}$ state and then populate the $^4\text{F}_{9/2}$ level via energy transfer from the excited Yb^{3+} ions, leading to the red $^4\text{F}_{9/2} \rightarrow ^4\text{I}_{15/2}$ emission.

NaYF_4 , representing complex rare earth fluoride (NaRF_4) compounds, is an ideal host material for upconversion (UC) phosphors, and $\beta\text{-NaYF}_4$ is the most efficient one up to now (Menyuk et al., 1972; Meyer and Wickleder, 2000). Haase et al. first prepared rare earth doped NaYF_4 NCs based on the coprecipitation process in with *N*-(2-hydroxyethyl)-ethylenediamine. The NCs showed efficient multicolor UC emissions under 980 nm, laser excitation (Heer et al., 2004). Capobianco et al. synthesized colloidal NaYF_4 NCs doped with $\text{Er}^{3+}/\text{Yb}^{3+}$ and $\text{Tm}^{3+}/\text{Yb}^{3+}$ by the thermo-decomposition method and observed visible green, red, and blue UC luminescence, respectively (Boyer et al., 2006, 2007a). Zhang et al. prepared hexagonal-phase core/shell $\text{NaYF}_4:\text{Yb},\text{Tm}@\text{NaYF}_4:\text{Yb},\text{Er}$ NCs synthesized by oleic acid assisted coprecipitation method followed by a seeded growth. A remarkable fluorescence enhancement was observed from the $^4\text{H}_{11/2}$, $^4\text{S}_{3/2}$, and $^4\text{F}_{9/2}$ to $^4\text{I}_{15/2}$ of Er^{3+} transitions (Qian and Zhang, 2008).

Chow et al. reported the IR-to-visible up-conversion fluorescent NCs of hexagonal $\text{NaYF}_4:20\%\text{Yb}^{3+}$, $2\%\text{Er}^{3+}$ and $\text{NaYF}_4:20\%\text{Yb}^{3+}$, $2\%\text{Tm}^{3+}$ prepared by decomposition of multi-trifluoroacetates in oleylamine. These materials showed intense green and blue UC emissions (Yi and Chow, 2006). Liu et al. tuned the UC emission colors based upon a single host source NaYF_4 NPs doped with Yb^{3+} , Tm^{3+} , and Er^{3+} . By precisely controlling the balance of emission intensity the luminescence could be tuned from visible to NIR under single-wavelength excitation (Figure 76) (Wang and Liu, 2008).

Using similar thermo-decomposition method, high quality $\text{NaGdF}_4:\text{Yb}^{3+}$, Er^{3+} NCs with hexagonal structure were synthesized by controlled precipitation in high boiling organic solvents (Aebischer et al., 2005). Both the green and red UC emissions were observed upon 977 nm laser excitation. Chen et al. obtained monodisperse, regular-shaped and well-crystallized rare earth-doped NaGdF_4 NCs with diverse morphologies. With different dopants, the NCs showed intense multicolor

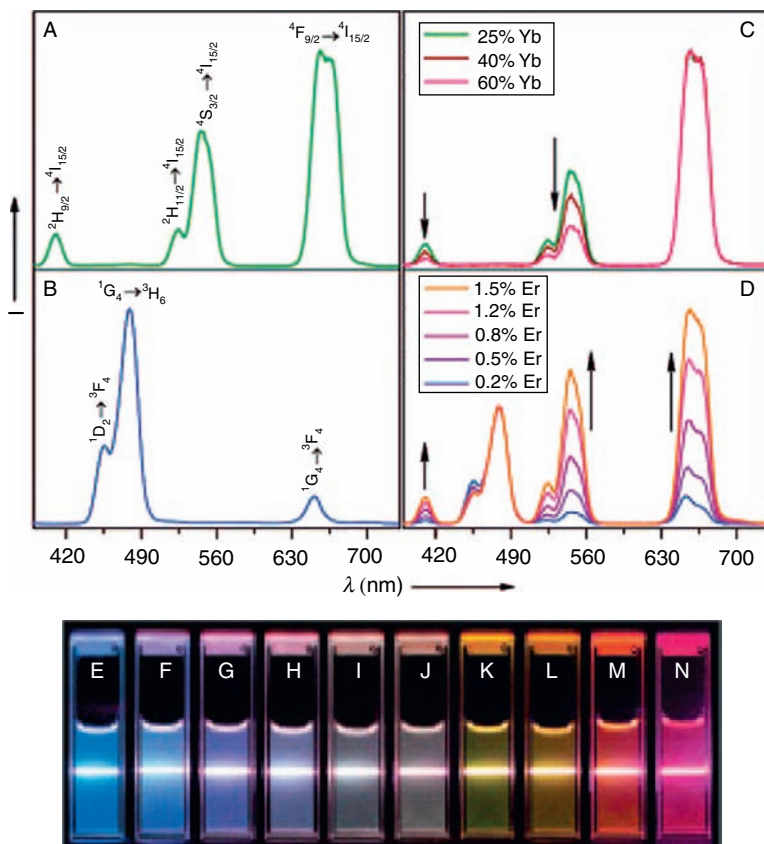


FIGURE 76 Up-conversion emission spectra of (A) NaYF₄: 18%Yb,2%Er, (B) NaYF₄:20% Yb,0.2%Tm, (C) NaYF₄:(25–60)%Yb,2%Er, and (D) NaYF₄:20%Yb,0.2%Tm,(0.2–1.5)%Er NPs. The luminescent photos showing corresponding colloidal solutions of (E) NaYF₄: 20% Yb,0.2%Tm, (F–J) NaYF₄:20%Yb,0.2%Tm,(0.2–1.5)%Er, and (K–N) NaYF₄:(18–60)%Yb,2%Er NCs. Reprinted with permission from Wang and Liu (2008). Copyright 2008 American Chemical Society.

down-conversion emissions under 254 nm UV excitation or up-conversion fluorescence under 980 nm excitation (Liu et al., 2009). Capobianco et al. prepared NaGdF₄: Ce³⁺, Tb³⁺ and NaGdF₄:Ce³⁺,Tb³⁺/NaYF₄ core/shell NCs by thermolysis of corresponding rare earth trifluoroacetate precursors in OA, OM and ODE mixture. Strong green luminescence was observed under UV excitation (Boyer et al., 2007b). More recently, Schäfer et al. reported the successful synthesis of Yb³⁺-Er³⁺ codoped KYF₄ NCs at 200 °C in *N*-(2-hydroxyethyl)-ethylenediamine (HEEDA) (Schäfer et al., 2008).

Besides recent developments in the synthesis controlling of the upconversion of luminescent NCs, the surface modification techniques for biological applications are also broadly studied. Generally, NCs must be water-soluble and have surface functional groups (such as $-\text{COOH}$, $-\text{NH}_2$, or $-\text{SH}$) for biomolecules conjugation. Zhang et al. used PVP as chelating agent and stabilizer to prepare monodisperse NaYF_4 NCs with multicolor UC luminescence. (Li and Zhang, 2006a). They also demonstrated the one-pot synthesis of polyethylenimine/ NaYF_4 NPs with lanthanide dopants, which were water soluble and biocompatible. The surface amino groups of polyethylenimine could be used for grafting of biomolecules (Li and Zhang, 2006b). Schäfer et al. treated $\text{NaYF}_4:\text{Yb}^{3+}$, Er^{3+} NCs with 1-hydroxyethane-1,1-diphosphonic acid (HEDP) to disperse the particles in aqueous solution (Schäfer et al., 2007). Chow et al. reported water soluble $\text{NaYF}_4:\text{Yb}^{3+}$, Er^{3+} (Tm^{3+})/ NaYF_4 /polymer core/shell/shell NPs with significant enhancement of UC fluorescence. These NPs were rendered with hydrophilicity and carboxylic functional groups by amphiphilic polymer coating, to be promising bio-probes (Yi and Chow, 2007). Capobianco et al. obtained $\text{NaGdF}_4:\text{Ho}^{3+}/\text{Yb}^{3+}$ NCs, whose green UC emission could be enhanced with increasing Ho^{3+} concentration. The ligand exchange with PAA could achieve hydrophilic NPs with the UC luminescence preserved (Naccache et al., 2009).

Li et al. developed a simple and versatile strategy for converting hydrophobic rare earth nanophosphors into water-soluble and carboxylic acid-functionalized analogues. The surface oleic acid ligands could be directly oxidized by the Lemieux-von Rudloff reagent, and the modified NCs kept the excellent luminescence and were further used as DNA labels (Figure 77) (Chen et al., 2008c).

Recently, Prasad et al. demonstrated the NIR-to-NIR up-conversion photoluminescence imaging of $\text{Yb}^{3+}\text{-Tm}^{3+}$ codoped NaYF_4 nanophosphors *in vitro* and *in vivo*. No apparent cytotoxicity was observed in the metabolizing process (Figure 78) (Nyk et al., 2008). Nann et al. developed a new series of UC NCs using cothermolysis method. The NCs were highly crystalline, colloidal, and uniformly sized, and showed four different spectrally resolvable UC spectra, applicable for multiplexing analysis. These NPs could be phase-transferred to polar solvents by SiO_2 encapsulation (one particle per silica sphere) (Ehlert et al., 2008). Li et al. synthesized uniform silica-coated $\text{NaYF}_4:20\%\text{Yb},2\%\text{Er}$ nanocomposites with incorporation of organic dye and folic acid. The folic acid served as targeting agent for human cells with folate receptor overexpressed. By the confocal microscopy imaging and quantitative flow cytometry analysis, they demonstrated the receptor mediated delivery of NPs for folate receptor-positive cell lines, such as KB cells (Hu et al., 2009).

Liu et al. used polyethylenimine (PEI) to stabilize R^{3+} and subsequently control the growth of NaYF_4 NCs. The as-obtained PEI-coated NCs were

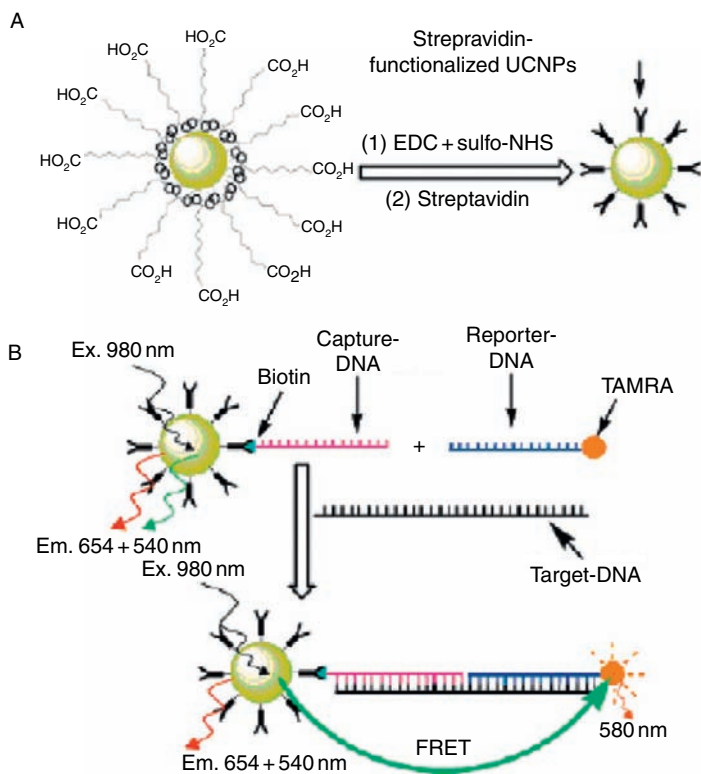


FIGURE 77 (A) Synthesis of streptavidin-functionalized $\text{NaYF}_4:\text{Yb,Er}$ up-converting NPs and (B) schematic of DNA nanosensors based on up-converting NPs. Reprinted with permission from Chen et al. (2008c). Copyright 2008 American Chemical Society.

dispersible in various solvents including water, ethanol, DMF, DMSO, and ethylene glycol. They also provide a platform for direct surface functionalization of biomolecules. The UC emission colors could be adjusted by varying the doping ratio and species of lanthanide ions (Wang and Liu, 2008).

A combination of useful optical and magnetic properties in a single material would enable simultaneous biolabeling/imaging and cell sorting/separation. Chen et al. prepared hybrid NPs possessing magnetic response, and UC fluorescence by coprecipitation of $\text{NaYF}_4:\text{Yb,Er}$ on superparamagnetic iron oxide NPs. The nanocomposites were further coated by SiO_2 shell and functionalized with streptavidin (Lu et al., 2004a). Zhang et al. prepared the $\text{Fe}_3\text{O}_4@\text{NaYF}_4:\text{R}^{3+}$ NCs by layer-by-layer assembly using a modified Stöber method (Stöber et al., 1968; Zhang et al., 2008g). Prasad et al. reported Gd^{3+} and $\text{Er}^{3+}/\text{Yb}^{3+}/\text{Eu}^{3+}$ codoped NaYF_4 nanoprobe combining optical and magnetic resonance imaging properties so as to provide the dual modality detection ability. The as-obtained nanophosphors

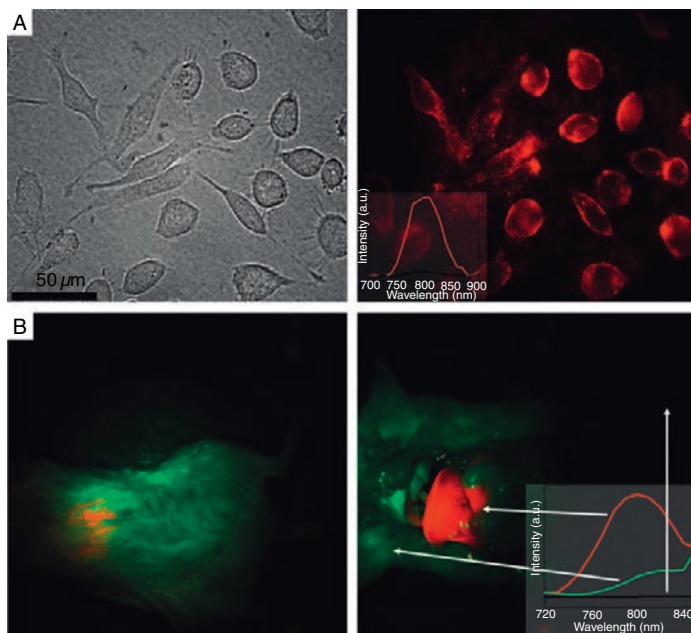


FIGURE 78 (A) *In vitro* transmission (left) and PL (right) images of Panc-1 cells treated with NaYF₄: 20%Yb,2%Tm NCs. (B) Whole body images of mouse injected intravenously with NaYF₄: 20%Yb,2%Tm NCs; intact mouse (left), the same mouse after dissection (right). Reprinted with permission from Nyk *et al.* (2008). Copyright 2008 Wiley-VCH.

were modified with biorecognition biomolecules such as anti-claudin-4 and anti-mesothelin, and showed *in vitro* targeting to cancer cells. It was also shown that the Gd³⁺ codoped within the nanophosphors strongly imparted T₁ (spin–lattice relaxation time) and T₂ (spin–spin relaxation time) values of MRI (Kumar *et al.*, 2009).

The current synthesis strategies mainly depend on trial-and-error approaches instead of rational systematic designs, so new methodologies for synthesizing functional rare earth NCs should meet special application-based requirements with a predesigned synthesis route. Further demands for diverse nanostructures of rare earth halides include environmental friendliness, scalability, versatility, and reliability. In addition, simulations of crystal growth behaviors, surface effect induced phases, morphology and property controls, and NCs assembly are essential for understanding of the structural characteristics, formation mechanisms, and shape control factors. However, the guiding principles of NC growth are a big challenge because of the complicated structures of rare earth halides.

The unique luminescence properties of rare earth halide NCs ensure their potential applications in optical devices. The underlying photophysical issues include the energy transfer processes within and between luminescent NCs; emission spectra related surface distortion and point symmetry sensitive luminescence, as well as the optical behavior of a single NC. On the other hand, high-quality rare earth halide NCs can serve as excellent building blocks, which are expected to be integrated into novel nanodevices with interesting properties both of the individual NCs and of the collective. The multifunctional nanostructures/nanodevices could also be designed in such ways. Moreover, these NC phosphors could play the role as active components in hybrid materials, and polymer and glass-based functional hybrids will be a shortcut to fabricate useful devices.

5. NANOMATERIALS OF RARE EARTH SULFIDES AND OXYSULFIDES

5.1 Rare earth sulfides

Among rare earth chalcogenide compounds, Eu(II) compounds, that is, EuX ($X = \text{S}, \text{Se}, \text{Te}$) is one of the most important series of magnetic semiconductors, which exhibit magnetic ordering ranging from ferromagnetism, to metamagnetism and antiferromagnetism. These compounds have been extensively studied since the 1960s (Wachter, 1972), and they continue to be of both theoretical and experimental interest. Due to the potential applications in optomagnetic and luminescent devices, EuS deserves particular attention. Bulk EuS is a ferromagnetic semiconductor material with rock salt structure. It has the Curie temperature (T_C) of 16.8 K, an energy gap of 1.6 eV, and spin splitting with the gap of 0.36 eV (Eastman et al., 1969; Hao et al., 1990; McGuire and Shafer, 1964). The 4f–5d electronic transition and spin configuration of Eu^{2+} could generate large optomagnetic properties, including Faraday and Kerr effects (Suits et al., 1966). Using physical synthesis methods, the obtained EuS nano-/microcrystals have been confirmed to possess optomagnetic behaviors mentioned above (Fumagalli et al., 1995; Gambino and Fumagalli, 1994; Tanaka et al., 2001). The chemical synthesis of bulk EuS employs the solid-state reaction of Eu (or Eu_2O_3) with S (or H_2S) at high temperature (Rard, 1985). As nanocrystalline semiconductor is of current interest, wet synthesis routes for colloidal EuS NPs are also being developed. The obtained nanoscale EuX ($X = \text{S}, \text{Se}, \text{Te}$) have been regarded as model systems to probe the relationship between the band gap energy and magnetic/optomagnetic properties.

Theoretically, EuS NPs have a size-dependent optical performance as the common characteristic for semiconductor material, but the

luminescence of bulk EuS is very weak and not suitable for applications. Chen *et al.* demonstrated luminescence enhancement of EuS clusters. By annealing mechanically milled EuS and zeolite powder in vacuum at 600 °C, EuS clusters could form in zeolite-Y supercages via solid-state diffusion. The product revealed a broad emission band in the range of 800–1400 nm, attributed to the $4f^65d^1(t_{2g}) \rightarrow 4f^7$ transition of Eu^{2+} . This luminescence was visible even at room temperature, while bulk EuS powder only showed luminescence at low temperature. Additionally, the emission of EuS-zeolite composites revealed a blue-shift from the spectrum of the bulk. This may be attributed to quantum-confinement effect, when EuS clusters were restrained by 0.65 nm sized zeolite supercages. This value was close to the calculated electron Bohr radius (0.35–0.75 nm) of EuS (Chen *et al.*, 2000).

Scholes *et al.* prepared EuS NPs via decomposition of single-source precursors in high boiling point organic solvent. Each metallic chelate precursor composed of one central Eu^{3+} ion, three sulfate source ligands such as diethyldithiocarbamate anion (Ddtc) or xanthate anion, and one chelating ligand such as 1,10-phenanthroline (Phen) or 2,2'-bipyridine (Bipy). The solvent phase was composed from oleylamine, trioctylphosphine, octadecene, and oleic acid. These solvent molecules also acted as stabilizing ligands for NPs. Similar to the QDs synthesis procedure, the reaction mixture was first incubated around 100 °C under vacuum to remove water and oxygen, then it was heated up to a predefined temperature (200–300 °C) for decomposition of precursors under argon protection. Under thermal environment, the Eu^{3+} ions were reduced into Eu(II) by oleylamine, followed by combining released sulfur for the nucleation of EuS. By varying the decomposition conditions and precursors, cube-, sphere-, or polygon-shaped EuS nanocrystals were obtained (Mirkovic *et al.*, 2005). In the following research, Scholes *et al.* have not observed size-dependence of optical properties of EuS NPs. Particle size change from 9 to 23 nm showed no effect on the absorption band positions, that is, the $4f^7 \rightarrow 4f^65d^1(t_{2g})$ transition at ca. 2.35 eV (Figure 79). This absorption peak (around 500 nm) was often mistaken for the excitation band of EuS. Actually, the absorption spectrum of 23 nm EuS colloidal NPs well corresponded to the reference data of bulk crystals, especially in low energy region. The derivation at the higher-energy region of the spectrum, such as the peak at approximately 4.9 eV, has been assigned to surface ligand absorption (Huxter *et al.*, 2008). The absence of quantum confinement effect was consistent with the estimated electron/hole Bohr radius for EuS, which was less than 1 nm (Chen *et al.*, 2000).

Gao *et al.* tried two methods to synthesize EuS NPs based on thermal decomposition of $\text{Eu}(\text{Phen})(\text{Ddtc})_3$ precursors. The direct decomposition of precursors in a nitrogen flowing furnace at 430 °C produced NPs in the range of 50–120 nm, while the decomposition in oleylamine at 200 °C

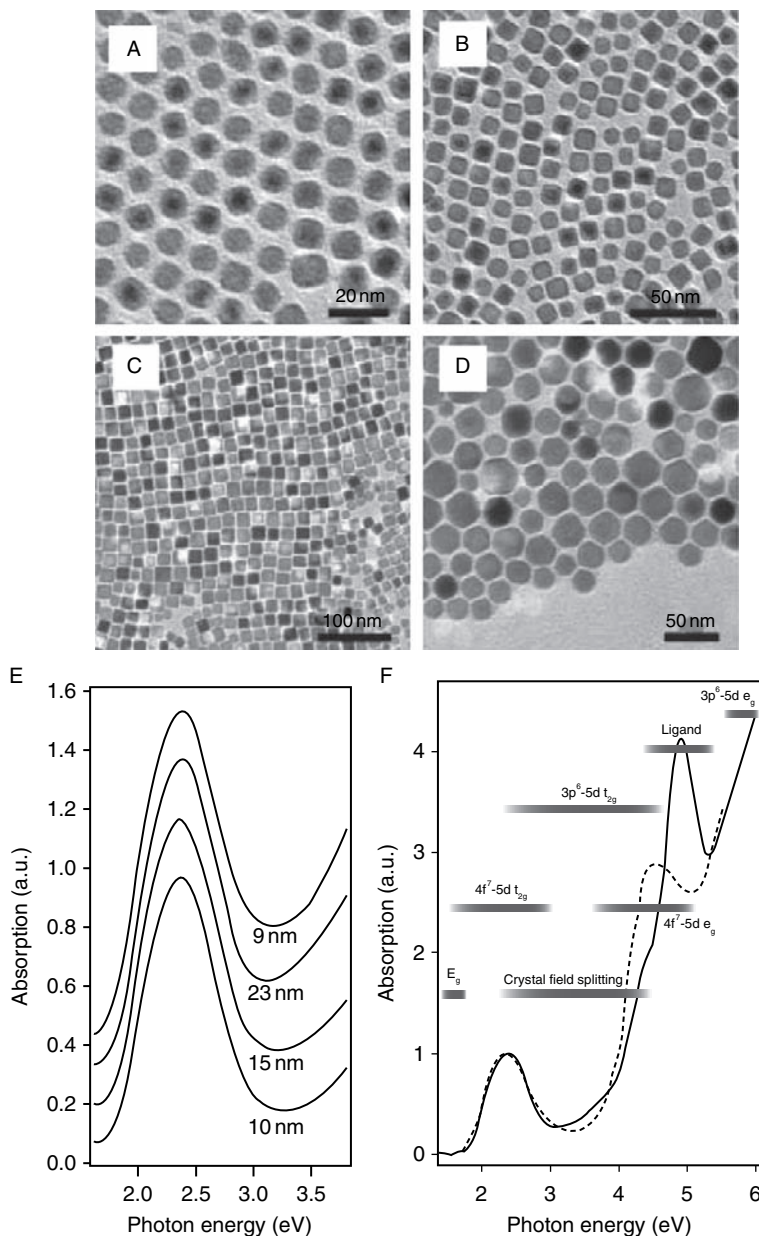


FIGURE 79 TEM images of the four samples of EuS NPs with average diameters of (A) 9 nm, (B) 10 nm, (C) 15 nm, (D) 23 nm; (E) normalized absorption spectra of EuS NPs plotted on an energy scale; (f) absorption spectrum of 23 nm EuS nanocrystals (solid line) and a reference bulk spectrum (dashed line). Reprinted with permission from Huxter et al. (2008). Copyright 2008 Wiley-VCH.

resulted in 5.5 nm NPs. The bigger EuS NPs revealed ferrimagnetic-like behavior as bulk materials did, whereas the smaller EuS NPs showed cluster glass-like behavior since the particle size was close to the single-domain scale. Moreover, a ferrimagnetic-like behavior was observed from the 5.5 nm EuS NPs after long-term exposure in air. This transition was caused by surface oxidized layer of Eu(III), which weakened the interparticle interactions (Zhao *et al.*, 2005). Gao's group subsequently synthesized monodisperse EuS nanocrystals with sizes ranging from 2.6 to 20 nm by a similar solution-phase decomposition method. These products could be self-assembled into 2D or 3D ordered superlattices. The particle size was controlled via varying the concentration of precursor and reaction temperature. In magnetic measurements, it was found that the coercive field values (H_C) strongly depended on the NPs size. When the size of EuS nanocrystals was close to the single-domain scale, the H_C reached the maximum value of 66 Oe. Below this critical size, the coercivity gradually decreased to zero. This variation confirmed their previous research (Zhao *et al.*, 2006a). Dickerson *et al.* also compared the magnetic properties of EuS nanocrystals with different size, which were synthesized via single-source precursor method. They found EuS nanocrystals with diameters between 2.0 and 100 nm showed reverse magnetization hysteresis curves at certain temperature (from 11 to 25 K), while sub-2.0-nm nanocrystals did not show this abnormality. This phenomenon was explained by the competition between the magnetic properties of strained surface Eu^{2+} and unstrained Eu^{2+} in core region. In the abnormal case, the surface Eu^{2+} ions tended to align the magnetic moments along their preferred directions, which could be different from the magnetic moment direction of the inner core. When the two proportions of magnetization were comparable, the magnetization hysteresis reversal became possible at certain temperature region. But in EuS nanoclusters (size below 2 nm), surface atoms were prevalent. Then the entire magnetization for a single cluster returned to a single mode and no reversal occurred (Redigolo *et al.*, 2006).

Stoll and coworkers tried to study the relationship between EuS band gap and its magnetic properties. The EuS nanocrystals were obtained from decomposition of $\text{Eu}(\text{S}_2\text{CN}^-\text{tBu}_2)_3\text{Phen}$ precursors in trioctylphosphine and oleylamine. Based on Arrott plots, they found that the ferromagnetic T_c for nano-sized EuS was 1–2 K lower than that of bulk material. Nevertheless, the size of nanocrystals (around 19 and 14 nm) was beyond the Bohr radius of EuS, so the band gap won't be changed too much. There may be other reasons responsible for the decrease of ordering temperature, such as lattice strain and surface effects, mentioned by the authors (Regulacio *et al.*, 2006). In the succeeding research, this group evaluated the role of quantum confinement and surface effects on size-dependent magnetic properties of EuS. For this goal, a series of smaller EuS nanocrystals (<10 nm) with controllable size were synthesized. The

preparation procedure was similar as before, except that the precursor was changed to $\text{NH}_2\text{Et}_2[\text{Eu}(\text{Ddte})_4]$ to avoid chelating ligands (Phen or Bipy). In optical absorption measurement, the peak value of $\text{Eu}^{2+} 4f^7(^8\text{S}_{7/2}) \rightarrow 4f^6(^7\text{F}_j)5d^1(t_{2g})$ transition shifted from 511 to 490 nm with decreasing particle size from 7.2 to 4.9 nm. However, only the motion of absorption edge (E_g , about 1.6 eV) could indicate quantum confinement, while it had a very small shift. They estimated that the Bohr radius for EuS was 1.2 nm, so the NPs were still too large to reveal unambiguous quantum confinement phenomenon. The T_c was calculated for different-sized EuS NPs by a classical equation. When considering the surface effects in the calculations only (assuming that the surface atoms had half the coordination number), the calculated T_c departed from the experimental data in the region of NPs sizes below 6 nm. Taking E_g changes together into calculation could correct for this deviation. The calculated T_c showed a sharp drop with decreasing NPs size to the confinement regime, which agreed with the tendency observed in the experimental data. This suggested that E_g variation (confinement effect) played an important role in magnetic properties of EuS nanocrystals (Regulacio et al., 2008).

Hasegawa et al. initiated the decomposition of precursors by uninterrupted photo irradiation for 3 days and obtained ca. 9 nm EuS NPs. The precursor, $\text{Na}[\text{Eu}(\text{Ddte})_4]$, absorbed the photons with compatible energy for its photolysis. The photolysis reaction produced S_2CNET_2 radical and simultaneously reduced Eu(III) to Eu(II). $\cdot\text{S}_2\text{CNET}_2$ radical also released S^{2-} , and they formed EuS NPs (Hasegawa et al., 2005). Hasegawa et al. also used microwave irradiation for thermal decomposition of $\text{PPh}_4[\text{Eu}(\text{S}_2\text{CNET}_2)_4]$ precursor. The reaction was held in refluxed acetonitrile under 80 °C, and ca. 9 nm EuS NPs were obtained. Strong luminescence around 350 nm was observed from the obtained EuS NPs at room temperature (Hasegawa et al., 2006).

Yanagida's group improved the liquid-ammonia-phase synthesis route and obtained EuS NPs. Europium metal was dissolved in liquid ammonia (−78 °C) to form a deep blue solution. Argon diluted H_2S gas was bubbled into the solution until its color turned to yellow. Then EuS NPs were collect by evaporating liquid ammonia away (Thongchant et al., 2003). Wada et al. reported a similar method, except that they used thiourea as the sulfur source (Kataoka et al., 2005). The thiourea was also considered as capping agent, while excessive thiourea limited the growth of EuS NPs. The average particle size was controlled between 7 and 14 nm by adjusting the thiourea amount. The authors observed a blue shift of the $4f^7(^8\text{S}_{7/2}) \rightarrow 4f^6(^7\text{F}_j)5d^1(t_{2g})$ absorption band accompanied by the decrease of the particle size. Since EuS has unique magneto-optical properties based on its 4f–5d electron transition and spin configuration, the product NPs were embedded inside a PMMA thin film for

Faraday effect test. The measured Faraday rotation peak wavelength showed a blue shift tendency with reduced NPs size.

In literature, europium (II) chalcogenide NPs have weaker magnetic properties compared with bulk counterparts because their size is often below the magnetic correlation distance. However, nanoscale europium (II) chalcogenides have confined electronic states and result in an increased optical transition cross-section. This probably enhances their magneto-optical performance. EuS NPs with different size could vary the Faraday rotation peak wavelength in the range of 580–640 nm (Kataoka *et al.*, 2005), but this value is still limited by the material resonance wavelength and magnetic susceptibility. Effective Faraday rotation phenomenon near 500 nm requires other europium chalcogenide NPs, which have wider band gap energy. EuSe material is an appropriate candidate, with 1.80 eV energy gap for the bulk materials. Hasegawa *et al.* prepared nanoscale EuSe in solution for the first time. A special organic selenium compound, $(PPh_4)[Se_2P(Ph)_2]$, was designed to reduce $Eu(NO_3)_3$ and simultaneously provide selenium. The preparation was held in hexadecylamine at 330 °C with nitrogen protection. EuSe NPs with size about 20 nm were obtained after a 4 h reaction (Adachi *et al.*, 2008). In the following study, Hasegawa and coworkers confirmed the

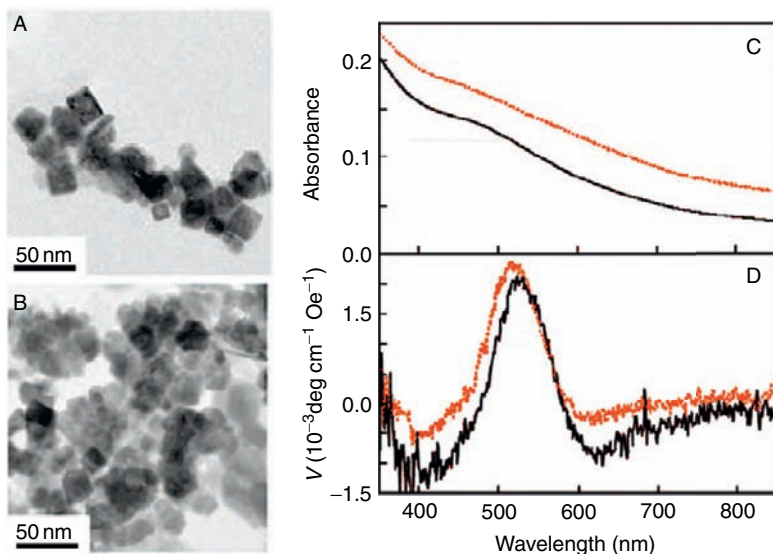


FIGURE 80 (A) $Eu_{1-x}Se$ sample 1 and (B) $Eu_{1-x}Se$ sample 2; (C) absorption and (D) Faraday rotation spectra of polymer thin films containing $Eu_{1-x}Se$ sample 1 NPs (black line) and sample 2 NPs (red line). Reprinted with permission from Hasegawa *et al.* (2008). Copyright 2008 American Chemical Society.

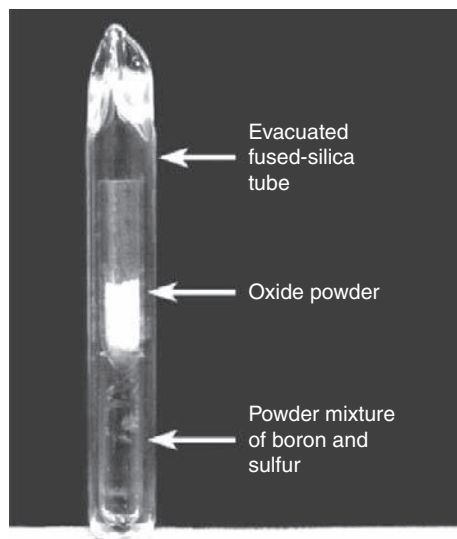


FIGURE 81 The reaction container (10 mm i.d.) and the reaction equations for boron sulfides-assisted synthesis of metal polysulfides and sulfides: $x\text{B}(s) + y\text{S}(g) \rightarrow a\text{B}_2\text{S}_3(g) + b\text{BS}_2(g) + c\text{S}(g)$; $m(\text{metal oxide})(s) + a\text{B}_2\text{S}_3(g) + b\text{BS}_2(g) + c\text{S}(g) \rightarrow p(\text{metal sulfide})(s) + q\text{B}_2\text{O}_3(v)$. The (s) stood for vitreous state. Reprinted with permission from Wu and Seo (2004). Copyright 2004 American Chemical Society.

composition of their products as Eu_{1-x}Se by quantitative EDX analysis (Hasegawa et al., 2008). The excess Se atoms were proposed to locate at the NPs surface, and the Eu defects might be neutralized by $\text{P}(\text{C}_6\text{H}_5)_4^+$ cations stacking on NPs. The magnetic measurements revealed that two samples of Eu_{1-x}Se NPs (synthesized from $\text{K}[\text{Se}_2\text{P}(\text{Ph})_2]$ and $(\text{PPh}_4)[\text{Se}_2\text{P}(\text{Ph})_2]$, respectively) displayed antiferromagnetic behavior. The magneto-optical properties of Eu_{1-x}Se NPs were measured in PMMA thin films, showing a Faraday rotation peak wavelength around 520 nm (Figure 80).

Beside rare earth monosulfide compounds, rare earth polysulfide nanomaterials have been reported in the literatures. Seo et al. explored new sulfiding agent for solid-state synthesis of rare earth polysulfide NPs. Initially, boron and sulfur powders formed B_2S_3 , BS_2 , and nonstoichiometric compounds as sulfo-source. Then, these boron sulfides evaporated for the sulfidation of Nd_2O_3 NPs (Figure 81). The reaction was carried out at 450°C , and NdS_2 products could maintain the original size of the oxide NPs (ca. 50 nm) without fusion. The unreacted sulfur, boron sulfides, and the by-product B_2O_3 were washed away by CS_2 and deionized water. When they used elemental sulfur alone, no neodymium sulfides formed with the same reaction conditions, except a small amount of $\text{Nd}_2\text{O}_2\text{S}$ (Wu et al., 2003b). This boron sulfides mediated sulfidation route has been

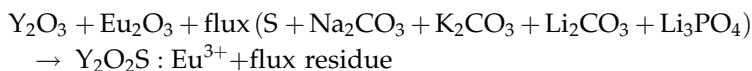
further extended for producing various nanoscale metal polysulfides and sulfides, including Y_2S_3 , and CeS_2 , NdS_2 , SmS_2 , EuS_2 , TbS_2 , and ErS_2 NPs (Wu and Seo, 2004).

5.2 Rare earth oxysulfides

Rare earth oxysulfide (R_2O_2S) compounds have hexagonal phase structure. They are known for the promising applications in field emission displays, and X-ray luminescent screens. For instance, $Y_2O_2S:Eu^{3+}$ is an important red photo-luminescent (PL) and cathodo-luminescent (CL) phosphor, and $Gd_2O_2S:Tb^{3+}$ is an X-ray excited green phosphor. In recent years, sub-micrometer sized $Y_2O_2S:Yb^{3+},Er^{3+}$ and $Y_2O_2S:Yb^{3+},Tm^{3+}$ particles have been used as up-conversion luminescence labels in DNA detection and immunoassays (Corstjens *et al.*, 2001; Corstjens *et al.*, 2003, 2005; Niedbala *et al.*, 2001; Rijke *et al.*, 2001; Zijlmans *et al.*, 1999). However, the synthesis procedures for metallic oxysulfides are still extremely rigorous. Solution phase coprecipitation routes could be denied first, because rare earth ions have stronger affinity to oxygen than to sulfur atoms. On the other hand, the currently used solid-state methods involve several time-consuming steps, that is, blending, calcinations (above 1000 °C), washing, milling, and classification. The washing and grinding process probably increases the surface defects on crystals, so the luminescent efficiencies of rare earth oxysulfides degrade. Moreover, the ideal morphology for practical phosphor is micrometer-scaled spheres with uniform size distribution. The classic synthesis strategy could not fulfill this point, thus new synthesis approaches for nano- and sub-micrometer sized R_2O_2S particles is an urgent issue for researches. This section summarizes the current developments on synthesis of R_2O_2S , including novel wet chemistry methods and improved solid-state methods. The optical properties of these phosphors are discussed later.

5.2.1 Solid state synthesis routes

Exclusion of water and oxygen is the primary criterion in rare earth oxysulfide synthesis procedures. This is generally analogous to the case of rare earth sulfides. The industry synthesis technology depends on sulfurizing rare earth oxide powders via solid-state reactions. For instance, the classical sulfide fusion method follows the schematic reaction:



The mixture is sintered in the range of 1100–1200 °C in nitrogen atmosphere. After elimination of the flux residue by acid washing,

$\text{Y}_2\text{O}_2\text{S}:\text{Eu}^{3+}$ crystals 5–10 μm in size are left (Chou et al., 2005). On this foundation, nano-/submicro-crystalline $\text{R}_2\text{O}_2\text{S}$ could be achieved after some technical improvements.

The morphology and properties of raw materials largely influence the manufacture of ceramics. If well-dispersed powders with high reactivity are used, the sulfurization will be much easier with decreasing calcination period and temperature. The relatively mild conditions also benefit the preservation of precursor morphology. Compared with rare earth oxides, rare earth hydroxides show more reactivity, because the dehydration process creates plenty of fresh sites for reaction. In a modified flux method from Kakihana's report, rare earth hydroxide processors and flux materials mixture was kept in different crucibles. And sulfur atmosphere came from the flux sublimation. The separation of the processors from the flux showed advantage for suppressing the overgrowth and sintering of NPs even above 1000 $^\circ\text{C}$. It also avoided the impurities of flux residue (Kawahara et al., 2006). Li et al. prepared well-crystallized $\text{R}(\text{OH})_3$ nanowires, nanotubes, and fullerene-like NCs via hydrothermal routes. These nanomaterials were applied in further dehydration, fluoridation or sulfidation processes (Wang and Li, 2003a). The obtained $\text{Y}_2\text{O}_2\text{S}:\text{Eu}^{3+}$ and $\text{Y}_2\text{O}_2\text{S}:\text{Yb}^{3+},\text{Er}^{3+}$ NCs maintained nanotube morphology even after 700 $^\circ\text{C}$ thermal treatment (Wang et al., 2003). Wu et al. used

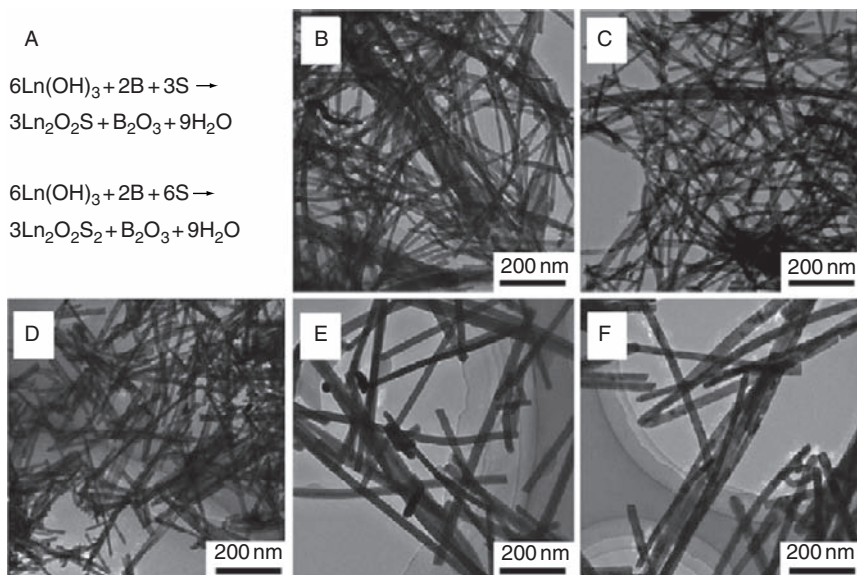


FIGURE 82 (A) The chemical equations for synthesizing $\text{Ln}_2\text{O}_2\text{S}$ and $\text{Ln}_2\text{O}_2\text{S}_2$; the TEM images of (B) $\text{La}_2\text{O}_2\text{S}$; (C) $\text{La}_2\text{O}_2\text{S}_2$; (D) $\text{La}_2\text{O}_2\text{S}:\text{Eu}$; (E) $\text{Nd}_2\text{O}_2\text{S}$; (F) $\text{Nd}_2\text{O}_2\text{S}_2$. Reprinted with permission from Huang et al. (2008b). Copyright 2008 American Chemical Society.

hydrothermally aged $\text{RE}(\text{OH})_3$ nanowires in boron–sulfur method and obtained $\text{Ln}_2\text{O}_2\text{S}$, $\text{Ln}_2\text{O}_2\text{S}_2$, and LnS_2 nanowires under mild conditions at 400–500 °C (Figure 82) (Huang *et al.*, 2008b). The sulfidation mechanism was the same as that for synthesizing rare earth sulfides (Wu *et al.*, 2003b). The reaction selectivity for $\text{Ln}_2\text{O}_2\text{S}$ or $\text{Ln}_2\text{O}_2\text{S}_2$ depended on the loading quantity of boron and sulfur. Stucchi *et al.* used monodispersed rare earth basic carbonate spheres as precursors, which were the hydrolysis product of RE chlorides and urea. Under argon protection, the sulfidization was held in horizontal tube furnace at 770 °C. The obtained $\text{Y}_2\text{O}_2\text{S}$ and $\text{Y}_2\text{O}_2\text{S}:\text{Eu}^{3+}$ spheres had uniform diameter of 0.4 and 0.2 μm , respectively. This value was consistent with the size of basic carbonate precursors. The emission of $\text{Y}_2\text{O}_2\text{S}:\text{Eu}^{3+}$ mainly located at the region of 580–630 nm with UV excitation. The assignments for different peaks agreed with the Eu^{3+} characteristic transitions with C_{3v} symmetry. The ${}^5\text{D}_0$ to ${}^7\text{F}_1$ transition was located at 626 nm, suggesting the absence of oxide impurity (the corresponding emission is at 611 nm) (Vila *et al.*, 1997). Hirai *et al.* (2002) prepared rare earth oxalate NPs as precursor, and obtained about 50 nm $\text{R}_2\text{O}_2\text{S}$ NPs after further decomposition in sulfur vapor (Hirai and Orikoshi, 2004).

In solid-state reaction, the dispersing medium has a minor influence on product morphology. Jagannathan's group developed a sol–gel polymer pyrolysis route to prepare $\text{R}_2\text{O}_2\text{S}$ nanomaterials. Urea and formaldehyde were added to the rare earth nitrates solution for a condensation reaction, and sulfur powders were dispersed in the polymer network. Then the dehydrated resin was thoroughly ground and heated at 500 °C to decompose. The pyrolysis of precursor resin could generate NH_4S_x vapors for the subsequent sulfidization (Dhanaraj *et al.*, 2003). In the following research, this group evolved the synthesis scheme into two steps. $\text{Y}_2\text{O}_3:\text{Eu}$ NPs were prepared via a similar sol–gel polymer pyrolysis route. Then they were used as precursors to react with $\text{Na}_2\text{S}_2\text{O}_3$ at 500 °C. The size of $\text{Y}_2\text{O}_2\text{S}:\text{Eu}^{3+}$ NPs was tunable between 7 and 14 nm depending on the precursors (Dhanaraj *et al.*, 2004). Serra *et al.* mixed rare earth nitrates, citric acid and ethylene glycol to form carbonized polymeric resin precursor. After sulfidization, agglomerates of 10–30 nm $\text{Y}_2\text{O}_2\text{S}:\text{Yb}^{3+}, \text{Er}^{3+}(\text{Tm}^{3+})$ NPs were obtained (Pires *et al.*, 2004). Sun *et al.* employed gelatin as the template gel and obtained $\text{R}_2\text{O}_2\text{S}$ product with relatively low aggregation. Rare earth nitrates were dissolved in gelatin sol before its coagulation. Then hydrolysis of R^{3+} was performed by soaking the gelatin gel in $\text{NH}_3 \cdot \text{H}_2\text{O}$ solution. The gelatin network well restricted rare earth hydroxides NPs with homogeneous size. For sulfuration, the hydroxides reacted with ammonium sulfate and produced $(\text{RO})_2\text{SO}_4$ in solid gel around 250–450 °C. In the last step, $(\text{RO})_2\text{SO}_4$ was reduced into $\text{R}_2\text{O}_2\text{S}$ under H_2 atmosphere at 750 °C. The obtained $\text{R}_2\text{O}_2\text{S}:\text{Tb}^{3+}/\text{Eu}^{3+}$ NPs revealed sizes ranging from 40 to 50 nm (Liu *et al.*, 2008c).

Combustion method was usually utilized to produce metal oxide compounds, including R_2O_3 nanomaterials (Sun et al., 2000). With special alteration, this methodology was also adapted for RE oxysulfides. In Bang's report, porous agglomerates of $A_2O_2S:R^{3+}$ ($A = Y, La, Gd$ and $R = Eu, Tb, Tm$) NPs were prepared via this method. Different rare earth nitrates were first mixed in stoichiometric amounts. Then the majority of water was removed at $100\text{ }^\circ\text{C}$, followed by adding $(CSNH_2)_2$ as both the fuel and sulfurizing agent. The mixture was ignited in an air tube furnace at a temperature around $300\text{--}350\text{ }^\circ\text{C}$. Afterward, the exothermic reaction of nitrates and organic fuel provided large amount of heat for the rapid formation of R_2O_2S . Due to the intense gas release, the particle growth was hindered while heat was transported away and locally temperature was quenched. Therefore, the product was a foamy network that composed of small primary NPs (Bang et al., 2004). Peng et al. replaced the expensive dithiooxamide by thiourea as sulfuration source, and introduced poly(vinyl alcohol) (PVA) into the combustion system to abate the agglomeration of products. TEM observation proved the existence of well-dispersed R_2O_2S NPs around 20 nm together with some agglomerates. Without PVA, the product dispersibility was much worse (Peng et al., 2005). Luo's group improved the classic combustion method by using liquid fuel. Rare earth nitrates and thioacetamide were solved in ethanol with a little of distilled water. Then the mixture was put into a preheated furnace ($400\text{ }^\circ\text{C}$) without drying. A relatively mild and slow combustion process was expected. The agglomerate of R_2O_2S NPs was further annealed at $1000\text{ }^\circ\text{C}$ for 2 h in a reducing atmosphere, so a small amount of impurity ($R_2O_2SO_4$) could be converted into R_2O_2S , and resulted in XRD-pure product (Luo and Cao, 2008).

5.2.2 Solution-phase synthesis routes

Due to the easy hydrolysis of rare earth ions, there was a big challenge for wet chemical synthesis of R_2O_3 or R_2O_2S NCs. Yu and coworkers developed a novel solvothermal pressure-relief process and accomplished the sulfidization of $La(OH)_3$. The reaction was conducted in a stainless steel autoclave containing $La(NO_3)_3 \cdot nH_2O$, thiourea and organic solvent (ethanol or pyridine). When the system reached $300\text{ }^\circ\text{C}$, the generated gas was slowly conducted out via a relief valve. This could decrease the concentration of NH_3 , H_2O , and CO_2 produced by thiourea, so as to avoid formation of lanthanum basic carbonate compounds. After a 4-h reaction, La_2O_2S NPs with an average size of 150 nm were obtained. The control solvothermal experiment validated the need for pressure-relief procedure (Yu et al., 1999). Qian et al. prepared nanoscale La_2O_2S from K_2S and freshly precipitated $La(OH)_3$ gel in $300\text{ }^\circ\text{C}$ solvothermal system. Using distilled water as solvent, La_2O_2S NPs around 10 nm were obtained. And ethylenediamine solvent system produced La_2O_2S nanorods with ca.

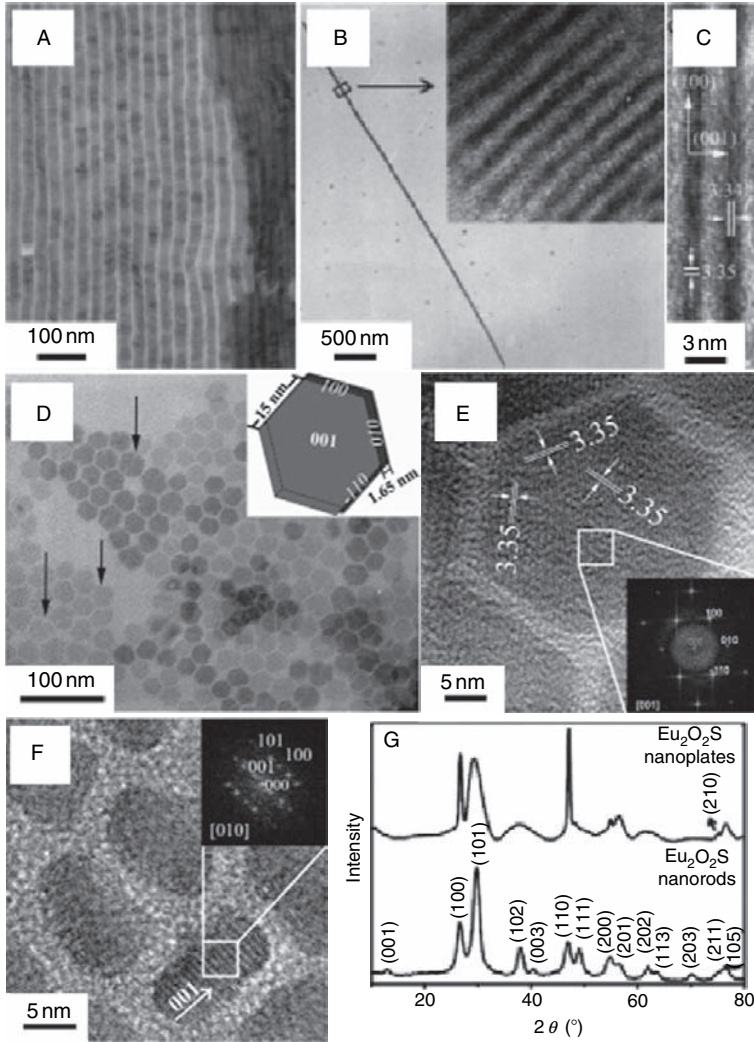


FIGURE 83 TEM images of $\text{Eu}_2\text{O}_2\text{S}$ nanoplates self-assembled into superlattice arrays (A) and (B) nanowire; (C) HRTEM images of the nanoplates standing on the side face. (D) TEM images of the lying nanoplates (inset: a schematic diagram of a hexagonal nanoplatform). (E) HRTEM image of the lying $\text{Eu}_2\text{O}_2\text{S}$ nanoplates (inset: FFT of the border region). (F) HRTEM image of $\text{Eu}_2\text{O}_2\text{S}$ short nanorods (inset: FFT). (G) Powder XRD patterns of nanoplates and nanorods. Reprinted with permission from Zhao *et al.* (2006b). Copyright 2006 American Chemical Society.

10 nm in diameter and 300 nm in length. This may be attributed to the basicity and chelating ability of ethylenediamine (Jiang et al., 2000). Gao's group followed the single-source precursors decomposition route and synthesized monodisperse R_2O_2S nanocrystals in high boiling point organic solvent (Zhao et al., 2006b). This approach came from their previous work on EuS NPs (Zhao and Gao, 2008). When oxygen was introduced into $\text{Ln}(\text{Phen})(\text{Ddtc})_3$ pyrolysis system, colloidal $\text{Ln}_2\text{O}_2\text{S}$ NPs were produced instead of LnS ($\text{Ln} = \text{Sm}, \text{Eu}, \text{Gd}$). In oleylamine/oleic acid/octadecene (OM/OA/ODE) mixture, $\text{Eu}_2\text{O}_2\text{S}$ formed hexagonal nanoplates with thickness ca. 1.65 nm, and in pure OM, the product morphology changed to short nanorods with dimensions of ca. 6.5 nm \times 10 nm (Figure 83). Compared with the previous methods, this synthetic protocol for $\text{RE}_2\text{O}_2\text{S}$ NPs was relatively mild and controllable.

5.2.3 Optical properties

The R^{3+} ions occupy the C_{3V} symmetry sites in the oxysulfide matrix. This is beneficial to the Eu^{3+} -based oxysulfide phosphors. In Stucchi's report, 200 nm $\text{Y}_2\text{O}_2\text{S}:\text{Eu}^{3+}$ (3.6% doping ratio) spheres revealed a dominant ${}^5\text{D}_0 \rightarrow {}^7\text{F}_2$ emission around 620 nm with $\lambda_{\text{ex}} = 311$ nm. The ${}^5\text{D}_0 \rightarrow {}^7\text{F}_2$ transition split into two peaks at 611 nm (medium) and 626 nm (strong), respectively. When the λ_{ex} changed to 265 nm (the characteristic excitation for $\text{Y}_2\text{O}_3:\text{Eu}^{3+}$), the split peak at 611 nm had no enhancement. This indicated that the impurity of yttrium oxides was negligible (Vila et al., 1997). Jagannathan et al. compared the luminescence properties of 20 nm irregular $\text{Y}_2\text{O}_2\text{S}:\text{Eu}^{3+}$ particles (7% doping ratio) and bulk material. Their emission spectra contained identical peak and Stark-splitting patterns, suggesting similar cationic site symmetry and chemical surroundings of Eu^{3+} ions. The intensity ratio of the ${}^5\text{D}_0 \rightarrow {}^7\text{F}_2$ transition with respect to the ${}^5\text{D}_0 \rightarrow {}^7\text{F}_1$ transition was decreased in $\text{Y}_2\text{O}_2\text{S}:\text{Eu}^{3+}$ NCs system. Moreover, nanosized $\text{Y}_2\text{O}_2\text{S}:\text{Eu}^{3+}$ showed a blue-shifted excitation band in relation to the bulk system. The excitation spectrum of oxysulfide compounds was composed of excitonic excitation band and $\text{Ln}^{3+}-\text{O}^{2-}/\text{S}^{2-}$ charge transfer band. The 5000 cm^{-1} blue shift of the band edge was attributed to quantum confinement effects, while the 2000 cm^{-1} blue shift of the charge transfer excitation was explained as a possible size-dependent change in the optical electronegativity (Dhanaraj et al., 2003). Similar blue shift phenomenon was observed in smaller $\text{Y}_2\text{O}_2\text{S}:\text{Eu}^{3+}$ NPs (Thirumalai et al., 2007, 2008b). Due to the considerable defect centers and surface states, 7 and 15 nm $\text{Y}_2\text{O}_2\text{S}:\text{Eu}^{3+}$ NPs revealed a dominant host-emission band at 450 nm (Dhanaraj et al., 2004).

Jagannathan et al. observed an ON/OFF luminescence blinking phenomenon from $\text{Y}_2\text{O}_2\text{S}:\text{Eu}^{3+}$ NPs (with diameter of ca. 7 nm). Yttrium oxysulfide has a band-gap of ca. 4.6 eV and belongs to large bandgap semiconductor, thus, the emission blinking could be explained by

diffusion controlled electron transfer model simulating QDs system (Nakkiran et al., 2007).

The optical performance of Eu^{3+} -doped $\text{La}_2\text{O}_2\text{S}$ and $\text{Gd}_2\text{O}_2\text{S}$ was generally analogous to that of $\text{Y}_2\text{O}_2\text{S}:\text{Eu}^{3+}$. With λ_{ex} at 330 nm, the room-temperature emissions of $\text{La}_2\text{O}_2\text{S}:\text{Eu}^{3+}$ nanowires showed ${}^5\text{D}_0 \rightarrow {}^7\text{F}_j$ ($j = 1, 2, 4$) transitions at 593 nm, 614/623 nm (two splits) and 701 nm, whereas the other three peaks (537, 555, and 585 nm) were identified as the ${}^5\text{D}_1 \rightarrow {}^7\text{F}_j$ ($j = 1, 2, 3$) transitions. The highest peak was located at 623 nm. All peak positions agreed well with those of bulk $\text{La}_2\text{O}_2\text{S}:\text{Eu}^{3+}$ (Huang et al., 2008b). Peng et al. researched the time-resolved emission spectra of 18 nm $\text{La}_2\text{O}_2\text{S}:\text{Eu}^{3+}$ NPs at 77 K. With a decrease in the delay time, a new emission peak appeared at the high-energy shoulder of the ${}^5\text{D}_0 \rightarrow {}^7\text{F}_2$ peak (593 nm), which meant the presence of a new luminescent center with a short lifetime. The author considered that this emission was contributed by surface Eu^{3+} ions in lower symmetry sites (Peng et al., 2005). The $\text{Gd}_2\text{O}_2\text{S}:\text{Eu}^{3+}$ nanotubes revealed the characteristic ${}^5\text{D}_0 \rightarrow {}^7\text{F}_j$ ($j = 1, 2, 4$) transitions of Eu^{3+} under 330 nm excitation. Referring to the data of bulk materials, a similar blue shift of excitation band was observed (Thirumalai et al., 2008a). The explanation could be found in the above discussion.

$\text{La}_2\text{O}_2\text{S}:\text{Tb}^{3+}$ NPs (ca. 50 nm) showed broad excitation band at 256 nm that was assigned to $4f^8 \rightarrow 4f^75d^1$ transition of Tb^{3+} . The emission of Tb^{3+} originated from its ${}^5\text{D}_4 \rightarrow {}^7\text{F}_j$ ($j = 3-6$) transitions. The main peak (the ${}^5\text{D}_4 \rightarrow {}^7\text{F}_4$ line) was located at 544 nm and resulted in the apparent green luminescence. It reached the maximum intensity at 8% doping ratio (Liu et al., 2008c). Cao et al. studied the luminescence of $\text{Gd}_2\text{O}_2\text{S}:\text{Tb}^{3+}$ NPs (ca. 50 nm) under UV light and X-ray excitation. With $\lambda_{\text{ex}} = 254$ nm, the doped Tb^{3+} showed the ${}^5\text{D}_3 \rightarrow {}^7\text{F}_j$ ($j = 4-6$) transitions in the region of 370–480 nm (blue) and the ${}^5\text{D}_4 \rightarrow {}^7\text{F}_j$ ($j = 3-6$) transitions in the region of 480–630 nm. In fact, the ${}^5\text{D}_3$ state of Tb^{3+} was quenched in $\text{La}_2\text{O}_2\text{S}$, because it was too close to the host charge-transfer states and induced nonradiative relaxation itself. In $\text{Gd}_2\text{O}_2\text{S}$, the host charge-transfer states were raised a little, so the emission from the ${}^5\text{D}_3$ state became visible but much weaker than that arising from the excited ${}^5\text{D}_4$ state. The ${}^5\text{D}_4 \rightarrow {}^7\text{F}_4$ transition provided the dominating emission (green) when the Tb^{3+} doping concentration was increased from 0.1% to 0.5% in $\text{Gd}_2\text{O}_2\text{S}$ NPs. The emission intensity for all peaks had the same dependence on Tb^{3+} concentration, whereas the maximum intensity appeared at the value of 0.25%. The X-ray excited emission of $\text{Gd}_2\text{O}_2\text{S}:\text{Tb}^{3+}$ NPs could be assigned to the same ${}^5\text{D}_3 \rightarrow {}^7\text{F}_j$ and ${}^5\text{D}_4 \rightarrow {}^7\text{F}_j$ transitions of Tb^{3+} . Only the peak positions and widths were slightly different. The optimal doping ratio was also 0.25% (Tian et al., 2007).

Rare earth oxysulfides are also fine host materials for Ln^{3+} -based up-conversion phosphors. The commonly used dopants in $\text{R}_2\text{O}_2\text{S}$ include the sensitizer Yb^{3+} , and the emitter Er^{3+} and Tm^{3+} ions (Figure 84). NIR

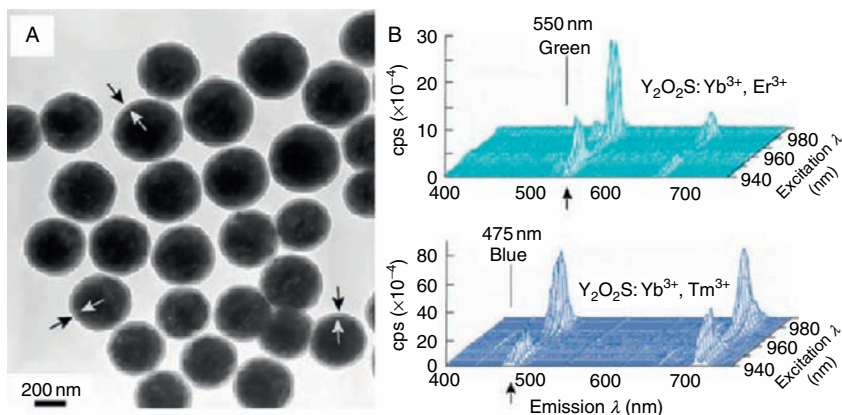


FIGURE 84 (A) TEM image of silica encapsulated $\text{Y}_2\text{O}_2\text{S}:\text{Yb},\text{Er}$ particles; (B) Emission and excitation spectra of green $\text{Y}_2\text{O}_2\text{S}:\text{Yb},\text{Er}$ and blue $\text{Y}_2\text{O}_2\text{S}:\text{Yb},\text{Tm}$ particles. Reprinted with permission from Corstjens et al. (2005). Copyright 2005 IEE.

photons with $\lambda = 980 \text{ nm}$ are absorbed by Yb^{3+} via its ${}^2\text{F}_{7/2} \rightarrow {}^2\text{F}_{5/2}$ transition, followed by energy transfer to $\text{Er}^{3+}/\text{Tm}^{3+}$ via two/three-photon luminescence process. The emission spectra of Er^{3+} compose of a green portion (${}^2\text{H}_{11/2}$, ${}^4\text{S}_{3/2} \rightarrow {}^4\text{I}_{15/2}$) and a red portion (${}^4\text{F}_{9/2} \rightarrow {}^4\text{I}_{15/2}$). Their intensity ratio was alterable related to the difference in doping concentration, dopant chemical environment, material crystallinity and surface properties. There was a related research on luminescent properties of $\text{Y}_2\text{O}_2\text{S}:\text{Yb}^{3+},\text{Er}^{3+}$ NPs, contributed by Serra's group (Pires et al., 2006). For comparison of literature data, the 200 nm dispersed $\text{Y}_2\text{O}_2\text{S}:\text{Yb}^{3+},\text{Er}^{3+}$ spheres had green-dominant up-conversion luminescence (Corstjens et al., 2005), while the aggregated $\text{Y}_2\text{O}_2\text{S}:\text{Yb}^{3+},\text{Er}^{3+}$ NPs (ca. 20 nm) displayed stronger red emission (Pires et al., 2004).

The $\text{Y}_2\text{O}_2\text{S}:\text{Yb}^{3+},\text{Er}^{3+}$ nanotubes reported by Li et al. showed red up-conversion luminescence at 650 nm, assigned to the $\text{F}_{9/2} \rightarrow \text{I}_{15/2}$ transition. Down-conversion emission occurred when these nanotubes were excited with 310 nm Xe sources. Additionally, there was a broad emission band centered at 730 nm in both up- and down-conversion spectra, assumed to be the $\text{I}_{9/2} \rightarrow \text{I}_{15/2}$ transition (Wang and Li, 2003). Tm-doped $\text{Y}_2\text{O}_2\text{S}$ up-conversion NPs emitted blue photons (with λ at ca. 475 nm) that came from $\text{G}_4 \rightarrow \text{F}_4$ transition, and also emitted red photons around 650 and 690 nm (Hirai and Orikoshi, 2004; Pires et al., 2004). $\text{Y}_2\text{O}_2\text{S}:\text{Ho}$ up-conversion NPs showed intense green emission related to the S_2 , $\text{F}_4 \rightarrow \text{I}_8$ transitions of Ho. The red emission from the $\text{F}_5 \rightarrow \text{I}_8$ transition was relatively weak (Hirai and Orikoshi, 2004).

Recently, Luo *et al.* observed up-conversion luminescence of praseodymium in nanosized oxysulfide matrix. In an imitation of the Yb /Er system, the up-conversion mechanism was presumed to be a double excitation by energy resonance transfer from Yb to Pr. The G_4 level of Pr was regarded as the metastable state. Excited state absorption (ESA) process was another possible mechanism, since the $G_4 \rightarrow P_0$ transition could match the 980 nm IR photon. With 980 nm laser excitation, $La_2O_2S:Yb,Pr$ nanocrystals exhibited green luminescence with peak at 508 nm and shoulder band at 500 nm, which was assigned to the $P_0 \rightarrow H_4$ electric dipole allowed transition of Pr ions. Other small peaks at 546, 638, and 665 nm were attributed to the P_0 to H_5 , H_6 , and F_2 transitions, respectively. Furthermore, there was a broad NIR emission band at ca. 830 nm. Its intensity was gradually weakened, by increasing the phosphor annealing temperature. Thus, this abnormal emission was considered as the manifestation of intrinsic defects or surface defects (Luo and Cao, 2008).

The cathodoluminescent properties of nanosized $La_2O_2S:Eu, Gd_2O_2S:Eu$, $Y_2O_2S:Tb, Gd_2O_2S:Tb$, and $La_2O_2S:Tm$ were researched in Bang's report. All emission peaks of these phosphors well corresponded with their photoluminescence characteristics. But Eu and Tb showed some differences on the minor emission peaks when they were doped in different host materials.

The appearance of these emission lines was dependent on the energy crossover between the f energy level of emitters and the charge transfer state of host (Bang *et al.*, 2004). The electron beam current density and temperature were important factors for cathodoluminescent performance. The detailed discussion of $Ln_2O_2S:Eu$ can be found in Yang's work (Bang *et al.*, 2007).

6. CONCLUSIONS AND PERSPECTIVES

In summary, rare earth nanomaterials have shown a great potential of their optical and catalytic properties for applications in the medical, nanodevices, catalysis, and fuel cells. A number of productive synthesis routes have been developed toward various rare earth nanomaterials. Well-defined rare earth compound based nanostructures have been extensively obtained via dry methods, aqueous solution based methods, as well as the nonaqueous solution based methods. The targets of obtaining pure phase, desired composition, controllable and uniform shapes and sizes, tuned surface status, and functionalization have been partially reached.

In this chapter, we discussed the synthesis and properties of rare earth inorganic nanomaterials. Due to the limited space, we did not discuss the metallic rare earth nanomaterials, however, Gd, Tb, Dy, Ho, Er, and Tm metals are ferromagnetic, each with a magnetic moment per atom

exceeding that of iron. Some {rare earth metals} show hydrogen-induced reversible changes in electrical and optical properties. These interesting properties make such materials highly suitable for a number of technological applications, including permanent magnets, data storage, magnetic refrigeration, diagnostics, hydrogen sensors and storage, and solid-state electrochromic devices. Although because of their high reduction potentials and extremely reactive nature, the preparation, storage, and application of nanosized rare earth particles require oxygen-free conditions, there have been a number of reports on the rare earth metal NCs and composites obtained through various methods, such as inert gas evaporation method (Aruna et al., 2004, 2005), magnetron sputtering (Yan et al., 2003b; Armitage et al., 1999), arc discharge methods (Si et al., 2003), pulsed laser deposition (PLD) (Bour et al., 2001), Ar ion sputtering (O'shea and Perera, 1999), as well as the solution based synthesis, such as the alkali reduction method (Nelson et al., 2002, 2003a,b). Therefore, we expect a bright future for these nanomaterials in the application fields in hydrogen storage, optoelectronics, and magnetic data storage.

Furthermore, studies on rare earth nanomaterials are on-going. Yet, the current synthesis routes are still limited in several aspects. Although the fabrication of many rare earth nanomaterials was successful, preparation of high quality nanocrystals and a variety of nanostructures in a number of systems, including Eu(II) associated materials, complex oxides of rare earth and transition metals, and rare earth soluble salts, remains a challenging topic, either because of the need for strict conditions during synthesis, storage, and application procedures, or because of the phase control and crystal growth process. High quality monodisperse nanocrystals with fewer defects and high applicability for usage in optical fields has been available for major rare earth compounds, however, the size, shape, and advanced nanostructures are only available for rather limited cases. When organic species are introduced for functionalization or modification for biological applications as well as solubility tuning, the fertile field of organic chemistry has been introduced, however, the current utilization of these possibilities is still quite limited.

When the emphasis is placed beyond a single nanocrystal, more complex nanostructures, including the hierarchical structures, mesostructures, aliened arrays, 2D or 3D ordered superlattices, have been taken into consideration. In this way, the bottom-up strategy in nanotechnology has been broadly implemented. The advanced assembly methods, such as generalized methods for fabrication, re-organization, defect introduction, and elimination are still highly desirable. With the current successes in evaporation induced self-assembly (EISA), Langmuir-Blodgett film assisted assembly, hard template assisted synthesis, and lattice compatibility induced heterostructures, there should be more confidence toward the fabrication of more and more advanced and complex assemblies.

However, the current outputs are still far from real applications or systematical property investigations and a systematic work is still required in the next decade or so. As for rare earth nanomaterials, their unique and reliable optical properties prove to be one of the most suitable building blocks for applications in future nanodevices, and will certainly play a crucial role here.

For the currently developed individual rare earth nanocrystals, several significant application fields will be more and more active, such as biomaterials and medical fields. For the current reported rare earth nanocrystals, some significant applications will be more and more active, such as in bio-imaging and bio-assay fields. Prior to rare earth NPs, fluorescent Ln chelates have been used in immunoassays, but they are prone to quenching in solvent environment. The inorganic crystal lattices provide much steadier microenvironment, so rare earth luminescent NPs have better optical performance to be bioprobes. Compared with traditional luminescent bioprobes, rare earth NPs have several unique advantages: (i) their luminescent lifetime is much longer than that of dyes and other organic species, so this benefits time-gated detection techniques in elimination of spontaneous fluorescence of biological specimens; (ii) no valence electron transitions are involved in the luminescence mechanism of Ln ions, ensuring high photostability under continual excitation; (iii) different from QDs, Ln ions show no size-dependence in the luminescence behavior, thus rigorous synthesis is unnecessary while the spectral purity could be preserved; (iv) by varying the Ln dopants and host matrixes, rare earth luminescent NPs could realize multicolor emission without overlap; (v) the unique up-conversion luminescence of Ln (i.e., Er, Tm, Ho, Pr, etc.) provides a new methodology for noninvasive biological imaging; (vi) combining paramagnetic Gd and other Ln emitters, rare earth nanomaterials could combine magnetic and optical properties, potentially leading to bifunctionalized probes for optical and magnetic resonance imaging. Moreover, the last two points mentioned above are already hot topics in bioprobe research offering numerous opportunities for functional rare earth NPs for further exploration.

Studies on the synthesis mechanism as well as of the obtained nanocrystals of rare earth nanomaterials would inevitably boost further studies in synthesis and applications of these advanced materials. The *in situ* and *ex situ* investigation methods, including optical spectra, electrochemical devices, as well as modern combined microscopy techniques will reveal the underlying, yet currently unknown aspects of synthetic or catalytic chemical processes, where a true optimization or new design routes will be discussed.

Modern computers have provided much needed power for theoretical studies utilizing various modeling and simulation techniques. Simulations of nanoscale objects requiring large models or surface/interface

based models will be one of the fields receiving most of the benefits. For rare earth compound based nanomaterials, the density functional theory based studies have been applied in limited capacity to surface structures and simple catalytic processes. For nanocrystals, only classical atomistic models are applicable, and most works are done only for ceria, though a number of successful examples have been established. In both ways, the multiscale simulations would be a great progress for the near future.

ACKNOWLEDGMENTS

We acknowledge the financial support from Natural Science Foundation of China (NSFC) and Ministry of Science and Technology (MoST) of China.

REFERENCES

- Abad, A., Almela, C., Corma, A., García, H., 2006. *Chem. Commun.* 3178.
- Abad, A., Corma, A., García, H., 2008. *Chem. Eur. J.* 14, 212.
- Adachi, T.A., Tanaka, A., Hasegawa, Y., Kawai, T., 2008. *Thin Solid Films* 516, 2460.
- Adschiri, T., Hakuta, Y., Sue, K., Arai, K., 2001. *J. Nanopart. Res.* 3, 227.
- Aebischer, A., Heer, S., Biner, D., Krämer, K., Haase, M., Güdel, H.U., 2005. *Chem. Phys. Lett.* 407, 124.
- Aguilar-Guerrero, V., Gates, B.C., 2007. *Chem. Commun.* 3210.
- Ahn, B.Y., Seok, S.I., Hong, S.I., Oh, J.S., Jung, H.K., Chung, W.J., 2006. *Opt. Mater.* 28, 374.
- Ahniyaz, A., Sakamoto, Y., Bergstrom, L., 2008. *Cryst. Growth Des.* 8, 1798.
- Akdeniz, Z., Önem, Z.C., Tosi, M.P., 2001. *Z. Naturforsch. A: Phys. Sci.* 56, 721.
- Aldorf, H.E., 1985. Rare Earth Halide Grease Compositions. US Patent No. 4, 507, 214.
- Alivisatos, A.P., 1996. *Science* 271, 933.
- Althues, H., Simon, P., Kaskel, S., 2007. *J. Mater. Chem.* 17, 758.
- Ananias, D., Ferdov, S., Paz, F.A.A., Ferreira, R.A.S., Ferreira, A., Geraldes, C., Carlos, L.D., Lin, Z., Rocha, J., 2008. *Chem. Mater.* 20, 205.
- Ansari, A.A., Singh, N.S.S.P., 2008. *J. Nanopart. Res.* 10, 703.
- Ansari, A.A., Solanki, P.R., Malhotra, B.D., 2008. *Appl. Phys. Lett.* 92, 263901.
- Anselmi-Tamburini, U., Maglia, F., Chioldelli, G., Tacca, A., Spinolo, G., Riello, P., Bucella, S., Munir, Z.A., 2006. *Adv. Funct. Mater.* 16, 2363.
- Aono, H., Tsuzaki, M., Kawaura, A., Sakamoto, M., Traversa, E., Sodaoka, Y., 2001. *J. Am. Ceram. Soc.* 84, 969.
- Armelaio, L., Barreca, D., Bottaro, G., Gasparotto, A., Maragno, C., Tondello, E., 2005. *Chem. Mater.* 17, 427.
- Armitage, R., Rubin, M., Richardson, T., O'Brien, N., Chen, Y., 1999. *Appl. Phys. Lett.* 75, 1863.
- Arney, D., Porter, B., Greve, B., Maggard, P. A., 2008. *J. Photochem. Photobiol. A* 199, 230.
- Aruna, I., Mehta, B.R., Malhotra, L.K., Shivaprasad, S.M., 2004. *Adv. Mater.* 16, 169.
- Aruna, I., Mehta, B.R., Malhotra, L.K., Shivaprasad, S.M., 2005. *Adv. Funct. Mater.* 15, 131.
- Assaaoudi, H., Ennaciri, A., Rulmont, A., Harcharras, M., 2000. *Phase Trans.* 72, 1.
- Au, C.T., Zhang, Y.Q., He, H., Lai, S.Y., Ng, C.F., 1997. *J. Catal.* 167, 354.
- Auzel, F., 2004. *Chem. Rev.* 104, 139.
- Avgouropoulos, G., Ioannides, T., 2003. *Appl. Catal. A* 244, 155.
- Azad, S., Marina, O.A., Wang, C.M., Saraf, L., Shutthanandan, V., McCready, D.E., El-Azab, A., Jaffe, J.E., Engelhard, M.H., Peden, C.H.F., Thevuthasan, S., 2005. *Appl. Phys. Lett.* 86, 131906.

- Babu, S., Schulte, A., Seal, S., 2008. *Appl. Phys. Lett.* 92, 123112.
- Bang, J., Abboudi, M., Abrams, B., Holloway, P.H., 2004. *J. Lumin.* 106, 177.
- Bang, J., Yang, H., Abrams, B., Holloway, P.H., 2007. *J. Lumin.* 126, 629.
- Bao, F., Wang, Y.S., Cheng, Y., Zheng, Y.H., 2006. *Mater. Lett.* 60, 389.
- Barreca, D., Gasparotto, A., Maragno, C., Tondello, E., Bontempi, E., Depero, L.E., Sada, C., 2005. *Chem. Vap. Depos.* 11, 426.
- Barreca, D., Gasparotto, A., Maccato, C., Maragno, C., Tondello, E., 2006. *Langmuir* 22, 8639.
- Barreca, D., Gasparotto, A., Maccato, C., Maragno, C., Tondello, E., Comini, E., Sberveglieri, G., 2007. *Nanotechnology* 18, 125502.
- Bazzi, R., Flores-Gonzalez, M.A., Louis, C., Lebbou, K., Dujardin, C., Brenier, A., Zhang, W., Tillement, O., Bernstein, E., Perriat, P., 2003. *J. Lumin.* 102–103, 445.
- Bazzi, R., Flores, M.A., Louis, C., Lebbou, K., Zhang, W., Dujardin, C., Roux, S., Mercier, B., Ledoux, G., Bernstein, E., Perriat, P., Tillement, O., 2004. *J. Colloid Interf. Sci.* 273, 191.
- Beaupaire, E., Buissette, V., Sauviat, M.P., Giaume, D., Lahlil, K., Mercuri, A., Casanova, D., Huignard, A., Martin, J.L., Gacoin, T., Boilot, J.P., Alexandrou, A., 2004. *Nano Lett.* 4, 2079.
- Behera, S.K., Sahu, P.K., Pratihari, S.K., Bhattacharyya, S., 2004. *Mater. Lett.* 58, 3710.
- Berger, D., Matei, C., Papa, F., Macovei, D., Fruth, V., Deloume, J.P., 2007. *J. Eur. Ceram. Soc.* 27, 4395.
- Bernal, S., Calvino, J.J., Cauqui, M.A., Gatica, J.M., Larese, C., Pères Omil, J.A., Pintado, J.M., 1999. *Catal. Today* 50, 175.
- Bierman, M.J., Van Heuvelen, K.M., Schmeisser, D., Brunold, T.C., Jin, S., 2007. *Adv. Mater.* 19, 2677.
- Bihari, B., Eilers, H., Tissue, B.M., 1997. *J. Lumin.* 75, 1.
- Blasse, G., Grabmaier, B.C., 1994. *Luminescent Materials*. Springer Verlag, Berlin.
- Boakye, E.E., Mogilevsky, P., Hay, R.S., 2005. *J. Am. Ceram. Soc.* 88, 2740.
- Bocchetta, P., Santamaria, M., Di Quarto, F., 2007. *Electrochem. Commun.* 683.
- Bondioli, F., Ferrari, A.M., Leonelli, C., Siligardi, C., Hart, N.A., Evans, N.G., 2001. *J. Mater. Chem.* 11, 2620.
- Borchert, Y., Sonstrom, P., Wilhelm, M., Borchert, H., Baumer, M., 2008. *J. Phys. Chem. C* 112, 3054.
- Bour, G., Reinholdt, A., Stepanov, A., Keutgen, C., Kreibitz, U., 2001. *Eur. Phys. J. D* 16, 219.
- Boyer, D., Bertrand-Chadeyron, G., Mahiou, R., Caperaa, C., Cousseins, J.C., 1999. *J. Mater. Chem.* 9, 211.
- Boyer, D., Bertrand, G., Mahiou, R., 2003. *J. Lumin.* 104, 229.
- Boyer, J.C., Vetrone, F., Cuccia, L.A., Capobianco, J.A., 2006. *J. Am. Chem. Soc.* 128, 7444.
- Boyer, J.C., Cuccia, L.A., Capobianco, J.A., 2007a. *Nano Lett.* 7, 847.
- Boyer, J.C., Gagnon, J., Cuccia, L.A., Capobianco, J.A., 2007b. *Chem. Mater.* 19, 3358.
- Brezesinski, T., Erpen, C., Iimura, K., Smarsly, B., 2005. *Chem. Mater.* 17, 1683.
- Brown, S.S., Im, H.J., Rondinone, A.J., Dai, S., 2005. *J. Colloid Interf. Sci.* 292, 127.
- Bruchez, M., Moronne, M., Gin, P., Weiss, S., Alivisatos, A.P., 1998. *Science* 281, 2013.
- Brunton, G., 1969. *Acta Crystallogr. B* 25, 600.
- Bu, W.B., Chen, H.R., Hua, Z.L., Liu, Z.C., Huang, W.M., Zhang, L.X., Shi, J.L., 2004. *Appl. Phys. Lett.* 85, 4307.
- Bu, W.B., Hua, Z., Chen, H.R., Shi, J.L., 2005. *J. Phys. Chem. B* 109, 14461.
- Bu, W.B., Zhang, L.X., Hua, Z.L., Chen, H.R., Shi, J.L., 2007. *Cryst. Growth Des.* 7, 2305.
- Buassi-Monroy, O.S., Luhrs, C.C., Chavez-Chavez, A., Michel, C.R., 2004. *Mater. Lett.* 58, 716.
- Bühler, G., Feldmann, C., 2006. *Angew. Chem. Int. Ed.* 45, 4864.
- Bühler, G., Feldmann, C., 2007. *Appl. Phys. A* 87, 631.
- Buissette, V., Huignard, A., Gacoin, T., Boilot, J.P., Aschehoug, P., Viana, B., 2003. *Surf. Sci.* 532–535, 444.

- Buissette, V., Moreau, M., Gacoin, T., Boilot, J.P., Chane-Ching, J.Y., Le Mercier, T., 2004. *Chem. Mater.* 16, 3767.
- Buissette, V., Giaume, D., Gacoin, T., Boilot, J.P., 2006a. *J. Mater. Chem.* 16, 529.
- Buissette, V., Moreau, M., Gacoin, T., Boilot, J.P., 2006b. *Adv. Funct. Mater.* 16, 351.
- Bumajdad, A., Zaki, M.I., Eastoe, J., Pasupulety, L., 2004. *Langmuir* 20, 11223.
- Burns, J.H., 1965. *Inorg. Chem.* 4, 881.
- Cabanas, A., Darr, J.A., Lester, E., Poliakoff, M., 2000. *Chem. Commun.* 901.
- Cao, Y.C., 2004. *J. Am. Chem. Soc.* 126, 7456.
- Cao, M.H., Hu, C.W., Wu, Q.Y., Guo, C.X., Qi, Y.J., Wang, E.B., 2005. *Nanotechnology* 16, 282.
- Capponetti, E., Saladino, M.L., Serra, F., Enzo, S., 2007a. *J. Mater. Sci.* 42, 4418.
- Capponetti, E., Enzo, S., Lasio, B., Saladino, M.L., 2007b. *Opt. Mater.* 29, 1240.
- Carrettin, S., Concepcion, P., Corma, A., Nieto, J.M.L., Puentes, V.F., 2004. *Angew. Chem. Int. Ed.* 43, 2538.
- Carrettin, S., Corma, A., Iglesias, M., Sánchez, F., 2005. *Appl. Catal. A* 291, 247.
- Casanova, D., Giaume, D., Beaurepaire, E., Gacoin, T., Boilot, J.P., Alexandrou, A., 2006a. *Appl. Phys. Lett.* 89, 253103.
- Casanova, D., Giaume, D., Gacoin, T., Boilot, J.P., Alexandrou, A., 2006b. *J. Phys. Chem. B* 110, 19264.
- Casanova, D., Giaume, D., Moreau, M., Martin, J.L., Gacoin, T., Boilot, J.P., Alexandrou, A., 2007. *J. Am. Chem. Soc.* 129, 12592.
- Chadeyron, G., Mahiou, R., ElGhozzi, M., Arbus, A., Zambon, D., Cousseins, J.C., 1997. *J. Lumin.* 72–74, 564.
- Chang, M.L., Tie, S.L., 2008. *Nanotechnology* 19, 075711.
- Chao, Z.S., Zhou, X.P., Wan, H.L., Tsai, K.R., 1995. *Appl. Catal. A* 130, 127.
- Charbonnière, L.J., Rehspringer, J.L., Ziessel, R., Zimmermann, Y., 2008. *New J. Chem.* 32, 1055.
- Chaudhury, S., Parida, S.C., Pillai, K.T., Mudher, K.D.S., 2007. *J. Solid State Chem.* 180, 2393.
- Chawla, K.K., Liu, H., Janczak-Rusch, J., Sambasivan, S., 2000. *J. Eur. Ceram. Soc.* 20, 551.
- Chen, L.M., 2006. *Mater. Lett.* 60, 1859.
- Chen, D., Xu, R., 1998. *Mater. Res. Bull.* 33, 409.
- Chen, W., Zhang, X.H., Huang, Y.N., 2000. *Appl. Phys. Lett.* 76, 2328.
- Chen, W., Joly, A.G., Kowalchuk, C.M., Malm, J.O., Huang, Y.N., Bovin, J.O., 2002. *J. Phys. Chem. B* 106, 7034.
- Chen, S.F., Yu, S.H., Yu, B., Ren, L., Yao, W.T., Cölfen, H., 2004. *Chem. Eur. J.* 10, 3050.
- Chen, J.P., Patil, S., Seal, S., McGinnis, J.F., 2006a. *Nat. Nanotech.* 1, 142.
- Chen, L.M., Liu, Y.N., Huang, K.L., 2006b. *Mater. Res. Bull.* 41, 158.
- Chen, W., Li, F., Liu, L., Liu, Y., 2006c. *J. Rare Earth* 24, 782.
- Chen, D.Q., Wang, Y.S., Ma, E., Yu, Y.L., Liu, F., Li, R.F., 2007a. *J. Appl. Phys.* 102, 023504.
- Chen, D.Q., Wang, Y.S., Yu, Y.L., Huang, P., 2007b. *Appl. Phys. Lett.* 91, 051920.
- Chen, G.Z., Sun, S.X., Song, X.Y., Yin, Z.L., Yu, H.Y., Fan, C.H., Zhao, W., 2007c. *J. Mater. Sci.* 42, 6977.
- Chen, W., Li, F., Yu, J., 2007d. *Mater. Lett.* 61, 397.
- Chen, D.Q., Wang, Y.S., Yu, Y.L., Huang, P., 2008a. *J. Phys. Chem. C* 112, 18943.
- Chen, L.M., Liu, G.C., Liu, Y.N., Huang, K.L., 2008b. *J. Mater. Process. Technol.* 198, 129.
- Chen, Z.G., Chen, H.L., Hu, H., Yu, M.X., Li, F.Y., Zhang, Q., Zhou, Z.G., Yi, T., Huang, C.H., 2008c. *J. Am. Chem. Soc.* 130, 3023.
- Cheng, C.S., Zhang, L., Zhang, Y.J., Jiang, S.P., 2008. *Solid State Ionics* 179, 282.
- Cherivin, C.N., Clapsaddle, B.J., Chiu, H.W., Gash, A.E., Satcher Jr., J.H., Kauzlarich, S.M., 2006. *Chem. Mater.* 18, 1928.
- Choi, B., Moon, B., Seo, H., Jeong, J., Lee, H., Seo, W., 2000. *Mater. Des.* 21, 567.
- Choi, H.J., Shin, J.H., Suh, K., Seong, H.K., Han, H.C., Lee, J.C., 2005. *Nano Lett.* 5, 2432.
- Chou, T.W., Mylswamy, S., Liu, R.S., Chuang, S.Z., 2005. *Solid State Commun.* 136, 205.

- Cizauskaite, S., Reichlova, V., Nenartaviciene, G., Beganskiene, A., Pinkas, J., Kareiva, A., 2007. *Mater. Chem. Phys.* 102, 105.
- Concepcion, P., Corma, A., Silvestre-Albero, J., Franco, V., Chane-Ching, J.Y., 2004. *J. Am. Chem. Soc.* 126, 5523.
- Conchon, F., Boulle, A., Girardot, C., Pignard, S., Guinebretiere, R., Dooryhee, E., Hodeau, J.-L., Weiss, F., Kresel, J., Berar, J.-F., 2007. *J. Phys. D: Appl. Phys.* 40, 4872.
- Cooke, A.H., Jones, D.A., Silva, J.F.A., Wells, M.R., 1975. *J. Phys. C* 8, 4083.
- Corma, A., Domine, M.E., 2005. *Chem. Commun.* 4042.
- Corstjens, P.L.A.M., Zuiderwijk, M., Brink, A., Li, S., Feindt, H., Niedbala, R.S., Tanke, H.J., 2001. *Clin. Chem.* 47, 1885.
- Corstjens, P.L.A.M., Zuiderwijk, M., Nilsson, M., Feindt, H., Niedbala, R.S., Tanke, H.J., 2003. *Anal. Biochem.* 312, 191.
- Corstjens, P.L.A.M., Li, S., Zuiderwijk, M., Kardos, K., Abrams, W.R., Niedbala, R.S., Tanke, H.J., 2005. *IEEE Proc. Nanobiotechnol.* 152, 64.
- Cress, C.D., Redino, C.S., Landia, B.J., Raffaele, R.P., 2008. *J. Solid State Chem.* 181, 2041.
- Cui, X.Z., Zhuang, W.D., Yu, Z.J., Xia, T., Huang, X.W., Li, H.W., 2008. *J. Alloys Compd.* 451, 280.
- Das, G.K., Tan, T.T.Y., 2008. *J. Phys. Chem. C* 112, 11211.
- Deheer, W.A., Chatelain, A., Ugarte, D., 1995. *Science* 270, 1179.
- Dekker, R., Klunder, D.J.W., Borreman, A., Diemeer, M.B.J.K., Driessen, W.A., Stouwdam, J.W., van Veggel, F.C.J.M., 2004. *Appl. Phys. Lett.* 85, 6104.
- Delgado, J.L., Herranz, M., Martin, N., 2008. *J. Mater. Chem.* 18, 1417.
- Deng, W.L., Flytzani-Stephanopoulos, M., 2006. *Angew. Chem. Int. Ed.* 45, 2285.
- Deng, H., Yang, S.H., Xiao, S., Gong, H.M., Wang, Q.Q., 2008. *J. Am. Chem. Soc.* 130, 2032.
- Deren, P.J., Weglarowicz, M.A., Mazur, P., Strek, W., 2007. *J. Lumin.* 122–123, 780.
- Deshpande, A.S., Pinna, N., Beato, P., Antonietti, M., Niederberger, M., 2004. *Chem. Mater.* 16, 2599.
- Devaraju, M.K., Yin, S., Sato, T., 2009. *Cryst. Growth Des.* 9, 2944.
- Dey, P., Nath, T.K., 2006. *Phys. Rev.* 73, 214425.
- Dezanneau, G., Sin, A., Roussel, H., Vincent, H., Audier, M., 2002a. *Solid State Commun.* 121, 133.
- Dezanneau, G., Isnard, O., Roussel, H., Sin, A., Audier, M., Vincent, H., 2002b. *Cryst. Eng.* 5, 347.
- Dezanneau, G., Sin, A., Roussel, H., Audier, M., Vincent, H., 2003. *J. Solid State Chem.* 173, 216.
- Dhanaraj, J., Jagannathan, R., Kutty, T.R.N., Lu, C.H., 2001. *J. Phys. Chem. B* 105, 11098.
- Dhanaraj, J., Jagannathan, R., Trivedi, D.C., 2003. *J. Mater. Chem.* 13, 1778.
- Dhanaraj, J., Geethalakshmi, M., Jagannathan, R., Kutty, T.R.N., 2004. *Chem. Phys. Lett.* 387, 23.
- Di Monte, R., Fornasiero, P., Kašpar, J., Graziani, M., Gatica, J.M., Bernal, S., Gomez-Herrero, A., 2000. *Chem. Commun.* 2167.
- Di Monte, R., Fornasiero, P., Desinan, S., Kašpar, J., Gatica, J.M., Calvino, J.J., Fonda, E., 2004. *Chem. Mater.* 16, 4273.
- Di, W.H., Wang, X.J., Zhu, P.F., Chen, B.J., 2007a. *J. Solid State Chem.* 180, 467.
- Di, W.H., Zhao, X.X., Lu, S.Z., Wang, X.J., Zhao, H.F., 2007b. *J. Solid State Chem.* 180, 2478.
- Diamante, P.R., van Veggel, F.C.J.M., 2005. *J. Fluoresc.* 15, 544.
- Diamante, P.R., Burke, R.D., van Veggel, F.C.J.M., 2006. *Langmuir* 22, 1782.
- Diaz-Guillen, J.A., Fuentes, A.F., Gallini, S., Colomer, M.T., 2007. *J. Alloys Compd.* 427, 87.
- DiMaio, J.R., Kokuoz, B., Ballato, J., 2006. *Opt. Express.* 14, 11412.
- Djerdj, I., Garnweitner, G., Su, D.S., Niederberger, M., 2007. *J. Solid State Chem.* 180, 2154.
- Dong, B., Song, H.W., Yu, H.Q., Zhang, H., Qin, R.F., Bai, X., Pan, G.H., Lu, S.Z., Wang, F., Fan, L.B., Dai, Q.L., 2008. *J. Phys. Chem. C* 112, 1435.

- Dong, G.P., Liu, X.F., Xiao, X.D., Qian, B., Ruan, J., Ye, S., Yang, H.C., Chen, D.P., Qiu, J.R., 2009. *Nanotechnology* 20, 055707.
- Dosev, D., Nichkova, M., Liu, M.Z., Guo, B., Liu, G.Y., Hammock, B.D., Kennedy, I.M., 2005. *J. Biomed. Opt.* 10, 064006.
- Dosev, D., Guo, B., Kennedy, I.M., 2006. *J. Aerosol Sci.* 37, 402.
- Dosev, D., Nichkova, M., Dumas, R.K., Gee, S.J., Hammock, B.D., Liu, K., Kennedy, I.M., 2007. *Nanotechnology* 18, 055102.
- Du, N., Zhang, H., Chen, B.G., Ma, X.Y., Yang, D.R., 2007. *J. Phys. Chem. C* 111, 12677.
- Du, Y.P., Zhang, Y.W., Sun, L.D., Yan, C.H., 2008. *J. Phys. Chem. C* 112, 405.
- Du, Y.P., Zhang, Y.W., Sun, L.D., Yan, C.H., 2009a. *J. Am. Chem. Soc.* 131, 3162.
- Du, Y.P., Zhang, Y.W., Sun, L.D., Yan, C.H., 2009b. unpublished results.
- Dutta, P., Dey, P., Nath, T.K., 2007. *J. Appl. Phys.* 102, 073906.
- Eastman, D.E., Holtzberg, F., Methfessel, S., 1969. *Phys. Rev. Lett.* 23, 226.
- Ehlert, O., Thomann, R., Darbandi, M., Nann, T., 2008. *ACS Nano* 2, 120.
- Eilers, H., Tissue, B.M., 1995. *Mater. Lett.* 24, 261.
- El-Toni, A.M., Yin, S., Hayasaka, Y., Sato, T., 2005. *J. Mater. Chem.* 15, 1293.
- El-Toni, A.M., Yin, S., Sato, T., 2006. *Appl. Surf. Sci.* 252, 5063.
- Eriksson, S., Nylén, U., Rojas, S., Boutonnet, M., 2004. *Appl. Catal. A* 265, 207.
- Evanics, F., Diamente, P.R., van Veggel, F.C.J.M., Stanisiz, G.J., Prosser, R.S., 2006. *Chem. Mater.* 18, 2499.
- Fan, S.S., Chapline, M.G., Franklin, N.R., Tomblor, T.W., Cassell, A.M., Dai, H.J., 1999. *Science* 283, 512.
- Fan, W.L., Zhao, W., You, L.P., Song, X.Y., Zhang, W.M., Yu, H.Y., Sun, S.X., 2004. *J. Solid State Chem.* 177, 4399.
- Fan, W.L., Song, X.Y., Bu, Y.X., Sun, S.X., Zhao, X., 2006. *J. Phys. Chem. B* 110, 23247.
- Fan, W.L., Bu, Y.X., Song, X.Y., Sun, S.X., Zhao, X., 2007a. *Cryst. Growth Des.* 7, 2361.
- Fan, W.L., Song, X.Y., Sun, S.X., Zhao, X., 2007b. *J. Solid State Chem.* 180, 284.
- Fang, Y.P., Xu, A.W., Song, R.Q., Zhang, H.X., You, L.P., Yu, J.C., Liu, H.Q., 2003a. *J. Am. Chem. Soc.* 125, 16025.
- Fang, Y.P., Xu, A.W., You, L.P., Song, R.Q., Yu, J.C., Zhang, H.X., Li, Q., Liu, H.Q., 2003b. *Adv. Funct. Mater.* 13, 955.
- Fang, Y.P., Xu, A.W., Dong, W.F., 2005a. *Small* 1, 967.
- Fang, Y.P., Xu, A.W., Qin, A.M., Yu, R.J., 2005b. *Cryst. Growth Des.* 5, 1221.
- Feldmann, C., 2003. *Adv. Funct. Mater.* 13, 101.
- Feng, J., Shan, G.M., Maquieira, A., Koivunen, M.E., Guo, B., Hammock, B.D., Kennedy, I.M., 2003. *Anal. Chem.* 75, 5282.
- Feng, X.D., Sayle, D.C., Wang, Z.L., Paras, M.S., Santora, B., Sutorik, A.C., Sayle, T.X.T., Yang, Y., Ding, Y., Wang, X.D., Her, Y.S., 2006. *Science* 312, 1504.
- Fernández-García, M., Martínez-Arias, A., Hanson, J.C., Rodriguez, J.A., 2004. *Chem. Rev.* 104, 4063.
- Fierro-Gonzalez, J.C., Bhirud, V.A., Gates, B.C., 2005. *Chem. Commun.* 5275.
- Firsching, F.H., Brune, S.N., 1991. *J. Chem. Eng. Data* 36, 93.
- Fisher, M.J., Wang, W.Z., Dorhout, P.K., Fisher, E.R., 2008. *J. Phys. Chem. C* 112, 1901.
- Fita, I., Markovich, V., Mogilyansky, D., Puzniak, R., Wisniewski, A., Titelman, L., Vrdam, L., Herskowitz, M., Varyukhin, V.N., Gorodetsky, G., 2008. *Phys. Rev. B* 77, 224421.
- Flytzani-Stephanopoulos, M., Sakkodin, M., Wang, Z., 2006. *Science* 312, 1508.
- Frolova-Borchert, Y.V., Sadykov, V.A., Alikina, G.M., Lukashevich, A.I., Moroz, E.M., Kochubey, D.I., Kriventsov, V.V., Zaikovskii, V.I., Zyryanov, V.V., Uvarov, N.F., 2006. *Solid State Ionics* 177, 2533.
- Fu, Q., Weber, A., Flytzani-Stephanopoulos, M., 2001. *Catal. Lett.* 77, 87.

- Fu, Q., Kudriavtseva, S., Saltsburg, H., Flytzani-Stephanopoulos, M., 2003a. *Chem. Eng. J.* 93, 41.
- Fu, Q., Saltsburg, H., Flytzani-Stephanopoulos, M., 2003b. *Science* 301, 935.
- Fu, Q., Deng, W.L., Saltsburg, H., Flytzani-Stephanopoulos, M., 2005. *Appl. Catal. B* 56, 57.
- Fujihara, S., Tokumo, K., 2005. *Chem. Mater.* 17, 5587.
- Fujihara, S., Koji, S., Kimura, T., 2004. *J. Mater. Chem.* 14, 1331.
- Fumagalli, P., Spaeth, C., Rudiger, U., 1995. *IEEE Trans. Magn.* 31, 3319.
- Gallini, S., Jurado, J.R., Colomer, M.T., 2005. *Chem. Mater.* 17, 4154.
- Galstyan, E., Lorenz, B., Martirosyan, K.S., Yen, F., Sun, Y.Y., Gospodinov, M.M., Chu, C.W., 2008. *J. Phys.: Condens. Matter* 20, 325241.
- Gambino, R.J., Fumagalli, P., 1994. *IEEE Trans. Magn.* 30, 4461.
- Gao, L., Wang, X., Chua, H.T., Kawi, S., 2006. *J. Solid State Chem.* 179, 2036.
- Gao, L., Chua, H.T., Kawi, S., 2008a. *J. Solid State Chem.* 181, 2804.
- Gao, L., Sun, G., Kawi, S., 2008b. *J. Solid State Chem.* 181, 7.
- Gedanken, A., 2004. *Ultrasonic Sonochem.* 11, 47.
- Geim, A.K., Novoselov, K.S., 2007. *Nat. Mater.* 3, 183.
- Ghosh, S., Rosenbaum, T.F., Aeppli, G., Coppersmith, S.N., 2003. *Nature* 425, 48.
- Ghosh, B., Kar, S., Brar, L.K., Raychaudhuri, A.K., 2005. *J. Appl. Phys.* 98, 094302.
- Ghosh, P., Oliva, J., De la Rosa, E., Haldar, K.K., Solis, D., Patra, A., 2008. *J. Phys. Chem. C* 112, 9650.
- Giannakas, A.E., Vaimakis, T.C., Ladavos, A.K., Trikalitis, P.N., Pomonis, P.J., 2003. *J. Colloid Interf. Sci.* 259, 244.
- Giannakas, A.E., Ladavos, A.K., Pomonis, P.J., 2004. *Appl. Catal. B* 49, 147.
- Giannakas, A.E., Leontiou, A.A., Ladavos, A.K., Pomonis, P.J., 2006. *Appl. Catal. A* 309, 254.
- Giaume, D., Buissette, V., Lahlil, K., Gacoin, T., Boilot, J.P., Casanova, D., Beaupreire, E., Sauviat, M.P., Alexandrou, A., 2005. *Prog. Solid State Chem.* 33, 99.
- Giaume, D., Poggi, M., Casanova, D., Mialon, G., Lahlil, K., Alexandrou, A., Gacoin, T., Boilot, J.P., 2008. *Langmuir* 24, 11018.
- Glaspell, G., Anderson, J., Wilkins, J.R., El-Shall, M.S., 2008. *J. Phys. Chem. C* 112, 11527.
- Gnanasekar, K.I., Jiang, X., Jiang, J.C., Aghasyan, M., Tiltsworth, R., Hormes, J., Rambabu, B., 2002. *Solid State Ionics* 148, 575.
- Godinho, M., Ribeiro, C., Longo, E., Leite, E.R., 2008. *Cryst. Growth Des.* 8, 384.
- Goldburt, E.T., Kulkarni, B., Bhargava, R.N., Taylor, J., Libera, M., 1997. *J. Lumin.* 72–74, 190.
- Goldys, E.M., Drozdowicz-Tomsia, K., Sun, J.J., Dosev, D., Kennedy, I.M., Yatsunenkov, S., Godlewski, M., 2006. *J. Am. Chem. Soc.* 128, 14498.
- Gonzalez-Ortega, J.A., Tejeda, E.M., Perea, N., Hirata, G.A., Bosze, E.J., McKittrick, J., 2005. *Opt. Mater.* 27, 1221.
- Gruehn, R., Glaum, R., 2000. *Angew. Chem. Int. Ed.* 39, 692.
- Gu, H., Soucek, M.D., 2007. *Chem. Mater.* 19, 1103.
- Gu, J.Q., Shen, J., Sun, L.D., Yan, C.H., 2008a. *J. Phys. Chem. C* 112, 6589.
- Gu, J.Q., Sun, L.D., Yan, Z.G., Yan, C.H., 2008b. *Chem. Asian J.* 3, 1857.
- Gu, M., Liu, Q., Mao, S.P., Mao, D., Chang, C.K., 2008c. *Cryst. Growth Des.* 8, 1422.
- Guan, H.M., Zhang, Y.J., 2004. *J. Solid State Chem.* 177, 781.
- Guan, M.Y., Sun, J.H., Han, M., Xu, Z., Tao, F.F., Yin, G., Wei, X.W., Zhu, J.M., Jiang, X.Q., 2007. *Nanotechnology* 18, 415602.
- Guillemin, N., Nistor, L.C., Fuess, H., Hahn, H., 1997. *Nanostruct. Mater.* 8, 545.
- Guo, Z.Y., Du, F.L., Li, G.C., Cui, Z.L., 2006. *Inorg. Chem.* 45, 4167.
- Guo, Z.Y., Du, F.L., Li, G.C., Cui, Z.L., 2008. *Cryst. Growth Des.* 8, 2674.
- Guzman, J., Corma, A., 2005. *Chem. Commun.* 743.
- Guzman, J., Carrettin, S., Fierro-Gonzalez, J.C., Hao, Y.L., Gates, B.C., Corma, A., 2005. *Angew. Chem. Int. Ed.* 44, 4778.
- Haase, M., Riwotzki, K., Meyssamy, H., Kornowski, A., 2000. *J. Alloys Compd.* 303–304, 191.

- Han, Z.H., Guo, N., Tang, K.B., Yu, S.H., Zhao, H.Q., Qian, Y.T., 2000. *J. Cryst. Growth* 219, 315.
- Han, W.Q., Wu, L.J., Zhu, Y.M., 2005. *J. Am. Chem. Soc.* 127, 12814.
- Han, M., Shi, N.E., Zhang, W.L., Li, B.J., Sun, J.H., Chen, K.J., Zhu, J.M., Wang, X., Xu, Z., 2008. *Chem. Eur. J.* 14, 1615.
- Hao, X., Moodera, J.S., Meservey, R., 1990. *Phys. Rev. B* 42, 8235.
- Hao, J.H., Studenikin, S.A., Cocivera, M., 2001. *J. Lumin.* 93, 313.
- Hasegawa, Y., Thongchant, S., Wada, Y., Tanaka, H., Kawai, T., Sakata, T., Mori, H., Yanagida, S., 2002. *Angew. Chem. Int. Ed.* 41, 2073.
- Hasegawa, Y., Afzaal, M., Brien, P.O., Wada, Y., Yanagida, S., 2005. *Chem. Commun.* 242.
- Hasegawa, Y., Okada, Y., Kataoka, T., Sakata, T., Mori, H., Wada, Y., 2006. *J. Phys. Chem. B* 110, 9008.
- Hasegawa, Y., Adachi, T.A., Tanaka, A., Afzaal, M., Brien, P.O., Doi, T., Hinatsu, Y., Fujita, K., Tanaka, K., Kawai, T., 2008. *J. Am. Chem. Soc.* 130, 5710.
- Heer, S., Lehmann, O., Haase, M., Gudel, H.U., 2003. *Angew. Chem. Int. Ed.* 42, 3179.
- Heer, S., Kompe, K., Gudel, H.U., Haase, M., 2004. *Adv. Mater.* 16, 2101.
- Henkes, A.E., Bauer, J.C., Sra, A.K., Johnson, R.D., Cable, R.E., Schaak, R.E., 2006. *Chem. Mater.* 18, 567.
- Hilderbrand, S.A., Shao, F.W., Salthouse, C., Mahmood, U., Weissleder, R., 2009. *Chem. Commun.* 4188.
- Hirai, T., Orikoshi, T., 2004. *J. Colloid Interface Sci.* 273, 470.
- Hirai, T., Hirano, T., Komasa, I., 2002. *J. Colloid Interface Sci.* 253, 62.
- Hirano, M., Inagaki, M., 2000. *J. Mater. Chem.* 10, 473.
- Hirano, M., Kato, E., 1999. *J. Am. Ceram. Soc.* 82, 786.
- Ho, C.M., Yu, J.C., Kwong, T., Mak, A.C., Lai, S.Y., 2005. *Chem. Mater.* 17, 4514.
- Hölsä, J., Säilynoja, E., Ylhä, P., Antic-Fidancev, E., Lemaître-Blaise, M., Porcher, P., 1998. *J. Chem. Soc. Faraday Trans.* 94, 481.
- Homola, J., Yee, S.S., Gauglitz, G., 1999. *Sens. Act. B* 54, 3.
- Hosono, E., Fujihara, S., Kimura, T., 2004. *Langmuir* 20, 3769.
- Hou, Z.Y., Yang, P.P., Li, C.X., Wang, L.L., Lian, H.Z., Quan, Z.W., Lin, J., 2008. *Chem. Mater.* 20, 6686.
- Hou, Z.Y., Wang, L.L., Lian, H.Z., Chai, R.T., Zhang, C.M., Cheng, Z.Y., Lin, J., 2009. *J. Solid State Chem.* 182, 698.
- Hreniak, D., Strek, W., Deren, P., Bednarkiewicz, A., Lukowiak, A., 2006. *J. Alloy Compd.* 408–412, 828.
- Hu, Z.S., Dong, J.X., Chen, G.X., He, J.Z., 2000. *Wear* 243, 43.
- Hu, C.G., Zhang, Z.W., Liu, H., Gao, P.X., Wang, Z.L., 2006a. *Nanotechnology* 17, 5983.
- Hu, Z.A., Wu, H.Y., Shang, X.L., Lu, R.J., Li, H.L., 2006b. *Mater. Res. Bull.* 41, 1045.
- Hu, Z.J., Ma, E., Wang, Y.S., Chen, D.P., 2006c. *Mater. Chem. Phys.* 100, 308.
- Hu, C.G., Liu, H., Dong, W.T., Zhang, Y.Y., Bao, G., Lao, C.S., Wang, Z.L., 2007. *Adv. Mater.* 19, 470.
- Hu, H., Chen, Z.G., Cao, T.Y., Zhang, Q., Yu, M.G., Li, F.Y., Yi, T., Huang, C.H., 2008a. *Nanotechnology* 19, 375702.
- Hu, H., Yu, M.X., Li, F.Y., Chen, Z.G., Gao, X., Xiong, L.Q., Huang, C.H., 2008b. *Chem. Mater.* 20, 7003.
- Hu, H., Xiong, L.Q., Zhou, J., Li, F.Y., Cao, T.Y., Huang, C.H., 2009. *Chem. Eur. J.* 15, 3577.
- Hua, R.N., Niu, J.H., Chen, B.J., Li, M.T., Yu, T.Z., Li, W.L., 2006. *Nanotechnology* 17, 1642.
- Huang, H., Gur, T.M., Saito, Y., Prinz, F., 2006a. *Appl. Phys. Lett.* 89, 143107.
- Huang, P.X., Wu, F., Zhu, B.L., Li, G.R., Wang, Y.L., Gao, X.P., Zhu, H.Y., Yan, T.Y., Huang, W.P., Zhang, S.M., Song, D.Y., 2006b. *J. Phys. Chem. B* 110, 1614.
- Huang, Q.L., Wang, M., Zhong, H.X., Chen, X.T., 2007. *Chin. J. Inorg. Chem.* 23, 1767.

- Huang, C.C., Lo, Y.W., Kuo, W.S., Hwu, J.R., Su, W.C., Shieh, D.B., Yeh, C.S., 2008a. *Langmuir* 24, 8309.
- Huang, Y.Z., Chen, L., Wu, L.M., 2008b. *Cryst. Growth Des.* 8, 739.
- Huignard, A., Gacoin, T., Boilot, J.P., 2000. *Chem. Mater.* 12, 1090.
- Huignard, A., Buissette, V., Laurent, G., Gacoin, T., Boilot, J.P., 2002. *Chem. Mater.* 14, 2264.
- Huignard, A., Buissette, V., Franville, A.C., Gacoin, T., Boilot, J.P., 2003. *J. Phys. Chem. B* 107, 6754.
- Huo, Z.Y., Chen, C., Chu, D., Li, H.H., Li, Y.D., 2007. *Chem. Eur. J.* 13, 7708.
- Huo, Z.Y., Chen, C., Liu, X.W., Chu, D.R., Li, H.H., Peng, Q., Li, Y.D., 2008. *Chem. Commun.* 3741.
- Huxter, V.M., Mirkovic, T., Nair, P.S., Scholes, G.D., 2008. *Adv. Mater.* 20, 2439.
- Iacconi, P., Junker, M., Guilhot, B., Huguenin, D., 2001. *Opt. Mater.* 17, 409.
- Iijima, S., 1991. *Nature* 354, 56.
- Ion, E., Malic, B., Kosec, M., 2007. *J. Sol-Gel Sci. Technol.* 44, 203.
- Jellison, G.E., Boatner, L.A., Chen, C., 2000. *Opt. Mater.* 15, 103.
- Jia, C.J., Sun, L.D., Luo, F., Jiang, X.C., Wei, L.H., Yan, C.H., 2004. *Appl. Phys. Lett.* 84, 5305.
- Jia, C.J., Sun, L.D., You, L.P., Jiang, X.C., Luo, F., Pang, Y.C., Yan, C.H., 2005. *J. Phys. Chem. B* 109, 3284.
- Jia, G., Yang, M., Song, Y.H., You, H.P., Zhang, H.J., 2009. *Cryst. Growth Des.* 9, 301.
- Jiang, Y., Wu, Y., Xie, Y., Qian, Y.T., 2000. *J. Am. Ceram. Soc.* 83, 2628.
- Jiang, X.C., Yan, C.H., Sun, L.D., Wei, Z.G., Liao, C.S., 2003. *J. Solid State Chem.* 175, 245.
- Jiang, J.C., Henry, L.L., Gnanasekar, K.I., Chen, C.L., Meletis, E.I., 2004a. *Nano Lett.* 4, 741.
- Jiang, X.C., Sun, L.D., Feng, W., Yan, C.H., 2004b. *Cryst. Growth Des.* 4, 517.
- Jiang, X.C., Sun, L.D., Yan, C.H., 2004c. *J. Phys. Chem. B* 108, 3387.
- Joseph, L.K., Dayas, K.R., Damodar, S., Krishnan, B., Krishnankutty, K., Nampoori, V.P.N., Radhakrishnan, P., 2008. *Spectrochim. Acta Part A* 71, 1281.
- Jung, H.K., Oh, J.S., Seok, S.I., Lee, T.H., 2005. *J. Lumin.* 114, 307.
- Kamimura, M., Miyamoto, D., Saito, Y., Soga, K., Nagasaki, Y., 2008. *Langmuir* 24, 8864.
- Kaneko, K., Inoke, K., Freitag, B., Hungria, A.B., Midgley, P.A., Hansen, T.W., Zhang, J., Ohara, S., Adschiri, T., 2007. *Nano Lett.* 7, 421.
- Karakoti, A.S., Kuchibhatla, S., Baer, D.R., Thevuthasan, S., Sayle, D.C., Seal, S., 2008. *Small* 4, 1210.
- Karbowiak, M., Mech, A., Bednarkiewicz, A., Streck, W., 2004. *J. Alloys Compd.* 380, 321.
- Karbowiak, M., Mech, A., Bednarkiewicz, A., Streck, W., Kepinski, L.J., 2005a. *Phys. Chem. Solids* 66, 1008.
- Karbowiak, M., Mech, A., Ke pin´ski, L., Mielcarek, W., Hubert, S., 2005b. *J. Alloys Compd.* 400, 67.
- Karmaoui, M., Ferreira, R.A.S., Mane, A.T., Carlos, L.D., Pinna, N., 2006. *Chem. Mater.* 18, 4493.
- Karmaoui, M., Mafra, L., Ferreira, R.A.S., Rocha, J., Carlos, L.D., Pinna, N., 2007. *J. Phys. Chem. C* 111, 2539.
- Kašpar, J., Fornasiero, P., Graziani, M., 1999. *Catal. Today* 50, 285.
- Kašpar, J., Graziani, M., Fornasiero, P., 2000. In: Gschneidner Jr., K.A., Eyring, L. (Eds.), *Handbook on the Physics and Chemistry of Rare Earths Volume 29*. Elsevier, Amsterdam, p. 159.
- Kataoka, T., Tsukahara, Y., Hasegawa, Y., Wada, Y., 2005. *Chem. Commun.* 6038.
- Kawahara, Y., Petrykin, V., Ichihara, T., Kijima, N., Kakihana, M., 2006. *Chem. Mater.* 18, 6303.
- Kelly, K.L., Coronado, E., Zhao, L.L., Schatz, G.C., 2003. *J. Phys. Chem. B* 107, 668.
- Kepinski, L., Hreniak, D., Streck, W., 2002a. *J. Alloys Compd.* 341, 203.
- Kepinski, L., Wolcyrz, M., Marchewka, M., 2002b. *J. Solid State Chem.* 168, 110.

- Kharrazi, S., Kundaliya, D.C., Gosavi, S.W., Kulkarni, S.K., Venkatesan, T., Ogale, S.B., Urban, J., Park, S., Cheong, S.-W., 2006. *Solid State Commun.* 138, 395.
- Kida, T., Guan, Q.Q., Minami, Y., Ma, T.L., Yoshida, A., 2003a. *J. Mater. Chem.* 13, 1186.
- Kida, T., Guan, Q.Q., Yoshida, A., 2003b. *Chem. Phys. Lett.* 371, 563.
- Kira, H., Tamura, H., Ando, Y., Onodera, M., Nakao, H., Murakami, Y., Tsuda, K., Ohoyama, K., Yamazaki, S., Tajiri, T., Deguchi, H., 2007. *J. Magn. Magn. Mater.* 310, 2480.
- Kleinogel, C., Gauckler, L.J., 2000. *Solid State Ionics* 135, 567.
- Kleinogel, C., Gauckler, L.J., 2001. *Adv. Mater.* 13, 1081.
- Kneipp, K., Wang, Y., Kneipp, H., Perelman, L.T., Itzkan, I., Dasari, R., Feld, M.S., 1997. *Phys. Rev. Lett.* 78, 1667.
- Kompe, K., Borchert, H., Storz, J., Lobo, A., Adam, S., Moller, T., Haase, M., 2003. *Angew. Chem. Int. Ed.* 42, 5513.
- Kompe, K., Lehmann, O., Haase, M., 2006. *Chem. Mater.* 18, 4442.
- Konishi, T., Shimizu, M., Kameyama, Y., Soga, K., 2007. *J. Mater. Sci. Mater. Electron.* 18, S183.
- Korsvik, C., Patil, S., Seal, S., Self, W.T., 2007. *Chem. Commun.* 1056.
- Krishnamoorthy, C., Sethupathi, K., Sankaranarayanan, V., 2007a. *Mater. Lett.* 61, 3254.
- Krishnamoorthy, C., Sethupathi, K., Sankaranarayanan, V., Nirmala, R., Malik, S.K., 2007b. *J. Alloys Compd.* 438, 1.
- Krishnan, V., Bottaro, G., Gross, S., Armelao, L., Tondello, E., Bertagnolli, H., 2005. *J. Mater. Chem.* 15, 2020.
- Kuchibhatla, S.V.N.T., Karakoti, A.S., Seal, S., 2007. *Nanotechnology* 18, 075303.
- Kuchibhatla, S.V.N.T., Karakoti, A.S., Sayle, D.C., Heinrich, H., Seal, S., 2009. *Cryst. Growth Des.* 9, 1614.
- Kumar, G.A., Chen, C.W., Ballato, J., Riman, R.E., 2007. *Chem. Mater.* 19, 1523.
- Kumar, R., Nyk, M., Ohulchansky, T.Y., Flask, C.A., Prasad, P.N., 2009. *Adv. Funct. Mater.* 19, 853.
- Kundu, A.K., Rautama, E.-L., Boullay, Ph., Caignaert, V., Pralong, V., Raveau, B., 2007. *Phys. Rev. B* 76, 184432.
- Lai, H., Bao, A., Yang, Y.M., Xu, W.W., Tao, Y.C., Yang, H., 2008. *Adv. J. Lumin.* 128, 521.
- Laporta, P., Taccheo, S., Longhi, S., Svelto, O., Svelto, C., 1999. *Opt. Mater.* 11, 269.
- Le Fur, Y., Khaidukov, N.M., Aleonard, S., 1992. *Acta Crystallogr. C* 48, 2062.
- Le, N.T.H., Calderon-Moreno, J.M., Popa, M., Crespo, D., Hong, L.V., Phuc, N.X., 2006. *J. Eur. Ceram. Soc.* 26, 403.
- Lebbou, K., Perriat, P., Tillement, O., 2005. *J. Nanosci. Nanotech.* 5, 1448.
- Lee, S.S., Byeon, S.H., 2006. *Mater. Sci. Eng. B—Solid State Mater. Adv. Technol.* 133, 77.
- Lee, J., Zhang, Q.W., Saito, F., 2001. *J. Solid State Chem.* 160, 469.
- Lee, J., Zhang, Q.W., Saito, F., 2003. *J. Alloys Compd.* 348, 214.
- Lee, S.S., Park, H.I., Joh, C.H., Byeon, S.H., 2007. *J. Solid State Chem.* 180, 3529.
- Lehmann, O., Meyssamy, H., Kompe, K., Schnablegger, H., Haase, M., 2003. *J. Phys. Chem. B* 107, 7449.
- Lehmann, O., Kompe, K., Haase, M., 2004. *J. Am. Chem. Soc.* 126, 14935.
- Lempicki, A., Berman, E., Wojtowicz, A.J., Balcerzyk, M., Boatner, L.A., 1993. *IEEE Trans. Nucl. Sci.* 40, 384.
- Lemyre, J.L., Ritcey, A.M., 2005. *Chem. Mater.* 17, 3040.
- Lezhnina, M.M., Jüstel, T., Kätker, H., Wiechert, D.U., Kynast, U.H., 2006. *Adv. Funct. Mater.* 16, 935.
- Li, D., Xia, Y.N., 2004. *Adv. Mater.* 16, 1151.
- Li, Q., Yam, V.W.W., 2007. *Angew. Chem. Int. Ed.* 46, 3486.
- Li, Z.Q., Zhang, Y., 2006a. *Angew. Chem. Int. Ed.* 45, 7732.
- Li, Z.Q., Zhang, Y., 2006b. *Nanotechnology* 17, 5786.
- Li, G.S., Feng, S.H., Li, L.P., 1996. *J. Solid State Chem.* 126, 74.

- Li, J.G., Ikegami, T., Mori, T., Wada, T., 2001. *Chem. Mater.* 13, 2913.
- Li, F., Yu, X., Chen, L., Pan, H., Xin, X., 2002. *J. Am. Ceram. Soc.* 85, 2177.
- Li, W.J., Wang, X., Li, Y.D., 2004. *Chem. Commun.* 164.
- Li, G.Z., Wang, Z.L., Yu, M., Quan, Z.W., Lin, J., 2006a. *J. Solid State Chem.* 179, 2698.
- Li, J.Y., Dai, H., Li, Q., Zhong, X.H., Ma, X.F., Meng, J., Cao, X.Q., 2006b. *Mater. Sci. Eng. B* 133, 209.
- Li, K.W., Wang, H., Yan, H., 2006c. *J. Mol. Catal. A: Chem.* 249, 65.
- Li, K.W., Wang, Y., Wang, H., Zhu, M., Yan, H., 2006d. *Nanotechnology* 17, 4863.
- Li, Z., Xue, H., Wang, X., Fu, X., 2006e. *J. Mol. Catal. A: Chem.* 260, 56.
- Li, C.X., Quan, Z.W., Yang, J., Yang, P.P., Lin, J., 2007a. *Inorg. Chem.* 46, 6329.
- Li, L., Jiang, W.G., Pan, H.H., Xu, X.R., Tang, Y.X., Ming, J.Z., Xu, Z.D., Tang, R.K., 2007b. *J. Phys. Chem. C* 111, 4111.
- Li, Z.H., Zeng, J.H., Li, Y.D., 2007c. *Small* 3, 438.
- Li, C.X., Liu, X.M., Yang, P.P., Zhang, C.M., Lian, H.Z., Lin, J., 2008a. *J. Phys. Chem. C* 112, 2904.
- Li, C.X., Quan, Z.W., Yang, P.P., Huang, S.S., Lian, H.Z., Lin, J., 2008b. *J. Phys. Chem. C* 112, 13395.
- Li, C.X., Quan, Z.W., Yang, P.P., Yang, J., Lian, H.Z., Lin, J., 2008c. *J. Mater. Chem.* 18, 1353.
- Li, C.X., Quan, Z.W., Yang, P.P., Zhang, X.M., Lian, H.Z., Lin, J., 2008d. *Cryst. Growth Des.* 8, 923.
- Li, C.X., Yang, J., Yang, P.P., Lian, H.Z., Lin, J., 2008e. *Chem. Mater.* 20, 4317.
- Li, G.C., Chao, K., Peng, H.R., Chen, K.Z., 2008f. *J. Phys. Chem. C* 112, 6228.
- Li, G.C., Chao, K., Peng, H.R., Chen, K.Z., Zhang, Z.K., 2008g. *J. Phys. Chem. C* 112, 16452.
- Li, H., Zhu, G.S., Ren, H., Li, Y., Hewitt, I.J., Qiu, S.L., 2008h. *Eur. J. Inorg. Chem.* 2033.
- Li, Z.X., Li, L.L., Yuan, Q., Feng, W., Xu, J., Sun, L.D., Song, W.G., Yan, C.H., 2008i. *J. Phys. Chem. C* 112, 18405.
- Lian, H., Zhang, M., Liu, J., Ye, Z., Yan, J., Shi, C.S., 2004. *Chem. Phys. Lett.* 395, 362.
- Liang, L., Xu, H.F., Su, Q., Konishi, H., Jiang, Y.B., Wu, M.M., Wang, Y.F., Xia, D.Y., 2004. *Inorg. Chem.* 43, 1594.
- Liang, S., Teng, F., Bulgan, G., Zhu, Y., 2007a. *J. Phys. Chem. C* 111, 16742.
- Liang, X., Wang, X., Zhuang, J., Peng, Q., Li, Y.D., 2007b. *Adv. Funct. Mater.* 17, 2757.
- Liang, X., Wang, X., Zhuang, J., Peng, Q., Li, Y.D., 2007c. *Inorg. Chem.* 46, 6050.
- Liang, X., Wang, X., Zhuang, Y., Xu, B., Kuang, S.M., Li, Y.D., 2008. *J. Am. Chem. Soc.* 130, 2736.
- Liao, X.H., Zhu, J.M., Zhu, J.J., Xu, J.Z., Chen, H.Y., 2001. *Chem. Commun.* 937.
- Liao, L., Mai, H.X., Yuan, Q., Lu, H.B., Li, J.C., Liu, C., Yan, C.H., Shen, Z.X., Yu, T., 2008. *J. Phys. Chem. C* 112, 9061.
- Lin, J.H., Sheptyakov, D., Wang, Y.X., Allenspach, P., 2004. *Chem. Mater.* 16, 2418.
- Lin, C.K., Yu, M., Pang, M.L., Lin, J., 2006. *Opt. Mater.* 28, 913.
- Lin, C.K., Kong, D.Y., Liu, X.M., Wang, H., Yu, M., Lin, J., 2007a. *Inorg. Chem.* 46, 2674.
- Lin, Y.S., Hung, Y., Lin, H.Y., Tseng, Y.H., Chen, Y.F., Mou, C.Y., 2007b. *Adv. Mater.* 19, 577.
- Liu, C.H., Chen, D.P., 2007a. *J. Mater. Chem.* 17, 3875.
- Liu, G.K., Chen, X.Y., 2007b. In: Gschneidner Jr., K.A., Bünzli, J.C.G., Pecharsky, V.K. (Eds.), *Handbook on the Physics and Chemistry of Rare Earths Volume 37*. Elsevier, Amsterdam, p. 99.
- Liu, W., Flytzani-Stephanopoulos, M., 1995a. *J. Catal.* 153, 304.
- Liu, W., Flytzani-Stephanopoulos, M., 1995b. *J. Catal.* 153, 317.
- Liu, J.F., Li, Y.D., 2007a. *Adv. Mater.* 19, 1118.
- Liu, J.F., Li, Y.D., 2007b. *J. Mater. Chem.* 17, 1797.
- Liu, P., Rodriguez, J.A., 2007. *J. Chem. Phys.* 126, 164705.
- Liu, L., Song, J.F., 2006. *Anal. Biochem.* 354, 22.
- Liu, G.X., Hong, G.Y., Wang, J.X., Dong, X.T., 2006. *Nanotechnology* 17, 3134.

- Liu, G.S., Zhang, Y., Yin, J., Zhang, W.F., 2008a. *J. Lumin.* 128, 2008.
- Liu, S.W., Xiu, Z.L., Xu, F.X., Yu, W.N., Yu, J.X., Feng, G.J., 2008b. *J. Alloys Compd.* 459, 407.
- Liu, Z.G., Sun, X.D., Xu, S.K., Lian, J.B., Li, X.D., Xiu, Z.M., Li, Q., Huo, D., Li, J.G., 2008c. *J. Phys. Chem. C* 112, 2353.
- Liu, C.H., Wang, H., Zhang, X.R., Chen, D.P., 2009. *J. Mater. Chem.* 19, 489.
- Losurdo, M., Sacchetti, A., Cappezuto, P., Bruno, G., Armelao, L., Barreca, D., Bottaro, G., 2005. *Appl. Phys. Lett.* 87, 061909.
- Louis, C., Bazzi, R., Flores, M.A., Zheng, W., Lebbou, K., Tillement, O., Mercier, B., Dujardin, C., Perriat, P., 2003. *J. Solid State Chem.* 173, 335.
- Lu, C.H., Wang, H.C., 2002. *Mater. Sci. Eng. B* 90, 138.
- Lu, H.C., Yi, G.S., Zhao, S.Y., Chen, D.P., Guo, L.H., Cheng, J., 2004a. *J. Mater. Chem.* 14, 1336.
- Lu, Z., Wang, J., Tang, Y., Li, Y., 2004b. *J. Solid State Chem.* 177, 3075.
- Luo, X.X., Cao, W.H., 2008. *J. Alloys Compd.* 460, 529.
- Luo, F., Jia, C.J., Song, W., Li, Z.F., Yan, C.H., 2004. *Solid State Commun.* 132, 595.
- Luo, F., Jia, C.J., Song, W., You, L.P., Yan, C.H., 2005. *Cryst. Growth Des.* 5, 137.
- Ma, J., Wu, Q.S., Ding, Y.P., Chen, Y., 2007a. *Cryst. Growth Des.* 7, 1553.
- Ma, L., Chen, W.X., Zhao, J., Zheng, Y.F., 2007b. *J. Cryst. Growth* 303, 590.
- Ma, L., Chen, W.X., Zheng, Y.F., Zhao, J., Xu, Z.D., 2007c. *Mater. Lett.* 61, 2765.
- Ma, J., Wu, Q.S., Ding, Y.P., 2008a. *J. Nanopart. Res.* 10, 775.
- Ma, Z., Yin, H.F., Overbury, S.H., Dai, S., 2008b. *Catal. Lett.* 126, 20.
- Madler, L., Stark, W.J., Pratsinis, S.E., 2002. *J. Mater. Res.* 17, 1356.
- Maensiri, S., Masingboon, C., Laokul, P., Jareonboon, W., Promarak, V., Anderson, P.L., Seraphin, S., 2007. *Cryst. Growth Des.* 7, 950.
- Mahajan, S.V., Dickerson, J.H., 2007. *Nanotechnology* 18, 325605.
- Mahapatra, S., Nayak, S.K., Madras, G., Row, T.N.G., 2008. *Ind. Eng. Chem. Res.* 47, 6509.
- Mahata, P., Aarathi, T., Madras, G., Natarajan, S., 2007. *J. Phys. Chem. C* 111, 1665.
- Mai, H.X., Sun, L.D., Zhang, Y.W., Si, R., Feng, W., Zhang, H.P., Liu, H.C., Yan, C.H., 2005. *J. Phys. Chem. B* 109, 24380.
- Mai, H.X., Zhang, Y.W., Si, R., Yan, Z.G., Sun, L.D., You, L.P., Yan, C.H., 2006. *J. Am. Chem. Soc.* 128, 6426.
- Mai, H.X., Zhang, Y.W., Sun, L.D., Yan, C.H., 2007. *Chem. Mater.* 19, 4514.
- Maicaneanu, S.A., Sayle, D.C., Watson, G.W., 2001. *Chem. Commun.* 289.
- Malandrino, G., Perdicaro, L.M.S., Fragalà, I.L., 2006. *Chem. Vap. Depos.* 12, 736.
- Malavasi, L., Mozzati, M.C., Polizzi, S., Azzoni, C.B., Flor, G., 2003. *Chem. Mater.* 15, 5036.
- Malavasi, L., Quartarone, E., Sanna, C., Lampis, N., Lehmann, A.G., Tealdi, C., Mozzati, M.C., Flor, G., 2006. *Chem. Mater.* 18, 5230.
- Mamontov, E., Egami, T., Brezny, R., Koranne, M., Tyagi, S., 2000. *J. Phys. Chem. B* 104, 11110.
- Markovich, V., Fita, I., Mogilyansky, D., Wisniewski, A., Puzniak, R., Titelman, L., Vradman, L., Herskowitz, M., Gorodetsky, G., 2007. *J. Phys.: Condens. Matter* 19, 346210.
- Markovich, V., Jung, G., Fita, I., Mogilyansky, D., Wu, X., Wisniewski, A., Puzniak, R., Froumin, N., Titelman, L., Vradman, L., Herskowitz, M., Gorodetsky, G., 2008a. *J. Phys. D: Appl. Phys.* 41, 185001.
- Markovich, V., Fita, I., Mogilyansky, D., Wisniewski, A., Puzniak, R., Titelman, L., Vradman, L., Herskowitz, M., Gorodetsky, G., 2008b. *Superlattices Microstruct.* 44, 476.
- Marrero-Lopez, D., Nunez, P., Abril, M., Lavin, V., Rodriguez-Mendoza, U.R., Rodriguez, V.D., 2004. *J. Non-Cryst. Solids* 345&346, 377.
- Marrero-Lopez, D., Canales-Vazquez, J., Ruiz-Morales, J.C., Rodriguez, A., Irvine, J.T.S., Nunez, P., 2005. *Solid State Ionics* 176, 1807.
- Marrero-Lopez, D., Perez-Coll, D., Ruiz-Morales, J.C., Canales-Vazquez, J., Martin-Sedeno, M.C., Nunez, P., 2007. *Electrochim. Acta* 52, 5219.

- Marrero-Lopez, D., Pena-Matinez, J., Ruiz-Morales, J.C., Nunez, P., 2008. *J. Solid State Chem.* 181, 253.
- Martin, P., Parker, S.C., Sayle, D.C., Watson, G.W., 2007. *Nano Lett.* 7, 543.
- Masui, T., Fujiwara, K., Machida, K., Adachi, G., Sakata, T., Mori, H., 1997. *Chem. Mater.* 9, 2197.
- Mathur, S., Shen, H., Lecerf, N., Kjekshus, A., Fjellvag, H., Goya, G.F., 2002. *Adv. Mater.* 14, 1405.
- Mathur, S., Veith, M., Rapalaviciute, R., Shen, H., Goya, G.F., Martins Filho, W.L., Berquo, T.S., 2004. *Chem. Mater.* 16, 1906.
- Maurel, F., Hytch, M.J., Knosp, B., Backhaus-Ricoult, M., 2000. *Eur. Phys. J. AP* 9, 205.
- McGuire, T.R., Shafer, M.W., 1964. *J. Appl. Phys.* 35, 984.
- Meiser, F., Cortez, C., Caruso, F., 2004. *Angew. Chem. Int. Ed.* 43, 5954.
- Mello, C.D., Dirksen, G.J., Folkerts, H.F., Meijerink, A., Blasse, G., 1995. *J. Phys. Chem. Solids* 56, 267.
- Meltzera, R.S., Zheng, H.R., Dejneka, M.J., 2004. *J. Lumin.* 107, 166.
- Meng, L., Yang, L.G., Zhou, B., Cai, C.X., 2009. *Nanotechnology* 20, 035502.
- Menyuk, N., Dwight, K., Pierce, J.W., 1972. *Appl. Phys. Lett.* 21, 159.
- Meyer, G., Staffel, T., 1986. *Z. Anorg. Allg. Chem.* 532, 31.
- Meyer, G., Wickleder, M.S., 2000. In: Gschneidner, K.A., Eyring, L. (Eds.), *Handbook on the Physics and Chemistry of Rare Earths*, Vol. 28, Ch. 177. Elsevier, Amsterdam, pp. 53–129.
- Meyssamy, H., Riwozki, K., Kornowski, A., Naused, S., Haase, M., 1999. *Adv. Mater.* 11, 840.
- Mialon, G., Gohin, M., Gacoïn, T., Boilot, J.P., 2008. *ACS Nano* 2, 2505.
- Miao, Z.J., Liu, Z.M., Ding, K.L., Han, B.X., Miao, S.D., An, G.M., 2007. *Nanotechnology* 18, 125605.
- Miritello, M., Lo Savio, R., Iacona, F., Franzo, G., Irrera, A., Piro, A.M., Bongiorno, C., Priolo, F., 2007. *Adv. Mater.* 19, 1582.
- Mirkovic, T., Hines, M.A., Nair, P.S., Scholes, G.D., 2005. *Chem. Mater.* 17, 3451.
- Mo, Z.L., Sun, Y.X., Chen, H., Zhang, P., Zuo, D.D., Liu, Y.Z., Li, H.J., 2005. *Polymer* 46, 12670.
- Moine, B., Mugnier, J., Boyer, D., Mahiou, R., Schamm, S., Zanchi, G., 2001. *J. Alloys Compd.* 323, 816.
- Moon, J., 2001. *J. Am. Ceram. Soc.* 84, 2531.
- Morales, L., Prado, F., Caneiro, A., Sanchez, R.D., Serquis, A., 2000. *J. Alloys Compd.* 302, 59.
- Morales, L., Caneiro, A., Vega, D., Zysler, R., Lanza, H., Mercader, R.C., 2002. *J. Solid State Chem.* 168, 100.
- Morgan, C.G., Mitchell, A.C., 2007. *Biosens. Bioelectron.* 22, 1769.
- Murray, C.B., Norris, D.J., Bawendi, M.G., 1993. *J. Am. Chem. Soc.* 115, 8706.
- Murray, E.P., Tsai, T., Barnett, S.A., 1999. *Nature* 400, 649.
- Murugan, B., Ramaswamy, A.V., 2007. *J. Am. Chem. Soc.* 129, 3062.
- Naccache, R., Vetrone, F., Mahalingam, V., Cuccia, L.A., Capobianco, J.A., 2009. *Chem. Mater.* 21, 717.
- Nagabhushana, B.M., Chandrappa, G.T., Chakradhar, R.P.S., Ramesh, K.P., Shivakumara, C., 2005. *Solid State Commun.* 136, 427.
- Nagabhushana, B.M., Chakradhar, R.P.S., Ramesh, K.P., Shivakumara, C., Chandrappa, G.T., 2006. *Mater. Res. Bull.* 41, 1735.
- Nagabhushana, B.M., Chakradhar, R.P.S., Ramesh, K.P., Shivakumara, C., Chandrappa, G.T., 2007. *Mater. Chem. Phys.* 102, 47.
- Nagabhushana, B.M., Chakradhar, R.P.S., Ramesh, K.P., Prasad, V., Shivakumara, C., Chandrappa, G.T., 2008. *J. Alloys Compd.* 450, 364.
- Nakajima, T., Žemva, B., Tressaud, A., 2000. *Advanced Inorganic Fluorides*. Elsevier, Amsterdam Ch. 10.
- Nakkiran, A., Thirumalai, J., Jagannathan, R., 2007. *Chem. Phys. Lett.* 436, 155.

- Nelson, J.A., Bennett, L.H., Wagner, M.J., 2002. *J. Am. Chem. Soc.* 124, 2979.
- Nelson, J.A., Brant, E.L., Wagner, M.J., 2003a. *Chem. Mater.* 15, 688.
- Nelson, J.A., Bennett, L.H., Wagner, M.J., 2003b. *J. Mater. Chem.* 13, 857.
- Nie, S.M., Emery, S.R., 1997. *Science* 275, 1102.
- Niedbala, R.S., Feindt, H., Kardos, K., Vail, T., Burton, J., Bielska, B., Li, S., Milunic, D., Bourdelle, P., Vallejo, R., 2001. *Anal. Biochem.* 293, 22.
- Nishihama, S., Hirai, T., Komasa, I., 2002. *J. Mater. Chem.* 12, 1053.
- Niu, X.S., Du, W.M., Du, W.P., Jiang, K., 2003. *J. Rare Earth.* 21, 630.
- Niu, X.S., Du, W.M., Du, W.P., Jiang, K., 2004a. *Chin. J. Chem. Phys.* 17, 79.
- Niu, X.S., Du, W.M., Du, W.P., 2004b. *Sens. Act. B* 99, 399.
- Niu, X.S., Du, W.M., Du, W.P., Jiang, K., 2005a. *Rare Met. Mater. Eng.* 34, 124.
- Niu, X.S., Li, H.H., Liu, G.G., 2005b. *J. Mol. Catal. A: Chem.* 232, 89.
- Niu, X.S., Li, H.H., Zhang, F., Liu, G.G., Jiang, K., 2005c. *J. Rare Earth* 23, 420.
- Niu, J.L., Azfer, A., Rogers, L.M., Wang, X.H., Kolattukudy, P.E., 2007. *Cardiovascular Res.* 73, 549.
- Norby, T., Christiansen, N., 1995. *Solid State Ion* 77, 240.
- Novoselov, K.S., Geim, A.K., Morozov, S.V., Jiang, D., Katsnelson, M.I., Grigorieva, I.V., Dubonos, S.V., Firsov, A.A., 2005. *Nature* 438, 197.
- Nyk, M., Kumar, R., Ohulchanskyy, T.Y., Bergey, E.J., Prasad, P.N., 2008. *Nano Lett.* 8, 3834.
- O'Shea, M.J., Perera, P., 1999. *J. Appl. Phys.* 85, 4322.
- Onoda, H., Nariai, H., Moriwaki, A., Maki, H., Motooka, I., 2002. *J. Mater. Chem.* 12, 1754.
- Ordunegui-Regil, E., Drot, R., Simoni, E., Ehrhardt, J.J., 2002. *Langmuir* 18, 7977.
- Ozgur, U., Alivov, Y.I., Liu, C., Teke, A., Reshchikov, M.A., Dogan, S., Avrutin, V., Cho, S.J., Morkoc, H., 2005. *J. Appl. Phys.* 98, 041301.
- Paek, J., Lee, C.H., Choi, J., Choi, S.Y., Kim, A., Lee, J.W., Lee, K., 2007. *Cryst. Growth Des.* 7, 1378.
- Pan, G.H., Song, H.W., Bai, X., Liu, Z.X., Yu, H.Q., Di, W.H., Li, S.W., Fan, L.B., Ren, X.G., Lu, S.Z., 2006. *Chem. Mater.* 18, 4526.
- Pan, G.H., Song, H.W., Bai, X., Fan, L.B., Yu, H.Q., Dai, Q.L., Dong, B., Qin, R.F., Li, S.W., Lu, S.Z., Ren, X.G., Zhao, H.F., 2007a. *J. Phys. Chem. C* 111, 12472.
- Pan, G.H., Song, H.W., Yu, L.X., Liu, Z.X., Bai, X., Lei, Y.Q., Fan, L.B., 2007b. *J. Lumin.* 122, 882.
- Panda, A.B., Glaspell, G., El-Shall, M.S., 2007. *J. Phys. Chem. C* 111, 1861.
- Park, S.D., Vohs, J.M., Gorte, R.J., 2000. *Nature* 404, 265.
- Park, S., Hwang, H.J., Moon, J., 2003. *Catal. Lett.* 87, 219.
- Patra, C.R., Alexandra, G., Patra, S., Jacob, D.S., Gedanken, A., Landau, A., Gofer, Y., 2005. *New J. Chem.* 29, 733.
- Patra, C.R., Bhattacharya, R., Patra, S., Basu, S., Mukherjee, P., Mukhopadhyay, D., 2007. *Clin. Chem.* 53, 2029.
- Patsalas, P., Logothetidis, S., Metaxa, C., 2002. *Appl. Phys. Lett.* 81, 466.
- Peng, H.S., Huang, S.H., You, F.T., Chang, J.J., Lu, S.Z., Cao, L., 2005. *J. Phys. Chem. B* 109, 5774.
- Perez, J.M., Asati, A., Nath, S., Kaittanis, C., 2008. *Small* 4, 552.
- Pinna, N., 2007. *J. Mater. Chem.* 17, 2769.
- Pinna, N., Garnweitner, G., Beato, P., Niederberger, M., Antonietti, M., 2005. *Small* 1, 112.
- Pires, A.M., Serra, O.A., Davolos, M.R., 2004. *J. Alloys Compd.* 374, 181.
- Pires, A.M., Heer, S., Güdel, H.U., Serra, O.A., 2006. *J. Fluoresc.* 16, 461.
- Popa, M., Frantti, J., Kakinaha, M., 2002a. *Solid State Ionics* 154–155, 135.
- Popa, M., Frantti, J., Kakinaha, M., 2002b. *Solid State Ionics* 154–155, 437.
- Popa, M., Hong, L.V., Kakinaha, M., 2003a. *Physics B* 327, 233.
- Popa, M., Hong, L.V., Kakinaha, M., 2003b. *Physics B* 327, 237.
- Prentice, L.H., Tyas, M.J., Burrow, M.F., 2006. *Dental Mater.* 22, 746.

- Purohit, R.D., Sharma, B.P., Pillai, K.T., Tyagi, A.K., 2001. *Mater. Res. Bull.* 36, 2711.
- Purwanto, A., Wang, W.N., Ogi, T., Lenggoro, I.W., Tanabe, E., Okuyama, K., 2008. *J. Alloys Compd.* 463, 350.
- Qi, X.W., Zhou, J., Yue, Z.X., Gui, Z.L., Li, L.T., 2002. *Mater. Chem. Phys.* 78, 25.
- Qi, L., Sehgal, A., Castaing, J.C., Chapel, J.P., Fresnais, J., Berret, J.F., Cousin, F., 2008. *ACS Nano* 2, 879.
- Qian, H.S., Zhang, Y., 2008. *Langmuir* 24, 12123.
- Qian, L.W., Zhu, J., Chen, Z., Gui, Y.C., Gong, Q., Yuan, Y.P., Zai, J.T., Qian, X.F., 2009. *Chem. Eur. J.* 15, 1233.
- Qin, R.F., Song, H.W., Pan, G.H., Bai, X., Dong, B., Xie, S.H., Liu, L.N., Dai, Q.L., Qu, X.S., Ren, X.G., Zhan, H.F., 2009. *Cryst. Growth Des.* 9, 1750.
- Qiu, S.Q., Dong, J.X., Chen, G.X., 1999. *Wear* 230, 35.
- Qiu, S.Q., Dong, J.X., Chen, G.X., 2000. *Powder Technol.* 113, 9.
- Rajesh, K., Mukundan, P., Pillai, P.K., Nair, V.R., Warriar, K.G.K., 2004. *Chem. Mater.* 16, 2700.
- Rajesh, K., Shajesh, P., Seidel, O., Mukundan, P., Warriar, K.G.K., 2007. *Adv. Funct. Mater.* 17, 1682.
- Rard, J.A., 1985. *Chem. Rev.* 85, 555.
- Ratnasamy, P., Srinivas, D., Satyanarayana, C.V.V., Manikandan, P., Senthil Kumaran, R.S., Sachin, M., Shetti, V.N., 2004. *J. Catal.* 221, 455.
- Redígolo, M.L., Koktysh, D.S., Rosenthal, S.J., Dickerson, J.H., Gai, Z., Gao, L., Shen, J., 2006. *Appl. Phys. Lett.* 89, 222501.
- Regulacio, M.D., Bussmann, K., Lewis, B., Stoll, S.L., 2006. *J. Am. Chem. Soc.* 128, 11173.
- Regulacio, M.D., Kar, S., Zuniga, E., Wang, G.B., Dollahon, N.R., Yee, G.T., Stoll, S.L., 2008. *Chem. Mater.* 20, 3368.
- Reisfeld, R., Jorgensen, C.K., 1977. *Laser and Excited State of Rare Earths*. Springer Verlag, Berlin.
- Ren, M., Lin, J.H., Dong, Y., Yang, L.Q., Su, M.Z., You, L.P., 1999. *Chem. Mater.* 11, 1576.
- Ribot, F., Escax, V., Roiland, C., Sanchez, C., Martins, J.C., Biesemans, M., Verbruggen, I., Willem, R., 2005. *Chem. Commun.* 1019.
- Rijke, F.v.-d., Zijlmans, H., Li, S., Vail, T., Raap, A.K., Niedbala, R.S., Tanke, H.J., 2001. *Nat. Biotechnol.* 19, 273.
- Riwotzki, K., Haase, M., 1998. *J. Phys. Chem. B* 102, 10129.
- Riwotzki, K., Haase, M., 2001. *J. Phys. Chem. B* 105, 12709.
- Riwotzki, K., Meyssamy, H., Kornowski, A., Haase, M., 2000. *J. Phys. Chem. B* 104, 2824.
- Riwotzki, K., Meyssamy, H., Schnablegger, H., Kornowski, A., Haase, M., 2001. *Angew. Chem. Int. Ed.* 40, 573.
- Robert, R., Romer, S., Reller, A., Weidenkaff, A., 2005. *Adv. Eng. Mater.* 7, 303.
- Ronda, C.R., 1997. *J. Lumin.* 72–74, 49.
- Rouanet, A., Serra, J.J., Allaf, K., Orlovskii, V.P., 1981. *Inorg. Mater.* 17, 76.
- Royer, S., Levasseur, B., Alamdari, H., Barbier Jr., J., Duprez, D., Kaliaguine, S., 2008. *Appl. Catal. B* 80, 51.
- Sadaoka, Y., Aono, H., Traversa, E., Sakamoto, M., 1998. *J. Alloys Compd.* 278, 135.
- Saha, S., Arya, S.K., Singh, S.P., Sreenivas, K., Malhotra, B.D., Gupta, V., 2009. *Biosens. Bioelectron.* 24, 2040.
- Sahu, P.K., Behera, S.K., Pratihari, S.K., Bhattacharyya, S., 2004. *Ceram. Int.* 30, 1231.
- Saradha, T., Muzhumathi, S., Subramania, A., 2008. *J. Solid State Electrochem.* 12, 143.
- Sathyamurthy, S., Leonard, K.J., Dabestani, R.T., Paranthaman, M.P., 2005. *Nanotechnology* 16, 1960.
- Sayle, T.X.T., Parker, S.C., Sayle, D.C., 2004. *Chem. Commun.* 2438.
- Sayle, T.X.T., Parker, S.C., Sayle, D.C., 2005. *Phys. Chem. Chem. Phys.* 7, 2936.
- Sayle, T.X.T., Parker, S.C., Sayle, D.C., 2006. *J. Mater. Chem.* 16, 1067.

- Sayle, D.C., Feng, X.D., Ding, Y., Wang, Z.L., Sayle, T.X.T., 2007a. *J. Am. Chem. Soc.* 129, 7924.
- Sayle, T.X.T., Parker, S.C., Sayle, D.C., 2007b. *Faraday Discuss.* 134, 377.
- Sayle, D.C., Seal, S., Wang, Z.W., Mangili, B.C., Price, D.W., Karakoti, A.S., Kuchibhatla, S.V.T.N., Hao, Q., Mobus, G., Xu, X.J., Sayle, T.X.T., 2008. *ACS Nano* 2, 1237.
- Schäfer, H., Ptacek, P., Kömpe, K., Haase, M., 2007. *Chem. Mater.* 19, 1396.
- Schäfer, H., Ptacek, P., Zerzouf, O., Haase, M., 2008. *Adv. Funct. Mater.* 18, 2913.
- Schuetz, P., Caruso, F., 2002. *Chem. Mater.* 14, 4509.
- Scirè, S., Minico, S., Crisafulli, C., Satriano, C., Pistone, A., 2003. *Appl. Catal. B* 40, 43.
- Sedmak, G., Hočevar, S., Levec, J., 2003. *J. Catal.* 213, 135.
- Shen, J., Sun, L.D., Yan, C.H., 2008a. *Dalton Trans.* 5687.
- Shen, Z.R., Zhang, G.J., Zhou, H.J., Sun, P.C., Li, B.H., Ding, D.T., Chen, T.H., 2008b. *Adv. Mater.* 20, 984.
- Shen, Z.R., Wang, J.G., Sun, P.C., Ding, D.T., Chen, T.H., 2009. *Chem. Commun.* 1742.
- Shi, J., Yan, R., Zhu, Y., Zhang, X., 2003. *Tanlanta* 6, 157.
- Shionoya, S., Yen, W.M., 1999. *Phosphor Handbook*. CRC Press, Boca Raton.
- Shlyakhtina, A.V., Abrantes, J.C.C., Larina, L.L., Shcherbakova, L.G., 2005. *Solid State Ionics* 176, 1653.
- Sholkapper, T.Z., Kurokawa, H., Jacobson, C.P., Visco, S.J., De Jonghe, L.C., 2007. *Nano Lett.* 7, 2136.
- Si, R., Flytzani-Stephanopoulos, M., 2008. *Angew. Chem. Int. Ed.* 47, 2884.
- Si, P.Z., Skorvanek, I., Kovac, J., Geng, D.Y., Zhao, X.G., Zhang, Z.D., 2003. *J. Appl. Phys.* 94, 6779.
- Si, R., Zhang, Y.W., Li, S.J., Lin, B.X., Yan, C.H., 2004. *J. Phys. Chem. B* 108, 12481.
- Si, R., Zhang, Y.W., You, L.P., Yan, C.H., 2005. *Angew. Chem. Int. Ed.* 44, 3256.
- Si, R., Zhang, Y.W., Zhou, H.P., Sun, L.D., Yan, C.H., 2007. *Chem. Mater.* 19, 18.
- Sivakumar, M., Gedanken, A., Zhong, W., Jiang, Y.H., Du, Y.W., Brukental, I., Bhattacharya, D., Yeshurun, Y., Nowik, I., 2004a. *J. Mater. Chem.* 14, 764.
- Sivakumar, M., Gedanken, A., Bhattacharya, D., Brukental, I., Yeshurun, Y., Zhong, W., Du, Y.W., Felner, I., Nowik, I., 2004b. *Chem. Mater.* 16, 3623.
- Sivakumar, S., van Veggel, F.C.J.M., Raudsepp, M., 2005. *J. Am. Chem. Soc.* 127, 12464.
- Sivakumar, S., Diamente, P.R., van Veggel, F.C.J.M., 2006. *Chem. Eur. J.* 12, 5878.
- Sivakumar, S., van Veggel, F.C.J.M., May, P.S., 2007a. *J. Am. Chem. Soc.* 129, 620.
- Sivakumar, S., van Veggel, F.C.J.M., Raudsepp, M., 2007b. *Chem. Phys. Chem.* 8, 1677.
- Soderlind, F., Fortin, M.A., Petoral Jr., R.M., Klasson, A., Veres, T., Engstrom, M., Uvadal, K., Kall, P.-O., 2008. *Nanotechnology* 19, 085608.
- Sommerdijk, J.L., Bril, A., 1974. *Philips Tech. Rev.* 34, 1.
- Song, H.W., Yu, L.X., Lu, S.Z., Wang, T., Liu, Z.X., Yang, L.M., 2004. *Appl. Phys. Lett.* 85, 470.
- Song, P., Hu, J.F., Qin, H.W., Zhang, L., Xue, T.F., Liu, X., Huang, S.X., Jiang, M.H., 2005. *J. Sol-Gel Sci. Technol.* 35, 65.
- Song, H.W., Yu, H.Q., Pan, G.H., Bai, X., Dong, B., Zhang, X.T., Hark, S.K., 2008. *Chem. Mater.* 20, 4762.
- Spanier, J.E., Robinson, R.D., Zheng, F., Chan, S.W., Herman, I.P., 2001. *Phys. Rev. B* 64, 245407.
- Stark, W.J., Madler, L., Maciejewski, M., Pratsinis, S.E., Baiker, A., 2003. *Chem. Commun.* 588.
- Stöber, W., Fink, A., Bohn, E., 1968. *J. Colloid Interface Sci.* 26, 62.
- Stouwdam, J.W., van Veggel, F.C.J.M., 2002. *Nano Lett.* 2, 733.
- Stouwdam, J.W., van Veggel, F.C.J.M., 2004. *Langmuir* 20, 11763.
- Stouwdam, J.W., Hebbink, G.A., Huskens, J., van Veggel, F., 2003. *Chem. Mater.* 15, 4604.
- Stouwdam, J.W., Raudsepp, M., van Veggel, F.C.J.M., 2005. *Langmuir* 21, 7003.
- Su, Y.G., Li, L.P., Li, G.S., 2008. *Cryst. Growth Des.* 8, 2678.
- Subramania, A., Saradha, T., Muzhumathi, S., 2007. *J. Power Sources* 167, 319.

- Sudarsan, V., Sivakumar, S., van Veggel, F.C.J.M., 2005. *Chem. Mater.* 17, 4736.
- Suh, K., Shin, J.H., Seo, S.J., Bae, B.S., 2008. *Appl. Phys. Lett.* 92, 121910.
- Suits, J.C., Argyle, B.E., Freiser, M.J., 1966. *J. Appl. Phys.* 37, 1391.
- Suljoti, E., Nagasono, M., Pietzsch, A., Hickmann, K., Trots, D.M., Haase, M., Wurth, W., Fohlisch, A., 2008. *J. Chem. Phys.* 128, 134706.
- Sun, L.D., Yao, J., Liu, C.H., Liao, C.S., Yan, C.H., 2000. *J. Lumin.* 87–89, 447.
- Sun, L.D., Zhang, Y.X., Zhang, J., Yan, C.H., Liao, C.S., Lu, Y.Q., 2002. *Solid State Commun.* 124, 35.
- Sun, C.W., Li, H., Wang, Z.X., Chen, L.Q., Huang, X.J., 2004. *Chem. Lett.* 33, 662.
- Sun, C.W., Li, H., Zhang, H.R., Wang, Z.X., Chen, L.Q., 2005. *Nanotechnology* 16, 1454.
- Sun, C.W., Sun, J., Xiao, G.L., Zhang, H.R., Qiu, X.P., Li, H., Chen, L.Q., 2006a. *J. Phys. Chem. B* 110, 13445.
- Sun, X.M., Liu, J.F., Li, Y.D., 2006b. *Chem. Eur. J.* 12, 2039.
- Sun, Y.J., Liu, H.J., Wang, X., Kong, X.G., Zhang, H., 2006c. *Chem. Mater.* 18, 2726.
- Sun, X., Zhang, Y.W., Du, Y.P., Yan, Z.G., Si, R., You, L.P., Yan, C.H., 2007. *Chem. Eur. J.* 13, 2320.
- Suyver, J.F., Aebischer, A., Biner, D., Gerner, P., Grimm, J., Heer, S., Krämer, K.W., Reinhard, C., Güdel, H.U., 2005. *Opt. Mater.* 27, 1111.
- Svensson, E.E., Nassos, S., Boutonnet, M., Jaras, S.G., 2006. *Catal. Today* 117, 484.
- Taghavinia, N., Lerondel, G., Makino, H., Yao, T., 2004. *Nanotechnology* 15, 1549.
- Takehita, S., Isobe, T., Niikura, S., 2008. *J. Lumin.* 128, 1515.
- Tamai, H., Ikeya, T., Nishiyama, F., Yasuda, H., Iida, K., Nojima, S., 2000. *J. Mater. Sci.* 35, 4945.
- Tanaka, K., Tatehata, N., Fujita, K., Hirao, K., 2001. *J. Appl. Phys.* 89, 2213.
- Tang, Q., Liu, Z.P., Li, S., Zhang, S.Y., Liu, X.M., Qian, Y.T., 2003. *J. Cryst. Growth* 259, 208.
- Tang, B., Zhuo, L.H., Ge, J.C., Wang, G.L., Shi, Z.Q., Niu, J.Y., 2005a. *Chem. Commun.* 3565.
- Tang, C.C., Bando, Y., Golberg, D., Ma, R.Z., 2005b. *Angew. Chem. Int. Ed.* 44, 576.
- Tang, C.C., Bando, Y., Liu, B.D., Golberg, D., 2005c. *Adv. Mater.* 17, 3005.
- Tans, S.J., Verschueren, A.R.M., Dekker, C., 1998. *Nature* 393, 49.
- Tao, F., Wang, Z.J., Yao, L.Z., Cai, W.L., Li, X.G., 2007a. *Cryst. Growth Des.* 7, 854.
- Tao, F., Wang, Z.J., Yao, L.Z., Cai, W.L., Li, X.G., 2007b. *J. Phys. Chem. C* 111, 3241.
- Tarnuzzer, R.W., Colon, J., Patil, S., Seal, S., 2005. *Nano Lett.* 5, 2573.
- Teng, F., Liang, S., Gaugeu, B., Zong, R., Yao, W., Zhu, Y., 2007. *Catal. Commun.* 8, 1748.
- Thammachart, M., Meeyoo, V., Risksomboon, T., Osuwan, S., 2001. *Catal. Today* 68, 53.
- Thess, A., Lee, R., Nikolaev, P., Dai, H.J., Petit, P., Robert, J., Xu, C.H., Lee, Y.H., Kim, S.G., Rinzler, A.G., Colbert, D.T., Scuseria, G.E., Tomanek, D., Fischer, J.E., Smalley, R.E., 1996. *Science* 273, 483.
- Thirumalai, J., Jagannathan, R., Trivedi, D.C., 2007. *J. Lumin.* 126, 353.
- Thirumalai, J., Chandramohan, R., Divakar, R., Mohandas, E., Sekar, M., Parameswaran, P., 2008a. *Nanotechnology* 19, 395703.
- Thirumalai, J., Chandramohan, R., Sekar, M., Rajachandrasekar, R., 2008b. *J. Nanopart. Res.* 10, 455.
- Thoma, R.E., Weaver, C.F., Friedman, H.A., Insley, H., Harris, L.A., Yakel, H.A., 1961. *J. Phys. Chem.* 65, 1096.
- Thoma, R.E., Insley, H., Hebert, G.M., 1966. *Inorg. Chem.* 5, 1222.
- Thongchant, S., Hasegawa, Y., Wada, Y., Yanagida, S., 2001. *Chem. Lett.* 1274.
- Thongchant, S., Hasegawa, Y., Wada, Y., Yanagida, S., 2003. *J. Phys. Chem. B* 107, 2193.
- Tian, Y., Cao, W.H., Luo, X.X., Fu, Y., 2007. *J. Alloys Compd.* 433, 313.
- Tien-Thao, N., Alamdari, H., Kaliaguine, S., 2008. *J. Solid State Chem.* 181, 2006.
- Tikhomirov, V.K., Furniss, D., Seddona, A.B., Reaney, I.M., Beggiora, M., Ferrari, M., Montagna, M., Rolli, R., 2002. *Appl. Phys. Lett.* 81, 1937.
- Tiwari, A., Rajeev, K.P., 1997. *J. Mater. Sci. Lett.* 16, 521.

- Tong, Y., Lu, L., Yang, X., Wang, X., 2008. *Solid State Sci.* 10, 1379.
- Traina, C.A., Schwartz, J., 2007. *Langmuir* 23, 9158.
- Traversa, E., Sakamoto, M., Sadaoka, Y., 1996. *J. Am. Ceram. Soc.* 79, 1401.
- Traversa, E., Nunziante, P., Sakamoto, M., Sadaoka, Y., Carotta, M.C., Martinelli, G., 1998. *J. Mater. Res.* 13, 1335.
- Traversa, E., Villanti, S., Gusmano, G., Aono, H., Sadaoka, Y., 1999. *J. Am. Ceram. Soc.* 82, 2442.
- Traversa, E., Nunziante, P., Sangaletti, L., Allieri, B., Depero, L.E., Aono, H., Sadaoka, Y., 2000. *J. Am. Ceram. Soc.* 83, 1087.
- Treacy, M.M.J., Ebbesen, T.W., Gibson, J.M., 1996. *Nature* 381, 678.
- Trovarelli, A., 2002. In: Hutchings, G.J. (Ed.), *Catalysis by Ceria and Related Materials*. Catalytic Science Series Imperial College Press, London.
- Trovarelli, A., Zamar, F., Llorca, J., de Leitenburg, C., Dolcetti, G., Kiss, J.T., 1997. *J. Catal.* 169, 490.
- Tsunekawa, S., Ishikawa, K., Li, Z.Q., Kawazoe, Y., Kasuya, A., 2000a. *Phys. Rev. Lett.* 85, 3440.
- Tsunekawa, S., Fukuda, T., Kasuya, A., 2000b. *J. Appl. Phys.* 87, 1318.
- Tukia, M., Holsa, J., Lastusaari, M., Niittykoski, J., 2005. *Opt. Mater.* 27, 1516.
- Uy, D., O'Neill, A.E., Xu, L., Weber, W.H., McCabe, R.W., 2003. *Appl. Catal. B* 41, 269.
- Van der Avert, P., Podkolzin, S.G., Manoilova, O., de Winne, H., Weckhuysen, B.M., 2004. *Chem. Eur. J.* 10, 1637.
- Vasyukiv, O., Sakka, Y., 2005. *Nano Lett.* 5, 2598.
- Vazquez-Vazquez, C., Lopez-Quintela, M.A., 2006. *J. Solid State Chem.* 179, 3229.
- Verdon, E., Devalette, M., Demazeau, G., 1995. *Mater. Lett.* 25, 127.
- Vetrone, F., Boyer, J.C., Capobianco, J.A., Speghini, A., Bettinelli, M., 2004. *Nanotechnology* 15, 75.
- Vila, L.D.D., Stucchi, E.B., Davolos, M.R., 1997. *J. Mater. Chem.* 7, 2113.
- Wachter, P., 1972. *CRC Crit. Rev. Solid State Sci.* 3, 189.
- Wakefield, G., Keron, H.A., Dobson, P.J., Hutchison, J.L., 1999a. *J. Colloid Interf. Sci.* 215, 179.
- Wakefield, G., Keron, H.A., Dobson, P.J., Hutchison, J.L., 1999b. *J. Phys. Chem. Solid.* 60, 503.
- Wakefield, G., Holland, E., Dobson, P.J., Hutchison, J.L., 2001. *Adv. Mater.* 13, 1557.
- Wang, Z.L., Feng, X.D., 2003. *J. Phys. Chem. B.* 107, 13563.
- Wang, X.J., Gao, M.Y., 2006. *J. Mater. Chem.* 16, 1360.
- Wang, X., Li, Y.D., 2002. *Angew. Chem. Int. Ed.* 41, 4790.
- Wang, X., Li, Y.D., 2003a. *Chem. Eur. J.* 9, 5627.
- Wang, H.C., Lu, C.H., 2002. *Mater. Res. Bull.* 37, 783.
- Wang, X., Li, Y.D., 2003b. *Angew. Chem. Int. Ed.* 42, 3497.
- Wang, L.Y., Li, Y.D., 2007. *Chem. Mater.* 19, 727.
- Wang, F., Liu, X.G., 2008. *J. Am. Chem. Soc.* 130, 5642.
- Wang, F., Liu, X.G., 2009. *Chem. Soc. Rev.* 38, 976.
- Wang, Z.L., Song, J.H., 2006. *Science* 312, 242.
- Wang, C.Y., Qian, Y.T., Xie, Y., Wang, C.S., Yang, L., Zhao, G.W., 1996. *Mater. Sci. Eng. B* 39, 160.
- Wang, Y.H., Uheda, K., Takizawa, H., Endo, T., 2001a. *Chem. Lett.* 3, 206.
- Wang, Z.W., Saxena, S.K., Pischedda, V., Liermann, H.P., Zha, C.S., 2001b. *Phys. Rev. B.* 64, 012102.
- Wang, C.Y., Zhang, W.Y., Qian, Y.T., 2002. *Mater. Sci. Eng. B* 94, 170.
- Wang, X., Sun, X.M., Yu, D.P., Zou, B.S., Li, Y.D., 2003. *Adv. Mater.* 15, 1442.
- Wang, F., Fan, X.P., Pi, D.B., Wang, M.Q., 2004a. *J. Solid State Chem.* 177, 3346.
- Wang, H., Meng, Y.Q., Yan, H., 2004b. *Inorg. Chem. Commun.* 7, 553.
- Wang, X., Zhuang, J., Li, Y.D., 2004c. *Eur. J. Inorg. Chem.* 946.
- Wang, Z.W., Zhao, Y.S., Schiferl, D., Zha, C.S., Downs, R.T., 2004d. *Appl. Phys. Lett.* 85, 124.

- Wang, H., Zhao, Z., Xu, C.M., Liu, J., 2005a. *Catal. Lett.* 102, 251.
- Wang, H.Z., Uehara, M., Nakamura, H., Miyazaki, M., Maeda, H., 2005b. *Adv. Mater.* 17, 2506.
- Wang, M., Huang, Q.L., Hong, J.M., Wu, W.H., Yu, Z., Chen, X.T., Xue, Z.L., 2005c. *Solid State Commun.* 136, 210.
- Wang, X., Zhuang, J., Peng, Q., Li, Y.D., 2005d. *Nature* 437, 121.
- Wang, D., Chu, X.F., Gong, M.L., 2006a. *Nanotechnology* 17, 5501.
- Wang, F., Zhang, Y., Fan, X.P., Wang, M.Q., 2006b. *J. Mater. Chem.* 16, 1031.
- Wang, F., Zhang, Y., Fan, X.P., Wang, M.Q., 2006c. *Nanotechnology* 17, 1527.
- Wang, H., Yu, M., Lin, C.K., Lin, J., 2006d. *J. Colloid Interface Sci.* 300, 176.
- Wang, M., Huang, Q.L., Hong, J.M., Chen, X.T., Xue, Z.L., 2006e. *Cryst. Growth Des.* 6, 2169.
- Wang, M., Huang, Q.L., Hong, J.M., Chen, X.T., Xue, Z.L., 2006f. *Cryst. Growth Des.* 6, 1972.
- Wang, S., Zhou, G., Lu, M., Zhou, Y., Wang, S., Yang, Z., 2006g. *J. Am. Ceram. Soc.* 89, 2956.
- Wang, X., Zhuang, J., Peng, Q., Li, Y.D., 2006h. *Inorg. Chem.* 45, 6661.
- Wang, Y.P., Yang, X., Lu, L., Wang, X., 2006i. *Thermochim. Acta* 443, 225.
- Wang, Z.L., Quan, Z.W., Jia, P.Y., Lin, C.K., Luo, Y., Chen, Y., Fang, J., Zhou, W., O'Connor, C.J., Lin, J., 2006j. *Chem. Mater.* 18, 2030.
- Wang, Y., Qin, W.P., Zhang, J.S., Cao, C.Y., Zhang, J.S., Jin, Y., Zhu, P.F., Wei, G.D., Wang, G.F., Wang, L.L., 2007. *J. Solid State Chem.* 180, 2268.
- Wang, J.C., Liu, Q., Liu, Q.F., 2007a. *Opt. Mater.* 29, 593.
- Wang, J.S., Hu, J., Tang, D.H., Liu, X.H., Zhen, Z., 2007b. *J. Mater. Chem.* 17, 1597.
- Wang, L.Y., Li, P., Li, Y.D., 2007c. *Adv. Mater.* 19, 3304.
- Wang, N., Zhang, Q.F., Chen, W., 2007d. *Cryst. Res. Technol.* 42, 138.
- Wang, S.M., Xiu, Z.L., Lu, M.K., Zhang, A.Y., Zhou, Y.Y., Yang, Z.S., 2007e. *Mater. Sci. Eng. B* 143, 90.
- Wang, Z.Y., Zhao, Z.B., Qiu, J.S., 2007f. *Chem. Mater.* 19, 3364.
- Wang, D.S., Xie, T., Peng, Q., Zhang, S.Y., Chen, J., Li, Y.D., 2008a. *Chem. Eur. J.* 14, 2507.
- Wang, F., Xue, X.J., Liu, X.G., 2008b. *Angew. Chem. Int. Ed.* 47, 906.
- Wang, G.F., Qin, W.P., Zhang, J.S., Cao, C.Y., Wang, L.L., Wei, G.D., Zhu, P.F., Kim, R., 2008c. *J. Phys. Chem. C* 112, 12161.
- Wang, L., Qian, B.B., Chen, H.Q., Liu, Y., Liang, A., 2008d. *Chem. Lett.* 37, 402.
- Wang, R., Crozier, P.A., Sharma, R., Adams, J.B., 2008e. *Nano Lett.* 8, 962.
- Wang, Y., Ren, J., Wang, Y., Zhang, F., Liu, X., Guo, Y., Lu, G., 2008f. *J. Phys. Chem. C* 112, 15293.
- Wang, L., Li, P., Wang, L.Y., 2009a. *Luminescence* 24, 39.
- Wang, L.Y., Yang, Z.H., Zhang, Y., Wang, L., 2009b. *J. Phys. Chem. C* 113, 3955.
- Waterhouse, G.I.N., Waterland, M.R., 2007. *Polyhedron* 26, 356.
- Waterhouse, G.I.N., Metson, J.B., Idriss, H., Sun-Waterhouse, D., 2008. *Chem. Mater.* 20, 1183.
- Weckhuysen, B.M., Rosynek, M.P., Lunsford, J.H., 1999. *Phys. Chem. Chem. Phys.* 1, 3157.
- Wegh, R.T., Donker, H., Oskam, K.D., Meijerink, A., 1999. *Science* 283, 663.
- Wei, Z.G., Sun, L.D., Liao, C.S., Jiang, X.C., Yan, C.H., 2002a. *J. Mater. Chem.* 12, 3665.
- Wei, Z.G., Sun, L.D., Liao, C.S., Yan, C.H., 2002b. *Appl. Phys. Lett.* 80, 1447.
- Wei, Z.G., Sun, L.D., Liao, C.S., Yin, J.L., Jiang, X.C., Yan, C.H., Lu, S.Z., 2002c. *J. Phys. Chem. B* 106, 10610.
- Wei, Z.G., Sun, L.D., Jiang, X.C., Liao, C.S., Yan, C.H., 2003a. *Chem. Mater.* 15, 3011.
- Wei, Z.G., Sun, L.D., Liao, C.S., Jiang, X.C., Yan, C.H., Tao, Y., Hou, X.Y., Ju, X., 2003b. *J. Appl. Phys.* 93, 9783.
- Wei, Y., Lu, F.Q., Zhang, X.R., Chen, D.P., 2007. *Mater. Lett.* 61, 1337.
- Wells, A.F., 1962. *Structural Inorganic Chemistry*. Clarendon, Oxford, p. 391.
- Wen, F., Li, W., Liu, Z., Kim, T., Yoo, K., Shin, S., Moon, J.H., Kim, J.H., 2005. *Solid State Commun.* 133, 417.

- Westbrook, C., 1999. Handbook of MRI Technique. Blackwell Science, Oxford.
- White, B., Chatterjee, S., Macam, E., Wachsmann, E., 2008. *J. Am. Ceram. Soc.* 91, 2024.
- Wickleder, M.S., 2002. *Chem. Rev.* 102, 2011.
- Williams, D.K., Yuan, H.B., Tissue, B.M., 1999. *J. Lumin.* 83–84, 297.
- Wright, C.S., Walton, R.I., Thompson, D., Fisher, J., Ashbrook, S.E., 2007. *Adv. Mater.* 19, 4500.
- Wu, L.M., Seo, D.K., 2004. *J. Am. Chem. Soc.* 126, 4676.
- Wu, J.H., Yan, B., 2008. *J. Alloys Compd.* 455, 485.
- Wu, H., Xu, H.F., Su, Q., Chen, T.H., Wu, M.M., 2003a. *J. Mater. Chem.* 13, 1223.
- Wu, L.M., Sharma, R., Seo, D.K., 2003b. *Inorg. Chem.* 42, 5798.
- Wu, G.S., Zhang, L.D., Cheng, B.C., Xie, T., Yuan, X.Y., 2004. *J. Am. Chem. Soc.* 126, 5976.
- Wu, X.C., Tao, Y.R., Dong, L., Zhu, J.J., Hu, Z., 2005. *J. Phys. Chem. B* 109, 11544.
- Wu, X.C., Tao, Y.R., Mao, C.J., Liu, D.J., Mao, Y.Q., 2006a. *J. Cryst. Growth* 290, 207.
- Wu, X.C., Tao, Y.R., Song, C.Y., Mao, C.J., Dong, L., Zhu, J.J., 2006b. *J. Phys. Chem. B* 15791.
- Wu, H., Engelhard, M.H., Wang, J., Fisher, D.R., Darrell, R., Lin, Y.H., 2008a. *J. Mater. Chem.* 18, 1779.
- Wu, Q., Chen, Y., Xiao, P., Zhang, F., Wang, X.Z., Hu, Z., 2008b. *J. Phys. Chem. C* 112, 9604.
- Xia, B., Lenggono, I.W., Okuyama, K., 2001. *J. Mater. Chem.* 11, 2925.
- Xia, G., Zhou, S., Zhang, J., Wang, S., Liu, Y., Xu, J., 2005. *J. Cryst. Growth* 283, 257.
- Xiao, S.G., Yang, X.L., Ding, J.W., Yan, X.H., 2007. *J. Phys. Chem. C* 111, 8161.
- Xing, Y., Li, M., Davis, S.A., Mann, S., 2006. *J. Phys. Chem. B* 110, 1111.
- Xiu, Z.L., Yang, Z.S., Lu, M.K., Liu, S.W., Zhang, H.P., Zhou, G.J., 2006. *Opt. Mater.* 29, 431.
- Xu, G.X., 2005. Rare Earths, 2nd ed. Metallurgy Industry Press, Beijing.
- Xu, A.W., Fang, Y.P., You, L.P., Liu, H.Q., 2003. *J. Am. Chem. Soc.* 125, 1494.
- Xu, H.Y., Wang, H., Meng, Y.Q., Yan, H., 2004. *Solid State Commun.* 130, 465.
- Xu, H.Y., Wang, H., Yan, H., 2007. *J. Hazard. Mater.* 144, 82.
- Xu, H., Hu, X.L., Zhang, L.Z., 2008. *Cryst. Growth Des.* 8, 2061.
- Xuan, Y.L., Hu, J., Xu, K.L., Hou, X.D., Lv, Y., 2009. *Sens. Act. B* 136, 218.
- Yabe, S., Sato, T., 2003. *J. Solid State Chem.* 171, 7.
- Yada, M., Mihara, M., Mouri, S., Kuroki, M., Kijima, T., 2002. *Adv. Mater.* 14, 309.
- Yada, M., Taniguchi, C., Torikai, T., Watari, T., Furuta, S., Katsuki, H., 2004. *Adv. Mater.* 16, 1448.
- Yan, R.X., Li, Y.D., 2005. *Adv. Funct. Mater.* 15, 763.
- Yan, C.H., Sun, L.D., Liao, C.S., Zhang, Y.X., Lu, Y.Q., Huang, S.H., Lu, S.Z., 2003a. *Appl. Phys. Lett.* 82, 3511.
- Yan, Z.C., Huang, Y.H., Zhang, Y., Okumura, H., Xiao, J.Q., Stoyanov, S., Skumryev, V., Hadjipanayis, G.C., 2003b. *Phys. Rev. B* 67, 054403, 1.
- Yan, Z.G., Zhang, Y.W., You, L.P., Si, R., Yan, C.H., 2004. *J. Cryst. Growth* 262, 408.
- Yan, R.X., Sun, X.M., Wang, X., Peng, Q., Li, Y.D., 2005. *Chem. Eur. J.* 11, 2183.
- Yan, W.F., Brown, S., Pan, Z.W., Mahurin, S.M., Overbury, S.H., Dai, S., 2006. *Angew. Chem. Int. Ed.* 45, 3614.
- Yan, L., Yu, R.B., Chen, J., Xing, X.R., 2008a. *Cryst. Growth Des.* 8, 1474.
- Yan, L., Yu, R.B., Liu, G.R., Xing, X.R., 2008b. *Scr. Mater.* 58, 707.
- Yanagida, T., Kanki, T., Vilquin, B., Tanaka, H., Kawai, T., 2004. *Phys. Rev. B* 70, 184437.
- Yanes, A.C., Del Castillo, J., Méndez-Ramos, J., Rodríguez, V.D., Torres, M.E., Arbiol, J., 2007. *Opt. Mater.* 29, 999.
- Yang, S.W., Gao, L., 2006. *J. Am. Chem. Soc.* 128, 9330.
- Yang, Z., Ren, M., Lin, J.H., Su, M.Z., Tao, Y., Wang, W., 2000. *Chem. J. Chin. Univ.* 21, 1339.
- Yang, H.S., Lee, H.K., Holloway, P.H., 2005a. *Nanotechnology* 16, 2794.
- Yang, Z., Huang, Y., Dong, B., Li, H.L., 2005b. *J. Solid State Chem.* 178, 1157.
- Yang, Z., Huang, Y., Dong, B., Li, H.L., 2006. *Mater. Res. Bull.* 41, 274.
- Yang, J., Quan, Z.W., Kong, D.Y., Liu, X.M., Lin, J., 2007a. *Cryst. Growth Des.* 7, 730.

- Yang, P.P., Huang, S.S., Kong, D.Y., Lin, J., Fu, H.G., 2007b. *Inorg. Chem.* 46, 3203.
- Yang, P.P., Quan, Z.W., Lu, L.L., Huang, S.S., Lin, J., Fu, H.G., 2007c. *Nanotechnology* 18, 235703.
- Yang, J., Li, C.X., Zhang, X.M., Quan, Z.W., Zhang, C.M., Li, H.Y., Lin, J., 2008a. *Chem. Eur. J.* 14, 4336.
- Yang, J., Zhang, C.M., Li, C.X., Yu, Y.N., Lin, J., 2008b. *Inorg. Chem.* 47, 7262.
- Yang, X.L., Xiao, S.G., Ding, J.W., Yan, X.H., 2008c. *J. Appl. Phys.* 103, 093101.
- Yang, J., Zhang, C.M., Peng, C., Li, C.X., Wang, L.L., Chai, R.T., Lin, J., 2009. *Chem. Eur. J.* 15, 4649.
- Ye, Q., Gao, Q., Zhang, X.R., Xu, B.Q., 2006. *Catal. Commun.* 7, 589.
- Ye, S.B., Zhu, J., Luo, J., Chen, X., Lakshminarayana, G., Qiu, J.R., 2008. *Opt. Express* 16, 8989.
- Yi, G.S., Chow, G.M., 2005. *J. Mater. Chem.* 15, 4460.
- Yi, G.S., Chow, G.M., 2006. *Adv. Funct. Mater.* 16, 2324.
- Yi, G.S., Chow, G.M., 2007. *Chem. Mater.* 19, 341.
- Yi, G.S., Lu, H.C., Zhao, S.Y., Ge, Y., Yang, W.J., Chen, D.P., Guo, L.H., 2004. *Nano Lett.* 4, 2191.
- Yi, N., Cao, Y., Su, Y., Dai, W.L., He, H.Y., Fan, K.N., 2005. *J. Catal.* 230, 249.
- You, F.T., Huang, S.H., Meng, C.X., Wang, D.W., Xu, J.H., Huang, Y., Zhang, G.B., 2007. *J. Lumin.* 122, 58.
- Yu, R., De Jonghe, L.C., 2007. *J. Phys. Chem. C* 111, 11003.
- Yu, S.H., Han, Z.H., Yang, J., Zhao, H.Q., Yang, R.Y., Xie, Y., Qian, Y.T., Zhang, Y.H., 1999. *Chem. Mater.* 11, 192.
- Yu, M., Lin, J., Wang, Z., Fu, J., Wang, S., Zhang, H.J., Han, Y.C., 2002. *Chem. Mater.* 14, 2224.
- Yu, M., Lin, J., Fu, J., Han, Y.C., 2003. *Chem. Phys. Lett.* 371, 178.
- Yu, L.X., Song, H.W., Lu, S.Z., Liu, Z.X., Yang, L.M., 2004a. *Chem. Phys. Lett.* 399, 384.
- Yu, L.X., Song, H.W., Lu, S.Z., Liu, Z.X., Yang, L.M., Kong, X.G., 2004b. *J. Phys. Chem. B* 108, 16697.
- Yu, L.X., Song, H.W., Liu, Z.X., Yang, L.M., Zheng, S., 2005a. *J. Phys. Chem. B* 109, 11450.
- Yu, M., Lin, J., Fang, J., 2005b. *Chem. Mater.* 17, 1783.
- Yu, T.K., Joo, J., Park, Y.I., Hyeon, T., 2005c. *Angew. Chem. Int. Ed.* 44, 7411.
- Yu, M., Wang, H., Lin, C.K., Li, G.Z., Lin, J., 2006a. *Nanotechnology* 17, 3245.
- Yu, T.K., Joo, J., Park, Y.I., Hyeon, T., 2006b. *J. Am. Chem. Soc.* 128, 1786.
- Yu, R.B., Yu, K.H., Wei, W., Xu, X.X., Qiu, X.M., Liu, S.Y., Huang, W., Tang, G., Ford, H., Peng, B., 2007. *Adv. Mater.* 19, 838.
- Yu, C.C., Yu, M., Li, C.X., Liu, X.M., Yang, J., Yang, P.P., Lin, J., 2008a. *J. Solid State Chem.* 182, 339.
- Yu, X.F., Chen, L.D., Li, M., Xie, M.Y., Zhou, L., Li, Y., Wang, Q.Q., 2008b. *Adv. Mater.* 20, 4118.
- Yuan, Q., Liu, Q., Song, W.G., Feng, W., Pu, W.L., Sun, L.D., Zhang, Y.W., Yan, C.H., 2007. *J. Am. Chem. Soc.* 129, 6698.
- Yuan, Q., Duan, H.H., Li, L.L., Sun, L.D., Zhang, Y.W., Yan, C.H., 2009. *J. Colloid. Interf. Sci.* 335, 151.
- Yuasa, M., Shimano, K., Teraoka, Y., Yamazoe, N., 2007. *Catal. Today* 126, 313.
- Yusupov, R.V., Kabanov, V., Mihailovic, D., Conder, K., Keller, H., Müller, K.A., 2007a. *Phys. C* 460-462, 801.
- Yusupov, R. V., Kabanov, V. V., Mihailovic, D., Conder, K., Müller, K. A., Keller, H., 2007b. *Phys. Rev.* 76, 024428.
- Zarur, A.J., Ying, J.Y., 2000. *Nature* 403, 65.
- Zeng, J.H., Su, J., Li, Z.H., Yan, R.X., Li, Y.D., 2005. *Adv. Mater.* 17, 2119.
- Zeng, J., Wang, H., Zhang, Y.C., Zhu, M.K., Yan, H., 2007. *J. Phys. Chem. C* 111, 11879.
- Zeng, J.H., Lou, T.J., Wang, Y.F., Guo, J.C., Di, D., Ma, R.L., 2009. *J. Phys. Chem. C* 113, 597.
- Zhang, Y.J., Guan, H.M., 2003. *J. Cryst. Growth* 256, 156.

- Zhang, Y., Li, Y.D., 2004. *J. Alloys Compd.* 384, 88.
- Zhang, J., Lin, J., 2004. *J. Cryst. Growth* 271, 207.
- Zhang, Y., Lu, M.H., 2007. *Nanotechnology* 18, 275603.
- Zhang, F., Zhao, D.Y., 2009. *ACS Nano* 3, 159.
- Zhang, Z.F., Liu, W.M., Xue, Q.J., 1998. *Wear* 218, 139.
- Zhang, Z.F., Liu, W.M., Xue, Q.J., 2001a. *Wear* 248, 48.
- Zhang, Z.F., Yu, L.G., Liu, W.M., Xue, Q.J., 2001b. *Tribol. Int.* 34, 83.
- Zhang, F., Chan, S.W., Spanier, J.E., Apak, E., Jin, Q., Robinson, R.D., Herman, I.P., 2002a. *Appl. Phys. Lett.* 80, 127.
- Zhang, Q.Y., Pita, K., Ye, W., Que, W.X., Kam, C.H., 2002b. *Chem. Phys. Lett.* 356, 161.
- Zhang, Y.W., Si, R., Liao, C.S., Yan, C.H., 2003a. *J. Phys. Chem. B* 107, 10159.
- Zhang, Y.W., Yan, Z.G., You, L.P., Si, R., Yan, C.H., 2003b. *Eur. J. Inorg. Chem.* 4099.
- Zhang, H.W., Fu, X.Y., Niu, S.Y., Sun, G.Q., Xin, Q., 2004a. *J. Solid State Chem.* 177, 2649.
- Zhang, H.W., Fu, X.Y., Niu, S.Y., Sun, G.Q., Xin, Q., 2004b. *Solid State Commun.* 132, 527.
- Zhang, M.F., Liu, J.M., Liu, Z.G., 2004c. *Appl. Phys. A* 79, 1753.
- Zhang, L., Hu, J.F., Qin, H.W., Song, P., Jiang, M.H., 2005a. *J. Inorg. Mater.* 20, 1385.
- Zhang, Y., Li, Y.D., Yin, Y.S., 2005b. *J. Alloys Compd.* 400, 222.
- Zhang, Y.W., Liu, J.H., Si, R., Yan, Z.G., Yan, C.H., 2005c. *J. Phys. Chem. B* 109, 18324.
- Zhang, Y.W., Sun, X., Si, R., You, L.P., Yan, C.H., 2005d. *J. Am. Chem. Soc.* 127, 3260.
- Zhang, H.P., Lü, M.K., Xiu, Z.L., Zhou, G.J., Wang, S.F., Zhou, Y.Y., Wang, S.M., 2006a. *Mater. Sci. Eng. B* 130, 151.
- Zhang, R., Villanueva, A., Alamdari, H., Kaliaguine, S., 2006b. *J. Mol. Catal. A: Chem.* 258, 22.
- Zhang, D.S., Fu, H.X., Shi, L.Y., Pan, C.S., Li, Q., Chu, Y.L., Yu, W.J., 2007a. *Inorg. Chem.* 46, 2446.
- Zhang, F., Wan, Y., Yu, T., Zhang, F.Q., Shi, Y.F., Xie, S.H., Li, Y.G., Xu, L., Tu, B., Zhao, D.Y., 2007b. *Angew. Chem. Int. Ed.* 46, 7976.
- Zhang, Q.Y., Yang, C.H., Jiang, Z.H., Ji, X.H., 2007c. *Appl. Phys. Lett.* 90, 061914.
- Zhang, Y.X., Guo, J., White, T., Thatt, T., Tan, Y., Xu, R., 2007d. *J. Phys. Chem. C* 111, 7893.
- Zhang, Z., Hu, C.G., Xiong, Y.F., Yang, R., Wang, Z.L., 2007e. *Nanotechnology* 18.
- Zhang, M.F., Fan, H., Xi, B.J., Wang, X.Y., Dong, C., Qian, Y.T., 2007f. *J. Phys. Chem. C* 111, 6652.
- Zhang, C., Chen, J., Zhou, Y.C., Li, D.Q., 2008a. *J. Phys. Chem. C* 112, 10083.
- Zhang, D.S., Huang, L., Zhang, J.P., Shi, L.Y., 2008b. *J. Mater. Sci.* 43, 5647.
- Zhang, F., Wan, Y., Shi, Y.F., Tu, B., Zhao, D.Y., 2008c. *Chem. Mater.* 20, 3778.
- Zhang, H.W., Fu, X.Y., Niu, S.Y., Xin, Q., 2008d. *J. Alloys Compd.* 457, 61.
- Zhang, K., Hu, W., Wu, Y., Liu, H., 2008e. *Physics B* 403, 1678.
- Zhang, L., Zhong, H., Zhang, W., Lu, L., Yang, X., Wang, X., 2008f. *J. Alloys Compd.* 463, 466.
- Zhang, M.F., Shi, S.J., Meng, J.X., Wang, X.Q., Fan, H., Zhu, Y.Y., Wang, X.Y., Qian, Y.T., 2008g. *J. Phys. Chem. C* 112, 2825.
- Zhang, W., Yang, T., Zhuang, X.M., Guo, Z.Y., Jiao, K., 2009. *Biosens. Bioelectron.* 24, 2417.
- Zhao, F., Gao, S., 2008. *J. Mater. Chem.* 18, 949.
- Zhao, F., Sun, H.L., Gao, S., Su, G., 2005. *J. Mater. Chem.* 15, 4209.
- Zhao, F., Sun, H.L., Su, G., Gao, S., 2006a. *Small* 2, 244.
- Zhao, F., Yuan, M., Zhang, W., Gao, S., 2006b. *J. Am. Chem. Soc.* 128, 11758.
- Zharkouskaya, A., Feldmann, C., Trampert, K., Heering, W., Lemmer, U., 2008. *Eur. J. Inorg. Chem.* 873.
- Zhou, X.D., Huebner, W., 2001. *Appl. Phys. Lett.* 79, 3512.
- Zhou, J.F., Wu, Z.S., Zhang, Z.J., Liu, W.M., Dang, H.X., 2001. *Wear* 249, 333.
- Zhou, Y.H., Lin, J., Wang, S.B., 2003. *J. Solid State Chem.* 171, 391.
- Zhou, K.B., Wang, X., Sun, X.M., Peng, Q., Li, Y.D., 2005. *J. Catal.* 229, 206.
- Zhou, K.B., Yang, Z.Q., Yang, S., 2007a. *Chem. Mater.* 19, 1215.
- Zhou, S., Shi, L., Zhao, J., He, L., Yang, H., Zhang, S., 2007b. *Phys. Rev. B* 76, 172407.

- Zhou, S., Zhao, J., Chu, S., Shi, L., 2007c. *Physics C* 451, 38.
- Zhou, H.P., Zhang, Y.W., Mai, H.X., Sun, X., Liu, Q., Song, W.G., Yan, C.H., 2008a. *Chem. Eur. J.* 14, 3380.
- Zhou, X.F., Zhao, Y., Cao, X.Y., Xue, X.F., Xu, D.P., Jiang, L., Su, W.H., 2008b. *Mater. Lett.* 62, 470.
- Zhou, Z.G., Hu, H., Yang, H., Yi, T., Huang, K.W., Yu, M.X., Li, F.Y., Huang, C.H., 2008c. *Chem. Commun.* 4786.
- Zhu, Y., Tan, R., Yi, T., Gao, S., Yan, C., Cao, L., 2000. *J. Alloys Compd.* 311, 16.
- Zhu, L., Liu, X.M., Liu, X.D., Li, Q., Li, J.Y., Zhang, S.Y., Meng, J., Cao, X.Q., 2006. *Nanotechnology* 17, 4217.
- Zhu, L., Li, J.Y., Li, Q., Liu, X.D., Meng, J., Cao, X.Q., 2007a. *Nanotechnology* 18, 055604.
- Zhu, L., Li, Q., Liu, X.D., Li, J.Y., Zhang, Y.F., Meng, J., Cao, X.Q., 2007b. *J. Phys. Chem. C* 111, 5898.
- Zhu, L., Li, Q., Li, J.Y., Liu, X.D., Meng, J., Cao, X.Q., 2007c. *J. Nanopart. Res.* 9, 261.
- Zhu, L., Liu, X.M., Meng, J., Cao, X.Q., 2007d. *Cryst. Growth Des.* 7, 2505.
- Zhu, G.Q., Liu, P., Liu, Y., Miao, H.Y., Zhou, J.P., 2008a. *J. Am. Ceram. Soc.* 91, 3423.
- Zhu, H.L., Yang, H., Jin, D.L., Wang, Z.K., Gu, X.Y., Yao, X.H., Yao, K.H., 2008b. *J. Nanopart. Res.* 10, 1149.
- Zhu, J.X., Gui, Z., Ding, Y.Y., 2008c. *Mater. Lett.* 62, 2373.
- Zhu, X.X., Zhang, Q.H., Li, Y.G., Wang, H.Z., 2008d. *J. Mater. Chem.* 18, 5060.
- Zhuang, J.L., Liang, L.F., Sung, H.H.Y., Yang, X.F., Wu, M.M., Williams, I.D., Feng, S.H., Su, Q., 2007. *Inorg. Chem.* 46, 5404.
- Zhuang, Z., Wang, X.P., Sun, A.H., Li, Y., Fang, Q.F., 2008. *J. Sol-Gel Sci. Technol.* 48, 315.
- Zhuravleva, N.G., Eliseev, A.A., Sapoletova, N.A., Lukashin, A.V., Kynast, U., Tretyakov Yu, D., 2005. *Mater. Sci. Eng. C* 25, 549.
- Zijlmans, H., Bonnet, J., Burton, J., Kardos, K., Vail, T., Niedbala, R.S., Tanke, H.J., 1999. *Anal. Biochem.* 267, 30.
- Zollfrank, C., Scheel, H., Brungs, S., Greil, P., 2008. *Cryst. Growth Des.* 8, 766.

AUTHOR INDEX

- Aarthi, T., see Mahata, P. 400
 Abad, A. 304
 Abboudi, M., see Bang, J. 443, 448
 Abdul-Sada, A.K., see Taylor, R. 105–106
 Abrams, B., see Bang, J. 443, 448
 Abrams, W.R., see Corstjens, P.L.A.M. 440, 446–447
 Abrantes, J.C.C., see Shlyakhtina, A.V. 390
 Abrefah, J. 105
 Abril, M., see Marrero-Lopez, D. 393
 Achiba, K., see Suzuki, T. 126
 Achiba, Y., see Akasaka, T. 115–116, 146
 Achiba, Y., see Hino, S. 122, 128, 133, 140
 Achiba, Y., see Kato, T. 116, 122, 124–125
 Achiba, Y., see Kawata, H. 119
 Achiba, Y., see Kessler, B. 132, 140
 Achiba, Y., see Kikuchi, K. 106, 109, 111, 115–116, 124, 128, 133, 144
 Achiba, Y., see Kobayashi, K. 114–115
 Achiba, Y., see Miyake, Y. 115
 Achiba, Y., see Poirier, M.D. 122, 132, 138, 140
 Achiba, Y., see Sato, W. 116
 Achiba, Y., see Suematsu, H. 114, 119
 Achiba, Y., see Suzuki, S. 102, 109, 122, 125
 Achiba, Y., see Suzuki, T. 116, 126, 128
 Achiba, Y., see Wakabayashi, T. 102–103, 109
 Adachi, G. 104
 Adachi, G., see Masui, T. 283, 289
 Adachi, T.A. 438
 Adachi, T.A., see Hasegawa, Y. 438
 Adam, S., see K mpe, K. 340, 343
 Adams, J.B., see Wang, R. 296
 Adelman, P., see Buerk, M. 134
 Adolphe, C., see Basancon, P. 260
 Adolphe, C., see Carr , D. 168–169, 197
 Adschiri, T. 283
 Adschiri, T., see Kaneko, K. 283, 383
 Aebischer, A. 428
 Aebischer, A., see Suyver, J.F. 426
 Aeppli, G., see Ghosh, S. 421
 Afzaal, M., see Hasegawa, Y. 437–438
 Aghasyan, M., see Gnanasekar, K.I. 397
 Aguilar-Guerrero, V. 303
 Ahn, B.Y. 346
 Ahniyaz, A. 291
 Aitken, J.A., see Iyer, R.G. 211, 226
 Ajie, H. 106
 Akachi, M., see Ito, Y. 121, 128, 132, 141
 Akasaka, T. 115–116, 146
 Akasaka, T., see Iiduka, Y. 117–118, 120, 137
 Akasaka, T., see Kato, T. 122, 124, 146
 Akasaka, T., see Kikuchi, K. 128, 130
 Akasaka, T., see Kobayashi, K. 115, 144
 Akasaka, T., see Nagase, S. 111–113, 115, 117, 122, 128, 138
 Akasaka, T., see Suzuki, T. 146
 Akasaka, T., see Yamamoto, K. 105–107, 123, 128–129
 Akdeniz, Z. 404–405
 Akeroyd, F.M. 3, 31
 Akiyama, K. 144
 Akiyama, K., see Kikuchi, K. 128, 130
 Alamdari, H., see Royer, S. 395
 Alamdari, H., see Tien-Thao, N. 395
 Alamdari, H., see Zhang, R. 395
 Aldorf, H.E. 415
 Aleandri, L.E. 170
 Alexandra, G., see Patra, C.R. 334
 Alexandrou, A., see Beaurepaire, E. 377–378
 Alexandrou, A., see Casanova, D. 378–379
 Alexandrou, A., see Giaume, D. 377, 379
 Alford, J.M., see Averitt, R.D. 105
 Alford, J.M., see Cagle, D.W. 144–145
 Alford, J.M., see Chai, Y. 97–99, 101, 105–106, 109, 114, 141
 Alford, J.M., see Ding, X. 116, 130, 132
 Alford, J.M., see Wang, L.S. 100, 111, 142
 Alford, M.J., see Guo, T. 100
 Alidzhanov, M.A., see Aliev, O.M. 169–170, 202
 Aliev, O.M. 169–170, 202
 Alikina, G.M., see Frolova-Borchert, Y.V. 402
 Alivisatos, A.P. 279
 Alivisatos, A.P., see Bruchez, M. 279
 Alivov, Y.I., see Ozgur, U. 279
 Allaf, K., see Rouanet, A. 331
 Allemand, P.M. 121
 Allen, K. 140
 Allenspach, P., see Lin, J.H. 379, 381

- Allieri, B., see Traversa, E. 400
 Almela, C., see Abad, A. 304
 Althues, H. 362
 Alvarez, M.M. 99, 110, 115–116
 Alvarez, M.M., see Allemand, P.M. 121
 Alvarez, M.M., see Gillan, E. 100
 Alvarez, M.M., see Yeretian, C. 99, 105, 109
 Ambe, F., see Sato, W. 116
 Ambruster, J.F., see Buerk, M. 134
 Amirov, A.S. 170, 205
 An, G.M., see Miao, Z.J. 406
 Ananias, D. 386
 Anderson, J., see Glaspell, G. 323
 Anderson, M.R. 116, 124, 126
 Anderson, P.L., see Maensiri, S. 285
 Ando, Y., see Bandow, S. 104
 Ando, Y., see Kira, H. 402
 Ando, Y., see Shinohara, H. 99–100, 105–107, 112–113, 116, 118, 122, 124, 138, 145
 Andreoni, W. 111–112, 115
 Andreoni, W., see Laasonen, K. 111–112, 138
 Andreoni, W., see Poirier, M.D. 122, 132, 138, 140
 Ansari, A.A. 306, 406
 Anselmi-Tamburini, U. 299
 Antic-Fidancev, E., see Hölsä J. 418
 Antonietti, M., see Deshpande, A.S. 295
 Antonietti, M., see Pinna, N. 313–314
 Anz, S.J., see Allemand, P.M. 121
 Aoki, M., see Hino, S. 114, 122, 133
 Aono, H. 400
 Aono, H., see Sadaoka, Y. 400
 Aono, H., see Traversa, E. 400
 Apak, E., see Zhang, F. 283
 Arai, K., see Adschiri, T. 283
 Arbiol, J., see Yanes, A.C. 415
 Arbus, A., see Chadeyron, G. 379
 Argyle, B.E., see Suits, J.C. 433
 Armelao, L. 399
 Armelao, L., see Krishnan, V. 399
 Armelao, L., see Losurdo, M. 399
 Armitage, R. 448
 Arney, D. 392
 Arnold, C. 54
 Arya, S.K., see Saha, S. 306
 Asai, K., see Sato, W. 116
 Asati, A., see Perez, J.M. 308
 Aschehoug, P., see Buissette, V. 375
 Ashbrook, S.E., see Wright, C.S. 295
 Assaoudi, H. 331
 Au, C.T. 418
 Audier, M., see Dezanneau, G. 396
 Auzel, F. 405
 Averitt, R.D. 105
 Avgouropoulos, G. 302
 Avrutin, V., see Ozgur, U. 279
 Awaga, K., see Ito, Y. 121, 128, 132, 141
 Ayuela, A., see Seifert, G. 122
 Azad, S. 299
 Azfer, A., see Niu, J.L. 308
 Azzoni, C.B., see Malavasi, L. 397
 Babu, S. 310
 Backhaus-Ricoult, M., see Maurel, F. 329
 Bae, B.S., see Suh, K. 386
 Baer, D.R., see Karakoti, A.S. 285, 297
 Bai, X., see Dong, B. 426
 Bai, X., see Pan, G.H. 359, 377, 381, 384
 Bai, X., see Qin, R.F. 407, 409–410
 Baiker, A., see Stark, W.J. 295
 Bakakin, V.V. 163
 Ballato, J., see DiMaio, J.R. 415
 Ballato, J., see Kumar, G.A. 407
 Balooch, M., see Abrefah, J. 105
 Bando, Y., see Tang, C.C. 286, 330–331, 334
 Bandow, S. 104, 123, 125
 Bandow, S., see Kato, T. 124
 Bandow, S., see Shinohara, H. 104, 106, 124, 128
 Bang, J. 443, 448
 Bao, F. 416
 Bao, G., see Hu, C.G. 313, 328, 407
 Barbier, J. Jr., see Royer, S. 395
 Barnaba, M., see Kessler, B. 132, 140
 Barnett, S.A., see Murray, E.P. 299
 Barnier, S., see Bugli, G. 163, 176
 Barreca, D. 305, 418
 Barreca, D., see Armelao, L. 399
 Barreca, D., see Losurdo, M. 399
 Bartl, A. 122, 128
 Bartl, A., see Dunsch, L. 128, 135, 140
 Bartl, A., see Knorr, S. 122
 Bartl, A., see Seifert, G. 122
 Basancon, P. 260
 Bassett, H. 71, 75
 Basu, S., see Patra, C.R. 350
 Batek, A., see Brauner, B. 34
 Battell-Quam, M., see Quam, G.N. 2
 Bauer, J.C., see Henkes, A.E. 389
 Baumer, M., see Borchert, Y. 326, 402
 Baur, E. 73
 Bawendi, M.G., see Murray, C.B. 279
 Bayley, T. 68–69

- Bazzi, R. 316
 Bazzi, R., see Louis, C. 312
 Beato, P., see Deshpande, A.S. 295
 Beato, P., see Pinna, N. 313–314
 Beaudry, B.J. 80
 Beaurepaire, E. 377–378
 Beaurepaire, E., see Casanova, D. 379
 Beaurepaire, E., see Giaume, D. 377
 Beck, R.D. 109
 Becker, C.H., see Moro, L. 100
 Bednarkiewicz, A., see Hreniak, D. 388
 Bednarkiewicz, A., see Karbowski, M. 421–422
 Bedworth, P.V., see Scrivens, W.A. 106
 Beganskiene, A., see Cizauskaite, S. 388
 Beggiora, M., see Tikhomirov, V.K. 416
 Behera, S.K. 388
 Behera, S.K., see Sahu, P.K. 388
 Ben-Amotz, D., see Roth, L.M. 109
 Benedicks, C. 51, 53
 Benesovsky, F., see Rieger, W. 175, 179
 Bennett, L.H., see Nelson, J.A. 449
 Bent, H.A. 2, 15, 83
 Benz, M., see Beck, R.D. 109
 Benz, M., see Ruebsam, M. 113, 122
 Berar, J.-F., see Conchon, F. 400
 Berg, O., see Noddack, W. 65
 Berger, D. 395
 Bergey, E.J., see Nyk, M. 430, 432
 Bergstrom, L., see Ahniyaz, A. 291
 Bernal, S. 279, 300
 Bernal, S., see Di Monte, R. 296
 Bernstein, E., see Bazzi, R. 316
 Berquo, T.S., see Mathur, S. 400
 Berret, J.F., see Qi, L. 288
 Bertagnolli, H., see Krishnan, V. 399
 Bertrand-Chadeyron, G., see Boyer, D. 380–381
 Bethune, D.S. 99, 109, 116
 Bethune, D.S., see Hoinkis, M. 123
 Bethune, D.S., see Johnson, R.D. 99, 121
 Bethune, D.S., see Macfarlane, R.M. 116, 132
 Bethune, D.S., see Poirier, M.D. 122, 132, 138, 140
 Bethune, D.S., see van Loosdrecht, P.H.M. 116, 124–125
 Bethune, D.S., see Wilson, R.J. 135
 Bethune, D.S., see Yannoni, C.S. 100, 105, 116, 118, 124
 Bettinelli, M., see Vetrone, F. 322
 Beyers, R. 110–111, 116–117, 137
 Bhargava, R.N., see Goldburt, E.T. 312, 321
 Bhattacharya, D., see Sivakumar, M. 400
 Bhattacharya, R., see Patra, C.R. 350
 Bhattacharyya, S., see Behera, S.K. 388
 Bhattacharyya, S., see Sahu, P.K. 388
 Bhirud, V.A., see Fierro-Gonzalez, J.C. 325
 Bielska, B., see Niedbala, R.S. 440
 Bierman, M.J. 325, 330
 Biesemans, M., see Ribot, F. 288
 Bihari, B. 321
 Bill, H., see Pilla, O. 122
 Billups, W.E., see Haufler, R.E. 101
 Biltz, H. 51–52
 Biner, D., see Aebischer, A. 428
 Biner, D., see Suyver, J.F. 426
 Binnemans, K. 1–87
 Blasse, G. 404
 Blasse, G., see Mello, C.D. 418
 Boakye, E.E. 336
 Boatner, L.A., see Jellison, G.E. 331
 Bocchetta, P. 328
 Boehm, M.C., see Schulte, J. 112–113
 Bohn, E., see Stöber, W. 431
 Bohr, N. 54–75
 Boilot, J.P., see Beaurepaire, E. 377–378
 Boilot, J.P., see Buissette, V. 321, 336, 343–344, 375
 Boilot, J.P., see Casanova, D. 378–379
 Boilot, J.P., see Giaume, D. 377, 379
 Boilot, J.P., see Huignard, A. 351–352, 367, 369
 Boilot, J.P., see Mialon, G. 354, 366
 Bondioli, F. 285
 Bongiorno, C., see Miritello, M. 386
 Bonnet, J., see Zijlmans, H. 440
 Bontempi, E., see Barreca, D. 418
 Borchert, H., see Borchert, Y. 326, 402
 Borchert, H., see Kömpe, K. 340, 343
 Borchert, Y. 326, 402
 Borreman, A., see Dekker, R. 415
 Bosze, E.J., see Gonzalez-Ortega, J.A. 385–386
 Bottaro, G., see Armelao, L. 399
 Bottaro, G., see Krishnan, V. 399
 Bottaro, G., see Losurdo, M. 399
 Boullay, Ph., see Kundu, A.K. 399
 Boulle, A., see Conchon, F. 400
 Bour, G. 449
 Bourdelle, P., see Niedbala, R.S. 440
 Boutonnet, M., see Eriksson, S. 289
 Boutonnet, M., see Svensson, E.E. 402
 Bovin, J.O., see Chen, W. 433–434

- Boyer, D. 380–381
 Boyer, D., see Moine, B. 379
 Boyer, J.C. 428
 Boyer, J.C., see Vetrone, F. 322
 Brant, E.L., see Nelson, J.A. 449
 Brar, L.K., see Ghosh, B. 400
 Brauner, B. 27–54, 63, 78, 86
 Brec, R., see Gauthier, G. 161, 173
 Brenier, A., see Bazzi, R. 316
 Brennan, T.D. 226
 Brezesinski, T. 291
 Brezny, R., see Mamontov, E. 304
 Bricogne, G. 111
 Brien, P.O., see Hasegawa, Y. 437–438
 Bril, A., see Sommerdijk, J.L. 405
 Bringer, A., see Kessler, B. 132, 140
 Brink, A., see Corstjens, P.L.A.M. 440
 Brink, C., see Lorents, D.C. 109
 Briscoe, H.V.A., see Friend, N.J. 54
 Brock, W.H. 39
 Brooks, N.M. 10, 24, 26
 Brown, I.D. 269
 Brown, S.S. 335, 350
 Brown, S.S., see Yan, W.F. 350
 Bruchez, M. 279
 Bruehwiler, P., see Pichler, T. 117, 132–133
 Brukental, I., see Sivakumar, M. 400
 Brune, S.N., see Firsching, F.H. 331
 Brungs, S., see Zollfrank, C. 333, 342
 Bruno, G., see Losurdo, M. 399
 Brunold, T.C., see Bierman, M.J. 325, 330
 Brunton, G. 419
 Bu, W.B. 334–335, 343
 Bu, Y.X., see Fan, W.L. 358–359, 371, 374
 Buassi-Monroy, O.S. 398
 Bucella, S., see Anselmi-Tamburini, U. 299
 Buerk, M. 134
 Buerk, M., see Hennrich, F.H. 115
 Bugli, G. 163, 176
 Bühler, G. 338–339
 Buissette, V. 321, 336, 343–344, 375
 Buissette, V., see Beaurepaire, E. 377–378
 Buissette, V., see Giaume, D. 377
 Buissette, V., see Huignard, A. 351–352, 367, 369
 Bulgan, G., see Liang, S. 396
 Bumajdad, A. 289
 Burbank, P., see van Loosdrecht, P.H.M. 116, 124–125
 Burbank, P.M., see Anderson, M.R. 116, 124, 126
 Burke, R.D., see Diamente, P.R. 412
 Burns, J.H. 419
 Burrow, M.F., see Prentice, L.H. 416
 Burton, J., see Niedbala, R.S. 440
 Burton, J., see Zijlmans, H. 440
 Bussmann, K., see Regulacio, M.D. 436
 Byrne, N.E., see Haufler, R.E. 101
 Cabanas, A. 295
 Cable, R.E., see Henkes, A.E. 389
 Cagle, D.W. 144–145
 Cai, C.X., see Meng, L. 350
 Cai, W.L., see Tao, F. 409
 Caignaert, V., see Kundu, A.K. 399
 Callahan, J.H., see Ross, M.M. 100
 Calvino, J.J., see Bernal, S. 279, 300
 Calvino, J.J., see Di Monte, R. 295
 Campbell, E.E.B. 102, 142
 Campbell, E.E.B., see Gromov, A. 142
 Campbell, E.E.B., see Krawez, N. 102
 Campbell, E.E.B., see Suzuki, S. 109
 Campbell, E.E.B., see Tellgmann, R. 102, 142
 Canales-Vazquez, J., see Marrero-Lopez, D. 393
 Caneiro, A., see Morales, L. 397
 Caneiro, A., see Morales, L. 397
 Cao, B.P. 100
 Cao, C.Y., see Wang, G.F. 409
 Cao, C.Y., see Wang, Y. 407
 Cao, L., see Peng, H.S. 323, 443, 445–446
 Cao, L., see Zhu, Y. 403
 Cao, M.H. 335, 364, 406, 446
 Cao, T.Y., see Hu, H. 406–407, 430
 Cao, W.H., see Luo, X.X. 443, 448
 Cao, W.H., see Tian, Y. 446
 Cao, X.Q., see Zhu, L. 335, 343, 364, 406
 Cao, X.Y., see Zhou, X.F. 400
 Cao, Y.C. 317
 Cao, Y.C., see Yi, N. 402
 Caperaa, C., see Boyer, D. 380
 Capobianco, J.A., see Boyer, J.C. 428
 Capobianco, J.A., see Naccache, R. 430
 Capobianco, J.A., see Vetrone, F. 322
 Cappezzuto, P., see Losurdo, M. 287
 Capponetti, E. 388
 Carlos, L.D., see Ananias, D. 386
 Carlos, L.D., see Karmaoui, M. 313
 Carotta, M.C., see Traversa, E. 400
 Carré, D. 168–170, 197, 202
 Carré, D., see Bugli, G. 163, 176
 Carré, D., see Lemoine, P. 170, 203, 262

- Carré, D., see Messain, D. 168, 200
 Carrettin, S. 302–303
 Carrettin, S., see Guzman, J. 302, 325
 Caruso, F., see Schuetz, P. 341, 343
 Casanova, D. 378–379
 Casanova, D., see Beaurepaire, E. 377–378
 Casanova, D., see Giaume, D. 377, 379
 Cassidy, C.J., see Roth, L.M. 109
 Cassell, A.M., see Fan, S.S. 279
 Castaing, J.C., see Qi, L. 288
 Cauqui, M.A., see Bernal, S. 279, 300
 Chadeyron, G. 379
 Chadwick, J. 67
 Chai, R.T., see Hou, Z.Y. 342
 Chai, R.T., see Yang, J. 323
 Chai, Y. 97–99, 101, 105–106, 109, 114, 141
 Chai, Y., see Guo, T. 100
 Chai, Y., see Haufler, R.E. 97, 101–102
 Chai, Y., see Pan, C. 105
 Chai, Y., see Wang, L.S. 100, 111, 142
 Chakradhar, R.P.S., see Nagabhushana, B. M. 396
 Chamberlain, J.E., see Wragg, J.L. 135
 Chambliss, D.D., see Wilson, R.J. 135
 Chan, S.W., see Spanier, J.E. 299
 Chan, S.W., see Zhang, F. 283
 Chander, M., see Li, Y.Z. 135
 Chandramohan, R., see Thirumalai, J. 445–446
 Chandrappa, G.T., see Nagabhushana, B.M. 396
 Chane-Ching, J.Y., see Buissette, V. 336
 Chane-Ching, J.Y., see Concepcion, P. 303
 Chang, A.H.H. 111
 Chang, C.K., see Gu, M. 330, 360, 375
 Chang, J.J., see Peng, H.S. 323, 443, 445–446
 Chang, M.L. 365–366
 Chao, K., see Li, G.C. 337, 354
 Chao, Z.S. 275–450
 Chapel, J.P., see Qi, L. 288
 Chapline, M.G., see Fan, S.S. 279
 Chaqour, S.M., see Tomas, A. 233
 Charbonnière, L.J. 412
 Chatelain, A., see Deheer, W.A. 279
 Chatterjee, S., see White, B. 404
 Chaudhury, S. 389
 Chavez-Chavez, A., see Buassi-Monroy, O.S. 398
 Chavy, C., see Joachim, C. 135, 137
 Chawla, K.K. 343
 Chen, B.G., see Du, N. 286
 Chen, B.J., see Di, W.H. 334
 Chen, B.J., see Hua, R.N. 418
 Chen, C., see Huo, Z.Y. 291, 336
 Chen, C., see Jellison, G.E. 331
 Chen, C.L., see Jiang, J.C. 400
 Chen, C.W., see Kumar, G.A. 407
 Chen, D. 391
 Chen, D.P., see Dong, G.P. 426
 Chen, D.P., see Hu, Z.J. 407, 416
 Chen, D.P., see Liu, C.H. 361–362, 371, 374, 426, 428
 Chen, D.P., see Lu, H.C. 430
 Chen, D.P., see Wei, Y. 412
 Chen, D.P., see Yi, G.S. 422
 Chen, D.Q. 280, 416–418
 Chen, G.X., see Hu, Z.S. 379, 407
 Chen, G.X., see Qiu, S.Q. 415
 Chen, G.Z. 288
 Chen, H., see Mo, Z.L. 328
 Chen, H.L., see Chen, Z.G. 430–431
 Chen, H.Q., see Wang, L. 348
 Chen, H.R., see Bu, W.B. 334–335, 343
 Chen, H.Y., see Liao, X.H. 284
 Chen, J.P. 308–309
 Chen, J.P., see Wang, D.S. 291
 Chen, J.P., see Yan, L. 288
 Chen, J.P., see Zhang, C. 411
 Chen, K.J., see Han, M. 319
 Chen, K.Z., see Li, G.C. 337, 354
 Chen, L., see Huang, Y.Z. 330, 441, 445
 Chen, L.D., see Yu, X.F. 414
 Chen, L.M. 313, 354–355, 361
 Chen, L.Q., see Sun, C.W. 287–288, 290, 325
 Chen, S.F. 287
 Chen, T.H., see Shen, Z.R. 313
 Chen, T.H., see Wu, H. 354
 Chen, W.X. 395, 433–434
 Chen, W.X., see Ma, L. 326, 408
 Chen, W.X., see Wang, N. 357
 Chen, X., see Ye, S.B. 415
 Chen, X.T., see Huang, Q.L. 411
 Chen, X.T., see Wang, M. 406, 422
 Chen, X.Y., see Liu, G.K. 279–280, 321, 361, 371–372, 375
 Chen, Y.F., see Armitage, R. 448
 Chen, Y.F., see Lin, Y.S. 329
 Chen, Y.F., see Ma, J. 380
 Chen, Y.F., see Wang, Z.L. 409
 Chen, Y.F., see Wu, Q. 408
 Chen, Z.G. 430–431
 Chen, Z.G., see Hu, H. 406–407, 412–413
 Chen, Z.G., see Qian, L.W. 355

- Cheng, B.C., see Wu, G.S. 312
 Cheng, C.S. 399
 Cheng, J., see Lu, H.C. 430
 Cheng, Y., see Bao, F. 416
 Cheng, Z.Y., see Hou, Z.Y. 342
 Chentsova, T.N., see Kedrov, B.M. 37
 Cheong, S.-W., see Kharrazi, S. 396
 Cherivin, C.N. 397–398
 Chibante, L.P.F., see Cagle, D.W. 144
 Chibante, L.P.F., see Chai, Y. 97–99, 101, 105–106, 109, 114, 141
 Chibante, L.P.F., see Haufler, R.E. 97, 101–102
 Chibante, L.P.F., see Li, Y.Z. 135
 Chiodelli, G., see Anselmi-Tamburini, U. 299
 Chiu, H.W., see Cherivin, C.N. 397–398
 Cho, S.J., see Ozgur, U. 279
 Choi, B. 421
 Choi, H.J. 386–387
 Choi, J., see Paek, J. 319
 Choi, S.Y., see Paek, J. 319
 Chou, T.W. 440
 Choudhury, A. 163
 Chow, G.M., see Yi, G.S. 406, 428, 430
 Christiansen, N., see Norby, T. 331
 Christuk, A.E. 239
 Chu, C.W., see Galstyan, E. 400
 Chu, D.R., see Huo, Z.Y. 291, 336
 Chu, S., see Zhou, S. 404
 Chu, X.F., see Wang, D. 400, 407
 Chu, Y.L., see Zhang, D.S. 288
 Chua, H.T., see Gao, L. 403, 434, 443
 Chuang, S.Z., see Chou, T.W. 440
 Chung, W.J., see Ahn, B.Y. 346
 Cioslowski, J. 111
 Ciufolini, M.A., see Haufler, R.E. 101
 Cizauskaite, S. 388
 Clapsaddle, B.J., see Cherivin, C.N. 397–398
 Clark, R.W. 3, 77
 Clark, T., see Mauser, H. 102
 Clemmer, D.E. 142
 Clemmer, D.E., see Shelimov, K.B. 142
 Cocco, D., see Kessler, B. 132, 140
 Cocivera, M., see Hao, J.H. 312
 Colbert, D.T., see Thess, A. 279
 Cölfen, H., see Chen, S.F. 287
 Collin, G. 209, 222
 Collin, G., see Michelet, A. 164, 168
 Collins, D.M. 111
 Colomer, M.T., see Diaz-Guillen, J.A. 342
 Colomer, M.T., see Gallini, S. 342
 Colon, J., see Tarnuzzer, R.W. 308
 Comini, E., see Barreca, D. 305
 Compton, R.N., see Ying, Z.C. 101, 103
 Conceicao, J., see Haufler, R.E. 97, 101–102
 Concepcion, P. 303
 Concepcion, P., see Carrettin, S. 302
 Conchon, F. 400
 Conder, K., see Yusupov, R.V. 403
 Cooke, A.H. 421
 Coppersmith, S.N., see Ghosh, S. 421
 Corbett, J.D., see Guloy, A.M. 163–164, 166–167, 175
 Corma, A. 302–304
 Corma, A., see Abad, A. 304
 Corma, A., see Carrettin, S. 302–303
 Corma, A., see Concepcion, P. 303
 Corma, A., see Guzman, J. 302, 325
 Coronado, E., see Kelly, K.L. 279
 Corstjens, P.L.A.M. 440, 446–447
 Coryell, C.D., see Marinsky, J.A. 67
 Cousin, F., see Qi, L. 288
 Cousseins, J.C., see Boyer, D. 380
 Cousseins, J.C., see Chadeyron, G. 379
 Cox, D.M. 105
 Cramm, S., see Kessler, B. 132, 140
 Cress, C.D. 312
 Crisafulli, C., see Scirè, S. 303
 Cronyn, M.W. 2
 Crookes, W. 4, 27–54
 Crowder, M.S., see Hoinkis, M. 123
 Crowder, M.S., see Yannoni, C.S. 100, 105, 116, 118, 124
 Crozier, P.A., see Wang, R. 296
 Cuberes, M.T. 135
 Cuccia, L.A., see Boyer, J.C. 428
 Cuccia, L.A., see Naccache, R. 430
 Cue, N., see Ding, J. 128
 Cui, X.Z. 380
 Cui, Z.L., see Guo, Z.Y. 287, 307
 Cummins, T.R., see Buerk, M. 134
 Curioni, A., see Andreoni, W. 111–112, 115
 Curl, R.F. 102
 Curl, R.F., see Haufler, R.E. 101
 Curl, R.F., see Heath, J. 97, 141
 Curl, R.F., see Kroto, H. 97
 Curl, R.F., see Weiss, F.D. 97
 Dai, H.J., see Fan, S.S. 279
 Dai, H.J., see Thess, A. 279
 Dai, Q.L., see Dong, B. 426
 Dai, Q.L., see Pan, G.H. 359

- Dai, Q.L., see Qin, R.F. 407, 409–410
 Dai, S., see Brown, S.S. 335, 350
 Dai, S., see Ma, Z. 350
 Dai, S., see Yan, W.F. 350
 Dai, W.L., see Yi, N. 402
 Damodar, S., see Joseph, L.K. 391
 Dang, H.X., see Zhou, J.F. 415
 Darbandi, M., see Ehlert, O. 430
 Darr, J.A., see Cabanas, A. 295
 Darrell, R., see Wu, H. 348
 Darriet Duale, M., see Michelet, A. 161
 Darwin, C.G., see Moseley, H.G.J. 57, 63
 Das, G.K. 323
 Dasari, R., see Kneipp, K. 279
 Dash, H.H. 80
 Daszkiewicz, M. 169, 197, 199, 242, 249
 Daszkiewicz, M. 157–270
 Daszkiewicz, M., see Gulay, L.D. 161,
 166–167, 188, 209, 242, 246
 Daszkiewicz, M., see Lychmanyuk, O.S. 159,
 164, 207–208
 Daszkiewicz, M., see Marchuk, O.V. 217
 Davis, S.A., see Xing, Y. 336
 Davolos, M.R., see Pires, A.M. 442, 446–447
 Davolos, M.R., see Vila, L.D.D. 442, 445
 Dayas, K.R., see Joseph, L.K. 391
 de Groot, F.M.F., see Pichler, T. 117, 132–133
 De Jonghe, L.C., see Sholklapper, T.Z. 300
 De Jonghe, L.C., see Yu, R. 331
 De la Rosa, E., see Ghosh, P. 336
 de Leitenburg, C., see Trovarelli, A. 293, 295
 de Saint-Giniez, D. 197
 de Vries, M.S., see Bethune, D.S. 99, 109
 de Vries, M.S., see Hoinkis, M. 123
 de Vries, M.S., see Johnson, R.D. 99, 121
 de Vries, M.S., see Macfarlane, R.M. 116, 132
 de Vries, M.S., see Wilson, R.J. 135
 de Vries, M.S., see Yannoni, C.S. 100, 105,
 116, 118, 124
 de Winne, H., see Van der Avert, P. 325
 Deguchi, H., see Kira, H. 402
 Deheer, W.A. 279
 Dejneka, M.J., see Meltzera, R.S. 415
 Dekker, C., see Tans, S.J. 279
 Dekker, R. 415
 DeKosky, R.K. 40
 Del Castillo, J., see Yanes, A.C. 415
 Delgado, J.L. 279
 Deloume, J.P., see Berger, D. 395
 Demazeau, G., see Verdon, E. 289
 Deng, H. 363, 373
 Deng, W.L. 302
 Deng, W.L., see Fu, Q. 301
 Dennis, T.J.S. 100, 103, 111, 129
 Dennis, T.J.S., see Hino, S. 114, 122, 133
 Dennis, T.J.S., see Krause, M. 133, 135
 Depero, L.E., see Barreca, D. 418
 Depero, L.E., see Traversa, E. 400
 Deren, P., see Hreniak, D. 388
 Deren, P.J. 388
 Deshpande, A.S. 295
 Desinan, S., see Di Monte, R. 295
 Devalette, M., see Verdon, E. 289
 Devaraju, M.K. 313
 Dey, P. 395
 Dey, P., see Dutta, P. 396
 Dezanneau, G. 396
 Dhanaraj, J. 312, 442, 445
 Di, D., see Zeng, J.H. 419
 Di, W.H. 333–334
 Di, W.H., see Pan, G.H. 377, 384
 Di Monte, R. 295–296
 Di Quarto, F., see Bocchetta, P. 328
 Diamante, P.R. 412
 Diamante, P.R., see Evanics, F. 418
 Diamante, P.R., see Sivakumar, S. 412
 Diaz-Guillen, J.A. 342
 Dickerson, J.H., see Mahajan, S.V. 320
 Dickerson, J.H., see Redigolo, M.L. 436
 Diederich, F., see Allemand, P.M. 121
 Diemeer, M.B.J.K., see Dekker, R. 415
 Diener, M.D. 105
 Diener, M.D., see Guo, T. 100
 Diener, M.D., see Wang, L.S. 100, 111, 142
 DiMaio, J.R. 415
 Ding, D.T., see Shen, Z.R. 313
 Ding, J.W. 116, 128, 130, 132
 Ding, J.W., see Wang, W. 126, 128
 Ding, J.W., see Xiao, S.G. 411
 Ding, J.W., see Yang, X.L. 411
 Ding, K.L., see Miao, Z.J. 406
 Ding, X. 116, 130, 132
 Ding, Y., see Feng, X.D. 298
 Ding, Y., see Sayle, D.C. 298
 Ding, Y.P., see Ma, J. 257, 380
 Ding, Y.Y., see Zhu, J.X. 328
 Dinse, K.P., see Knapp, C. 102, 124, 128
 Dinse, K.P., see Ruetsam, M. 113, 122
 Dinse, K.P., see Schulte, J. 112–113
 Dirksen, G.J., see Mello, C.D. 418
 DiSalvo, F.J., see Poduska, K.M. 210–211
 Divakar, R., see Thirumalai, J. 446
 Djerdj, I. 329
 Dobson, P.J., see Wakefield, G. 312, 316

- Dogan, S., see Ozgur, U. 279
 Doi, T., see Hasegawa, Y. 438
 Dolcetti, G., see Trovarelli, A. 293, 295
 Dollahon, N.R., see Regulacio, M.D. 437
 Domine, M.E., see Corma, A. 302–304
 Dong, B. 426
 Dong, B., see Pan, G.H. 359
 Dong, B., see Qin, R.F. 407, 409–410
 Dong, B., see Yang, Z. 401–402
 Dong, C., see Zhang, M.F. 408
 Dong, G.P. 426
 Dong, J.X., see Hu, Z.S. 379, 407
 Dong, J.X., see Qiu, S.Q. 415
 Dong, L., see Wu, X.C. 358–359
 Dong, W.F., see Fang, Y.P. 343
 Dong, W.T., see Hu, C.G. 313, 328, 407
 Dong, X.T., see Liu, G.X. 329, 365
 Dong, Y., see Ren, M. 379
 Donker, H., see Wegh, R.T. 417
 Dooryhee, E., see Conchon, F. 400
 Dorhout, P.K. 165, 186
 Dorhout, P.K., see Choudhury, A. 163
 Dorhout, P.K., see Fisher, M.J. 337
 Dorn, H.C. 116
 Dorn, H.C., see Anderson, M.R. 116, 124, 126
 Dorn, H.C., see Klute, R.C. 106
 Dorn, H.C., see Macfarlane, R.M. 116, 132
 Dorn, H.C., see van Loosdrecht, P.H.M. 116, 124–125
 Dosev, D. 312, 323–324
 Dosev, D., see Goldys, E.M. 312, 322
 Downs, R.T., see Wang, Z.W. 298
 Driessen, W.A., see Dekker, R. 415
 Drot, R., see Ordonez-Regil, E. 331
 Drozdowicz-Tomsia, K., see Goldys, E.M. 312, 322
 Druce, G. 27
 Du, F.L., see Guo, Z.Y. 287, 307
 Du, N. 286
 Du, W.M., see Niu, X.S. 397
 Du, W.P., see Niu, X.S. 397
 Du, Y.P. 275–450
 Du, Y.P., see Sun, X. 410
 Du, Y.W., see Sivakumar, M. 400
 Duale, M., see Perez, G. 161–162
 Duan, H.H., see Yuan, Q. 282
 Dubai, O., see Krause, M. 120
 Dubonos, S.V., see Novoselov, K.S. 279
 Dugourd, P., see Sugai, T. 120
 Dugué, J., see Bugli, G. 163, 176
 Dujardin, C., see Bazzi, R. 316
 Dujardin, C., see Louis, C. 312
 Dumas, R.K., see Dosev, D. 324
 Dunsch, L. 128–129, 133, 135, 140
 Dunsch, L., see Bartl, A. 122, 128
 Dunsch, L., see Kirbach, U. 128–129, 135
 Dunsch, L., see Knorr, S. 122
 Dunsch, L., see Krause, M. 135
 Dunsch, L., see Mauser, H. 102
 Dunsch, L., see Petra, A. 128
 Dunsch, L., see Pichler, T. 117, 132–133
 Dunsch, L., see Seifert, G. 122
 Duprez, D., see Royer, S. 395
 Dutta, P. 396
 Dwight, K., see Menyuk, N. 428
 Eastman, D.E. 433
 Eastoe, J., see Bumajdad, A. 289
 Eberhardt, W., see Kessler, B. 132, 140
 Ebbesen, T.W., see Treacy, M.M.J. 279
 Eckert, D., see Dunsch, L. 135, 140
 Egami, T., see Mamontov, E. 304
 Ehlert, O. 430
 Ehrhardt, G.J., see Cagle, D.W. 144
 Ehrhardt, J.J., see Ordonez-Regil, E. 331
 Eilers, H. 312
 Eilers, H., see Bihari, B. 321
 El-Azab, A., see Azad, S. 299
 ElGhozzi, M., see Chadeyron, G. 379
 Eliseev, A.A. 158
 Eliseev, A.A., see Zhuravleva, N.G. 411
 Elkind, J.L., see Weiss, F.D. 97
 El-Shall, M.S., see Glaspell, G. 323
 El-Shall, M.S., see Panda, A.B. 317
 El-Toni, A.M. 311
 Emery, S.R., see Nie, S.M. 279
 Emura, S., see Kubozono, Y. 142
 Endo, T., see Wang, Y.H. 380
 Engelhard, M.H., see Azad, S. 299
 Engelhard, M.H., see Wu, H. 348
 Engstrom, M., see Soderlind, F. 398
 Ennaciri, A., see Assaouidi, H. 331
 Enoki, T., see Inakuma, M. 141
 Enzo, S., see Capponetti, E. 388
 Erata, T., see Akasaka, T. 115
 Eriksson, S. 289
 Ermler, W.C., see Chang, A.H.H. 111
 Erpen, C., see Brezesinski, T. 291
 Escax, V., see Ribot, F. 288
 Esch, F., see Kessler, B. 132, 140
 Etienne, J., see Mazurier, A. 163, 168, 172
 Etienne, J., see Michelet, A. 161

- Evain, M., see Gauthier, G. 161, 173
 Evanics, F. 418
 Evans, C.H. 4, 6
 Evans, N.G., see Bondioli, F. 285
 Evenson, C.R. 165, 186
- Fan, C.H., see Chen, G.Z. 288
 Fan, H., see Zhang, M.F. 408, 431
 Fan, K.N., see Yi, N. 402
 Fan, L.B., see Dong, B. 426
 Fan, L.B., see Pan, G.H. 359, 377, 381, 384
 Fan, S.S. 279
 Fan, W.L. 357–359, 363, 371, 374
 Fan, X.P., see Wang, F. 385, 407, 412
 Fang, J., see Wang, Z.L. 409
 Fang, J., see Yu, M. 365
 Fang, Q.F., see Zhuang, Z. 394
 Fang, Y.P. 313, 326, 329–330, 333–334, 342–343
 Fang, Y.P., see Xu, A.W. 328–330
 Feindt, H., see Corstjens, P.L.A.M. 440
 Feindt, H., see Niedbala, R.S. 440
 Feld, M.S., see Kneipp, K. 279
 Feldmann, C. 291, 338
 Feldmann, C., see Bühler, G. 338–339
 Feldmann, C., see Zharkouskaya, A. 338
 Felner, I., see Sivakumar, M. 400
 Feng, G.J., see Liu, S.W. 342
 Feng, J. 323–324
 Feng, S.H., see Zhuang, J.L. 422
 Feng, W. 275–450
 Feng, W., see Jiang, X.C. 380–381
 Feng, W., see Li, Z.X. 291–292
 Feng, W., see Mai, H.X. 284, 286, 304, 306
 Feng, W., see Yuan, Q. 296
 Feng, X.D. 298
 Feng, X.D., see Sayle, D.C. 298
 Feng, X.D., see Wang, Z.L. 298, 441
 Ferdov, S., see Ananias, D. 386
 Fernandes, L., see Rolla, L. 64
 Fernández-García, M. 282
 Ferrari, A.M., see Bondioli, F. 285
 Ferrari, M., see Tikhomirov, V.K. 416
 Ferreira, A., see Ananias, D. 386
 Ferreira, R.A.S., see Ananias, D. 386
 Ferreira, R.A.S., see Karmaoui, M. 313
 Fierro-Gonzalez, J.C. 325
 Fierro-Gonzalez, J.C., see Guzman, J. 302, 325
 Filimonyuk, J.O., see Gulay, L.D. 166, 215–216, 227
- Fink, A., see Stöber, W. 431
 Fink, J., see Pichler, T. 117, 132–133
 Firsching, F.H. 331
 Firsov, A.A., see Novoselov, K.S. 279
 Fischer, J.E., see Thess, A. 279
 Fisher, A., see Hennrich, F.H. 115
 Fisher, D.R., see Wu, H. 348
 Fisher, E.R., see Fisher, M.J. 337
 Fisher, J., see Wright, C.S. 295
 Fisher, K., see Miyake, Y. 115
 Fisher, M.J. 337
 Fita, I. 399
 Fita, I., see Markovich, V. 397
 Fjellvag, H., see Mathur, S. 400
 Flahaut, J. 265
 Flahaut, J., see Basancon, P. 260
 Flahaut, J., see de Saint-Giniey, D. 197
 Flahaut, J., see Michelet, A. 162–164, 168
 Flanagan, S., see Haufler, R.E. 101
 Flask, C.A., see Kumar, R. 431
 Fleischmann, E.D., see Cioslowski, J. 111
 Flor, G., see Malavasi, L. 397, 400
 Flores, M.A., see Bazzi, R. 316
 Flores, M.A., see Louis, C. 312
 Flores-Gonzalez, M.A., see Bazzi, R. 316
 Flytzani-Stephanopoulos, M. 299–300, 302
 Flytzani-Stephanopoulos, M., see Deng, W. L. 302
 Flytzani-Stephanopoulos, M., see Fu, Q. 292, 300–301, 325
 Flytzani-Stephanopoulos, M., see Liu, W. 300
 Flytzani-Stephanopoulos, M., see Si, R. 304, 306
 Fohlich, A., see Suljoti, E. 341
 Folkerts, H.F., see Mello, C.D. 418
 Follath, R., see Pichler, T. 117, 132–133
 Fonda, E., see Di Monte, R. 295
 Ford, H., see Yu, R.B. 323
 Fornasiero, P., see Di Monte, R. 295–296
 Fornasiero, P., see Kašpar, J. 281, 295, 304
 Fortin, M.A., see Soderlind, F. 398
 Fostiropoulos, K., see Kraetschmer, W. 97, 105
 Fouassier, C., see Gauthier, G. 161, 173
 Fowler, P.W. 110–111
 Fowler, P.W., see Manolopoulos, D.E. 111
 Fragalá, I.L., see Malandrino, G. 418–419
 Francis, A.H., see Savina, M. 106
 Franco, V., see Concepcion, P. 303
 Franklin, N.R., see Fan, S.S. 279
 Frantti, J., see Popa, M. 397

- Franville, A.C., see Huignard, A. 351–352, 369
 Franzen, H.F., see Kim, S.-J. 260
 Franzen, H.F., see Zhang, Y. 261
 Franzo, G., see Miritello, M. 386
 Freiser, B.S., see Huang, Y. 110
 Freiser, B.S., see Roth, L.M. 109
 Freiser, M.J., see Suits, J.C. 433
 Freitag, B., see Kaneko, K. 283, 383
 Fresnais, J., see Qi, L. 288
 Friedman, H.A., see Thoma, R.E. 419
 Friend, N.J. 54
 Froehner, J., see Bartl, A. 122
 Froehner, J., see Dunsch, L. 128, 135, 140
 Frolova-Borchert, Y.V. 402
 Froumin, N., see Markovich, V. 397
 Fruth, V., see Berger, D. 395
 Fu, H.G., see Yang, P.P. 365
 Fu, H.X., see Zhang, D.S. 288
 Fu, J., see Yu, M. 336, 343, 365
 Fu, Q. 292, 300–301, 325
 Fu, X.Y., see Zhang, H.W. 366, 373–374
 Fu, Y., see Tian, Y. 446
 Fuchs, D. 138
 Fuchs, D., see Beck, R.D. 109
 Fuchs, D., see Buerk, M. 134
 Fuchs, D., see Hennrich, F.H. 115
 Fuchs, D., see Ruebsam, M. 113, 122
 Fuentes, A.F., see Diaz-Guillen, J.A. 341
 Fuess, H., see Guillou, N. 293
 Fujihara, S. 390, 418–419
 Fujihara, S., see Hosono, E. 419
 Fujii, N., see Inoue, T. 121
 Fujii, Y., see Kawata, H. 119
 Fujii, Y., see Suematsu, H. 114, 119
 Fujita, K., see Hasegawa, Y. 438
 Fujita, K., see Tanaka, K. 433
 Fujita, W., see Ito, Y. 121, 128, 132, 141
 Fujiwara, K., see Masui, T. 283, 289
 Fukuda, T., see Tsunekawa, S. 298
 Fumagalli, P. 433
 Fumagalli, P., see Gambino, R.J. 433
 Funasaka, H. 139
 Funasaka, H., see Akasaka, T. 115, 146
 Funasaka, H., see Kato, T. 122, 124–125, 146
 Funasaka, H., see Suzuki, T. 126, 128, 146
 Funasaka, H., see Yamamoto, K. 105–107, 123–124, 128–129
 Fure, J., see Chai, Y. 97–99, 101, 105–106, 109, 114, 141
 Furniss, D., see Tikhomirov, V.K. 416
 Furuta, S., see Yada, M. 313–314
 Fuzhong, Z., see Adachi, G. 104
 Fye, J.L., see Hunter, J. 142
 Fye, J.L., see Sugai, T. 120
 Gacoin, T., see Beaurepaire, E. 377–378
 Gacoin, T., see Buissette, V. 321, 336, 343–344, 375
 Gacoin, T., see Casanova, D. 378–379
 Gacoin, T., see Giaume, D. 377, 379
 Gacoin, T., see Huignard, A. 351–352, 367, 369
 Gacoin, T., see Mialon, G. 354, 366
 Gagnon, J., see Boyer, J.C. 428
 Gai, Z., see Redigolo, M.L. 436
 Gallini, S. 342
 Gallini, S., see Diaz-Guillen, J.A. 342
 Galstyan, E. 400
 Gambino, R.J. 433
 Gao, L. 403, 434, 443
 Gao, L., see Redigolo, M.L. 436
 Gao, L., see Yang, S.W. 290
 Gao, M.Y., see Wang, X.J. 279, 333
 Gao, P.X., see Hu, C.G. 294, 407
 Gao, Q., see Ye, Q. 306
 Gao, S., see Zhao, F. 434, 436, 443–444
 Gao, S., see Zhu, Y. 403
 Gao, X., see Hu, H. 407, 412–413
 Gao, X.P., see Huang, P.X. 326
 García, H., see Abad, A. 304
 Garnweitner, G., see Djerdj, I. 329
 Garnweitner, G., see Pinna, N. 313–314
 Gash, A.E., see Cherivin, C.N. 397–398
 Gasparotto, A., see Armelao, L. 399
 Gasparotto, A., see Barreca, D. 305, 418
 Gates, B.C., see Aguilar-Guerrero, V. 303
 Gates, B.C., see Fierro-Gonzalez, J.C. 325
 Gates, B.C., see Guzman, J. 302, 325
 Gatica, J.M., see Bernal, S. 279, 300
 Gatica, J.M., see Di Monte, R. 295–296
 Gauckler, L.J., see Kleinlogel, C. 279, 293
 Gaugeu, B., see Teng, F. 400
 Gauglitz, G., see Homola, J. 279
 Gauthier, G. 161, 173
 Ge, J.C., see Tang, B. 286
 Ge, Y., see Yi, G.S. 422
 Gedanken, A. 335
 Gedanken, A., see Patra, C.R. 334
 Gedanken, A., see Sivakumar, M. 400
 Gee, S.J., see Dosev, D. 324
 Geethalakshmi, M., see Dhanaraj, J. 442, 445

- Geim, A.K. 279
 Geim, A.K., see Novoselov, K.S. 279
 Geng, D.Y., see Si, P.Z. 448
 Geraldès, C., see Ananias, D. 386
 Gerner, P., see Suyver, J.F. 426
 Ghosh, B. 400
 Ghosh, P. 336
 Ghosh, S. 421
 Giannakas, A.E. 400
 Giaume, D. 377, 379
 Giaume, D., see Beaurepaire, E. 377–378
 Giaume, D., see Buissette, V. 321, 343
 Giaume, D., see Casanova, D. 378–379
 Gibson, J.M., see Treacy, M.M.J. 279
 Gibson, J.R., see Anderson, M.R. 116, 124, 126
 Gilb, S., see Hennrich, F.H. 115
 Gillan, E.G. 100
 Gillan, E.G., see Alvarez, M.M. 99, 110, 115–116
 Gillan, E.G., see Yerezian, C. 99, 105, 109
 Gimzewski, J.K. 110, 137
 Gimzewski, J.K., see Cuberes, M.T. 135
 Gimzewski, J.K., see Joachim, C. 135, 137
 Gin, P., see Bruchez, M. 279
 Girardot, C., see Conchon, F. 400
 Glaspell, G. 323
 Glaspell, G., see Panda, A.B. 317
 Glaum, R., see Gruehn, R. 418
 Glendenin, L.E., see Marinsky, J.A. 67
 Gnanasekar, K.I. 397
 Gnanasekar, K.I., see Jiang, J.C. 400
 Godinho, M. 286
 Godlewski, M., see Goldys, E.M. 312, 322
 Godly, E.W. 98
 Gofer, Y., see Patra, C.R. 334
 Gohin, M., see Mialon, G. 354, 366
 Golberg, D., see Tang, C.C. 286, 330–331, 334
 Goldburt, E.T. 312, 321
 Golden, M.S., see Pichler, T. 117, 132–133
 Goldschmidt, V.M. 75
 Goldys, E.M. 312, 322
 Gomez-Herrero, A., see Di Monte, R. 296
 Gong, H.M., see Deng, H. 363, 373
 Gong, M.L., see Wang, D. 400, 407
 Gong, Q., see Qian, L.W. 355
 Gonzalez-Ortega, J.A. 385–386
 Gordin, M.D. 9, 12, 26
 Gorin, G. 57
 Gorodetsky, G., see Fita, I. 399
 Gorodetsky, G., see Markovich, V. 397
 Gorte, R.J., see Park, S.D. 299
 Gosavi, S.W., see Kharrazi, S. 396
 Gospodinov, M.M., see Galstyan, E. 400
 Goubitz, K., see Helmholdt, R.B. 163
 Goya, G.F., see Mathur, S. 400
 Grabmaier, B.C., see Blasse, G. 404
 Graziani, M., see Di Monte, R. 296
 Graziani, M., see Kašpar, J. 281, 295, 304
 Grazioli, C., see Pichler, T. 117, 132–133
 Greil, P., see Zollfrank, C. 333, 342
 Greve, B., see Arney, D. 392
 Grigorieva, I.V., see Novoselov, K.S. 279
 Grimm, A., see Prandtl, W. 65
 Grimm, J., see Suyver, J.F. 426
 Gromov, A. 142
 Gromov, A., see Krawez, N. 102
 Gross, S., see Krishnan, V. 399
 Gruehn, R. 418
 Grupp, A., see Knorr, S. 122
 Gschneidner, K.A. Jr., see Beaudry, B.J. 80
 Gu, H. 291–292
 Gu, J.Q. 348, 350, 356
 Gu, M. 330, 360, 375
 Gu, X.Y., see Zhu, H.L. 360
 Gu, Z.N., see Okazaki, T. 128
 Guan, H.M. 333
 Guan, H.M., see Zhang, Y.J. 333
 Guan, M.Y. 335
 Guan, Q.Q., see Kida, T. 401
 Güdel, H.U., see Aebischer, A. 428
 Güdel, H.U., see Heer, S. 340, 346–347, 428
 Güdel, H.U., see Pires, A.M. 446
 Güdel, H.U., see Suyver, J.F. 426
 Gui, Y.C., see Qian, L.W. 355
 Gui, Z.L., see Qi, X.W. 395
 Gui, Z.L., see Zhu, J.X. 328
 Guillhot, B., see Iacconi, P. 331
 Guillou, N. 293
 Guinebretiere, R., see Conchon, F. 400
 Guittard, M. 164–165
 Guittard, M., see Carré, D. 168–169, 197
 Guittard, M., see Flahaut, J. 265
 Guittard, M., see Jaulmes, S. 165, 181
 Guittard, M., see Lemoine, P. 170, 203, 262
 Guittard, M., see Likforman, A. 170, 203
 Guittard, M., see Loireau-Lozac'h, A. 164
 Guittard, M., see Patrie, M. 166–167, 170
 Guittard, M., see Tomas, A. 203, 233
 Gulay, L.D. 161–163, 166–167, 169–170, 188, 191, 193, 197, 199, 207–213, 215–217, 227–229, 233, 235–236, 238–240, 242, 246, 249

- Gulay, L.D., see Daszkiewicz, M. 160, 165, 209–213, 224–225
 Gulay, L.D., see Huch, M.R. 170, 220, 242, 244
 Gulay, L.D., see Hvaleba, N.V. 166, 216
 Gulay, L.D., see Lychmanyuk, O.S. 159, 161, 164, 207–208, 211
 Gulay, L.D., see Marchuk, O.V. 167, 191, 216–217
 Gulay, L.D., see Shemet, V.Ya. 166, 187, 193, 207–208, 212, 216–217, 230, 232
 Guloy, A.M. 163–164, 166–167, 175
 Guo, B., see Dosev, D. 312, 323–324
 Guo, B., see Feng, J. 323–324
 Guo, C.X., see Cao, M.H. 335, 364, 406, 446
 Guo, G.-C., see Lin, S.-H. 210
 Guo, G.-C., see Zeng, H.-Y. 163–165, 168, 213
 Guo, J.C., see Zhang, Y.X. 319
 Guo, J.C., see Zeng, J.H. 419
 Guo, L.H., see Lu, H.C. 430
 Guo, L.H., see Yi, G.S. 422
 Guo, N., see Han, Z.H. 287
 Guo, T. 100–112
 Guo, T., see Chai, Y. 97–99, 101, 105–106, 109, 114, 141
 Guo, T., see Wang, L.S. 100, 111, 142
 Guo, Y., see Wang, Y. 400–401
 Guo, Z.Y. 287, 307
 Guo, Z.Y., see Zhang, W. 307, 423
 Gupta, V., see Saha, S. 306
 Gur, T.M., see Huang, H. 294
 Guseinov, G.G. 169, 197
 Guseinov, G.G., see Amirov, A.S. 170, 205
 Gusmano, G., see Traversa, E. 400
 Guymont, M., see Tomas, A. 233
 Guzman, J. 302, 325

 Haase, M. 338, 346, 353, 367, 428
 Haase, M., see Aebischer, A. 428
 Haase, M., see Heer, S. 340, 346–347, 428
 Haase, M., see Kömpe, K. 340, 343
 Haase, M., see Meyssamy, H. 332–333, 343, 346
 Haase, M., see Riwozki, K. 338–339, 341, 343–344, 346, 353, 360, 366–368, 373, 375, 395
 Haase, M., see Schäfer, H. 428, 430
 Haase, M., see Suljoti, E. 341

 Habashi, F. 2
 Hadjipanayis, G.C., see Yan, Z.C. 448
 Hahn, H., see Guillou, N. 293
 Haigh, C.W. 57
 Hakuta, Y., see Adschiri, T. 283
 Halas, N.J., see Averitt, R.D. 105
 Halasyamani, P.S., see Poduska, K.M. 210–211
 Haldar, K.K., see Ghosh, P. 336
 Haley, M.M., see Haufler, R.E. 101
 Hamaya, N., see Suematsu, H. 114, 119
 Hamilton, D.C. 80
 Hammock, B.D., see Dosev, D. 323–324
 Hammock, B.D., see Feng, J. 323–324
 Han, B.X., see Miao, Z.J. 406
 Han, H.C., see Choi, H.J. 386–387
 Han, M. 319
 Han, M., see Guan, M.Y. 335
 Han, W.Q. 286–287
 Han, Y.C., see Yu, M. 336, 343, 365
 Han, Z.H. 287
 Han, Z.H., see Yu, S.H. 443
 Hansen, K., see Yeretjian, C. 99, 105, 109
 Hansen, T.W., see Kaneko, K. 283, 383
 Hanson, J.C., see Fernández-Garciá, M. 282
 Hao, J.H. 312
 Hao, Q., see Sayle, D.C. 297
 Hao, X. 433
 Hao, Y.L., see Guzman, J. 302, 325
 Harbrecht, B.J., see Zhang, Y. 261
 Harcharras, M., see Assaoudi, H. 331
 Hare, J.P., see Taylor, R. 105–106
 Harris, J.A. 64
 Harris, L.A., see Thoma, R.E. 419
 Hart, N.A., see Bondioli, F. 285
 Hartenbach, I. 209
 Hasegawa, M., see Nishibori, E. 114–115, 117–120, 122, 137
 Hasegawa, S., see Hino, S. 122, 128, 140
 Hasegawa, Y. 137–138, 325, 437–438
 Hasegawa, Y., see Adachi, T.A. 438
 Hasegawa, Y., see Kataoka, T. 437
 Hasegawa, Y., see Sakurai, T. 110, 135
 Hasegawa, Y., see Thongchant, S. 325, 437
 Hashizume, T. 135, 137–138
 Hashizume, T., see Hasegawa, Y. 137–138
 Hashizume, T., see Sakurai, T. 110, 135
 Hashizume, T., see Shinohara, H. 103, 110, 117, 124, 128, 139–138
 Hashizume, T., see Wang, X.D. 110, 116–117, 136–138
 Hatakeyama, R., see Hirata, T. 102

- Hatscher, S.T. 162, 173
 Haufler, R.E. 97, 101–102
 Haufler, R.E., see Chai, Y. 97–99, 101, 105–106, 109, 114, 141
 Haufler, R.E., see Guo, T. 100
 Haufler, R.E., see Ying, Z.C. 101, 103
 Hauge, R.H., see Haufler, R.E. 101
 Hauge, R.H., see Pan, C. 105
 Hay, R.S., see Boakye, E.E. 336
 Hayasaka, Y., see El-Toni, A.M. 311
 Hayashi, N., see Bandow, S. 123, 125
 Hayashi, N., see Kato, T. 124
 Hayashi, N., see Shinohara, H. 104, 106–107, 110, 116–117, 124, 136, 145
 Hayashibara, T., see Kubozono, Y. 100, 142
 He, H.Y., see Au, C.T. 418
 He, H.Y., see Yi, N. 402
 He, J.Z., see Hu, Z.S. 379, 407
 He, L., see Zhou, S. 398
 Heath, J.R. 97, 141
 Heath, J.R., see Kroto, H. 97
 Hebbink, G.A., see Stouwdam, J.W. 343–345
 Hebert, G.M., see Thoma, R.E. 420
 Heer, S. 340, 346–347, 428
 Heer, S., see Aebischer, A. 428
 Heer, S., see Pires, A.M. 446
 Heer, S., see Suyver, J.F. 426
 Heering, W., see Zharkouskaya, A. 338
 Heid, R., see Lebedkin, S. 133–135
 Heilbron, J.L., see Heimann, P.M. 57
 Heimann, P.M. 57–61, 64
 Heinrich, H., see Kuchibhatla, S.V.N.T. 298
 Helmholtz, R.B. 163
 Henkes, A.E. 389
 Hennrich, F.H. 115
 Henry, L.L., see Jiang, J.C. 400
 Her, Y.S., see Feng, X.D. 298
 Herman, I.P., see Spanier, J.E. 299
 Herman, I.P., see Zhang, F. 283
 Herranz, M., see Delgado, J.L. 279
 Herskowitz, M., see Fita, I. 399
 Herskowitz, M., see Markovich, V. 397
 Hertel, I.V., see Campbell, E.E.B. 102, 142
 Hertel, I.V., see Suzuki, S. 109
 Hertel, I.V., see Tellgmann, R. 102, 142
 Hettich, R.L., see Ying, Z.C. 101, 103
 Hewitt, I.J., see Li, H. 335
 Hickmann, K., see Suljoti, E. 341
 Hilderbrand, S.A. 324
 Hill, P.M. 187
 Hinatsu, Y., see Hasegawa, Y. 438
 Hines, M.A., see Mirkovic, T. 434
 Hino, S. 114, 122, 128, 133, 140
 Hirai, T. 442, 447
 Hirai, T., see Nishihama, S. 335
 Hirano, M. 283
 Hirano, T., see Hirai, T. 442
 Hirao, K., see Tanaka, K. 433
 Hiraoka, K., see Kubozono, Y. 142
 Hirata, G.A., see Gonzalez-Ortega, J.A. 385–386
 Hirata, T. 102
 Hirsch, A., see Mauser, H. 102
 Hite, G.E., see Schmalz, T.G. 110
 Ho, C.M. 291
 Hodeau, J.-L., see Conchon, F. 400
 Hoffman, K.R. 132
 Hoffmann, R.-D., see Pocha, R. 162, 166, 173, 186
 Hogg, J.T. 56, 58, 60
 Hoinkis, M. 123
 Hoinkis, M., see Yannoni, C.S. 100, 105, 116, 118, 124
 Hölsä, J. 418
 Holczer, K., see Alvarez, M.M. 99, 110, 115–116
 Holczer, K., see Yeretzyan, C. 99, 105, 109
 Holland, E., see Wakefield, G. 312
 Holler, E.R., see Krusic, P.J. 121
 Holloway, P.H., see Bang, J. 443, 448
 Holloway, P.H., see Yang, H.S. 320
 Holmyard, E.J. 54
 Hölsä, J., see Tukia, M. 380
 Holtzberg, F., see Eastman, D.E. 433
 Homola, J. 279
 Honda, Y., see Tanaka, N. 110
 Hong, G.Y., see Liu, G.X. 329, 365
 Hong, J.M., see Wang, M. 406, 422
 Hong, L.V., see Popa, M. 397
 Hong, S.I., see Ahn, B.Y. 346
 Hopkins, B.S., see Harris, J.A. 64
 Hormes, J., see Gnanasekar, K.I. 397
 Horn, E., see Iiduka, Y. 118, 120
 Hoševár, S., see Sedmak, G. 303
 Hoshino, T., see Akasaka, T. 115
 Hosono, E. 419
 Hou, X.D., see Xuan, Y.L. 306
 Hou, X.Y., see Wei, Z.G. 383
 Hou, Z.Y. 342, 365, 376
 Hreniak, D. 388
 Hreniak, D., see Kepinski, L. 386
 Hu, C.G. 294, 313, 328, 407
 Hu, C.G., see Zhang, Z. 294
 Hu, C.W., see Cao, M.H. 335, 364, 406, 446

- Hu, H. 406–407, 412–413, 430
 Hu, H., see Chen, Z.G. 430–431
 Hu, H., see Zhou, Z.G. 415–416
 Hu, J.F., see Wang, J.S. 415
 Hu, J.F., see Xuan, Y.L. 306
 Hu, J.F., see Zhang, L. 398
 Hu, W., see Zhang, K. 389
 Hu, X.L., see Xu, H. 400
 Hu, Z., see Pichler, T. 117, 132–133
 Hu, Z., see Wu, Q. 408
 Hu, Z., see Wu, X.C. 359
 Hu, Z.A. 401, 407
 Hu, Z.J. 407, 416
 Hu, Z.S. 379, 407
 Hua, R.N. 418
 Hua, Z.L., see Bu, W.B. 334–335, 343
 Huang, C.C. 337
 Huang, C.H., see Chen, Z.G. 430–431
 Huang, C.H., see Hu, H. 406–407, 412–413, 430
 Huang, C.H., see Zhou, Z.G. 415–416
 Huang, F.Q. 211
 Huang, F.Q., see Mitchell, K. 259
 Huang, F.Q., see Wu, L.-B. 209
 Huang, H. 130, 294
 Huang, J.-S., see Lin, S.-H. 210
 Huang, J.-S., see Zeng, H.-Y. 163–165, 168, 213
 Huang, K.L., see Chen, L.M. 313, 355, 361
 Huang, K.W., see Zhou, Z.G. 415–416
 Huang, L., see Zhang, D.S. 287
 Huang, P.X. 326
 Huang, P.X., see Chen, D.Q. 280, 416–418
 Huang, Q.L. 411
 Huang, Q.L., see Wang, M. 406, 422
 Huang, S.H., see Peng, H.S. 323, 443, 445–446
 Huang, S.H., see Yan, C.H. 369
 Huang, S.H., see You, F.T. 385
 Huang, S.S., see Yang, P.P. 365
 Huang, W., see Yu, R.B. 323
 Huang, W.M., see Bu, W.B. 335
 Huang, W.P., see Huang, P.X. 326
 Huang, X.J., see Sun, C.W. 288, 325
 Huang, X.W., see Cui, X.Z. 380
 Huang, Y. 110
 Huang, Y., see Roth, L.M. 109
 Huang, Y., see Yang, Z. 401–402
 Huang, Y., see You, F.T. 385
 Huang, Y.H., see Yan, Z.C. 448
 Huang, Y.N., see Chen, W. 433–434
 Huang, Y.Z. 330, 441, 445
 Hubert, S., see Karbowski, M. 422
 Huch, M.R. 169–170, 197, 199, 220, 242, 244, 249
 Huch, M.R., see Gulay, L.D. 170, 242, 246
 Hudgins, R., see Sugai, T. 120
 Huebner, W., see Zhou, X.D. 298
 Huffman, D.R., see Kraetschmer, W. 97, 105
 Huffman, D.R., see Wragg, J.L. 135
 Hughbanks, T., see Ungerer, J.R. 118, 125
 Huguenin, D., see Iacconi, P. 331
 Huignard, A. 351–352, 367, 369
 Huignard, A., see Beaurepaire, E. 377–378
 Huignard, A., see Buissette, V. 375
 Hulman, M. 133
 Hulman, M., see Krause, M. 120, 133, 135
 Hung, Y., see Lin, Y.S. 329
 Hungria, A.B., see Kaneko, K. 283, 383
 Hunt, M.R.C., see Pichler, T. 117, 132–133
 Hunter, J.M. 142
 Hunter, J.M., see Clemmer, D.E. 142
 Hunziker, H.E., see Wilson, R.J. 135
 Huo, D., see Liu, Z.G. 442, 446
 Huo, Z.Y. 291, 336
 Huskens, J., see Stouwdam, J.W. 343–345
 Hutchison, J.L., see Wakefield, G. 312, 316
 Huxter, V.M. 434–435
 Hvaleba, N.V. 166, 216
 Hvelplund, P., see Lorents, D.C. 109
 Hwang, H.J., see Park, S. 391
 Hwu, J.R., see Huang, C.C. 337
 Hyeon, T., see Yu, T.K. 292, 294, 317
 Hytch, M.J., see Maurel, F. 329
 Iacconi, P. 331
 Iacona, F., see Miritello, M. 386
 Ibers, J.A., see Aleandri, L.E. 170
 Ibers, J.A., see Brennan, T.D. 226
 Ibers, J.A., see Christuk, A.E. 239
 Ibers, J.A., see Huang, F.Q. 211
 Ibers, J.A., see Mitchell, K. 259
 Ibers, J.A., see Tougait, O. 171
 Ichihara, T., see Kawahara, Y. 441
 Idriss, H., see Waterhouse, G.I.N. 310
 Iglesias, M., see Carretin, S. 302–303
 Iida, K., see Tamai, H. 350
 Iiduka, Y. 117–118, 120, 137
 Iijima, S. 278
 Iimura, K., see Brezesinski, T. 291
 Ikemoto, I., see Kawata, H. 119
 Ikemoto, I., see Kikuchi, K. 106, 128, 130, 133

- Ikemoto, I., see Suematsu, H. 114, 119
 Ikeya, T., see Tamai, H. 350
 Im, H.J., see Brown, S.S. 335, 350
 Imanaka, N., see Adachi, G. 104
 Inagaki, M., see Hirano, M. 283
 Inagaki, M., see Shinohara, H. 124
 Inakuma, M. 105, 107, 124, 128–129, 141
 Inakuma, M., see Hino, S. 114, 122, 133
 Inakuma, M., see Kato, T. 124
 Inakuma, M., see Krause, M. 133, 135
 Inakuma, M., see Kuroki, K. 105
 Inakuma, M., see Pichler, T. 117, 132–133
 Inakuma, M., see Saito, Y. 104
 Inakuma, M., see Shinohara, H. 104, 106, 124, 137–138
 Inakuma, M., see Sugai, T. 120
 Inakuma, M., see Takahashi, T. 116, 133
 Inakuma, M., see Takata, M. 111, 113, 118–119, 122
 Inakuma, M., see Wan, S.M. 100
 Inoke, K., see Kaneko, K. 283, 383
 Inokuchi, H., see Bandow, S. 123, 125
 Inokuchi, H., see Shinohara, H. 124
 Inoshita, T. 138
 Inoshita, T., see Watanabe, H. 138
 Inoue, T. 121, 142
 Inoue, T., see Nishibori, E. 114–115, 117–120, 122, 137
 Insley, H., see Thoma, R.E. 419–420
 Ioannides, T., see Avgouropoulos, G. 302
 Ion, E. 390
 Ipatova, E.N., see Bakakin, V.V. 163
 Irrera, A., see Miritello, M. 386
 Irvine, J.T.S., see Marrero-Lopez, D. 393
 Ishibashi, Y., see Kumazawa, S. 111
 Ishida, H., see Kubozono, Y. 100, 142
 Ishiguro, T., see Yamamoto, K. 124
 Ishihara, M., see Nishibori, E. 114–115, 117–120, 122, 137
 Ishikawa, K., see Tsunekawa, S. 298
 Isnard, O., see Dezanneau, G. 396
 Isobe, T., see Takeshita, S. 352, 369–370
 Ito, A., see Takahashi, T. 116, 133
 Ito, T., see Shimotani, H. 116
 Ito, Y. 121, 128, 132, 141
 Ito, Y., see Nishibori, E. 114–115, 117–120, 122, 137
 Itzkan, I., see Kneipp, K. 279
 Iwasa, Y., see Shimotani, H. 116
 Iwasaki, K., see Hino, S. 114, 122, 128, 133, 140
 Iyer, R.G. 211, 226
 Jacob, D.S., see Patra, C.R. 334
 Jacobson, C.P., see Sholklipper, T.Z. 300
 Jaffe, J.E., see Azad, S. 299
 Jagannathan, R., see Dhanaraj, J. 312, 442, 445
 Jagannathan, R., see Nakkiran, A. 445
 Jagannathan, R., see Thirumalai, J. 445
 Janczak-Rusch, J., see Chawla, K.K. 343
 Janet, C. 73–74, 76, 83
 Jaras, S.G., see Svensson, E.E. 402
 Jareonboon, W., see Maensiri, S. 285
 Jarrold, M.F., see Clemmer, D.E. 142
 Jarrold, M.F., see Hunter, J. 142
 Jarrold, M.F., see Shelimov, K.B. 142
 Jarrold, M.F., see Sugai, T. 120
 Jaulmes, S. 165, 179, 181, 184–185
 Jaulmes, S., see Guittard, M. 165
 Jaulmes, S., see Julien-Pouzol, M. 165
 Jellison, G.E. 331
 Jensen, M.A., see Hamilton, D.C. 80
 Jensen, N., see Lorents, D.C. 109
 Jensen, W.B. 2–3, 11, 77–78, 80
 Jeong, J., see Choi, B. 421
 Ji, X.H., see Zhang, Q.Y. 385
 Jia, C.J. 356–357, 371–372
 Jia, C.J., see Luo, F. 357–358
 Jia, G. 313
 Jia, P.Y., see Wang, Z.L. 409
 Jiang, D., see Novoselov, K.S. 279
 Jiang, J.C. 400
 Jiang, J.C., see Gnanasekar, K.I. 397
 Jiang, K., see Niu, X.S. 397
 Jiang, L., see Zhou, X.F. 400
 Jiang, M.H., see Zhang, L. 398
 Jiang, S.P., see Cheng, C.S. 399
 Jiang, X., see Gnanasekar, K.I. 397
 Jiang, X.C. 380–381, 383, 385
 Jiang, X.C., see Jia, C.J. 356–357, 371–372
 Jiang, X.C., see Wei, Z.G. 380, 382–383
 Jiang, X.Q., see Guan, M.Y. 335
 Jiang, Y. 443
 Jiang, Y.B., see Liang, L. 409, 422
 Jiang, Y.H., see Sivakumar, M. 400
 Jiang, Z.H., see Zhang, Q.Y. 385
 Jiao, K., see Zhang, W. 307, 423
 Jin, C., see Chai, Y. 97–99, 101, 105–106, 109, 114, 141
 Jin, C., see Haufler, R.E. 97, 101–102
 Jin, C., see Ying, Z.C. 101, 103
 Jin, D.L., see Zhu, H.L. 360
 Jin, Q., see Zhang, F. 283
 Jin, S., see Bierman, M.J. 325, 330

- Jin, Y., see Wang, Y. 407
 Jinno, K. 106
 Joachim, C. 135, 137
 Jobic, S., see Gauthier, G. 161, 173
 Johnson, R.D. 99, 121
 Johnson, R.D., see Bethune, D.S. 99, 109
 Johnson, R.D., see Henkes, A.E. 389
 Johnson, R.D., see Hoinkis, M. 123
 Johnson, R.D., see van Loosdrecht, P.H.M. 116, 124–125
 Johnson, R.D., see Wilson, R.J. 135
 Johnson, R.D., see Yannoni, C.S. 100, 105, 116, 118, 124
 Johrendt, D. 162, 164, 173, 177
 Johrendt, D., see Pocha, R. 162, 166, 173, 186
 Johrendt, D., see Tampier, M. 164, 177
 Joly, A.G., see Chen, W. 433–434
 Jones, D.A., see Cooke, A.H. 421
 Jones, H.C. 53
 Jonsson, M., see Gromov, A. 142
 Joo, J., see Yu, T.K. 292, 294, 317
 Joseph, L.K. 391
 Ju, X., see Wei, Z.G. 383
 Julien-Pouzol, M. 165
 Julien-Pouzol, M., see Guittard, M. 164
 Julien-Pouzol, M., see Jaulmes, S. 165, 181, 184–185
 Jung, Ch., see Pichler, T. 117, 132–133
 Jung, G., see Markovich, V. 397
 Jung, H.K. 346
 Jung, H.K., see Ahn, B.Y. 346
 Junker, M., see Iacconi, P. 331
 Jurado, J.R., see Gallini, S. 342
- Kabanov, V.V., see Yusupov, R.V. 403
 Kaczorowski, D., see Gulay, L.D. 167, 212, 229, 239
 Kahr, B., see Roth, L.M. 109
 Kai, T., see Dennis, T.J.S. 100, 103, 111, 129
 Kai, T., see Nakane, T. 103, 129
 Kai, T., see Wang, C.R. 120
 Kainosho, M., see Miyake, Y. 115
 Kaittanis, C., see Perez, J.M. 308
 Kakihana, M., see Kawahara, Y. 441
 Kakinaha, M., see Popa, M. 397
 Kako, M., see Akasaka, T. 115
 Kaliaguine, S., see Royer, S. 395
 Kaliaguine, S., see Tien-Thao, N. 395
 Kaliaguine, S., see Zhang, R. 395
 Kall, P.-O., see Soderlind, F. 398
 Kam, C.H., see Zhang, Q.Y. 385
- Kameyama, Y., see Konishi, T. 419
 Kamimura, M. 324
 Kanatzidis, M.G., see Iyer, R.G. 211, 226
 Kanazawa, Y., see Kato, H. 144
 Kanazawa, Y., see Mikawa, M. 144–145
 Kaneko, K. 283, 383
 Kaner, R.B., see Alvarez, M.M. 99, 110, 115–116
 Kaner, R.B., see Gillan, E. 100
 Kaner, R.B., see Yeretizian, C. 99, 105, 109
 Kanki, T., see Yanagida, T. 400
 Kappes, M.M., see Beck, R.D. 109
 Kappes, M.M., see Buerk, M. 134
 Kappes, M.M., see Hennrich, F.H. 115
 Kappes, M.M., see Ruebsam, M. 113, 122
 Kar, S., see Ghosh, B. 400
 Kar, S., see Regulacio, M.D. 437
 Karakoti, A.S. 285, 297
 Karakoti, A.S., see Kuchibhatla, S.V.N.T. 298
 Karakoti, A.S., see Sayle, D.C. 297
 Karbowiak, M. 421–422
 Kardos, K., see Corstjens, P.L.A.M. 440, 446–447
 Kardos, K., see Niedbala, R.S. 440
 Kardos, K., see Zijlmans, H. 440
 Kareiva, A., see Cizauskaite, S. 388
 Karmaoui, M. 313
 Kashino, S., see Kubozono, Y. 100, 142
 Kaskel, S., see Althues, H. 362
 Kašpar, J. 281, 295, 304
 Kašpar, J., see Di Monte, R. 295–296
 Kasuya, A., see Tsunekawa, S. 298
 Kasuya, D., see Suzuki, S. 102
 Kasuya, D., see Wakabayashi, T. 102–103, 109
 Kataoka, T. 437
 Kataoka, T., see Hasegawa, Y. 437
 Kataura, H., see Suzuki, S. 102
 Kato, E., see Hirano, M. 283
 Kato, H. 144
 Kato, H., see Inakuma, M. 141
 Kato, H., see Mikawa, M. 144–145
 Kato, T. 116, 122, 124–125, 146
 Kato, T., see Akasaka, T. 115–116, 146
 Kato, T., see Iiduka, Y. 118, 120
 Kato, T., see Shinohara, H. 100, 104–106, 113, 116, 118, 122, 124, 128
 Kato, T., see Suzuki, S. 122, 125
 Kato, T., see Suzuki, T. 116, 126, 146
 Katsnelson, M.I., see Novoselov, K.S. 279
 Katsuki, H., see Yada, M. 313–314
 Katz, G. 83

- Kauzlarich, S.M., see Cherivin, C.N. 397–398
 Kawahara, H., see Yamamoto, K. 116–117, 137
 Kawahara, M., see Tanaka, N. 110
 Kawahara, Y. 441
 Kawai, T., see Adachi, T.A. 438
 Kawai, T., see Hasegawa, Y. 325, 438
 Kawai, T., see Yanagida, T. 400
 Kawata, H. 119
 Kawata, H., see Suematsu, H. 114, 119
 Kawata, S., see Suzuki, S. 122, 125
 Kawaura, A., see Aono, H. 400
 Kawazoe, Y., see Ohtsuki, T. 144
 Kawazoe, Y., see Tsunekawa, S. 298
 Kawi, S., see Gao, L. 403, 434, 443
 Kedrov, B.M. 37
 Keller, H., see Yusupov, R.V. 403
 Kelly, K.L. 279
 Kennedy, I.M., see Dosev, D. 312, 323–324
 Kennedy, I.M., see Feng, J. 323–324
 Kennedy, I.M., see Goldys, E.M. 312, 322
 Kepinski, L.J. 386
 Kepinski, L.J., see Karbowiak, M. 421–422
 Keron, H.A., see Wakefield, G. 316
 Kessler, B. 132, 140
 Keutgen, C., see Bour, G. 449
 Kharrazi, S. 396
 Khemani, K., see Allemand, P.M. 121
 Khemani, K.C. 105
 Kichuchi, K., see Kato, T. 116, 122, 124–125
 Kida, T. 401
 Kijima, N., see Kawahara, Y. 441
 Kijima, T., see Yada, M. 313
 Kikuchi, K. 106, 109, 111, 115–116, 124, 128, 130, 133, 144
 Kikuchi, K., see Akasaka, T. 115–116, 146
 Kikuchi, K., see Hino, S. 122, 128, 133, 140
 Kikuchi, K., see Kawata, H. 119
 Kikuchi, K., see Kobayashi, K. 114–115
 Kikuchi, K., see Miyake, Y. 115
 Kikuchi, K., see Ohtsuki, T. 144
 Kikuchi, K., see Sato, W. 116
 Kikuchi, K., see Suematsu, H. 114, 119
 Kikuchi, K., see Suzuki, S. 122, 125
 Kikuchi, K., see Suzuki, T. 116, 126, 128
 Kikuchi, K., see Wakabayashi, T. 102–103, 109
 Kikuchi, K., see Watanuki, T. 114, 119, 140
 Kim, A., see Paek, J. 319
 Kim, J.H., see Wells, A.F. 384
 Kim, R., see Wang, G.F. 409
 Kim, S.G., see Thess, A. 279
 Kim, S.-J. 260
 Kim, T., see Wells, A.F. 384
 Kimura, T. 109–110
 Kimura, T., see Fujihara, S. 418–419
 Kimura, T., see Hosono, E. 419
 Kira, H. 402
 Kirbach, U. 128–129, 135
 Kirbach, U., see Bartl, A. 122, 128
 Kirbach, U., see Dunsch, L. 128–129, 135
 Kirbach, U., see Knorr, S. 122
 Kirbach, U., see Pichler, T. 117, 132–133
 Kishida, M., see Shinohara, H. 124, 128, 137–138
 Kishida, M., see Tanaka, N. 110
 Kiss, J.T., see Trovarelli, A. 293, 295
 Kitagawa, H., see Bandow, S. 123, 125
 Kitagawa, H., see Shinohara, H. 124
 Kitaura, R., see Ito, Y. 121, 128, 132, 141
 Kjekshus, A., see Mathur, S. 400
 Kjeldgaard, L., see Pichler, T. 117, 132–133
 Klasson, A., see Soderlind, F. 398
 Klee, W. 201–202
 Klein, D.J., see Schmalz, T.G. 110
 Kleinlogel, C. 279, 293
 Klunder, D.J.W., see Dekker, R. 415
 Klute, R.C. 106
 Knapp, C. 102, 124, 128
 Knapp, C.P., see Ruebsam, M. 113, 122
 Kneipp, H., see Kneipp, K. 279
 Kneipp, K. 279
 Knorr, S. 122
 Knosp, B., see Maurel, F. 329
 Knupfer, M., see Pichler, T. 117, 132–133
 Knupfer, M., see Poirier, M.D. 122, 132, 138, 140
 Kobayashi, K. 114–115, 135, 144–115
 Kobayashi, K., see Akasaka, T. 115–116, 146
 Kobayashi, K., see Hennrich, F.H. 115
 Kobayashi, K., see Hino, S. 114, 122, 133
 Kobayashi, K., see Iiduka, Y. 118, 120
 Kobayashi, K., see Kato, T. 122, 124, 146
 Kobayashi, K., see Kikuchi, K. 128, 144
 Kobayashi, K., see Miyake, Y. 115
 Kobayashi, K., see Sato, W. 116
 Kobayashi, K., see Suzuki, T. 116, 146
 Kobayashi, K., see Wan, S.M. 100
 Kobayashi, Y., see Nakane, T. 103, 129
 Kobayashi, Y., see Wang, C.R. 120
 Kobayashi, Y., see Yamamoto, K. 116–117, 137
 Koch, A., see Allemand, P.M. 121

- Kochubey, D.I., see Frolova-Borchert, Y.V. 402
- Kodama, T., see Shinohara, H. 100, 105, 113, 116, 118, 122, 124
- Koivunen, M.E., see Feng, J. 323–324
- Koji, S., see Fujihara, S. 418–419
- Kojima, Y., see Miyake, Y. 115
- Kojima, Y., see Suzuki, S. 109, 125
- Koktysh, D.S., see Redígolo, M.L. 436
- Kokuoz, B., see DiMaio, J.R. 415
- Kolattukudy, P.E., see Niu, J.L. 308
- Koldun, L.V., see Gulay, L.D. 166, 215–216, 227
- Kolodkine, P. 9
- Komada, T., see Kikuchi, K. 128, 130
- Komasawa, I., see Hirai, T. 442
- Komasawa, I., see Nishihama, S. 335
- Kömpe, K. 340, 343
- Kömpe, K., see Heer, S. 428
- Kömpe, K., see Schäfer, H. 430
- Kong, D.Y., see Lin, C.K. 380
- Kong, D.Y., see Yang, J. 313
- Kong, D.Y., see Yang, P.P. 365
- Kong, X.G., see Sun, Y.J. 354
- Kong, X.G., see Yu, L.X. 346
- Konishi, H., see Liang, L. 409, 422
- Konishi, T. 419
- Koo, H.-J., see Gauthier, G. 161, 173
- Koranne, M., see Mamontov, E. 304
- Kornowski, A., see Haase, M. 338, 346, 353, 367, 428
- Kornowski, A., see Meyssamy, H. 332–333, 343, 346
- Kornowski, A., see Riwozki, K. 338–339, 341, 343–344, 346, 366, 368, 395
- Korsvik, C. 308
- Kosec, M., see Ion, E. 390
- Kotzyba, G., see Tampier, M. 177
- Kovac, J., see Si, P.Z. 448
- Kowalchuk, C.M., see Chen, W. 433–434
- Kraetschmer, W. 97, 105
- Kraetschmer, W., see Krawez, N. 102
- Kraetschmer, W., see Wragg, J.L. 135
- Kragh, H. 55, 59
- Krämer, K.W., see Aebischer, A. 428
- Krämer, K.W., see Suyver, J.F. 426
- Krause, M. 120, 133, 135
- Krause, M., see Dunsch, L. 133, 135
- Krawez, N. 102
- Krawez, N., see Campbell, E.E.B. 102, 142
- Krawez, N., see Tellgmann, R. 102, 142
- Kreibig, U., see Bour, G. 449
- Kresel, J., see Conchon, F. 400
- Kresse, G., see Krause, M. 120
- Krishnamoorthy, C. 398
- Krishnan, B., see Joseph, L.K. 391
- Krishnan, V. 399
- Krishnankutty, K., see Joseph, L.K. 391
- Kriventsov, V.V., see Frolova-Borchert, Y.V. 402
- Kroto, H.W. 97, 110
- Kroto, H.W., see Heath, J. 97, 141
- Kroto, H.W., see Taylor, R. 105–106
- Krusic, P.J. 121
- Kuang, S.M., see Liang, X. 295
- Kubota, Y., see Kumazawa, S. 111
- Kubozono, Y. 100, 142
- Kuchibhatla, S.V.N.T. 298
- Kuchibhatla, S.V.N.T., see Karakoti, A.S. 285, 297
- Kuchibhatla, S.V.T.N., see Sayle, D.C. 297
- Kudriavtseva, S., see Fu, Q. 300
- Kuk, Y., see Hashizume, T. 135, 138
- Kulkarni, B., see Goldburn, E.T. 312, 321
- Kulkarni, S.K., see Kharrazi, S. 396
- Kumar, G.A. 407
- Kumar, R. 431
- Kumar, R., see Nyk, M. 430, 432
- Kumazawa, S. 111
- Kundaliya, D.C., see Kharrazi, S. 396
- Kundu, A.K. 399
- Kuo, W.S., see Huang, C.C. 337
- Kuran, P., see Dunsch, L. 128–129, 133, 135, 140
- Kuran, P., see Krause, M. 135
- Kuran, P., see Pichler, T. 117, 132–133
- Kurbanov, T.K., see Aliev, O.M. 169–170, 202
- Kurbatov, J.D. 66
- Kurbatov, J.D., see Law, H.B. 66
- Kuriyama, T., see Kuroki, K. 105
- Kurokawa, H., see Sholkapper, T.Z. 300
- Kuroki, K. 105
- Kuroki, M., see Yada, M. 313
- Kutty, T.R.N., see Dhanaraj, J. 312, 442, 445
- Kuwano, see Kobayashi, K. 114–115
- Kuzmany, H., see Hulman, M. 133
- Kuzmany, H., see Krause, M. 120, 133, 135
- Kuzmany, H., see Pichler, T. 117, 132–133
- Kuzmichyeva, G.M., see Eliseev, A.A. 158
- Kwong, K.P., see Wan, S.M. 100
- Kwong, T., see Ho, C.M. 291
- Kynast, U., see Zhuravleva, N.G. 411

- Laasonen, K. 111–112, 138
 Laasonen, K., see Poirier, M.D. 122, 132, 138, 140
 Ladavos, A.K., see Giannakas, A.E. 400
 Lahlil, K., see Beaurepaire, E. 377–378
 Lahlil, K., see Giaume, D. 377, 379
 Lai, S.Y., see Au, C.T. 418
 Lai, S.Y., see Ho, C.M. 291
 Laing, M. 2–3, 77, 80, 85–86
 Lakshminarayana, G., see Ye, S.B. 415
 Lamb, L.D., see Kraetschmer, W. 97, 105
 Lampis, N., see Malavasi, L. 400
 Landau, A., see Patra, C.R. 334
 Landia, B.J., see Cress, C.D. 312
 Lanza, H., see Morales, L. 397
 Lao, C.S., see Hu, C.G. 313, 328, 407
 Laokul, P., see Maensiri, S. 285
 Larese, C., see Bernal, S. 279, 300
 Larina, L.L., see Shlyakhtina, A.V. 390
 Laruelle, P., see Basancon, P. 260
 Laruelle, P., see Collin, G. 209, 222
 Laruelle, P., see de Saint-Giniez, D. 197
 Laruelle, P., see Flahaut, J. 265
 Laruelle, P., see Jaulmes, S. 165, 181
 Laruelle, P., see Messain, D. 200, 268
 Laruelle, P., see Michelet, A. 163–164, 168
 Lasio, B., see Capponetti, E. 388
 Lassesson, A., see Gromov, A. 142
 Lastusaari, M., see Tukia, M. 380
 Lauffer, R.B. 145
 Laurent, G., see Huignard, A. 351–352, 367, 369
 Lavelle, L. 3, 77, 80
 Lavin, V., see Marrero-Lopez, D. 393
 Law, H.B. 66
 Le Mercier, T., see Buissette, V. 336
 Lebbou, K., see Bazzi, R. 316
 Lebbou, K., see Louis, C. 312
 Lebedkin, S. 133–135
 Lecerf, N., see Mathur, S. 400
 Ledoux, G., see Bazzi, R. 316
 Lee, C.H., see Paek, J. 319
 Lee, H.K., see Choi, B. 421
 Lee, H.K., see Yang, H.S. 320
 Lee, J.C., see Choi, H.J. 386–387
 Lee, J.W., see Paek, J. 319
 Lee, K., see Paek, J. 319
 Lee, R., see Thess, A. 279
 Lee, T.H., see Jung, H.K. 346
 Lee, Y.H., see Thess, A. 279
 Legner, S., see Pichler, T. 117, 132–133
 Lehmann, A.G., see Malavasi, L. 400
 Lehmann, O., see Heer, S. 340, 346–347
 Lehmann, O., see Kömpe, K. 343
 Lei, Y.Q., see Pan, G.H. 381, 384
 Leite, E.R., see Godinho, M. 286
 Lemaître-Blaise, M., see Hölsä, J. 418
 Lemmer, U., see Zharkouskaya, A. 338
 Lemoine, P. 170, 203, 262
 Lenggoro, I.W., see Purwanto, A. 388–389
 Lenggoro, I.W., see Xia, B. 294
 Leone, M. 41
 Leonelli, C., see Bondioli, F. 285
 Leontiou, A.A., see Giannakas, A.E. 400
 Lerondel, G., see Taghavinia, N. 385
 Lesk, A.M. 57
 Lester, E., see Cabanas, A. 295
 Levasseur, B., see Royer, S. 395
 Levec, J., see Sedmak, G. 303
 Lewis, B., see Regulacio, M.D. 436
 Li, B.H., see Shen, Z.R. 313
 Li, B.J., see Han, M. 319
 Li, C.X. 407, 422
 Li, C.X., see Hou, Z.Y. 365, 376
 Li, C.X., see Yang, J. 323, 380–381, 385
 Li, C.X., see Yu, C.C. 335
 Li, D.Q., see Zhang, C. 411
 Li, F.Y., see Chen, W. 395
 Li, F.Y., see Chen, Z.G. 430–431
 Li, F.Y., see Hu, H. 406–407, 412–413, 430
 Li, F.Y., see Zhou, Z.G. 415–416
 Li, G.C. 337, 354
 Li, G.C., see Guo, Z.Y. 287, 307
 Li, G.R., see Huang, P.X. 326
 Li, G.S., see Su, Y.G. 423
 Li, G.Z., see Yu, M. 343
 Li, H. 335
 Li, H., see Sun, C.W. 287–288, 290, 325
 Li, H.H., see Huo, Z.Y. 291, 336
 Li, H.H., see Niu, X.S. 397
 Li, H.J., see Mo, Z.L. 328
 Li, H.L., see Hu, Z.A. 401, 407
 Li, H.L., see Yang, Z. 401–402
 Li, H.W., see Cui, X.Z. 380
 Li, H.Y., see Yang, J. 380–381
 Li, J.C., see Liao, L. 306–307
 Li, J.G., see Liu, Z.G. 442, 446
 Li, J.Y., see Zhu, L. 335, 343, 364, 406
 Li, L.L., see Li, Z.X. 291–292
 Li, L.L., see Yuan, Q. 282
 Li, L.P., see Su, Y.G. 423
 Li, L.T., see Qi, X.W. 395
 Li, M., see Xing, Y. 336
 Li, M., see Yu, X.F. 414

- Li, M.T., see Hua, R.N. 418
 Li, P., see Wang, L. 412
 Li, P., see Wang, L.Y. 407
 Li, Q., see Fang, Y.P. 313, 326, 330, 342
 Li, Q., see Liu, Z.G. 442, 446
 Li, Q., see Zhang, D.S. 288
 Li, Q., see Zhu, L. 335, 343, 364, 406
 Li, R.F., see Chen, D.Q. 416
 Li, S., see Corstjens, P.L.A.M. 440, 446–447
 Li, S., see Niedbala, R.S. 440
 Li, S., see Rijke, F.v.-d. 440
 Li, S., see Tang, Q. 328
 Li, S.J., see Si, R. 304–305
 Li, S.W., see Pan, G.H. 359, 377, 384
 Li, W., see Wells, A.F. 384
 Li, W.L., see Hua, R.N. 418
 Li, X.D., see Liu, Z.G. 442, 446
 Li, X.G., see Tao, F. 409
 Li, X.Y., see Wang, W. 126, 128
 Li, Y., see Li, H. 335
 Li, Y., see Lu, Z. 390
 Li, Y., see Yu, X.F. 414
 Li, Y., see Zhuang, Z. 394
 Li, Y.D., see Huo, Z.Y. 291, 336
 Li, Y.D., see Liang, X. 295, 422
 Li, Y.D., see Liu, J.F. 279–280, 321, 361–362, 371–372, 374–375
 Li, Y.D., see Sun, X.M. 288
 Li, Y.D., see Wang, D.S. 291
 Li, Y.D., see Wang, L.Y. 407, 422, 424
 Li, Y.D., see Wang, X. 287, 290, 313, 326–328, 330, 361, 406, 408, 441
 Li, Y.D., see Yan, R.X. 333, 409
 Li, Y.D., see Zeng, J.H. 422
 Li, Y.D., see Zhang, Y. 379
 Li, Y.D., see Zhou, K.B. 304
 Li, Y.G., see Zhang, F. 423, 425
 Li, Y.G., see Zhu, X.X. 411
 Li, Y.Z. 135
 Li, Z.F., see Luo, F. 357
 Li, Z.H., see Zeng, J.H. 422
 Li, Z.Q., see Tsunekawa, S. 298
 Li, Z.X. 291–292
 Lian, H.Z. 409, 422
 Lian, H.Z., see Hou, Z.Y. 342, 365, 376
 Lian, H.Z., see Li, C.X. 407, 422
 Lian, J.B., see Liu, Z.G. 442, 446
 Lian, Y., see Okazaki, T. 128
 Liang, A., see Wang, L. 348
 Liang, L.F. 409, 422
 Liang, L.F., see Zhuang, J.L. 422
 Liang, S. 396
 Liang, S., see Teng, F. 400
 Liang, X. 422
 Liang, X. 295, 422
 Liao, C.S., see Jiang, X.C. 380, 385
 Liao, C.S., see Sun, L.D. 362, 442
 Liao, C.S., see Wei, Z.G. 380, 382–383
 Liao, C.S., see Yan, C.H. 369
 Liao, C.S., see Zhang, Y.W. 290
 Liao, L. 306–307
 Liao, X.H. 284
 Libby, W.F. 66
 Libera, M., see Goldburtt, E.T. 312, 321
 Liermann, H.P., see Wang, Z.W. 298
 Likforman, A. 170, 203
 Likforman, A., see Lemoine, P. 170, 203
 Lin, B.X., see Si, R. 304–305
 Lin, C.K. 379–380
 Lin, C.K., see Wang, H. 365, 373
 Lin, C.K., see Wang, Z.L. 409
 Lin, C.K., see Yu, M. 343
 Lin, H.Y., see Lin, Y.S. 329
 Lin, J.H. 379, 381
 Lin, J.H., see Hou, Z.Y. 342, 365, 376
 Lin, J.H., see Li, C.X. 407, 422
 Lin, J.H., see Lin, C.K. 380
 Lin, J.H., see Ren, M. 379
 Lin, J.H., see Wang, H. 365, 373
 Lin, J.H., see Wang, Z.L. 409
 Lin, J.H., see Yang, J. 313, 323, 380–381, 385
 Lin, J.H., see Yang, P.P. 365
 Lin, J.H., see Yang, Z. 379
 Lin, J.H., see Yu, C.C. 335
 Lin, J.H., see Yu, M. 336, 343, 365
 Lin, J.H., see Zhang, J. 381
 Lin, J.H., see Zhou, Y.H. 322
 Lin, N., see Ding, J. 128
 Lin, S.-H. 210
 Lin, S.-H., see Tellgmann, R. 102, 142
 Lin, Y.H., see Wu, H. 348
 Lin, Y.S. 329
 Lin, Z., see Ananias, D. 386
 Ling, Y., see Hasegawa, Y. 137–138
 Little, H.F.V., see Friend, N.J. 54
 Liu, B.D., see Tang, C.C. 331, 334
 Liu, C.H. 361–362, 371, 374, 426, 428
 Liu, C.H., see Liao, L. 306–307
 Liu, C.H., see Ozgur, U. 279
 Liu, C.H., see Sun, L.D. 442
 Liu, D.J., see Wu, X.C. 359
 Liu, F., see Chen, D.Q. 416
 Liu, G.C., see Chen, L.M. 313, 361
 Liu, G.G., see Niu, X.S. 397

- Liu, G.K. 279–280, 321, 361,
 371–372, 375
 Liu, G.R., see Yan, L. 326, 328
 Liu, G.S. 322
 Liu, G.X. 329, 365
 Liu, G.Y., see Dosev, D. 323–324
 Liu, H., see Chawla, K.K. 343
 Liu, H., see Hu, C.G. 294, 313, 328, 407
 Liu, H., see Zhang, K. 389
 Liu, H.C., see Mai, H.X. 284, 286, 304, 306
 Liu, H.J., see Sun, Y.J. 354
 Liu, H.Q., see Fang, Y.P. 313, 326, 329–330,
 333–334, 342
 Liu, H.Q., see Xu, A.W. 328–330
 Liu, J., see Lian, H. 409, 422
 Liu, J., see Wang, H. 397
 Liu, J.F. 279–280, 321, 361–362, 371–372,
 374–375
 Liu, J.F., see Sun, X.M. 288
 Liu, J.H., see Zhang, Y.W. 327
 Liu, J.M., see Zhang, M.F. 396
 Liu, K., see Dosev, D. 324
 Liu, L.N. 329, 365
 Liu, L.N., see Chen, W. 395
 Liu, L.N., see Qin, R.F. 407, 409–410
 Liu, M.T., see Iiduka, Y. 118, 120
 Liu, M.Z., see Dosev, D. 323–324
 Liu, P. 304
 Liu, P., see Zhu, G.Q. 400
 Liu, Q.F., see Gu, M. 330, 360, 375
 Liu, Q.F., see Wang, J.C. 327, 408
 Liu, Q.F., see Yuan, Q. 296
 Liu, Q.F., see Zhou, H.P. 291, 293
 Liu, R.S., see Chou, T.W. 440
 Liu, S.W. 342
 Liu, S.W., see Xiu, Z.L. 346
 Liu, S.Y., see Yu, R.B. 323
 Liu, W.M. 300
 Liu, W.M., see Zhang, Z.F. 329, 415
 Liu, W.M., see Zhou, J.F. 415
 Liu, X., see Wang, Y. 400–401
 Liu, X.D., see Zhu, L. 335, 343, 364, 406
 Liu, X.F., see Dong, G.P. 426
 Liu, X.G., see Wang, F. 360, 376, 426, 428–430
 Liu, X.H., see Wang, J.S. 415
 Liu, X.M., see Lin, C.K. 380
 Liu, X.M., see Tang, Q. 328
 Liu, X.M., see Yang, J. 313
 Liu, X.M., see Yu, C.C. 335
 Liu, X.M., see Zhu, L. 335, 343, 406
 Liu, X.W., see Huo, Z.Y. 291
 Liu, Y., see Chen, W. 395
 Liu, Y., see Heath, J. 97, 141
 Liu, Y., see Wang, L. 348
 Liu, Y., see Xia, G. 388
 Liu, Y., see Zhu, G.Q. 400
 Liu, Y.N., see Chen, L.M. 313, 355, 361
 Liu, Y.Z., see Mo, Z.L. 328
 Liu, Z., see Wells, A.F. 384
 Liu, Z.C., see Bu, W.B. 335
 Liu, Z.G. 442, 446
 Liu, Z.G., see Zhang, M.F. 396
 Liu, Z.M., see Miao, Z.J. 406
 Liu, Z.P., see Tang, Q. 328
 Liu, Z.X., see Pan, G.H. 377, 381, 384
 Liu, Z.X., see Song, H.W. 346
 Liu, Z.X., see Yu, L.X. 343, 346
 Llorca, J., see Trovarelli, A. 293, 295
 Lo Savio, R., see Mirirtello, M. 386
 Lo, Y.W., see Huang, C.C. 337
 Lobo, A., see Kömpe, K. 340, 343
 Logothetidis, S., see Patsalas, P. 310
 Loireau-Lozac'h, A. 164
 Longo, E., see Godinho, M. 286
 Lopez-Quintela, M.A., see Vazquez-
 Vazquez, C. 400
 Lorents, D.C. 109
 Lorents, D.C., see Moro, L. 100
 Lorenz, B., see Galstyan, E. 400
 Losurdo, M. 399
 Lou, T.J., see Zeng, J.H. 419
 Louis, C. 312
 Louis, C., see Bazzi, R. 316
 Lu, C.H. 287
 Lu, C.H., see Dhanaraj, J. 312
 Lu, C.H., see Wang, H.C. 287, 290,
 390, 430
 Lu, F.Q., see Wei, Y. 412
 Lu, G., see Wang, Y. 400–401
 Lu, H.B., see Liao, L. 306–307
 Lu, H.C. 430
 Lu, H.C., see Yi, G.S. 422
 Lu, L.L., see Tong, Y. 392
 Lu, L.L., see Wang, Y.P. 395
 Lu, L.L., see Yang, P.P. 365
 Lu, L.L., see Zhang, L. 390
 Lu, M., see Wang, S. 390
 Lu, M.H., see Zhang, Y. 406
 Lu, M.K., see Wang, S.M. 392
 Lu, M.K., see Xiu, Z.L. 346
 Lu, M.K., see Zhang, H.P. 370
 Lu, R.J., see Hu, Z.A. 401, 407
 Lu, S.Z., see Di, W.H. 333
 Lu, S.Z., see Dong, B. 426

- Lu, S.Z., see Pan, G.H. 359, 377, 384
 Lu, S.Z., see Peng, H.S. 323, 443, 445–446
 Lu, S.Z., see Song, H.W. 346
 Lu, S.Z., see Wei, Z.G. 383
 Lu, S.Z., see Yan, C.H. 369
 Lu, S.Z., see Yu, L.X. 346
 Lu, X., see Shi, Z.Q. 120
 Lu, Y.Q., see Sun, L.D. 362
 Lu, Y.Q., see Yan, C.H. 369
 Lu, Z. 390
 Luhrs, C.C., see Buassi-Monroy, O.S. 398
 Lukashevich, A.I., see Frolova-Borchert, Y.V. 402
 Lukashin, A.V., see Zhuravleva, N.G. 411
 Lukowiak, A., see Hreniak, D. 388
 Lunsford, J.H., see Weckhuysen, B.M. 325
 Luo, F. 357–358
 Luo, F., see Jia, C.J. 356–357, 371–372
 Luo, J., see Ye, S.B. 415
 Luo, X.X. 443, 448
 Luo, X.X., see Tian, Y. 446
 Luo, Y., see Wang, Z.L. 409
 Lv, Y., see Xuan, Y.L. 306
 Lychmanyuk, O.S. 159, 161, 164, 207–208, 211
 Lychmanyuk, O.S., see Daszkiewicz, M. 209–212, 225
 Lychmanyuk, O.S., see Gulay, L.D. 161–163, 208–211, 217, 228–229
 Lykke, K.R., see Soderholm, L. 109
 Lytle, F.W., see Soderholm, L. 109
- Ma, E., see Chen, D.Q. 416
 Ma, E., see Hu, Z.J. 407, 416
 Ma, J. 257, 380
 Ma, L. 326, 408
 Ma, R.L., see Zeng, J.H. 419
 Ma, R.Z., see Tang, C.C. 286, 330
 Ma, T.L., see Kida, T. 401
 Ma, X.Y., see Du, N. 286
 Ma, Z. 350
 Macam, E., see White, B. 404
 Maccato, C., see Barreca, D. 305
 MacDonald, D.C., see Kurbatov, J.D. 66
 Macfarlane, R.M. 116, 132
 Machida, K., see Masui, T. 283, 289
 Maciejewski, M., see Stark, W.J. 295
 Macovei, D., see Berger, D. 395
 Madelung, E. 82–83
 Madler, L. 294
 Madler, L., see Stark, W.J. 295
- Madras, G., see Mahapatra, S. 364
 Madras, G., see Mahata, P. 400
 Maeda, H., see Kubozono, Y. 100, 142
 Maeda, H., see Wang, H.Z. 319
 Maeda, Y., see Iiduka, Y. 117–118, 120, 137
 Maensiri, S. 285
 Mafra, L., see Karmaoui, M. 313
 Maggard, P.A., see Arney, D. 392
 Maglia, F., see Anselmi-Tamburini, U. 299
 Mahajan, S.V. 320
 Mahalingam, V., see Naccache, R. 430
 Mahapatra, S. 364
 Mahata, P. 400
 Mahiou, R., see Boyer, D. 380–381
 Mahiou, R., see Chadeyron, G. 379
 Mahiou, R., see Moine, B. 379
 Mahmood, U., see Hilderbrand, S.A. 324
 Mahurin, S.M., see Yan, W.F. 350
 Mai, H.X. 284, 286, 304, 306, 341, 424–425
 Mai, H.X., see Liao, L. 306–307
 Mai, H.X., see Zhou, H.P. 291, 293
 Maicaneanu, S.A. 296
 Mak, A.C., see Ho, C.M. 291
 Maki, H., see Onoda, H. 331, 350
 Makino, H., see Taghavinia, N. 385
 Malandrino, G. 418–419
 Malavasi, L. 397, 400
 Malhotra, B.D., see Ansari, A.A. 306, 406
 Malhotra, B.D., see Saha, S. 306
 Malhotra, L.K., see Aruna, I. 448
 Malhotra, R., see Moro, L. 100
 Malic, B., see Ion, E. 390
 Malik, S.K., see Krishnamoorthy, C. 398
 Malm, J.O., see Chen, W. 433–434
 Malone, B., see Krusic, P.J. 121
 Mamedov, F.H., see Guseinov, G.G. 169, 197
 Mamedov, H.S., see Guseinov, G.G. 169, 197
 Mamedov, Kh.S., see Amirov, A.S. 170, 205
 Mamontov, E. 304
 Mane, A.T., see Karmaoui, M. 313
 Mangili, B.C., see Sayle, D.C. 297
 Manikandan, P., see Ratnasamy, P. 303
 Maniwa, Y., see Miyake, Y. 115
 Maniwa, Y., see Watanuki, T. 114, 119, 140
 Mann, S., see Xing, Y. 336
 Manoilova, O., see Van der Avert, P. 325
 Manolopoulos, D.E. 111
 Manolopoulos, D.E., see Fowler, P.W. 110–111
 Mao, C.J., see Wu, X.C. 358–359
 Mao, D., see Gu, M. 330, 360, 375
 Mao, J.-G., see Lin, S.-H. 210

- Mao, S.P., see Gu, M. 330, 360, 375
 Mao, Y.Q., see Wu, X.C. 359
 Maquieira, A., see Feng, J. 323–324
 Maragno, C., see Armelao, L. 399
 Maragno, C., see Barreca, D. 305, 418
 Marchewka, M., see Kepinski, L. 386
 Marchuk, O.V. 166–167, 191, 215–217
 Marchuk, O.V., see Daszkiewicz, M. 160
 Margrave, J.L., see Haufler, R.E. 101
 Margrave, J.L., see Pan, C. 105
 Marina, O.A., see Azad, S. 299
 Marinsky, J.A. 63, 67
 Markovich, V. 397
 Markovich, V., see Fita, I. 399
 Marrero-Lopez, D. 393–394
 Martin, G., see Savina, M. 106
 Martin, J.L., see Beaurepaire, E. 377–378
 Martin, J.L., see Casanova, D. 379
 Martin, N., see Delgado, J.L. 279
 Martin, P. 297
 Martinelli, G., see Traversa, E. 400
 Martínez-Arias, A., see Fernández-García, M. 282
 Martins Filho, W.L., see Mathur, S. 400
 Martins, J.C., see Ribot, F. 288
 Martin-Sedeno, M.C., see Marrero-Lopez, D. 393
 Martirosyan, K.S., see Galstyan, E. 400
 Maruyama, S., see Haufler, R.E. 97, 101–102
 Maruyama, Y., see Kikuchi, K. 124, 128
 Maruyama, Y., see Ohtsuki, T. 144
 Maruyama, Y., see Suzuki, T. 116, 126, 146
 Maruyama, Y., see Yamamoto, K. 105, 107, 123, 129
 Masingboon, C., see Maensiri, S. 285
 Masui, T. 283, 289
 Masumoto, K., see Ohtsuki, T. 144
 Matei, C., see Berger, D. 395
 Mathur, S. 400
 Matsumoto, K., see Hino, S. 122, 128, 140
 Mattauch, J. 65–66
 Maurel, F. 329
 Maurin, M., see Ribes, M. 173
 Mauser, H. 102
 May, P.S., see Sivakumar, S. 414
 Mazur, P., see Deren, P.J. 388
 Mazurier, A. 163, 168, 172
 Mazurier, A., see Michelet, A. 164, 168
 Mazurs, E. 2
 Mc Nair, H.M., see Klute, R.C. 106
 McCabe, R.W., see Uy, D. 350
 McClure, S.M., see Guo, T. 100
 McClure, S.M., see Wang, L.S. 100, 111, 142
 McCreedy, D.E., see Azad, S. 299
 McElvany, S.W. 100
 McElvany, S.W., see Ross, M.M. 100
 McGinnis, J.F., see Chen, J.P. 308–309
 McGuire, T.R. 433
 McKittrick, J., see Gonzalez-Ortega, J.A. 385–386
 Mech, A., see Karbowski, M. 421–422
 Meeyoo, V., see Thammachart, M. 295
 Mehring, M., see Knorr, S. 122
 Mehta, B.R., see Aruna, I. 448
 Meier, M.S. 106
 Meijer, G., see Wilson, R.J. 135
 Meijerink, A., see Mello, C.D. 418
 Meijerink, A., see Wegh, R.T. 417
 Meisel, K. 191
 Meletis, E.I., see Jiang, J.C. 400
 Mello, C.D. 418
 Meltzera, R.S. 415
 Mendeleev, D.I. 2–3, 7–27, 38, 45–48, 82
 Mendelejeff, D. 14–15, 17, 19–20, 23, 26
 Mendelejew, D. 22
 Méndez-Ramos, J., see Yanes, A.C. 415
 Meng, C.X., see You, F.T. 385
 Meng, J.X., see Zhang, M.F. 431
 Meng, J.X., see Zhu, L. 335, 343, 364, 406
 Meng, L. 350
 Meng, Y.Q., see Wang, H. 364
 Meng, Y.Q., see Xu, H.Y. 364
 Menyuk, N. 428
 Mercader, R.C., see Morales, L. 397
 Mercier, B., see Bazzi, R. 316
 Mercier, B., see Louis, C. 312
 Mercuri, A., see Beaurepaire, E. 377–378
 Merle, R.B., see Hoffman, K.R. 132
 Merz, H. 80
 Meservey, R., see Hao, X. 433
 Messain, D. 168, 200
 Metaxa, C., see Patsalas, P. 310
 Methfessel, S., see Eastman, D.E. 433
 Metson, J.B., see Waterhouse, G.I.N. 310
 Meyer, G. 404–405, 418, 428
 Meyer, S. 51, 53
 Meyerhoff, M.E., see Savina, M. 106
 Meyssamy, H. 332–333, 343, 346
 Meyssamy, H., see Haase, M. 338, 346, 353, 367, 428
 Meyssamy, H., see Riwozki, K. 338–339, 341, 343–344, 346, 366, 368, 395
 Mialon, G. 354, 366

- Mialon, G., see Giaume, D. 379
 Miao, H.Y., see Zhu, G.Q. 400
 Miao, S.D., see Miao, Z.J. 406
 Miao, Z.J. 406
 Michel, C.R., see Buassi-Monroy, O.S. 398
 Michel, R.H., see Beck, R.D. 109
 Michel, R.H., see Buerk, M. 134
 Michel, R.H., see Hennrich, F.H. 115
 Michel, R.H., see Ruebsam, M. 113, 122
 Michelet, A. 161–164, 168
 Midgley, P.A., see Kaneko, K. 283, 383
 Mielcarek, W., see Karbowski, M. 422
 Mieno, T. 104
 Mieno, T., see Hirata, T. 102
 Mihailovic, D., see Yusupov, R.V. 403
 Mihara, M., see Yada, M. 313
 Mikawa, M. 144–145
 Milanovich, N., see Savina, M. 106
 Milunic, D., see Niedbala, R.S. 440
 Min, K.S., see Alvarez, M.M. 99, 110, 115–116
 Min, K.S., see Gillan, E. 100
 Min, K.S., see Poduska, K.M. 210–211
 Min, K.S., see Yeretzi, C. 99, 105, 109
 Minami, Y., see Kida, T. 401
 Minico, S., see Scirè, S. 303
 Miritello, M. 386
 Mirkovic, T. 434
 Mirkovic, T., see Huxter, V.M. 434–435
 Mitani, T., see Bandow, S. 123, 125
 Mitani, T., see Shinohara, H. 124
 Mitchell, A.C., see Morgan, C.G. 323
 Mitchell, K. 259
 Miwa, N., see Mikawa, M. 144–145
 Miyake, Y. 115
 Miyamae, T., see Hino, S. 114, 122, 133
 Miyamoto, D., see Kamimura, M. 324
 Miyazaki, M., see Wang, H.Z. 319
 Miyazaki, T., see Hino, S. 122, 128, 133, 140
 Mizorogi, N., see Iiduka, Y. 117–118, 120, 137
 Mizutani, T., see Ito, Y. 121, 128, 132, 141
 Mo, Z.L. 328
 Mobus, G., see Sayle, D.C. 297
 Mogilevsky, P., see Boakye, E.E. 336
 Mogilyansky, D., see Fita, I. 399
 Mogilyansky, D., see Markovich, V. 397
 Mohandas, E., see Thirumalai, J. 446
 Moine, B. 379
 Moller, T., see Kömpe, K. 340, 343
 Monaghan, P.K., see Puddephatt, R.J. 2
 Montagna, M., see Tikhomirov, V.K. 416
 Moodera, J.S., see Hao, X. 433
 Moon, B., see Choi, B. 421
 Moon, J.H. 391
 Moon, J.H., see Park, S. 391
 Moon, J.H., see Wells, A.F. 384
 Morales, L. 397
 Moreau, M., see Buissette, V. 336, 344
 Moreau, M., see Casanova, D. 379
 Morgan, C.G. 323
 Mori, H., see Hasegawa, Y. 325, 437
 Mori, H., see Masui, T. 283, 289
 Moriwaki, A., see Onoda, H. 331, 350
 Morkoc, H., see Ozgur, U. 279
 Moro, L. 100
 Moronne, M., see Bruchez, M. 279
 Moroz, E.M., see Frolova-Borchert, Y.V., 402
 Morozov, S.V., see Novoselov, K.S. 279
 Mosel, B.D., see Pocha, R. 162, 166, 173, 186
 Mosel, B.D., see Tampier, M. 177
 Moseley, H.G.J. 54–75
 Motooka, I., see Onoda, H. 331, 350
 Mou, C.Y., see Lin, Y.S. 329
 Mouri, S., see Yada, M. 313
 Mozzati, M.C., see Malavasi, L. 397, 400
 Mudher, K.D.S., see Chaudhury, S. 389
 Mueller, K.H., see Dunsch, L. 135, 140
 Mugnier, J., see Moine, B. 379
 Mukherjee, P., see Patra, C.R. 350
 Mukhopadhyay, D., see Patra, C.R. 350
 Mukundan, P., see Rajesh, K. 337, 350
 Müller, A.C., see Hartenbach, I. 209
 Müller, K.A., see Yusupov, R.V. 403
 Munir, Z.A., see Anselmi-Tamburini, U., 299
 Murakami, Y., see Kawata, H. 119
 Murakami, Y., see Kira, H. 402
 Murakami, Y., see Suematsu, H. 114, 119
 Murray, C.B. 279
 Murray, E.P. 299
 Murugan, B. 303
 Muzhumathi, S., see Saradha, T. 394
 Muzhumathi, S., see Subramania, A. 394
 Mylswamy, S., see Chou, T.W. 440
 Naccache, R. 430
 Nagabhushana, B.M. 396
 Nagasaki, Y., see Kamimura, M. 324
 Nagase, S. 111–113, 115, 117, 122, 128, 138
 Nagase, S., see Akasaka, T. 115, 146
 Nagase, S., see Hennrich, F.H. 115
 Nagase, S., see Hino, S. 114, 122, 133
 Nagase, S., see Iiduka, Y. 117–118, 120, 137
 Nagase, S., see Kato, T. 122, 124, 146

- Nagase, S., see Kobayashi, K. 135, 144–115
 Nagase, S., see Miyake, Y. 115
 Nagase, S., see Suzuki, T. 116, 146
 Nagase, S., see Wan, S.M. 100
 Nagasono, M., see Suljoti, E. 341
 Nair, P.S., see Huxter, V.M. 434–435
 Nair, P.S., see Mirkovic, T. 434
 Nair, V.R., see Rajesh, K. 337, 350
 Nakahara, H., see Kikuchi, K. 128, 130, 144
 Nakahara, H., see Kobayashi, K. 114–115
 Nakahara, H., see Sato, W. 116
 Nakahara, N., see Kikuchi, K. 106, 128, 133
 Nakahodo, T., see Iiduka, Y. 117–118, 120, 137
 Nakai, T., see Kubozono, Y. 142
 Nakajima, K., see Iiduka, Y. 117, 120, 137
 Nakajima, T. 405
 Nakamura, H., see Wang, H.Z. 319
 Nakamura, J., see Shinohara, H. 144
 Nakamura, T., see Ito, Y. 121, 128, 132, 141
 Nakane, T. 103, 129
 Nakane, T., see Hino, S. 114, 122, 133
 Nakane, T., see Shinohara, H. 128
 Nakane, T., see Wan, S.M. 100
 Nakane, T., see Xu, Z. 100, 108, 129
 Nakao, H., see Kawata, H. 119
 Nakao, H., see Kira, H. 402
 Nakao, Y., see Kikuchi, K. 106, 109, 111, 115–116, 124, 128, 133
 Nakao, Y., see Suzuki, S. 125
 Nakao, Y., see Suzuki, T. 116, 126, 128
 Nakao, Y., see Watanuki, T. 114, 119, 140
 Nakkiran, A. 445
 Nampoori, V.P.N., see Joseph, L.K. 391
 Nann, T., see Ehlert, O. 430
 Narazaki, M., see Mikawa, M. 144–145
 Nariai, H., see Onoda, H. 331, 350
 Nassos, S., see Svensson, E.E. 402
 Natarajan, S., see Mahata, P. 400
 Nath, S., see Perez, J.M. 308
 Nath, T.K., see Dey, P. 395
 Nath, T.K., see Dutta, P. 396
 Naused, S., see Meyssamy, H. 332–333, 343, 346
 Nayak, S.K., see Mahapatra, S. 364
 Nelson, H.H., see Ross, M.M. 100
 Nelson, J.A. 449
 Nenartaviciene, G., see Cizauskaite, S. 388
 Neudeck, A., see Petra, A. 128
 Newell, L.C. 54
 Ng, C.F., see Au, C.T. 418
 Nguyen, S., see Yeretziyan, C. 99, 105, 109
 Ni, K., see Kobayashi, K. 114–115
 Nichkova, M., see Dosev, D. 323–324
 Nie, S.M. 279
 Niedbala, R.S. 440
 Niedbala, R.S., see Corstjens, P.L.A.M. 440, 446–447
 Niedbala, R.S., see Rijke, F.v.-d. 440
 Niedbala, R.S., see Zijlmans, H. 440
 Niederberger, M., see Deshpande, A.S. 295
 Niederberger, M., see Djerdj, I. 329
 Niederberger, M., see Pinna, N. 313–314
 Nieto, J.M.L., see Carretin, S. 302
 Niikura, S., see Takeshita, S. 352, 369–370
 Niinistö, L. 4
 Niittykoski, J., see Tukka, M. 380
 Nikolaev, P., see Thess, A. 279
 Nilges, T., see Hartenbach, I. 209
 Nilson, L.F. 3, 8, 31, 36
 Nilsson, M., see Corstjens, P.L.A.M. 440
 Nirmala, R., see Krishnamoorthy, C. 398
 Nishibori, E. 114–115, 117–120, 122, 137
 Nishibori, E., see Ito, Y. 121, 128, 132, 141
 Nishibori, E., see Shimotani, H. 116
 Nishibori, E., see Takata, M. 110–111, 113, 116–120, 122, 128, 135, 137, 139
 Nishibori, E., see Wang, C.R. 120
 Nishihama, S. 335
 Nishina, Y., see Hashizume, T. 135, 137–138
 Nishina, Y., see Wang, X.D. 110, 116–117, 135–138
 Nishiyama, F., see Tamai, H. 350
 Nistor, L.C., see Guillou, N. 293
 Niu, J.H., see Hua, R.N. 418
 Niu, J.L. 308
 Niu, J.Y., see Tang, B. 286
 Niu, S.Y., see Zhang, H.W. 366, 373–374
 Niu, X.S. 397
 Noddack, W. 65
 Noël, R. 200
 Nojima, K., see Inoue, T. 121
 Nojima, S., see Tamai, H. 350
 Nomura, M., see Kikuchi, K. 109, 111, 115–116
 Norby, T. 331
 Norris, B.J., see Hoffman, K.R. 132
 Norris, D.J., see Murray, C.B. 279
 Norris, J.F. 54
 Novaro, O. 2
 Novoselov, K.S. 279
 Novoselov, K.S., see Geim, A.K. 279
 Nowik, I., see Sivakumar, M. 400
 Nowotny, H., see Rieger, W. 175, 179

- Nuecker, N., see Buerk, M. 134
 Nunez, P., see Marrero-Lopez, D. 393–394
 Nunziante, P., see Traversa, E. 400
 Nuroh, K. 80
 Nyk, M. 430, 432
 Nyk, M., see Kumar, R. 431
 Nylén, U., see Eriksson, S. 289
- O'Brien, N., see Armitage, R. 448
 O'Brien, S.C., see Haufler, R.E. 101
 O'Brien, S.C., see Heath, J. 97, 141
 O'Brien, S.C., see Kroto, H. 97
 O'Brien, S.C., see Weiss, F.D. 97
 O'Connor, C.J., see Wang, Z.L. 409
 Oda, Y., see Funasaka, H. 139
 Odom, G.K., see Guo, T. 100–112
 Ogale, S.B., see Kharrazi, S. 396
 Ogawa, T. 142
 Ogi, T., see Purwanto, A. 388–389
 Oguri, F., see Suzuki, T. 126, 128
 Oh, J.S., see Ahn, B.Y. 346
 Oh, J.S., see Jung, H.K. 346
 Ohara, S., see Kaneko, K. 283, 383
 Ohkohchi, M., see Shinohara, H. 100, 105, 113, 116, 118, 122, 124
 Ohkohchi, M., see Bandow, S. 104
 Ohkohchi, M., see Shinohara, H. 99, 105–107, 112, 116, 122, 138, 145
 Ohkubo, Y., see Sato, W. 116
 Ohnishi, S., see Inoshita, T. 138
 Ohno, K., see Ohtsuki, T. 144
 Ohno, M., see Inakuma, M. 105, 107, 124, 128–129
 Ohno, M., see Shinohara, H. 124, 137–138
 Ohno, M., see Takata, M. 110–111, 119–120, 128, 135, 139
 Ohno, T., see Guo, T. 100
 Ohno, Y., see Ito, Y. 121, 128, 132, 141
 Ohoyama, K., see Kira, H. 402
 Ohta, T., see Kubozono, Y. 100, 142
 Ohtsuki, T. 144
 Ohulchanskyy, T.Y., see Kumar, R. 431
 Ohulchanskyy, T.Y., see Nyk, M. 430, 432
 Okada, Y., see Hasegawa, Y. 437
 Okazaki, T. 128
 Okazaki, T., see Cao, B.P. 100
 Okazaki, T., see Inoue, T. 121
 Okazaki, T., see Ito, Y. 121, 128, 132, 141
 Okazaki, T., see Shi, Z.J. 128
 Okuba, S., see Ito, Y. 121, 128, 132, 141
- Okumura, H., see Yan, Z.C. 448
 Okumura, M., see Kato, H. 144
 Okumura, M., see Mikawa, M. 144–145
 Okuyama, K., see Purwanto, A. 388–389
 Okuyama, K., see Xia, B. 294
 Olander, D. R., see Abrefah, J. 105
 Olekseyuk, I.D. 166, 215, 227–228, 236
 Olekseyuk, I.D., see Gulay, L.D. 163, 166–167, 170, 191, 193, 208–213, 215–217, 227–229, 233, 235, 238, 240
 Olekseyuk, I.D., see Huch, M.R. 170, 220, 242, 244
 Olekseyuk, I.D., see Hvaleba, N.V., 166, 216
 Olekseyuk, I.D., see Lychmanyuk, O.S. 159, 161, 164, 207–208, 211
 Olekseyuk, I.D., see Marchuk, O.V. 167, 191, 216–217
 Olekseyuk, I.D., see Shemet, V.Ya. 166, 187, 193, 207–208, 212, 216–217, 230, 232
 Oliva, J., see Ghosh, P. 336
 O'Neill, A.E., see Uy, D. 350
 Önem, Z.C., see Akdeniz, Z. 404–405
 Onoda, H. 331, 350
 Onodera, M., see Kira, H. 402
 Ordonez-Regil, E. 331
 Orikoshi, T., see Hirai, T. 442, 447
 Orlovskii, V.P., see Rouanet, A. 331
 O'Shea, M.J. 449
 Oshima, K., see Kubozono, Y. 100, 142
 Oshiyama, A., see Inoshita, T. 138
 Oskam, K.D., see Wegh, R.T. 417
 Ostrovskii, D., see Gromov, A. 142
 Ostwald, W. 53
 Osuwan, S., see Thammachart, M. 295
 Overbury, S.H., see Ma, Z. 350
 Overbury, S.H., see Yan, W.F. 350
 Ozgur, U. 279
- Paek, J. 319
 Palazzi, M., see Tomas, A. 233
 Pan, C.S. 105
 Pan, C.S., see Haufler, R.E. 101
 Pan, C.S., see Zhang, D.S. 288
 Pan, G.H. 359, 377, 381, 384
 Pan, G.H., see Dong, B. 426
 Pan, G.H., see Qin, R.F. 407, 409–410
 Pan, Z.W., see Yan, W.F. 350
 Panda, A.B. 317
 Paneth, F.A. 18, 62–63
 Pang, M.L., see C.K. 379
 Pang, M.L., see Lin, C.K. 379

- Pang, Y.C., see Jia, C.J. 357, 371–372
 Papa, F., see Berger, D. 395
 Parameswaran, P., see Thirumalai, J. 446
 Paras, M.S., see Feng, X.D. 298
 Pardo, M.P., see Flahaut, J. 265
 Pardo, M.P., see Patrie, M. 166–167, 170
 Parida, S.C., see Chaudhury, S. 389
 Park, C.H. 109, 111
 Park, S.D. 299, 391
 Park, S.D., see Kharrazi, S. 396
 Park, Y.I., see Yu, T.K. 292, 294, 317
 Parker, D.H., see Soderholm, L. 109
 Parker, S.C., see Martin, P. 297
 Parker, S.C., see Sayle, T.X.T. 283, 285, 296–297
 Parkinson, B.A., see Krusic, P.J. 121
 Parrinello, M., see Laasonen, K. 111–112, 138
 Parrinello, M., see Poirier, M.D. 122, 132, 138, 140
 Pasupulety, L., see Bumajdad, A. 289
 Patil, S., see Chen, J.P. 308–309
 Patil, S., see Korsvik, C. 308
 Patil, S., see Tarnuzzer, R.W. 308
 Patra, A., see Ghosh, P. 336
 Patra, C.R. 334, 350
 Patra, S., see Patra, C.R. 334, 350
 Patrie, M. 166–167, 170
 Patrin, J.P., see Li, Y.Z. 135
 Patsalas, P. 310
 Pavlicek, F., see Brauner, B. 34
 Paz, F.A.A., see Ananias, D. 386
 Pères Omil, J.A., see Bernal, S. 279, 300
 Peden, C.H.F., see Azad, S. 299
 Peiser, H.S., see Hill, P.M. 187
 Pena-Matinez, J., see Marrero-Lopez, D. 394
 Peng, B., see Yu, R.B. 323
 Peng, C., see Yang, J. 323
 Peng, H.R., see Li, G.C. 337, 354
 Peng, H.S. 323, 443, 445–446
 Peng, Q., see Huo, Z.Y. 291
 Peng, Q., see Liang, X. 422
 Peng, Q., see Wang, D.S. 291
 Peng, Q., see Wang, X. 361, 406
 Peng, Q., see Yan, R.X. 333
 Peng, Q., see Zhou, K.B. 304
 Perdicaro, L.M.S., see Malandrino, G. 418–419
 Perea, N., see Gonzalez-Ortega, J.A. 385–386
 Perelman, L.T., see Kneipp, K. 279
 Perera, P., see O’Shea, M.J. 449
 Perez, G. 161–162
 Perez, G., see Michelet, A. 161
 Perez, J.M. 308
 Perez-Coll, D., see Marrero-Lopez, D. 393
 Perriat, P., see Bazzi, R. 316
 Perriat, P., see Louis, C. 312
 Perrier, C. 66
 Petit, P., see Thess, A. 279
 Petoral, R.M. Jr., see Soderlind, F. 398
 Petra, A. 128
 Petrykin, V., see Kawahara, Y. 441
 Pettersson, O., see Nilson, L.F. 3, 31, 36
 Philippot, E., see Ribes, M. 173
 Pi, D.B., see Wang, F. 385
 Pichler, T. 117, 132–133
 Pichler, T., see Hulman, M. 133
 Pickering, H., see Hasegawa, Y. 137–138
 Pierce, J.W., see Menyuk, N. 428
 Pietraszko, A., see Daszkiewicz, M. 160, 209–213, 224
 Pietraszko, A., see Gulay, L.D. 161, 163, 166–167, 170, 191, 193, 208–213, 215–217, 227–229, 235, 239, 242, 246
 Pietraszko, A., see Huch, M.R. 242, 244
 Pietraszko, A., see Lychmanyuk, O.S. 159, 164, 207–208
 Pietraszko, A., see Marchuk, O.V. 217
 Pietraszko, A., see Shemet, V.Ya. 166, 187, 207, 212, 217, 230, 232
 Pietzak, B., see Knapp, C. 102
 Pietzak, B., see Mauser, H. 102
 Pietzsch, A., see Suljoti, E. 341
 Pignard, S., see Conchon, F. 400
 Pilla, O. 122
 Pillai, K.T., see Chaudhury, S. 389
 Pillai, K.T., see Purohit, R.D. 293–294
 Pillai, P.K., see Rajesh, K. 337, 350
 Pinkas, J., see Cizauskaite, S. 388
 Pinna, N. 313–314
 Pinna, N., see Deshpande, A.S. 295
 Pinna, N., see Karmaoui, M. 313
 Pintado, J.M., see Bernal, S. 279, 300
 Pires, A.M. 442, 446–447
 Piro, A.M., see Miritello, M. 386
 Pischedda, V., see Wang, Z.W. 298
 Pissarjevski, O. 9
 Pistone, A., see Scirè, S. 303
 Pita, K., see Zhang, Q.Y. 385
 Pitzer, R.M., see Chang, A.H.H. 111
 Plant, S.R. 132
 Plueschau, M., see Ruebsam, M., 113, 122
 Pocha, R. 162, 166, 173, 186
 Pocha, R., see Johrendt, D. 162, 164, 173
 Podkolzin, S.G., see Van der Avert, P. 325

- Poduska, K.M. 210–211
 Poggi, M., see Giaume, D. 379
 Poirier, M.D. 122, 132, 138, 140
 Poliakov, M., see Cabanas, A. 295
 Polizzi, S., see Malavasi, L. 397
 Pomonis, P.J., see Giannakas, A.E. 400
 Pool, M.L. 66
 Pool, M.L., see Kurbatov, J.D. 66
 Pool, M.L., see Law, H.B. 66
 Popa, M. 397
 Porcher, P., see Hölsä, J. 418
 Porter, B., see Arney, D. 392
 Pöttgen, R., see Pocha, R. 162, 166,
 173, 186
 Pöttgen, R., see Tampier, M. 177
 Prado, F., see Morales, L. 397
 Pralong, V., see Kundu, A.K. 399
 Prandtl, W. 65
 Prasad, P.N., see Kumar, R. 431
 Prasad, P.N., see Nyk, M. 430, 432
 Prasad, V., see Nagabhushana, B.M. 396
 Pratihari, S.K., see Behera, S.K. 388
 Pratihari, S.K., see Sahu, P.K. 388
 Prato, M., see Khemani, K.C. 105
 Pratsinis, S.E., see Madler, L. 294
 Pratsinis, S.E., see Stark, W.J. 295
 Prentice, L.H. 416
 Price, D.W., see Sayle, D.C. 297
 Prinz, F., see Huang, H. 294
 Priolo, F., see Miritello, M. 386
 Probst, C. 80
 Promarak, V., see Maensiri, S. 285
 Prosser, R.S., see Evanics, F. 418
 Ptacek, P., see Schäfer, H. 428, 430
 Pu, W.L., see Yuan, Q. 296
 Puddephatt, R.J. 2
 Puntès, V.F., see Carretin, S. 302
 Puzosky, A.A., see Ying, Z.C. 101, 103
 Purohit, R.D. 293–294
 Purwanto, A. 388–389
 Puzniak, R., see Markovich, V. 397
 Puzniak, R., see Fita, I. 399
- Qi, L. 288
 Qi, X.W. 395
 Qi, Y.J., see Cao, M.H. 335, 364, 406, 446
 Qian, B.B., see Dong, G.P. 426
 Qian, B.B., see Wang, L. 348
 Qian, H.S. 428
 Qian, L.W. 355
 Qian, X.F., see Qian, L.W. 355
- Qian, Y.T., see Han, Z.H. 287
 Qian, Y.T., see Jiang, Y. 443
 Qian, Y.T., see Tang, Q. 328
 Qian, Y.T., see Wang, C.Y. 290
 Qian, Y.T., see Yu, S.H. 443
 Qian, Y.T., see Zhang, M.F. 408, 431
 Qin, A.M., see Fang, Y.P. 334
 Qin, H.W., see Zhang, L. 398
 Qin, R.F. 407, 409–410
 Qin, R.F., see Dong, B. 426
 Qin, R.F., see Pan, G.H. 359
 Qin, W.P., see Wang, G.F. 409
 Qin, W.P., see Wang, Y. 407
 Qiu, J.R., see Dong, G.P. 426
 Qiu, J.R., see Ye, S.B. 415
 Qiu, J.S., see Wang, Z.Y. 409
 Qiu, S.L., see Li, H. 335
 Qiu, S.Q. 415
 Qiu, X.M., see Yu, R.B. 323
 Qiu, X.P., see Sun, C.W. 287
 Qu, X.S., see Qin, R.F. 407, 409–410
 Quam, G.N. 2
 Quan, Z.W., see Hou, Z.Y. 365, 376
 Quan, Z.W., see Li, C.X. 422
 Quan, Z.W., see Wang, Z.L. 409
 Quan, Z.W., see Yang, J. 313, 380–381
 Quan, Z.W., see Yang, P.P. 365
 Quartarone, E., see Malavasi, L. 400
 Que, W.X., see Zhang, Q.Y. 385
 Quill, L.L., see Kurbatov, J.D. 66
 Quill, L.L., see Law, H.B. 66
 Quill, L.L., see Pool, M.L. 66
- Raap, A.K., see Rijke, F.v.-d. 440
 Radhakrishnan, P., see Joseph, L.K. 391
 Raffaele, R.P., see Cress, C.D. 312
 Rait, J.R., see Hill, P.M. 187
 Rajachandrasekar, R., see Thirumalai, J. 445
 Rajeev, K.P., see Tiwari, A. 396
 Rajesh, K. 337, 350
 Ramaswamy, A.V., see Murugan, B. 303
 Rambabu, B., see Gnanasekar, K.I. 397
 Ramesh, K.P., see Nagabhushana, B.M. 396
 Rapalaviciute, R., see Mathur, S. 400
 Rard, J.A. 433
 Ratnasamy, P. 303
 Raudsepp, M., see Sivakumar, S. 414
 Raudsepp, M., see Stouwdam, J.W. 353, 371,
 374
 Rautama, E.-L., see Kundu, A.K. 399
 Raveau, B., see Kundu, A.K. 399

- Raychaudhuri, A.K., see Ghosh, B. 400
 Reaney, I.M., see Tikhomirov, V.K. 416
 Redígolo, M.L. 436
 Redino, C.S., see Cress, C.D. 312
 Regulacio, M.D. 436–437
 Rehspringer, J.L., see Charbonnière, L.J. 412
 Reichlova, V., see Cizauskaite, S. 388
 Reinhard, C., see Suyver, J.F. 426
 Reinholdt, A., see Bour, G. 449
 Reisfeld, R. 404
 Reller, A., see Robert, R. 399
 Ren, H., see Li, H. 335
 Ren, J., see Wang, Y. 400–401
 Ren, L., see Chen, S.F. 287
 Ren, M. 379
 Ren, M., see Yang, Z. 379
 Ren, X.G., see Pan, G.H. 359, 377, 384
 Ren, X.G., see Qin, R.F. 407, 409–410
 Renker, B., see Lebedkin, S. 133–135
 Reshchikov, M.A., see Ozgur, U. 279
 Retgers, J.W. 51–52
 Reynolds, J.E. 42
 Ribeiro, C., see Godinho, M. 286
 Ribes, M. 173
 Ribot, F. 288
 Richards, T.W. 70
 Richard-Schneider, S., see Hennrich, F.H. 115
 Richardson, T., see Armitage, R. 448
 Rieger, W. 175, 179
 Riello, P., see Anselmi-Tamburini, U. 299
 Rietschel, H., see Fuchs, D. 138
 Rietschel, H., see Lebedkin, S. 133–135
 Rietschel, H., see Ruebsam, M. 113, 122
 Rietveld, H.M. 111
 Rijke, F.v.-d. 440
 Riman, R.E., see Kumar, G.A. 407
 Rinzler, A.G., see Thess, A. 279
 Risksomboon, T., see Thammachart, M. 295
 Riwozki, K. 338–339, 341, 343–344, 346, 353, 360, 366–368, 373, 375, 395
 Riwozki, K., see Haase, M. 338, 346, 353, 367, 428
 Riwozki, K., see Meyssamy, H. 332–333, 343, 346
 Robert, J., see Thess, A. 279
 Robert, R. 399
 Robinson, R.D., see Spanier, J.E. 299
 Robinson, R.D., see Zhang, F. 283
 Robotti, N., see Leone, M. 41
 Rocha, J., see Ananias, D. 386
 Rocha, J., see Karmaoui, M. 313
 Rockenbauer, A., see Seifert, G. 122
 Rockenberger, J., see Beck, R.D. 109
 Rodriguez, A., see Marrero-Lopez, D. 393
 Rodriguez, J.A., see Fernández-García, M. 282
 Rodriguez, J.A., see Liu, P. 304
 Rodríguez, V.D., see Marrero-Lopez, D. 393
 Rodríguez, V.D., see Yanes, A.C. 415
 Rodriguez-Mendoza, U.R., see Marrero-Lopez, D. 393
 Rogers, L.M., see Niu, J.L. 308
 Roiland, C., see Ribot, F. 288
 Rojas, S., see Eriksson, S. 289
 Rolla, L. 64
 Rolli, R., see Tikhomirov, V.K. 416
 Romer, S., see Robert, R. 399
 Ronda, C.R. 379
 Rondinone, A.J., see Brown, S.S. 335, 350
 Rosen, A. 111, 138
 Rosenbaum, T.F., see Ghosh, S. 421
 Rosenhahn, C., see Tampier, M. 177
 Rosenthal, S.J., see Redígolo, M.L. 436
 Ross, M.M. 100
 Rosynek, M.P., see Weckhuysen, B.M. 325
 Roth, L.M. 109
 Rouanet, A. 331
 Roussel, H., see Dezanneau, G. 396
 Roux, S., see Bazzi, R. 316
 Row, T.N.G., see Mahapatra, S. 364
 Royer, S. 395
 Ruan, J., see Dong, G.P. 426
 Rubin, M., see Armitage, R. 448
 Rubin, Y., see Allemand, P.M. 121
 Ruda, I.R., see Daszkiewicz, M. 160
 Rudiger, U., see Fumagalli, P. 433
 Rudolf, P., see Pichler, T. 117, 132–133
 Rudolf, G. 51
 Ruebsam, M. 113, 122
 Ruiz-Morales, J.C., see Marrero-Lopez, D. 393–394
 Rulmont, A., see Assaoui, H. 331
 Ruoff, R.S., see Moro, L. 100
 Ruoff, R.S., see Wan, S.M. 100
 Russell, H. Jr., see Yost, D.M. 75
 Rustamov, P.G., see Aliev, O.M. 169–170, 202
 Rutherford, E. 54, 59
 Sacchetti, A., see Losurdo, M. 399
 Sachin, M., see Ratnasamy, P. 303
 Sada, C., see Barreca, D. 418

- Sadaoka, Y. 400
 Sadaoka, Y., see Traversa, E. 400
 Sadykov, V.A., see Frolova-Borchert, Y.V. 402
 Saha, S. 306
 Sahu, P.K. 388
 Sahu, P.K., see Behera, S.K. 388
 Säilynoja, E., see Hölsä J. 418
 Saito, I., see Kikuchi, K. 106, 128, 133
 Saito, S. 111, 138
 Saito, Y. 95–146
 Saito, Y., see Bandow, S. 104, 123, 125
 Saito, Y., see Hashizume, T. 135, 137–138
 Saito, Y., see Huang, H. 294
 Saito, Y., see Jinno, K. 106
 Saito, Y., see Kamimura, M. 324
 Saito, Y., see Kato, T. 124
 Saito, Y., see Shinohara, H. 99–100, 104–107, 110, 112–113, 116–118, 122, 124, 128, 136, 138, 145
 Saito, Y., see Takata, M. 110–111, 119–120, 128, 135, 139
 Saito, Y., see Wang, X.D. 110, 116–117, 135–138
 Sakai, A., see Hasegawa, Y. 137–138
 Sakamoto, M., see Aono, H. 400
 Sakamoto, M., see Sadaoka, Y. 400
 Sakamoto, M., see Traversa, E. 400
 Sakamoto, Y., see Ahniyaz, A. 291
 Sakata, M. 111
 Sakata, M., see Ito, Y. 121, 128, 132, 141
 Sakata, M., see Kumazawa, S. 111
 Sakata, M., see Nishibori, E. 114–115, 117–120, 122, 137
 Sakata, M., see Shimotani, H. 116
 Sakata, M., see Shinohara, H. 103
 Sakata, M., see Takata, M. 110–111, 113, 116–120, 122, 128, 135, 137, 139
 Sakata, M., see Wang, C.R. 120
 Sakata, T., see Hasegawa, Y. 325, 437
 Sakata, T., see Masui, T. 283, 289
 Sakbodin, M., see Flytzani-Stephanopoulos, M. 299–300, 302
 Sakka, Y., see Vasyilkiv, O. 294–295
 Sakuraba, A., see Iiduka, Y. 118, 120
 Sakurai, K., see Funasaka, H. 139
 Sakurai, K., see Yamamoto, K. 124
 Sakurai, T. 110, 135
 Sakurai, T., see Hashizume, T. 135, 137–138
 Sakurai, T., see Shinohara, H. 103, 110, 117, 124, 128, 136–138
 Sakurai, T., see Wang, X.D. 135–136
 Saladino, M.L., see Capponetti, E. 388
 Salem, J.R., see Bethune, D.S. 99, 109
 Salem, J.R., see Hoinkis, M. 123
 Salem, J.R., see Johnson, R.D. 99, 121
 Salem, J.R., see Yannoni, C.S. 100, 105, 116, 118, 124
 Salmanov, S.M., see Aliev, O.M. 169–170, 202
 Salthouse, C., see Hilderbrand, S.A. 324
 Saltsburg, H., see Fu, Q. 300–301, 325
 Sambasivan, S., see Chawla, K.K. 343
 Sampson, M.P., see Pan, C. 105
 Sanchez, C., see Ribot, F. 288
 Sanchez, F., see Carretin, S. 302–303
 Sanchez, R.D., see Morales, L. 397
 Sanderson, R.T. 80
 Sangaletti, L., see Traversa, E. 400
 Sankaranarayanan, V., see Krishnamoorthy, C. 398
 Sanna, C., see Malavasi, L. 400
 Santamaria, M., see Bocchetta, P. 328
 Santora, B., see Feng, X.D. 298
 Sapoletova, N.A., see Zhuravleva, N.G. 411
 Saradha, T. 394
 Saradha, T., see Subramania, A. 394
 Saraf, L., see Azad, S. 299
 Satcher, J.H. Jr., see Cherivin, C.N. 397–398
 Sato, H., see Bandow, S. 123, 125
 Sato, H., see Shinohara, H. 99–100, 104–107, 110, 112–113, 116–118, 122, 124, 136, 138, 145
 Sato, M., see Sakata, M. 111
 Sato, N., see Hirata, T. 102
 Sato, T., see Devaraju, M.K. 313
 Sato, T., see El-Toni, A.M. 311
 Sato, T., see Yabe, S. 311
 Sato, W. 116
 Satriano, C., see Scirè, S. 303
 Satyanarayana, C.V.V., see Ratnasamy, P. 303
 Sauviat, M.P., see Beaurepaire, E. 377–378
 Sauviat, M.P., see Giaume, D. 377
 Savina, M. 106
 Sawada, S., see Saito, S. 111, 138
 Saxena, S.K., see Wang, Z.W. 298
 Sayle, D.C. 297–298
 Sayle, D.C., see Feng, X.D. 298
 Sayle, D.C., see Karakoti, A.S. 285, 297
 Sayle, D.C., see Kuchibhatla, S.V.N.T. 298
 Sayle, D.C., see Maicaneanu, S.A. 296
 Sayle, D.C., see Martin, P. 297

- Sayle, D.C., see Sayle, T.X.T. 283, 285, 296–297
- Sayle, T.X.T. 283, 285, 296–297
- Sayle, T.X.T., see Feng, X.D. 298
- Sayle, T.X.T., see Sayle, D.C. 297–298
- Sberveglieri, G., see Barreca, D. 305
- Scerri, E.R. 2–3, 59, 63, 77, 79–80
- Schaak, R.E., see Henkes, A.E. 389
- Schäfer, H. 428, 430
- Schäfer, H., see Klee, W. 201–202
- Schamm, S., see Moine, B. 379
- Schandert, B., see Bartl, A. 122
- Schatz, G.C., see Kelly, K.L. 279
- Scheel, H., see Zollfrank, C. 333, 342
- Scheller, D., see Dunsch, L. 128–129, 135
- Schenk, H., see Helmholdt, R.B. 163
- Schiba, Y., see Watanuki, T. 114, 119, 140
- Schiferl, D., see Wang, Z.W. 298
- Schlebusch, see Kessler, B. 132, 140
- Schleid, T., see Hartenbach, I. 209
- Schlittler, R.R., see Cuberes, M.T. 135
- Schlittler, R.R., see Joachim, C. 135, 137
- Schmalz, T.G. 110
- Schmeisser, D., see Bierman, M.J. 325, 330
- Schmidt, M., see Buerk, M. 134
- Schnablegger, H., see Riwozki, K. 338–339, 343–344, 346, 366, 368, 395
- Schober, H., see Lebedkin, S. 133–135
- Scholes, G.D., see Huxter, V.M. 434–435
- Scholes, G.D., see Mirkovic, T. 434
- Schuetz, P. 341, 343
- Schulte, A., see Babu, S. 310
- Schulte, J. 112–113
- Schuppler, S., see Buerk, M. 134
- Schwartz, J., see Traina, C.A. 323
- Schwarz, W.H.E., see Wang, S.G. 2
- Schwedler, J.T., see Roth, L.M. 109
- Schweitzer, P., see Ruebsam, M. 113, 122
- Scirè, S. 303
- Scrivens, W.A. 106
- Scuseria, G.E. 100
- Scuseria, G.E., see Guo, T. 100–112
- Scuseria, G.E., see Thess, A. 279
- Scuseria, G.E., see Wang, L.S. 100, 111, 142
- Seaborg, G.T. 4, 73, 75–76
- Seal, S., see Babu, S. 310
- Seal, S., see Chen, J.P. 308–309
- Seal, S., see Karakoti, A.S. 285, 297
- Seal, S., see Korsvik, C. 308
- Seal, S., see Kuchibhatla, S.V.N.T. 298
- Seal, S., see Sayle, D.C. 297
- Seal, S., see Tarnuzzer, R.W. 308
- Seddona, A.B., see Tikhomirov, V.K. 416
- Sedmak, G. 303
- Sègre, E., see Perrier, C. 66
- Sehgal, A., see Qi, L. 288
- Seidel, O., see Rajesh, K. 350
- Seifert, G. 122
- Seifert, G., see Bartl, A. 122
- Seifert, G., see Krause, M. 120
- Seits, W.A., see Schmalz, T.G. 110
- Sekar, M., see Thirumalai, J. 445–446
- Selegue, J.P., see Meier, M.S. 106
- Self, W.T., see Korsvik, C. 308
- Senthil Kumaran, R.S., see Ratnasamy, P. 303
- Seo, D.K., see Wu, L.M. 312, 439, 441
- Seo, H., see Choi, B. 421
- Seo, S.J., see Suh, K. 386
- Seo, W., see Choi, B. 421
- Seok, S.I., see Ahn, B.Y. 346
- Seok, S.I., see Jung, H.K. 346
- Seong, H.K., see Choi, H.J. 386–387
- Seraphin, S., see Maensiri, S. 285
- Serquis, A., see Morales, L. 397
- Serra, F., see Capponetti, E. 388
- Serra, J.J., see Rouanet, A. 331
- Serra, O.A., see Pires, A.M. 442, 446–447
- Sethupathi, K., see Krishnamoorthy, C. 398
- Shafer, M.W., see McGuire, T.R. 433
- Shajesh, P., see Rajesh, K. 350
- Shan, G.M., see Feng, J. 323–324
- Shang, X.L., see Hu, Z.A. 401, 407
- Shannon, R.D. 159
- Shao, F.W., see Hilderbrand, S.A. 324
- Sharma, B.P., see Purohit, R.D. 293–294
- Sharma, R., see Wang, R. 296
- Sharma, R., see Wu, L.M. 439, 441
- Shcherbakova, L.G., see Shlyakhtina, A.V. 390
- Shelimov, K.B. 142
- Shelimov, K.B., see Clemmer, D.E. 142
- Shemet, V.Ya. 166, 187, 193, 207–208, 212, 216–217, 227–228, 230, 232, 236
- Shemet, V.Ya., see Daszkiewicz, M. 165, 213, 224
- Shemet, V.Ya., see Gulay, L.D. 166–167, 188, 193, 212–213, 215–216, 227–229, 233, 238
- Shemet, V.Ya., see Marchuk, O.V. 167, 191, 216–217
- Shen, H., see Mathur, S. 400
- Shen, J. 275–450
- Shen, J., see Gu, J.Q. 348, 350, 356

- Shen, J., see Redígolo, M.L. 436
 Shen, Z.R. 313
 Shen, Z.X., see Liao, L. 306–307
 Shepard, J.H. 74
 Sheptyakov, D., see Lin, J.H. 379, 381
 Shetti, V.N., see Ratnasamy, P. 303
 Shi, C.S., see Lian, H. 409, 422
 Shi, J.L. 403
 Shi, J.L., see Bu, W.B. 334–335, 343
 Shi, L.Y., see Zhang, D.S. 287–288
 Shi, L.Y., see Zhou, S. 398, 404
 Shi, N.E., see Han, M. 319
 Shi, S.J., see Zhang, M.F. 431
 Shi, Y.F., see Zhang, F. 409, 423, 425
 Shi, Z.J. 128
 Shi, Z.Q. 120
 Shi, Z.Q., see Tang, B. 286
 Shida, T., see Shinohara, H. 100, 105, 113, 116, 118, 122, 124
 Shieh, D.B., see Huang, C.C. 337
 Shimada, T., see Shi, Z.J. 128
 Shimano, K., see Yuasa, M. 400
 Shimizu, M., see Konishi, T. 419
 Shimotani, H. 116
 Shin, J.H., see Choi, H.J. 386–387
 Shin, J.H., see Suh, K. 386
 Shin, S., see Wells, A.F. 384
 Shinohara, H. 95–146
 Shinohara, H., see Bandow, S. 104, 123, 125
 Shinohara, H., see Cao, B.P. 100
 Shinohara, H., see Dennis, T.J.S. 100, 103, 111, 129
 Shinohara, H., see Hasegawa, Y. 137–138
 Shinohara, H., see Hashizume, T. 135, 137–138
 Shinohara, H., see Hino, S. 114, 122, 133
 Shinohara, H., see Hulman, M. 133
 Shinohara, H., see Inakuma, M. 105, 107, 124, 128–129, 141
 Shinohara, H., see Inoue, T. 121
 Shinohara, H., see Ito, Y. 121, 128, 132, 141
 Shinohara, H., see Kato, H. 144
 Shinohara, H., see Kato, T. 124
 Shinohara, H., see Kimura, T. 109–110
 Shinohara, H., see Krause, M. 120, 133, 135
 Shinohara, H., see Kuroki, K. 105
 Shinohara, H., see Mikawa, M. 144–145
 Shinohara, H., see Nakane, T. 103, 129
 Shinohara, H., see Nishibori, E. 114–115, 117–120, 122, 137
 Shinohara, H., see Ogawa, T. 142
 Shinohara, H., see Okazaki, T. 128
 Shinohara, H., see Pichler, T. 117, 132–133
 Shinohara, H., see Saito, Y. 104
 Shinohara, H., see Sakurai, T. 110, 135
 Shinohara, H., see Shi, Z.J. 128
 Shinohara, H., see Shi, Z.Q. 120
 Shinohara, H., see Shimotani, H. 116
 Shinohara, H., see Sugai, T. 120
 Shinohara, H., see Tagmatarchis, N. 128
 Shinohara, H., see Takahashi, T. 116, 133
 Shinohara, H., see Takata, M. 110–111, 113, 116–120, 122, 128, 135, 137, 139
 Shinohara, H., see Tanaka, N. 110
 Shinohara, H., see Wan, S.M. 100
 Shinohara, H., see Wang, C.R. 120
 Shinohara, H., see Wang, X.D. 110, 116–117, 135–138
 Shinohara, H., see Xu, Z. 100, 108, 129
 Shinohara, H., see Yamamoto, K. 116–117, 137
 Shionoya, S. 404
 Shiromaru, H., see Kikuchi, K. 106, 128, 133
 Shiromaru, H., see Suzuki, S. 102, 109, 122
 Shiromaru, H., see Wakabayashi, T. 102–103, 109
 Shivakumara, C., see Nagabhushana, B.M. 396
 Shivaprasad, S.M., see Aruna, I. 448
 Shlyakhtina, A.V. 390
 Shnulin, A.N., see Amirov, A.S. 170, 205
 Shnulin, A.N., see Guseinov, G.G. 169, 197
 Sholklapper, T.Z. 300
 Shutthanandan, V., see Azad, S. 299
 Si, P.Z. 448
 Si, R. 304–306, 317–318
 Si, R., see Mai, H.X. 284, 286, 304, 306, 424–425
 Si, R., see Sun, X. 410
 Si, R., see Yan, Z.G. 332, 334
 Si, R., see Zhang, Y.W. 290, 327, 332–333, 410–411
 Siekhaus, W. J., see Abrefah, J. 105
 Siligardi, C., see Bondioli, F. 285
 Silva, J.F.A., see Cooke, A.H. 421
 Silvestre-Albero, J., see Concepcion, P. 303
 Simon, P., see Althues, H. 362
 Simoni, E., see Ordonez-Regil, E. 331
 Sin, A., see Dezanneau, G. 396
 Singh, N.S.S.P., see Ansari, A.A. 406
 Singh, S.P., see Saha, S. 306
 Sivakumar, A. 400
 Sivakumar, M. 400

- Sivakumar, S. 412, 414
 Sivakumar, S., see Sudarsan, V. 414
 Skorvanek, I., see Si, P.Z. 448
 Skumryev, V., see Yan, Z.C. 448
 Smalley, R.E. 103
 Smalley, R.E., see Chai, Y. 97–99, 101, 105–106, 109, 114, 141
 Smalley, R.E., see Curl, R.F. 102
 Smalley, R.E., see Guo, T. 100
 Smalley, R.E., see Haufler, R.E. 97, 101–102
 Smalley, R.E., see Heath, J. 97, 141
 Smalley, R.E., see Li, Y.Z. 135
 Smalley, R.E., see Thess, A. 279
 Smalley, R.E., see Wang, L.S. 100, 111, 142
 Smalley, R.E., see Weiss, F.D. 97
 Smalley, R.F., see Kroto, H. 97
 Smarsly, B., see Brezesinski, T. 291
 Smith, A. 53
 Smith, C.A., see Diener, M.D. 105
 Sodaoka, Y., see Aono, H. 400
 Soderholm, L. 109
 Soderlind, F. 398
 Soga, K., see Kamimura, M. 324
 Soga, K., see Konishi, T. 419
 Sogabe, T., see Kubozono, Y. 100, 142
 Solanki, P.R., see Ansari, A.A. 306, 406
 Solis, D., see Ghosh, P. 336
 Solov'eva, L.P., see Bakakin, V.V. 163
 Somers, R.C., see Mitchell, K. 259
 Sommerdijk, J.L. 405
 Song, C.Y., see Wu, X.C. 358
 Song, D.Y., see Huang, P.X. 326
 Song, H.W. 346
 Song, H.W., see Dong, B. 426
 Song, H.W., see Pan, G.H. 359, 377, 381, 384
 Song, H.W., see Qin, R.F. 407, 409–410
 Song, H.W., see Yu, L.X. 343, 346
 Song, J.F., see Liu, L. 329, 365
 Song, J.H., see Wang, Z.L. 279
 Song, P., see Zhang, L. 398
 Song, R.Q., see Fang, Y.P. 313, 326, 329–330, 333–334, 342
 Song, W.G., see Li, Z.X. 291–292
 Song, W.G., see Luo, F. 357–358
 Song, W.G., see Yuan, Q. 296
 Song, W.G., see Zhou, H.P. 291, 293
 Song, X.Y., see Chen, G.Z. 288
 Song, X.Y., see Fan, W.L. 357–359, 363, 371, 374
 Song, Y.H., see Jia, G. 313
 Sonneveld, E.J., see Helmholdt, R.B. 163
 Sonstrom, P., see Borchert, Y. 326, 402
 Soucek, M.D., see Gu, H. 291–292
 Spaeth, C., see Fumagalli, P. 433
 Spanier, J.E. 299
 Spanier, J.E., see Zhang, F. 283
 Speghini, A., see Vetrone, F. 322
 Spek, A.L. 168
 Spinolo, G., see Anselmi-Tamburini, U. 299
 Sra, A.K., see Henkes, A.E. 389
 Srdanov, G., see Allemand, P.M. 121
 Sreenivas, K., see Saha, S. 306
 Srinivas, D., see Ratnasamy, P. 303
 Staffel, T., see Meyer, G. 418
 Stanisz, G.J., see Évanics, F. 418
 Stark, W.J. 295
 Stark, W.J., see Madler, L. 294
 Steele, B.D. 70
 Stepanov, A., see Bour, G. 449
 Stępień-Damm, J., see Gulay, L.D. 167
 Stępień-Damm, J., see Gulay, L.D. 163, 166–167, 193, 208–210, 212–213, 215–217, 227–229, 235, 240
 Stępień-Damm, J., see Lychmanyuk, O.S. 159, 164, 207–208
 Stępień-Damm, J., see Shemet, V.Ya. 27, 166, 187, 207, 212, 230, 232
 Stevenson, S. 107, 116, 120, 124
 Stevenson, S., see Anderson, M.R. 116, 124, 126
 Stevenson, S., see Macfarlane, R.M. 116, 132
 Stevenson, S., see van Loosdrecht, P.H.M. 116, 124–125
 Stewart, A.W. 48
 Stewart, P.J. 2–3, 74, 77
 Stöber, W. 431
 Stoll, S.L., see Regulacio, M.D. 436–437
 Storz, J., see Kömpe, K. 340, 343
 Stouwdam, J.W. 343–345, 353, 371, 374, 406, 412
 Stouwdam, J.W., see Dekker, R. 415
 Stoyanov, S., see Yan, Z.C. 448
 Strek, W., see Deren, P.J. 388
 Strek, W., see Hreniak, D. 388
 Strek, W., see Karbowski, M. 421–422
 Strek, W., see Kepinski, L. 386
 Stucchi, E.B., see Vila, L.D.D. 442, 445
 Studenikin, S.A., see Hao, J.H. 312
 Su, D.S., see Djerdj, I. 329
 Su, G., see Zhao, F. 434, 436
 Su, J., see Zeng, J.H. 422
 Su, M.Z., see Ren, M. 379
 Su, M.Z., see Yang, Z. 379
 Su, Q., see Liang, L. 409, 422

- Su, Q., see Wu, H. 354
 Su, Q., see Zhuang, J.L. 422
 Su, T., see Yeretzián, C. 99, 105, 109
 Su, W.C., see Huang, C.C. 337
 Su, W.H., see Zhou, X.F. 400
 Su, Y.G. 423
 Su, Y.G., see Yi, N. 402
 Subramania, A. 394
 Subramania, A., see Saradha, T. 394
 Sudarsan, V. 414
 Sue, K., see Adschiri, T. 283
 Sueki, K. 130, 144
 Sueki, K., see Kikuchi, K. 128, 130, 144
 Sueki, K., see Kobayashi, K. 114–115
 Sueki, K., see Ohtsuki, T. 144
 Sueki, K., see Sato, W. 116
 Suematsu, H. 114, 119
 Suematsu, H., see Kawata, H. 119
 Suematsu, H., see Watanuki, T. 114, 119, 140
 Suematsu, T., see Inoue, T. 121
 Suenaga, K., see Cao, B.P. 100
 Suenaga, K., see Okazaki, T. 128
 Suenaga, K., see Shi, Z.J. 128
 Sugai, T. 120
 Sugai, T., see Inoue, T. 121
 Sugai, T., see Ito, Y. 121, 128, 132, 141
 Sugai, T., see Kimura, T. 109–110
 Sugai, T., see Nakane, T. 103, 129
 Sugai, T., see Nishibori, E. 114–115, 117–120, 122, 137
 Sugai, T., see Ogawa, T. 142
 Sugai, T., see Shi, Z.J. 128
 Sukanuma, T., see Suzuki, S. 102
 Sugiyama, K., see Funasaka, H. 139
 Suh, K. 386
 Suh, K., see Choi, H.J. 386–387
 Suits, J.C. 433
 Suljoti, E. 341
 Sun, A.H., see Zhuang, Z. 394
 Sun, C.W. 287–288, 290, 325
 Sun, G.Q., see Gao, L. 403, 434, 443
 Sun, G.Q., see Zhang, H.W. 366
 Sun, H.L., see Zhao, F. 434, 436
 Sun, J.H., see Guan, M.Y. 335
 Sun, J.H., see Han, M. 319
 Sun, J.H., see Sun, C.W. 287
 Sun, J.J., see Goldys, E.M. 312, 322
 Sun, L.D. 362, 442
 Sun, L.D., see Du, Y.P. 419–420, 424, 426
 Sun, L.D., see Gu, J.Q. 348, 350, 356
 Sun, L.D., see Jia, C.J. 356–357, 371–372
 Sun, L.D., see Jiang, X.C. 380–381, 383, 385
 Sun, L.D., see Li, Z.X. 291–292
 Sun, L.D., see Mai, H.X. 284, 286, 304, 306, 341, 424–425
 Sun, L.D., see Shen, J. 356, 412
 Sun, L.D., see Si, R. 317
 Sun, L.D., see Wei, Z.G. 380, 382–383
 Sun, L.D., see Yan, C.H. 369
 Sun, L.D., see Yuan, Q. 282, 296
 Sun, P.C., see Shen, Z.R. 313
 Sun, S.X., see Chen, G.Z. 288
 Sun, S.X., see Fan, W.L. 357–359, 363, 371, 374
 Sun, X. 410
 Sun, X., see Zhang, Y.W. 410–411
 Sun, X., see Zhou, H.P. 291, 293
 Sun, X.D., see Liu, Z.G. 442, 446
 Sun, X.M. 288
 Sun, X.M., see Wang, X. 441
 Sun, X.M., see Yan, R.X. 333
 Sun, X.M., see Zhou, K.B. 304
 Sun, Y.J. 354
 Sun, Y.X., see Mo, Z.L. 328
 Sun, Y.Y., see Galstyan, E. 400
 Sung, H.H.Y., see Zhuang, J.L. 422
 Sun-Waterhouse, D., see
 Waterhouse, G.I.N. 310
 Sutorik, A.C., see Feng, X.D. 298
 Suyver, J.F. 426
 Suzuki, S. 102, 109, 122, 125
 Suzuki, S., see Kato, T. 116, 122, 124–125
 Suzuki, S., see Kessler, B. 132, 140
 Suzuki, S., see Kikuchi, K. 106, 124, 128, 133, 144
 Suzuki, S., see Miyake, Y. 115
 Suzuki, S., see Sato, W. 116
 Suzuki, S., see Suzuki, T. 126, 128
 Suzuki, S., see Wakabayashi, T. 102–103, 109
 Suzuki, T. 116, 126, 128, 146
 Suzuki, T., see Akasaka, T. 115–116, 146
 Suzuki, T., see Kato, T. 122, 124–125
 Suzuki, T., see Kikuchi, K. 124, 128
 Suzuki, T., see Yamamoto, K. 105, 107, 123, 129
 Svensson, E.E. 402
 Szabadváry, F. 4
 Tacca, A., see Anselmi-Tamburini, U. 299
 Tacke, I., see Noddack, W. 65
 Taghavinia, N. 385
 Tagmatarchis, N. 128

- Tajiri, T., see Kira, H. 402
 Takabayashi, Y., see Kubozono, Y. 142
 Takahashi, H., see Hino, S. 122, 128, 140
 Takahashi, T. 116, 133
 Takahashi, T., see Akasaka, T. 146
 Takahashi, T., see Funasaka, H. 139
 Takahashi, T., see Kato, T. 122, 124–125, 146
 Takahashi, T., see Suzuki, T. 126, 128, 146
 Takahashi, T., see Yamamoto, K. 105–107, 123, 128–129
 Takata, M. 110–111, 113, 116–120, 122, 128, 135, 137, 139
 Takata, M., see Ito, Y. 121, 128, 132, 141
 Takata, M., see Nishibori, E. 114–115, 117–120, 122, 137
 Takata, M., see Shimotani, H. 116
 Takata, M., see Shinohara, H. 103
 Takata, M., see Wang, C.R. 120
 Takeshita, S. 352, 369–370
 Takizawa, H., see Wang, Y.H. 380
 Tamai, H. 350
 Tampier, M. 164, 177
 Tampier, M., see Johrendt, D. 177
 Tampier, M., see Pocha, R. 162, 166, 173, 186
 Tamura, H., see Kira, H. 402
 Tan, R., see Zhu, Y. 403
 Tan, T.T.Y., see Das, G.K. 323
 Tan, Y., see Zhang, Y.X. 319
 Tanabe, E., see Purwanto, A. 388–389
 Tanaka, A., see Adachi, T.A. 438
 Tanaka, A., see Hasegawa, Y. 438
 Tanaka, H., see Hasegawa, Y. 325
 Tanaka, H., see Yanagida, T. 400
 Tanaka, K. 433
 Tanaka, K., see Hasegawa, Y. 438
 Tanaka, M., see Kumazawa, S. 111
 Tanaka, N. 110
 Tang, B. 286
 Tang, C.C. 286, 330–331, 334
 Tang, D.H., see Wang, J.S. 415
 Tang, G., see Yu, R.B. 323
 Tang, K.B., see Han, Z.H. 287
 Tang, Q. 328
 Tang, Y., see Lu, Z. 390
 Taniguchi, C., see Yada, M. 313–314
 Taninaka, A., see Inakuma, M. 141
 Taninaka, A., see Kato, H. 144
 Taninaka, A., see Nishibori, E. 114–115, 117–120, 122, 137
 Taninaka, A., see Shimotani, H. 116
 Tanke, H.J., see Corstjens, P.L.A.M. 440, 446–447
 Tanke, H.J., see Zijlmans, H. 440
 Tans, S.J. 279
 Tansho, M., see Yamamoto, K. 116–117, 137
 Tao, F. 409
 Tao, F.F., see Guan, M.Y. 335
 Tao, Y.R., see Wei, Z.G. 383
 Tao, Y.R., see Wu, X.C. 358–359
 Tao, Y.R., see Yang, Z. 379
 Tarnuzzer, R.W. 308
 Tatehata, N., see Tanaka, K. 433
 Taylor, J., see Goldburt, E.T. 312, 321
 Taylor, R. 105–106
 Taylor, R., see Godly, E.W. 98
 Tealdi, C., see Malavasi, L. 400
 Tejada, E.M., see Gonzalez-Ortega, J.A. 385–386
 Teke, A., see Ozgur, U. 279
 Tellgmann, R. 102, 142
 Tellgmann, R., see Campbell, E.E.B. 102, 142
 Tellgmann, R., see Krawez, N. 102
 Tellgmann, R., see Suzuki, S. 109
 Teng, F. 400
 Teng, F., see Liang, S. 396
 Teraoka, Y., see Yuasa, M. 400
 Terauchi, I., see Nishibori, E. 114–115, 117–120, 122, 137
 Thammachart, M. 295
 Thatt, T., see Zhang, Y.X. 319
 Thess, A. 103, 279
 Thevuthasan, S., see Azad, S. 299
 Thevuthasan, S., see Karakoti, A.S. 285, 297
 Thirumalai, J. 445–446
 Thirumalai, J., see Nakkiran, A. 445
 Thoma, R.E. 419–420
 Thomann, R., see Ehlert, O. 430
 Thompsett, D., see Wright, C.S. 295
 Thomsen, J. 55–56, 68, 70
 Thongchant, S. 325, 437
 Thongchant, S., see Hasegawa, Y. 325
 Thrash, T.P., see Cagle, D.W. 144
 Thyssen, P. 1–87
 Tian, Y. 446
 Tie, S.L., see Chang, M.L. 365–366
 Tien, J., see Cagle, D.W. 144–145
 Tien-Thao, N. 395
 Tikhomirov, V.K. 416
 Tillement, O., see Bazzi, R. 316
 Tillement, O., see Louis, C. 312
 Tiltsworth, R., see Gnanasekar, K.I. 397
 Tissue, B.M., see Bihari, B. 321
 Tissue, B.M., see Eilers, H. 312
 Tissue, B.M., see Williams, D.K. 321–322

- Titelman, L., see Fita, I. 399
 Titelman, L., see Markovich, V. 397
 Tittel, F.K., see Heath, J. 97, 141
 Tiwari, A. 396
 Tokumo, K., see Fujihara, S. 390, 419
 Tomanek, D., see Thess, A. 279
 Tomanek, D., see Wang, Y. 100
 Tomas, A. 203, 233
 Tomas, A., see Lemoine, P. 170, 203
 Tomblor, T.W., see Fan, S.S. 279
 Tomiyama, T., see Dennis, T.J.S. 100, 103, 111, 129
 Tomiyama, T., see Inoue, T. 121
 Tomiyama, T., see Nakane, T. 103, 129
 Tomiyama, T., see Wang, C.R. 120
 Tomiyama, T., see Yamamoto, K. 116–117, 137
 Tomura, K., see Kobayashi, K. 114–115
 Tondello, E., see Armelao, L. 399
 Tondello, E., see Barreca, D. 305, 418
 Tondello, E., see Krishnan, V. 399
 Tong, Y. 392
 Torikai, T., see Yada, M. 313–314
 Torres, M.E., see Yanes, A.C. 415
 Tosi, M.P., see Akdeniz, Z. 404–405
 Tougait, O. 171
 Tour, M.J., see Scrivens, W.A. 106
 Traina, C.A. 323
 Trampert, K., see Zharkouskaya, A. 338
 Traversa, E. 400
 Traversa, E., see Aono, H. 400
 Traversa, E., see Sadaoka, Y. 400
 Treacy, M.M.J. 279
 Tressaud, A., see Nakajima, T. 405
 Tretyakov Yu, D., see Zhuravleva, N.G. 411
 Trifonov, D.N. 19, 22–23, 34, 37, 63, 70
 Trifonov, V.D., see Trifonov, D.N. 63
 Trikalitis, P.N., see Giannakas, A.E. 400
 Trivedi, D.C., see Dhanaraj, J. 442, 445
 Trivedi, D.C., see Thirumalai, J. 445
 Trojer, F. 176
 Trots, D.M., see Suljoti, E. 341
 Trovarelli, A. 281, 293, 295
 Tsai, K.R., see Chao, Z.S. 418
 Tsai, T., see Murray, E.P. 299
 Tseng, Y.H., see Lin, Y.S. 329
 Tso, T.S.C., see Wan, S.M. 100
 Tsuchiya, T., see Iiduka, Y. 117–118, 120, 137
 Tsuda, K., see Kira, H. 402
 Tsukahara, Y., see Kataoka, T. 437
 Tsunekawa, S. 298
 Tsuzaki, M., see Aono, H. 400
 Tu, B., see Zhang, F. 409, 423, 425
 Tugia, M. 380
 Turner, W.E.S., see Friend, N.J. 54
 Tyagi, A.K., see Purohit, R.D. 293–294
 Tyagi, S., see Mamontov, E. 304
 Tyas, M.J., see Prentice, L.H. 416
 Uehara, M., see Wang, H.Z. 319
 Ugarte, D., see Deheer, W.A. 279
 Uheda, K., see Wang, Y.H. 380
 Ukita, S., see Kubozono, Y. 100, 142
 Ulmer, K., see Merz, H. 80
 Umeda, B., see Takata, M. 110–111, 113, 116–117, 119–120, 122, 128, 135, 137, 139
 Umishita, K., see Hino, S. 114, 122, 133
 Ungerer, J.R. 118, 125
 Urbain, G. 59, 63
 Urban, J., see Kharrazi, S. 396
 Urland, W., see Hatscher, S.T. 162, 173
 Utsumi, H., see Inoue, T. 121
 Uvadal, K., see Soderlind, F. 398
 Uvarov, N.F., see Frolova-Borchert, Y.V. 402
 Uy, D. 350
 Vail, T., see Niedbala, R.S. 440
 Vail, T., see Rijke, F.v.-d. 440
 Vail, T., see Zijlmans, H. 440
 Vaimakis, T.C., see Giannakas, A.E. 400
 Vallejo, R., see Niedbala, R.S. 440
 Van den Broek, A.J. 59
 Van der Avert, P. 325
 Van Heuvelen, K.M., see Bierman, M.J. 325, 330
 van Hommes, E., see Mauser, H. 102
 van Loosdrecht, P.H.M. 116, 124–125
 van Loosdrecht, P.H.M., see Macfarlane, R.M. 116, 132
 van Spronsen, J. 2–3, 26, 59
 van Veggel, F.C.J.M., see Dekker, R. 415
 van Veggel, F.C.J.M., see Diamante, P.R., 412
 van Veggel, F.C.J.M., see Evancis, F. 418
 van Veggel, F.C.J.M., see Sivakumar, S. 412, 414
 van Veggel, F.C.J.M., see Stouwdam, J.W. 343–345, 353, 371, 374, 406, 412

- van Veggel, F.C.J.M., see Sudarsan, V. 414
 Varyukhin, V.N., see Fita, I. 399
 Vasyukiv, O. 294–295
 Vazquez-Vazquez, C. 400
 Vega, D., see Morales, L. 397
 Veirs, D.K., see Diener, M.D. 105
 Veith, M., see Mathur, S. 400
 Venable, F.P. 2
 Venkatesan, T., see Kharrazi, S. 396
 Verbruggen, I., see Ribot, F. 288
 Verdon, E. 289
 Veres, T., see Soderlind, F. 398
 Verschueren, A.R.M., see Tans, S.J. 279
 Vetrone, F. 322
 Vetrone, F., see Boyer, J.C. 428
 Vetrone, F., see Naccache, R. 430
 Viana, B., see Buissette, V. 375
 Vietze, K., see Krause, M. 120
 Vila, L.D.D. 442, 445
 Villanti, S., see Traversa, E. 400
 Villanueva, A., see Zhang, R. 395
 Villar, G.E.J. 80
 Vilquin, B., see Yanagida, T. 400
 Vincent, H., see Dezanneau, G. 396
 Visco, S.J., see Sholklipper, T.Z. 300
 Vohs, J.M., see Park, S.D. 299
 Vovan, T., see Noël, R. 200
 Vradamn, L., see Fita, I. 399
 Vradman, L., see Markovich, V. 397
- Wachsman, E., see White, B. 404
 Wachter, P. 433
 Wada, Y., see Hasegawa, Y. 325, 437
 Wada, Y., see Kataoka, T. 437
 Wada, Y., see Thongchant, S. 325, 437
 Waelchli, M., see Akasaka, T. 115
 Waestberg, B., see Rosen, A. 111, 138
 Wagner, M.J., see Nelson, J.A. 449
 Waiblinger, M., see Knapp, C. 102
 Wakabayashi, T. 102–103, 109
 Wakabayashi, T., see Kikuchi, K. 106, 128, 133
 Wakabayashi, T., see Suzuki, S. 125
 Wakahara, T., see Iiduka, Y. 117–118, 120, 137
 Wakefield, G. 312, 316
 Walabayashi, T., see Suzuki, S. 109
 Walker, J. 54
 Walton, R.I., see Wright, C.S. 295
 Wan, H.L., see Chao, Z.S. 418
 Wan, S.M. 100
 Wan, Y., see Zhang, F. 409, 423, 425
 Wang, C., see Krause, M. 120
 Wang, C.M., see Azad, S. 299
 Wang, C.R. 120
 Wang, C.R., see Shi, Z.Q. 120
 Wang, C.S., see Wang, C.Y. 290
 Wang, C.Y. 290
 Wang, D. 400, 407
 Wang, D.S. 291
 Wang, D.W., see You, F.T. 385
 Wang, E.B., see Cao, M.H. 335, 364, 406, 446
 Wang, F. 360, 376, 385, 407, 412, 426, 428–430
 Wang, F., see Dong, B. 426
 Wang, G.B., see Regulacio, M.D. 437
 Wang, G.F. 409
 Wang, G.F., see Wang, Y. 407
 Wang, G.L., see Tang, B. 286
 Wang, H. 364–365, 373, 397
 Wang, H., see Lin, C.K. 380
 Wang, H., see Liu, C.H. 426, 428
 Wang, H., see Xu, H.Y. 364
 Wang, H., see Yu, M. 343
 Wang, H., see Zeng, J. 391–392
 Wang, H.C. 287, 290
 Wang, H.C., see Lu, C.H. 287
 Wang, H.Z. 319
 Wang, H.Z., see Zhu, X.X. 411
 Wang, J., see Lu, Z. 390
 Wang, J., see Wu, H. 348
 Wang, J.C. 327, 408
 Wang, J.G., see Shen, Z.R. 313
 Wang, J.S. 415
 Wang, J.X., see Liu, G.X. 329, 365
 Wang, L. 348, 412
 Wang, L., see Chai, Y. 97–99, 101, 105–106, 109, 114, 141
 Wang, L., see Wang, L.Y. 415
 Wang, L.L., see Hou, Z.Y. 342, 365, 376
 Wang, L.L., see Wang, G.F. 409
 Wang, L.L., see Wang, Y. 407
 Wang, L.L., see Yang, J. 323
 Wang, L.S. 100, 111, 142
 Wang, L.S., see Haufler, R.E. 97, 101–102
 Wang, L.Y. 407, 415, 422, 424
 Wang, L.Y., see Wang, L. 412
 Wang, M.Q. 406, 422
 Wang, M.Q., see Huang, Q.L. 411
 Wang, M.Q., see Wang, F. 385, 407, 412
 Wang, N. 357
 Wang, Q.Q., see Deng, H. 363, 373
 Wang, Q.Q., see Yu, X.F. 414
 Wang, R. 296

- Wang, S. 390
 Wang, S., see Wang, S. 390
 Wang, S., see Xia, G. 388
 Wang, S., see Yu, M. 365
 Wang, S.B., see Zhou, Y.H. 322
 Wang, S.F., see Zhang, H.P. 370
 Wang, S.G. 2
 Wang, S.M. 392
 Wang, S.M., see Zhang, H.P. 370
 Wang, T., see Song, H.W. 346
 Wang, W. 126, 128
 Wang, W., see Yang, Z. 379
 Wang, W.N., see Purwanto, A. 388–389
 Wang, W.Z., see Fisher, M.J. 337
 Wang, X. 287, 290, 313, 326–328, 330, 361, 406, 408, 441
 Wang, X., see Gao, L. 403, 434, 443
 Wang, X., see Han, M. 319
 Wang, X., see Liang, X. 295, 422
 Wang, X., see Sun, Y.J. 354
 Wang, X., see Tong, Y. 392
 Wang, X., see Wang, Y.P. 395
 Wang, X., see Yan, R.X. 333
 Wang, X., see Zhang, L. 390
 Wang, X., see Zhou, K.B. 304
 Wang, X.D. 110, 116–117, 135–138
 Wang, X.D., see Feng, X.D. 298
 Wang, X.D., see Hashizume, T. 135, 137–138
 Wang, X.D., see Sakurai, T. 110, 135
 Wang, X.D., see Shinohara, H. 110, 117, 128, 136
 Wang, X.H., see Niu, J.L. 308
 Wang, X.J. 279, 333
 Wang, X.J., see Di, W.H. 333–334
 Wang, X.P., see Zhuang, Z. 394
 Wang, X.Q., see Zhang, M.F. 431
 Wang, X.Y., see Zhang, M.F. 408, 431
 Wang, X.Z., see Wu, Q. 408
 Wang, Y. 100, 400–401, 407
 Wang, Y., see Kneipp, K. 279
 Wang, Y., see Wang, Y. 400–401
 Wang, Y.F., see Liang, L. 409, 422
 Wang, Y.F., see Zeng, J.H. 419
 Wang, Y.H. 380
 Wang, Y.L., see Huang, P.X. 326
 Wang, Y.P. 395
 Wang, Y.S., see Bao, F. 416
 Wang, Y.S., see Chen, D.Q. 280, 416–418
 Wang, Y.S., see Hu, Z.J. 407, 416
 Wang, Y.X., see Lin, J.H. 379, 381
 Wang, Z., see Flytzani-Stephanopoulos, M. 299–300, 302
 Wang, Z., see Yu, M. 365
 Wang, Z.J., see Tao, F. 409
 Wang, Z.K., see Zhu, H.L. 360
 Wang, Z.L. 279, 298, 409, 441
 Wang, Z.L., see Feng, X.D. 298
 Wang, Z.L., see Hu, C.G. 294, 313, 328, 407
 Wang, Z.L., see Sayle, D.C. 298
 Wang, Z.L., see Zhang, Z. 294
 Wang, Z.W. 298
 Wang, Z.W., see Sayle, D.C. 297
 Wang, Z.X., see Sun, C.W. 288, 290, 325
 Wang, Z.Y. 409
 Warriar, K.G.K., see Rajesh, K. 337, 350
 Wasserman, E., see Krusic, P.J. 121
 Watanabe, H. 138
 Watanabe, M., see Kobayashi, K. 114–115
 Watanuki, T. 114, 119, 140
 Watanuki, T., see Kawata, H. 119
 Watari, T., see Yada, M. 313–314
 Waterhouse, G.I.N. 310
 Waterland, M.R., see Waterhouse, G.I.N. 310
 Watson, G.W., see Maicaneanu, S.A. 296
 Watson, G.W., see Martin, P. 297
 Weaver, C.F., see Thoma, R.E. 419
 Weaver, J.H. 99, 112, 116, 122, 138
 Weaver, J.H., see Guo, T. 100
 Weaver, J.H., see Poirier, M.D. 122, 132, 138, 140
 Weaver, J.W., see Li, Y.Z. 135
 Weber, A., see Fu, Q. 292, 300
 Weber, W.H., see Uy, D. 350
 Weckhuysen, B.M. 325
 Weckhuysen, B.M., see Van der Avert, P. 325
 Weeks, M.E. 4, 59, 63
 Wegh, R.T. 417
 Weglarowicz, M.A., see Deren, P.J. 388
 Wei, G.D., see Wang, G.F. 409
 Wei, G.D., see Wang, Y. 407
 Wei, L.H., see Jia, C.J. 356, 371
 Wei, W., see Yu, R.B. 323
 Wei, X.W., see Guan, M.Y. 335
 Wei, Y. 412
 Wei, Z.G. 380, 382–383
 Wei, Z.G., see Jiang, X.C. 380, 385
 Weiden, N., see Knapp, C. 124, 128
 Weidinger, A., see Knapp, C. 102
 Weidinger, A., see Mauser, H. 102
 Weis, P., see Beck, R.D. 109
 Weiss, F.D. 97
 Weiss, F.D., see Conchon, F. 400
 Weiss, S., see Bruchez, M. 279
 Weissleder, R., see Hilderbrand, S.A. 324

- Wells, A.F. 418
 Wells, M.R., see Cooke, A.H. 421
 Wen, F., see Wells, A.F. 384
 Wendin, G., see Nuroh, K. 80
 Wendt, H.R., see Wilson, R.J. 135
 Weng, L., see Ding, J. 128
 Werner, A. 71–72, 81
 Westbrook, C. 418
 Whangbo, M.-H., see Gauthier, G. 161, 173
 Whetten, R.L., see Allemand, P.M. 121
 Whetten, R.L., see Alvarez, M.M. 99, 110, 115–116
 Whetten, R.L., see Gillan, E. 100
 Whetten, R.L., see Yeretizian, C. 99, 105, 109
 White, B. 404
 White, G.D., see Clark, R.W. 3, 77
 White, H.W., see Wragg, J.L. 135
 White, T., see Zhang, Y.X. 319
 Wickleder, M.S. 331, 404–405, 428
 Wickleder, M.S., see Meyer, G. 404–405, 428
 Wiley, J.B., see Yeretizian, C. 99, 105, 109
 Wilhelm, M., see Borchert, Y. 326, 402
 Wilkins, J.R., see Glaspell, G. 323
 Willem, R., see Ribot, F. 288
 Williams, D.K. 321–322
 Williams, I.D., see Zhuang, J.L. 422
 Wilson, L.J., see Cagle, D.W. 144–145
 Wilson, L.J., see Haufler, R.E. 101
 Wilson, R.J. 135
 Wisniewski, A., see Fita, I. 399
 Wisniewski, A., see Markovich, V. 397
 Wittig, J., see Probst, C. 80
 Wittmann, G., see Macfarlane, R.M. 116, 132
 Wolcyrz, M., see Gulay, L.D. 167, 191, 210–211, 216–217, 227–228, 240
 Wolcyrz, M., see Kepinski, L. 386
 Wolf, M., see Dunsch, L. 135, 140
 Wong, T., see Wan, S.M. 100
 Wragg, J.L. 135
 Wright, C.S. 295
 Wright, J.C., see Ding, X. 116, 130, 132
 Wu, F., see Huang, P.X. 326
 Wu, G.S. 312
 Wu, H.Y. 348, 354
 Wu, H.Y., see Hu, Z.A. 401, 407
 Wu, J.H. 356, 375
 Wu, L.-B. 209
 Wu, L.J., see Han, W.Q. 286–287
 Wu, L.M. 312, 439, 441
 Wu, L.M., see Huang, Y.Z. 330, 441, 445
 Wu, M.M., see Liang, L. 409, 422
 Wu, M.M., see Wu, H. 354
 Wu, M.M., see Zhuang, J.L. 422
 Wu, P., see Christuk, A.E. 239
 Wu, Q. 408
 Wu, Q.S., see Ma, J. 257, 380
 Wu, Q.Y., see Cao, M.H. 335, 364, 406, 446
 Wu, W.H., see Wang, M. 422
 Wu, X.C. 358–359
 Wu, X.C., see Markovich, V. 397
 Wu, X.C., see Shi, Z.Q. 120
 Wu, Y., see Jiang, Y. 443
 Wu, Y., see Zhang, K. 389
 Wu, Z.S., see Zhou, J.F. 415
 Wudl, F., see Allemand, P.M. 121
 Wudl, F., see Khemani, K.C. 105
 Wurth, W., see Suljoti, E. 341
 Wurzb, P., see Soderholm, L. 109
 Wyruboff, G. 36
- Xi, B.J., see Zhang, M.F. 408
 Xia, B. 294
 Xia, D.Y., see Liang, L. 409, 422
 Xia, G. 388
 Xia, T., see Cui, X.Z. 380
 Xiao, G.L., see Sun, C.W. 287
 Xiao, J.Q., see Savina, M. 106
 Xiao, J.Q., see Yan, Z.C. 448
 Xiao, P., see Wu, Q. 408
 Xiao, S.G. 411
 Xiao, S.G., see Deng, H. 363, 373
 Xiao, S.G., see Yang, X.L. 411
 Xiao, X.D., see Dong, G.P. 426
 Xiao, Z., see Haufler, R.E. 101
 Xie, M.Y., see Yu, X.F. 414
 Xie, S.H., see Qin, R.F. 407, 409–410
 Xie, S.H., see Zhang, F. 423, 425
 Xie, T., see Wang, D.S. 291
 Xie, T., see Wu, G.S. 312
 Xie, Y., see Jiang, Y. 443
 Xie, Y., see Wang, C.Y. 290
 Xie, Y., see Yu, S.H. 443
 Xin, Q., see Zhang, H.W. 366, 373–374
 Xing, X.R., see Yan, L. 288, 326, 328
 Xing, Y. 336
 Xiong, L.Q., see Hu, H. 407, 412–413, 430
 Xiong, Y.F., see Zhang, Z. 294
 Xiu, Z.L. 346
 Xiu, Z.L., see Liu, S.W. 342
 Xiu, Z.L., see Wang, S.M. 392
 Xiu, Z.L., see Zhang, H.P. 370
 Xiu, Z.M., see Liu, Z.G. 442, 446

- Xu, A.W. 328–330
 Xu, A.W., see Fang, Y.P. 313, 326, 329–330, 333–334, 342–343
 Xu, B.Q., see Liang, X. 295
 Xu, B.Q., see Ye, Q. 306
 Xu, C.H., see Thess, A. 279
 Xu, C.M., see Wang, H. 397
 Xu, D.P., see Zhou, X.F. 400
 Xu, F.X., see Liu, S.W. 342
 Xu, G.X. 279
 Xu, H. 400
 Xu, H.F., see Liang, L. 409, 422
 Xu, H.F., see Wu, H. 354
 Xu, H.Y. 364
 Xu, J., see Li, Z.X. 291–292
 Xu, J., see Xia, G. 388
 Xu, J.H., see You, F.T. 385
 Xu, J.Z., see Liao, X.H. 284
 Xu, K.L., see Xuan, Y.L. 306
 Xu, L., see Uy, D. 350
 Xu, L., see Zhang, F. 423, 425
 Xu, R., see Chen, D. 391
 Xu, R., see Zhang, Y.X. 319
 Xu, S.K., see Liu, Z.G. 442, 446
 Xu, X.J., see Sayle, D.C. 297
 Xu, X.X., see Yu, R.B. 323
 Xu, Z.D. 100, 108, 129
 Xu, Z.D., see Guan, M.Y. 335
 Xu, Z.D., see Han, M. 319
 Xu, Z.D., see Ma, L. 408
 Xu, Z.D., see Nakane, T. 103, 129
 Xu, Z.D., see Wan, S.M. 100
 Xuan, Y.L. 306
 Xue, Q., see Wang, X.D. 110, 116–117, 136–138
 Xue, Q.J., see Zhang, Z.F. 329, 415
 Xue, Q.K., see Sakurai, T. 110, 135
 Xue, X.F., see Zhou, X.F. 400
 Xue, X.J., see Wang, F. 360, 376
 Xue, Z.L., see Wang, M. 406, 422

 Yabe, S. 311
 Yada, M. 313–314
 Yagi, K., see Shinohara, H. 144
 Yakel, H.A., see Thoma, R.E. 419
 Yamaguchi, H., see Bandow, S. 123, 125
 Yamaguchi, H., see Shinohara, H. 106–107, 116, 124, 145
 Yamamoto, E., see Hulman, M. 133
 Yamamoto, E., see Nakane, T. 103, 129
 Yamamoto, E., see Pichler, T. 117, 132–133
 Yamamoto, E., see Takata, M. 116–117, 119, 137
 Yamamoto, K. 105–107, 116–117, 123–124, 128–129, 137
 Yamamoto, K., see Akasaka, T. 115, 146
 Yamamoto, K., see Funasaka, H. 139
 Yamamoto, K., see Kato, T. 122, 124–125, 146
 Yamamoto, K., see Suzuki, T. 126, 128, 146
 Yamamoto, Y., see Takata, M. 118–119
 Yamauchi, K., see Suzuki, S. 122
 Yamazaki, H., see Kubozono, Y. 100, 142
 Yamazaki, S., see Hasegawa, Y. 137–138
 Yamazaki, S., see Kira, H. 402
 Yamazaki, S., see Shinohara, H. 124, 137–138
 Yamazoe, N., see Yuasa, M. 400
 Yan, B., see Wu, J.H. 356, 375
 Yan, C.H. 275–450
 Yan, C.H., see Du, Y.P. 419–420, 424, 426
 Yan, C.H., see Gu, J.Q. 348, 350, 356
 Yan, C.H., see Jia, C.J. 356–357, 371–372
 Yan, C.H., see Jiang, X.C. 380–381, 383, 385
 Yan, C.H., see Li, Z.X. 291–292
 Yan, C.H., see Liao, L. 306–307
 Yan, C.H., see Luo, F. 357–358
 Yan, C.H., see Mai, H.X. 284, 286, 304, 306, 341, 424–425
 Yan, C.H., see Shen, J. 356, 412
 Yan, C.H., see Si, R. 304–305, 317–318
 Yan, C.H., see Sun, L.D. 362, 442
 Yan, C.H., see Sun, X. 410
 Yan, C.H., see Wei, Z.G. 380, 382–383
 Yan, C.H., see Yan, Z.G. 332, 334
 Yan, C.H., see Yuan, Q. 282, 296
 Yan, C.H., see Zhang, Y.W. 290, 327, 332–333, 410–411
 Yan, C.H., see Zhou, H.P. 291, 293
 Yan, C.H., see Zhu, Y. 403
 Yan, H., see Wang, H. 364
 Yan, H., see Xu, H.Y. 364
 Yan, H., see Zeng, J. 391–392
 Yan, J., see Lian, H. 409, 422
 Yan, L. 288, 326, 328
 Yan, R.X. 333, 409
 Yan, R.X., see Shi, J. 403
 Yan, R.X., see Zeng, J.H. 422
 Yan, T.Y., see Huang, P.X. 326
 Yan, W.F. 350
 Yan, X.H., see Xiao, S.G. 411
 Yan, X.H., see Yang, X.L. 411
 Yan, Z.C. 448
 Yan, Z.G. 275–450
 Yan, Z.G., see Gu, J.Q. 348

- Yan, Z.G., see Mai, H.X. 424–425
 Yan, Z.G., see Sun, X. 410
 Yan, Z.G., see Zhang, Y.W. 327, 332–333
 Yanagida, S., see Hasegawa, Y. 325, 437
 Yanagida, S., see Thongchant, S. 325, 437
 Yanagida, T. 400
 Yanes, A.C. 415
 Yang, C.H., see Zhang, Q.Y. 385
 Yang, D.R., see Du, N. 286
 Yang, H., see Bang, J. 448
 Yang, H., see Zhou, S. 398
 Yang, H., see Zhou, Z.G. 415–416
 Yang, H., see Zhu, H.L. 360
 Yang, H.C., see Dong, G.P. 426
 Yang, H.S. 320
 Yang, J. 313, 323, 380–381, 385
 Yang, J., see Li, C.X. 407, 422
 Yang, J., see Yu, C.C. 335
 Yang, J., see Yu, S.H. 443
 Yang, L., see Wang, C.Y. 290
 Yang, L.G., see Meng, L. 350
 Yang, L.M., see Song, H.W. 346
 Yang, L.M., see Yu, L.X. 343, 346
 Yang, L.Q., see Ren, M. 379
 Yang, M., see Jia, G. 313
 Yang, P.P. 365
 Yang, P.P., see Hou, Z.Y. 365, 376
 Yang, P.P., see Li, C.X. 422
 Yang, P.P., see Yu, C.C. 335
 Yang, R.Y., see Yu, S.H. 443
 Yang, R.Y., see Zhang, Z. 294
 Yang, S., see Ding, J. 116, 128, 130, 132
 Yang, S., see Huang, H. 130
 Yang, S., see Wang, W. 126, 128
 Yang, S., see Zhou, K.B. 286
 Yang, S.H., see Deng, H. 363, 373
 Yang, S.W. 290
 Yang, T., see Zhang, W. 307, 423
 Yang, W.J., see Yi, G.S. 422
 Yang, X., see Tong, Y. 392
 Yang, X., see Wang, Y.P. 395
 Yang, X., see Zhang, L. 390
 Yang, X.F., see Zhuang, J.L. 422
 Yang, X.L. 411
 Yang, X.L., see Xiao, S.G. 411
 Yang, Y., see Feng, X.D. 298
 Yang, Z. 379, 401–402
 Yang, Z., see Wang, S. 390
 Yang, Z.H., see Wang, L.Y. 415
 Yang, Z.Q., see Zhou, K.B. 286
 Yang, Z.S., see Wang, S.M. 392
 Yang, Z.S., see Xiu, Z.L. 346
 Yannoni, C.S. 100, 105, 116, 118, 124
 Yannoni, C.S., see Bethune, D.S. 99, 109
 Yannoni, C.S., see Hoinkis, M. 123
 Yannoni, C.S., see Johnson, R.D. 99, 121
 Yao, J., see Sun, L.D. 442
 Yao, K.H., see Zhu, H.L. 360
 Yao, L.Z., see Tao, F. 409
 Yao, T., see Taghavinia, N. 385
 Yao, W.T., see Chen, S.F. 287
 Yao, W.T., see Teng, F. 400
 Yao, X.H., see Zhu, H.L. 360
 Yasuda, H., see Tamai, H. 350
 Yatsunencko, S., see Goldys, E.M. 312, 322
 Ye, Q. 306
 Ye, S.B. 415
 Ye, S.B., see Dong, G.P. 426
 Ye, W., see Zhang, Q.Y. 385
 Ye, Z., see Lian, H. 409, 422
 Yee, G.T., see Regulacio, M.D. 437
 Yee, S.S., see Homola, J. 279
 Yeh, C.S., see Huang, C.C. 337
 Yen, F., see Galstyan, E. 400
 Yen, W.M., see Shionoya, S. 404
 Yeretzian, C. 99, 105, 109
 Yeretzian, C., see Gillan, E. 100
 Yeshurun, Y., see Sivakumar, M. 400
 Yi, G.S. 406, 422, 428, 430
 Yi, G.S., see Lu, H.C. 430
 Yi, N. 402
 Yi, T., see Chen, Z.G. 430–431
 Yi, T., see Hu, H. 406–407
 Yi, T., see Zhou, Z.G. 415–416
 Yi, T., see Zhu, Y. 403
 Yin, G., see Guan, M.Y. 335
 Yin, H.F., see Ma, Z. 350
 Yin, J.L., see Liu, G.S. 322
 Yin, J.L., see Wei, Z.G. 383
 Yin, S., see Devaraju, M.K. 313
 Yin, S., see El-Toni, A.M. 311
 Yin, Y.S., see Zhang, Y. 379
 Yin, Z.L., see Chen, G.Z. 288
 Ying, J.Y., see Zarur, A.J. 283
 Ying, Z.C. 101, 103
 Ylhä, P., see Hölsä, J. 418
 Yntema, L.F. 64
 Yntema, L.F., see Harris, J.A. 64
 Yokawa, T., see Kato, H. 144
 Yokoyama, S., see Saito, Y. 104
 Yomiyama, T., see Wang, C.R. 120
 Yoo, K., see Wells, A.F. 384
 Yoshida, A., see Kida, T. 401
 Yoshida, T., see Wang, C.R. 120

- Yost, D.M. 75
 You, F.T. 385
 You, F.T., see Peng, H.S. 323, 443, 445–446
 You, H.P., see Jia, G. 313
 You, L.P., see Fan, W.L. 357
 You, L.P., see Fang, Y.P. 313, 326, 329–330, 333–334, 342
 You, L.P., see Jia, C.J. 357, 371–372
 You, L.P., see Luo, F. 357–358
 You, L.P., see Mai, H.X. 424–425
 You, L.P., see Si, R. 317–318
 You, L.P., see Sun, X. 410
 You, L.P., see Xu, A.W. 328–330
 You, L.P., see Yan, Z.G. 332, 334
 You, L.P., see Zhang, Y.W. 332–333, 410–411
 Yoza, K., see Iiduka, Y. 118, 120
 Yu, B., see Chen, S.F. 287
 Yu, C.C. 335
 Yu, D.H., see Lorents, D.C. 109
 Yu, D.P., see Wang, X. 441
 Yu, H.Q., see Dong, B. 426
 Yu, H.Q., see Pan, G.H. 359, 377, 384
 Yu, H.Y., see Chen, G.Z. 288
 Yu, H.Y., see Fan, W.L. 357
 Yu, J., see Chen, W. 395
 Yu, J.C., see Fang, Y.P. 313, 326, 329–330, 333–334, 342
 Yu, J.C., see Ho, C.M. 291
 Yu, J.X., see Liu, S.W. 342
 Yu, K.H., see Yu, R.B. 323
 Yu, L.G., see Zhang, Z.F. 415
 Yu, L.X. 343, 346
 Yu, L.X., see Pan, G.H. 381, 384
 Yu, L.X., see Song, H.W. 346
 Yu, M. 336, 343, 365
 Yu, M., see Lin, C.K. 379–380
 Yu, M., see Wang, H. 365, 373
 Yu, M., see Yu, C.C. 335
 Yu, M.G., see Hu, H. 406–407
 Yu, M.X., see Chen, Z.G. 430–431
 Yu, M.X., see Hu, H. 407, 412–413
 Yu, M.X., see Zhou, Z.G. 415–416
 Yu, R. 331
 Yu, R.B. 323
 Yu, R.B., see Yan, L. 288, 326, 328
 Yu, R.J., see Fang, Y.P. 334
 Yu, S.H. 443
 Yu, S.H., see Chen, S.F. 287
 Yu, S.H., see Han, Z.H. 287
 Yu, T., see Liao, L. 306–307
 Yu, T., see Zhang, F. 423, 425
 Yu, T.K. 292, 294, 317
 Yu, T.Z., see Hua, R.N. 418
 Yu, W.J., see Zhang, D.S. 288
 Yu, W.N., see Liu, S.W. 342
 Yu, X.F. 414
 Yu, Y.L., see Chen, D.Q. 280, 416–418
 Yu, Y.N., see Yang, J. 380, 385
 Yu, Z.J., see Cui, X.Z. 380
 Yu, Z.J., see Wang, M. 422
 Yuan, H.B., see Williams, D.K. 321–322
 Yuan, M., see Zhao, F. 443–444
 Yuan, Q. 282, 296
 Yuan, Q., see Li, Z.X. 291–292
 Yuan, Q., see Liao, L. 306–307
 Yuan, X.Y., see Wu, G.S. 312
 Yuan, Y.P., see Qian, L.W. 355
 Yuasa, M. 400
 Yue, Z.X., see Qi, X.W. 395
 Yurov, V.Y., see Wang, X.D. 110, 116–117, 136–138
 Yusupov, R.V. 403
 Zai, J.T., see Qian, L.W. 355
 Zaikovskii, V.I., see Frolova-Borchert, Y.V. 402
 Zaki, M.I., see Bumajdad, A. 289
 Zamar, F., see Trovarelli, A. 293, 295
 Zambon, D., see Chadeyron, G. 379
 Zanchi, G., see Moine, B. 379
 Zang, J., see Wang, L.S. 100, 111, 142
 Zarur, A.J. 283
 Žemva, B., see Nakajima, T. 405
 Zeng, H.-Y. 163–165, 168, 213
 Zeng, J.H. 391–392, 419, 422
 Zerbetto, F., see Hulman, M. 133
 Zerzouf, O., see Schäfer, H. 428
 Zha, C.S., see Wang, Z.W. 298
 Zhan, H.F., see Qin, R.F. 407, 409–410
 Zhang, A.Y., see Wang, S.M. 392
 Zhang, C.M. 275–450
 Zhang, C.M., see Hou, Z.Y. 342
 Zhang, C.M., see Yang, J. 323, 380–381, 385
 Zhang, D.S. 287–288
 Zhang, F.Q. 283, 409, 423, 425
 Zhang, F.Q., see Niu, X.S. 397
 Zhang, F.Q., see Wang, Y. 400–401
 Zhang, F.Q., see Wu, Q. 408
 Zhang, F.Q., see Zhang, F. 423, 425
 Zhang, G.B., see You, F.T. 385
 Zhang, G.J., see Shen, Z.R. 313
 Zhang, H., see Dong, B. 426
 Zhang, H., see Du, N. 286

- Zhang, H., see Sun, Y.J. 354
 Zhang, H.J., see Jia, G. 313
 Zhang, H.J., see Yu, M. 365
 Zhang, H.P. 370
 Zhang, H.P., see Mai, H.X. 284, 286, 304, 306
 Zhang, H.P., see Xiu, Z.L. 346
 Zhang, H.R., see Sun, C.W. 287, 290
 Zhang, H.W. 366, 373–374
 Zhang, H.W., see Wan, S.M. 100
 Zhang, H.X., see Fang, Y.P. 313, 326, 329–330, 333–334, 342
 Zhang, J. 381
 Zhang, J., see Kaneko, K. 283, 383
 Zhang, J., see Sun, L.D. 362
 Zhang, J., see Xia, G. 388
 Zhang, J.P., see Zhang, D.S. 287
 Zhang, J.S., see Wang, G.F. 409
 Zhang, J.S., see Wang, Y. 407
 Zhang, K. 389
 Zhang, L. 390, 398
 Zhang, L., see Cheng, C.S. 399
 Zhang, L.D., see Wu, G.S. 312
 Zhang, L.X., see Bu, W.B. 334–335
 Zhang, L.Z., see Xu, H. 400
 Zhang, M., see Lian, H. 409, 422
 Zhang, M.F. 396, 408, 431
 Zhang, P., see Mo, Z.L. 328
 Zhang, Q., see Chen, Z.G. 430–431
 Zhang, Q., see Heath, J. 97, 141
 Zhang, Q., see Hu, H. 406–407
 Zhang, Q.F., see Wang, N. 357
 Zhang, Q.H., see Zhu, X.X. 411
 Zhang, Q.Y. 385
 Zhang, R. 395
 Zhang, S., see Zhou, S. 398
 Zhang, S.M., see Huang, P.X. 326
 Zhang, S.Y., see Tang, Q. 328
 Zhang, S.Y., see Wang, D.S. 291
 Zhang, S.Y., see Zhu, L. 335, 343
 Zhang, W. 307, 423
 Zhang, W., see Bazzi, R. 316
 Zhang, W., see Zhang, L. 390
 Zhang, W., see Zhao, F. 443–444
 Zhang, W.F., see Liu, G.S. 322
 Zhang, W.L., see Han, M. 319
 Zhang, W.M., see Fan, W.L. 357
 Zhang, W.Y., see Wang, C.Y. 290
 Zhang, X., see Shi, J. 403
 Zhang, X.H., see Chen, W. 433–434
 Zhang, X.M., see Li, C.X. 422
 Zhang, X.M., see Yang, J. 380–381
 Zhang, X.R., see Liu, C.H. 426, 428
 Zhang, X.R., see Wei, Y. 412
 Zhang, X.R., see Ye, Q. 306
 Zhang, Y. 261, 379, 406
 Zhang, Y., see Qian, H.S. 428
 Zhang, Y., see Wang, F. 407, 412
 Zhang, Y., see Wang, L.Y. 415
 Zhang, Y., see Yan, Z.C. 448
 Zhang, Y.C., see Zeng, J. 391–392
 Zhang, Y.F., see Zhu, L. 406
 Zhang, Y.H., see Yu, S.H. 443
 Zhang, Y.J. 333
 Zhang, Y.J., see Cheng, C.S. 399
 Zhang, Y.J., see Guan, H.M. 333
 Zhang, Y.Q., see Au, C.T. 418
 Zhang, Y.W. 290, 327, 332–333, 410–411
 Zhang, Y.W., see Du, Y.P. 419–420, 424, 426
 Zhang, Y.W., see Mai, H.X. 284, 286, 304, 306, 341, 424–425
 Zhang, Y.W., see Si, R. 304–305, 317–318
 Zhang, Y.W., see Sun, X. 410
 Zhang, Y.W., see Yan, Z.G. 332, 334
 Zhang, Y.W., see Yuan, Q. 282, 296
 Zhang, Y.W., see Zhou, H.P. 291, 293
 Zhang, Y.X. 319
 Zhang, Y.X., see Sun, L.D. 362
 Zhang, Y.X., see Yan, C.H. 369
 Zhang, Y.Y., see Hu, C.G. 313, 328, 407
 Zhang, Z. 294
 Zhang, Z.D., see Si, P.Z. 448
 Zhang, Z.F. 329, 415
 Zhang, Z.J., see Zhou, J.F. 415
 Zhang, Z.K., see Li, G.C. 337
 Zhang, Z.W., see Hu, C.G. 294, 407
 Zhao, D.Y., see Zhang, F. 409, 423, 425
 Zhao, F. 434, 436, 443–444
 Zhao, G.W., see Wang, C.Y. 290
 Zhao, H.F., see Di, W.H. 333
 Zhao, H.F., see Pan, G.H. 359
 Zhao, H.Q., see Han, Z.H. 287
 Zhao, H.Q., see Yu, S.H. 443
 Zhao, J., see Ma, L. 326, 408
 Zhao, J., see Zhou, S. 398, 404
 Zhao, L.L., see Kelly, K.L. 279
 Zhao, S.Y., see Lu, H.C. 430
 Zhao, S.Y., see Yi, G.S. 422
 Zhao, W., see Chen, G.Z. 288
 Zhao, W., see Fan, W.L. 357
 Zhao, X., see Fan, W.L. 358–359, 363, 371, 374
 Zhao, X.G., see Si, P.Z. 448
 Zhao, X.X., see Di, W.H. 333
 Zhao, Y.S., see Wang, Z.W. 298

- Zhao, Y.S., see Zhou, X.F. 400
 Zhao, Z.B., see Wang, H. 397
 Zhao, Z.B., see Wang, Z.Y. 409
 Zharkouskaya, A. 338
 Zhen, Z., see Wang, J.S. 415
 Zheng, F.-K., see Spanier, J.E. 299
 Zheng, F.-K., see Zeng, H.-Y. 163–165, 168, 213
 Zheng, H.R., see Meltzera, R.S. 415
 Zheng, S., see Yu, L.X. 343
 Zheng, W., see Louis, C. 312
 Zheng, Y.F., see Ma, L. 326, 408
 Zheng, Y.H., see Bao, F. 416
 Zhong, H.X., see Huang, Q.L. 411
 Zhong, H.X., see Zhang, L. 390
 Zhong, W., see Sivakumar, M. 400
 Zhou, B., see Meng, L. 350
 Zhou, G.J., see Wang, S. 390
 Zhou, G.J., see Xiu, Z.L. 346
 Zhou, G.J., see Zhang, H.P. 370
 Zhou, H.J., see Shen, Z.R. 313
 Zhou, H.P. 291, 293
 Zhou, H.P., see Si, R. 317
 Zhou, J., see Hu, H. 407, 430
 Zhou, J., see Qi, X.W. 395
 Zhou, J.F. 415
 Zhou, J.P., see Zhu, G.Q. 400
 Zhou, K.B. 286, 304
 Zhou, L., see Yu, X.F. 414
 Zhou, S. 398, 404
 Zhou, S., see Xia, G. 388
 Zhou, W., see Wang, Z.L. 409
 Zhou, X.D. 298
 Zhou, X.F. 400
 Zhou, X.P., see Chao, Z.S. 418
 Zhou, Y., see Wang, S. 390
 Zhou, Y.C., see Zhang, C. 411
 Zhou, Y.H. 322
 Zhou, Y.Y., see Wang, S.M. 392
 Zhou, Y.Y., see Zhang, H.P. 370
 Zhou, Z.G. 415–416
 Zhou, Z.G., see Chen, Z.G. 430–431
 Zhu, B.L., see Huang, P.X. 326
 Zhu, G.Q. 400
 Zhu, G.S., see Li, H. 335
 Zhu, H.L. 360
 Zhu, H.Y., see Huang, P.X. 326
 Zhu, J., see Qian, L.W. 355
 Zhu, J., see Ye, S.B. 415
 Zhu, J.J., see Liao, X.H. 284
 Zhu, J.J., see Wu, X.C. 358–359
 Zhu, J.M., see Guan, M.Y. 335
 Zhu, J.M., see Han, M. 319
 Zhu, J.M., see Liao, X.H. 284
 Zhu, J.X. 328
 Zhu, L. 335, 343, 364, 406
 Zhu, M.K., see Zeng, J. 391–392
 Zhu, P.F., see Di, W.H. 334
 Zhu, P.F., see Wang, G.F. 409
 Zhu, P.F., see Wang, Y. 407
 Zhu, X.X. 411
 Zhu, Y. 403
 Zhu, Y., see Liang, S. 396
 Zhu, Y., see Shi, J. 403
 Zhu, Y., see Teng, F. 400
 Zhu, Y.M., see Han, W.Q. 286–287
 Zhu, Y.Y., see Zhang, M.F. 431
 Zhuang, J.L. 422
 Zhuang, J.L., see Liang, X. 422
 Zhuang, J.L., see Wang, X. 326, 361, 406
 Zhuang, W.D., see Cui, X.Z. 380
 Zhuang, X.M., see Zhang, W. 307, 423
 Zhuang, Y., see Liang, X. 295
 Zhuang, Z. 394
 Zhuo, L.H., see Tang, B. 286
 Zhuravleva, N.G. 411
 Ziessel, R., see Charbonnière, L.J. 412
 Zijlmans, H. 440
 Zijlmans, H., see Rijke, F.v.-d. 440
 Zimmermann, Y., see Charbonnière, L.J. 412
 Zmiy, O.F., see Hvaleba, N.V. 166, 216
 Zollfrank, C. 333, 342
 Zong, R., see Teng, F. 400
 Zou, B.S., see Wang, X. 441
 Zuiderwijk, M., see Corstjens, P.L.A.M. 440, 446–447
 Zuniga, E., see Regulacio, M.D. 437
 Zuo, D.D., see Mo, Z.L. 328
 Zyryanov, V.V., see Frolova-Borchert, Y.V. 402
 Zysler, R., see Morales, L. 397

SUBJECT INDEX

- ab initio* theoretical calculation, 138
Acetylacetonate, 317
Actinide series, 75, 76
Aerosol synthesis, 388
AFM. *See* Atomic force microscope
Alkalide reduction method, 448
Am@C₈₂, 144
Anodic aluminum oxide, 312, 401
Antiferromagnetic-like interactions, 141
Antiferromagnetism, 433
Arc discharge method, 448
Ar ion sputtering, 449
Arrhenius, Carl Axel, 4
Arrhenius-like behaviour, 134
Asteriod hypothesis, 46
Atomic force microscope (AFM), 397
Atomistic simulation, 296, 297
Au(110), 137
Au(111), 135
Automotive pollution control, 403
Avidin, 323, 347, 348
- Band gap, 146, 404, 436, 437
Bastnäs mine, 5
β-decay, 144
⁷Be@C₆₀, 144
Berzelian atomic weights, 13
Berzelius, Jöns Jacob, 5
Bioapplications, 307
Biofunctionalization, 344, 346, 348
Bioimaging, 450
 probe, 321, 323
Biotin, 323, 347, 348
2,2'-Bipyridine (Bipy), 434
BiVO₄, 369
BMIMPF₆, 307
B₂O₃, 439
Bohr, Niels 54
Bohr
 atomic theory, 54
 radius, 433, 434, 436
Brauner, Bohuslav, 27
Brillouin function, 139
- Bucky periodic table, 101
Bunsenium, 33
Bunsen, Robert Wilhelm, 7
Butanol, 409
1-Butyl-3-methylimidazolium
 hexafluorophosphate, 411
- C₆₀, 97
C₇₂, 100
C₇₄, 100
Ca@C₆₀, 100
Ca@C₈₂, 108
Ca@C₈₂ (I-IV), 131
Ca@C₈₄, 109
CaF₂, 122
Cage isomerization, 135
Carbide metallofullerenes, 40
Carbon nanotubes, 278, 279, 400, 403
Cataluminescence, 306
Catalysis, 296, 299, 300, 306
Cathodoluminescence, 375
 phosphor, 439
CBD. *See* Chemical bath deposition
CCl₄, 289, 325
CdS, 401
Ce(NO₃)₃, 406
Ce(OH)₃, 282, 285, 330
Ce₂@C₁₀₀, 109
Ce@C₈₂, 109
Ce(OH)CO₃, 285, 287
CeF₃, 30, 406, 407, 409, 411, 424
CeF₄, 30
CeF₄H₂O, 30
Celtium, 59–61, 63
CeO₂, 22, 281–295, 297, 298, 302–307,
 310, 317, 318, 320, 325, 326, 330,
 337, 354, 386
Ce₂O₃, 22
CePO₄, 335–337, 339, 340, 343–345,
 348, 350
Ceria, 5
Ceria-zirconia, 19–21, 23, 28, 281
CeS₂, 439

- CeVO₄, 351, 354, 355, 357, 358, 361, 363, 364, 373
 Ce_{1-x}Zr_xO₂, 295, 296, 305
 Charge transfer (CT), 345, 352, 369, 370, 383, 388
 Chemical bath deposition (CBD), 419
 Chemical vapor deposition (CVD), 399, 400, 418
 Chemiluminescence, 403
 Citric acid method, 396, 400
 Cleve, Per Theodor, 8
 Closed-packed fullerenes, 136
 Cluster, 138
 beam, 97
¹³C NMR, 115, 137
 Cobaltite, 394
 Coercive field, 434
 Coercivity, 395, 403
 Colloidal synthesis, 315–317
 Columbium
 Combustion, 282, 294, 299, 302, 303, 311, 312, 322
 fluorination method, 411
 method, 442
 Composite hydroxide
 mediated, 294
 method, 294, 328
 rods, 97
 Confocal
 fluorescence microscopy, 350
 microscopy imaging, 430
 Construction methodology of the periodic table, 15
 CO oxidation, 23, 24, 26, 27, 29, 47, 49, 71, 119, 281
 Copper surface, 137
 Co-precipitation, 440
 method, 312, 388
 Core shell structure, 411, 415
 Crookes, Sir William, 39
 Cronstedt, Axel Frederik, 5
 Crystal field symmetry, 371
 Crystallographic relationships, 265
 ErCuPbS₃, 265
 ErCuPbSe₃, 265
 Er₅CuPb₃Se₁₁, 266
 Er₂EuS₄, 267
 Er₂PbS₄, 267
 LaCuPbS₃, 265
 La₂S₃, 265
 lead chalcogenides, 258, 269
 Lu_{3.33}CuPb_{1.5}Se₇, 266
 R₃MZX₇, 252, 262
 role of voids, 269
 R₂Se₃–Cu₂Se–PbSe systems, 268
 R₂X₃–Cu₂X–PbX systems, 258
 R₂X₃–PbX systems, 258, 267
 Sc₂PbS₄, 267
 substitution, 260, 268–269
 Tm₂PbSe₄, 267
 Tm₈S₁₁, 266
 YbLaS₃, 265
 Y_{3.33}CuPb_{1.5}S₇, 266
 Y_{4.2}Pb_{0.7}Se₇, 266
 Y₆Pb₂Se₁₁, 266
 Y₅Se₇, 266
 Crystal structure of rare-earth metals, 80
 CS₂, 306, 439
¹³C satellite structures, 122
 CS₂ extraction, 105
 CT. *See* Charge transfer
 CTAB (hexadecyltrimethylammonium bromide), 348, 362, 381, 390, 391, 402, 409, 422, 423
 Cu(111), 135
 1×1, 137
 CuO–CeO₂, 302
 Curie
 constant, 140
 law, 140
 temperature, 325, 396, 433
 Curie–Weiss
 behavior, 139
 curve, 140
 CV. *See* Cyclic voltammetry
 CVD. *See* Chemical vapor deposition
 Cyclic
 voltammetry (CV), 126
 voltammograms, 126
 Cyclohexane, 409, 415, 420
 Cyclonium, 66

 Damarium, 7
 Danium, 62
 Data storage, 448
 de Boisbaudran, Paul–Emile Lecoq, 8
 de Marignac, Jean Charles Galissard, 7
 Decipium, 7, 8
 Dehydrogenation reactions, 357
 Delafontaine, Marc, 8
 Demarçay, Eugène–Anatole, 8
 Demonium, 7
 Density of state (DOS), 140
 Dextran T–10, 308

- Diagnostics, 448
 Diarylethene, 415
 Didymium, 7
 Dielectric constants, 388
 Diethylene glycol, 409, 411, 412, 426
 DiF_5 , 30
 Differential pulse voltammograms, 127
 Differentiating electron, 80
 Dimerization, 138
 Dimers, 137
 Dimethyldichlorosilane (DMDCS), 323
 Di_2O_3 , 28
 Di_2O_5 , 28
 Dip-coating, 336, 365
 Dipole moments, 138
 Divalent metallofullerenes, 128, 129
 DMDCS. *See* Dimethyldichlorosilane
 DNA, 412, 430, 431
 D_2O , 352
 DOS. *See* Density of states
 Downconversion, 404, 417
 Drift-time distribution, 142
 Dy@C_{82} , 126
 Dynamic light scattering, 347
 DyPO_4 , 333
 $\text{Dy}_2\text{Ti}_2\text{O}_7$, 390

 EDTA. *See* Ethylenediaminetetraacetic acid
 EISA. *See* Evaporation induced self-assembly
 eka
 aluminium, 22
 boron, 22
 silicon, 22
 Ekeberg, Anders Gustav, 4
 Electric furnace, 102
 Electrochemistry, 126
 Electron donor, 126
 Electronic configurations, 80
 Electron
 donor, 126
 spin-echo envelope modulation techniques (ESEEM), 122
 spin resonance (ESR), 99
 transfers, 111
 Electrospinning, 342, 365, 381, 392, 394, 400, 426
 Elemental group, 40
 Elementoids, 40
 Elution behaviour, 130
 Endohedral metallofullerenes, 97
 Energy level diagram, 126, 127

 Enzyme, 350
 Epitaxial growth, 394, 400
 Erbium, 7
 $\text{Er}_2\text{@C}_{82}$, 116
 Er@C_{82} , 126
 $\text{Er}_2\text{C}_2\text{@C}_{82}$, 121
 ErF_3 , 416
 ErS_2 , 439
 $\text{Er}_2\text{Si}_2\text{O}_7$, 386, 387
 Er_2SiO_5 , 386
 ESEEM. *See* Electron spin-echo envelope modulation techniques
 ESR. *See* Electron spin resonance
 Ethylenediamine, 290
 Ethylenediaminetetraacetic acid (EDTA), 333, 337, 356-358, 380-382, 391, 408, 422
 $\text{Eu}(\text{NO}_3)_3$, 406, 422
 Eu@C_{74} , 135
 EuF_3 , 406, 407, 411, 422
 EuO , 48, 52
 Eu_2O_3 , 312, 316, 318, 323, 325, 330, 422, 433, 440
 EuPO_4 , 54, 56, 63, 71
 EuS , 433-437, 443
 EuS_2 , 439
 EuSe , 437
 $\text{Eu}_2\text{Ti}_2\text{O}_7$, 389
 EuVO_4 , 361
 Euxenium, 7
 Evaporation induced self-assembly (EISA), 449
 EXAFS. *See* Extended X-ray absorption fine structure
 Excited state absorption, 447
 Extended X-ray absorption fine structure (EXAFS), 109

 Faraday
 effect, 437
 rotation, 437
 Far IR, 135
 5f electrons, 76
 Fe_3O_4 , 415, 430
 Fermi level, 132, 394
 Ferrocene, 126
 Ferromagnetic-paramagnetic transition temperature, 395, 396
 Ferromagnetism, 433
 FITC. *See* Fluorescein isothiocyanate
 Flame, 294, 295, 298, 312
 assisted spray pyrolysis, 388

- Flat-panel display, 420
 Florentium, 7
 Fluorescein isothiocyanate (FITC), 412
 Fluorescence resonance energy transfer (FRET), 348, 377
 Fluorescent labeling, 323
 Flux method, 440
 Formaldehyde, 403
 FRET. *See* Fluorescence resonance energy transfer
 FT-ICR mass spectrum, 99
 Fuel cell, 299
 Fullerenes, 97, 279
- GaAs(110), 135
¹⁵⁹Ga@C₈₂, 144
 Gadolin, Johan, 4
 Gadolinite, 7
 Gas condensation, 292
 Gd(OH)₃, 359
 GdAlO₃, 388, 389
 Gd₃Al₅O₁₂, 389
 Gd₄Al₂O₉, 389
 GdBO₃, 380, 384
 Gd@C₈₂, 110
 Gd@C₈₂(OH)₄₀, 145
¹⁵³Gd@C₈₂, 144
 Gd-DTPA, 145
 GdF₃, 418
 GdFeO₃, 398
 Gd₂O₃, 312, 317, 319–321, 323, 324, 422
 Er doped, 319
 Eu doped, 324
 GdOCl, 419
 Gd₂O₂S
 Tb³⁺, 439, 446, 448
 GdPO₄, 337
 GdVO₄, 355, 356, 359, 360, 365, 375
 Glucose oxidase, 306
 Glycerol, 389, 409
 Glycol, 409, 412, 430
 Graphene, 279
 Group 2 metallofullerenes, 129
 Group 3 metallofullerenes, 128
 Growth mechanism, 142
- Hafnium, 7
 Hard-sphere collision model, 143
 Hard template assisted synthesis, 449
 Heterobimetallic precursor, 400
 Heterometallic rare-earth oxide, 387
- Heterostructure, 138
 Hexadecylamine, 419, 421, 438
 1-Hexadecyl-3-methylimidazolium bromide, 291
 HfO₂, 414
 hfs. *See* Hyperfine splitting
 High-boiling solvent, 289, 311, 315–317, 319, 410, 434, 443
 Higher oxides, 28
 High-performance liquid chromatography (HPLC), 102
 High-resolution transmission electron microscopy (HRTEM), 110
 High spin state, 124
 High-temperature
 flux method, 400
 fuel cell, 389
 laser-furnace, 102
 Hisinger, Wilhelm, 5
 History of the discovery of the rare-earth elements, 4
 Ho@C₈₂, 122, 126
 Homologous accommodation methodology, 24
 HOMO-LUMO, 115
 gaps, 146
 HPLC. *See* High-performance liquid chromatography
 HRTEM, 137. *See* High-resolution transmission electron microscopy
 Hybridized states, 132
 Hydrogen storage, 449
 Hydrothermal, 406
 method, 282–283, 285–288, 295, 311–313, 327, 329, 330, 347–348, 351, 353, 356, 359–362, 367, 374, 380, 381, 384, 391, 396, 400
 Hyperfine
 parameters, 125
 satellites, 121
 spectra, 121
 splitting (hfs), 99
- I_h-C₈₀ cage, 115
 Illinium, 64
 Immunoassay, 323, 449
 Impregnation method, 402
 Incognitum, 7
 Inert gas evaporation method, 448
 In₂O₃, 414

- in situ* ESR, 128
 Intergroup accommodation methodology, 67
 Interperiodic accommodation methodology, 87
 Intramolecular dynamics, 125
 Intraperiodic accommodation methodology, 51
 Inverse susceptibility, 139
 In vivo imaging, 324
 Ionic
 conductivity, 387, 389, 393, 418
 liquid, 289, 291, 337–339
 IPR. *See* Isolated–pentagon rule
 Isobars, 65
 Isolated–pentagon rule (IPR), 110
 Isothermal R_2X_3 – M_2X – In_2X_3 sections, 219
 Er_2S_3 – Cu_2S – In_2S_3 , 220, 244
 Er_2Se_3 – Cu_2Se – In_2Se_3 , 220, 246
 La_2S_3 – Cu_2S – In_2S_3 , 220, 243
 La_2Se_3 – Cu_2Se – In_2Se_3 , 220, 245
 Pr_2S_3 – Cu_2S – In_2S_3 , 220, 244
 Pr_2Se_3 – Cu_2Se – In_2Se_3 , 220, 246
 R_2Se_3 – M_2Se – In_2Se_3 , 221
 Y_2S_3 – Cu_2S – In_2S_3 , 220, 243
 Y_2Se_3 – Cu_2Se – In_2Se_3 , 29, 120, 220, 245
 Isothermal R_2X_3 – M_2X – PbX sections, 214
 Dy_2S_3 – Cu_2S – PbS , 216, 231
 Dy_2Se_3 – Cu_2Se – $PbSe$, 216, 235
 Dy_2Te_3 – Ag_2Te – $PbTe$, 217, 241
 Dy_2Te_3 – Cu_2Te – $PbTe$, 217, 238
 Er_2S_3 – Cu_2S – PbS , 216, 232
 Er_2Se_3 – Cu_2Se – $PbSe$, 216, 236
 Er_2Te_3 – Cu_2Te – $PbTe$, 217, 239
 Ho_2S_3 – Cu_2S – PbS , 216, 232
 Ho_2Se_3 – Cu_2Se – $PbSe$, 216, 235
 Ho_2Te_3 – Cu_2Te – $PbTe$, 216, 239
 Lu_2S_3 – Cu_2S – PbS , 216, 237
 Pr_2S_3 – Cu_2S – PbS , 215, 230
 Pr_2Se_3 – Ag_2Se – $PbSe$, 217, 240
 Pr_2Se_3 – Cu_2Se – $PbSe$, 216, 234
 R_2Te_3 – Cu_2Te – $PbTe$, 218
 R_2X_3 – Ag_2X – PbX , 218
 R_2X_3 – Cu_2X – PbX , 218
 Sc_2Se_3 – Cu_2Se – $PbSe$, 216, 233
 Tb_2S_3 – Cu_2S – PbS , 215, 231
 Tb_2Se_3 – Cu_2Se – $PbSe$, 216, 234
 Tb_2Te_3 – Ag_2Te – $PbTe$, 217, 241
 Tb_2Te_3 – Cu_2Te – $PbTe$, 217, 238
 Tm_2Se_3 – Cu_2Se – $PbSe$, 216, 236
 Tm_2Te_3 – Cu_2Te – $PbTe$, 217, 240
 Y_2S_3 – Cu_2S – PbS , 215, 230
 Y_2Se_3 – Cu_2Se – $PbSe$, 216, 233
 Y_2Te_3 – Cu_2Te – $PbTe$, 217, 237
 Isothermal R_2X_3 – M_2X – ZX_2 sections, 206
 Er_2S_3 – Cu_2S – SnS_2 , 207, 222
 Er_2Se_3 – Cu_2Se – $SnSe_2$, 208, 225
 Ho_2S_3 – Cu_2S – GeS_2 , 207, 218
 Ho_2S_3 – Cu_2S – SiS_2 , 207, 215
 Ho_2Se_3 – Cu_2Se – $GeSe_2$, 207, 219
 Ho_2Se_3 – Cu_2Se – $SiSe_2$, 207, 216
 La_2S_3 – Cu_2S – SnS_2 , 207, 221
 La_2Se_3 – Cu_2Se – $SnSe_2$, 208, 224
 Lu_2S_3 – Cu_2S – SnS_2 , 208, 226
 Pr_2S_3 – Cu_2S – GeS_2 , 207, 217
 Pr_2S_3 – Cu_2S – SiS_2 , 207, 214
 Pr_2Se_3 – Cu_2Se – $GeSe_2$, 207, 219
 Pr_2Se_3 – Cu_2Se – $SiSe_2$, 207, 216
 R_2X_3 – Cu_2X – ZX_2 , 27, 208
 Sc_2Se_3 – Cu_2Se – $SnSe_2$, 207, 223
 Sm_2S_3 – Cu_2S – SnS_2 , 207, 221
 Sm_2Se_3 – Cu_2Se – $SnSe_2$, 208, 225
 Tb_2S_3 – Cu_2S – SnS_2 , 207, 222
 Y_2S_3 – Cu_2S – GeS_2 , 207, 217
 Y_2S_3 – Cu_2S – SiS_2 , 207, 214
 Y_2S_3 – Cu_2S – SnS_2 , 207, 220
 Y_2S_3 – Cu_2S – SnS , 27, 118, 207, 220
 Y_2Se_3 – Cu_2Se – $GeSe_2$, 207, 218
 Y_2Se_3 – Cu_2Se – $SiSe_2$, 207, 215
 Y_2Se_3 – Cu_2Se – $SnSe_2$, 207, 224
 Y_2Se_3 – Cu_2Se – $SnSe_2$, 207, 223
 Y_2Te_3 – Cu_2Te – $SnTe$, 208, 226
 Y_2Te_3 – Cu_2Te – $SnTe_2$, 208, 226
 IUPAC nomenclature, 98

 Jahn–Teller distortion, 396, 398
 Janet, Charles, 73
 circular system 73
 Janet periodic table, 83

 KBF_4 , 406
 $K@C_{60}$, 102
 $3KF_2CeF_4 \cdot 2H_2O$, 30
 $KGdF_4$, 422
 Kirchhoff, Gustav, 7
 Klaproth, Martin Heinrich, 5
 Klechkowski's rule, 82
 $KMnO_4$, 344, 345
 $K[Se_2P(Ph)_2]$, 438
 KYF_4 , 428

 $La(CF_3COO)_3$, 409, 410
 $La(OH)_3$, 327–330, 443
 $LaAlO_3$, 388
 $LaBaCo_2O_6$, 399

- LaBO₃, 380
 LaC₂, 104
 La₂@C₈₀, 99
 LaC₆₀, 97
 La@C₆₀, 97
 La@C₇₀, 97
 La@C₇₆, 109
 La@C₇₈, 109
 La@C₈₀, 109
 La@C₈₂, 97
 La@C₈₂(CS₂)_{1.5}, 114
 La@C₉₀, 125
 LaCl₃, 80
 LaCoO₃, 394, 395, 398–403
 La₂CuO₄, 403, 404
 LaF₃, 406, 408–416
 LaFeO₃, 395, 398, 400, 401
 Laing's periodic table, 85
¹⁴⁰La-labelled La@C₈₂, 144
 LaMnO₃, 395, 402
 La₂Mo₂O₉, 393, 394
 Langmuir–Blodgett film, 361, 449
 LaNi₅, 329
 LaNiO₃, 394, 399, 401, 402
¹³⁹La NMR, 115
 Lanthana, 7
 Lanthanide
 contraction, 25
 coordination polymer foam, 313
 Lanthanum i-propoxide, 329
 La₂O₃, 29, 288, 321, 325
 LaOBr, 419
 LaOCl, 419, 421
 LaOF, 418, 420
 La₂O₂S, 441, 443, 445–448
 LaPO₄, 331–333, 335–348, 350
 Laser
 furnace method, 141
 vaporization, 97
 vaporization cluster–beam, 141
 LaVO₄, 351, 352, 356, 357, 359, 361–363,
 371–374
 La_{1-x}Ce_xMnO₃, 398
 La_{1-x}Sr_xMnO₃, 395, 397
 (LaY)@C₈₀, 100
 La₂Zr₂O₇, 390–393
 LC. *See* Liquid chromatography
 Left-step table, 83
 Lemieux–von Rudloff reagent, 430
 Li@C₆₀, 102
 Light wave circuit, 405
 Liquid chromatography (LC), 106
 Lithography, 336, 365
 Long forms of the periodic table, 81
 LRET. *See* Luminescence resonance
 energy transfer
¹⁷⁵Lu, 124
 Lu(OH)₃, 327
 Lu@C₈₂, 126
 LuCl₃, 80
 Luminescence resonance energy transfer
 (LRET), 347, 348
 Luminol, 403
 LuMnO₃, 400
 Lu₂O₃, 80, 288, 321, 323, 327
 LuPO₄, 340, 347, 348
 LuVO₄, 361

 Madelung rule, 82
 Magic number, 97, 141
 anisotropy, 125
 moment, 139
 properties, 139
 refrigeration, 448
 resonance imaging (MRI), 144
 resonance imaging (MRI) contrast agent,
 418
 semiconductors, 433
 susceptibility, 404, 437
 Magnetization, 139
 hysteresis reversal, 436
 Magnetoimpedance behavior, 396
 Magnetron sputtering, 448
 Mass spectrum, 97
 Material resonance wavelength, 437
 Mattauach rule, 65, 66
 Maximum entropy method (MEM), 111
 electron density, 111
 M@C₆₀, 98
 MCM-41, 402
 M@C₆₀ mystery, 143
 M@C_{2n}, 98
 Mechanical milling, 292, 295
 Mechanochemical method, 419
 Medical applications, 146
 Medium-long forms of the periodic table, 81
 Melting point of rare-earth metals, 80
 MEM. *See* Maximum entropy method
 Mendeleev, Dmitrii Ivanovich, 8, 37
 line, 15
 method, 24
 methodology, 37
 active rare-earth research, 25

- attempted system, 9
- natural system of elements, 19
- Meso-elements, 44
- Mesoporous, 296
- Meta-elements, 38
- Metal carbides, 104
- Metal-fingerprint, 135
- Metal-insulator transition, 395
- Metallic rare-earth nanomaterials, 448
- Metallofullerene chemistry, 144
- Metalorganic chemical vapor deposition (MOCVD) method, 418
- Metal-to-cage vibrations, 135
- Metamagnetism, 433
- Methyl orange, 364, 390, 391
- Meyer, Julius Lothar, 26
- MgO, 402
- Microemulsion method, 283, 285, 289, 335, 351, 360, 362, 400, 402, 405, 409, 418
- Microwave, 55, 60, 72, 83, 111, 121
- Mighty pendulum, 42
- Mixed-metal organic framework, 400
- Mobility, 143
- MOCVD. *See* Metalorganic chemical vapor deposition method
- Molecular dynamics, 283, 285, 296, 298
- Molten-salt flux synthesis, 392
- Monoclinic, 111
- Mono-metallofullerenes, 124
- Mosander, Carl Gustaf, 6
- Mosandrum, 7
- Moseley, Henry, 54
- Moseley's law, 4
- MRI. *See* Magnetic resonance imaging
- Multiscale simulations, 450

- NaBF₄, 406, 407
- NaEuF₄, 422
- Na₅Eu₉F₃₂, 422
- NaF, 405, 406, 408, 422–424, 426
- NaGdF₄, 428, 430
- NaLuF₄, 422
- Nanocasting strategy, 400
- Nanoclusters, 302
- Nanoscale electronic devices, 146
- Na₂S, 401
- Na₂S₂O₃, 442
- Na₂SO₃, 401
- Natural groups, 15
- NaYbF₄, 422
- NaYF₄, 346, 422–425, 427–432
- N@C₆₀, 102
- Nd@C₈₂, 126
- NdF₃, 415, 416
- Nd₂O₃, 439
- Nd₂O₂S, 439, 441
- NdS₂, 439
- NdVO₄, 358, 361, 363, 364, 371, 373
- NdYAG laser, 102
- Near-infrared, 346, 367, 372–374, 385, 404, 412, 414, 421, 426–428, 430
- Neutron powder diffraction, 379
- NEXAFS, 341
- NH₄ClO₄, 395
- NH₄F, 405, 406, 409, 416
- Nickelate, 394
- Nilson, Lars Fredrik, 8
- Non-aqueous solution method, 289
- Non-IPR metallofullerenes, 120
- Non-stoichiometry, 160, 168, 252
- Np@C₈₂, 144
- NpO₂, 76
- Nuclear
 - reaction, 144
 - spin quantum number, 121
 - spin relaxation, 124
 - waste, 331, 389

- Oceanium, 62
- Octadecene, 317, 410, 419, 424, 434, 443
- Octadecylamine, 290, 291, 317, 319, 320, 419, 421
- Octane, 289
- 1-Octyl-3-methylimidazolium
 - hexafluorophosphate, 411
 - tetrafluoroborate, 411
- Oleic acid, 290–292, 311, 317, 319, 320, 323, 341, 361, 363, 374, 375, 382, 406, 410, 412, 415, 419, 422, 423, 428, 430, 434, 443
- Oleylamine, 341, 363, 419, 421, 424, 428, 434, 436, 443
- Optical waveguide amplifier, 405, 415
- Optoelectronics, 449
- OSC. *See* Oxygen storage capacity
- Oxygen
 - monitoring sensor, 389
 - storage capacity (OSC), 286, 295, 299, 304, 305

- PAH. *See* Poly(alkylamine hydrochloride)
- Paramagnetic, 139
- Patterson symmetry, 119
- Pauli paramagnetism, 140
- PbFCl, 419
- PEG. *See* Poly(ethylene glycol)
- Pentabromobenzyl (5-PBB), 107

- Pentagonal–dodecahedral, 115
 1–Pentanol, 409
 Pentavalency of didymium, 28
 Periodic
 law, 2, 9, 11, 18
 system of the elements, 2
 table, 1
 Permanent magnets, 448
 1,10–phenanthroline (Phen), 434
 Philippium, 7
 Phosphino polyacrylic acid (P–PAA), 355
 Photon echo signal, 415
 PLD. *See* Pulsed laser deposition
 PMMA. *See* Poly(methyl methacrylate)
 Poly(alkylamine hydrochloride) (PAH), 415
 Poly(ethylene glycol) (PEG), 284, 285, 288,
 324, 328
 Poly(methyl methacrylate) (PMMA), 310, 328
 Poly(sodium 4–styrenesulfonate) (PSS), 415
 Polycyclic polyynes, 142
 Polyol hydrolysis method, 409
 Polyol method, 289, 291, 405
 Polyvinyl pyrrolidone (PVP), 291, 355, 392,
 393, 407, 424, 429
 Positive electrodes, 104
 Pr(OH)₃, 326
 Pr@C₈₂, 126
 PrF₃, 408
 Primary
 classification, 15
 elements, 16
 group, 15
 Pr₆O₁₁, 326
 Process of genesis, 41
 Promethium, 8
 Propellant synthesis, 397
 Protein, 347, 379
 Protyle, 41
 Prout's hypothesis, 41
 PrVO₄, 361, 364
 PSS. *See* Poly(sodium 4–styrenesulfonate)
 Pulsed laser
 ablation, 385–386, 397, 400
 laser deposition (PLD), 400, 448–449
 PuO₂, 76
 PVP. *See* Polyvinyl pyrrolidone
 Pyridine, 105

 Quantitative flow cytometry analysis, 430
 Quantum confinement effect, 433, 434,
 436, 445
 Quantum cutting, 415, 417

 Quantum dot, 346
 Quantum efficiency, 331, 389
 Quaternary systems
 R–M–In–X, 219
 R–M–Pb–X, 214
 R–M–Z–X, 206

 Radiant matter spectroscopy, 40
 Radioactivity, 144
 Radiochromatographic techniques, 144
 Radio frequency magnetron sputtering, 400
 Radioimmunoassay, 348
 Radiotracers, 144
 Raman spectroscopy, 133
 Rare earth
 aluminates, 388
 benzoylacetate, 317
 borate, 379
 chalcogenide, 433
 germanium chalcogenides, 163
 indium chalcogenides, 169
 chalcogenide ionic radius, 159
 lead chalcogenides, 166
 silicon chalcogenides, 161
 chalcogenide synthesis, 159
 tin chalcogenides, 165
 crisis, 27, 77
 cuprate, 403
 halide, 404, 405, 432
 hydroxide, 326, 329
 manganite, 394
 molybdate, 392
 monosulfide, 438
 oxysalt, 329, 387
 oxysulfide, 439
 phosphate, 329, 331–336, 338, 343, 348, 350
 polysulfide, 438
 silicate, 385, 386
 γ-ray spectrometry, 144
 R@C₈₂, 100
 Recoil energy, 144
 Refractive index, 331
 Relaxivity, 145
 Retention time, 130
 Rietveld analysis, 111
 Rietveld/MEM analysis, 118
 Ring isomers, 142
 Rogerium, 7
 Rotational diffusion, 134

 SAM. *See* Self-assembled monolayer
 SBA–15, 365, 402, 409

- Scandium metallofullerenes, 106
- Sc₂@C₇₄, 100, 107
- Sc₂@C₈₂, 100, 107
- Sc₂@C₈₄, 100
- Sc₂@C₈₆, 120
- Sc₃@C₈₂, 100
- Sc₄@C₈₂, 100
- Sc@C₆₀, 101
- Sc@C₈₂, 100
- Sc₂C₂@C₆₈, 120
- Sc₂C₂@C₈₂, 107
- Sc₂C₂@C₈₄, 120
- Sc₂C₂@C_{2n-2}, 120
- ScCl₃, 80
- ScF₃, 410
- Scintillator, 331, 385
- Sc_n@C₈₂, 105
- Sc_nC₂@C₈₀, 105
- ⁴⁵Sc NMR, 115
- ScOOH, 327
- Sc₃ trimer, 118
- SDS. *See* Sodium dodecyl sulfate
- Seaborg's actinide concept, 75
- Secondary
 - classification, 16
 - elements, 13
 - group, 16
- Second rare-earth series, 75
- Self-assembled monolayer (SAM), 110
- Self-hydrolysis process, 419
- Self-propagating high temperature synthesis, 391
- SERS. *See* Surface enhanced Raman scattering
- Si(100), 135
- Si(111), 135
- Si₃N₄, 415
- Single
 - source precursor, 405, 410, 418–419
 - wall carbon nanotube (SWNT), 307
 - wavelength excitation, 428
- Singly occupied molecular orbital (SOMO), 132
- SiO₂, 365, 366, 369, 375, 377, 379, 380, 386, 387, 407, 414, 415, 418, 430
- Sm₂O₃, 317
- SmS₂, 439
- SmVO₄, 361
- Sodium
 - bis(2-ethylhexyl) sulfosuccinate, 288, 289
 - dodecyl sulfate (SDS), 291, 313, 363
 - malate, 354
 - tartrate, 354
- Sol-gel method, 292, 295, 303, 306, 311, 312, 326, 336, 342, 346, 351, 365, 366, 380–382, 385, 388–390, 394, 396–399, 401, 404
- Solid electrolyte, 389
- Solid state
 - electrochromic device, 448
 - laser, 404
 - reaction, 440
- Solvent extraction, 105
- Solvent-free crystals, 141
- Solvothermal method, 287, 289, 290, 313, 323
- SOMO. *See* Singly occupied molecular orbital
- Sonochemistry, 350, 355, 400
- Soxhlet extraction, 105
- Spatial hindrance, 254
- Spin
 - coating, 361, 394
 - density, 122
 - lattice relaxation, 124
 - splitting, 433
 - susceptibility, 140
- SQUID magnetometer, 139
- Stearic acid method, 392
- Stokes shift, 377, 378
- Structure type
 - β-BaLaCuSe₃, 239, 255
 - CaFe₂O₄, 187, 189
 - β-CaSiO₃, 176, 179
 - Ce₃Al_{1.67}S₇, 197, 198
 - Ce₆Si₄S₁₇, 173, 174
 - Dy₃Ge_{1.25}S₇, 168, 171
 - ErCuPbS₃, 240, 256
 - Er₅CuPb₃Se₁₁, 235, 252
 - Er₂PbS₄, 188, 190
 - Eu₂GeS₄, 176, 180
 - Eu₂SnS₄, 186, 187
 - Eu₂SnS₅, 181, 183
 - Eu₃Sn₂S₇, 184
 - Eu₅Sn₃S₁₂, 185
 - Eu₂SnSe₅, 186, 188
 - Hf₅CuSn₃, 175, 178
 - La₄Ag₂In₄S₁₃, 249, 260
 - La₃Ag_{0.82}SnS₇, 224, 230
 - La₂CuInS₅, 244, 246
 - La₂CuInSe₅, 246, 259
 - LaCuPbS₃, 243, 257
 - La₃CuSiS₇, 222, 224
 - La₂GeS₅, 168, 171

- Structure type (*cont.*)
 La₄Ge₃S₁₂, 172, 173
 La₃InS₆, 195–196
 La_{3.92}In_{4.76}S₁₃, 199
 La₂SnS₅, 179, 182
 Lu_{3.33}CuPb_{1.5}Se₇, 238, 254
 Nd₄In₅S₁₃, 197
 Pb_{1.75}Ag_{0.5}GeS₄, 226, 249
 R₃MZX₇, 262
 SrAl₂Se₄, 201–202
 Sr₂GeS₄, 173, 176
 Sr₂Ge₂Se₅, 177, 181
 Tb₃Ag_{0.59}GeS₇, 225, 248
 Tb₃In₅S₁₂, 202–203
 Tb₄Si₃S₁₂, 173, 177
 Th₃P₄, 191–192
 Tm₂PbSe₄, 191–192
 U₃ScS₆, 200–201
 Yb_{1.84}Fe_{1.23}S₄, 233, 251
 Yb₂FeS₄, 203–204
 YbIn₂S₄, 205, 207
 Yb₁₈In_{7.33}S₃₆, 203, 205
 Y_{3.33}CuPb_{1.5}S₇, 236, 238
 Y₂Cu_{0.20}Sn_{0.95}S₅, 232, 250
 Y₃Cu_{0.64}Sn_{1.09}S₇, 230, 250
 Y_{4.2}Pb_{0.7}Se₇, 193, 194
 Y₆Pb₂Se₁₁, 193, 195
- Sublimation, 140
 method, 105
- Superatoms, 137
- Superconducting oxide, 394
- Superconductivity of rare-earth metals, 80
- Superlattices, 290, 317, 320, 434, 449
- Superoxide dismutase, 308
- Surface enhanced Raman scattering (SERS), 279
- Surface
 modification, 323, 325
 plasmon resonance, 279
- Susceptibility, 139
- SWNT. *See* Single wall carbon nanotube
- Synchrotron X-ray diffraction (XRD), 110, 111, 114
- Tb(NO₃)₃, 406
 Tb(OH)₃, 326, 330
 Tb@C₈₂, 126
 TbF₃, 406
 TbMnO₃, 396
 Tb₂O₃, 316, 326
 Tb₄O₇, 325, 326, 330
 TbPO₄, 333, 341, 350
- TbS₂, 439
- Temperature-programmed reduction (TPR), 295, 300, 302
- Terbia, 7
- Ternary systems
 R–Ag–Te, 218
 R–Cu–X, 218
 R–Ge–X, 160
 R–In–X, 168
 R–Pb–X, 160
 R–Si–X, 160
 R–Sn–X, 160
- Terrace edges, 137
- Terre ochroite, 5
- 4-Tert-butyl benzyl alcohol, 313, 314
- Tetralvalency of cerium, 28
- Theoretical modeling, 280
- Thermal conductivity, 331, 389
- Thermal expansion coefficient, 387, 389
- Thermolysis method, 410, 423, 430
- Thiourea, 437, 443
- ThO₂, 76
- Three way catalysts (TWC), 295, 303
- Tm@C₈₂, 122
- Tm@C₈₂ (A, B, C), 129
- TmVO₄, 361
- TOA. *See* Trioctylamine
- TOPO. *See* Trioctylphosphine oxide
- TPP. *See* Tripolyphosphate
- TPR. *See* Temperature-programmed reduction
- Transitional function of primary groups, 17
- 1,2,4-Trichlorobenzene, 105
- Trioctylamine (TOA), 320
- Trioctylphosphine, 434, 436
 oxide (TOPO), 311, 316, 319, 320, 337, 411
- Tripolyphosphate (TPP), 336, 344
- Trisodium citrate, 354, 407, 422
- Tungstate, 392
- TWC. *See* Three way catalysts
- T1-weighted MRI, 145
- Two-stage HPLC method, 106
- UC. *See* Upconversion
- U@C₆₀, 100
- U@C₈₂, 144
- UHV-STM. *See* Ultra-high vacuum scanning tunneling microscopy
- Ultra-high vacuum scanning tunneling microscopy (UHV-STM), 110
- Ultrasonic extraction, 105
- Ultraviolet photoelectron spectroscopy (UPS), 113, 122, 132

- Ultraviolet-visible-near IR
 (UV-Vis-NIR) absorption, 128
 UO₂, 76
 Upconversion (UC), 323, 324, 404–407, 416,
 417, 419, 426–428, 430
 UPS. *See* Ultraviolet photoelectron
 spectroscopy
 Ursubstanz, 47
 UV-Vis-NIR. *See* Ultraviolet-visible-near IR
- Vacuum ultraviolet (VUV), 377, 379, 381,
 383–385, 404, 417
 Valencies of the rare earths, 14, 22, 35
 Vanadate, 343, 351, 352, 358, 360, 361
 Van den Broek, Antonius, 59
 van der Waals
 distance, 138
 interaction, 136
 Vibrational
 modes, 134
 structures, 133
 Victorium, 7
 Voids in the structures, 269
 coordination number, 269
 filling, 269
 origin, 269
 von Welsbach, Carl Auer, 46
 VUV. *See* Vacuum ultraviolet
- Water
 gas shift reaction (WGS), 281, 299–302,
 304, 306
 protons, 145
 soluble, 145
 Werner, Alfred, 71
 WGS. *See* Water gas shift reaction
 Wyruboff, Grégoire, 36
- X-ray
 absorption spectrum, 117
 spectra of elements, 56
 X-ray structural data, 119
- Y₃Al₅O₁₂, 388
 Y₄Al₂O₉, 388
- Y₃Al₅O₁₂ garnet, 388
 YbF₃, 416
 YbMnO₃, 400
 YBO₃, 377, 379–384
 YbOOH, 327
 YbPO₄, 336, 340
 (Y@C₈₂)₂, 137
 Y₂@C₈₂, 99
 Y@C₈₂, 99
 Y₂C₂@C₈₂, 121
 YCl₃, 80, 408, 409
 (Y@C₈₂)_n, 138
 YCoO₃, 398
 YF₃, 408–411, 415
 YMnO₃, 396
 Y₂O₃, 80
 Eu doped, 312, 313, 319, 321, 322
 Sm doped, 322
 Tb doped, 312, 313, 319, 321
 Yb,Er doped, 324
 Y₂O₂S, 439–442, 445–448
 Eu doped, 312, 440–442, 445
 YPO₄, 333, 341, 342, 346
 Y₂S₃, 439
 Y₂Si₂O₇, 385
 Y₂SiO₅, 385, 386
 Y₂Sn₂O₇, 390, 391
 Y₂Ti₂O₇, 389, 390
 Ytterby, 4
 Yttria, 4
 stabilized zirconia, 281
 Yttrium
 barium copper oxide, 281
 isopropoxide, 313
 YVO₄, 346, 347, 351–356, 358, 359,
 361, 362, 364–371, 373–375, 377,
 378, 384
- ZBLAN, 405
 ZDDP. *See* Zinc
 di-iso-amyl-octyl-dithiophosphate
 Zinc di-iso-amyl-octyl-dithiophosphate
 (ZDDP), 415
 ZnO, 279
 ZrO₂, 414